Complexity

Applications of Delay Differential Equations in Biological Systems 2021

Lead Guest Editor: F. A. Rihan
Guest Editors: C. Rajivganthi, Majid Bani-Yaghoub, and Shanmugam Lakshmanan

Applications of Delay Differential Equations in Biological Systems 2021

Complexity

Applications of Delay Differential Equations in Biological Systems 2021

Lead Guest Editor: F. A. Rihan
Guest Editors: C. Rajivganthi, Majid Bani-Yaghoub, and Shanmugam Lakshmanan

Contents

Contents

Hindawi
Complexity
Volume 2023, Article ID 9852348, 1 page
https://doi.org/10.1155/2023/9852348

Retraction

Retracted: A Comparison of Finite Difference and Finite Volume Methods with Numerical Simulations: Burgers Equation Model

Complexity

Received 15 August 2023; Accepted 15 August 2023; Published 16 August 2023

This article has been retracted by Hindawi following an investigation undertaken by the publisher [1]. This investigation has uncovered evidence of one or more of the following indicators of systematic manipulation of the publication process:

(1) Discrepancies in scope
(2) Discrepancies in the description of the research reported
(3) Discrepancies between the availability of data and the research described
(4) Inappropriate citations
(5) Incoherent, meaningless and/or irrelevant content included in the article
(6) Peer-review manipulation

The presence of these indicators undermines our confidence in the integrity of the article's content and we cannot, therefore, vouch for its reliability. Please note that this notice is intended solely to alert readers that the content of this article is unreliable. We have not investigated whether authors were aware of or involved in the systematic manipulation of the publication process.

Wiley and Hindawi regrets that the usual quality checks did not identify these issues before publication and have since put additional measures in place to safeguard research integrity.

We wish to credit our own Research Integrity and Research Publishing teams and anonymous and named external researchers and research integrity experts for contributing to this investigation.

The corresponding author, as the representative of all authors, has been given the opportunity to register their agreement or disagreement to this retraction. We have kept a record of any response received.

References

[1] A. H. Ali, A. S. Jaber, M. T. Yaseen, M. Rasheed, O. Bazighifan, and T. A. Nofal, "A Comparison of Finite Difference and Finite Volume Methods with Numerical Simulations: Burgers Equation Model," *Complexity*, vol. 2022, Article ID 9367638, 9 pages, 2022.

Hindawi
Complexity
Volume 2022, Article ID 7236824, 21 pages
https://doi.org/10.1155/2022/7236824

Research Article

A Detailed Study of a Fractal-Fractional Transmission Dynamical Model of Viral Infectious Disease with Vaccination

Kamal Shah[1,2] **Muhammad Sinan**[3] **Thabet Abdeljawad**[1,4] **M.A. El-Shorbagy**[5,6] **Bahaaeldin Abdalla**[1] **and Marwan S. Abualrub**[7]

[1]*Department of Mathematics and Sciences, Prince Sultan University, Riyadh 11586, Saudi Arabia*
[2]*Department of Mathematics, University of Malakand, Chakdara Dir (L), Khyber Pakhtunkhwa 18000, Pakistan*
[3]*School of Mathematical Sciences, University of Electronic Science and Technology of China, Chengdu 611731, China*
[4]*Department of Medical Research, China Medical University, Taichung 40402, Taiwan*
[5]*Department of Mathematics, College of Science and Humanities in Al-Kharj, Prince Sattam Bin Abdulaziz University, Al-Kharj 11942, Saudi Arabia*
[6]*Department of Basic Engineering Science, Faculty of Engineering, Menoufia University, Shebin El-Kom 32511, Egypt*
[7]*Mathematics Department (Prep.Programm) Faculty of Science, Khalifa University, P.O. Box 127788, Abu Dhabi, UAE*

Correspondence should be addressed to Thabet Abdeljawad; tabdeljawad@psu.edu.sa

Received 6 May 2022; Revised 29 May 2022; Accepted 22 September 2022; Published 14 November 2022

Academic Editor: Chongyang Liu

This article is devoted to investigate a mathematical model consisting on susceptible, exposed, infected, quarantined, vaccinated, and recovered compartments of COVID-19. The concerned model describes the transmission mechanism of the disease dynamics with therapeutic measures of vaccination of susceptible people along with the cure of the infected population. In the said study, we use the fractal-fractional order derivative to understand the dynamics of all compartments of the proposed model in more detail. Therefore, the first model is formulated. Then, two equilibrium points disease-free (DF) and endemic are computed. Furthermore, the basic threshold number is also derived. Some sufficient conditions for global asymptotical stability are also established. By using the next-generation matrix method, local stability analysis is developed. We also attempt the sensitivity analysis of the parameters of the proposed model. Finally, for the numerical simulations, the Adams–Bashforth method is used. Using some available data, the results are displayed graphically using various fractal-fractional orders to understand the mechanism of the dynamics. In addition, we compare our numerical simulation with real data in the case of reported infected cases.

1. Introduction

Various viral infectious diseases have greatly affected human life in the past. Some famous viral infectious diseases were known as swine flu, influenza, SARs, MERs, etc. Recently, coronavirus disease 2019 (COVID-19) has greatly affected human life all over the world. The said infection has been reported for the first time in Wuhan, China, in December 2019. After three months, the disease took the form of a pandemic which was announced by the WHO in April 2020 (see [1]). Recent estimates issued by the WHO showed that the full death toll associated directly or indirectly with the COVID-19 pandemic between 1 January 2020 and 31 December 2021 was approximately 14.9 million (see details in [2]). Approximately, more than six hundred million people have got infections (see [3, 4]). Since the outbreak surrounded the whole globe, each nation in the world has taken its own measures. Some countries have imposed a strict curfew and precautionary measures including wearing face masks, keeping social distance, and avoiding large gatherings. Europe has been seriously affected along with USA, Brazil, Iran, and India. Initially it was reported that the disease has been transmitted from some animals to humans because the virus was first identified in a man who was working in a fish market. After that, various researchers proved that bats are not a unique source and the mentioned

disease may be transmitted from other animals, person to person, and dogs (see [5, 6]).

Epidemiology is the most important branch of medical science and it has been very well developed in recent times. In the said area, various infectious diseases are investigated for treatment, controlling, curing, etc. Moreover, virology is a sub-branch, particularly dealing with virus and their transmitted diseases. Here, we remark that infectious diseases are investigated via various tools and methods. Biomathematics and bio-informatics engineering have attracted researchers recently more than in the past. It is worth mentioning that mathematical models are powerful tools to describe various real-world problems. Therefore, modeling infectious diseases is a hot area of research at the present time. In the said area, the dynamics of various infectious diseases are explained by using various differential or integral equations (some studies we refer to as [7–9]). Mathematical models help us to investigate various diseases for prediction and controlling procedures, to save society from great loss. Inspired by the aforesaid importance of mathematical models, researchers have formulated various real-world infectious diseases, we refer some as (see [10–15] and [16]). COVID-19 has been transmitted nearly to every part of the Earth and affected every nation of the world. The health conditions and economical situation of well-developed counties have been disturbed very well. In recent times, the world needs effective medication for the said diseases to save the lives of people. In this regard, great trials have been performed on vaccine preparation so far (for such detail, we refer [17]). Some authors have identified that COVID-19 vaccination in low and middle-income nations is extremely cost-effective and even price-saving (see [18]). The infection can be minimized all over the world by providing a vaccine to all nations of the world without any obstacles. Because by doing so, we can secure the next generation from the deadly virus. Moreover, some measures, like treatment, and vaccination, nonpharmaceutical precautionary measures, for instance, quarantine of confirmed cases, isolation, face masks, hand washing, social distancing, and avoiding gathering, should be imposed to reduce the transmission. Currently, some versions of the virus have been identified which indicate a new threat to human life. However, researchers have proved that the currently available vaccine is useful in medication. Moreover, it has been proved that vaccinated people if infected can easily be recovered compared to nonvaccinated people. However, this is not a permanent solution. Therefore, preparing proper vaccines and their availability without any bound in every society at a low price will be the best solution. Although, in some people, the vaccine has shown some adverse reactions. However, with the passage of time, things will become relaxed.

Most real-world problems are nonlinear in nature. In the same line, most epidemiological processes or phenomena are modeled in the form of nonlinear equations under traditional order derivatives or difference equations. As ordinary differential operators are local in nature and cannot produce the global dynamical behavior of the phenomenon, researchers are increasingly using fractional order derivatives in mathematical models (for instance, see [19–22], and [23]). A significant amount of work has been performed in this regard. Some well-known studies are referred here as [24–28], and [26]. In current times, in almost every discipline including fluid dynamics, bio-engineering, control theory, epidemiology, and rheology, the concept of fractional calculus is increasingly used to study various processes and phenomenons (see [29–32]). On the other hand, the said area has been exploited in engineering sides also recently (see [33–35]). Here it is worth mentioning that fractal geometry can be used as a powerful tool to investigate complex phenomena and every irregular picture in nature properly. Furthermore, fractal curves and surfaces are treated by using fractal dimensions to investigate their roughness. Because natural graphs are analyzed by using fractal interpolation (see some details in [36]). In previous times, due to the complex nature of fractional calculus, researchers have studied fractal surfaces through classical integer order calculus. Recently, many researchers have used the fractal-fractional order concept to investigate various real-world problems relating to epidemiology and physics, and chemical sciences. Here, we refer to some good work as [37].

Due to the ability to explain complex nature and preserve memory concepts, the idea of fractal calculus is widely used in the mathematical modeling of various diseases (details can be seen in [38]). For dealing with problems involving the fractal-fractional order derivatives, the traditional analytical and numerical techniques have been updated (see [39, 40], and [41]). Moreover, various numerical methods used for fractional derivatives have been applied to treat fractal-fractional problems. For instance, Adams–Bashforth procedure has been updated for dealing classical and fractal-fractional order problems (see [42–49]). Also, some authors have investigated other infectious diseases models like [50–54], and [55]. Authors [56] studied the psychological effects of staying home due to the COVID-19 pandemic. For instance, the authors applied a novel fractal-fractional order operator to the mathematical model of optimal control for malaria, where the derivative is defined in the Caputo sense. Two control variables have been introduced, as well as the necessary optimality condition in order to minimize the low-risk and high-risk infectious humans. Furthermore, the optimal control has been studied and results were simulated using a numerical scheme (see [57, 58]). In the same fashion, the author [59] proposed a compartmental mathematical model to acquire a better understanding of COVID-19's future dynamics. The problem has been described as a highly nonlinear coupled system of classical order ODEs, which has then been generalized using the fractal-fractional derivative with the Mittag-Leffler kernel. For recent work on fractional order models, see [60], and [61]. Moreover, the boundedness and non-negativity of the model have been established as well. Here it should be kept in mind that authors [62] studied the backward bifurcation of a vaccination model with nonlinear incidence. Authors [63] studied a COVID-19 model. Authors [64] studied some stability results in control process by using fractional derivative. For more applications of fractional derivative, we refer [65]. Using mathematical models and the concept of fractional calculus, we refer some

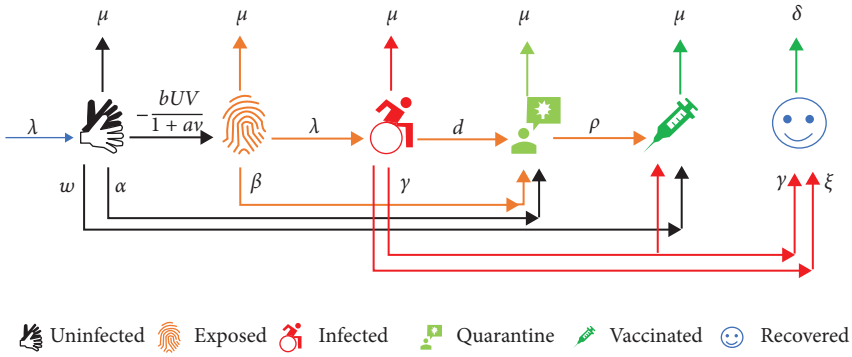

Figure 1: Compartment diagram of COVID–19.

recent work like [66–69], and [70]. Also authors investigated a fractional order model for HIV infection in [71].

Motivated by the aforesaid discussion, we formulate the proposed model under the fractal-fractional order derivative. We investigate the proposed mathematical model with the vaccinated class by considering the available therapeutic measures, vaccination of susceptible, and curing of infected/hospitalized people. Our considered model involves some important epidemiological and biological features of the said disease like inhibitory effect, death rates due to infection and nature, birth rate, and different vaccination rates. A flow chart of our study is given in Figure 1.

Considering the compartmental diagram, the model is formulated as

$$\left.\begin{aligned}
{}^{\mathrm{FFP}}_{0}\mathscr{D}^{\upsilon,\pi}U(t) &= \Lambda - \frac{bUV}{1+aV} - (\omega+\mu+\alpha)U,\\
{}^{\mathrm{FFP}}_{0}\mathscr{D}^{\upsilon,\pi}V(t) &= \frac{bUV}{1+aV} - (\lambda+\mu+\beta)V,\\
{}^{\mathrm{FFP}}_{0}\mathscr{D}^{\upsilon,\pi}W(t) &= \lambda V - (\mu+\xi+\gamma+d)W,\\
{}^{\mathrm{FFP}}_{0}\mathscr{D}^{\upsilon,\pi}Q(t) &= \alpha U + \beta V + dW - (\mu+\rho)Q,\\
{}^{\mathrm{FFP}}_{0}\mathscr{D}^{\upsilon,\pi}X_v &= \omega U + \rho Q + \gamma W - \mu X_v,\\
{}^{\mathrm{FFP}}_{0}\mathscr{D}^{\upsilon,\pi}Y &= \xi W + \gamma W - \delta Y.
\end{aligned}\right\} \quad (1)$$

Symbols involved in model (1) are described in Table 1. Also, the nomenclature and their dimensions are described in Table 2.

Using various tools of mathematical analysis, we establish global and local stability. The said analysis is established by the Lyapunov method and next-generation matrix method. Moreover, by using the Pontryagin maximum principle, we develop some results about the optimal control procedure. Furthermore, sensitivity analysis is also investigated about the parameters involved in our proposed model. Some results for numerical stability are derived by using the Ulam–Hyers concept. We also perform numerical simulation for our considered model by using a numerical method based on the Adams–Bashforth method to investigate multiphase behaviors under various fractal-fractional order derivatives. Here, we remark that multistep methods are increasingly used because these procedures are more efficient than the earlier methods like the Euler method. Moreover, the derivation of the Adams–Bashforth method can be performed in a number of ways. By using numerical interpolation and numerical integration, one can easily derive the aforesaid method. Therefore, we use the aforesaid scheme to simulate our model by using some numerical values of the parameters and initial data given in Table 1. A graphical presentation of some real data and discussion are provided.

Table 1: The compartments and their description involved in model (1) with initial values.

Variables	Physical representation	Initial values
U	The uninfected class	2500
V	The exposed class	20
W	The infected class	70
Q	The quarantine class	3
X_v	The vaccinated class	10
Y	The recovered class	20

Table 2: The parameters and their description involved in model (1).

Variables	Physical representation	Dimension
Λ	Birth rate	month^{-1}
ξ	COVID-19 death rate	month^{-1}
μ	Natural death rate	month^{-1}
a	Inhibitory effect rate	month^{-1}
b	Saturation constant	month^{-1}
β	Infection rate from exposed class	month^{-1}
α	Rate of quarantine from susceptible class	month^{-1}
β	Rate of quarantine from exposed class	month^{-1}
d	Quarantine from infected class	month^{-1}
ω	Vaccination rate of susceptible	month^{-1}
γ	Vaccination rate of infected	month^{-1}
ρ	Vaccination rate of quarantine	month^{-1}

2. Preliminaries

In this section, we recall the fractional-fractional operators as given below.

Definition 1 (see [61]). Let the function v be differentiable in the opened interval (a, b), then the fractional-fractional derivative with υ and π are fractal and fractional orders, respectively, in the Caputo sense with power law is given as

$$
\begin{aligned}
{}^{\mathrm{FFP}}_{a}\mathscr{D}^{\upsilon,\pi}_{\mathrm{t}}v(\mathrm{t}) &= \frac{1}{\Gamma[m-\pi]}\int_a^{\mathrm{t}}\frac{\mathrm{d}v(\xi)}{\mathrm{d}\xi^{\upsilon}}(\mathrm{t}-\xi)^{m-\pi-1}\mathrm{d}\xi,\\
& m-1<\pi\le m, 0<m-1<\upsilon\le m, \qquad (2)\\
\frac{\mathrm{d}v(\xi)}{\mathrm{d}\xi^{\upsilon}} &= \lim_{\mathrm{t}-\xi}\frac{v(\mathrm{t})-v(\xi)}{\mathrm{t}^{\upsilon}-\xi^{\upsilon}}.
\end{aligned}
$$

Here, v is continuous over the interval (a, b).

Definition 2 (see [61]). The fractal-fractional integral of a function v with fractal order $\upsilon > 0$ and fractional order $\pi > 0$ is defined as

$$
{}^{\mathrm{FFP}}_{0}\mathscr{I}^{\upsilon,\pi}_{\mathrm{t}}v(\mathrm{t}) = \frac{\upsilon}{\Gamma(\pi)}\int_0^{\mathrm{t}}\xi^{\lambda-1}v(\xi)(\mathrm{t}-\xi)^{\pi-1}\mathrm{d}\xi, \qquad (3)
$$

where v is continuous over the interval (a, b).

Definition 3. Consider the fractal-fractional nonlinear ODE, such that

$$
{}^{\mathrm{FFP}}_{0}\mathscr{D}^{\upsilon,\pi}g(t) = v(t,u(t)), \text{with} g(0) = g_0. \qquad (4)
$$

From [45], the resultant Adams–Bashforth scheme for (4) can be written as

$$
\begin{aligned}
g(l+1) = g_0 + \frac{\upsilon\hbar^{\pi}}{\Gamma(\pi+2)}\sum_{j=0}^{f}\Big[t^{\upsilon-1}_{(j)}g\big(w_{(j)},t_j\big)\times\big((f+1-j)^{\upsilon}(f-j+2+v)-(f-j)^{\upsilon}(f-j+2+2v)\big)\\
- t^{\upsilon-1}_{(j-1)}v\big(w_{(j-1)},t_{(j-1)}\big)\big((f+1-j)^{\upsilon}+1-(f-j)^{\upsilon}(f-j+1+v)\big)\Big].
\end{aligned} \qquad (5)
$$

3. Equilibrium Points and Stability

This section is enriched with various stability results and equilibrium points.

3.1. Equilibrium Points. The disease-free equilibrium point is given by

$$
\mathscr{E}^0 = \big(U^0, 0, 0, 0, X^0_{\nu}, 0\big), \qquad (6)
$$

where

$$
\begin{aligned}
U^0 &= \frac{\lambda}{(\omega+\mu+\alpha)},\\
X^0_{\nu} &= \frac{\omega}{\mu(\omega+\mu+\alpha)},
\end{aligned} \qquad (7)
$$

while the positive disease-endemic equilibrium is computed in terms of one class such that

$$
\mathscr{E}^* = (U^*, V^*, W^*, Q^*, X^*_V, Y^*), \qquad (8)
$$

where

$$
\left.
\begin{aligned}
V^* &= \frac{U^*(\omega+\mu+\alpha)-\lambda}{\lambda+\mu+\beta},\\
W^* &= \frac{\lambda U^*(\omega+\mu+\alpha)-\lambda^2}{(\mu+\xi+\gamma+d)(\lambda+\mu+\beta)},\\
Q^* &= \frac{1}{\mu+\rho}\left[\alpha U^* + \frac{\beta U^*(\omega+\mu+\alpha)-\lambda}{\lambda+\mu+\beta} + \frac{d\lambda\, U^*(\omega+\mu+\alpha)-\lambda^2}{(\mu+\xi+\gamma+d)(\lambda+\mu+\beta)}\right],\\
X^*_V &= \frac{\rho}{\mu(\mu+\rho)}\left[\frac{\beta U^*(\omega+\mu+\alpha)-\lambda}{(\lambda+\mu+\beta)} + \frac{d\lambda\, U^*(\omega+\mu+\alpha)-\lambda^2}{(\mu+\xi+\gamma+d)(\lambda+\mu+\beta)} + \alpha U^*\right],\\
Y^* &= \frac{\xi+\gamma}{\delta}\left[\frac{\lambda U^*(\omega+\mu+\alpha)-\lambda^2}{(\mu+\xi+\gamma+d)(\lambda+\mu+\beta)}\right].
\end{aligned}
\right\} \qquad (9)
$$

3.2. Basic Reproduction Number

$$\frac{dZ}{dt}|_{E^0} = F - V. \tag{10}$$

The nonlinear and linear terms of the infected classes in matrices F and V, respectively, are given as

$$F = \begin{pmatrix} \frac{UVb}{Va+1} \\ 0 \\ 0 \\ 0 \end{pmatrix}, \tag{11}$$

$$V = \begin{pmatrix} V(\beta+\lambda+\mu) \\ W(d+\gamma+\mu+\xi) - V\lambda \\ Q(\mu+\rho) - V\beta - W\ d - U\alpha \\ X_v\mu - Q\rho - U\omega - W\gamma \end{pmatrix}.$$

Now, the Jacobian matrix of F and V is given by

$$F = \begin{pmatrix} U^0 b & 0 & 0 & 0 \\ 0 & 0 & 0 & 0 \\ 0 & 0 & 0 & 0 \\ 0 & 0 & 0 & 0 \end{pmatrix}, \tag{12}$$

$$V = \begin{pmatrix} \beta+\lambda+\mu & 0 & 0 & 0 \\ -\lambda & d+\gamma+\mu+\xi & 0 & 0 \\ -\beta & -d & \mu+\rho & 0 \\ 0 & -\gamma & -\rho & \mu \end{pmatrix}.$$

Calculating the inverse of matrix V and the next-generation matrix $G(E^0)$, such that

$$V^{-1} = \begin{pmatrix} \frac{1}{\beta+\lambda+\mu} & 0 & 0 & 0 \\ \frac{\lambda}{(\beta+\lambda+\mu)(d+\gamma+\mu+\xi)} & \frac{1}{d+\gamma+\mu+\xi} & 0 & 0 \\ \frac{\beta\ d+\beta\gamma+\beta\mu+d\lambda+\beta\xi}{(\mu+\rho)(\beta+\lambda+\mu)(d+\gamma+\mu+\xi)} & \frac{d}{(\mu+\rho)(d+\gamma+\mu+\xi)} & \frac{1}{\mu+\rho} & 0 \\ \frac{\beta\ d\rho+\beta\gamma\rho+\gamma\lambda\mu+\beta\mu\rho+d\lambda\ \rho+\gamma\lambda\rho+\beta\rho\xi}{\mu(\mu+\rho)(\beta+\lambda+\mu)(d+\gamma+\mu+\xi)} & \frac{\gamma\mu+d\rho+\gamma\rho}{\mu(\mu+\rho)(d+\gamma+\mu+\xi)} & \frac{\rho}{\mu(\mu+\rho)} & \frac{1}{\mu}. \end{pmatrix}. \tag{13}$$

Thus, the nonzero and largest eigenvalue is the basic reproduction number $\mathscr{R}_0$, which is

$$R_0 = \frac{b\lambda}{(\omega+\mu+\alpha)(\beta+\lambda+\mu)}. \tag{14}$$

3.3. Stability Analysis

Lemma 1 (see [60]). *Let A be a 2×2 matrix, then the eigenvalues of the matrix A are negative in real part if $trace(A) < 0$, and $det(A) > 0$.*

Theorem 1. *The COVID-19 model at the disease-free equilibrium point E^0, is locally asymptotically stable if $\mathscr{R}_0 < 1$, otherwise unstable.*

Proof 1. The Jacobian matrix of system (1) at disease-free equilibrium point E^0 is given by

$$J(E^0) = \begin{pmatrix} -\alpha-\mu-\omega & -U^0 b & 0 & 0 & 0 & 0 \\ 0 & U^0 b-\lambda-\mu-\beta & 0 & 0 & 0 & 0 \\ 0 & \lambda & -d-\gamma-\mu-\xi & 0 & 0 & 0 \\ \alpha & \beta & d & -\mu-\rho & 0 & 0 \\ \omega & 0 & \gamma & \rho & -\mu & 0 \\ 0 & 0 & \gamma+\xi & 0 & 0 & -\delta \end{pmatrix}. \tag{15}$$

Following the characteristic equation of the Jacobian matrix (14), we have

$$\begin{aligned}&(\varepsilon+\delta)(\varepsilon+\mu)(\varepsilon+(\mu+\rho))(\varepsilon+(d+\gamma+\mu+\xi))\\&(\varepsilon+(\alpha+\mu+\omega))\left(\varepsilon-\left(\lambda+\mu+\beta-U^{0}b\right)\right)=0.\end{aligned}\tag{16}$$

Thus, the eigenvalues of the characteristic (16) are given by

$$\left.\begin{aligned}\varepsilon_1&=-\delta,\\\varepsilon_2&=-\mu,\\\varepsilon_3&=-(\mu+\rho),\\\varepsilon_4&=-(d+\gamma+\mu+\xi),\\\varepsilon_5&=-(\alpha+\mu+\omega),\\\varepsilon_6&=(\lambda+\mu+\beta)[R_0-1].\end{aligned}\right\}.\tag{17}$$

As a result, all eigenvalues of the Jacobian matrix (15) are negative for $(\lambda+\mu+\beta)[R_0-1]<0$, such that $R_0<1$. Hence, model (1) is locally asymptotically stable around a disease-free equilibrium point. □

Theorem 2. *The COVID-19 model at the disease-endemic equilibrium point E^* is locally asymptotically stable if $R_0>1$, otherwise unstable.*

Proof 2. The Jacobian matrix of system (1) at disease-endemic equilibrium point E^* is given by

$$J_1(E^*)=\begin{pmatrix}-(\alpha+\mu+\omega)-\dfrac{V^*b}{V^*a+1} & -\dfrac{U^*b}{(V^*a+1)^2} & 0 & 0 & 0 & 0\\ \dfrac{V^*b}{V^*a+1} & \dfrac{U^*b}{V^*a+1}-(\lambda+\mu+\beta)-\dfrac{U^*V^*ab}{(V^*a+1)^2} & 0 & 0 & 0 & 0\\ 0 & \lambda & -(d+\gamma+\mu+\xi) & 0 & 0 & 0\\ \alpha & \beta & d & -(\mu+\rho) & 0 & 0\\ \omega & 0 & \gamma & \rho & -\mu & 0\\ 0 & 0 & \gamma+\xi & 0 & 0 & -\delta\end{pmatrix},\tag{18}$$

$$(\varepsilon+\delta)(\varepsilon+\mu)(\varepsilon+(\mu+\rho))(\varepsilon+(d+\gamma+\mu+\xi))(\varepsilon+(\alpha+\mu+\omega))=0.$$

Thus, eigenvalues of the characteristic (16) are given by

$$\left.\begin{aligned}\varepsilon_1&=-\delta,\\\varepsilon_2&=-\mu,\\\varepsilon_3&=-(\mu+\rho),\\\varepsilon_4&=-(d+\gamma+\mu+\xi).\end{aligned}\right\}.\tag{19}$$

However, the reduced matrix takes the form

$$J_2(E^*)=\begin{pmatrix}-(\alpha+\mu+\omega)-\dfrac{V^*b}{V^*a+1} & -\dfrac{U^*b}{(V^*a+1)^2}\\ \dfrac{V^*b}{V^*a+1} & \dfrac{U^*b}{V^*a+1}-(\lambda+\mu+\beta)-\dfrac{U^*V^*ab}{(V^*a+1)^2}\end{pmatrix}.\tag{20}$$

The matrix (20) possesses negative eigenvalues if the trace $(J_2(E^*))$ is negative and determinant $(J_2(E^*))$ is positive, such that

$$\text{Trace}\left(J_2\left(E^*\right)\right) = -(\alpha+\mu+\omega) - \frac{V^*b}{V^*a+1} - (\lambda+\mu+\beta) - \frac{U^*b}{1+aV^*}\left(\frac{aV^*}{1+aV^*} - 1\right) < 0,$$

$$\text{Determinant}\left(J_2\left(E^*\right)\right) = \frac{b}{(1+aV^*)}\left((\alpha+\mu+\omega) + \frac{V^*b}{V^*a+1} + (\lambda+\mu+\beta) + \frac{U^*b}{1+aV^*}\left(\frac{aV^*}{1+aV^*} - 1\right)\right)\left(\frac{U^*}{1+aV^*} - V\right) > 0. \tag{21}$$

The determinant is positive if $U^*b/V^*a + 1 > U^*V^*ab/(V^*a+1)^2$. Hence, model (1) is locally asymptotically stable around the disease-endemic equilibrium point with negative eigenvalues of $J_1(E^*)$ and $R_0 > 1$. □

4. Globally Asymptotical Stability

Theorem 3. *For nonautonomous fractional order system, let* $\overline{a} = 0$ *be an equilibrium point, such that*

$$^{\text{FFP}}D_t^{\upsilon,\pi}\overline{a}(t) = g(t,\overline{a}), \overline{a}\left(t_0\right) = \overline{a}_0. \tag{22}$$

Let $\Lambda \subseteq R^n$ be a domain which contains $\overline{a} = 0$. Let $\mathscr{L}(t,\overline{a})$: $[t_0,\infty] \times \Lambda \longrightarrow R$ be a continuously differentiable function such that $\overline{w}_1(\overline{a}) \le \overline{v}(t,\overline{a}) \le \overline{w}_2(u)$ and $^{\text{FFP}}D_t^{\upsilon}\mathscr{L}(t,\overline{a}) \le -\overline{w}_3(\overline{a})$, for $t \ge 0, \overline{a} \in \Omega$,where continuous positive definite functions $\overline{w}_1(\overline{a}), \overline{w}_2(\overline{a})$, and $\overline{w}_3(\overline{a})$ on Λ and $\mathscr{L}$ is Lyapunov candidate function, then, $\overline{a} = 0$, is globally asymptotically stable.

Lemma 2. *For the fractal-fractional order, we use the lemma defined for fractional order ODE from [42, 60]. At any instant of time* $t \ge t_0$, *assume a continuous differentiable function* $\overline{a}$ *as*

$$\frac{1}{2}\,^{FFP}D_t^{\upsilon,\pi}\overline{a}^2(\mathbf{t}) \le {}^{FFP}D_{\mathbf{t}}^{\upsilon,\pi}\overline{a}(t), \text{for all} \upsilon, \pi \in (0,1). \tag{23}$$

Theorem 4. *Equilibrium point* E^* *is globally asymptotically stable.*

Proof 3. We consider the quadratic Lyapunov function to derive the Lyapunov candidate function for fractional order differential equation.

$$\mathscr{L}\left(\overline{a}_1, \overline{a}_2, \overline{a}_3, \ldots, \overline{a}_n\right) = \sum_{k=1}^{n} \frac{s_k}{2}\left(\overline{a}_k(t) - \overline{a}^*\right)^2. \tag{24}$$

We define the Lyapunov candidate function as

$$\begin{aligned}\mathscr{L}\left(U(t),V(t),W(t),Q(t),X_v(t),Y(t)\right) &= \frac{1}{2}\left(U(t)-U^*\right) + \frac{1}{2}\left(V(t)-V^*\right) + \frac{1}{2}\left(W(t)-W^*\right) + \frac{1}{2}\left(Q(t)-Q^*\right) \\ &+ \frac{1}{2}\left(X_v(t)-X_v^*\right) + \frac{1}{2}\left(Y(t)-Y^*\right).\end{aligned} \tag{25}$$

The linearity property is given as

$$\begin{aligned}&{}_0^{\text{FFP}}D_t^{\upsilon,\pi}\mathscr{L}\left(U(t),V(t),W(t),Q(t),X_v(t),Y(t)\right) \\ &= \frac{1}{2}\left[{}_0^{\text{FFP}}D_t^{\upsilon,\pi}\left(U(t)-U^*\right) + {}_0^{\text{FFP}}D_t^{\upsilon,\pi}\left(V(t)-V^*\right) + {}_0^{\text{FFP}}D_t^{\upsilon,\pi}\left(W(t)-W^*\right) + {}_0^{\text{FFP}}D_t^{\upsilon,\pi}\left(Q(t)-Q^*\right) + {}_0^{\text{FFP}}D_t^{\upsilon,\pi}\left(X_v(t)-X_v^*\right) + {}_0^{\text{FFP}}D_t^{\upsilon,\pi}\left(Y(t)-Y^*\right)\right].\end{aligned} \tag{26}$$

Using Lemma 2, we have

$$
\begin{aligned}
{}_{0}^{\mathrm{FFP}}D_{t}^{\upsilon,\pi}\mathscr{L}\left(U(t),V(t),W(t),Q(t),X_{\nu}(t),Y(t)\right) &= {}_{0}^{\mathrm{FFP}}D_{t}^{\upsilon,\pi}\left(U(t)-U^{*}\right)+{}_{0}^{\mathrm{FFP}}D_{t}^{\upsilon,\pi}\left(V(t)-V^{*}\right)\\
&+{}_{0}^{\mathrm{FFP}}D_{t}^{\upsilon,\pi}\left(W(t)-W^{*}\right)+{}_{0}^{\mathrm{FFP}}D_{t}^{\upsilon,\pi}\left(Q(t)-Q^{*}\right)+{}_{0}^{\mathrm{FFP}}D_{t}^{\upsilon,\pi}\left(X_{\nu}(t)-X_{\nu}^{*}\right)\\
&+{}_{0}^{\mathrm{FFP}}D_{t}^{\upsilon,\pi}\left(Y(t)-Y^{*}\right)\leq\lambda-\mu\left(N(t)-N^{*}\right)-\mu\left(Y(t)-Y^{*}\right)-\delta\left(Y(t)-Y^{*}\right),
\end{aligned}
\tag{27}
$$

which further implies that

$$
{}_{0}^{\mathrm{FFP}}D_{t}^{\upsilon,\pi}\mathscr{L}\left(U(t),V(t),W(t),Q(t),X_{\nu}(t),Y(t)\right)\leq\lambda-\mu\left(N(t)-N^{*}\right)-\mu\left(Y(t)-Y^{*}\right)-\delta\left(Y(t)-Y^{*}\right).
\tag{28}
$$

□

4.1. Global Stability at Disease-Free Equilibrium Point E^0. Using disease-free equilibrium point, $N^0 = (\Lambda/\mu)$ in the last equation of the proposed model, one has

$$
\begin{aligned}
&{}_{0}^{\mathrm{FFP}}D_{t}^{\upsilon,\pi}\mathscr{L}\left(U(t),V(t),W(t),Q(t),X_{\nu}(t),Y(t)\right)\\
&\leq\lambda-\mu\left(N(t)-N^{0}\right)-\mu\left(Y(t)-Y^{0}\right)-\delta\left(Y(t)-Y^{0}\right)\\
&\leq\lambda-\mu\left(N(t)-\frac{\lambda}{\mu}\right)-Y(t)(\mu+\delta)\leq-\overline{w}(\overline{a}(t)).
\end{aligned}
\tag{29}
$$

The last inequality (29) is negative if $\overline{w}(\overline{a}(t))>0$, such that if $\lambda>\mu(N(t)-\lambda/\mu)+Y(t)(\mu+\delta)$. Hence, model (1) is globally asymptotically stable around disease-free equilibrium point, E^0 with N^0.

4.2. Global Stability at Disease-Endemic Equilibrium Point E^*. For global stability around disease-endemic equilibrium point E^* and N^*, we have

$$
\begin{aligned}
&{}_{0}^{\mathrm{FFP}}D_{t}^{\upsilon,\pi}\mathscr{L}\left(U(t),V(t),W(t),Q(t),X_{\nu}(t),Y(t)\right)\\
&\leq\lambda-\mu\left(N(t)-N^{*}\right)-\mu\left(Y(t)-Y^{*}\right)-\delta\left(Y(t)-Y^{*}\right),
\end{aligned}
\tag{30}
$$

where

$$
\begin{aligned}
N^{*} &= \frac{\lambda-Y^{*}(\mu+\delta)}{\mu},\\
Y^{*} &= \frac{\xi+\gamma}{\delta}\left[\frac{\lambda U^{*}(\omega+\mu+\alpha)-\lambda^{2}}{(\mu+\xi+\gamma+d)(\lambda+\mu+\beta)}\right].
\end{aligned}
\tag{31}
$$

From (30) and (31), we obtain

$$
\begin{aligned}
&{}_{0}^{\mathrm{FFP}}D_{t}^{\upsilon,\pi}\mathscr{L}\left(U(t),V(t),W(t),Q(t),X_{\nu}(t),Y(t)\leq 2\lambda-\mu N(t)\right)\\
&\quad-Y^{*}(\mu+\delta),\\
&\quad-Y(t)(\mu+\delta)-\frac{\xi+\gamma}{\delta}\left[\frac{\lambda U^{*}(\omega+\mu+\alpha)-\lambda^{2}}{(\mu+\xi+\gamma+\mathrm{d})(\lambda+\mu+\beta)}\right](\mu+\delta),\\
&\leq-\overline{w}(\overline{a}(t)).
\end{aligned}
\tag{32}
$$

The last inequality (32) is negative if $\overline{w}(\overline{a}(t))$ is positive such that, if $2\lambda>\mu N(t)+Y^{*}(\mu+\delta)+Y\ (t)(\mu+\delta)+\xi+\gamma/\delta[\lambda U^{*}(\omega+\mu+\alpha)-\lambda^{2}/(\mu+\xi+\gamma+\mathrm{d})(\lambda+\mu+\beta)](\mu+\delta)$. Hence, model (1) is globally asymptotically stable around disease-endemic equilibrium point, E^* with N^*.

5. Sensitivity Analysis

$$
\mathbb{S}_{p}^{R_0}=\frac{p}{R_0}\left[\frac{\partial R_0}{\partial p}\right].
\tag{33}
$$

Now, according to the (33) relation, we have

$$
\left.
\begin{aligned}
S_{\nu}^{R_0} &= \frac{b}{R_0}\left[\frac{\lambda}{(\beta+\lambda+\mu)(\alpha+\mu+\omega)}\right]>0,\\
S_{\tau}^{R_0} &= \frac{\lambda}{R_0}\left[\frac{b(\beta+\mu)}{(\beta+\lambda+\mu)^{2}(\alpha+\mu+\omega)}\right]>0,\\
S_{\vartheta}^{R_0} &= -\frac{\omega}{R_0}\left[\frac{b\lambda}{(\beta+\lambda+\mu)(\alpha+\mu+\omega)^{2}}\right]<0,\\
S_{\chi}^{R_0} &= -\frac{\mu}{R_0}\left[\frac{b\lambda(\alpha+\beta+\lambda+2\mu+\omega)}{(\beta+\lambda+\mu)^{2}(\alpha+\mu+\omega)^{2}}\right]<0,\\
S_{\varrho_1}^{R_0} &= -\frac{\alpha}{R_0}\left[\frac{b\lambda}{(\beta+\lambda+\mu)(\alpha+\mu+\omega)^{2}}\right]<0,\\
S_{\upsilon}^{R_0} &= -\frac{\beta}{R_0}\left[\frac{b\lambda}{(\beta+\lambda+\mu)^{2}(\alpha+\mu+\omega)}\right]<0.
\end{aligned}
\right\}.
\tag{34}
$$

Here, in Figures 2–7, we have described graphically the dynamics of sensitivity analysis of various parameters, respectively.

Furthermore, we present Table 3 for the sensitivity index of each parameter associated with R_0 based on system (34).

Considering Table 3, the change in the value of each parameter in the basic reproduction number causes an increase or decrease in the value of the basic reproduction number R_0. Hence, it directly affects the spread in the population while keeping the values of the remaining

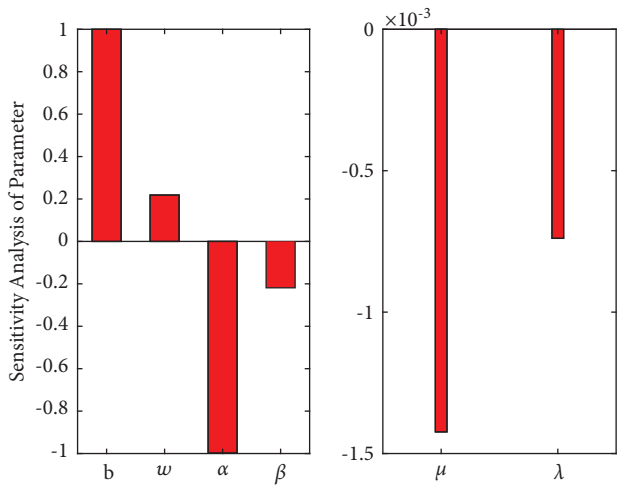

Figure 2: The dynamics of sensitivity analysis based on R_0 with respect to each parameter associated with R_0.

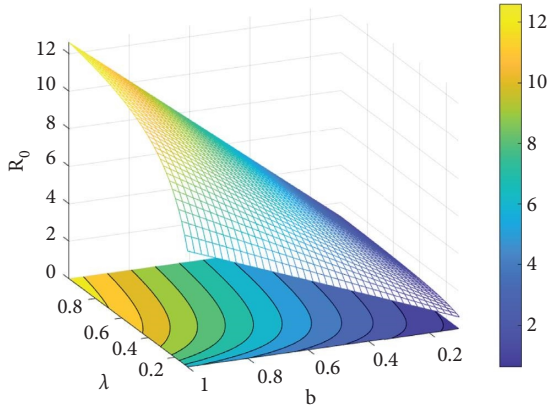

Figure 3: The dynamics of sensitivity analysis with respect to parameters λ and b with R_0.

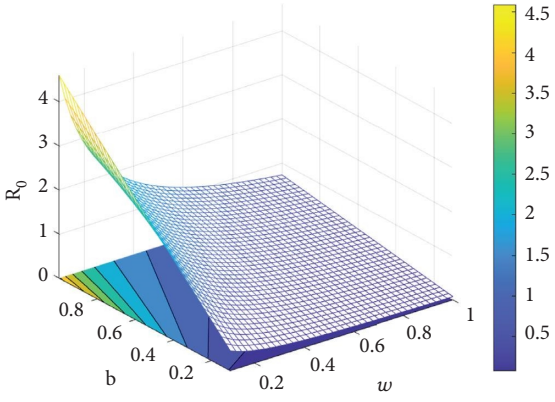

Figure 4: The dynamics of sensitivity analysis with respect to parameters ω and b with R_0.

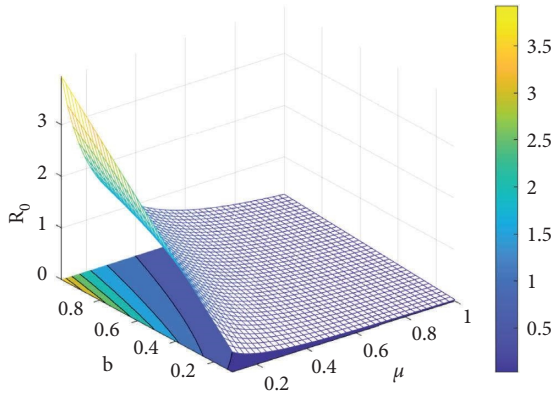

Figure 5: The dynamics of sensitivity analysis with respect to parameters μ and b with R_0.

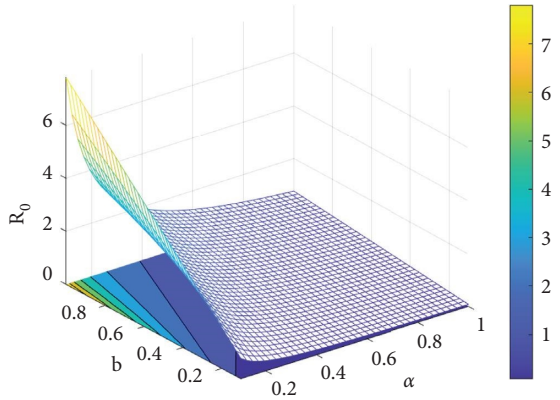

Figure 6: The dynamics of Sensitivity Analysis with respect to parameters α and b with R_0.

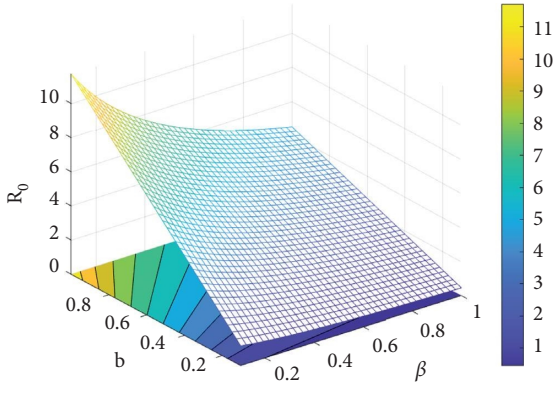

Figure 7: The dynamics of sensitivity analysis with respect to parameters β and b with R_0.

Table 3: Sensitivity of the R_0 versus proposed parameters.

Parameter	Sensitivity index	Value	Parameter	Sensitivity index	Value
b	$\mathbf{s}_b^{R_0}$	1.0000	ω	$\mathbf{s}_\omega^{R_0}$	0.2188
α	$\mathbf{s}_\alpha^{R_0}$	−0.9979	β	$\mathbf{s}_\beta^{R_0}$	−0.2187
μ	$\mathbf{s}_\mu^{R_0}$	−0.0014	λ	$\mathbf{s}_\lambda^{R_0}$	−0.0007

parameters constant. Furthermore, in Table 3, if the sensitivity index $\mathbf{s}_p^{R_0}$ for parameter p goes negatively, then there is an inverse effect on R_0. The parameters show the negative effect must be minimized for the sake of the spread of infection in the population. Moreover, the sensitivity index of b is positive at its peak.

6. Ulam–Hyers Stability

Stability theory is an important branch of the qualitative theory of differential equations. As we know, the computation of exact solutions to some problems is quite challenging to obtain. Therefore, various numerical techniques were developed to find a solution. In this regard, we check the stability of the given problem. We can find various types of stability in literature, including Lyapunov, exponential, and asymptotic. But the most important type of stability, which is first introduced by Ulam in 1940 is called Ulam stability. He posed a problem about the stability of functional equations. The proper introduction was given by Hyers in 1941. Therefore, this stability was named Ulam–Hyers stability (see [72, 73]). The said stability results have been extended and generalized by researchers for difference and functional equations in different directions. From a numerical and optimization point of view, Ulam–Hyers stability is essential because it provides a bridge between the exact and numerical solutions. The said stability is most useful and also easy to establish for the approximated solution o model (1). Therefore, in this section, by the use of nonlinear functional analysis, some adequate conditions are constructed for the mentioned stability of the proposed model (1).

$$\left.\begin{aligned}
{}^{\mathrm{FFP}}_{0}D^{\nu,\pi}U(t) &= \Lambda - \frac{bUV}{1+aV} - (\omega-\mu+\alpha)U,\\
{}^{\mathrm{FFP}}_{0}D^{\nu,\pi}W(t) &= \frac{bUV}{1+aV} - (\lambda+\mu+\beta)V,\\
{}^{\mathrm{FFP}}_{0}D^{\nu,\pi}Q(t) &= \lambda V - (\mu+\xi+\gamma+d)W,\\
{}^{\mathrm{FFP}}D^{\nu,\pi}X(t) &= \alpha U + \beta V + \alpha W - (\mu+\rho)Q,\\
{}^{\mathrm{FFP}}D^{\nu,\pi}_{0}Y(t) &= \omega U + \rho Q + \gamma W - \mu X_v,\\
&= \xi W + \gamma W - \delta Y.
\end{aligned}\right\}. \tag{35}$$

We express model (35) as

$$\left.\begin{aligned}
f_1(t,U,D,W,Q,X,Y) &= \Lambda - \frac{bUV}{1+aV} - (\omega-\mu+\alpha)U,\\
f_2(t,U,D,W,Q,X,Y) &= \frac{bUV}{1+aV} - (\lambda+\mu+\beta)V,\\
f_3(t,U,D,W,Q,X,Y) &= \lambda V - (\mu+\xi+\gamma+d)W,\\
f_4(t,U,D,W,Q,X,Y) &= \alpha U + \beta V + dW - (\mu+\rho)Q,\\
f_5(t,U,D,W,Q,X,Y) &= \omega U + \rho Q + \gamma W - \mu X_v,\\
f_6(t,U,D,W,Q,X,Y) &= \xi W + \gamma W - \delta Y.
\end{aligned}\right\}. \tag{36}$$

The proposed problem (35) can be reformulated in the following form:

$$\left.\begin{aligned}
{}^{c}_{0}D^{\pi}U(t) &= \nu t^{\nu-1} f_1(t,U,D,W,Q,X,Y),\\
{}^{c}_{0}D^{\pi}V(t) &= \nu t^{\nu-1} f_2(t,U,D,W,Q,X,Y),\\
{}^{c}_{0}D^{\pi}V(t) &= \nu t^{\nu-1} f_3(t,U,D,W,Q,X,Y),\\
{}^{c}_{0}D^{\pi}V(t) &= \nu t^{\nu-1} f_4(t,U,D,W,Q,X,Y),\\
{}^{c}_{0}D^{\pi}V(t) &= \nu t^{\nu-1} f_5(t,U,D,W,Q,X,Y),\\
{}^{c}_{0}D^{\pi}V(t) &= \nu t^{\nu-1} f_6(t,U,D,W,Q,X,Y).
\end{aligned}\right\}. \tag{37}$$

With the help of (36), we can write the considered system (33) as

$$\begin{aligned}
{}^{c}_{0}D^{\pi}K(t) &= \nu t^{\nu-1}\mathscr{F}(t,K(t)), 0<\nu<1, 0<\pi<1,\\
K(0) &= K_0.
\end{aligned} \tag{38}$$

On applying the integral, we get the solution of (38) as

$$K(t) = K_0(\mathrm{t}) + \frac{\nu}{\Gamma(\pi)}\int_0^t x^{\nu-1}(t-x)^{\pi-1}\mathscr{F}(x,K(x))\mathrm{d}x, \tag{39}$$

where

$$K(t)=\begin{Bmatrix} U(t)\\ V(t)\\ W(t)\\ Q(t)\\ X(t)\\ Y(t)\end{Bmatrix}, K_0(t)=\begin{Bmatrix} U_0\\ V_0\\ W_0\\ Q_0\\ X_0\\ Y_0\end{Bmatrix},$$

$$\mathfrak{F}(t,K(t))=\begin{Bmatrix} f_1(t,U,D,W,Q,X,Y),\\ f_2(t,U,D,W,Q,X,Y),\\ f_3(t,U,D,W,Q,X,Y),\\ f_4(t,U,D,W,Q,X,Y),\\ f_5(t,U,D,W,Q,X,Y),\\ f_6(t,U,D,W,Q,X,Y).\end{Bmatrix} \tag{40}$$

For Ulam–Hyers stability, let $\wp \in C(\mathfrak{F})$, which is a small perturbation independent of solution. In addition, $|\wp(t)| \le \varepsilon$, for $\varepsilon > 0$; ${}_0^{\mathrm{FFP}}D^{\nu,\pi}K(t) = \mathfrak{F}(t,K(t)) + \wp(t)$.

Lemma 3. *The solution of the perturbed problem,*

$$\begin{aligned} {}_0^cD^{\pi}K(t) &= \nu t^{\nu-1}\mathfrak{F}(t,K(t)) + \wp(t),\\ K(0) &= K_0, \end{aligned} \tag{41}$$

satisfies the following relation

$$\left|K(t) - \left(K_0(t) + \frac{\nu}{\Gamma(\pi)}\int_0^t x^{\nu-1}(t-x)^{\pi-1}\mathfrak{F}(x,K(x))\mathrm{d}x\right)\right| \le \Delta\varepsilon. \tag{42}$$

Proof 4. According to (37), the solution of (39) is given by

$$K(t) = K_0(t) + \frac{\nu}{\Gamma(\pi)}\int_0^t x^{\nu-1}(t-x)^{\pi-1}[\mathfrak{F}(x,K(x))x + \wp(t)]\mathrm{d}x. \tag{43}$$

Using $|\wp(t)| \le \varepsilon$ in (43), one can easily get the relation (41). □

Theorem 5. *Inview of the inequality (42), and hypothesis given in (44), if the condition $\Delta\mathfrak{L}_{\mathfrak{F}} < 1$ holds, then the solution of problem (33) is Ulam–Hyers stable, where*

$$|\mathfrak{F}(x,K) - \mathfrak{F}(x,\overline{K})| \le \mathfrak{Q}_{\mathfrak{F}}|K - \overline{K}|, \mathfrak{L}_{\mathfrak{F}} > 0. \tag{44}$$

Proof 5. Suppose $\mathscr{W}$ is a unique solution and K be any other solution of (37) in Banach space $\mathfrak{B}$; then,

$$\begin{aligned} |K(t) - \mathscr{W}(t)| &= \left|K(t) - \left(\mathscr{W}_0(t) + \frac{\nu}{\Gamma(\pi)}\int_0^t x^{\nu-1}(t-x)^{\pi-1}\mathfrak{F}(x,\mathscr{W}(x))\mathrm{d}x\right)\right|,\\ &\le \left|K(t) - \left(K_0(t) + \frac{\nu}{\Gamma(\pi)}\int_0^t x^{\nu-1}(t-x)^{\pi-1}\mathfrak{F}(x,K(x))\mathrm{d}x\right)\right|\\ &\quad + \left|\left(K_0(t) + \frac{\nu}{\Gamma(\pi)}\int_0^t x^{\nu-1}(t-x)^{\pi-1}\mathfrak{F}(x,K(x))\mathrm{d}x\right)\right.\\ &\quad \left. - \left(\mathscr{W}_0(t) + \frac{\nu}{\Gamma(\pi)}\int_0^t x^{\nu-1}(t-x)^{\pi-1}\mathfrak{F}(x,\mathscr{W}(x))\mathrm{d}x\right)\right|\\ &\le \Delta\varepsilon + \mathfrak{L}_{\mathfrak{F}}\|K - \mathscr{W}\|. \end{aligned} \tag{45}$$

From (45), we can write

$$\|K - \mathscr{W}\| \le \mathfrak{U}_{\nu,\pi}\varepsilon, \tag{46}$$

where $\mathfrak{A} > 0, \forall K \in \mathfrak{B}$. Thus, from the result (43), we conclude that (33) is Ulam–Hyers stable. □

7. Numerical Scheme

Nonlinear problems are more difficult than linear ones to solve analytically. Therefore, researchers have implemented efficient and accurate numerical schemes for the treatment of nonlinear problems to explore the dynamics of real-world

problems more precisely. To tackle this nonlinear problem, from definition (3), we use the Adams–Bashforth scheme for the justification of our work.

$$
\begin{aligned}
U(l+1) &= U(0) + \frac{v\hbar^{\pi}}{\Gamma(\pi+2)} \sum_{j=0}^{f} \left[t_{(j)}^{v-1} u\left(U_{(j)}, t_j\right) \right. \\
&\quad \times \left((f+1-j)^{v} (f-j+2+v) - (f-j)^{v} (f-j+2+2v) \right) \\
&\quad \left. - t_{(j-1)}^{v-1} v\left(U_{(j-1)}, t_{(j-1)}\right) \left((f+1-j)^{v} + 1 - (f-j)^{v} (f-j+1+v) \right) \right], \\
V(l+1) &= V(0) + \frac{v\hbar^{\pi}}{\Gamma(\pi+2)} \sum_{j=0}^{f} \left[t_{(j)}^{v-1} u\left(V_{(j)}, t_j\right) \right. \\
&\quad \times \left((f+1-j)^{v} (f-j+2+v) - (f-j)^{v} (f-j+2+2v) \right) \\
&\quad \left. - t_{(j-1)}^{v-1} v\left(V_{(j-1)}, t_{(j-1)}\right) \left((f+1-j)^{v} + 1 - (f-j)^{v} (f-j+1+v) \right) \right], \\
W(l+1) &= W(0) + \frac{v\hbar^{\pi}}{\Gamma(\pi+2)} \sum_{j=0}^{f} \left[t_{(j)}^{v-1} u\left(W_{(j)}, t_j\right) \right. \\
&\quad \times \left((f+1-j)^{v} (f-j+2+v) - (f-j)^{v} (f-j+2+2v) \right) \\
&\quad \left. - t_{(j-1)}^{v-1} v\left(W_{(j-1)}, t_{(j-1)}\right) \left((f+1-j)^{v} + 1 - (f-j)^{v} (f-j+1+v) \right) \right], \\
Q(l+1) &= Q(0) + \frac{v\hbar^{\pi}}{\Gamma(\pi+2)} \sum_{j=0}^{f} \left[t_{(j)}^{v-1} u\left(Q_{(j)}, t_j\right) \right. \\
&\quad \times \left((f+1-j)^{v} (f-j+2+v) - (f-j)^{v} (f-j+2+2v) \right) \\
&\quad \left. - t_{(j-1)}^{v-1} v\left(Q_{(j-1)}, t_{(j-1)}\right) \left((f+1-j)^{v} + 1 - (f-j)^{v} (f-j+1+v) \right) \right], \\
X_{v}(l+1) &= X_{v}(0) + \frac{v\hbar^{\pi}}{\Gamma(\pi+2)} \sum_{j=0}^{f} \left[t_{(j)}^{v-1} u\left(X_{v\,(j)}, t_j\right) \right. \\
&\quad \times \left((f+1-j)^{v} (f-j+2+v) - (f-j)^{v} (f-j+2+2v) \right) \\
&\quad \left. - t_{(j-1)}^{v-1} v\left(X_{v^{(j-1)}}, t_{(j-1)}\right) \left((f+1-j)^{v} + 1 - (f-j)^{v} (f-j+1+v) \right) \right], \\
Y(l+1) &= Y(0) + \frac{v\hbar^{\pi}}{\Gamma(\pi+2)} \sum_{j=0}^{f} \left[t_{(j)}^{v-1} u\left(Y_{(j)}, t_j\right) \right. \\
&\quad \times \left((f+1-j)^{v} (f-j+2+v) - (f-j)^{v} (f-j+2+2v) \right) \\
&\quad \left. - t_{(j-1)}^{v-1} v\left(Y_{(j-1)}, t_{(j-1)}\right) \left((f+1-j)^{v} + 1 - (f-j)^{v} (f-j+1+v) \right) \right].
\end{aligned}
\tag{47}
$$

Table 4: Table for numerical values of parameters.

Symbol	Description of parameter	Dimension	Value
Λ	Recruitment rate [49]	Month^{-1}	$10000/50 \times 365$
μ	Natural death rate. [49]	Month^{-1}	$1/50 \times 365$
b	Transmission rate	Month^{-1}	0.00019
a	Psychological effect on human, [55]	Month^{-1}	0.0701
ξ	Recovery rate of infected population, [48]	Month^{-1}	0.01
α	Period of quarantine in susceptible population.	Month^{-1}	0.0701
β	Period of quarantine in exposed population	Month^{-1}	0.13
d	Period of quarantine in infected population	Month^{-1}	0.0701
ω	Vaccination rate of susceptible population	Month^{-1}	0.0001
γ	Vaccination rate of infected population	Month^{-1}	0.00001
ρ	Vaccination rate of quarantine population	Month^{-1}	0.0002
δ	Death rate of recovered population	Month^{-1}	0.002

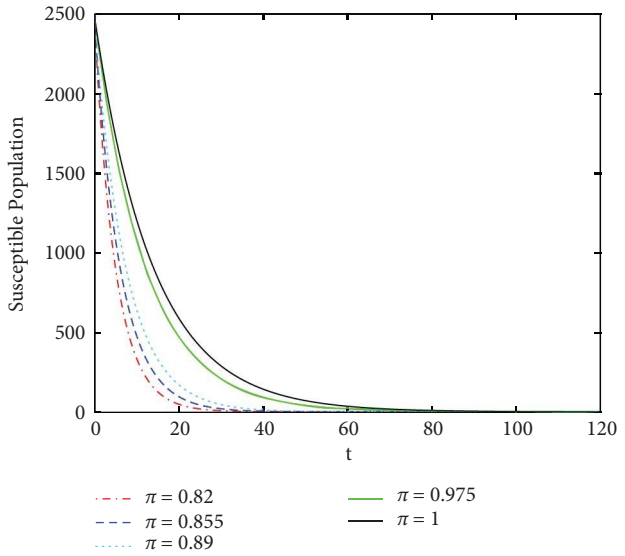

Figure 8: The dynamics of susceptible human population for various fractional orders π and for fractal order $\upsilon = 0.5$.

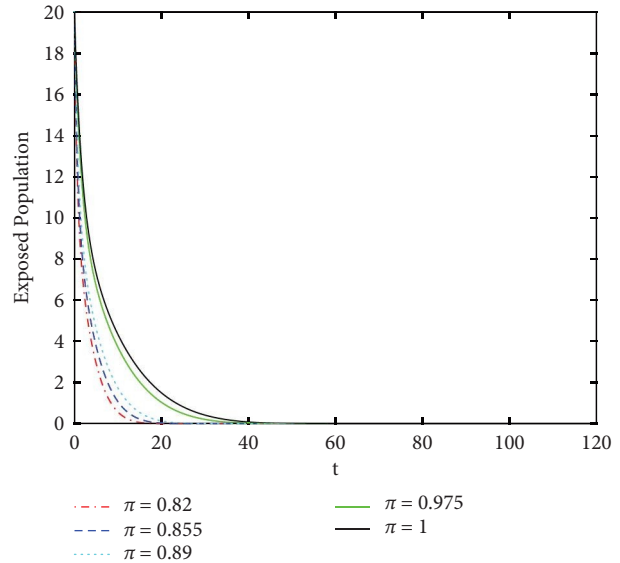

Figure 9: The dynamics of exposed human population for various fractional orders υ and for fractal order $\pi = 0.5$.

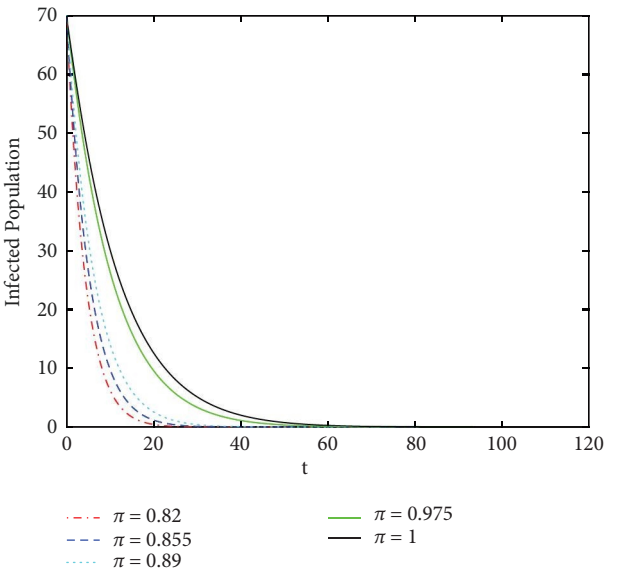

Figure 10: The dynamics of infected human population for various fractional orders υ and for fractal order $\pi = 0.5$.

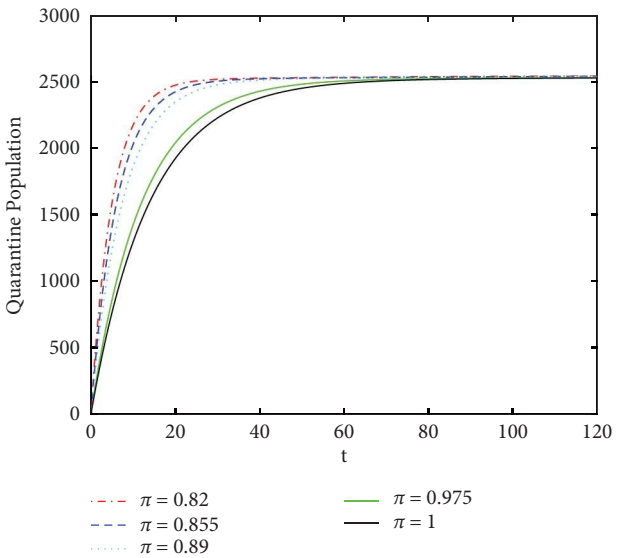

Figure 11: The dynamics of quarantine human population for various fractional orders υ and for fractal order $\pi = 0.5$.

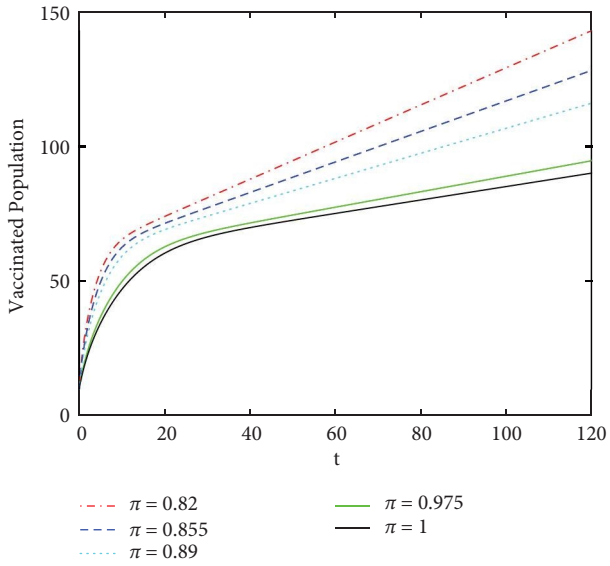

Figure 12: The dynamics of vaccinated human population for various fractional orders υ and for fractal order $\pi = 0.5$.

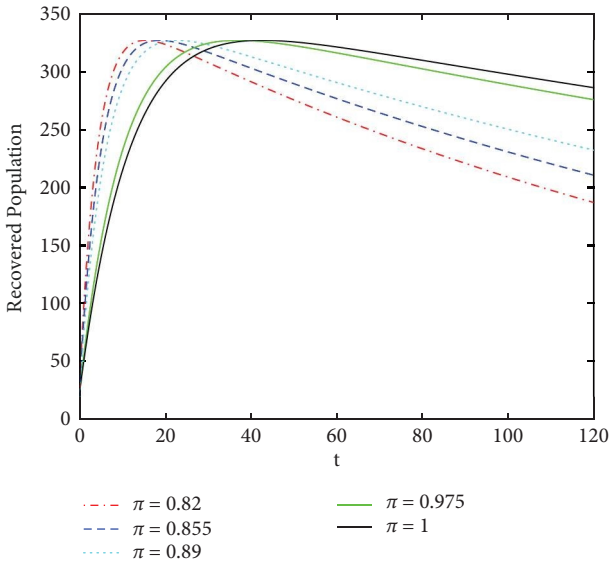

Figure 13: The dynamics of recovered human population for various fractional orders υ and for fractal order $\pi = 0.5$.

Remark 1. Here it should be kept in mind that the Adams–Bashforth method preserves the basic type of numerical stability associated with the usual one-step numerical methods including Euler, backward Euler, and trapezoidal. Furthermore, it is a $(l+1)$-step explicit method, and whose truncation error is of size $O(h^{l+2})$. For detailed convergence and stability of the Adams–Bashforth method, we refer for the readers to see [74].

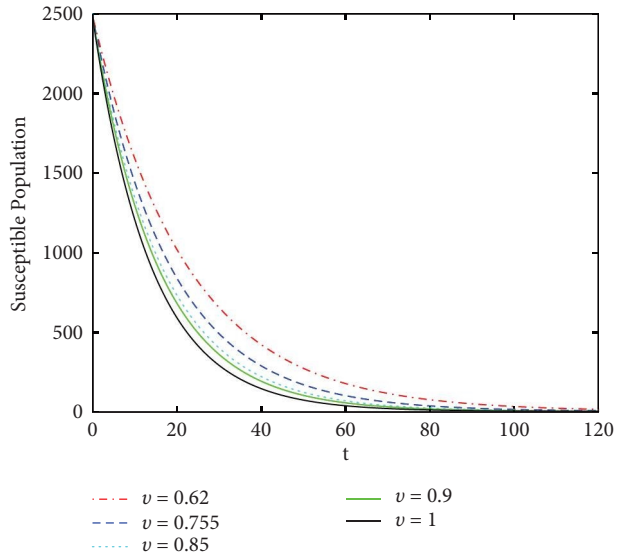

Figure 14: The dynamics of susceptible human population for various fractal orders π and for fractional order $\upsilon = 0.5$.

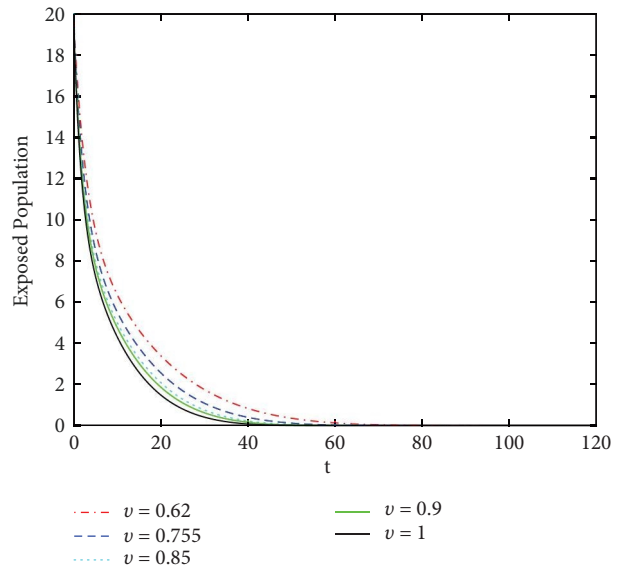

Figure 15: The dynamics of exposed human population for various fractal orders π and for fractional order $\upsilon = 0.5$.

8. Numerical Results and Discussion

To simulate our model, we use the numerical values given in Table 4.

In this section, we explain the dynamics of the proposed model from graphical results such that the bar chart (2) shows the quantity of sensitivity index of parameters associated with R_0, in which two parameters b and α have a

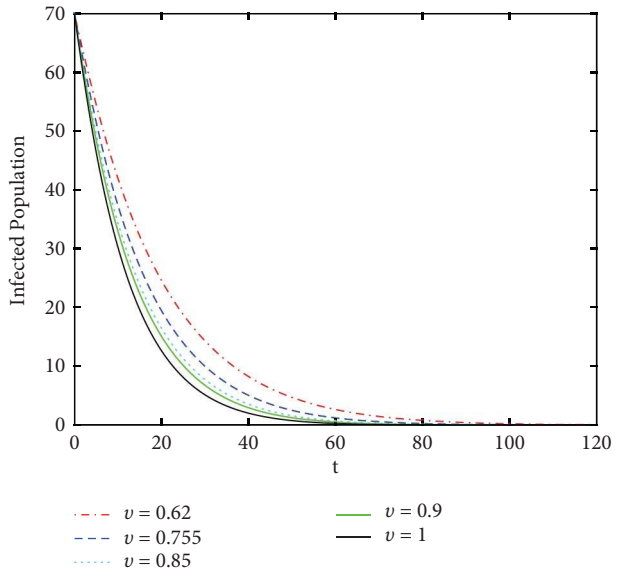

Figure 16: The dynamics of infected human population for various fractal orders π and for fractional order $\upsilon = 0.5$.

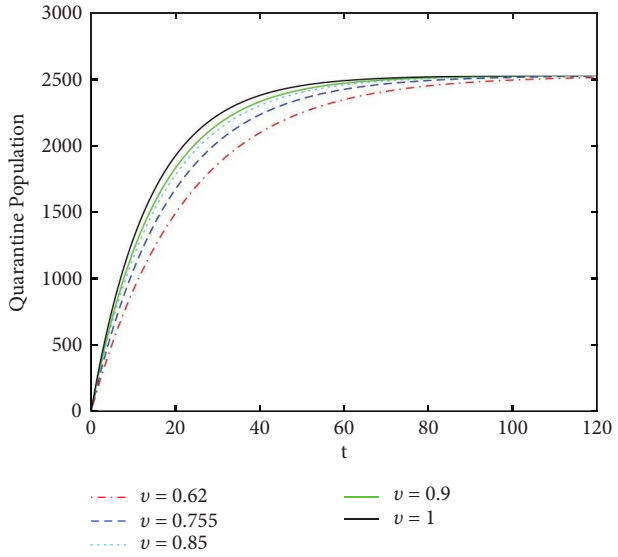

Figure 17: The dynamics of quarantine human population for various fractal orders π and for fractional order $\upsilon = 0.5$.

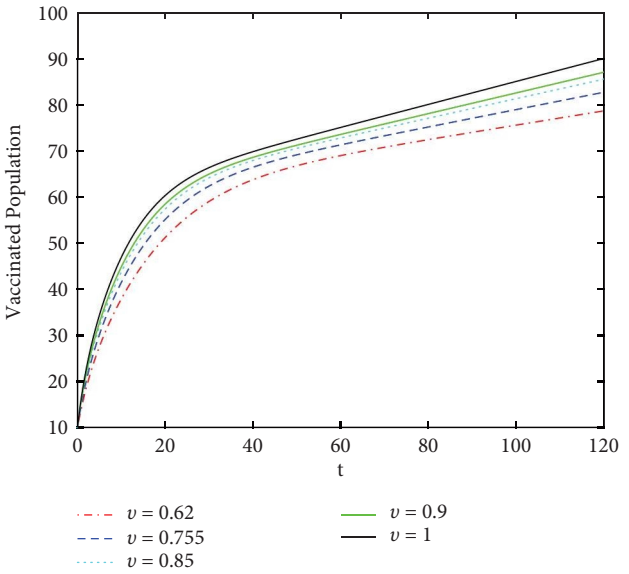

Figure 18: The dynamics of vaccinated human population for various fractal orders π and for fractional order $\upsilon = 0.5$.

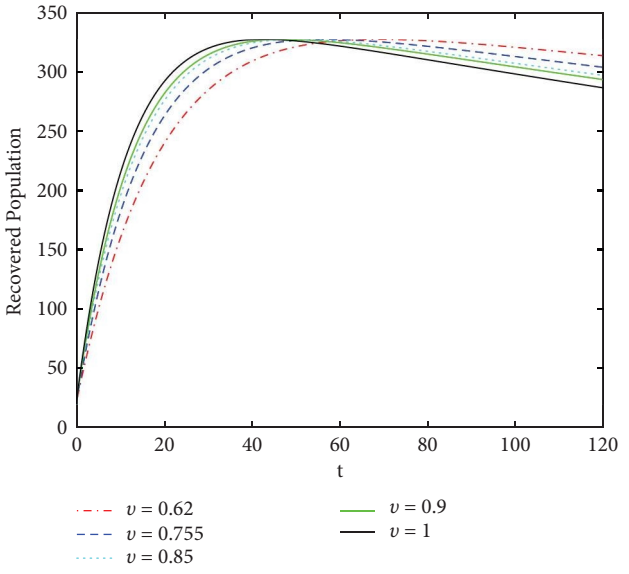

Figure 19: The dynamics of recovered human population for various fractal orders π and for fractional order $\upsilon = 0.5$.

large effect on R_0. From Figures 3–7, we see the dynamics of R_0 by using numerical values of parameters λ, ω, μ, α, and β. Furthermore, Figures 8–13 show the stable behavior of susceptible, exposed, infected, quarantine, vaccinated, and recovered population, respectively, with a variation in fractal order π and using value of fractional order $\upsilon = 0.5$. Moreover, Figures 14–19 show the behavior of the model with each compartment under different fractional order and using value of fractal order $\pi = 0.5$. While in Figures 20, 21, 22, 23, 24, and 25, we plot the solution for different fractal-fractional order. Here, we compared the real available reported cases of infection in Pakistan for 200 days from 15th March 2021 to 30th September 2021. The details about the COVID-19 situation in Pakistan can be found in [75, 76], and [77]. Also, some real data in comparison with fractional order simulation has been plotted in [78] recently. We see

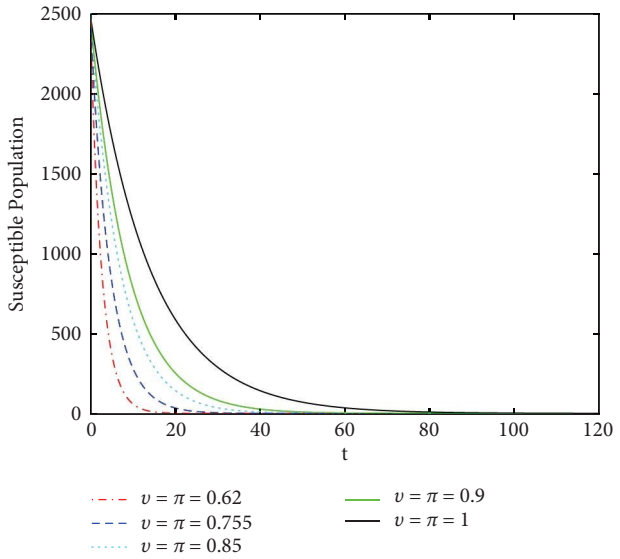

Figure 20: The dynamics of susceptible human population for various fractal-fractional orders.

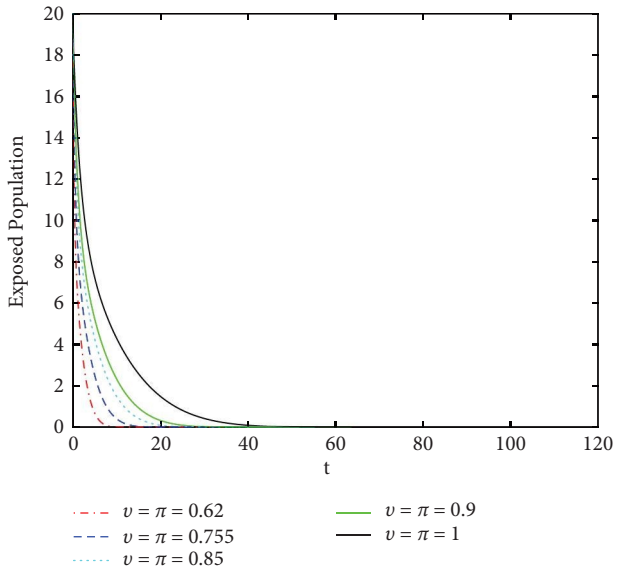

Figure 21: The dynamics of exposed human population for various fractal-fractional orders.

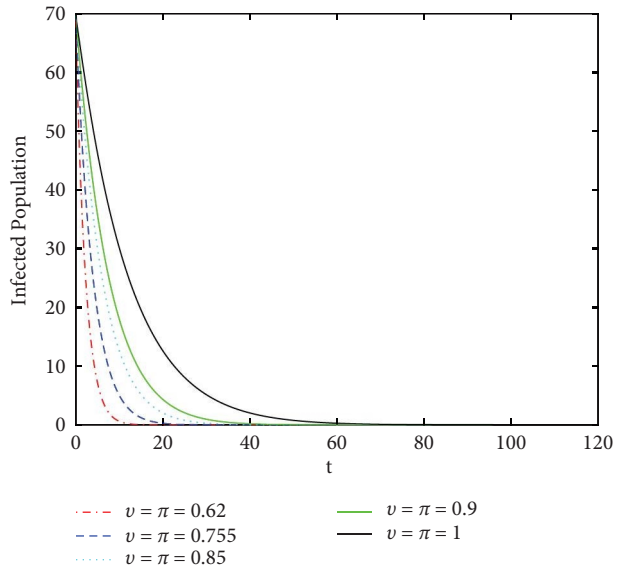

Figure 22: The dynamics of infected human population for various fractal-fractional orders.

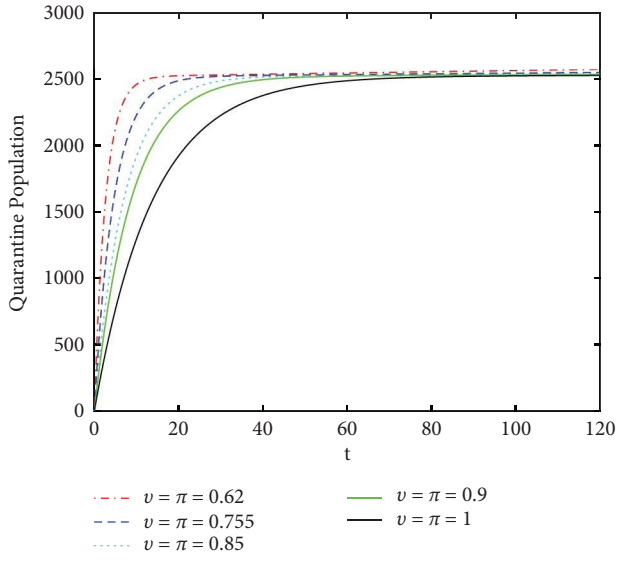

Figure 23: The dynamics of quarantine human population for various fractal-fractional orders.

that the numerical simulation at two different fractional orders coincides very well with the plot of real data as shown in Figure 26. The graphical results also reveal that when the fractal υ and fractional π orders approach 1, then model 1 is reduced to the classical order model.

From Figure 26, it is clear that the real data plot and the simulated data graph are closely related. Moreover,

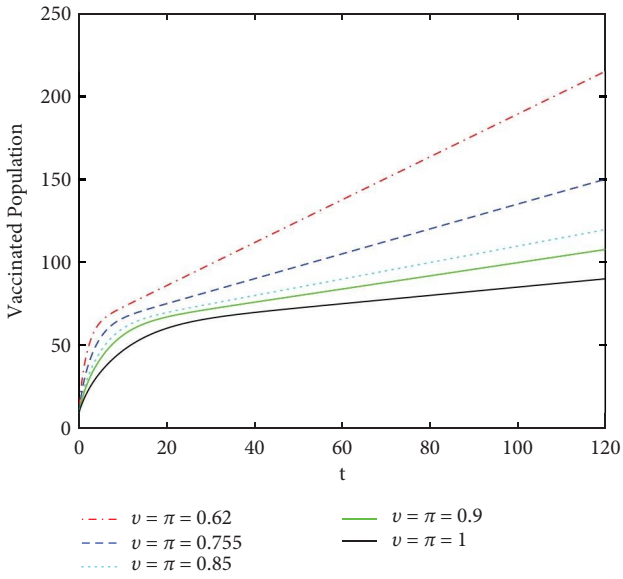

Figure 24: The dynamics of vaccinated human population for various fractal-fractional orders.

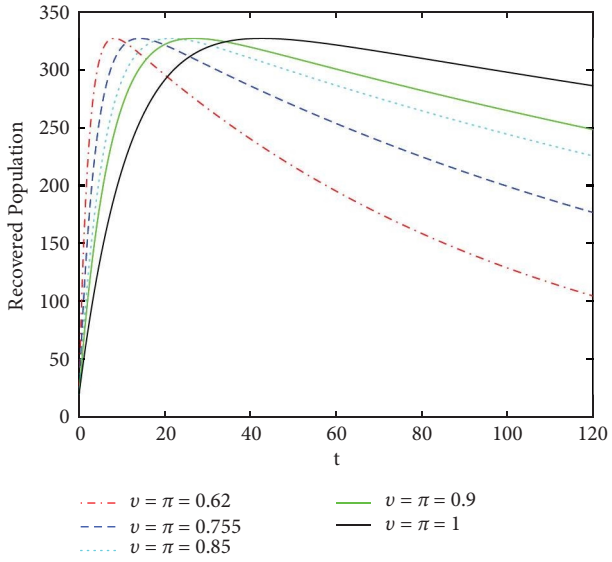

Figure 25: The dynamics of recovered human population for various fractal-fractional orders.

by fitting the real data, we can obtain the numerical values of the parameters of model 1 given in Table 4. Moreover, the model is numerically stable and takes less time and memory during simulation using the Adams–Bashforth scheme due to the nonlinearity and complexity of the problem.

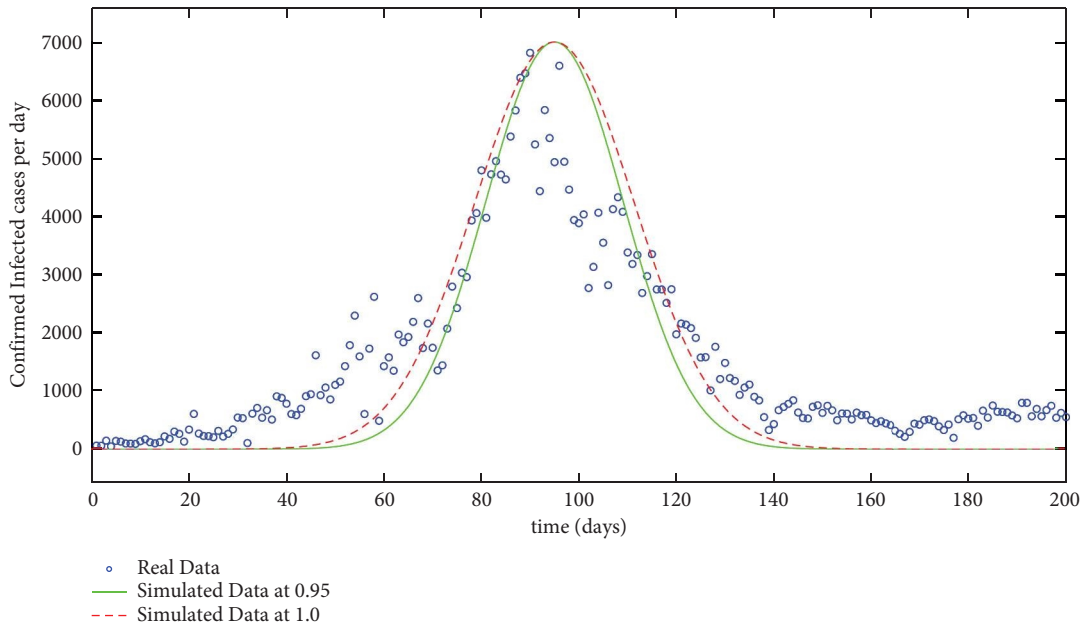

Figure 26: Comparison between real reported infected cases with simulated data at two different fractional orders.

9. Conclusion

We have studied the compartmental model of COVID-19 which has been consisting of susceptible, infected, quarantined, vaccinated, and recovered human populations. The model has been specifically proposed for the implementation of a vaccinated class. The fractal-fractional calculus has been used to understand the dynamics of fractal order π and fractional order υ. We have also investigated some results devoted to local and global stability for the proposed model based on the Jacobian matrix and the Lyapunov function method. Both local and global type stabilities have been demonstrated under the disease-free and endemic equilibrium points by showing that $R_0 < 1$ and $R_0 > 1$, respectively. For the sensitivity analysis of each parameter, we have investigated global sensitivity analysis to justify the said feature. Furthermore, some results necessary for numerical stability based on the Ulam–Hyers concept have also been studied. Numerical simulations have been presented by means of the Adams–Bashforth scheme. Some discussion about the convergence and numerical stability of the proposed method has been given in Remark 1. Numerical results have been displayed in different fractional orders graphically to understand the dynamics of the model. We have given a comparison between real reported and simulated data in the case of the infected class. Both curves are closely agreed which shows the efficiency of the proposed numerical method. The given detail can be extended to more complex dynamical systems in the future.

Data Availability

All the data used in the paper are included in the manuscript.

Conflicts of Interest

The authors declare that they have no conflicts of interest regarding this work.

Authors' Contributions

All authors have contributed equally.

Acknowledgments

Kamal Shah, Thabet Abdeljawad, and Bahaaeldin Abdalla are thankful to the Prince Sultan University for paying the APC and support through TAS research lab.

References

[1] World Health Organization (WHO), "Naming the coronavirus disease (COVID-19) and the virus that causes it, Archived from the original on 28 February 2020," 2020, https://www.who.int/emergencies/diseases/novel-cor.

[2] Million-Excess-Deaths-Were-Associated, "Million-excess-deaths-were-associated," 2022, https://www.who.int/news/item/05-05-2022-14.9-million-excess-deaths-were-associated-with-the-covid-19-pandemic-in-2020-and-2021.

[3] S. Zhao, S. S. Musa, Q. Lin et al., "Estimating the unreported number of novel coronavirus (2019-nCoV) cases in China in the first half of January 2020, a data-driven Modelling analysis of the early outbreak," *Journal of Clinical Medicine*, vol. 9, no. 2, p. 388, 2020.

[4] I. Nesteruk, "Statistics based predictions of coronavirus 2019-nCoV spreading in mainland China," *medRxiv*, vol. 4, no. 1, pp. 1988-1989, 2020.

[5] D. S. I. Hui, E. I Azhar, T. A. Madani et al., "The continuing 2019-nCoV epidemic threat of novel coronaviruses to global

health-The latest 2019 novel coronavirus outbreak in Wuhan, China," *International Journal of Infectious Diseases*, vol. 91, no. 6, pp. 264–266, 2020.

[6] S. Zhao, Q. Lin, J. Ran et al., "Preliminary estimation of the basic reproduction number of novel coronavirus (2019-nCoV) in China, from 2019 to 2020: a data-driven analysis in the early phase of the outbreak," *International Journal of Infectious Diseases*, vol. 92, pp. 214–217, 2020.

[7] K. Shah, R. U. Din, W. Deebani, P. Kumam, and Z. Shah, "On nonlinear classical and fractional order dynamical system addressing COVID-19," *Results in Physics*, vol. 24, Article ID 104069, 2021.

[8] F. Mainardi, "An historical perspective on fractional calculus in linear viscoelasticity," *Fractional Calculus and Applied Analysis*, vol. 15, no. 4, pp. 712–717, 2012.

[9] N. S. Goel, S. C. Maitra, and E. W. Montroll, "On the Volterra and other nonlinear models of interacting populations," *Reviews of Modern Physics*, vol. 43, no. 2, pp. p231–276, 1971.

[10] P. Zhou, X. L. Yang, X. G. Wang et al., "A pneumonia outbreak associated with a new coronavirus of probable bat origin," *Nature*, vol. 579, no. 7798, pp. 270–273, 2020.

[11] Q. Li, X. Guan, P. Wu et al., "Early transmission dynamics in Wuhan, China, of novel coronavirus infected pneumonia," *New England Journal of Medicine*, vol. 382, no. 13, pp. 1199–1207, 2020.

[12] I. I. Bogoch, A. Watts, A. Thomas-Bachli, C. Huber, M. U. G. Kraemer, and K. Khan, "Pneumonia of unknown aetiology in Wuhan, China: potential for international spread via commercial air travel," *Journal of Travel Medicine*, vol. 27, no. 2, Article ID taaa008, 2020.

[13] A. B. Gumel, S. Ruan, T. Day et al., "Modelling strategies for controlling SARS out breaks," *Proceedings of the Royal Society of London B*, vol. 271, no. 1554, pp. 2223–2232, 2004.

[14] A. Atangana and S. İğret Araz, "Modeling third waves of Covid-19 spread with piecewise differential and integral operators: Turkey, Spain and Czechia," *Results in Physics*, vol. 29, Article ID 104694, 2021.

[15] A. Atangana, "Modelling the spread of COVID-19 with new fractal-fractional operators: can the lockdown save mankind before vaccination?" *Chaos, Solitons & Fractals*, vol. 136, Article ID 109860, 2020.

[16] A. Atangana and S. İğret Araz, "Mathematical model of COVID-19 spread in Turkey and South Africa: theory, methods, and applications," *Advances in Difference Equations*, vol. 2020, no. 1, pp. 659–689, 2020.

[17] R. Prieto Curiel and H. González Ramírez, "Vaccination strategies against COVID-19 and the diffusion of anti- vaccination views," *Scientific Reports*, vol. 11, no. 1, p. 6626, 2021.

[18] C. A. B. Pearson, F. Bozzani, and S. R. Procter, *Health Impact and Cost-Effectiveness of COVID-19 Vaccination in Sindh Province Pakistan*, medRxiv, Spring Harbor, NY, USA, 2021.

[19] J. T. Wu, K. Leung, and G. M. Leung, "Nowcasting and forecasting the potential domestic and international spread of the 2019-nCoV outbreak originating in Wuhan, China: a modelling study," *The Lancet*, vol. 395, no. 10225, pp. 689–697, 2020.

[20] M. S. Arshad, D. Baleanu, M. B. Riaz, and M. Abbas, "A novel 2-stage fractional Runge-Kutta method for a TimeFractional logistic growth model," *Discrete Dynamics in Nature and Society*, vol. 2020, Article ID 1020472, 8 pages, 2020.

[21] T. Abdeljawad, Q. M. Al-Mdallal, and F. Jarad, "Fractional logistic models in the frame of fractional operators generated by conformable derivatives, Chaos," *Solitons & Fractals*, vol. 119, pp. 94–101, 2019.

[22] F. Liu and K. Burrage, "Novel techniques in parameter estimation for fractional dynamical models arising from biological systems," *Computers & Mathematics with Applications*, vol. 62, no. 3, pp. 822–833, 2011.

[23] M. T. Hoang and O. F. Egbelowo, "Dynamics of a fractional-order hepatitis b epidemic model and its solutions by non-standard numerical schemes," *Mathematical Modelling and Analysis of Infectious Diseases*, vol. 2020, pp. 127–153, 2020.

[24] M. A. Khan and A. Atangana, "Modeling the dynamics of novel coronavirus (2019-nCov) with fractional derivative," *Alexandria Engineering Journal*, vol. 59, no. 4, pp. 2379–2389, 2020.

[25] M. A. Khan, A. Atangana, E. Alzahrani, and Fatmawati, "The dynamics of COVID-19 with quarantined and isolation," *Advances in Difference Equations*, vol. 2020, no. 1, pp. 425–522, 2020.

[26] S. Boccaletti, W. Ditto, G. Mindlin, and A. Atangana, "Modeling and forecasting of epidemic spreading: the case of Covid-19 and beyond," *Chaos, Solitons & Fractals*, vol. 135, Article ID 109794, 2020.

[27] E. Atangana and A. Atangana, "Facemasks simple but powerful weapons to protect against COVID-19 spread: can they have sides effects?" *Results in Physics*, vol. 19, Article ID 103425, 2020.

[28] S. T. Thabet, M. S. Abdo, K. Shah, and T. Abdeljawad, "Study of transmission dynamics of COVID-19 mathematical model under ABC fractional order derivative," *Results in Physics*, vol. 19, Article ID 103507, 2020.

[29] J. T. Machado, V. Kiryakova, and F. Mainardi, "Recent history of fractional calculus," *Communications in Nonlinear Science and Numerical Simulation*, vol. 16, no. 3, pp. 1140–1153, 2011.

[30] F. C. Meral, T. J. Royston, and R. Magin, "Fractional calculus in viscoelasticity: an experimental study," *Communications in Nonlinear Science and Numerical Simulation*, vol. 15, no. 4, pp. 939–945, 2010.

[31] R. L. Magin, "Fractional calculus in bioengineering, part 1," *Critical Reviews in Biomedical Engineering*, vol. 32, no. 1, pp. 1–104, 2004.

[32] M. Dalir and M. Bashour, "Applications of fractional calculus," *Applied Mathematical Sciences*, vol. 4, no. 21, pp. 1021–1032, 2010.

[33] L. M. Richard, *Fractional Calculus in Bioengineering*, Begell House, Danbury, Connecticut, 2006.

[34] A. Y. Rossikhin and M. V. Shitikova, "Applications of Fractional Calculus to Dynamic Problems of Linear and Nonlinear Hereditary Mechanics of Solids," *Appl. Mech. Rev*, vol. 50, pp. 15–67, 1997.

[35] F. Mainardi, "Fractional calculus," in *Fractals and Fractional Calculus in Continuum Mechanics*Springer, Berlin, Germany, 1997.

[36] B. B. Mandelbrot, "How long is the coast of Britain? Statistical self-similarity and fractional dimension," *Science*, vol. 156, no. 3775, pp. 636–638, 1967.

[37] B. B. Mandelbrot, D. E. Passoja, and A. J. Paullay, "Fractal character of fracture surfaces of metals," *Nature*, vol. 308, no. 5961, pp. 721-722, 1984.

[38] P. R. Massopust, "Fractal surfaces," *Journal of Mathematical Analysis and Applications*, vol. 151, no. 1, pp. 275–290, 1990.

[39] Q. W. Ran and X. Y. Tan, *Wavelet Analysis, Fractional Fourier Transformation and Application*, National Defence Industry Press, Beijing, China, 2002.

[40] M. F. Barnsley, *Fractals Everywhere*, Elsevier, Singapore, 2009.

[41] Z. Sha and H. J. Ruan, *Fractals and Fitting*, Zhen jiang University Press, Hangzhou, China, 2005.

[42] I. Ahmed, I. A. Baba, A. Yusuf, P. Kumam, and W. Kumam, "Analysis of Caputo fractional-order model for COVID-19 with lockdown," *Advances in Difference Equations*, vol. 2020, no. 1, pp. 394–414, 2020.

[43] R. B. Vinter, J. Baillieul, and T. Samad, *Optimal Control and Pontryagin's Maximum Principle, Encyclopedia of Systems and Control*, pp. 950–956, Springer, Berlin, Germany, 2015.

[44] M. J. Mardanov and Y. A. Sharifov, "Pontryagin's maximum principle for the optimal control problems with multipoint boundary conditions," *Abstract and Applied Analysis*, vol. 2015, Article ID 428042, 6 pages, 2015.

[45] L. Zhang, M. U. Rahman, Q. Haidong, and M. Arfan, "Fractal-fractional anthroponotic cutaneous leishmania model study in sense of Caputo derivative," *Alexandria Engineering Journal*, vol. 61, no. 6, pp. 4423–4433, 2022.

[46] R. M. Anderson and R. M. May, *Infectious Diseases of Humans: Dynamics and Control*, Oxford University Press, Oxford, UK, 1992.

[47] P. K. Anderson, A. A. Cunningham, N. G. Patel, F. J. Morales, P. R. Epstein, and P. Daszak, "Emerging infectious diseases of plants: pathogen pollution, climate change and agro-technology drivers," *Trends in Ecology & Evolution*, vol. 19, no. 10, pp. 535–544, 2004.

[48] Y. Gu, M. A. Khan, Y. S. Hamed, and B. F. Felemban, "A comprehensive mathematical model for SARS-CoV-2 in Caputo derivative," *Fractal and Fractional*, vol. 5, no. 4, p. 271, 2021.

[49] Z. H. Shen, Y. M. Chu, M. A. Khan, S. Muhammad, O. A. Al-Hartomy, and M. Higazy, "Mathematical modeling and optimal control of the COVID-19 dynamics," *Results in Physics*, vol. 31, Article ID 105028, 2021.

[50] N. H. J. M. Chitnis, J. M. Hyman, and J. M. Cushing, "Determining important parameters in the spread of malaria through the sensitivity analysis of a mathematical model," *Bulletin of Mathematical Biology*, vol. 70, no. 5, pp. 1272–1296, 2008.

[51] C. Castillo-Chavez and B. Song, "Dynamical models of tuberculosis and their applications," *Mathematical Biosciences and Engineering*, vol. 1, no. 2, pp. 361–404, 2004.

[52] L. S. Pontryagin, *Mathematical Theory of Optimal Processes*, CRC Press, Boca Raton, FA, USA, 1987.

[53] M. Martcheva, *An Introduction to Mathematical Epidemiology*, vol. 61, pp. 9–31, Springer, Berlin, Germany, 2015.

[54] W. H. Fleming and R. W. Rishel, *Deterministic and Stochastic Optimal Control*, Springer Science & Business Media, Berlin, Germany, 2012.

[55] S. Liu, L. Pang, S. Ruan, and X. Zhang, "Global dynamics of avian influenza epidemic models with psychological effect," *Computational and Mathematical Methods in Medicine*, vol. 2015, Article ID 913726, 12 pages, 2015.

[56] F. Bozdag, "The psychological effects of staying home due to the COVID-19 pandemic," *The Journal of General Psychology*, vol. 148, no. 3, pp. 226–248, 2021.

[57] N. H. Sweilam, S. M. Al-Mekhlafi, and A. Almutairi, "Fractal fractional optimal control for a novel malaria mathematical model; a numerical approach," *Results in Physics*, vol. 19, Article ID 103446, 2020.

[58] N. H. Sweilam, S. M. Al-Mekhlafi, and D. G. Mohamed, "Novel chaotic systems with fractional differential operators: numerical approaches," *Chaos, Solitons & Fractals*, vol. 142, Article ID 110475, 2021.

[59] A. Malik, M. Alkholief, F. M. Aldakheel et al., "Sensitivity analysis of COVID-19 with quarantine and vaccination: a fractal-fractional model," *Alexandria Engineering Journal*, vol. 61, no. 11, pp. 8859–8874, 2022.

[60] M. Sinan, K. Shah, P. Kumam et al., "Fractional order mathematical modeling of typhoid fever disease," *Results in Physics*, vol. 32, Article ID 105044, 2022.

[61] A. Atangana, "Fractal-fractional differentiation and integration: c," *Chaos, Solitons & Fractals*, vol. 102, pp. 396–406, 2017.

[62] B. Buonomo and D. Lacitignola, "On the backward bifurcation of a vaccination model with nonlinear incidence," *Nonlinear Analysis Modelling and Control*, vol. 16, no. 1, pp. 30–46, 2011.

[63] H. Lu, Y. Ding, S. Gong, and S. Wang, "Mathematical modeling and dynamic analysis of SIQR model with delay for pandemic COVID-19," *Mathematical Biosciences and Engineering*, vol. 18, no. 4, pp. 3197–3214, 2021.

[64] D. Matignon, "Stability results for fractional differential equations with applications to control processing," *Comput. Eng. Sys. Appl.*vol. 2, no. 1, pp. 963–968, 1996.

[65] C. Li and Y. Ma, "Fractional dynamical system and its linearization theorem," *Nonlinear Dynamics*, vol. 71, no. 4, pp. 621–633, 2013.

[66] A. S. Shaikh, I. N. Shaikh, and K. S. Nisar, "A mathematical model of COVID-19 using fractional derivative: outbreak in India with dynamics of transmission and control," *Advances in Difference Equations*, vol. 2020, no. 1, pp. 373–419, 2020.

[67] P. Kumar, V. S. Erturk, and M. Murillo-Arcila, "A new fractional mathematical modelling of COVID-19 with the availability of vaccine," *Results in Physics*, vol. 24, Article ID 104213, 2021.

[68] M. Mohammad and A. Trounev, "On the dynamical modeling of COVID-19 involving Atangana-Baleanu fractional derivative and based on Daubechies framelet simulations," *Chaos, Solitons & Fractals*, vol. 140, Article ID 110171, 2020.

[69] A. A. M. Arafa, M. Khalil, and A. Sayed, "A non-integer variable order mathematical model of human immunodeficiency virus and malaria coinfection with time delay," *Complexity*, vol. 2019, pp. 1–13, 2019.

[70] A. M. A. El-Sayed, A. A. M. Arafa, M. Khali, and A. Sayed, "Backward bifurcation in a fractional order epidemiological model," *Progress in Fractional Differentiation and Applications*, vol. 3, no. 4, pp. 281–287, 2017.

[71] A. A. M. Arafa, S. Z. Rida, and M. Khalil, "A fractional-order model of HIV infection: numerical solution and comparisons with data of patients," *International Journal of Biomathematics*, vol. 07, no. 04, Article ID 1450036, 2014.

[72] A. Ali, M. Y. Khan, M. Sinan et al., "Theoretical and numerical analysis of novel COVID-19 via fractional order mathematical model," *Results in Physics*, vol. 20, Article ID 103676, 2021.

[73] P. Kumam, A. Ali, K. Shah, and R. A. Khan, "Existence results and Hyers-Ulam stability to a class of nonlinear arbitrary order differential equations," *The Journal of Nonlinear Science and Applications*, vol. 10, no. 06, pp. 2986–2997, 2017.

[74] H. Ramos, "Formulation and analysis of a class of direct implicit integration methods for special second-order IVPs in predictor-corrector modes," in *Recent Advances in Differential Equations and Applications*, pp. 33–61, Springer, Berlin, Germany, 2019.

[75] Worldometers, "Worldometers," 2022, https://www.worldometers.info/world-population/pakistan-population.
[76] Coronatracker, "Coronatracker," 2021, https://www.coronatracker.com/country/pakistan/.
[77] Current Information, "Current information about COVID-19 in Pakistan," 2021, https://www.worldometers.info.
[78] K. Shah, T. Abdeljawad, and R. Ud Din, "To study the transmission dynamic of SARS-CoV-2 using nonlinear saturated incidence rate," *Physica A: Statistical Mechanics and Its Applications*, vol. 604, Article ID 127915, 2022.

Hindawi
Complexity
Volume 2022, Article ID 9752628, 17 pages
https://doi.org/10.1155/2022/9752628

Research Article

Dynamical Analysis of Posttreatment HIV-1 Infection Model

M. Pradeesh,[1] **A. Manivannan**,[2] **S. Lakshmanan**,[2] **F. A. Rihan**,[3] **and Prakash Mani**[1]

[1]*Division of Mathematics, School of Advanced Sciences, Vellore Institute of Technology, Vellore, India*
[2]*Division of Mathematics, School of Advanced Sciences, Vellore Institute of Technology, Chennai, India*
[3]*Department of Mathematical Sciences, Faculty of Science, UAE University, Al-Ain, UAE*

Correspondence should be addressed to Prakash Mani; prakashgru88@gmail.com

Received 30 May 2022; Revised 29 July 2022; Accepted 8 August 2022; Published 8 October 2022

Academic Editor: Abdellatif Ben Makhlouf

This paper aims to explore the dynamic characteristics of the post treatment human immunodeficiency virus (HIV) type-1 model by proposing the theoretical frameworks. Distinct from the previous works, this study explores the effect of effector cells, loss of functional effector cells, and two types of anti-retroviral therapies such as reverse transcriptase inhibitors (RTIs) and protease inhibitors (PIs) and also the effect of intracellular time delay. Based on the Routh—Hurwitz criterion and eigenvalue analysis, the stability of the proposed HIV-1 model is analyzed. To reveal the significance of time delay, the Hopf-type bifurcation analysis is performed. The optimal control algorithm is designed by choosing the antiviral therapies such as RTI and PI as control parameters. Numerical simulations are performed to validate the effectiveness of the proposed theoretical frameworks.

1. Introduction

According to the World Health Organization (WHO), 680,000 individuals died from HIV-1-related diseases worldwide in 2020, ranging from 480,000 to 1.0 million, while 1.5 million people were newly infected with HIV-1. Antiretroviral therapy (ART) has drastically reduced the number of people infected with HIV during the 1990s, with 27.5 million (approximately) people undergoing treatment in 2020. Because of antiretroviral medication, the HIV infection rate has decreased by 49% over the last two decades, from 2000 to 2020. Despite the researcher's valiant efforts in terms of treatment options and drugs, a cure for HIV-1 remains a pipe dream, necessitating lifelong treatment. Mathematical models have been demonstrated to be a useful tool for comprehending the dynamics of disease progression, identifying key determinants, and evaluating the efficacy of antiretroviral therapy.

During the 1990s, HIV was thought to be a lethal disease, similar to other lentiviruses, because HIV remains within the host without causing symptoms and progresses to a chronic stage known as acquired immunodeficiency virus (AIDS), with a nearly ten-year delay between HIV and AIDS. In this case, mathematical modeling of HIV can help in estimating the lifespan of infected cells, evaluating therapeutic efficacy, and realizing that new virions require a host with deoxyribonucleic acid (DNA) to replicate. Currently, a variety of therapy options are available to help people with HIV get better. However, controlling the virus is the only option available and curing the disease still requires seamless efforts in the research domain.

Mathematical models have been created to investigate the dynamic properties of cell populations using parameters including latent reservoirs, immunological responses, total carrying capacity, and time-delayed fractional differential operators based on literature reviews (see [1–5]). Immature infected cells also known as latent stage are those that have been infected but are not yet infectious, which is considered in the present study. Immune responses such as CD4+ T-cells/CD8+ T-cells are activated when a foreign agent enters the body, causing the body's alarm system to go into overdrive [6, 7].

When systems are in motion, there will always be a degree of lag time. Time delays are inevitable because it has

an ability to cause a significant impact on cell populations. When modeling the kinetics of HIV-1 infection, two types of delays are taken into account. One situation is that the uninfected cells interact with infected/free virions and there is an intracellular temporal delay. Besides, after a foreign agent has been ingested, immune response cells must be activated, which results in a delay in the immunological response. This study aims to explore the effect of intracellular time delay with respect to infected cell population [8, 9]. Initially, ART is given to every primarily infected HIV person, but based on the stage of infection the level of drugs may be redefined. However, it is a challenging task with respect to the immune boosters which may vary in the individual. Besides, it can be seen that, if there is a change in the period of drugs provided, then it will reflect in the virion populations. Hence, this study explores the effect of antiretroviral therapies which are suggested as posttreatment for a long period of time. The proposed model's stability analysis will provide some insights into disease progression in relation to the system parameters such as infection rate and time delays. Followed by, bifurcation analysis is used to determine the threshold value of the significant parameter that has the potential to cause fluctuations in the cell population. The optimal control algorithm is designed by selecting cell populations, which aids in better understanding and extraction of system parameters, resulting in cell populations with stable staining [10–13]. Recently, the models were proposed on Zika virus, HIV, SARS-CoV-2, and other viral dynamics models such as maize streak virus in maize spread by leaf hopper mostly in Africa, canine distemper virus, and rabies epidemics in red fox with respect to significant factors such as vaccination parameter involved models and optimal control strategies (for more details, refer [14–22]). Distinct from the existing models, the present study focuses on considering the effect of time delays and two kinds of antiretroviral therapies. The overall contribution is listed in the following:

(1) This paper models the dynamics of HIV-1 infection by considering the factors such as healthy CD4+ cells, latent reservoirs, infected cells, free virions, and immune responses also considering the effect of time delay.

(2) Positivity and boundedness of solutions of the differential model are proved. The reproduction number is determined through the next-generation matrix, which helps to identify the community spread.

(3) Conditions for the existence of Hopf bifurcation are proved by choosing the intracellular time delay as a bifurcation parameter.

(4) Optimal control algorithm is designed to ensure the stabilization of the proposed model.

(5) Numerical simulations are performed to validate the proposed theoretical frameworks.

2. Model of Posttreatment HIV-1 Viral Dynamics

The schematic representation of our model is given below.

$$\begin{aligned}
\dot{x}(t) &= s - \gamma x(t) - \left(1 - \varepsilon_1(t)\right)\beta x(t) y(t-\tau),\\
\dot{l}(t) &= \alpha_L\left(1 - \varepsilon_1(t)\right)\beta x(t) y(t) + \left(\rho - a - d_L\right) l(t),\\
\dot{y}(t) &= \left(1 - \alpha_L\right)\left(1 - \varepsilon_1(t)\right)\beta x(t) y(t) + a l(t)\\
&\quad - \delta y(t) - m y(t) z(t),\\
\dot{u}(t) &= \left(1 - \varepsilon_2(t)\right) p y(t) - c u(t),\\
\dot{z}(t) &= b_z \frac{y(t)}{K_B + y(t)} z(t) - d_z \frac{(t)}{K_D + y(t)} z(t) - \mu z(t).
\end{aligned} \tag{1}$$

In model (1), the first equation represents the rate of change in the susceptible cell populations, where s denotes the rate of production, γ is decay rate and $\varepsilon_1, \varepsilon_2$ denotes the efficacy of antiretroviral therapies. Consider that $\varepsilon_i(t)$, where $i = 1, 2$, in $[0, 1]$; if $\varepsilon_i = 1$, where $i = 1, 2.$, then cent percent the treatment is effective which makes the infection zero, and if $\varepsilon_i(t) = 0$, $i = 1, 2$, then, no progress in the therapy. β represents the rate of infection between the infected and uninfected cell population. τ stands for intracellular time delay. The second equation describes the state of latent infection; that is, target cells are infected but not yet infectious. Suppose if the infected cells are matured enough to infect the susceptible cells. ρ, α_L, and d_L are scalars. The third equation explains the rate of change in the infectious cell population with the death rate δ, migrated from latent infection a, removing the infection by immune responses at the rate of m. The fourth equation explores the rate of change in the free virions; the rate of proliferation from the infection is given by p and the decay rate is c. Finally, the production of effector cells can have the maximum proliferation in an infected cell with a maximum rate b_z and is given by the term $b_z(y(t)/y(t) + K_B)z(t)$. The loss of functional effector cells is defined by $d_z(y(t)/y(t) + K_D)z(t)$, with an assumption $K_D > K_B$.

2.1. Positivity and Boundedness. In order to ensure the convergence of the solutions of the model, it becomes necessary to ensure that solutions of the state variables in model (1) are positive and ultimately bounded.

Theorem 1. *Assume that* $(x(t), l(t), y(t), u(t), z(t))$ *be a solution of the proposed model (1) with the initial conditions* $x(t) > 0, l(t) > 0, y(t) > 0, u(t) > 0, z(t) > 0$. *It is positive and ultimately bounded for* $t > 0$.

Proof. Consider the proof regarding $x(t) > 0$ for all $t > 0$. In this regard, assume that there exists $t_1 > 0$, which implies $x(t_1) = 0, x(t) > 0, t \in [0, t_1)$ such that $\dot{x}(t) \le 0$. From (1), it is clear that $\dot{x}(t_1) = s$, $s > 0$, which is a contradiction and leads to the proof that $x(t) > 0$, $\forall t > 0$.

Similarly, the proof can be extended for all the remaining state equations.

$$
\begin{aligned}
l(t) &= l(0)e^{-(a+d_L-\rho)t} + \int_0^t \alpha_L(1-\epsilon_1(t))\beta x(\xi)y(\xi)e^{(a+d_L-\rho)(\xi-t)}\mathrm{d}\xi,\\
z(t) &= z(0)e^{\int_0^t (b_z y(\xi)/K_B + y(\xi)z(\xi) - d_z y(\xi)/K_D + y(\xi)z(\xi) - \mu)\mathrm{d}\xi},\\
y(t) &= y(0)e^{-\delta t} + \int_0^t ((1-\alpha_L)(1-\epsilon_1(t))\beta x(\xi)y(\xi) + al(\xi)\\
&\quad - my(\xi)z(\xi))e^{-\delta(\xi-t)}\mathrm{d}\xi,\\
u(t) &= u(0)e^{-ct} + \int_0^t (1-\epsilon_2(t))ye^{c(\xi-t)}\mathrm{d}\xi.
\end{aligned}
\tag{2}
$$

Now, to prove $\{l(t),\ y(t),\ u(t),\ z(t)\} > 0,\ \forall t > 0$. And consider that $t_2 > 0$ and define

$$
\min\{l(t_2), y(t_2), u(t_2), z(t_2)\} = 0. \tag{3}
$$

If $l(t_2) = 0$, $l(t) > 0$ for $t \in [0, t_2)$ and $y(t) > 0$, $u(t) > 0$, $z(t) > 0$ for $t \in [0, t_2)$, $\dot{l}(t_2) = 0$, then we have $\dot{l}(t_2) = \alpha_L(1-\epsilon_1(t))\beta x(t_2)y(t_2) > 0$, which is a contradiction.

If $y(t_2) = 0$, $y(t) > 0$ for $t \in [0, t_2)$ and $\{l(t),\ u(t),\ z(t)\} > 0$ for $t \in [0, t_2)$ with $\dot{y}(t_2) \le 0$. However, from (1), one can have $\dot{y}(t_2) = al(t_2) > 0$.

Similarly, for $u(t_2) = 0$ and $z(t_2) = 0$ is also a contradiction. Thus, $\{x(t), l(t), y(t), u(t), z(t)\} > 0,\ \forall t > 0$. To proceed with ensuring the boundedness of the solutions, we extend the results of the positivity of the solution for model (1).

$$
\dot{x}(t) \le s - \gamma x(t). \tag{4}
$$

Taking the limits will lead to

$$
\lim_{t\longrightarrow\infty} \sup(x(t)) \le \frac{s}{\gamma}. \tag{5}
$$

Let $H(t) = x(t) + l(t) + y(t)$

$$
\begin{aligned}
\dot{H}(t) &= \dot{x}(t) + \dot{l}(t) + \dot{y}(t)\\
\dot{H}(t) &= s - \gamma x(t) - (1-\varepsilon_1(t))\beta x(t)y(t)\\
&\quad + \alpha_L(1-\varepsilon_1(t))\beta x(t)y(t) + (\rho - a - d_L)l(t)\\
&\quad + (1-\alpha_L)(1-\varepsilon_1(t))\beta x(t)y(t)\\
&\quad + al(t) - \delta y(t) - my(t)z(t)\\
&\le s - \Upsilon x(t) + (\rho - d_L)l(t) - \delta y(t)\\
&\le s + \sigma H(t).
\end{aligned}
\tag{6}
$$

Define that $\sigma = \min\{\gamma, (\rho - d_L), \delta\}$ and

$$
\lim_{t\longrightarrow\infty} \sup(H(t)) \le \frac{s}{\sigma}, \tag{7}
$$

To prove the ultimate boundedness of free virions, the same approach is followed:

$$
\begin{aligned}
\dot{u}(t) &= py(t) - cu(t) = p\left(\frac{s}{\sigma}(1-\epsilon_2(t))\right) - cu(t)\\
\lim_{t\to\infty}\sup(u(t)) &\le \frac{ps(1-\epsilon_2(t))}{\sigma c}.
\end{aligned}
\tag{8}
$$

Since $u(t)$ cannot be negative, if $\epsilon_2(t) = 0$, then $\sup(u(t)) = 0$. Similarly, for $z(t)$, we get

$$
\begin{aligned}
\dot{z}(t) &= b_z\frac{y(t)}{K_B + y(t)}z(t) - d_z\frac{(t)}{K_D + y(t)}z(t) - \mu z(t),\\
\frac{\dot{z}(t)}{z} &= b_z\frac{y(t)}{K_B + y(t)} - d_z\frac{y(t)}{K_D + y(t)} - \mu.
\end{aligned}
\tag{9}
$$

Applying integration on both sides

$$
\lim_{t\longrightarrow\infty} \sup(z(t)) \le b_z\Omega_1 - d_z\Omega_2 - \mu, \tag{10}
$$

where

$$
\begin{aligned}
\Omega_1 &= b_z\frac{(s/\sigma)}{K_B + (s/\sigma)},\\
\Omega_2 &= d_z\frac{(s/\sigma)}{K_D + (s/\sigma)}.
\end{aligned}
\tag{11}
$$

Hence, it is proved that all the state variables solutions are ultimately bounded.

Consider

$$
\begin{aligned}
\Delta = \Big\{&(x, l, y, u, z) \in C_+^5 :\ \|x(t)\| \le \frac{s}{\sigma}, \|l(t)\|\\
&\le \frac{s}{\sigma}, \|y(t)\| \le \frac{s}{\sigma}, \left\|u(t)\right\| \le \frac{ps(1-\varepsilon_2(t))}{\sigma c}\\
&\|z(t)\| \le b_z\Omega_1 - d_z\Omega_2 - \mu\},
\end{aligned}
\tag{12}
$$

where σ, Ω_1, and Ω_2 are given in the above equation. From the given theorem, it is clear that, within the region, Δ is a positive invariant. □

3. Equilibria

This section describes the derivation of equilibria of PTC HIV model based on three cases such as disease-free, immune-free equilibrium, and endemic equilibrium.

(i) Model (1) without infection exhibits disease-free equilibrium $E_0 = (x_0, 0, 0, 0, 0)$, where $x_0 = s/d$.

(ii) If $R_0 > 1$, model (1) has an immune-free equilibrium $E_1 = (x_1, l_1, y_1, u_1, 0)$ with the coefficients

$$
\begin{aligned}
x_1 &= \frac{\delta(a + d_L - \rho)}{\beta(1-\epsilon_1(t))[a\alpha_L + (1-\alpha_L)(a + d_L - \rho)]},\\
l_1 &= \frac{\alpha_L\beta(1-\epsilon_1(t))x_1y_1}{a + d_L - \rho},\\
u_1 &= \frac{p(1-\epsilon_2(t))_1}{c},\\
y_1 &= \frac{d(R_0 - 1)}{\beta(1-\epsilon_1(t))}.
\end{aligned}
\tag{13}
$$

(iii) The endemic equilibrium of the system $E_2(x_+, l_+, y_+, u_+, z_+)$ is given by

$$
\begin{aligned}
x_+ &= \frac{s}{\gamma + \beta(1-\epsilon_1(t))y_+},\\
l_+ &= \frac{\alpha_L(1-\epsilon_1(t))\beta x_+ y_+}{a + d_L - \rho}\\
y_+ &= \frac{-(K_y) + \sqrt{(K_y)^2 - 4(I)(C)}}{2I},\\
u_+ &= p_+\left(\frac{1-\epsilon_2(t)}{c, z_+ = \dfrac{(a+d_L-\rho)(1-\alpha_L)(1-\epsilon_1(t))\beta x_+ + a\alpha_L(1-\epsilon_1(t))\beta x_+ y_+ - \delta(a+d_L-\rho)}{m(a+d_L-\rho)}},\right.
\end{aligned}
\tag{14}
$$

with $K_y = K_D b_z - d_z K_B - \mu K_B - \mu K_D$ and $I = b_z - d_z - \mu$, $C = -\mu K_B K_D$.

3.1. Basic Reproduction Number. In epidemiology, a basic reproduction number is the average number of persons an affected person can transmit the secondary infection. The basic reproduction number is an indicator that helps to determine the community spread of infection, which can be calculated using the next generation matrix. For the proposed model, the basic reproduction number, say, R_0, is determined for various situations and described in the following sections.

3.1.1. For Disease-Free Equilibrium. The basic reproduction number of the model without a viral latent reservoir is

$$
\begin{aligned}
(1-\epsilon_1(t))\beta x(t) y(t) - \delta y(t) > 0,\\
\left((1-\epsilon_1(t))\beta x(t) - \delta\right) y(t) > 0.
\end{aligned}
\tag{15}
$$

Since $y(t) \neq 0$, then

$$
R_0 = (1-\epsilon_1(t))\beta \cdot \frac{s}{\gamma} \cdot \frac{1}{\delta}. \tag{16}
$$

3.1.2. For Immune-Free Equilibrium. The basic reproduction number of the model with immune-free equilibrium is

$$
\begin{aligned}
\mathscr{F} &= \begin{pmatrix} \alpha_L(1-\varepsilon_1(t))\beta x(t) y(t) \\ (1-\alpha_L)(1-\varepsilon_1(t))\beta x(t) y(t) \end{pmatrix},\\
\mathscr{V} &= \begin{pmatrix} (\rho - a - d_L) l(t) \\ a l(t) - \delta y(t) \end{pmatrix}.
\end{aligned}
\tag{17}
$$

Then, $\mathscr{F}$ and $\mathscr{V}$ help us to find the next generation matrix FV^{-1} as calculated:

$$
\begin{aligned}
F &= \begin{pmatrix} 0 & \alpha_L(1-\varepsilon_1(t))\beta x(t) \\ 0 & (1-\alpha_L)(1-\varepsilon_1(t))\beta x(t) \end{pmatrix},\\
V &= \begin{pmatrix} \rho - a - d_L & 0 \\ a & -\delta \end{pmatrix},\\
V^{-1} &= \frac{1}{-\delta(\rho - a - d_L)} \begin{pmatrix} -\delta & 0 \\ -a & \rho - a - d_L \end{pmatrix},\\
FV^{-1} &= \begin{pmatrix} 0 & \alpha_L(1-\varepsilon_1(t))\beta x(t) \\ 0 & (1-\alpha_L)(1-\varepsilon_1(t))\beta x(t) \end{pmatrix} \cdot \frac{1}{-\delta(\rho - a - d_L)} \begin{pmatrix} -\delta & 0 \\ -a & \rho - a - d_L \end{pmatrix},\\
&= \begin{pmatrix} \dfrac{-a\alpha_L(1-\varepsilon_1(t))\beta x(t)}{\delta(a+d_L-\rho)} & \dfrac{-\alpha_L(1-\varepsilon_1(t))\beta x(t)}{\delta} \\ \dfrac{-a(1-\alpha_L)(1-\varepsilon_1(t))\beta x(t)}{\delta(a+d_L-\rho)} & \dfrac{-(1-\varepsilon_1(t))(1-\alpha_L)\beta x(t)}{\delta} \end{pmatrix}.
\end{aligned}
\tag{18}
$$

Now, the characteristic equation for the above matrix is

$$\lambda^2 - \left[\frac{-a\alpha_L(1-\varepsilon_1(t))\beta x(t)}{\delta(a+d_L-\rho)} - \frac{(1-\varepsilon_1(t))(1-\alpha_L)\beta x(t)}{\delta}\right],$$
$$\lambda + \left(\frac{-\alpha_L(1-\varepsilon_1(t))\beta x(t)}{\delta}\right)\left(\frac{-a(1-\alpha_L)(1-\varepsilon_1(t))\beta x(t)}{\delta(a+d_L-\rho)}\right) = 0, \tag{19}$$

where $x_0 = s/\Upsilon$, then the basic reproduction number is given by

$$R_0 = (1-\varepsilon_1(t))\cdot\beta\cdot\left[(1-\alpha_L) + \frac{a\alpha_L}{a+d_L-\rho}\right]\cdot\frac{s}{\Upsilon}\cdot\frac{1}{\delta}. \tag{20}$$

3.1.3. For Endemic Equilibrium. The basic reproduction number of the model with endemic equilibrium is given by

$$\mathscr{F} = \begin{pmatrix} \alpha_L(1-\varepsilon_1(t))\beta x(t)y(t) \\ (1-\alpha_L)(1-\varepsilon_1(t))\beta x(t)y(t) \end{pmatrix},$$
$$\mathscr{V} = \begin{pmatrix} (\rho - a - d_L)l(t) \\ al(t) - \delta y(t) \end{pmatrix}. \tag{21}$$

Then, $\mathscr{F}$ and $\mathscr{V}$ help us to find the next generation matrix FV^{-1} as calculated below:

$$F = \begin{pmatrix} 0 & \alpha_L(1-\varepsilon_1(t))\beta x(t) \\ 0 & (1-\alpha_L)(1-\varepsilon_1(t))\beta x(t) \end{pmatrix},$$
$$V = \begin{pmatrix} \rho - a - d_L & 0 \\ a & -\delta \end{pmatrix},$$
$$V^{-1} = \frac{1}{-\delta(\rho - a - d_L)}\begin{pmatrix} -\delta & 0 \\ -a & \rho - a - d_L \end{pmatrix},$$
$$FV^{-1} = \begin{pmatrix} 0 & \alpha_L(1-\varepsilon_1(t))\beta x(t) \\ 0 & (1-\alpha_L)(1-\varepsilon_1(t))\beta x(t) \end{pmatrix}\cdot\frac{1}{-\delta(\rho - a - d_L)}\begin{pmatrix} -\delta & 0 \\ -a & \rho - a - d_L \end{pmatrix},$$
$$= \begin{pmatrix} \dfrac{-a\alpha_L(1-\varepsilon_1(t))\beta x(t)}{\delta(a+d_L-\rho)} & \dfrac{-\alpha_L(1-\varepsilon_1(t))\beta x(t)}{\delta} \\ \dfrac{-a(1-\alpha_L)(1-\varepsilon_1(t))\beta x(t)}{\delta(a+d_L-\rho)} & \dfrac{-(1-\varepsilon_1(t))(1-\alpha_L)\beta x(t)}{\delta} \end{pmatrix}. \tag{22}$$

Now, the characteristic equation for the above matrix is

$$\lambda^2 - \left[\frac{-a\alpha_L(1-\varepsilon_1(t))\beta x(t)}{\delta(a+d_L-\rho)} - \frac{(1-\varepsilon_1(t))(1-\alpha_L)\beta x(t)}{\delta}\right],$$
$$\lambda + \left(\frac{-\alpha_L(1-\varepsilon_1(t))\beta x(t)}{\delta}\right)\left(\frac{-a(1-\alpha_L)(1-\varepsilon_1(t))\beta x(t)}{\delta(a+d_L-\rho)}\right) = 0. \tag{23}$$

The basic reproduction number is calculated from the next generation matrix is given by

$$\lambda = \frac{2Is\beta(1-\varepsilon_1(t))[a\alpha_L + (a+d_L-\rho)(1-\alpha_L)]}{\delta(a+d_L-\rho)\left\{2I\gamma + \beta(1-\varepsilon_1(t))\left[-\left(K_y + \sqrt{(K_y)^2 - 4IC}\right]\right]\right\}}, \tag{24}$$

where K_y, I, and C are described above. The spectral radius or the largest eigenvalue of the next generation matrix is called the basic reproduction number.

4. Stability Analysis

Let $E_2(x_+, l_+, y_+, u_+, z_+)$ be any arbitrary positive equilibrium of the system (1). Then, the Jacobian matrix was

evaluated at positive equilibrium's E_2 in the view of biological aspects. This leads us to the following characteristic polynomial. The plus signs are ignored for the convenience of calculations.

$$J = \begin{pmatrix} -\gamma - (1-\varepsilon_1(t))\beta y & 0 & -(1-\varepsilon_1(t))\beta x e^{-\lambda\tau} & 0 & 0 \\ \alpha_L(1-\varepsilon_1(t))\beta y & \rho - a - d_L & \alpha_L(1-\varepsilon_1(t))\beta x & 0 & 0 \\ \beta y(1-\alpha_L)(1-\varepsilon_1(t)) & a & a_{33} & 0 & -my \\ 0 & 0 & p(1-\varepsilon_2(t)) & -c & 0 \\ 0 & 0 & a_{53} & 0 & a_{55} \end{pmatrix}, \tag{25}$$

where $a_{33} = \beta x(1-\alpha_L)(1-\varepsilon_1(t)) - mz - \delta$, $a_{53} = (b_z z/K_B + y) - (d_z z/ K_D + y) - (b_z yz/(K_B + y)^2) + (d_z yz/(K_D + y)^2)$ and $a_{55} = (b_z y/K_B + y) - \mu - (d_z y/K_D + y)$

4.1. Stability Analysis of the Model without Time Delay. The characteristic polynomial without delay is given by

$$\lambda^5 + P_1\lambda^4 + P_2\lambda^3 + P_3\lambda^2 + P_4\lambda + P_5 = 0. \tag{26}$$

Routh–Hurwitz criterion: define n^{th} root-based Routh–Hurwitz matrix as follows:

$$H_n = \begin{pmatrix} P_1 & 1 & 0 & 0 & \cdots & 0 \\ P_3 & P_2 & P_1 & 1 & \cdots & 0 \\ P_5 & P_4 & P_3 & P_2 & \cdots & 1 \\ \vdots & \vdots & \vdots & & & \\ 0 & 0 & 0 & 0 & \cdots & P_n \end{pmatrix}, \tag{27}$$

where $P_j = 0$, if $j > n$. When $n = 5$, the matrix is simplified into

$$H_5 = \begin{pmatrix} P_1 & 1 & 0 & 0 & 0 \\ P_3 & P_2 & P_1 & 1 & 0 \\ P_5 & P_4 & P_3 & P_2 & 1 \\ 0 & 0 & P_5 & P_4 & P_3 \\ 0 & 0 & 0 & 0 & P_5 \end{pmatrix}. \tag{28}$$

Suppose all the roots of the characteristic polynomial with negative real part, then the determinant of Routh–Hurwitz matrices are positive and vice versa. That is, $\det H_I > 0, 1 = 1, 2, \ldots, 5$. This can be employed to verify the proof of Theorem 1. The necessary and sufficient condition to exist for the negative real part for equation (6) is $P_1 > 0, P_1P_2 - P_3 > 0, P_1(P_2P_3 - P_1P_4) + (P_3^2 - P_1P_5) > 0, P_1[P_2(P_3P_4 - P_2P_5) - P_1(P_4^2) + P_4P_5] - [P_3(P_3P_4 - P_2P_5) + P_1(P_4P_5) + P_5^2] > 0,$ and $\det(H_5) > 0$.

The expansion of the coefficients P_1, P_2, P_3, P_4, P_5 is given in Appendix.

4.2. Stability Analysis of the Model with Time Delay. The characteristic polynomial of the Jacobian is

$$\begin{aligned} &\lambda^5 + Q_1\lambda^4 + Q_2\lambda^3 + Q_3\lambda^2 + Q_4\lambda + Q_5 \\ &+e^{-\lambda\tau}\left(R_1\lambda^3 + R_2\lambda^2 + R_3\lambda + R_4\right) = 0. \end{aligned} \tag{29}$$

The coefficients Q_i, $i = 1, 2, 3, 4, 5$, and R_i, $i = 1, 2, 3, 4$, are given in Appendix. We rewrite the above equation as

$$Q(\lambda) + e^{-\lambda\tau}R(\lambda) = 0. \tag{30}$$

Suppose some of the eigenvalues are purely imaginary, that is, $\lambda = i\omega$, then the characteristic equation becomes

$$\begin{aligned} &(i\omega)^5 + Q_1(i\omega)^4 + Q_2(i\omega)^3 + Q_3(i\omega)^2 + Q_4(i\omega) \\ &+ Q_5 + e^{-i\omega\tau}\left(R_1(i\omega)^3 + R_2(i\omega)^2 + R_3(i\omega) + R_4\right) = 0, \\ &i\omega^5 + Q_1\omega^4 - iQ_2\omega^3 - Q_3\omega^2 + iQ_4\omega + Q_5 \\ &+ e^{-i\omega\tau}\left(-R_1 i\omega^3 - R_2\omega^2 + iR_3\omega + R_4\right) = 0, \\ &i\left(\omega^5 - Q_2\omega^3 + Q_4\omega\right) + \left(Q_1\omega^4 - Q_3\omega^2 + Q_5\right) \\ &+ (\cos\omega\tau - i\sin\omega\tau)\left(-iR_1\omega^3 - R_2\omega^2 + iR_3\omega + R_4\right) = 0, \\ &i\left(\omega^5 - Q_2\omega^3 + Q_4\omega\right) + \left(Q_1\omega^4 - Q_3\omega^2 + Q_5\right) \\ &+ (\cos\omega\tau - i\sin\omega\tau)\left(i\left(-R_1\omega^3 + R_3\omega\right) - R_2\omega^2 + R_4\right) = 0. \end{aligned} \tag{31}$$

Equating real and imaginary parts in the above equation:

$$\begin{aligned} \omega^5 - Q_2\omega^3 + Q_4\omega + \cos\omega\tau\left(-R_1\omega^3 - R_3\omega\right) \\ - i\sin\omega\tau\left(-R_2\omega^2 + R_4\right) = 0, \end{aligned} \tag{32}$$

$$\begin{aligned} Q_1\omega^4 - Q_3\omega^2 + Q_5 + \cos\omega\tau\left(-R_2\omega^2 + R_4\right) \\ + i\sin\omega\tau\left(-R_1\omega^3 + R_3\omega\right) = 0. \end{aligned} \tag{33}$$

Squaring and adding equations (32) and (33), we get

$$\begin{aligned}&\left(\omega^5 - Q_2\omega^3 + Q_4\omega\right)^2 + \left(Q_1\omega^4 - Q_3\omega^2 + Q_5\right)^2\\&= \cos^2\omega\tau\left(-R_2\omega^2 + R_4\right)^2 + \sin^2\omega\tau\left(-R_1\omega^3 + R_3\omega\right)^2\\&\quad + \cos^2\omega\tau\left(-R_1\omega^3 + R_3\omega\right)^2 + \sin^2\omega\tau\left(-R_2\omega^2 + R_4\right)^2\Big], \quad (34)\\&\left(\omega^5 - Q_2\omega^3 + Q_4\omega\right)^2 + \left(Q_1\omega^4 - Q_3\omega^2 + Q_5\right)^2\\&= \left(-R_1\omega^3 + R_3\omega\right)^2 + \left(-R_2\omega^2 + R_4\right)^2.\end{aligned}$$

Simplifying the above equations leads to the following: $-\omega^{10} + (-Q_1^2 + 2Q_2)\omega^8 + (-Q_2^2 + R_1^2 - 2Q_4 + 2Q_1Q_3)\omega^6 + (-Q_3^2 + R_2^2 - 2Q_1Q_5 + 2Q_2Q_4 - 2R_1R_3)\omega^4 + (-Q_4^2 + R_3^2 + 2Q_3Q_5 - 2R_2R4)\omega^2 - Q_5^2 + R_4^2 = 0.$

Since this is the differential equation of order 10, we get almost "10" roots such as $\omega_1 = z_1, \omega_2 = z_2, \omega_3 = z_3, \omega_4 = z_4, \omega_5 = z_5, \omega_6 = z_6, \omega_7 = z_7, \omega_8 = z_8, \omega_9 = z_9,$ and $\omega_{10} = z_{10}$.

Eliminating $\cos\omega\tau$ from equations (32) and (33), we get

$$\begin{aligned}\sin\omega\tau &= \frac{\left(\omega^5 - Q_2\omega^3 + Q_4\omega\right)A - \left(Q_1\omega^4 - Q_3\omega^2 + Q_5\right)B}{A^2 + B^2},\\\omega\tau &= \sin^{-1}\left(\frac{\left(\omega^5 - Q_2\omega^3 + Q_4\omega\right)A - \left(Q_1\omega^4 - Q_3\omega^2 + Q_5\right)B}{A^2 + B^2}\right), \quad (35)\\\tau^i &= \frac{1}{\omega}\sin^{-1}\left(\frac{\left(\omega^5 - Q_2\omega^3 + Q_4\omega\right)A - \left(Q_1\omega^4 - Q_3\omega^2 + Q_5\right)B}{A^2 + B^2}\right),\end{aligned}$$

where $i = 0, 1, 2, \ldots,$ $A = (R_4 - R_2\omega^2)$ and $B = (-R_1\omega^3 + R_3\omega)$.

Hence, for $\tau = 0$, E_2 is asymptotically stable by Routh–Hurwitz criterion [1], E_2 remains stable for $\tau < \tau^0$; we choose

$$\tau^0 = \min\left(\tau^j\right), \quad (36)$$

which completes the proof.

5. Hopf Bifurcation Analysis

In general, any physical system will reflect the changes in the qualitative behavior subject to states and parameters changes; for instance, changes in the rate of infection will reflect in the cell populations. Hence, determining the significant parameters that have an ability to affect the stability of the systems is considered bifurcation parameters. By choosing bifurcation parameters, various kinds of solution nature can be realized; among that Hopf-type bifurcation explores the point where solution trajectories cross the origin, say, from negative to positive, in which the system has purely imaginary eigenvalues. The present model possesses the Hopf-type bifurcation while the bifurcation parameter exceeds the threshold value. The process of deriving the stability conditions and proving the existence of Hopf bifurcation are given below.

Theorem 2. *Consider that the characteristic polynomial is of the form*

$$f_0(\lambda) + f_1(\lambda)e^{-\lambda\tau} = 0, \quad (37)$$

where f_0 and f_1 are continuously differentiable with respect to λ. One of the roots is $\lambda(\tau) = \alpha(\tau) + i\omega(\tau)$, where $\lambda(\tau)$ is continuously differentiable with respect to τ, and satisfies $\alpha(\tau_0) = 0$ and $\omega(\tau_0) = \omega_0$ for a positive real number t_0. Denote

$$\phi(\omega) = \left|f_0(i\omega)\right|^2 - \left|f_1(i\omega)\right|^2, \quad (38)$$

which results in

$$\operatorname{sign}\left[\frac{d\operatorname{Re}(\lambda)}{d\tau}\Big|_{\tau=\tau_0}\right] = \operatorname{sign}\left[\left(\frac{1}{2\omega}\frac{d\phi}{d\omega}\right)\Big|_{\omega=\omega_0}\right]. \quad (39)$$

Proof. Consider equation (38), and by taking the derivative of $|f_0(i\omega)|^2$ with respect to ω, will lead to

$$\begin{aligned}\frac{d}{d\omega}\left(\left|f_0(i\omega)\right|^2\right) &= \frac{d}{d\omega}\left\{\left[\operatorname{Re}f_0(i\omega)\right]^2 + \left[\operatorname{Im}f_0(i\omega)\right]^2\right\}\\&= 2\operatorname{Re}f_0(i\omega).\operatorname{Re}\left[f_0'(i\omega)i\right] + 2\operatorname{Im}f_0f_0(i\omega).\operatorname{Im}\left[f_0'(i\omega)i\right] \quad (40)\\&= 2\operatorname{Re}\left[\overline{f_0(i\omega)}f_0'(i\omega)i\right]\\&= -2\operatorname{Im}\left[\overline{f_0(i\omega)}f_0'(i\omega)\right].\end{aligned}$$

Then,

$$\begin{aligned}\frac{1}{2\omega}.\frac{d\phi}{d\omega} &= \frac{d}{d\omega}\left(\left|f_0(i\omega)\right|^2 - \left|f_1(i\omega)\right|^2\right)\\&= \frac{1}{\omega}\operatorname{Im}\left[\overline{f_1(i\omega)}f_1'(i\omega) - \overline{f_0(i\omega)}f_0'(i\omega)\right] \quad (41)\\&= \operatorname{Im}\left[\left|f_1(i\omega)\right|^2\frac{f_1'(i\omega)}{\omega f_1(i\omega)} - \left|f_0(i\omega)\right|^2\frac{f_0'(i\omega)}{\omega f_0(i\omega)}\right].\end{aligned}$$

Since $|f_0(i\omega_0)|^2 = |f_1(i\omega_0)|^2$, we have

$$\left(\frac{1}{2\omega}.\frac{d\phi}{d\omega}\right)\Big|_{\omega=\omega_0} = \left|f_0(i\omega_0)\right|^2\operatorname{Im}\left[\frac{f_1'(i\omega_0)}{\omega_0 f_1(i\omega_0)} - \frac{f_0'(i\omega_0)}{\omega_0 f_0(i\omega_0)}\right]. \quad (42)$$

Now, we turn to the left side of (38), calculating the derivative of both sides of $f_0(\lambda) + f_1e^{-\lambda\tau} = 0$ with respect to τ, we obtain

$$f_0'(\lambda)\frac{d\lambda}{d\tau}+f_1'(\lambda)\frac{d\lambda}{d\tau}e^{-\lambda\tau}-\left(\lambda+\tau\frac{d\lambda}{d\tau}f_1(\lambda)e^{-\lambda\tau}\right)=0. \quad (43)$$

Thus,

$$\left[\frac{d\lambda}{d\tau}\right]^{-1}=\frac{f_0'(\lambda)+f_1(\lambda)e^{-\lambda\tau}-\tau f_1(\lambda)e^{-\lambda\tau}}{\lambda f_1(\lambda)e^{-\lambda\tau}}=\frac{f_0'(\lambda)e^{\lambda\tau}+f_1'(\lambda)}{\lambda f_1(\lambda)}-\frac{\tau}{\lambda}. \quad (44)$$

Since $f_0(i\omega_0)+f_1(i\omega_0)e^{-i\omega_0\tau_0}=0$, we have

$$\begin{aligned}\mathrm{Re}\left[\frac{d\lambda}{d\tau}\Big|_{\tau=\tau_0}\right]^{-1}&=\mathrm{Re}\left[\frac{f_0'(i\omega_0)e^{i\omega_0\tau_0}+f_1'(i\omega_0)}{\omega_0 f_1(i\omega_0)}\right]\\&=\mathrm{Re}\left[\frac{f_0'(i\omega_0)}{\omega_0 f_0(i\omega_0)}i\right]+\mathrm{Re}\left[-\frac{f_1'(i\omega_0)}{\omega_0 f_1(i\omega_0)}i\right]\\&=\mathrm{Im}\left[\frac{f_1'(i\omega_0)}{\omega_0 f_1(i\omega_0)}-\frac{f_0'(i\omega_0)}{\omega_0 f_0(i\omega_0)}\right].\end{aligned} \quad (45)$$

Therefore,

$$\begin{aligned}\mathrm{sign}\left[\frac{d\mathrm{Re}(\lambda)}{d\tau}\Big|_{\tau=\tau_0}\right]&=\mathrm{sign}\mathrm{Re}\left[\frac{d\lambda}{d\tau}\Big|_{\tau=\tau_0}\right]\\&=\mathrm{sign}\mathrm{Re}\left[\frac{d\lambda}{d\tau}\Big|_{\tau=\tau_0}\right]^{-1}\\&=\mathrm{sign}\left[\left(\frac{1}{2\omega}\frac{d\phi}{d\omega}\right)\Big|_{\omega=\omega_0}\right].\end{aligned} \quad (46)$$

The proof is completed. □

6. Optimal Control Design

Considering (1), based on two variables such as RTI and PI as controls, namely, ε_1 and ε_2. Here, ε_1 represents the drug reverse transcriptase, and it safeguards the healthy CD4+ from infection, so that the healthy immune cells are maintained in the right proportion. Also, ε_2 is represented the drug protease inhibitors, which maintains the release of the free virions to burst which are active and fully infected. In general, the treatment is initiated with an antiretroviral drug or the combination of two or more drugs, which creates some side effects while using a regular basis. Since the decision of choosing the drug combination is complex and, in this regard, an optimal strategy is a useful tool to understand the situation and make decisions. Now, optimal control provides different options with respect to estimating the costs of the drugs used for the therapies and observing the drug's effectiveness for the disease. The therapy should last long as the optimal control helps us to find the suitable drug combination for the disease. Formulating the optimization problem based on optimal pair, existence is discussed in the following sections.

6.1. The Optimization Problem. In order to state the optimization problem, we first consider ε_1 and ε_2 vary with time.

$$\begin{aligned}\dot{x}(t)&=s-\gamma x(t)-(1-\varepsilon_1(t))\beta x(t)y(t),\\\dot{l}(t)&=\alpha_L(1-\varepsilon_1(t))\beta x(t)y(t)+(\rho-a-d_L)l(t),\\\dot{y}(t)&=(1-\alpha_L)(1-\varepsilon_1(t))\beta x(t)y(t)\\&\quad+al(t)-\delta y(t)-my(t)z(t),\\\dot{u}(t)&=p(1-\varepsilon_2(t))y(t)-cu(t),\\\dot{z}(t)&=b_z\frac{y(t)}{K_B+y(t)}z(t)-d_z\frac{y(t)}{K_D+y(t)}z(t)-\mu z(t).\end{aligned} \quad (47)$$

The optimization problem is designed in terms of maximizing the following objective function constructed from the model parameters:

$$J(\varepsilon_1,\varepsilon_2)=\int_0^{t_f}x(t)+z(t)+u(t)-\left[\frac{A_1}{2}\varepsilon_1^2(t)+\frac{A_2}{2}\varepsilon_2^2(t)\right]dt. \quad (48)$$

Here, the upper bound t_f denotes the period of the treatment and assumptions $A_1>0$ and $A_2>0$, respectively, stand for benefit and treatment costs. The scalars $\varepsilon_1(t)$ and $\varepsilon_2(t)$ are bounded and Lebesgue integrable. The objective of the control is to increase the uninfected cell populations through immune cells and decrease the cell count of free virions and infected cells. Hence, $(\varepsilon_1^*,\varepsilon_2^*)$ is the control pair that needs to be investigated. We assume that the control pair is nonempty, convex, and closed and it is integrable in the objective functional.

$$J(\varepsilon_1^*,\varepsilon_2^*)=\max\{J(\varepsilon_1,\varepsilon_2):\ (\varepsilon_1,\varepsilon_2)\in U\}, \quad (49)$$

where U is the control set defined by $U=\{\varepsilon_1(t),\varepsilon_2(t):\ \varepsilon_i(t)\}$ measurable, $0\le\varepsilon_i\le 1, t\in[0,t_f], i=1,2$.

6.2. Optimal System. In order to investigate the properties of the optimal system, the Pontryagin's minimum principle given in [13] is utilized and it provides necessary stability conditions for the designed optimal control problem. The advantage of the principle is that it handles (47)–(49) in terms of maximizing a Hamiltonian H through ε_1 and ε_2

$$\begin{aligned}&H(t,x,l,y,u,z,y_\tau,\varepsilon_1,\varepsilon_2,\lambda)\\&\quad=\frac{A_1}{2}\varepsilon_1^2+\frac{A_2}{2}\varepsilon_2^2-x-u-z+\sum_{i=0}^{5}\lambda_i f_i,\end{aligned} \quad (50)$$

with

$$\begin{aligned}f_1&=s-\gamma x-(1-\varepsilon_1)\beta x y_\tau\\f_2&=\alpha_L(1-\varepsilon_1)\beta x y+(\rho-a-d_L)l,\\f_3&=(1-\alpha_L)(1-\varepsilon_1)\beta x y+al-\delta y-myz,\\f_4&=p(1-\varepsilon_2)y-cu,\\f_5&=b_z\frac{y}{K_B+y}z-d_z\frac{y}{K_D+y}z-\mu z.\end{aligned} \quad (51)$$

Based on the above discussion, the following theorem can be derived.

Theorem 3. *For any optimal control ε_1^*, ε_2^*, and solutions x^*, l^*, y^*, u^*, z^* of the corresponding state system (1), there exists adjoint variables λ_1, λ_2, λ_3, λ_4, and λ_5 satisfying the equations*

$$\begin{aligned}
\lambda_1'(t) &= 1 + \lambda_1(t)\left(\Upsilon + \beta\left(1-\varepsilon_1(t+\tau)y(t)\right) + \lambda_2(t)\left(\alpha_L\left(\varepsilon_1-1\right)\beta y(t)\right) + \lambda_3(t)\left(1-\alpha_L\right)\left(\varepsilon_1-1\right)\beta y(t)\right)\\
\lambda_2'(t) &= \lambda_2(t)\left(-\rho + a + d_L\right) - \lambda_3(t)(a),\\
\lambda_3'(t) &= \lambda_1(t)\beta x(t)\left[1-\left(\varepsilon_1(t+\tau)\right)\right] + \lambda_2(t)\left[\alpha_l\left(\varepsilon_1(t)-1\right)\beta x(t)\right],\\
&\quad + \lambda_3(t)\left[\left(1-\alpha_L\right)\left(\varepsilon_1(t)-1\right)\beta x(t) + \delta + mz(t)\right] + \lambda_4(t)\rho\left(\varepsilon_2(t)-1\right),\\
&\quad + \lambda_5(t)\left[-\frac{b_z z(t)}{k_B + y(t)} + \frac{d_z z(t)}{k_D + y(t)} + \frac{b_z y(t) z(t)}{\left(k_B + y(t)\right)^2} - \frac{d_z y(t) z(t)}{\left(k_D + y(t)\right)^2}\right],\\
\lambda_4'(t) &= 1 + c\lambda_4(t),\\
\lambda_5'(t) &= 1 + \lambda_3(t)\left(\mathrm{m}y(t)\right) + \lambda_5(t)\left[d_z\frac{y(t)}{K_D + y(t)} - b_z\frac{y(t)}{K_B + y(t)} + \mu\right],
\end{aligned} \tag{52}$$

with the transversality conditions

$$\lambda_i\left(t_f\right) = 0, i = 1, \ldots, 5. \tag{53}$$

Moreover, the optimal control is given by

$$\begin{aligned}
\varepsilon_1^* &= \min\left(1, \max\left(0, -\frac{\beta}{A_1}\left[\lambda_1 x^*(t) y_\tau^*\right]\right)\right),\\
\varepsilon_2^* &= \min\left(1, \max\left(0, \frac{p}{A_2}\left[\lambda_4 y^*(t)\right]\right)\right).
\end{aligned} \tag{54}$$

Proof. The adjoint equations and transversality conditions can be obtained by using Pontryagin's minimum principle with delay, such that suppose if consider the equation in the vector for $X = (\lambda_1, \lambda_2, \lambda_3, \lambda_4, \lambda_5)$.

$$\begin{aligned}
\lambda_1'(t) &= -\begin{pmatrix}\frac{\partial(\dot{x}(t))}{\partial x(t)} & \frac{\partial(\dot{l}(t))}{\partial x(t)} & \frac{\partial(\dot{y}(t))}{\partial x(t)} & \frac{\partial(\dot{u}(t))}{\partial x(t)} & \frac{\partial(\dot{z}(t))}{\partial x(t)}\end{pmatrix} X^T - \frac{\partial H}{\partial x},\\
\lambda_2'(t) &= -\begin{pmatrix}\frac{\partial(\dot{x}(t))}{\partial l(t)} & \frac{\partial(\dot{l}(t))}{\partial l(t)} & \frac{\partial(\dot{y}(t))}{\partial l(t)} & \frac{\partial(\dot{u}(t))}{\partial l(t)} & \frac{\partial(\dot{z}(t))}{\partial l(t)}\end{pmatrix} X^T - \frac{\partial H}{\partial l},\\
\lambda_3'(t) &= -\begin{pmatrix}\frac{\partial(\dot{x}(t))}{\partial y(t)} & \frac{\partial(\dot{l}(t))}{\partial y(t)} & \frac{\partial(\dot{y}(t))}{\partial y(t)} & \frac{\partial(\dot{u}(t))}{\partial y(t)} & \frac{\partial(\dot{z}(t))}{\partial y(t)}\end{pmatrix} X^T - \frac{\partial H}{\partial y},\\
\lambda_4'(t) &= -\begin{pmatrix}\frac{\partial(\dot{x}(t))}{\partial u(t)} & \frac{\partial(\dot{l}(t))}{\partial u(t)} & \frac{\partial(\dot{y}(t))}{\partial u(t)} & \frac{\partial(\dot{u}(t))}{\partial u(t)} & \frac{\partial(\dot{z}(t))}{\partial u(t)}\end{pmatrix} X^T - \frac{\partial H}{\partial u},\\
\lambda_5'(t) &= -\begin{pmatrix}\frac{\partial(\dot{x}(t))}{\partial z(t)} & \frac{\partial(\dot{l}(t))}{\partial z(t)} & \frac{\partial(\dot{y}(t))}{\partial z(t)} & \frac{\partial(\dot{u}(t))}{\partial z(t)} & \frac{\partial(\dot{z}(t))}{\partial z(t)}\end{pmatrix} X^T - \frac{\partial H}{\partial z}.
\end{aligned} \tag{55}$$

The optimal control ε_1^* and ε_2^* can be solved from the optimality conditions

$$\frac{\partial H}{\partial \varepsilon_1}(t) = 0, \frac{\partial H}{\partial \varepsilon_2}(t) = 0. \tag{56}$$

That is,

$$\frac{\partial H}{\partial \varepsilon_1}(t) = A_1\varepsilon_1 + \beta\left(x(t)y_\tau\right)\lambda_1 = 0,$$
$$\frac{\partial H}{\partial \varepsilon_2}(t) = A_2\varepsilon_2 - \lambda_4 p y(t) = 0. \tag{57}$$

Consider the optimal controls ε_1^* and ε_2^* defined in (54) are bounded. If we substitute ε_1^* and ε_2^* in systems (47) and (52), we obtain the following optimality system:

$$\begin{aligned}
\dot{x}(t) &= s - \Upsilon x^*(t) - \left(1-\varepsilon_1^*(t)\right)\beta x^*(t)y^*(t-\Gamma),\\
\dot{l}^*(t) &= \alpha_L\left(1-\varepsilon_1^*(t)\right)\beta x^*(t)y^*(t) + \left(\rho - a - d_L\right)l^*(t),\\
\dot{y}^*(t) &= \left(1-\alpha_L\right)\left(1-\varepsilon_1^*(t)\right)\beta x^*(t)y^*(t) + al^*(t) - \delta y^*(t) - my^*(t)z^*(t),\\
\dot{u}^*(t) &= p\left(1-\varepsilon_2^*(t)\right)y^*(t) - cu^*(t),\\
\dot{z}^*(t) &= b_z\frac{y^*(t)}{K_B + y^*(t)}z^*(t) - d_z\frac{y^*(t)}{K_D + y^*(t)}z^*(t) - \mu z^*(t),\\
\lambda_1'(t) &= 1 + \lambda_1(t)\left(\Upsilon + \beta\left(1-\varepsilon_1(t+\tau)y(t)\right) + \lambda_2(t)\left(\alpha_L\left(\varepsilon_1 - 1\right)\beta y(t)\right)\right.\\
&\quad \left. + \lambda_3(t)\left(1-\alpha_L\right)\left(\varepsilon_1 - 1\right)\beta y(t)\right),\\
\lambda_2'(t) &= \lambda_2(t)\left(-\rho + a + d_L\right) - \lambda_3(t)(a),\\
\lambda_3'(t) &= \lambda_1(t)\beta x(t)\left[1 - \left(\varepsilon_1(t+\tau)\right)\right] + \lambda_2(t)\left[\alpha_l\left(\varepsilon_1(t) - 1\right)\beta x(t)\right]\\
&\quad + \lambda_3(t)\left[\left(1-\alpha_L\right)\left(\varepsilon_1(t) - 1\right)\beta x(t) + \delta + mz(t)\right] + \lambda_4(t)\rho\left(\varepsilon_2(t) - 1\right)\\
&\quad + \lambda_5(t)\left[-\frac{b_z z(t)}{k_B + y(t)} + \frac{d_z z(t)}{k_D + y(t)} + \frac{b_z y(t)z(t)}{\left(k_B + y(t)\right)^2} - \frac{d_z y(t)z(t)}{\left(k_D + y(t)\right)^2}\right],\\
\lambda_4'(t) &= 1 + c\lambda_4(t),\\
\lambda_5'(t) &= 1 + \lambda_3(t)\left(my(t)\right) + \lambda_5(t)\left[d_z\frac{y(t)}{K_D + y(t)} - b_z\frac{y(t)}{K_B + y(t)} + \mu\right],\\
\varepsilon_1^* &= \min\left(1, \max\left(0, -\frac{\beta}{A_1}\left[\lambda_1 x^*(t)y_\tau^*\right]\right)\right),\\
\varepsilon_2^* &= \min\left(1, \max\left(0, \frac{p}{A_2}\left[\lambda_4 y^*(t)\right]\right)\right),\\
\lambda_i\left(t_f\right) &= 0, \quad i = 1, \ldots, 5.
\end{aligned} \tag{58}$$

The significance of stability conditions, validating the existence of Hopf bifurcation properties, and effect of the optimal controller are explored in the following section. □

7. Numerical Simulation

This section describes the numerical evaluations of the proposed model (1) by choosing the experimental range of parameter values provided in Table 1. The simulations are performed through Runge–Kutta fourth-order numerical approximation scheme. The outcomes of the cell simulations corresponding to cell populations are demonstrated through phase-space diagrams. Figures 1 and 2 illustrate the solution behavior of cell populations within the threshold and exceeding the threshold of time delay, respectively. Also, Figure 3 explores the effect of optimal control design, in which the objective is achieved by increasing the number of uninfected cell populations and diminishing the number of virions. In addition, Figures 4–7 provide insights by comparing the controlled and uncontrolled system states such as uninfected, infected, latent, and free virions, respectively. Figures 2 shows the interpretation of variables of the

Table 1: Parameter values and their sources.

Notations	Values	References
s	10^5 cells/mL/day	[23]
γ	0.01	—
β	1.5×10^{-6} (mL/day)	[24, 25]
δ	1 day^{-1}	[26]
N	2000	[27, 28]
p	2000 day^{-1}	—
C	23 day^{-1}	[29]
ϵ	0.001	—
A	0.001 day^{-1}	—
d_L	0.004 day^{-1}	[30]
$t_{1/2}$	44 months	[31]
ρ	0.0045 day^{-1}	[32]
α_L	10^{-6}	—
s_z	1 cells/mL/day	—
b_z	1 day^{-1}	[33]
K_B	0.1 cells/mL	[34]
d_z	2 day^{-1}	[35]
K_D	5 cells/mL	[34]
μ	0.0002 day^{-1}	—
M	0.42 mL/cells/day	—

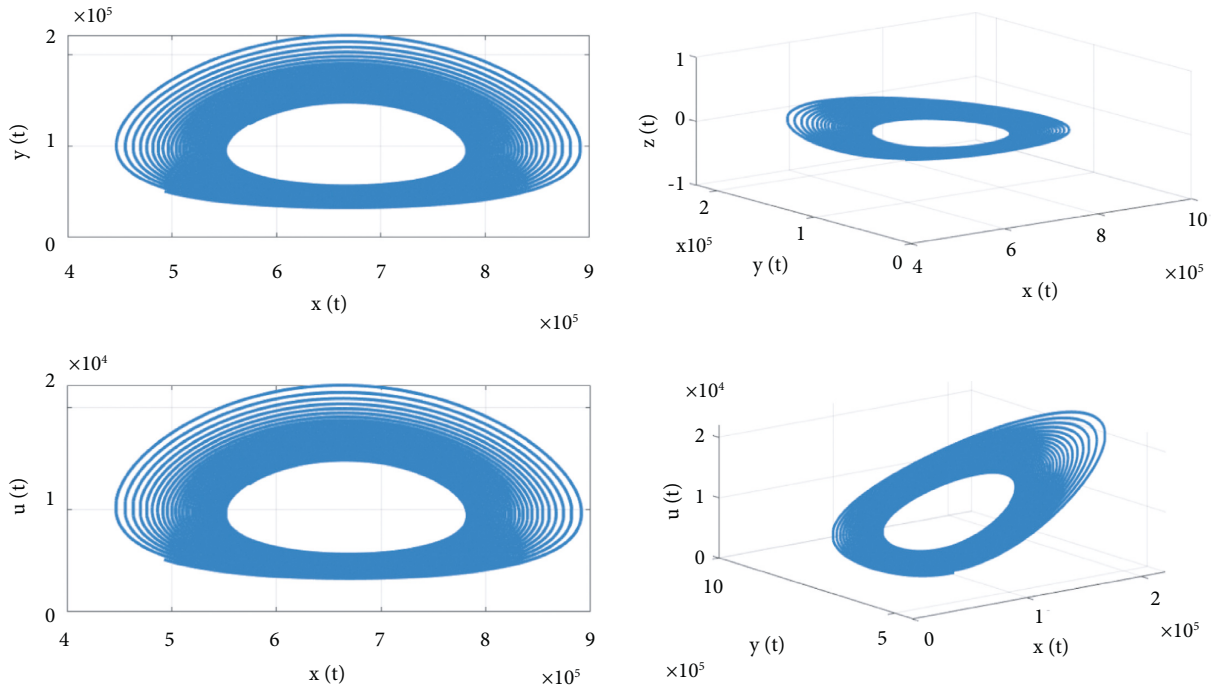

Figure 1: Unstable responses for the time delay $\tau > 0.93$.

equilibrium when $\tau < 0.93$. The top left corner in the panel of Figure 2 evidence the rate of change in healthy CD4+ and infected cells and the bottom left depicts the uninfected cells and the free virions. Similarly, the phase portrait of all the cell populations such as uninfected and infected cells with free virions and immune cells is accordingly picturized. The drug parameter $\varepsilon_1(t)$ and the transmission rate β have a high influence on the stability of the equilibrium. That is, for $0 \le \varepsilon_1(t) \le 0.6$, the equilibrium is stable. For $1.5 \times 10^{-7} \le \beta \le 1.5 \times 10^{-6}$, the equilibrium remains stable. When the transmission rate gets higher or lesser, it loses the stability of equilibrium, where α_L, r, μ, and a also affect the stability when it increases rapidly. The rest of the parameters are having less significance in terms of stability when compared with the remaining parameters.

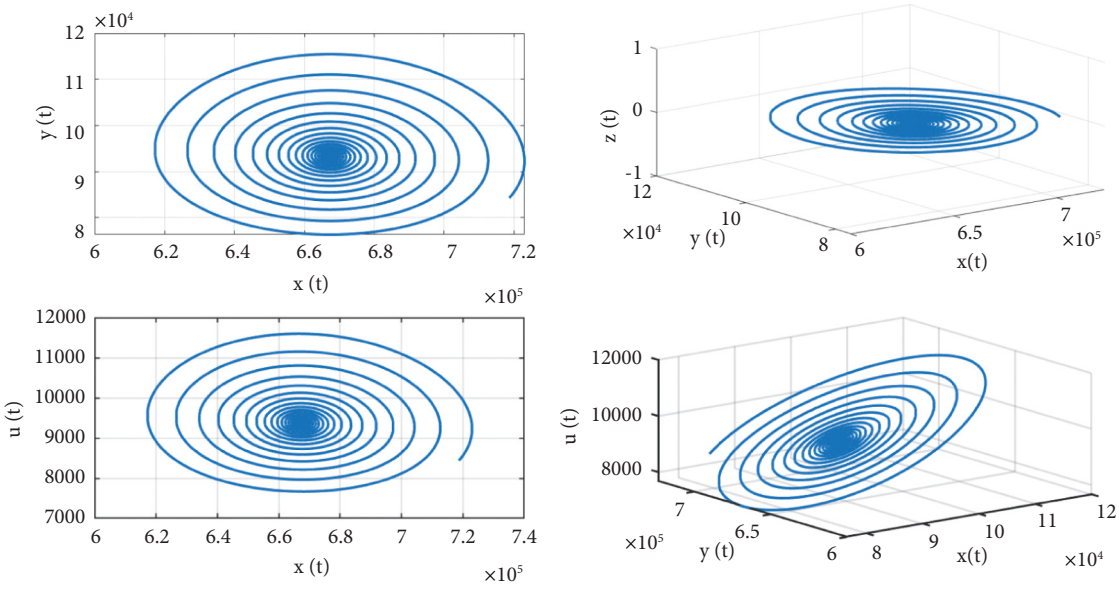

Figure 2: Stable responses for the time delay $\tau < 0.93$.

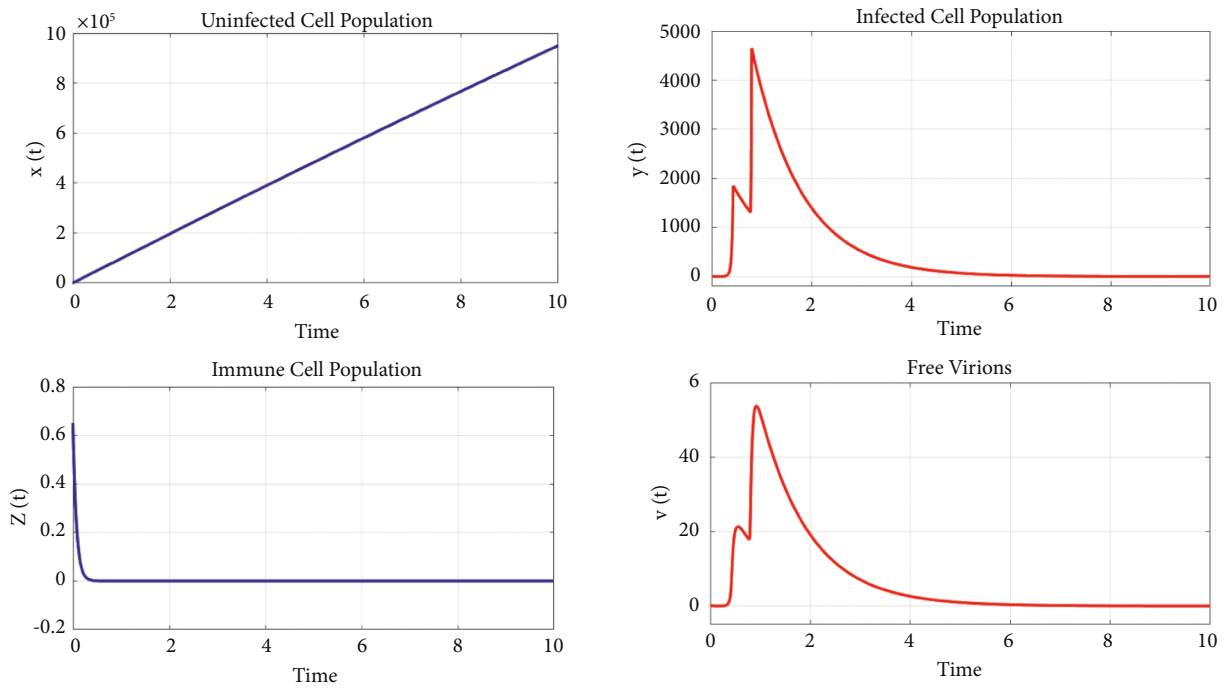

Figure 3: Optimal control-based state responses with respect to time.

Figure 1 represents the state trajectories where the equilibrium point loses its stability due to time delay that makes the transmission rate slow. If the drug is already administered into the body, the drug starts to function among the cells; there is a period for the drug to make progress and with respect to time delays, it becomes necessary to have the effect of time response, and if the drug efficacy is not up to expectation, then the endemic equilibrium will loose the stability.

Figure 8 shows that the uninfected cells start to bifurcate as τ crosses the value 0.93.

Figures 3 represents the uninfected cell population after the optimal control is established. The top figures show the

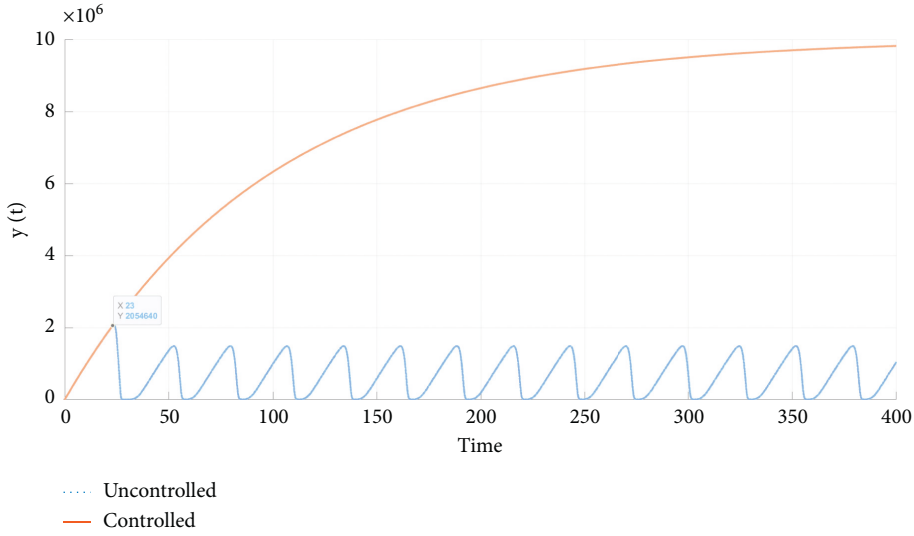

Figure 4: Comparison of controlled and uncontrolled susceptible cell populations.

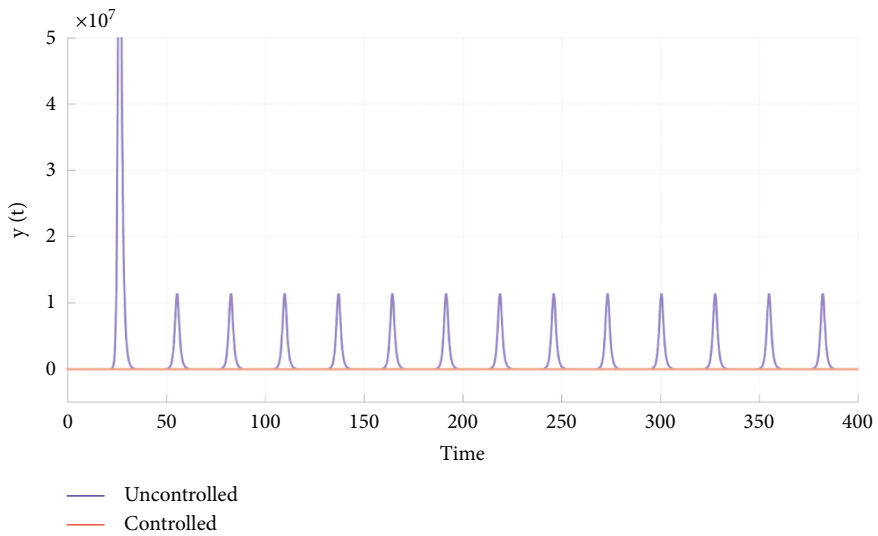

Figure 5: Comparison of controlled and uncontrolled infected cell populations.

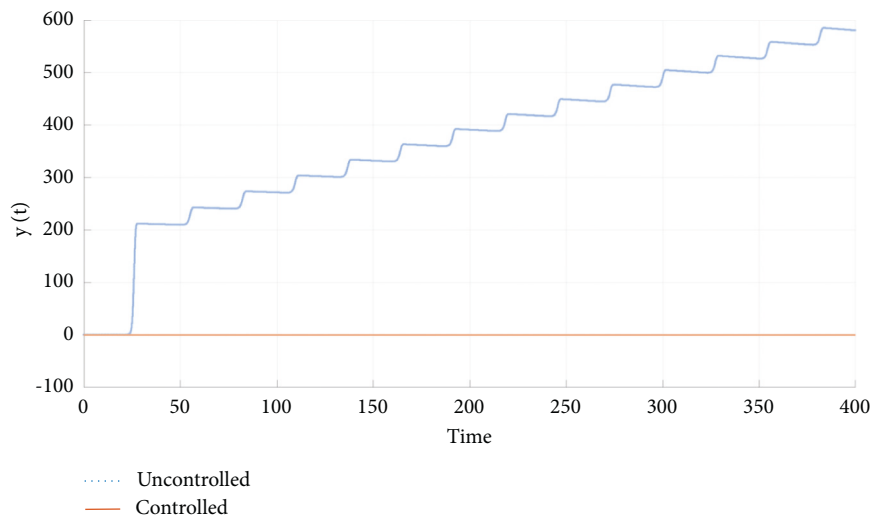

Figure 6: Comparison of controlled and uncontrolled latent cell populations.

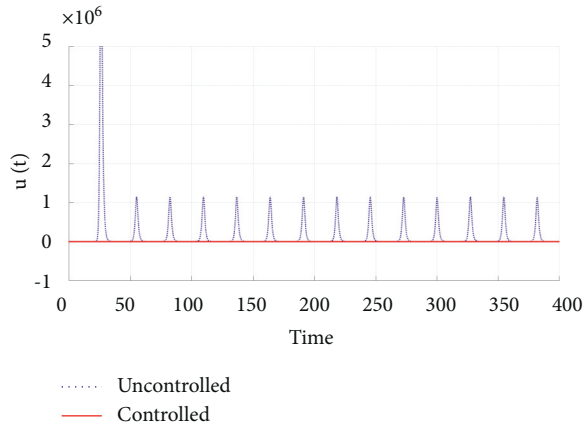

Figure 7: Comparison of controlled and uncontrolled free virions.

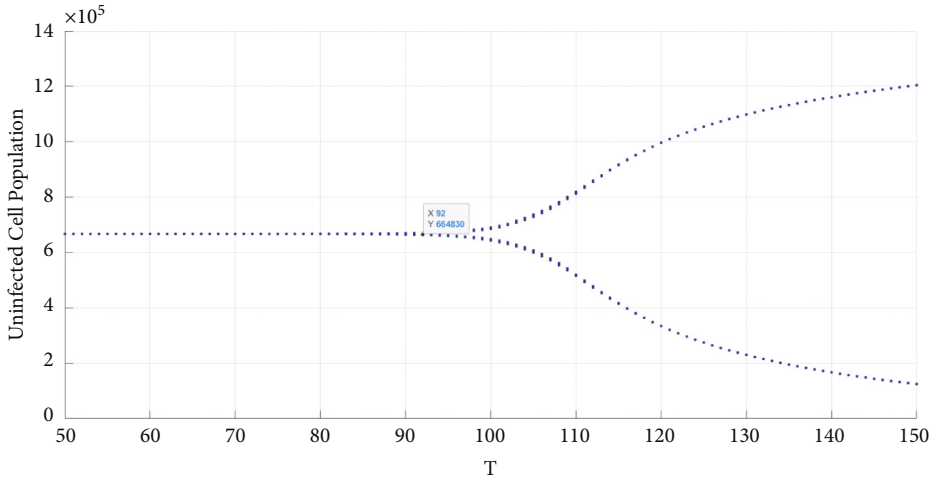

Figure 8: Bifurcation behavior for time delay with respect to uninfected cell populations.

increasing cell population of the uninfected cells and the reducing rate of the infected cells; it is visible after a certain stage the immune cells maintained in proportion, with no increasing number of cells. Similarly, the free virions are depleted in the process.

Figures 4–7 provide the comparisons between controlled and uncontrolled susceptible cell populations, infected cell populations, latent cell populations, and free virions. The graphs exhibit the controlled cell population after the implementation of optimal control.

8. Conclusion

The aim of the paper is to explore the dynamical analysis of posttreatment HIV-1 infection with respect to various significant parameters such as the effect of time delays, two different kinds of antiretroviral therapies, and loss of functional effector cells. By employing the Routh–Hurwitz criterion, the stability properties of the model with respect to discrete-type constant time-delay which is chosen as a bifurcation parameter have been presented. To ensure the effect of time delays, the existence of Hopf-type bifurcation in the behavior of solutions has been proved through proving the corresponding transversality conditions. To reveal the effect of combination of drug therapies, along with those parameters, the situation is modeled as an optimal control problem in terms of the objective function. Through objective function, the results explore the maximization in the number of uninfected cell population and minimization in the number of infected cells and corresponding results are picturized in the numerical section. In the future direction, the model can be extended in terms of fractional order differential operator, considering continuous-type time-delays, stochastic disturbances, and impulse in the antiviral therapy, which also plays a significant role in the system dynamics.

Appendix

The coefficient of system variables is provided in the following:

$$
\begin{aligned}
&\mathrm{C}_{11}\\
&\mathrm{C}_{22} = \rho - a - d_L; \mathrm{C}_{23}\\
&C_{53} = \frac{b_z z}{K_B + y} - \frac{d_z z}{K_D + y} - \frac{b_z yz}{(K_B + y)^2} + \frac{b_z yz}{(K_D + y)^2}; C55\\
&Q_1 = (c - C_{22} - C_{33} - C_{55} - C_{11})\\
&Q_2 = (C_{11}C_{22} - C_{11}c - C_{22}c - C_{33}cC_{23}a + C_{11}C_{33} + C_{22}C_{33} + C_{11}C_{55}C_{22}C_{55})\\
&\quad + C_{33}C_{55} - C_{35}C_{53}\\
&Q_3 = (C_{11}C_{35}C_{53} - C_{11}C_{22}C_{55} - C_{11}C_{33}C_{55} - C_{11}C_{22}C_{33} - C_{22}C_{33}C_{55}\\
&\quad + C_{22}C_{35}C_{53} + C_{11}C_{23}a + C_{23}C_{55}a + C_{11}C_{22}c + C_{11}C_{33}c + C_{22}C_{33}c\\
&\quad + C_{11}C_{55}c + C_{22}C_{55}c + C_{33}C_{55}c - C_{35}C_{53}c - C_{23}ac)\\
&\quad Q_4 (C_{11}C_{22}C_{33}C_{55} - C_{11}C_{22}C_{35}C_{53} - C_{11}C_{23}C_{55}a - C_{11}C_{22}C_{33}c\\
&\quad - C_{11}C_{22}C_{55}c - C_{11}C_{33}C_{55}c + C_{11}C_{35}C_{53}c - C_{22}C_{33}C_{55}c\\
&\quad + C_{22}C_{35}C_{53}c + C_{11}C_{23}ac + C_{23}C_{55}ac)\\
&Q_5 = C_{11}C_{22}C_{33}C_{55}c - C_{11}C_{22}C_{35}C_{53}c - C_{11}C_{23}C_{55}ac\\
&R_1 = -C_{13}C_{31}\\
&R_2 = (C_{13}C_{22}C_{31} + C_{13}C_{31}C_{55} - C_{13}C_{21}a - C_{13}C_{31}c),\\
&R_3 = (C_{13}C_{21}C_{55}a - C_{13}C_{22}C_{31}C_{55} + C_{13}C_{22}C_{31}c + C_{13}C_{31}C_{55}c - C_{13}C_{21}ac)\\
&R_4 = -C_{13}C_{22}C_{31}C_{55}c + C_{13}C_{21}C_{55}ac\\
&P_1 = (c - C_{22} - C_{33} - C_{55} - C_{11}),\\
&P_2 = (C_{11}C_{22} - C_{11}c - C22c - C_{33}c - C_{55}c - C_{23}a + C_{11}C_{33} - C_{13}C_{31}\\
&\quad + C_{22}C_{33} + C_{11}C_{55} + C_{22}C_{55} + C_{33}C_{55} - C_{35}C_{53}),\\
&P_3 = (C_{13}C_{22}C_{31} - C_{11}C_{22}C_{33} - C_{11}C_{22}C_{55} - C_{11}C_{33}C_{55} + C_{11}C_{35}C_{53}\\
&\quad + C_{13}C_{31}C_{55} - C_{22}C_{33}C_{55} + C_{22}C_{35}C_{53} + C_{11}C_{23}a\\
&\quad - C_{13}C_{21}a + C_{23}C_{55}a + C_{11}C_{22}c + C_{11}C_{33}c\\
&\quad - C_{13}C_{31}c + C_{22}C_{33}c + C_{11}C_{55}c + C_{22}C_{55}c\\
&\quad + C_{33}C_{55}c - C_{35}C_{53}c - C_{23}ac),\\
&P_4 = (C_{11}C_{22}C_{33}C_{55} - C_{11}C_{22}C_{35}C_{53} - C_{13}C_{22}C_{31}C_{55} - C_{11}C_{23}C_{55}a + C_{13}C_{21}C_{55}a - C_{11}C_{22}C_{33}c\\
&\quad + C_{13}C_{22}C_{31}c - C_{11}C_{22}C_{55}c - C_{11}C_{33}C_{55}c + C_{11}C_{35}C_{53}c + C_{13}C_{31}C_{55}c\\
&\quad - C_{22}C_{33}C_{55}c + C_{22}C_{35}C_{53}c + C_{11}C_{23}ac - C_{13}C_{21}ac + C_{23}C_{55}ac),\\
&P_5 = C_{11}C_{22}C_{33}C_{55}c - C_{11}C_{22}C_{35}C_{53}c - C_{13}C_{22}C_{31}C_{55}c - C_{11}C_{23}C_{55}ac + C_{13}C_{21}C_{55}ac.
\end{aligned}
\tag{A.1}
$$

Data Availability

All the data are available within the article.

Conflicts of Interest

The authors declare that there are no conflicts of interest.

References

[1] M. Prakash, R. Rakkiyappan, A. Manivannan, and J. Cao, "Dynamical analysis of antigen-driven t-cell infection model with multiple delays," *Applied Mathematics and Computation*, vol. 354, pp. 266–281, 2019.

[2] T. Wang, Z. Hu, and F. Liao, "Stability and hopf bifurcation for a virus infection model with delayed humoral immunity response," *Journal of Mathematical Analysis and Applications*, vol. 411, no. 1, pp. 63–74, 2014.

[3] X. Wang, S. Tang, X. Song, and L. Rong, "Mathematical analysis of an hiv latent infection model including both virus-to-cell infection and cell-to-cell transmission," *Journal of Biological Dynamics*, vol. 11, no. sup2, pp. 455–483, 2017.

[4] T. K. Ayele, E. F. Doungmo Goufo, and S. Mugisha, "Mathematical modeling of hiv/aids with optimal control: a case study in Ethiopia," *Results in Physics*, vol. 26, Article ID 104263, 2021.

[5] A. M. Elaiw, N. H. AlShamrani, and A. D. Hobiny, "Mathematical modeling of hiv/htlv co-infection with ctl-mediated immunity," *AIMS Mathematics*, vol. 6, no. 2, pp. 1634–1676, 2021.

[6] Z. Liu, L. Wang, and R. Tan, "Spatiotemporal dynamics for a diffusive hiv-1 infection model with distributed delays and ctl immune response," *Discrete & Continuous Dynamical Systems-B*, vol. 27, no. 5, p. 2767, 2022.

[7] L. Noël, R. Tubiana, A. Simon et al., "Low immune response rate of hiv-infected patients to a single injection of hepatitis a vaccine," *Infectious Disease News*, vol. 51, no. 1, pp. 94–96, 2021.

[8] N. H. AlShamrani, "Stability of an htlv-hiv coinfection model with multiple delays and ctl-mediated immunity," *Advances in Difference Equations*, vol. 2021, no. 1, pp. 270–357, 2021.

[9] H. Liu and J.-F. Zhang, "Dynamics of two time delays differential equation model to hiv latent infection," *Physica A: Statistical Mechanics and Its Applications*, vol. 514, pp. 384–395, 2019.

[10] H.-D. Kwon, J. Lee, and S.-D. Yang, "Optimal control of an age-structured model of hiv infection," *Applied Mathematics and Computation*, vol. 219, no. 5, pp. 2766–2779, 2012.

[11] J. Danane and K. Allali, "Optimal control of an HIV model with CTL cells and latently infected cells," *Numerical Algebra, Control and Optimization*, vol. 10, no. 2, pp. 207–225, 2020.

[12] G. Akudibillah, A. Pandey, and J. Medlock, "Optimal control for hiv treatment," *Mathematical Biosciences and Engineering*, vol. 16, no. 1, pp. 373–396, 2019.

[13] F. A. Rihan, S. Lakshmanan, and H. Maurer, "Optimal control of tumour-immune model with time-delay and immuno-chemotherapy," *Applied Mathematics and Computation*, vol. 353, pp. 147–165, 2019.

[14] A. Zeb, P. Kumar, V. S. Erturk, and T. Sitthiwirattham, "A new study on two different vaccinated fractional-order covid-19 models via numerical algorithms," *Journal of King Saud University Science*, vol. 34, no. 4, Article ID 101914, 2022.

[15] K. N. Nabi, P. Kumar, and V. S. Erturk, "Projections and fractional dynamics of COVID-19 with optimal control strategies," *Chaos, Solitons & Fractals*, vol. 145, Article ID 110689, 2021.

[16] K. N. Nabi, H. Abboubakar, and P. Kumar, "Forecasting of COVID-19 pandemic: from integer derivatives to fractional derivatives," *Chaos, Solitons & Fractals*, vol. 141, Article ID 110283, 2020.

[17] P. Kumar, V. S. Erturk, M. Vellappandi, H. Trinh, and V. Govindaraj, "A study on the maize streak virus epidemic model by using optimized linearization-based predictor-corrector method in Caputo sense," *Chaos, Solitons & Fractals*, vol. 158, Article ID 112067, 2022.

[18] P. Kumar, V. S. Erturk, A. Yusuf, K. S. Nisar, and S. F. Abdelwahab, "A study on canine distemper virus (cdv) and rabies epidemics in the red fox population via fractional derivatives," *Results in Physics*, vol. 25, Article ID 104281, 2021.

[19] S. Abbas, S. Tyagi, P. Kumar, V. S. Ertürk, and S. Momani, "Stability and Bifurcation Analysis of a Fractional-Order Model of Cell-To-Cell Spread of Hiv-1 with a Discrete Time Delay," *Mathematical Methods in the Applied Sciences*, vol. 45, 2022.

[20] N. Iqbal and Y. Karaca, "Complex fractional-order hiv diffusion model based on amplitude equations with turing patterns and turing instability," *Fractals*, vol. 29, no. 05, Article ID 2140013, 2021.

[21] S. Hussain, E. N. Madi, N. Iqbal, T. Botmart, Y. Karaca, and W. W. Mohammed, "Fractional dynamics of vector-borne infection with sexual transmission rate and vaccination," *Mathematics*, vol. 9, no. 23, p. 3118, 2021.

[22] F. Arif, Z. Majeed, J. U. Rahman, N. Iqbal, and J. Kafle, "Mathematical Modeling and Numerical Simulation for the Outbreak of Covid-19 Involving Loss of Immunity and Quarantined Class," *Computational and Mathematical Methods in Medicine*, vol. 2022, Article ID 3816492, 2022.

[23] M. Salgado, S. A. Rabi, K. A. O'Connell et al., "Prolonged control of replication-competent dual-tropic human immunodeficiency virus-1 following cessation of highly active antiretroviral therapy," *Retrovirology*, vol. 8, no. 1, pp. 97–14, 2011.

[24] W. Stöhr, S. Fidler, M. McClure et al., "Duration of hiv-1 viral suppression on cessation of antiretroviral therapy in primary infection correlates with time on therapy," *PLoS One*, vol. 8, no. 10, Article ID e78287, 2013.

[25] O. Lambotte, F. Boufassa, Y. Madec et al., "Hiv controllers: a homogeneous group of hiv-1—infected patients with spontaneous control of viral replication," *Clinical Infectious Diseases*, vol. 41, no. 7, pp. 1053–1056, 2005.

[26] K. A. O'Connell, J. R. Bailey, and J. N. Blankson, "Elucidating the elite: mechanisms of control in hiv-1 infection," *Trends in Pharmacological Sciences*, vol. 30, no. 12, pp. 631–637, 2009.

[27] J. N. Blankson, "Effector mechanisms in hiv-1 infected elite controllers: highly active immune responses?" *Antiviral Research*, vol. 85, no. 1, pp. 295–302, 2010.

[28] B. D. Walker, "Elite control of hiv infection: implications for vaccines and treatment," *Topics in HIV Medicine a publication of the International AIDS Society USA*, vol. 15, no. 4, pp. 134–136, 2007.

[29] A. Sáez-Cirión, C. Lacabaratz, O. Lambotte et al., "Hiv controllers exhibit potent cd8 t cell capacity to suppress hiv infection ex vivo and peculiar cytotoxic t lymphocyte activation phenotype," *Proceedings of the National Academy of Sciences*, vol. 104, no. 16, pp. 6776–6781, 2007.

[30] J. F. Okulicz, V. C. Marconi, M. L. Landrum et al., "Clinical outcomes of elite controllers, viremic controllers, and long-

term nonprogressors in the us department of defense hiv natural history study," *Journal of Infectious Diseases*, vol. 200, no. 11, pp. 1714–1723, 2009.

[31] S. Grabar, H. Selinger-Leneman, S. Abgrall, G. Pialoux, L. Weiss, and D. Costagliola, "Prevalence and comparative characteristics of long-term nonprogressors and hiv controller patients in the French hospital database on hiv," *AIDS*, vol. 23, no. 9, pp. 1163–1169, 2009.

[32] D. D. Richman, D. M. Margolis, M. Delaney, W. C. Greene, D. Hazuda, and R. J. Pomerantz, "The challenge of finding a cure for hiv infection," *Science*, vol. 323, no. 5919, pp. 1304–1307, 2009.

[33] N. Chomont, M. El-Far, P. Ancuta et al., "Hiv reservoir size and persistence are driven by t cell survival and homeostatic proliferation," *Nature Medicine*, vol. 15, no. 8, pp. 893–900, 2009.

[34] T.-W. Chun, D. Engel, M. M. Berrey, T. Shea, L. Corey, and A. S. Fauci, "Early establishment of a pool of latently infected, resting cd4+ t cells during primary hiv-1 infection," *Proceedings of the National Academy of Sciences*, vol. 95, no. 15, pp. 8869–8873, 1998.

[35] J. Ananworanich, A. Schuetz, C. Vandergeeten et al., "Impact of multi-targeted antiretroviral treatment on gut t cell depletion and hiv reservoir seeding during acute hiv infection," *PLoS One*, vol. 7, no. 3, Article ID e33948, 2012.

Hindawi
Complexity
Volume 2022, Article ID 6078567, 19 pages
https://doi.org/10.1155/2022/6078567

Research Article

A Flexible Extension of Reduced Kies Distribution: Properties, Inference, and Applications in Biology

Muqrin A. Almuqrin,[1] **Ahmed M. Gemeay**,[2] **M. M. Abd El-Raouf**,[3] **Mutua Kilai**,[4] **Ramy Aldallal**,[5] **and Eslam Hussam**[6]

[1]*Department of Mathematics, Faculty of Science in Zulfi, Majmaah University, Al Majma'ah 11952, Saudi Arabia*
[2]*Department of Mathematics, Faculty of Science, Tanta University, Tanta 31527, Egypt*
[3]*Basic and Applied Science Institute, Arab Academy for Science, Technology and Maritime Transport (AASTMT), Alexandria, Egypt*
[4]*Department of Mathematics, Pan-African Institute of Basic Science Technology and Innovation, Nairobi, Kenya*
[5]*Department of Accounting, College of Business Administration in Hawtat Bani Tamim, Prince Sattam bin Abdulaziz University, Hawtat Bani Tamim, Saudi Arabia*
[6]*Department of Mathematics, Faculty of Science, Helwan University, Cairo, Egypt*

Correspondence should be addressed to Mutua Kilai; kilai.mutua1@students.jkuat.ac.ke

Received 17 May 2022; Revised 25 June 2022; Accepted 27 July 2022; Published 5 October 2022

Academic Editor: Fathalla A. Rihan

The extended reduced Kies distribution (ExRKD), which is an asymmetric flexible extension of the reduced Kies distribution, is the subject of this research. Some of its most basic mathematical properties are deduced from its formal definitions. We computed the ExRKD parameters using eight well-known methods. A full simulation analysis was done that allows the study of these estimators' asymptotic behavior. The efficiency and applicability of the ExRKD are investigated via the modeling of COVID-19 and milk data sets, which demonstrates that the ExRKD delivers a better match to the data sets when compared to competing models.

1. Introduction

In order to emulate real-world applications, several authors have proposed ways for adding shape characteristics to standard distributions. In particular, statisticians and data modelers are highly interested in the new distributions that are formed by the extra parameter of a good generator(s). Deriving distributions with limit support is becoming an increasingly popular topic of study among researchers. The necessity for modeling and analyzing bounded data may be seen in a variety of real-world domains, including medicine, politics, and psychology. There are a variety of natural and artificial phenomena that are quantified in terms of indices, percentages, proportions, rates, and ratios. All of these measurements are circumscribed by a certain interval, which is typically the unit interval. According to the literature, a number of distributions with support on the unit interval have been presented, which are derived from transformations of the cumulative distribution function (CDF). Many writers have developed and examined unit distributions such as unit Teissier distribution [1], exponentiated Top–p–Leone distribution [2], log-Lindley distribution [3], transformed gamma distribution [4], Cosine-sine distribution [5], power log-Lindley distribution, power logarithmic distribution and unit Weibull distribution [6, 7, 8], respectivly.

In 2013, Kumar and Dharmaja [9] proposed the reduced Kies distribution (RKD) with CDF and probability density function (PDF) defined, respectively, as follows:

$$F(x) = 1 - e^{-(x/1-x)^{\alpha}},\ 0 < x < 1,$$
$$f(x) = \frac{\alpha e^{-(x/1-x)^{\alpha}} (x/1-x)^{\alpha}}{(1-x)x}. \tag{1}$$

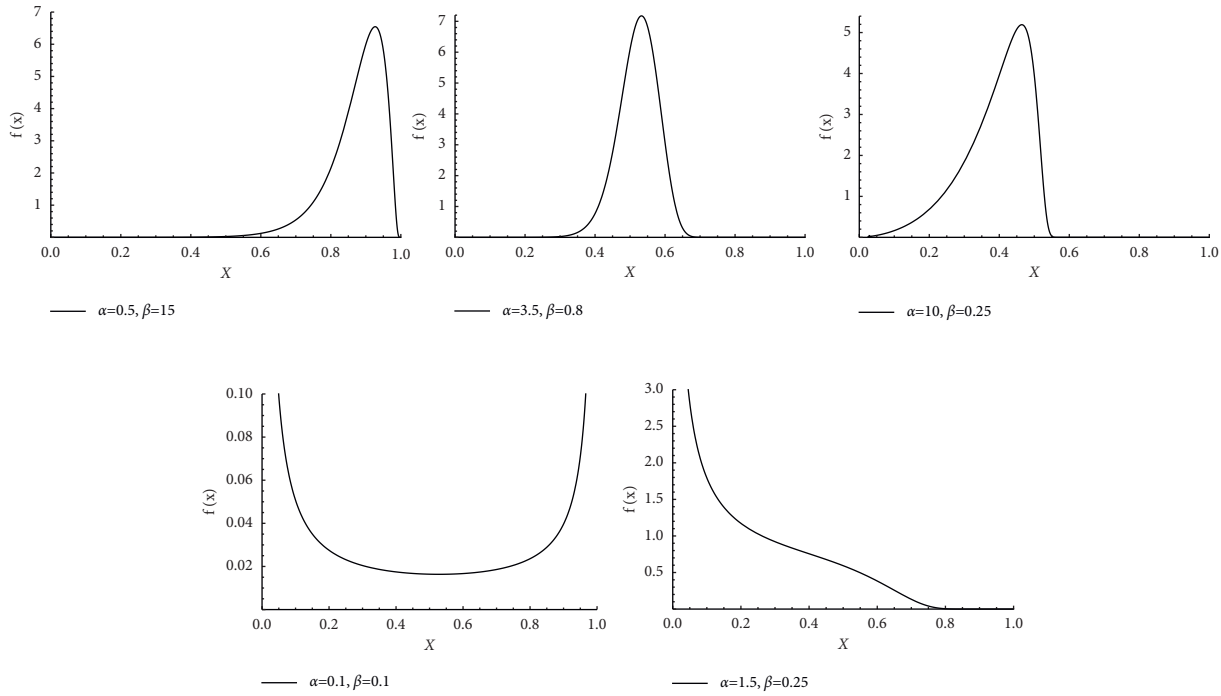

Figure 1: Plots of the PDF of the ExRKD with various parametric values.

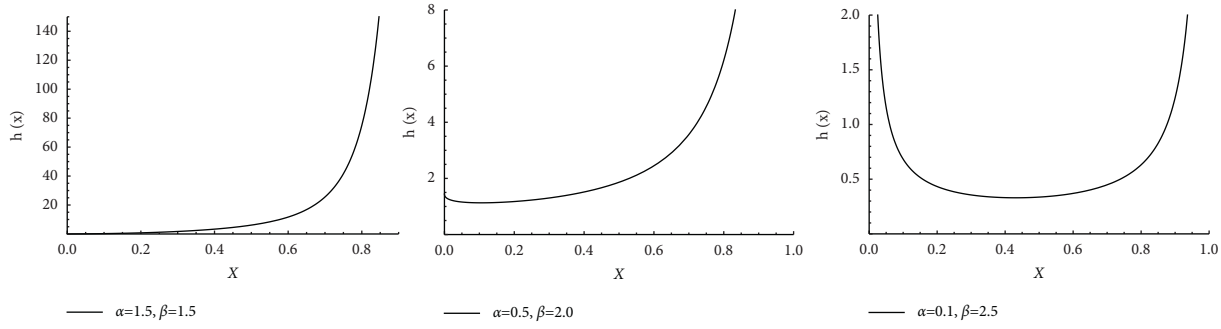

Figure 2: Plots of the HF of the ExRKD with various parametric values.

Our motivation for developing a new flexible version of the RKD, which we refer to as the extended reduced Kies distribution (ExRKD), is to provide greater flexibility in fitting real-world data sets. Furthermore, the article's main objectives are as follows: The first objective is dedicated to the investigation of a novel version of the RKD based on the weighted-G (WD-G) family [10], which is referred to as the ExRKD. The essential distributional characteristics of the ExRKD are thoroughly studied. The ExRKD is endowed with a variety of favorable characteristics. According to the following section, it is capable of handling a variety of PDF and hazard function(HF) shapes. The second goal is to investigate the estimate of the ExRKD parameters using conventional techniques. As a result, eight different estimating methodologies are used for this objective. On the basis of empirical simulation findings, we investigate and rate the performance of various estimators in order to establish a guideline for selecting the most appropriate estimation technique for estimating the ExRKD parameters.

The rest of the paper is divided into six sections, which are as follows: In Section 2, we define the ExRKD and plot its PDF and HF. Section 3 delves into the fundamental characteristics of ExRKD. In Section 4, the parameters of the model are determined using traditional estimation methods. The findings of the simulation are presented in Section 5. Section 6 is dedicated to the analysis of real-world data. Finally, in Section 7, some concluding observations are presented.

2. Formulation of ExRK Distribution

In this section, we define the CDF and the PDF of ExRK distribution, respectively, by using the WD-G family of [10] and CDF in equation (1) as follows:

Table 1: Simulation values of BIAS, MSE, and MRE for $\alpha = 0.25, \beta = 0.75$.

n	Est.	Est. Par.	MLE	ADE	CVME	MPSE	LSE	PCE	RTADE	WLSE
25	BIAS	$\widehat{\alpha}$	$0.081622^{\{4\}}$	$0.065258^{\{3\}}$	$0.122917^{\{8\}}$	$0.053236^{\{1\}}$	$0.090325^{\{7\}}$	$0.084864^{\{6\}}$	$0.062003^{\{2\}}$	$0.082455^{\{5\}}$
		$\widehat{\beta}$	$0.16451^{\{1\}}$	$0.187985^{\{4\}}$	$0.215351^{\{6\}}$	$0.167454^{\{2\}}$	$0.216096^{\{7\}}$	$0.217825^{\{8\}}$	$0.185377^{\{3\}}$	$0.195407^{\{5\}}$
	MSE	$\widehat{\alpha}$	$0.009973^{\{2\}}$	$0.014156^{\{3\}}$	$0.070766^{\{8\}}$	$0.007123^{\{1\}}$	$0.030151^{\{7\}}$	$0.015345^{\{5\}}$	$0.01441^{\{4\}}$	$0.028916^{\{6\}}$
		$\widehat{\beta}$	$0.04479^{\{1\}}$	$0.057887^{\{4\}}$	$0.074164^{\{7\}}$	$0.046973^{\{2\}}$	$0.073642^{\{6\}}$	$0.078046^{\{8\}}$	$0.055738^{\{3\}}$	$0.060312^{\{5\}}$
	MRE	$\widehat{\alpha}$	$0.326489^{\{4\}}$	$0.261031^{\{3\}}$	$0.491669^{\{8\}}$	$0.212945^{\{1\}}$	$0.3613^{\{7\}}$	$0.339455^{\{6\}}$	$0.248012^{\{2\}}$	$0.329821^{\{5\}}$
		$\widehat{\beta}$	$0.219347^{\{1\}}$	$0.250647^{\{4\}}$	$0.287134^{\{6\}}$	$0.223272^{\{2\}}$	$0.288128^{\{7\}}$	$0.290433^{\{8\}}$	$0.247169^{\{3\}}$	$0.260543^{\{5\}}$
	$\sum$ ranks		$13^{\{2\}}$	$21^{\{4\}}$	$43^{\{8\}}$	$9^{\{1\}}$	$41^{\{6.5\}}$	$41^{\{6.5\}}$	$17^{\{3\}}$	$31^{\{5\}}$
50	BIAS	$\widehat{\alpha}$	$0.053746^{\{7\}}$	$0.039116^{\{3\}}$	$0.058017^{\{8\}}$	$0.032691^{\{1\}}$	$0.050696^{\{5\}}$	$0.05304^{\{6\}}$	$0.038016^{\{2\}}$	$0.046704^{\{4\}}$
		$\widehat{\beta}$	$0.10746^{\{1\}}$	$0.126549^{\{3\}}$	$0.148825^{\{7\}}$	$0.110671^{\{2\}}$	$0.144277^{\{6\}}$	$0.159685^{\{8\}}$	$0.126768^{\{4\}}$	$0.133584^{\{5\}}$
	MSE	$\widehat{\alpha}$	$0.005371^{\{5\}}$	$0.003024^{\{3\}}$	$0.010234^{\{8\}}$	$0.002024^{\{1\}}$	$0.006508^{\{7\}}$	$0.004869^{\{4\}}$	$0.002743^{\{2\}}$	$0.005481^{\{6\}}$
		$\widehat{\beta}$	$0.019585^{\{1\}}$	$0.027016^{\{4\}}$	$0.035223^{\{7\}}$	$0.021115^{\{2\}}$	$0.033684^{\{6\}}$	$0.040851^{\{8\}}$	$0.024993^{\{3\}}$	$0.028816^{\{5\}}$
	MRE	$\widehat{\alpha}$	$0.214985^{\{7\}}$	$0.156463^{\{3\}}$	$0.232068^{\{8\}}$	$0.130764^{\{1\}}$	$0.202786^{\{5\}}$	$0.212161^{\{6\}}$	$0.152064^{\{2\}}$	$0.186816^{\{4\}}$
		$\widehat{\beta}$	$0.14328^{\{1\}}$	$0.168731^{\{3\}}$	$0.198433^{\{7\}}$	$0.147561^{\{2\}}$	$0.19237^{\{6\}}$	$0.212914^{\{8\}}$	$0.169024^{\{4\}}$	$0.178112^{\{5\}}$
	$\sum$ ranks		$22^{\{4\}}$	$19^{\{3\}}$	$45^{\{8\}}$	$9^{\{1\}}$	$35^{\{6\}}$	$40^{\{7\}}$	$17^{\{2\}}$	$29^{\{5\}}$
75	BIAS	$\widehat{\alpha}$	$0.050815^{\{8\}}$	$0.028764^{\{2\}}$	$0.04524^{\{7\}}$	$0.024581^{\{1\}}$	$0.041811^{\{5\}}$	$0.044249^{\{6\}}$	$0.029942^{\{3\}}$	$0.035437^{\{4\}}$
		$\widehat{\beta}$	$0.084779^{\{2\}}$	$0.09661^{\{3\}}$	$0.121307^{\{6\}}$	$0.082531^{\{1\}}$	$0.127078^{\{8\}}$	$0.122239^{\{7\}}$	$0.109596^{\{4\}}$	$0.110472^{\{5\}}$
	MSE	$\widehat{\alpha}$	$0.002684^{\{4\}}$	$0.001601^{\{2\}}$	$0.004687^{\{8\}}$	$0.001066^{\{1\}}$	$0.003741^{\{7\}}$	$0.003194^{\{5\}}$	$0.001627^{\{3\}}$	$0.003236^{\{6\}}$
		$\widehat{\beta}$	$0.01297^{\{2\}}$	$0.016376^{\{3\}}$	$0.023753^{\{6\}}$	$0.012253^{\{1\}}$	$0.025487^{\{8\}}$	$0.024522^{\{7\}}$	$0.019014^{\{4\}}$	$0.019493^{\{5\}}$
	MRE	$\widehat{\alpha}$	$0.20326^{\{8\}}$	$0.115057^{\{2\}}$	$0.180961^{\{7\}}$	$0.098323^{\{1\}}$	$0.167245^{\{5\}}$	$0.176996^{\{6\}}$	$0.119769^{\{3\}}$	$0.141747^{\{4\}}$
		$\widehat{\beta}$	$0.113039^{\{2\}}$	$0.128814^{\{3\}}$	$0.161743^{\{6\}}$	$0.110041^{\{1\}}$	$0.169437^{\{8\}}$	$0.162985^{\{7\}}$	$0.146128^{\{4\}}$	$0.147296^{\{5\}}$
	$\sum$ ranks		$26^{\{4\}}$	$15^{\{2\}}$	$40^{\{7\}}$	$6^{\{1\}}$	$41^{\{8\}}$	$38^{\{6\}}$	$21^{\{3\}}$	$29^{\{5\}}$
100	BIAS	$\widehat{\alpha}$	$0.045262^{\{8\}}$	$0.024581^{\{2\}}$	$0.034583^{\{5\}}$	$0.019686^{\{1\}}$	$0.036614^{\{6\}}$	$0.039413^{\{7\}}$	$0.026108^{\{3\}}$	$0.028806^{\{3\}}$
		$\widehat{\beta}$	$0.071516^{\{2\}}$	$0.080407^{\{3\}}$	$0.103425^{\{6\}}$	$0.07047^{\{1\}}$	$0.108323^{\{8\}}$	$0.107061^{\{7\}}$	$0.090832^{\{4\}}$	$0.094763^{\{5\}}$
	MSE	$\widehat{\alpha}$	$0.000995^{\{2\}}$	$0.00122^{\{4\}}$	$0.002207^{\{6\}}$	$0.000703^{\{1\}}$	$0.002658^{\{8\}}$	$0.002532^{\{7\}}$	$0.001175^{\{3\}}$	$0.001517^{\{5\}}$
		$\widehat{\beta}$	$0.009947^{\{2\}}$	$0.011883^{\{3\}}$	$0.017578^{\{6\}}$	$0.009252^{\{1\}}$	$0.018299^{\{7\}}$	$0.018385^{\{8\}}$	$0.013158^{\{4\}}$	$0.014533^{\{5\}}$
	MRE	$\widehat{\alpha}$	$0.181047^{\{8\}}$	$0.098322^{\{2\}}$	$0.138331^{\{5\}}$	$0.078745^{\{1\}}$	$0.146455^{\{6\}}$	$0.157654^{\{7\}}$	$0.104431^{\{3\}}$	$0.115222^{\{4\}}$
		$\widehat{\beta}$	$0.095354^{\{2\}}$	$0.107209^{\{3\}}$	$0.1379^{\{6\}}$	$0.09396^{\{1\}}$	$0.144431^{\{8\}}$	$0.142748^{\{7\}}$	$0.12111^{\{4\}}$	$0.12635^{\{5\}}$
	$\sum$ ranks		$24^{\{4\}}$	$17^{\{2\}}$	$34^{\{6\}}$	$6^{\{1\}}$	$43^{\{7.5\}}$	$43^{\{7.5\}}$	$21^{\{3\}}$	$28^{\{5\}}$
125	BIAS	$\widehat{\alpha}$	$0.042024^{\{8\}}$	$0.021384^{\{2\}}$	$0.03378^{\{7\}}$	$0.01728^{\{1\}}$	$0.029932^{\{5\}}$	$0.033378^{\{6\}}$	$0.02344^{\{3\}}$	$0.025707^{\{4\}}$
		$\widehat{\beta}$	$0.058643^{\{2\}}$	$0.070858^{\{3\}}$	$0.097561^{\{7\}}$	$0.057506^{\{1\}}$	$0.092583^{\{6\}}$	$0.098095^{\{8\}}$	$0.083185^{\{4\}}$	$0.084214^{\{5\}}$
	MSE	$\widehat{\alpha}$	$0.000518^{\{1\}}$	$0.000934^{\{3\}}$	$0.002101^{\{8\}}$	$0.000548^{\{2\}}$	$0.00163^{\{6\}}$	$0.00184^{\{7\}}$	$0.000936^{\{4\}}$	$0.001198^{\{5\}}$
		$\widehat{\beta}$	$0.007231^{\{2\}}$	$0.009414^{\{3\}}$	$0.015016^{\{7\}}$	$0.006427^{\{1\}}$	$0.013678^{\{6\}}$	$0.015056^{\{8\}}$	$0.010814^{\{4\}}$	$0.011244^{\{5\}}$
	MRE	$\widehat{\alpha}$	$0.168094^{\{8\}}$	$0.085536^{\{2\}}$	$0.135121^{\{7\}}$	$0.069119^{\{1\}}$	$0.119729^{\{5\}}$	$0.133511^{\{6\}}$	$0.093762^{\{3\}}$	$0.102828^{\{4\}}$
		$\widehat{\beta}$	$0.07819^{\{2\}}$	$0.094477^{\{3\}}$	$0.130082^{\{7\}}$	$0.076675^{\{1\}}$	$0.123444^{\{6\}}$	$0.130793^{\{8\}}$	$0.110913^{\{4\}}$	$0.112286^{\{5\}}$
	$\sum$ ranks		$23^{\{4\}}$	$16^{\{2\}}$	$43^{\{7.5\}}$	$7^{\{1\}}$	$34^{\{6\}}$	$43^{\{7.5\}}$	$22^{\{3\}}$	$28^{\{5\}}$
150	BIAS	$\widehat{\alpha}$	$0.033995^{\{8\}}$	$0.018661^{\{2\}}$	$0.027968^{\{6\}}$	$0.015277^{\{1\}}$	$0.027097^{\{5\}}$	$0.031338^{\{7\}}$	$0.020924^{\{3\}}$	$0.023931^{\{4\}}$
		$\widehat{\beta}$	$0.054205^{\{1\}}$	$0.061158^{\{3\}}$	$0.087696^{\{8\}}$	$0.056196^{\{2\}}$	$0.087088^{\{6\}}$	$0.087545^{\{7\}}$	$0.075761^{\{4\}}$	$0.079985^{\{5\}}$
	MSE	$\widehat{\alpha}$	$0.000394^{\{1\}}$	$0.000717^{\{3\}}$	$0.001377^{\{7\}}$	$0.000438^{\{2\}}$	$0.001307^{\{6\}}$	$0.001591^{\{8\}}$	$0.000727^{\{4\}}$	$0.001063^{\{5\}}$
		$\widehat{\beta}$	$0.006265^{\{2\}}$	$0.007217^{\{4\}}$	$0.011789^{\{6\}}$	$0.006085^{\{1\}}$	$0.011989^{\{7\}}$	$0.012343^{\{8\}}$	$0.009136^{\{4\}}$	$0.010003^{\{5\}}$
	MRE	$\widehat{\alpha}$	$0.155981^{\{8\}}$	$0.074646^{\{2\}}$	$0.111872^{\{6\}}$	$0.061109^{\{1\}}$	$0.10839^{\{5\}}$	$0.125352^{\{7\}}$	$0.083695^{\{3\}}$	$0.095722^{\{4\}}$
		$\widehat{\beta}$	$0.072274^{\{1\}}$	$0.081543^{\{3\}}$	$0.116927^{\{8\}}$	$0.074928^{\{2\}}$	$0.116118^{\{6\}}$	$0.116727^{\{7\}}$	$0.101014^{\{4\}}$	$0.106646^{\{5\}}$
	$\sum$ ranks		$21^{\{3\}}$	$16^{\{2\}}$	$41^{\{7\}}$	$9^{\{1\}}$	$35^{\{6\}}$	$44^{\{8\}}$	$22^{\{4\}}$	$28^{\{5\}}$

$$F(x) = \frac{\log\left(\left(1 - e^{-(x/1-x)^{\alpha}}\right)^{\beta} + 1\right)}{\log(2)},$$
$$f(x) = \frac{\alpha\beta(x/1-x)^{\alpha-1}\left(1 - e^{-(x/1-x)^{\alpha}}\right)^{\beta}}{(x-1)^2\log(2)\left(e^{(x/1-x)^{\alpha}} - 1\right)\left(\left(1 - e^{-(x/1-x)^{\alpha}}\right)^{\beta} + 1\right)}. \quad (2)$$

Its hazard function is defined as follows:

$$h(x) = \frac{f(x)}{S(x)} = \frac{\alpha\beta(1/x-1)^{-\alpha}\left(1 - e^{-(x/1-x)^{\alpha}}\right)^{\beta}}{(x-1)x\left(e^{(x/1-x)^{\alpha}} - 1\right)\left(\left(1 - e^{-(x/1-x)^{\alpha}}\right)^{\beta} + 1\right)\left(\log(2) - \log\left(\left(1 - e^{-(x/1-x)^{\alpha}}\right)^{\beta} + 1\right)\right)}, \quad (3)$$

Table 2: Simulation values of BIAS, MSE, and MRE for $\alpha = 0.75, \beta = 1.5$.

n	Est.	Est. Par.	MLE	ADE	CVME	MPSE	LSE	PCE	RTADE	WLSE
25	BIAS	$\widehat{\alpha}$	$0.117882^{\{3\}}$	$0.112061^{\{2\}}$	$0.165051^{\{8\}}$	$0.107679^{\{1\}}$	$0.145588^{\{7\}}$	$0.123216^{\{5\}}$	$0.120017^{\{4\}}$	$0.129074^{\{6\}}$
		$\widehat{\beta}$	$0.259965^{\{2\}}$	$0.271556^{\{3\}}$	$0.299962^{\{8\}}$	$0.244616^{\{1\}}$	$0.278657^{\{5\}}$	$0.275586^{\{4\}}$	$0.296926^{\{7\}}$	$0.284412^{\{6\}}$
	MSE	$\widehat{\alpha}$	$0.028782^{\{5\}}$	$0.022124^{\{2\}}$	$0.118446^{\{8\}}$	$0.019317^{\{1\}}$	$0.052388^{\{7\}}$	$0.027362^{\{4\}}$	$0.026159^{\{3\}}$	$0.034504^{\{6\}}$
		$\widehat{\beta}$	$0.108514^{\{2\}}$	$0.119873^{\{3\}}$	$0.148218^{\{7\}}$	$0.099379^{\{1\}}$	$0.12962^{\{5\}}$	$0.121339^{\{4\}}$	$0.150547^{\{8\}}$	$0.137926^{\{6\}}$
	MRE	$\widehat{\alpha}$	$0.157176^{\{3\}}$	$0.149415^{\{2\}}$	$0.220068^{\{8\}}$	$0.143572^{\{1\}}$	$0.194117^{\{7\}}$	$0.164288^{\{5\}}$	$0.160023^{\{4\}}$	$0.172099^{\{6\}}$
		$\widehat{\beta}$	$0.17331^{\{2\}}$	$0.181037^{\{3\}}$	$0.199975^{\{8\}}$	$0.163077^{\{1\}}$	$0.185771^{\{5\}}$	$0.183724^{\{4\}}$	$0.197951^{\{7\}}$	$0.189608^{\{6\}}$
	$\sum$ ranks		$17^{\{3\}}$	$15^{\{2\}}$	$47^{\{8\}}$	$6^{\{1\}}$	$36^{\{6.5\}}$	$26^{\{4\}}$	$33^{\{5\}}$	$36^{\{6.5\}}$
50	BIAS	$\widehat{\alpha}$	$0.07402^{\{1\}}$	$0.077653^{\{3\}}$	$0.104456^{\{8\}}$	$0.077545^{\{2\}}$	$0.093938^{\{7\}}$	$0.080405^{\{5\}}$	$0.077729^{\{4\}}$	$0.081263^{\{6\}}$
		$\widehat{\beta}$	$0.181696^{\{2\}}$	$0.185623^{\{3\}}$	$0.209063^{\{8\}}$	$0.176866^{\{1\}}$	$0.202077^{\{7\}}$	$0.193209^{\{5\}}$	$0.201481^{\{6\}}$	$0.187236^{\{4\}}$
	MSE	$\widehat{\alpha}$	$0.009703^{\{2\}}$	$0.010413^{\{3\}}$	$0.022908^{\{8\}}$	$0.009263^{\{1\}}$	$0.015877^{\{7\}}$	$0.010442^{\{4\}}$	$0.010491^{\{5\}}$	$0.011499^{\{6\}}$
		$\widehat{\beta}$	$0.05272^{\{2\}}$	$0.05428^{\{3\}}$	$0.070501^{\{8\}}$	$0.049971^{\{1\}}$	$0.065014^{\{6\}}$	$0.059947^{\{5\}}$	$0.066791^{\{7\}}$	$0.058^{\{4\}}$
	MRE	$\widehat{\alpha}$	$0.098694^{\{1\}}$	$0.103538^{\{3\}}$	$0.139274^{\{8\}}$	$0.103394^{\{2\}}$	$0.12525^{\{7\}}$	$0.107207^{\{5\}}$	$0.103639^{\{4\}}$	$0.10835^{\{6\}}$
		$\widehat{\beta}$	$0.121131^{\{2\}}$	$0.123749^{\{3\}}$	$0.139376^{\{8\}}$	$0.117911^{\{1\}}$	$0.134718^{\{7\}}$	$0.128806^{\{5\}}$	$0.134321^{\{6\}}$	$0.124824^{\{4\}}$
	$\sum$ ranks		$10^{\{2\}}$	$18^{\{3\}}$	$48^{\{8\}}$	$8^{\{1\}}$	$41^{\{7\}}$	$29^{\{4\}}$	$32^{\{6\}}$	$30^{\{5\}}$
75	BIAS	$\widehat{\alpha}$	$0.061778^{\{2\}}$	$0.062994^{\{4\}}$	$0.076351^{\{8\}}$	$0.060783^{\{1\}}$	$0.074807^{\{7\}}$	$0.068885^{\{6\}}$	$0.062589^{\{3\}}$	$0.066892^{\{5\}}$
		$\widehat{\beta}$	$0.145697^{\{2\}}$	$0.154409^{\{3\}}$	$0.170298^{\{8\}}$	$0.142167^{\{1\}}$	$0.160494^{\{6\}}$	$0.158044^{\{5\}}$	$0.163073^{\{7\}}$	$0.155157^{\{4\}}$
	MSE	$\widehat{\alpha}$	$0.006557^{\{4\}}$	$0.006518^{\{2\}}$	$0.010007^{\{8\}}$	$0.005551^{\{1\}}$	$0.00954^{\{7\}}$	$0.007545^{\{5\}}$	$0.006529^{\{3\}}$	$0.007606^{\{6\}}$
		$\widehat{\beta}$	$0.033801^{\{2\}}$	$0.037605^{\{3\}}$	$0.046341^{\{8\}}$	$0.031609^{\{1\}}$	$0.042229^{\{6\}}$	$0.039689^{\{5\}}$	$0.042514^{\{7\}}$	$0.038408^{\{4\}}$
	MRE	$\widehat{\alpha}$	$0.08237^{\{2\}}$	$0.083992^{\{4\}}$	$0.101801^{\{8\}}$	$0.081043^{\{1\}}$	$0.099742^{\{7\}}$	$0.091846^{\{6\}}$	$0.083452^{\{3\}}$	$0.089189^{\{5\}}$
		$\widehat{\beta}$	$0.097131^{\{2\}}$	$0.102939^{\{3\}}$	$0.113532^{\{8\}}$	$0.094778^{\{1\}}$	$0.106996^{\{6\}}$	$0.105363^{\{5\}}$	$0.108715^{\{7\}}$	$0.103438^{\{4\}}$
	$\sum$ ranks		$14^{\{2\}}$	$19^{\{3\}}$	$48^{\{8\}}$	$6^{\{1\}}$	$39^{\{7\}}$	$32^{\{6\}}$	$30^{\{5\}}$	$28^{\{4\}}$
100	BIAS	$\widehat{\alpha}$	$0.050862^{\{1\}}$	$0.05658^{\{4\}}$	$0.064863^{\{7\}}$	$0.052378^{\{2\}}$	$0.065046^{\{8\}}$	$0.056738^{\{5\}}$	$0.054369^{\{3\}}$	$0.057854^{\{6\}}$
		$\widehat{\beta}$	$0.125442^{\{2\}}$	$0.132155^{\{4\}}$	$0.143719^{\{7\}}$	$0.121916^{\{1\}}$	$0.14539^{\{8\}}$	$0.137344^{\{5\}}$	$0.138746^{\{6\}}$	$0.132091^{\{3\}}$
	MSE	$\widehat{\alpha}$	$0.00431^{\{2\}}$	$0.005302^{\{5\}}$	$0.006966^{\{7\}}$	$0.004103^{\{1\}}$	$0.007192^{\{8\}}$	$0.005069^{\{4\}}$	$0.004964^{\{3\}}$	$0.005772^{\{6\}}$
		$\widehat{\beta}$	$0.024675^{\{2\}}$	$0.02777^{\{3\}}$	$0.033143^{\{8\}}$	$0.02385^{\{1\}}$	$0.032864^{\{7\}}$	$0.029737^{\{5\}}$	$0.029878^{\{6\}}$	$0.02827^{\{4\}}$
	MRE	$\widehat{\alpha}$	$0.067816^{\{1\}}$	$0.07544^{\{4\}}$	$0.086484^{\{7\}}$	$0.069837^{\{2\}}$	$0.086727^{\{8\}}$	$0.075651^{\{5\}}$	$0.072491^{\{3\}}$	$0.077139^{\{6\}}$
		$\widehat{\beta}$	$0.083628^{\{2\}}$	$0.088104^{\{4\}}$	$0.095813^{\{7\}}$	$0.081277^{\{1\}}$	$0.096926^{\{8\}}$	$0.091563^{\{5\}}$	$0.092498^{\{6\}}$	$0.088061^{\{3\}}$
	$\sum$ ranks		$10^{\{2\}}$	$24^{\{3\}}$	$43^{\{7\}}$	$8^{\{1\}}$	$47^{\{8\}}$	$29^{\{6\}}$	$27^{\{4\}}$	$28^{\{5\}}$
125	BIAS	$\widehat{\alpha}$	$0.046076^{\{1\}}$	$0.049459^{\{4\}}$	$0.059037^{\{8\}}$	$0.046894^{\{2\}}$	$0.056816^{\{7\}}$	$0.0516^{\{6\}}$	$0.048696^{\{3\}}$	$0.049737^{\{5\}}$
		$\widehat{\beta}$	$0.111973^{\{2\}}$	$0.116232^{\{3\}}$	$0.129633^{\{8\}}$	$0.109042^{\{1\}}$	$0.127908^{\{7\}}$	$0.123999^{\{6\}}$	$0.123779^{\{5\}}$	$0.117006^{\{4\}}$
	MSE	$\widehat{\alpha}$	$0.003409^{\{2\}}$	$0.003916^{\{4\}}$	$0.005662^{\{8\}}$	$0.003354^{\{1\}}$	$0.005285^{\{7\}}$	$0.004201^{\{6\}}$	$0.003831^{\{3\}}$	$0.004026^{\{5\}}$
		$\widehat{\beta}$	$0.019726^{\{2\}}$	$0.022038^{\{4\}}$	$0.026632^{\{8\}}$	$0.019442^{\{1\}}$	$0.026065^{\{7\}}$	$0.023897^{\{5\}}$	$0.024712^{\{6\}}$	$0.0218^{\{3\}}$
	MRE	$\widehat{\alpha}$	$0.061434^{\{1\}}$	$0.065945^{\{4\}}$	$0.078717^{\{8\}}$	$0.062525^{\{2\}}$	$0.075755^{\{7\}}$	$0.0688^{\{6\}}$	$0.064928^{\{3\}}$	$0.066316^{\{5\}}$
		$\widehat{\beta}$	$0.074648^{\{2\}}$	$0.077488^{\{3\}}$	$0.086422^{\{8\}}$	$0.072695^{\{1\}}$	$0.085272^{\{7\}}$	$0.082666^{\{6\}}$	$0.082519^{\{5\}}$	$0.078004^{\{4\}}$
	$\sum$ ranks		$10^{\{2\}}$	$22^{\{3\}}$	$48^{\{8\}}$	$8^{\{1\}}$	$42^{\{7\}}$	$35^{\{6\}}$	$25^{\{4\}}$	$26^{\{5\}}$
150	BIAS	$\widehat{\alpha}$	$0.040845^{\{1\}}$	$0.044847^{\{3\}}$	$0.054291^{\{8\}}$	$0.041118^{\{2\}}$	$0.052331^{\{7\}}$	$0.045308^{\{4\}}$	$0.045597^{\{5\}}$	$0.046057^{\{6\}}$
		$\widehat{\beta}$	$0.102559^{\{2\}}$	$0.10974^{\{3\}}$	$0.116942^{\{8\}}$	$0.09909^{\{1\}}$	$0.114989^{\{6\}}$	$0.111479^{\{4\}}$	$0.115777^{\{7\}}$	$0.111507^{\{5\}}$
	MSE	$\widehat{\alpha}$	$0.002734^{\{2\}}$	$0.003241^{\{3\}}$	$0.004805^{\{8\}}$	$0.002593^{\{1\}}$	$0.004415^{\{7\}}$	$0.003332^{\{5\}}$	$0.003284^{\{4\}}$	$0.003443^{\{6\}}$
		$\widehat{\beta}$	$0.01668^{\{2\}}$	$0.019294^{\{3\}}$	$0.021686^{\{8\}}$	$0.015809^{\{1\}}$	$0.02074^{\{6\}}$	$0.019633^{\{4\}}$	$0.021631^{\{7\}}$	$0.019823^{\{5\}}$
	MRE	$\widehat{\alpha}$	$0.05446^{\{1\}}$	$0.059797^{\{3\}}$	$0.072388^{\{8\}}$	$0.054825^{\{2\}}$	$0.069775^{\{7\}}$	$0.06041^{\{4\}}$	$0.060797^{\{5\}}$	$0.061409^{\{6\}}$
		$\widehat{\beta}$	$0.068372^{\{2\}}$	$0.07316^{\{3\}}$	$0.077961^{\{8\}}$	$0.06606^{\{1\}}$	$0.076659^{\{6\}}$	$0.074319^{\{4\}}$	$0.077185^{\{7\}}$	$0.074338^{\{5\}}$
	$\sum$ ranks		$10^{\{2\}}$	$18^{\{3\}}$	$48^{\{8\}}$	$8^{\{1\}}$	$39^{\{7\}}$	$25^{\{4\}}$	$35^{\{6\}}$	$33^{\{5\}}$

where $S(x)$ is its survival function (SF). Figures 1 and 2 show the possible plots of the PDF and the HF of the ExRKD, respectively.

3. Statistical Properties

3.1. Quantile Function. To get the quantile function (QF) of the ExRKD, one must first determine the inverse function of the CDF of the ExRKD, which is used to have randomly generated data sets from our proposed model and it is defined as follows:

$$Q = 1 - \frac{1}{\left(-\log\left(1 - \left(2^{p} - 1\right)^{1/\beta}\right)\right)^{1/\alpha} + 1}, \quad 0 < p < 1. \tag{4}$$

3.2. Linear Representation. In this subsection, we derive linear representations of the CDF and PDF of the ExRKD that are helpful in many calculations.

For $-1 < x \leq 1$, we define the following expansion:

$$\log(1 + x) = \sum_{w=1}^{\infty} (-1)^{w+1} \frac{x^{w}}{w}. \tag{5}$$

By using last relation to CDF of ExRKD in equation (3), we have

$$F(x) = \sum_{w=1}^{\infty} \Phi_{w} G_{w}(x), \tag{6}$$

and its corresponding PDF is defined as follows:

Table 3: Simulation values of BIAS, MSE, and MRE for $\alpha = 1.5, \beta = 0.75$.

n	Est.	Est. Par.	MLE	ADE	CVME	MPSE	LSE	PCE	RTADE	WLSE
25	BIAS	$\widehat{\alpha}$	$0.403938^{\{5\}}$	$0.394719^{\{3\}}$	$0.599086^{\{8\}}$	$0.353052^{\{1\}}$	$0.522094^{\{7\}}$	$0.360686^{\{2\}}$	$0.398035^{\{4\}}$	$0.501736^{\{6\}}$
		$\widehat{\beta}$	$0.171923^{\{1\}}$	$0.184513^{\{4\}}$	$0.208659^{\{7\}}$	$0.178267^{\{2\}}$	$0.208677^{\{8\}}$	$0.178345^{\{3\}}$	$0.189428^{\{5\}}$	$0.205418^{\{6\}}$
	MSE	$\widehat{\alpha}$	$0.477018^{\{3\}}$	$0.493378^{\{4\}}$	$1.376029^{\{8\}}$	$0.357452^{\{2\}}$	$0.929049^{\{6\}}$	$0.354195^{\{1\}}$	$0.674488^{\{5\}}$	$1.012718^{\{7\}}$
		$\widehat{\beta}$	$0.046371^{\{1\}}$	$0.052691^{\{4\}}$	$0.069169^{\{7\}}$	$0.051124^{\{3\}}$	$0.069188^{\{8\}}$	$0.050753^{\{2\}}$	$0.05782^{\{5\}}$	$0.065421^{\{6\}}$
	MRE	$\widehat{\alpha}$	$0.269292^{\{5\}}$	$0.263146^{\{3\}}$	$0.399391^{\{8\}}$	$0.235368^{\{1\}}$	$0.348063^{\{7\}}$	$0.240457^{\{2\}}$	$0.265356^{\{4\}}$	$0.334491^{\{6\}}$
		$\widehat{\beta}$	$0.229231^{\{1\}}$	$0.246018^{\{4\}}$	$0.278212^{\{7\}}$	$0.237689^{\{2\}}$	$0.278236^{\{8\}}$	$0.237793^{\{3\}}$	$0.252571^{\{5\}}$	$0.27389^{\{6\}}$
	$\sum$ ranks		$16^{\{3\}}$	$22^{\{4\}}$	$45^{\{8\}}$	$11^{\{1\}}$	$44^{\{7\}}$	$13^{\{2\}}$	$28^{\{5\}}$	$37^{\{6\}}$
50	BIAS	$\widehat{\alpha}$	$0.221619^{\{2\}}$	$0.23885^{\{5\}}$	$0.34319^{\{8\}}$	$0.209574^{\{1\}}$	$0.328961^{\{7\}}$	$0.228378^{\{3\}}$	$0.237229^{\{4\}}$	$0.285926^{\{6\}}$
		$\widehat{\beta}$	$0.118107^{\{2\}}$	$0.132868^{\{4\}}$	$0.154687^{\{8\}}$	$0.116901^{\{1\}}$	$0.151413^{\{7\}}$	$0.131583^{\{3\}}$	$0.134993^{\{5\}}$	$0.14188^{\{6\}}$
	MSE	$\widehat{\alpha}$	$0.102835^{\{4\}}$	$0.105831^{\{5\}}$	$0.334914^{\{8\}}$	$0.075844^{\{1\}}$	$0.289094^{\{7\}}$	$0.088987^{\{2\}}$	$0.10164^{\{3\}}$	$0.212808^{\{6\}}$
		$\widehat{\beta}$	$0.021414^{\{2\}}$	$0.028344^{\{4\}}$	$0.036168^{\{7\}}$	$0.02138^{\{1\}}$	$0.036571^{\{8\}}$	$0.026762^{\{3\}}$	$0.028403^{\{5\}}$	$0.031995^{\{6\}}$
	MRE	$\widehat{\alpha}$	$0.147746^{\{2\}}$	$0.159233^{\{5\}}$	$0.228793^{\{8\}}$	$0.139716^{\{1\}}$	$0.219307^{\{7\}}$	$0.152252^{\{3\}}$	$0.158153^{\{4\}}$	$0.190618^{\{6\}}$
		$\widehat{\beta}$	$0.157476^{\{2\}}$	$0.177158^{\{4\}}$	$0.206249^{\{8\}}$	$0.155867^{\{1\}}$	$0.201884^{\{7\}}$	$0.175444^{\{3\}}$	$0.17999^{\{5\}}$	$0.189173^{\{6\}}$
	$\sum$ ranks		$14^{\{2\}}$	$27^{\{5\}}$	$47^{\{8\}}$	$6^{\{1\}}$	$43^{\{7\}}$	$17^{\{3\}}$	$26^{\{4\}}$	$36^{\{6\}}$
75	BIAS	$\widehat{\alpha}$	$0.169662^{\{2\}}$	$0.193867^{\{5\}}$	$0.270825^{\{8\}}$	$0.165032^{\{1\}}$	$0.25135^{\{7\}}$	$0.178703^{\{4\}}$	$0.177601^{\{3\}}$	$0.209395^{\{6\}}$
		$\widehat{\beta}$	$0.093936^{\{1\}}$	$0.106846^{\{5\}}$	$0.128505^{\{8\}}$	$0.094145^{\{2\}}$	$0.120559^{\{7\}}$	$0.10356^{\{3\}}$	$0.105625^{\{4\}}$	$0.108721^{\{6\}}$
	MSE	$\widehat{\alpha}$	$0.053903^{\{2\}}$	$0.066424^{\{5\}}$	$0.144329^{\{8\}}$	$0.044168^{\{1\}}$	$0.131125^{\{7\}}$	$0.054543^{\{3\}}$	$0.056073^{\{4\}}$	$0.093976^{\{6\}}$
		$\widehat{\beta}$	$0.013993^{\{2\}}$	$0.017994^{\{5\}}$	$0.025477^{\{8\}}$	$0.013988^{\{1\}}$	$0.02418^{\{7\}}$	$0.01686^{\{3\}}$	$0.01753^{\{4\}}$	$0.018504^{\{6\}}$
	MRE	$\widehat{\alpha}$	$0.113108^{\{2\}}$	$0.129245^{\{5\}}$	$0.18055^{\{8\}}$	$0.110022^{\{1\}}$	$0.167567^{\{7\}}$	$0.119135^{\{4\}}$	$0.118401^{\{3\}}$	$0.139597^{\{6\}}$
		$\widehat{\beta}$	$0.125248^{\{1\}}$	$0.142461^{\{5\}}$	$0.17134^{\{8\}}$	$0.125526^{\{2\}}$	$0.160746^{\{7\}}$	$0.138081^{\{3\}}$	$0.140833^{\{4\}}$	$0.144962^{\{6\}}$
	$\sum$ *Ranks*		$10^{\{2\}}$	$30^{\{5\}}$	$48^{\{8\}}$	$8^{\{1\}}$	$42^{\{7\}}$	$20^{\{3\}}$	$22^{\{4\}}$	$36^{\{6\}}$
100	BIAS	$\widehat{\alpha}$	$0.143207^{\{2\}}$	$0.170465^{\{6\}}$	$0.207384^{\{7\}}$	$0.13941^{\{1\}}$	$0.216216^{\{8\}}$	$0.156581^{\{3\}}$	$0.16659^{\{5\}}$	$0.164009^{\{4\}}$
		$\widehat{\beta}$	$0.084284^{\{2\}}$	$0.092792^{\{4\}}$	$0.104823^{\{7\}}$	$0.080592^{\{1\}}$	$0.107247^{\{8\}}$	$0.092391^{\{3\}}$	$0.096125^{\{6\}}$	$0.093657^{\{5\}}$
	MSE	$\widehat{\alpha}$	$0.037562^{\{2\}}$	$0.053^{\{6\}}$	$0.094128^{\{7\}}$	$0.028895^{\{1\}}$	$0.127587^{\{8\}}$	$0.039867^{\{3\}}$	$0.046498^{\{4\}}$	$0.052543^{\{5\}}$
		$\widehat{\beta}$	$0.011233^{\{2\}}$	$0.013858^{\{4\}}$	$0.017662^{\{7\}}$	$0.010207^{\{1\}}$	$0.018116^{\{8\}}$	$0.013373^{\{3\}}$	$0.0143^{\{6\}}$	$0.014001^{\{5\}}$
	MRE	$\widehat{\alpha}$	$0.095471^{\{2\}}$	$0.113644^{\{6\}}$	$0.138256^{\{7\}}$	$0.09294^{\{1\}}$	$0.144144^{\{8\}}$	$0.104387^{\{3\}}$	$0.11106^{\{5\}}$	$0.10934^{\{4\}}$
		$\widehat{\beta}$	$0.112378^{\{2\}}$	$0.123722^{\{4\}}$	$0.139764^{\{7\}}$	$0.107456^{\{1\}}$	$0.142995^{\{8\}}$	$0.123189^{\{3\}}$	$0.128166^{\{6\}}$	$0.124876^{\{5\}}$
	$\sum$ *Ranks*		$12^{\{2\}}$	$30^{\{5\}}$	$42^{\{7\}}$	$6^{\{1\}}$	$48^{\{8\}}$	$18^{\{3\}}$	$32^{\{6\}}$	$28^{\{4\}}$
125	BIAS	$\widehat{\alpha}$	$0.125323^{\{1\}}$	$0.140446^{\{4\}}$	$0.196285^{\{8\}}$	$0.12934^{\{2\}}$	$0.186987^{\{7\}}$	$0.143845^{\{5\}}$	$0.138527^{\{3\}}$	$0.145408^{\{6\}}$
		$\widehat{\beta}$	$0.071757^{\{1\}}$	$0.081591^{\{3\}}$	$0.096374^{\{8\}}$	$0.072325^{\{2\}}$	$0.094955^{\{7\}}$	$0.083968^{\{6\}}$	$0.082654^{\{4\}}$	$0.082885^{\{5\}}$
	MSE	$\widehat{\alpha}$	$0.028017^{\{2\}}$	$0.03325^{\{4\}}$	$0.076361^{\{8\}}$	$0.026108^{\{1\}}$	$0.071163^{\{7\}}$	$0.034206^{\{5\}}$	$0.032985^{\{3\}}$	$0.037533^{\{6\}}$
		$\widehat{\beta}$	$0.008159^{\{1\}}$	$0.010109^{\{3\}}$	$0.014827^{\{8\}}$	$0.008263^{\{2\}}$	$0.014461^{\{7\}}$	$0.011302^{\{6\}}$	$0.010758^{\{4\}}$	$0.010818^{\{5\}}$
	MRE	$\widehat{\alpha}$	$0.083548^{\{1\}}$	$0.093631^{\{4\}}$	$0.130857^{\{8\}}$	$0.086227^{\{2\}}$	$0.124658^{\{7\}}$	$0.095896^{\{5\}}$	$0.092351^{\{3\}}$	$0.096939^{\{6\}}$
		$\widehat{\beta}$	$0.095675^{\{1\}}$	$0.108788^{\{3\}}$	$0.128498^{\{8\}}$	$0.096433^{\{2\}}$	$0.126606^{\{7\}}$	$0.111957^{\{6\}}$	$0.110205^{\{4\}}$	$0.110513^{\{5\}}$
	$\sum$ *Ranks*		$7^{\{1\}}$	$21^{\{3.5\}}$	$48^{\{8\}}$	$11^{\{2\}}$	$42^{\{7\}}$	$33^{\{5.5\}}$	$21^{\{3.5\}}$	$33^{\{5.5\}}$
150	BIAS	$\widehat{\alpha}$	$0.115159^{\{1\}}$	$0.134124^{\{5\}}$	$0.172374^{\{8\}}$	$0.115194^{\{2\}}$	$0.163079^{\{7\}}$	$0.13224^{\{4\}}$	$0.120341^{\{3\}}$	$0.135241^{\{6\}}$
		$\widehat{\beta}$	$0.065425^{\{1\}}$	$0.073621^{\{3\}}$	$0.086416^{\{8\}}$	$0.065783^{\{2\}}$	$0.083708^{\{7\}}$	$0.075534^{\{4\}}$	$0.075598^{\{5\}}$	$0.076739^{\{6\}}$
	MSE	$\widehat{\alpha}$	$0.023219^{\{2\}}$	$0.031351^{\{6\}}$	$0.054339^{\{8\}}$	$0.020216^{\{1\}}$	$0.048258^{\{7\}}$	$0.028359^{\{4\}}$	$0.023266^{\{3\}}$	$0.030862^{\{5\}}$
		$\widehat{\beta}$	$0.006828^{\{1\}}$	$0.008545^{\{3\}}$	$0.011775^{\{8\}}$	$0.006833^{\{2\}}$	$0.011559^{\{7\}}$	$0.00896^{\{4\}}$	$0.00901^{\{5\}}$	$0.009189^{\{6\}}$
	MRE	$\widehat{\alpha}$	$0.076773^{\{1\}}$	$0.089416^{\{5\}}$	$0.114916^{\{8\}}$	$0.076796^{\{2\}}$	$0.10872^{\{7\}}$	$0.08816^{\{4\}}$	$0.080227^{\{3\}}$	$0.09016^{\{6\}}$
		$\widehat{\beta}$	$0.087233^{\{1\}}$	$0.098162^{\{3\}}$	$0.115221^{\{8\}}$	$0.087711^{\{2\}}$	$0.11161^{\{7\}}$	$0.100712^{\{4\}}$	$0.100798^{\{5\}}$	$0.102319^{\{6\}}$
	$\sum$ *Ranks*		$7^{\{1\}}$	$25^{\{5\}}$	$48^{\{8\}}$	$11^{\{2\}}$	$42^{\{7\}}$	$24^{\{3.5\}}$	$24^{\{3.5\}}$	$35^{\{6\}}$

$$f(x) = \sum_{w=1}^{\infty} \Phi_w g_w(x), \tag{7}$$

where $\Phi_w = (-1)^{w+1}/w \log(2)$ and $G_w(x) = (1 - e^{-(x/1-x)^{\alpha}})^{\beta w}$ follow the exponentiated reduced Kies distribution (ERKD) [14] with parameters α and βw.

3.3. Moments. The ExRKD's k^{th} moments have the following form:

$$\begin{aligned} \mu_k' &= E\left(X^k\right) = \int_0^{\infty} x^k f(x)\mathrm{d}x \\ &= \sum_{w=1}^{\infty} \Phi_w \int_0^{\infty} x^k g_w(x)\mathrm{d}x = \sum_{w=1}^{\infty} \Phi_w B_k, \end{aligned} \tag{8}$$

where B_k is the k^{th} moments of ERKD, see [14] which is defined. With the values of $k = 1, 2, 3$, and 4, we get the first four moments around the origin of the ExRKD, which are then used to derive the coefficients of skewness and kurtosis, respectively.

Table 4: Simulation values of BIAS, MSE, and MRE for $\alpha = 2.5, \beta = 2.5$.

n	Est.	Est. Par.	MLE	ADE	CVME	MPSE	LSE	PCE	RTADE	WLSE
25	BIAS	$\widehat{\alpha}$	$0.304119^{\{4\}}$	$0.296276^{\{1\}}$	$0.385635^{\{8\}}$	$0.301092^{\{3\}}$	$0.357767^{\{7\}}$	$0.299733^{\{2\}}$	$0.329087^{\{5\}}$	$0.331094^{\{6\}}$
		$\widehat{\beta}$	$0.411856^{\{6\}}$	$0.401001^{\{3\}}$	$0.461255^{\{7\}}$	$0.365757^{\{1\}}$	$0.410637^{\{5\}}$	$0.370429^{\{2\}}$	$0.461765^{\{8\}}$	$0.406516^{\{4\}}$
	MSE	$\widehat{\alpha}$	$0.173413^{\{4\}}$	$0.150549^{\{3\}}$	$0.286677^{\{8\}}$	$0.135627^{\{1\}}$	$0.233482^{\{7\}}$	$0.141902^{\{2\}}$	$0.195735^{\{5\}}$	$0.216509^{\{6\}}$
		$\widehat{\beta}$	$0.281335^{\{4\}}$	$0.26855^{\{3\}}$	$0.363038^{\{7\}}$	$0.214857^{\{1\}}$	$0.299694^{\{6\}}$	$0.228874^{\{2\}}$	$0.38591^{\{8\}}$	$0.289853^{\{5\}}$
	MRE	$\widehat{\alpha}$	$0.121648^{\{4\}}$	$0.118511^{\{1\}}$	$0.154254^{\{8\}}$	$0.120437^{\{3\}}$	$0.143107^{\{7\}}$	$0.119893^{\{2\}}$	$0.131635^{\{5\}}$	$0.132438^{\{6\}}$
		$\widehat{\beta}$	$0.164742^{\{6\}}$	$0.1604^{\{3\}}$	$0.184502^{\{7\}}$	$0.146303^{\{1\}}$	$0.164255^{\{5\}}$	$0.148172^{\{2\}}$	$0.184706^{\{8\}}$	$0.162606^{\{4\}}$
	$\sum$ *Ranks*		$28^{\{4\}}$	$14^{\{3\}}$	$45^{\{8\}}$	$10^{\{1\}}$	$37^{\{6\}}$	$12^{\{2\}}$	$39^{\{7\}}$	$31^{\{5\}}$
50	BIAS	$\widehat{\alpha}$	$0.20402^{\{1\}}$	$0.211866^{\{3\}}$	$0.254903^{\{8\}}$	$0.209012^{\{2\}}$	$0.239911^{\{7\}}$	$0.215345^{\{4\}}$	$0.218514^{\{5\}}$	$0.220951^{\{6\}}$
		$\widehat{\beta}$	$0.277733^{\{3\}}$	$0.277755^{\{4\}}$	$0.298225^{\{7\}}$	$0.258464^{\{2\}}$	$0.291377^{\{6\}}$	$0.25659^{\{1\}}$	$0.312824^{\{8\}}$	$0.27948^{\{5\}}$
	MSE	$\widehat{\alpha}$	$0.069994^{\{2\}}$	$0.075141^{\{4\}}$	$0.110322^{\{8\}}$	$0.067262^{\{1\}}$	$0.092775^{\{7\}}$	$0.071149^{\{3\}}$	$0.076677^{\{5\}}$	$0.082901^{\{6\}}$
		$\widehat{\beta}$	$0.124769^{\{3\}}$	$0.127553^{\{4\}}$	$0.151987^{\{7\}}$	$0.105374^{\{1\}}$	$0.141063^{\{6\}}$	$0.105421^{\{2\}}$	$0.163508^{\{8\}}$	$0.127786^{\{5\}}$
	MRE	$\widehat{\alpha}$	$0.081608^{\{1\}}$	$0.084746^{\{3\}}$	$0.101961^{\{8\}}$	$0.083605^{\{2\}}$	$0.095964^{\{7\}}$	$0.086138^{\{4\}}$	$0.087406^{\{5\}}$	$0.08838^{\{6\}}$
		$\widehat{\beta}$	$0.111093^{\{3\}}$	$0.111102^{\{4\}}$	$0.11929^{\{7\}}$	$0.103385^{\{2\}}$	$0.116551^{\{6\}}$	$0.102636^{\{1\}}$	$0.12513^{\{8\}}$	$0.111792^{\{5\}}$
	$\sum$ *Ranks*		$13^{\{2\}}$	$22^{\{4\}}$	$45^{\{8\}}$	$10^{\{1\}}$	$39^{\{6.5\}}$	$15^{\{3\}}$	$39^{\{6.5\}}$	$33^{\{5\}}$
75	BIAS	$\widehat{\alpha}$	$0.166547^{\{1\}}$	$0.170835^{\{4\}}$	$0.196685^{\{7\}}$	$0.169062^{\{2\}}$	$0.20057^{\{8\}}$	$0.169818^{\{3\}}$	$0.175179^{\{5\}}$	$0.182211^{\{6\}}$
		$\widehat{\beta}$	$0.22025^{\{3\}}$	$0.225596^{\{4\}}$	$0.24252^{\{7\}}$	$0.207421^{\{1\}}$	$0.241819^{\{6\}}$	$0.212417^{\{2\}}$	$0.249624^{\{8\}}$	$0.23013^{\{5\}}$
	MSE	$\widehat{\alpha}$	$0.045789^{\{3\}}$	$0.04581^{\{4\}}$	$0.06405^{\{7\}}$	$0.042931^{\{1\}}$	$0.066407^{\{8\}}$	$0.044833^{\{2\}}$	$0.048791^{\{5\}}$	$0.053745^{\{6\}}$
		$\widehat{\beta}$	$0.077378^{\{3\}}$	$0.081369^{\{4\}}$	$0.093009^{\{6\}}$	$0.069242^{\{1\}}$	$0.094038^{\{7\}}$	$0.070275^{\{2\}}$	$0.101808^{\{8\}}$	$0.084736^{\{5\}}$
	MRE	$\widehat{\alpha}$	$0.066619^{\{1\}}$	$0.068334^{\{4\}}$	$0.078674^{\{7\}}$	$0.067625^{\{2\}}$	$0.080228^{\{8\}}$	$0.067927^{\{3\}}$	$0.070072^{\{5\}}$	$0.072885^{\{6\}}$
		$\widehat{\beta}$	$0.0881^{\{3\}}$	$0.090238^{\{4\}}$	$0.097008^{\{7\}}$	$0.082968^{\{1\}}$	$0.096728^{\{6\}}$	$0.084967^{\{2\}}$	$0.09985^{\{8\}}$	$0.092052^{\{5\}}$
	$\sum$ *Ranks*		$14^{\{2.5\}}$	$24^{\{4\}}$	$41^{\{7\}}$	$8^{\{1\}}$	$43^{\{8\}}$	$14^{\{2.5\}}$	$39^{\{6\}}$	$33^{\{5\}}$
100	BIAS	$\widehat{\alpha}$	$0.141906^{\{2\}}$	$0.146114^{\{3\}}$	$0.169241^{\{7\}}$	$0.140648^{\{1\}}$	$0.173418^{\{8\}}$	$0.153637^{\{6\}}$	$0.152786^{\{4\}}$	$0.153514^{\{5\}}$
		$\widehat{\beta}$	$0.190564^{\{3\}}$	$0.195179^{\{4\}}$	$0.210297^{\{7\}}$	$0.180092^{\{1\}}$	$0.196464^{\{5\}}$	$0.18454^{\{2\}}$	$0.220167^{\{8\}}$	$0.201465^{\{6\}}$
	MSE	$\widehat{\alpha}$	$0.032574^{\{2\}}$	$0.033924^{\{3\}}$	$0.046013^{\{7\}}$	$0.030339^{\{1\}}$	$0.047511^{\{8\}}$	$0.036331^{\{4\}}$	$0.03827^{\{5\}}$	$0.038545^{\{6\}}$
		$\widehat{\beta}$	$0.057766^{\{3\}}$	$0.062308^{\{5\}}$	$0.071568^{\{7\}}$	$0.051122^{\{1\}}$	$0.062295^{\{4\}}$	$0.052888^{\{2\}}$	$0.077332^{\{8\}}$	$0.063063^{\{6\}}$
	MRE	$\widehat{\alpha}$	$0.056763^{\{2\}}$	$0.058446^{\{3\}}$	$0.067697^{\{7\}}$	$0.056259^{\{1\}}$	$0.069367^{\{8\}}$	$0.061455^{\{6\}}$	$0.061114^{\{4\}}$	$0.061406^{\{5\}}$
		$\widehat{\beta}$	$0.076225^{\{3\}}$	$0.078072^{\{4\}}$	$0.084119^{\{7\}}$	$0.072037^{\{1\}}$	$0.078586^{\{5\}}$	$0.073816^{\{2\}}$	$0.088067^{\{8\}}$	$0.080586^{\{6\}}$
	$\sum$ *Ranks*		$15^{\{2\}}$	$22^{\{3.5\}}$	$42^{\{8\}}$	$6^{\{1\}}$	$38^{\{7\}}$	$22^{\{3.5\}}$	$37^{\{6\}}$	$34^{\{5\}}$
125	BIAS	$\widehat{\alpha}$	$0.118476^{\{1\}}$	$0.134094^{\{5\}}$	$0.155452^{\{8\}}$	$0.125452^{\{2\}}$	$0.147565^{\{7\}}$	$0.130606^{\{3\}}$	$0.132839^{\{4\}}$	$0.134527^{\{6\}}$
		$\widehat{\beta}$	$0.167993^{\{2\}}$	$0.176812^{\{5\}}$	$0.180364^{\{6\}}$	$0.165227^{\{1\}}$	$0.180729^{\{7\}}$	$0.170747^{\{3\}}$	$0.194579^{\{8\}}$	$0.171912^{\{4\}}$
	MSE	$\widehat{\alpha}$	$0.023258^{\{1\}}$	$0.029345^{\{6\}}$	$0.038982^{\{8\}}$	$0.024233^{\{2\}}$	$0.034698^{\{7\}}$	$0.026704^{\{3\}}$	$0.028139^{\{4\}}$	$0.028436^{\{5\}}$
		$\widehat{\beta}$	$0.046381^{\{3\}}$	$0.050439^{\{5\}}$	$0.051135^{\{6\}}$	$0.042368^{\{1\}}$	$0.052449^{\{7\}}$	$0.044546^{\{2\}}$	$0.062435^{\{8\}}$	$0.047364^{\{4\}}$
	MRE	$\widehat{\alpha}$	$0.04739^{\{1\}}$	$0.053638^{\{5\}}$	$0.062181^{\{8\}}$	$0.050181^{\{2\}}$	$0.059026^{\{7\}}$	$0.052243^{\{3\}}$	$0.053136^{\{4\}}$	$0.053811^{\{6\}}$
		$\widehat{\beta}$	$0.067197^{\{2\}}$	$0.070725^{\{5\}}$	$0.072145^{\{6\}}$	$0.066091^{\{1\}}$	$0.072292^{\{7\}}$	$0.068299^{\{3\}}$	$0.077832^{\{8\}}$	$0.068765^{\{4\}}$
	$\sum$ *Ranks*		$10^{\{2\}}$	$31^{\{5\}}$	$42^{\{7.5\}}$	$9^{\{1\}}$	$42^{\{7.5\}}$	$17^{\{3\}}$	$36^{\{6\}}$	$29^{\{4\}}$
150	BIAS	$\widehat{\alpha}$	$0.112162^{\{1\}}$	$0.121655^{\{4\}}$	$0.139967^{\{8\}}$	$0.114556^{\{2\}}$	$0.137315^{\{7\}}$	$0.120293^{\{3\}}$	$0.122264^{\{5\}}$	$0.122876^{\{6\}}$
		$\widehat{\beta}$	$0.159623^{\{3\}}$	$0.163072^{\{5\}}$	$0.168161^{\{6\}}$	$0.152283^{\{2\}}$	$0.168542^{\{7\}}$	$0.150036^{\{1\}}$	$0.180895^{\{8\}}$	$0.161729^{\{4\}}$
	MSE	$\widehat{\alpha}$	$0.0203^{\{2\}}$	$0.022597^{\{3\}}$	$0.031855^{\{8\}}$	$0.020019^{\{1\}}$	$0.029988^{\{7\}}$	$0.022608^{\{4\}}$	$0.023563^{\{5\}}$	$0.023642^{\{6\}}$
		$\widehat{\beta}$	$0.039966^{\{3\}}$	$0.041972^{\{4\}}$	$0.045767^{\{6\}}$	$0.037165^{\{2\}}$	$0.046095^{\{7\}}$	$0.035307^{\{1\}}$	$0.051321^{\{8\}}$	$0.04252^{\{5\}}$
	MRE	$\widehat{\alpha}$	$0.044865^{\{1\}}$	$0.048662^{\{4\}}$	$0.055987^{\{8\}}$	$0.045823^{\{2\}}$	$0.054926^{\{7\}}$	$0.048117^{\{3\}}$	$0.048906^{\{5\}}$	$0.049151^{\{6\}}$
		$\widehat{\beta}$	$0.063849^{\{3\}}$	$0.065229^{\{5\}}$	$0.067264^{\{6\}}$	$0.060913^{\{2\}}$	$0.067417^{\{7\}}$	$0.060014^{\{1\}}$	$0.072358^{\{8\}}$	$0.064692^{\{4\}}$
	$\sum$ *Ranks*		$13^{\{2.5\}}$	$25^{\{4\}}$	$42^{\{7.5\}}$	$11^{\{1\}}$	$42^{\{7.5\}}$	$13^{\{2.5\}}$	$39^{\{6\}}$	$31^{\{5\}}$

The e^{th} central moment of X, say μ_n, is determined as follows:

$$\mu_e = E(x-\mu)^e = \sum_{w=0}^{\infty} (-1)^w \binom{e}{w} \mu_1'^w \mu'_{e-w}. \tag{9}$$

The cumulants (H_c) of X can be obtained as follows:

$$H_c = \mu'_c - \sum_{w=0}^{c-1} \binom{c-1}{w-1} w_r \mu'_{c-r}. \tag{10}$$

The moment generating function of the ExRKD takes the following form:

$$M(t) = \sum_{m=0}^{\infty} \sum_{w=1}^{\infty} \Phi_w \frac{t^m}{m!} B_m, \tag{11}$$

and its characteristic function is generated by substituting *it* for t in the last equation.

Table 5: Simulation values of BIAS, MSE, and MRE for $\alpha = 5, \beta = 7$.

n	Est.	Est. Par.	MLE	ADE	CVME	MPSE	LSE	PCE	RTADE	WLSE
25	BIAS	$\widehat{\alpha}$	$0.424125^{\{3\}}$	$0.418816^{\{1\}}$	$0.502114^{\{8\}}$	$0.453139^{\{4\}}$	$0.471347^{\{7\}}$	$0.420383^{\{2\}}$	$0.457444^{\{5\}}$	$0.470156^{\{6\}}$
		$\widehat{\beta}$	$1.213283^{\{3\}}$	$1.26109^{\{4\}}$	$1.52221^{\{7\}}$	$1.134502^{\{1\}}$	$1.331473^{\{5\}}$	$1.142832^{\{2\}}$	$1.552684^{\{8\}}$	$1.34303^{\{6\}}$
	MSE	$\widehat{\alpha}$	$0.313475^{\{4\}}$	$0.295721^{\{2\}}$	$0.401758^{\{8\}}$	$0.306792^{\{3\}}$	$0.351378^{\{6\}}$	$0.281471^{\{1\}}$	$0.338885^{\{5\}}$	$0.369043^{\{7\}}$
		$\widehat{\beta}$	$2.888571^{\{3\}}$	$2.973171^{\{4\}}$	$4.691322^{\{7\}}$	$2.170101^{\{2\}}$	$3.443173^{\{5\}}$	$2.132579^{\{1\}}$	$5.549997^{\{8\}}$	$3.520322^{\{6\}}$
	MRE	$\widehat{\alpha}$	$0.084825^{\{3\}}$	$0.083763^{\{1\}}$	$0.100423^{\{8\}}$	$0.090628^{\{4\}}$	$0.094269^{\{7\}}$	$0.084077^{\{2\}}$	$0.091489^{\{5\}}$	$0.094031^{\{6\}}$
		$\widehat{\beta}$	$0.173326^{\{3\}}$	$0.180156^{\{4\}}$	$0.217459^{\{7\}}$	$0.162072^{\{1\}}$	$0.19021^{\{5\}}$	$0.163262^{\{2\}}$	$0.221812^{\{8\}}$	$0.191861^{\{6\}}$
	$\sum$ *Ranks*		$19^{\{4\}}$	$16^{\{3\}}$	$45^{\{8\}}$	$15^{\{2\}}$	$35^{\{5\}}$	$10^{\{1\}}$	$39^{\{7\}}$	$37^{\{6\}}$
50	BIAS	$\widehat{\alpha}$	$0.289599^{\{2\}}$	$0.293456^{\{3\}}$	$0.350989^{\{7\}}$	$0.307804^{\{5\}}$	$0.359051^{\{8\}}$	$0.287945^{\{1\}}$	$0.321541^{\{6\}}$	$0.30213^{\{4\}}$
		$\widehat{\beta}$	$0.784693^{\{2\}}$	$0.821394^{\{4\}}$	$0.952284^{\{7\}}$	$0.773842^{\{1\}}$	$0.92615^{\{6\}}$	$0.786926^{\{3\}}$	$1.047538^{\{8\}}$	$0.833305^{\{5\}}$
	MSE	$\widehat{\alpha}$	$0.137515^{\{3\}}$	$0.136897^{\{2\}}$	$0.200054^{\{7\}}$	$0.145307^{\{4\}}$	$0.201669^{\{8\}}$	$0.125261^{\{1\}}$	$0.16455^{\{6\}}$	$0.149501^{\{5\}}$
		$\widehat{\beta}$	$1.051162^{\{3\}}$	$1.156676^{\{4\}}$	$1.844135^{\{7\}}$	$0.959457^{\{1\}}$	$1.446362^{\{6\}}$	$0.960695^{\{2\}}$	$2.032209^{\{8\}}$	$1.257739^{\{5\}}$
	MRE	$\widehat{\alpha}$	$0.05792^{\{2\}}$	$0.058691^{\{3\}}$	$0.070198^{\{7\}}$	$0.061561^{\{5\}}$	$0.07181^{\{8\}}$	$0.057589^{\{1\}}$	$0.064308^{\{6\}}$	$0.060426^{\{4\}}$
		$\widehat{\beta}$	$0.112099^{\{2\}}$	$0.117342^{\{4\}}$	$0.136041^{\{7\}}$	$0.110549^{\{1\}}$	$0.132307^{\{6\}}$	$0.112418^{\{3\}}$	$0.149648^{\{8\}}$	$0.119044^{\{5\}}$
	$\sum$ *Ranks*		$14^{\{2\}}$	$20^{\{4\}}$	$42^{\{7\}}$	$17^{\{3\}}$	$42^{\{7\}}$	$11^{\{1\}}$	$42^{\{7\}}$	$28^{\{5\}}$
75	BIAS	$\widehat{\alpha}$	$0.238391^{\{2\}}$	$0.248294^{\{3\}}$	$0.276135^{\{8\}}$	$0.248778^{\{4\}}$	$0.273071^{\{7\}}$	$0.228686^{\{1\}}$	$0.272073^{\{6\}}$	$0.250092^{\{5\}}$
		$\widehat{\beta}$	$0.688096^{\{5\}}$	$0.679673^{\{4\}}$	$0.768152^{\{6\}}$	$0.631936^{\{1\}}$	$0.783999^{\{7\}}$	$0.63501^{\{2\}}$	$0.855302^{\{8\}}$	$0.677334^{\{3\}}$
	MSE	$\widehat{\alpha}$	$0.089056^{\{2\}}$	$0.098175^{\{5\}}$	$0.123015^{\{8\}}$	$0.096679^{\{3\}}$	$0.122167^{\{7\}}$	$0.084542^{\{1\}}$	$0.117451^{\{6\}}$	$0.097492^{\{4\}}$
		$\widehat{\beta}$	$0.769224^{\{5\}}$	$0.747234^{\{3\}}$	$1.006987^{\{6\}}$	$0.63311^{\{2\}}$	$1.039185^{\{7\}}$	$0.624892^{\{1\}}$	$1.238218^{\{8\}}$	$0.750067^{\{4\}}$
	MRE	$\widehat{\alpha}$	$0.047678^{\{2\}}$	$0.049659^{\{3\}}$	$0.055227^{\{8\}}$	$0.049756^{\{4\}}$	$0.054614^{\{7\}}$	$0.045737^{\{1\}}$	$0.054415^{\{6\}}$	$0.050018^{\{5\}}$
		$\widehat{\beta}$	$0.098299^{\{5\}}$	$0.097096^{\{4\}}$	$0.109736^{\{6\}}$	$0.090277^{\{1\}}$	$0.112^{\{7\}}$	$0.090716^{\{2\}}$	$0.122186^{\{8\}}$	$0.096762^{\{3\}}$
	$\sum$ *Ranks*		$21^{\{3\}}$	$22^{\{4\}}$	$42^{\{7\}}$	$15^{\{2\}}$	$42^{\{7\}}$	$8^{\{1\}}$	$42^{\{7\}}$	$24^{\{5\}}$
100	BIAS	$\widehat{\alpha}$	$0.207156^{\{2\}}$	$0.217747^{\{5\}}$	$0.244345^{\{8\}}$	$0.206672^{\{1\}}$	$0.233912^{\{7\}}$	$0.209156^{\{3\}}$	$0.232231^{\{6\}}$	$0.212134^{\{4\}}$
		$\widehat{\beta}$	$0.618257^{\{5\}}$	$0.594219^{\{4\}}$	$0.692723^{\{7\}}$	$0.549872^{\{1\}}$	$0.644486^{\{6\}}$	$0.579368^{\{2\}}$	$0.738799^{\{8\}}$	$0.593609^{\{3\}}$
	MSE	$\widehat{\alpha}$	$0.066763^{\{3\}}$	$0.07673^{\{5\}}$	$0.094387^{\{8\}}$	$0.064204^{\{1\}}$	$0.08983^{\{7\}}$	$0.066149^{\{2\}}$	$0.086771^{\{6\}}$	$0.071822^{\{4\}}$
		$\widehat{\beta}$	$0.623719^{\{5\}}$	$0.576807^{\{3\}}$	$0.809345^{\{7\}}$	$0.479949^{\{1\}}$	$0.711039^{\{6\}}$	$0.510618^{\{2\}}$	$0.906671^{\{8\}}$	$0.585592^{\{4\}}$
	MRE	$\widehat{\alpha}$	$0.041431^{\{2\}}$	$0.043549^{\{5\}}$	$0.048869^{\{8\}}$	$0.041334^{\{1\}}$	$0.046782^{\{7\}}$	$0.041831^{\{3\}}$	$0.046446^{\{6\}}$	$0.042427^{\{4\}}$
		$\widehat{\beta}$	$0.088322^{\{5\}}$	$0.084888^{\{4\}}$	$0.09896^{\{7\}}$	$0.078553^{\{1\}}$	$0.092069^{\{6\}}$	$0.082767^{\{2\}}$	$0.105543^{\{8\}}$	$0.084801^{\{3\}}$
	$\sum$ *Ranks*		$22^{\{3.5\}}$	$26^{\{5\}}$	$45^{\{8\}}$	$6^{\{1\}}$	$39^{\{6\}}$	$14^{\{2\}}$	$42^{\{7\}}$	$22^{\{3.5\}}$
125	BIAS	$\widehat{\alpha}$	$0.175227^{\{1\}}$	$0.183615^{\{4\}}$	$0.212005^{\{8\}}$	$0.181934^{\{3\}}$	$0.205874^{\{6\}}$	$0.177247^{\{2\}}$	$0.208815^{\{7\}}$	$0.189139^{\{5\}}$
		$\widehat{\beta}$	$0.483692^{\{1\}}$	$0.531625^{\{4\}}$	$0.596861^{\{7\}}$	$0.518691^{\{3\}}$	$0.580656^{\{6\}}$	$0.511083^{\{2\}}$	$0.652667^{\{8\}}$	$0.55218^{\{5\}}$
	MSE	$\widehat{\alpha}$	$0.050023^{\{1\}}$	$0.054502^{\{4\}}$	$0.072149^{\{8\}}$	$0.051608^{\{3\}}$	$0.069579^{\{7\}}$	$0.05096^{\{2\}}$	$0.067353^{\{6\}}$	$0.05644^{\{5\}}$
		$\widehat{\beta}$	$0.394679^{\{1\}}$	$0.445153^{\{4\}}$	$0.570226^{\{7\}}$	$0.416821^{\{3\}}$	$0.521715^{\{6\}}$	$0.414464^{\{2\}}$	$0.664917^{\{8\}}$	$0.483635^{\{5\}}$
	MRE	$\widehat{\alpha}$	$0.035045^{\{1\}}$	$0.036723^{\{4\}}$	$0.042401^{\{8\}}$	$0.036387^{\{3\}}$	$0.041175^{\{6\}}$	$0.035449^{\{2\}}$	$0.041763^{\{7\}}$	$0.037828^{\{5\}}$
		$\widehat{\beta}$	$0.069099^{\{1\}}$	$0.075946^{\{4\}}$	$0.085266^{\{7\}}$	$0.074099^{\{3\}}$	$0.082951^{\{6\}}$	$0.073012^{\{2\}}$	$0.093238^{\{8\}}$	$0.078883^{\{5\}}$
	$\sum$ *Ranks*		$6^{\{1\}}$	$24^{\{4\}}$	$45^{\{8\}}$	$18^{\{3\}}$	$37^{\{6\}}$	$12^{\{2\}}$	$44^{\{7\}}$	$30^{\{5\}}$
150	BIAS	$\widehat{\alpha}$	$0.16481^{\{1\}}$	$0.177895^{\{5\}}$	$0.197563^{\{8\}}$	$0.170441^{\{2\}}$	$0.195316^{\{7\}}$	$0.174931^{\{4\}}$	$0.183598^{\{6\}}$	$0.170571^{\{3\}}$
		$\widehat{\beta}$	$0.464907^{\{3\}}$	$0.483013^{\{5\}}$	$0.550978^{\{7\}}$	$0.442317^{\{1\}}$	$0.520645^{\{6\}}$	$0.455147^{\{2\}}$	$0.559226^{\{8\}}$	$0.48077^{\{4\}}$
	MSE	$\widehat{\alpha}$	$0.042474^{\{1\}}$	$0.048229^{\{5\}}$	$0.062796^{\{8\}}$	$0.044627^{\{2\}}$	$0.059323^{\{7\}}$	$0.046728^{\{4\}}$	$0.052764^{\{6\}}$	$0.045857^{\{3\}}$
		$\widehat{\beta}$	$0.352247^{\{3\}}$	$0.374937^{\{4\}}$	$0.495016^{\{7\}}$	$0.313611^{\{1\}}$	$0.429923^{\{6\}}$	$0.321892^{\{2\}}$	$0.517236^{\{8\}}$	$0.375403^{\{5\}}$
	MRE	$\widehat{\alpha}$	$0.032962^{\{1\}}$	$0.035579^{\{5\}}$	$0.039513^{\{8\}}$	$0.034088^{\{2\}}$	$0.039063^{\{7\}}$	$0.034986^{\{4\}}$	$0.03672^{\{6\}}$	$0.034114^{\{3\}}$
		$\widehat{\beta}$	$0.066415^{\{3\}}$	$0.069002^{\{5\}}$	$0.078711^{\{7\}}$	$0.063188^{\{1\}}$	$0.074378^{\{6\}}$	$0.065021^{\{2\}}$	$0.079889^{\{8\}}$	$0.068681^{\{4\}}$
	$\sum$ *Ranks*		$12^{\{2\}}$	$29^{\{5\}}$	$45^{\{8\}}$	$9^{\{1\}}$	$39^{\{6\}}$	$18^{\{3\}}$	$42^{\{7\}}$	$22^{\{4\}}$

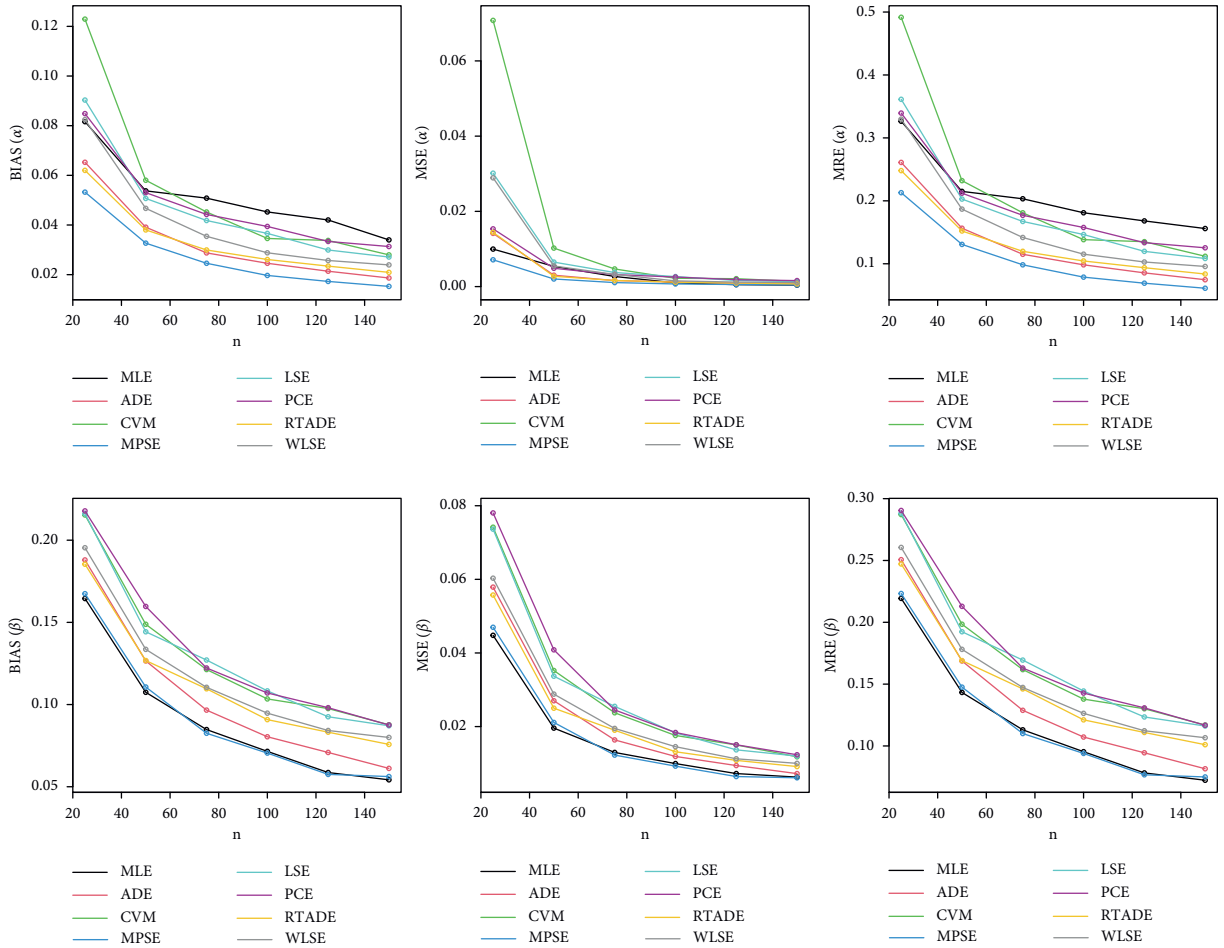

Figure 3: Graphical representation of BIAS, MSE, and MRE values in Table 1.

3.4. Order Statistics. The PDF and CDF of the ith order statistic for the ExRKD are defined, respectively, as follows:

$$f_{i:n}(x) = \frac{n!}{(i-1)!(n-i)!}[F(x)]^{i-1}[1-F(x)]^{n-i}f(x) = \alpha\beta n!\log^{-i}(2)\left(\frac{x}{1-x}\right)^{\alpha-1} \times \frac{\left(1-e^{-(x/1-x)^{\alpha}}\right)^{\beta}\log^{i-1}\left(\left(1-e^{-(x/1-x)^{\alpha}}\right)^{\beta}+1\right)\left(1-\log\left(\left(1-e^{-(x/1-x)^{\alpha}}\right)^{\beta}+1\right)/\log(2)\right)^{n-i}}{(x-1)^2\,\Gamma(i)\left(e^{(x/1-x)^{\alpha}}-1\right)\Gamma(-i+n+1)\left(\left(1-e^{-(x/1-x)^{\alpha}}\right)^{\beta}+1\right)},$$

$$F_{i:n}(x) = \sum_{r=i}^{n}\binom{n}{r}(F(x))^{r}(1-F(x))^{n-r} = \frac{\log^{-i}(2)\Gamma(n+1)\log^{i}\left(\left(1-e^{-(x/1-x)^{\alpha}}\right)^{\beta}+1\right)\left(1-\log\left(\left(1-e^{-(x/1-x)^{\alpha}}\right)^{\beta}+1\right)/\log(2)\right)^{n-i}T}{\Gamma(-i+n+1)}, \tag{12}$$

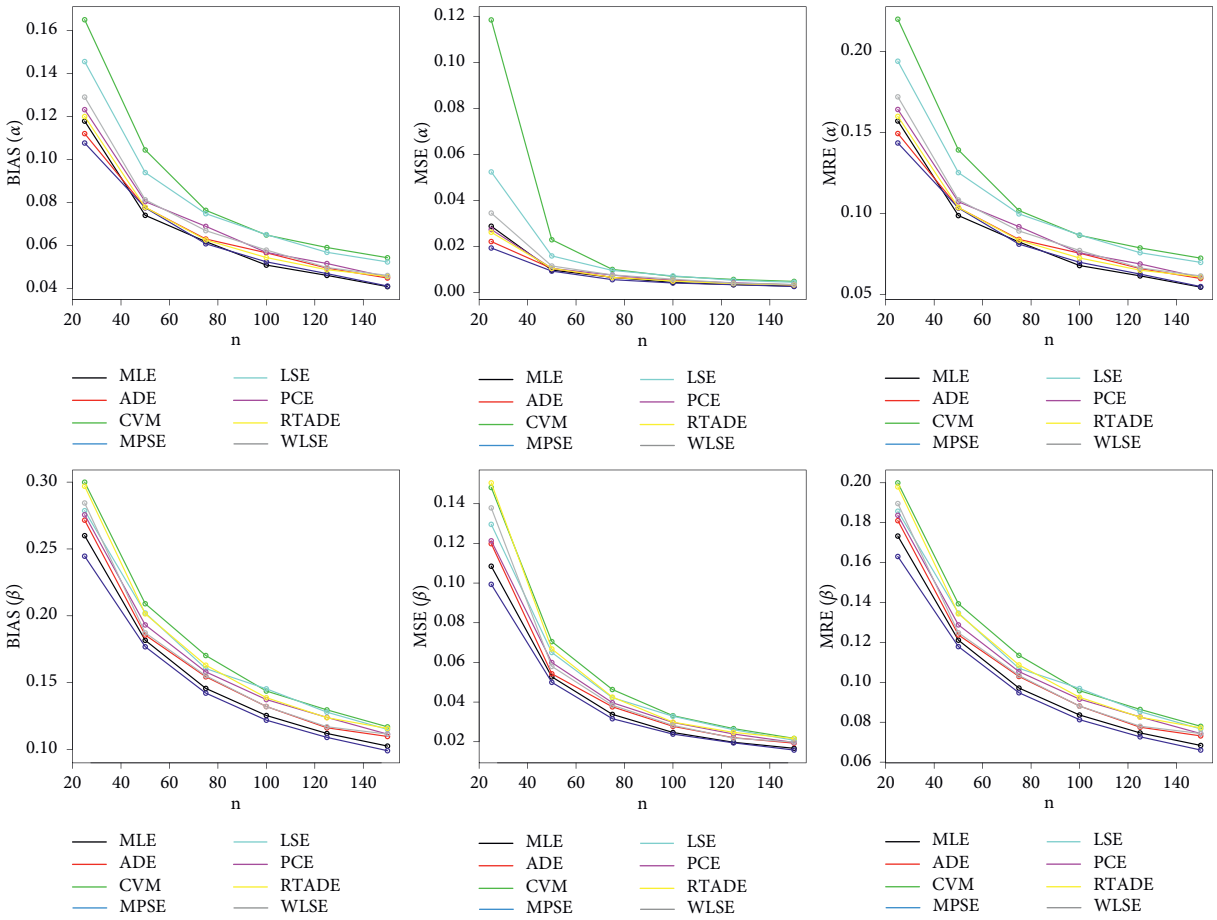

Figure 4: Graphical representation of BIAS, MSE, and MRE values in Table 2.

where $T = {}_2\widetilde{F}_1(1, i-n; i+1; \log(2)/\log(1/2((1-e^{-(x/1-x)^{\alpha}})^{\beta}+1))+1)$ is a regularized hypergeometric function.

4. Estimation Methods

This section discusses how to estimate the ExRK model parameters using several classical estimation approaches by maximization or minimization of the considered function. For more details, see [15–19].

For $x_1, \ldots, x_n$ defined as a random sample from ExRK distribution, maximum likelihood estimation (MLE) obtains estimators of ExRK distribution by maximizing the log-likelihood function specified in the following equation:

$$l = \beta \sum_{i=1}^{n} \log\left(1 - e^{-\left(x_i/1-x_i\right)^{\alpha}}\right) - \sum_{i=1}^{n} \log\left(\left(1 - e^{-\left(x_i/1-x_i\right)^{\alpha}}\right)^{\beta} + 1\right) - \sum_{i=1}^{n} \log\left(e^{\left(x_i/1-x_i\right)^{\alpha}} - 1\right)$$
$$+ (\alpha - 1) \sum_{i=1}^{n} \log\left(\frac{x_i}{1-x_i}\right) - \sum_{i=1}^{n} \log\left((x_i - 1)^2\right) + n \log\left(\frac{\alpha\beta}{\log(2)}\right). \tag{13}$$

For $x_1 \leq \cdots \leq x_n$ defined as a sorted random sample from ExRK distribution, Anderson–Darling estimation (ADE) obtains estimators of ExRK distribution by minimizing the function specified in the following equation:

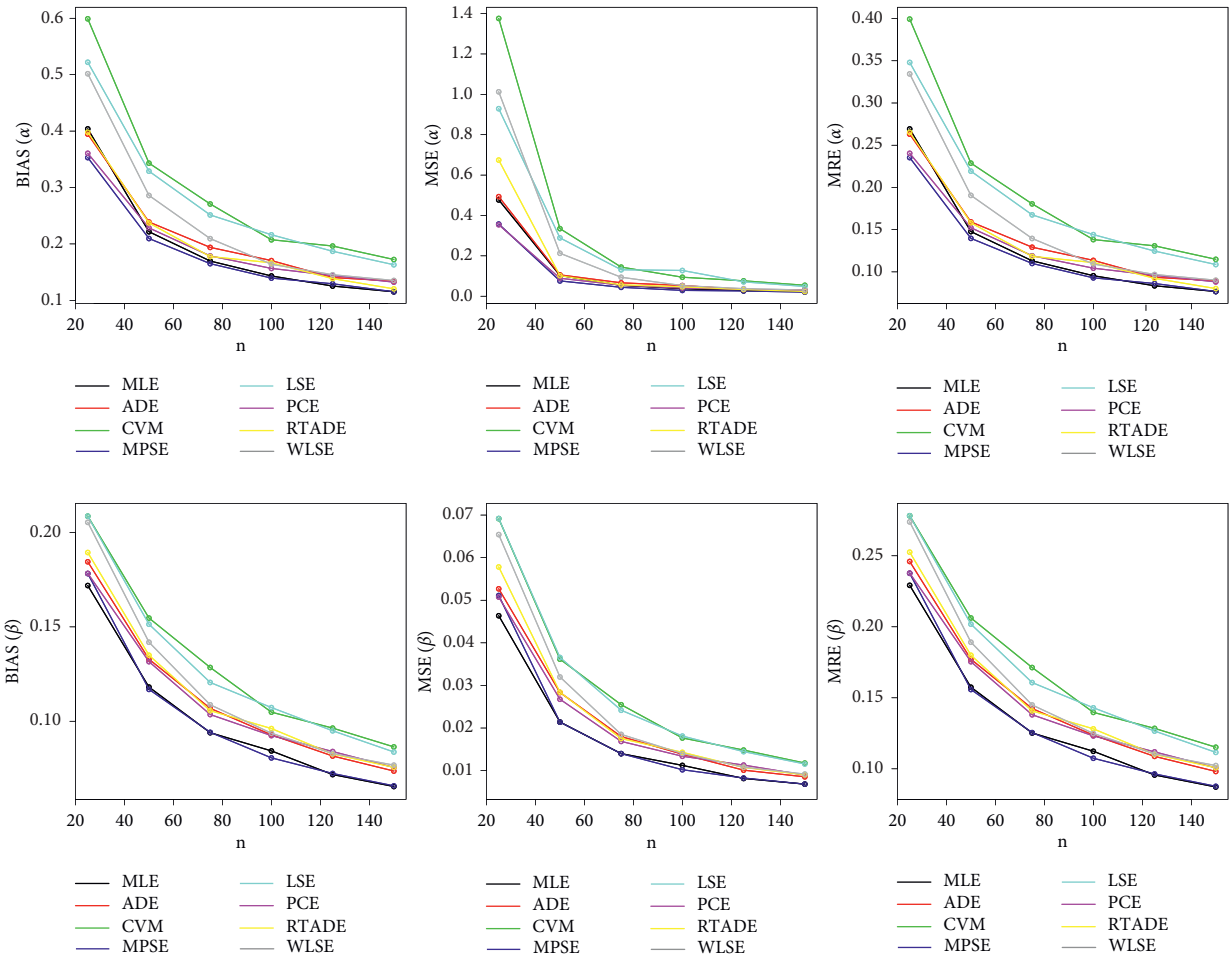

Figure 5: Graphical representation of BIAS, MSE, and MRE values in Table 3.

$$A = -n - \frac{1}{n}\sum_{i=1}^{n}(2i-1)\left[\log F(x_i) + \log S(x_i)\right]$$
$$= -n - \frac{1}{n}\sum_{i=1}^{n}(2i-1)\left[\log\left(\frac{\log\left(\left(1-e^{-\left(x_i/1-x_i\right)^{\alpha}}\right)^{\beta}+1\right)}{\log(2)}\right) + \log\left(1-\frac{\log\left(\left(1-e^{-\left(x_i/1-x_i\right)^{\alpha}}\right)^{\beta}+1\right)}{\log(2)}\right)\right]. \quad (14)$$

For $x_1 \le \cdots \le x_n$, defined as a sorted random sample from ExRK distribution, Cramér–von Mises estimation (CVME) obtains estimators of ExRK distribution by minimizing the function specified in the following equation:

$$C = -\frac{1}{12n} + \sum_{i=1}^{n}\left[F(x_i) - \frac{2i-1}{2n}\right]^2$$
$$= -\frac{1}{12n} + \sum_{i=1}^{n}\left[\frac{\log\left(\left(1-e^{-\left(x_i/1-x_i\right)^{\alpha}}\right)^{\beta}+1\right)}{\log(2)} - \frac{2i-1}{2n}\right]^2. \quad (15)$$

For $x_1 \le \cdots \le x_n$, defined as a sorted random sample from ExRK distribution, maximum product of spacings estimation (MPSE) obtains estimators of ExRK distribution by maximizing the function specified in the following equation:

$$MP = \frac{1}{n+1}\sum_{i=1}^{n+1}\log H_i, \quad (16)$$

where

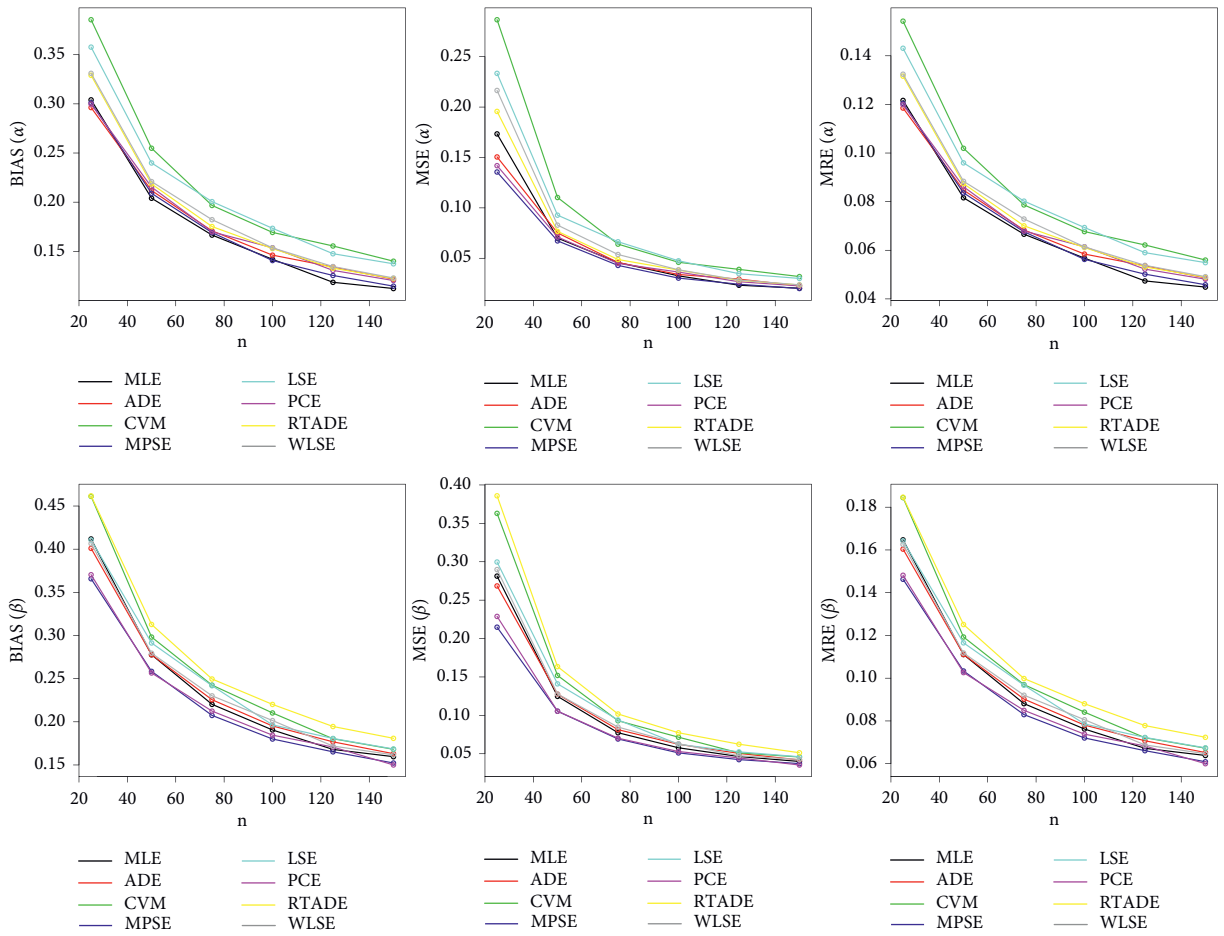

Figure 6: Graphical representation of BIAS, MSE, and MRE values in Table 4.

$$H_i = F\left(x_{(i)}\right) - F\left(x_{(i-1)}\right) = \frac{\log\left(\left(1 - e^{-\left(x_i/1-x_i\right)^{\alpha}}\right)^{\beta} + 1\right)}{\log(2)} - \frac{\log\left(\left(1 - e^{-\left(x_{i-1}/1-x_{i-1}\right)^{\alpha}}\right)^{\beta} + 1\right)}{\log(2)}. \tag{17}$$

For $x_1 \le \cdots \le x_n$, defined as a sorted random sample from ExRK distribution, least-squares estimation (LSE) obtains estimators of ExRK distribution by minimizing the function specified in the following equation:

$$V = \sum_{i=1}^{n}\left[F(x_i) - \frac{i}{n+1}\right]^2 = \sum_{i=1}^{n}\left[\frac{\log\left(\left(1 - e^{-\left(x_i/1-x_i\right)^{\alpha}}\right)^{\beta} + 1\right)}{\log(2)} - \frac{i}{n+1}\right]^2. \tag{18}$$

For $x_1 \le \cdots \le x_n$, defined as a sorted random sample from ExRK distribution, percentile estimation (PCE) obtains estimators of ExRK distribution by minimizing the function specified in the following equation:

$$PC = \sum_{i=1}^{n}\left[x_i - Q(k_i)\right]^2 = \sum_{i=1}^{n}\left[x_i - 1 + \frac{1}{\left(-\log\left(1 - (2^p - 1)^{1/\beta}\right)\right)^{1/\alpha} + 1}\right]^2, k_i = \frac{i}{n+1}. \tag{19}$$

For $x_1 \le \cdots \le x_n$, defined as a sorted random sample from ExRK distribution, right-tail Anderson–Darling estimation (RTADE) obtains estimators of ExRK distribution by minimizing the function specified in the following equation:

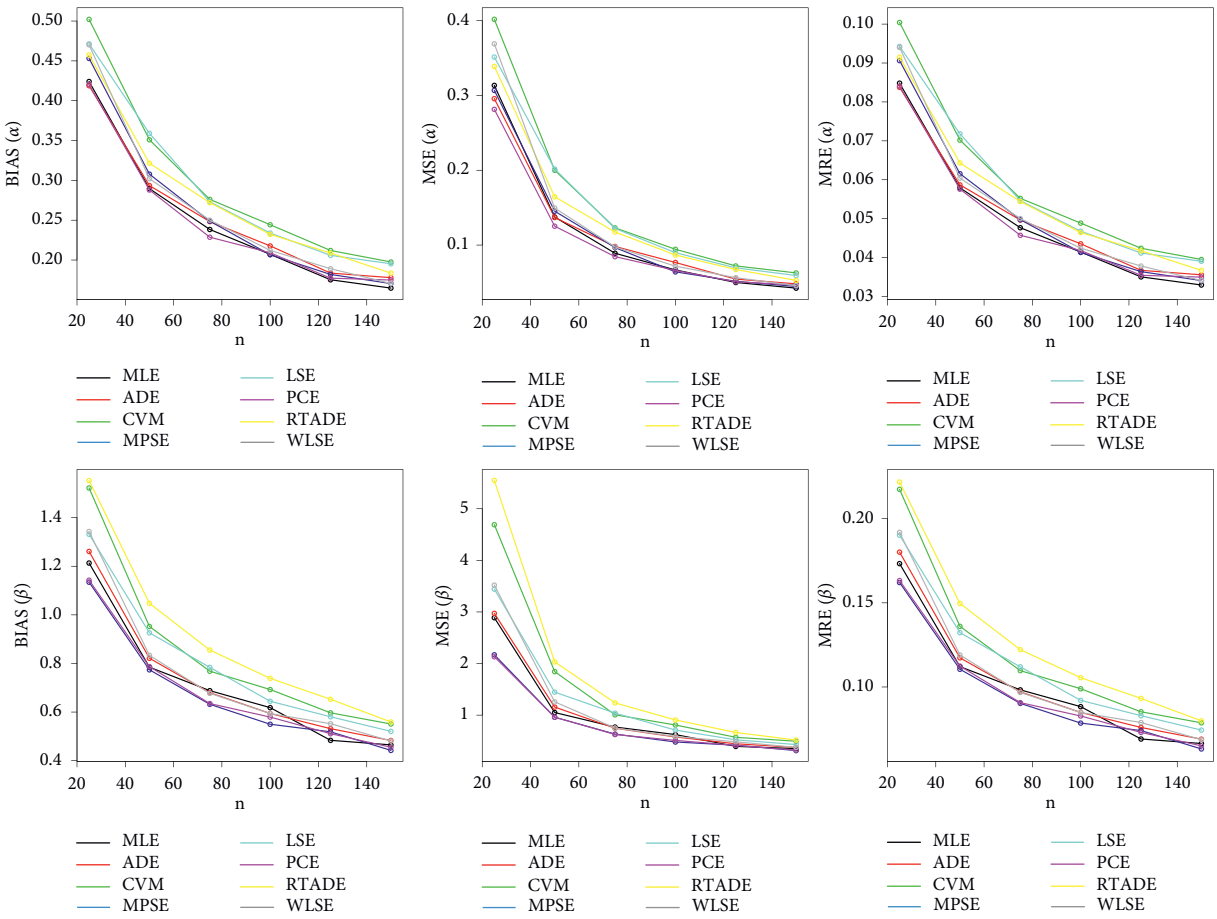

Figure 7: Graphical representation of BIAS, MSE, and MRE values in Table 5.

$$R = \frac{n}{2} - 2\sum_{i=1}^{n} F(x_i) - \frac{1}{n}\sum_{i=1}^{n}(2i-1)\log S(x_{n+1-i})$$

$$= \frac{n}{2} - 2\sum_{i=1}^{n}\left(\frac{\log\left(\left(1-e^{-\left(x_i/1-x_i\right)^{\alpha}}\right)^{\beta}+1\right)}{\log(2)}\right)$$

$$-\frac{1}{n}\sum_{i=1}^{n}(2i-1)\log\left(\frac{\log\left(\left(1-e^{-\left(x_{n+1-i}/1-x_{n+1-i}\right)^{\alpha}}\right)^{\beta}+1\right)}{\log(2)}\right). \tag{20}$$

For $x_1 \le \cdots \le x_n$, defined as a sorted random sample from ExRK distribution, weighted least-squares estimation (WLSE) obtains estimators of ExRK distribution by minimizing the function specified in the following equation:

$$W = \sum_{i=1}^{n}\frac{(n+1)^2(n+2)}{i(n-i+1)}\left[F(x_i) - \frac{i}{n+1}\right]^2$$

$$= \sum_{i=1}^{n}\frac{(n+1)^2(n+2)}{i(n-i+1)} \tag{21}$$

$$\bullet\left[\frac{\log\left(\left(1-e^{-\left(x_i/1-x_i\right)^{\alpha}}\right)^{\beta}+1\right)}{\log(2)} - \frac{i}{n+1}\right]^2.$$

Table 6: Partial and overall ranks of all the methods of estimation of proposed distribution by various values of model parameters.

Parameter	n	MLE	ADE	CVME	MPSE	LSE	PCE	RTADE	WLSE
$\alpha = 0.25, \beta = 0.75$	25	2.0	4.0	8.0	1.0	6.5	6.5	3.0	5.0
	50	4.0	3.0	8.0	1.0	6.0	7.0	2.0	5.0
	75	4.0	2.0	7.0	1.0	8.0	6.0	3.0	5.0
	100	4.0	2.0	6.0	1.0	7.5	7.5	3.0	5.0
	125	4.0	2.0	7.5	1.0	6.0	7.5	3.0	5.0
	150	3.0	2.0	7.0	1.0	6.0	8.0	4.0	5.0
$\alpha = 0.75, \beta = 1.5$	25	3.0	2.0	8.0	1.0	6.5	4.0	5.0	6.5
	50	2.0	3.0	8.0	1.0	7.0	4.0	6.0	5.0
	75	2.0	3.0	8.0	1.0	7.0	6.0	5.0	4.0
	100	2.0	3.0	7.0	1.0	8.0	6.0	4.0	5.0
	125	2.0	3.0	8.0	1.0	7.0	6.0	4.0	5.0
	150	2.0	3.0	8.0	1.0	7.0	4.0	6.0	5.0
$\alpha = 1.5, \beta = 0.75$	25	3.0	4.0	8.0	1.0	7.0	2.0	5.0	6.0
	50	2.0	5.0	8.0	1.0	7.0	3.0	4.0	6.0
	75	2.0	5.0	8.0	1.0	7.0	3.0	4.0	6.0
	100	2.0	5.0	7.0	1.0	8.0	3.0	6.0	4.0
	125	1.0	3.5	8.0	2.0	7.0	5.5	3.5	5.5
	150	1.0	5.0	8.0	2.0	7.0	3.5	3.5	6.0
$\alpha = 2.5, \beta = 2.5$	25	4.0	3.0	8.0	1.0	6.0	2.0	7.0	5.0
	50	2.0	4.0	8.0	1.0	6.5	3.0	6.5	5.0
	75	2.5	4.0	7.0	1.0	8.0	2.5	6.0	5.0
	100	2.0	3.5	8.0	1.0	7.0	3.5	6.0	5.0
	125	2.0	5.0	7.5	1.0	7.5	3.0	6.0	4.0
	150	2.5	4.0	7.5	1.0	7.5	2.5	6.0	5.0
$\alpha = 5, \beta = 7$	25	4.0	3.0	8.0	2.0	5.0	1.0	7.0	6.0
	50	2.0	4.0	7.0	3.0	7.0	1.0	7.0	5.0
	75	3.0	4.0	7.0	2.0	7.0	1.0	7.0	5.0
	100	3.5	5.0	8.0	1.0	6.0	2.0	7.0	3.5
	125	1.0	4.0	8.0	3.0	6.0	2.0	7.0	5.0
	150	2.0	5.0	8.0	1.0	6.0	3.0	7.0	4.0
$\sum$ ranks		75.5	108.0	229.5	38.0	205.0	119.0	153.5	151.5
Overall rank		2	3	8	1	7	4	6	5

Table 7: List of the compared distributions.

Distribution	Abbreviation	Author(s)
Reduced Kies distribution	RKD	Kumar and Dharmaja [14]
Exponentiated Topp–Leone distribution	ETLD	Pourdarvish et al. [2]
Topp–Leone distribution	TLD	Topp and Leone [13]
Log-Lindley distribution	LLD	Gómez-Déniz et al. [3]
Power log-Lindley distribution	PLLD	Abd El-Bar et al. [6]
Cosine-sine distribution	CSD	Abd El-Bar et al. [6]
Power logarithmic distribution	PLD	Abd El-Bar et al. [7]
Transformed gamma distribution	TGD	Grassia [4]
Log-gamma distribution	LGD	Amini et al. [11]
Log-weighted power distribution	LWPD	Chesneau [12]
Transmuted power distribution	TPD	Chesneau [12]
Beta distribution	BD	

Table 8: Numerical values for analyzing the milk real data set.

Model	$-L$	C_1	C_2	C_3	C_4	GoF_1	GoF_2	GoF_3	$GoF_3(p)$	Est. parameters (SEs)
ExRKD	−27.1801	−50.3602	−50.2448	−45.0146	−48.1932	0.619746	0.0962025	0.0733981	0.611643	$\widehat{\alpha} = 0.975641\,(0.0721869)$ $\widehat{\beta} = 1.72127\,(0.167809)$
RKD	−22.1004	−42.2008	−42.1627	−39.528	−41.1173	4.93197	1.00894	0.177934	0.00228316	$\widehat{a} = 1.09136\,(0.0688131)$
BD	−23.7772	−43.5545	−43.4391	−38.2088	−41.3874	1.38527	0.22823	0.0909919	0.338375	$\widehat{a} = 2.41252\,(0.314491)$ $\widehat{b} = 2.82967\,(0.374422)$
ETLD	−23.3428	−42.6856	−42.5702	−37.3399	−40.5185	1.54214	0.263196	0.0950351	0.288614	$\widehat{a} = 2.46832\,(0.301618)$ $\widehat{b} = 1.30496\,(0.179222)$
TLD	−21.5262	−41.0524	−41.0143	−38.3796	−39.9689	1.88132	0.284751	0.0972409	0.263762	$\widehat{a} = 2.08023\,(0.201103)$
LLD	−20.7039	−37.4077	−37.2923	−32.0621	−35.2407	2.18556	0.338619	0.103804	0.199137	$\widehat{\beta} = 2.22468\,(0.0812055)$ $\widehat{\lambda} = 1 \times 10^{-9}\,(0.0519599)$
PLLD	−20.6977	−35.3954	−35.1624	−27.3769	−32.1448	2.18706	0.338862	0.103846	0.198773	$\widehat{\alpha} = 55.9927\,(17.2231)$ $\widehat{\sigma} = 0.0397265\,(0.0100298)$ $\widehat{\lambda} = 0.00551514\,(0.128159)$
CSD	−6.56401	−11.128	−11.0899	−8.45519	−10.0445	15.0079	3.28194	0.304419	< 0.00001	$\widehat{\lambda} = 1.18423 \times 10^{-9}\,(7.99982 \times 10^{-7})$
PLD	−20.7039	−35.4077	−35.1747	−27.3892	−32.1571	2.18556	0.338618	0.103804	0.199136	$\widehat{\alpha} = 1.22468\,(0.152076)$ $\widehat{\beta} = 0.00140746\,(6.03799)$ $\widehat{\delta} = 810216\,(249258)$
TGD	−23.1814	−44.3627	−44.3246	−41.6899	−43.2792	1.98331	0.378296	0.120438	0.0897177	$\widehat{\sigma} = 2.83623\,(0.193881)$
LGD	−20.7039	−39.4077	−39.3696	−36.7349	−38.3242	2.18556	0.338618	0.103804	0.199136	$\widehat{\sigma} = 2.22468\,(0.152076)$
LWPD	−20.7039	−37.4077	−37.2923	−32.0621	−35.2407	2.18556	0.338618	0.103804	0.199136	$\widehat{\alpha} = 2.22468\,(0.372222)$ $\widehat{\lambda} = 1.0\,(0.414309)$
TPD	−20.434	−36.8681	−36.7527	−31.5224	−34.701	2.42687	0.379845	0.11484	0.118918	$\widehat{\alpha} = 1.66014\,(0.253083)$ $\widehat{\lambda} = 1.0\,(0.549492)$

Table 9: Numerical values for analyzing the COVID-19 real data set.

Model	$-L$	C_1	C_2	C_3	C_4	GoF_1	GoF_2	GoF_3	$GoF_3(p)$	Est. parameters (SEs)
ExRKD	−58.7972	−113.594	−113.404	−109.215	−111.864	0.900701	0.155322	0.106187	0.446282	$\widehat{\alpha} = 0.817392$ (0.0475411) $\widehat{\beta} = 8.2891$ (1.03689)
RKD	8.72551	19.451	19.5135	21.6407	20.3163	53.0981	10.4062	0.616969	< 0.00001	$\widehat{a} = 0.664682$ (0.051041)
BD	−57.5743	−111.149	−110.958	−106.769	−109.418	1.05197	0.178341	0.114785	0.349424	$\widehat{a} = 12.7943$ (2.2291) $\widehat{b} = 4.89941$ (0.826972)
ETLD	−56.7872	−109.574	−109.384	−105.195	−107.844	1.23021	0.214243	0.12548	0.249774	$\widehat{a} = 15.3167$ (2.19208) $\widehat{b} = 1.86404$ (0.348079)
TLD	−51.5544	−101.109	−101.046	−98.9191	−100.244	2.04752	0.27752	0.18133	0.0260671	$\widehat{a} = 10.5284$ (1.29596)
LLD	−46.7273	−89.4547	−89.2642	−85.0753	−87.7242	3.39896	0.509096	0.220321	0.00329848	$\widehat{\beta} = 5.96527$ (0.376555) $\widehat{\lambda} = 9.40395 \times 10^{-9}$ (0.0200914)
PLLD	−46.7271	−87.4542	−87.0671	−80.8853	−84.8585	3.39834	0.508938	0.220297	0.003303	$\widehat{\alpha} = 814.282$ (266.225) $\widehat{\sigma} = 0.0073251$ (0.0020101) $\widehat{\lambda} = 0.001136$ (0.778915)
CSD	32.6342	67.2684	67.3309	69.4581	68.1337	76.827	13.4103	0.6956	< 0.00001	$\widehat{\lambda} = 1.18423 \times 10^{-9}$ (1.01859×10^{-7})
PLD	−46.7273	−87.4547	−87.0676	−80.8857	−84.8589	3.39896	0.509096	0.220321	0.00329848	$\widehat{\alpha} = 4.96527$ (0.51921) $\widehat{\beta} = 0.001398$ (13.1574) $\widehat{\delta} = 1.31665 \times 10^{7}$ (4.30822×10^{6})
TGD	−26.0342	−50.0683	−50.0058	−47.8787	−49.2031	9.06226	1.64558	0.273367	0.000103993	$\widehat{\sigma} = 1.46942$ (0.127897)
LGD	−46.7273	−91.4547	−91.3922	−89.265	−90.5894	3.39896	0.509096	0.220321	0.00329848	$\widehat{\sigma} = 5.96527$ (0.51921)
LWPD	−46.7273	−89.4547	−89.2642	−85.0753	−87.7242	3.39896	0.509096	0.220321	0.00329849	$\widehat{\alpha} = 5.96527$ (1.40819) $\widehat{\lambda} = 1.0$ (0.715182)
TPD	−45.3289	−86.6579	−86.4674	−82.2785	−84.9274	3.73667	0.565396	0.226964	0.00222829	$\widehat{\alpha} = 4.38457$ (0.777979) $\widehat{\lambda} = 1.0$ (0.759)

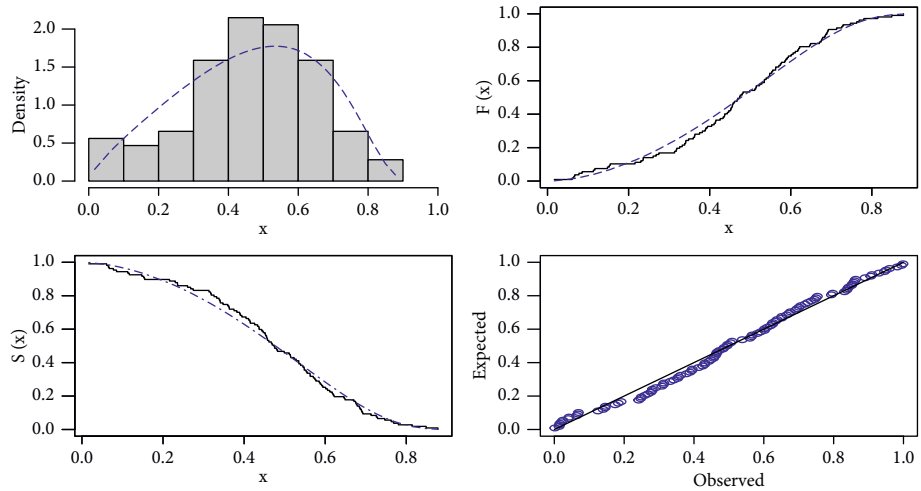

Figure 8: Histogram of the milk data set with the fitted PDF, CDF, SF, and P–P plots.

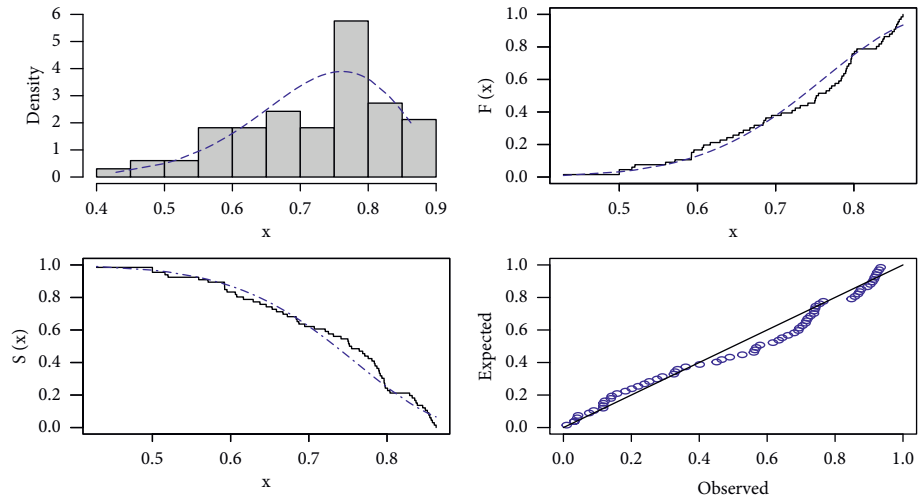

Figure 9: Histogram of the COVID-19 data set with the fitted PDF, CDF, SF, and P–P plots.

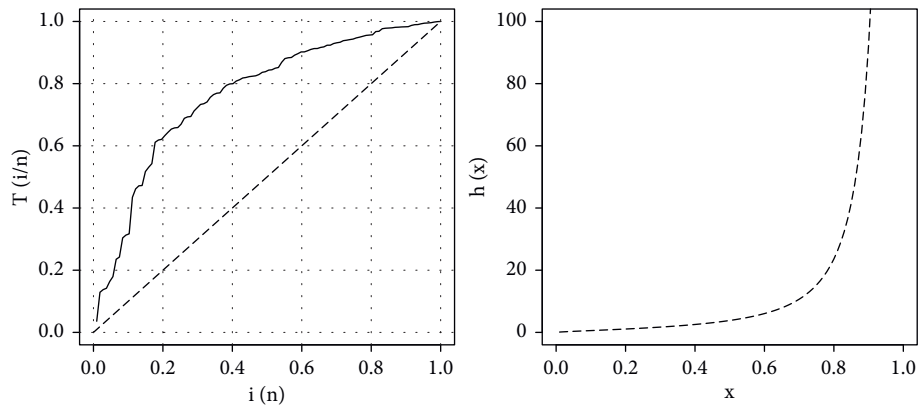

Figure 10: TTT plot and fitted HRF of ExRK model for the milk data set.

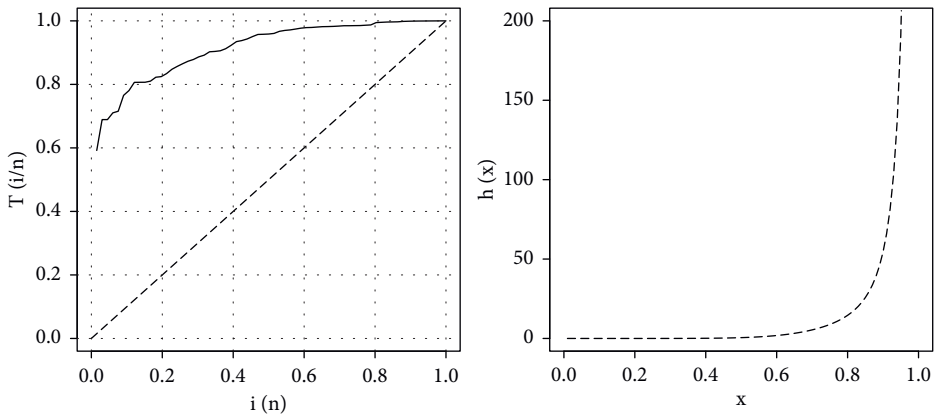

Figure 11: TTT plot and fitted HRF of ExRK model for the COVID-19 data set.

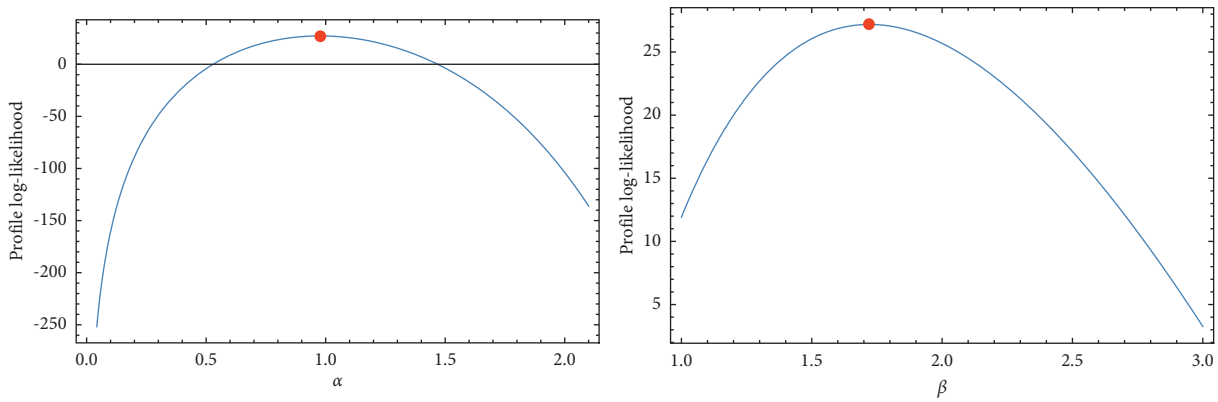

Figure 12: The profile of the log-likelihood functions for α and β of the milk data set.

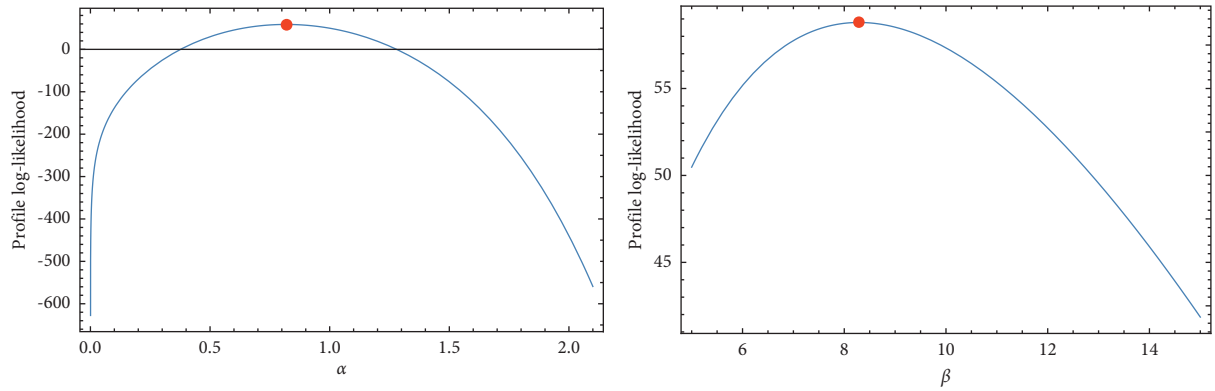

Figure 13: The profile of the log-likelihood functions for α and β of the COVID-19 data set.

5. Numerical Simulation

In order to find estimators of our proposed model using data sets are generated at random, all of the estimation techniques discussed in the previous section will be employed in this section. Our goal is to examine both the performance of these estimation methods and the behavior of the model estimators that we have presented in this research. In addition, we will assess the effectiveness of these strategies using various measures such as average of bias (BIAS),

$|\text{Bias}(\widehat{\omega})| = 1/H \sum_{i=1}^{H} |\widehat{\omega} - \omega|$; mean squared errors (MSE), $\text{MSE} = 1/H \sum_{i=1}^{H} (\widehat{\omega} - \omega)^2$; and mean relative errors (MRE), $\text{MRE} = 1/H \sum_{i=1}^{H} |\widehat{\omega} - \omega|/\omega$, $\omega = (\alpha, \beta)$. Using the simulation, you can figure out what the most reasonable estimation method for the model parameters would be. In our simulation, we generated one thousand ($H = 1000$) samples of size $n = 25$, 50, 75, 100, 125, and 150.

The results of simulations are presented in Tables 1–5, while the graphical representations of these tables, which correlate to the numerical results of simulations, are shown in Figures 3–7, respectively. The power value reveals how effective a technique is in comparison to all other techniques. Our estimators' partial and overall rankings are displayed in Table 6.

5.1. Simulation Outcomes. Based on the results of the simulation and the ranking tables, we reach the following conclusion:

(i) Almost all of the estimators exhibit the property of consistency in their results.

(ii) As sample size rises, the BIAS of all estimators decreases for all techniques of estimation, regardless of method.

(iii) As sample size rises, the MSE of all estimators decreases for all techniques of estimation, regardless of method.

(iv) As sample size rises, the MRE of all estimators decreases for all techniques of estimation, regardless of method.

(v) The most preferred technique for estimation is to use the maximum spacing product. If researchers have data that matches our proposed model, we recommend that they use this technique.

6. Real Data Analysis

Real-world data is used to demonstrate the distribution's adaptability in this section. The first real data set consists of 107 observations about the total milk production in the first birth of 107 cows from SINDI race which was studied by Cordeiro and dos Santos Brito [20]. The second real data set consists of 66 observations which refer to the rates of recovery from COVID-19 infections in Spain (from the 3rd of March to the 7th of May, 2020).

In order to show the flexibility of our proposed model, we compare it with well-known models. All of the compared models are specified in Table 7 for $0 < x < 1$.

In order to choose the most appropriate model for the real-world data set, we use a set of analytical criteria, including Akaike information criterion (C_1), correct Akaike information criterion (C_2), Bayesian information criterion (C_3), and Hannan–Quinn information criterion (C_4). In addition, we consider a variety of goodness-of-fit statistics in our selection, such as Anderson–Darling (GoF_1), Cramér–von Mises (GoF_2), and Kolmogorov–Smirnov (GoF_3) with its p value ($GoF_3(p)$).

As demonstrated in Tables 8 and 9, the analytical measures, as well as the MLE and corresponding standard errors (SE), are provided for the real data sets that were under consideration for evaluation. As a result, we may conclude that the ExRK model performs much better than the other comparable models. Additionally, the P–P plot and the estimated PDF, CDF, and SF plots are used to fit the proposed ExRK model to the milk and the COVID-19 data sets shown in Figures 8 and 9. Using the milk and the COVID-19 data sets, the suggested model was shown to be a good fit. TTT and estimated HRF of the ExRK model plots are shown in Figures 10 and 11 for the two real data sets, respectively. The behavior of the log-likelihood function, which is a unimodal function, with estimated parameters is shown in Figures 12 and 13 for the two real data sets.

7. Conclusion

An extension of the reduced Kies distribution, which is discussed in more depth and detailed , is built in this paper as a statistical model. Its PDF may be left- or right-skewed, symmetrical, decreasing, or even a "bathtub" form. Some of its most notable statistical properties are explored through mathematical analysis. Eight traditional estimating methods are discussed in details, and these methods are used to estimate the ExRKD parameters. Simulation findings show that the proposed estimators perform quite well. In addition, the ExRKD's practical use is discussed by examining its performance in comparison to well known models using real-world data sets.

Data Availability

The data used to support the findings of this study are included in the paper.

Conflicts of Interest

The authors declare that they have no conflicts of interest.

Acknowledgments

The authors would like to thank the Deanship of Scientific Research at Majmaah University for supporting this work under project R-2022-240.

References

[1] A. Krishna, R. Maya, C. Chesneau, and M. R. Irshad, "The unit teissier distribution and its applications," *Mathematical and Computational Applications*, vol. 27, no. 1, p. 12, 2022.

[2] A. Pourdarvish, S. M. T. K. Mirmostafaee, and K. Naderi, "The exponentiated topp-leone distribution: properties and application," *Journal of Applied Environmental and Biological Sciences*, vol. 5, no. 7, pp. 251–256, 2015.

[3] E. Gómez-Déniz, M. A. Sordo, and E. Calderín-Ojeda, "The log–lindley distribution as an alternative to the beta regression model with applications in insurance," *Insurance: Mathematics and Economics*, vol. 54, pp. 49–57, 2014.

[4] A. Grassia, "On a family of distributions with argument between 0 and 1 obtained by transformation of the gamma and derived compound distributions," *Australian Journal of Statistics*, vol. 19, no. 2, pp. 108–114, 1977.
[5] A. M. T. Abd El-Bar, H. S. Bakouch, and S. Chowdhury, "A new trigonometric distribution with bounded support and an application," *Revista de la Unión Matemática Argentina*, vol. 62, no. 2, pp. 459–473, 2021.
[6] A. M. T. Abd El-Bar, W. B. F. da Silva, and A. D. C. Nascimento, "An extended log-lindley-g family: properties and experiments in repairable data," *Mathematics*, vol. 9, no. 23, p. 3108, 2021.
[7] A. M. T. Abd El-Bar, M. d. C. S. Lima, and M. Ahsanullah, "Some inferences based on a mixture of power function and continuous logarithmic distribution," *Journal of Taibah University for Science*, vol. 14, no. 1, pp. 1116–1126, 2020.
[8] J. Mazucheli, A. F. B. Menezes, L. B. Fernandes, R. P. De Oliveira, and M. E. Ghitany, "The unit-weibull distribution as an alternative to the kumaraswamy distribution for the modeling of quantiles conditional on covariates," *Journal of Applied Statistics*, vol. 47, no. 6, pp. 954–974, 2020.
[9] C. S. Kumar and S. H. S. Dharmaja, "On reduced Kies distribution," *Collection of Recent Statistical Methods and Applications*, pp. 111–123, 2013.
[10] H. Bakouch, C. Chesneau, and M. Enany, "A weighted general family of distributions: theory and practice," *Computational and Mathematical Methods*, p. e1135, 2020.
[11] M. Amini, S. M. T. K. MirMostafaee, and J. Ahmadi, "Log-gamma-generated families of distributions," *Statistics*, vol. 48, no. 4, pp. 913–932, 2014.
[12] C. Chesneau, "On a logarithmic weighted power distribution: theory, modelling and applications," *Journal of Mathematical Sciences: Advances and Applications*, vol. 67, no. 1, pp. 1–59, 2021.
[13] C. W. Topp and F. C. Leone, "A family of j-shaped frequency functions," *Journal of the American Statistical Association*, vol. 50, no. 269, pp. 209–219, 1955.
[14] C. S. Kumar and S. H. S. Dharmaja, "The exponentiated reduced kies distribution: properties and applications," *Communications in Statistics - Theory and Methods*, vol. 46, no. 17, pp. 8778–8790, 2017.
[15] A. E. A. M. Teamah, A. A. Elbanna, and A. M. Gemeay, "Heavy-tailed log-logistic distribution: properties, risk measures and applications," *Statistics, Optimization & Information Computing*, vol. 9, no. 4, pp. 910–941, 2021.
[16] H. M. Alshanbari, A. Al-Aziz Hosni El-Bagoury, A. M. Gemeay, E. H. Hafez, and A. S. Eldeeb, "A flexible extension of pareto distribution: properties and applications," *Computational Intelligence and Neuroscience*, 2021.
[17] M. Aba Oud and M. Almuqrin, "On the early detecting of the covid-19 outbreak," *The Journal of Infection in Developing Countries*, vol. 15, no. 11, pp. 1625–1629, 2021.
[18] F. H. Riad, E. Hussam, A. M. Gemeay, R. A. Aldallal, and A. ZAfify, "Classical and bayesian inference of the weighted-exponential distribution with an application to insurance data," *Mathematical Biosciences and Engineering*, vol. 19, no. 7, pp. 6551–6581, 2022.
[19] A. Z. Afify, A. M. Gemeay, N. M. Alfaer, G. M. Cordeiro, and E. H. Hafez, "Power-modified kies-exponential distribution: properties, classical and bayesian inference with an application to engineering data," *Entropy*, vol. 24, no. 7, p. 883, 2022.
[20] G. M. Cordeiro and R. dos Santos Brito, "The beta power distribution," *Brazilian journal of probability and statistics*, vol. 26, no. 1, pp. 88–112, 2012.

Hindawi
Complexity
Volume 2022, Article ID 9705690, 19 pages
https://doi.org/10.1155/2022/9705690

WILEY | Hindawi

Research Article

Optimal Algorithms for Nonlinear Equations with Applications and Their Dynamics

Amir Naseem,[1] **M. A. Rehman**,[1] **and Nasr Al Din Ide**[2]

[1]*Department of Mathematics, University of Management and Technology, Lahore 54770, Pakistan*
[2]*Department of Mathematics, Faculty of Science, Aleppo University, Aleppo, Syria*

Correspondence should be addressed to Amir Naseem; amir.kasuri89@gmail.com and Nasr Al Din Ide; ide1112002@yahoo.ca

Received 16 May 2022; Accepted 18 August 2022; Published 27 September 2022

Academic Editor: Shanmugam Lakshmanan

In the present work, we introduce two novel root-finding algorithms for nonlinear scalar equations. Among these algorithms, the second one is optimal according to Kung-Traub's conjecture. It is established that the newly proposed algorithms bear the fourth- and sixth-order of convergence. To show the effectiveness of the suggested methods, we provide several real-life problems associated with engineering sciences. These problems have been solved through the suggested methods, and their numerical results proved the superiority of these methods over the other ones. Finally, we study the dynamics of the proposed methods using polynomiographs created with the help of a computer program using six cubic-degree polynomials and then give a detailed graphical comparison with similar existing methods which shows the supremacy of the presented iteration schemes with respect to convergence speed and other dynamical aspects.

1. Introduction

A huge number of complicated problems in mathematics and engineering disciplines are directly connected to the solution of transcendental and algebraic nonlinear equations of the form:

$$\varphi(x) = 0, \tag{1}$$

where the real-valued function φ is defined on the open connected set. Mostly, the direct solution of these problems is not possible to find via analytical methods, and ultimately, we have to move towards the iterative algorithms. By an algorithm, we mean a sequence of finite number of steps to achieve the required goal (solution) of the given problem. The repetition of these steps is called iterations. In the process of iterative algorithms, we always need a starting point to initialize the iteration process. This starting point is usually called the initial guess that is rectified after each iteration till the required accuracy is gained.

In literature, there is a plethora of root-finding iterative algorithms for the problems related to the nonlinear equations. The oldest, classical, and most widely used algorithm was suggested by Newton–Raphson in 1690 [1]. Geometrically, the derivation of Newton's algorithm was purely based on the concept of slope of the line. This method requires two evaluations per iteration and possesses the quadratic convergence order. For many years, Newton's method has been implemented successfully for root-finding of nonlinear problems. After that, Gutierrez and Hernández [2] presented a new family of Chebyshev–Halley type methods in Banach spaces which were utilized for root-finding of nonlinear problems. In 1993, Argyros et al. [3] discussed the applications of Halley method in Banach space. After few years, Chun [4] constructed Newton-like iteration methods which were purely designed for finding one-dimensional nonlinear equations' solution. After the construction of one step Newton-like iterative algorithms, a huge class of researchers tried to modify it and suggested a broad range of root-finding algorithms with the help of different mathematical techniques and established a class of multistep algorithm. For further details of the multistep algorithm, one can see Amiri et al. [5], Behl et al. [6], Naseem et al. [7], and Ozyapici [8]. The motivation behind these modifications is to attain higher-order and more efficient algorithms.

Ostrowski [9] and Traub [10] in the twentieth century introduced the concept of multistep iteration schemes and proposed two-step fourth-order iteration schemes with Newton's iteration method as a predictor. In 2006, Aslam Noor and Inayat Noor [11] introduced some new three-step iterative schemes and proved their third-order convergence. After that, Golbabi and Javidi [12] in 2007 presented a new cubically convergent method whose derivation is totally based on the homotopy-perturbation method. By utilizing the new series expansion of the nonlinear function, Noor et al. [13], in 2012, constructed and then analyzed some novel two-step iteration methods and discussed some special cases. These suggested schemes possessed the convergence of quadratic and cubic orders and were actually the modified form of Newton's algorithm. Kumar et al. [14] presented a novel class of sixth-order parameter-based methods for finding zeros of one-dimensional nonlinear equations in 2018. In 2019, Said Solaiman et al. [15] proposed derivative free optimal fourth-order and eighth-order versions of King's approach by combining the composition technique with rational interpolation, as well as the Pade's concept of approximation. In 2020, Chand et al. [16] developed some novel PotraPtak type optimal sixth- and eighth-order iteration methods by utilizing the idea of weight functions on the PotraPtak method for determining the approximate zeros of nonlinear models and applied them on some real-life engineering problems. The authors also analyzed the stability of the suggested schemes via basins of attraction for some cubic and quadratic polynomials. Naseem et al. [17] recently constructed and analyzed some novel ninth-order iteration schemes by implementing the idea of variational iteration and then investigated the dynamical behaviour via polynomiographs of different complex polynomials.

The main contributions of the present research are given as follows:

(i) We developed and examined two novel predictor corrector type iterative techniques, namely, Algorithm 1 and Algorithm 2, in which Newton's method is used in the predictor step.

(ii) We demonstrated that these newly created approaches have fourth- and sixth-order of convergence and are more efficient than the other well-known iterative methods of the same type.

(iii) The suggested approaches were used to solve several test cases in order to evaluate their validity and accuracy.

(iv) We compare the polynomiographs of newly proposed techniques to those of existing methods of the same category in terms of time and other dynamical aspects. The exhibited polynomiographs contain highly fascinating and attractive patterns that represent many polynomial characteristics.

The remaining sections of the paper are arranged as follows:

In Section 2, we have constructed two novel algorithms. The convergence criteria for the constructed algorithms have been discussed in Section 3. In Section 4, we solved different test problems for assuring the validity of the constructed methods. Section 5 includes the graphical properties of the constructed algorithms, and Section 6 contains the conclusion.

2. Construction of New Optimal Root-Finding Algorithms

By employing the technique of modified homotopy perturbation, Golbabai and Javidi [12] introduced the following iteration formula:

$$x_{p+1} = x_p - \frac{\varphi(x_p)}{\varphi'(x_p)} - \frac{\varphi^2(x_p)\varphi''(x_p)}{2\left[\varphi\prime^3(x_p) - \varphi(x_p)\varphi'(x_p)\varphi\prime\prime(x_p)\right]}, \tag{2}$$

which is a third-order iteration method, usually known as Javidi's method. In [18], Rafiq and Rafiullah considered Newton's iteration method in the predictor step and presented a new two-step Javidi's iteration method given as

$$y_p = x_p - \frac{\varphi(x_p)}{\varphi'(x_p)}, p = 0, 1, 2, \ldots,$$

$$x_{p+1} = y_p - \frac{\varphi(y_p)}{\varphi'(y_p)} - \frac{\varphi^2(y_p)\varphi''(y_p)}{2\left[\varphi'^3(y_p) - \varphi(y_p)\varphi'(y_p)\varphi''(y_p)\right]}. \tag{3}$$

To make it optimal, we consider the following approximations of first and second derivatives:

$$\varphi'(y_p) \approx \varphi'(x_p),$$

$$\varphi''(y_p) \approx \frac{4\varphi(x_p) + 10\varphi(y_p)}{y_p - x_p}, \tag{4}$$

$$= \eta(x_p, y_p).$$

Using the above approximations in (3), we gain new optimal root-finding algorithms having the following iterative form:

Algorithm 1.For a given x_0, compute the approximate solution x_{p+1} by the following iterative schemes:

$$y_p = x_p - \frac{\varphi(x_p)}{\varphi'(x_p)}, \quad p = 0, 1, 2, \ldots,$$

$$x_{p+1} = y_p - \frac{\varphi(y_p)}{\varphi'(y_p)} - \frac{\varphi^2(y_p)\eta(x_p, y_p)}{2\left[\varphi'^3(y_p) - \varphi(y_p)\varphi'(y_p)\eta(x_p, y_p)\right]}, \tag{5}$$

which is fourth-order optimal root-finding algorithm for nonlinear scalar equations and it utilizes three functional evaluations per iteration. It should be noted that all the terms that appeared in the denominator of Algorithm 1 must not

be zero; otherwise, the method will fail to find the approximate solution to the given problem. To achieve better convergence, we utilize the same idea as described above and add one more step as Newton's method which results in the following iterative method:

$$y_p = x_p - \frac{\varphi(x_p)}{\varphi'(x_p)}, p = 0, 1, 2, \ldots,$$

$$z_p = y_p - \frac{\varphi(y_p)}{\varphi'(x_p)} - \frac{\varphi^2(y_p)\eta(x_p, y_p)}{2\left[\varphi'^3(x_p) - \varphi(y_p)\varphi'(x_p)\eta(x_p, y_p)\right]}, \quad (6)$$

$$x_{p+1} = z_p - \frac{\varphi(z_p)}{\varphi'(z_p)}.$$

The above iteration scheme gains optimal order but does not fulfill the Kung and Traub's conjecture [19]; to fulfill this conjecture, we consider the following approximations:

$$\varphi'(z_p) \approx \frac{\varphi'(x_p)}{G(u_p, v_p, w_p)}, \quad (7)$$

where

$$\begin{aligned} G &= G(u_p, v_p, w_p), \\ &= 1 + 2u_p(1 + 3u_p + 3u_p^2) + v_p + 4w_p, \\ u_p &= \frac{\varphi(y_p)}{\varphi(x_p)}, v_p = \frac{\varphi(z_p)}{\varphi(y_p)}, w_p = \frac{\varphi(z_p)}{\varphi(x_p)}. \end{aligned} \quad (8)$$

With the help of the above approximations in (6), we are able to suggest the following algorithm:

Algorithm 2.For a given x_0, compute the approximate solution x_{p+1} by the following iterative schemes:

$$y_p = x_p - \frac{\varphi(x_p)}{\varphi'(x_p)}, \quad p = 0, 1, 2, \ldots,$$

$$z_p = y_p - \frac{\varphi(y_p)}{\varphi'(x_p)} - \frac{\varphi^2(y_p)\eta(x_p, y_p)}{2\left[\varphi'^3(x_p) - \varphi(y_p)\varphi'(x_p)\eta(x_p, y_p)\right]},$$

$$x_{p+1} = z_p - G\frac{\varphi(z_p)}{\varphi'(x_p)},$$

$$\text{where } G = G(u_p, v_p, w_p) = 1 + 2u_p(1 + 3u_p + 3u_p^2) + v_p + 4w_p, \quad (9)$$

which is a three-step optimal root-finding algorithm, having sixth convergence order and utilizing only four functional evaluations per iteration. One must keep in mind that all the terms that appeared in the denominator of Algorithm 2 must not be vanished at the initial guess in the given domain; otherwise, the method will not work properly to find the approximate solution of the given problem.

3. Convergence Analysis

This section of the paper contains the convergence analysis of the suggested iteration methods.

Theorem 1. *Suppose α be the actual root of equation $\varphi(x) = 0$. If $\varphi(x)$ is differentiable near α, Algorithm 1 is of fourth-order convergence.*

Proof. To prove the theorem, suppose α be the exact root of the equation $\varphi(x) = 0$ and e_p be p th-iteration's error, where $e_p = x_p - \alpha$, and with the help of Taylor's series expansion around $x = \alpha$, we obtain

$$\begin{aligned} \varphi(x_p) = \varphi'(\alpha)e_p + \frac{1}{2!}\varphi''(a)e_p^2 + \frac{1}{3!}\varphi'''(a)e_p^3 + \frac{1}{4!}\varphi^{(vi)}(a)e_p^4 + \frac{1}{5!}\varphi^{(v)}(a)e_p^5 \\ + \frac{1}{6!}\varphi^{(vi)}(\alpha)e_p^6 + O(e_p^7), \end{aligned} \quad (10)$$

$$\varphi(x_p) = \varphi'(a)\left[e_p + d_2e_p^2 + d_3e_p^3 + d_4e_p^4 + d_5e_p^5 + d_6e_p^6 + O(e_p^7)\right],$$

$$\varphi'(x_p) = \varphi'(\alpha)\left[1 + 2d_2e_p + 3d_3e_p^2 + 4d_4e_p^3 + 5d_5e_p^4 + 6d_6e_p^5 + 7d_7e_p^6 + O(e_p^7)\right], \quad (11)$$

where

$$\mathrm{d}_p = \frac{1}{p!}\frac{\varphi^{(p)}(\alpha)}{\varphi'(\alpha)}. \quad (12)$$

With the help of (10) and (11), we get

$$y_p = \varphi'(\alpha)\left[\alpha + d_2 e_p^2 + \left(2d_3 - 2d_2^2\right)e_p^3 + \left(3d_4 - 7d_2 d_3 + 4d_2^3\right)e_p^4 + \left(-6d_3^2 + 20d_3 d_2^2 - 10d_2 d_4 + 4d_5 - 8d_2^4\right)e_p^5 + \left(-17d_4 d_3 + 28d_4 d_2^2 - 13d_2 d_5 + 5d_6 + 33d_2 d_3^2 - 52d_3 d_2^3 + 16d_2^5\right)e_p^6 + O\left(e_p^7\right)\right]. \tag{13}$$

$$\varphi\left(y_p\right) = \varphi'(\alpha)\left[d_2 e_p^2 + \left(2d_3 - 2d_2^2\right)e_p^3 + \left(5d_2^3 - 7d_2 d_3 + 4d_4\right)e_p^4 + \left[-24d_3^2 + 12d_3 d_2^4 - 10d_2 d_4 + 4d_5 - 6d_3^2\right)e_p^5 + \left(-73d_4 d_2^3 + 34d_4 d_2^2 - 28d_2^5 + 37d_2 d_3^2 + 17d_4 d_3 13d_2 d_5 + 5d_6\right)e_p^6 + O\left(e_p^7\right)\right]. \tag{14}$$

With the help of (10), (13), and (14), we get

$$\begin{aligned}\eta\left(x_p, y_p\right) = \varphi'(\alpha)\Big[&4e^{-1} + 22d_2 + \left(40d_3 + 4d_2^2\right)e_p + \left(26d_2 d_3 - 4d_2^3 + 58d_4\right)e_p^2 \\ &+ \left(76d_5 + 44d_2 d_4 + 36d_3^2 - 40d_3 d_2^2 + 4d_2^4\right)e_p^3 + \left(94d_6 + 62d_2 d_5 + 118d_4 d_3\right. \\ &\left. - 58d_4 d_2^2 - 102d_2 d_3^2 + 64d_3 d_2^3 - 4d_2^5\right)e_p^4 + \left(112d_7 t + n80qd_2 hd_{6+} x1647d_5 Cd_3\right) \\ &- 76d_5 d_2^2 + 96d_4^2 + 72d_4 d_2^3 + 252d_3^2 d_2^2 - 108d_3 d_2^4 - 288d_4 d_2 d_3 - 76d_3^3 \\ &+ 4d_2^6\Big)e_p^5 + \left(130d_8 + 98d_2 d_7 - 314d_4 d_3^2 + 378d_2 d_3^3 - 596d_3^2 d_2^3 + 192d_3 d_2^5\right. \\ &- 200d_2 d_4^2 + 266d_4 d_5 - 76d_4 d_2^4 + 90d_5 d_2^3 - 94d_6 d_2^2 - 372d_3 d_2 d_5 + 596d_3 d_4 d_2^2 \\ &\left. - 4d_2^7 210d_3 d_6\right)e_p^6 + O\left(e_p^7\right)\Big].\end{aligned} \tag{15}$$

Using equations (10)–(15) in Algorithm 1, we obtain

$$x_{p+1} = \alpha - \left(8d_2^3 + d_2 d_3\right)e_p^4 + O\left(e^5\right), \tag{16}$$

which implies that

$$e_{p+1} = \alpha - \left(8d_2^3 + d_2 d_3\right)e_p^4 + O\left(e^5\right). \tag{17}$$

The above equations confirms that Algorithm 1 is of fourth-order convergence. □

Theorem 2. *Suppose α be the actual root of $\varphi(x) = 0$. If $\varphi(x)$ is differentiable near α, Algorithm 2 is of sixth-order convergence.*

Proof. From equations (10)–(15) with the same assumptions of the previous theorem, we have

$$\begin{aligned}\eta\left(x_p, y_p\right) = \varphi'(\alpha)\Big[&2d_2 + (6d_2 d_3 - 2d_4)e_p^2 + \left(12d_3^2 - 12d_3 d_2^2 + 4d_2 d_4 - 4d_5\right)e_p^3 + \left(2d_2 d_5\right. \\ &\left. - 26d_3 d_4 - 42d_2 d_3^2 + 24d_3 d_2^3 + 2d_4 d_2^2 - 6d_6\right)e_p^4 + \left(-48d_4 d_2 d_3 + 12d_4^2 - 24d_4 d_2^3\right. \\ &\left. + 28d_5 d_3 + 4d_5 d_2^2 + 120d_3^2 d_2^2 - 48d_3 d_2^4 - 8d_7 - 36d_3^3\right)e_p^5 + \left(-60d_5 d_2 d_3 + 28d_4 d_3 d_2^2\right. \\ &\left. - 2d_2 d_7 + 22d_5 d_4 - 10d_5 d_2^3 + 30d_6 d_3 + 6d_6 d_2^2 + 20d_2 d_4^2 - 86d_4 d_3^2 + 88d_4 d_2^4\right. \\ &\left. + 198d_2 d_3^3 - 312d_3^2 d_2^3 + 96d_3 d_2^5 - 10d_8\right)e_p^6 + O\left(e_p^7\right)\Big].\end{aligned} \tag{18}$$

where $G = G\left(u_p, v_p, w_p\right)$

$= 1 + 2u_p\left(1 + 3u_p + 3u_p^2\right) + v_p + 4w_p,$

$$z_p = \varphi'(\alpha)\left[\alpha + \left(-8d_2^3 - c2d_3\right)e_p^4 + \left(-2d_2d_4 - 46d_3d_2^2 + 22d_2^4 - 2d_3^2\right)e_p^5 + \left(-3d_2d_5 - 7d_4d_3 - 69d_4d_2^2 - 90d_2d_3^2 + 124d_3d_2^3 - 118d_2^5\right)e_p^6 + \left(-272d_4d_2d_3 - 4d_2d_6 - 10d_5d_3 - 92d_5d_2^2 + 164d_4d_2^3 + 220d_3^2d_2^2 - 1028d_3d_2^4 - 6d_4^2 - 60d_3^3 + 388d_2^6\right)e_p^7 + \left(-364d_3d_2d_5 + 529d_3d_4d_2^2 - 5d_2d_7 - 274d_4d_3^2 + 93d_2d_3^3 - 3681d_3^2d_2^3 + 3586d_3d_2^5 - 206d_2d_4^2 - 17d_4d_5 - 1502d_4d_2^4 + 203d_5d_2^3 - 115d_6d_2^2 - 13d_3d_6 - 1743d_2^7\right)e_p^8 + O\left(e_p^9\right)\right], \tag{19}$$

$$\varphi\left(z_p\right) = \varphi'(\alpha)\left[\left(-8d_2^3 - c2d_3\right)e_p^4 + \left(-2d_2d_4 - 46d_3d_2^2 + 22d_2^4 - 2d_3^2\right)e_p^5 + \left(-3d_2d_5 - 7d_4d_3 - 69d_4d_2^2 - 90d_2d_3^2 + 124d_3d_2^3 - 118d_2^5\right)e_p^6 + \left(-272d_4d_2d_3 - 4d_2d_6 - 10d_5d_3 - 92d_5d_2^2 + 164d_4d_2^3 + 220d_3^2d_2^2 - 1028d_3d_2^4 - 6d_4^2 - 60d_3^3 + 388d_2^6\right)e_p^7 + \left(-364d_3d_2d_5 + 529d_3d_4d_2^2 - 5d_2d_7 - 274d_4d_3^2 + 93d_2d_3^3 - 3681d_3^2d_2^3 + 3586d_3d_2^5 - 206d_2d_4^2 - 17d_4d_5 - 1502d_4d_2^4 + 203d_5d_2^3 - 115d_6d_2^2 - 13d_3d_6 - 1743d_2^7\right)e_p^8 + O\left(e_p^9\right)\right], \tag{20}$$

$$u_p = \varphi'(\alpha)\left[\alpha + \left(2d_3 - 3d_2^2\right)e_p^4 + \left(8d_2^3 - 10d_2d_3 + 3d_4\right)e_p^5 + \left(37d_3d_2^2 - 20d_2^4 - 14d_2d_4 + 4d_5 - 8d_3^2\right)e_p^6 + \left(-118d_3d_2^3 + 51d_4d_2^2 + 48d_2^5 + 55d_2d_3^2 - 18d_2d_5 + 5d_622d_4d_3\right)e_p^5 + \left(150d_4d_2d_3 + 6d_7 - 22d_2d_6 - 28d_5d_3 + 65d_5d_2^2 - 163d_4d_2^3 - 252d_3^2d_2^2 + 344d_3d_2^4 - 15d_4^2 + 26d_3^3 - 112d_2^6\right)e_p^6 + \left(190d_3d_2d_5 - 693d_3d_4d_2^2 + 7d_8 - 26d_2d_7 + 105d_4d_3^2 - 228d_2d_3^3 + 952d_3^2d_2^3 - 944d_3d_2^5 + 102d_2d_4^2 - 38d_4d_5 + 480d_4d_2^4 - 207d_5d_2^3 + 79d_6d_2^2 - 34d_3d_6 + 256d_2^7\right)e_p^7 + \left(258d_4d_2d_5 - 936d_4d_2d_3^2 + 2660d_4d_3d_2^3 - 876d_5d_3d_2^2 + 230d_6d_2d_3 + 8d_9 - 30d_2d_8 - 46d_4d_6 + 141d_4^2d_3 - 477d_4^2d_2^2 - 1336d_4d_2^5 + 132d_5d_2^3 + 607d_5d_2^4 - 40d_7d_3 + 93d_7d_2^2 - 251d_6d_2^3 + 1254d_3^2d_2^2 - 3200d_3^2d_2^4 + 2480d_3d_2^6 - 24d_5^2 - 72d_3^4 - 576d_2^8\right)e_p^8 + O\left(e_p^9\right)\right], \tag{21}$$

$$v_p = \varphi'(\alpha)\left[\left(-8d_2^2 - c3\right)e_p^4 + \left(-2d_4 - 32d_2d_3 + 6d_2^3\right)e_p^5 + \left(-66d_2^4 - 3d_3d_2^2 - 49d_2d_4 - 33d_3^2 - 3d_5\right)e_p^6 + \left(-102d_4d_3 - 4d_6 - 66d_2d_5 - 22d_4d_2^2 - 88d_2d_3^2 - 520d_3d_2^3 + 130d_2^5\right)e_p^5 + \left(-138d_5d_3 - 339d_4d_2d_3 - 5d_7 - 117d_3^3 - 1645d_3^2d_2^2771d_3d_2^4 - 79d_4^2 - 795d_4d_3^2 - 42d_5d_2^2 - 83d_2d_6 - 793d_2^6\right)e_p^6 + \left(-214d_4d_5 - 608d_4d_3^2 - 5138d_3d_4d_2^2 - 506d_3d_2d_5 - 174d_3d_6 - 6d_8 + 312d_2d_4^2 + 914d_4d_2^4 - 1066d_5d_2^3 - 100d_2d_7 - 62d_6d_2^2 - 2464d_2d_3^3 + 828d_3^2d_2^3 - 8702d_3d_2^5 + 2686d_2^7\right)e_p^7 + \left(-915d_4d_2d_5 - 869d_5d_3^2 - 6964d_5d_3d_2^2 - 210d_7d_3 - 270d_4d_6 - 673d_6d_2d_3 - 1038d_4^2d_3 - 11738d_4d_2d_3^2 + 347d_4d_3d_2^3 - 7d_9 + 28970d_3d_2^6 - 145d_5^2 + 1030d_5d_2^4 - 117d_2d_8 - 82d_7d_2^2 - 1338d_6d_2^3 - 4034d_4^2d_2^2 - 12825d_4d_2^5 - 1453d_3^4 - 3392d_3^3d_2^2 - 41833d_3^2d_2^4 - 13161d_2^8\right)e_p^8 + O\left(e_p^9\right)\right], \tag{22}$$

$$w_p = \varphi'(\alpha)\left[\left(-8d_2^3 - c2d_3\right)e_p^4 + \left(-2d_2d_4 - 45d_3d_2^2 + 30d_2^4 - 2d_3^2\right)e_p^5 + \left(177d_3d_2^3 - 87d_2d_3^2 - 3d_2d_5 - 7d_4d_3 - 67d_4d_2^2 - 148d_2^5\right)e_p^6 + \left(239d_4d_2^3 - 262d_4d_2d_3 - 4d_2d_6 - 10d_5d_3 - 89d_5d_2^2 + 352d_3^2d_2^2e_p^5 + 1235d_3d_2^4 - 6d_4^2 - 58d_3^3 + 536d_2^6\right)e_p^6 + \left(-350d_3d_2d_5 + 903d_3d_4d_2^2 - 5d_2d_7 - 265d_4d_3^2 + 238d_2d_3^3 - 4209d_3^2d_2^3 + 4985d_3d_2^5 - 198d_2d_4^2 - 17d_4d_5 - 1771d_4d_2^4 + 300d_5d_2^3 - 111d_6d_2^2 - 13d_3d_6 - 2215d_2^7\right)e_p^7 + \left(-530d_4d_2d_5 + 768d_4d_2d_3^2 - 12203d_4d_3d_2^3 + 1096d_5d_3d_2^2 - 438d_6d_2d_3 - 6d_2d_8 - 22d_4d_6 - 405d_4^2d_3 + 563d_4^2d_2^2 + 6931d_4d_2^5 - 356d_5d_3^2 - 2300d_5d_2^4 - 16d_7d_3 - 133d_7d_2^2 + 361d_6d_2^3 - 7436d_3^3d_2^2 + 18656d_3^2d_2^4 - 25327d_3d_2^6 - 12d_5^2 + 4d_3^4 + 8609d_2^8\right)e_p^8 + O\left(e_p^9\right)\right], \tag{23}$$

$$
\begin{aligned}
G(u_p, v_p, w_p) = \varphi'(\alpha)\big[1 &+ 2d_2e_p + \left(3d_3 - 8d_2^2\right)e_p^4 + \left(-40d_2^3 - 32d_2d_3 + 4d_4\right)e_p^5 + \left(5d_5 - 49d_2d\right.\\
&-265d_3d_2^2 + 33d_3^2 + 110d_2^4\big)e_p^6 + \left(6d_6 - 66d_2d_5 - 102d_4d_3 - 410d_4d_2^2 - 590d_2d_3^2\right.\\
&+552d_3d_2^3 - 588d_2^5\big)e_p^6 + \left(-1831d_4d_2d_3 + 7d_7 - 83d_2d_6 - 138d_5d_3 - 556d_5d_2^2\right.\\
&+663d_4d_2^3 + 615d_3^2d_2^2 - 5023d_3d_2^4 - 79d_4^2 - 441d_3^3 + 1421d_2^6\big)e_p^7 + \left(-2486d_3d_2d_5\right.\\
&+784d_3d_4d_2^2 + 8d_8 - 100d_2d_7 - 2058d_4d_3^2 - 672d_2d_3^3 - 18094d_3^2d_2^3 + 11042d_3d_2^5\\
&-1422d_2d_4^2 - 214d_4d_5 - 7286d_4d_2^4 + 776d_5d_2^3 - 702d_6d_2^2 - 174d_3d_6 - 5182d_2^7\big)e_p^7\\
&+\left(-3863d_4d_2d_5 - 5330d_4d_2d_3^2 - 53693d_4d_3d_2^3 + 348d_5d_3d_2^2 - 3141d_6d_2d_3 + 9d_9\right.\\
&-117d_2d_8 - 270d_4d_6 - 3204d_4^2d_3 - 228d_4^2d_2^2 + 14345d_4d_2^5 - 2797d_5d_3^2 - 9554d_5d_2^4\\
&-210d_7d_3 - 848d_7d_2^2 + 888d_6d_2^3 - 35200d_3^3d_2^2 + 28233d_3^2d_2^4 - 58240d_3d_2^6 - 145d_5^2\\
&\left.-1149d_3^4 + 14579d_2^8\big)e_p^8 + O\left(e_p^9\right)\right].
\end{aligned}
\tag{24}
$$

Using equations (10)–(24) in Algorithm 2, we get

$$
x_{p+1} = \alpha + \left(-8d_3d_2^3 - 64d_2^5\right)e_p^6 + O\left(e^7\right), \tag{25}
$$

which implies that

$$
e_{p+1} = \alpha + \left(-8d_3d_2^3 - 64d_2^5\right)e_p^6 + O\left(e^7\right). \tag{26}
$$

The above equations confirm that Algorithm 2 is of sixth-order convergence. □

4. Numerical Comparisons and Applications

To demonstrate the applicability and effectiveness of our newly devised iterative approaches, we present five real-world engineering problems and one very important and well-known nonlinear problem in this section. The devised iterative approaches are compared to the following existing two-step iterative algorithms:

4.1. Noor's Method One (NM1). For the given initial guess x_0, calculate the approximate solution x_{p+1} using the iteration schemes as follows:

$$
\begin{aligned}
x_{p+1} &= x_p - \frac{\varphi(x_p)}{\varphi'(x_p)}, \quad p = 0, 1, 2, 3, \ldots,\\
x_{p+1} &= x_p - \frac{\varphi(x_p)}{\varphi'(x_p)} + \left[\frac{\varphi(x_p)}{\varphi'(x_p)}\right]\frac{\varphi'(y_p)}{\varphi'(x_p)},
\end{aligned}
\tag{27}
$$

which is the second-order convergent method, known as Noor's method one [11] for solving nonlinear scalar equations.

4.2. Chun's Method (CM). For a given initial guess x_0, determine the approximate root x_{p+1} with the iteration schemes:

$$
\begin{aligned}
y_p &= x_p - \frac{\varphi(x_p)}{\varphi'(x_p)}, \quad p = 0, 1, 2, 3, \ldots,\\
x_{p+1} &= x_p - \frac{\varphi(x_p)}{\varphi'(x_p)} + \left[1 + \frac{\varphi(y_p)}{\varphi(x_p)} + 2\left(\frac{\varphi(y_p)}{\varphi(x_p)}\right)^2\right],
\end{aligned}
\tag{28}
$$

which is the fourth-order convergent Chun's method [20] for solving nonlinear scalar equations.

4.3. Chand's Method (CHM). For the given initial guess x_0, calculate the approximate solution x_{p+1} using the iteration schemes:

$$
\begin{aligned}
y_p &= x_p - \frac{\varphi(x_p)}{\varphi'(x_p)}, \quad p = 0, 1, 2, 3, \ldots,\\
x_{p+1} &= x_p - \frac{\varphi(x_p) + \varphi(y_p)}{\varphi'(x_p)} + \left[1 + 2\left(\frac{\varphi(y_p)}{\varphi(x_p)}\right)^2\right],
\end{aligned}
\tag{29}
$$

which is the fourth-order two-step Chand's method [16] for solving nonlinear scalar equations.

4.4. Noor's Method Two (NM2). For the given initial guess x_0, calculate the approximate solution x_{p+1} using the iteration schemes:

$$
\begin{aligned}
y_p &= x_p - \frac{\varphi(x_p)}{\varphi'(x_p)}, \quad p = 0, 1, 2, 3, \ldots,\\
z_p &= -\frac{\varphi(x_p)}{\varphi'(x_p)},\\
x_{p+1} &= x_p - \frac{\varphi(x_p)}{\varphi'(x_p)} + \left[1 + \frac{\varphi(y_p + z_p)}{\varphi(x_p)}\right],
\end{aligned}
\tag{30}
$$

which is three-step cubic-order Noor's method two [13] for solving nonlinear scalar equations.

4.5. Yun's Method (YM). For the given initial guess x_0, calculate the approximate solution x_{p+1} using the iteration schemes:

$$\begin{aligned} y_p &= x_p - \frac{\varphi(x_p)}{\varphi'(x_p)}, \quad p = 0, 1, 2, 3, \ldots, \\ z_p &= -\frac{\varphi(y_p)}{\varphi'(x_p)}, \\ x_{p+1} &= x_p - \frac{\varphi(x_p)}{\varphi'(x_p)} + -\frac{\varphi(y_p)}{\varphi'(x_p)} - \frac{\varphi(y_p + z_p)}{\varphi(x_p)}, \end{aligned} \tag{31}$$

which is the three-step Yun's method [21] for solving nonlinear scalar equations, having the convergence of fourth order. We evaluate the following test examples to conduct a numerical comparison of the above-described methods with our proposed algorithms:

Example 1. Kinetic problem equation.

The equation of kinetic problem has the following form:

$$e^{21000/T} = 1.11 \times 10^{11} T^2, \tag{32}$$

Where Trepresents the temperature of the given system. (32) has been derived from the stirred reactor with the cooling coils [22]. By taking $T = x$, (32) may be rewritten in form of the following nonlinear function:

$$\varphi_1(x) = x^{-2} e^{21000/x} - 1.11 \times 10^{11}, \tag{33}$$

which can be used to find the temperature of the system. We start the iteration process with the initial guess $x_0 = 430$, and the related results from various iteration techniques are shown in Table 1.

Example 2. Planck's radiation law.

The Planck's radiation law [23] is used to compute the energy density within an isothermal black body with the standard form as

$$\varphi(\sigma) = \frac{8\pi cP}{\sigma^5 \left(e^{cP/\sigma kT} - 1\right)}. \tag{34}$$

Assume that we want to determine the wavelength sigma_1 that corresponds to maximal energy density $\varphi(\sigma_1)$. We use $x = cP/\sigma kT$ to turn the aforementioned problem into a nonlinear equation, which has the following nonlinear equation:

$$1 - \frac{x}{5} = e^{-x}, \tag{35}$$

which can be converted into the form of nonlinear function as follows:

$$\varphi_2(x) = e^{-x} + \frac{x}{5} - 1. \tag{36}$$

The maximal wavelength of the radiation is represented by the estimated root of the aforementioned function φ_2. To begin the iteration process, we take the starting guess $x_0 = 0.2$, and the relevant results from various iteration methods are shown in Table 2.

Example 3. Adiabatic flame temperature equation.

The equation of adiabatic flame temperature has the following form:

$$\varphi_3(x) = \Delta H - a_1(298 - x) - \frac{a_2}{2}\left(298^2 - x^2\right) - \frac{a_3}{3}\left(298^3 - x^3\right), \tag{37}$$

where we take $\Delta H = -57798, a_1 = 7.256, a_2 = 0.002298,$ and $a_3 = 0.00000283$. For more information, one may see [24, 25] and the references are cited therein. The aforementioned function φ_3 is actually a third-degree polynomial, and according to algebra's fundamental theorem, it must have three unique roots (zeros) and $\alpha = 4305.309913666125563040198929 45$ is a simple one among them that we estimated using the proposed algorithms with the starting guess $x_0 = 2000$, and the numerical results are presented in Table 3.

Example 4. Beam designing model.

We consider the problem of beam positioning from [26], which yields a nonlinear function as

$$\varphi_4(x) = x^4 + 4x^3 - 24x^2 + 16x + 16. \tag{38}$$

The given function φ_4 is actually a four-degree polynomial, and it must have precisely four roots (zeros) in the light of fundamental theorem of algebra. We choose the starting guess $x_0 = -0.75$ to approximate the required root using the proposed algorithms, and the numerical results are shown in Table 4.

Example 5. Open channel flow problem.

In fluid dynamics, Manning's equation (27) deals with the water flow with the following standard form:

$$\text{water flow} = F = \frac{\sqrt{\text{sar}}^{2/3}}{N}. \tag{39}$$

In (39), the symbol s stands for the slope, a stands for the area, r stands for the hydraulic radius, and n stands for Manning's roughness coefficient. For a channel with the rectangular-shape of width w and depth x, we may have

$$a = wx, \& r = \frac{wx}{w + 2x}. \tag{40}$$

Using these values in (39), we obtain

$$F = \frac{\sqrt{s}\, wx}{N}\left(\frac{wx}{w + 2x}\right)^{2/3}. \tag{41}$$

In order to compute water's depth in a channel, we rewrite (41) in the following nonlinear form:

Table 1: Numerical comparison of various root-finding algorithms for the problem φ_1.

Method $\varphi_1(x)$, $x_0 = 430.000$	N	x_{p+1}	$\lvert\varphi(x_{p+1})\rvert$	$\sigma = \lvert x_{p+1} - x_p\rvert$	CPU time
NM1	12	551.773824930326599636215866007540	$7.093691e-23$	$4.808708e-16$	3.065
CM	10	551.773824930326599636215866007312	$1.837158e-18$	$9.899467e-07$	3.128
CHM	10	551.773824930326599636215866007540	$2.258490e-46$	$1.218702e-13$	3.190
NM2	15	551.773824930326599636215866007540	$2.913370e-27$	$3.081698e-18$	3.253
YM	10	551.773824930326599636215865875416	$1.064742e-15$	$4.946704e-06$	3.331
Algorithm 1	9	551.773824930326599636215866007540	$1.608420e-26$	$1.509462e-08$	2.626
Algorithm 2	8	551.773824930326599636215866007540	$8.779657e-72$	$2.409901e-13$	2.704

Table 2: Numerical comparison of various root-finding algorithms for the problem φ_2.

Method $\varphi_2(x)$, $x_0 = 0.20$	N	x_{p+1}	$\lvert\varphi(x_{p+1})\rvert$	$\sigma = \lvert x_{p+1} - x_p\rvert$	CPU time
NM1	5	0.00000000000000000000003947489	$3.157991e-24$	$2.513162e-12$	3.521
CM	3	−0.00000000000000000000000000000	$1.571613e-40$	$1.158532e-10$	3.600
CHM	3	−0.00000000000000000000000000000	$1.750456e-48$	$1.380631e-12$	3.663
NM2	5	−0.00000000000000000000000019832	$1.586544e-26$	$1.781316e-13$	3.707
YM	3	−0.00000000000000000000000000000	$2.329495e-42$	$4.155449e-11$	3.403
Algorithm 1	3	0.00000000000000000000000000000	$2.160782e-52$	$2.134128e-13$	2.934
Algorithm 2	2	0.00000000000000000000232846266	$1.862770e-22$	$1.814949e-04$	2.986

Table 3: Numerical comparison of various root-finding algorithms for the problem φ_3.

Method $\varphi_3(x)$, $x_0 = 2000.00$	N	x_{p+1}	$\lvert\varphi(x_{p+1})\rvert$	$\sigma = \lvert x_{p+1} - x_p\rvert$	CPU time
NM1	11	4305.309913666125563020922754179909	$4.316939e-16$	$4.270236e-07$	3.281
CM	4	4305.309913666125563040198929446342	$2.174776e-55$	$6.493737e-12$	3.329
CHM	3	4305.309913666125563040198929446342	$5.855416e-30$	$1.704358e-05$	3.391
NM2	6	4305.309913666125563040199102978796	$3.886295e-21$	$1.281244e-09$	3.322
YM	4	4305.309913666125563040198929446342	$5.772631e-71$	$8.594129e-16$	3.468
Algorithm 1	4	4305.309913666125563040198928972873	$1.060344e-23$	$1.332626e-05$	2.516
Algorithm 2	3	4305.309913666125563040116005825452	$1.857091e-18$	$6.740210e-01$	2.547

Table 4: Numerical comparison of various root-finding algorithms for the problem φ_4.

Method $\varphi_4(x)$, $x_0 = -0.75$	N	x_{p+1}	$\lvert\varphi(x_{p+1})\rvert$	$\sigma = \lvert x_{p+1} - x_p\rvert$	CPU time
NM1	4	−0.535898384862245344805625149808	$3.035870e-15$	$1.028354e-08$	3.650
CM	3	−0.535898384862245412945107316988	$4.071744e-45$	$2.889668e-12$	3.712
CHM	3	−0.535898384862245412945107316988	$1.105351e-48$	$4.228953e-13$	3.743
NM2	5	−0.535898384862245412945107316989	$2.255247e-29$	$8.863356e-16$	3.808
YM	3	−0.535898384862245412945107316988	$1.563471e-46$	$1.345709e-12$	3.854
Algorithm 1	3	−0.535898384862245412945838932746	$3.259623e-20$	$9.586839e-08$	2.670
Algorithm 2	2	−0.535898384862245404466362113905	$3.777599e-16$	$1.027830e-03$	2.732

$$\varphi_5(x) = \frac{\sqrt{swx}}{N}\left(\frac{wx}{w+2x}\right)^{2/3} - F. \tag{42}$$

In (42), the parameters haven been chosen as $w = 4.572m$, $s = 0.017$, $F = 14.15m^3/s$, and $N = 0.0015$. We start the iteration process with the initial guess $x_0 = 0.1$, and the related results from various iteration techniques are shown in Table 5.

Example 6. A well-known nonlinear problem.

To analyze the proposed methods, we consider the following very important and well-known nonlinear problem:

$$x = \tan x. \tag{43}$$

The above equation in the form of nonlinear function φ_6 can be rewritten as

$$\varphi_6(x) = x - \tan x. \tag{44}$$

Table 5: Numerical comparison among different algorithms for the problem φ_5.

Method $\varphi_5(x)$, $x_0 = 0.10$	N	x_{p+1}	$\lvert\varphi(x_{p+1})\rvert$	$\sigma = \lvert x_{p+1} - x_p\rvert$	CPU time
NM1	7	1.46509122029582464237602073145 3	2.422027$e-24$	1.334423$e-12$	2.943
CM	4	1.46509122029582464237602109248 6	2.481534$e-24$	2.175366$e-06$	3.391
CHM	4	1.46509122029582464237602450984 2	4.889610$e-23$	4.918775$e-06$	3.468
NM2	6	1.46509122029582464238381925535 9	1.059172$e-19$	2.790535$e-10$	3.431
YM	4	1.46509122029582464237602090977 9	4.475999$e-35$	5.351749$e-09$	3.593
Algorithm 1	4	1.46509122029582464237602090982 5	6.277761$e-28$	3.483992$e-07$	2.826
Algorithm 2	3	1.46509122029582464237602090977 9	8.454782$e-89$	5.011500$e-15$	2.920

We start the iteration process with the initial guess $x_0 = 1.0$, and the related results from various iteration techniques are shown in Table 6.

The machine used for computing numerical results has the following specifications:

(i) 64 bit operating system

(ii) x64-based processor with Core(TM) m3-7Y30 CPU@1.00 GHz 1.61 GHz

(iii) 8 GB of memory

We use the accuracy $\varepsilon = 10^{-15}$ in the stopping criteria $\lvert x_{p+1} - x_p\rvert < \varepsilon$ for the all aforementioned problems. We used the computer application Maple 13 to compute all of the numerical results and can be observed in Tables 1–6.

Tables 1–6 represent the detailed comparison of the suggested root-finding methods with the other above-described methods for the engineering and arbitrary problems φ_1–φ_6. In the columns of the above-presented tables, N stands for the consumption of the iterations for different methods, $\lvert\varphi(x)\rvert$ stands for the modulus value of $\varphi(x)$, x_{p+1} represents the final estimation, $\lvert x_{p+1} - x_p\rvert$ stands for the positive distance between the two consecutive estimations, and the last columns gives us the information about the CPU time consumption in seconds for different methods in comparison.

The careful examination of the obtained results in Tables 1–6 certifies that the proposed root-finding algorithms are showing better efficiency and performance which justified the supremacy of the suggested root-finding algorithms with respect to CPU-time consumption, accuracy, convergence-speed, no. of iterations, and computational order of convergence against the other comparable methods.

5. Dynamical Representation

In this section, we investigate the dynamical aspects of different algorithms with the aid of polynomiographs created through different algorithms for complex polynomials of different degrees. To generate polynomiographs of different complex polynomials by means of a computer program, we have to choose an initial rectangle $\mathscr{R}$ which contains the polynomial's roots. Then, corresponding to each starting point w_0 in the region, we execute an iterative process and then colour the point corresponding to w_0 that relies on the approximate convergence of the truncated orbit to a root. The discretization of $\mathscr{R}$ is completely responsible for the image's resolution quality. For instance, if we discretize $\mathscr{R}$ into a 2000 by 2000 grid, the output is a high-resolution picture.

We know that any complex polynomial q having degree n has exactly n-roots, and from the fundamental theorem of algebra, it may be uniquely defined as

$$q(w) = c_n w^n + c_{n-1} w^{n-1} + \cdots + c_1 w + c_0. \tag{45}$$

or by its zeros (roots) $\{w_1, w_2, \ldots, w_{n-1}, w_p\}$:

$$q(w) = (w - w_1)(w - w_2)\cdots(w - w_p). \tag{46}$$

where $\{c_n, c_{n-1}, \ldots, c_1, c_0\}$ are the complex coefficients.

The iterative algorithms can be easily applied to the both representations of the complex polynomial q. The polynomial's degree depicts the number of basins of attraction. The location of basins can be managed by changing the position of roots in the complex plane manually. The polynomiographs' colours depends upon the no. of iterations needed to attain the approximate solution of some polynomial with a given accuracy and a chosen scheme of iteration.

The main algorithm for drawing polynomiographs is given in Algorithm.

In Algorithm 3, the convergence test $(w_p + 1, w_p, \epsilon)$ would be considered true in case of convergence and vice versa. The following is the standard form of the widely used convergence test:

$$\left|w_{p+1} - w_p\right| < \epsilon. \tag{47}$$

In (47), w_p and w_{p+1} are the consecutive estimations in the iteration procedure, and the symbol $\varepsilon > 0$ stands for the accuracy. In this article, we also use the stopping criteria (47). We created visually appealing and intriguing polynomiographs using newly developed root-finding methods and compared them with the polynomiographs of the other similar methods. The colour of polynomiographs is determined by the no. of iterations required to estimate the roots of a polynomial with a certain precision ε. A huge number of similar graphics may be made by changing the value of the parameter k, where k specifies the maximum no. of iterations. The work on polynomiography was first initiated by Kalantri [28–30] who described its artistic applications in different fields of science and arts. Gdawiec et al. [31, 32] put forward the work of Kalantri and presented fractal patterns of polynomial root-finding methods. Scott et al. [33], in 2011, worked on the basis of attraction for different existing methods and compared them with respect to their basis. In

Table 6: Numerical comparison among different algorithms for the problem φ_6.

Method $\varphi_6(x)$, $x_0 = 0.10$	N	x_{p+1}	$\lvert\varphi(x_{p+1})\rvert$	$\sigma = \lvert x_{p+1} - x_p\rvert$	CPU time
NM1	15	0.00002608876646998465898868 5903	5.918878$e-15$	2.809559$e-05$	2.728
CM	16	0.00002818293639540981813247 4046	7.461695$e-15$	2.714568$e-05$	2.791
CHM	16	0.00001601522608756049175252 9952	1.369235$e-15$	1.653393$e-05$	2.822
NM2	22	0.00002182070311849458609793 9226	3.463259$e-15$	1.420995$e-05$	2.460
YM	16	0.00002655497860302085053013 4645	6.241897$e-15$	2.583725$e-05$	2.907
Algorithm 1	15	0.00001877077528720948812608 5980	2.204578$e-15$	2.149290$e-05$	2.600
Algorithm 2	8	0.00001819989851890705509229 3023	2.009489$e-15$	6.032757$e-05$	2.663

Input: $q \in C$—polynomial, $A \subset C$—area, k—max. no. of iterations, I—iteration method, ϵ—accuracy, colormap $[0 \ldots C-1]$—colormap with C colors.
Output: polynomiograph corresponding to polynomial q.
for $w_0 \in A$ do
  $i = 0$
  while $i \leq k$ do
    $w_{p+1} = I(w_p)$
    if $|w_{p+1} - w_p| < \epsilon$, then
      break
    $i = i + 1$
Colour w_0 by means of colormap.

Algorithm 3: Polynomiograph's generation.

this sense, the polynomiography gives us a new way to analyze the graphical behaviors of different existing methods in the literature.

We investigate the following complex polynomials for the aim of generating polynomiographs using the suggested methods, and we compare them with other well-known two-step iteration methods.

$$q_1(w) = w^3 - 1, q_2(w) = w^3 - w.i - 1, q_3(w), = w^3 + w.i + 1, q_4(w) = w^3 - w^2 + w - 1, \quad (48)$$
$$q_5(w) = w^3 + w^2 + w + 1, q_6(w) = w^3.i - w^2 + i.$$

The colormap that has been used for the coloring of iterations in the generation of polynomiographs is presented in Figure 1:

Example 7. Polynomiographs corresponding to polynomial $q_1(w)$ through various numerical algorithms.

In this example, we investigate and compare the dynamical results obtained through different iteration schemes with our presented algorithms by considering the cubic polynomial $w^3 - 1$ which possesses three distinct simple zeros: $1, -1/2 - \sqrt{3}/2i$, and $-1/2 + \sqrt{3}/2i$. We executed all the algorithms to achieve the simple zeros of the considered polynomials, and the results can be visualized in Figures 2–8.

Example 8. Polynomiographs corresponding to polynomial $q_2(w)$ through various numerical algorithms.

This example includes the dynamical comparison of the suggested iteration schemes with different similar-nature iterative algorithms by taking the cubic complex polynomial $w^3 - w.i - 1$. The degree of this complex polynomial is three, and according to the fundamental theorem of algebra, it has exactly three roots which are all simple and given as $(1/6)3[4 + (4/9)\sqrt{81 + 12i}]^{2/3} + 4i/4 + (4/9)\sqrt{81 + 12i}^{1/3}$, $(1/12)[3i(4 + (4/9)\sqrt{81 + 12i})^{2/3} + 4] \quad \sqrt{3} - 3[4 + (4/9)\sqrt{81 + 12i}]^{2/3} - 4i/4 + (4/9)\sqrt{81 + 12i}^{1/3}$, and $(1/12)[3i(4 + (4/9)\sqrt{81 + 12i})^{2/3} - 4] \quad \sqrt{3} - 3[4 + (4/9) \quad \sqrt{81 + 12i}]^{2/3} - 4i/4 + (4/9)\sqrt{81 + 12i}^{1/3}$. Using computer program, we executed all the iteration processes, and the corresponding results can be seen in Figures 9–15.

Example 9. Polynomiographs corresponding to polynomial $q_3(w)$ through various numerical algorithms.

We consider the complex polynomial $w^3 + w.i + 1$ in this experiment for analyzing the behaviors of different iteration schemes graphically. For this purpose, we generated the polynomiographs of the considered polynomials whose simple zeros are $(1/6)3[4 + (4/9) \quad \sqrt{81 + 12i}]^{2/3} + 4i/4 + (4/9)\sqrt{81 + 12i}^{1/3}$ and $(1/12)[3i(4 + (4/9)\sqrt{81 + 12i})^{2/3} + 4]\sqrt{3} - 3[4 + (4/9)\sqrt{81 + 12i}]^{2/3} - 4i/4 + (4/9)\sqrt{81} \quad +12i^{1/3}(1/12)[3i(4 + (4/9) \quad \sqrt{81 + 12i})^{2/3} - 4] \quad \sqrt{3} - 3[4 + (4/9)\sqrt{81 + 12i}]^{2/3} \quad -4i/4 + (4/9)\sqrt{81 + 12i}^{1/3}$, and the corresponding dynamic results are presented in Figures 16–22.

Example 10. Polynomiographs corresponding to polynomial $q_4(w)$ through various numerical algorithms.

In this example, we show the dynamics of different iteration schemes in the form of polynomiographs by taking the complex polynomial $w^3 - w^2 + w - 1$, whose simple zeros are 1, i, and $-i$ that can be visualized easily on the complex planes of the corresponding polynomiographs that are shown in Figures 23–29.

Example 11. Polynomiographs corresponding to polynomial $q_5(w)$ through various numerical algorithms.

In the eleventh example, we take the polynomial $w^3 + w^2 + w + 1$, having simple zeros -1, i, and $-i$. To draw the polynomiographs, we executed all the iteration schemes with the help of computer program, and the corresponding graphical objects can be visualized in Figures 30–36.

Example 12. Polynomiographs corresponding to polynomial $q_6(w)$ through various numerical algorithms.

In the last and final experiment, we show the graphical representations of different iteration schemes by generating

Figure 1: The colormap used for generating polynomiographs.

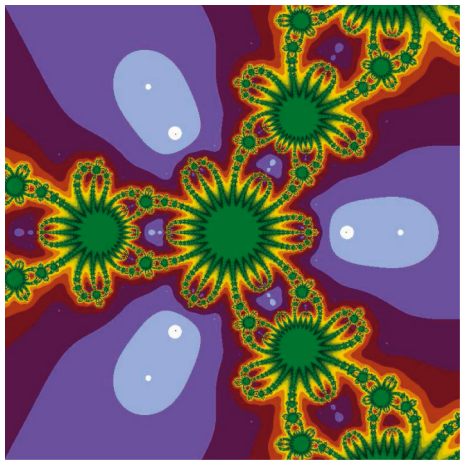

Figure 2: Polynomiograph for $q_1(w)$ using NM1.

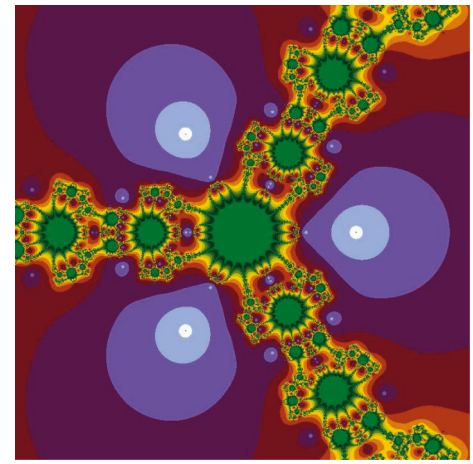

Figure 5: Polynomiograph for $q_1(w)$ using NM2.

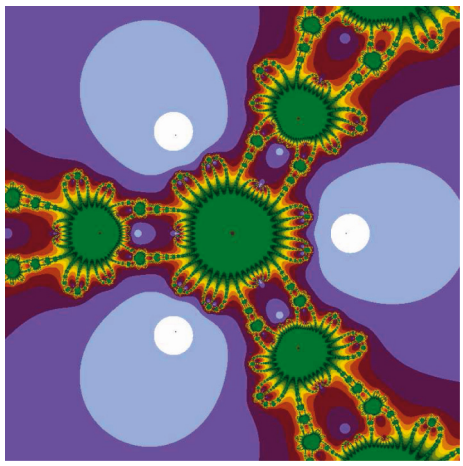

Figure 3: Polynomiograph for $q_1(w)$ using CM.

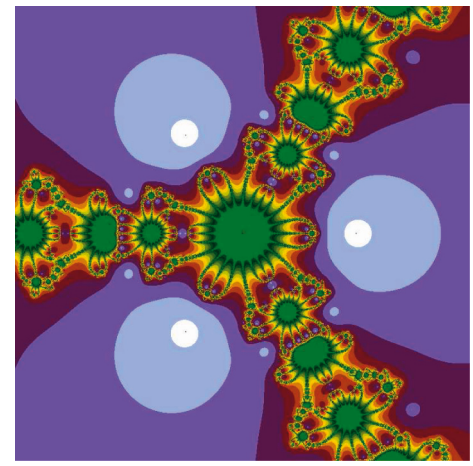

Figure 6: Polynomiograph for $q_1(w)$ using YM.

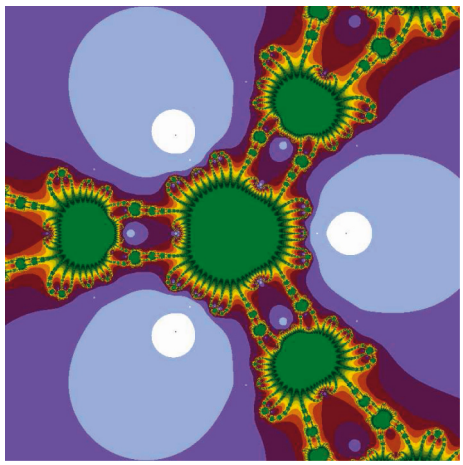

Figure 4: Polynomiograph for $q_1(w)$ using CHM.

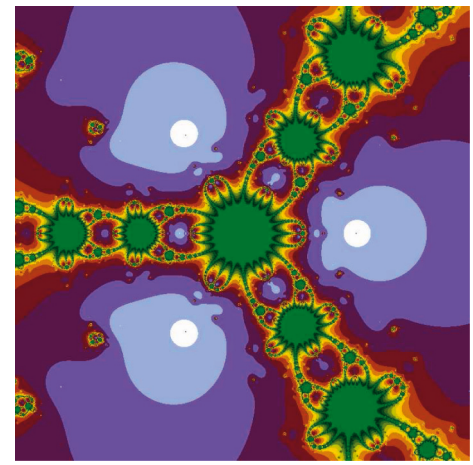

Figure 7: Polynomiograph for $q_1(w)$ using Algorithm 1.

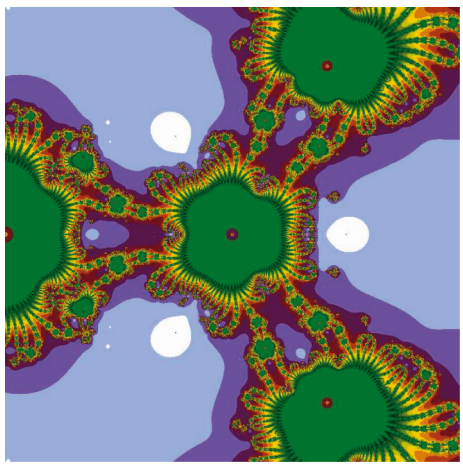

Figure 8: Polynomiograph for $q_1(w)$ using Algorithm 2.

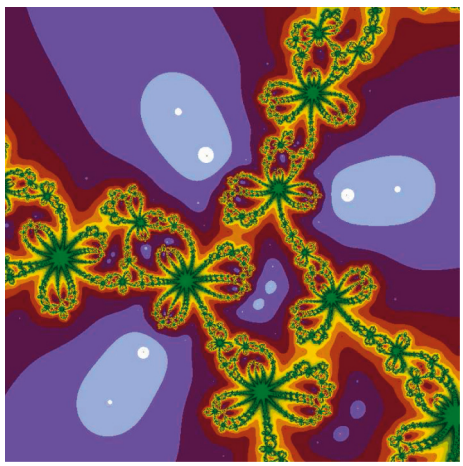

Figure 9: Polynomiograph for $q_2(w)$ using NM1.

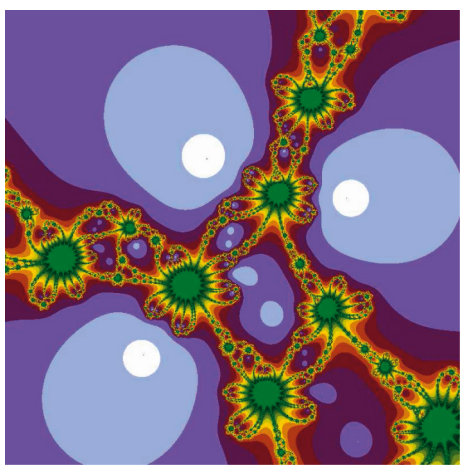

Figure 10: Polynomiograph for $q_2(w)$ using CM.

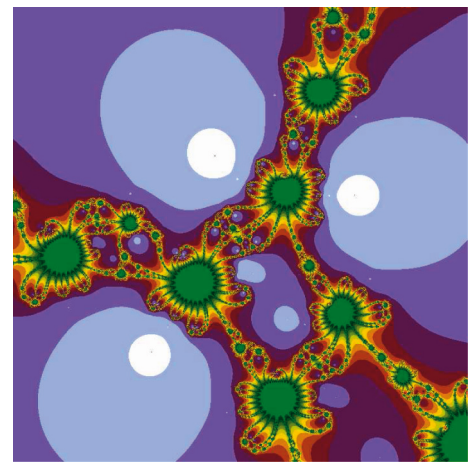

Figure 11: Polynomiograph for $q_2(w)$ using CHM.

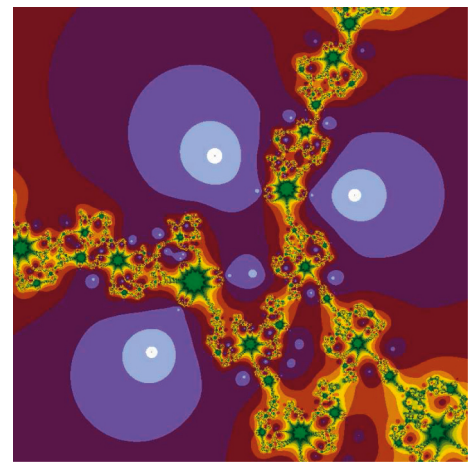

Figure 12: Polynomiograph for $q_2(w)$ using NM2.

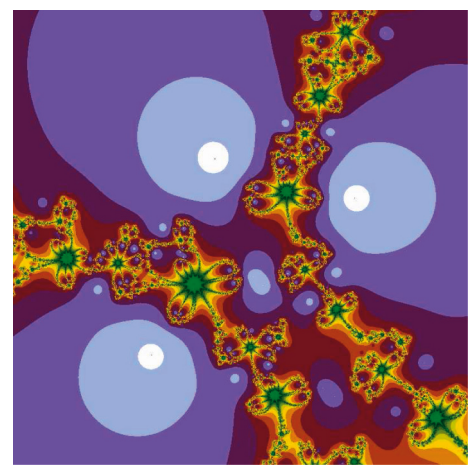

Figure 13: Polynomiograph for $q_2(w)$ using YM.

the polynomiographs of the complex polynomial $w^3.i - w^2 + i$ whose simple zeros are $[-108+8i+12\sqrt{81-12i}]^{2/3} - 4 - 2i[-108+8i+12\sqrt{81-12i}]^{1/}$ $3/6[-108+8i+12\sqrt{81-12i}]^{1/3}$, $[-108+8i+12\sqrt{81-12i}]^{2/3}+4+4i$ $[-108+8i+12\sqrt{81-12i}]^{1/3}+i\sqrt{3}[-108+8i+12\sqrt{81-12i}]^{2/3}+4i\sqrt{3}/-12[-108+8i+12\sqrt{81-12i}]^{1/3}$, and $[-108+8i+$

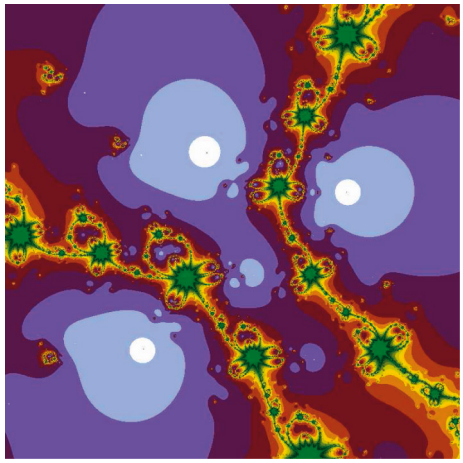

Figure 14: Polynomiograph for $q_2(w)$ using Algorithm 1.

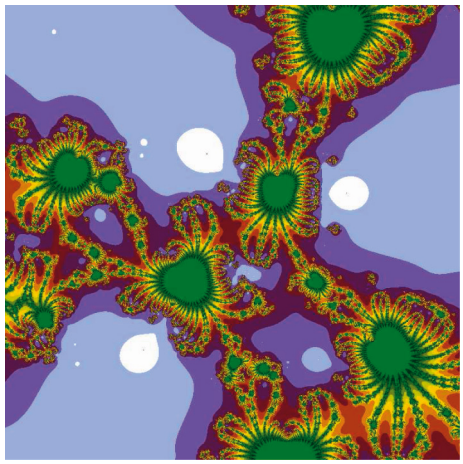

Figure 15: Polynomiograph for $q_2(w)$ using Algorithm 2.

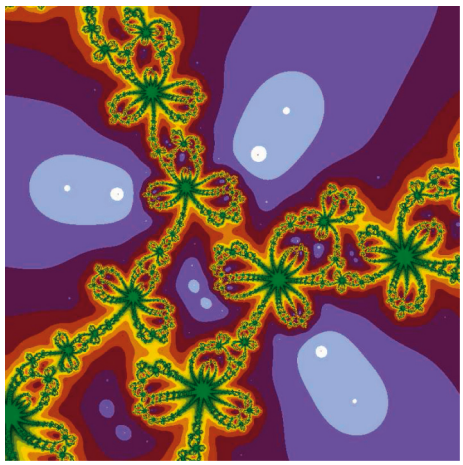

Figure 16: Polynomiograph for $q_3(w)$ using NM1.

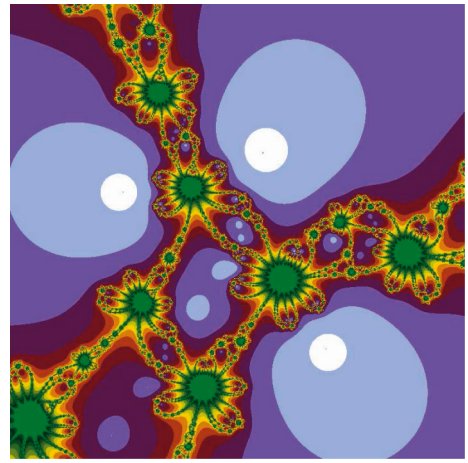

Figure 17: Polynomiograph for $q_3(w)$ using CM.

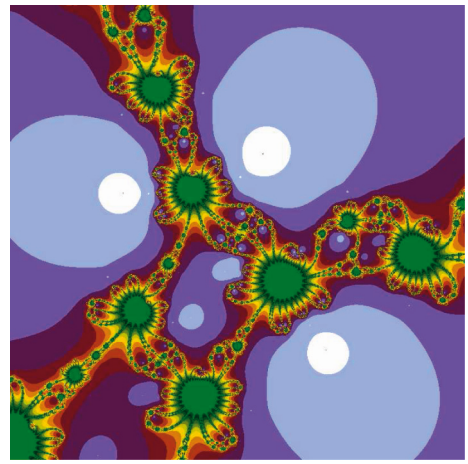

Figure 18: Polynomiograph for $q_3(w)$ using CHM.

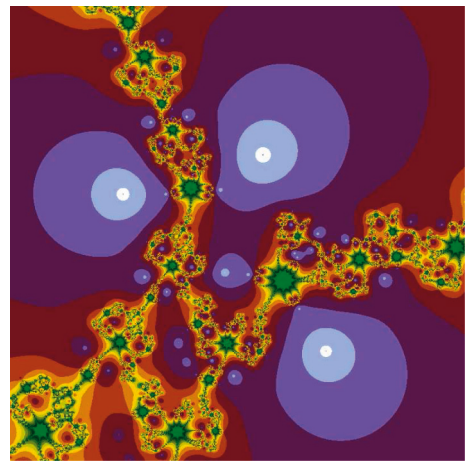

Figure 19: Polynomiograph for $q_3(w)$ using NM2.

$12\sqrt{81-12i}]^{2/3} - 4 + 4i[-108+8i+12\sqrt{81-12i}]^{1/3} + i\sqrt{3}[-108+8i+12\sqrt{81-12i}]^{2/3} + 4i\sqrt{3}/-12[-108+8i+12\sqrt{81-12i}]^{1/3}$. For this purpose, we ran all the iteration schemes with the aid of computer program and the corresponding graphs can be seen in Figures 37–43.

In all six experiments, we considered the different cubic complex polynomials for examining the graphical aspects of the suggested iteration schemes. In all the obtained images, the regions of convergence for the suggested iteration schemes possess the larger convergence areas than the other

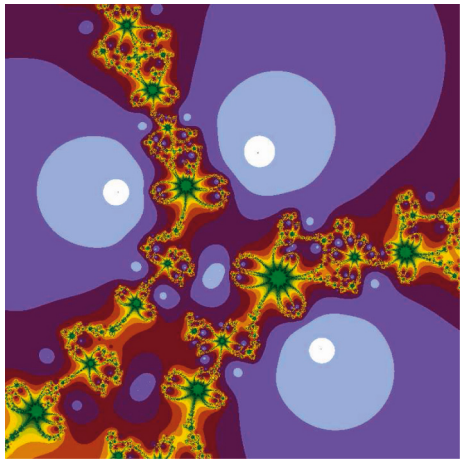

Figure 20: Polynomiograph for $q_3(w)$ using YM.

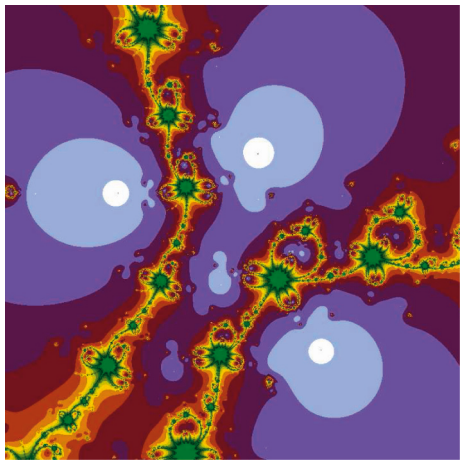

Figure 21: Polynomiograph for $q_3(w)$ using Algorithm 1.

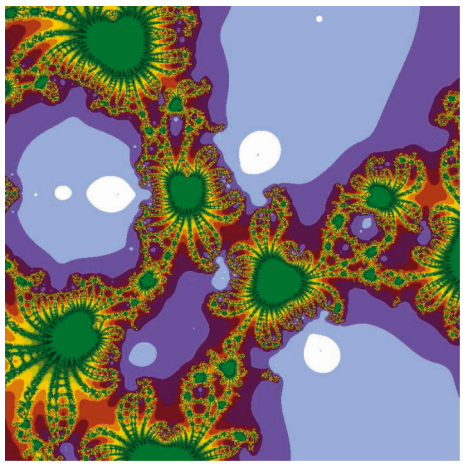

Figure 22: Polynomiograph for $q_3(w)$ using Algorithm 2.

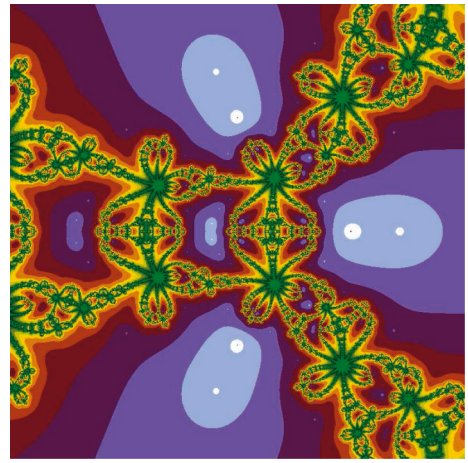

Figure 23: Polynomiograph for $q_4(w)$ using NM1.

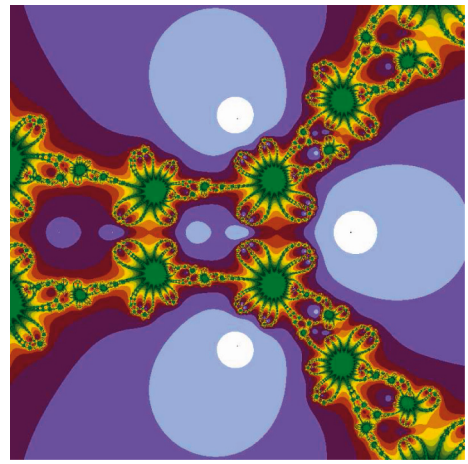

Figure 24: Polynomiograph for $q_4(w)$ using CM.

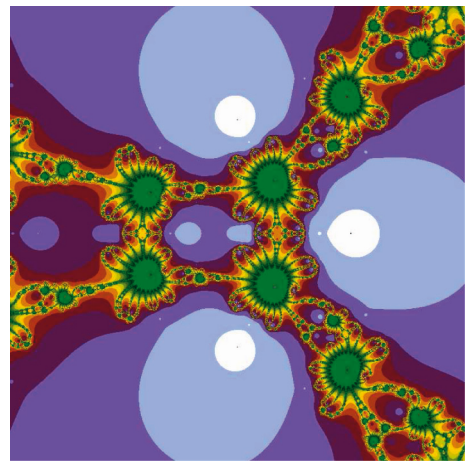

Figure 25: Polynomiograph for $q_4(w)$ using CHM.

comparable methods which certified the efficiency and better convergence of our proposed algorithms. The colour tones represent the performance and efficiency of the considered algorithm used to build the polynomiograph. The two important aspects which can be exhibited by these graphical objects are the convergence-speed and the dynamics of the

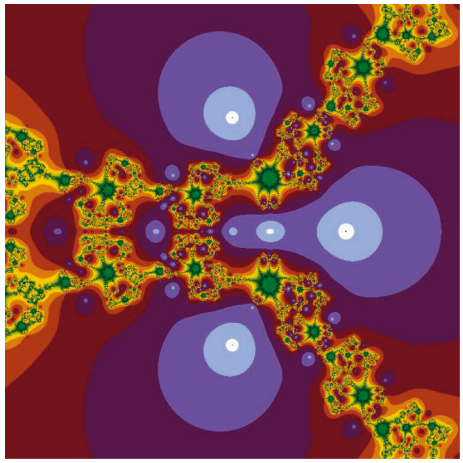

Figure 26: Polynomiograph for $q_4(w)$ using NM2.

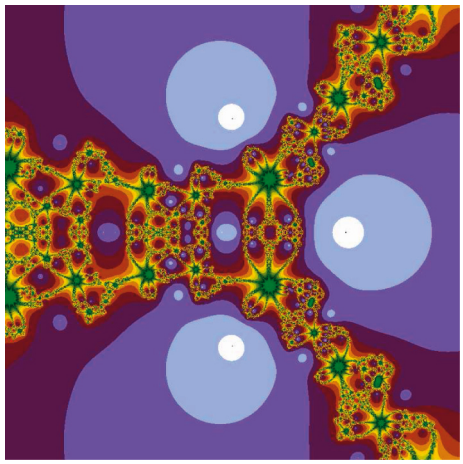

Figure 27: Polynomiograph for $q_4(w)$ using YM.

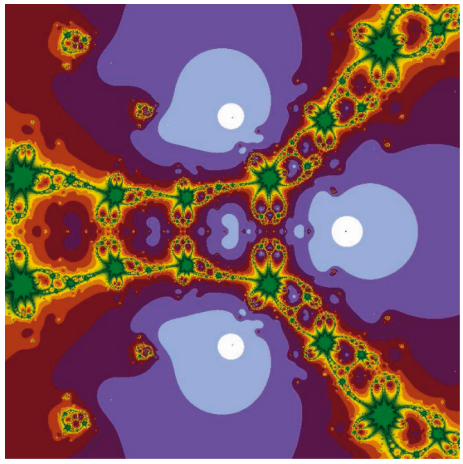

Figure 28: Polynomiograph for $q_4(w)$ using Algorithm 1.

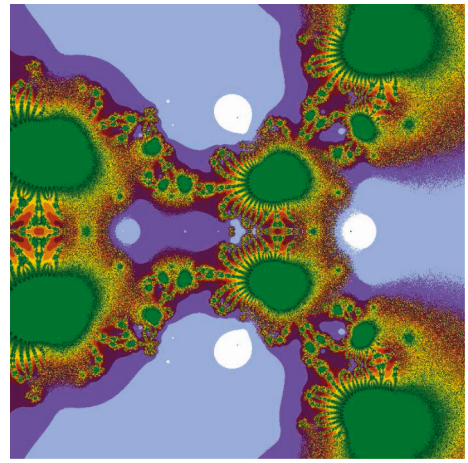

Figure 29: Polynomiograph for $q_4(w)$ using Algorithm 2.

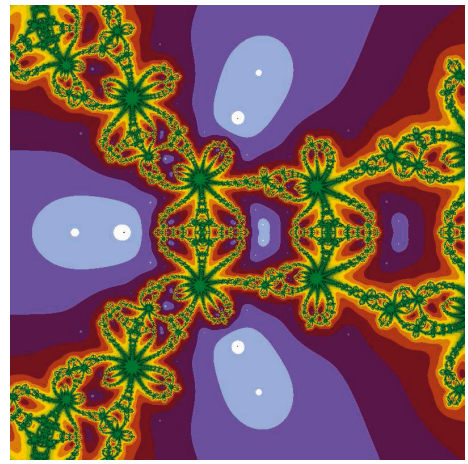

Figure 30: Polynomiograph for $q_5(w)$ using NM1.

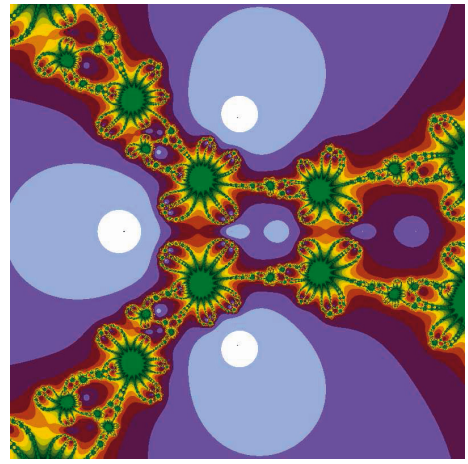

Figure 31: Polynomiograph for $q_5(w)$ using CM.

considered iteration techniques used to build these graphs. The first may be shown by examining the image's colour tones. The darkness of the colours in the presented images demonstrates fast convergence with less number of iterations, i.e., the darker the image, the more efficient the approach, and the given images demonstrate the superiority of

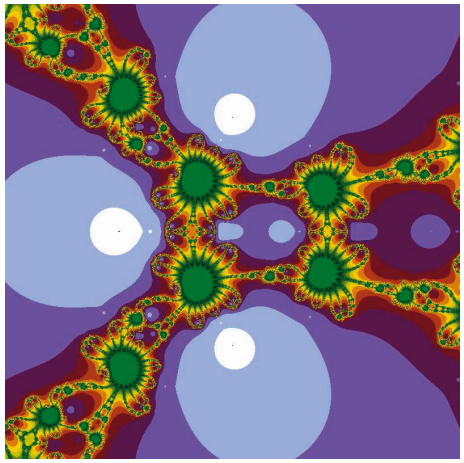

Figure 32: Polynomiograph for $q_5(w)$ using CHM.

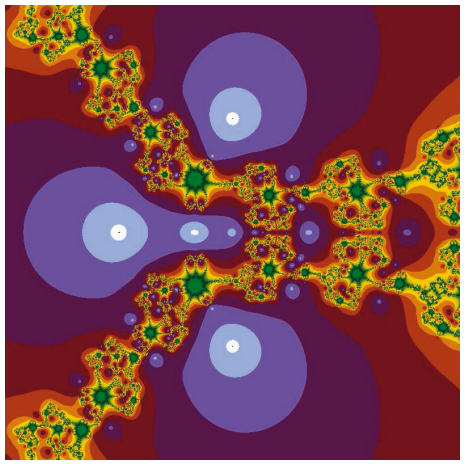

Figure 33: Polynomiograph for $q_5(w)$ using NM2.

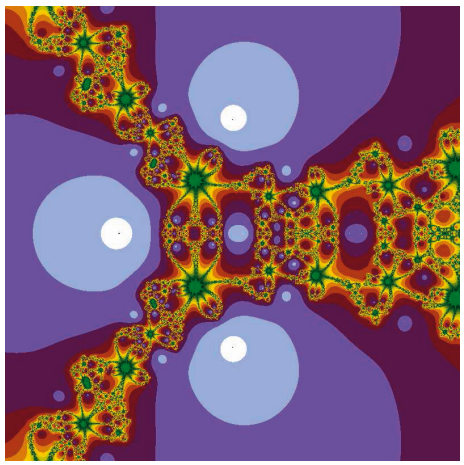

Figure 34: Polynomiograph for $q_5(w)$ using YM.

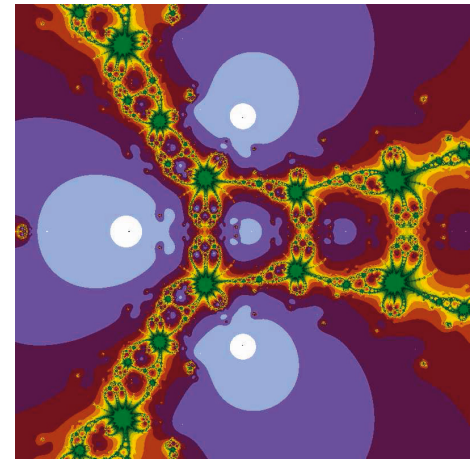

Figure 35: Polynomiograph for $q_5(w)$ using Algorithm 1.

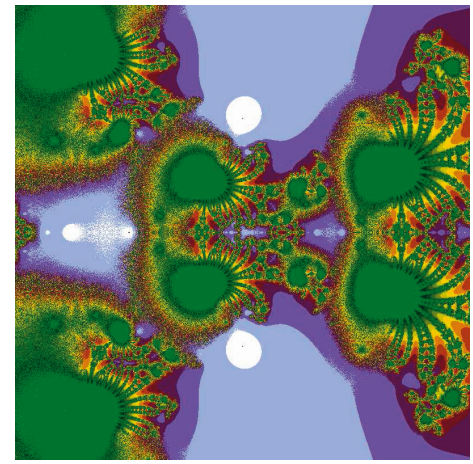

Figure 36: Polynomiograph for $q_5(w)$ using Algorithm 2.

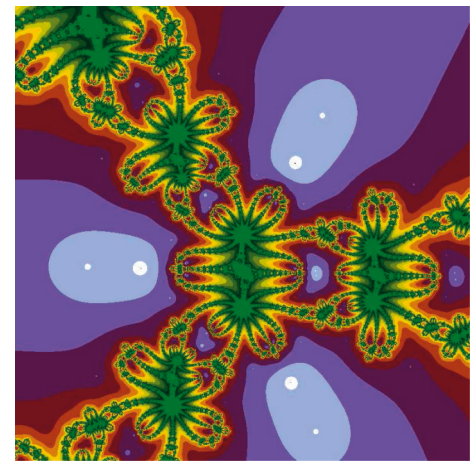

Figure 37: Polynomiograph for $q_6(w)$ using NM1.

the suggested methods. The second aspect may be examined by observing the colour fluctuation of the drawn polynomiographs. The regions with a limited variety of colours have low dynamics, whereas the regions with a great diversity of colours have high dynamics. The black colour in the displayed graphical representations demonstrates the

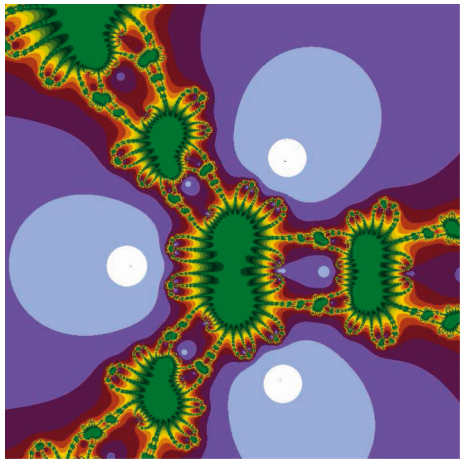

Figure 38: Polynomiograph for $q_6(w)$ using CM.

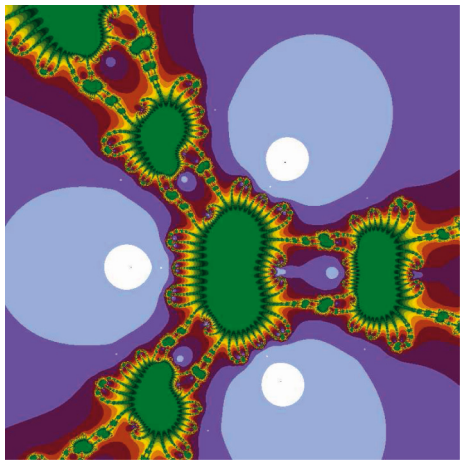

Figure 39: Polynomiograph for $q_6(w)$ using CHM.

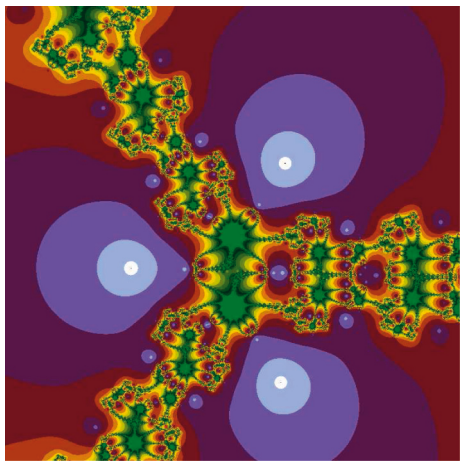

Figure 40: Polynomiograph for $q_6(w)$ using NM2.

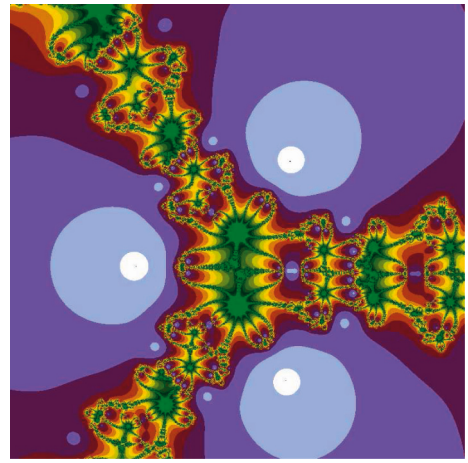

Figure 41: Polynomiograph for $q_6(w)$ using YM.

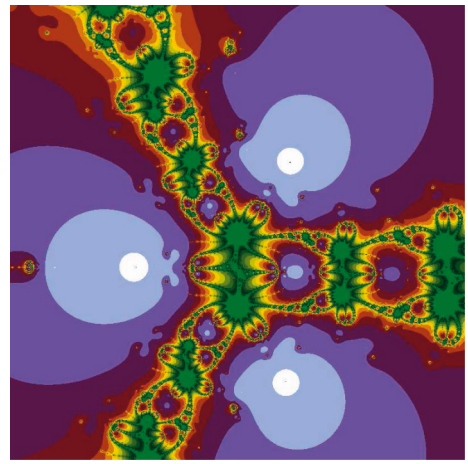

Figure 42: Polynomiograph for $q_6(w)$ using Algorithm 1.

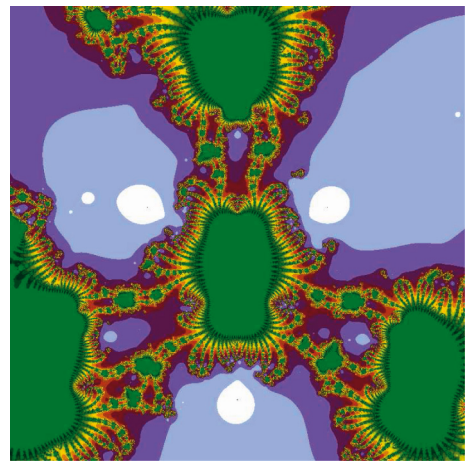

Figure 43: Polynomiograph for $q_6(w)$ using Algorithm 2.

method's deficiency by locating those precise locations where the solution cannot be obtained for the specified no. of iterations with the defined precision. The same-coloured regions in the figures show the same amount of iterations spent by different iteration strategies to approximate the answer and provide a comparable perspective of the contour

lines on the map. All of the graphics were created using the computer program Mathematica 12.0 with the accuracy $\epsilon = 0.01$, and the upper bound of the no. of iterations $m = 15$.

6. Conclusions

In this study, we have established and analyzed two novel optimal root-finding algorithms for nonlinear functions. The convergence criterion of the presented algorithms has been discussed and verified that the suggested iterative algorithms bear fourth- and sixth-order convergence. To exhibit the applicability of the suggested algorithms, some real-life engineering applications have also been added and solved whose numerical results confirmed that the proposed algorithms are time-efficient and consumed less iterations to achieve the required solution and more accurate to the exact solution. The dynamics of the provided methods demonstrating the greater convergence area in comparison with the other comparable methods. These dynamics also highlighted the proposed algorithms' quicker convergence speed and other dynamical properties, proving their superiority over the others in comparison.

Data Availability

All data required for this paper are included within this paper.

Conflicts of Interest

The authors do not have any conflicts of interest.

Authors' Contributions

All authors contributed equally in this paper.

References

[1] R. L. Burden and J. D. Faires, *Numerical Analysis*, Brooks/Cole Publishing Company, Monterey, CA, USA, 6th edition, 1997.

[2] J. M. Gutiérrez and M. A. Hernández, "A family of Chebyshev-Halley type methods in Banach spaces," *Bulletin of the Australian Mathematical Society*, vol. 55, no. 1, pp. 113–130, 1997.

[3] I. Argyros, D. Chen, and Q. Qian, "A note on the Halley method in Banach spaces," *Applied Mathematics and Computation*, vol. 58, no. 2-3, pp. 215–224, 1993.

[4] C. Chun, "Construction of Newton-like iteration methods for solving nonlinear equations," *Numerische Mathematik*, vol. 104, no. 3, pp. 297–315, 2006.

[5] A. Amiri, A. Cordero, M. T. Darvishi, and J. R. Torregrosa, "A fast algorithm to solve systems of nonlinear equations," *Journal of Computational and Applied Mathematics*, vol. 354, pp. 242–258, 2019.

[6] R. Behl, M. Salimi, M. Ferrara, S. Sharifi, and S. K. Alharbi, "Some real-life applications of a newly constructed derivative free iterative scheme," *Symmetry*, vol. 11, no. 2, p. 239, 2019.

[7] A. Naseem, M. A. Rehman, and T. Abdeljawad, "Higher-order root-finding algorithms and their basins of attraction," *Journal of Mathematics*, vol. 2020, Article ID 5070363, 11 pages, 2020.

[8] A. Özyapıcı, "Effective numerical methods for non-linear equations," *International Journal of Applied and Computational Mathematics*, vol. 6, no. 2, p. 35, 2020.

[9] A. M. Ostrowski, *Solution of Equations and Systems of Equations*, Academic Press, Cambridge, MA, USA, 1966.

[10] J. F. Traub, *Iterative Methods for the Solution of Equations*, Chelsea Publishing Company, New York, NY, USA, 1982.

[11] M. Aslam Noor and K. Inayat Noor, "Three-step iterative methods for nonlinear equations," *Applied Mathematics and Computation*, vol. 183, no. 1, pp. 322–327, 2006.

[12] A. Golbabai and M. Javidi, "A third-order Newton type method for nonlinear equations based on modified homotopy perturbation method," *Applied Mathematics and Computation*, vol. 191, no. 1, pp. 199–205, 2007.

[13] M. A. Noor, K. I. Noor, and K. Aftab, "Some new iterative methods for solving nonlinear equations," *World Applied Sciences Journal*, vol. 20, no. 6, pp. 870–874, 2012.

[14] A. Kumar, P. Maroju, R. Behl, D. K. Gupta, and S. S. Motsa, "A family of higher order iterations free from second derivative for nonlinear equations in R," *Journal of Computational and Applied Mathematics*, vol. 330, pp. 215–224, 2018.

[15] O. Said Solaiman, S. A. Abdul Karim, and I. Hashim, "Optimal fourth- and eighth-order of convergence derivative-free modifications of King's method," *Journal of King Saud University - Science*, vol. 31, no. 4, pp. 1499–1504, 2019.

[16] P. B. Chand, F. I. Chicharro, N. Garrido, and P. Jain, "Design and complex dynamics of potra-pták-type optimal methods for solving nonlinear equations and its applications," *Mathematics*, vol. 7, no. 10, p. 942, 2019.

[17] A. Naseem, M. A. Rehman, and T. Abdeljawad, "Some new iterative algorithms for solving one-dimensional non-linear equations and their graphical representation," *IEEE Access*, vol. 9, pp. 8615–8624, 2021.

[18] A. Rafiq and M. Rafiullah, "Some multi-step iterative methods for solving nonlinear equations," *Computers & Mathematics with Applications*, vol. 58, no. 8, pp. 1589–1597, 2009.

[19] H. T. Kung and J. F. Traub, "Optimal order of one-point and multipoint iteration," *Journal of the ACM*, vol. 21, no. 4, pp. 643–651, 1974.

[20] C. Chun, "Some variants of King's fourth-order family of methods for nonlinear equations," *Applied Mathematics and Computation*, vol. 190, no. 1, pp. 57–62, 2007.

[21] J. H. Yun, "A note on three-step iterative method for nonlinear equations," *Applied Mathematics and Computation*, vol. 202, no. 1, pp. 401–405, 2008.

[22] M. ShachamShacham and E. Kehat, "An iteration method with memory for the solution of a non-linear equation," *Chemical Engineering Science*, vol. 27, no. 11, pp. 2099–2101, 1972.

[23] M. Planck, *The Theory of Heat Radiation. Translated by Masius, M*, Blakiston's Son & Co, Philadelphia, PA, USA, 2nd edition, 1914.

[24] M. Shacham, "An improved memory method for the solution of a nonlinear equation," *Chemical Engineering Science*, vol. 44, no. 7, pp. 1495–1501, 1989.

[25] M. Shacham and E. Kehat, "Converging interval methods for the iterative solution of a non-linear equation," *Chemical Engineering Science*, vol. 28, no. 12, pp. 2187–2193, 1973.

[26] C. S. Chapra, *Applied Numerical Methods with MATLAB for Engineers and Scientists*, McGraw-Hill, New York, NY, USA, 2010.

[27] R. Manning, "On the flow of water in open channels and pipes," *Transactions of the Institution of Civil Engineers of Ireland*, vol. 20, pp. 161–207, 1891.
[28] B. Kalantari, "Polynomiography: from the fundamental theorem of algebra to art," *Leonardo*, vol. 38, no. 3, pp. 233–238, 2005.
[29] B. Kalantari and E. H. Lee, "Newton-Ellipsoid polynomiography," *Journal of Mathematics and the Arts*, vol. 13, no. 4, pp. 336–352, 2019.
[30] B. Kalantari, "An invitation to polynomiography via exponential series," 2017, https://arxiv.org/abs/1707.09417.
[31] K. Gdawiec, W. Kotarski, and A. Lisowska, "Visual analysis of the Newton's method with fractional order derivatives," *Symmetry*, vol. 11, no. 9, p. 1143, 2019.
[32] K. Gdawiec, "Fractal patterns from the dynamics of combined polynomial root finding methods," *Nonlinear Dynamics*, vol. 90, no. 4, pp. 2457–2479, 2017.
[33] M. Scott, B. Neta, and C. Chun, "Basin attractors for various methods," *Applied Mathematics and Computation*, vol. 218, no. 6, pp. 2584–2599, 2011.

Hindawi
Complexity
Volume 2022, Article ID 3846904, 15 pages
https://doi.org/10.1155/2022/3846904

Research Article

Modeling and Dynamics of the Fractional Order SARS-CoV-2 Epidemiological Model

Tahir Khan,[1,2] **Roman Ullah**,[2] **Ali Yousef**,[3] **Gul Zaman**,[4] **Qasem M. Al-Mdallal**,[5] **and Yasser Alraey**[6]

[1]*Department of Mathematics and Statistics, Woman University Swabi, Khyber Pakhtunkhwa, Pakistan*
[2]*Department of Computing, Muscat College Muscat, Muscat, Oman*
[3]*Department of Mathematics, Kuwait College of Science and Technoloy, Safat 13133, P. O. Box 27235, Kuwait*
[4]*Department of Mathematics, University of Malakand, Chakdara Dir Lower, Khyber Pakhtunkhwa, Pakistan*
[5]*Department of Mathematical Sciences, UAE University, P. O. Box 15551, Al-Ain, UAE*
[6]*Department of Clinical Laboratory Sciences, Central Research Laboratory, College of Applied Medical Sciences, King Khalid University, Abha, Saudi Arabia*

Correspondence should be addressed to Qasem M. Al-Mdallal; q.almdallal@uaeu.ac.ae

Received 12 February 2022; Revised 3 July 2022; Accepted 26 July 2022; Published 27 September 2022

Academic Editor: M. De Aguiar

We propose a theoretical study to investigate the spread of the SARS-CoV-2 virus, reported in Wuhan, China. We develop a mathematical model based on the characteristic of the disease and then use fractional calculus to fractionalize it. We use the *Caputo-Fabrizio* operator for this purpose. We prove that the considered model has positive and bounded solutions. We calculate the threshold quantity of the proposed model and discuss its sensitivity analysis to find the role of every epidemic parameter and the relative impact on disease transmission. The threshold quantity (reproductive number) is used to discuss the steady states of the proposed model and to find that the proposed epidemic model is stable asymptotically under some constraints. Both the global and local properties of the proposed model will be performed with the help of the mean value theorem, *Barbalat's lemma,* and linearization. To support our analytical findings, we draw some numerical simulations to verify with graphical representations.

1. Introduction

The coronavirus family causes infections in humans, beginning with a common cold and progressing to SARS. Two coronavirus epidemics have been recorded in the preceding twenty years [1–3]. SARS was one of them, and it created a large-scale outbreak in several nations. Approximately, 8000 people were affected by this outbreak, with 800 of them dying. In December 2019, a serious respiratory sickness outbreak began in Wuhan, China [4]. In early January 2020, the causal agent, a new coronavirus, was identified and isolated from a single patient (COVID-19). According to scientific evidence, animals were the earliest source of virus transmission, although the majority of cases are caused by infected humans contacting susceptible humans. The spread of this virus is a hot topic that has touched practically every corner of the globe and has been reported in over 200 countries. According to current records, there have been over 401,288,380 confirmed cases, with 5,783,182 deaths occurring till February 9th 2022. According to the WHO, this is a public health emergency. The World Health Organization (WHO) has designated it a public health emergency of worldwide concern due to the severity of the condition. This virus appears to be highly contagious, spreading rapidly to nearly every country on the planet, prompting the declaration of a global pandemic. It signifies that it is a highly major public health threat, with symptoms such as cough, fever, lethargy, and breathing problems after infection.

Fractional computing is an emerging area of mathematics and attracted the attention of researchers. Because of the wide applications to express the axioms of heritage and recall different physical situations that occur in various fields of applied science. Many classical models have been shown with less accuracy in prediction about the temporal dynamics of the disease, while on the other hand, models with noninteger order provide better information in allocating and preserving data for large-scale analysis [5–7]. Moreover, the derivative of integer order does not find the dynamics between two various points [8, 9]. Furthermore, the comparison of integer and noninteger order epidemic models reveals that models with noninteger order are the generalization of integer order and provide more and accurate dynamics rather than the classical order, (for detail see [9–11]). A model with noninteger order demonstrating the complex dynamics of a biological system has been proposed by Asma et al. [12]. A fractional-order epidemic model has been investigated to explore the dynamics of toxoplasmosis in feline and human populations [13]. Another study has been reported and studied the stability analysis of pests in tea with fractional order [14]. Similarly, many authors studied dynamics of infectious diseases with fractional-order derivatives, for e.g., Hadamard and Caputo and Rieman and Liouville [15–19]. For the solution of Caputofractional order, epidemiological models of many iterative and numerical methods have been developed; however, the complications of singular kernel arise. So, Caputo and Fabrizio presented an idea based on the nonsingular kernel to overcome the limitation that arises in the above fractional-order derivatives [20].

Coronavirus disease 2019 (COVID-19) is one of the top infectious diseases among other ones and therefore has been recognized as a global threat by World Health Organization (WHO). Due to novel characteristics of the coronavirus disease various researchers have taken a keen interest. Several researchers formulated various epidemiological models to study the dynamics of communicable diseases (see for instance [21–25]). The current pandemic of novel coronavirus disease is also a burning issue and many biologists and mathematicians reported different studies. For example, Wu et al. introduced a model to describe the transmission of the disease based on reported data from 31.12.2019 to 28.01.2020 [26]. Imai et al. studied the transmission of the disease with the help of computational modeling to estimate the disease outbreak in Wuhan, whose main focus was on the human-to-human transmission [27]. Another study has been investigated by Zhu et al. [28] to analyze the infectivity of the novel coronavirus. The dynamical analysis of the novel disease of COVID-19 under the effect of the carrier with environmental contamination has been performed by Hattaf et al. [29]. All the reported studies indicate that bats and minks may be two animal hosts of the novel coronavirus. Similarly, many more studies have been reported on the dynamics of a novel coronavirus, for instance, see [30, 31]. Nevertheless, the literature reveals that the work proposed is an excellent contribution, however, it could be possible to improve further by incorporating some interesting and important factors related to the novel coronavirus disease.

The spreading of coronavirus disease globally rises from the human-to-human transmission, while the initial source of the disease was an animal/reservoir. The characteristic of SARS-CoV-2 confirms that various infection phases are significant and affect the transmission. The role of asymptomatic is notable because with no symptoms it becomes the major source of transmission of the infection. So, a small number of this population leads to a big disaster. We develop a mathematical model according to the novel disease of coronavirus and keeping in view the aesthetic of the virus. To do this, first, we formulate the model and then fractionalize it to perform the fractional type analysis of the proposed model. The fractional derivative used in this study is a particular case of the new generalized Hattaf fractional (GHF) derivative [32, 33]. We show that the proposed fractional-order epidemiological model is bounded and possesses positive solutions. We also find the steady states of the epidemic problem and discuss asymptotic stabilities. For this, we use the dynamical systems theory. Particularly, we utilize the *linearization*, *mean value theorem*, and *Barbalat's Lemma*. Moreover, the sensitivity analysis will be performed for the threshold parameter to find the impact of each epidemic parameter involved in the model mechanism. We use the sensitivity index formula for this purpose. We perform the numerical visualization of the analytical results to verify the theocratical part and show the effectiveness of the control strategy. We also show the difference between integer and noninteger order epidemiological cases.

2. Formulation of the Model with Fractional Analysis

The proposed problem is formulated by taking into account the characteristics of the novel coronavirus illness. We divide the total human population $N_h(t)$ into four various compartments and assume that $M(t)$ represents the reservoir. In the proposed study, we also consider several transmission routes, such as from human-to-human and from a reservoir-to-human. Before we show the model, we make the following assumption:

(i) The parameters and variables involved in the model are positive or non-negative values

(ii) The inflow of newborn are susceptible

(iii) The novel disease is transmitted by several routes, such as from latent and symptomatic individuals as well as from reservoirs and so accordingly incorporated.

(iv) Those who have a strong immune system got natural recovery

(v) Two types of recoveries i.e., from latent and symptomatic populations are taken

(vi) The death rate due to disease is taken in the symptomatic infected compartment

As a result of combining all the above assumptions, the following system of nonlinear differential equations emerges:

$$\begin{cases} \dfrac{dS_h(t)}{dt} = \Lambda - \beta_1 S_h(t) L_h(t) - \gamma\beta_2 S_h(t) I_h(t) - \psi\beta_3 S_h(t) M(t) - dS_h(t), \\ \dfrac{dL_h(t)}{dt} = \beta_1 S_h(t) L_h(t) + \gamma\beta_2 S_h(t) I_h(t) + \psi\beta_3 S_h(t) M(t) - (\gamma_1 + \gamma_2 + d) L_h(t), \\ \dfrac{dI_h(t)}{dt} = \gamma_1 L_h(t) - (\gamma_3 + d + d_1) I_h(t), \dfrac{dR_h(t)}{dt} = \gamma_3 I_h(t) + \gamma_2 L_h(t) - dR_h(t), \\ \dfrac{dM(t)}{dt} = \eta_2 I_h(t) + \eta_1 L_h(t) - \alpha M(t). \end{cases} \tag{1}$$

and the initial population sizes are assumed to be as follows:

$$S_h(0) > 0, L_h(0) \geq 0, I_h(0) \geq 0, R_h(0) \geq 0, M(0) \geq 0. \tag{2}$$

In the proposed epidemiological model, the parameters described as Λ is the new birth rate, and the disease transmission rates are symbolized by, β_1, β_2, and β_3, which represent the transmission from latent, symptomatic, and reservoir, respectively. We also denote the reduced transmission coefficient by γ and ψ, while γ_1 is the moving ratio of latent to infected and γ_2 denotes the recovery rate. We also denote the recovery rate under treatment by γ_3, while d is the natural mortality. The disease-induced rate is d_1. Furthermore, η_1 and η_2 are the two ratios that contribute production of the virus in the seafood market. We denote the removing rate of the virus with α.

2.1. Fractional-Order Epidemiological Model. Let σ be the fractional-order parameter $0 < \sigma < 1$. We will extend the model to its associate fractional order. First, we give some fundamental concepts that will be used in getting our findings.

Definition 1. (see [9]). Let $T > 0$ and assume that $\phi \in H^1(0, T)$, if $n - 1 < \sigma < n$ and $\sigma > 0$ such that $n \in \mathbb{N}$, then the derivative in the sense of *Caputo* as well as the *Caputo-Fabrizio* with σ order are given as follows:

$$\begin{aligned} {}^{CF}D^{\sigma}_{0,t}\{\varphi(t)\} &= \frac{K(\sigma)}{(1-\sigma)} \int_0^t \varphi'(u) \exp\left(\frac{(u-t)\sigma}{1-\sigma}\right) du, \\ {}^{C}D^{\sigma}_{0,t}\{\varphi(t)\} &= \frac{1}{\Gamma(-\sigma+n)} \int_0^t (t-u)^{-1+n-\sigma} \varphi^n(u) du, \end{aligned} \tag{3}$$

where *CF* and *C* are used for the representation of *Caputo-Fabrizio* and *Caputo,* respectively, while $t > 0$ and $K(\sigma)$ are the normalization function, and $K(0) = 0 = K(1)$.

Definition 2 see [9]). (If $0 < \sigma < 1$ and $\varphi(t)$ varies with time t, then the integral is described as follows:

$${}^{RL}J^{\sigma}_{0,t}\{\varphi(t)\} = \frac{1}{\Gamma(\sigma)} \int_0^t (t-z)^{\sigma-1} \varphi(u) du. \tag{4}$$

The above integral is known as the Riemann–Liouville integral.

$${}^{CF}J^{\sigma}_{0,t}\{\varphi(t)\} = \frac{2}{(2-\sigma)K(\sigma)} \left\{ (1-\sigma)\varphi(t) + \sigma \int_0^t \varphi(u) du \right\}. \tag{5}$$

The integral defined by Equation (5) is said to be the Caputo-Fabrizio-Caputo (CF) integral.

Since σ is the fractional order, and using the notion $\rangle_1 = \gamma_1^{\sigma} + \gamma_2^{\sigma} + d^{\sigma}$ and $\varrho_2 = \gamma_3^{\sigma} + d^{\sigma} + d_1^{\sigma}$ for the shake of simplicity, therefore the fractional order model looks like the following equation:

$$\begin{cases} {}^{CF}D^{\sigma}_{0,t} S_h(t) = \Lambda^{\sigma} - \beta_1^{\sigma} L_h(t) S_h(t) - \gamma^{\sigma}\beta_2^{\sigma} I_h(t) S_h(t) - \psi^{\sigma}\beta_3^{\sigma} M(t) S_h(t) - d^{\sigma} S_h(t), \\ {}^{CF}D^{\sigma}_{0,t} L_h(t) = \beta_1^{\sigma} L_h(t) S_h(t) + \gamma^{\sigma}\beta_2^{\sigma} I_h(t) S_h(t) + \psi^{\sigma}\beta_3^{\sigma} M(t) S_h(t) - \varrho_1 L_h(t), \\ {}^{CF}D^{\sigma}_{0,t} I_h(t) = \gamma_1^{\sigma} L_h(t) - \varrho_2 I_h(t), \\ {}^{CF}D^{\sigma}_{0,t} R_h(t) = \gamma_3^{\sigma} I_h(t) + \gamma_2^{\sigma} L_h(t) - d^{\sigma} R_h(t), \\ {}^{CF}D^{\sigma}_{0,t} M(t) = \eta_2^{\sigma} I_h(t) + \eta_1^{\sigma} L_h(t) - \alpha^{\sigma} M(t). \end{cases} \tag{6}$$

We show that the proposed fractional-order epidemic model as reported by the above system is both biologically and mathematically feasible. For this, we discuss the positivity and boundedness of the model (6), which proves that the underconsidered problem is well-posed. We also investigate that the dynamics of the proposed model are confined to a certain region invariant positively. The following *Lemmas* is established for this purpose.

Lemma 1. *Since* $(S_h(t), L_h(t), I_h(t), R_h(t), M(t)$ *are the proposed model (6) solutions and let us consider that it possessing non-negative initial sizes of population, then* $(S_h(t), L_h(t), I_h(t), R_h(t), M(t)$ *are non-negative for all* $t \geq 0$.

Proof. Since, σ is the fractional order and assuming that G represents the fractional operator with order σ, then system (1) leads to

$$\begin{cases} GD^{\sigma}_{0,t}\left(S_h(t)\right) = \Lambda^{\sigma} - \left(\beta_1^{\omega} L_h(t) + \gamma^{\sigma}\beta_2^{\sigma} I_h(t) + \psi^{\sigma}\beta_3^{\sigma} M(t) + d^{\sigma}\right) S_h(t), \\ GD^{\sigma}_{0,t}\left(L_h(t)\right) = \left(\beta_1^{\sigma} L_h(t) + \gamma^{\sigma}\beta_2^{\sigma} I_h(t) + \psi^{\sigma}\beta_3^{\sigma} M(t)\right) S_h(t) - \varrho_1 L_h(t), \\ GD^{\sigma}_{0,t}\left(I_h(t)\right) = \gamma_1^{\sigma} L_h(t) - \varrho_2 I_h(t), \\ GD^{\sigma}_{0,t}\left(R_h(t)\right) = \gamma_2^{\sigma} L_h(t) + \gamma_3^{\sigma} I_h(t) - d^{\sigma} R_h(t), GD^{\sigma}_{0,t}\left(M(t)\right) = \eta_1^{\sigma} L_h(t) + \eta_2^{\sigma} I_h(t) - \alpha^{\sigma} M(t). \end{cases} \tag{7}$$

This implies that

$$\begin{cases} GD^{\sigma}_{0,t} S_h(t)\big|_{\kappa(S_h)} = \Lambda^{\sigma} > 0, \\ GD^{\sigma}_{0,t} L_h(t)\big|_{\kappa(L_h)} = \left(\beta_1^{\sigma} L_h(t) + \gamma^{\sigma}\beta_2^{\sigma} I_h(t) + \psi^{\sigma}\beta_3^{\sigma} M(t)\right) S_h(t) \geq 0, \\ GD^{\sigma}_{0,t} I_h(t)\big|_{\kappa(I_h)} = \gamma_1^{\sigma} L_h(t) \geq 0, GD^{\sigma}_{0,t} R_h(t)\big|_{\kappa(R_h)} = \gamma_2^{\sigma} L_h(t) + \gamma_3^{\sigma} I_h(t) \geq 0, \\ GD^{\sigma}_{0,t} M(t)\big|_{\kappa(M)} = \eta_1^{\sigma} L_h(t) + \eta_2^{\sigma} I_h(t) \geq 0, \end{cases} \tag{8}$$

where $\kappa(\xi) = \{\xi = 0$ and S_h, L_h, I_h, R_h, M are in $C(R_+ \times R_+)$ and $\xi \in \{S_h, L_h, I_h, R_h, M\}$, respectively. Following the methodology proposed in [34] and consequently used by *Qureshi* et al. [35], we reach to the conclusion that the solutions are non-negative for all non-negative t. □

Lemma 2. *Let us assume that the* Ω *is the feasible region of the model (6), then within it, the model that is under consideration is invariant and the feasible region is given by*

$$\Omega = \left\{ \begin{array}{c} \left(S_h(t), L_h(t), I_h(t), R_h(t), M(t)\right) \in R_+^5 \colon S_h + L_h{}' \\ +I_h + R_h \leq \left(\dfrac{\Lambda}{d}\right)^{\sigma}, \\ M(t) \leq \dfrac{\Lambda^{\sigma}\left(\eta_1^{\sigma} + \eta_2^{\sigma}\right)}{d^{\sigma}\alpha^{\sigma}} \end{array} \right\}. \tag{9}$$

Proof. Let $N_h(t)$ represent the total human population, then the use of the proposed fractional model leads to the assertion is given by the following equation:

$$GD^{\sigma}_{0,t} N_h(t) + d^{\sigma} N_h(t) \leq \Lambda^{\sigma} N_h(t). \tag{10}$$

Solving equation (10), we get the following equation:

$$N_h(t) \leq N_h(0) E_{\omega}\left(-d^{\sigma} t^{\sigma}\right) + \left(\frac{\Lambda}{d}\right)^{\sigma}\left(1 - E_{\sigma}\left(-d^{\sigma} t^{\sigma}\right)\right). \tag{11}$$

It could be also noted that $L_h, I_h \leq N_h$, so the last equation of the fractional model (6) looks like the following equation:

$$GD^{\sigma}_{0,t} M(t) + \alpha^{\sigma} M(t) \leq \frac{\left(\eta_1^{\sigma} + \eta_2^{\sigma}\right)\Lambda^{\sigma}}{\alpha^{\sigma} d^{\sigma}}. \tag{12}$$

The solution of (12) leads to the following equation:

$$M(t) \leq M(0) E_{\sigma}\left(-\alpha^{\sigma} t^{\sigma}\right) + \left(\frac{\Lambda^{\sigma}\left(\eta_1^{\sigma} + \eta_2^{\sigma}\right)}{d^{\sigma}\alpha^{\sigma}}\right)\left(1 - E_{\sigma}\left(-\alpha^{\sigma} t^{\sigma}\right)\right). \tag{13}$$

In (11) and (13), $E(.)$ denotes the *Mittag-Leffler* function and $E_{\sigma}(Z) = \sum_{n=0}^{\infty} \Gamma(\sigma i + 1)/Z^n$. Furthermore, it is obvious that when times grows without bound then (11) and (13) gives that $N_h(t) \longrightarrow (\Lambda/d)^{\sigma}$ and $M(t) \longrightarrow (\Lambda(\eta_1^{\sigma} + \eta_2^{\sigma})/d^{\sigma}\alpha^{\sigma})$. Thus, if $N_h(0) \leq (\Lambda/d)^{\sigma}$ and $M(0) \leq (\Lambda^{\sigma}(\eta_1^{\sigma} + \eta_2^{\sigma})/d^{\sigma}\alpha^{\sigma})$, then $N_h(t) \leq (\Lambda/d)^{\sigma}$ and $M(t) \leq (\Lambda^{\sigma}(\eta_1^{\sigma} + \eta_2^{\sigma})/d^{\sigma}\alpha^{\sigma})$ for every $t > 0$, while if $N_h(0) > (\Lambda/d)^{\sigma}$ and $M(0) > (\Lambda^{\sigma}(\eta_1^{\sigma} + \eta_2^{\sigma})/d^{\sigma}\alpha^{\sigma})$, then N_h and M contained in Ω and will never leave. So, the dynamics of the fractional epidemic model can be investigated in feasible region Ω. □ □

3. Stability Analysis

In this section, we will examine the stability of fractional epidemiological model (6). We find the steady states first and threshold parameter (*basic reproductive number*) of the fractional model to investigate the stability conditions. We use the notion X_1 for disease-free equilibrium calculating at steady state with $L_h = I_h = R_h = M = 0$. It is easily stated

that the component of X_1 looks like $S_{h0} = \Lambda^{\omega}/d^{\omega}$ and $L_{h0} = I_{h0} = R_{h0} = M = 0$. We now use the disease-free state and find the threshold parameter. This quantity represents the maximum epidemic potential of a pathogen, which describes what would happen if an infectious agent were to enter a susceptible community, and therefore is an estimate based on an idealized scenario. The effective threshold quantity depends on the nature of the population's current susceptibility. This measure the potential transmission, which is likely lower than the basic reproduction number, depends on various factors e.g., whether some individuals have immunity due to prior exposure to the pathogen or whether some individuals are vaccinated against the disease. Therefore, this quantity is effective and changes over time and is an estimate based on a more realistic situation within the population. We calculate this quantity i.e., the threshold quantity (R_0) of the proposed model by following [36], therefore following the next generation matrix approach, we calculate the associated matrices i.e., F and V as given by the following equation:

$$F = \begin{pmatrix} \beta_1^{\sigma} S_{h0} & \gamma^{\sigma}\beta_2^{\sigma} S_{h0} & \psi^{\sigma}\beta_3^{\sigma} S_{h0} \\ 0 & 0 & 0 \\ 0 & 0 & 0 \end{pmatrix}, V = \begin{pmatrix} \varrho_1 & 0 & 0 \\ 0 & \varrho_2 & 0 \\ -\eta_1^{\sigma} & -\eta_2^{\sigma} & \alpha^{\sigma} \end{pmatrix}. \tag{14}$$

The associated threshold quantity of model (6) is the spectral radius of the matrix $(\overline{K} = FV^{-1})$ is as $R_0 = R_1 + R_2 + R_3$, where

$$R_1 = \frac{\Lambda^{\sigma}\beta_1^{\sigma}}{d^{\sigma}\varrho_1}, R_2 = \frac{\Lambda^{\sigma}\beta_2^{\sigma}\gamma^{\sigma}\gamma_1^{\sigma}}{d^{\sigma}\varrho_1\varrho_2}, R_3 = \frac{\Lambda^{\sigma}\beta_3^{\sigma}\psi^{\sigma}\eta_1^{\sigma}}{\alpha^{\sigma}d^{\sigma}\varrho_1} + \frac{\Lambda^{\sigma}\beta_3^{\sigma}\psi^{\sigma}\eta_2^{\sigma}\gamma_1^{\sigma}}{\alpha^{\sigma}d^{\sigma}\varrho_1\varrho_2}. \tag{15}$$

It could be noted that the threshold quantity consists of three parts that describe various transmission routes. One may observe, that there is a transmission from an infected human, while the other from reservoirs.

Similarly, we use the above quantity (R_0) and assume that X_2 is the endemic equilibrium of the fractional order model, then the components are calculated by solving system (6) simultaneously at steady state. We also set $S_h = S_h^*$, $L_h = L_h^*$, $I_h = I_h^* R_h = R_h^*$, and $M = M^*$ for the sake of convenience, then the corresponding endemic equilibrium leads to $X_2 = (S_h^*, L_h^*, I_h^*, R_h^*, M^*)$, whoso components are defined by the following equation:

$$\begin{aligned} S_h^* &= \frac{\varrho_1\varrho_2\alpha^{\sigma}}{\beta_1^{\sigma}\varrho_2\alpha^{\sigma} + \alpha^{\sigma}\gamma_1^{\sigma}\gamma^{\sigma}\beta_2^{\sigma} + \psi^{\sigma}\beta_3^{\sigma}\eta_1^{\sigma}\varrho_2 + \eta_2^{\sigma}\gamma_1^{\sigma}\psi^{\sigma}\beta_3^{\sigma}}, \\ L_h^* &= \frac{\alpha^{\sigma}d^{\sigma}\varrho_2\varrho_1(R_0 - 1)}{q_2(\beta_1^{\sigma}\varrho_2\alpha^{\sigma} + \alpha^{\sigma}\gamma^{\sigma}\gamma_1^{\sigma}\beta_2^{\sigma} + \psi^{\sigma}\beta_3^{\sigma}\eta_1^{\sigma}\varrho_2 + \eta_2^{\sigma}\gamma_1^{\sigma}\psi^{\sigma}\beta_3^{\sigma})}, \\ I_h^* &= \frac{\gamma_1^{\sigma}}{\varrho_2}L_h^*, R_h^* = \frac{1}{d^{\sigma}\varrho_2}(\gamma_2^{\sigma}\varrho_2 + \gamma_1^{\sigma}\gamma_3^{\sigma})L_h^*, \\ M^* &= \frac{1}{\alpha^{\sigma}\varrho_2}(\eta_1^{\sigma}\varrho_2^{\sigma} + \gamma_1^{\sigma}\eta_2^{\sigma})L_h^*. \end{aligned} \tag{16}$$

The endemic equilibrium reveals that X_2 exists only if $R_0 > 1$. For this, we sate the following result.

Lemma 3. *The endemic equilibrium $X_2 = (S_h^*, L_h^*, I_h^*, R_h^*, M^*)$ for the proposed problem (6) exists only whenever, the threshold quantity (R_0) is greater than unity.*

We use the linear stability analysis to discuss the temporal dynamics of the fractional model (6) around X_1 and X_2. So we have the following results.

Theorem 1. *If the threshold quantity (R_0) is less than unity, then the local, as well as global dynamics of the problem, is asymptotically stable around $X_1 = (S_{h0}, 0, 0, 0, 0)$.*

Proof. Following Theorem 3 reported in [37] to obtain the required results. Since it is clear that all other compartments of the proposed model do not depend explicitly on the recovered class, so we study the dynamics of the model for only the three-compartment, which will be enough for the whole model. Let $A(X_1)$ be the Jacobian matrix of the proposed model (6) around X_1; then,

$$A(X_1) = \begin{pmatrix} -d^{\sigma} & -\frac{\beta_1^{\sigma}\Lambda^{\sigma}}{d^{\sigma}} & -\frac{\gamma^{\sigma}\beta_2^{\sigma}\Lambda^{\sigma}}{d^{\sigma}} & -\frac{\psi^{\sigma}\beta_3^{\sigma}\Lambda^{\sigma}}{d^{\sigma}} \\ 0 & \frac{\beta_1^{\sigma}\Lambda^{\sigma}}{d^{\sigma}} - \varrho_1 & \frac{\gamma^{\sigma}\beta_2^{\sigma}\Lambda^{\sigma}}{d^{\sigma}} & \frac{\psi^{\sigma}\beta_3^{\sigma}\Lambda^{\sigma}}{d^{\sigma}} \\ 0 & \gamma_1^{\sigma} & -\varrho_2 & 0 \\ 0 & \eta_1^{\sigma} & \eta_2^{\sigma} & -\alpha^{\sigma} \end{pmatrix}. \tag{17}$$

The calculation shows that $A(X_1)$, obviously has two negative eigenvalue i.e., $\lambda_1 = -d^{\sigma}$ and $\lambda_2 = -\alpha^{\sigma}$. To find the nature of the remaining, we take the matrix given by the following equation:

$$A(X_1) = \begin{pmatrix} \frac{\beta_1^{\sigma}\Lambda^{\sigma}}{d^{\sigma}} - \varrho_1 & \frac{\gamma^{\sigma}\beta_2^{\sigma}\Lambda^{\sigma}}{d^{\sigma}} \\ \gamma_1^{\sigma} & -\varrho_2 \end{pmatrix}. \tag{18}$$

It is sufficient for the Routh–Hurwitz criteria that H_1: $\text{trace}(A(x_1)) < 0$, and $\det(A(X_1)) > 0$ holds. We calculate the $\text{trace}(A(x_1))$ and $\det(A(X_1))$, such that

$$\text{trace}(A(X_1)) = -\varrho_1(1 - R_1) - \varrho_2, \tag{19}$$

$$\det(A(X_1)) = q_2 q_3(1 - (R_1 + R_2)). \tag{20}$$

It can be noted from the above equations (19)–(20) that trace(A(X1))<0 and det(A(X1))>0, if R1+R2<1.. So the Routh–Hurwitz criteria are satisfied if $R_0 < 1$. It proves the conclusion that the local dynamics of the model (6) is asymptotically stable, if $R_0 < 1$. □

The application of linear stability analysis is utilized to find the dynamics of the proposed model (6) around its

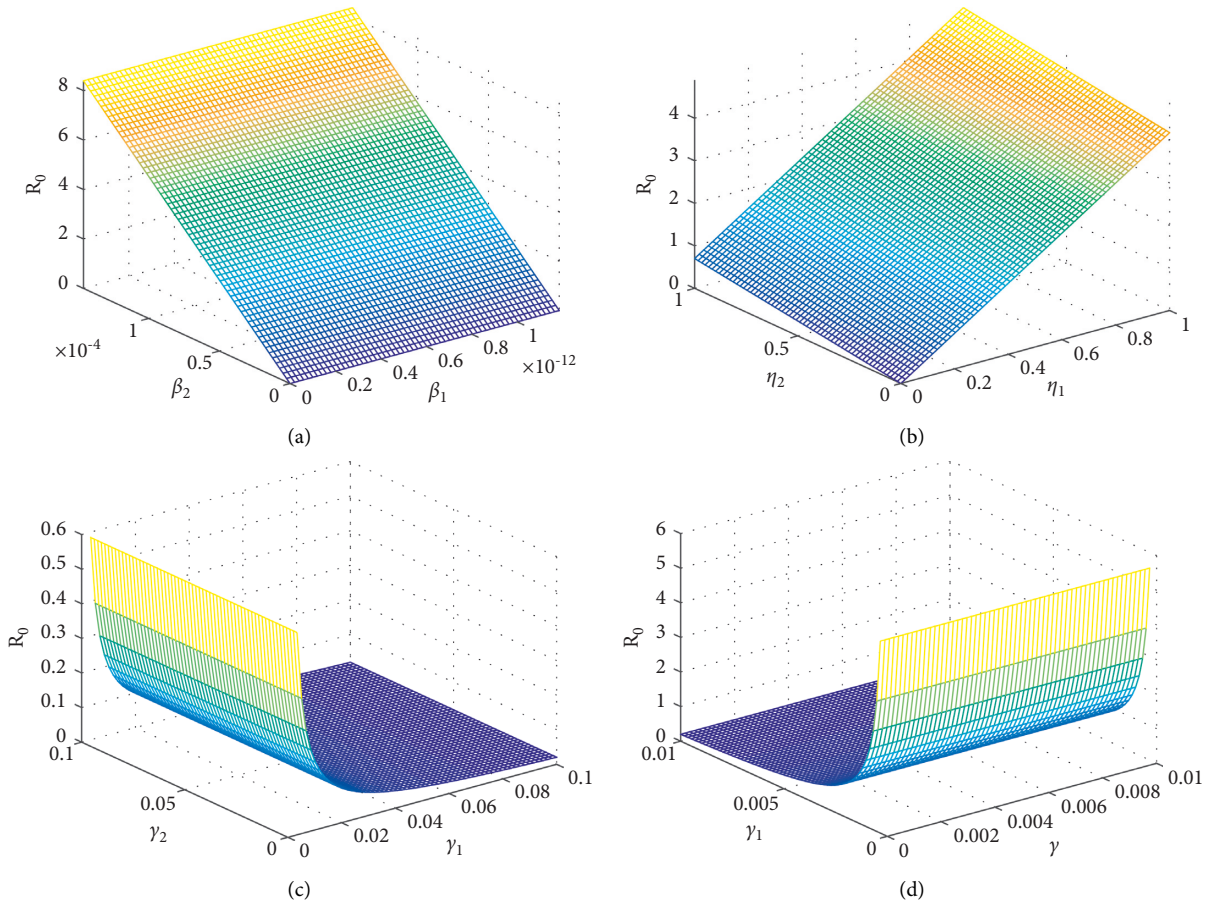

FIGURE 1: The graphical results demonstrate the local sensitivity analysis of the threshold quantity (R_0) with respect to the model parameters β_1, β_2, η_1, η_2, γ_1, γ_2, and γ. For this we use the parametric values as follows: $\Pi = 0.2453$, $\psi = 0.00180$, $\beta_1 = 0.0001847$, $\gamma_3 = 0.09960$, $\gamma = 0.8631$, $\gamma_4 = 0.01470$, $\beta_2 = 0.0004615$, $\mu_1 = 0.00130$, $\mu_0 = 0.00002$, $\mu_2 = 0.00230$, $\gamma_1 = 0.2381$, $\eta_1 = 0.00200$, $\gamma_2 = 1.3184$, and $\eta_2 = 0.00005$. (a)R_0 verses β_1 and β_2. (b)R_0 verses η_1 and η_2. (c)R_0 verses γ_1 and γ_2. (d)R_0 verses γ and γ_1.

associated endemic equilibrium (16). For this, we describe the result as follows. □

Theorem 2. *If the threshold quantity (R_0) is greater than unity i.e., $R_0 > 1$, then the local as well as the global dynamics of the endemic equilibrium, $X_2 = (S_h^*, L_h^*, I_h^*, R_h^*, M^*)$ is asymptotically stable.*

Proof. Using the theory of a dynamical system, we discuss the local dynamics of the proposed system around the endemic equilibrium. Let $A(X_2)$ be the Jacobian matrix of system (6) around X_2; then,

$$A(X_*) = \begin{pmatrix} -(d^\sigma + \beta_1^\sigma L_h^* + \gamma^\sigma \beta_2^\sigma I_h^* + \psi^\sigma \beta_3^\sigma M^*) & -\beta_1^\sigma S_h^* & -\gamma^\sigma \beta_2^\sigma S_h^* & -\psi^\sigma \beta_3^\sigma S_h^* \\ \beta_1^\sigma L_h^* + \gamma^\sigma \beta_2^\sigma I_h^* + \psi^\sigma \beta_3^\sigma M^* & \psi^\sigma \beta_3^\sigma S_h^* - \varrho_1 & \beta_2^\sigma S_h^* & \\ 0 & \gamma_1^\sigma & -\varrho_2 & 0 \\ 0 & \eta_1^\sigma & \eta_2^\sigma & -\alpha^\sigma \end{pmatrix}. \tag{21}$$

We find the characteristic polynomial of the matrix (21), such that

$$p(\lambda) = \lambda^4 + k_1\lambda^3 + k_2\lambda^2 + k_3\lambda + k_4, \tag{22}$$

where

$$
\begin{aligned}
k_1 &= \left((\alpha^\sigma + d^\sigma + \varrho_1)\left(\beta_1^\sigma \varrho_2 \alpha^\sigma + \alpha^\sigma \gamma_1^\sigma \gamma^\sigma \beta_2^\sigma + \psi^\sigma \beta_3^\sigma \eta_1^\sigma \varrho_2 + \eta_2^\sigma \gamma_1^\sigma \psi^\sigma \beta_3^\sigma\right) + \varrho_1\left(\alpha^\sigma \gamma_1^\sigma \gamma^\sigma \beta_2^\sigma + \psi^\sigma \beta_3^\sigma \eta_1^\sigma \varrho_2\right.\right.\\
&\quad \left.\left. + \eta_2^\sigma \gamma_1^\sigma \psi^\sigma \beta_3^\sigma + \left(\beta_1^\sigma \alpha^\sigma d^\sigma \varrho_2 + \alpha^\sigma d^\sigma \gamma_1^\sigma \gamma^\sigma \beta_2^\sigma + \psi^\sigma \beta_3^\sigma \left(\eta_1^\sigma \varrho_2 + \eta_2^\sigma \gamma_1^\sigma\right) d^\sigma\right)(R_0 - 1),\right.\right.\\
k_2 &= \alpha^{2\sigma} d^\sigma \beta_1^\sigma \varrho_2 + d^\sigma \varrho_2^2 \beta_1^\sigma \alpha^\sigma + \alpha^{2\sigma} \varrho_2^2 \beta_1^\sigma + \alpha^\sigma d^\sigma \psi^\sigma \beta_3^\sigma \eta_1^\sigma \varrho_2 + \alpha^\sigma d^\sigma \eta_2^\sigma \gamma_1^\sigma \psi^\sigma \beta_3^\sigma + \alpha^\sigma \varrho_1 \eta_2^\sigma \gamma_1^\sigma \psi^\sigma \beta_3^\sigma\\
&\quad + \alpha^\sigma \varrho_2 \eta_2^\sigma \gamma_1^\sigma \psi^\sigma \beta_3^\sigma + d^\sigma \varrho_1 \alpha^\sigma \gamma_1^\sigma \gamma^\sigma \beta_2^\sigma + d^\sigma \varrho_1 \psi^\sigma \beta_3^\sigma \eta_1^\sigma \varrho_2 + d^\sigma \varrho_1 \eta_2^\sigma \gamma_1^\sigma \psi^\sigma \beta_3^\sigma + d^\sigma \varrho_2 \alpha^\sigma \gamma_1^\sigma \gamma^\sigma \beta_2^\sigma\\
&\quad + d^\sigma \varrho_2 \eta_2^\sigma \gamma_1^\sigma \psi^\sigma \beta_3^\sigma + \varrho_1 \varrho_2 \eta_2^\sigma \gamma_1^\sigma \psi^\sigma \beta_3^\sigma + \alpha^{2\sigma} d^\sigma \gamma_1^\sigma \gamma^\sigma \beta_2^\sigma + \alpha^{2\sigma} \gamma_1^\sigma \gamma^\sigma \beta_2^\sigma + \alpha^{2\sigma} \varrho_2 \gamma_1^\sigma \gamma^\sigma \beta_2^\sigma\\
&\quad + \alpha^\sigma \varrho_2^2 \psi^\sigma \beta_3^\sigma \eta_1^\sigma + d^\sigma \varrho_2^2 \psi^\sigma \beta_3^\sigma \eta_1^\sigma + \varrho_2 \varrho_3^2 \psi^\sigma \beta_3^\sigma \eta_1^\sigma + d^\sigma \left(\alpha^{3\sigma} \beta_1^{2\sigma} \varrho_2^2 + \varrho_2^3 \beta_1^{2\sigma} \alpha^{2\sigma} + \varrho_2^4 \alpha^{4\sigma} \beta_1^{2\sigma}\right.\\
&\quad + 2\beta_3^\sigma \psi^\sigma \varrho_2^3 \eta_1^\sigma \beta_1^\sigma \alpha^\sigma + 2\beta_3^{2\sigma} \psi^{2\sigma} \varrho_2^2 \eta_1^\sigma \eta_2^\sigma \gamma_1^\sigma + 2\alpha^{3\sigma} \beta_1^\sigma \varrho_2 \gamma_1^\sigma \gamma^\sigma \beta_2^\sigma + 2\varrho_2^2 \beta_1^\sigma \alpha^{2\sigma} \gamma_1^\sigma \gamma^\sigma \beta_2^\sigma\\
&\quad + 2\varrho_2^3 \alpha^{4\sigma} \beta_1^\sigma \gamma_1^\sigma \gamma^\sigma \beta_2^\sigma + 2\varrho_2^4 \alpha^{3\sigma} \beta_1^\sigma \psi^\sigma \beta_3^\sigma \eta_1^\sigma + \varrho_2^2 \alpha^{2\sigma} \eta 2^{2\sigma} \gamma_1^{2\sigma} \psi^{2\sigma} \beta_3^{2\sigma} + \gamma_1^\sigma \alpha^{2\sigma} \varrho_2 \varrho_1 \beta_2^{2\sigma} \gamma^\sigma\\
&\quad + \alpha^\sigma \beta_3^{2\sigma} \psi^{2\sigma} \eta_1^{2\sigma} \varrho_2^2 + \alpha^\sigma \beta_3^{2\sigma} \psi^{2\sigma} \gamma_1^{2\sigma} \eta_2^{2\sigma} + \beta_3^{2\sigma} \psi^{2\sigma} \varrho_1 \eta_1^{2\sigma} \varrho_2^2 + \beta_3^{2\sigma} \psi^{2\sigma} \varrho_1 \gamma_1^{2\sigma} \eta_2^{2\sigma} + \beta_3^{2\sigma} \psi^{2\sigma} \varrho_2 \gamma_1^{2\sigma} \eta_2^{2\sigma}\\
&\quad + \varrho_2^2 \alpha^{4\sigma} \gamma_1^{2\sigma} \gamma^{2\sigma} \beta_2^{2\sigma} + \varrho_2^4 \alpha^{2\sigma} \psi^{2\sigma} \beta_3^{2\sigma} \eta_1^{2\sigma} + \varrho_1 \alpha^{2\sigma} \gamma_1^{2\sigma} \gamma^{2\sigma} \beta_2^{2\sigma} + q_3 \alpha^{2\sigma} \gamma_1^{2\sigma} \gamma^{2\sigma} \beta_2^{2\sigma} + 2\alpha^{2\sigma} \beta_3^\sigma \psi^\sigma \eta_1^\sigma q_3^2 \beta_1^\sigma\\
&\quad + 2\alpha^{2\sigma} \beta_3^\sigma \psi^\sigma \eta_1^\sigma \varrho_2 \gamma_1^\sigma \gamma^\sigma \beta_2^\sigma + 2\alpha^\sigma \beta_3^{2\sigma} \psi^{2\sigma} \eta_1^\sigma \varrho_2 \eta_2^\sigma \gamma_1^\sigma + 2\alpha^{2\sigma} \beta_3^\sigma \psi^\sigma \gamma_1^\sigma \eta_2^\sigma \beta_1^\sigma \varrho_2 + 2\alpha^{2\sigma} \beta_3^\sigma \psi^\sigma \gamma_1^{2\sigma} \eta_2^\sigma \gamma^\sigma \beta_2^\sigma\\
&\quad + \beta_3^\sigma \psi^\sigma \varrho_1 \eta_1 \varrho_2^2 \beta_1^\sigma \alpha^\sigma + 2\beta_3^\sigma \psi^\sigma \varrho_1 \eta_1^\sigma \varrho_2 \alpha^\sigma \gamma_1^\sigma \gamma^\sigma \beta_2^\sigma + 2\beta_3^{2\sigma} \psi^{2\sigma} \varrho_1 \eta_1^\sigma \varrho_2 \eta_2^\sigma \gamma_1^\sigma + \beta_3^\sigma \psi^\sigma \varrho_1 \gamma_1^\sigma \eta_2^\sigma \beta_1^\sigma \varrho_2 \alpha^\sigma\\
&\quad + 2\beta_3^\sigma \psi^\sigma \varrho_1 \gamma_1^{2\sigma} \eta_2^\sigma \alpha^\sigma \gamma^\sigma \beta_2^\sigma + 2\beta_3^\sigma \psi^\sigma \varrho_2^2 \eta_1^\sigma \alpha^\sigma \gamma_1^\sigma \gamma^\sigma \beta_2^\sigma + 2\beta_3^\sigma \psi^\sigma \varrho_2^2 \gamma_1^\sigma \eta_2^\sigma \beta_1^\sigma \alpha^\sigma + 2\beta_3^\sigma \psi^\sigma \varrho_2 \gamma_1^{2\sigma} \eta_2^\sigma \alpha^\sigma \gamma^\sigma \beta_2^\sigma\\
&\quad + \varrho_1 \beta_1^\sigma \varrho_2 \alpha^{2\sigma} \gamma_1^\sigma \gamma^\sigma \beta_2^\sigma + 2\varrho_2^3 \alpha^{3\sigma} \beta_1^\sigma \eta_2^\sigma \gamma_1^\sigma \psi^\sigma \beta_3^\sigma + 2\varrho_2^3 \alpha^{3\sigma} \gamma_1^\sigma \gamma^\sigma \beta_2^\sigma \psi^\sigma \beta_3^\sigma \eta_1^\sigma + 2\varrho_2^2 \alpha^{3\sigma} \gamma_1^{2\sigma} \gamma^\sigma \beta_2^\sigma \eta_2^\sigma \psi^\sigma \beta_3^\sigma\\
&\quad + 2\varrho_2^{3\sigma} \alpha^{2\sigma} \psi^{2\sigma} \beta_3^{2\sigma} \eta_1^\sigma \eta_2^\sigma \gamma_1^\sigma + \varrho_1 \varrho_2^2 \alpha^\sigma \beta_2^\sigma \beta_3^\sigma \psi^\sigma \eta_1^\sigma + \varrho_2 \varrho_3 \alpha^\sigma \beta_2^\sigma \beta_3^\sigma \psi^\sigma \gamma_1^\sigma \eta_2^\sigma + \beta_3^{2\sigma} \psi^{2\sigma} \varrho_2^3 \eta_1^{2\sigma}\\
&\quad + \alpha^{3\sigma} \gamma_1^{2\sigma} \gamma^{2\sigma} \beta_2^{2\sigma} (R_0 - 1),\\
k_3 &= d\left(\beta_1^\sigma \varrho_2 \alpha^\sigma + \alpha^\sigma \gamma_1^\sigma \gamma^\sigma \beta_2^\sigma + \psi^\sigma \beta_3^\sigma \eta_1^\sigma \varrho_2 + \eta_2^\sigma \gamma_1^\sigma \psi^\sigma \beta_3^\sigma\right)\left(\psi^\sigma \varrho_1 \eta_1^\sigma \beta_3^\sigma \varrho_2^2 + \psi^\sigma \varrho_2 \beta_3^\sigma \alpha^\sigma q^\sigma \eta_1^\sigma + \psi^\sigma \varrho_2 \beta_3^\sigma \varrho_1 \eta_2^\sigma \gamma_1^\sigma\right.\\
&\quad + \psi^\sigma \beta_3^\sigma \varrho_1 \alpha^\sigma \gamma_1^\sigma \eta_2^\sigma + \psi^\sigma \beta_3^\sigma \alpha^\sigma \varrho_2 \eta_2^\sigma \gamma_1^\sigma + \varrho_2^2 \varrho_1 \alpha^\sigma \beta_2^\sigma + \alpha^{2\sigma} \varrho_2^2 \beta_1^\sigma + \varrho_2 \varrho_1 \alpha^\sigma \gamma^\sigma \gamma_1^\sigma \beta_3^\sigma - \varrho_1 \varrho_2 \alpha^\sigma \gamma_1^\sigma \gamma^\sigma \beta_2^\sigma\\
&\quad + \varrho_2 \alpha^{2\sigma} \gamma_1^\sigma \gamma^\sigma \beta_2^\sigma + \varrho_1 \varrho_2 \alpha^{2\sigma} \beta_2^\sigma + \gamma_1^\sigma \alpha^{2\sigma} \varrho_1 \beta_2^\sigma \gamma^\sigma + \gamma_1^\sigma \alpha^\sigma (R_0 - 1) + \left(d^\sigma \varrho_1 \varrho_2^2 \psi^\sigma \beta_3^\sigma \eta_1^\sigma\right.\\
&\quad + d^\sigma \varrho_1 \varrho_2 \eta_2^\sigma \gamma_1^\sigma \psi^\sigma \beta_3^\sigma + \alpha^{2\sigma} d^\sigma \varrho_2^2 \beta_1^\sigma + \gamma_1^\sigma \alpha^{2\sigma} d^\sigma \beta_2^\sigma \gamma^\sigma \varrho_2 + \alpha^\sigma d^\sigma \varrho_2^2 \psi^\sigma \beta_3^\sigma \eta_1^\sigma + \alpha^\sigma d^\sigma \varrho_2 \eta_2^\sigma \gamma_1^\sigma \psi^\sigma \beta_3^\sigma\\
&\quad + \gamma_1^\sigma \alpha^{2\sigma} d^\sigma \beta_2^\sigma \gamma^\sigma \varrho_1 + \alpha^\sigma d^\sigma \varrho_1 \eta_2^\sigma \gamma_1^\sigma \psi^\sigma \beta_3^\sigma + \alpha^\sigma \varrho_1 \varrho_2^2 \psi^\sigma \beta_3^\sigma \eta_1^\sigma - \varrho_1 \varrho_2^2 \alpha^\sigma (\beta_1^\sigma \varrho_2 \alpha^\sigma + \alpha^\sigma \gamma_1^\sigma \gamma^\sigma \beta_2^\sigma\\
&\quad \left.\left. + \psi^\sigma \beta_3^\sigma \eta_1^\sigma \varrho_2 + \eta_2^\sigma \gamma_1^\sigma \psi^\sigma \beta_3^\sigma\right), \text{ and}\right.\\
k_4 &= d^\sigma \varrho_2 \varrho_3 \alpha^{2\sigma} \left(\varrho_2^2 \beta_2^\sigma \beta_3^\sigma \gamma^\sigma \gamma_1^\sigma \psi^\sigma \alpha^{3\sigma} + \varrho_2^2 \beta_1^\sigma \beta_2^\sigma \alpha^\sigma + \varrho_2^2 \beta_2^\sigma \beta_3^\sigma \psi^\sigma \eta_1^\sigma + \varrho_2 \gamma_1^\sigma \beta_2^{2\sigma} \gamma^\sigma \alpha^\sigma + \varrho_2 \beta_2^\sigma \beta_3^\sigma \psi^\sigma \gamma_1^\sigma \eta_2^\sigma\right.\\
&\quad + \varrho_2 \gamma_1^\sigma \beta_2^\sigma \beta_3^\sigma \eta_1^\sigma \gamma^\sigma \psi^\sigma + \varrho_2 \beta_3^{2\sigma} \gamma^\sigma \gamma_1^\sigma \psi^\sigma \eta_1^\sigma + \gamma_1^{2\sigma} \beta^\sigma - 2\beta_3^\sigma \gamma^{2\sigma} \alpha^\sigma + \beta_3^{2\sigma} \gamma^\sigma \gamma_1^{2\sigma} \psi^\sigma \eta_2^\sigma\\
&\quad \left. + \gamma_1^{2\sigma} \beta_2^\sigma \beta_3^\sigma \eta_2^\sigma \gamma^\sigma \psi^\sigma (R_0 - 1).\right.
\end{aligned}
\tag{23}
$$

Eigenvalues (roots) of (22) are negative or having negative real parts, if (H_0): $k_i > 0$, $i = 1, 2, \ldots, 4$ and $\delta > 0$ holds, where

$$
\Delta_4 = \begin{pmatrix} k_1 & 1 & 0 & 0 \\ k_3 & k_2 & k_1 & 1 \\ 0 & k_4 & k_3 & k_2 \\ 0 & 0 & 0 & k_4 \end{pmatrix}. \tag{24}
$$

It could be noted, from the above equations, that obviously H_0 holds, if $R_0 > 1$. Thus, we conclude that the local dynamics of the proposed model (6) at endemic equilibrium (X_2) is asymptotically stable, if the threshold quantity is greater than unity. □

Theorem 3. *If $R_0 \le 1$, then the point X_1 of the model (6) is globally asymptotically stable, while the same holds for X_2 whenever $R_0 > 1$.*

Proof. To perform the global analysis of the proposed fractional order epidemiological model, first we assume that $X(t) = (S_h(t), L_h(t), I_h(t), R_h(t), M(t))$ and if $t \longrightarrow \infty$, then it has finite limit, therefore by following the result 3.1 in [38], then from first equation of the model (7), we may write the following equation:

$$
CFD_{0,t}^{\alpha} S_h(t) \le \Lambda^\sigma - d^\sigma S_h(t). \tag{25}
$$

Since for every $\phi \le \phi e^t$, so by following the result Theorem 1 in [38] with the application of *mean value theorem*, the above (25) may leads to the following equation:

$$
\left\| S_h(t) \right\| \le aU \exp\left[-\{(-d)\} + 1\right]t, t \ge T, \tag{26}
$$

Table 1: The results represent the sensitivity indices of epidemic parameters.

Parameter	Index value	Parameter	Index value
β_1	0.1075×10^{-7}	β_2	0.999999
γ_1	−0.995739	η_2	0.004176
γ	0.3489×10^{-8}	γ_2	−0.00387
γ_3	−0.00029	η_1	0.995823

where $a = \|S_h(0)\|e^{-T} + KT^{\sigma}e^{-T}/\sigma\Gamma(\sigma) + \Lambda^{\sigma}$, and $U > 0$. Consequently, we may derive the following equation:

$$\lim_{t\longrightarrow\infty} S_h(t) \leq U\Lambda^{\sigma}. \tag{27}$$

Similarly, lim of $L_h(t)$, $I_h(t)$, $R_h(t)$, and $M(t)$ can be proved. We also assume that

$$\lim_{t\longrightarrow\infty} X(t) = \left(S_h^{\infty}, L_h^{\infty}, I_h^{\infty}, R_h^{\infty}, M^{\infty}\right),$$
$$\vartheta(X) = \begin{pmatrix} \psi_1(X) \\ \psi_2(X) \\ \psi_3(X) \\ \psi_4(X) \\ \psi_5(X) \end{pmatrix} = \begin{pmatrix} \Lambda^{\sigma} - \left(\beta_1^{\sigma}L_h(t) + \gamma^{\sigma}\beta_2^{\sigma}I_h(t) + \psi^{\sigma}\beta_3^{\sigma}M(t) + d^{\sigma}\right)S_h(t), \\ \left(\beta_1^{\sigma}L_h(t) + \gamma^{\sigma}\beta_2^{\sigma}I_h(t) + \psi^{\sigma}\beta_3^{\sigma}M(t)S_h(t) - \varrho_1 L_h(t), \\ \gamma_1^{\sigma}L_h(t) - \varrho_2 I_h(t), \\ \gamma_2^{\sigma}L_h(t) + \gamma_3^{\sigma}I_h(t) - dR_h(t), \\ \eta_1^{\sigma}L_h(t) + \eta_2^{\sigma}I_h(t) - \alpha^{\sigma}M(t) \end{pmatrix}. \tag{28}$$

Thus, in the light of *mean value theorem*, there exists constants $C_1 > 0, C_2 > 0$, such that

$$\|\vartheta(X)\| \leq C_1 + C_2\|X\|. \tag{29}$$

So, Theorem 2.1 and 1 in [39] implies that $CFD_{0,t}^{\alpha}(S_h(t), L_h(t), I_h(t), R_h(t), M(t))$ is uniformly continuous. Thus, the application of *Barbalat's Lemma* (see for detail, [40]) gives the following equation:

$$\lim_{t\longrightarrow\infty}{}^{CF}D_{0,t}^{\alpha}(X(t)) = (0,0,0,0,0,0). \tag{30}$$

Consequently,

$$\begin{cases} \Lambda^{\sigma} - \left(\beta_1^{\sigma}L_h(t) + \gamma^{\sigma}\beta_2^{\sigma}I_h(t) + \psi^{\sigma}\beta_3^{\sigma}M(t) + d^{\sigma}\right)S_h(t) = 0, \\ \left(\beta_1^{\sigma}L_h(t) + \gamma^{\sigma}\beta_2^{\sigma}I_h(t) + \psi^{\sigma}\beta_3^{\sigma}M(t)\right)S_h(t) - \varrho_1 L_h(t) = 0, \gamma_1^{\sigma}L_h(t) - \varrho_2 I_h(t) = 0, \\ \gamma_2^{\sigma}L_h(t) + \gamma_3^{\sigma}I_h(t) - d^{\sigma}R_h(t) = 0, \eta_1^{\sigma}L_h(t) + \eta_2^{\sigma}I_h(t) - \alpha^{\sigma}M(t) = 0. \end{cases} \tag{31}$$

Therefore, $(S_h^{\infty}, L_h^{\infty}, I_h^{\infty}, R_h^{\infty}, M^{\infty})$ is the equilibrium of model (6) and by the similar procedure as adopted in [41], we reach to the following equation:

$$\lim_{t\longrightarrow\infty}(X(t)) = X_1 \text{ or } \lim_{t\longrightarrow\infty}(X(t)) = X_2. \tag{32}$$

So, it could be concluded that the disease endemic state X_2 does not exists if $R_0 < 1$, and so $\lim X(t) = X_1$ whenever t approaches ∞ and if $R_0 = 1$ then $X_2 = X_1$, and $\lim X(t) = X_1$ as t approaches ∞, while on the other hand whenever $R_0 > 1$, then X_2 exists and thus $\lim X(t) = X_2$ as t tend to ∞. □

4. Numerical Simulation

In this section, we present the numerical simulation of the proposed epidemic problem. We divided the section into two subsections in which we discuss the sensitivity analysis of every epidemic parameter and its relative impact on disease transmission. We also discuss the temporal dynamics for the long run and present the significance of fractional parameters.

4.1. Sensitivity Analysis. We discuss the local sensitivity analysis of the model parameters to define the relation between threshold quantity and the epidemic parameters. This allows us to measure the relative impact of every epidemic parameter on disease transmission. We follow the work presented in [42] to perform the sensitivity analysis. Using the sensitivity index formula, we get the sensitivity indices as given in Table 1. It may be noted from the sensitivity indices that the set of parameters $S_1 = \{\beta_1, \beta_2, \eta_1, \eta_2, \gamma\}$ has a direct relation with threshold quantity, which means that increase in the value of these

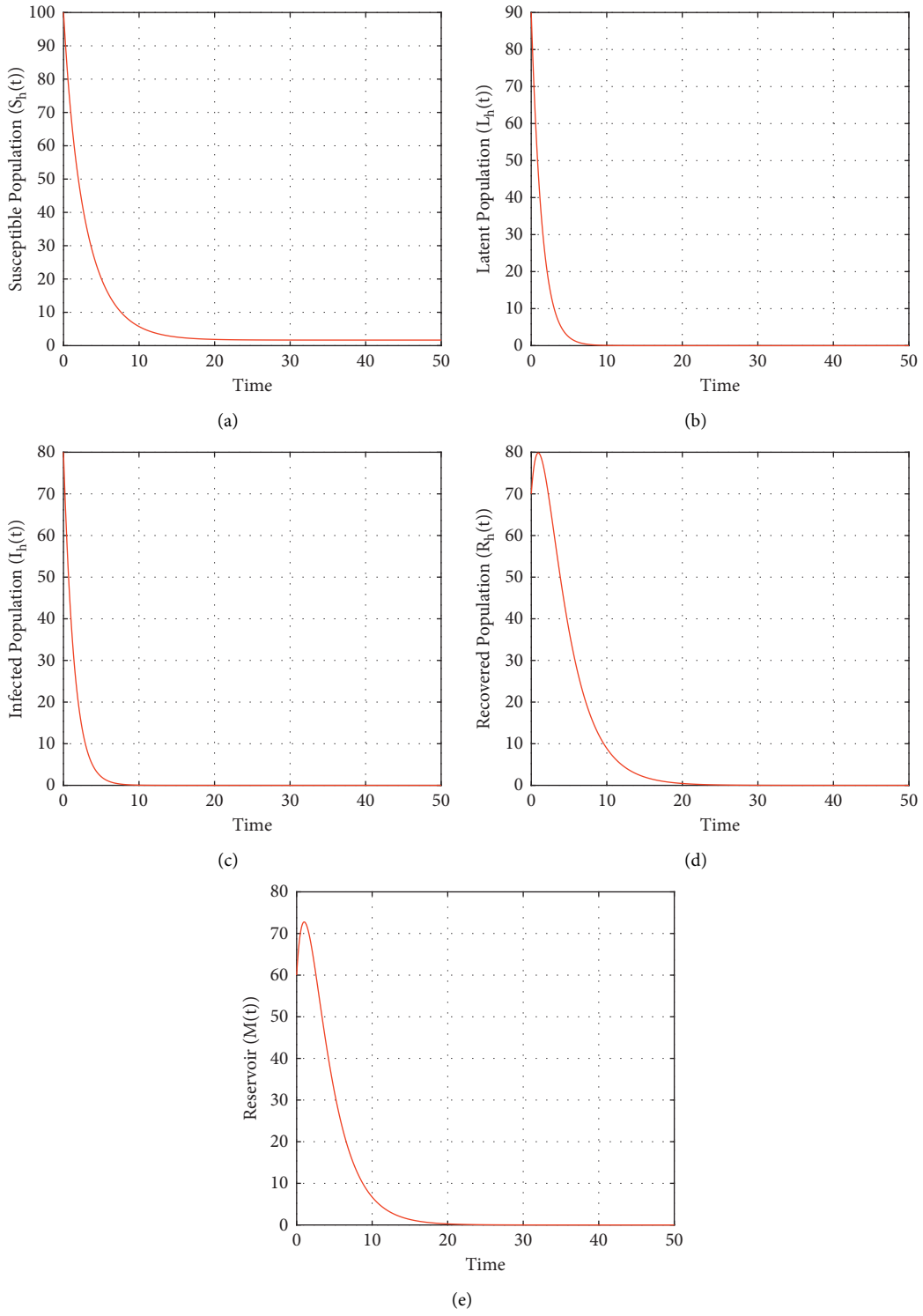

FIGURE 2: The results visualize the dynamics of the fractional order model around the disease-free state (X_1), where the value of epidemic parameters are chosen as: $\Lambda = 0.5$, $\beta_1 = 0.0011$, $\beta_2 = 0.00000005$, $\beta_3 = 0.0001$, $d = 0.3$, $\gamma_1 = 0.0000001$, $\gamma_2 = 0.5$, $\gamma_3 = 0.005$, $d_1 = 0.02$, $\eta_1 = 0.2$, $\eta_2 = 0.6$, and $\alpha = 0.6$. In this case, the value of the threshold parameter is less than unity i.e., $R_0 < 1$.(a) Susceptible–$S_h(t)$. (b) Latent–$L_h(t)$. (c) Infected–$I_h(t)$. (d) Recovered–$R_h(t)$. (e) Reservoir–. $M(t)$.

parameters causes an increase in the value of the threshold quantity of the model. On the other hand, there is an inverse relationship between the set of parameters $\{\gamma_1, \gamma_2, \gamma_3\}$ and so an increase in these parameters will cause a decrease in the value of threshold quantity. The highest sensitivity index parameter is β_2 having the sensitivity index 0.999999, which means that an increase in the value of this parameter say by 10% would increase the value of the threshold quantity by

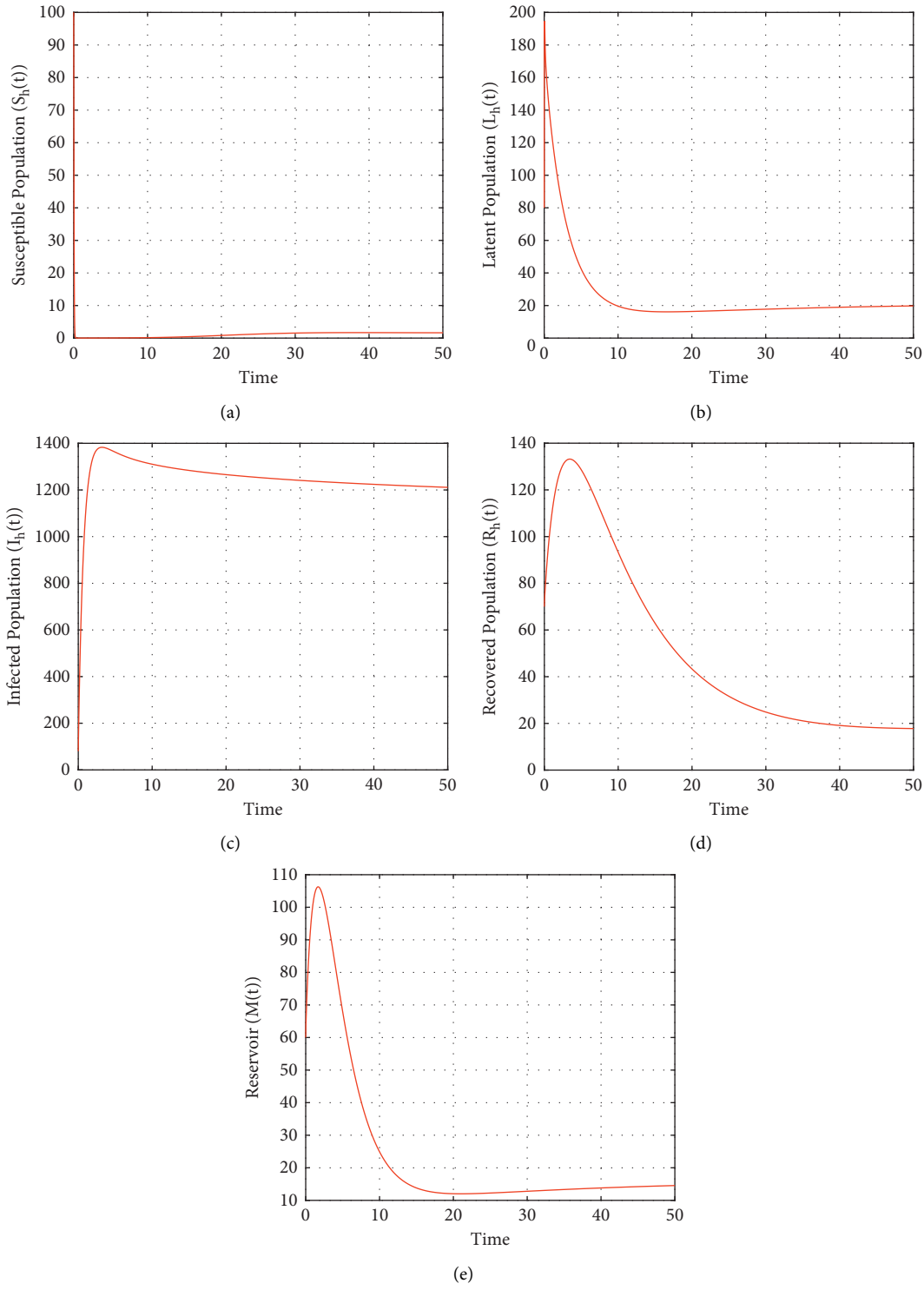

FIGURE 3: The results visualizes the dynamics of the proposed model at endemic state (X_2), where the value of the epidemic parameters are: $\Lambda = 0.5$, $\beta_1 = 0.11$, $\beta_2 = 0.00005$, $\beta_3 = 0.1$, $d = 0.1$, $\gamma_1 = 0.001$, $\gamma_2 = 0.2$, $\gamma_3 = 0.3$, $d_1 = 0.2$, $\eta_1 = 0.3$, $\eta_2 = 0.5$, and $\alpha = 0.4$. In this case, the value of the reproductive number is greater than unity i.e., $R_0 > 1$. (a) Susceptible–$S_h(t)$. (b) Latent–$L_h(t)$. (c) Infected–$I_h(t)$. (d) Recovered–$R_h(t)$. (e) Reservoir–$M(t)$.

9.99999%, as shown in Figure 1(a). Similarly the collectively impact of other parameters of S_1 is approximately 9.89%, if their values increase or decrease by 10%, as shown in Figures 1(a) and 1(b). Moreover, the parameters of S_2 have a negative relation and therefore its collectively impact is 9.94% whenever the value of the parameters given in S2 increases or decreases by 10 % (see Figures 1(c) and Figures 1(d)). More precisely, if the value of the parameters of S_2 are

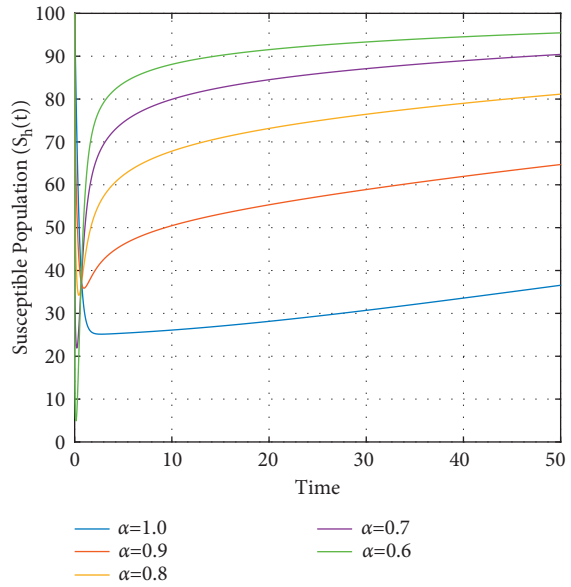

FIGURE 4: The graph visualizes the temporal dynamics of the susceptible for long run against various value of (σ), while the value of epidemic parameters are: $\Lambda = 0.4$, $\beta_1 = 0.011$, $\beta_2 = 0.005$, $\psi = 0.016$, $\beta_3 = 0.01$, $d = 0.01\,\gamma_1 = 0.05$, $\gamma_2 = 0.05$, $\gamma_3 = 0.05$, $d_1 = 0.002$, $\eta_1 = 0.01$, $\eta_2 = 0.06$, and $\alpha = 0.06$. We also used the initial population sizes: $(100, 90, 80, 70, 60)$.

increased by 10%, the basic reproductive number will be decreased by 9.94%, while if one decreases the value of the parameters, the threshold quantity will be increased by 9.94%.

4.2. Verification of Stability Results. We find out the numerical simulation to verify the theocratical work carried out for the fractional-order SARS-CoV-2 transmission epidemiological model (6). To show the validity of the analytical findings we present the large-scale simulation. There are not many choices like the traditional numerical methods to choose various schemes for the numerical simulation of fractional-order models [43], therefore extensive attention is required to formulate new and convenient techniques for the simulation of fractional models. We follow a numerical scheme formulated in [18, 44]. We assume the time step $h = 10^{-3}$ for integration with the simulation interval $[0, t]$, $n = T/h$ and $n \in \mathbb{N}$. We also assume that $u = 0, 1, 2, \ldots, n$, therefore the discretization for the proposed model looks like the following equation:

$$
\begin{aligned}
CFS_{h(u+1)} &= S_h(0) + \{\Lambda^\sigma - (\beta_1^\sigma L_h(t) + \gamma^\sigma \beta_2^\sigma I_h(t) + \psi^\sigma \beta_3^\sigma M(t) + d^\sigma) S_h(t)\}(1-\alpha) \\
&\quad + \alpha h \sum_{k=0}^{u} \{\Lambda^\sigma - (\beta_1^\sigma L_h(t) + \gamma^\sigma \beta_2^\sigma I_h(t) + \psi^\sigma \beta_3^\sigma M(t) + d^\sigma) S_h(t)\}, \\
CFL_{h(u+1)} &= L_h(0) + \{(\beta_1^\sigma L_h(t) + \gamma^\sigma \beta_2^\sigma I_h(t) + \psi^\sigma \beta_3^\sigma M(t) S_h(t) - \varrho_1 L_h(t)\}(1-\alpha) \\
&\quad + \alpha h \sum_{k=0}^{u} \{(\beta_1^\sigma L_h(t) + \gamma^\sigma \beta_2^\sigma I_h(t) + \psi^\sigma \beta_3^\sigma M(t) S_h(t) - \varrho_1 L_h(t)\}, \\
CFI_{h(u+1)} &= (1-\alpha)\{\gamma_1^\sigma L_h(t) - \varrho_2 I_h(t)\} + \alpha h \sum_{k=0}^{u} \{\gamma_1^\sigma L_h(t) - \varrho_2 I_h(t)\}, \\
&\quad + I_h(0), \\
CFR_{h(u+1)} &= (1-\alpha)\{\gamma_2^\sigma L_h(t) + \gamma_3^\sigma I_h(t) - d^\sigma R_h(t)\} + \alpha h \sum_{k=0}^{u} \{\gamma_2^\sigma L_h(t) + \gamma_3^\sigma I_h(t) - d^\sigma R_h(t)\}, \\
&\quad + R_h(0), \\
CFM_{(u+1)} &= (1-\alpha)\{\eta_1^\sigma L_h(t) + \eta_2^\sigma I_h(t) - \alpha^\sigma M(t)\} + M(0) + \alpha h \sum_{k=0}^{u} \{\eta_1^\sigma L_h(t) + \eta_2^\sigma I_h(t) - \alpha^\sigma M(t)\}.
\end{aligned}
\tag{33}
$$

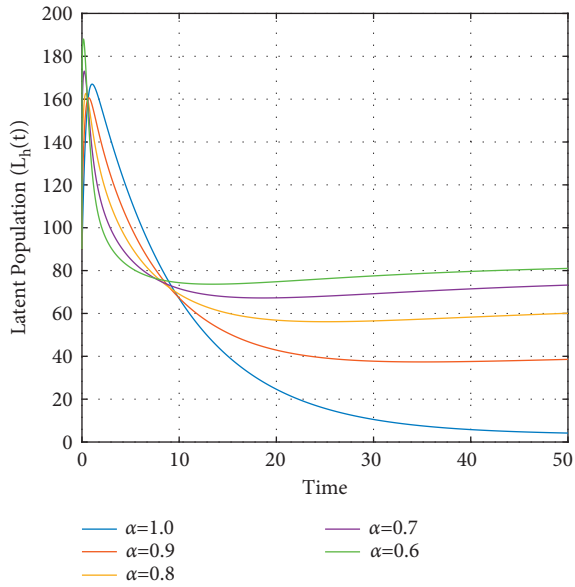

Figure 5: The plot demonstrate the dynamical behaviour of the latent individuals against the epidemic parameters having values: $\Lambda = 0.4$, $\beta_1 = 0.011$, $\beta_2 = 0.005$, $\psi = 0.016$, $\beta_3 = 0.01$, $d = 0.01\,\gamma_1 = 0.05$, $\gamma_2 = 0.05$, $\gamma_3 = 0.05$, $d_1 = 0.002$, $\eta_1 = 0.01$, $\eta_2 = 0.06$, and $\alpha = 0.06$, and different values of fractional parameter (σ), while the initial sizes for compartmental population are $(100, 90, 80, 70, 60)$.

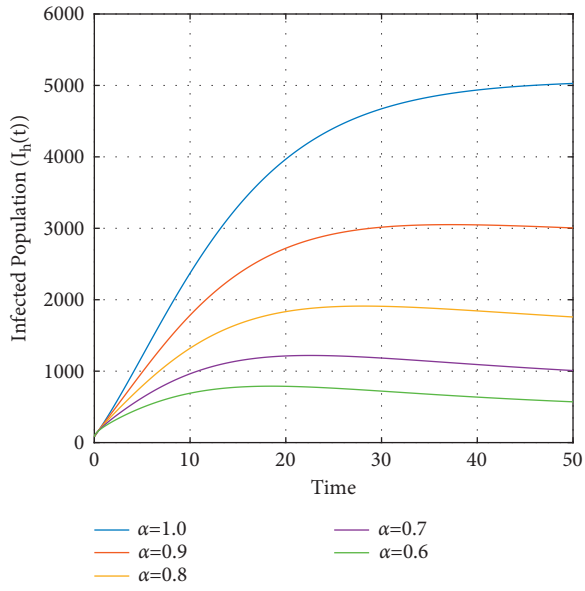

Figure 6: The graph represents the temporal dynamics of infected individuals against the fractional parameter (σ) and model parameters value are: $\Lambda = 0.4$, $\beta_1 = 0.011$, $\beta_2 = 0.005$, $\psi = 0.016$, $\beta_3 = 0.01$, $d = 0.01\,\gamma_1 = 0.05$, $\gamma_2 = 0.05$, $\gamma_3 = 0.05$, $d_1 = 0.002$, $\eta_1 = 0.01$, and $\eta_2 = 0.06$, while the sizes of compartmental population are $(100, 90, 80, 70, 60)$.

Furthermore, we chose the value of epidemic parameters biologically while the initial population sizes are assumed to be non-negative values $(100, 90, 80, 70, 60)$. We use the MATLAB software package to execute the model for

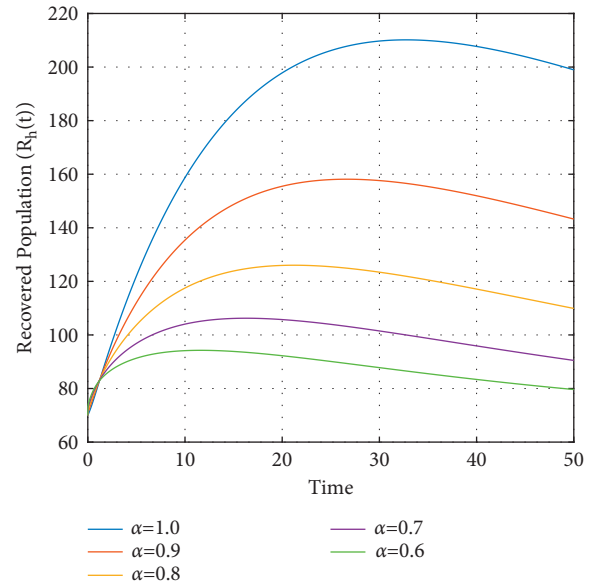

Figure 7: The graph describes the dynamics of the recovered individuals for different value of the fractional parameter (σ) and model parameters value are: $\Lambda = 0.4$, $\beta_1 = 0.011$, $\beta_2 = 0.005$, $\psi = 0.016$, $\beta_3 = 0.01$, $d = 0.01\,\gamma_1 = 0.05$, $\gamma_2 = 0.05$, $\gamma_3 = 0.05$, $d_1 = 0.002$, $\eta_1 = 0.01$, and $\eta_2 = 0.06$, while the initial guess are $(100, 90, 80, 70, 60)$.

numerical simulations. We justify the stabilities results to show the dynamics of the disease-free and endemic states as given in Figures 2 and 3. This investigates the graphical verification of the dynamics of the considered problem around disease-free state X_1. Besides from a mathematical point of view, the biological interpretation reveals that whenever the value of the threshold parameter is less than unity, each solution curve of S_h will tend to its equilibrium position as shown in Figure 2(a). This shows that there will be always a susceptible population. Moreover, the dynamics of the other compartments around the disease-free state are depicted in Figures 2(b)–2(d), and which describe that the solution curves will tend to the associated equilibrium position and remain stable. So it could be noted that the elimination of the contagious disease of the novel coronavirus from the community depends on the value of R_0, and the disease could be easily eliminated if $R_0 < 1$. Furthermore, the dynamics of the fractional-order model around endemic equilibrium are shown in Figures 3(a)–3(e), which respectively show the temporal dynamics of susceptible, latent, infected, recovered, and reservoirs. From these results, we observed that if proper control measures are not adopted the disease will attain the endemic position. It is clear that the susceptible population decreases from the beginning and then has no effect after some time and so becomes stable as shown in Figure 3(a). The dynamics of the latent population state that there will be a sudden increase in the initial period of infection, while then decreases after some unit of time and become stable, as shown in Figure 3(b), which verifies that there will be always latent population. Similarly, the dynamics of the infected population are shown in Figure 3(c). This reveals that the infected ratio increases day by day and

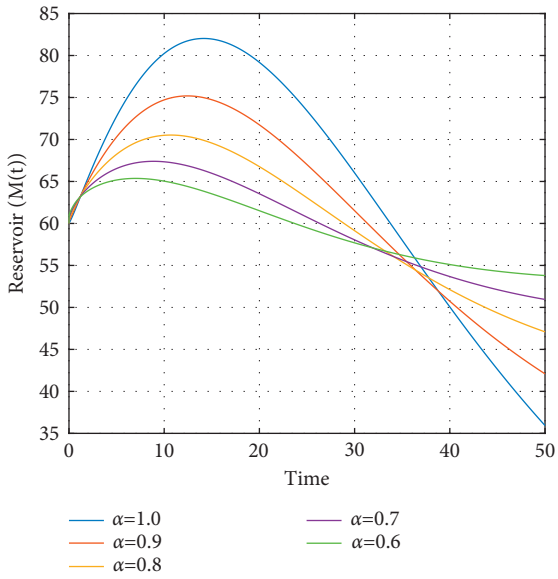

FIGURE 8: The graph describes the dynamics of the ratio of reservoir for different value of the fractional parameter (σ), and the model parameters value are: $\Lambda = 0.4$, $\beta_1 = 0.011$, $\beta_2 = 0.005$, $\psi = 0.016$, $\beta_3 = 0.01$, $d = 0.01$ $\gamma_1 = 0.05$, $\gamma_2 = 0.05$, $\gamma_3 = 0.05$, $d_1 = 0.002$, $\eta_1 = 0.01$, and $\eta_2 = 0.06$, while the initial guess are $(100, 90, 80, 70, 60)$.

reaches its endemic position in a few units of time. Furthermore, the simulation of the model for recovered population and reservoir is given in Figures 3(d)–3(e). All these results suggest that if no proper control measure is implemented, the disease will attain its endemic position whenever the value of the threshold quantity (R_0) is greater than unity.

We also show the significance of the fractional-order via disease transmission as shown in Figures 4–8, which respectively visualizes the temporal dynamics of S_h, A_h, I_h, R_h, and M. Particularly, the temporal dynamics of the susceptible are shown in Figure 4. We noted a significant impact of the fractional order on the transmission dynamics of susceptible individuals that if the fractional parameter σ increases than the number of susceptible individuals decreases as shown in Figure 4. The long run of the latent, infected, and the recovered population for various orders of fractional order are presented in Figures 5–7. We noted that there is a strong influence of (σ) on disease transmission. The temporal dynamics of the reservoir are presented in Figure 8. Thus, we investigate that the *CF* model gives more accurate dynamics of the disease and provides valuable outputs instead of classical models.

5. Conclusion

We investigated the dynamics of SARS-CoV-2 with asymptomatic, symptomatic, and quarantined individuals using an epidemic model. First, the formulation of the model is proposed, and then consequently fractionalized due to the increasing development in fractional calculus. Particularly, we used the well-known *Caputo-Fabrizio* operator for the said purposes. Both the biological and mathematical feasibilities are discussed in detail for the proposed model and proved that the problem is well-passed. We also calculated the threshold parameter and performed stabilities of the fractional model. The detailed sensitivity is also discussed and quantified the role of every epidemic parameter and its relative impact on the disease transmission. We showed that the proposed model is stable in both local and global sense. Finally, we gave some graphical representations and showed the validations of the obtained results. We also presented the relative impact of the fractional parameter on the various groups of the compartmental populations graphically and proved that the major outcome of the reported work is that the fractional-order *CF* epidemic models are more appropriate and the best choice rather than the classical order. We believe that the findings of this work will be helpful for the audience working in the field of mathematical epidemiology.

Data Availability

No data were used to support this study.

Conflicts of Interest

The authors declare that they have no conflicts of interest.

Acknowledgments

The authors would like to acknowledge and express their gratitude to the United Arab Emirates University, Al Ain, UAE, for providing financial support with Grant No. 12S086. In addition, the authors are thankful for the financial support of King Khalid University, Institute for Research and Counseling Studies Administration of Contracts, under grant 24-S-2020.

References

[1] E. I. Azhar, S. A. E. Kafrawy, S. A. Farraj et al., "Evidence for camel-to-human transmission of mers coronavirus," *New England Journal of Medicine*, vol. 370, no. 26, pp. 2499–2505, 2014.

[2] Y. Kim, S. Lee, C. Chu, S. Choe, S. Hong, and Y. Shin, "The characteristics of middle eastern respiratory syndrome coronavirus transmission dynamics in South Korea," *Osong public health and research perspectives*, vol. 7, no. 1, pp. 49–55, 2016.

[3] J. A. Al-Tawfiq, K. Hinedi, J. Ghandour et al., "Middle east respiratory syndrome coronavirus: a case-control study of hospitalized patients," *Clinical Infectious Diseases*, vol. 59, no. 2, pp. 160–165, 2014.

[4] J. A. Backer, D. Klinkenberg, and J. Wallinga, "Incubation period of 2019 novel coronavirus (2019-ncov) infections among travellers from wuhan, China, 20–28 january 2020," *Euro Surveillance*, vol. 25, no. 5, 2020.

[5] A. Atangana, "Modelling the spread of covid-19 with new fractal-fractional operators: can the lockdown save mankind before vaccination?" *Chaos, Solitons & Fractals*, vol. 136, Article ID 109860, 2020.

[6] A. Atangana and S. İğret Araz, "Nonlinear equations with global differential and integral operators: existence,

uniqueness with application to epidemiology," *Results in Physics*, vol. 20, Article ID 103593, 2021.

[7] Q. Haidong, M. ur Rahman, M. Arfan, M. Salimi, S. Salahshour, and A. Ahmadian, "Fractal–fractional dynamical system of typhoid disease including protection from infection," *Engineering with Computers*, pp. 1–10, 2021.

[8] S. G. Samko, "Fractional integrals and derivatives, theory and applications," CRC, Boca Raton, 1987.

[9] D. Baleanu, Z. B. Güvenç, and J. T. Machado, *New Trends in Nanotechnology and Fractional Calculus Applications*, Springer, Germany, 2010.

[10] D. Baleanu, J. A. T. Machado, and A. C. Luo, *Fractional Dynamics and Control*, Springer Science & Business Media, Germany, 2011.

[11] D. Baleanu, K. Diethelm, E. Scalas, and J. J. Trujillo, "Fractional calculus: models and numerical methods," *World Scientific*, vol. 3, 2012.

[12] N. Ali, N. Ali, G. Zaman, A. Zeb, V. S. Erturk, and I. H. Jung, "Dynamical analysis of approximate solutions of hiv-1 model with an arbitrary order," *Complexity*, vol. 2019, pp. 1–7, Article ID 9715686, 2019.

[13] Z. U. A. Zafar, N. Ali, and D. Baleanu, "Dynamics and numerical investigations of a fractional-order model of toxoplasmosis in the population of human and cats," *Chaos, Solitons & Fractals*, vol. 151, Article ID 111261, 2021.

[14] Z. U. A. Zafar, Z. Shah, N. Ali, E. O. Alzahrani, and M. Shutaywi, "Mathematical and stability analysis of fractional order model for spread of pests in tea plants," *Fractals*, vol. 29, no. 1, Article ID 2150008, 2021.

[15] H. M Srivastava, K. M Saad, J. F Gómez-Aguilar, and A. A Almadiy, "Some new mathematical models of the fractional-order system of human immune against iav infection," *Mathematical Biosciences and Engineering*, vol. 17, no. 5, pp. 4942–4969, 2020.

[16] N. H. Tuan, H. Mohammadi, and S. Rezapour, "A mathematical model for COVID-19 transmission by using the Caputo fractional derivative," *Chaos, Solitons & Fractals*, vol. 140, Article ID 110107, 2020.

[17] K. M. Owolabi and A. Atangana, "Numerical approximation of nonlinear fractional parabolic differential equations with Caputo–Fabrizio derivative in Riemann–Liouville sense," *Chaos, Solitons & Fractals*, vol. 99, pp. 171–179, 2017.

[18] D. Baleanu, A. Jajarmi, and M. Hajipour, "On the nonlinear dynamical systems within the generalized fractional derivatives with mittag–leffler kernel," *Nonlinear Dynamics*, vol. 94, no. 1, pp. 397–414, 2018.

[19] D. Baleanu, H. Mohammadi, and S. Rezapour, "Analysis of the model of hiv-1 infection of cd4+ t-cell with a new approach of fractional derivative," *Advances in Difference Equations*, vol. 71, no. 1, pp. 1–17, 2020.

[20] M. Caputo and M. Fabrizio, "A new definition of fractional derivative without singular kernel," *Progr. Fract. Differ. Appl*, vol. 1, no. 2, pp. 1–13, 2015.

[21] Y. Wang and J. Cao, "Global dynamics of a network epidemic model for waterborne diseases spread," *Applied Mathematics and Computation*, vol. 237, pp. 474–488, 2014.

[22] T. Khan, G. Zaman, and M. I. Chohan, "The transmission dynamic and optimal control of acute and chronic hepatitis b," *Journal of Biological Dynamics*, vol. 11, no. 1, pp. 172–189, 2017.

[23] N. Ali, G. Zaman, and M. I. Chohan, "Global stability of a delayed hiv-1 model with saturations response," *Applied Mathematics & Information Sciences*, vol. 11, no. 1, pp. 189–194, 2017.

[24] G. Zaman, Y. Han Kang, and I. H. Jung, "Stability analysis and optimal vaccination of an sir epidemic model," *Biosystems*, vol. 93, no. 3, pp. 240–249, 2008.

[25] H. Abboubakar, J. Claude Kamgang, and D. Tieudjo, "Backward bifurcation and control in transmission dynamics of arboviral diseases," *Mathematical Biosciences*, vol. 278, pp. 100–129, 2016.

[26] J. T. Wu, K. Leung, and G. M. Leung, "Nowcasting and forecasting the potential domestic and international spread of the 2019-ncov outbreak originating in wuhan, China: a modelling study," *The Lancet*, vol. 395, pp. 689–697, Article ID 10225, 2020.

[27] N. Imai, A. Cori, I. Dorigatti et al., *Report 3: Transmissibility of 2019-ncov*Imperial College London, London, U.k, 2020.

[28] H. Zhu, Q. Guo, M. Li et al., *Host and Infectivity Prediction of Wuhan 2019 Novel Coronavirus Using Deep Learning Algorithm*, bioRxiv, New York, NY, U.S.A, 2020.

[29] K. Hattaf, A. A. Mohsen, J. Harraq, and N. Achtaich, "Modeling the dynamics of covid-19 with carrier effect and environmental contamination," *International Journal of Modeling, Simulation, and Scientific Computing*, vol. 12, no. 3, Article ID 2150048, 2021.

[30] C. Rothe, M. Schunk, P. Sothmann et al., "Transmission of 2019-ncov infection from an asymptomatic contact in Germany," *New England Journal of Medicine*, vol. 382, no. 10, pp. 970-971, 2020.

[31] J. M. Read, J. R. Bridgen, D. A. Cummings, A. Ho, and C. P. Jewell, *Novel Coronavirus 2019-ncov: Early Estimation of Epidemiological Parameters and Epidemic Predictions*, MedRxiv, New York, NY, U.S.A, 2020.

[32] K. Hattaf, "A new generalized definition of fractional derivative with non-singular kernel," *Computation*, vol. 8, no. 2, p. 49, 2020.

[33] K. Hattaf, "On some properties of the new generalized fractional derivative with non-singular kernel," *Mathematical Problems in Engineering*, vol. 2021, pp. 2021–2026, Article ID 1580396, 2021.

[34] X. Yang, L. Chen, and J. Chen, "Permanence and positive periodic solution for the single-species nonautonomous delay diffusive models," *Computers & Mathematics with Applications*, vol. 32, no. 4, pp. 109–116, 1996.

[35] S. Qureshi, E. Bonyah, and A. A. Shaikh, "Classical and contemporary fractional operators for modeling diarrhea transmission dynamics under real statistical data," *Physica A: Statistical Mechanics and Its Applications*, vol. 535, Article ID 122496, 2019.

[36] D. Earn, F. Brauer, P. van den Driessche, and J. Wu, *Mathematical Epidemiology*, Spriger, Germany, 2008.

[37] P. T. Karaji and N. Nyamoradi, "Analysis of a fractional sir model with general incidence function," *Applied Mathematics Letters*, vol. 108, Article ID 106499, 2020.

[38] L. Kexue and P. Jigen, "Laplace transform and fractional differential equations," *Applied Mathematics Letters*, vol. 24, no. 12, pp. 2019–2023, 2011.

[39] W. Lin, "Global existence theory and chaos control of fractional differential equations," *Journal of Mathematical Analysis and Applications*, vol. 332, no. 1, pp. 709–726, 2007.

[40] F. Wang and Y. Yang, "Correction: fractional order BARBALAT'S lemma and its applications in the stability of fractional order nonlinear systems," *Mathematical Modelling and Analysis*, vol. 22, no. 4, pp. 503–513, 2017.

[41] K. Hattaf, N. Yousfi, and A. Tridane, "Mathematical analysis of a virus dynamics model with general incidence rate and

cure rate," *Nonlinear Analysis: Real World Applications*, vol. 13, no. 4, pp. 1866–1872, 2012.

[42] G. T. Tilahun, O. D. Makinde, and D. Malonza, "Co-dynamics of pneumonia and typhoid fever diseases with cost effective optimal control analysis," *Applied Mathematics and Computation*, vol. 316, pp. 438–459, 2018.

[43] H. Ramos, Z. Kalogiratou, T. Monovasilis, and T. E. Simos, "An optimized two-step hybrid block method for solving general second order initial-value problems," *Numerical Algorithms*, vol. 72, no. 4, pp. 1089–1102, 2016.

[44] C. Li and F. Zeng, *Numerical methods for fractional calculus*, Chapman and Hall/CRC, Boca Raton, FL, U.S.A, 2019.

Hindawi
Complexity
Volume 2022, Article ID 7635696, 17 pages
https://doi.org/10.1155/2022/7635696

Research Article

Analytical Investigation of Some Dynamical Systems by ZZ Transform with Mittag–Leffler Kernel

Mounirah Areshi,[1] Muhammad Naeem ,[2] and Noorolhuda Wyal [3]

[1]*Department of Mathematics, Faculty of Science, University of Tabuk, P.O. Box 741, Tabuk 71491, Saudi Arabia*
[2]*Deanship of Joint First Year Umm Al-Qura University Makkah, Mecca, P.O. Box 715, Saudi Arabia*
[3]*Department of Mathematics, Kabul Polytechnic University, Kabul, Afghanistan*

Correspondence should be addressed to Muhammad Naeem; mfaridoon@uqu.edu.sa and Noorolhuda Wyal; noorolhuda.wyal@kpu.edu.af

Received 6 January 2022; Revised 16 June 2022; Accepted 12 July 2022; Published 24 September 2022

Academic Editor: Shanmugam Lakshmanan

In this work, ZZ transformation is combined with the Adomian decomposition method to solve the dynamical system of fractional order. The derivative of fractional order is represented in the Atangana–Baleanu derivative. The numerical examples are combined for their approximate-analytical solution. It is explored using graphs that indicate that the actual and approximation results are close to each other, demonstrating the method's usefulness. Fractional-order solutions are the most in line with the dynamics of the targeted problems, and they provide an endless number of options for an optimal mathematical model solution for a particular physical phenomenon. This analytical approach produces a series form solution that is quickly convergent to exact solutions. The acquired results suggest that the novel analytical solution technique is simple to use and very successful at assessing complicated problems that arise in related fields of research and technology.

1. Introduction

Because of their extensive applications in many science and engineering disciplines, fractional differential equations have sparked much attention in recent years. Critical phenomena well characterize differential equations of fractional order in electromagnetics, finance, viscoelasticity, acoustics, material science, and electrochemistry. Barkai et al. [1], Mainardi [2], Tadjeran and Meerschaert [3], Meerschaert et al. [4], and Magin et al. [5] just released a review article on fractional signals and systems, including control theory applications. The edited volume of Machado contains several applications of fractional calculus, such as image processing [6]. The importance and necessity of fractional calculus can be seen in several applications in transdisciplinary disciplines. Miller and Ross [7], Oldham and Spanier [8], Podlubny [9], Kilbas et al. [10], Samko et al. [11], Caponetto [12], and Diethelm [13] have all authored essential studies on the fractional derivative and fractional differential equations. A review study on the recent history of fractional calculus was written by Machado et al. [14]. An article on recent developments in the theory of abstract differential equations with fractional derivatives was published by Hernandez et al. [15]. These publications provide a systematic explanation of fractional calculus, including the existence and uniqueness of solutions and various analytical methods for solving fractional differential equations, such as Green's function method, power series approach, Mellin transform method, and others. No method in the literature produces a precise solution for nonlinear fractional differential equations (16) and (17). Using linearization or perturbation approaches, only approximate answers can be obtained. All of these push us to develop a numerical approach for fractional differential equations that is both efficient and accurate [18–21]. Chaos theory, heat transfer, variational issues, and other fields have used the Atangana–Baleanu fractional differential extensively. Recently, a fractional-differential mask based on a fractional Gaussian kernel with Atangana–Baleanu

fractional differential has been published in the literature for the detection of blood vessels in retinal pictures, with the suggested method's efficacy compared to other well-known approaches. Furthermore, it discusses the underlying differences between power-law, exponential-law, and Mittag–Leffler kernels, as well as their potential applications in diverse domains.

This paper establishes a connection between the Aboodh transformation (AT), ZZ transformation (ZZT), and Laplace transformation (LT), with several applications mentioned in [22–24]. The ZZT was then employed to define fractional Atangana–Baleanu Caputo operators and characterize Riemann–Liouville senses using theorems. Later, we solved several test problems stated in the Atangana–Baleanu sense using this ZZ transform. The current author's contributions to this study are (i) applying the ZZ transform to solve fractional differential equations expressed in the Atangana–Baleanu derivative and (ii) establishing the connection between the Laplace, Aboodh, and ZZ transformations. A few well-known transforms that the ZZ transform generalizes can be related to other well-known transforms. Divide the ZZ transform by the adjusted variable to get the natural transform. Relationships with other integral transformations are also included in this work in terms of theorems. This transformation has the advantage of converging to the Sumudu transformation, which is advantageous when solving fractional differential equations with variable coefficients, such as [25–27].

Adomian (1980) established the Adomian decomposition technique (ADM), an efficient method for finding explicit and numerical solutions to a larger and more general class of differential systems representing real-world issues [28–30]. This strategy effectively addresses initial and boundary value problems, linear and nonlinear, ordinary and partial differential equations, and stochastic systems. Furthermore, this approach does not require any linearization or perturbation. ADM has been used extensively in the last two decades since it yields approximate analytical solutions for nonlinear problems, and there has been much interest in utilizing it to solve fractional differential equations (31)–(33).

The ZZ decomposition method has the following advantages with respect to Adomian decomposition method:

(i) ZZ decomposition method required small calculations as compared to the Adomian decomposition method

(ii) The fractional derivative is simplified by using the ZZ transformation first and then applying decomposition method while it is not the case if we use the Adomian decomposition method directly

(iii) The initial conditions/boundary conditions are used directly in the ZZ decomposition method, and it mostly avoids the extra calculations of Adomian polynomials

The novelty of the present work is to deal with the analytical solutions of important fractional-order some dynamical systems. The fractional-order of some dynamical systems have many applications in physical sciences, and therefore, different graphs are presented to show various dynamics of fractional parabolic equations. The solutions are obtained in rather simpler way as compared to other techniques. The current study has been structured as follows: in Section 2, some basic notions of basic definitions of ZZ transformation are described. In Section 3, we give an analysis of the suggested technique. In Section 4, we provide current solutions which suggested equations explaining how to implemented the suggested technique. Finally, the conclusion is provided.

2. Preliminaries

Definition 1. The function set of the Aboodh transform (AT) is defined as

$$B = \{h(\rho):\ \exists M, n_1, n_2 > 0, |h(\rho)| < Me^{-s\rho}\}, \tag{1}$$

and is given as [22, 23]

$$A\{h(\rho)\} = \frac{1}{\varsigma}\int_0^{\infty} h(\rho)e^{-\varsigma\rho}d\rho\ , \rho > 0 \text{ and } n_1 \le \varsigma \le n. \tag{2}$$

Theorem 1. *Now, we consider G and F as the Aboodh and Laplace transforms of $h(\rho) \in B$; then [24, 25],*

$$G(\varsigma) = \frac{F(\varsigma)}{\varsigma}. \tag{3}$$

Zafar [26] was the first to develop the ZZ transform. It is mixture of the Laplace and Aboodh integral transforms. The ZZ transform is expressed in the following.

Definition 2 (ZZ transform). Suppose that $h(\rho)\forall\rho \ge 0$ is a function, then the ZZ transformation $Z(\varrho, \varsigma)$ of $h(\rho)$ is defined as [26]

$$ZZ(h(\rho)) = Z(\varrho, \varsigma) = \varsigma\int_0^{\infty} h(\varrho\rho)e^{-\varsigma\rho}d\rho. \tag{4}$$

The ZZ transformation is linear, just as the Aboodh and Laplace transforms. The MLF is a function that is given as an extension of the exponential term.

$$E_\delta(z) = \sum_{m=0}^{\infty}\frac{z^m}{\Gamma(1+m\delta)}, \mathrm{Re}(\delta) > 0. \tag{5}$$

Definition 3. The Atangana–Baleanu Caputo derivative of a function $\nu(\varphi, \rho) \in H^1(a, b)$; then, for $\delta \in (0, 1)$, it is defined as [27]

$${}^{ABC}_{a}D^{\delta}_{\rho}\nu(\varphi, \rho) = \frac{\psi(\delta)}{1-\delta}\int_a^{\rho}\nu'(\varphi, \rho)E_\delta\left(\frac{-\delta(\rho-\eta)^\delta}{1-\delta}\right)d\eta. \tag{6}$$

Definition 4. Let the Riemann–Liouville Atangana–Baleanu derivative $\nu(\varphi, \rho) \in H^1(a, b)$; then, for $\delta \in (0, 1)$, it is given as [27]

$$ {}_{a}^{ABR}D_{\rho}^{\delta}\nu(\varphi,\eta)=\frac{\psi(\delta)}{1-\delta}\frac{\mathrm{d}}{\mathrm{d}\rho}\int_{a}^{\rho}\nu(\varphi,\eta)E_{\delta}\left(\frac{-\delta(\rho-\eta)^{\delta}}{1-\delta}\right)\mathrm{d}\eta, \tag{7} $$

with the condition $\psi(0)=\psi(1)=1$, $\psi(\delta)$ is a function, and $b>a$.

Theorem 2. *The Laplace transform of Riemann–Liouville Atangana–Baleanu derivative and Atangana–Baleanu Caputo are, respectively, defined as [27]*

$$ \mathrm{L}\left\{{}_{a}^{ABC}D_{\rho}^{\delta}\nu(\varphi,\rho)\right\}(\varsigma)=\frac{\psi(\delta)}{1-\delta}\frac{\varsigma^{\delta}L\{\nu(\varphi,\rho)\}-\varsigma^{\delta-1}\nu(\varphi,0)}{\varsigma^{\delta}+\delta/1-\delta} \tag{8} $$

and

$$ L\left\{{}_{a}^{ABR}D_{\rho}^{\delta}\nu(\varphi,\rho)\right\}(\varsigma)=\frac{\psi(\delta)}{1-\delta}\frac{\varsigma^{\delta}L\{\nu(\varphi,\rho)\}}{\varsigma^{\delta}+\delta/1-\delta}. \tag{9} $$

The theorems that follow are based on the idea that $h(\rho)\in H^{1}(a,b), b>a$, and $\delta\in(0,1)$.

Theorem 3. *The Aboodh transformation of Atangana–Baleanu Riemann–Liouville derivative is defined as [25]*

$$ G(\varsigma)=A\left\{{}_{a}^{ABR}D_{\rho}^{\delta}\nu(\varphi,\rho)\right\}(\varsigma)=\frac{1}{\varsigma}\left[\frac{\psi(\delta)}{1-\delta}\frac{\varsigma^{\delta}L\{\nu(\varphi,\rho)\}}{\varsigma^{\delta}+\delta/1-\delta}\right]. \tag{10} $$

Proof 1. Using Theorem 1 and equation (3), we arrive to the required solution. The relationship among the transforms of ZZ and Aboodh is given in the following theorem. □

Theorem 4. *The Aboodh transform of Atangana–Baleanu Caputo derivative is defined as [25]*

$$ \begin{aligned} G(\varsigma)&=A\left\{{}_{a}^{ABC}D_{\rho}^{\delta}\nu(\varphi,\rho)\right\}(\varsigma)\\ &=\frac{1}{\varsigma}\left[\frac{\psi(\delta)}{1-\delta}\frac{\varsigma^{\delta}L\{\nu(\varphi,\rho)\}-\varsigma^{\delta-1}\nu(\varphi,0)}{\varsigma^{\delta}+\delta/1-\delta}\right]. \end{aligned} \tag{11} $$

Proof 2. Using Theorem 1 and equation (2), we can discover the desired solution. □

Theorem 5. *If $Z(\varrho,\varsigma)$ and $G(\varsigma)$ are the Aboodh and ZZ transforms of $h(\rho)\in B$, then we obtain the following [25]:*

$$ Z(\varrho,\varsigma)=\frac{\varsigma^{2}}{\varrho^{2}}G\left(\frac{\varsigma}{\varrho}\right). \tag{12} $$

Proof 3. (The ZZ transform definitions). We get

$$ Z(\varrho,\varsigma)=\varsigma\int_{0}^{\infty}h(\varrho\rho)e^{-\varsigma\rho}d\rho. \tag{13} $$

Put $\varrho\rho=\rho$ in (13); we get

$$ Z(\varrho,\varsigma)=\frac{\varsigma}{\varrho}\int_{0}^{\infty}h(\rho)e^{-\frac{\pi z}{\varrho}}d\rho\ . \tag{14} $$

The right-hand side of (14) may be expressed as

$$ Z(\varrho,\varsigma)=\frac{\varsigma}{\varrho}F\left(\frac{\varsigma}{\varrho}\right), \tag{15} $$

where $F(.)$ expresses the Laplace transformation of $h(\rho)$. Using Theorem 1, (15) can be defined as

$$ Z(\varrho,\varsigma)=\frac{\varsigma}{\varrho}F\left(\frac{\varsigma}{\varrho}\right)\left(\frac{\varsigma}{\varrho}\right)\times\left(\frac{\varsigma}{\varrho}\right)=\left(\frac{\varsigma}{\varrho}\right)^{2}G\left(\frac{\varsigma}{\varrho}\right), \tag{16} $$

where $G(.)$ defines the Aboodh transform of $h(\rho)$. □

Theorem 6. *ZZ transformation of $h(\rho)=\rho^{\delta-1}$ is defined as*

$$ Z(\varrho,\varsigma)=\Gamma(\delta)\left(\frac{\varrho}{\varsigma}\right)^{\delta-1} \tag{17} $$

Proof 4. The Aboodh transformation of $h(\rho)=\rho^{\delta}, \delta\geq 0$, is

$$ \begin{aligned} G(s)&=\frac{\Gamma(\delta)}{\varsigma^{\delta+1}},\\ \text{now, } G\left(\frac{\varsigma}{\varrho}\right)&=\frac{\Gamma(\delta)\varrho^{\delta+1}}{\varsigma^{\delta+1}}. \end{aligned} \tag{18} $$

Applying (17), we achieve

$$ Z(\varrho,\varsigma)=\frac{\varsigma^{2}}{\varrho^{2}}G\left(\frac{\varsigma}{\varrho}\right)=\frac{\varsigma^{2}}{\varrho^{2}}\frac{\Gamma(\delta)\varrho^{\delta+1}}{\varsigma^{\delta+1}}=\Gamma(\delta)\left(\frac{\varrho}{\varsigma}\right)^{\delta-1}. \tag{19} $$

□

Theorem 7. *Let $\delta,\omega\in C$ and $Re(\delta)>0$; then, the ZZ transformation of $E_{\delta}(\omega\rho^{\delta})$ is defined as [25]*

$$ ZZ\left\{\left(E_{\delta}\left(\omega\rho^{\delta}\right)\right)\right\}=Z(\varrho,\varsigma)=\left(1-\omega\left(\frac{\varrho}{\varsigma}\right)^{\delta}\right)^{-1}. \tag{20} $$

Proof 5. We know that Aboodh transform of $E_{\delta}(\omega\rho^{\delta})$ is defined as

$$ G(\varsigma)=\frac{F(\varsigma)}{\varsigma}=\frac{\varsigma^{\delta-1}}{\varsigma\left(\varsigma^{\delta}-\omega\right)}. \tag{21} $$

So,

$$ G\left(\frac{\varsigma}{\varrho}\right)=\frac{(\varsigma/\varrho)^{\delta-1}}{(\varsigma/\varrho)\left((\varsigma/\varrho)^{\delta}-\omega\right)}. \tag{22} $$

Applying Theorem 9, we achieve

$$Z(\varrho,\varsigma)=\left(\frac{\varsigma}{\varrho}\right)^2 G\left(\frac{\varsigma}{\varrho}\right)=\left(\frac{\varsigma}{\varrho}\right)^2\frac{(\varsigma/\varrho)^{\delta-1}}{(\varsigma/\varrho)\left((\varsigma/\varrho)^{\delta}-\omega\right)}$$
$$=\frac{(\varsigma/\varrho)^{\delta}}{(\varsigma/\varrho)^{\delta}-\omega}=\left(1-\omega(\varrho/\varsigma)^{\delta}\right)^{-1}. \tag{23}$$

□

Theorem 8. *If $Z(\varrho,\varsigma)$ and $G(s)$ are the Aboodh and ZZ transforms of $h(\rho)$, then the Atangana–Baleanu Caputo ZZ transformation derivative is defined as [25]*

$$ZZ\left\{{}_0^{ABC}D_\rho^\delta h(\rho)\right\}=\left[\frac{\psi(\delta)}{1-\delta}\frac{\left(\left(\varsigma^{\delta+2}/\varrho^{\delta+2}\right)\right)G(\varsigma/\varrho)-\left(\varsigma^{\delta}/\varrho^{\delta}\right)f(0)}{\left(\varsigma^{\delta}/\varrho^{\delta}\right)+(\delta/1-\delta)}\right]. \tag{24}$$

Proof 6. Applying equations (1) and (5), we get

$$G\left(\frac{\varsigma}{\varrho}\right)==\frac{\varrho}{\varsigma}\left[\frac{\psi(\delta)}{1-\delta}\frac{(\varsigma/\varrho)^{\delta+1}G(\varsigma/\varrho)-(\varsigma/\varrho)^{\delta-1}f(0)}{(\varsigma/\varrho)^{\delta}+\delta/1-\delta}\right]. \tag{25}$$

So, the Atangana–Baleanu Caputo of ZZ transformation is defined as

$$Z(\varrho,\varsigma)=\left(\frac{\varsigma}{\varrho}\right)^2 G\left(\frac{\varsigma}{\varrho}\right)$$
$$=\left(\frac{\varsigma}{\varrho}\right)^2\frac{\varrho}{\varsigma}\left[\frac{\psi(\delta)}{1-\delta}\frac{(\varsigma/\varrho)^{\delta+1}G(\varsigma/\varrho)-(\varsigma/\varrho)^{\delta-1}f(0)}{(\varsigma/\varrho)^{\delta}+(\delta/1-\delta)}\right]$$
$$=\left[\frac{\psi(\delta)}{1-\delta}\frac{(\varsigma/\varrho)^{\delta+2}G(\varsigma/\varrho)-(\varsigma/\varrho)^{\delta}f(0)}{(\varsigma/\varrho)^{\delta}+(\delta/1-\delta)}\right]. \tag{26}$$

□

Theorem 9. *Let us suppose that $Z(\varrho,\varsigma)$ and $G(s)$ are the Aboodh and ZZ transforms of $h(\rho)$. Then, the Atangana–Baleanu Riemann–Liouville ZZ transform derivative is defined as [25]*

$$ZZ\left\{{}_0^{ABR}D_\rho^\delta f(\rho)\right\}=\left[\frac{\psi(\delta)}{1-\delta}\frac{5^{\delta+2}/\varrho^{\delta+2}G(\varsigma/\varrho)}{\varsigma^{\mu}/\varrho^{\mu}+(\delta/1-\delta)}\right]. \tag{27}$$

Proof 7. Applying equations (1) and (4), we get

$$G\left(\frac{\varsigma}{\varrho}\right)=\frac{\varrho}{\varsigma}\left[\frac{\psi(\delta)}{1-\delta}\frac{(\varsigma/\varrho)^{\delta+1}G(\varsigma/\varrho)}{(\varsigma/\varrho)^{\delta}+\delta/1-\delta}\right]. \tag{28}$$

From (16), the ZZ transform of Riemann–Liouville Atangana–Baleanu is defined as

$$Z(\varrho,\varsigma)=\left(\frac{\varsigma}{\varrho}\right)^2 G\left(\frac{\varsigma}{\varrho}\right)$$
$$=\left(\frac{\varsigma}{\varrho}\right)^2\left(\frac{\varrho}{\varsigma}\right)\left[\frac{\psi(\delta)}{1-\delta}\frac{(\varsigma/\varrho)^{\delta+1}G(\varsigma/\varrho)}{(\varsigma/\varrho)^{\delta}+(\delta/1-\delta)}\right]$$
$$=\left[\frac{\psi(\delta)}{1-\delta}\frac{(\varsigma/\varrho)^{\delta+2}G(\varsigma/\varrho)}{(\varsigma/\varrho)^{\delta}+(\delta/1-\delta)}\right]. \tag{29}$$

□

3. Idea of MDM

Consider the fractional order partial differential equation by MDM:

$$D_\rho^\delta\nu(\varphi,\rho)=\overline{\mathscr{H}}_1(\nu,\varphi)+\mathscr{N}_1(\nu,\varphi),0<\delta\le 1, \tag{30}$$

with the initial condition

$$\nu(\varphi,0)=\xi(\varphi), \tag{31}$$

where $D_\rho^\delta=\partial^\delta/\partial\rho^\delta$ is the Atangana–Baleanu fractional derivative of order δ; $\overline{\mathscr{H}}_1$ is linear and $\mathscr{N}_1$ nonlinear terms, respectively. On both sides, we use ZZ transformation of (30), to achieve

$$\mathscr{Z}\left[D_\rho^\delta\nu(\varphi,\rho)\right]=\mathscr{Z}\left[\overline{\mathscr{H}}_1(\nu,\varphi)+\mathscr{N}_1(\nu,\varphi)\right]. \tag{32}$$

By the differentiation property of ZZ transformation, we get

$$\psi(\delta)\left(1-\delta+\delta\left(\frac{\varrho}{\varsigma}\right)^{\delta}\right)\{\nu(\varphi,\rho)\}-\frac{\varrho}{\varsigma}\nu(\varphi,0)$$
$$=\mathscr{Z}\left[\overline{\mathscr{H}}_1(\nu,\varphi)+\mathscr{N}_1(\nu,\varphi)\right]. \tag{33}$$

(33) implies that

$$\nu(\varphi,\rho)=\frac{\varrho}{\varsigma}\nu(\varphi,0)$$
$$+\left(1-\delta+\delta\left(\frac{\varrho}{\varsigma}\right)^{\delta}\right)\psi(\delta)\mathscr{Z}\left[\overline{\mathscr{H}}_1(\nu,\varphi)+\mathscr{N}_1(\nu,\varphi)\right]. \tag{34}$$

Applying the ZZ inverse transformation of (34), we get

$$\nu(\varphi,\rho)=\nu(\varphi,0)$$
$$+\mathscr{Z}^{-1}\left[\left(1-\delta+\delta\left(\frac{\varrho}{\varsigma}\right)^{\delta}\right)\psi(\delta)\mathscr{Z}\left\{\overline{\mathscr{H}}_1(\nu,\varphi)+\mathscr{N}_1(\nu,\varphi)\right\}\right]. \tag{35}$$

MDM determines the infinite sequence's result of $\nu(\varphi,\rho)$:

$$\nu(\varphi,\rho)=\sum_{m=0}^{\infty}\nu_m(\varphi,\rho). \tag{36}$$

The nonlinear functions can be found with the help of Adomian polynomials $\mathscr{N}_1$ which is expressed as

$$\mathscr{N}_1(\nu,\varphi)=\sum_{m=0}^{\infty}\mathscr{A}_m. \tag{37}$$

The Adomian polynomials can show all types of nonlinearity as

$$\mathscr{A}_m=\frac{1}{m!}\left[\frac{\partial^m}{\partial\ell^m}\left\{\mathscr{N}_1\left(\sum_{k=0}^{\infty}\ell^k\nu_k,\sum_{k=0}^{\infty}\ell^k\varphi_k\right)\right\}\right]_{\ell=0}. \tag{38}$$

Putting (36) and (38) into (35), it gives

$$\sum_{m=0}^{\infty}\nu_m(\varphi,\rho)=\nu(\varphi,0)+\mathscr{Z}^{-1}\left[\frac{\left(1-\delta+\delta(\varsigma/\varrho)^{\delta}\right)}{\psi(\delta)}\mathscr{Z}\left\{\overline{\mathscr{H}}_1\left(\sum_{m=0}^{\infty}\nu_m,\sum_{m=0}^{\infty}\varphi_m\right)+\sum_{m=0}^{\infty}\mathscr{A}_m\right\}\right]. \tag{39}$$

The following terms are described:

$$\nu_0(\varphi,\rho)=\nu(\varphi,0),$$

$$\nu_1(\varphi,\rho)=\mathscr{Z}^{-1}\left[\frac{\left(1-\delta+\delta(\varrho/\varsigma)^{\delta}\right)}{\psi(\delta)}\mathscr{Z}\left\{\overline{\mathscr{H}}_1(\nu_0,\varphi_0)+\mathscr{A}_0\right\}\right]. \tag{40}$$

The general form for $m\geq 1$ is determined as

$$\nu_{m+1}(\varphi,\rho)=\mathscr{Z}^{-1}\left[\frac{\left(1-\delta+\delta(\varrho/\varsigma)^{\delta}\right)}{\psi(\delta)}\mathscr{Z}\left\{\overline{\mathscr{H}}_1(\nu_m,\varphi_m)+\mathscr{A}_m\right\}\right]. \tag{41}$$

4. Numerical Examples

Example 1. Here, we take the following FPDE:

$$\begin{cases} D_{\rho}^{\delta}(\mu)-\dfrac{\partial\nu}{\partial\zeta}+\nu+\mu=0, \\ \\ D_{\rho}^{\delta}(\nu)-\dfrac{\partial\mu}{\partial\zeta}+\nu+\mu=0,\delta,\in(0,1], \end{cases}. \tag{42}$$

with initial source

$$\begin{cases} \mu(\zeta,0)=\sinh(\zeta) \\ \nu(\zeta,0)=\cosh(\zeta) \end{cases}. \tag{43}$$

The exact result at $\delta=1$ is (1) $\mu(\varphi,\rho)=\sinh(\varphi-\rho)$ and (2) $\nu(\varphi,\rho)=\cosh(\varphi+\rho)$.

Applying ZZT (42), we get

$$\mathscr{Z}\left\{\frac{\partial^{\delta}\mu}{\partial\rho^{\delta}}\right\}=\mathscr{Z}\left\{\frac{\partial\nu}{\partial\varphi}-\nu-\mu\right\},\mathscr{Z}\left\{\frac{\partial^{\delta}\nu}{\partial\rho^{\delta}}\right\}=\mathscr{Z}\left\{\frac{\partial\mu}{\partial\varphi}-\nu-\mu\right\},$$

$$\frac{\psi(\delta)}{\left(1-\delta+\delta(\varrho/\varsigma)^{\delta}\right)}\mathscr{Z}\{\mu(\varphi,\rho)\}-\frac{\varrho}{\varsigma}\mu(\varphi,0)=\mathscr{Z}\left\{\frac{\partial\nu}{\partial\varphi}-\nu-\mu\right\}, \tag{44}$$

$$\frac{\psi(\delta)}{\left(1-\delta+\delta(\varrho/\varsigma)^{\delta}\right)}\mathscr{Z}\{\nu(\varphi,\rho)\}-\frac{\varrho}{\varsigma}\nu(\varphi,0)=\mathscr{Z}\left\{\frac{\partial\mu}{\partial\varphi}-\nu-\mu\right\}.$$

We get

$$\mathscr{Z}\{\mu(\varphi,\rho)\}=\frac{\varrho}{\varsigma}\{\mu(\varphi,0)\}+\frac{\left(1-\delta+\delta(\varrho/\varsigma)^{\delta}\right)}{\psi(\delta)}\mathscr{Z}\left\{\frac{\partial\nu}{\partial\varphi}-\nu-\mu\right\},$$

$$\mathscr{Z}\{\nu(\varphi,\rho)\}=\frac{\varrho}{\varsigma}\{\nu(\varphi,0)\}+\frac{\left(1-\delta+\delta(\varrho/\varsigma)^{\delta}\right)}{\psi(\delta)}\mathscr{Z}\left\{\frac{\partial\mu}{\partial\varphi}-\nu-\mu\right\}. \tag{45}$$

Applying the inverse ZZT to (45), we get

$$\mu(\varphi,\rho)=\mu(\varphi,0)+\mathscr{Z}^{-1}\left[\frac{\left(1-\delta+\delta(\varrho/\varsigma)^{\delta}\right)}{\psi(\delta)}\mathscr{Z}\left[\frac{\partial\nu}{\partial\varphi}-\nu-\mu\right]\right],$$

$$\nu(\varphi,\rho)=\nu(\varphi,0)+\mathscr{Z}^{-1}\left[\frac{\left(1-\delta+\delta(\varrho/\varsigma)^{\delta}\right)}{\psi(\delta)}\mathscr{Z}\left[\frac{\partial\mu}{\partial\varphi}-\nu-\mu\right]\right]. \tag{46}$$

Decomposition results for $\mu(\varphi,\rho)$ and $\nu(\varphi,\rho)$ can be expressed as

$$\mu(\varphi,\rho)=\sum_{\aleph=0}^{\infty}\mu_{\aleph}(\varphi,\rho),\text{and}\nu(\varphi,\rho)=\sum_{\aleph=0}^{\infty}\nu_{\aleph}(\varphi,\rho),$$

$$\sum_{\aleph=0}^{\infty}\mu_{\aleph}(\varphi,\rho)=\mu(\varphi,0)+\mathscr{Z}^{-1}\left[\frac{\left(1-\delta+\delta(\varrho/\varsigma)^{\delta}\right)}{\psi(\delta)}\mathscr{Z}\left[\frac{\partial\sum_{\aleph=0}^{\infty}\nu_{\aleph}(\varphi,\rho)}{\partial\varphi}-\sum_{\aleph=0}^{\infty}\nu_{\aleph}(\varphi,\rho)-\sum_{\aleph=0}^{\infty}\mu_{\aleph}(\varphi,\rho)\right]\right], \tag{47}$$

$$\sum_{\aleph=0}^{\infty}\nu_{\aleph}(\varphi,\varphi,\rho)=\nu(\varphi,0)+\mathscr{Z}^{-1}\left[\frac{\left(1-\delta+\delta(\varrho/\varsigma)^{\delta}\right)}{\psi(\delta)}\mathscr{Z}\left[\frac{\partial\sum_{\aleph=0}^{\infty}\mu_{\aleph}(\varphi,\rho)}{\partial\varphi}-\sum_{\aleph=0}^{\infty}\nu_{\aleph}(\varphi,\rho)-\sum_{\aleph=0}^{\infty}\mu_{\aleph}(\varphi,\rho)\right]\right].$$

Furthermore,

$$\sum_{\aleph=0}^{\infty}\mu_{\aleph}(\varphi,\rho)=\sinh(\varphi)+\mathscr{Z}^{-1}\left[\frac{\left(1-\delta+\delta(\varrho/\varsigma)^{\delta}\right)}{\psi(\delta)}\mathscr{Z}\left[\frac{\partial\sum_{\aleph=0}^{\infty}\nu_{\aleph}(\varphi,\rho)}{\partial\varphi}-\sum_{\aleph=0}^{\infty}\nu_{\aleph}(\varphi,\rho)-\sum_{\aleph=0}^{\infty}\mu_{\aleph}(\varphi,\rho)\right]\right],$$
$$\sum_{\aleph=0}^{\infty}\nu_{\aleph}(\varphi,\rho)=\cosh(\varphi)+\mathscr{Z}^{-1}\left[\frac{\left(1-\delta+\delta(\varrho/\varsigma)^{\delta}\right)}{\psi(\delta)}\mathscr{Z}\left[\frac{\partial\sum_{\aleph=0}^{\infty}\mu_{\aleph}(\varphi,\rho))}{\partial\varphi}-\sum_{\aleph=0}^{\infty}\nu_{\aleph}(\varphi,\rho)-\sum_{\aleph=0}^{\infty}\mu_{\aleph}(\varphi,\rho)\right]\right]. \tag{48}$$

The component comparison in (48) provides the following recursive MDM algorithm:

$$\mu_0(\varphi,\rho)=\sinh(\varphi),\nu_0(\varphi,\rho)=\cosh(\varphi). \tag{49}$$

For $\aleph=0$,

$$\mu_1(\varphi,\rho)=-\cosh(\varphi)\frac{1}{\psi(\delta)}\left[1-\delta+\frac{\delta\rho^{\delta}}{\Gamma(\delta+1)}\right],\nu_1(\varphi,\rho)=-\sinh(\varphi)\frac{1}{\psi(\delta)}\left[1-\delta+\frac{\delta\rho^{\delta}}{\Gamma(\delta+1)}\right]. \tag{50}$$

For $\aleph=1$,

$$\begin{aligned}\mu_2(\varphi,\rho)&=-\cosh(\varphi)\frac{(1}{(\mathrm{B}(\delta))^2}\left[(1-\delta)^2+\frac{2\delta(1-\delta)\rho^{\delta}}{\Gamma(\delta+1)}+\frac{\delta^2\rho^{2\delta}}{\Gamma(2\delta+1)}\right]\\&+\sinh(\varphi)\frac{1}{(\mathrm{B}(\delta))^2}\left[(1-\delta)^2+\frac{2\delta(1-\delta)\rho^{\delta}}{\Gamma(\delta+1)}+\frac{\delta^2\rho^{2\delta}}{\Gamma(2\delta+1)}\right]\\&+\cosh(\varphi)\frac{1}{(\mathrm{B}(\delta))^2}\left[(1-\delta)^2+\frac{2\delta(1-\delta)\rho^{\delta}}{\Gamma(\delta+1)}+\frac{\delta^2\rho^{2\delta}}{\Gamma(2\delta+1)}\right],\\\nu_2(\varphi,\rho)&=-\sinh(\varphi)\frac{1}{(\mathrm{B}(\delta))^2}\left[(1-\delta)^2+\frac{2\delta(1-\delta)\rho^{\delta}}{\Gamma(\delta+1)}+\frac{\delta^2\rho^{2\delta}}{\Gamma(2\delta+1)}\right]\\&+\cosh(\varphi)\frac{1}{(\mathrm{B}(\delta))^2}\left[(1-\delta)^2+\frac{2\delta(1-\delta)\rho^{\delta}}{\Gamma(\delta+1)}+\frac{\delta^2\rho^{2\delta}}{\Gamma(2\delta+1)}\right]\\&+\sinh(\varphi)\frac{1}{(\mathrm{B}(\delta))^2}\left[(1-\delta)^2+\frac{2\delta(1-\delta)\rho^{\delta}}{\Gamma(\delta+1)}+\frac{\delta^2\rho^{2\delta}}{\Gamma(2\delta+1)}\right].\end{aligned} \tag{51}$$

For $\aleph=2$,

$$\mu_3(\varphi,\rho)=-\cosh(\varphi)\frac{\rho^{3\delta}}{\Gamma(3\delta+1)},\nu_3(\varphi,\rho)=\sinh(\varphi)\frac{\rho^{3\delta}}{\Gamma(3\delta+1)}. \tag{52}$$

$$\vdots$$

Similar to $\aleph>2$, MDM can be used to determine the remaining terms of μ_m and ν_m. In general, MDM's solution is as follows:

$$\mu(\varphi,\rho)=\sum_{\aleph=0}^{\infty}\mu_{\aleph}(\varphi,\rho)=\mu_0(\varphi)+\mu_1(\varphi)+\mu_2(\varphi)+\mu_3(\varphi)+\cdots,$$

$$\nu(\varphi,\rho)=\sum_{\aleph=0}^{\infty}\nu_{\aleph}(\varphi,\rho)=\nu_0(\varphi)+\nu_1(\varphi)+\nu_2(\varphi)+\nu_3(\varphi)+\cdots,$$

$$\begin{aligned}\mu(\varphi,\rho)&=\sum_{\aleph=0}^{\infty}\mu_{\aleph}(\varphi)\\&=\sinh(\varphi)-\cosh(\varphi)\frac{1}{\psi(\delta)}\left[1-\delta+\frac{\delta\rho^{\delta}}{\Gamma(\delta+1)}\right]-\cosh(\varphi)\frac{1}{(\mathrm{B}(\delta))^2}\left[(1-\delta)^2+\frac{2\delta(1-\delta)\rho^{\delta}}{\Gamma(\delta+1)}+\frac{\delta^2\rho^{2\delta}}{\Gamma(2\delta+1)}\right]\\&\quad+\sinh(\varphi)\frac{1}{(\mathrm{B}(\delta))^2}\left[(1-\delta)^2+\frac{2\delta(1-\delta)\rho^{\delta}}{\Gamma(\delta+1)}+\frac{\delta^2\rho^{2\delta}}{\Gamma(2\delta+1)}\right]+\cosh(\varphi)\frac{1}{(\mathrm{B}(\delta))^2}\left[(1-\delta)^2\right.\\&\quad\left.+\frac{2\delta(1-\delta)\rho^{\delta}}{\Gamma(\delta+1)}+\frac{\delta^2\rho^{2\delta}}{\Gamma(2\delta+1)}\right]\cdots,\end{aligned}$$

$$\begin{aligned}\nu(\varphi,\rho)&=\sum_{\aleph=0}^{\infty}\nu_{\aleph}(\varphi)\\&=\cosh(\varphi)-\sin(\varphi)\frac{1}{\psi(\delta)}\left[1-\delta+\frac{\delta\rho^{\delta}}{\Gamma(\delta+1)}\right]-\sinh(\varphi)\frac{1}{(\mathrm{B}(\delta))^2}\left[(1-\delta)^2+\frac{2\delta(1-\delta)\rho^{\delta}}{\Gamma(\delta+1)}+\frac{\delta^2\rho^{2\delta}}{\Gamma(2\delta+1)}\right]\\&\quad+\cosh(\varphi)\frac{1}{(\mathrm{B}(\delta))^2}\left[(1-\delta)^2+\frac{2\delta(1-\delta)\rho^{\delta}}{\Gamma(\delta+1)}+\frac{\delta^2\rho^{2\delta}}{\Gamma(2\delta+1)}\right]+\sinh(\varphi)\frac{1}{(\mathrm{B}(\delta))^2}\left[(1-\delta)^2\right.\\&\quad\left.+\frac{2\delta(1-\delta)\rho^{\delta}}{\Gamma(\delta+1)}+\frac{\delta^2\rho^{2\delta}}{\Gamma(2\delta+1)}\right]\cdots,\end{aligned}\tag{53}$$

$$\begin{aligned}\mu(\varphi,\rho)&=\sinh(\varphi)\left[1+\frac{1}{(\mathrm{B}(\delta))^2}\left[(1-\delta)^2+\frac{2\delta(1-\delta)\rho^{\delta}}{\Gamma(\delta+1)}+\frac{\delta^2\rho^{2\delta}}{\Gamma(2\delta+1)}\right]+\cdots\right]\\&\quad-\cosh(\varphi)\left[\frac{1}{\psi(\delta)}\left[1-\delta+\frac{\delta\rho^{\delta}}{\Gamma(\delta+1)}\right]+\frac{1}{(\mathrm{B}(\delta))^2}\left[(1-\delta)^2+\frac{2\delta(1-\delta)\rho^{\delta}}{\Gamma(\delta+1)}+\frac{\delta^2\rho^{2\delta}}{\Gamma(2\delta+1)}\right]\right.\\&\quad\left.-\frac{1}{(\mathrm{B}(\delta))^2}\left[(1-\delta)^2+\frac{2\delta(1-\delta)\rho^{\delta}}{\Gamma(\delta+1)}+\frac{\delta^2\rho^{2\delta}}{\Gamma(2\delta+1)}\right]+\cdots\right],\end{aligned}$$

$$\begin{aligned}\nu(\varphi,\rho)&=\cosh(\varphi)\left[1+\frac{1}{(\mathrm{B}(\delta))^2}\left[(1-\delta)^2+\frac{2\delta(1-\delta)\rho^{\delta}}{\Gamma(\delta+1)}+\frac{\delta^2\rho^{2\delta}}{\Gamma(2\delta+1)}\right]+\cdots\right]\\&\quad-\sinh(\varphi)\left[\frac{1}{\psi(\delta)}\left[1-\delta+\frac{\delta\rho^{\delta}}{\Gamma(\delta+1)}\right]+\frac{1}{(\mathrm{B}(\delta))^2}\left[(1-\delta)^2+\frac{2\delta(1-\delta)\rho^{\delta}}{\Gamma(\delta+1)}+\frac{\delta^2\rho^{2\delta}}{\Gamma(2\delta+1)}\right]\right.\\&\quad\left.-\frac{1}{(\mathrm{B}(\delta))^2}\left[(1-\delta)^2+\frac{2\delta(1-\delta)\rho^{\delta}}{\Gamma(\delta+1)}+\frac{\delta^2\rho^{2\delta}}{\Gamma(2\delta+1)}\right]+\cdots\right].\end{aligned}$$

Set $\delta = 1$ in (42); we get

$$\begin{aligned}\mu(\varphi,\rho) &= \sinh(\varphi)\left[1+\frac{\rho^2}{(2)!}+\frac{\rho^4}{(4!)}+\cdots\right]-cosh(\varphi)\left[\frac{\rho}{(1!)}+\frac{\rho^3}{(3!)}+\frac{\rho^5}{(5!)}+\cdots\right]=\sinh(\varphi-\rho),\\ \nu(\varphi,\rho) &= \cosh(\varphi)\left[1+\frac{\rho^2}{(2)!}+\frac{\rho^4}{(4!)}+\cdots\right]-sinh(\varphi)\left[\frac{\rho}{(1!)}+\frac{\rho^3}{(3!)}+\frac{\rho^5}{(5!)}+\cdots\right]=\cosh(\varphi+\rho).\end{aligned} \tag{54}$$

The exact results are at $\delta = 1$.

$$\begin{aligned}\mu(\varphi,\rho) &= sinh(\varphi-\rho),\\ \nu(\varphi,\rho) &= cosh(\varphi+\rho).\end{aligned} \tag{55}$$

We analyze the solution figures of the problem, which have been investigated by applying the ZZ decomposition method in the sense of the Atangana–Baleanu operator. Figure 1 represents the three-dimensional solution-figures for variables μ of example 1 at fractional order $\delta = 1$ and 0.8, respectively; Figure 2 represents different fractional order of $\delta = 0.6$ and 0.4; and Figure 3 represents that at δ. In Figure 4, different fractional order with respect to φ and ρ. It is observed that the ZZ decomposition method solution-figures are identical and in close contact with each other. In the same way, Figures 5–8 show different fractional order graphs of δ at ν of Example 1.

Example 2. Here, we take the following FPDE:

$$\begin{cases} D_\rho^\delta(\mu)+\nu_\varphi\omega_\chi-\nu_\chi\omega_\varphi=-\mu,\\ D_\rho^\delta(\nu)+\mu_\chi\omega_\varphi+\mu_\chi\omega_\varphi=\nu,\\ D_\rho^\delta(\omega)+\mu_\varphi\nu_\chi+\mu_\chi\nu_\varphi=\omega, \delta\in(0,1], \end{cases} \tag{56}$$

with initial sources

$$\begin{cases} \mu(\varphi,\chi,0)=\exp^{\varphi+\chi},\\ \nu(\varphi,\chi,0)=\exp^{\varphi-\chi},\\ \omega(\varphi,\chi,0)=\exp^{-\varphi+\chi}. \end{cases} \tag{57}$$

The exact solution at $\delta = 1$ is

$$\begin{cases} \mu(\varphi,\chi,\rho)=\exp^{\varphi+\chi-\rho},\\ \nu(\varphi,\chi,\rho)=\exp^{\varphi-\chi+\rho},\\ \omega(\varphi,\chi,\rho)=\exp^{-\varphi+\chi+\rho}. \end{cases} \tag{58}$$

Using ZZT equation (33), it can be written as

$$\begin{aligned} \mathcal{Z}\left\{\frac{\partial^\delta\mu}{\partial\rho^\delta}\right\}=\mathcal{Z}\{-\mu+\nu_\varphi\omega_\chi-\nu_\chi\omega_\varphi\}, \mathcal{Z}\left\{\frac{\partial^\delta\nu}{\partial\rho^\delta}\right\}=\mathcal{Z}\{\nu-\mu_\chi\omega_\varphi-\mu_\chi\omega_\varphi\},\\ \mathcal{Z}\left\{\frac{\partial^\delta\omega}{\partial\rho^\delta}\right\}=\mathcal{Z}\{\omega-\mu_\varphi\nu_\chi-\mu_\chi\nu_\varphi\},\\ \frac{\psi(\delta)}{\left(1-\delta+\delta(\varrho/\varsigma)^\delta\right)}\mathcal{Z}\{\mu(\varphi,\chi,\rho)\}-\frac{\varrho}{\varsigma}\mu(\varphi,\chi,0)=\mathcal{Z}\{-\mu+\nu_\varphi\omega_\chi-\nu_\chi\omega_\varphi\},\\ \frac{\psi(\delta)}{\left(1-\delta+\delta(\varrho/\varsigma)^\delta\right)}\mathcal{Z}\{\nu(\varphi,\chi,\rho)\}-\frac{\varrho}{\varsigma}\nu(\varphi,\chi,0)=\mathcal{Z}\{\nu-\mu_\chi\omega_\varphi-\mu_\chi\omega_\varphi\},\\ \frac{\psi(\delta)}{\left(1-\delta+\delta(\varrho/\varsigma)^\delta\right)}\mathcal{Z}\{\omega(\varphi,\varphi,\rho)\}-\frac{\varrho}{\varsigma}\omega(\varphi,\chi,0)=\mathcal{Z}\{\omega-\mu_\varphi\nu_\chi-\mu_\chi\nu_\varphi\}. \end{aligned} \tag{59}$$

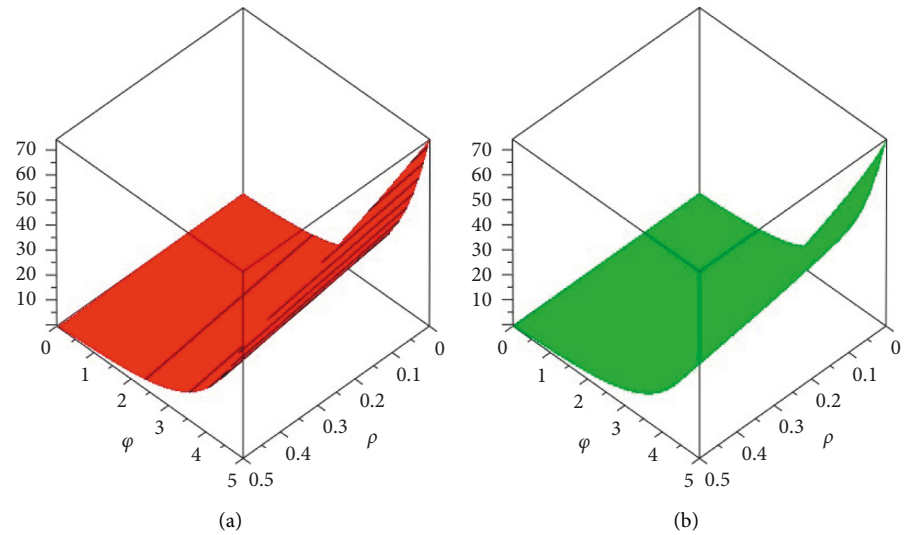

Figure 1: (a) The exact and approximate solution at $\delta = 1$ and (b) second fractional order at $\delta = 0.8$.

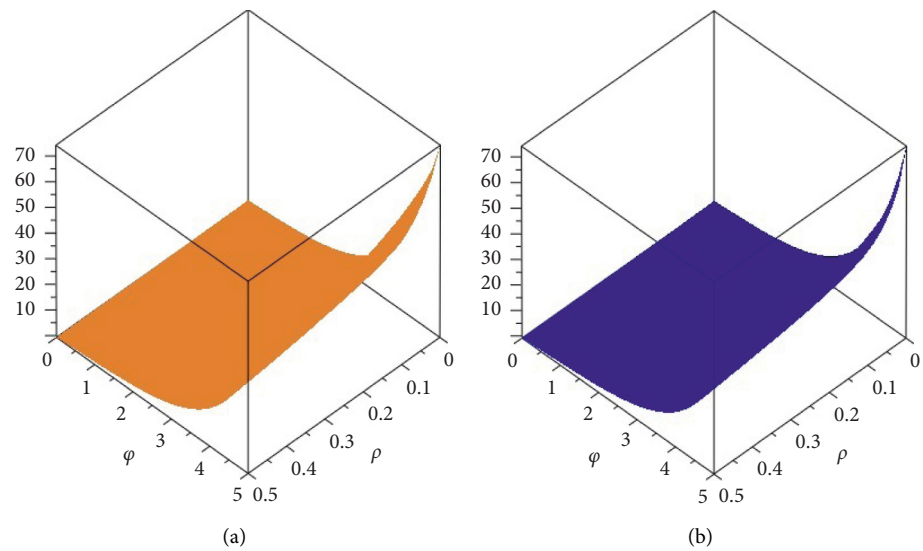

Figure 2: The graph shows the fractional order at $\delta = 0.6$ and 0.4.

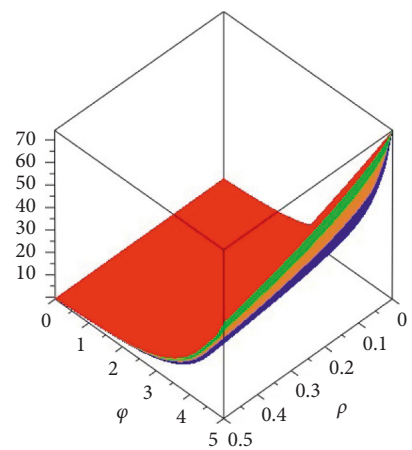

Figure 3: The graph shows different fractional orders of δ.

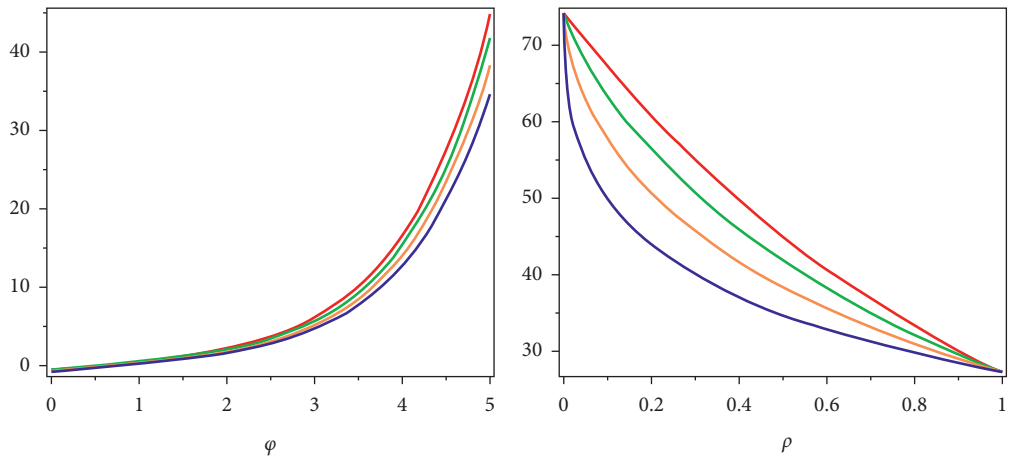

Figure 4: The graph of the two dimensions of different fractional orders at δ with respect to φ and ρ.

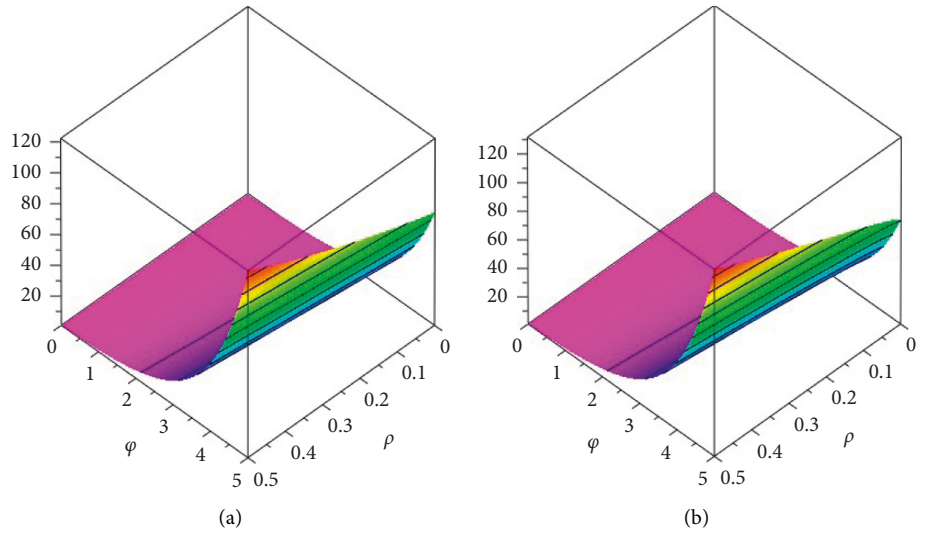

Figure 5: (a) The exact and approximate solution at $\delta = 1$ and (b) second fractional order at $\delta = 0.8$.

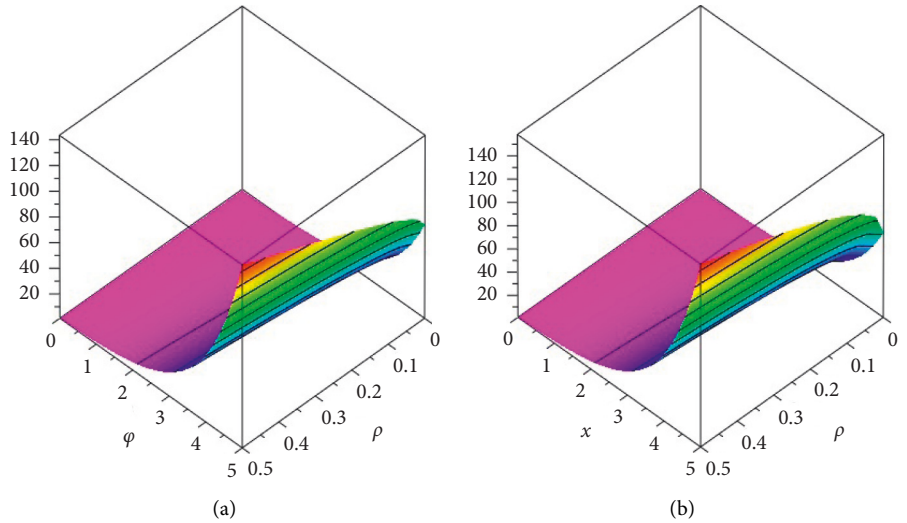

Figure 6: The graph shows the fractional order at $\delta = 0.6$ and 0.4.

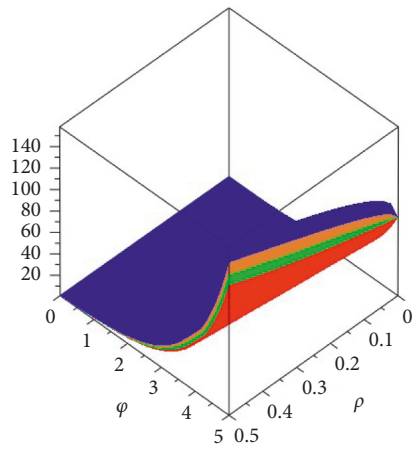

Figure 7: The graph shows different fractional orders of δ.

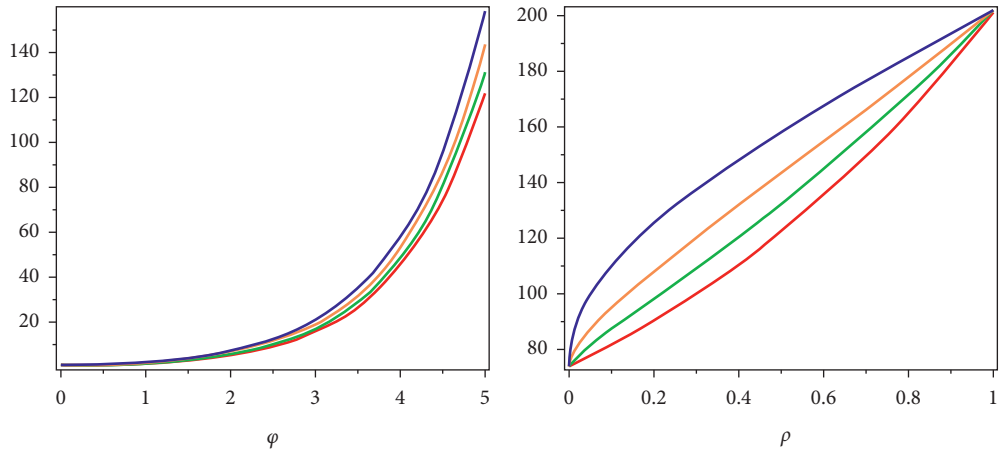

Figure 8: The graph of the two dimensions of different fractional orders at δ with respect to φ and ρ.

After simplification, we obtain

$$\begin{aligned}
\frac{\psi(\delta)}{\left(1-\delta+\delta(\varrho/\varsigma)^{\delta}\right)}\mathcal{Z}\{\mu(\varphi,\chi,\rho)\} &= \frac{\varrho}{\varsigma}\mu(\varphi,\chi,0)+\mathcal{Z}\{-\mu+\nu_{\varphi}\omega_{\chi}-\nu_{\chi}\omega_{\varphi}\},\\
\frac{\psi(\delta)}{\left(1-\delta+\delta(\varrho/\varsigma)^{\delta}\right)}\mathcal{Z}\{\nu(\varphi,\chi,\rho)\} &= \frac{\varrho}{\varsigma}\nu(\varphi,\chi,0)+\mathcal{Z}\{\nu-\mu_{\chi}\omega_{\varphi}-\mu_{\chi}\omega_{\varphi}\},\\
\frac{\psi(\delta)}{\left(1-\delta+\delta(\varrho/\varsigma)^{\delta}\right)}\mathcal{Z}\{\omega(\varphi,\varphi,\rho)\} &= \frac{\varrho}{\varsigma}\omega(\varphi,\chi,0)+\mathcal{Z}\{\omega-\mu_{\varphi}\nu_{\chi}-\mu_{\chi}\nu_{\varphi}\},\\
\mathcal{Z}\{\mu(\varphi,\chi,\rho)\} &= \frac{\varrho}{\varsigma}\mu(\varphi,\chi,0)+\frac{\left(1-\delta+\delta(\varrho/\varsigma)^{\delta}\right)}{\psi(\delta)}\mathcal{Z}\{-\mu+\nu_{\varphi}\omega_{\chi}-\nu_{\chi}\omega_{\varphi}\},\\
\mathcal{Z}\{\nu(\varphi,\chi,\rho)\} &= \frac{\varrho}{\varsigma}\nu(\varphi,\chi,0)+\frac{\left(1-\delta+\delta(\varrho/\varsigma)^{\delta}\right)}{\psi(\delta)}\mathcal{Z}\{\nu-\mu_{\chi}\omega_{\varphi}-\mu_{\chi}\omega_{\varphi}\},\\
\mathcal{Z}\{\omega(\varphi,\varphi,\rho)\} &= \frac{\varrho}{\varsigma}\omega(\varphi,\chi,0)+\frac{\left(1-\delta+\delta(\varrho/\varsigma)^{\delta}\right)}{\psi(\delta)}\mathcal{Z}\{\omega-\mu_{\varphi}\nu_{\chi}-\mu_{\chi}\nu_{\varphi}\}.
\end{aligned} \tag{60}$$

Taking inverse ZZT of (60), we obtain

$$\mu(\varphi,\chi,\rho)=\mu(\varphi,\chi,0)+\mathscr{Z}^{-1}\left[\frac{\left(1-\delta+\delta(\varrho/\varsigma)^{\delta}\right)}{\psi(\delta)}\mathscr{Z}\left\{-\mu+\nu_{\varphi}\omega_{\chi}-\nu_{\chi}\omega_{\varphi}\right\}\right],$$
$$\nu(\varphi,\chi,\rho)=\nu(\varphi,\chi,0)+\mathscr{Z}^{-1}\left[\frac{\left(1-\delta+\delta(\varrho/\varsigma)^{\delta}\right)}{\psi(\delta)}\mathscr{Z}\left\{\nu-\mu_{\chi}\omega_{\varphi}-\mu_{\chi}\omega_{\varphi}\right\}\right], \tag{61}$$
$$\omega(\varphi,\chi,\rho)=\omega(\varphi,\chi,0)+\mathscr{Z}^{-1}\left[\frac{\left(1-\delta+\delta(\varrho/\varsigma)^{\delta}\right)}{\psi(\delta)}\mathscr{Z}\left\{\omega-\mu_{\varphi}\nu_{\chi}-\mu_{\chi}\nu_{\varphi}\right\}\right].$$

Assume decomposition solutions for variables $\mu(\varphi,\chi,\rho)$, $\nu(\varphi,\chi,\rho)$, and $\omega(\varphi,\chi,\rho)$, it can be written as

$$\mu(\varphi,\chi,\rho)=\sum_{\aleph=0}^{\infty}\mu_{\aleph}(\varphi,\chi,\rho),\nu(\varphi,\chi,\rho)=\sum_{\aleph=0}^{\infty}\nu_{\aleph}(\varphi,\chi,\rho),\text{and}\omega(\varphi,\chi,\rho)=\sum_{\aleph=0}^{\infty}\omega_{\aleph}(\varphi,\chi,\rho). \tag{62}$$

Remember that $\nu_{\varphi}\omega_{\chi}=\sum_{\aleph=0}^{\infty}\mathscr{A}_m$, $\nu_{\chi}\omega_{\varphi}=\sum_{\aleph=0}^{\infty}\mathscr{B}_{\aleph}$, $\mu_{\varphi}\omega_{\chi}=\sum_{\aleph=0}^{\infty}\mathscr{C}_{\aleph}$, $\mu_{\chi}\omega_{\varphi}=\sum_{\aleph=0}^{\infty}\mathscr{D}_{\aleph},\mu_{\varphi}\nu_{\chi}=\sum_{\aleph=0}^{\infty}\mathscr{E}_{\aleph}$, and $\mu_{\chi}\nu_{\varphi}=\sum_{\aleph=0}^{\infty}\mathscr{F}_{\aleph}$ are the Adomian polynomials and the nonlinear terms were characterized, which can be further simplified as

$$\sum_{\aleph=0}^{\infty}\mu_{\aleph}(\varphi,\chi,\rho)=\mu(\varphi,\chi,0)+\mathscr{Z}^{-1}\left[\frac{\left(1-\delta+\delta(\varrho/\varsigma)^{\delta}\right)}{\psi(\delta)}\mathscr{Z}\left[-\sum_{\aleph=0}^{\infty}\mu_{\aleph}(\varphi,\chi,\rho)+\left(\sum_{\aleph=0}^{\infty}\mathscr{A}_{\aleph}-\sum_{\aleph=0}^{\infty}\mathscr{B}_{\aleph}\right)\right]\right],$$
$$\sum_{\aleph=0}^{\infty}\nu_{\aleph}(\varphi,\chi,\rho)=\nu(\varphi,\chi,0)+\mathscr{Z}^{-1}\left[\frac{\left(1-\delta+\delta(\varrho/\varsigma)^{\delta}\right)}{\psi(\delta)}\mathscr{Z}\left[\sum_{\aleph=0}^{\infty}\nu_{\aleph}(\varphi,\chi,\rho)-\left(\sum_{\aleph=0}^{\infty}\mathscr{C}_{\aleph}+\sum_{\aleph=0}^{\infty}\mathscr{D}_{\aleph}\right)\right]\right], \tag{63}$$
$$\sum_{\aleph=0}^{\infty}\omega_{\aleph}(\varphi,\chi,\rho)=\omega(\varphi,\varphi,\delta,0)+\mathscr{Z}^{-1}\left[\frac{\left(1-\delta+\delta(\varrho/\varsigma)^{\delta}\right)}{\psi(\delta)}\mathscr{Z}\left[\sum_{\aleph=0}^{\infty}\omega_{\aleph}(\varphi,\chi,\rho)-\left(\sum_{\aleph=0}^{\infty}\mathscr{Z}_{\aleph}+\sum_{\aleph=0}^{\infty}\mathscr{F}_{\aleph}\right)\right]\right].$$

Using (38), the nonlinearity in the given problem can be expressed as

$$\mathscr{A}_0=\frac{\partial\nu_0}{\partial\varphi}\frac{\partial\omega_0}{\partial\chi},\mathscr{A}_1=\frac{\partial\nu_0}{\partial\varphi}\frac{\partial\omega_1}{\partial\chi}+\frac{\partial\nu_1}{\partial\varphi}\frac{\partial\omega_0}{\partial\chi},\mathscr{B}_0=\frac{\partial\nu_0}{\partial\chi}\frac{\partial\omega_0}{\partial\varphi},\mathscr{B}_1=\frac{\partial\nu_0}{\partial\chi}\frac{\partial\omega_1}{\partial\varphi}+\frac{\partial\nu_0}{\partial\varphi}\frac{\partial\omega_1}{\partial\chi},$$
$$\mathscr{C}_0=\frac{\partial\mu_0}{\partial\varphi}\frac{\partial\omega_0}{\partial\chi},\mathscr{C}_1==\frac{\partial\mu_1}{\partial\varphi}\frac{\partial\omega_0}{\partial\chi}+\frac{\partial\mu_0}{\partial\varphi}\frac{\partial\omega_1}{\partial\chi},\mathscr{D}_0=\frac{\partial\mu_0}{\partial\chi}\frac{\partial\omega_0}{\partial\varphi},\mathscr{D}_1=\frac{\partial\mu_0}{\partial\chi}\frac{\partial\omega_1}{\partial\varphi}+\frac{\partial\mu_1}{\partial\chi}\frac{\partial\omega_0}{\partial\varphi}, \tag{64}$$
$$\mathscr{E}_0=\frac{\partial\mu_0}{\partial\varphi}\frac{\partial\nu_0}{\partial\varphi},\mathscr{E}_1=\frac{\partial\mu_1}{\partial\varphi}\frac{\partial\nu_0}{\partial\chi}+\frac{\partial\mu_0}{\partial\varphi}\frac{\partial\nu_1}{\partial\chi},\mathscr{F}_0=\frac{\partial\mu_0}{\partial\chi}\frac{\partial\nu_0}{\partial\varphi},\mathscr{F}_1=\frac{\partial\mu_1}{\partial\chi}\frac{\partial\nu_0}{\partial\varphi}+\frac{\partial\mu_0}{\partial\varphi}\frac{\partial\nu_1}{\partial\chi}.$$

The component comparison provides the following recursive MDM algorithm:

$$\begin{aligned}
&\mu_0(\varphi,\chi,\rho)=\mu(\varphi,\chi,0),\nu_0(\varphi,\chi,\rho)=\nu(\varphi,\chi,0),\omega_0(\varphi,\chi,\rho)=\omega(\varphi,\chi,0),\\
&\mu_1(\varphi,\chi,\rho)=\mathscr{Z}^{-1}\left[\frac{\left(1-\delta+\delta(\varrho/\varsigma)^{\delta}\right)}{\psi(\delta)}\mathscr{Z}\left[-\mu_0(\varphi,\chi,\rho)+\left[\mathscr{A}_0-\mathscr{B}_0\right]\right]\right],\\
&\nu_1(\varphi,\chi,\rho)=\mathscr{Z}^{-1}\left[\frac{\left(1-\delta+\delta(\varrho/\varsigma)^{\delta}\right)}{\psi(\delta)}\mathscr{Z}\left[\nu_0(\varphi,\chi,\rho)-\left[\mathscr{C}_0+\mathscr{D}_0\right]\right]\right],\\
&\omega_1(\varphi,\chi,\rho)=\mathscr{Z}^{-1}\left[\frac{\left(1-\delta+\delta(\varrho/\varsigma)^{\delta}\right)}{\psi(\delta)}\mathscr{Z}\left[\omega_0(\varphi,\chi,\rho)-\left[\mathscr{E}_0+\mathscr{F}_0\right]\right]\right],\\
&\mu_{\aleph+1}(\varphi,\chi,\rho)=\mathscr{Z}^{-1}\left[\frac{\left(1-\delta+\delta(\varrho/\varsigma)^{\delta}\right)}{\psi(\delta)}\mathscr{Z}\left[-\mu_{\aleph}(\varphi,\chi,\rho)+\left[\mathscr{A}_{\aleph}-\mathscr{B}_{\aleph}\right]\right]\right],\\
&\nu_{\aleph+1}(\varphi,\chi,\rho)=\mathscr{Z}^{-1}\left[\frac{\left(1-\delta+\delta(\varrho/\varsigma)^{\delta}\right)}{\psi(\delta)}\mathscr{Z}\left[\nu_{\aleph}(\varphi,\chi,\rho)-\left[\mathscr{C}_{\aleph}+\mathscr{D}_{\aleph}\right]\right]\right],\\
&\omega_{\aleph+1}(\varphi,\chi,\rho)=\mathscr{Z}^{-1}\left[\frac{\left(1-\delta+\delta(\varrho/\varsigma)^{\delta}\right)}{\psi(\delta)}\mathscr{Z}\left[\omega_{\aleph}(\varphi,\chi,\rho)-\left[\mathscr{E}_{\aleph}+\mathscr{F}_{\aleph}\right]\right]\right],\\
&\mu_0(\varphi,\chi,\rho)=\exp^{\varphi+\chi},\nu_0(\varphi,\chi,\rho)=\exp^{\varphi-\chi},\omega_0(\varphi,\chi,\rho)=\exp^{-\varphi+\chi}.
\end{aligned}\tag{65}$$

For $\aleph=0$,

$$\begin{aligned}
&\mu_1(\varphi,\chi,\rho)=-\exp^{\varphi+\chi}\frac{1}{\psi(\delta)}\left[1-\delta+\frac{\delta\rho^{\delta}}{\Gamma(\delta+1)}\right],\\
&\nu_1(\varphi,\chi,\rho)=\exp^{\varphi-\chi}\frac{1}{\psi(\delta)}\left[1-\delta+\frac{\delta\rho^{\delta}}{\Gamma(\delta+1)}\right],\\
&\omega_1(\varphi,\chi,\rho)=\exp^{-\varphi+\chi}\frac{1}{\psi(\delta)}\left[1-\delta+\frac{\delta\rho^{\delta}}{\Gamma(\delta+1)}\right].
\end{aligned}\tag{66}$$

For $\aleph=1$,

$$\begin{aligned}
&\mu_2(\varphi,\chi,\rho)=\exp^{\varphi+\chi}\frac{1}{(\mathrm{B}(\delta))^2}\left[(1-\delta)^2+\frac{2\delta(1-\delta)\rho^{\delta}}{\Gamma(\delta+1)}+\frac{\delta^2\rho^{2\delta}}{\Gamma(2\delta+1)}\right],\\
&\nu_2(\varphi,\chi,\rho)=\exp^{\varphi-\chi}\frac{1}{(\mathrm{B}(\delta))^2}\left[(1-\delta)^2+\frac{2\delta(1-\delta)\rho^{\delta}}{\Gamma(\delta+1)}+\frac{\delta^2\rho^{2\delta}}{\Gamma(2\delta+1)}\right],\\
&\omega_2(\varphi,\chi,\rho)=\exp^{-\varphi+\chi}\frac{1}{(\mathrm{B}(\delta))^2}\left[(1-\delta)^2+\frac{2\delta(1-\delta)\rho^{\delta}}{\Gamma(\delta+1)}+\frac{\delta^2\rho^{2\delta}}{\Gamma(2\delta+1)}\right].
\end{aligned}\tag{67}$$

For $\aleph=2$,

$$\begin{aligned}
&\mu_3(\varphi,\chi,\rho)=-\exp^{\varphi+\chi}\frac{1}{(\mathrm{B}(\delta))^3}\left[(1-\delta)^3+\frac{3\delta(1-\delta)^2\rho^{\delta}}{\Gamma(\delta+1)}+\frac{\delta^2(1-\delta)\rho^{2\delta+1}}{\Gamma(2\delta+2)}+\frac{2\delta^2(1-\delta)\rho^{2\delta}}{\Gamma(2\delta+1)}+\frac{\delta^3\rho^{2\delta+1}}{\Gamma(2\delta+2)}\right],\\
&\nu_3(\varphi,\chi,\rho)=\exp^{\varphi-\chi}\frac{1}{(\mathrm{B}(\delta))^3}\left[(1-\delta)^3+\frac{3\delta(1-\delta)^2\rho^{\delta}}{\Gamma(\delta+1)}+\frac{\delta^2(1-\delta)\rho^{2\delta+1}}{\Gamma(2\delta+2)}+\frac{2\delta^2(1-\delta)\rho^{2\delta}}{\Gamma(2\delta+1)}+\frac{\delta^3\rho^{2\delta+1}}{\Gamma(2\delta+2)}\right],\\
&\omega_3(\varphi,\chi,\rho)=\exp^{-\varphi+\chi}\frac{1}{(\mathrm{B}(\delta))^3}\left[(1-\delta)^3+\frac{3\delta(1-\delta)^2\rho^{\delta}}{\Gamma(\delta+1)}+\frac{\delta^2(1-\delta)\rho^{2\delta+1}}{\Gamma(2\delta+2)}+\frac{2\delta^2(1-\delta)\rho^{2\delta}}{\Gamma(2\delta+1)}+\frac{\delta^3\rho^{2\delta+1}}{\Gamma(2\delta+2)}\right].
\end{aligned}\tag{68}$$

$\vdots$

In same manner, the remaining terms of $\mu_{\aleph}$, $\nu_{\aleph}$, and $\omega_{\aleph}$ for $(\aleph>3)$ can be calculated easily by using MDM. The general solution of MDM is given by

$$\mu(\varphi,\chi,\rho)=\sum_{\aleph=0}^{\infty}\mu_{\aleph}(\varphi,\chi,\rho)=\mu_0(\varphi,\chi,\rho)+\mu_1(\varphi,\chi,\rho)+\mu_2(\varphi,\chi,\rho)+\mu_3(\varphi,\chi,\rho)+\cdots,$$

$$\nu(\varphi,\chi,\rho)=\sum_{\aleph=0}^{\infty}\nu_{\aleph}(\varphi,\chi,\rho)=\nu_0(\varphi,\chi,\rho)+\nu_1(\varphi,\chi,\rho)+\nu_2(\varphi,\chi,\rho)+\nu_3(\varphi,\chi,\rho)+\cdots,$$

$$\omega(\varphi,\chi,\rho)=\sum_{\aleph=0}^{\infty}\omega_{\aleph}(\varphi,\chi,\rho)=\omega_0(\varphi,\chi,\rho)+\omega_1(\varphi,\chi,\rho)+\omega_2(\varphi,\chi,\rho)+\omega_3(\varphi,\chi,\rho)+\cdots,$$

$$\begin{aligned}
\mu(\varphi,\chi,\rho)=\sum_{\aleph=0}^{\infty}\mu_{\aleph}(\varphi,\chi,\rho)=&\ \exp^{\varphi+\chi}-\exp^{\varphi+\chi}\frac{1}{\psi(\delta)}\left[1-\delta+\frac{\delta\rho^{\delta}}{\Gamma(\delta+1)}\right]\\
&+\exp^{\varphi+\chi}\frac{1}{(\mathrm{B}(\delta))^2}\left[(1-\delta)^2+\frac{2\delta(1-\delta)\rho^{\delta}}{\Gamma(\delta+1)}+\frac{\delta^2\rho^{2\delta}}{\Gamma(2\delta+1)}\right]-\exp^{\varphi+\chi}\frac{1}{(\mathrm{B}(\delta))^3}\\
&\cdot\left[(1-\delta)^3+\frac{3\delta(1-\delta)^2\rho^{\delta}}{\Gamma(\delta+1)}+\frac{\delta^2(1-\delta)\rho^{2\delta+1}}{\Gamma(2\delta+2)}+\frac{2\delta^2(1-\delta)\rho^{2\delta}}{\Gamma(2\delta+1)}+\frac{\delta^3\rho^{2\delta+1}}{\Gamma(2\delta+2)}\right]\\
\cdots,\nu(\varphi,\chi,\rho)=\sum_{\aleph=0}^{\infty}\mu_{\aleph}(\varphi,\chi,\rho)=&\ \exp^{\varphi-\chi}+\exp^{\varphi-\chi}\frac{1}{\psi(\delta)}\left[1-\delta+\frac{\delta\rho^{\delta}}{\Gamma(\delta+1)}\right]+\exp^{\varphi-\chi}\frac{1}{(\mathrm{B}(\delta))^2}\\
&\left[(1-\delta)^2+\frac{2\delta(1-\delta)\rho^{\delta}}{\Gamma(\delta+1)}+\frac{\delta^2\rho^{2\delta}}{\Gamma(2\delta+1)}\right]\\
&+\exp^{\varphi-\chi}\frac{1}{(\mathrm{B}(\delta))^3}\left[\begin{array}{c}(1-\delta)^3\\+\frac{3\delta(1-\delta)^2\rho^{\delta}}{\Gamma(\delta+1)}+\frac{\delta^2(1-\delta)\rho^{2\delta+1}}{\Gamma(2\delta+2)}+\frac{2\delta^2(1-\delta)\rho^{2\delta}}{\Gamma(2\delta+1)}+\frac{\delta^3\rho^{2\delta+1}}{\Gamma(2\delta+2)}\end{array}\right]\\
+\cdots,\omega(\varphi,\chi,\rho)=\sum_{\aleph=0}^{\infty}\mu_{\aleph}(\varphi,\chi,\rho)=&\ \exp^{-\varphi+\chi}+\exp^{-\varphi+\chi}\frac{1}{\psi(\delta)}\left[1-\delta+\frac{\delta\rho^{\delta}}{\Gamma(\delta+1)}\right]\\
&+\exp^{-\varphi+\chi}\frac{1}{(\mathrm{B}(\delta))^2}\left[(1-\delta)^2+\frac{2\delta(1-\delta)\rho^{\delta}}{\Gamma(\delta+1)}+\frac{\delta^2\rho^{2\delta}}{\Gamma(2\delta+1)}\right]\\
&+\exp^{-\varphi+\chi}\frac{1}{(\mathrm{B}(\delta))^3}\left[(1-\delta)^3+\frac{3\delta(1-\delta)^2\rho^{\delta}}{\Gamma(\delta+1)}+\frac{\delta^2(1-\delta)\rho^{2\delta+1}}{\Gamma(2\delta+2)}+\frac{2\delta^2(1-\delta)\rho^{2\delta}}{\Gamma(2\delta+1)}+\frac{\delta^3\rho^{2\delta+1}}{\Gamma(2\delta+2)}\right]+\cdots,
\end{aligned}\tag{69}$$

$$\mu(\varphi,\chi,\rho)=\exp^{\varphi+\chi}\left[\begin{array}{c}1-\frac{1}{\psi(\delta)}\left[1-\delta+\frac{\delta\rho^{\delta}}{\Gamma(\delta+1)}\right]+\frac{1}{(\mathrm{B}(\delta))^2}\left[(1-\delta)^2+\frac{2\delta(1-\delta)\rho^{\delta}}{\Gamma(\delta+1)}+\frac{\delta^2\rho^{2\delta}}{\Gamma(2\delta+1)}\right]-\\ \frac{1}{(\mathrm{B}(\delta))^3}\left[(1-\delta)^3+\frac{3\delta(1-\delta)^2\rho^{\delta}}{\Gamma(\delta+1)}+\frac{\delta^2(1-\delta)\rho^{2\delta+1}}{\Gamma(2\delta+2)}+\frac{2\delta^2(1-\delta)\rho^{2\delta}}{\Gamma(2\delta+1)}+\frac{\delta^3\rho^{2\delta+1}}{\Gamma(2\delta+2)}\right]+\cdots\end{array}\right],$$

$$\nu(\varphi,\chi,\rho)=\exp^{\varphi-\chi}\left[\begin{array}{c}1+\frac{1}{\psi(\delta)}\left[1-\delta+\frac{\delta\rho^{\delta}}{\Gamma(\delta+1)}\right]+\frac{1}{(\mathrm{B}(\delta))^2}\left[(1-\delta)^2+\frac{2\delta(1-\delta)\rho^{\delta}}{\Gamma(\delta+1)}+\frac{\delta^2\rho^{2\delta}}{\Gamma(2\delta+1)}\right]+\\ \frac{1}{(\mathrm{B}(\delta))^3}\left[(1-\delta)^3+\frac{3\delta(1-\delta)^2\rho^{\delta}}{\Gamma(\delta+1)}+\frac{\delta^2(1-\delta)\rho^{2\delta+1}}{\Gamma(2\delta+2)}+\frac{2\delta^2(1-\delta)\rho^{2\delta}}{\Gamma(2\delta+1)}+\frac{\delta^3\rho^{2\delta+1}}{\Gamma(2\delta+2)}\right]+\cdots\end{array}\right],$$

$$\omega(\varphi,\chi,\rho)=\exp^{-\varphi+\chi}\left[\begin{array}{c}1+\frac{1}{\psi(\delta)}\left[1-\delta+\frac{\delta\rho^{\delta}}{\Gamma(\delta+1)}\right]+\frac{1}{(\mathrm{B}(\delta))^2}\left[(1-\delta)^2+\frac{2\delta(1-\delta)\rho^{\delta}}{\Gamma(\delta+1)}+\frac{\delta^2\rho^{2\delta}}{\Gamma(2\delta+1)}\right]+\\ \frac{1}{(\mathrm{B}(\delta))^3}\left[(1-\delta)^3+\frac{3\delta(1-\delta)^2\rho^{\delta}}{\Gamma(\delta+1)}+\frac{\delta^2(1-\delta)\rho^{2\delta+1}}{\Gamma(2\delta+2)}+\frac{2\delta^2(1-\delta)\rho^{2\delta}}{\Gamma(2\delta+1)}+\frac{\delta^3\rho^{2\delta+1}}{\Gamma(2\delta+2)}\right]\cdots\end{array}\right].$$

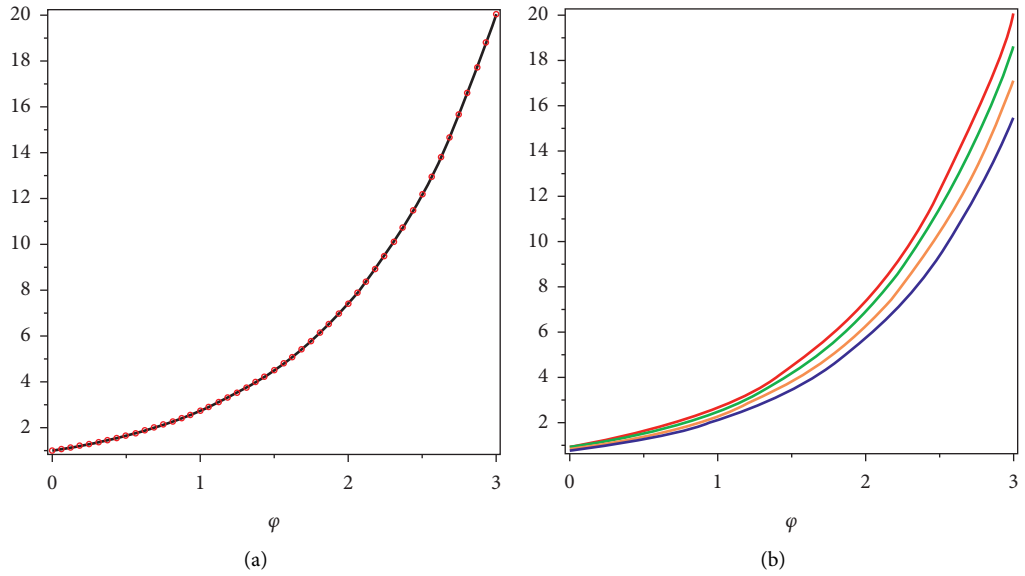

Figure 9: (a) The exact and approximate solution at $\delta = 1$ and (b) the different fractional order of δ.

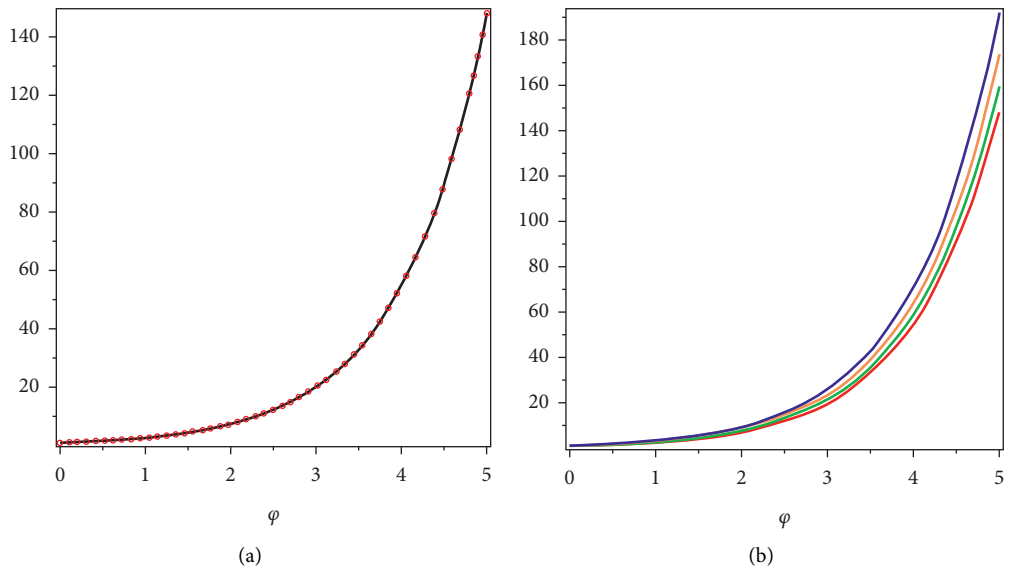

Figure 10: (a) The exact and approximate solution at $\delta = 1$ and (b) the different fractional order of δ.

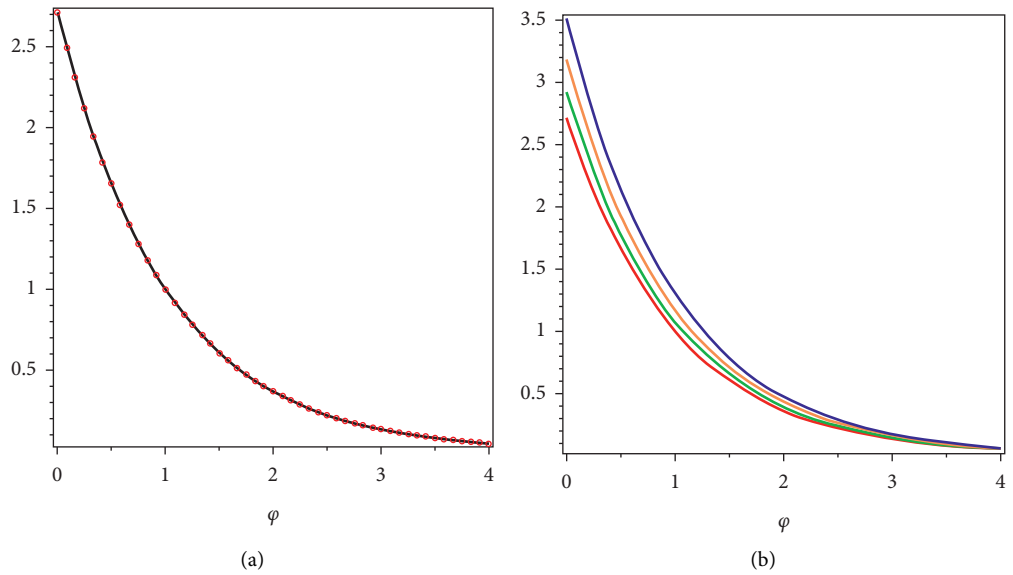

FIGURE 11: (a) The exact and approximate solution at $\delta = 1$ and (b) the different fractional order of δ.

Setting $\delta = 1$ in (69), we get

$$\begin{aligned}
\mu(\varphi,\chi,\rho) &= \exp^{\varphi+\chi}\left[1-\frac{\rho}{\Gamma(2)}+\frac{\rho^2}{\Gamma(3)}-\frac{\rho^3}{\Gamma(4)}\cdots\right],\\
\nu(\varphi,\chi,\rho) &= \exp^{\varphi-\chi}\left[1+\frac{\rho}{\Gamma(2)}+\frac{\rho^2}{\Gamma(3)}+\frac{\rho^3}{\Gamma(4)}\cdots\right],\\
\omega(\varphi,\chi,\rho) &= \exp^{-\varphi+\chi}\left[1+\frac{\rho}{\Gamma(2)}+\frac{\rho^2}{\Gamma(3)}+\frac{\rho^3}{\Gamma(4)}\cdots\right].\\
\mu(\varphi,\chi,\rho) &= \exp^{\varphi+\chi}\left[1-\frac{\rho}{1!}+\frac{\rho^2}{2!}-\frac{\rho^3}{3!}\cdots\right],\\
\nu(\varphi,\chi,\rho) &= \exp^{\varphi-\chi}\left[1+\frac{\rho}{1!}+\frac{\rho^2}{2!}+\frac{\rho^3}{3!}\cdots\right],\\
\omega(\varphi,\chi,\rho) &= \exp^{-\varphi+\chi}\left[1+\frac{\rho}{1!}+\frac{\rho^2}{2!}+\frac{\rho^3}{3!}\cdots\right],
\end{aligned} \tag{70}$$

which is the MDM solution in closed form of equation (34). When $\delta = 1$,

$$\begin{aligned}
\mu(\varphi,\chi,\rho) &= \exp^{\varphi+\chi-\rho},\\
\nu(\varphi,\chi,\rho) &= \exp^{\varphi-\chi+\rho},\\
\omega(\varphi,\chi,\rho) &= \exp^{-\varphi+\chi+\rho}.
\end{aligned} \tag{71}$$

We analyze the solution-figures of the problem, which have been investigated by applying the ZZ decomposition method in the sense of the Atangana–Baleanu operator. Figure 9 represents the two-dimensional solution-figures for variables μ of example 2 and second graph of different fractional order δ. Figure 10 represents the two-dimensional solution-figures for variables ν of example 2 and second graph of different fractional-order δ. Figure 11 represents the two-dimensional solution-figures for variables ω of example 2 and second graph of different fractional-order δ. It is observed that the ZZ decomposition method solution-figures are identical and in close contact with each other.

5. Conclusion

In this paper, some important system of fractional partial differential equations is considered for its analytical solution using the ZZ decomposition method. It has been demonstrated from the figures that the present techniques have the greater tendency to analyze the results of the given models. The problems results at different time fractional are investigated which cover the various aspects of the proposed models and proposed method. The results at different fractional orders are suggested and shown a very closed convergence phenomena of the fractional results towards integer order solutions. The graph has shown a very consistent relation between the integer and fractional orders results. It is noted that the effective and straight-forward solution of the ZZ decomposition method implies its applicability to solve other fractional partial differential equations.

Data Availability

The numerical data used to support the findings of this study are included within the article.

Conflicts of Interest

The authors declare that there are no conflicts of interest regarding the publication of this article.

Acknowledgments

The authors would like to thank the Deanship of Scientific Research at Umm Al-Qura University for supporting this work under Grant Code number: 22UQU4310396DSR18.

References

[1] E. Barkai, R. Metzler, and J. Klafter, "From continuous time random walks to the fractional Fokker-Planck equation," *Physical Review A*, vol. 61, no. 1, pp. 132–138, 2000.

[2] F. Mainardi, *Fractional Calculus and Waves in Linear Viscoelasticity: An Introduction to Mathematical Models*, World Scientific Imperial College Press, London, 2010.

[3] C. Tadjeran and M. M. Meerschaert, "A second-order accurate numerical method for the two-dimensional fractional diffusion equation," *Journal of Computational Physics*, vol. 220, no. 2, pp. 813–823, 2007.

[4] M. M. Meerschaert, D. A. Benson, H. P. Scheffler, and P. Becker-Kern, "Governing equations and solutions of anomalous random walk limits," *Physical Review A*, vol. 66, no. 6, 2002.

[5] R. Magin, M. D. Ortigueira, I. Podlubny, and J. Trujillo, "On the fractional signals and systems," *Signal Processing*, vol. 91, no. 3, pp. 350–371, 2011.

[6] J. T. Machado, D. Baleanu, and A. C. Luo, *Discontinuity and Complexity in Nonlinear Physical Systems*, Springer International Publishing, New York City, 2014.

[7] K. S. Miller and B. Ross, *An Introduction to the Fractional Calculus and Fractional Differential Equations*, John Wiley & Sons, New York, NY, USA, 1993.

[8] K. Oldham and J. Spanier, *The Fractional Calculus Theory and Applications of Differentiation and Integration to Arbitrary Order*, Elsevier, California, 1974.

[9] I. Podlubny, *Fractional Differential Equations: An Introduction to Fractional Derivatives, Fractional Differential Equations to Methods of Their Solution and Some of Their Applications*, Elsevier, Amsterdam, Netherlands, 1998.

[10] A. A. Kilbas, H. M. Srivastava, and J. J. Trujillo, *Theory and applications of fractional differential equations*, Elsevier, vol. 204, 2006.

[11] S. G. Samko, A. A. Kilbas, and O. I. Marichev, *Fractional integrals and derivatives*Vol. 1, Gordon and breach science publishers, Yverdon; Gordan and Breach, Switzerland, 1993.

[12] R. Caponetto, *Fractional order systems: modeling and control applications*, Vol. 72, World Scientific Publishing Company, Singapore, 2010.

[13] K. Diethelm, *The Analysis of Fractional Differential Equations: An Application-Oriented Exposition Using Differential Operators of Caputo Type*, Springer Science & Business Media, Berlin, Germany, 2010.

[14] J. T. Machado, V. Kiryakova, and F. Mainardi, "Recent history of fractional calculus," *Communications in Nonlinear Science and Numerical Simulation*, vol. 16, no. 3, pp. 1140–1153, 2011.

[15] E. Hernandez, D. ORegan, and K. Balachandran, "On recent developments in the theory of abstract differential equations with fractional derivatives," *Nonlinear Analysis: Theory, Methods & Applications*, vol. 73, no. 10, pp. 3462–3471, 2010.

[16] N. Iqbal, A. Akgul, R. Shah, A. Bariq, M. Mossa Al-Sawalha, and A. Ali, "On solutions of fractional-order gas dynamics equation by effective techniques," *Journal of Function Spaces*, pp. 1–14, 2022.

[17] M. K. Alaoui, R. Fayyaz, A. Khan, and M. S. Abdo, "Analytical Investigation of Noyes-Field Model for Time-Fractional Belousov-Zhabotinsky Reaction," *Complexity*, 2021.

[18] M. Meddahi, H. Jafari, and M. N. Ncube, "New general integral transform via Atangana-Baleanu derivatives," *Advances in Difference Equations*, vol. 2021, no. 1, pp. 385–414, 2021.

[19] H. Jafari, "A new general integral transform for solving integral equations," *Journal of Advanced Research*, vol. 32, pp. 133–138, 2021.

[20] H. Jafari, H. K. Jassim, D. Baleanu, and Y. M. Chu, "On the approximate solutions for a system of coupled Korteweg-de Vries equations with local fractional derivative," *Fractals*, vol. 29, no. 05, Article ID 2140012, 2021.

[21] H. Jafari, J. G. Prasad, P. Goswami, and R. S. Dubey, "Solution of the local fractional generalized KDV equation using homotopy analysis method," *Fractals*, vol. 29, no. 05, Article ID 2140014, 2021.

[22] K. S. Aboodh, "Application of new transform "Aboodh Transform" to partial differential equations," *Global Journal of Pure and Applied Mathematics*, vol. 10, no. 2, pp. 249–254, 2014.

[23] K. Suliman Aboodh, "Solving fourth order parabolic PDE with variable coefficients using Aboodh transform homotopy perturbation method," *Pure and Applied Mathematics Journal*, vol. 4, no. 5, pp. 219–224, 2015.

[24] R. M. Jena, S. Chakraverty, D. Baleanu, and M. M. Alqurashi, "New aspects of ZZ transform to fractional operators with Mittag-Leffler kernel," *Frontiers in Physics*, vol. 8, p. 352, 2020.

[25] L. Riabi, K. Belghaba, M. H. Cherif, and D. Ziane, "Homotopy perturbation method combined with ZZ transform to solve some nonlinear fractional differential equations," *International Journal of Analysis and Applications*, vol. 17, no. 3, pp. 406–419, 2019.

[26] Z. U. A. Zafar, "Application of ZZ transform method on some fractional differential equations," *International Journals of Advanced Engineering & Global Technology*, vol. 4, pp. 1355–1363, 2016.

[27] A. Atangana and D. Baleanu, "New fractional derivatives with nonlocal and non-singular kernel: theory and application to heat transfer model," *Thermal Science*, vol. 20, no. 2, pp. 763–769, 2016.

[28] K. Nonlaopon, M. Naeem, A. M. Zidan, A. Alsanad, and A. Gumaei, "Numerical Investigation of the Time-Fractional Whitham-Broer-Kaup Equation Involving without Singular Kernel Operators," *Complexity*, 2021.

[29] N. H. Aljahdaly, A. Akgul, R. Shah, I. Mahariq, and J. Kafle, "A comparative analysis of the fractional-order coupled Korteweg-De Vries equations with the Mittag-Leffler law," *Journal of Mathematics*, pp. 1–30, 2022.

[30] N. A. Shah, H. A. Alyousef, S. A. El-Tantawy, R. Shah, and J. D. Chung, "Analytical investigation of fractional-order korteweg-de-vries-type equations under atangana-baleanu-caputo operator: modeling nonlinear waves in a plasma and fluid," *Symmetry*, vol. 14, no. 4, p. 739, 2022.

[31] A. M. Wazwaz, "A reliable modification of Adomian decomposition method," *Applied Mathematics and Computation*, vol. 102, no. 1, pp. 77–86, 1999.

[32] R. Shah, H. Khan, M. Arif, and P. Kumam, "Application of Laplace Adomian decomposition method for the analytical solution of third-order dispersive fractional partial differential equations," *Entropy*, vol. 21, no. 4, p. 335, 2019.

[33] H. Thabet and S. Kendre, "New modification of Adomian decomposition method for solving a system of nonlinear fractional partial differential equations," *International Journal of Advances in Applied Mathematics and Mechanics*, vol. 6, pp. 1–13, 2019.

Hindawi
Complexity
Volume 2022, Article ID 7845765, 15 pages
https://doi.org/10.1155/2022/7845765

Research Article

A New Flexible Logarithmic-X Family of Distributions with Applications to Biological Systems

Ibrahim Alkhairy,[1] **Humaira Faqiri**,[2] **Zubir Shah**,[3] **Hassan Alsuhabi**,[1] **M. Yusuf**,[4] **Ramy Aldallal**,[5] **Nicholas Makumi**,[6,7] **and Fathy H. Riad**[8,9]

[1]*Department of Mathematics, Al-Qunfudah University College, Umm Al-Qura University, Mecca, Saudi Arabia*
[2]*Education Faculty, Farah Institute of Higher Education, Farah, Afghanistan*
[3]*Department of Statistics, Abdul Wali Khan University, Mardan, Pakistan*
[4]*Department of Mathematics, Faculty of Science, Helwan University, Helwan, Egypt*
[5]*Department of Accounting, College of Business Administration in Hawtat Bani Tamim, Prince Sattam bin Abdulaziz University, Saudi Arabia*
[6]*Pan African University, Institute for Basic Sciences, Technology and Innovation (PAUSTI), Nairobi, Kenya*
[7]*Department of Statistics and Actuarial Sciences, JKUAT, Nairobi, Kenya*
[8]*Mathematics Department, College of Science, Jouf University, P.O. Box 2014, Sakaka, Saudi Arabia*
[9]*Department of Mathematics, Faculty of Science, Minia University, Minia 61519, Egypt*

Correspondence should be addressed to Nicholas Makumi; nicholas.makumi@jkuat.ac.ke

Received 25 May 2022; Revised 15 June 2022; Accepted 13 July 2022; Published 30 August 2022

Academic Editor: Fathalla A. Rihan

Probability distributions play an essential role in modeling and predicting biomedical datasets. To have the best description and accurate prediction of the biomedical datasets, numerous probability distributions have been introduced and implemented. We investigate a novel family of lifetime probability distributions to represent biological datasets in this paper. The proposed family is called a new flexible logarithmic-X (NFLog-X) family. The suggested NFLog-X family is obtained by applying the T-X method together with the exponential model having the PDF $m(t) = e^{-t}$. Based on the NFLog-X approach, a three parameters probability distribution, namely, a new flexible logarithmic-Weibull (NFLog-Wei) distribution is introduced. The method of maximum likelihood estimation is adopted for estimating the parameters of the NFLog-X family. In the end, we examine three different biological datasets in order to give a thorough numerical research that illustrates the NFLog-Wei distribution. Comparisons are made between the analytical goodness-of-fit metrics of the suggested distribution. We made comparison with the (i) alpha power transformed Weibull, (ii) exponentiated Weibull, (iii) Weibull, (iv) flexible reduced logarithmic-Weibull, and (v) Marshall–Olkin Weibull distributions. After performing the analyses, we observe that the proposed method outclassed other competitive distributions.

1. Introduction

Probability distributions are frequently used to model the lifetime phenomena in applied sectors [1]. In the literature of distributions theory, the most frequently used distributions to model the lifetime phenomena are the exponential (Exp), Rayleigh (Ray), and Weibull (Wei) distributions. However, when the lifetime phenomena are complex, then these probability distributions are not suitable to model and predict the data accurately (Ahmad et al. [2] and Liao et al. [3]). For example, the Exp distribution is concerned with describing data that have a constant HF (hazard function). On the other hand, the Ray distribution is used to model data with an increasing HF. Similarly, the Wei distribution having the Exp and Ray as the special models is one of the popular probability distributions (Sarhan and Zaindin [4] and Huo et al. [5]). The Weibull

model offers/provides the features of both the Exp and Ray probability distributions and has widely been used in modeling lifetime phenomena with monotone failure rates. However, when the lifetime phenomena have a monotone (increasing, decreasing, and constant) HF, then, the Weibull distribution is the best choice to use (Almalki and Yuan [6] and Liu et al. [7]).

In the field of biomedical sciences, authors have shown greater interest and published numerous papers to propose new distributions. In the past decade, researchers' efforts have been devoted to deriving new families of probability distributions. The new probability distributions have been constructed by adding one or more new additional parameters to the baseline models (El-Morshedy et al. [8]; Guerra et al. [9]; Reyad et al. [10]; Bantan et al. [11]; Eghwerido et al. [12]; Eghwerido and Agu [13]; Alzaatreh et al. [14]; Lahcene [15]; ElSherpieny and Almetwally [16]; Roozegar et al. [17]; Klakattawi et al. [18]; Hussein et al. [19]; and Kilai et al. [20]).

Recently, Ahmad et al. [21] studied a Z-family by adding a new parameter. We can write the distribution function (DF) $F(x;\beta,\lambda)$ of the Z-family through the following equation:

$$F(x;\beta,\boldsymbol{\lambda}) = 1 - \frac{1 - K(x;\boldsymbol{\lambda})}{\beta^{K(x;\boldsymbol{\lambda})}}, \quad x \in \mathbb{R}, \tag{1}$$

such that $\beta > 0$ can be considered as an extra parameter.

Wang et al. [22] developed another method called, a NG-X (new generalized-X) family by the following DF:

$$F(x;\theta,\boldsymbol{\lambda}) = 1 - \frac{[1 - K(x;\boldsymbol{\lambda})]^{\theta}}{e^{K(x;\boldsymbol{\lambda})}}, \quad x \in \mathbb{R}, \tag{2}$$

where $\theta > 0$.

Mohammed et al. [23] proposed another new approach to develop new probability distribution for modeling lifetime events. They named their proposed method, a NLT-X (new lifetime-X) distributions. The DF $F(x;\eta,\lambda)$ of the NLT-X distributions is given by the following equation:

$$F(x;\eta,\boldsymbol{\lambda}) = 1 - \left(\frac{1 - K(x;\boldsymbol{\lambda})}{e^{K(x;\boldsymbol{\lambda})}}\right)^{\eta}, \quad x \in \mathbb{R}, \tag{3}$$

with an additional parameter $\eta > 0$.

We additionally propose a new class of probability distribution in this paper by implementing the T-X method. The new class is called a NFLog-X family of distributions. Using the proposed NFLog-X approach, we can formulate an upgraded version of the Wei distribution whicnh can be presented and dubbed as NFLog-Wei distribution. The proposed NFLog-Wei distribution offers a close fit to the healthcare datasets.

2. The Proposed Method

Here, we propose a new method to introduce new updated and modified versions of the lifetime distributions. By incorporating the exponential model, having the PDF $m(t) = e^{-t}$ with the T-X method (Alzaatreh et al. [24]), the suggested approach is presented.

Let us assume that we have a RV (random variable), represented by T, considered as a baseline RV with PDF $m(t)$, where $T \in [\pi_1, \pi_2]$ for $-\infty < \pi_1 < \pi_2 < \infty$. Let X be another RV with DF $K(x;\lambda)$. Let suppose $G[K(x;\lambda)]$ considered as a function in the DF, meeting each of the three requirements outlined below:

(i) $G[K(x;\lambda)] \in [\pi_1, \pi_2]$.

(ii) $G[K(x;\lambda)]$ is a differentiable and IF (increasing function).

(iii) $G[K(x;\lambda)] \longrightarrow \pi_1$ as $x \longrightarrow -\infty$ and $G[K(x;\lambda)] \longrightarrow \pi_2$ as $x \longrightarrow \infty$.

According to Alzaatreh et al. [24], the DF $F(x)$ of the T-X family is as follows:

$$F(x) = \int_{\pi_1}^{G[K(x;\boldsymbol{\lambda})]} m(t)\mathrm{d}t, \tag{4}$$

with PDF given by

$$f(x) = m(G[K(x;\boldsymbol{\lambda})])\frac{d}{dx}G[K(x;\boldsymbol{\lambda})]. \tag{5}$$

Now, setting $G[K(x;\lambda)] = -\log(1 - (\delta^2 K(x;\lambda)/[\delta - \log(K(x;\lambda))]^2)s)$ and using $m(t) = e^{-t}$, exists in (1), we can obtain easilythe DF $F(x;\delta,\lambda)$ of the NFLog-X distributions, represented as below

$$F(x;\delta,\boldsymbol{\lambda}) = \frac{\delta^2 K(x;\boldsymbol{\lambda})}{[\delta - \log(K(x;\boldsymbol{\lambda}))]^2}, \quad x \in \mathbb{R}, \tag{6}$$

with

$$f(x;\delta,\boldsymbol{\lambda}) = \frac{\delta^2 k(x;\boldsymbol{\lambda})}{[\delta - \log(K(x;\boldsymbol{\lambda}))]^3}[2 + \delta - \log(K(x;\boldsymbol{\lambda}))], \tag{7}$$

where $(d/dx)K(x;\lambda) = k(x;\lambda)$.

Related to equations (2) and (3), the SF (survival function) $S(x;\lambda) = 1 - K(x;\lambda)$, HF (hazard function) $h(x;\lambda) = (k(x;\lambda)/S(x;\lambda))$, and cumulative HF $K(x;\lambda) = -\log[1 - K(x;\lambda)]$ are represented by the equations in the preceding:

$$\begin{aligned} S(x;\delta,\boldsymbol{\lambda}) &= 1 - \frac{\delta^2 K(x;\boldsymbol{\lambda})}{[\delta - \log(K(x;\boldsymbol{\lambda}))]^2}, \\ h(x;\delta,\boldsymbol{\lambda}) &= \frac{\delta^2 k(x;\boldsymbol{\lambda})[2 + \delta - \log(K(x;\boldsymbol{\lambda}))]}{[\delta - \log(K(x;\boldsymbol{\lambda}))]^2 - \delta^2 K(x;\boldsymbol{\lambda})[\delta - \log(K(x;\boldsymbol{\lambda}))]}, \end{aligned} \tag{8}$$

and

$$H(x;\delta,\boldsymbol{\lambda}) = -\log\left(1 - \frac{\delta^2 K(x;\boldsymbol{\lambda})}{[\delta - \log(K(x;\boldsymbol{\lambda}))]^2}\right), \tag{9}$$

on the same order.

In this article, we implement the NFLog-X distributions approach and introduce the NFLog-Wei distribution. Section 4 offers the expression of the DF, PDF, SF, HF, and CHF of the NFLog-Wei distribution.

3. The Identifiability Property

The identifiability property is a very useful statistical property that ensures precise inferences. Here, we derive the identifiability property of the NFLog-X distributions. Let δ_1 and δ_2 be the two parameters having DFs $F(x;\delta_1,\lambda)$ and $F(x;\delta_2,\lambda)$, respectively. The parameter δ is identifiable, if $\delta_1 = \delta_2$. Mathematically, we have

$$F(x;\delta_1,\boldsymbol{\lambda}) = F(x;\delta_2,\boldsymbol{\lambda}). \tag{10}$$

Incorporating equation (2) in equation (4), we get

$$\frac{\delta_1^2 K(x;\boldsymbol{\lambda})}{\left[\delta_1 - \log(K(x;\boldsymbol{\lambda}))\right]^2} = \frac{\delta_2^2 K(x;\boldsymbol{\lambda})}{\left[\delta_2 - \log(K(x;\boldsymbol{\lambda}))\right]^2}. \tag{11}$$

Taking square root of equation (5), we get

$$\begin{aligned}
\frac{\delta_1\sqrt{K(x;\boldsymbol{\lambda})}}{\left[\delta_1 - \log(K(x;\boldsymbol{\lambda}))\right]} &= \frac{\delta_2\sqrt{K(x;\boldsymbol{\lambda})}}{\left[\delta_2 - \log(K(x;\boldsymbol{\lambda}))\right]},\\
\delta_1\sqrt{K(x;\boldsymbol{\lambda})}\left[\delta_2 - \log(K(x;\boldsymbol{\lambda}))\right] &= \delta_2\sqrt{K(x;\boldsymbol{\lambda})}\left[\delta_1 - \log(K(x;\boldsymbol{\lambda}))\right],\\
\delta_1\delta_2\sqrt{K(x;\boldsymbol{\lambda})} - \delta_1\sqrt{K(x;\boldsymbol{\lambda})}\log(K(x;\boldsymbol{\lambda})) &= \delta_1\delta_2\sqrt{K(x;\boldsymbol{\lambda})} - \delta_2\sqrt{K(x;\boldsymbol{\lambda})}\log(K(x;\boldsymbol{\lambda})),\\
-\delta_1\sqrt{K(x;\boldsymbol{\lambda})}\log(K(x;\boldsymbol{\lambda})) &= -\delta_2\sqrt{K(x;\boldsymbol{\lambda})}\log(K(x;\boldsymbol{\lambda})),\\
\delta_1\sqrt{K(x;\boldsymbol{\lambda})}\log(K(x;\boldsymbol{\lambda})) &= \delta_2\sqrt{K(x;\boldsymbol{\lambda})}\log(K(x;\boldsymbol{\lambda})),\\
\delta_1 &= \delta_2.
\end{aligned} \tag{12}$$

From equation (6), we can see that $\delta_1 = \delta_2$. Therefore, the parameter δ is identifiable.

4. The NFLog-Wei Distribution

Consider the DF $K(x;\lambda)$ and PDF $k(x;\lambda)$ of the two parameters $(\alpha > 0, \beta > 0)$ traditional Wei model are given, respectively, by

$$K(x;\boldsymbol{\lambda}) = 1 - e^{-\beta x^{\alpha}}, \tag{13}$$

and

$$k(x;\boldsymbol{\lambda}) = \alpha\beta x^{\alpha-1}e^{-\beta x^{\alpha}}, \tag{14}$$

where $\lambda = (\alpha,\beta)$.

Using equation (8) in equation (2), we get the DF $F(x;\delta,\lambda)$ of the NFLog-Wei distribution given by

$$F(x;\delta,\boldsymbol{\lambda}) = \frac{\delta^2\left(1 - e^{-\beta x^{\alpha}}\right)}{\left[\delta - \log\left(1 - e^{-\beta x^{\alpha}}\right)\right]^2}, \tag{15}$$

with SF $S(x;\delta,\lambda)$

$$S(x;\delta,\boldsymbol{\lambda}) = 1 - \frac{\delta^2\left(1 - e^{-\beta x^{\alpha}}\right)}{\left[\delta - \log\left(1 - e^{-\beta x^{\alpha}}\right)\right]^2}. \tag{16}$$

Some plots of $F(x;\delta,\lambda)$ and $S(x;\delta,\lambda)$ of the NFLog-Wei model are provided in Figure 1. The plots of $F(x;\delta,\lambda)$ and $S(x;\delta,\lambda)$ are obtained for (i) $\delta = 2.8, \beta = 1.0, \alpha = 1.2$ (red curve), (ii) $\delta = 1.2, \beta = 1.0, \alpha = 1.8$ (green curve), and (iii) $\delta = 0.8, \beta = 0.5, \alpha = 2.5$ (blue curve).

Corresponding to $F(x;\delta,\lambda)$ in equation (9), the PDF $f(x;\delta,\lambda)$ is as follows:

$$f(x;\delta,\boldsymbol{\lambda}) = \frac{\delta^2\alpha\beta x^{\alpha-1}e^{-\beta x^{\alpha}}}{\left[\delta - \log\left(1 - e^{-\beta x^{\alpha}}\right)\right]^3}\left[2 + \delta - \log\left(1 - e^{-\beta x^{\alpha}}\right)\right], \quad x > 0. \tag{17}$$

Different plots for the PDF $f(x;\delta,\lambda)$ of the NFLog-Wei model are shown in Figure 2. The plots of $f(x;\delta,\lambda)$ are obtained for (i) $\delta = 1.4, \beta = 1.0, \alpha = 0.4$ (red curve), (ii) $\delta = 7.3, \beta = 1.2, \alpha = 2.6$ (green curve), (iii) $\delta = 0.1, \beta = 0.3, \alpha = 3.2$ (black curve), and (iv) $\delta = 0.4, \beta = 0.8, \alpha = 2.4$ (blue curve).

From Figure 2, we can see that the PDF $f(x;\delta,\lambda)$ of the NFLog-Wei model has four different patterns, including (i) decreasing or reverse in the form of J-shaped but reversed shown in (red curve), (ii) left-skewed (green curve), (iii) right-skewed (black curve), and (iv) symmetrical (blue curve).

Furthermore, the HF $h(x;\delta,\lambda)$ and CHF $H(x;\delta,\lambda)$ of the NFLog-Wei distribution are given by the following equations:

$$h(x;\delta,\boldsymbol{\lambda}) = \frac{\delta^2\alpha\beta x^{\alpha-1}e^{-\beta x^{\alpha}}\left[2 + \delta - \log\left(1 - e^{-\beta x^{\alpha}}\right)\right]}{\left(\left[\delta - \log\left(1 - e^{-\beta x^{\alpha}}\right)\right]^2 - \delta^2\left(1 - e^{-\beta x^{\alpha}}\right)\right)\left[\delta - \log\left(1 - e^{-\beta x^{\alpha}}\right)\right]}, \quad x > 0, \tag{18}$$

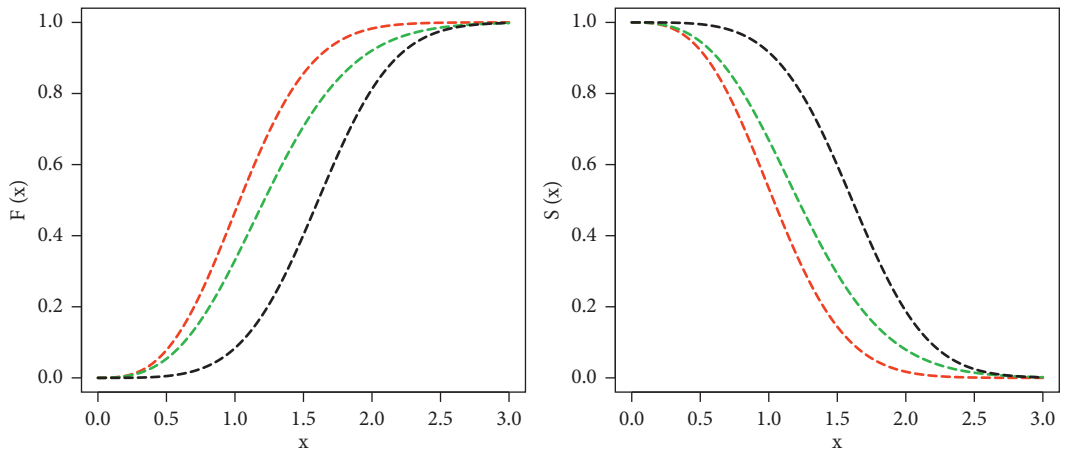

Figure 1: Graphical representation of $F(x;\delta,\lambda)$ and $S(x;\delta,\lambda)$.

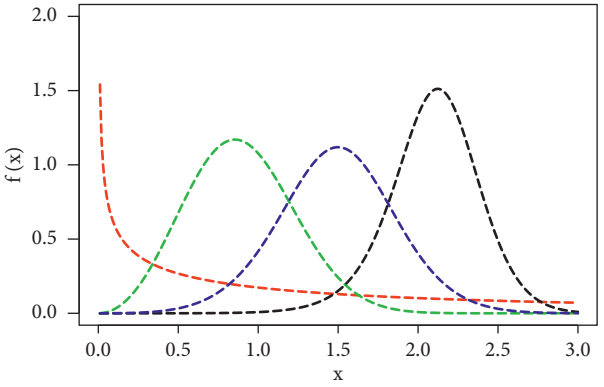

Figure 2: Visual display of $f(x;\delta,\lambda)$.

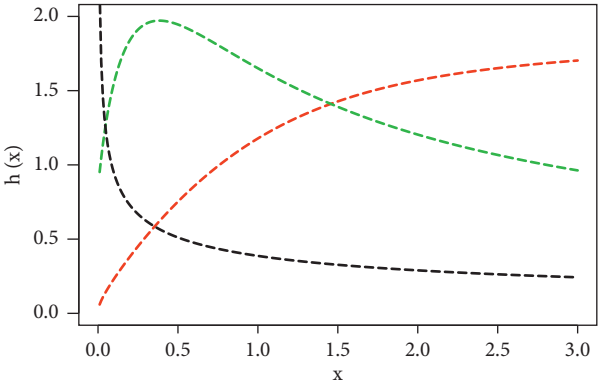

Figure 3: Visual display of $h(x;\delta,\lambda)$.

and

$$H(x;\delta,\boldsymbol{\lambda}) = -\log\left(1-\frac{\delta^2\left(1-e^{-\beta x^{\alpha}}\right)}{\left[\delta-\log\left(1-e^{-\beta x^{\alpha}}\right)\right]^2}\right), \quad x>0, \tag{19}$$

respectively.

Different plots for the HF $h(x;\delta,\lambda)$ of the NFLog-Wei distribution are provided in Figure 3. The plots of $h(x;\delta,\lambda)$ are obtained for (i) $\delta = 1.3, \beta = 1.4, \alpha = 1.1$ (red curve), (ii) $\delta = 0.1, \beta = 4.7, \alpha = 0.4$ (green curve), and (iii) $\delta = 4.1, \beta = 0.9, \alpha = 0.5$ (black curve).

From Figure 3, we can see that the HF $h(x;\delta,\lambda)$ of the NFLog-Wei distribution has three different patterns, including (i) increasing (red curve), (ii) unimodal (green curve), and (iii) reverse J-shaped (black curve).

Despite the prominent advantages of the NFLog-Wei distribution over the other distributions, the NFLog-Wei model has also disadvantages, for example

(i) The NFLog-Wei distribution is a continuous distribution used to evaluate continuous datasets. Consequently, the suggested NFLog-Wei distribution cannot be utilized to assess discrete data sets.

(ii) Because of the NFLog-Weidistribution PDF's complicated structure, the expressions of its estimators cannot be reduced to a simple, closed form easily represented. Therefore, the numerical estimates of the estimators can be obtained with the help of computer software.

(iii) Due to the complexity of the PDF of the NFLog-Wei distribution, additional computing work is necessary to determine its mathematical features.

5. Estimation and Simulation

Here, we obtain the MLEs $(\widehat{\delta}_{MLE}, \widehat{\lambda}_{MLE})$ of the NFLog-X distributions. In addition, we do provide a comprehensive Monte–Carlo simulation study (MCSS) for assessing the performances of $\widehat{\delta}_{MLE}$ and $\widehat{\lambda}_{MLE}$.

5.1. Estimation. In the research that has been conducted on the topic, a number of different strategies and procedures for estimating the parameters of probability models have been proposed and put into practice. Among them, the MLE is one of the most usually adopted methods. Here, we implement this method to obtain the $\widehat{\delta}_{MLE}$ and $\widehat{\lambda}_{MLE}$.

Let $x_1, x_2, \ldots, x_n$ be a set of observed values of size n taken from the PDF $f(x;\delta,\lambda)$. Then, the corresponding likelihood function (LF) $\varphi(x;\delta,\lambda)$ is obtained as follows:

$$\varphi(x;\delta,\boldsymbol{\lambda}) = \prod_{i=1}^{n} \frac{\delta^2 k(x_i;\boldsymbol{\lambda})}{[\delta - \log(K(x_i;\boldsymbol{\lambda}))]^3}[2+\delta-\log(K(x_i;\boldsymbol{\lambda}))]. \quad (20)$$

Corresponding to $\varphi(x;\delta,\lambda)$, the log LF $\ell(\Phi)$ is obtained as follows:

$$\begin{aligned}\ell(\boldsymbol{\Phi}) = 2n\log\delta + \sum_{i=1}^{n}\log k(x_i;\boldsymbol{\lambda}) \\ + \sum_{i=1}^{n}\log[2+\delta-\log(K(x_i;\boldsymbol{\lambda}))] \\ - 3\sum_{i=1}^{n}\log[\delta-\log(K(x_i;\boldsymbol{\lambda}))].\end{aligned} \quad (21)$$

Using $\ell(\Phi)$, the following equation will provide the partial derivatives:

$$\begin{aligned}\frac{\partial}{\partial\delta}\ell(\boldsymbol{\Phi}) = \frac{2n}{\delta} + \sum_{i=1}^{n}\frac{1}{[2+\delta-\log(K(x_i;\boldsymbol{\lambda}))]} \\ - 3\sum_{i=1}^{n}\frac{1}{[\delta-\log(K(x_i;\boldsymbol{\lambda}))]},\end{aligned} \quad (22)$$

and

$$\begin{aligned}\frac{\partial}{\partial\boldsymbol{\lambda}}\ell(\boldsymbol{\Phi}) = \sum_{i=1}^{n}\frac{\partial/\partial\boldsymbol{\lambda}k(x_i;\boldsymbol{\lambda})}{k(x_i;\boldsymbol{\lambda})} - \sum_{i=1}^{n}\frac{[K(x_i;\boldsymbol{\lambda})]^{-1}\partial/\partial\boldsymbol{\lambda}K(x_i;\boldsymbol{\lambda})}{[2+\delta-\log(K(x_i;\boldsymbol{\lambda}))]} \\ + 3\sum_{i=1}^{n}\frac{[K(x_i;\boldsymbol{\lambda})]^{-1}\partial/\partial\boldsymbol{\lambda}K(x_i;\boldsymbol{\lambda})}{[\delta-\log(K(x_i;\boldsymbol{\lambda}))]},\end{aligned} \quad (23)$$

respectively, where $\Phi = (\delta,\lambda)$.

On solving $(\partial/\partial\partial)\ell(\Phi) = 0$ and $\partial/\partial\lambda\ell(\Phi) = 0$, we obtain $\widehat{\delta}_{MLE}$ and $\widehat{\lambda}_{MLE}$, respectively.

5.2. Simulation. In this second subsection, a comprehensive MCSS is conducted to assess the behaviors of $\widehat{\delta}_{MLE}$ and $\widehat{\lambda}_{MLE}$ of the NFLog-Wei distribution. The RNs (random numbers) are successfully generated from the PDF $f(x;\delta,\lambda)$ via the inverse DF method. The outcome of the simulation are acquired for a total of four groups and sets (Set I, Set II, Set III, and Set IV) of parameters values, given by Set I: $\alpha = 0.6$, $\beta = 2.3$, and $\delta = 3.5$, Set II: $\alpha = 1.3$, $\beta = 3.8$, and $\delta = 4.6$, Set III: $\alpha = 3.0$, $\beta = 4.0$, and $\delta = 4.5$, and Set IV: $\alpha = 3.4$, $\beta = 2.5$, and $\delta = 3.5$.

To check performances of $\widehat{\delta}_{MLE}$ and $\widehat{\lambda}_{MLE}$, two statistical measures are considered. These measures include the (i) mean square error (MSE) and (ii) bias. The numerical values of the MSE and bias are, respectively, computed as follows:

$$\frac{1}{n}\sum_{i=1}^{n}(\widehat{\delta}-\delta)^2, \quad (24)$$

and

$$\frac{1}{n}\sum_{i=1}^{n}(\widehat{\delta}-\delta). \quad (25)$$

The values of the MSE and bias are also computed for λ.

Corresponding to Set I: $\alpha = 0.6$, $\beta = 2.3$, and $\delta = 3.5$ and Set II: $\alpha = 1.3$, $\beta = 3.8$, and $\delta = 4.6$, we can easily see the outcomes resulted from doing the simulation in Table 1. Whereas, in link to Set III: $\alpha = 3.0$, $\beta = 4.0$, $\delta = 4.5$ and Set IV: $\alpha = 3.4$, $\beta = 2.5$, $\delta = 3.5$, the outcomes of the simulation are shown in Table 2.

Based on the findings of the simulation, which are shown in Tables 1 and 2, we can see that as the size of n increases.

(i) The estimated values of $\widehat{\lambda}_{MLE}$ and $\widehat{\delta}_{MLE}$ tend to be stable.

(ii) The MSEs of $\widehat{\lambda}_{MLE}$ and $\widehat{\delta}_{MLE}$ decrease.

(iii) The biases of $\widehat{\lambda}_{MLE}$ and $\widehat{\delta}_{MLE}$ decay to zero.

6. Applications

By doing an analysis on three different biomedical datasets, the purpose of this article is to demonstrate the utility of the NFLog-Wei distribution (Table 3).

We compare the NFLog-Wei distribution with the Wei model and three other traditional and new probability distributions, as an example of these distributions, the Marshall–Olkin Weibull (MO-Wei) studied by Marshall and Olkin [25], APT-Wei (alpha power transformed Weibull) proposed by Dey et al. [26], and a flexible reduced logarithmic-Weibull (FRLog-Wei) distribution, introduced by Liu et al. [7]. The DFs of the competitive probability distributions are outlined below:

(i) The APT-Wei distribution is obtained by the following equation:

$$K(x;\alpha_1,\boldsymbol{\lambda}) = \frac{\alpha_1^{\left(1-e^{-\beta x^{\alpha}}\right)}-1}{\alpha_1-1}, \quad (26)$$

where $\alpha_1 \neq 1, \alpha_1 > 0$.

(ii) The MO-Wei distribution is represented by the equation that is as follows:

$$K(x;\gamma,\boldsymbol{\lambda}) = \frac{\left(1-e^{-\beta x^{\alpha}}\right)}{\gamma+(1-\gamma)\left(1-e^{-\beta x^{\alpha}}\right)}, \quad (27)$$

where $\gamma > 0$.

(iii) The FRLog-Wei distribution is represented by the equation that is as follows:

$$K(x;\sigma,\boldsymbol{\lambda}) = 1 - \frac{\log\left(1+\sigma-\sigma\left(1-e^{-\beta x^{\alpha}}\right)\right)}{\log(1+\sigma)}, \quad (28)$$

where $\sigma > 0$.

To determine the optimum model among the fitted distributions, we consider different goodness-of-fit measures (analytical measures). It is generally agreed that

Table 1: The results of conducting a simulation using the NFLog-Wei distribution utilizing sets I and II.

n	Est.	Set I: $\alpha = 0.6$, $\beta = 2.3$, and $\delta = 3.5$			Set II:$\alpha = 1.3$, $\beta = 3.8$, and $\delta = 4.6$		
		MLE	MSE	Bias	MLE	MSE	Bias
25	$\widehat{\alpha}$	1.359714	3.352142	0.959714	1.470587	1.916907	0.070586
	$\widehat{\beta}$	2.558740	2.272587	0.258740	4.107370	1.019913	0.507369
	$\widehat{\delta}$	3.932950	1.830509	0.432950	4.536813	0.659791	−0.263187
50	$\widehat{\alpha}$	1.261625	2.610044	0.861625	1.324459	1.355837	−0.075540
	$\widehat{\beta}$	2.527184	2.103823	0.227184	4.074657	0.827990	0.474657
	$\widehat{\delta}$	3.854091	1.742594	0.354091	4.428739	0.809154	−0.371261
75	$\widehat{\alpha}$	1.249921	2.380179	0.849921	1.304567	1.105549	−0.095432
	$\widehat{\beta}$	2.373155	1.660890	0.073155	4.027904	0.720244	0.427903
	$\widehat{\delta}$	3.903062	1.633956	0.403062	4.434167	0.722466	−0.365833
100	$\widehat{\alpha}$	1.121601	1.880341	0.721601	1.311440	1.055909	−0.088560
	$\widehat{\beta}$	2.409936	1.568806	0.109935	3.990797	0.645796	0.390796
	$\widehat{\delta}$	3.827443	1.488893	0.327443	4.464805	0.678206	−0.335194
200	$\widehat{\alpha}$	0.937715	1.208062	0.537715	1.268340	0.643048	−0.131660
	$\widehat{\beta}$	2.367964	1.106299	0.067963	3.910828	0.469170	0.310828
	$\widehat{\delta}$	3.755479	1.181334	0.255478	4.493781	0.563858	−0.306218
300	$\widehat{\alpha}$	0.846743	0.925916	0.446743	1.229159	0.517821	−0.170841
	$\widehat{\beta}$	2.330760	0.853094	0.030759	3.896567	0.414911	0.296567
	$\widehat{\delta}$	3.718240	0.963105	0.218240	4.481787	0.556714	−0.318213
400	$\widehat{\alpha}$	0.820652	0.786768	0.420652	1.249808	0.489246	−0.150192
	$\widehat{\beta}$	2.268908	0.698790	−0.031091	3.869472	0.370287	0.269471
	$\widehat{\delta}$	3.744079	0.849120	0.244079	4.507406	0.504602	−0.292593
500	$\widehat{\alpha}$	0.726767	0.635959	0.326767	1.240931	0.413434	−0.159069
	$\widehat{\beta}$	2.321649	0.575961	0.021649	3.834327	0.293431	0.234327
	$\widehat{\delta}$	3.652565	0.701084	0.152564	4.531517	0.424718	−0.268482
600	$\widehat{\alpha}$	0.666051	0.491945	0.266051	1.280216	0.402240	−0.119784
	$\widehat{\beta}$	2.309838	0.453986	0.009838	3.803557	0.258676	0.203557
	$\widehat{\delta}$	3.629989	0.587730	0.129989	4.559654	0.384078	−0.240346
700	$\widehat{\alpha}$	0.701362	0.504666	0.301362	1.299725	0.378063	−0.100275
	$\widehat{\beta}$	2.256093	0.430943	−0.043907	3.790054	0.250775	0.190053
	$\widehat{\delta}$	3.694393	0.588829	0.194392	4.590190	0.345656	−0.209809
800	$\widehat{\alpha}$	0.642816	0.378790	0.242816	1.270926	0.336466	−0.129073
	$\widehat{\beta}$	2.255541	0.350091	−0.044459	3.789066	0.208206	0.189066
	$\widehat{\delta}$	3.658857	0.464875	0.158856	4.586876	0.324176	−0.213124
900	$\widehat{\alpha}$	0.652121	0.396530	0.252121	1.307186	0.327404	−0.092814
	$\widehat{\beta}$	2.257956	0.353270	−0.042043	3.755260	0.186083	0.155260
	$\widehat{\delta}$	3.668265	0.508969	0.168265	4.618437	0.274431	−0.181562
1000	$\widehat{\alpha}$	0.597530	0.304498	0.197530	1.296956	0.316957	−0.123043
	$\widehat{\beta}$	2.292465	0.316204	−0.017534	3.791939	0.188118	0.171938
	$\widehat{\delta}$	3.518328	0.415432	0.118328	4.600692	0.302786	−0.199307

the best competing model is the probability model that achieves the lowest values of these analytical metrics. The numerical values of the analytical measure are computed as follows:

(i) The CM test statistic is computed as follows:

$$\sum_{i=1}^{n}\left(\frac{2i-1}{2n} - K\left(x_i;\boldsymbol{\lambda}\right)\right)^2 + \frac{1}{12n}. \tag{29}$$

(ii) The AD test statistic is calculated as follows:

$$-n - \frac{1}{n}\sum_{i=1}^{n}(2i-1)\left[\log K\left(x_i;\boldsymbol{\lambda}\right) + \log\left(1 - K\left(x_i;\boldsymbol{\lambda}\right)\right)\right]. \tag{30}$$

(iii) The KS test statistic is derived as follows:

$$\sup_x\left[K_n\left(x;\boldsymbol{\lambda}\right) - K\left(x;\boldsymbol{\lambda}\right)\right]. \tag{31}$$

(iv) The AIC is obtained as follows:

$$2m - 2\ell\left(\boldsymbol{\Phi}\right). \tag{32}$$

(v) The BIC is calculated as follows:

$$m\log\left(n\right) - 2\ell\left(\boldsymbol{\Phi}\right). \tag{33}$$

(vi) The HQIC is obtained as follows:

Table 2: The results of conducting a simulation using the NFLog-Wei distribution with sets III and IV.

n	Est.	Set III: $\alpha = 3.0$, $\beta = 4.0$, and $\delta = 4.5$			Set IV: $\alpha = 3.4$, $\beta = 2.5$, and $\delta = 3.5$		
		MLE	MSE	Bias	MLE	MSE	Bias
25	$\widehat{\alpha}$	2.381875	2.794807	−0.118124	3.410283	4.557224	−0.489717
	$\widehat{\beta}$	4.296184	0.720145	0.396183	3.035897	1.458385	0.6358970
	$\widehat{\delta}$	4.518220	0.628748	−0.281780	3.427576	0.913335	−0.172423
50	$\widehat{\alpha}$	2.319224	2.574264	−0.180776	3.413811	4.507704	−0.486189
	$\widehat{\beta}$	4.275190	0.585435	0.375189	2.935012	1.212232	0.535011
	$\widehat{\delta}$	4.516319	0.584158	−0.283680	3.348358	0.754218	−0.251642
75	$\widehat{\alpha}$	2.343670	2.636672	−0.156330	3.337658	4.571121	−0.562342
	$\widehat{\beta}$	4.249329	0.527632	0.3493285	2.898243	1.057149	0.498242
	$\widehat{\delta}$	4.486865	0.607032	−0.313134	3.294626	0.669432	−0.305374
100	$\widehat{\alpha}$	2.337194	2.565672	−0.162806	3.206369	4.830113	−0.693630
	$\widehat{\beta}$	4.208815	0.470883	0.308815	2.913587	1.014642	0.513587
	$\widehat{\delta}$	4.486939	0.573087	−0.313060	3.261691	0.674156	−0.338309
200	$\widehat{\alpha}$	2.345233	2.217673	−0.154767	3.317303	4.219805	−0.582696
	$\widehat{\beta}$	4.155143	0.343410	0.255143	2.768109	0.635353	0.368108
	$\widehat{\delta}$	4.498184	0.533703	−0.301816	3.319766	0.477188	−0.280234
300	$\widehat{\alpha}$	2.256714	2.014241	−0.243285	3.294189	3.997942	−0.605811
	$\widehat{\beta}$	4.173869	0.327524	0.273868	2.718230	0.445176	0.318229
	$\widehat{\delta}$	4.490608	0.520666	−0.309391	3.331029	0.382241	−0.268971
400	$\widehat{\alpha}$	2.296481	1.781173	−0.203519	3.377208	3.613586	−0.522792
	$\widehat{\beta}$	4.124638	0.263154	0.224638	2.656047	0.327071	0.256046
	$\widehat{\delta}$	4.531144	0.433862	−0.268856	3.369713	0.300703	−0.230287
500	$\widehat{\alpha}$	2.279038	1.641563	−0.220962	3.427285	3.272158	−0.472715
	$\widehat{\beta}$	4.109448	0.235986	0.209448	2.610146	0.231249	0.210146
	$\widehat{\delta}$	4.541954	0.404543	−0.258045	3.406040	0.236117	−0.193959
600	$\widehat{\alpha}$	2.290175	1.499904	−0.209825	3.427226	3.213429	−0.472773
	$\widehat{\beta}$	4.081241	0.204391	0.181240	2.600575	0.209351	0.200574
	$\widehat{\delta}$	4.554415	0.362888	−0.245585	3.412186	0.215645	−0.187813
700	$\widehat{\alpha}$	2.326864	1.380761	−0.173135	3.430730	3.088489	−0.469269
	$\widehat{\beta}$	4.066115	0.175150	0.166115	2.584588	0.177430	0.184588
	$\widehat{\delta}$	4.590552	0.327957	−0.209447	3.421499	0.197229	−0.178501
800	$\widehat{\alpha}$	2.323243	1.338615	−0.176757	3.447615	3.004778	−0.452385
	$\widehat{\beta}$	4.058958	0.160689	0.158958	2.578249	0.163990	0.178248
	$\widehat{\delta}$	4.593206	0.306266	−0.206794	3.427515	0.180315	−0.172485
900	$\widehat{\alpha}$	2.332042	1.424302	−0.167957	3.597858	2.660379	−0.302141
	$\widehat{\beta}$	4.059840	0.169700	0.159839	2.541229	0.131273	0.141229
	$\widehat{\delta}$	4.583009	0.321603	−0.216991	3.462147	0.151573	−0.137853
1000	$\widehat{\alpha}$	2.296988	0.802130	−0.203012	3.415560	1.019690	−0.444440
	$\widehat{\beta}$	4.054148	0.095211	0.154147	2.512916	0.084999	0.092915
	$\widehat{\delta}$	4.519912	0.088924	−0.210088	3.490555	0.089363	−0.159445

Table 3: The medical datasets.

No.	Observations of the datasets	References
Data 1	12.20, 23.56, 23.74, 25.87, 31.98, 37, 41.35, 47.38, 55.46, 58.36, 63.47, 68.46, 78.26, 74.47, 81.43, 84, 92, 94, 110, 112, 119, 127, 130, 133, 140, 146, 155, 159, 173, 179, 194, 195, 209, 249, 281, 319, 339, 432, 469, 519, 633, 725, 817, 1776	Ceren et al. [29]
Data 2	10, 33, 44, 56, 59, 72, 74, 77, 92, 93, 96, 100, 100, 102, 105, 107, 107, 108, 108, 108, 109, 112, 113, 115, 116, 120, 121, 122, 122, 124, 130, 134, 136, 139, 144, 146, 153, 159, 160, 163, 163, 168, 171, 172, 176, 183, 195, 196, 197, 202, 213, 215, 216, 222, 230, 231, 240, 245, 251, 253, 254, 255, 278, 293, 327, 342, 347, 361, 402, 432, 458, 555	Bjerkedal [28]
Data 3	0.080, 0.200, 0.400, 0.500, 0.510, 0.810, 0.900, 1.050, 1.190, 1.260, 1.350, 1.400, 1.460, 1.760, 2.020, 2.020, 2.070, 2.090, 2.230, 2.260, 2.460, 2.540, 2.620, 2.640, 2.690, 2.690, 2.750, 2.830, 2.870, 3.020, 3.250, 3.310, 3.360, 3.360, 3.480, 3.520, 3.570, 3.640, 3.700, 3.820, 3.880, 4.180, 4.230, 4.260, 4.330, 4.340, 4.400, 4.500, 4.510, 4.870, 4.980, 5.060, 5.090, 5.170, 5.320, 5.320, 5.340, 5.410, 5.410, 5.490, 5.620, 5.710, 5.850, 6.250, 6.540, 6.760, 6.930, 6.940, 6.970, 7.090, 7.260, 7.280, 7.320, 7.390, 7.590, 7.620, 7.630, 7.660, 7.870, 7.930, 8.260, 8.370, 8.530, 8.650, 8.660, 9.020, 9.220, 9.470, 9.740, 10.06, 10.34, 10.66, 10.75, 11.25, 11.64, 11.79, 11.98, 12.02, 12.03, 12.07, 12.63, 13.11, 13.29, 13.80, 14.24, 14.76, 14.77, 14.83, 15.96, 16.62, 17.12, 17.14, 17.36, 18.10, 19.13, 20.28, 21.73, 22.69, 23.63, 25.74, 25.82, 26.31, 32.15, 34.26, 36.66, 43.01, 46.12, 79.05	Aldeni et al. [27]

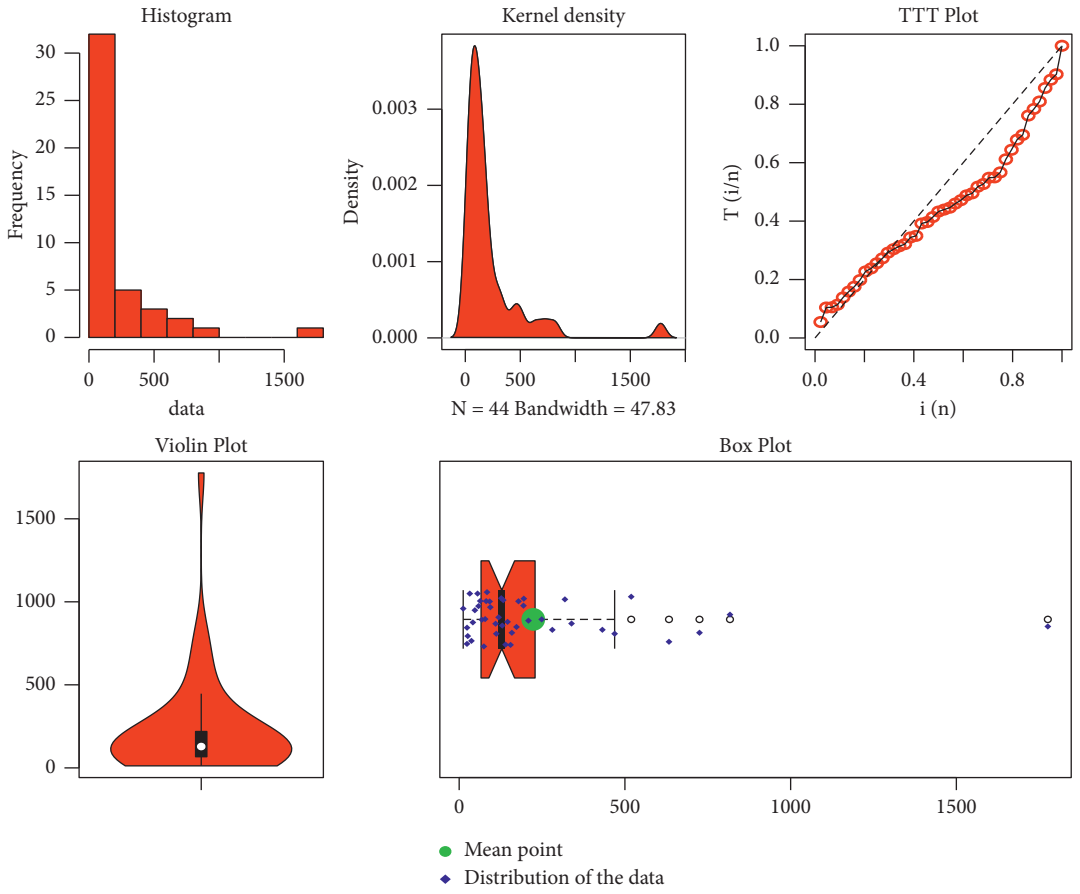

Figure 4: Basic plots of Data 1.

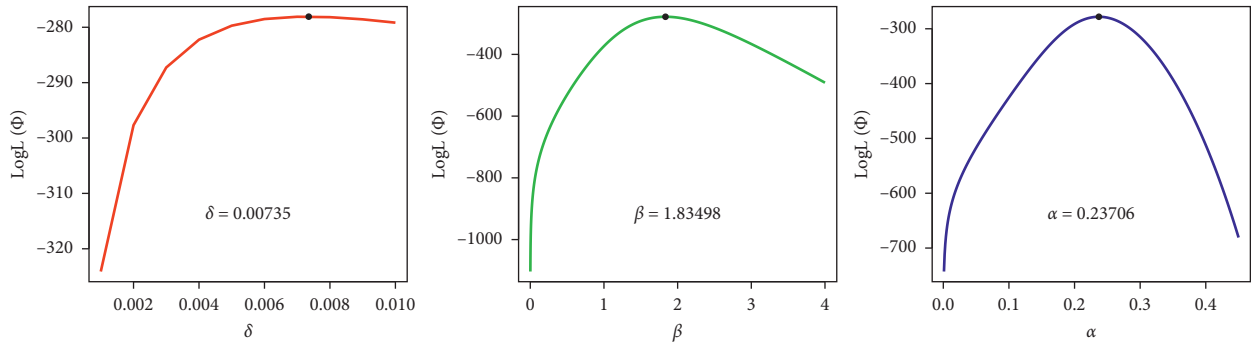

Figure 5: The profiles of the log LF of the NFLog-Wei distribution using Data 1.

Table 4: The values of $\widehat{\alpha}_{MLE}, \widehat{\beta}_{MLE}, \widehat{\delta}_{MLE}, \widehat{\alpha}_{1MLE}, \widehat{\gamma}_{MLE}$, and $\widehat{\sigma}_{MLE}$ of the fitted models using Data 1.

Models	$\widehat{\alpha}_{MLE}$	$\widehat{\beta}_{MLE}$	$\widehat{\delta}_{MLE}$	$\widehat{\alpha}_{1MLE}$	$\widehat{\gamma}_{MLE}$	$\widehat{\sigma}_{MLE}$
NFLog-Wei	1.83498	0.23706	0.00735	—	—	—
APT-Wei	0.99270	0.00326	—	0.24503	—	—
FRLog-Wei	0.76184	0.02859	—	—	—	5.72175
Weibull	0.93131	0.00677	—	—	—	—
MO-Wei	2.41759	0.00303	—	—	0.50752	—

Table 5: The values of CM, AD, KS, and P value of the fitted models for Data 1.

Models	CM	AD	KS	P value
NFLog-Wei	0.02815	0.18922	0.06204	0.9919
APT-Wei	0.09338	0.55387	0.10551	0.6723
FRLog-Wei	0.19103	1.09553	0.13355	0.3789
Weibull	0.13983	0.81427	0.12612	0.4494
MO-Wei	0.09492	0.56181	0.11255	0.5933

Table 6: The values of AIC, BIC, CAIC, and HQIC of the fitted models for Data 1.

Models	AIC	BIC	CAIC	HQIC
NFLog-Wei	562.1700	567.5226	562.7700	564.1550
APT-Wei	567.7712	573.1238	568.3712	569.7562
FRLog-Wei	572.8833	578.2359	573.4833	574.8683
Weibull	567.6941	571.2625	567.9868	569.0175
MO-Wei	568.2084	573.5610	568.8084	570.1934

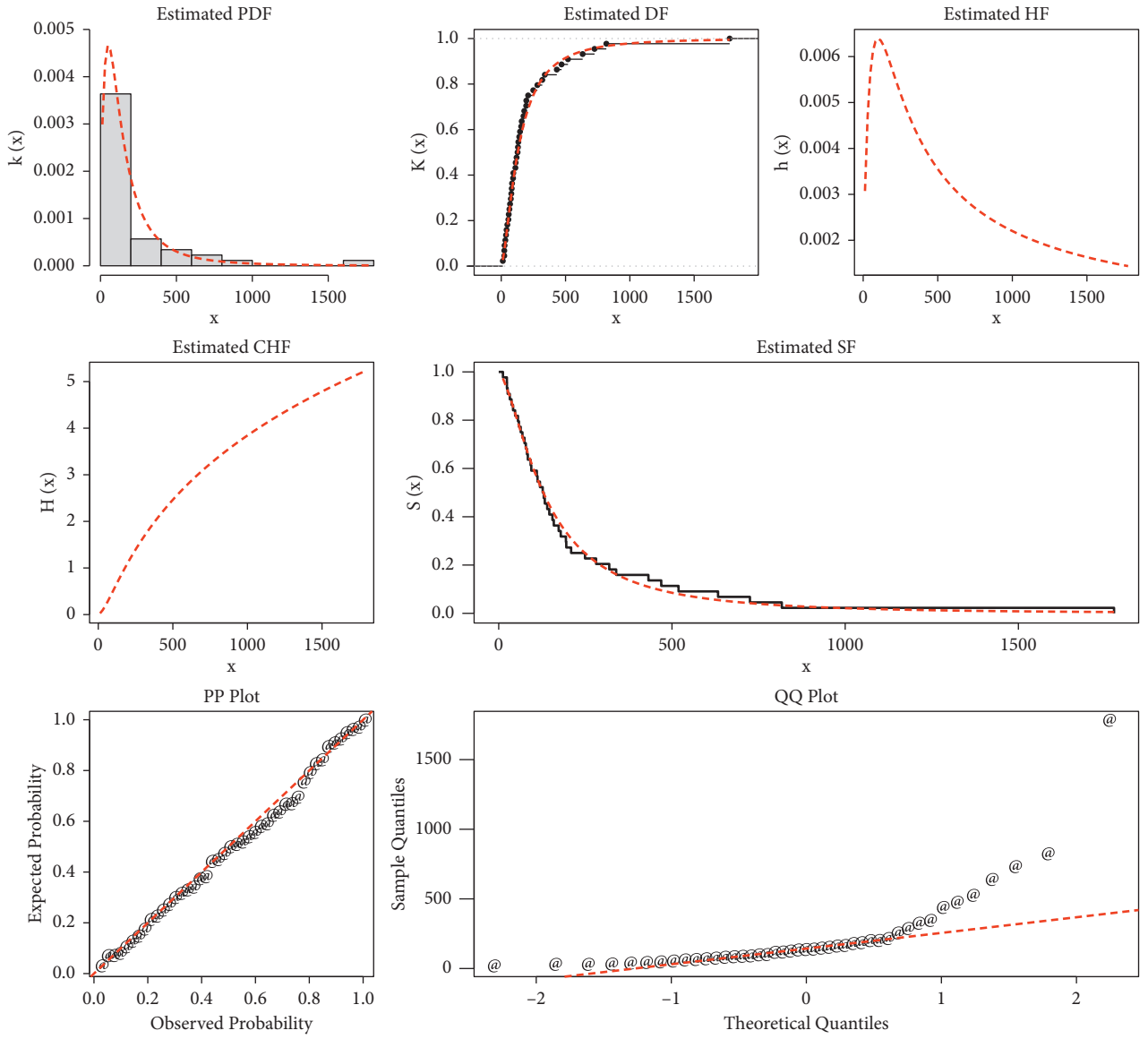

Figure 6: Visual illustration of the NFLog-Wei model using Data 1.

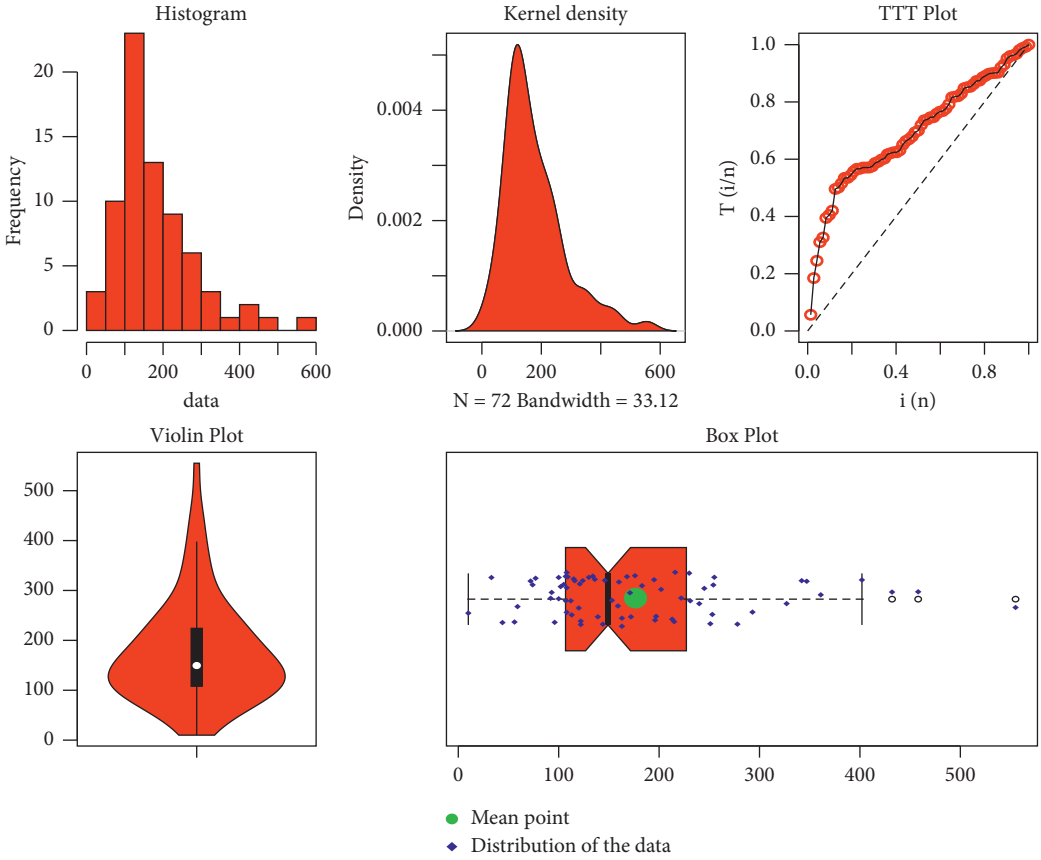

Figure 7: Basic plots of Data 2.

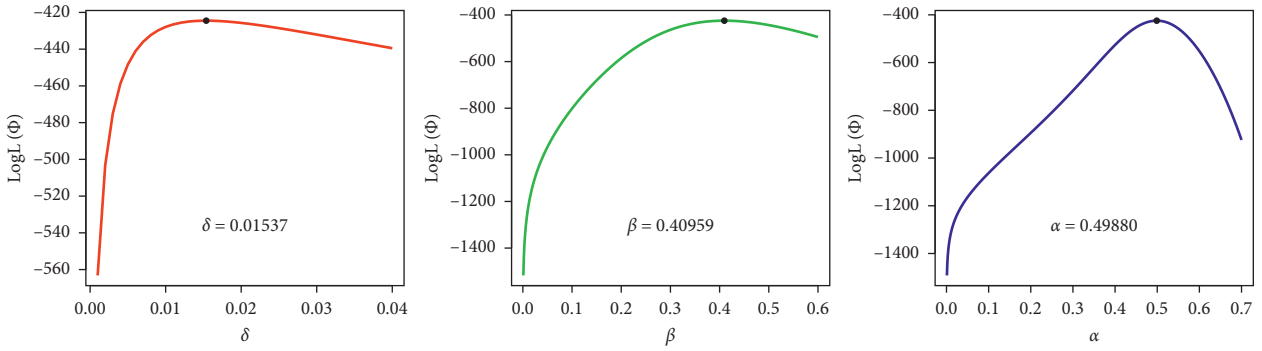

Figure 8: The profiles of the log LF of the NFLog-Wei distribution using Data 2.

Table 7: The values of $\widehat{\alpha}_{MLE}, \widehat{\beta}_{MLE}, \widehat{\delta}_{MLE}, \widehat{\alpha_1}_{MLE}, \widehat{\gamma}_{MLE}$, and $\widehat{\sigma}_{MLE}$ of the fitted models using Data 2.

Models	$\widehat{\alpha}_{MLE}$	$\widehat{\beta}_{MLE}$	$\widehat{\delta}_{MLE}$	$\widehat{\alpha_1}_{MLE}$	$\widehat{\gamma}_{MLE}$	$\widehat{\sigma}_{MLE}$
NFLog-Wei	0.01537	0.40959	0.49880	—	—	—
APT-Wei	1.19003	0.00325	—	6.81765	—	—
FRLog-Wei	1.20746	0.00354	—	—	—	11.84593
Weibull	1.19177	0.00208	—	—	—	—
MO-Wei	1.24252	0.00240	—	—	2.37148	—

Table 8: The values of CM, AD, KS, and P value of the fitted models for Data 2.

Models	CM	AD	KS	P value
NFLog-Wei	0.06315	0.37584	0.07504	0.81220
APT-Wei	0.13802	0.80373	0.17147	0.20986
FRLog-Wei	0.20630	1.20443	0.17744	0.19768
Weibull	0.10908	0.65947	0.25498	0.17134
MO-Wei	0.16136	0.94136	0.17256	0.20469

Table 9: The values of AIC, BIC, CAIC, and HQIC of the fitted probability models for Data 2.

Models	AIC	BIC	CAIC	HQIC
NFLog-Wei	854.9775	861.8075	855.3304	857.6965
APT-Wei	864.1267	870.9567	864.4797	866.8458
FRLog-Wei	868.2720	875.1020	868.6249	870.9910
Weibull	877.7535	882.3068	877.9274	879.5662
MO-Wei	865.7111	872.5411	866.0641	868.4302

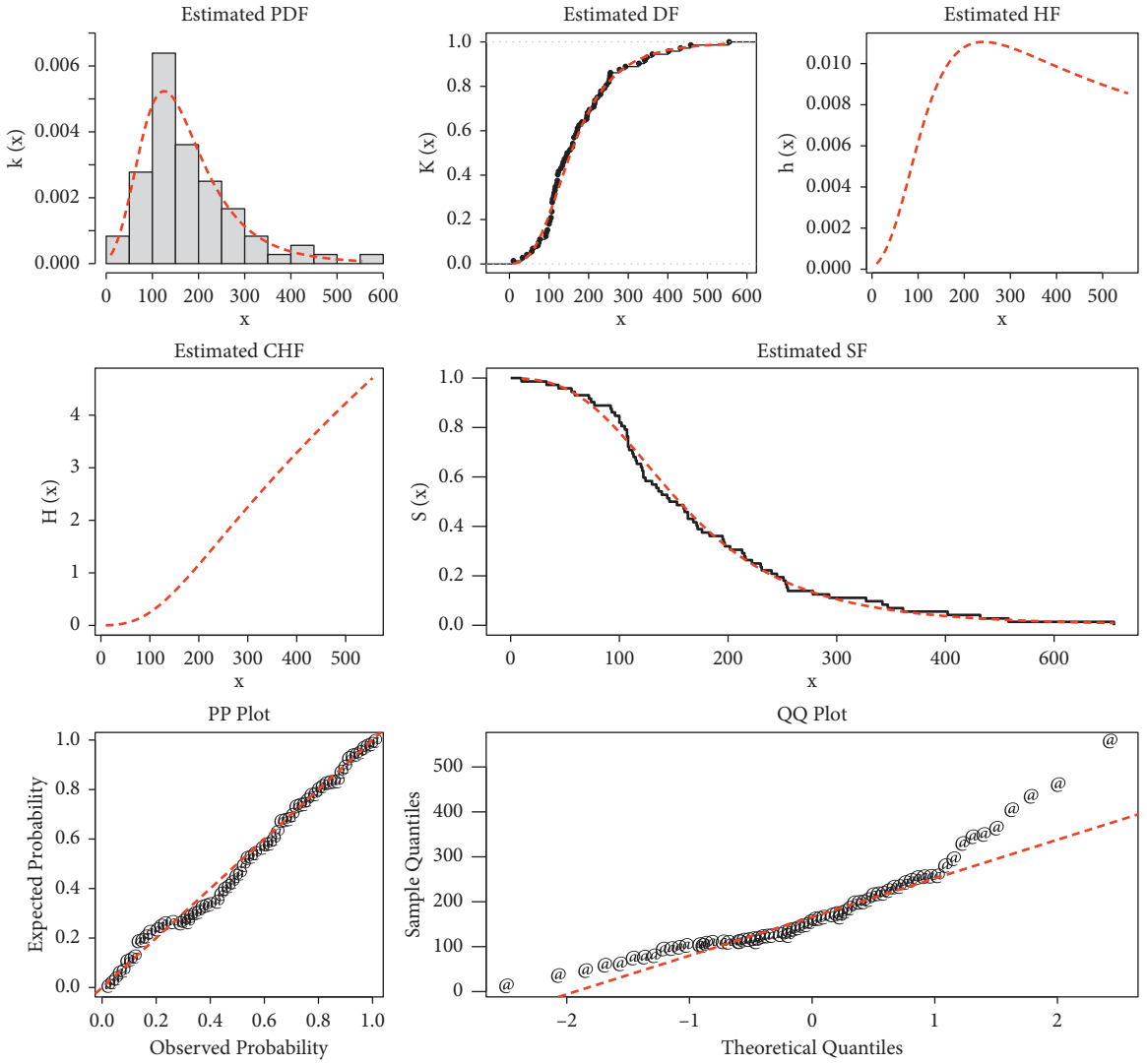

Figure 9: Visual illustration of the NFLog-Wei distribution using Data 2.

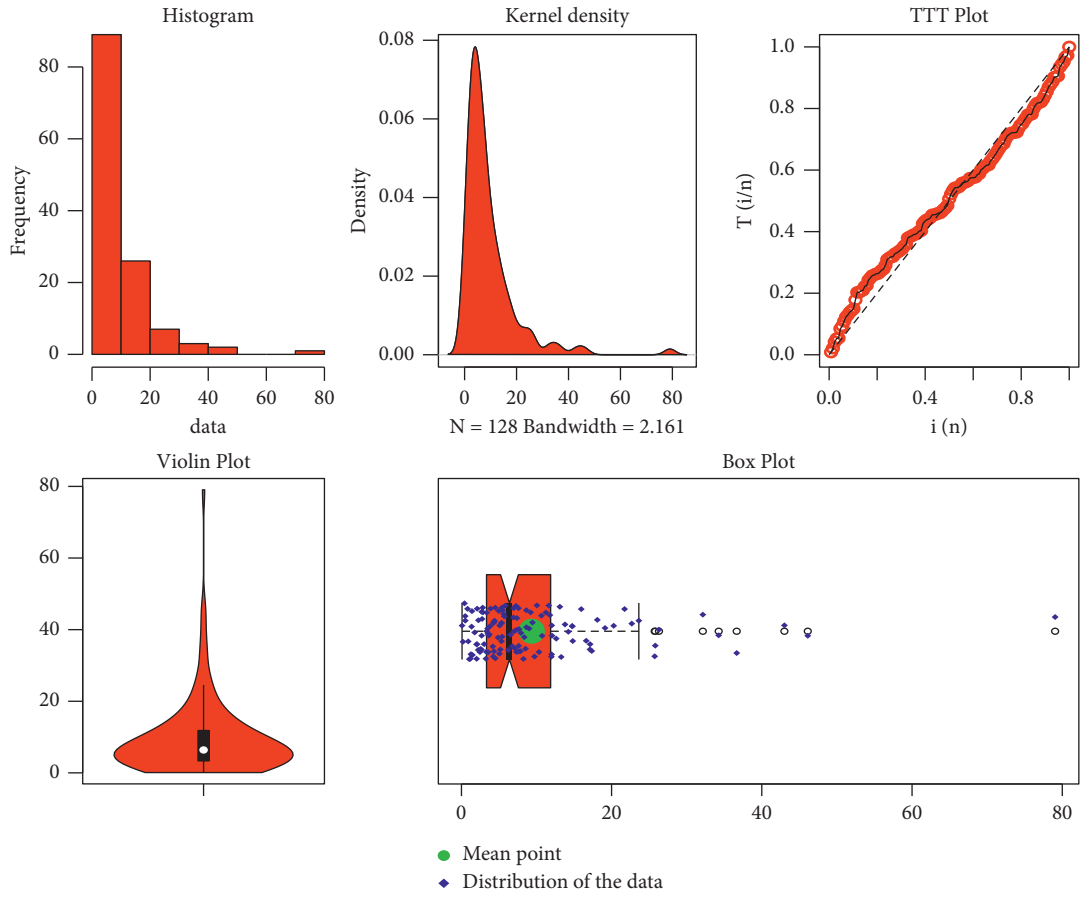

Figure 10: Basic plots of Data 3.

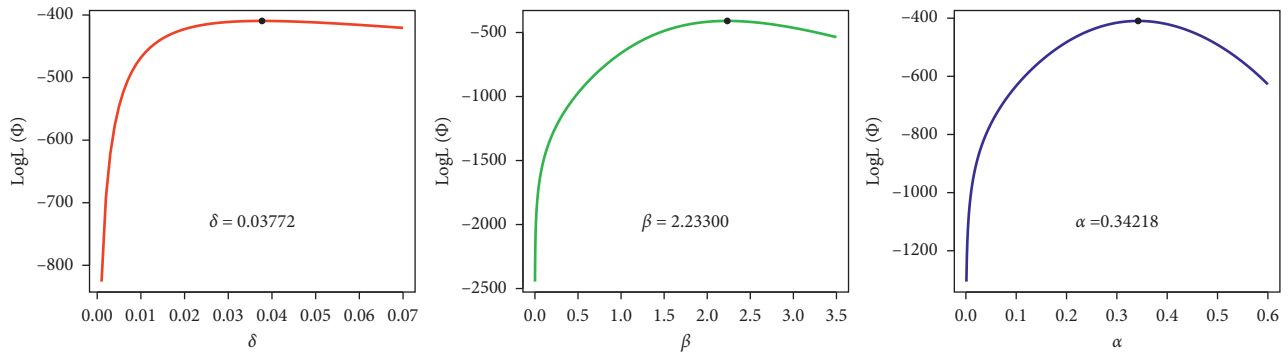

Figure 11: The profiles of the log LF of the NFLog-Wei distribution using Data 3.

Table 10: The values of $\widehat{\alpha}_{MLE}, \widehat{\beta}_{MLE}, \widehat{\delta}_{MLE}, \widehat{\alpha_1}_{MLE}, \widehat{\gamma}_{MLE}$, and $\widehat{\sigma}_{MLE}$ of the fitted models using Data 3.

Models	$\widehat{\alpha}_{MLE}$	$\widehat{\beta}_{MLE}$	$\widehat{\delta}_{MLE}$	$\widehat{\alpha_1}_{MLE}$	$\widehat{\gamma}_{MLE}$	$\widehat{\sigma}_{MLE}$
NFLog-Wei	0.03770	2.23388	0.34211	—	—	—
APT-Wei	1.26652	0.01661	—	0.01490	—	—
FRLog-Wei	1.27348	0.03210	—	—	—	0.81243
Weibull	1.04777	0.09390	—	—	—	—
MO-Wei	1.50855	0.00673	—	—	0.11186	—

Table 11: The values of CM, AD, KS, and P value of the fitted models for Data 3.

Models	CM	AD	KS	P value
NFLog-Wei	0.01562	0.10017	0.03054	0.9998
APT-Wei	0.04227	0.25411	0.04660	0.9437
FRLog-Wei	0.09868	0.61203	0.06859	0.5836
Weibull	0.13135	0.78639	0.06999	0.5573
MO-Wei	0.03150	0.22134	0.04008	0.9863

Table 12: The values of AIC, BIC, CAIC, and HQIC of the fitted models for Data 3.

Models	AIC	BIC	CAIC	HQIC
NFLog-Wei	824.9405	833.4966	825.1340	828.4169
APT-Wei	826.3801	834.9362	826.5737	829.8565
FRLog-Wei	832.5411	841.0972	832.7346	836.0175
Weibull	832.1738	837.8778	832.2698	834.4913
MO-Wei	826.5740	835.1301	826.7675	830.0504

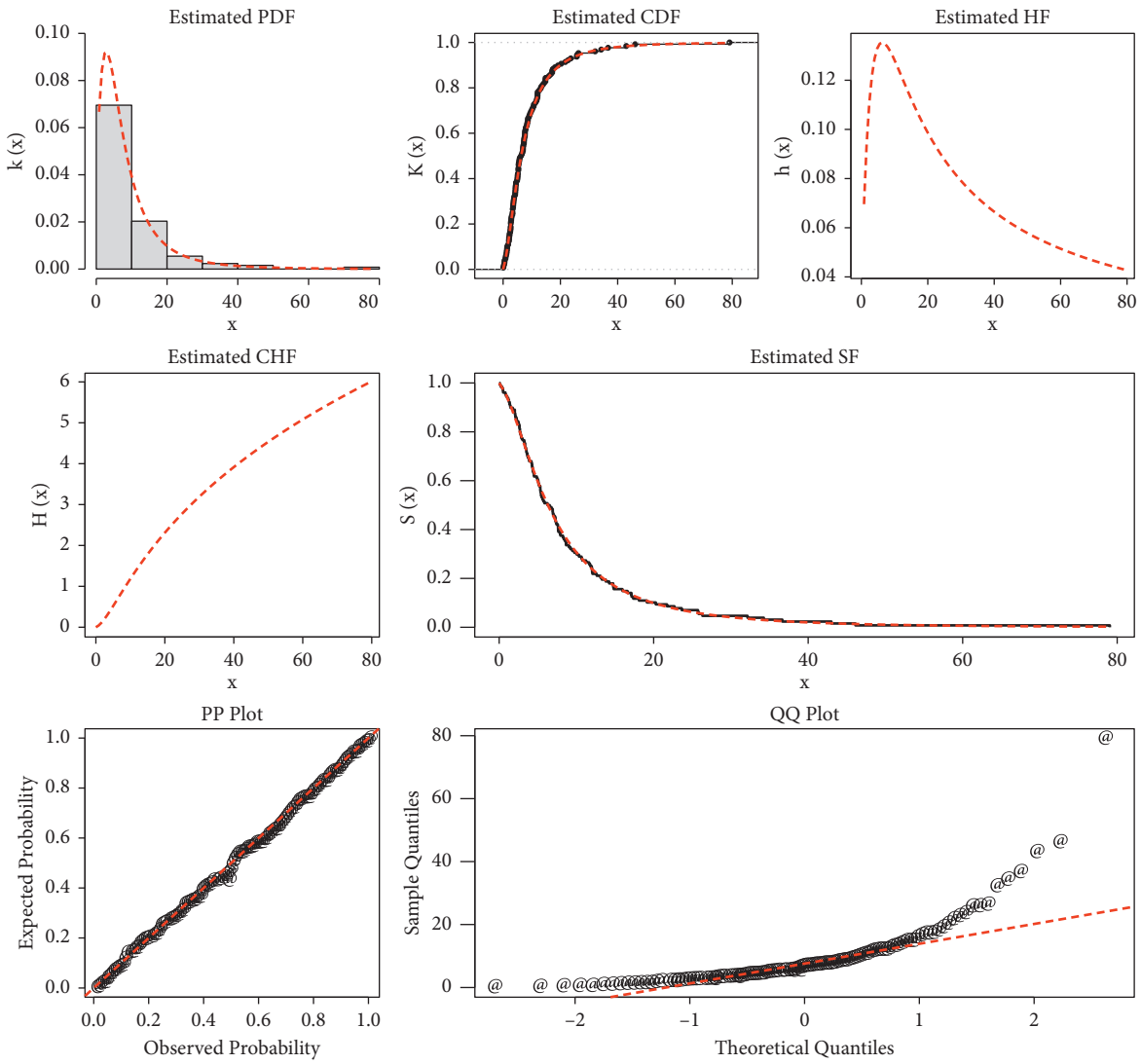

Figure 12: Visual illustration of the NFLog-Wei distribution using Data 3.

$$2m \log[\log(n)] - 2\ell(\mathbf{\Phi}). \tag{34}$$

(vii) The CAIC is derived as follows:

$$\frac{2mn}{n-m-1} - 2\ell(\mathbf{\Phi}). \tag{35}$$

6.1. Data 1. The first dataset (Data 1) consists of forty-four observations. The lengths of time that patients managed to stay alive may be seen here in this dataset. The key measures (summary measures) of Data 1 are as follows: skewness = 3.38382, minimum = 12.20, 1st quartile = 67.21, median = 128.50, mean = 223.48, 3rd quartile = 219.00, maximum = 1776.00, kurtosis = 16.5596, variance = 93286.41, and range = 1763.8. Corresponding to Data 1, some basic plots and the profiles of the MLEs of the NFLog-Wei distribution are presented in Figures 4 and 5, respectively.

Furthermore, for Data 1, the numerical values of the NFLog-Wei distribution and other competing models are presented in Table 4. The numerical values of the analytical measures of the competing probability models are provided in Tables 5 and 6. In justification of the numerical depiction that may be seen in Tables 5 and 6, confirm the best fitting of the NFLog-Wei model to Data 1. Figure 6 presents a graphic representationof the NFLog-Wei model. We can see that the plots shown in Figure 6 also confirm the close-fitting (best fitting) of the NFLog-Wei model to Data 1.

6.2. Data 2. The second dataset (Data 2) consists of seventy-two observations. The following are the important indicators of Data 2: minimum = 10.0, 1st quartile = 108.0, median = 149.5, mean = 176.8, 3rd quartile = 224.0, maximum = 555.0, skewness = 1.341284, kurtosis = 4.988524, variance = 10705.1, and range = 545. As in Figure 7, we can provide some summary graphs in relation to Data 2. Using Data 2, the profiles of the MLEs of the NFLog-Wei distribution are shown in Figure 8.

We also applied the NFLog-Wei distribution and other competing probability models to Data 2. Corresponding to this dataset, the numerical values of the competing probability distributions can be easily shown in Table 7. Also, the metrics of the analysis measures of the distributions that were "fitted" are already provided in Tables 8 and 9. The numerical results, in Tables 8 and 9, demonstrate that the NFLog-Wei distribution has the least results of the analytical metrics. This fact supports the best fitting power of the NFLog-Wei distribution to the guinea pigs infected dataset. In addition, Figure 9 illustrates the NFLog-Wei distribution graphically. The plots in Figure 9 support the close fit (best fit) of the NFLog-Wei distribution to the guinea pig-infected dataset.

6.3. Data 3. The third dataset (Data 3) consists of one hundred and twenty-eight observations. The key measures of Data 3 are as follows: skewness = 0.634064, median = 5.320, minimum = 0.080, 1st quartile = 2.830, mean = 6.017, 3rd quartile = 8.370, maximum = 15.960, kurtosis = 2.5349, variance = 15.66289, and range = 15.88. Figure 10 depicts many major charts that correspond to Data 3. In link to this dataset, the profiles of the MLEs of the NFLog-Wei distribution are displayed in Figure 11.

Again, we applied the NFLog-Wei distribution and the competing distributions to Data 3. Corresponding to Data 3, the numerical results of the fitted probability models can be found in Table 10. The numerical values of the statistical tests of the competing probability models are given in Tables 11 and 12. In light of the numerical findings presented in the Tables 11 and 12, we can observe that the NFLog-Wei is the best competing probability model for Data 3. To support the best fitting power of the NFLog-Wei distribution to Data 3, a graphical illustration is also presented in Figure 12. The visual illustration provided in Figure 12 supports the best fit capability of the NFLog-Wei distribution to Data 3.

7. Conclusion

In this study, a novel family of probability models was presented. The proposed family was named a new flexible logarithmic-X family. A subcase of the NFLog-X family was studied in detail. The unknown parameters of the NFLog-X family of distributions were computed using the maximum likelihood method. Furthermore, a MCSS was carried out to assess the performances of $\widehat{\delta}_{MLE}$ and $\widehat{\lambda}_{MLE}$ of the NFLog-X family. Finally, three applications (real-life datasets) to the biomedical datasets were presented to illustrate the potentiality and flexibility of the NFLog-X method. The comparison of the NFLog-X method was made with the Wei distribution and its three other well-known distributions including the APT-Wei, FRLog-Wei, and MO-Wei distributions. On the basis of eight analytic metrics, it is demonstrated that the NFLog-Wei distribution is the optimal probability distribution for modeling the medical datasets.

In the future, we are motivated to introduce further flexible forms of the NFLog-X distributions for data modeling in various sectors. We are also motivated to study the bivariate and multivariate extensions of the NFLog-X distributions [27–29] and also in the upcoming stage of this research, we will use the newly invented family of distributions in addition to the suggested distribution to analyse the censored sample technique. In order to create randomised censored samples based on the new distribution, we will carry out research on a variety of censoring techniques, including the type-I and type-II censored sample. The scope of our analysis might be increased to encompass the implementation of the suggested model to various accelerated life testing scenarios, such as constant and partially constant tests, and perhaps even outcomes of progressive load accelerated life tests.

Data Availability

In the paper, the datasets are listed.

Conflicts of Interest

It is stated by the authors that they have no competing interests.

Acknowledgments

The authors would like to thank the Deanship of Scientific Research at the Umm Al-Qura University for supporting this work by grant code (22UQU4300011DSR01).

References

[1] A. Hassan, A. Rashid, and N. Akhtar, "Exponentiated quasi power Lindley power series distribution with applications in medical science," *Journal of Applied Mathematics, Statistics and Informatics*, vol. 16, no. 1, pp. 37–60, 2020.

[2] Z. Ahmad, M. Elgarhy, and G. G. Hamedani, "A new Weibull-X family of distributions: properties, characterizations and applications," *Journal of Statistical Distributions and Applications*, vol. 5, no. 1, pp. 1–18, 2018.

[3] Q. Liao, Z. Ahmad, E. Mahmoudi, and G. G. Hamedani, "A new flexible bathtub-shaped modification of the Weibull model: properties and applications," *Mathematical Problems in Engineering*, vol. 2020, p. 11, Article ID 3206257, 2020.

[4] A. M. Sarhan and M. Zaindin, "Modified Weibull distribution. APPS," *Applied Sciences*, vol. 11, pp. 123–136, 2009.

[5] X. Huo, S. K. Khosa, Z. Ahmad, Z. Almaspoor, M. Ilyas, and M. Aamir, "A new lifetime exponential-X family of distributions with applications to reliability data," *Mathematical Problems in Engineering*, vol. 2020, Article ID 1316345, 2020.

[6] S. J. Almalki and J. Yuan, "A new modified Weibull distribution," *Reliability Engineering & System Safety*, vol. 111, pp. 164–170, 2013.

[7] Y. Liu, M. Ilyas, S. K. Khosa et al., "A flexible reduced logarithmic-X family of distributions with biomedical analysis," *Computational and Mathematical Methods in Medicine*, vol. 2020, Article ID 4373595, 2020.

[8] M. El-Morshedy, F. S. Alshammari, Y. S. Hamed, M. S. Eliwa, and H. M. Yousof, "A new family of continuous probability distributions," *Entropy*, vol. 23, no. 2, p. 194, 2021.

[9] R. R. Guerra, F. A. Peña-Ramírez, and M. Bourguignon, "The unit extended Weibull families of distributions and its applications," *Journal of Applied Statistics*, vol. 48, no. 16, pp. 3174–3192, 2021.

[10] H. Reyad, M. Ç. Korkmaz, A. Z. Afify, G. G. Hamedani, and S. Othman, "The Fréchet Topp Leone-G family of distributions: properties, characterizations and applications," *Annals of Data Science*, vol. 8, no. 2, pp. 345–366, 2021.

[11] R. A. Bantan, C. Chesneau, F. Jamal, I. Elbatal, and M. Elgarhy, "The truncated burr X-G family of distributions: properties and applications to actuarial and financial data," *Entropy*, vol. 23, no. 8, p. 1088, 2021.

[12] J. T. Eghwerido, E. Efe-Eyefia, and S. C. Zelibe, "The transmuted alpha power-G family of distributions," *Journal of Statistics and Management Systems*, vol. 24, no. 5, pp. 965–1002, 2021.

[13] J. T. Eghwerido and F. I. Agu, "The shifted Gompertz-G family of distributions: properties and applications," *Mathematica Slovaca*, vol. 71, no. 5, pp. 1291–1308, 2021.

[14] A. Alzaatreh, M. A. Aljarrah, M. Smithson et al., "Truncated family of distributions with applications to time and cost to start a business," *Methodology and Computing in Applied Probability*, vol. 23, no. 1, pp. 5–27, 2021.

[15] B. Lahcene, "A new extended-gamma family of distributions: properties and applications," *Journal of Applied Mathematics and Computation*, vol. 5, no. 1, pp. 9–17, 2021.

[16] E. A. ElSherpieny and E. M. Almetwally, "The exponentiated generalized alpha power family of distribution: properties and applications," *Pakistan Journal of Statistics and Operation Research*, vol. 18, pp. 349–367, 2022.

[17] R. Roozegar, G. Tekle, and G. Hamedani, "A new generalized-X family of distributions: applications, characterization and a mixture of random effect models," *Pakistan Journal of Statistics and Operation Research*, vol. 18, pp. 483–504, 2022.

[18] H. Klakattawi, D. Alsulami, M. A. Elaal, S. Dey, and L. Baharith, "A new generalized family of distributions based on combining Marshal-Olkin transformation with T-X family," *PloS One*, vol. 17, no. 2, Article ID e0263673, 2022.

[19] M. Hussein, H. Elsayed, and G. M. Cordeiro, "A new family of continuous distributions: properties and estimation," *Symmetry*, vol. 14, no. 2, p. 276, 2022.

[20] M. Kilai, G. A. Waititu, W. A. Kibira, H. M. Alshanbari, and M. El-Morshedy, "A new generalization of Gull Alpha Power Family of distributions with application to modeling COVID-19 mortality rates," *Results in Physics*, vol. 36, Article ID 105339, 2022.

[21] Z. Ahmad, E. Mahmoudi, and O. Kharazmi, "On modeling the earthquake insurance data via a new member of the TX family," *Computational Intelligence and Neuroscience*, vol. 2020, Article ID 7631495, 2020.

[22] W. Wang, Z. Ahmad, O. Kharazmi, C. B. Ampadu, E. H. Hafez, and M. M. Mohie El-Din, "New generalized-x family: modeling the reliability engineering applications," *Plos One*, vol. 16, no. 3, Article ID e0248312, 2021.

[23] H. S. Mohammed, Z. Ahmad, A. T. Ahmad et al., "Statistical modelling for Bladder cancer disease using the NLT-W distribution," *AIMS Mathematics*, vol. 6, no. 9, pp. 9262–9276.

[24] A. Alzaatreh, C. Lee, and F. Famoye, "A new method for generating families of continuous distributions," *Metron*, vol. 71, no. 1, pp. 63–79, 2013.

[25] A. W. Marshall and I. Olkin, "A new method for adding a parameter to a family of distributions with application to the exponential and Weibull families," *Biometrika*, vol. 84, no. 3, pp. 641–652, 1997.

[26] S. Dey, V. K. Sharma, and M. Mesfioui, "A new extension of Weibull distribution with application to lifetime data," *Annals of Data Science*, vol. 4, no. 1, pp. 31–61, 2017.

[27] M. Aldeni, C. Lee, and F. Famoye, "Families of distributions arising from the quantile of generalized lambda distribution," *Journal of Statistical Distributions and Applications*, vol. 4, no. 1, pp. 1–18, 2017.

[28] T. Bjerkedal, "Acquisition of resistance in Guinea pigs infected with different doses of virulent tubercle Bacilli1," *American Journal of Epidemiology*, vol. 72, no. 1, pp. 130–148, 1960.

[29] Ü. N. A. L. Ceren, S. Cakmakyapan, and Ö. Z. E. L. Gamze, "Alpha power inverted exponential distribution: properties and application," *Gazi University Journal of Science*, vol. 31, no. 3, pp. 954–965, 2018.

Hindawi
Complexity
Volume 2022, Article ID 1753992, 8 pages
https://doi.org/10.1155/2022/1753992

Research Article

A New Technique for Solving Neutral Delay Differential Equations Based on Euler Wavelets

Mutaz Mohammad [1] **and Alexander Trounev** [2]

[1] *Zayed University, Abu Dhabi, UAE*
[2] *Kuban State Agrarian University, Krasnodar, Russia*

Correspondence should be addressed to Mutaz Mohammad; mutaz.mohammad@zu.ac.ae

Received 27 May 2022; Accepted 24 July 2022; Published 29 August 2022

Academic Editor: Fathalla A. Rihan

An effective numerical scheme based on Euler wavelets is proposed for numerically solving a class of neutral delay differential equations. The technique explores the numerical solution via Euler wavelet truncated series generated by a set of functions and matrix inversion of some collocation points. Based on the operational matrix, the neutral delay differential equations are reduced to a system of algebraic equations, which is solved through a numerical algorithm. The effectiveness and efficiency of the technique have been illustrated by several examples of neutral delay differential equations. The main advantages and key role of using the Euler wavelets in this work lie in the performance, accuracy, and computational cost of the proposed technique.

1. Introduction

We consider the following neutral delay differential equation (NDDE) given by.

$$u'(t) = gt, u(t), u(t-\theta(t,u(t))), \quad u'(t-\eta(t,u(t))),\ t_1 \le t \le t_g, \tag{1}$$

$$u(t) = \phi(t),\ t \le t_1,\ \ (\phi \text{ is the initial function}). \tag{2}$$

such that

$$g\colon \left[t_1, t_g\right] \times R \times R \times R \circledR R, \tag{3}$$

is a differentiable function, θ and η are continuous functions defined on $[t_1, t_g] \times \mathbb{R}$, provided that.

$$t - \theta(t,u(t)) < t_g, t - \eta(t,u(t)) < t_g. \tag{4}$$

Recently, delay differential equations (DDEs) and NDDE have been given much interest in engineering and science including physics, chemistry, and biology, for e.g., one of the rich sources of such applications can be found in [1–3]. More interesting examples and rigorous treatment are presented in [4–7]. In [8–13], the authors developed various issues of numerical modeling involving DDEs.

The proposed problem 1 and (2) is a special class of DDE, which appears in a wide range of applications such as the mathematical modeling of ecology, electronics, and control of ships and aircraft. It is obvious that these kinds of NDDE cannot be solved exactly. Hence, it is crucial to develop efficient numerical techniques to simulate solutions of such equations. Many researchers reported several techniques in this development, for example, Runge–Kutta method has been used in [14], variational iteration method in [15], and other numerical schemes and properties can be found in [7, 16, 17].

2. The Numerical Approach Based on Euler Wavelet

Wavelet expansions and its generalization, such as framelets, have been successful in numerical simulation in many areas of applications in real-world phenomena [18]. This is largely due to the fact that wavelets have the right structure to capture the sparsity in linear systems. Note that the great

hopes in developing wavelet-based representations and theory of turbulent flows have not been materialized. Euler wavelet approximation would have the right approximating structure to be efficient for a general NDDE due to the orthogonality of the envisaged wavelets in the proposed framework. To solve the proposed problem, we use Euler wavelets generated via Euler polynomials and presented in [19].

The Euler polynomial $U_k(x)$ is defined based on the generating function that has the form.

$$\sum_{k=0}^{\infty} \frac{U_k(x)t^k}{k!} = \frac{e^{xt}}{e^t + 1}. \tag{5}$$

The first few Euler polynomials are given below, and the graphical presentation of some of these functions is presented in Figure 1.

$$\begin{aligned} U_0(x) &= 1, \\ U_1(x) &= x - \frac{1}{2}, \\ U_2(x) &= x^2 - x, \\ U_3(x) &= x^3 - \frac{3x^2}{2} + \frac{1}{4}, \\ U_4(x) &= x^4 - 2x^3 + x, \\ U_5(x) &= x^5 - \frac{5x^4}{2} + \frac{5x^2}{2} - \frac{1}{2}, \\ U_6(x) &= x^6 - 3x^5 + 5x^3 - 3x, \\ U_7(x) &= x^7 - \frac{7x^6}{2} + \frac{35x^4}{4} - \frac{21x^2}{2} + \frac{17}{8}. \end{aligned} \tag{6}$$

Let us define the Euler polynomials $U_1(x), U_2(x)$ and the needed functions in the following numerical scheme:

$$U_1(t) = -\frac{1}{2} + x, U_2(x) = -x + x^2, \tag{7}$$

$$I_1^1 = \int_0^x U_1(t)\mathrm{d}t, \tag{8}$$

$$I_2^1 = \int_0^x U_2(t)\mathrm{d}t, \tag{9}$$

$$I_1^2 = \int_0^x I_1^1(t)\mathrm{d}t, \tag{10}$$

$$I_2^2 = \int_0^x I_2^1(t)\mathrm{d}t. \tag{11}$$

Let Ξ be the set of all functions given in equations (3)–(8). For any function $\tau \in \Xi$, we define the function $\varphi(x)$ as follows:

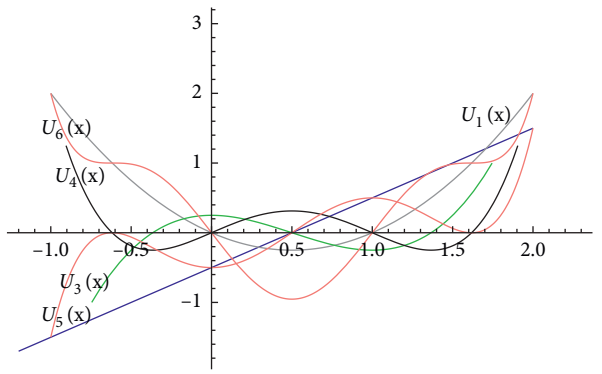

Figure 1: The graphs of the first few Euler polynomials U_1 through U_5.

$$\varphi(t) = \tau\chi_{[0,1]}(t), \tag{12}$$

where $\chi_{[0,1]}$ is the indicator function on [0,1]. Assume that,

$$\begin{aligned} \varphi_1 &= U_1, \\ \varphi_2 &= U_2, \\ \varphi_{1,1} &= I_1^1, \\ \varphi_{2,1} &= I_2^1, \\ \varphi_{1,2} &= I_1^2, \\ \varphi_{2,2} &= I_2^2. \end{aligned} \tag{13}$$

We define the following set of wavelets, where $j,k \in \mathbb{Z}$ as,

$$\begin{aligned} \varphi_1(j,k,t) &= \varphi_1\left(2^j t - k\right), \\ \varphi_2(j,k,t) &= \varphi_2\left(2^j t - k\right), \\ \varphi(j,k,t) &= \left(\varphi_1(j,k,t) + \varphi_2(j,k,t)\right), \\ \varphi^{1,1}(j,k,t) &= \varphi_{1,1}\left(2^j t - k\right), \\ \varphi^{1,2}(j,k,t) &= \varphi_{1,2}\left(2^j t - k\right), \\ \varphi^{2,1}(j,k,t) &= \varphi_{2,1}\left(2^j t - k\right), \\ \varphi^{2,2}(j,k,t) &= \varphi_{2,2}\left(2^j t - k\right), \\ \varphi^1(j,k,t) &= \frac{\left(\varphi^{1,1}(j,k,t) + \varphi^{2,1}(j,k,t)\right)}{j}, \\ \varphi^2(j,k,t) &= \frac{\left(\varphi^{2,1}(j,k,t) + \varphi^{2,2}(j,k,t)\right)}{j^2}. \end{aligned} \tag{14}$$

Recall that, see for example., [20], a function $\tau \in L_2(\mathbb{R})$ can be expanded using the following series,

$$\tau(x) = \sum_{\ell=1}^{2} \sum_{j,k \in \mathbb{Z}}^{\infty} d^{\ell}(j,k)\varphi^{\ell}(j,k,x), \tag{15}$$

where,

$$d^{\ell}(j,k) = \langle \tau, \varphi^{\ell}(j,k,x)\rangle = \int_{\mathbb{R}} \tau(x)\varphi^{\ell}(j,k,x)w(x)\mathrm{d}x, \tag{16}$$

In which $\langle\cdot,\cdot\rangle$ denotes the usual inner product over the space $L_2(\mathbb{R})$ and w is a proper weight function.

One may truncate (16) by $\tau_{n,M}$ where,

$$\tau_{n,M}(t) = \sum_{\ell=1}^{2}\sum_{j=0}^{n}\sum_{k=0}^{M-1} d^{\ell}(j,k)\varphi^{\ell}(j,k,t). \tag{17}$$

Therefore,

$$\left\|\tau - \tau_{n,M}\right\|_2^2 = \left\|\sum_{\ell=1}^{2}\sum_{j\geq n+1}\sum_{k\geq M+1} d^{\ell}(j,k)\varphi^{\ell}(j,k,t)\right\|_2^2. \tag{18}$$

Notice that,

$$\left|\langle d^{\ell}(j,k)\rangle\right| \leq \max_t |\tau|\left\|\varphi^{\ell}(j,k,t)\right\|_1. \tag{19}$$

Hence based on Bessel inequality,

$$\left\|f - f_{n,M}\right\|_2^2 \leq \max_t |\tau|\left\|\varphi^{\ell}(j,k,t)\right\|_1 \sum_{\ell=1}^{2}\sum_{j\geq n+1}\sum_{k=M} |d^{\ell}(j,k). \tag{20}$$

To solve the proposed problem, similar to the method in [19], we construct a vector Ξ_τ of length $M = 2^{n+1}, n \in \mathbb{N}$, such that

$$\Xi_\tau = \left[\varphi_\tau, \sigma^{\kappa}(1,0,x), \ldots, \sigma^{\kappa}\left(2^j,k,x\right), \ldots, \sigma^{\kappa}\left(2^n, 2^{n-1}, x\right),\right.$$
$$\left. j = 0,1,2,\ldots,n; k = 0,1,2,\ldots,2^{j-1}\right], \tag{21}$$

where,

$$\begin{cases} \varphi_\tau = 1, \sigma^{\kappa} = \varphi & \text{when } \tau = U_1, U_2,\ \kappa = 1, \\ \varphi_\tau = x, \sigma^{\kappa} = \varphi^1 & \text{when } \tau = I_1^1, I_2^1,\ \kappa = j, \\ \varphi_\tau = \dfrac{x^2}{2}, \sigma^{\kappa} = \varphi^2 & \text{when } \tau = I_1^2, I_2^2,\ \kappa = j^2. \end{cases} \tag{22}$$

As an illustration, when $n = 2$, we have the following equations:

(i) When $\varphi_\tau = 1, \kappa = 1$, we have the following equation:

$$\Xi_\tau = \begin{cases} [1,0,\ldots,0] & x \in \mathbb{R} - [0,1) \\ \left[1, x^2 - 0.5, 0, 4x^2 - 4x + 0.5, 0, 0, 0, 16x^2 - 24x + 8.5\right] & x \in [0.75,1) \\ \left[1, x^2 - 0.5, 0, x^2 - 4x + 0.5, 0, 0, 16x^2 - 16x + 3.5, 0\right] & x \in [0.5, 0.75) \\ \left[1, x^2 - 0.5, 4x^2 - 0.5, 0, 0, 0.5 - 8x + 16x^2, 0, 0\right] & x \in [0.25, 0.5) \\ \left[1, x^2 - 0.5, 4x^2 - 0.5, 0, 16x^2 - 0.5, 0, 0, 0\right] & \text{True} \end{cases}. \tag{23}$$

(ii) When $\varphi_\tau = x, \kappa = j$, we have the following equation:

$$\Xi_\tau = \begin{cases} [x,0,\ldots,0] & x \in \mathbb{R} - [0,1) \\ \left[x, \dfrac{x^3}{3} - \dfrac{x}{2}, 0, \dfrac{4x^3}{3} - 2x^2 + \dfrac{x}{2} + \dfrac{1}{12}, 0, 0, 0, \dfrac{16x^3}{3} - 12x^2 + \dfrac{17x}{2} - \dfrac{15}{8}\right] & x \in [0.75,1) \\ \left[x, \dfrac{x^3}{3} - \dfrac{x}{2}, 0, \dfrac{4x^3}{3} - 2x^2 + \dfrac{x}{2} + 0.0833333, 0, 0, \dfrac{16x^3}{3} - 8x^2 + \dfrac{7x}{2} - \dfrac{5}{12}, 0\right] & x \in [0.5, 0.75) \\ \left[x, \dfrac{x^3}{3} - \dfrac{x}{2}, \dfrac{4x^3}{3} - \dfrac{x}{2}, 0, 0, \dfrac{16x^3}{3} - 4x^2 + \dfrac{x}{2} + \dfrac{1}{24}, 0, 0\right] & x \in [0.25, 0.5) \\ \left[x, \dfrac{x^3}{3} - \dfrac{x}{2}, \dfrac{4x^3}{3} - \dfrac{x}{2}, 0, \dfrac{16x^3}{3} - \dfrac{x}{2}, 0, 0, 0\right] & \text{True} \end{cases}. \tag{24}$$

(iii) When $\varphi_\tau = x^2/2, \kappa = j^2$, we have the following equation:

$$\Xi_\tau = \begin{cases} \left[0.5x^2, 0, \ldots, 0\right] & x \in \mathbb{R} - [0,1) \\ \left[0.5x^2, \frac{x^4}{12} - \frac{x^2}{4}, 0, \frac{x^4}{3} - \frac{2x^3}{3} + \frac{x^2}{4} + \frac{x}{12} - \frac{1}{24}, 0, 0, 0, \frac{4x^4}{3} - 4x^3 + \frac{17x^2}{4} - \frac{15x}{8} + \frac{9}{32}\right] & x \in [0.75,1) \\ \left[0.5x^2, \frac{x^4}{12} - \frac{x^2}{4}, 0, \frac{x^4}{3} - \frac{2x^3}{3} + \frac{x^2}{4} + \frac{x}{12} - \frac{1}{24}, 0, 0, \frac{4x^4}{3} - \frac{8x^3}{3} + \frac{7x^2}{4} - \frac{5x}{12} + \frac{1}{48}, 0\right] & x \in [0.5,0.75) \\ \left[0.5x^2, \frac{x^4}{12} - \frac{x^2}{4}, \frac{x^4}{3} - \frac{x^2}{4}, 0, 0, 48x^4 - 28x^3 - \frac{47x^2}{12} + \frac{11x}{24} - \frac{1}{96}, 0, 0\right] & x \in [0.25,0.5) \\ \left[0.5x^2, \frac{x^4}{12} - \frac{x^2}{4}, \frac{x^4}{3} - \frac{x^2}{4}, 0, \frac{4x^4}{3} - \frac{x^2}{4}, 0, 0, 0\right] & \text{True} \end{cases}. \tag{25}$$

Now, let us define the solution of equations (1) and (2) via the form of matrices based on the above approach. Assume the Euler wavelet truncated expansion given by equation (10) to be defined as follows:

$$u'(t) = \sum_{\ell=1}^{2}\sum_{j=0}^{n}\sum_{k=0}^{M-1} d^\ell(j,k)\varphi^\ell(j,k,t). \tag{26}$$

Then,

$$u(t) = u(0) + \sum_{\ell=1}^{2}\sum_{j=0}^{n}\sum_{k=0}^{M-1}\int_0^t \mathrm{d}^\ell(j,k)\varphi^\ell(j,k,x)\mathrm{d}x. \tag{27}$$

Additionally,

$$u'(t-\eta(t,u((t)))) = \sum_{\ell=1}^{2}\sum_{j=0}^{n}\sum_{k=0}^{M-1}\mathrm{d}^\ell(j,k)\varphi^\ell(j,k,t-\eta(t,u(t))). \tag{28}$$

Note that from (28), we have the following equation:

$$u(t-\theta(t,u(t))) = u(0) + \sum_{\ell=1}^{2}\sum_{j=0}^{n}\sum_{k=0}^{M-1}\int_0^t \mathrm{d}^\ell(j,k)\varphi^\ell (j,k,x-\theta(x,u(x)))\mathrm{d}x. \tag{29}$$

Assume that $I_{j,k}^\ell(t) = \int_0^t \varphi^\ell(j,k,x)\mathrm{d}x$. Substituting equations (11)–(14) in equations (1) and (2) yields,

$$\begin{aligned} &\sum_{\ell=1}^{2}\sum_{j=0}^{n}\sum_{k=0}^{M-1}\mathrm{d}^\ell(j,k)\varphi^\ell(j,k,t-\eta(t,u(t))) \\ &= g\Bigg(t, u(0) + \sum_{\ell=1}^{2}\sum_{j=0}^{n}\sum_{k=0}^{M-1} d^\ell(j,k)I_{j,k}^\ell(t), u(0) + \sum_{\ell=1}^{2}\sum_{j=0}^{n}\sum_{k=0}^{M-1}\mathrm{d}^\ell(j,k)I_{j,k}^\ell(t), \\ &\sum_{\ell=1}^{2}\sum_{j=0}^{n}\sum_{k=0}^{M-1} d^\ell(j,k)\varphi^\ell(j,k,t-\eta(t,u(t))) \end{aligned} \tag{30}$$

The needed functions for the numerical scheme are ready to be used and so we define,

$$M = 2^{1+n}, n = 1,2,\ldots, \tag{31}$$

As a collocation node where

$$\begin{aligned} s_i &= \frac{s_{i-1}+1}{M}, i = 1,2,\ldots,M; t_i \\ &= \frac{1}{2}\left(s_{i-1} + s_i\right), i = 1,2,\ldots,M. \end{aligned} \tag{32}$$

Hence, by substituting the proposed collocation points to the equation above, we get the following equation:

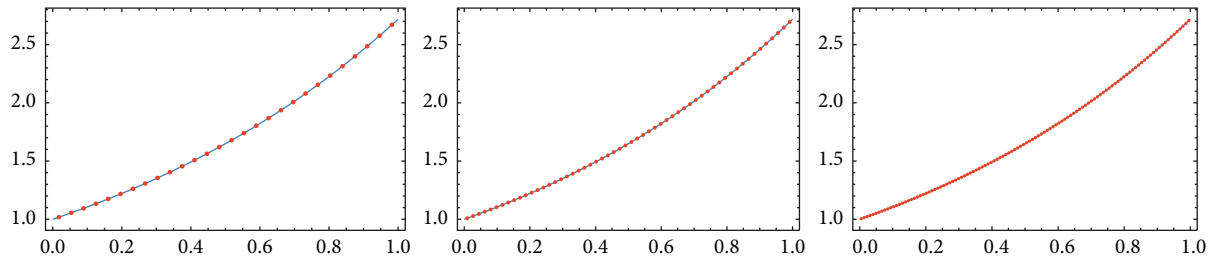

Figure 2: Illustration of example 1 for the analytical and numerical solution (dots) computed with 28, 56, and 112 collocation points.

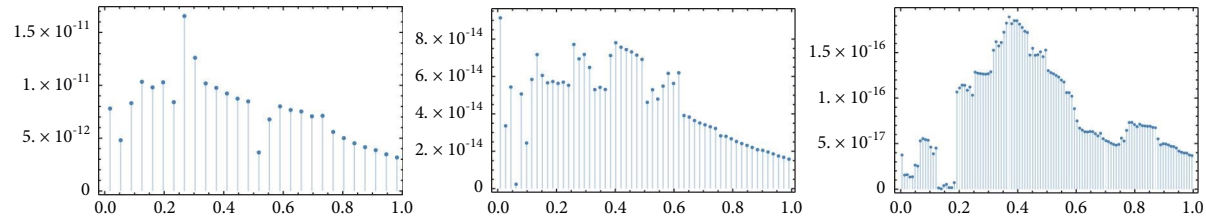

Figure 3: Absolute maximum errors in example 1 when $M = 3, 4, 5$, respectively.

$$u(0) + \sum_{\ell=1}^{2}\sum_{j=0}^{n}\sum_{k=0}^{M-1} d^{\ell}(j,k) I_{j,k}^{\ell}(t_i),$$

$$g\Bigg(t_i, u(0) + \sum_{\ell=1}^{2}\sum_{j=0}^{n}\sum_{k=0}^{M-1} d^{\ell}(j,k) I_{j,k}^{\ell}(t_i),$$

$$u(0) + \sum_{\ell=1}^{2}\sum_{j=0}^{n}\sum_{k=0}^{M-1} d^{\ell}(j,k) I_{j,k}^{\ell}(t_i), \tag{33}$$

$$\sum_{\ell=1}^{2}\sum_{j=0}^{n}\sum_{k=0}^{M-1} d^{\ell}(j,k)\varphi^{\ell}(j,k,t_i - \eta(t,u(t_i)))\Bigg).$$

Note that implementing the collocation division generates a system of algebraic equations that can be solved easily, for example using Mathematica software 13.0 to produce the unknown coefficients $d^{\ell}(j,k)$ needed to find an approximate solution given by (28).

3. Numerical Illustration

In this part, we illustrate some examples of the proposed NDDE problem based on the presented numerical scheme and obtain some maximum absolute errors. The numerical evidences showed high accuracy compared with the exact ones. Six examples will be illustrated. For examples 1–3 from [21], we got an absolute error decreasing from 10^{-12} by 28 collocation points to 10^{-18} by 112 collocation points. In example 4, we got zero absolute error. Thorough out the presented figures and numerical results, the algorithm demonstrates the accuracy and excellent agreement between the numerical solutions and the exact ones.

Table 1: Some numerical evidences for the errors in example 1, with 28 collocation points.

x	Error bound
0.0178571	7.79821×10^{-12}
0.0535714	4.80194×10^{-12}
0.0892857	8.30580×10^{-12}
0.1250000	1.03304×10^{-11}
0.1607140	9.80105×10^{-12}
0.8035710	5.00178×10^{-12}
0.8392860	4.51461×10^{-12}
0.8750000	4.14158×10^{-12}
0.9107140	3.86313×10^{-12}
0.9464290	3.46967×10^{-12}
0.9821430	3.16769×10^{-12}

Example 1. Let's take the following NDDE

$$\frac{du}{dt} + (\cos(t))^{1/2}\left(u'\left(t^{1/2}\right) - e^{t^{1/2}}\right) + \left(\sin\left(t^{1/2}\right) + e^{t}\right)\left(u(\sin(t)) - e^{\sin(t)}\right) = e^{t}, 0 \le t \le 1. \tag{34}$$

The initial condition for this formulation is given by,

$$u(t) = e^{t}, \ t \le 0. \tag{35}$$

The exact solution is defined as follows:

$$u(t) = e^{t}. \tag{36}$$

The exact and approximate solutions for different number of collocation points are presented in Figures 2 and 3, where the agreement between the approximate and exact functions and the error bounds are clearly improved gradually when the order of the partial sum of the truncated Euler series expansion enlarges. In Table 1, we show the error bound resulted for example 1.

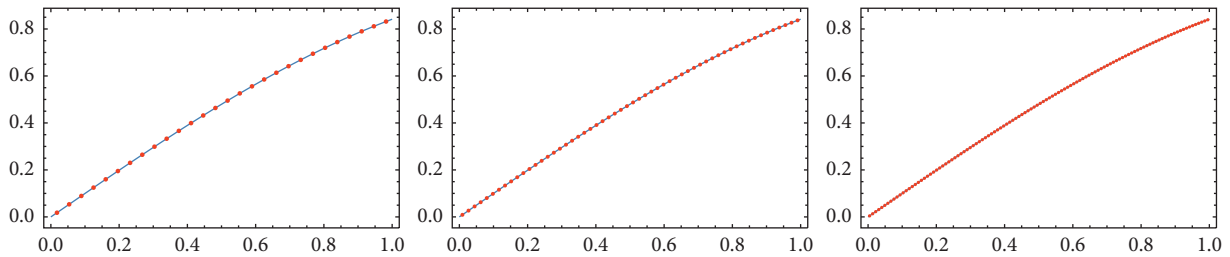

Figure 4: Illustration of Example 2 for the analytical and numerical solution (dots) computed with 28, 56, and 112 collocation points.

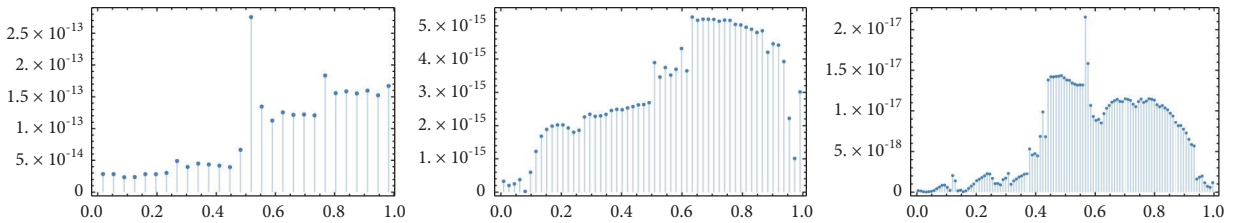

Figure 5: Absolute maximum errors in Example 2 when $M = 3, 4, 5$, respectively.

Example 2. Here we take the NDDE

$$\frac{du}{dt} + t^{1/2}\left(u'\left(e^{-t/2}\right) - u\left(t^{1/2}e^{-t}\right) + u(t) - \cos\left(e^{-t/2}\right) - \sin\left(t^{1/2}e^{-t}\right) + \sin(t)\right) = \cos(t), 0 \le t \le 1, \tag{37}$$

where the initial condition is as follows:

$$u(t) = \sin(t), \ t \le 0. \tag{38}$$

The exact solution is as follows:

$$u(t) = \sin(t). \tag{39}$$

Similarly, both the exact and approximate solutions for different number of collocation points are depicted in Figures 4 and 5 and we illustrate the error bound for example 1 in Table 2, where again the improvement of the numerical approximation is clearly shown in the graphical and numerical evidences.

Example 3. Consider the following NDDE

$$\frac{du}{dt} - \frac{1}{2}u'\left(\frac{4}{5}t\right) - \frac{1}{10}u\left(\frac{4}{5}\right) - u(t) + \left(\frac{4}{5}t - \frac{1}{2}\right)e^{\frac{4}{5}t} = e^{-t}, 0 \le t \le 1, \tag{40}$$

where the initial condition for this formulation is given by,

$$u(0) = 0, \ t \le 0. \tag{41}$$

The exact solution is given by,

$$u(t) = te^{-t}. \tag{42}$$

Another graphical and numerical evidences are presented in Figures 6, 7, and Table 3.

Table 2: Some numerical evidences for the errors in example 2, with 28 collocation points.

x	Error bound
0.0178571	2.84662×10^{-14}
0.0535714	2.83601×10^{-14}
0.0892857	2.34596×10^{-14}
0.1250000	2.36812×10^{-14}
0.1607140	2.83169×10^{-14}
0.8035710	1.55746×10^{-13}
0.8392860	1.58554×10^{-13}
0.8750000	1.55258×10^{-13}
0.9107140	1.59703×10^{-13}
0.9464290	1.52353×10^{-13}
0.9821430	1.67129×10^{-12}

Example 4. Consider the following NDDE arising in electrodynamics

$$\frac{du}{dt} - 3\left(t^2 + \frac{t}{6} + 2\right)u\left(\frac{t}{6}\right) = \left(-\frac{t^4}{12} + \frac{193t^3}{360} + \frac{3749t^2}{588} + \frac{30t}{7} - 1\right) - u'(t) - 4(t+2)u\left(\frac{t}{4}\right) + 5tu\left(\frac{t}{5}\right) + 2u\left(\frac{t}{7}\right), \ 0 \le t \le 1, \tag{43}$$

where the initial condition for this formulation is given by,

$$u(0) = 2, \ t \le 0. \tag{44}$$

The exact solution is given by

$$u(t) = 2 + t - t^2. \tag{45}$$

The approximate solution u_e for 7 collocation points is given by

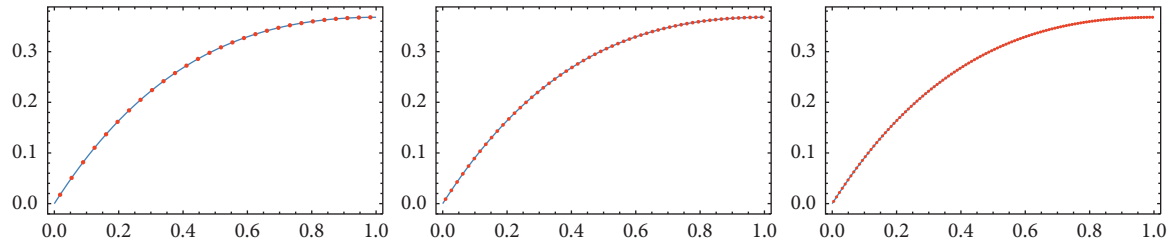

Figure 6: Illustration of Example 3 for the analytical and numerical solution (dots) computed with 28, 56, and 112 collocation points.

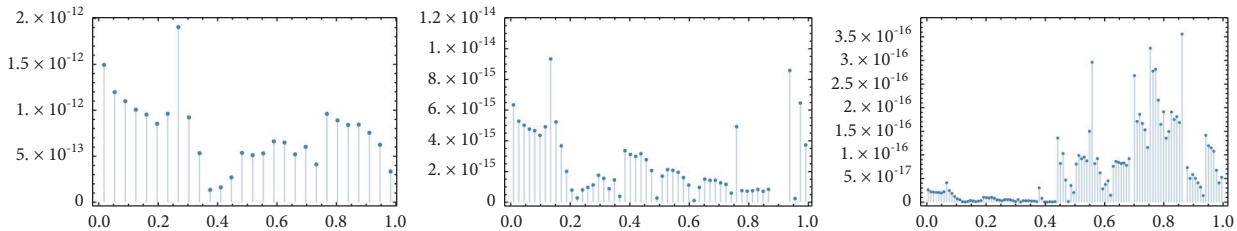

Figure 7: Absolute maximum errors in Example 3 when $M = 3, 4, 5$, respectively.

Table 3: Some numerical evidences for the errors in Example 3, with 28 collocation points.

x	Error bound
0.0178571	1.49479×10^{-12}
0.0535714	1.19775×10^{-12}
0.0892857	1.09876×10^{-12}
0.1250000	1.00640×10^{-12}
0.1607140	9.53904×10^{-13}
0.8035710	8.90010×10^{-13}
0.8392860	8.40772×10^{-13}
0.8750000	8.43603×10^{-13}
0.9107140	7.55229×10^{-13}
0.9464290	6.25056×10^{-13}
0.9821430	3.33067×10^{-12}

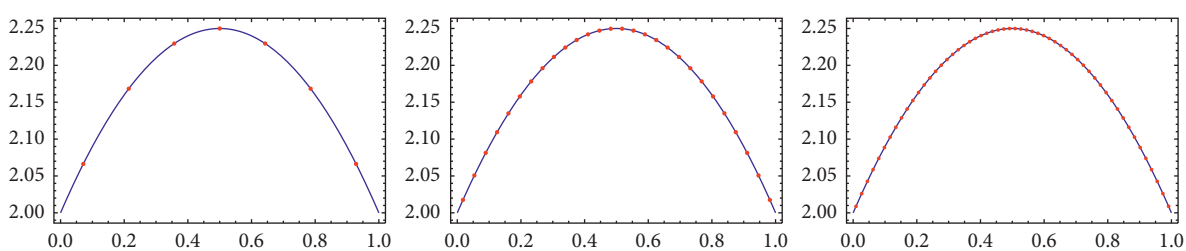

Figure 8: Illustration of example 4 for the analytical and numerical solution (dots) computed with 28, 56, and 112 collocation points.

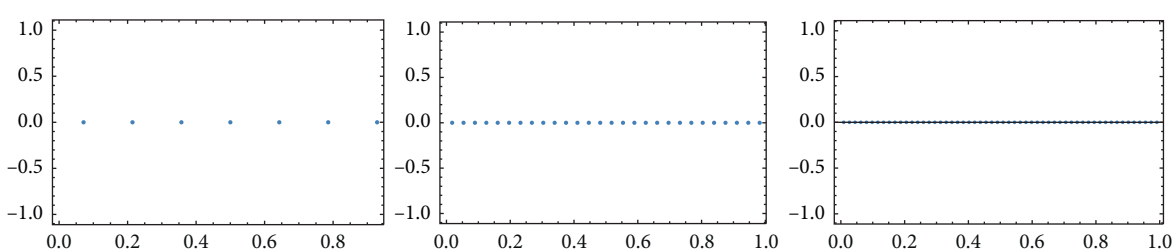

Figure 9: Absolute maximum errors in example 4 when $M = 1, 4, 5$, respectively.

$$u_e(t) = 2 + t - t^2 - 2.14603 \times 10^{-37} t^3 + 6.49387 \times 10^{-37} t^4 - 1.02869 \times 10^{-36} t^5 + 8.05867 \times 10^{-37} t^6 - 2.46105 \times 10^{-37} t^7. \quad (46)$$

Lastly, we depict the graph of the approximate and exact solutions in Figure 8, where the accuracy is presented in Figure 9.

4. Conclusion

In this presented work, a new numerical scheme based on a certain wavelet settings generated by the Euler functions is proposed. The collocation technique has been implemented on the neutral delay differential equations. We demonstrated the Euler wavelet truncated expansions to convert the resulted equations to a system of algebraic equations. We illustrated the work by solving numerically a set of problems, which arise in many scientific areas. The numerical results achieved an exceptional absolute error among other methods known in the literature. The error and approximate solutions of the given problems have been depicted by some figures to show the accuracy of the algorithm.

The main advantage of the presented algorithm is to shed some lights on the use of Euler wavelets and to develop a suitable computational technique for the numerical treatment of neural delay differential equations on a side, and on the effectiveness, efficiency of the technique in the performance, accuracy, and computational cost even with a small number of collocation points, on the other side.

Data Availability

No data were used to support this study.

Conflicts of Interest

The authors declare that they have no conflicts of interest.

Acknowledgments

This study was supported by Zayed University and UAE University Fund # 12S107UAEU-ZU-2022.

References

[1] F. A. Rihan, *Delay Differential Equations and Applications to Biology*, Springer, Berlin, Germany, 2021.

[2] F. A. Rihan, E. H. Doha, M. I. Hassan, and N. M. Kamel, *Numerical Treatments for Volterra Delay Integro-differential Equations*, vol. 9, no. 3, pp. 292–308, 2009.

[3] G. A. Bocharov and F. A. Rihan, "Numerical modeling in biosciences using delay differential equations," *Journal of Computational and Applied Mathematics*, vol. 125, no. 1-2, pp. 183–199, 2000.

[4] Y. Kyrychko and S. Hogan, "On the use of delay equations in engineering applications," *Journal of Vibration and Control*, vol. 16, pp. 943–960, 2010.

[5] V. Kolmanovskii and A. Myshkis, *Introduction to the Theory and Applications of Functional Differential Equations*, Springer, Berlin, Germany, 1999.

[6] D. Nagy, L. Bencsik, and T. Insperger, "Experimental estimation of tactile reaction delay during stick balancing using cepstral analysis," *Mechanical Systems and Signal Processing*, vol. 138, 2020.

[7] C. Jamilla, R. Mendoza, and V. Mendoza, "Explicit solution of a Lotka-Sharpe-McKendrick system involving neutral delay differential equations using the R-Lambert W function," *Mathematical Biosciences and Engineering*, vol. 17, pp. 5686–5708, 2020.

[8] B. Pao, C. Liu, and G. Yin, *Topics in Stochastic Analysis and Nonparametric Estimation*, Science Business Media, New York, 2008.

[9] R. Driver, "Ordinary and delay differential equations," *Applied Mathematical Sciences*, pp. 225–331, Springer-Verlag, New York-Heidelberg, 1977.

[10] K. Gopalsamy, "Stability and oscillations in delay differential equations of population dynamics," *Mathematics and its Applications*, vol. 74, pp. 394–461, Kluwer Academic Publishers Group, Dordrecht, 1992.

[11] E. Lelarsmee, A. Ruehli, and S. Vincentelli, "The waveform relaxation method for time domain analysis of large scale integrated circuits," *IEEE Trans. CAD*, vol. 1, no. 3, pp. 131–145, 1982.

[12] J. Hale, *Theory of Functional Differential Equations*, Springer, NY, USA, 1977.

[13] O. Bazighifan and T. Abdeljawad, "Improved approach for studying oscillatory properties of fourth-order advanced differential equations with p-laplacian like operator," *Mathematics*, vol. 8, no. 5, p. 821, 2020.

[14] A. Bellen and M. Zennaro, "Adaptive integration of delay differential equations," *Advances in time-delay systems*, Springer, Berlin, 2004.

[15] W. Wang, Y. Zhang, and S. Li, "Stability of continuous Runge–Kutta-type methods for nonlinear neutral delay-differential equations," *Applied Mathematical Modelling*, vol. 33, no. 8, pp. 3319–3329, 2009.

[16] M. Maleki and A. Davari, "Analysis of an adaptive collocation solution for retarded and neutral delay systems," *Numerical Algorithms*, vol. 88, pp. 67–91, 2021.

[17] L. Berezansky and E. Braverman, "Asymptotic properties of neutral type linear systems," *Journal of Mathematical Analysis and Applications*, vol. 497, 2021.

[18] M. Mohammad and A. Trounev, "On the dynamical modeling of Covid-19 involving Atangana-Baleanu fractional derivative and based on Daubechies framelet simulations, Chaos," *Solitons & Fractals*, vol. 140, 2020.

[19] M. Mohammad, A. Trounev, and M. Alshbool, "A novel numerical method for solving fractional diffusion-wave and nonlinear fredholm and volterra integral equations with zero absolute error," *Axioms*, vol. 10, no. 3, p. 165, 2021.

[20] M. Mohammad and E. B. Lin, "Gibbs phenomenon in tight framelet expansions," *Communications in Nonlinear Science and Numerical Simulation*, vol. 55, pp. 84–92, 2018.

[21] A. Raza and A. Khan, "Haar wavelet series solution for solving neutral delay differential equations," *Journal of King Saud University Science*, vol. 31, pp. 1070–1076, 2019.

Hindawi
Complexity
Volume 2022, Article ID 1325825, 9 pages
https://doi.org/10.1155/2022/1325825

Research Article

New Statistical Approaches for Modeling the COVID-19 Data Set: A Case Study in the Medical Sector

Mohammed M. A. Almazah,[1,2] **Kalim Ullah**,[3] **Eslam Hussam**,[4] **Md. Moyazzem Hossain**,[5] **Ramy Aldallal**,[6] **and Fathy H. Riad**[7,8]

[1]*Department of Mathematics, College of Sciences and Arts (Muhyil), King Khalid University, Muhyil 61421, Saudi Arabia*
[2]*Department of Mathematics and Computer, College of Sciences, Ibb University, Ibb 70270, Yemen*
[3]*Foundation University Medical College, Foundation University School of Health Sciences, DHA-I, Islamabad 44000, Pakistan*
[4]*Department of Mathematics, Faculty of Science, Helwan University, Cairo, Egypt*
[5]*Department of Statistics, Jahangirnagar University, Savar, Dhaka 1342, Bangladesh*
[6]*Department of Accounting, College of Business Administration in Hawtat Bani Tamim, Prince Sattam bin Abdulaziz University, Saudi Arabia*
[7]*Mathematics Department, College of Science, Jouf University, P. O. Box 2014, Sakaka, Saudi Arabia*
[8]*Department of Mathematics, Faculty of Science, Minia University, Minia 61519, Egypt*

Correspondence should be addressed to Md. Moyazzem Hossain; hossainmm@juniv.edu

Received 26 May 2022; Revised 27 July 2022; Accepted 3 August 2022; Published 19 August 2022

Academic Editor: Fathalla A. Rihan

Statistical distributions have great applicability for modeling data in almost every applied sector. Among the available classical distributions, the inverse Weibull distribution has received considerable attention. In the practice of distribution theory, numerous methods have been studied and suggested/introduced to increase the flexibility level of the traditional probability distributions. In this paper, we implement different distribution methods to obtain five new different versions of the inverse Weibull model. The new modifications of the inverse Weibull model are called the logarithm transformed-inverse Weibull, a flexible reduced logarithmic-inverse Weibull, the weighted TX-inverse Weibull, a new generalized-inverse Weibull, and the alpha power transformed extended-inverse Weibull distributions. To illustrate the flexibility and applicability of the new modifications of the inverse Weibull model, a biomedical data set is analyzed. The data set consists of 108 observations and represents the mortality rate of the COVID-19-infected patients. The practical application shows that the new generalized-inverse Weibull is the best modification of the inverse Weibull distribution.

1. Introduction

In the practice of distribution theory, one of the important tasks is to devise an efficient statistical model for real phenomena of nature. Generally, the statistical distributions are implemented to analyze real-life situations that are uncertain and endangered. For example, the probability distributions are frequently applied to analyze data in (i) engineering and related sectors [1], (ii) healthcare engineering [2], (iii) the economic and financial sector [3], (iv) hydrology [4], (v) education [5], (vi) metrology [6], (vii) biological sector [7], and (viii) sports [8].

Due to the applicability of the probability distributions in applied areas/sectors, numerous approaches (probability models) have been proposed and studied. For example, Afify et al. [9] proposed the MOPG-Weibull distribution for analyzing the engineering data set. For further studies related to the engineering sector (i.e., data modeling in the engineering-related area), we refer to studies by Almarashi et al. [10] and Strzelecki [11].

Klakattawi [12] implemented a new extended Weibull (NE-Weibull) model for statistical analysis of the data sets related to cancer patients. For more studies related to the biomedical/healthcare data sets (i.e., data modeling in the

biomedical-related area), we refer to studies by Ahmad et al. [13]; Plana et al. [14]; Xin et al. [15]; and Martinez et al. [16].

Tung et al. [17] proposed the arcsine-Weibull (ASin-Weibull) distribution for analyzing data sets in the business and financial sectors. For more studies related to the financial data sets (i.e., data modeling in the financial-related area), we refer to studies by Zhao et al. [18]; Alfaro et al. [19]; Abubakar and Sabri [20]; and Rana et al. [21].

Bakouch et al. [22] implemented the Gumbel model for analyzing the hydrology data set. Singh et al. [23] provided the assessment of groundwater quality data in Nigeria. Hassan et al. [24] implemented the truncated power Lomax (TP-Lomax) distribution for analyzing the flood data set. For other studies related to the hydrology data sets, we refer to studies by Karahacane et al. [25]; Dodangeh et al. [26]; and Tegegne et al. [27].

Among the above fields (engineering, education, hydrology, and healthcare sectors), statistical distributions are frequently implemented to analyze the biomedical data sets. Since December 2019, researchers have proposed and implemented new probability models for analyzing and predicting the COVID-19 events (Baleanu et al. [28]; Özköse and Yavuz, *M*. (2022), Khan et al. [29]; Lella and Pja [30]; Mohan et al. [31]; and Singh et al. [32]).

Maurya et al. [33] proposed a new method called the logarithm transformed (LT) family for introducing flexible probability distributions. Let X has the LT family, if its DF (distribution function) $R(x;\psi)$ is

$$R(x;\boldsymbol{\psi}) = 1 - \frac{\log[2 - M(x;\boldsymbol{\psi})]}{\log 2}, \tag{1}$$

where $x \in \mathbb{R}$ and $M(x;\psi)$ is a baseline DF.

Liu et al. [34] introduced a useful method, namely, a FRL-X (flexible reduced logarithmic-X) family for obtaining the modified versions of the existing distributions. Let X has the FRL-X distributions, if its DF $R(x;\beta,\psi)$ is

$$R(x;\boldsymbol{\psi},\beta) = 1 - \frac{\log[1 - \beta M(x;\boldsymbol{\psi}) + \beta]}{\log(\beta + 1)}, \tag{2}$$

where $\beta \in \mathbb{R}^+$ is an additional parameter.

Ahmad et al. [35] proposed another new class of probability distributions, called the weighted T-X (WT-X) family of distributions. The DF $R(x;\psi)$ of the WT-X distributions is

$$R(x;\boldsymbol{\psi}) = 1 - \frac{1 - M(x;\boldsymbol{\psi})}{e^{M(x;\boldsymbol{\psi})}}, \tag{3}$$

with PDF $r(x;\psi)$ given by

$$r(x;\boldsymbol{\psi}) = [2 - M(x;\boldsymbol{\psi})]\frac{m(x;\boldsymbol{\psi})}{e^{M(x;\boldsymbol{\psi})}}, \tag{4}$$

where $m(x;\psi) = d/dxM(x;\psi)$.

Wang et al. [36] studied a NG-X (new generalized-X) family with DF $R(x;\psi,\theta)$, provided by

$$R(x;\boldsymbol{\psi},\theta) = 1 - e^{-M(x;\boldsymbol{\psi})}[1 - M(x;\boldsymbol{\psi})]^{\theta}, \tag{5}$$

where $\theta \in \mathbb{R}^+$ is the additional parameter.

Bo et al. [37] proposed another useful method, namely, the APTEx-X (alpha power-transformed extended-X) family of distributions. The DF $R(x;\psi,\alpha_1)$ of the APTEx-X family is

$$R(x;\boldsymbol{\psi},\alpha_1) = \frac{\alpha_1^{\left(1-\left(1-M(x;\boldsymbol{\psi})/e^{M(x;\boldsymbol{\psi})}\right)\right)} - 1}{\alpha_1 - 1}, \tag{6}$$

where $\alpha_1 \neq 1, \alpha_1 \in \mathbb{R}^+$ is an additional parameter.

In the next section, we obtain different modifications of the inverse Weibull (IW) distribution by implementing the approaches defined in Eqs. (1)–(6). For every new modified form of the IW model, the plots of the PDF are also obtained.

2. Some New Modifications of the Inverse Weibull Distribution

This section offers some new different extensions of the IW distribution by incorporating the well-known approaches described in Section 1. Consider the DF $M(x;\psi)$, PDF $m(x;\psi)$, SF (survival function) $S(x;\psi)$, HF (hazard function) $h(x;\psi)$, and cumulative HF $H(x;\psi)$ of the IW distribution (with parameters $\alpha \in \mathbb{R}^+$ and $\psi \in \mathbb{R}^+$) given by

$$\begin{aligned} M(x;\boldsymbol{\psi}) &= e^{-\psi/x^{\alpha}}, \\ m(x;\boldsymbol{\psi}) &= \frac{\alpha\psi}{x^{\alpha+1}}e^{-(\psi/x^{\alpha})}, \\ S(x;\boldsymbol{\psi}) &= 1 - e^{-(\psi/x^{\alpha})}, \\ h(x;\boldsymbol{\psi}) &= \frac{\left(\alpha\psi/x^{\alpha+1}\right)}{e^{-(\psi/x^{\alpha})}\left(1 - e^{-(\psi/x^{\alpha})}\right)}, \end{aligned} \tag{7}$$

$$H(x;\boldsymbol{\psi}) = -\log\left(1 - e^{-(\psi/x^{\alpha})}\right), \tag{8}$$

respectively, where $\psi = (\alpha,\psi)$.

2.1. The Logarithm Transformed-Inverse Weibull Distribution. Here, we implement the LT family approach (see (1)) to introduce a new version of the IW model. The new version of the IW model is called the logarithmic transformed-inverse Weibull (LT-IW) distribution. The DF of the LT-IW distribution is obtained by using (7) in (1). Let X has the LT-IW model, if its DF is expressed by

$$R(x;\boldsymbol{\psi}) = 1 - \frac{\log\left[2 - e^{-(\psi/x^{\alpha})}\right]}{\log 2}, \quad x \in \mathbb{R}^+, \alpha, \delta \in \mathbb{R}^+. \tag{9}$$

Associating to Eq. (9), the PDF $r(x;\psi)$, SF $\overline{R}(x;\psi)$, and HF $h(x;\psi)$ of the LT-IW model are given by

$$r(x;\psi) = \frac{\left(\alpha\psi/x^{\alpha+1}\right)e^{-\left(\psi/x^{\alpha}\right)}}{(\log 2)\left[2 - e^{-\left(\psi/x^{\alpha}\right)}\right]},$$

$$\overline{R}(x;\psi) = \frac{\log\left[2 - e^{-\left(\psi/x^{\alpha}\right)}\right]}{\log 2}, \tag{10}$$

$$h(x;\psi) = \frac{\left(\alpha\psi/x^{\alpha+1}\right)e^{-\left(\psi/x^{\alpha}\right)}}{\left(\log\left[2 - e^{-\left(\psi/x^{\alpha}\right)}\right]\right)\left[2 - e^{-\left(\psi/x^{\alpha}\right)}\right]}, \tag{11}$$

respectively.

The PDF plots of the LT-IW model are provided in Figure 1. The plots of the LT-IW model in Figure 1 are obtained for $\alpha = 0.2, \psi = 0.5$ (red line), $\alpha = 3.4, \psi = 0.4$ (green line), $\alpha = 2.5, \psi = 0.5$ (black line), and $\alpha = 2.1, \psi = 1.5$ (blue line).

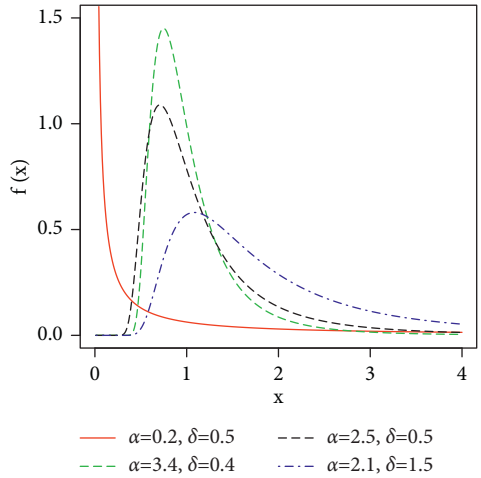

Figure 1: PDF plots of the LT-IW distribution.

2.2. A Flexible Reduced Logarithmic-Inverse Weibull Distribution. Here, we use the FRL-X approach (see (2)) to introduce a novel generalized version of the IW distribution. The new updated form of the IW distribution is called the FRL-IW distribution. The DF of the FRL-IW model is obtained by using Eq. (7) in (2). Let X has the FRL-IW distribution, if its DF is given by

$$R(x;\psi,\beta) = 1 - \frac{\log\left[1 - \beta e^{-\left(\psi/x^{\alpha}\right)} + \beta\right]}{\log(\beta + 1)}, \tag{12}$$

$$x \in \mathbb{R}^{+}, \alpha, \psi, \beta \in \mathbb{R}^{+}.$$

Corresponding to Eq. (12), the PDF $r(x;\beta,\psi)$, SF $\overline{R}(x;\beta,\psi)$, and HF $h(x;\beta,\psi)$ of the FRL-IW model are given by

$$r(x;\beta,\psi) = \frac{\beta\left(\alpha\psi/x^{\alpha+1}\right)e^{-\left(\psi/x^{\alpha}\right)}\left[\log(1+\beta)\right]^{-1}}{\left[1 + \beta - \beta e^{-\left(\psi/x^{\alpha}\right)}\right]},$$

$$\overline{R}(x;\beta,\psi) = \log\left[1 + \beta - \beta e^{-\left(\psi/x^{\alpha}\right)}\right]\left[\log(1+\beta)\right]^{-1}, \tag{13}$$

$$h(x;\beta,\psi) = \frac{\beta\left(\alpha\psi/x^{\alpha+1}\right)e^{-\left(\psi/x^{\alpha}\right)}}{\left(\log\left[1 + \beta - \beta e^{-\left(\psi/x^{\alpha}\right)}\right]\right)\left[1 + \beta - \beta e^{-\left(\psi/x^{\alpha}\right)}\right]}, \tag{14}$$

respectively.

Different plots of $r(x;\beta,\psi)$ of the FRL-IW distribution are presented in Figure 2. The plots of $r(x;\beta,\psi)$ in Figure 2 are obtained for $\alpha = 1.2, \psi = 0.4, \beta = 1.2$ (red line), $\alpha = 3.4$, $\psi = 0.7, \beta = 2.5$ (green line), $\alpha = 2.5, \psi = 0.9, \beta = 2.8$ (black line), and $\alpha = 3.1, \psi = 0.3, \beta = 0.9$ (blue line).

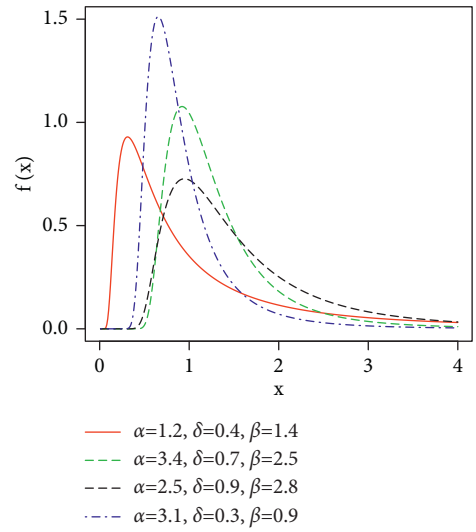

Figure 2: Different plots $r(x;\beta,\psi)$ of the FRL-IW distribution.

2.3. The Weigted TX-Inverse Weibull Distribution. In this section, we apply the WT-X distribution approach to propose a modified version of the IW distribution, called the weighted TX-inverse Weibull (WT X-IW) distribution. The DF of the WT X-IW distribution is obtained by using Eq. (7) in (3). Let X has the WT X-IW model, if its DF is

$$R(x;\psi) = 1 - \frac{1 - e^{-\left(\psi/x^{\alpha}\right)}}{e^{e^{-\left(\psi/x^{\alpha}\right)}}}, \quad x \in \mathbb{R}^{+}, \alpha, \psi \in \mathbb{R}^{+}. \tag{15}$$

In link to (15), the PDF $r(x;\psi)$, SF $\overline{R}(x;\psi)$, and HF $h(x;\psi)$ of the WT X-IW model are given by

$$r(x;\psi) = \left[2 - e^{-\left(\psi/x^{\alpha}\right)}\right]\frac{\left(\alpha\psi/x^{\alpha+1}\right)e^{-\left(\psi/x^{\alpha}\right)}}{e^{e^{-\left(\psi/x^{\alpha}\right)}}},$$

$$\overline{R}(x;\psi) = \frac{1 - e^{-\left(\psi/x^{\alpha}\right)}}{e^{e^{-\left(\psi/x^{\alpha}\right)}}}, \tag{16}$$

$$h(x;\psi) = \left[2 - e^{-\psi/x^{\alpha}}\right]\frac{\left(\alpha\psi/x^{\alpha+1}\right)e^{-\left(\psi/x^{\alpha}\right)}}{1 - e^{-\left(\psi/x^{\alpha}\right)}}, \tag{17}$$

respectively.

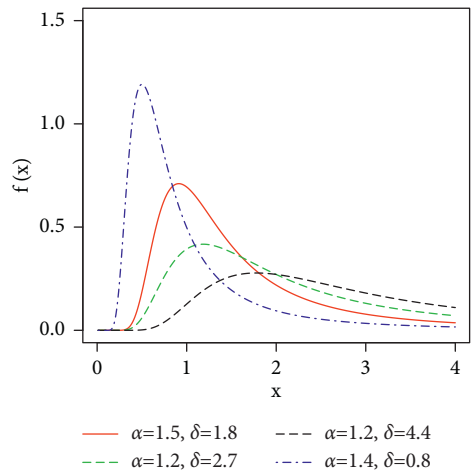

Figure 3: Some possible plots for the PDF of the WTX-IW distribution.

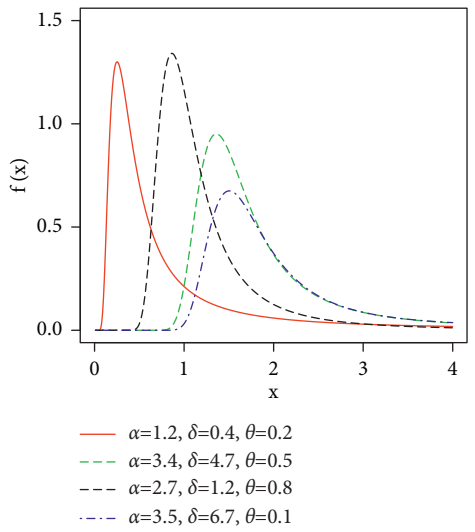

Figure 4: Some possible PDF plots of the NG-IW distribution.

Some possible plots for the PDF of the WTX-IW model are sketched in Figure 3. The plots in Figure 3 are sketched for $\alpha = 1.5, \psi = 1.8$ (red line), $\alpha = 1.2, \psi = 2.7$ (green line), $\alpha = 1.2, \psi = 4.4$ (black line), and $\alpha = 1.4, \psi = 0.8$ (blue line).

2.4. A New Generalized-Inverse Weibull Distribution. In this section, we incorporate a NG-X method and introduce another extended form of the IW distribution. The new extended form of the IW model is called a NG-IW (new generalized-inverse Weibull) model. The DF of the NG-IW model is obtained by using Eq. (7) in (5). Let X has the NG-IW model, if its DF is given by

$$R(x;\theta,\psi) = 1 - \frac{\left[1 - e^{-(\psi/x^{\alpha})}\right]^{\theta}}{e^{e^{-(\psi/x^{\alpha})}}}, \quad x \in \mathbb{R}^{+}, \alpha, \psi, \theta \in \mathbb{R}^{+}. \tag{18}$$

In link to (8), the PDF $r(x;\theta,\psi)$, SF $\overline{R}(x;\theta,\psi)$, and HF $h(x;\theta,\psi)$ of the NG-IW model are, respectively, given by

$$r(x;\theta,\psi) = \frac{\alpha\psi e^{-(\psi/x^{\alpha})}}{x^{\alpha+1}}\left[1 - e^{-(\psi/x^{\alpha})}\right]^{\theta-1}\frac{\left[(1+\theta) - e^{-(\psi/x^{\alpha})}\right]}{e^{e^{-(\psi/x^{\alpha})}}},$$

$$\overline{R}(x;\theta,\psi) = \frac{\left[1 - e^{-(\psi/x^{\alpha})}\right]^{\theta}}{e^{e^{-(\psi/x^{\alpha})}}}, \tag{19}$$

$$h(x;\theta,\psi) = \frac{\alpha\psi e^{-(\psi/x^{\alpha})}}{x^{\alpha+1}\left[1 - e^{-(\psi/x^{\alpha})}\right]}\left[(1+\theta) - e^{-(\psi/x^{\alpha})}\right]. \tag{20}$$

Some possible PDF $r(x;\theta,\psi)$ plots of the NG-IW distribution are sketched in Figure 4. The plots of $r(x;\theta,\psi)$ in Figure 4 are sketched for $\alpha = 1.2, \psi = 0.4, \theta = 0.2$ (red line), $\alpha = 3.4, \psi = 4.7, \theta = 0.5$ (green line), $\alpha = 2.7, \psi = 1.2, \theta = 0.8$ (black line), and $\alpha = 3.5, \psi = 6.7, \theta = 0.1$ (blue line).

2.5. The Alpha Power-Transformed Extended-Inverse Weibull Distribution. This section offers another new extension/generalization of the IW model called the alpha power transformed extended-inverse Weibull (APTE-IW) model. The DF of the APTE-IW distribution is obtained by using Eq. (7) in (6). Let X has the APTE-IW model, if its DF is

$$R(x;\alpha_1,\psi) = \frac{\alpha_1^{\left(1-1-e^{-(\psi/x^{\alpha})}/e^{e^{-(\psi/x^{\alpha})}}\right)} - 1}{\alpha_1 - 1}, \tag{21}$$

$$x \in \mathbb{R}^{+}, \alpha_1 \neq 1, \alpha_1, \alpha, \delta \in \mathbb{R}^{+}.$$

In link to (21), the PDF $r(x;\alpha_1,\psi)$, SF $\overline{R}(x;\alpha_1,\psi)$, and HF $h(x;\alpha_1,\psi)$ of the APTE-IW model are given by

$$r(x;\alpha_1,\psi) = \frac{(\log\alpha)\alpha\psi/x^{\alpha+1}e^{-(\psi/x^{\alpha})}\alpha_1^{\left(1-\left(1-e^{-(\psi/x^{\alpha})}/e^{e^{-(\psi/x^{\alpha})}}\right)\right)}}{(\alpha_1 - 1)\left[2 - e^{-(\psi/x^{\alpha})}\right]^{-1}},$$

$$\overline{R}(x;\alpha_1,\psi) = \frac{\alpha_1 - \alpha_1^{\left(1-\left(1-e^{-(\psi/x^{\alpha})}/e^{e^{-(\psi/x^{\alpha})}}\right)\right)}}{\alpha_1 - 1}, \tag{22}$$

$$h(x;\alpha_1,\psi) = \frac{(\log\alpha)\left(\alpha\psi/x^{\alpha+1}\right)e^{-(\psi/x^{\alpha})}\alpha_1^{\left(1-1-e^{-(\psi/x^{\alpha})}/e^{e^{-(\psi/x^{\alpha})}}\right)}}{\left(\alpha_1 - \alpha_1^{\left(1-1-e^{-(\psi/x^{\alpha})}/e^{e^{-(\psi/x^{\alpha})}}\right)}\right)\left[2 - e^{-(\psi/x^{\alpha})}\right]^{-1}}, \tag{23}$$

respectively.

Some possible PDF $r(x;\alpha_1,\psi)$ plots of the APTE-IW distribution are provided in Figure 5. The plots of $r(x;\alpha_1,\psi)$ in Figure 5 are sketched for $\alpha = 1.2, \psi = 2.1, \theta = 2.2$ (red line), $\alpha = 1.5, \psi = 0.8, \theta = 3.2$ (green line), $\alpha = 1.7, \psi = 1.2, \theta = 3.8$ (black line), and $\alpha = 1.8, \psi = 2.1, \theta = 2.1$ (blue line).

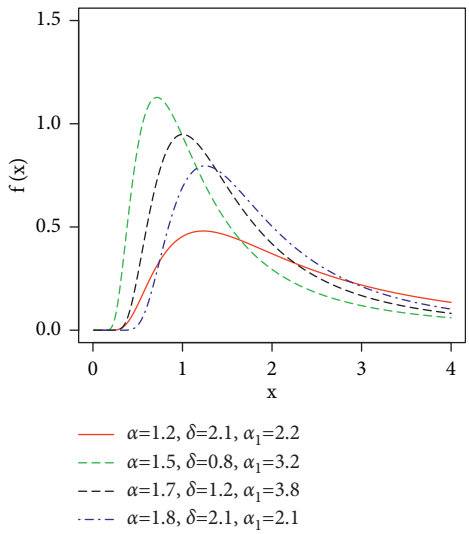

FIGURE 5: Some possible PDF plots of the APTE-IW distribution.

3. Data Analysis

Here, we demonstrate the applicability of the updated versions of the IW distribution. All the proposed updated versions of the IW distribution are applied to a data set concerned with the COVID-19 pandemic. These data are recorded between March 4, 2022, and July 20, 2020 [38].

The considered data set has one hundred eight observations and is given by 1.041, 1.205, 1.402, 1.800, 1.815, 1.923, 2.058, 2.065, 2.070, 2.077, 2.326, 2.352, 2.438, 2.500, 2.506, 2.601, 2.926, 2.988, 3.027, 3.029, 3.215, 3.218, 3.219, 3.228, 3.233, 3.257, 3.286, 3.298, 3.327, 3.336, 3.359, 3.395, 3.440, 3.499, 3.537, 3.632, 3.751, 3.778, 3.922, 4.089, 4.120, 4.292, 4.344, 4.424, 4.557, 4.648, 4.661, 4.697, 4.730, 4.909, 4.949, 5.143, 5.242, 5.317, 5.392, 5.406, 5.442, 5.459, 5.854, 5.985, 6.015, 6.105, 6.122, 6.140, 6.182, 6.327, 6.370, 6.412, 6.535, 6.560, 6.625, 6.656, 6.697, 6.814, 6.968, 7.151, 7.260, 7.267, 7.486, 7.630, 7.840, 7.854, 7.903, 8.108, 8.325, 8.551, 8.696, 8.813, 8.826, 9.284, 9.391, 9.550, 9.935, 10.035, 10.043, 10.158, 10.383, 10.685, 10.855, 11.665, 12.042, 12.878, 13.220, 14.604, 14.962, and 16.498.

The summary values of the COVID-19 data are given by minimum = 1.041, maximum = 16.498, range = 15.457, mean = 5.822, variance = 10.56173, standard derivation- = 3.249882, skewness = 0.9732453, 1^{st} quartile = 3.289, $2^{n\,d}$ quartile or median = 5.279, $3^{r\,d}$ quartile = 7.594, interquartile range = 4.305, and kurtosis = 3.666136. Furthermore, some summary plots of the data set are presented in Figure 6.

Here, we consider four frequently used analytical measures (statistical tests or statistical procedures) to show which probability distribution better fits the biomedical data. These measures are given by the following:

(i) The AIC:

$$\text{AIC} = 2p - 2\pi(\mathbf{\upsilon}). \tag{24}$$

(ii) The BIC:

$$\text{BIC} = p\,\log(m) - 2\pi(\mathbf{\upsilon}). \tag{25}$$

(iii) The CAIC:

$$\text{CAIC} = \frac{2mp}{m-p-1} - 2\pi(\mathbf{\upsilon}). \tag{26}$$

(iv) The HQIC:

$$\text{HQIC} = 2p\,\log(\log(m)) - 2\pi(\mathbf{\upsilon}). \tag{27}$$

In a general sense, the above-mentioned analytical measures are used for comparative analysis. A statistical model that has smaller values of the statistical tests is considered the most suitable model among other competing statistical models.

Table 1 gives the MLEs $(\widehat{\alpha}_{MLE}, \widehat{\psi}_{MLE}, \widehat{\beta}_{MLE}, \widehat{\theta}_{MLE}, \widehat{\alpha_1}_{MLE})$ of the competitive probability models using the COVID-19 data set. The analytical measures for the COVID-19 data using the considered probability models are presented in Table 2.

Based on the reported results in Table 2, it is obvious that the NG-IW model provides the best fit to the biomedical data. For the NG-IW model, the values of the considered test statistics are AIC = 531.7657, CAIC = 532.0010, BIC = 539.7561, and HQIC = 535.0043. Based on the numerical results in Table 2, the second appropriate model is the FRL-IW distribution. For the FRL-IW model, we have AIC = 546.7329, CAIC = 546.9682, BIC = 554.7232, and HQIC = 549.9714. The $3^{r\,d}$ best model is the LT-IW distribution. For the LT-IW model, AIC = 549.0155, CAIC = 549.1321, BIC = 554.3424, and HQIC = 551.1746. The 4^{th} best model is the WTX-IW distribution. For the WTX-IW model, AIC = 551.7866, CAIC = 551.9032, BIC = 557.1135, and HQIC = 553.9457. The 5^{th} best model is the APTE-IW distribution. For the APTE-IW model, AIC = 553.3800, CAIC = 553.6043, BIC = 561.5085, and HQIC = 556.6775.

As we have seen that the NG-IW model provides a close fit to the biomedical data. Therefore, we provide the profiles of the log-likelihood function (LLF) of the NG-IW distribution. Based on the $\widehat{\alpha}_{MLE}$, $\widehat{\psi}_{MLE}$, and $\widehat{\theta}_{MLE}$, the LLF profiles of the NG-IW distribution are obtained in Figure 7. The graphs in Figure 7 confirm the unique values of the $\widehat{\alpha}_{MLE}$, $\widehat{\psi}_{MLE}$, and $\widehat{\theta}_{MLE}$.

After the numerical illustration of the NG-IW model using the COVID-19 data set (see Table 2), next we show visually that the NG-IW model provides the best fit to the COVID-19 data set. For the visual illustration of the NG-IW model, the plots of the fitted PDF $r(x;\widehat{\theta},\widehat{\psi})$, DF $R(x;\widehat{\theta},\widehat{\psi})$, SF $\overline{R}(x;\widehat{\theta},\widehat{\psi})$, HF $h(x;\widehat{\theta},\widehat{\psi})$, cumulative HF $H(x;\widehat{\theta},\widehat{\psi})$, probability-probability (PP), and QQ (quantile-quantile) are obtained in Figure 8. The plots of $r(x;\widehat{\theta},\widehat{\psi})$, $R(x;\widehat{\theta},\widehat{\psi})$, $\overline{R}(x;\widehat{\theta},\widehat{\psi})$, $h(x;\widehat{\theta},\widehat{\psi})$, and $H(x;\widehat{\theta},\widehat{\psi})$ are obtained using the following expressions:

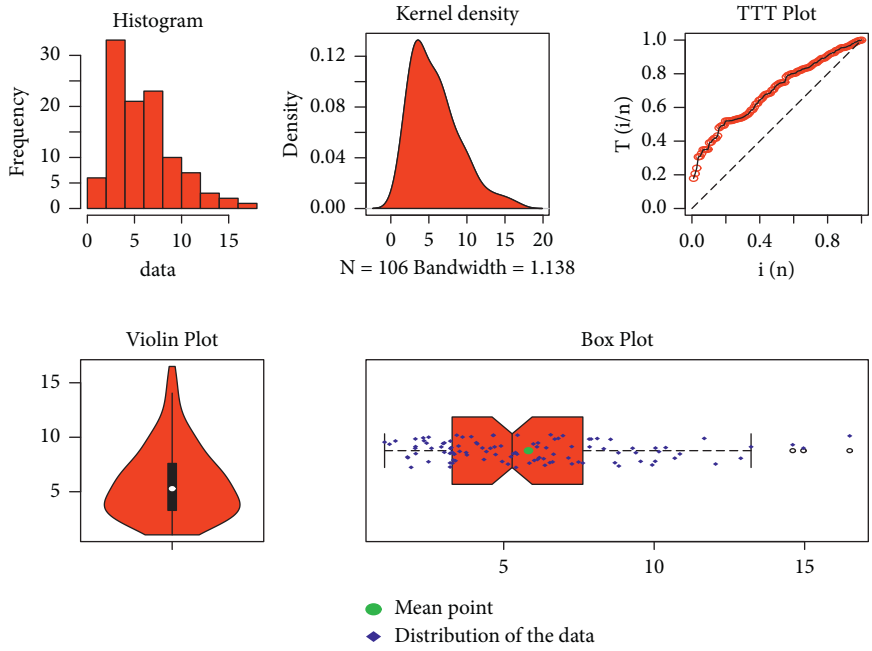

Figure 6: Some summary plots of the COVID-19 data set.

Table 1: The values of the maximum likelihood estimators of the fitted models using the COVID-19 data set.

Distributions	$\widehat{\alpha}$	$\widehat{\psi}$	$\widehat{\beta}$	$\widehat{\theta}$	$\widehat{\alpha}_1$
LT-IW	1.829195	8.721454	—	—	—
FRL-IW	2.291612	8.003594	11.582096	—	—
WTX-IW	1.339224	9.164487	—	—	—
NG-IW	0.705908	8.586715	—	9.655237	—
APTE-IW	0.633391	8.119927	—	—	12.65028

Table 2: The values of the analytical measures of the fitted models using the COVID-19 data set.

Distributions	AIC	CAIC	BIC	HQIC
LT-IW	549.0155	549.1321	554.3424	551.1746
FRL-IW	546.7329	546.9682	554.7232	549.9714
WTX-IW	551.7866	551.9032	557.1135	553.9457
NG-IW	531.7657	532.0010	539.7561	535.0043
APTE-IW	553.3800	553.6043	561.5085	556.6775

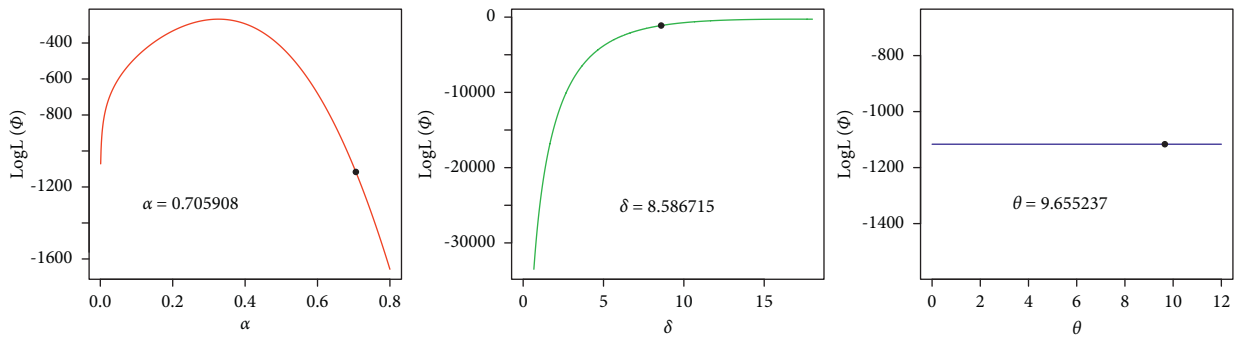

Figure 7: The profiles of the log LF of the NG-IW distribution using the COVID-19 data set.

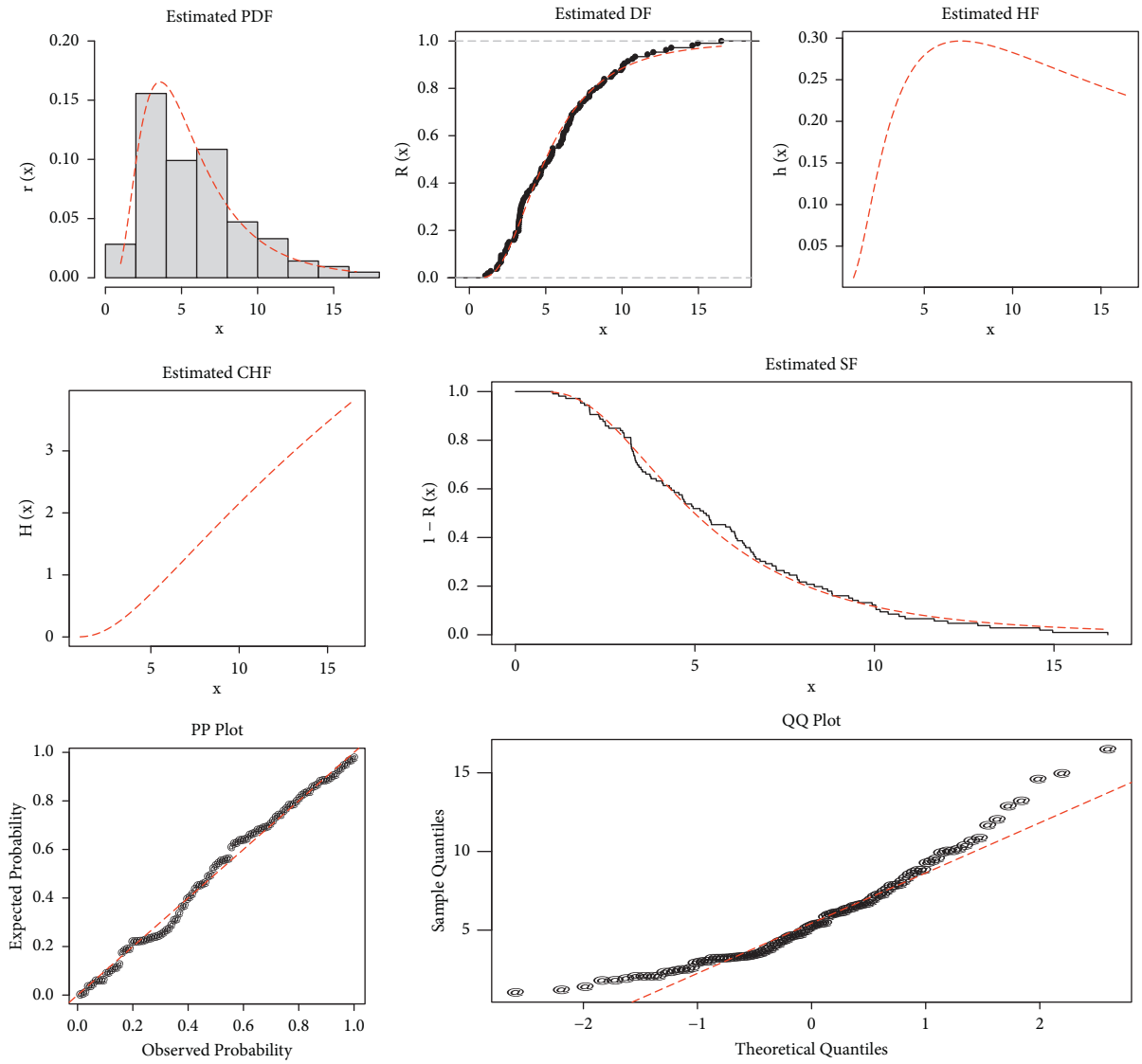

Figure 8: Visual illustration of the NG-IW distribution using the COVID-19 data set.

$$
\begin{aligned}
r(x;\widehat{\theta},\widehat{\psi}) &= \frac{6.061430\, e^{-8.586715/x^{0.705908}}}{x^{1.705908}}\left[1-e^{-8.586715/x^{0.705908}}\right]^{8.655237} \times \frac{\left[(10.655237)-e^{-8.586715/x^{0.705908}}\right]}{e^{e^{-8.586715/x^{0.705908}}}},\\
R(x;\widehat{\theta},\widehat{\psi}) &= 1-\frac{\left[1-e^{-8.586715/x^{0.705908}}\right]^{9.655237}}{e^{e^{-8.586715/x^{0.705908}}}},\\
\overline{R}(x;\widehat{\theta},\widehat{\psi}) &= \frac{\left[1-e^{-8.586715/x^{0.705908}}\right]^{9.655237}}{e^{e^{-8.586715/x^{0.705908}}}},\\
h(x;\theta,\psi) &= \frac{6.061430\, e^{-8.586715/x^{0.705908}}}{x^{1.705908}\left[1-e^{-8.586715/x^{0.705908}}\right]}\left[(10.655237)-e^{-8.586715/x^{0.705908}}\right],
\end{aligned}
\tag{28}
$$

$$
H(x;\widehat{\theta},\widehat{\psi}) = -\log\left(\frac{\left[1-e^{-8.586715/x^{0.705908}}\right]^{9.655237}}{e^{e^{-8.586715/x^{0.705908}}}}\right),
\tag{29}
$$

respectively.

The empirical and fitted plots in Figure 8 reveal that the NG-IW distribution provides a close fit to the COVID-19 data set.

4. Concluding Remarks

In recent times, statistical models have been frequently used to analyze data in applied sectors, such as engineering, hydrology, education, finance, and biomedical sectors. To provide the best description of the phenomena under consideration, a number of statistical models have been introduced and implemented. Among these models, the IW distribution has received considerable attention. Therefore, numerous modifications of the IW distribution have been proposed and applied. In this paper, we introduced five different modifications of the IW distribution for modeling real-life data sets. Finally, the new modified forms of the IW distribution were applied to real-life data taken from the biomedical sector. The practical application showed that the NG-IW distribution was the best candidate model for analyzing the COVID-19 data set.

In the future, we are motivated to implement the LT-IW, FRL-IW, WTX-IW, NG-IW, and APTE-IW models in other applied sectors. Furthermore, the bivariate extensions of the LT-IW, FRL-IW, WTX-IW, NG-IW, and APTE-IW models can also be introduced to deal with the bivariate data sets. Bayesian estimation of the LT-IW, FRL-IW, WTX-IW, NG-IW, and APTE-IW models using different types of censored samples can be discussed [39].

Data Availability

All data are included in the paper.

Conflicts of Interest

The authors declare no conflicts of interest.

Acknowledgments

The first author acknowledges the support of Deanship of Scientific Research at King Khalid University for funding this work through Larg Groups (a project under grant no. RGP.2/34/43).

References

[1] L. Pan, L. Novák, D. Lehký, D. Novák, and M. Cao, "Neural network ensemble-based sensitivity analysis in structural engineering: comparison of selected methods and the influence of statistical correlation," *Computers & Structures*, vol. 242, Article ID 106376, 2021.

[2] E. Gholipour, B. Vizvári, T. Babaqi, and S. Takács, "Statistical analysis of the Hungarian COVID-19 victims," *Journal of Medical Virology*, vol. 93, no. 12, pp. 6660–6670, 2021.

[3] S. Dutta and K. Saini, "Statistical assessment of hybrid blockchain for SME sector," *WSEAS Transactions on Systems and Control*, vol. 16, pp. 83–95, 2021.

[4] B. Moccia, C. Mineo, E. Ridolfi, F. Russo, and F. Napolitano, "Probability distributions of daily rainfall extremes in Lazio and Sicily, Italy, and design rainfall inferences," *Journal of Hydrology: Regional Studies*, vol. 33, Article ID 100771, 2021.

[5] E. Artigao, A. Vigueras-Rodríguez, A. Honrubia-Escribano, S. Martín-Martínez, and E. Gómez-Lázaro, "Wind resource and wind power generation assessment for education in engineering," *Sustainability*, vol. 13, no. 5, p. 2444, 2021.

[6] M. Aslam, "Testing average wind speed using sampling plan for Weibull distribution under indeterminacy," *Scientific Reports*, vol. 11, no. 1, pp. 7532–7539, 2021.

[7] F. A. Rihan, *Delay Differential Equations and Applications to Biology*, Springer, Singapore, 2021.

[8] G. Shengjie, A. Craig, and G. T. Mekiso, "A new alpha power Weibull model for analyzing time-to-event data: a case study from football," *Mathematical Problems in Engineering*, vol. 2022, pp. 1–10, 2022.

[9] A. Z. Afify, D. Kumar, and I. Elbatal, "Marshall–Olkin power generalized Weibull distribution with applications in engineering and medicine," *Journal of Statistical Theory and Applications*, vol. 19, no. 2, pp. 223–237, 2020.

[10] A. M. Almarashi, A. Algarni, and M. Nassar, "On estimation procedures of stress-strength reliability for Weibull distribution with application," *PLoS One*, vol. 15, no. 8, Article ID e0237997, 2020.

[11] P. Strzelecki, "Determination of fatigue life for low probability of failure for different stress levels using 3-parameter Weibull distribution," *International Journal of Fatigue*, vol. 145, Article ID 106080, 2021.

[12] H. S. Klakattawi, "Survival analysis of cancer patients using a new extended Weibull distribution," *PLoS One*, vol. 17, no. 2, Article ID e0264229, 2022.

[13] Z. Ahmad, Z. Almaspoor, F. Khan, and M. El-Morshedy, "On predictive modeling using a new flexible Weibull distribution and machine learning approach: analyzing the COVID-19 data," *Mathematics*, vol. 10, no. 11, p. 1792, 2022.

[14] D. Plana, G. Fell, B. M. Alexander, A. C. Palmer, and P. K. Sorger, "Cancer patient survival can be parametrized to improve trial precision and reveal time-dependent therapeutic effects," *Nature Communications*, vol. 13, no. 1, pp. 873–913, 2022.

[15] Y. Xin, Y. Zhou, and G. T. Mekiso, "A New Generalized-Family for Analyzing the COVID-19 Data Set: a Case Study," *Mathematical Problems in Engineering*, p. 1, Article ID 1901526, 2022.

[16] E. Z. Martinez, B. C. L. de Freitas, J. A. Achcar, D. C. Aragon, and M. V. de Oliveira Peres, "Exponentiated Weibull models applied to medical data in presence of right-censoring, cure fraction and covariates. Statistics," *Optimization & Information Computing*, vol. 10, no. 2, pp. 548–571, 2022.

[17] Y. Liang Tung, Z. Ahmad, and E. Mahmoudi, "The arcsine-X family of distributions with applications to financial sciences," *Computer Systems Science and Engineering*, vol. 39, no. 3, pp. 351–363, 2021.

[18] W. Zhao, S. K. Khosa, Z. Ahmad, M. Aslam, and A. Z. Afify, "Type-I heavy tailed family with applications in medicine, engineering and insurance," *PLoS One*, vol. 15, no. 8, Article ID e0237462, 2020.

[19] N. M. Alfaer, A. M. Gemeay, H. M. Aljohani, and A. Z. Afify, "The extended log-logistic distribution: inference and actuarial applications," *Mathematics*, vol. 9, no. 12, p. 1386, 2021.

[20] H. Abubakar and S. R. M. Sabri, "A simulation study on modified Weibull distribution for modelling of investment return," *Pertanika Journal of Science & Technology*, vol. 29, no. 4, pp. 2767–2790, 2021.

[21] M. S. Rana, S. H. Shahbaz, M. Q. Shahbaz, and M. M. Rahman, "Pareto-weibull distribution with properties and applications: a member of pareto-X family," *Pakistan Journal of Statistics and Operation Research*, vol. 18, pp. 121–132, 2022.

[22] H. S. Bakouch, C. Chesneau, and O. A. Elsamadony, "The Gumbel kernel for estimating the probability density function with application to hydrology data," *Journal of Digital Information Management*, vol. 3, no. 4, pp. 261–269, 2021.

[23] V. V. Singh, A. A. Suleman, A. Ibrahim, U. A. Abdullahi, and S. A. Suleiman, "Assessment of probability distributions of groundwater quality data in Gwale area, north-western Nigeria," *Annals of Optimization Theory and Practice*, vol. 3, no. 1, pp. 37–46, 2020.

[24] A. S. Hassan, M. A. Sabry, and A. M. Elsehetry, "Truncated power Lomax distribution with application to flood data," *Journal of Statistics Applications & Probability*, vol. 9, pp. 347–359, 2020.

[25] H. Karahacane, M. Meddi, F. Chebana, and H. A. Saaed, "Complete multivariate flood frequency analysis, applied to northern Algeria," *Journal of Flood Risk Management*, vol. 13, no. 4, Article ID e12619, 2020.

[26] E. Dodangeh, V. P. Singh, B. T. Pham, J. Yin, G. Yang, and A. Mosavi, "Flood frequency analysis of interconnected rivers by copulas," *Water Resources Management*, vol. 34, no. 11, pp. 3533–3549, 2020.

[27] G. Tegegne, A. M. Melesse, D. H. Asfaw, and A. W. Worqlul, "Flood frequency analyses over different basin scales in the Blue Nile River basin, Ethiopia," *Hydrology*, vol. 7, no. 3, p. 44, 2020.

[28] D. Baleanu, M. Hassan Abadi, A. Jajarmi, K. Zarghami Vahid, and J. J. Nieto, "A new comparative study on the general fractional model of COVID-19 with isolation and quarantine effects," *Alexandria Engineering Journal*, vol. 61, no. 6, pp. 4779–4791, 2022.

[29] M. A. Khan, R. Khan, F. Algarni, I. Kumar, A. Choudhary, and A. Srivastava, "Performance evaluation of regression models for COVID-19: a statistical and predictive perspective," *Ain Shams Engineering Journal*, vol. 13, no. 2, Article ID 101574, 2022.

[30] K. K. Lella and A. Pja, "Automatic diagnosis of COVID-19 disease using deep convolutional neural network with multi-feature channel from respiratory sound data: cough, voice, and breath," *Alexandria Engineering Journal*, vol. 61, no. 2, pp. 1319–1334, 2022.

[31] S. Mohan, A. Abugabah, A. Abugabah et al., "An approach to forecast impact of Covid-19 using supervised machine learning model," *Software: Practice and Experience*, vol. 52, no. 4, pp. 824–840, 2022.

[32] P. Singh and A. Gupta, "Generalized SIR (GSIR) epidemic model: an improved framework for the predictive monitoring of COVID-19 pandemic," *ISA Transactions*, vol. 124, pp. 31–40, 2022.

[33] S. K. Maurya, A. Kaushik, R. K. Singh, S. K. Singh, and U. Singh, "A new method of proposing distribution and its application to real data," *Imperial Journal of Interdisciplinary Research*, vol. 2, no. 6, pp. 1331–1338, 2016.

[34] Y. Liu, M. Ilyas, S. K. Khosa et al., "A flexible reduced logarithmic-X family of distributions with biomedical analysis," *Computational and Mathematical Methods in Medicine*, vol. 2020, p. 1, 2020.

[35] Z. Ahmad, E. Mahmoudi, G. G. Hamedani, and O. Kharazmi, "New methods to define heavy-tailed distributions with applications to insurance data," *Journal of Taibah University for Science*, vol. 14, no. 1, pp. 359–382, 2020.

[36] W. Wang, Z. Ahmad, O. Kharazmi, C. B. Ampadu, E. H. Hafez, and M. M. Mohie El-Din, "New generalized-x family: modeling the reliability engineering applications," *PLoS One*, vol. 16, no. 3, Article ID e0248312, 2021.

[37] W. Bo, Z. Ahmad, A. R. Alanzi, A. I. Al-Omari, E. H. Hafez, and S. F. Abdelwahab, "The current COVID-19 pandemic in China: an overview and corona data analysis," *Alexandria Engineering Journal*, vol. 61, no. 2, pp. 1369–1381, 2022.

[38] H. M. Almongy, E. M. Almetwally, H. M. Aljohani, A. S. Alghamdi, and E. H. Hafez, "A new extended Rayleigh distribution with applications of COVID-19 data," *Results in Physics*, vol. 23, Article ID 104012, 2021.

[39] F. Özköse and M. Yavuz, "Investigation of interactions between COVID-19 and diabetes with hereditary traits using real data: a case study in Turkey," *Computers in Biology and Medicine*, vol. 141, Article ID 105044, 2022.

Hindawi
Complexity
Volume 2022, Article ID 8961352, 8 pages
https://doi.org/10.1155/2022/8961352

Research Article

An Analysis of the Theta-Method for Pantograph-Type Delay Differential Equations

Fathalla A. Rihan[1] **and Ahmed F. Rihan**[2]

[1]*Department of Mathematical Sciences, College of Science, United Arab Emirats University, Al-Ain 15551, UAE*
[2]*Department of Electrical Engineering, College of Engineering, United Arab Emirates University, Al-Ain 15551, UAE*

Correspondence should be addressed to Fathalla A. Rihan; frihan@uaeu.ac.ae

Received 26 May 2022; Accepted 25 July 2022; Published 13 August 2022

Academic Editor: Ning Cai

The pantograph equation arises in electrodynamics as a delay differential equation (DDE). In this article, we provide the ϑ-method for numerical solutions of pantograph equations. We investigate the stability conditions for the numerical schemes. The theoretical results are verified by numerical simulations. The theoretical results and numerical simulations show that implicit or partially implicit ϑ-methods, with $\vartheta > (1/2)$, are effective in resolving stiff pantograph problems.

1. Introduction

Pantograph equations are a special kind of functional differential equations with proportional delays [1]. The name pantograph was derived in 1971 from the work of Ockendon and Tayler [2]. Over the past few years, pantograph equations have gained increasing importance in the investigation of various scientific models. These arise in industrial applications and in a variety of fields of pure and applied mathematics, such as electrodynamics, control systems, number theory, probability, and quantum mechanics. Since most of these types of differential equations cannot be solved analytically, researchers have developed numerical methods to solve them. There are a lot of research articles in the solution methods of pantograph equations, such as the exponential approximation [3], Taylor method [4], collocation method using Hermite polynomials [5], and improved Morgan-Voyce collocation method [6]. Legendre wavelet solutions are discussed in [7], and homotopy perturbation method is examined in Ref. [8]. The variational iteration method is discussed in Ref. [9], and the homotopy analysis method is discussed in Ref. [10]. The authors in Ref. [11] discuss the modified Chebyshev collocation method for pantograph equations. A pseudospectral method based on the Legendre principle is examined in Ref. [12], and a modified procedure based on the residual power series method is explored in [13]. Other spectral methods and recent research about numerical treatments of pantograph equations exist in Refs. [14–17].

Despite the fact that there are several polynomial approximation methods, such as spectral and pseudospectral methods, a comprehensive study of step methods for solving pantograph delay differential equations is lacking. In this article, we present some numerical schemes using the ϑ-method to solve pantograph equations numerically and stability conditions for such schemes. Although the maximum order of ϑ-methods is 2, the numerical schemes are very suitable and effective for pantograph equations in a long-run time interval [18–20].

The general delay differential equations (DDEs) take the following form:

$$y'(t) = \mathscr{F}(t, y(t), y(\gamma(t))), \quad t \geq t_0,\ y(t) = \psi(t),\ t \leq t_0, \tag{1}$$

where $\mathscr{F}$: $[t_0, +\infty) \times \mathbb{C}^n \times \mathbb{C}^n \longrightarrow \mathbb{C}^n$ and $y(t)$: $[t_0, +\infty) \times \mathbb{R}^+ \longrightarrow \mathbb{C}^n$. Time delay can be a constant, time-dependent, or state-dependent. A classic case that has been discussed in many papers is when $\gamma(t) = t - \tau$, and τ is positive. The pantograph equations are functional differential equations

whose delays are proportional, where $0 \le \gamma(t) \le t$, $\gamma(0) = 0$. Differential equations with variable or proportional delays are more difficult to solve numerically than equations with constant delays.

The purpose of this article is to consider a nonlinear pantograph type of DDE:

$$\begin{aligned} y'(t) &= \mathscr{F}(t, y(t), y(\lambda t)), \quad t \ge t_0,\ \lambda \in (0,1), \\ y(t) &= \psi(t), \quad t \in [\lambda t_0, t_0]. \end{aligned} \tag{2}$$

The lag function $\gamma(t) = \lambda t$, and $\psi \in [\lambda t_0, t_0]$ is a continuous initial function. We remark that this kind of equation plays an interesting role in modeling many phenomena including biological and nonlinear dynamical systems. Considering the numerical aspect, it is important to identify how the numerical methods preserve the qualitative behavior of the analytic solutions. Herein, we investigate the stability properties of ϑ-methods when applied to pantograph delay differential equations.

This study is organized as follows. Analytical stability conditions are discussed in Section 2. In Section 3, we provide continuous ϑ-methods for the pantograph equation. Numerical stability analysis and conditions of the asymptotic stability are discussed in Section 4. Some numerical simulations showing the effectiveness of the theoretical results are provided in Section 5, and concluding remarks are given in Section 6.

2. Nonlinear Stability

One of the important characteristics of differential equation (2) is the sensitivity of a particular solution to small changes in the "parameters," which occur in the equation, or in the "initial conditions," that gives rise to a definition of stability. If we consider another system, defined by the same function $\mathscr{F}(t, u(t), u(\lambda t))$ of (2) but with another initial condition, then

$$\begin{aligned} u'(t) &= \mathscr{F}(t, u(t), u(\lambda t)), \quad t \ge t_0, \\ u(t) &= \phi(t), \quad t \in [\lambda t_0, t_0]. \end{aligned} \tag{3}$$

$y_0 \ne u_0$. Assume that $\langle u, v \rangle$ is the inner product of vectors $u, v \in \mathbb{C}^N$, such that $\|u\| = \langle u, u \rangle^{1/2}$.

Definition 1. The solution of (1) is asymptotically stable, with respect to perturbing the initial function, if $\|y(t) - u(t)\| \longrightarrow 0$ for $t \longrightarrow \infty$. The solution ξ-exponentially stable (or algebraically decay [19]) if $\|y(t) - u(t)\| \le Ke^{-\xi(t-t_0)}$, where $\xi > 0$ (see [1], Chapter 3).

Theorem 1 (Halanay inequality [21]). *Suppose that $\alpha > \beta > 0$ and $p(t)$ be a continuous nonnegative function on $[\lambda t_0, t_0)$ satisfying the inequality:*

$$p'(t) \le -\alpha p(t) + \beta \sup_{\lambda t \le s \le t} p(s), \quad t \ge t_0. \tag{4}$$

Then,

$$p(t) \le Ge^{-\xi(t-t_0)}, \quad t \ge t_0, \tag{5}$$

where $G = sup_{\lambda t_0 \le t \le t_0} p(t)$ (depends on the initial condition), and ξ is the unique positive solution of

$$\mathscr{H}(\xi) := \xi - \alpha + \beta e^{\xi(1-\lambda)}. \tag{6}$$

Theorem 2. *The solution of (1) is ξ-exponentially stable (algebraically decay) if*

$$\rho_1(t) + q\rho_2(t) \le 0, \quad 0 \le q < 1, \tag{7}$$

where

$$\begin{aligned} \rho_1(t) &\ge \sup_{\substack{u, y, \widetilde{y} \in \mathbb{C}^n \\ y \ne \widetilde{y}}} \frac{\mathrm{Re}\langle (\mathscr{F}(t, y, u) - \mathscr{F}(t, \widetilde{y}, u), y - \widetilde{y}) \rangle}{\|y - \widetilde{y}\|^2}, \\ \rho_2(t) &\ge \sup_{\substack{y, u, \widetilde{u} \in \mathbb{C}^n \\ u \ne \widetilde{u}}} \frac{\|\mathscr{F}(t, y, u) - \mathscr{F}(t, y, \widetilde{u})\|}{\|u - \widetilde{u}\|}. \end{aligned} \tag{8}$$

Proof. Assume for the inner product $\langle ., . \rangle$ on $\mathbb{C}^n$ such that (6) holds. For every $t \ge t_0$, we have (see [22])

$$\begin{aligned} \frac{1}{2}\frac{\mathrm{d}}{\mathrm{d}t}\|y(t) - u(t)\|^2 &= \mathrm{Re}\langle y'(t) - u'(t), y(t) - u(t) \rangle \\ &= \mathrm{Re}\langle \mathscr{F}(t, y(t), y(\lambda t)) \\ &\quad - \mathscr{F}(t, u(t), u(\lambda t)), y(t) - u(t) \rangle \\ &= \mathrm{Re}\langle \mathscr{F}(t, y(t), y(\lambda t)) \\ &\quad - \mathscr{F}(t, y(t), u(\lambda t)), y(t) - u(t) \rangle \\ &\quad + \mathrm{Re}\langle \mathscr{F}(t, y(t), u(\lambda t)) \\ &\quad - \mathscr{F}(t, u(t), u(\lambda t)), y(t) - u(t) \rangle. \end{aligned} \tag{9}$$

It follows from the definitions of $\rho_1(t)$ and $\rho_2(t)$, and from the Schwartz inequality that

$$\begin{aligned} \frac{1}{2}\frac{\mathrm{d}}{\mathrm{d}t}\|y(t) - u(t)\|^2 &\le \rho_1(t)\|y(t) - u(t)\|^2 \\ &\quad + \|\mathscr{F}(t, y(t) \\ &\le \rho_1(t)\|y(t) - u(t)\|^2 + \rho_2(t)\|y(\lambda t) \\ &\quad - u(\lambda t)\|\|y(t) - u(t)\|. \end{aligned} \tag{10}$$

Define

$$Y(t) := \|y(t) - u(t)\|. \tag{11}$$

Note that $Y(t) > 0$ for every $t > t_0$ because we assume that the function f is such that (2) has unique solution $y(t)$ for every initial condition $y(t_0) = y_0$. Then,

$$\frac{1}{2}\frac{\mathrm{d}}{\mathrm{d}t}\|y(t)-u(t)\|^2 = \|y(t)-u(t)\|\frac{\mathrm{d}}{\mathrm{d}t}\|y(t)-u(t)\| = Y(t)Y'(t), \tag{12}$$

so we have

$$Y(t)Y'(t) \le \rho_1(t)Y^2(t) + \rho_2(t)\|Y(\lambda t)\|Y(t), \tag{13}$$

and hence,

$$Y'(t) \le \rho_1(t)Y(t) + \rho_2(t)\sup_{\lambda t\le s\le t} Y(s). \tag{14}$$

Applying Theorem 1 to the above inequality yields the following:

$$Y(t) \le \mathrm{G}e^{-\xi(t-t_0)}, \quad t \ge t_0. \tag{15}$$

Here, G depends only on the initial conditions $\|\psi(t)-\phi(t)\|$. □

Corollary 1. *For the scalar linear case, let* $\mathscr{F}(t, y(t), y(\lambda t)) = \alpha y(t) + \beta y(\lambda t)$. *Then, the solution of* $y'(t) = \alpha y(t) + \beta y(\lambda t)$, *with* $\rho_1(t) = Re(\alpha)$ *and* $\rho_2(t) = |\beta|$, *is algebraically asymptotically stable (see [23]).*

3. Continuous ϑ-Methods for Pantograph Equations

Here, we study a discretization of pantograph equation (2). Let $0 < \lambda < 1$ be a positive real and $\mathscr{T} \equiv \{t_0, t_1, \ldots, t_n, \ldots\}$ be the assigned mesh points, with the property that $t_n \longrightarrow \infty$ as $n \longrightarrow \infty$. Let $h_n = t_{n+1} - t_n$, where $n = 0, 1, \ldots$. be the nonconstant step-size. We divide the whole interval if the solution $[0, T)$ into bounded subintervals

$$I_k = \left(\lambda^{-k}r, \lambda^{-k-1}r\right], \quad k \ge 0,\ r \text{ is a positive integer.} \tag{16}$$

We then partition any of them into a fixed number m of subintervals of the same size using the grid points, such that

$$0 = t_0 < t_l < t_2 < \cdots < t_p = r < t_{p+1} < \cdots < t_{p+m} = \lambda^{-1}r, \quad t_{p+(k+1)m} = \lambda^{-k-1}r,\ k = 0, 1, \ldots \tag{17}$$

Let $\widetilde{y}_n$ denote an approximate to the exact solution $y(t)$ of (2) at t_n. Then, applying the linear ϑ-method to (2) yields

$$\widetilde{y}_{n+1} = \widetilde{y}_n + h_n\left[\vartheta\mathscr{F}\left(t_{n+1}, \widetilde{y}_{n+1}, \widehat{y}\left(\lambda t_{n+1}\right)\right) + (1-\vartheta)\mathscr{F}\left(t_n, \widetilde{y}_n, \widehat{y}\left(\lambda t_n\right)\right)\right], \tag{18}$$

where $\widehat{y}(t)$ extends the values of the numerical solution to nonmesh points. Since, for $\lambda \in (0, 1)$, it is usually the case that $\lambda t_n \notin \mathscr{T}$, we shall then require a densely defined approximation via linear interpolation:

$$\widehat{y}(t) = \frac{t_{n+1}-t}{h_n}\widetilde{y}_n + \frac{t-t_n}{h_n}\widetilde{y}_{n+1}, \quad t_n \le t < t_{n+1},\ n = 0, 1. \ldots. \tag{19}$$

To find the solution at nonmesh points, assuming a uniform constant step-size $h_n = h$, we have dense outputs for $y(\lambda t)$:

$$\widehat{y}(\lambda t_n) = (\lfloor \lambda n\rfloor + 1 - \lambda n)y_{\lfloor \lambda n\rfloor} + (\lambda n - \lfloor \lambda n\rfloor \lambda n)y_{\lfloor \lambda n\rfloor+1}\ n = 0, 1. \ldots, \tag{20}$$

where $\lfloor . \rfloor$ is denoting the integer part, so that $t_{\lfloor \lambda n\rfloor} < \lambda t_n < t_{\lfloor \lambda n\rfloor+1}$. Furthermore, we define the global mesh by partitioning every primary interval into a fixed number m of subintervals of the same size, so that the mesh points are defined by the following recursion formula:

$$h_{n+1} = \frac{1-\lambda}{m\lambda^{\lfloor n/m\rfloor+1}}, \quad n = 0, 1, \ldots, \text{ with grid } t_n = \lambda^{-1}t_{n-m},\ n > m. \tag{21}$$

Therefore, when $\vartheta = 1$, it corresponds to the so-called backward (or implicit) Euler method. However, when $\vartheta = 0$, it corresponds to the forward method. Both of them are of 1–stage RK methods. Normally, the order of ϑ methods is 1, but for $\vartheta = 1/2$, which corresponds to the trapezium rule method, the order is 2.

Consider the following scalar linear pantograph equation:

$$y'(t) = \alpha y(t) + \beta y(\lambda t), \quad \lambda \in (0, 1),\ t > t_0, \qquad y(t) = \psi(t), \quad \lambda t_0 \le t \le t_0. \tag{22}$$

Applying the ϑ– method for (22), with a constant step-size $h = t_{n+1} - t_n$, yields

$$\widetilde{y}_{n+1} - \widetilde{y}_n = \alpha h\left[\vartheta\widetilde{y}_{n+1} + (1-\vartheta)\widetilde{y}_n\right] + \beta h\left[\vartheta\widetilde{y}_{n+1-m} + (1-\vartheta)\widetilde{y}_{n-m}\right]. \tag{23}$$

This generates the sequence $\{\widetilde{y}_n\}_{n\ge 1}$, when given $\widetilde{y}_{-\ell} = \psi(\lambda(\ell h - t_0))$, for $\ell \in \{0, 1, \ldots, N\}$.

We also should mention that, in both analytical and numerical terms, delay differential equations with infinite lags and those with finite lags exhibit remarkable differences [24]. Let us compare (22) with the DDE:

$$y'(t) = \alpha y(t) + \beta y(t-\tau), \quad \tau \in (0, \infty). \tag{24}$$

Solution to (22) is an analytic function on $[0, \infty)$, while solution to (24) is initially nonsmooth and becomes smoother as t increases. The solution of (22) decays algebraically, whereas the solution of (24) decays exponentially (see [18, 25, 26]).

4. Numerical Stability

In this section, we can use the discrete Halanay inequality [21] to examine the stability conditions of the discrete schemes for linear pantograph (22).

Theorem 3. *Given* $\alpha + |\beta| < 0$ *and* ξ_h *is the solution of the characteristic equations (see [21]):*

$$\xi_h^{m+1} - (1-\alpha h)\xi_h^m - \beta h = 0, \tag{25}$$

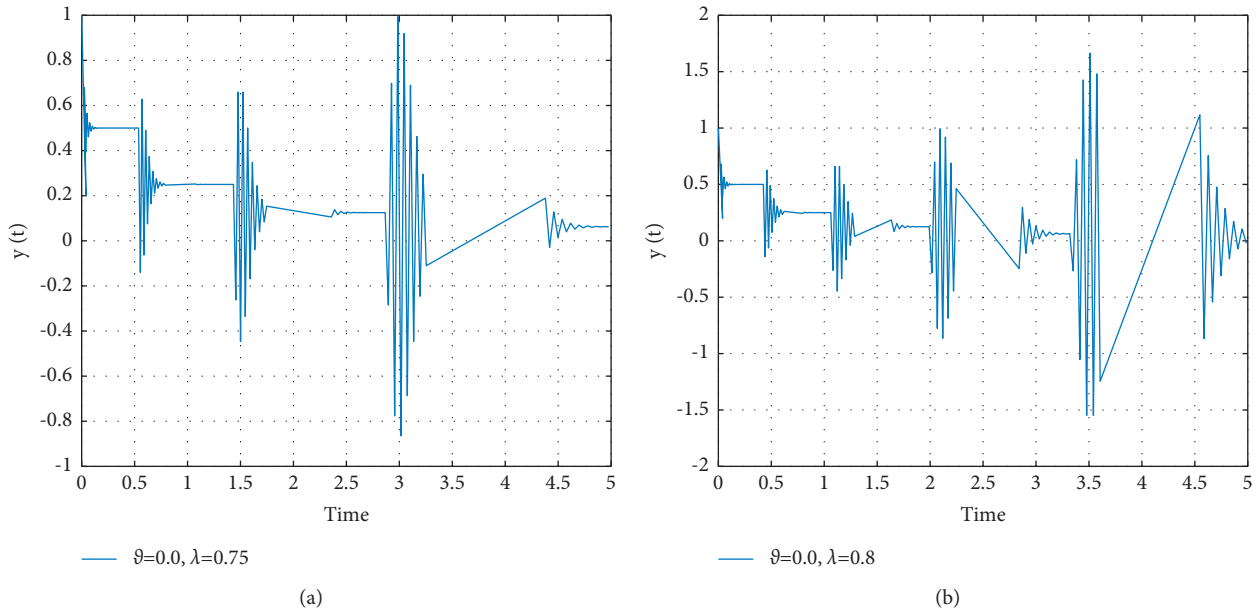

Figure 1: Numerical simulations of model (36) when $\vartheta = 0$, and $\lambda = 0.75$ (a), $\lambda = 0.8$ (b).

where $m \in \mathcal{N}$ is a positive integer number, and $0 < \alpha h < 1$. Assume that $\{\widetilde{p}_n\}_{-m}^{\infty}$ is a sequence, satisfying numbers satisfies the recurrence relation:

$$\frac{\widetilde{z}_{n+1} - \widetilde{z}_n}{h} \leq -\alpha_h \widetilde{z} + \beta_h \max_{\ell \in \mathcal{T}} \widetilde{z}_{n-\ell}, \quad \text{for } n \in \mathbb{N}, \tag{26}$$

where $0 \leq \beta_h < \alpha_h, 0 < \alpha_h h < 1$. Then, $\widetilde{z}_n \leq \mathcal{G}_h e^{-\xi_h (t_n - t_0)}$, where $\xi_h > 0$ are the values that occur in (25) and $\mathcal{G}_h \max_{\ell \in \mathcal{T}} \widetilde{p}\ell$.

4.1. Stability of ϑ–Method. From the auxiliary polynomial, it is possible to compute (asymptotic) stability regions of recurrence relations (23):

$$\xi^{m+1} - \varrho_0 \xi^m - \varrho_1 \xi - \varrho_2 = 0, \tag{27}$$

where

$$\begin{aligned} \varrho_0 &= \frac{1 + (1 - \vartheta)\alpha h}{1 - \vartheta \alpha h}, \\ \varrho_1 &= \frac{\vartheta \beta h}{1 - \vartheta \alpha h}, \\ \varrho_2 &= \frac{(1 - \vartheta)\beta h}{1 - \vartheta \alpha h}, \end{aligned} \tag{28}$$

$$1 - \vartheta \alpha h \neq 0,$$

such that the roots of (27) must satisfy the condition $|\xi_i| < 1$.

A small perturbation in the initial conditions $\{\widetilde{y}_{-\ell}\}_{\ell \in \mathcal{T}}$ in (23) leads to a consequence variation $\{\delta \widetilde{y}_\ell\}_{\ell \geq 1}$, satisfying

$$\delta \widetilde{y}_{n+1} = \varrho_0 \delta \widetilde{y}_n + \varrho_1 \delta \widetilde{y}_{n+1-m} + \varrho_2 \delta \widetilde{y}_{n-m}, \quad n \geq 0. \tag{29}$$

One can get [22].

$$\begin{aligned} \delta \widetilde{y}_{n+1}^2 - \delta \widetilde{y}_n^2 = {} & \left(\varrho_0^2 - 1\right)\delta \widetilde{y}_n^2 + 2\varrho_0 \varrho_1 \delta \widetilde{y}_n^2 \delta \widetilde{y}_{n+1-m}^2 + 2\varrho_0 \varrho_2 \delta \widetilde{y}_n^2 \delta \widetilde{y}_{n-m}^2 \\ & + 2\varrho_1 \varrho_2 \delta \widetilde{y}_{n+1-m}^2 \delta \widetilde{y}_{n-m}^2 + \varrho_1^2 \delta \widetilde{y}_{n+1-m}^2 + \varrho_2^2 \delta \widetilde{y}_{n-m}^2. \end{aligned} \tag{30}$$

If $\mathcal{U}V \neq 0$, then $|\mathcal{S}UV| \leq 1/2(\mathcal{U}^2 + \mathcal{S}^2\mathcal{V}^2)$, with equally if $\mathcal{S} = \mathcal{U}/\mathcal{V}v$. Thus, $|\mathcal{U}V| = \inf_{\mathcal{S} \in (0,\infty)} (1/2\mathcal{S})\ (\mathcal{U}^2 + \mathcal{S}^2\mathcal{V}^2) \leq ((\mathcal{U}^2/r) + r\mathcal{V}^2)$ for all $r \in (0, \infty)$. Therefore,

$$\left|\varrho_i \varrho_j \delta \widetilde{y}_l \delta \widetilde{y}_m\right| \leq \frac{\left|\varrho_i \varrho_j\right|}{2}\left(\frac{\delta \widetilde{y}_l^2}{r_{lm}} + r_{lm} \delta \widetilde{y}_m^2\right), \tag{31}$$

for all arbitrary $r_{lm} \in (0, \infty)$.

From (30) and (31), one can get

$$\begin{aligned} \delta \widetilde{y}_{n+1}^2 - \delta \widetilde{y}_n^2 \leq {} & \left(\varrho_0^2 - 1\right)\delta \widetilde{y}_n^2 + \left|\varrho_0 \varrho_1\right|\left(\frac{\delta \widetilde{y}_n^2}{r_1} + r_1 \delta \widetilde{y}_{n+1-m}^2\right) \\ & + \left|\varrho_0 \varrho_2\right|\left(\frac{\delta \widetilde{y}_n^2}{r_2} + r_2 \delta \widetilde{y}_{n-m}^2\right) \\ & + \left|\varrho_1 \varrho_2\right|\left(\frac{\delta \widetilde{y}_{n-m+1}^2}{r_3} + r_3 \delta \widetilde{y}_{n-m}^2\right) \\ & + \varrho_1^2 \delta \widetilde{y}_{n+1-m}^2 + \varrho_2^2 \delta \widetilde{y}_{n-m}^2, \end{aligned} \tag{32}$$

for the arbitrary numbers $r_1, r_2, r_3 \in (0, \infty)$. Therefore,

$$\frac{\delta \widetilde{y}_{n+1}^2 - \delta \widetilde{y}_n^2}{h} \leq -A_h^\natural \delta \widetilde{y}_n^2 + B_h^\natural \max_{\ell \in \mathcal{T}} \delta \widetilde{y}_{n-\ell}^2, \tag{33}$$

where

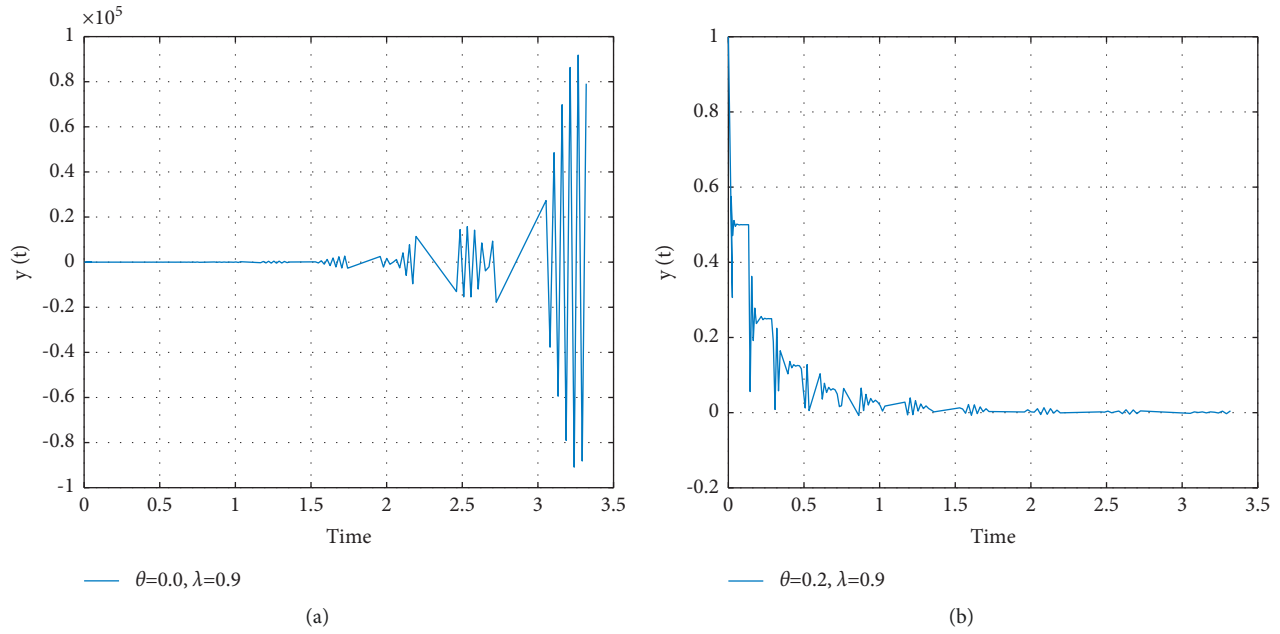

Figure 2: Numerical simulations of model (36) with $\vartheta = 0.0$ (a) and $\vartheta = 0.2$ (b), when $\lambda = 0.9$.

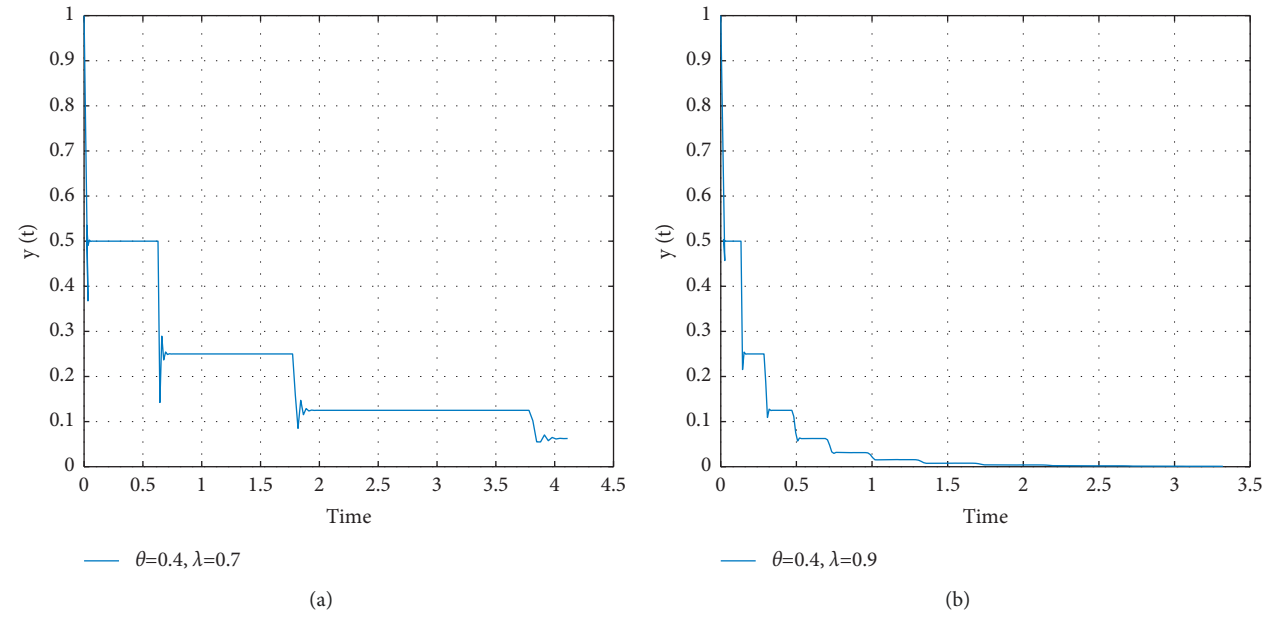

Figure 3: Numerical simulations of model (36) with $\vartheta = 0.4$ and different values of $\lambda = 0.7$ (a) and $\lambda = 0.9$ (b).

$$A_h^{\natural} \equiv A_h^{\natural}(r_1, r_2) = -\frac{1}{h}\left(\varrho_0^2 - 1 + \frac{|\varrho_0\varrho_1|}{r_1} + \frac{|\varrho_0\varrho_2|}{r_2}\right). \tag{34}$$

For $r_3 = 1$,

$$B_h^{\natural} \equiv B_h^{\natural}(r_1, r_2) = \frac{1}{h}\left(|\varrho_0\varrho_1|r_1 + |\varrho_0\varrho_2|r_2 + \left(|\varrho_1| + |\varrho_2|\right)^2\right). \tag{35}$$

We have following theorem and remarks.

Theorem 4. *From inequality (33), using equation (26) of Theorem 3, if* $0 \le B_h^{\natural} < A_h^{\natural}$ *and* $hA_h^{\natural} \in (0, 1)$ *with any positive values of* r_1, r_2*, the recurrence relation (23) is* $\xi-$ *exponentially stable.*

Remark 1. The ϑ-method, as applied to equation (2) is asymptotically stable if and only $\vartheta > 1/2$.

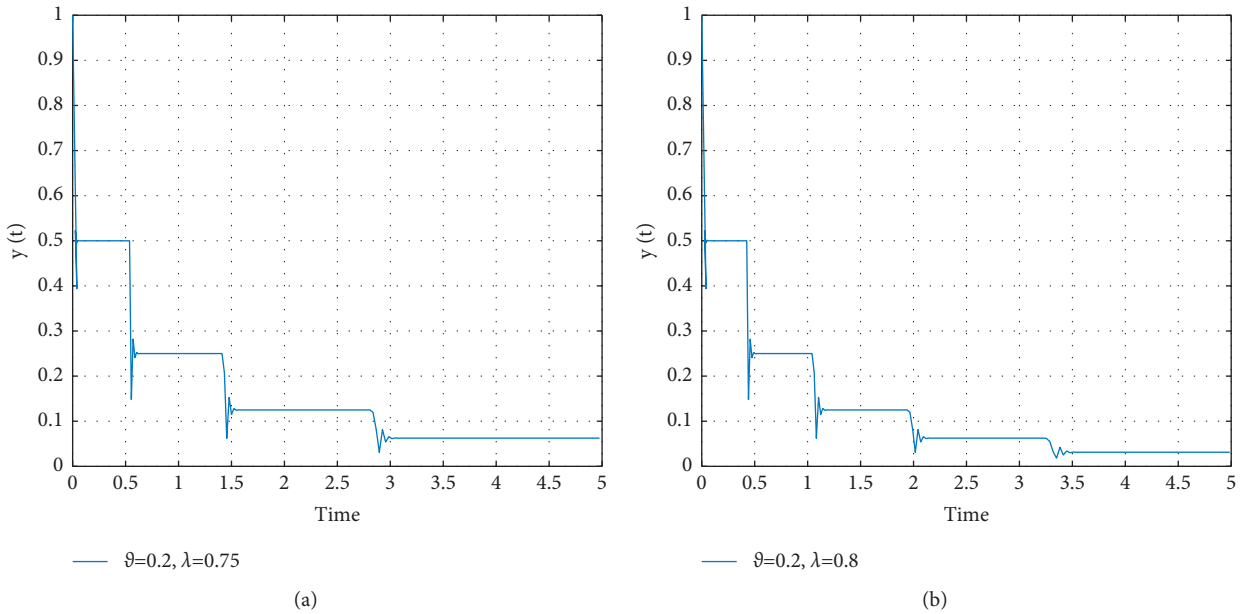

Figure 4: Numerical simulations of model (36) with $\vartheta = 0.2$ and $\lambda = 0.75$ (a), $\lambda = 0.8$ (b).

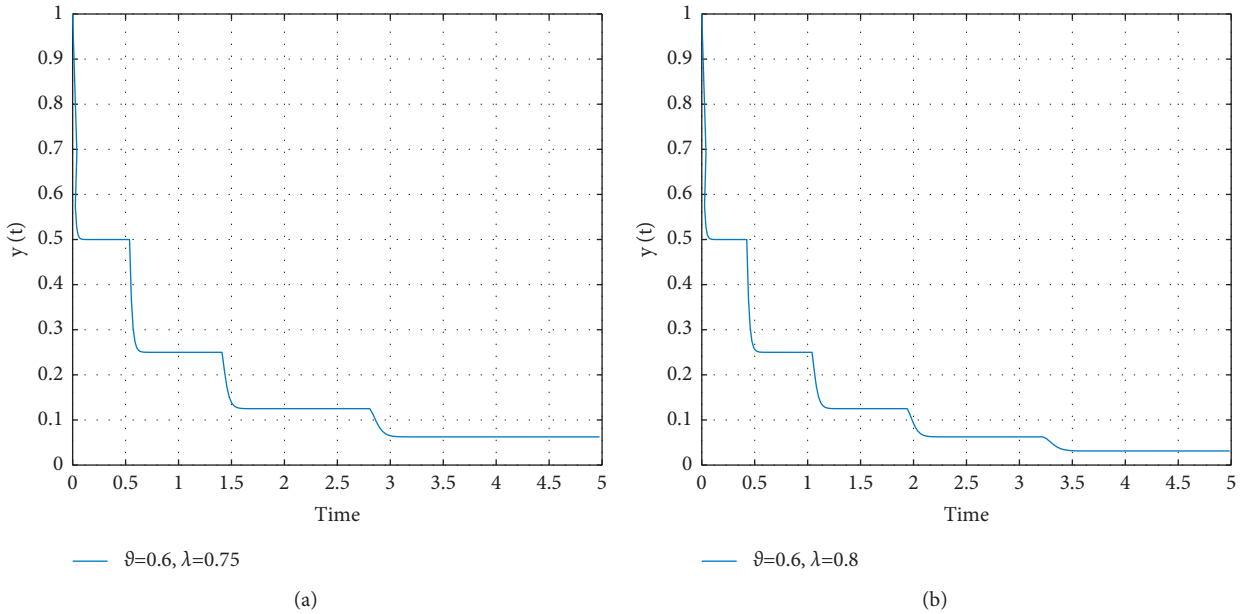

Figure 5: Numerical simulations of model (36) with $\vartheta = 0.6$, with $\lambda = 0.75$ (a), $\lambda = 0.8$ (b).

It is important to mention that explicit methods are easy to implement and are recommended for solving nonstiff problems. For stiff problems, however, the standard explicit methods with poor stability properties suffer a lot from step-size reduction and turn out to be inefficient in terms of overall computational costs [27–29].

Remark 2. In order to solve stiff problems numerically, we should use implicit or partially implicit ϑ-method's schemes.

5. Numerical Examples and Simulations

We present an example with some numerical simulations to illustrate the previous results.

Example 1. Consider the initial-value problem (IVP):

$$y'(t) = -40y(t) + 20y(\lambda t), \quad y(t) = 1 \text{ for } t \in [\lambda t_0, t_0]. \tag{36}$$

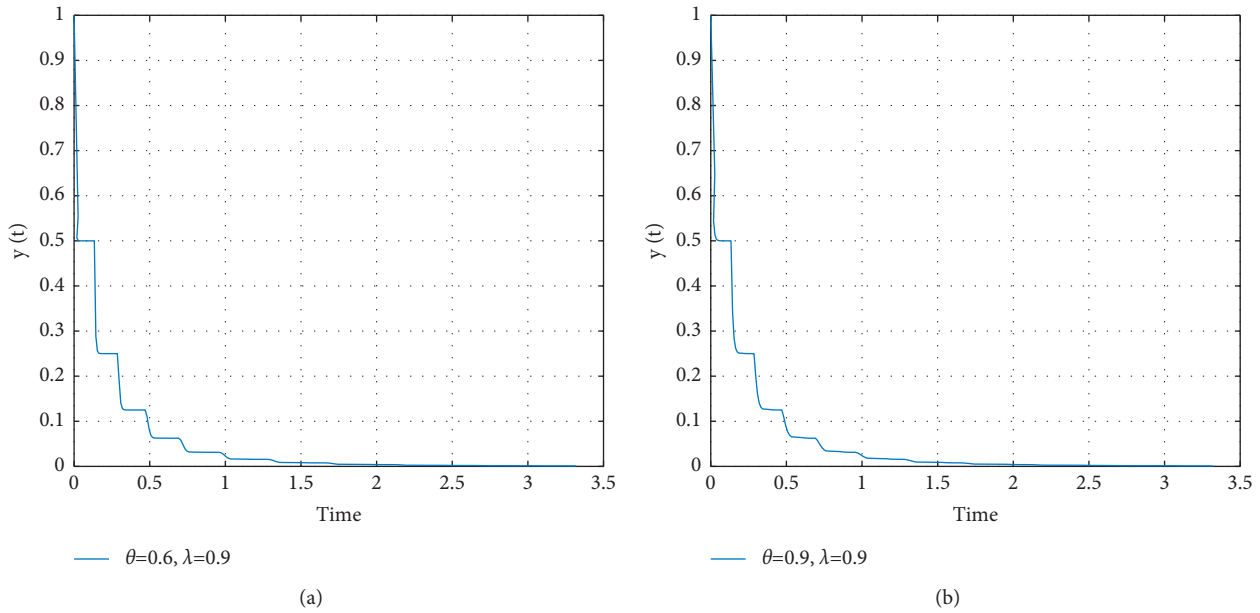

Figure 6: Numerical simulations of model (36) with $\vartheta = 0.6$ (a) and $\vartheta = 0.9$ (b), when $\lambda = 0.9$.

This IVP is considered a stiff problem. This problem can also be considered a singularly perturbed and stiff problem $\varepsilon y'(t) = \alpha y(t) + \beta y(\lambda t)$, with $\varepsilon = 0.01$, $\alpha = -0.4$, $\beta = 0.2$. Since $\alpha + |\beta| < 0$, where $\alpha = -40$, $\beta = 20$, the analytical solution is asymptotically stable. We apply the ϑ-method scheme to (36) with different values of $\vartheta = 0.0, 0.2, 0.6$. The mesh points are given by

$$\begin{aligned} 0 = t_0 < t_l < t_2 < \cdots < t_p \\ = r < t_{p+1} < \cdots < t_{p+m} \\ = \lambda^{-1} r, \quad t_{p+(k+1)m} = \lambda^{-k-1} r,\ k = 0, 1, \ldots \end{aligned} \tag{37}$$

Figures 1 and 2 show the numerical simulations of model (36) with a full explicit scheme $\vartheta = 0$ and partially explicit with $\vartheta = 0.2$, for $\lambda = 0.75, 0,8, 0.9$. Although $\alpha + |\beta| < 0$, the numerical solutions when $\vartheta = 0$ are unstable. Usually, the asymptotic and stability of explicit numerical schemes are restricted by step-size, which is given in terms of λ. As the step-size decreases, the numerical approximation solutions become more asymptotic. Figure 3 shows the numerical simulations with fixed ϑ and different values of delays. Time delays significantly increase the stability of differential equations.

Figure 4 displays numerical simulations when $\vartheta < 0.5\,(= 0.2)$ with $\lambda = 0.75$ and $\lambda = 0.8$. The asymptotic and stability behavior are improved with bigger λ, and numerical solution is getting smoother with long-run time. However, Figures 5 and 6 show the numerical simulation with partially implicit scheme, with $\vartheta = 0.6, 0.9 > 0.5$, with different values of $\lambda = 0.75, 0.8, 0.9$. The solution is asymptotically stable regardless of the size of the step-size. The numerical schemes are unconditionally asymptotically stable with $\vartheta > 1/2$.

6. Conclusion

Time delays significantly increase the complexity and stability of differential equations. It is possible for a delay to stabilize an otherwise unstable system or unstabilize a stable one. We developed and discussed an efficient numerical scheme for solving pantograph-type delay differential equations using the ϑ-method. Some stability conditions of analytical and numerical solutions of the problem have been investigated. From the theoretical results, numerical simulations can conclude that the ϑ-method, applied to pantograph equations, is a reliable method and asymptotically stable if and only if $\vartheta > 1/2$, regardless of the step-size of the scheme, especially with respect to the long-time behavior of the solutions. For $\vartheta < 1/2$, the stability of the numerical solution is almost unstable. Most of pantograph equations are stiff problems, and it is recommended to use an implicit or partially implicit sachems.

We can extend the stability analysis, in the coming research, to other classes of higher-order Runge-Kutta methods with pantograph equations. The schemes can also be extended to stochastic pantograph delay differential equations [30, 31].

Data Availability

The authors confirm that the data supporting the findings of this study are available within the article.

Conflicts of Interest

The authors declare no conflicts of interest.

Acknowledgments

This research was funded by the UAEU Research, fund # 12S005-2021.

References

[1] F. A. Rihan, *Delay Differential Equations and Applications to Biology*, Springer, New York, NY, USA, 2021.

[2] J. R. Ockendon and A. B. Tayler, "The dynamics of a current collection system for an electric locomotive," *Proceedings of the Royal Society of London. Series A, Mathematical and Physical Sciences*, vol. 322, no. 1551, pp. 447–468, 1971.

[3] Ş. Yüzbaşi and M. Sezer, "An exponential approximation for solutions of generalized pantograph-delay differential equations," *Applied Mathematical Modelling*, vol. 37, no. 22, pp. 9160–9173, 2013.

[4] M. Sezer and A. Akyüz-Daşcioğlu, "A taylor method for numerical solution of generalized pantograph equations with linear functional argument," *Journal of Computational and Applied Mathematics*, vol. 200, no. 1, pp. 217–225, 2007.

[5] S. Yalçinbaş, M. Aynigül, and M. Sezer, "A collocation method using Hermite polynomials for approximate solution of pantograph equations," *Journal of the Franklin Institute*, vol. 348, no. 6, pp. 1128–1139, 2011.

[6] Ô. İlhan, "An improved Morgan-Voyce Collocation method for numerical solution of generalized pantograph equations," *Journal of Scientific and Engineering Research*, vol. 10, pp. 320–332, 2017.

[7] S. Gümgüm, D. E. Özdek, G. Ôzaltun, and N. Bildik, "Legendre wavelet solution of neutral differential equations with proportional delays," *Journal of Applied Mathematics and Computing*, vol. 61, no. 1-2, pp. 389–404, 2019.

[8] J. Biazar and B. Ghanbari, "The homotopy perturbation method for solving neutral functional-differential equations with proportional delays," *Journal of King Saud University Science*, vol. 24, no. 1, pp. 33–37, 2012.

[9] X. Chen and L. Wang, "The variational iteration method for solving a neutral functional-differential equation with proportional delays," *Computers & Mathematics with Applications*, vol. 59, no. 8, pp. 2696–2702, 2010.

[10] M. G. Sakar, "Numerical solution of neutral functional-differential equations with proportional delays," *An International Journal of Optimization and Control: Theories & Applications*, vol. 7, no. 2, pp. 186–194, 2017.

[11] C. Yang, "Modified Chebyshev collocation method for pantograph-type differential equations," *Applied Numerical Mathematics*, vol. 134, pp. 132–144, 2018.

[12] H. Jafari, M. Mahmoudi, and M. H. Noori Skandari, "A new numerical method to solve pantograph delay differential equations with convergence analysis," *Advances in Difference Equations*, vol. 2021, no. 1, p. 129, 2021.

[13] F. N. Anakira, A. Jameel, M. Hijazi, A. K. Alomari, and N. Man, "A new approach for solving multi-pantograph type delay differential equations," *International Journal of Electrical and Computer Engineering*, vol. 12, no. 2, p. 1859, 2022.

[14] Z. Sabir, M. A. Z. Raja, J. L. G. Guirao, and T. Saeed, "Swarm intelligence procedures using meyer wavelets as a neural network for the novel fractional order pantograph singular system," *Fractal and Fractional*, vol. 5, no. 4, p. 277, 2021.

[15] Z. Sabir, M. A. Z. Raja, J. L. G. Guirao, and T. Saeed, "Meyer wavelet neural networks to solve a novel design of fractional order pantograph lane-emden differential model," *Chaos, Solitons & Fractals*, vol. 152, Article ID 111404, 2021.

[16] Z. Sabir, H. A. Wahab, and J. L. G. Guirao, "A novel design of Gudermannian function as a neural network for the singular nonlinear delayed, prediction and pantograph differential models," *Mathematical Biosciences and Engineering*, vol. 19, no. 1, pp. 663–687, 2021.

[17] I. Ahmad, G. U. Nieto, J. J. annd Rahman, and K. Shah, "Existence and stability for fractional order pantograph equations with nonlocal conditions," *The Electronic Journal of Differential Equations*, vol. 132, no. 1–16, 2020.

[18] A. Iserles, "On the generalized pantograph functional-differential equation," *European Journal of Applied Mathematics*, vol. 4, no. 1, pp. 1–38, 1993.

[19] Y. Liu, "Stability analysis of θ-methods for neutral functional-differential equations," *Numerische Mathematik*, vol. 70, pp. 473–485, 1995.

[20] J. Cermak, "The stability and asymptotic properties of the θ-methods for the pantograph equation," *IMA Journal of Numerical Analysis*, vol. 31, no. 4, pp. 1533–1551, 2011.

[21] A. Halanay, *Differential Equations– Stability, Oscillations, Time Lags*, Academic Press, New York, NY, USA, 1966.

[22] F. A. Rihan, "Stability concepts of numerical solutions of delay differential equations," in *Delay Differential Equations and Applications to Biology. Forum for Interdisciplinary Mathematics*Springer, New York, NY, USA, 2021.

[23] A. Bellen, N. Guglielmi, and L. Torelli, "Asymptotic stability properties of θ-methods for the pantograph equation," *Applied Numerical Mathematics*, vol. 24, no. 2, pp. 279–293, 1997.

[24] C. T. H. Baker, C. A. H. Paul, and D. R. Willé, "Issues in the numerical solution of evolutionary delay differential equations," *Advances in Computational Mathematics*, vol. 3, pp. 171–196, 1995.

[25] In', M. N. Spijker, and M. N. Spijker, "Stability analysis of numerical methods for delay differential equations," *Numerische Mathematik*, vol. 59, no. 1, pp. 807–814, 1991.

[26] A. Iserles, "Numerical analysis of delay differential equations with variable delays," *Annals of Numerical Mathematics*, vol. 1, no. 133, p. 152, 1994.

[27] G. Bocharov, G. Marchuk, and A. Romanyukha, "Numerical solution by LMMs of stiff delay differential systems modelling an immune response," *Numerische Mathematik*, vol. 73, no. 2, pp. 131–148, 1996.

[28] F. A. Rihan, E. H. Doha, M. I. Hassan, and N. M. Kamel, "Mono-implicit Runge-Kutta method for delay differential equations," *Journal of the Egyptian Mathematical Society*, vol. 17, no. 2, pp. 213–232, 2009.

[29] J. R. Cash and A. Singhal, "Mono-implicit runge—kutta formulae for the numerical integration of stiff differential systems," *IMA Journal of Numerical Analysis*, vol. 2, pp. 211–227, 1982.

[30] H. Zhang, Y. Xiao, and F. Guo, "Convergence and stability of a numerical method for nonlinear stochastic pantograph equations," *Journal of the Franklin Institute*, vol. 351, no. 6, pp. 3089–3103, 2014.

[31] X. Yang, Z. Yang, and Y. Xiao, "Asymptotical mean-square stability of linear θ–methods for stochastic pantograph differential equations: variable stepsize and transformation approach," *International Journal of Applied and Computational Mathematics*, vol. 99, no. 4, pp. 759–770, 2022.

Hindawi
Complexity
Volume 2022, Article ID 4717663, 25 pages
https://doi.org/10.1155/2022/4717663

Research Article

Novel Numerical Estimates of the Pneumonia and Meningitis Epidemic Model via the Nonsingular Kernel with Optimal Analysis

Saima Rashid[1], **Bushra Kanwal**[2], **Abdulaziz Garba Ahmad**[3], **Ebenezer Bonyah**[4] and **S.K. Elagan**[5,6]

[1]*Department of Mathematics, Government College University, Faisalabad 38000, Pakistan*
[2]*Department of Mathematics, COMSATS University, Islamabad, Pakistan*
[3]*Department of Mathematics, National Mathematical Centre Abuja, Abuja 900211, Nigeria*
[4]*Department of Mathematics Education, University of Education, Winneba, Kumasi Campus, Ghana*
[5]*Department of Mathematics and Computer Sciences, Faculty of Science Menoufia University, Shebin, Elkom 32511, Egypt*
[6]*Department of Mathematics and Statistics, College of Science, Taif University, P. O. Box 11099, Taif 21944, Saudi Arabia*

Correspondence should be addressed to Ebenezer Bonyah; ebonyah@aamusted.edu.gh

Received 10 April 2022; Accepted 30 May 2022; Published 31 July 2022

Academic Editor: Fathalla A. Rihan

In this article, we investigated a deterministic model of pneumonia-meningitis coinfection. Employing the Atangana–Baleanu fractional derivative operator in the Caputo framework, we analyze a seven-component approach based on ordinary differential equations (DEs). Furthermore, the invariant domain, disease-free as well as endemic equilibria, and the validity of the model's potential results are all investigated. According to controller design evaluation and modelling, the modulation technique devised is effective in diminishing the proportion of incidences in various compartments. A fundamental reproducing value is generated by exploiting the next generation matrix to assess the properties of the equilibrium. The system's reliability is further evaluated. Sensitivity analysis is used to classify the impact of each component on the spread or prevention of illness. Using simulation studies, the impacts of providing therapy have been determined. Additionally, modelling the appropriate configuration demonstrated that lowering the fractional order from 1 necessitates a rapid initiation of the specified control technique at the largest intensity achievable and retaining it for the bulk of the pandemic's duration.

1. Introduction

Fractional calculus has gained popularity over the years for representing a plethora of new challenges in fields such as computational virology, quantum theory, technology, and numerous others, wherein fractional-order (FO) operators are either singular (Caputo derivative and Riemann–Liouville (RL) fractional derivatives) or nonsingular (Atangana–Baleanu and Caputo–Fabrizio derivatives) [1–4].

However, the variation between integer-order and FO derivatives is that the integer-order derivative depicts the functionality of a complex nonlinear network for the entirety of the period, whereas the FO derivative operator represents a characteristic of a logistic scheme for the enormous moment. Furthermore, the integer-order derivative reflects a dynamic state's spatial information, while the FO derivative formulation of a complex process encompasses the project process domain [5–8]. On the other hand, in modelling specific cases, implementing derivation operators via noninteger values is critical for articulating generational requirements and the reliability of memories as a key component of various systems [9, 10].

Therefore, the advent of multiple meanings of a fractional derivative is fascinating and creates an incentive to identify the intricacies of natural surroundings in the context that certain challenges in existence pursue the index law for the RL fractional operator, some also implement the Mittag-Leffler (ML) rules for the Atangana–Baleanu fractional

derivative operator, and many others try to emulate the exponentially decaying law for the Caputo–Fabrizio fractional operator or an amalgamation of such regulations [11, 12].

Furthermore, the fact that many nonlinear mechanisms in connection to complex processes are discovered to be nonlocal with protracted recollection in time, and that inherently fractional derivation operators can characterize such kinds of mechanisms more appropriately than integer derivatives, has resulted in a rapid boost in the description of various nonlinear dynamic structures utilizing fractional-order derivatives [13]. In other respects, fractional-order operators are the ideal way to characterize or reveal crucial characteristics of several complex processes.

Pneumonia, which is classified as an infectious agent, is responsible for the loss of individual lives worldwide due to the inhalation of potential pathogens, primarily *Streptococcus pyogenes* [14]. Other disorders susceptible to infection include meningitis, respiratory ailments, and nasal congestion, among others (see Figure 1).

Infections can occur in adults, including infants to adults, and pneumonia turns severe whenever the immune system is weakened, as it is in vulnerable populations, as well as when it is co-infected with several other infections, such as meningitis [15]. Meningitis is a contagious bacterial ailment of the membrane that surrounds the cerebrum and spinal cord [16] (see Figures 2(a)and 2(b)).

Meningitis is caused by viral illness in 80 percent of cases, which is caused by pneumococcal pneumonia, streptococci, and *Neisseria meningitidis*. A majority of the research was carried out to determine the governing strategies of contagious ailments in a population (see [17–19]). In order to analyze the evolution of contagious infections in a population, various researchers have designed simulations to examine the evolution of various contagious infections. The authors [20, 21] also mentioned the co-dynamics of pneumonia and waterborne illness infections [22], as well as economic evaluation and optimal monitoring. The findings of this investigation demonstrated that among the suggested techniques, preventing infectious disease and treating pneumonia seem to be the most cost-effective. Many researchers have examined co-infection of communicable ailments with HIV and pneumonia co-infection [23], while Akinyi et al. [24] looked into bacterial meningitis and plasmodium co-infection.

To the best of our knowledge, since its invention in 2016 by Atangana and Baleanu [2], the innovative fractional derivative operator has been significantly employed in a multitude of disciplines of scientific innovation [25, 26]. For a short period of time, modelling using the nonsingular fractional derivatives culminates in a stochastic, deterministic, and physical process [27–29]. Atangana [30] presented the extension of rate of change concept from local to nonlocal operators with applications. Baleanu et al. [31] constructed a fractional framework for a malignant cell's ability to use information and assessed how chemotherapeutics influenced the system. As a consequence of the observations, the optimum modulation technique was found to be effective. Sene [32] studied the formulation of the governing equations of a fractional diffusion equation in the setting of the fractional operator with a Rabotnov fractional exponential kernel. Zhao [33] presented the fuzzy-based strategy to suppress the novel coronavirus (2019-NCOV) massive outbreak.

To approach the ABC fractional derivative, Owolabi [34] adopted a two-step family of Adams–Bashforth procedures to perform evaluation and modelling techniques on a problem. Demirci et al. [35] took into account an SEIR fractional model and its experimental validation. In [36], the SEIRA mathematical model is examined using the ABC fractional derivative operator with the ML kernel. Thus, we can conclude from the above-mentioned research that fractional derivatives have several implications in numerical techniques and in the study of real-world processes. The newly formed Atangana–Baleanu fractional operator, notably, has gained appreciation and acceptance as a result of its variety of uses in ecological, chemical, and biomedical sciences, as well as a variety of other complex studies.

In this research, we investigate a pneumonia and meningitis ($\mathbb{P}$) mathematical formulation with a dominating interaction incidence, which is inspired by the aforesaid considerations. The fractional derivative formulation of the system is generated, and its analytical simulation is estimated by applying the newly reported Atangana–Baleanu fractional derivative and Toufik–Atangana numerical solutions [37]. The $\mathbb{P}$ epidemiological theory utilizing the Atangana–Baleanu fractional derivative has not previously been examined, to the best of the researchers' expertise. The researchers further claim that in the relevant research, robust regulation characterization of mathematical formulae in the context of Atangana–Baleanu fractional operators is infrequent in the earlier research. As a response, we examine the sensitivity characterization of the $\mathbb{P}$ model in this article.

2. Depiction of the Model

In this part, the ABC fractional derivative form of the $\mathbb{P}$ epidemic mathematical systems is introduced. Let us just continue with a review of the ML kernels' notions and their concerning consequences.

Definition 1 (see [2]). For $\beta \in [0,1]$, $\mathbf{c} < \mathbf{d}$ and $\mathscr{F}_1 \in H^1(\mathbf{c}, \mathbf{d})$; then, the ABC derivative of fractional-order for $\mathscr{F}_1$ is presented as

$$ {}^{ABC}D^{\beta}\mathscr{F}_1(\zeta) = \frac{\mathbb{M}(\beta)}{(1-\beta)} \int_c^{\zeta} \frac{d\mathscr{F}_1}{d\zeta} E_{\beta}\left(\frac{\beta}{\beta-1}(\zeta - >)^{\beta}\right) d >, \quad (1) $$

where $\mathbb{M}(\beta)$is a normalization mapping that satisfying $\mathbb{M}(0) = \mathbb{M}(1) = 1$and the Mittag–Leffler function is denoted by $E_{\beta}(z_1)$ defined as

$$ E_{\beta}(z_1) = \sum_{\gamma=0}^{\infty} \frac{z_1^{\gamma}}{\Gamma(\beta\gamma + 1)}, \beta, z_1 \in \mathbb{C}, \Re(\beta) > 0. \quad (2) $$

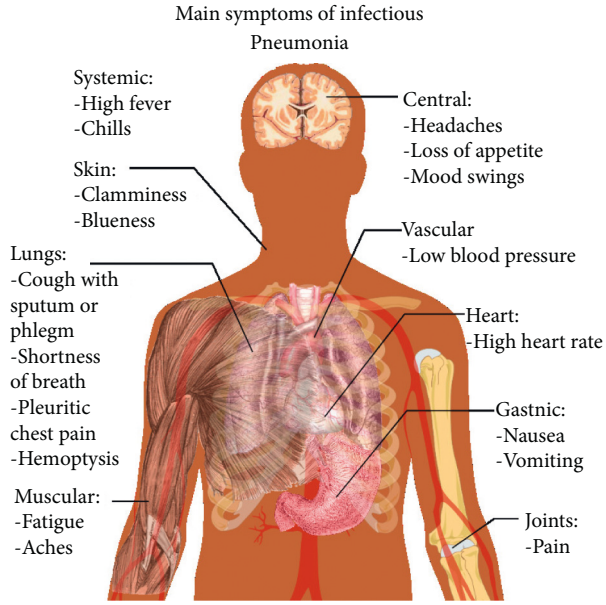

Figure 1: Basic indications of infectious pneumonia.

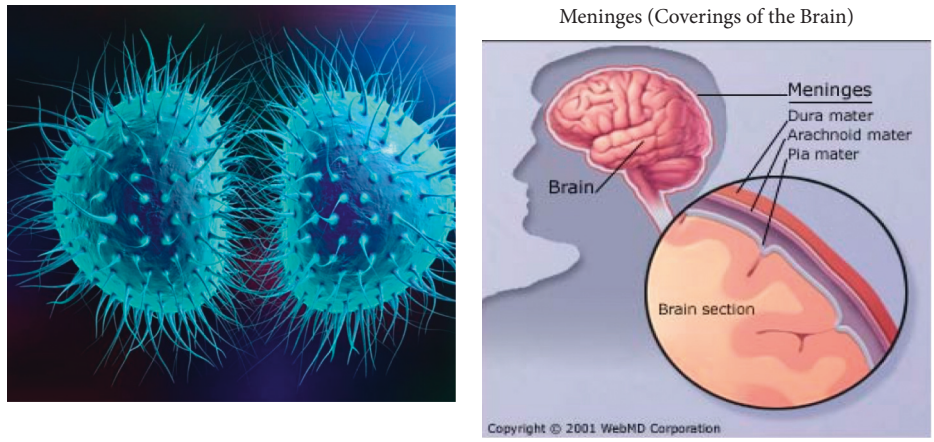

(a) (b)

Figure 2: (a) Bacterial meningitis. (b) Anatomy of meningitis.

Definition 2 (see [2]). For $\beta \in [0,1]\beta \in [0,1]$, $c < d$ and $\mathcal{F}_1 \in H^1(c,d)$; then, the AB fractional integral of $\mathcal{F}_1$ is presented as

$$ {}_c^{AB}I_\zeta^\beta \mathcal{F}_1(\zeta) = \frac{(1-\beta)}{\mathbb{M}(\beta)}\mathcal{F}_1(\zeta) + \frac{\beta}{\Gamma(\beta)\mathbb{M}(\beta)}\int_c^\zeta \mathcal{F}_1(\varrho)(\zeta-\varrho)^{\beta-1}d\varrho. \tag{3}$$

Lemma 1 (see [38]) (Newton–Leibniz identity). *For $\mathcal{F}_1 \in \mathbb{C}^1(c,d)$, the ABC fractional derivative and integral for $\mathcal{F}_1$ hold:*

$$ {}_c^{AB}I_\zeta^\beta\left({}_c^{AB}D_\zeta^\beta \mathcal{F}_1(\zeta)\right) = \mathcal{F}_1(\zeta) - \mathcal{F}_1(c). \tag{4}$$

Lemma 2 (see [39]). *For $c < d, \mathcal{F}_1, \mathcal{F}_2 \in H^1(c,d)$, then the ABC fractional derivative holds for the subsequent variant:*

$$\left\| {}_c^{AB}D_\zeta^\beta \mathcal{F}_1(\zeta) - {}_c^{AB}D_\zeta^\beta \mathcal{F}_2(\zeta)\right\| \le H\left\|\mathcal{F}_1(\zeta) - \mathcal{F}_2(\zeta)\right\|. \tag{5}$$

Our next result is the generalized mean-value theorem, which is mainly due to [40].

Lemma 3 (see [40]). *Let there be a function $h_1(\varrho) \in \mathbb{C}[c,d]$ and also suppose ${}_0^{AB}D_\zeta^\beta h(\varrho) \in \mathbb{C}[c,q_2], \beta \in (0,1]$. Then, $h_1(\varrho) = h_1(c) + 1/\Gamma(\beta){}_0^{ABC}D_\zeta^\beta h_1(\theta)(\varrho - \mathbf{c})^\beta, \theta \in [0,\varrho]$.*

Followed by Lemma 3, for $\beta \in (0,1]$, if $h_1(\varrho) \in [0,d], {}_0^{AB}D_\zeta^\beta h_1(\varrho) \in (0,d]$, and ${}_0^{ABC}\mathbf{D}_\zeta^\beta h_1(\varrho) \ge 0$ for all $\varrho \in (0,\mathbf{d}]$, then the mapping $h_1(\varrho)$ is increasing. Otherwise, $h_1(\varrho)$ is said to be decreasing for all $\varrho \in [0,d]$.

We shall now continue on to the system's development. The numerical framework for this

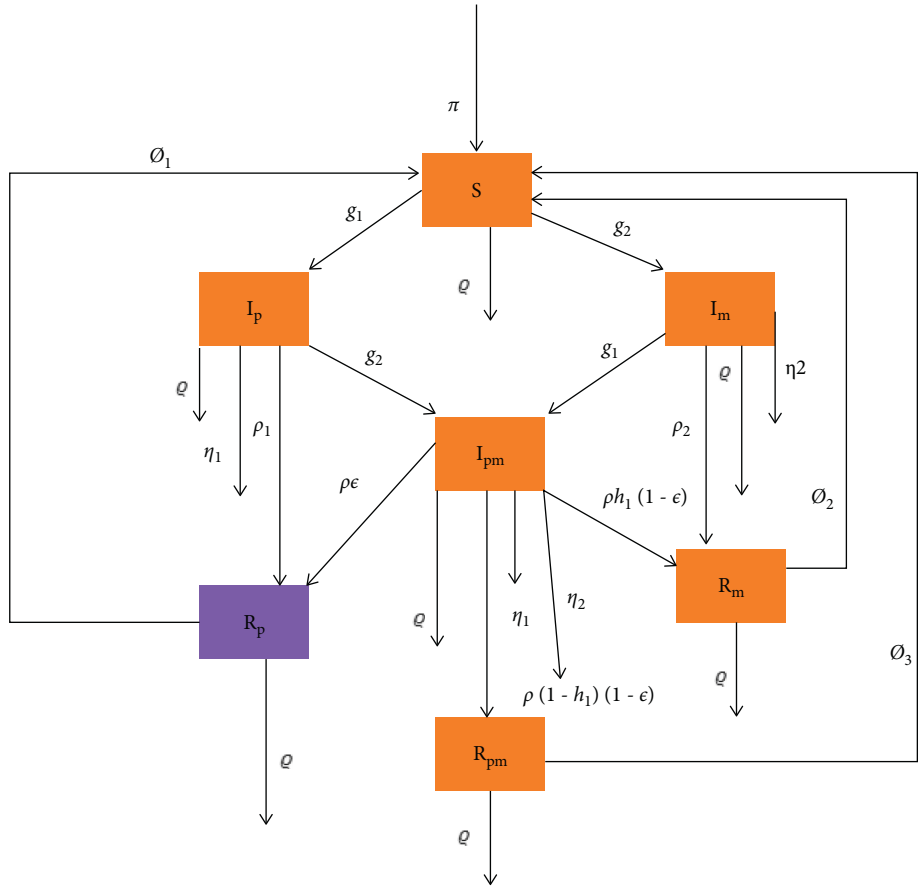

Figure 3: Flowchart for *PM* co-infection model.

investigation has been developed utilizing the sequence chart below (Figure 3).

The numerical approach with numerical approximation employed in this work is represented by the governing formulae, which are predicated on the workflow.

$$\begin{cases} \dot{S}(\zeta) = \pi + \phi_1 R_p + \phi_2 R_m + \phi_3 R_{pm} - (g_1 + g_2 + \varrho)S, \\ \dot{\mathbf{I}}_p\ (\zeta) = g_1 \mathbf{S} - (g_2 + \varrho + \rho_1 + \eta_1)\mathbf{I}_p, \\ \dot{\mathbf{I}}_m\ (\zeta) = g_2 \mathbf{S} - (g_1 + \varrho + \rho_2 + \eta_2)\mathbf{I}_m, \\ \dot{\mathbf{I}}_{pm}\ (\zeta) = g_2 \mathbf{I}_p + g_1 \mathbf{I}_m - (\rho + \varrho + \eta_1 + \eta_2)\mathbf{I}_{pm}, \\ \dot{\mathbf{R}}_p\ (\zeta) = \rho_1 \mathbf{I}_p + \epsilon\rho \mathbf{I}_{pm} - (\phi_1 + \varrho)\mathbf{R}_p, \\ \dot{\mathbf{R}}_m\ (\zeta) = \rho_2 \mathbf{I}_m + \epsilon\rho h_1 (1 - \epsilon)\mathbf{I}_{pm} - (\phi_2 + \varrho)\mathbf{R}_m, \\ \dot{\mathbf{R}}_{pm}\ (\zeta) = \rho (1 - h_1)(1 - \epsilon)\mathbf{I}_{pm} - (\phi_3 + \varrho)\mathbf{R}_{pm}. \end{cases} \tag{6}$$

Here, we examine a community that is diversified in this scenario. In this framework, we explore the probabilistic seven-dimensional global species. In this framework, we explore the probabilistic seven dimensional global species such as sensitive group (**S**), pneumonia virulent ($\mathbf{I}_p$), meningitis epidemic ($\mathbf{I}_m$), pneumonia and meningitis co-infectious ($\mathbf{I}_{pm}$), pneumonia healed ($\mathbf{R}_p$), meningitis regained ($\mathbf{R}_m$), and pneumonia-meningitis co-infectious retrieved are the numerous subgroups. ($\mathbf{R}_{pm}$). Susceptible are recruited with rate of Π through birth or immigration, and their number increases from individuals that come from subclasses of pneumonia recovered, meningitis recovered, and coinfectious recovered by losing their temporary immunity with rate of ϕ_1, ϕ_2, and ϕ_3, respectively. In the entire susceptible population, individuals can get pneumonia with contact rate of q_1 from a pneumonia-only infected or coinfected person with force of infection of pneumonia $g_1 = q_1 (\mathbf{I}_p + \mathbf{I}_{pm})/\mathcal{N}$ and join $\mathbf{I}_p$ compartment. In a similar way, individuals can get meningitis by a contact rate of q_2 from a meningitis-only infected or coinfected person with force of infection of meningitis $g_2 = q_2 (\mathbf{I}_m + \mathbf{I}_{pm})/\mathcal{N}$ and join $\mathbf{I}_m$ compartment. Pneumonia-only infected individuals also can get an additional meningitis infection with a force of infection g_2 and join coinfected compartment ($\mathbf{I}_{pm}$). Participants emerge from meningitis merely affected by a segment when attacked by pneumonia using g_1 a high intensity of transmission to boost the post-operative subsystem. Patients who have only been afflicted with pneumonia may recuperate at a frequency of ρ_1 approximately and can represent the pneumonia only cured category ($\mathbf{I}p$). As a result, meningitis-only people who are contaminated recover at a rate of ρ_2 and are assigned to the meningitis-only healed group ($\mathbf{I}_{pm}$). People in the immune-compromised class also retrieve at a speed ρ, but they either heal just from pneumonia ailment and enter pneumonia only retrieved storage area, with the possibility of $\rho(1 - \epsilon)$, or revive just from meningitis ailment and participate in meningitis

only retrieved zone with the plausibility of $\rho h_1(1-\epsilon)$, or restore from all these maladies and participate in co-infected recapture zone with a likely hood of $\rho(1-\epsilon)(1-h_1)$. Furthermore, ϱ represents the natural death rate. Furthermore, η_1 is the relative risk induced entirely by pneumonia, and η_2 is the number of fatalities due to meningitis.

2.1. Model Configuration. In this part, we investigate the framework's descriptive characteristics. We segmented the comprehensive framework into various DEs as presented in (5), which are estimates for pneumonia and meningitis ($\mathbb{P}$), to make the process easier.

The combination of DEs describes formal system (6) that incorporates the hypotheses, the saturate interaction frequency, and the flowchart (Figure 3) and analyzes model (6) by ABC fractional derivative.

$$\begin{cases} {}_0^{AB}\mathbf{D}_\zeta^\beta \mathbf{S}(\zeta) = \Theta_1(\zeta, \mathbf{S}), \\ {}_0^{AB}\mathbf{D}_\zeta^\beta \mathbf{I}_p(\zeta) = \Theta_2\left(\zeta, \mathbf{I}_p\right), \\ {}_0^{AB}\mathbf{D}_\zeta^\beta \mathbf{I}_m(\zeta) = \Theta_3(t_3, \mathbf{I}_m), \\ {}_0^{AB}\mathbf{D}_\zeta^\beta \mathbf{I}_{pm}(\zeta) = \Theta_4\left(\zeta, \mathbf{I}_{pm}\right), \\ {}_0^{AB}\mathbf{D}_\zeta^\beta \mathbf{R}_p(\zeta) = \Theta_5\left(\zeta, \mathbf{R}_p\right), \\ {}_0^{AB}\mathbf{D}_\zeta^\beta \mathbf{R}_m(\zeta) = \Theta_6(\zeta, \mathbf{R}_m), \\ {}_0^{AB}\mathbf{D}_\zeta^\beta \mathbf{R}_{pm}(\zeta) = \Theta_7\left(\zeta, \mathbf{I}_{pm}\right), \end{cases} \tag{7}$$

where the kernels are set as follows:

$$\begin{cases} \Theta_1(\zeta, \mathbf{S}) = \pi + \phi_1 \mathbf{R}_p + \phi_2 \mathbf{R}_m + \phi_3 \mathbf{R}_{pm} - (g_1 + g_2 + \varrho)\mathbf{S}, \\ \Theta_2\left(\zeta, \mathbf{I}_p\right) = g_1 \mathbf{S} - (g_2 + \varrho + \rho_1 + \eta_1)\mathbf{I}_p, \\ \Theta_3(\zeta, \mathbf{I}_m) = g_2 \mathbf{S} - (g_1 + \varrho + \rho_2 + \eta_2)\mathbf{I}_m, \\ \Theta_4\left(\zeta, \mathbf{I}_{pm}\right) = g_2 \mathbf{I}_p + g_1 \mathbf{I}_m - (\rho + \varrho + \eta_1 + \eta_2)\mathbf{I}_{pm}, \\ \Theta_5\left(\zeta, \mathbf{R}_p\right) = \rho_1 \mathbf{I}_p + \epsilon\rho \mathbf{I}_{pm} - (\phi_1 + \varrho)\mathbf{R}_p, \\ \Theta_6(\zeta, \mathbf{R}_m) = \rho_2 \mathbf{I}_m + \epsilon\rho h_1(1-\epsilon)\mathbf{I}_{pm} - (\phi_2 + \varrho)\mathbf{R}_m, \\ \Theta_7\left(\zeta, \mathbf{R}_{pm}\right) = \rho(1-h_1)(1-\epsilon)\mathbf{I}_{pm} - (\phi_3 + \varrho)\mathbf{R}_{pm}, \end{cases} \tag{8}$$

subject to the nonnegative initial values $\mathbf{S}(0) = \mathbf{S}_0, \mathbf{I}_p(0) = \mathbf{I}_{p0}, \mathbf{I}_m(0) = \mathbf{I}_{m0}$,
$\mathbf{I}_{pm}(0) = \mathbf{I}_{pm0}, \mathbf{R}_p(0) = \mathbf{R}_{p0}, \mathbf{R}_m(0) = \mathbf{R}_{m0}, \mathbf{R}_{pm}(0) = \mathbf{R}_{pm0}$.

Thus, in the absence of disease, the differential equation of the total population size is $d\mathcal{N}/d\zeta = \pi - \varrho \mathrm{N} - \eta_1(\mathbf{I}_p + \mathbf{I}_{pm}) - \eta_2(\mathbf{I}_m + \mathbf{I}_{pm})$. Table 1 summarizes the characteristics that were considered in the analysis (7).

2.2. Consequences on the Existence-Uniqueness. Here, employing the Banach fixed point f_p theorem for contraction mapping, the existence-uniqueness of the result for the ABC fractional model suggested in (7) is demonstrated. Before actually moving on, it is important to remember the two additional theorems. For further details, see [41] and the references cited therein.

We continue as follows to demonstrate the method's existence-uniqueness. We acquire framework (7) while we implement the AB fractional integral.

$$\% \begin{cases} \mathbf{S}(\zeta) - \mathbf{S}(0) = \dfrac{1-\beta}{\mathbb{M}(\beta)}\Theta_1(\zeta, \mathbf{S}) + \dfrac{\beta}{\mathbb{M}(\beta)\Gamma(\beta)}\displaystyle\int_0^\zeta \Theta_1(\varsigma, \mathbf{S})(\zeta - \varsigma)^{\beta-1} d\varsigma, \\ \mathbf{I}_p(\zeta) - \mathbf{I}_p(0) = \dfrac{1-\beta}{\mathbb{M}(\beta)}\Theta_2\left(\zeta, \mathbf{I}_p\right) + \dfrac{\beta}{\mathbb{M}(\beta)\Gamma(\beta)}\displaystyle\int_0^\zeta \Theta_2\left(\varsigma, \mathbf{I}_p\right)(\zeta - \varsigma)^{\beta-1} d\varsigma, \\ \mathbf{I}_m(\zeta) - \mathbf{I}_m(0) = \dfrac{1-\beta}{\mathbb{M}(\beta)}\Theta_3(\zeta, \mathbf{I}_m) + \dfrac{\beta}{\mathbb{M}(\beta)\Gamma(\beta)}\displaystyle\int_0^\zeta \Theta_3(\varsigma, \mathbf{I}_m)(\zeta - \varsigma)^{\beta-1} d\varsigma, \\ \mathbf{I}_{pm}(\zeta) - \mathbf{I}_{pm}(0) = \dfrac{1-\beta}{\mathbb{M}(\beta)}\Theta_4\left(\zeta, \mathbf{I}_{pm}\right) + \dfrac{\beta}{\mathbb{M}(\beta)\Gamma(\beta)}\displaystyle\int_0^\zeta \Theta_4\left(\varsigma, \mathbf{I}_{pm}\right)(\zeta - \varsigma)^{\beta-1} d\varsigma, \\ \mathbf{R}_p(\zeta) - \mathbf{R}_p(0) = \dfrac{1-\beta}{\mathbb{M}(\beta)}\Theta_5\left(\zeta, \mathbf{R}_p\right) + \dfrac{\beta}{\mathbb{M}(\beta)\Gamma(\beta)}\displaystyle\int_0^\zeta \Theta_5\left(\varsigma, \mathbf{R}_p\right)(\zeta - \varsigma)^{\beta-1} d\varsigma, \\ \mathbf{R}_m(\zeta) - \mathbf{R}_m(0) = \dfrac{1-\beta}{\mathbb{M}(\beta)}\Theta_6\left(\zeta, \mathbf{R}_p\right) + \dfrac{\beta}{\mathbb{M}(\beta)\Gamma(\beta)}\displaystyle\int_0^\zeta \Theta_6\left(\varsigma, \mathbf{R}_p\right)(\zeta - \varsigma)^{\beta-1} d\varsigma, \\ \mathbf{R}_{pm}(\zeta) - \mathbf{R}_{pm}(0) = \dfrac{1-\beta}{\mathbb{M}(\beta)}\Theta_7\left(\zeta, \mathbf{R}_{pm}\right) + \dfrac{\beta}{\mathbb{M}(\beta)\Gamma(\beta)}\displaystyle\int_0^\zeta \Theta_7\left(\varsigma, \mathbf{R}_{pm}\right)(\zeta - \varsigma)^{\beta-1} d\varsigma. \end{cases} \tag{9}$$

Table 1: Explanation of attributed values assumed in the model.

Symbols	Value	References
ϕ_1	0.003–0.1	[20]
ϕ_2	0.00904–0.99	[16]
ϕ_3	0.01	Supposed
q_1	0.007–0.6	[22]
q_2	0.9	[16]
η_1	0.006–0.5	Estimated
η_2	0.002–0.2	Estimated
ρ	0.1	[20]
h_1	0.5–1.0	[22]
ϵ	0.5–1.0	[22]
ϱ	0.01	Supposed
ρ_1	0.9	Supposed
ρ_2	0.8	Supposed

Surmise that the collection $\mathfrak{B} = \Lambda(\mathfrak{F}) \times \Lambda(\mathfrak{F}) \times \Lambda(\mathfrak{F}) \times \Lambda(\mathfrak{F}) \times \Lambda(\mathfrak{F}) \times \Lambda(\mathfrak{F}) \times \Lambda(\mathfrak{F})$, where $\Lambda(\mathfrak{F}) = \mathbf{C}[0, \overline{T}]$ indicates real-valued continuous mappings for the Banach space on $\mathfrak{F} = [0, \overline{T}]$ considering the norm presented as $\|(\mathbf{S}, \mathbf{I}_p, \mathbf{I}_m, \mathbf{I}_{pm}, \mathbf{R}_p, \mathbf{R}_m, \mathbf{R}_{pm})\| = \|\mathbf{S}\| + \|\mathbf{I}_p\| + \|\mathbf{I}_m\| + \|\mathbf{I}_{pm}\| + \|\mathbf{R}_p\| + \|\mathbf{R}_m\| + \|\mathbf{R}_{pm}\|$, where $\|\mathbf{S}\| = \sup_{\zeta\in\mathfrak{F}}|\mathbf{S}(\zeta)|$, $\|\mathbf{I}_p\| = \sup_{\zeta\in\mathfrak{F}}|\mathbf{I}_p(\zeta)|$, $\|\mathbf{I}_m\| = \sup_{\zeta\in\mathfrak{F}}|\mathbf{I}_m(\zeta)|$, $\|\mathbf{I}_{pm}\| = \sup_{\zeta\in\mathfrak{F}}|\mathbf{I}_{pm}(\zeta)|$, $\|\mathbf{R}_p\| = \sup_{\zeta\in\mathfrak{F}}|\mathbf{R}_p(\zeta)|$, $\|\mathbf{R}_m\| = \sup_{\zeta\in\mathfrak{F}}|\mathbf{R}_m(\zeta)|$, and $\|\mathbf{R}_{pm}\| = \sup_{\zeta\in\mathfrak{F}}|\mathbf{R}_{pm}(\zeta)|$.

The contraction and the Lipschitz hypothesis are the foundations of our following theorem.

Theorem 1. *For the following kernels $\Theta_\ell, \ell = 1, 2, \ldots, 7$ in (7), there exists $\mathbb{L}_\ell > 0, \ell = 1, 2, \ldots 7$, such that*

$$\begin{cases} \left\|\Theta_1(\zeta, \mathbf{S}) - \Theta_1(\zeta, \mathbf{S}_1)\right\| \le \mathbb{L}_1\left\|\mathbf{S}(\zeta) - \mathbf{S}_1(\zeta)\right\|, \\ \left\|\Theta_2\left(\zeta, \mathbf{I}_p\right) - \Theta_2\left(\zeta, \mathbf{I}_{p1}\right)\right\| \le \mathbb{L}_2\left\|\mathbf{I}_p(\zeta) - \mathbf{I}_{p1}(\zeta)\right\|, \\ \left\|\Theta_3(\zeta, \mathbf{I}_m) - \Theta_3(\zeta, \mathbf{I}_{m1})\right\| \le \mathbb{L}_3\left\|\mathbf{I}_m(\zeta) - \mathbf{I}_{m1}(\zeta)\right\|, \\ \left\|\Theta_4\left(\zeta, \mathbf{I}_{pm}\right) - \Theta_4\left(\zeta, \mathbf{I}_{pm}\right)\right\| \le \mathbb{L}_4\left\|\mathbf{I}_{pm}(\zeta) - \mathbf{I}_{pm}(\zeta)\right\|, \\ \left\|\Theta_5\left(\zeta, \mathbf{R}_p\right) - \Theta_5\left(\zeta, \mathbf{R}_{p1}\right)\right\| \le \mathbb{L}_5\left\|\mathbf{R}_p(\zeta) - \mathbf{R}_{p1}(\zeta)\right\|, \\ \left\|\Theta_6(\zeta, \mathbf{R}_m) - \Theta_6(\zeta, \mathbf{R}_{m1})\right\| \le \mathbb{L}_6\left\|\mathbf{R}_m(\zeta) - \mathbf{R}_{m1}(\zeta)\right\|, \\ \left\|\Theta_7\left(\zeta, \mathbf{R}_{pm}\right) - \Theta_7\left(\zeta, \mathbf{R}_{pm}\right)\right\| \le \mathbb{L}_7\left\|\mathbf{R}_{pm}(\zeta) - \mathbf{R}_{pm}(\zeta)\right\|, \end{cases} \tag{10}$$

are contractions for $\mathbb{L}_\ell \in [0, 1), \ell = 1, 2, \ldots, 7$.

Proof. In order to satisfy Lipschitz assumptions, we have

$$\begin{aligned} \left\|\Theta_1(\zeta, \mathbf{S}) - \Theta_1(\zeta, \mathbf{S}_1)\right\| &= \pi + \phi_1\mathbf{R}_p + \phi_2\mathbf{R}_m + \phi_3\mathbf{R}_{pm} - (g_1 + g_2 + \varrho)\mathbf{S} - \left(\pi + \phi_1\mathbf{R}_p + \phi_2\mathbf{R}_m + \phi_3\mathbf{R}_{pm} - (g_1 + g_2 + \varrho)\mathbf{S}_1\right\| \\ &= \left\|-(g_1 + g_2 + \varrho)(\mathbf{S} - \mathbf{S}_1)\right\| \le (g_1 + g_2 + \varrho)\left\|\mathbf{S} - \mathbf{S}_1\right\| \le \mathbb{L}_1\left\|\mathbf{S} - \mathbf{S}_1\right\|, \end{aligned} \tag{11}$$

where $\mathbb{L}_1 = q_1(\mathscr{K}_2 + \mathscr{K}_4)/\mathscr{N} + q_2(\mathscr{K}_3 + \mathscr{K}_4)/\mathscr{N} + \varrho$, $\|\mathbf{S}\| = \sup_{\zeta\in\mathfrak{F}}|\mathbf{S}(\zeta)| = \mathscr{K}_1$, $\|\mathbf{I}_p\| = \sup_{\zeta\in\mathfrak{F}}|\mathbf{I}_p(\zeta)| = \mathscr{K}_2$, $\|\mathbf{I}_m\| = \sup_{\zeta\in\mathfrak{F}}|\mathbf{I}_m(\zeta)| = \mathscr{K}_3$, $\|\mathbf{I}_{pm}\| = \sup_{\zeta\in\mathfrak{F}}|\mathbf{I}_{pm}(\zeta)| = \mathscr{K}_4$, $\|\mathbf{R}_p\| = \sup_{\zeta\in\mathfrak{F}}|\mathbf{R}_p(\zeta)| = \mathscr{K}_5$, $\|\mathbf{R}_m\| = \sup_{\zeta\in\mathfrak{F}}|\mathbf{R}_m(\zeta)| = \mathscr{K}_6$, and $\|\mathbf{R}_{pm}\| = \sup_{\zeta\in\mathfrak{F}}|\mathbf{R}_{pm}(\zeta)| = \mathscr{K}_7$.

It is worth noting that $\Theta_1(\zeta, \mathbf{S}_1)$ holds the Lipschitz assumption containing Lipschitz constant $\mathbb{L}_1 = q_1(\mathscr{K}_2 + \mathscr{K}_4)/\mathscr{N} + q_2(\mathscr{K}_3 + \mathscr{K}_4)/\mathscr{N} + \varrho$. Furthermore, if $\mathbb{L}_1 \in [0, 1)$, then $\Theta_1(\zeta, \mathbf{S}_1)$ is a contraction.

Analogously, we can analyze the existence consequences of $\mathbb{L}_\ell, \ell = 2, 3, \ldots, 7$ and the contraction technique for

$\Theta_2(\zeta, \mathbf{I}_p), \Theta_3(\zeta, \mathbf{I}_m), \Theta_4(\zeta, \mathbf{I}_{pm}), \Theta_5(\zeta, \mathbf{R}_p), \Theta_6(\zeta, \mathbf{R}_m)$, and $\Theta_7(\zeta, \mathbf{R}_{pm})$ for $\mathbb{L}_\ell \in [0,1), \ell = 2, 3, \ldots, 7$.

At $\zeta = \zeta_n, n = 1, 2, \ldots$, introduce the subsequent recursive version of (9):

$$\begin{cases} \mathbf{S}_{\mathbf{n}}(\zeta) = \frac{1-\beta}{\mathbb{M}(\beta)}\Theta_1(\zeta, \mathbf{S}_{\mathbf{n}-1}) + \frac{\beta}{\mathbb{M}(\beta)\Gamma(\beta)}\int_0^\zeta \Theta_1(\varsigma, \mathbf{S}_{\mathbf{n}-1})(\zeta-\varsigma)^{\beta-1}d\varsigma, \\ \mathbf{I}_{p_{\mathbf{n}}}(\zeta) = \frac{1-\beta}{\mathbb{M}(\beta)}\Theta_2\left(\zeta, \mathbf{I}_{p_{\mathbf{n}-1}}\right) + \frac{\beta}{\mathbb{M}(\beta)\Gamma(\beta)}\int_0^\zeta \Theta_2\left(\varsigma, \mathbf{I}_{p_{\mathbf{n}-1}}\right)(\zeta-\varsigma)^{\beta-1}d\varsigma, \\ \mathbf{I}_{m_{\mathbf{n}}}(\zeta) = \frac{1-\beta}{\mathbb{M}(\beta)}\Theta_3\left(\zeta, \mathbf{I}_{m_{\mathbf{n}-1}}\right) + \frac{\beta}{\mathbb{M}(\beta)\Gamma(\beta)}\int_0^\zeta \Theta_3\left(\varsigma, \mathbf{I}_{m_{\mathbf{n}-1}}\right)(\zeta-\varsigma)^{\beta-1}d\varsigma, \\ \mathbf{I}_{pm_{\mathbf{n}}}(\zeta) = \frac{1-\beta}{\mathbb{M}(\beta)}\Theta_4\left(\zeta, \mathbf{I}_{pm_{\mathbf{n}-1}}\right) + \frac{\beta}{\mathbb{M}(\beta)\Gamma(\beta)}\int_0^\zeta \Theta_4\left(\varsigma, \mathbf{I}_{pm_{\mathbf{n}-1}}\right)(\zeta-\varsigma)^{\beta-1}d\varsigma, \\ \mathbf{R}_{p_{\mathbf{n}}}(\zeta) = \frac{1-\beta}{\mathbb{M}(\beta)}\Theta_5\left(\zeta, \mathbf{R}_{p_{\mathbf{n}-1}}\right) + \frac{\beta}{\mathbb{M}(\beta)\Gamma(\beta)}\int_0^\zeta \Theta_5\left(\varsigma, \mathbf{R}_{p_{\mathbf{n}-1}}\right)(\zeta-\varsigma)^{\beta-1}d\varsigma, \\ \mathbf{R}_{m_{\mathbf{n}}}(\zeta) = \frac{1-\beta}{\mathbb{M}(\beta)}\Theta_6\left(\zeta, \mathbf{R}_{m_{\mathbf{n}-1}}\right) + \frac{\beta}{\mathbb{M}(\beta)\Gamma(\beta)}\int_0^\zeta \Theta_6\left(\varsigma, \mathbf{R}_{m_{\mathbf{n}-1}}\right)(\zeta-\varsigma)^{\beta-1}d\varsigma, \\ \mathbf{R}_{pm_{\mathbf{n}}}(\zeta) = \frac{1-\beta}{\mathbb{M}(\beta)}\Theta_7\left(\zeta, \mathbf{R}_{pm_{\mathbf{n}-1}}\right) + \frac{\beta}{\mathbb{M}(\beta)\Gamma(\beta)}\int_0^\zeta \Theta_7\left(\varsigma, \mathbf{R}_{pm_{\mathbf{n}-1}}\right)(\zeta-\varsigma)^{\beta-1}d\varsigma, \end{cases} \tag{12}$$

subject to ICs $\mathbf{S}(0) = \mathbf{S}_0, \mathbf{I}_p(0) = \mathbf{I}_{p0}, \mathbf{I}_m(0) = \mathbf{I}_{m0}, \mathbf{I}_{pm}(0) = \mathbf{I}_{pm0}, \mathbf{R}_p(0) = \mathbf{R}_{p0}, \mathbf{R}_m(0) = \mathbf{R}_{m0}, \mathbf{R}_{pm}(0) = \mathbf{R}_{pm0}$.

In (12), the variations of successive components are written in the following form:

$$\begin{aligned}
\Xi_{1\mathbf{n}}(\zeta) &= \mathbf{S}_{\mathbf{n}}(\zeta) - \mathbf{S}_{\mathbf{n}-1}(\zeta) = \frac{1-\beta}{\mathbb{M}(\beta)}\left(\Theta_1(\zeta, \mathbf{S}_{\mathbf{n}-1}) - \Theta_1(\zeta, \mathbf{S}_{\mathbf{n}-2})\right) + \frac{\beta}{\Gamma(\beta)\mathbb{M}(\beta)}\int_0^\zeta \left(\Theta_1(\varsigma, \mathbf{S}_{\mathbf{n}-1}) - \Theta_1(\varsigma, \mathbf{S}_{\mathbf{n}-2})\right)(\zeta-\varsigma)^{\beta-1}d\varsigma, \\
\Xi_{2\mathbf{n}}(\zeta) &= \mathbf{I}_{p_{\mathbf{n}}}(\zeta) - \mathbf{I}_{p_{\mathbf{n}-1}}(\zeta) = \frac{1-\beta}{\mathbb{M}(\beta)}\left(\Theta_2\left(\zeta, \mathbf{I}_{p_{\mathbf{n}-1}}\right) - \Theta_2\left(\zeta, \mathbf{I}_{p_{\mathbf{n}-2}}\right)\right) + \frac{\beta}{\Gamma(\beta)\mathbb{M}(\beta)}\int_0^\zeta \left(\Theta_2\left(\varsigma, \mathbf{I}_{p_{\mathbf{n}-1}}\right) - \Theta_2\left(\varsigma, \mathbf{I}_{p_{\mathbf{n}-2}}\right)\right)(\zeta-\varsigma)^{\beta-1}d\varsigma, \\
\Xi_{3\mathbf{n}}(\zeta) &= \mathbf{I}_{m_{\mathbf{n}}}(\zeta) - \mathbf{I}_{m_{\mathbf{n}-1}}(\zeta) = \frac{1-\beta}{\mathbb{M}(\beta)}\left(\Theta_3\left(\zeta, \mathbf{I}_{m_{\mathbf{n}-1}}\right) - \Theta_3\left(\zeta, \mathbf{I}_{m_{\mathbf{n}-2}}\right)\right) + \frac{\beta}{\Gamma(\beta)\mathbb{M}(\beta)}\int_0^\zeta \left(\Theta_3\left(\varsigma, \mathbf{I}_{m_{\mathbf{n}-1}}\right) - \Theta_3\left(\varsigma, \mathbf{I}_{m_{\mathbf{n}-2}}\right)\right)(\zeta-\varsigma)^{\beta-1}d\varsigma, \\
\Xi_{4\mathbf{n}}(\zeta) &= \mathbf{I}_{pm_{\mathbf{n}}}(\zeta) - \mathbf{I}_{pm_{\mathbf{n}-1}}(\zeta) = \frac{1-\beta}{\mathbb{M}(\beta)}\left(\Theta_4\left(\zeta, \mathbf{I}_{pm_{\mathbf{n}-1}}\right) - \Theta_4\left(\zeta, \mathbf{I}_{pm_{\mathbf{n}-2}}\right)\right) + \frac{\beta}{\Gamma(\beta)\mathbb{M}(\beta)}\int_0^\zeta \left(\Theta_4\left(\varsigma, \mathbf{I}_{pm_{\mathbf{n}-1}}\right) - \Theta_4\left(\varsigma, \mathbf{I}_{pm_{\mathbf{n}-2}}\right)\right)(\zeta-\varsigma)^{\beta-1}d\varsigma, \\
\Xi_{5\mathbf{n}}(\zeta) &= \mathbf{R}_{p_{\mathbf{n}}}(\zeta) - \mathbf{R}_{p_{\mathbf{n}-1}}(\zeta) = \frac{1-\beta}{\mathbb{M}(\beta)}\left(\Theta_5\left(\zeta, \mathbf{R}_{p_{\mathbf{n}-1}}\right) - \Theta_5\left(\zeta, \mathbf{R}_{p_{\mathbf{n}-2}}\right)\right) + \frac{\beta}{\Gamma(\beta)\mathbb{M}(\beta)}\int_0^\zeta \left(\Theta_5\left(\varsigma, \mathbf{R}_{p_{\mathbf{n}-1}}\right) - \Theta_5\left(\varsigma, \mathbf{R}_{p_{\mathbf{n}-2}}\right)\right)(\zeta-\varsigma)^{\beta-1}d\varsigma, \\
\Xi_{6\mathbf{n}}(\zeta) &= \mathbf{R}_{m_{\mathbf{n}}}(\zeta) - \mathbf{R}_{m_{\mathbf{n}-1}}(\zeta) = \frac{1-\beta}{\mathbb{M}(\beta)}\left(\Theta_2\left(\zeta, \mathbf{R}_{m_{\mathbf{n}-1}}\right) - \Theta_6\left(\zeta, \mathbf{R}_{m_{\mathbf{n}-2}}\right)\right) + \frac{\beta}{\Gamma(\beta)\mathbb{M}(\beta)}\int_0^\zeta \left(\Theta_6\left(\varsigma, \mathbf{R}_{m_{\mathbf{n}-1}}\right) - \Theta_6\left(\varsigma, \mathbf{R}_{m_{\mathbf{n}-2}}\right)\right)(\zeta-\varsigma)^{\beta-1}d\varsigma, \\
\Xi_{7\mathbf{n}}(\zeta) &= \mathbf{R}_{pm_{\mathbf{n}}}(\zeta) - \mathbf{R}_{pm_{\mathbf{n}-1}}(\zeta) = \frac{1-\beta}{\mathbb{M}(\beta)}\left(\Theta_7\left(\zeta, \mathbf{R}_{pm_{\mathbf{n}-1}}\right) - \Theta_7\left(\zeta, \mathbf{R}_{pm_{\mathbf{n}-2}}\right)\right) + \frac{\beta}{\Gamma(\beta)\mathbb{M}(\beta)}\int_0^\zeta \left(\Theta_7\left(\varsigma, \mathbf{R}_{pm_{\mathbf{n}-1}}\right) - \Theta_7\left(\varsigma, \mathbf{R}_{pm_{\mathbf{n}-2}}\right)\right)(\zeta-\varsigma)^{\beta-1}d\varsigma.
\end{aligned} \tag{13}$$

Implementing the norm on the aforementioned system (13), we have

$$\begin{aligned}
\left\|\Xi_{1\mathbf{n}}(\zeta)\right\| &= \left\|\mathbf{S}_{\mathbf{n}}(\zeta)-\mathbf{S}_{\mathbf{n}-1}(\zeta)\right\| = \frac{1-\beta}{\mathbb{M}(\beta)}\left\|\Theta_1(\zeta,\mathbf{S}_{\mathbf{n}-1})-\Theta_1(\zeta,\mathbf{S}_{\mathbf{n}-2})\right\| + \frac{\beta}{\Gamma(\beta)\mathbb{M}(\beta)}\int_0^{\zeta}\left\|\Theta_1(\varsigma,\mathbf{S}_{\mathbf{n}-1})-\Theta_1(\varsigma,\mathbf{S}_{\mathbf{n}-2})\right\|(\zeta-\varsigma)^{\beta-1}d\varsigma,\\
\left\|\Xi_{2\mathbf{n}}(\zeta)\right\| &= \left\|\mathbf{I}_{p_{\mathbf{n}}}(\zeta)-\mathbf{I}_{p_{\mathbf{n}-1}}(\zeta)\right\| = \frac{1-\beta}{\mathbb{M}(\beta)}\left\|\Theta_2\left(\zeta,\mathbf{I}_{p_{\mathbf{n}-1}}\right)-\Theta_2\left(\zeta,\mathbf{I}_{p_{\mathbf{n}-2}}\right)\right\| + \frac{\beta}{\Gamma(\beta)\mathbb{M}(\beta)}\int_0^{\zeta}\left\|\Theta_2\left(\varsigma,\mathbf{I}_{p_{\mathbf{n}-1}}\right)-\Theta_2\left(\varsigma,\mathbf{I}_{p_{\mathbf{n}-2}}\right)\right\|(\zeta-\varsigma)^{\beta-1}d\varsigma,\\
\left\|\Xi_{3\mathbf{n}}(\zeta)\right\| &= \left\|\mathbf{I}_{m_{\mathbf{n}}}(\zeta)-\mathbf{I}_{m_{\mathbf{n}-1}}(\zeta)\right\| = \frac{1-\beta}{\mathbb{M}(\beta)}\left\|\Theta_3\left(\zeta,\mathbf{I}_{m_{\mathbf{n}-1}}\right)-\Theta_3\left(\zeta,\mathbf{I}_{m_{\mathbf{n}-2}}\right)\right\| + \frac{\beta}{\Gamma(\beta)\mathbb{M}(\beta)}\int_0^{\zeta}\left\|\Theta_3\left(\varsigma,\mathbf{I}_{m_{\mathbf{n}-1}}\right)-\Theta_3\left(\varsigma,\mathbf{I}_{m_{\mathbf{n}-2}}\right)\right\|(\zeta-\varsigma)^{\beta-1}d\varsigma,\\
\left\|\Xi_{4\mathbf{n}}(\zeta)\right\| &= \left\|\mathbf{I}_{pm_{\mathbf{n}}}(\zeta)-\mathbf{I}_{pm_{\mathbf{n}-1}}(\zeta)\right\| = \frac{1-\beta}{\mathbb{M}(\beta)}\left\|\Theta_4\left(\zeta,\mathbf{I}_{pm_{\mathbf{n}-1}}\right)-\Theta_4\left(\zeta,\mathbf{I}_{pm_{\mathbf{n}-2}}\right)\right\| + \frac{\beta}{\Gamma(\beta)\mathbb{M}(\beta)}\int_0^{\zeta}\left\|\Theta_4\left(\varsigma,\mathbf{I}_{pm_{\mathbf{n}-1}}\right)-\Theta_4\left(\varsigma,\mathbf{I}_{pm_{\mathbf{n}-2}}\right)\right\|(\zeta-\varsigma)^{\beta-1}d\varsigma,\\
\left\|\Xi_{5\mathbf{n}}(\zeta)\right\| &= \left\|\mathbf{R}_{p_{\mathbf{n}}}(\zeta)-\mathbf{R}_{p_{\mathbf{n}-1}}(\zeta)\right\| = \frac{1-\beta}{\mathbb{M}(\beta)}\left\|\Theta_5\left(\zeta,\mathbf{R}_{p_{\mathbf{n}-1}}\right)-\Theta_5\left(\zeta,\mathbf{R}_{p_{\mathbf{n}-2}}\right)\right\| + \frac{\beta}{\Gamma(\beta)\mathbb{M}(\beta)}\int_0^{\zeta}\left\|\Theta_5\left(\varsigma,\mathbf{R}_{p_{\mathbf{n}-1}}\right)-\Theta_5\left(\varsigma,\mathbf{R}_{p_{\mathbf{n}-2}}\right)\right\|(\zeta-\varsigma)^{\beta-1}d\varsigma,\\
\left\|\Xi_{6\mathbf{n}}(\zeta)\right\| &= \left\|\mathbf{R}_{m_{\mathbf{n}}}(\zeta)-\mathbf{R}_{m_{\mathbf{n}-1}}(\zeta)\right\| = \frac{1-\beta}{\mathbb{M}(\beta)}\left\|\Theta_2\left(\zeta,\mathbf{R}_{m_{\mathbf{n}-1}}\right)-\Theta_6\left(\zeta,\mathbf{R}_{m_{\mathbf{n}-2}}\right)\right\| + \frac{\beta}{\Gamma(\beta)\mathbb{M}(\beta)}\int_0^{\zeta}\left\|\Theta_6\left(\varsigma,\mathbf{R}_{m_{\mathbf{n}-1}}\right)-\Theta_6\left(\varsigma,\mathbf{R}_{m_{\mathbf{n}-2}}\right)\right\|(\zeta-\varsigma)^{\beta-1}d\varsigma,\\
\left\|\Xi_{7\mathbf{n}}(\zeta)\right\| &= \left\|\mathbf{R}_{pm_{\mathbf{n}}}(\zeta)-\mathbf{R}_{pm_{\mathbf{n}-1}}(\zeta)\right\| = \frac{1-\beta}{\mathbb{M}(\beta)}\left\|\Theta_7\left(\zeta,\mathbf{R}_{pm_{\mathbf{n}-1}}\right)-\Theta_7\left(\zeta,\mathbf{R}_{pm_{\mathbf{n}-2}}\right)\right\| + \frac{\beta}{\Gamma(\beta)\mathbb{M}(\beta)}\int_0^{\zeta}\left\|\Theta_7\left(\varsigma,\mathbf{R}_{pm_{\mathbf{n}-1}}\right)-\Theta_7\left(\varsigma,\mathbf{R}_{pm_{\mathbf{n}-2}}\right)\right\|(\zeta-\varsigma)^{\beta-1}d\varsigma\,.
\end{aligned} \tag{14}$$

In addition, the first identity in (14) can be simplified to the representations:

$$\begin{aligned}
\Xi_{1\mathbf{n}}(\zeta) = \left\|\mathbf{S}_{\mathbf{n}}(\zeta)-\mathbf{S}_{\mathbf{n}-1}(\zeta)\right\| &= \frac{1-\beta}{\mathbb{M}(\beta)}\left\|\Theta_1(\zeta,\mathbf{S}_{\mathbf{n}-1})-\Theta_1(\zeta,\mathbf{S}_{\mathbf{n}-2})\right\| + \frac{\beta}{\Gamma(\beta)\mathbb{M}(\beta)}\int_0^{\zeta}\left\|\Theta_1(\varsigma,\mathbf{S}_{\mathbf{n}-1})-\Theta_1(\varsigma,\mathbf{S}_{\mathbf{n}-2})\right\|(\zeta-\varsigma)^{\beta-1}d\varsigma\\
&\le \mathbb{L}_1\frac{1-\beta}{\mathbb{M}(\beta)}\left\|\mathbf{S}_{\mathbf{n}-1}-\mathbf{S}_{\mathbf{n}-2}\right\| + \frac{\beta\mathbb{L}_1}{\Gamma(\beta)\mathbb{M}(\beta)}\int_0^{\zeta}\left\|\mathbf{S}_{\mathbf{n}-1}-\mathbf{S}_{\mathbf{n}-2}\right\|(\zeta-\varsigma)^{\beta-1}d\varsigma \le \mathbb{L}_1\left\|\Xi_{1(\mathbf{n}-1)}(\zeta)\right\|\left|\frac{1-\beta}{\mathbb{M}(\beta)}+\frac{\zeta^{\beta}}{\mathbb{M}(\beta)}\right|.
\end{aligned} \tag{15}$$

Ultimately, we have

$$\left\|\Xi_{1\mathbf{n}}(\zeta)\right\| \le \mathbb{L}_1\left\|\Xi_{1(\mathbf{n}-1)}(\zeta)\right\|\left|\frac{1-\beta}{\mathbb{M}(\beta)}+\frac{\zeta^{\beta}}{\mathbb{M}(\beta)}\right|. \tag{16}$$

Repeating the same procedure, the subsequent terms of (14) can be simplified to the following:

$$\begin{aligned}
\left\|\Xi_{2\mathbf{n}}(\zeta)\right\| &\leq \mathbb{L}_2\left\|\Xi_{2(\mathbf{n}-1)}(\zeta)\right\|\left|\frac{1-\beta}{\mathbb{M}(\beta)}+\frac{\zeta^{\beta}}{\mathbb{M}(\beta)}\right|,\\
\left\|\Xi_{3\mathbf{n}}(\zeta)\right\| &\leq \mathbb{L}_3\left\|\Xi_{3(\mathbf{n}-1)}(\zeta)\right\|\left|\frac{1-\beta}{\mathbb{M}(\beta)}+\frac{\zeta^{\beta}}{\mathbb{M}(\beta)}\right|,\\
\left\|\Xi_{4\mathbf{n}}(\zeta)\right\| &\leq \mathbb{L}_4\left\|\Xi_{4(\mathbf{n}-1)}(\zeta)\right\|\left|\frac{1-\beta}{\mathbb{M}(\beta)}+\frac{\zeta^{\beta}}{\mathbb{M}(\beta)}\right|,\\
\left\|\Xi_{5\mathbf{n}}(\zeta)\right\| &\leq \mathbb{L}_5\left\|\Xi_{5(\mathbf{n}-1)}(\zeta)\right\|\left|\frac{1-\beta}{\mathbb{M}(\beta)}+\frac{\zeta^{\beta}}{\mathbb{M}(\beta)}\right|,\\
\left\|\Xi_{6\mathbf{n}}(\zeta)\right\| &\leq \mathbb{L}_6\left\|\Xi_{6(\mathbf{n}-1)}(\zeta)\right\|\left|\frac{1-\beta}{\mathbb{M}(\beta)}+\frac{\zeta^{\beta}}{\mathbb{M}(\beta)}\right|,\\
\left\|\Xi_{7\mathbf{n}}(\zeta)\right\| &\leq \mathbb{L}_7\left\|\Xi_{7(\mathbf{n}-1)}(\zeta)\right\|\left|\frac{1-\beta}{\mathbb{M}(\beta)}+\frac{\zeta^{\beta}}{\mathbb{M}(\beta)}\right|.
\end{aligned} \tag{17}$$

□

Theorem 2. *The fractional $\mathbb{P}$ model presented in (7) has a solution if $\mathcal{U}_0$ holds the variant*

$$\left(\frac{1-\beta}{\mathbb{M}(\beta)}+\frac{\mathcal{U}_0^{\beta}}{\mathbb{M}(\beta)\Gamma(\beta)}\right)\mathbb{L}_{\ell}<1, \ell=1,2,\ldots,7. \tag{18}$$

Proof. By means of (16) and (19), we have

$$\begin{aligned}
\left\|\Xi_{1\mathbf{n}}(\zeta)\right\| &\leq \|\mathbf{S}(0)\|\left\{\mathbb{L}_1\left(\frac{1-\beta}{\mathbb{M}(\beta)}+\frac{\zeta^{\beta}}{\mathbb{M}(\beta)}\right)\right\}^{\mathbf{n}},\\
\left\|\Xi_{2\mathbf{n}}(\zeta)\right\| &\leq \left\|\mathbf{I}_p(0)\right\|\left\{\mathbb{L}_2\left(\frac{1-\beta}{\mathbb{M}(\beta)}+\frac{\zeta^{\beta}}{\mathbb{M}(\beta)}\right)\right\}^{\mathbf{n}},\\
\left\|\Xi_{3\mathbf{n}}(\zeta)\right\| &\leq \left\|\mathbf{I}_m(0)\right\|\left\{\mathbb{L}_3\left(\frac{1-\beta}{\mathbb{M}(\beta)}+\frac{\zeta^{\beta}}{\mathbb{M}(\beta)}\right)\right\}^{\mathbf{n}},\\
\left\|\Xi_{4\mathbf{n}}(\zeta)\right\| &\leq \left\|\mathbf{I}_{pm}(0)\right\|\left\{\mathbb{L}_4\left(\frac{1-\beta}{\mathbb{M}(\beta)}+\frac{\zeta^{\beta}}{\mathbb{M}(\beta)}\right)\right\}^{\mathbf{n}},\\
\left\|\Xi_{5\mathbf{n}}(\zeta)\right\| &\leq \left\|\mathbf{R}_p(0)\right\|\left\{\mathbb{L}_5\left(\frac{1-\beta}{\mathbb{M}(\beta)}+\frac{\zeta^{\beta}}{\mathbb{M}(\beta)}\right)\right\}^{\mathbf{n}},\\
\left\|\Xi_{6\mathbf{n}}(\zeta)\right\| &\leq \left\|\mathbf{R}_m(0)\right\|\left\{\mathbb{L}_6\left(\frac{1-\beta}{\mathbb{M}(\beta)}+\frac{\zeta^{\beta}}{\mathbb{M}(\beta)}\right)\right\}^{n},
\end{aligned}$$

$$\left\|\Xi_{7\mathbf{n}}(\zeta)\right\| \leq \left\|\mathbf{R}_{pm}(0)\right\|\left\{\mathbb{L}_7\left(\frac{1-\beta}{\mathbb{M}(\beta)}+\frac{\zeta^{\beta}}{\mathbb{M}(\beta)}\right)\right\}^{\mathbf{n}}, \tag{19}$$

Theorem 1 verifies the validity of the solution (the existence of a f_p), and which shows that the mappings $\mathbf{S}(\zeta)$, $\mathbf{I}_p(\zeta)$, $\mathbf{I}_m(\zeta)$, $\mathbf{I}_{pm}(\zeta)$, $\mathbf{R}_p(\zeta)$, $\mathbf{R}_m(\zeta)$, and $\mathbf{R}_{pm}(\zeta)$ are solution of the model (7).

Let us begin by defining which requirements are satisfied:

$$\begin{cases}
\mathbf{S}(\zeta)-\mathbf{S}(0)=\mathbf{S}_{\mathbf{n}}-\widetilde{B_{1\mathbf{n}}}(\zeta),\\
\mathbf{I}_p(\zeta)-\mathbf{I}_p(0)=\mathbf{I}_{p_{\mathbf{n}}}-\widetilde{B_{2\mathbf{n}}}(\zeta),\\
\mathbf{I}_m(\zeta)-\mathbf{I}_m(0)=\mathbf{I}_{m_{\mathbf{n}}}-\widetilde{B_{3\mathbf{n}}}(\zeta),\\
\mathbf{I}_{pm}(\zeta)-\mathbf{I}_{pm}(0)=\mathbf{I}_{pm_{\mathbf{n}}}-\widetilde{B_{4\mathbf{n}}}(\zeta),\\
\mathbf{R}_p(\zeta)-\mathbf{R}_p(0)=\mathbf{R}_{p_{\mathbf{n}}}-\widetilde{B_{5\mathbf{n}}}(\zeta),\\
\mathbf{R}_m(\zeta)-\mathbf{R}_m(0)=\mathbf{R}_{m_{\mathbf{n}}}-\widetilde{B_{6\mathbf{n}}}(\zeta),\\
\mathbf{R}_{pm}(\zeta)-\mathbf{R}_{pm}(0)=\mathbf{R}_{pm_{\mathbf{n}}}-\widetilde{B_{7\mathbf{n}}}(\zeta).
\end{cases} \tag{20}$$

Utilizing the fact of (20), we find

$$\begin{aligned}
\left\|B_{1\mathbf{n}}(\zeta)\right\| &\leq \frac{1-\beta}{\mathbb{M}(\beta)}\left\|\Theta_1(\zeta,\mathbf{S}_{\mathbf{n}})-\Theta_1(\zeta,\mathbf{S}_{\mathbf{n}-1})\right\|\\
&\quad+\frac{\beta}{\Gamma(\beta)\mathbb{M}(\beta)}\int_0^{\zeta}\left\|\Theta_1(\varsigma,\mathbf{S}_{\mathbf{n}})-\Theta_1(\varsigma,\mathbf{S}_{\mathbf{n}-1})\right\|(\zeta-\varsigma)^{\beta-1}d\varsigma\\
&\leq \mathbb{L}_1\frac{1-\beta}{\mathbb{M}(\beta)}\left\|\mathbf{S}_{\mathbf{n}}-\mathbf{S}_{\mathbf{n}-1}\right\|+\frac{\beta^{\mathbf{n}}\mathbb{L}_1}{\Gamma(\beta)\mathbb{M}(\beta)}\left\|\mathbf{S}_{\mathbf{n}}-\mathbf{S}_{\mathbf{n}-1}\right\|.
\end{aligned} \tag{21}$$

Iteratively performing the technique yields

$$\left\|B_{1\mathbf{n}}(\zeta)\right\| \leq \mathbb{L}_1^{\mathbf{n}}\left\{\frac{1-\beta}{\mathbb{M}(\beta)}+\mathbb{L}_1^{\mathbf{n}}\frac{\zeta^{\beta}}{\Gamma(\beta)\mathbb{M}(\beta)}\right\}^{\mathbf{n}+1}\left\|\mathbf{S}_{\mathbf{n}}-\mathbf{S}_{\mathbf{n}-1}\right\|^{\mathbf{n}}. \tag{22}$$

$\zeta=\mathcal{U}_0^{\beta}$ gives

$$\left\|B_{1\mathbf{n}}(\zeta)\right\| \leq \mathbb{L}_1^{\mathbf{n}}\left\{\frac{1-\beta}{\mathbb{M}(\beta)}+\frac{\zeta^{\beta}}{\Gamma(\beta)\mathbb{M}(\beta)}\right\}^{\mathbf{n}+1}\left\|\mathbf{S}_{\mathbf{n}}-\mathbf{S}_{\mathbf{n}-1}\right\|^{\mathbf{n}}. \tag{23}$$

Since, the expression can be formulated as

$$\left\|B_{1\mathbf{n}}(\zeta)\right\|\mapsto 0. \tag{24}$$

Take limit to (23) as $\mathbf{n}\mapsto\infty$. Clearly, observe that $\|B_{1\mathbf{n}}(\zeta)\|\mapsto 0$ for $\zeta^{\beta}(1-\beta/\mathbb{M}(\beta)+\zeta^{\beta}/\Gamma(\beta)\mathbb{M}(\beta))\mathbb{L}_1<1$. Identically, we can illustrate $\|B_{\ell\mathbf{n}}(\zeta)\|\mapsto 0$, for $\ell=2,3,\ldots,7$; then, $(1-\beta/\mathbb{M}(\beta)+\zeta^{\beta}/\Gamma(\beta)\mathbb{M}(\beta))\mathbb{L}_{\ell}<1, \ell=1,2,\ldots,7$.

This completes the proof. □

Here, the Banach f_p theorem asserts the validity of the result of system (7) by Theorems 1 and 2. Theorem 3 verifies the solution's uniqueness.

Theorem 3. *Let there be a unique solution of the fractional $\mathbb{P}$ model (7) given that*

$$\left(\frac{1-\beta}{\mathbb{M}(\beta)}+\frac{\zeta^{\beta}}{\Gamma(\beta)\mathbb{M}(\beta)}\right)\mathbb{L}_{\ell}<1, \ell=1,2,\ldots,7. \tag{25}$$

Proof. Suppose that $\mathbf{S}_1, \mathbf{I}_{p_1}, \mathbf{I}_{m_1}, \mathbf{I}_{pm_1}, \mathbf{R}_{p_1}, \mathbf{R}_{m_1}$, and $\mathbf{R}_{pm_1}$ are another solution to fractional $\mathbb{P}$ model (7). Then,

$$\mathbb{S}(\zeta)-\mathbb{S}_1(\zeta)=\frac{1-\beta}{\mathbb{M}(\beta)}\left(\Theta_1(\zeta,\mathbf{S})-\Theta_1(\zeta,\mathbf{S}_1)\right)+\frac{\beta}{\mathbb{M}(\beta)\Gamma(\beta)}\int_0^{\zeta}\left(\Theta_1(\varsigma,\mathbf{S})-\Theta_1(\varsigma,\mathbf{S}_1)\right)(\zeta-\varsigma)^{\beta-1}d\varsigma. \tag{26}$$

Employing the norm to the aforesaid equation, we have

$$\left\|\mathbb{S}(\zeta)-\mathbb{S}_1(\zeta)\right\|\leq\frac{1-\beta}{\mathbb{M}(\beta)}\left\|\mathbf{S}-\mathbf{S}_1\right\|\mathbb{L}_1+\frac{\zeta^{\beta}}{\mathbb{M}(\beta)\Gamma(\beta)}\left\|\mathbf{S}-\mathbf{S}_1\right\|. \tag{27}$$

Since $(1-(1-\beta/\mathbb{M}(\beta)+\zeta^{\beta}/\Gamma(\beta)\mathbb{M}(\beta))\mathbb{L}_1)>0$, we acquire $\|\mathbf{S}-\mathbf{S}_1\|=0$. Consequently, we have $\mathbf{S}=\mathbf{S}_1$. Repeating the same process, we can prove that $\mathbf{I}_p=\mathbf{I}_{p_1}, \mathbf{I}_m=\mathbf{I}_{m_1}, \mathbf{I}_{pm}=\mathbf{I}_{pm_1}, \mathbf{R}_p=\mathbf{R}_{p_1}, \mathbf{R}_m=\mathbf{R}_{m_1}$, and $\mathbf{R}_{pm}=\mathbf{R}_{pm_1}$. This completes the proof. □

3. Qualitative Analysis

Several key aspects of the developed framework, including boundedness, the existence of equilibria, and fundamental reproductive quantity, will be outlined and discussed.

3.1. Positively Invariant and Boundedness. In order to find the invariant domain, we surmise the overall population $\mathcal{N}=\mathbf{S}+\mathbf{I}_p+\mathbf{I}_m+\mathbf{I}_{pm}+\mathbf{R}_p+\mathbf{R}_m+\mathbf{R}_{pm}$.

Let the domain of the fractional $\mathbb{P}$ model (7) that is epidemiologically sustainable determined by

$$\mathcal{O}=:\left\{\left(\mathbf{S},\mathbf{I}_p,\mathbf{I}_m,\mathbf{I}_{pm},\mathbf{R}_p,\mathbf{R}_m,\mathbf{R}_{pm}\right)\in\mathbb{R}_+^7:\ 0\leq\mathbf{S}+\mathbf{I}_p+\mathbf{I}_m+\mathbf{I}_{pm}+\mathbf{R}_p+\mathbf{R}_m+\mathbf{R}_{pm}\leq\mathcal{N}\leq\frac{\pi}{\varrho}\right\}. \tag{28}$$

In order to prove that the collection $\mathcal{O}$ is positively invariant, apply Lemma 1, and we have

$$\begin{cases}
{}_0^{ABC}\mathbf{D}_{\zeta}^{\beta}\mathbf{S}(\zeta)|_{\mathbf{S}=0}=\pi\geq 0,\\
{}_0^{ABC}\mathbf{D}_{\zeta}^{\beta}\mathbf{I}_p(\zeta)|_{\mathbf{I}_p=0}=g_1\mathbf{S}\geq 0,\\
{}_0^{ABC}\mathbf{D}_{\zeta}^{\beta}\mathbf{I}_m(\zeta)|_{\mathbf{I}_m=0}=g_2\mathbf{S}\geq 0,\\
{}_0^{ABC}\mathbf{D}_{\zeta}^{\beta}\mathbf{I}_{pm}(\zeta)|_{\mathbf{I}_{pm}=0}=g_2\mathbf{I}_p+g_1\mathbf{I}_m\geq 0,\\
{}_0^{ABC}\mathbf{D}_{\zeta}^{\beta}\mathbf{R}_p(\zeta)|_{\mathbf{R}_p=0}=\rho_1\mathbf{I}_p+\epsilon\rho\mathbf{I}_{pm}\geq 0,\\
{}_0^{ABC}\mathbf{D}_{\zeta}^{\beta}\mathbf{R}_m(\zeta)|_{\mathbf{R}_m=0}=\rho_2\mathbf{I}_m+\epsilon\rho h_1(1-\epsilon)\mathbf{I}_{pm}\geq 0,\\
{}_0^{ABC}\mathbf{D}_{\zeta}^{\beta}\mathbf{R}_{pm}(\zeta)|_{\mathbf{R}_{pm}=0}=\rho\left(1-h_1\right)(1-\epsilon)\mathbf{I}_{pm}\geq 0.
\end{cases} \tag{29}$$

It is clear from (29) that every outcome of (7) is positive and will be in $\mathbb{R}_+^7$. Therefore, the set $\mathcal{O}$ presented in (28) is positively invariant for fractional $\mathbb{P}$ model (7).

Additionally, to prove the boundedness of the solutions of the fractional $\mathbb{P}$ framework, we proceed by aggregating all of the system's components, offering

$${}_0^{ABC}\mathbf{D}_{\zeta}^{\beta}\mathcal{N}(\zeta)=\pi-\varrho\mathrm{N}-\eta_1\left(\mathbf{I}_p+\mathbf{I}_{pm}\right)-\eta_2\left(\mathbf{I}_m+\mathbf{I}_{pm}\right)\leq\pi-\varrho\mathrm{N}. \tag{30}$$

Using the Laplace transform, we have

$$\begin{aligned}\mathscr{L}\left({}_0^{ABC}\mathbf{D}_{\zeta}^{\beta}\mathcal{N}(\zeta)+-\varrho\mathrm{N}\right)&\leq\mathscr{L}(\pi)\mathscr{L}(\mathcal{N})\left((1-\lambda)s_1^{\beta}-\frac{\lambda\beta}{1-\beta}\right)-\omega^{\beta-1}\mathcal{N}(0)\leq\frac{1-\beta}{\mathbb{M}(\beta)}\left(\omega^{\beta}+\frac{\beta}{1-\beta}\right)\frac{\pi}{\omega}\\&\leq\left(1-\frac{\lambda\beta}{(1-\lambda)(1-\beta)\omega^{\beta}}\right)\left\{\frac{1-\beta}{(1-\lambda)\mathbb{M}(\beta)}\left(1+\frac{\beta}{(1-\beta)\omega^{\beta}}\frac{\pi}{\omega}\right)+\frac{\mathcal{N}(0)}{(1-\lambda)\omega}\right\},\end{aligned} \tag{31}$$

where $\lambda = (\beta - 1)\varrho/\mathbb{M}(\beta)$. In view of inverse Laplace transform, we have

$$\mathcal{N}(\zeta) = \frac{\pi}{\varrho} - \frac{\pi}{\varrho(1-\lambda)}\frac{d}{d\zeta}\int_0^{\zeta} E_{\beta}\left(\frac{\lambda\beta(\zeta - x_1)^{\beta}}{(1-\lambda)(1-\beta)}\right)dx_1 + \frac{1}{1-\lambda}E_{\beta}\left(\frac{\lambda\beta\zeta^{\beta}}{(1-\lambda)(1-\beta)}\right)\mathcal{N}(0), \tag{32}$$

where $E_{\beta,\gamma}$ presents the ML function. Based on the assumption that the ML function exhibits asymptotic nature,

$$E_{\beta,\gamma}(\widetilde{z}) \approx \frac{\sum_{\mathcal{J}=1}^{w}\widetilde{z}^{-\lambda}}{\Gamma(\gamma - \beta\mathcal{J}) + \mathcal{O}\left(|\widetilde{z}|^{-w-1}\right)}, |\widetilde{z}| \mapsto \infty, \frac{\beta\pi}{2} < |\arg(\widetilde{z})| \le \pi. \tag{33}$$

It is not really hard to perceive that $\mathcal{N}(\zeta) \mapsto \pi/\varrho$, and this concludes that system (7) is biologically sustainable in the domain.

3.2. Disease-Free Equilibrium ($\mathcal{DFE}$). Set $\mathbf{I}_p = 0, \mathbf{I}_m = 0$, and $\mathbf{I}_{pm} = 0$ in (6); then, $\mathcal{DFE}$ reduces to $\widetilde{E}_0 = (\pi/\varrho, 0, 0, 0, 0, 0, 0)$.

3.3. Fundamental Reproductive Number. Assume that the infected component of system (6) is

$$\begin{aligned}
\dot{\mathbf{I}}_p(\zeta) &= g_1\mathbf{S} - (g_2 + \varrho + \rho_1 + \eta_1)\mathbf{I}_p,\\
\dot{\mathbf{I}}_m(\zeta) &= g_2\mathbf{S} - (g_1 + \varrho + \rho_2 + \eta_2)\mathbf{I}_m,\\
\dot{\mathbf{I}}_{pm}(\zeta) &= g_2\mathbf{I}_p + g_1\mathbf{I}_m - (\rho + \varrho + \eta_1 + \eta_2)\mathbf{I}_{pm}.
\end{aligned} \tag{34}$$

As in [42], it is constructed employing the next generation matrix. For this, we construct the matrix $\mathcal{F}$ and $\mathcal{V}$ as follows:

$$\mathcal{F} = \begin{bmatrix} \frac{q_1\pi}{\varrho} & 0 & \frac{q_1\pi}{\varrho} \\ 0 & \frac{q_2\pi}{\varrho} & \frac{q_2\pi}{\varrho} \\ 0 & 0 & 0 \end{bmatrix} \text{and } \mathcal{V} = \begin{bmatrix} \rho_1 + \eta_1 + \varrho & 0 & 0 \\ 0 & \rho_2 + \eta_2 + \varrho & 0 \\ 0 & 0 & \rho + \eta_1 + \eta_2 + \varrho \end{bmatrix},$$

$$\mathcal{F}\mathcal{V}^{-1} = \begin{bmatrix} \frac{q_1\pi}{\varrho(\rho_1 + \eta_1 + \varrho)} & 0 & \frac{q_1\pi}{\varrho(\rho_1 + \eta_1 + \eta_1 + \varrho)} \\ 0 & \frac{q_2\pi}{\varrho(\rho_2 + \eta_2 + \varrho)} & \frac{q_2\pi}{\varrho(\rho + \eta_1 + \eta_2 + \varrho)} \\ 0 & 0 & 0 \end{bmatrix}. \tag{35}$$

The eigenvalues of the system are $\lambda_1 = 0$, $\lambda_2 = q_1\pi/\varrho(\rho_1 + \eta_1 + \varrho) = \mathfrak{R}_{0p}$, $\lambda_3 = q_2\pi/\varrho(\rho_2 + \eta_2 + \varrho) = \mathfrak{R}_{0m}$. Clearly, we see that $\mathfrak{R}_0 = \max\{\mathfrak{R}_{0p}, \mathfrak{R}_{0m}\}$ is the fundamental reproductive number.

3.4. Local Stability of $\mathcal{DFE}$

Theorem 4. *Let there be a $\mathcal{DEF}$ point which is locally asymptotically stable if $\mathfrak{R}_0 < 1$. Also, if $\mathfrak{R}_0 > 1$, then it is unstable.*

Proof. For $\mathscr{DFE}$, the Jacobian matrix of $\mathbb{P}$ model (6) is presented as where

$$\mathbb{J}_{\widetilde{E_0}} = \begin{bmatrix} \mathrm{R}_{3\times3} & \mathscr{Q}_{3\times4} \\ \mathscr{R}_{4\times3} & \mathscr{S}_{4\times4} \end{bmatrix}, \tag{36}$$

$$\mathrm{R}_{3\times3} = \begin{bmatrix} -\varrho, & \frac{-q_1\pi}{\varrho}, & 0, \\ 0, & \frac{-q_1\pi}{\varrho-(\rho_1+\eta_1+\varrho)}, & 0, \\ 0, & 0, & \frac{q_2\pi}{\varrho-(\rho_2+\eta_2+\varrho)}, \end{bmatrix},$$

$$\mathscr{Q}_{3\times4} = \begin{bmatrix} \frac{-q_2\pi}{\varrho} & \phi_1 & \phi_2 & \phi_3 \\ \frac{-q_2\pi}{\varrho} & 0 & 0 & 0 \\ 0 & 0 & 0 & 0 \\ -(\rho+\eta_1+\eta_2+\varrho) & 0 & 0 & 0 \end{bmatrix}, \tag{37}$$

$$\mathscr{R}_{4\times3} = \begin{bmatrix} 0 & 0 & 0 \\ 0 & \phi_1 & 0 \\ 0 & 0 & \phi_2 \\ 0 & 0 & 0 \end{bmatrix}, \mathscr{S}_{4\times4} = \begin{bmatrix} \rho e & -(\varrho+\phi_1) & 0 & 0 \\ \rho h_1(1-\epsilon) & 0 & -(\varrho+\phi_2) & 0 \\ \rho(1-h_1)(1-\epsilon) & 0 & 0 & -(\varrho+\phi_3) \end{bmatrix}.$$

By the virtue of (36), one can acquire the subsequent characteristic polynomial as

$$D(\lambda) = -(\varrho+\lambda)(\phi_1+\varrho+\lambda)(\phi_2+\varrho+\lambda)(\rho+\eta_1+\eta_2+\varrho+\lambda)(\phi_3+\varrho+\lambda)\left(\frac{-q_1\pi}{\varrho+\rho_1+\eta_1+\varrho+\lambda}\right) \times\left(\frac{-q_2\pi}{\varrho+\rho_2+\eta_2+\varrho+\lambda}\right). \tag{38}$$

After simplification, we get

$$\lambda_1 = -, \lambda_2 = -(\phi_1+), \lambda_3 = -(\phi_2+), \lambda_4 = -(\rho+\eta_1+\eta_2+), \lambda_5 = -(+\phi_3), \lambda_6 = -(\rho+\eta_1+\eta_1+\varrho), \lambda_7 = -(\rho+\eta_1+\eta_1+\varrho). \tag{39}$$

Since $\lambda_6, \lambda_7 < 0$, that is, $\rho_1 + \eta_1 + \varrho < q_1\pi/\varrho$ and $\rho_2 + \eta_2 + \varrho < q_2\pi/\varrho$, this yields that $\mathfrak{R}_{0p} < 1$. Analogously, $\rho_2 + \eta_2 + \varrho < q_2\pi/\varrho$ shows that $\mathfrak{R}_{0m} < 1$. This concludes that $\mathfrak{R}_0 = \max\{\mathfrak{R}_{0p}, \mathfrak{R}_{0m}\} < 1$ which shows that $\mathcal{FE}$ is locally asymptotically stable. □

3.5. Global Stability of $\mathcal{DFE}$. Here, we employ the mechanism described in [22] to examine the global stability of $\mathcal{DFE}$. To begin, rewrite $\mathbb{P}$ model (6) as

$$\begin{aligned} \dot{\chi}_1(\zeta) &= \mathcal{Y}_1(\chi_1, \chi_2), \\ \dot{\chi}_2(\zeta) &= \mathcal{Y}_2(\chi_1, \chi_2), \end{aligned} \tag{40}$$

subject to $\mathcal{Y}_2(\chi_1, 0) = 0$. It is worth mentioning that $\chi_1 = \{\mathbf{S}, \mathbf{R}_p, \mathbf{R}_m, \mathbf{R}_{pm}\}$ represents the uncontaminated population while $\chi_2 = \{\mathbf{I}_p, \mathbf{I}_m, \mathbf{I}_{pm}\}$ indicate the contaminated population, respectively. Furthermore, the $\mathcal{FE}$ of the $\mathbb{P}$ model is presented by $\mathcal{V} = (\overline{\chi}, 0)$. This demonstrates that $\mathcal{V} = (\overline{\chi}, 0)$ is globally asymptotically stable equilibrium for $\mathbb{P}$ framework given that $\mathfrak{R}_0 < 1$ (by Theorem 1) and the subsequent assumptions hold:

(i) For $\dot{\chi}_1(\zeta) = \mathcal{Y}_1(\chi_1, 0), \overline{\chi}$ is globally asymptotically stable.

(ii) $\mathcal{Y}_2(\chi_1, \chi_2) = \mathcal{A}\chi_2 - \widetilde{\mathcal{Y}}_2(\chi_1, \chi_2), \widetilde{\mathcal{Y}}_2(\chi_1, \chi_2) \geq 0$ for $(\chi_1, \chi_2) \in \mathcal{O}$.

The preceding hypothesis applies if $\mathbb{P}$ model (6) satisfies the aforementioned requirements.

Theorem 5. *If* (**i**) *and* (**ii**) *hold, then* $\mathcal{V} = (\overline{\chi}, 0)$ *is globally asymptotically stable equilibrium given that* $\mathfrak{R}_0 < 1$.

Proof. By means of $\mathbb{P}$ model, we can write

$$\mathcal{Y}_1(\chi_1, \chi_2) = \begin{bmatrix} \pi + \phi_1\mathbf{R}_p + \phi_2\mathbf{R}_m + \phi_3\mathbf{R}_{pm} - (g_1 + g_2 + \varrho)\mathbf{S} \\ \rho_1\mathbf{I}_p + \epsilon\rho\mathbf{I}_{pm} - (\phi_1 + \varrho)\mathbf{R}_p \\ \rho_2\mathbf{I}_m + \epsilon\rho h_1(1-\epsilon)\mathbf{I}_{pm} - (\phi_2 + \varrho)\mathbf{R}_m \\ \rho(1-h_1)(1-\epsilon)\mathbf{I}_{pm} - (\phi_3 + \varrho)\mathbf{R}_{pm} \end{bmatrix}, \tag{41}$$

and

$$\mathcal{Y}_2(\chi_1, \chi_2) = \begin{bmatrix} g_1\mathbf{S} - (g_2 + \varrho + \rho_1 + \eta_1)\mathbf{I}_p, \\ g_2\mathbf{S} - (g_1 + \varrho + \rho_2 + \eta_2)\mathbf{I}_m, \\ g_2\mathbf{I}_p + g_1\mathbf{I}_m - (\rho + \varrho + \eta_1 + \eta_2)\mathbf{I}_{pm}. \end{bmatrix}. \tag{42}$$

□

Suppose the system is diminished to

$$\dot{\chi}_1(\zeta)|_{\chi_2=0} = \begin{bmatrix} \pi - \varrho\mathbf{S} \\ 0 \\ 0 \\ 0 \end{bmatrix}. \tag{43}$$

It is clear by expression (43) that $\overline{\chi} = (\pi\varrho, 0)$ is the global asymptotic state.

This is reinforced by the result, which is as follows:

$$\mathbf{S} = \frac{\pi}{\varrho} + \left(\mathbf{S}(0) - \frac{\pi}{\varrho}\right)\exp(-\varrho\zeta). \tag{44}$$

When $\zeta \mapsto \infty$, the solution follows $\mathbf{S} \mapsto \pi/\varrho$. This implies the global convergence of (43) in $\mathcal{O}$.

Consider

$$\mathcal{A} = \begin{bmatrix} q_1 - \rho_1 - \eta_1 - \varrho & 0 & q_1 \\ 0 & -(\rho_2 + \eta_2 + \varrho) & 0 \\ 0 & 0 & -(\rho + \eta_1 + \eta_1 + \varrho) \end{bmatrix}. \tag{45}$$

Then, $\mathcal{Y}_2(\chi_1, \chi_2)$ can be expressed as

$$\widetilde{\mathcal{Y}}_2(\chi_1, \chi_2) = \begin{bmatrix} q_1(\mathbf{I}_m + \mathbf{I}_{pm})\left(\dfrac{1-\mathbf{S}}{\mathcal{N}}\right) + g_2\mathbf{I}_p \\ g_1\mathbf{I}_m \\ -(g_1\mathbf{I}_m + g_2\mathbf{I}_p) \end{bmatrix}, \tag{46}$$

which illustrates that $\widetilde{\mathcal{Y}}_2(\chi_1, \chi_2) < 0$, and this suggests that the secondary assumption (ii) is not provided, and $\mathcal{V} = (\overline{\chi}, 0)$ may not be globally asymptotically stable when $\mathfrak{R}_0 < 1$.

3.6. Sensitivity Analysis. Through sensitivity analysis, the most important components for the development and regulation of transmission in the population are identified. We employ the strategies provided in [43] to accomplish this. With consideration to a factor, assume x_1, the responsiveness factor of $\mathfrak{R}_0$, is determined by $\psi_{x_1}^{\mathfrak{R}_0} = \partial\mathfrak{R}_0/\partial x_1 x_1/\mathfrak{R}_0$. As $\mathfrak{R}_0 = \max\{\mathfrak{R}_{0p}, \mathfrak{R}_{0m}\}$, the sensitivity evaluation of $\mathfrak{R}_{0p}$ and $\mathfrak{R}_{0m}$ is conducted individually as follows:

$$\begin{aligned}
\psi_{q_1^{\mathfrak{R}_0}} &= \frac{\partial \mathfrak{R}_0}{\partial q_1}\frac{q_1}{\mathfrak{R}_0} = \frac{\pi q_1 \varrho(\rho_1+\beta_1+\varrho)}{q_1\pi\varrho(\rho_1+\beta_1+\varrho)} = 1>0,\\
\psi_{\eta_1^{\mathfrak{R}_0}} &= \frac{\partial \mathfrak{R}_0}{\partial \eta_1}\frac{\eta_1}{\mathfrak{R}_0} = -\frac{\eta_1}{(\rho_1+\beta_1+\varrho)}<0,\\
\psi_{\rho_1^{\mathfrak{R}_0}} &= \frac{\partial \mathfrak{R}_0}{\partial \rho_1}\frac{\rho_1}{\mathfrak{R}_0} = -\frac{\rho_1}{(\rho_1+\beta_1+\varrho)}<0,\\
\psi_{\varrho^{\mathfrak{R}_0}} &= \frac{\partial \mathfrak{R}_0}{\partial \varrho_1}\frac{\varrho_1}{\mathfrak{R}_0} = -\frac{(\rho_1+\eta_1+2\varrho)}{(\rho_1+\beta_1+\varrho)}<0,\\
\psi_{q_2^{\mathfrak{R}_0}} &= \frac{\partial \mathfrak{R}_0}{\partial q_2}\frac{q_2}{\mathfrak{R}_0} = \frac{\pi q_2 \varrho(\rho_2+\beta_2+\varrho)}{q_1\pi\varrho(\rho_2+\beta_2+\varrho)} = 1>0,\\
\psi_{\eta_2^{\mathfrak{R}_0}} &= \frac{\partial \mathfrak{R}_0}{\partial \eta_2}\frac{\eta_2}{\mathfrak{R}_0} = -\frac{\eta_2}{(\rho_2+\beta_2+\varrho)}<0,\\
\psi_{\rho_2^{\mathfrak{R}_0}} &= \frac{\partial \mathfrak{R}_0}{\partial \rho_2}\frac{\rho_2}{\mathfrak{R}_0} = -\frac{\rho_2}{(\rho_2+\beta_2+\varrho)}<0,\\
\psi_{\varrho^{\mathfrak{R}_0}} &= \frac{\partial \mathfrak{R}_0}{\partial \varrho}\frac{\varrho}{\mathfrak{R}_0} = -\frac{\rho_2+\eta_2+2\varrho}{(\rho_2+\beta_2+\varrho)}<0.
\end{aligned} \tag{47}$$

The analysis shows that characteristics with highly accurate index values, especially q_1 and q_2, have a huge promise for spreading bacterial viruses, meningitis, and their co-infections in the congregation even though they boost their corresponding propagation quantity, which seems to be the mean value of supplementary illnesses. If the estimated quantities containing a negative sensitivity value are improved while the quantities of the other characteristics remain stable, the factors having a negative sensitivity level contribute significantly to reducing the spread of $\mathbb{P}$ in the population.

3.7. Numerical Approaches of $\mathbb{PM}$ Model. Here, we leverage the Toufik–Atangana [37] approach to generate a systematic formula for scheme (7) in this part.

In consideration of the first component of (7), we find

$$\begin{cases} {}_0^{ABC}\mathbf{D}_\zeta^\beta \mathbf{S}(\zeta) = \nabla_1(\zeta, \mathbf{S}(\zeta)), \mathbf{S}(0) = \mathbf{S}_0. \end{cases} \tag{48}$$

Observing (9), one can calculate for (48) in the problem described in the following:

$$\begin{aligned}
\mathbf{S}(\zeta) = \mathbf{S}(0) &+ \frac{1-\beta}{\mathbb{M}(\beta)}\nabla_1(\zeta, \mathbf{S}(\zeta)) + \frac{\beta}{\mathbb{M}(\beta)\Gamma(\beta)}\\
&\int_0^\zeta \nabla_1(\varsigma, \mathbf{S}(\varsigma))(\zeta-\varsigma)^{\beta-1}d\varsigma.
\end{aligned} \tag{49}$$

Utilizing Lagrange's interpolating polynomial technique on $[\zeta_\wp, \zeta_{\wp+1}]$ to $\nabla_1(\mathbf{y}, \mathbf{S}(\mathbf{y})) = \pi/(g_1+g_2+\varrho) - (\phi_1\mathbf{R_p}(\mathbf{y}) + \phi_2\mathbf{R_m}(\mathbf{y}) + \phi_3\mathbf{R_{pm}}(\mathbf{y}))/(g_1+g_2+\varrho) - \mathbf{S}(\mathbf{y})$, then we have

$$\begin{aligned}
\mathbf{S}_\wp \approx \frac{1}{\hbar}\Big[&\big(\mathbf{y}-\zeta_{\wp-1}\big)\nabla_1\big(\zeta_\wp, \mathbf{S}\big(\zeta_\wp\big), \mathbf{I}_p\big(\zeta_\wp\big), \mathbf{I}_m\big(\zeta_\wp\big), \mathbf{I}_{pm}\big(\zeta_\wp\big), \mathbf{R}_p\big(\zeta_\wp\big), \mathbf{R}_m\big(\zeta_\wp\big), \mathbf{R}_{pm}\big(\zeta_\wp\big)\big)\\
&-\big(\mathbf{y}-\zeta_\wp\big)\nabla_1\big(\zeta_{\wp-1}, \mathbf{S}\big(\zeta_{\wp-1}\big), \mathbf{I}_p\big(\zeta_{\wp-1}\big), \mathbf{I}_m\big(\zeta_{\wp-1}\big), \mathbf{I}_{pm}\big(\zeta_{\wp-1}\big), \mathbf{R}_p\big(\zeta_{\wp-1}\big), \mathbf{R}_m\big(\zeta_{\wp-1}\big), \mathbf{R}_{pm}\big(\zeta_{\wp-1}\big)\big)\Big],
\end{aligned} \tag{50}$$

where $\hbar = \zeta_\wp - \zeta_{\wp-1}$.

Inserting (49) into (50), we have

$$\begin{aligned}\mathbf{S}(\zeta_{\mathbf{n}+1}) &= \mathbf{S}(0)+\frac{1-\beta}{\mathbb{M}(\beta)}\nabla_1\left(\zeta_\wp,\mathbf{S}\left(\zeta_\wp\right),\mathbf{I}_p\left(\zeta_\wp\right),\mathbf{I}_m\left(\zeta_\wp\right),\mathbf{I}_{pm}\left(\zeta_\wp\right),\mathbf{R}_p\left(\zeta_\wp\right),\mathbf{R}_m\left(\zeta_\wp\right),\mathbf{R}_{pm}\left(\zeta_\wp\right)\right)\\&+\frac{\beta}{\mathbb{M}(\beta)\Gamma(\beta)}\sum_{\kappa=1}^{\mathbf{n}}\begin{cases}\dfrac{\nabla_1\left(\zeta_\kappa,\mathbf{S}(\zeta_\kappa),\mathbf{I}_p(\zeta_\kappa),\mathbf{I}_m(\zeta_\kappa),\mathbf{I}_{pm}(\zeta_\kappa),\mathbf{R}_p(\zeta_\kappa),\mathbf{R}_m(\zeta_\kappa),\mathbf{R}_{pm}(\zeta_\kappa)\right)}{\hbar}\\\times\displaystyle\int_{\zeta_\kappa}^{\zeta_{\kappa+1}}(\mathbf{y}-\zeta_{\kappa-1})(\zeta_{\mathbf{n}+1}-\mathbf{y})^{\beta-1}d\mathbf{y}\\-\dfrac{\nabla_1\left(\zeta_{\kappa-1},\mathbf{S}(\boldsymbol{\zeta}_{\kappa-1}),\mathbf{I}_p(\zeta_{\kappa-1}),\mathbf{I}_m(\zeta_{\kappa-1}),\mathbf{I}_{pm}(\zeta_{\kappa-1}),\mathbf{R}_p(\zeta_{\kappa-1}),\mathbf{R}_m(\zeta_{\kappa-1}),\mathbf{R}_{pm}(\zeta_{\kappa-1})\right)}{\hbar}\\\times\displaystyle\int_{\zeta_\kappa}^{\zeta_{\kappa+1}}(\mathbf{y}-\zeta_{\kappa-1})(\zeta_{\mathbf{n}+1}-\mathbf{y})^{\beta-1}d\mathbf{y}.\end{cases}\\&=\mathbf{S}(0)+\frac{1-\beta}{\mathbb{M}(\beta)}\nabla_1\left(\zeta_{\mathbf{n}},\mathbf{S}(\zeta_{\mathbf{n}}),\mathbf{I}_p(\zeta_{\mathbf{n}}),\mathbf{I}_m(\zeta_{\mathbf{n}}),\mathbf{I}_{pm}(\zeta_{\mathbf{n}}),\mathbf{R}_p(\zeta_{\mathbf{n}}),\mathbf{R}_m(\zeta_{\mathbf{n}}),\mathbf{R}_{pm}(\zeta_{\mathbf{n}})\right)\\&+\frac{\beta}{\mathbb{M}(\beta)\Gamma(\beta)}\sum_{\kappa=1}^{\mathbf{n}}\left(\begin{cases}\dfrac{\nabla_1\left(\zeta_\kappa,\mathbf{S}(\zeta_\kappa),\mathbf{I}_p(\zeta_\kappa),\mathbf{I}_m(\zeta_\kappa),\mathbf{I}_{pm}(\zeta_\kappa),\mathbf{R}_p(\zeta_\kappa),\mathbf{R}_m(\zeta_\kappa),\mathbf{R}_{pm}(\zeta_\kappa)\right)}{\hbar}\mathfrak{I}_{\kappa-1}\\-\dfrac{\nabla_1\left(\zeta_{\kappa-1},\mathbf{S}(\zeta_{\kappa-1}),\mathbf{I}_p(\zeta_{\kappa-1}),\mathbf{I}_m(\zeta_{\kappa-1}),\mathbf{I}_{pm}(\zeta_{\kappa-1}),\mathbf{R}_p(\zeta_{\kappa-1}),\mathbf{R}_m(\zeta_{\kappa-1}),\mathbf{R}_{pm}(\zeta_{\kappa-1})\right)}{\hbar}\mathfrak{I}_\kappa\end{cases}\right),\end{aligned}\tag{51}$$

where

$$\begin{aligned}\mathfrak{I}_{\kappa-1}&=\int_{\zeta_\kappa}^{\zeta_{\kappa+1}}(\mathbf{y}-\zeta_{\kappa-1})(\zeta_{\mathbf{n}+1}-\mathbf{y})^{\beta-1}d\mathbf{y}\\&=-\frac{1}{\beta}\left\{(\zeta_{\kappa+1}-\zeta_{\kappa-1})(\zeta_{\mathbf{n}+1}-\zeta_{\kappa+1})^{\beta}-(\zeta_\kappa-\zeta_{\kappa-1})(\zeta_{\mathbf{n}+1}-\zeta_\kappa)^{\beta}\right\}-\frac{1}{\beta(\beta+1)}\left\{(\zeta_{\mathbf{n}+1}-\zeta_{\kappa+1})^{\beta+1}(\zeta_{\mathbf{n}+1}-\zeta_{\kappa+1})^{\beta}-(\zeta_{\mathbf{n}+1}-\zeta_\kappa)^{\beta+1}\right\},\end{aligned}\tag{52}$$

and

$$\begin{aligned}\mathfrak{I}_\kappa&=\int_{\zeta_\kappa}^{\zeta_{\kappa+1}}(\mathbf{y}-\zeta_{\kappa-1})(\zeta_{\mathbf{n}+1}-\mathbf{y})^{\beta-1}d\mathbf{y}\\&=-\frac{1}{\beta}\left\{(\zeta_{\kappa+1}-\zeta_{\kappa-1})(\zeta_{\mathbf{n}+1}-\zeta_{\kappa+1})^{\beta}\right\}\\&-\frac{1}{\beta(\beta+1)}\left\{(\zeta_{\mathbf{n}+1}-\zeta_{\kappa+1})^{\beta+1}-(\zeta_{\mathbf{n}+1}-\zeta_\kappa)^{\beta+1}\right\}.\end{aligned}\tag{53}$$

Also, utilizing $\zeta_\kappa=\kappa\hbar$ into (52) and (53) represents

$$\mathfrak{I}_{\kappa-1}=\frac{\hbar^{\beta+1}}{\beta(\beta+1)}\left\{(\mathbf{n}+1-\kappa)^{\beta}(\mathbf{n}-\kappa+2+\beta)-(\mathbf{n}-\kappa)^{\beta}(\mathbf{n}-\kappa+2+2\beta)\right\},\tag{54}$$

and

$$\mathfrak{I}_\kappa=\frac{\hbar^{\beta+1}}{\beta(\beta+1)}\left\{(\mathbf{n}+1-\kappa)^{\beta+1}-(\mathbf{n}-\kappa)^{\beta}(\mathbf{n}-\kappa+1+\beta)\right\}.\tag{55}$$

Eventually, we can write (56) in the form of (54) and (55) as follows:

$$\mathbf{S}(\zeta_{\mathbf{n}+1}) = \mathbf{S}(\zeta_0) + \frac{1-\beta}{\mathbb{M}(\beta)}\nabla_1\left(\zeta_{\mathbf{n}}, \mathbf{S}(\zeta_{\mathbf{n}}), \mathbf{I}_p(\zeta_{\mathbf{n}}), \mathbf{I}_m(\zeta_{\mathbf{n}}), \mathbf{I}_{pm}(\zeta_{\mathbf{n}}), \mathbf{R}_p(\zeta_{\mathbf{n}}), \mathbf{R}_m(\zeta_{\mathbf{n}}), \mathbf{R}_{pm}(\zeta_{\mathbf{n}})\right),$$

$$+\frac{\beta}{\mathbb{M}(\beta)\Gamma(\beta)}\sum_{\kappa=1}^{\mathbf{n}}\left(\begin{cases}\dfrac{\nabla_1\left(\zeta_\kappa, \mathbf{S}(\zeta_\kappa), \mathbf{I}_p(\zeta_\kappa), \mathbf{I}_m(\zeta_\kappa), \mathbf{I}_{pm}(\zeta_\kappa), \mathbf{R}_p(\zeta_\kappa), \mathbf{R}_m(\zeta_\kappa), \mathbf{R}_{pm}(\zeta_\kappa)\right)}{\Gamma(\beta+2)} \\ \times\hbar^\beta\left\{(\mathbf{n}+1-\kappa)^\beta(\mathbf{n}-\kappa+2+\beta) - (\mathbf{n}-\kappa)^\beta(\mathbf{n}-\kappa+2+2\beta)\right\} \\ -\dfrac{\nabla_1\left(\zeta_{\kappa-1}, \mathbf{S}(\zeta_{\kappa-1}), \mathbf{I}_p(\zeta_{\kappa-1}), \mathbf{I}_m(\zeta_{\kappa-1}), \mathbf{I}_{pm}(\zeta_{\kappa-1}), \mathbf{R}_p(\zeta_{\kappa-1}), \mathbf{R}_m(\zeta_{\kappa-1}), \mathbf{R}_{pm}(\zeta_{\kappa-1})\right)}{\hbar} \\ \times\hbar^\beta\left\{(\mathbf{n}+1-\kappa)^\beta(\mathbf{n}-\kappa+2+\beta) - (\mathbf{n}-\kappa)^\beta(\mathbf{n}-\kappa+2+2\beta)\right\}\end{cases}\right). \tag{56}$$

Additionally, the formulations for the remaining model factors are as follows:

$$\mathbf{I}_p(\zeta_{\mathbf{n}+1}) = \mathbf{I}_p(\zeta_0) + \frac{1-\beta}{\mathbb{M}(\beta)}\nabla_2\left(\zeta_{\mathbf{n}}, \mathbf{S}(\zeta_{\mathbf{n}}), \mathbf{I}_p(\zeta_{\mathbf{n}}), \mathbf{I}_m(\zeta_{\mathbf{n}}), \mathbf{I}_{pm}(\zeta_{\mathbf{n}}), \mathbf{R}_p(\zeta_{\mathbf{n}}), \mathbf{R}_m(\zeta_{\mathbf{n}}), \mathbf{R}_{pm}(\zeta_{\mathbf{n}})\right)$$

$$+\frac{\beta}{\mathbb{M}(\beta)\Gamma(\beta)}\sum_{\kappa=1}^{\mathbf{n}}\left(\begin{cases}\dfrac{\nabla_2\left(\zeta_\kappa, \mathbf{S}(\zeta_\kappa), \mathbf{I}_p(\zeta_\kappa), \mathbf{I}_m(\zeta_\kappa), \mathbf{I}_{pm}(\zeta_\kappa), \mathbf{R}_p(\zeta_\kappa), \mathbf{R}_m(\zeta_\kappa), \mathbf{R}_{pm}(\zeta_\kappa)\right)}{\Gamma(\beta+2)} \\ \times\hbar^\beta\left\{(\mathbf{n}+1-\kappa)^\beta(\mathbf{n}-\kappa+2+\beta) - (\mathbf{n}-\kappa)^\beta(\mathbf{n}-\kappa+2+2\beta)\right\} \\ -\dfrac{\nabla_2\left(\zeta_{\kappa-1}, \mathbf{S}(\zeta_{\kappa-1}), \mathbf{I}_p(\zeta_{\kappa-1}), \mathbf{I}_m(\zeta_{\kappa-1}), \mathbf{I}_{pm}(\zeta_{\kappa-1}), \mathbf{R}_p(\zeta_{\kappa-1}), \mathbf{R}_m(\zeta_{\kappa-1}), \mathbf{R}_{pm}(\zeta_{\kappa-1})\right)}{\hbar} \\ \times\hbar^\beta\left\{(\mathbf{n}+1-\kappa)^\beta(\mathbf{n}-\kappa+2+\beta) - (\mathbf{n}-\kappa)^\beta(\mathbf{n}-\kappa+2+2\beta)\right\}\end{cases}\right),$$

$$\mathbf{I}_m(\zeta_{\mathbf{n}+1}) = \mathbf{I}_m(\zeta_0) + \frac{1-\beta}{\mathbb{M}(\beta)}\nabla_3\left(\zeta_{\mathbf{n}}, \mathbf{S}(\zeta_{\mathbf{n}}), \mathbf{I}_p(\zeta_{\mathbf{n}}), \mathbf{I}_m(\zeta_{\mathbf{n}}), \mathbf{I}_{pm}(\zeta_{\mathbf{n}}), \mathbf{R}_p(\zeta_{\mathbf{n}}), \mathbf{R}_m(\zeta_{\mathbf{n}}), \mathbf{R}_{pm}(\zeta_{\mathbf{n}})\right)$$

$$+\frac{\beta}{\mathbb{M}(\beta)\Gamma(\beta)}\sum_{\kappa=1}^{\mathbf{n}}\left(\begin{cases}\dfrac{\nabla_3\left(\zeta_\kappa, \mathbf{S}(\zeta_\kappa), \mathbf{I}_p(\zeta_\kappa), \mathbf{I}_m(\zeta_\kappa), \mathbf{I}_{pm}(\zeta_\kappa), \mathbf{R}_p(\zeta_\kappa), \mathbf{R}_m(\zeta_\kappa), \mathbf{R}_{pm}(\zeta_\kappa)\right)}{\Gamma(\beta+2)} \\ \times\hbar^\beta\left\{(\mathbf{n}+1-\kappa)^\beta(\mathbf{n}-\kappa+2+\beta) - (\mathbf{n}-\kappa)^\beta(\mathbf{n}-\kappa+2+2\beta)\right\} \\ -\dfrac{\nabla_3\left(\zeta_{\kappa-1}, \mathbf{S}(\zeta_{\kappa-1}), \mathbf{I}_p(\zeta_{\kappa-1}), \mathbf{I}_m(\zeta_{\kappa-1}), \mathbf{I}_{pm}(\zeta_{\kappa-1}), \mathbf{R}_p(\zeta_{\kappa-1}), \mathbf{R}_m(\zeta_{\kappa-1}), \mathbf{R}_{pm}(\zeta_{\kappa-1})\right)}{\hbar} \\ \times\hbar^\beta\left\{(\mathbf{n}+1-\kappa)^\beta(\mathbf{n}-\kappa+2+\beta) - (\mathbf{n}-\kappa)^\beta(\mathbf{n}-\kappa+2+2\beta)\right\},\end{cases}\right),$$

$$\mathbf{I}_{pm}(\zeta_{\mathbf{n}+1}) = \mathbf{I}_{pm}(\zeta_0) + \frac{1-\beta}{\mathbb{M}(\beta)}\nabla_4\left(\zeta_{\mathbf{n}}, \mathbf{S}(\zeta_{\mathbf{n}}), \mathbf{I}_p(\zeta_{\mathbf{n}}), \mathbf{I}_m(\zeta_{\mathbf{n}}), \mathbf{I}_{pm}(\zeta_{\mathbf{n}}), \mathbf{R}_p(\zeta_{\mathbf{n}}), \mathbf{R}_m(\zeta_{\mathbf{n}}), \mathbf{R}_{pm}(\zeta_{\mathbf{n}})\right)$$

$$+\frac{\beta}{\mathbb{M}(\beta)\Gamma(\beta)}\sum_{\kappa=1}^{\mathbf{n}}\left(\begin{cases}\dfrac{\nabla_4\left(\zeta_\kappa, \mathbf{S}(\zeta_\kappa), \mathbf{I}_p(\zeta_\kappa), \mathbf{I}_m(\zeta_\kappa), \mathbf{I}_{pm}(\zeta_\kappa), \mathbf{R}_p(\zeta_\kappa), \mathbf{R}_m(\zeta_\kappa), \mathbf{R}_{pm}(\zeta_\kappa)\right)}{\Gamma(\beta+2)} \\ \times\hbar^\beta\left\{(\mathbf{n}+1-\kappa)^\beta(\mathbf{n}-\kappa+2+\beta) - (\mathbf{n}-\kappa)^\beta(\mathbf{n}-\kappa+2+2\beta)\right\} \\ -\dfrac{\nabla_4\left(\zeta_{\kappa-1}, \mathbf{S}(\zeta_{\kappa-1}), \mathbf{I}_p(\zeta_{\kappa-1}), \mathbf{I}_m(\zeta_{\kappa-1}), \mathbf{I}_{pm}(\zeta_{\kappa-1}), \mathbf{R}_p(\zeta_{\kappa-1}), \mathbf{R}_m(\zeta_{\kappa-1}), \mathbf{R}_{pm}(\zeta_{\kappa-1})\right)}{\hbar} \\ \times\hbar^\beta\left\{(\mathbf{n}+1-\kappa)^\beta(\mathbf{n}-\kappa+2+\beta) - (\mathbf{n}-\kappa)^\beta(\mathbf{n}-\kappa+2+2\beta)\right\},\end{cases}\right), \tag{57}$$

$$\mathbf{R}_p(\zeta_{\mathbf{n}+1}) = \mathbf{R}_p(\zeta_0) + \frac{1-\beta}{\mathbb{M}(\beta)}\nabla_5\big(\zeta_{\mathbf{n}}, \mathbf{S}(\zeta_{\mathbf{n}}), \mathbf{I}_p(\zeta_{\mathbf{n}}), \mathbf{I}_m(\zeta_{\mathbf{n}}), \mathbf{I}_{pm}(\zeta_{\mathbf{n}}), \mathbf{R}_p(\zeta_{\mathbf{n}}), \mathbf{R}_m(\zeta_{\mathbf{n}}), \mathbf{R}_{pm}(\zeta_{\mathbf{n}})\big)$$
$$+ \frac{\beta}{\mathbb{M}(\beta)\Gamma(\beta)}\sum_{\kappa=1}^{\mathbf{n}}\left\{\begin{array}{l}\dfrac{\nabla_5\big(\zeta_\kappa, \mathbf{S}(\zeta_\kappa), \mathbf{I}_p(\zeta_\kappa), \mathbf{I}_m(\zeta_\kappa), \mathbf{I}_{pm}(\zeta_\kappa), \mathbf{R}_p(\zeta_\kappa), \mathbf{R}_m(\zeta_\kappa), \mathbf{R}_{pm}(\zeta_\kappa)\big)}{\Gamma(\beta+2)} \\ \times\hbar^\beta\big\{(\mathbf{n}+1-\kappa)^\beta(\mathbf{n}-\kappa+2+\beta) - (\mathbf{n}-\kappa)^\beta(\mathbf{n}-\kappa+2+2\beta)\big\} \\ -\dfrac{\nabla_5\big(\zeta_{\kappa-1}, \mathbf{S}(\zeta_{\kappa-1}), \mathbf{I}_p(\zeta_{\kappa-1}), \mathbf{I}_m(\zeta_{\kappa-1}), \mathbf{I}_{pm}(\zeta_{\kappa-1}), \mathbf{R}_p(\zeta_{\kappa-1}), \mathbf{R}_m(\zeta_{\kappa-1}), \mathbf{R}_{pm}(\zeta_{\kappa-1})\big)}{\hbar} \\ \times\hbar^\beta\big\{(\mathbf{n}+1-\kappa)^\beta(\mathbf{n}-\kappa+2+\beta) - (\mathbf{n}-\kappa)^\beta(\mathbf{n}-\kappa+2+2\beta)\big\},\end{array}\right\},$$

$$\mathbf{R}_m(\zeta_{\mathbf{n}+1}) = \mathbf{R}_m(\zeta_0) + \frac{1-\beta}{\mathbb{M}(\beta)}\nabla_6\big(\zeta_{\mathbf{n}}, \mathbf{S}(\zeta_{\mathbf{n}}), \mathbf{I}_p(\zeta_{\mathbf{n}}), \mathbf{I}_m(\zeta_{\mathbf{n}}), \mathbf{I}_{pm}(\zeta_{\mathbf{n}}), \mathbf{R}_p(\zeta_{\mathbf{n}}), \mathbf{R}_m(\zeta_{\mathbf{n}}), \mathbf{R}_{pm}(\zeta_{\mathbf{n}})\big)$$
$$+ \frac{\beta}{\mathbb{M}(\beta)\Gamma(\beta)}\sum_{\kappa=1}^{\mathbf{n}}\left\{\begin{array}{l}\dfrac{\nabla_6\big(\zeta_\kappa, \mathbf{S}(\zeta_\kappa), \mathbf{I}_p(\zeta_\kappa), \mathbf{I}_m(\zeta_\kappa), \mathbf{I}_{pm}(\zeta_\kappa), \mathbf{R}_p(\zeta_\kappa), \mathbf{R}_m(\zeta_\kappa), \mathbf{R}_{pm}(\zeta_\kappa)\big)}{\Gamma(\beta+2)} \\ \times\hbar^\beta\big\{(\mathbf{n}+1-\kappa)^\beta(\mathbf{n}-\kappa+2+\beta) - (\mathbf{n}-\kappa)^\beta(\mathbf{n}-\kappa+2+2\beta)\big\} \\ -\dfrac{\nabla_6\big(\zeta_{\kappa-1}, \mathbf{S}(\zeta_{\kappa-1}), \mathbf{I}_p(\zeta_{\kappa-1}), \mathbf{I}_m(\zeta_{\kappa-1}), \mathbf{I}_{pm}(\zeta_{\kappa-1}), \mathbf{R}_p(\zeta_{\kappa-1}), \mathbf{R}_m(\zeta_{\kappa-1}), \mathbf{R}_{pm}(\zeta_{\kappa-1})\big)}{\hbar} \\ \times\hbar^\beta\big\{(\mathbf{n}+1-\kappa)^\beta(\mathbf{n}-\kappa+2+\beta) - (\mathbf{n}-\kappa)^\beta(\mathbf{n}-\kappa+2+2\beta)\big\},\end{array}\right\}, \tag{58}$$

$$\mathbf{R}_{pm}(\zeta_{\mathbf{n}+1}) = \mathbf{R}_{pm}(\zeta_0) + \frac{1-\beta}{\mathbb{M}(\beta)}\nabla_7\big(\zeta_{\mathbf{n}}, \mathbf{S}(\zeta_{\mathbf{n}}), \mathbf{I}_p(\zeta_{\mathbf{n}}), \mathbf{I}_m(\zeta_{\mathbf{n}}), \mathbf{I}_{pm}(\zeta_{\mathbf{n}}), \mathbf{R}_p(\zeta_{\mathbf{n}}), \mathbf{R}_m(\zeta_{\mathbf{n}}), \mathbf{R}_{pm}(\zeta_{\mathbf{n}})\big)$$
$$+ \frac{\beta}{\mathbb{M}(\beta)\Gamma(\beta)}\sum_{\kappa=1}^{\mathbf{n}}\left\{\begin{array}{l}\dfrac{\nabla_7\big(\zeta_\kappa, \mathbf{S}(\zeta_\kappa), \mathbf{I}_p(\zeta_\kappa), \mathbf{I}_m(\zeta_\kappa), \mathbf{I}_{pm}(\zeta_\kappa), \mathbf{R}_p(\zeta_\kappa), \mathbf{R}_m(\zeta_\kappa), \mathbf{R}_{pm}(\zeta_\kappa)\big)}{\Gamma(\beta+2)} \\ \times\hbar^\beta\big\{(\mathbf{n}+1-\kappa)^\beta(\mathbf{n}-\kappa+2+\beta) - (\mathbf{n}-\kappa)^\beta(\mathbf{n}-\kappa+2+2\beta)\big\} \\ -\dfrac{\nabla_7\big(\zeta_{\kappa-1}, \mathbf{S}(\zeta_{\kappa-1}), \mathbf{I}_p(\zeta_{\kappa-1}), \mathbf{I}_m(\zeta_{\kappa-1}), \mathbf{I}_{pm}(\zeta_{\kappa-1}), \mathbf{R}_p(\zeta_{\kappa-1}), \mathbf{R}_m(\zeta_{\kappa-1}), \mathbf{R}_{pm}(\zeta_{\kappa-1})\big)}{\hbar} \\ \times\hbar^\beta\big\{(\mathbf{n}+1-\kappa)^\beta(\mathbf{n}-\kappa+2+\beta) - (\mathbf{n}-\kappa)^\beta(\mathbf{n}-\kappa+2+2\beta)\big\}.\end{array}\right\}.$$

3.8. Results and Discussion. In this section, simulation studies for the resulting structure ($\mathbb{P}$ co-infection model) are carried out, taking into consideration the ABC derivative fractional operator having ML kernel. We employed MATLAB 2022 to assess the influence of several factors in the proliferation as well as to prevent $\mathbb{P}$ co-infection. For modelling purposes, the model parameters in Table 1 are considered.

In Figure 4, by maintaining the interaction rate stable, $q_1 = 0.9$, we evaluated the influence of ρ_1 in reducing the amount of pneumonia exclusively infected people. Figures 5 and 6 show that as the quantity of ρ_1 increases, the proportion of pneumonia exclusively susceptible people decreases. Figure 5, 6, and 7 indicate that the proportion of instances in categories $\mathbf{I}_p, \mathbf{I}_m, \mathbf{I}_{pm}, \mathbf{R}_p, \mathbf{R}_m, \mathbf{R}_{pm}$ decreased dramatically when contrasted to Figures 4–7, which were replicated lacking the control approach. For various orders of the fractional derivative β, the trajectories have varying asymptotic behaviour. As a result, authorities and regulators should focus on maximizing the levels of the survival rate, either by addressing sick populations or by increasing specific susceptibility to the pneumonia virus.

In Figure 8, we can observe that ρ_2 is essential to minimize the meningitis development. The proportion of

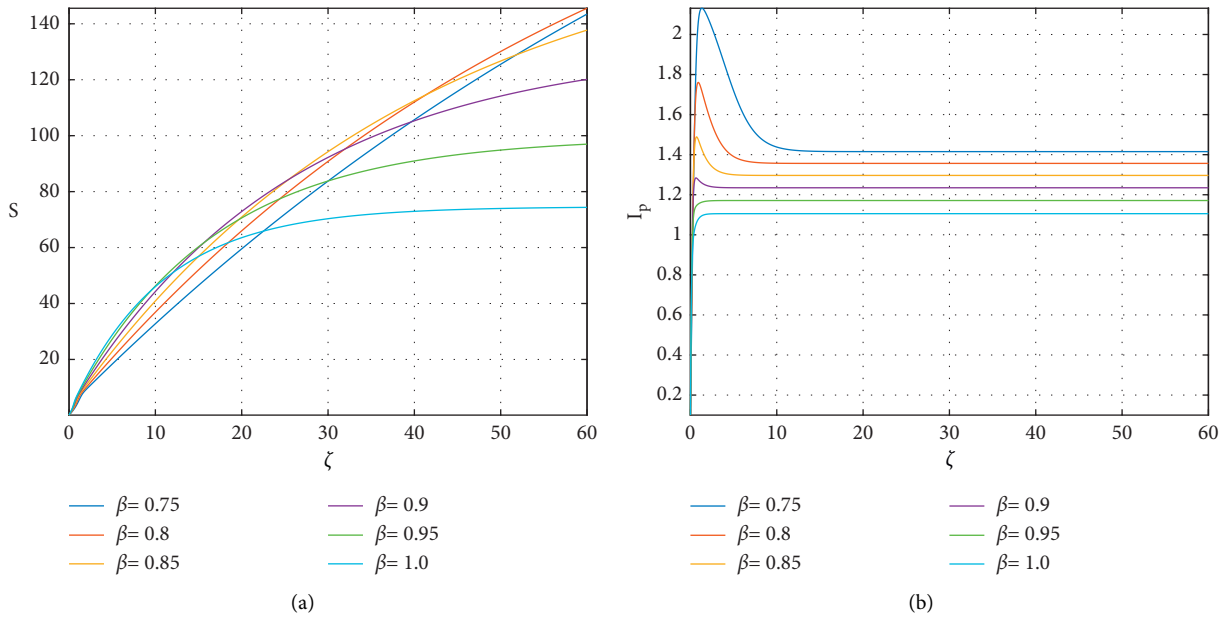

FIGURE 4: Two-dimensional illustration of the susceptible class **S** and pneumonia infectious $\mathbf{I}_p$ when $q_1 = 0.9$ with multiple fractional orders $\beta \in [0, 1]$.

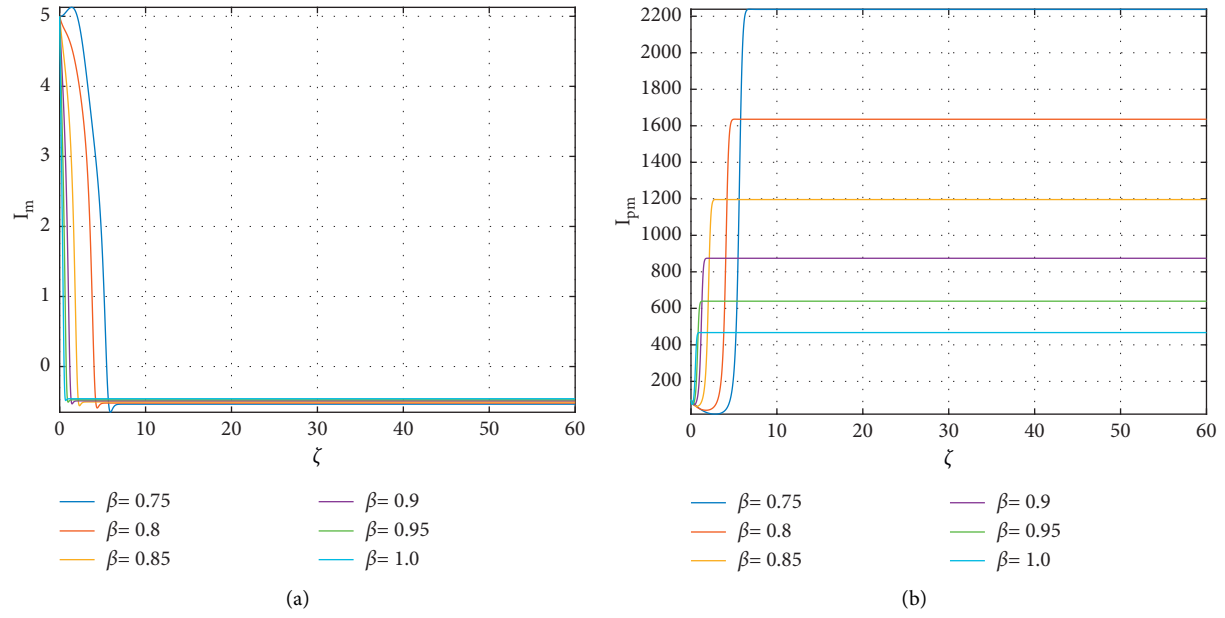

FIGURE 5: Two-dimensional illustration of the meningitis infectious $\mathbf{I}_m$ and $\mathbb{PM}$ co-infection $\mathbf{I}_{pm}$ when $q_1 = 0.9$ with multiple fractional orders $\beta \in [0, 1]$.

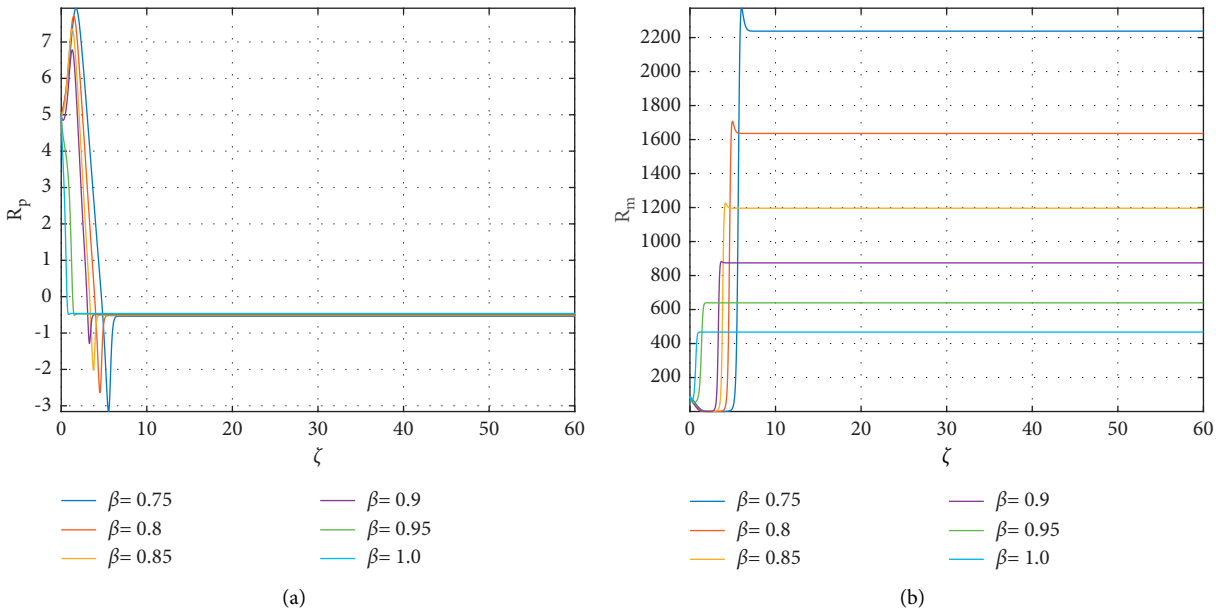

FIGURE 6: Two-dimensional illustration of the pneumonia recovered $\mathbf{R}_p$ and meningitis recovered $\mathbf{R}_m$ when $q_1 = 0.9$ with multiple fractional orders $\beta \in [0, 1]$.

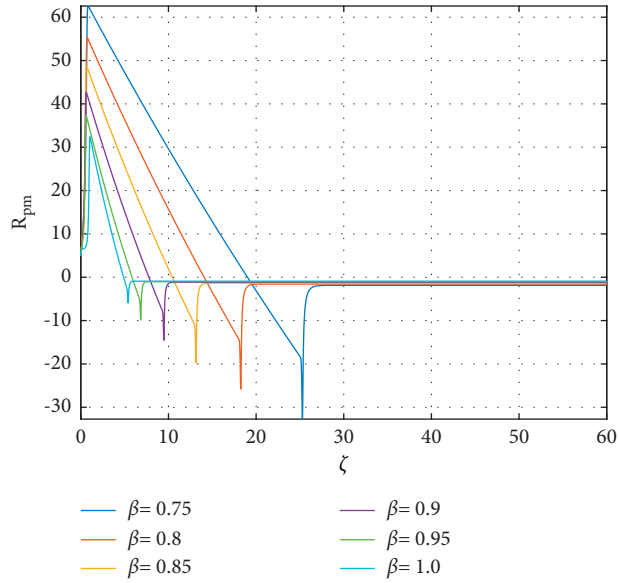

FIGURE 7: Two-dimensional illustration of the ℙℳ co-infection recovered $\mathbf{R}_{pm}$ when $q_1 = 0.9$ with multiple fractional orders $\beta \in [0, 1]$.

contagious community owing to meningitis decreases as the level of ρ_2 increases from 0.1 to 0.9, but the interaction rate stays unchanged at $q_2 = 0.06$. Figures 9, 10, and 11 indicate that the proportion of instances in categories $\mathbf{I}_p, \mathbf{I}_m, \mathbf{I}_{pm}, \mathbf{R}_p, \mathbf{R}_m, \mathbf{R}_{pm}$ decreased dramatically when contrasted to Figures 8–11, which were replicated inducing the control approach. Therefore, the outbreak spreads gradually as the fractional order diminishes from 1, and the majority of

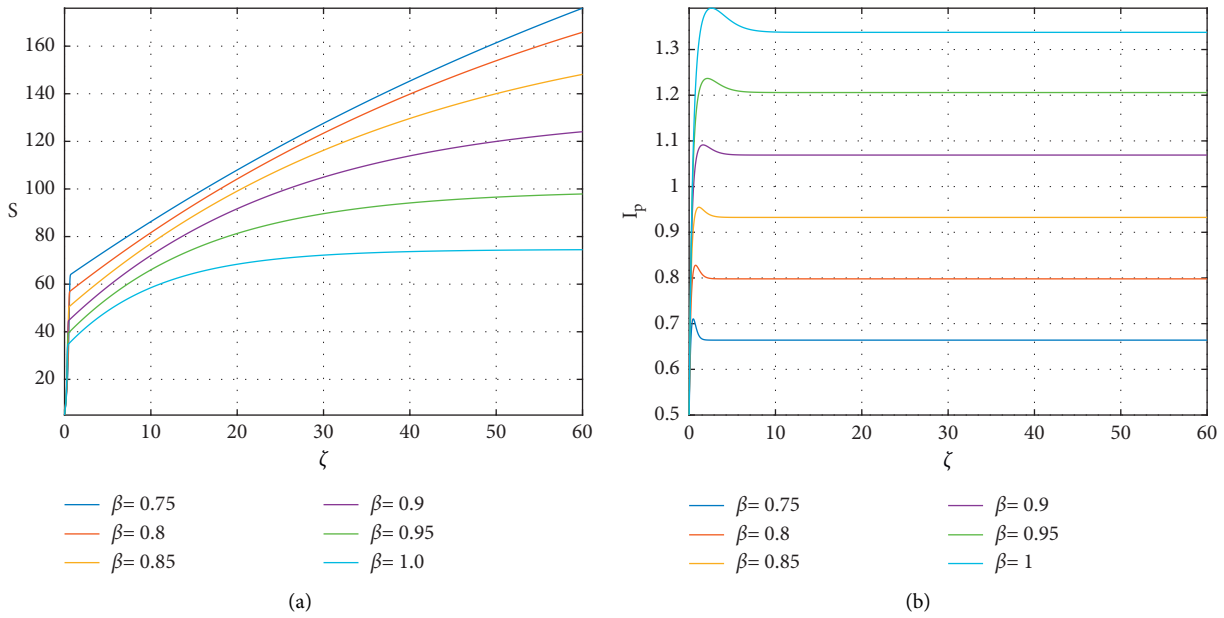

FIGURE 8: Two-dimensional illustration of the susceptible class **S** and pneumonia infectious $\mathbf{I}_p$ when $q_2 = 0.06$, $\rho_2 \in [0.1, 0.9]$ with multiple fractional orders $\beta \in [0, 1]$.

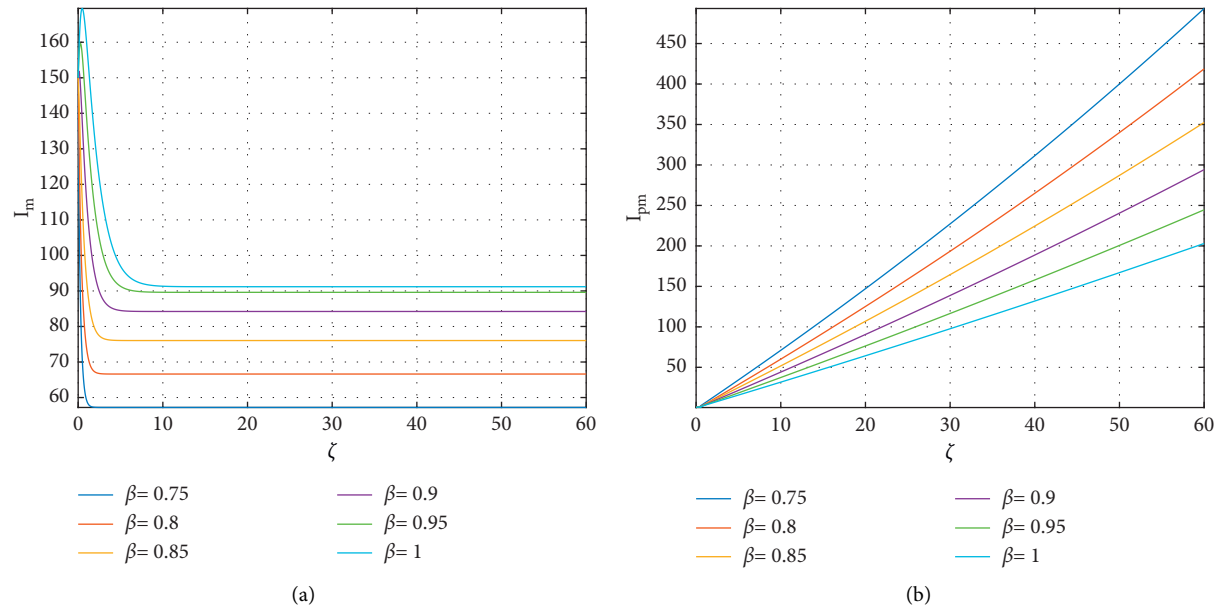

FIGURE 9: Two-dimensional illustration of the meningitis infectious $\mathbf{I}_m$ and $\mathbb{PM}$ co-infectious $\mathbf{I}_{pm}$ when $q_2 = 0.06$, $\rho_2 \in [0.1, 0.9]$ with multiple fractional orders $\beta \in [0, 1]$.

patients at the apex drops significantly (Figures 8–11). Consequently, normal individuals or the administration must pay special consideration to healing the afflicted individuals in their locality when combating the meningitis infection.

In Figure 12, the meningitis connection incidence q_2 and the success percentage of the co-infectious community ρ are both assumed unchanged. Figure 13 demonstrates that as the interaction frequency of pneumonia improves, the co-infectious numbers boost, implying that the proliferation of

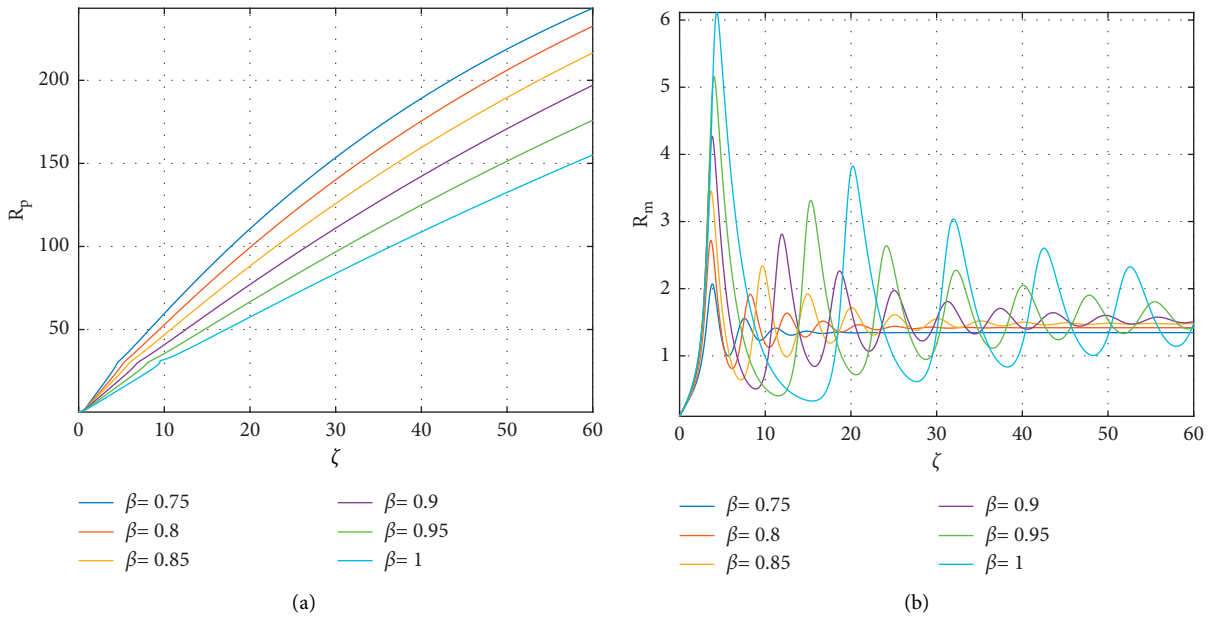

FIGURE 10: Two-dimensional illustration of the pneumonia recovered $\mathbf{R}_p$ and meningitis recovered $\mathbf{R}_m$ when $q_2 = 0.06$, $\rho_2 \in [0.1, 0.9]$ with multiple fractional orders $\beta \in [0, 1]$.

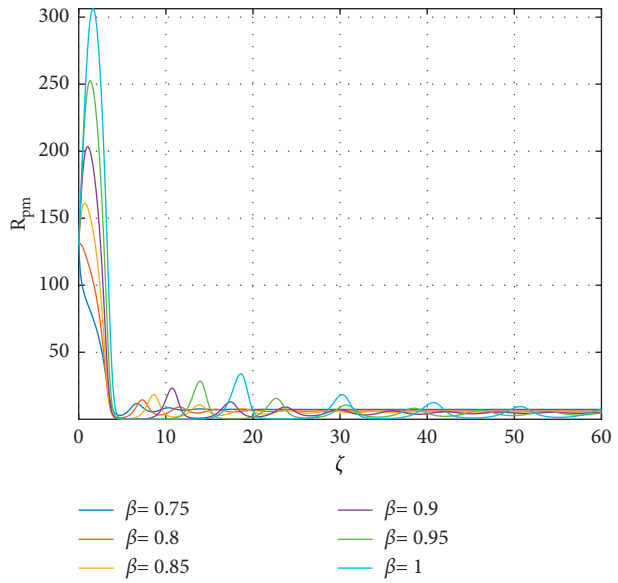

FIGURE 11: Two-dimensional illustration of the $\mathbb{R}_{pm}$ co-infectious recovered $\mathbf{R}_{pm}$ when $q_2 = 0.06$, $\rho_2 \in [0.1, 0.9]$ with multiple fractional orders $\beta \in [0, 1]$.

pneumonia and meningitis co-infection will expand as well. According to Figure 14, it is critical to reduce the incidence and prevalence of pneumonia in order to prevent co-infection. As a result, organizations should aim to minimize the interaction risk of pneumonia by quarantining sick individuals or implementing an effective mitigation technique to limit the spread of co-infection in the population.

The influence of the survival incidence of $\mathbb{P}$ on the co-infectious community was investigated. According to the scenario characterization in Section 2, co-infectious

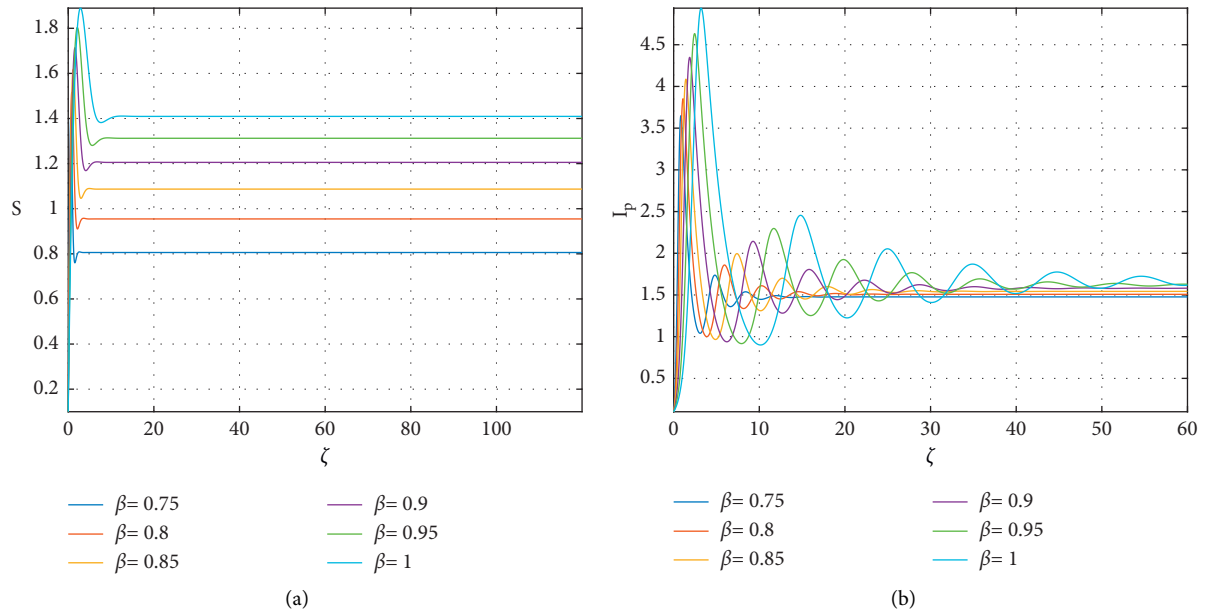

FIGURE 12: Two-dimensional illustration of the susceptible class **S** and pneumonia infectious $\mathbf{I}_p$ with varying contact rate q_2 and recovery rate co-infection ρ for multiple fractional orders $\beta \in [0, 1]$.

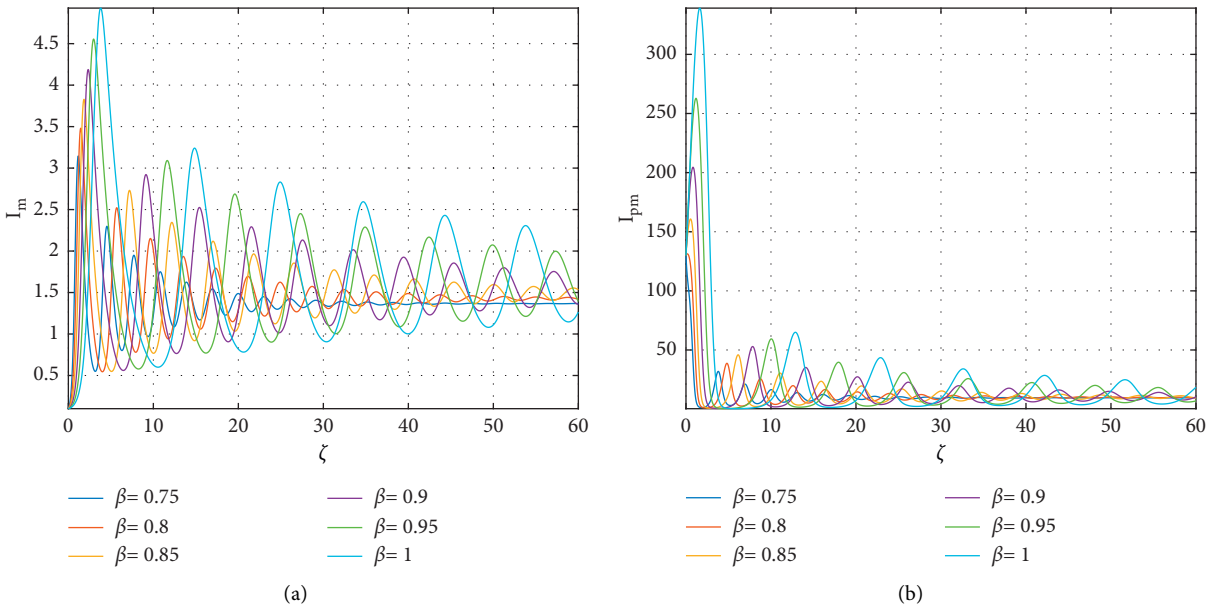

FIGURE 13: Two-dimensional illustration of the meningitis infection $\mathbf{I}_m$ and $\mathbb{PM}$ infectious $\mathbf{I}_{pm}$ with varying contact rate q_2 and recovery rate co-infection ρ for multiple fractional orders $\beta \in [0, 1]$.

populations generally heal from pneumonia solely or resume the corresponding healed section, alleviating the symptoms or additional processes. As a result, Figure 15 indicates that boosting the co-infectious majority's survival intensity has a significant impact on eliminating both infections in the region.

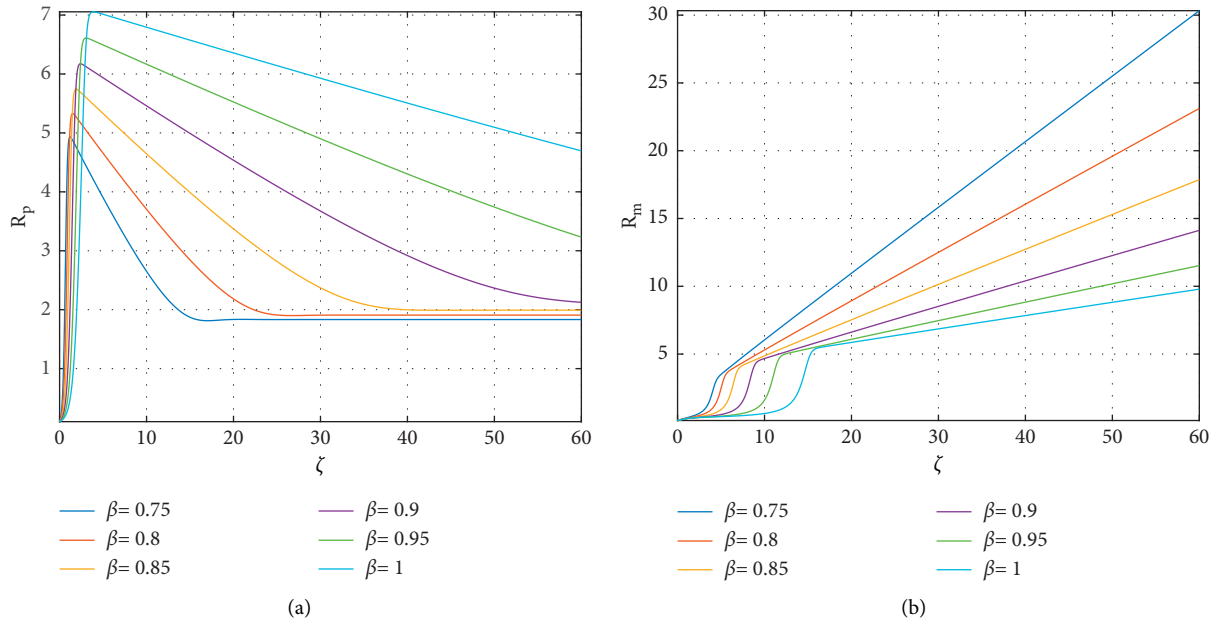

FIGURE 14: Two-dimensional illustration of the pneumonia recovered $\mathbf{R}_p$ and meningitis recovered $\mathbf{R}_m$ with varying contact rate q_2 and recovery rate co-infection ρ for multiple fractional orders $\beta \in [0, 1]$.

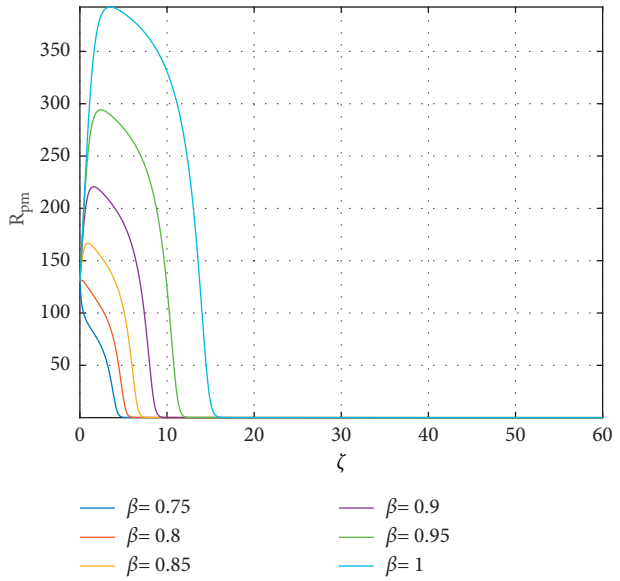

FIGURE 15: Two-dimensional illustration of the $\mathbb{PM}$ recovered $\mathbf{R}_{pm}$ with varying contact rate q_2 and recovery rate co-infection ρ for multiple fractional orders $\beta \in [0, 1]$.

4. Conclusion

This research examines seven-dimensional pneumonia and meningitis. The Atangana–Baleanu fractional derivative is applied to describe the integer-order framework, and the Banach contraction hypothesis is employed to assess the presence of systems in the fractional formulation of the numerical method. The Atangana–Baleanu fractional operator featuring generational characteristics is responsible for this beneficial outcome. The findings of this article argue that formal frameworks utilizing the Atangana–Baleanu fractional operator can effectively disclose the underlying or realistic features of real-world situations. This hypothesis can be supported by continuing research into the effects of various fractional operators, including such fractal-fractional derivatives, and reporting the performance of the Atangana–Baleanu fractional operator outcome on the relatively similar system or additional relevant epidemiological concepts. The paucity of a comparison of the present findings for the SEAIR paradigm employing the Atangana–Baleanu fractional operator versus findings acquired for the equivalent system assuming alternative fractional operators could potentially represent a deficit for ongoing studies.

Data Availability

No data were used to support this study.

Conflicts of Interest

The authors declare that they have no conflicts of interest.

Authors' Contributions

S. Rashid provided the main ideas of the article, constructed the main results, and submitted the article. B. Kanwal drafted the manuscript and provided the qualitative analysis. A. G. Ahmad presented the existence and uniqueness analysis with their illustration. E. Bonyah provided the solution of example and completed the final revision. S. K. Elagan presented the qualitative analysis of the proposed model. All authors read and approved the final manuscript.

References

[1] M. Caputo and M. Fabrizio, "A new definition of fractional derivative without singular kernel," *Prog. Fract. Differ. Appl.*vol. 73, no. 13, 2015.

[2] A. Atangana and D. Baleanu, "New fractional derivatives with nonlocal and non-singular kernel: theory and application to heat transfer model," *Thermal Science*, vol. 20, no. 2, pp. 763–769, 2016.

[3] R. Scherer, S. L. Kalla, Y. Tang, and J. Huang, "The Grünwald-Letnikov method for fractional differential equations," *Computers & Mathematics with Applications*, vol. 62, no. 3, pp. 902–917, 2011.

[4] C. Li, d. Qian, and Y. Q. Chen, "On riemann-liouville and Caputo derivatives," *Discrete Dynamics in Nature and Society*, vol. 2011, Article ID 562494, 15 pages, 2011.

[5] T. Li and Y. Wang, "Stability of a class of fractional-order nonlinear systems," *Discrete Dynamics in Nature and Society*, vol. 2014, Article ID 724270, 14 pages, 2014.

[6] H. Durur, A. Yokus, and K. A. Abro, "A non-linear analysis and fractionalized dynamics of Langmuir waves and ion sound as an application to acoustic waves," *International Journal of Modelling and Simulation*, pp. 1–7, 2020.

[7] A. Yokus, H. Durur, D. Kaya, H. Ahmad, and T. A. Nofal, "Numerical comparison of Caputo and Conformable derivatives of time fractional Burgers-Fisher equation," *Results in Physics*, vol. 25, Article ID 104247, 2021.

[8] H. Durur, O. Tasbozan, and A. Kurt, "New analytical solutions of conformable time fractional bad and good modified Boussinesq equations," *Applied Mathematics and Nonlinear Sciences*, vol. 5, no. 1, pp. 447–454, 2020.

[9] H. Khan, J. F. Gómez-Aguilar, A. Alkhazzan, and A. Khan, "A fractional order HIV-TB coinfection model with nonsingular Mittag-Leffler Law," *Mathematical Methods in the Applied Sciences*, vol. 43, no. 6, pp. 3786–3806, 2020.

[10] C. T. Deressa and G. F. Duressa, "Analysis of Atangana-Baleanu fractional-order SEAIR epidemic model with optimal control," *Advances in Difference Equations*, vol. 2021, no. 1, 2021.

[11] A. Atangana and J. F. Gómez-Aguilar, "Hyperchaotic behaviour obtained via a nonlocal operator with exponential decay and Mittag-Leffler laws," *Chaos, Solitons & Fractals*, vol. 102, pp. 285–294, 2017.

[12] A. Atangana and K. M. Owolabi, "New numerical approach for fractional differential equations," *Mathematical Modelling of Natural Phenomena*, vol. 13, no. 1, p. 3, 2018.

[13] T. Zdzislaw, "Matlab solutions of chaotic fractional order circuits," *Matlab Solutions of Chaotic Fractional Order Circuits. Engineering Education and Research Using MATLAB Engineering Education and Research Using MATLAB*, ' Intech Open, 2011.

[14] A. McLuckie, *Respiratory Disease and its Management*, p. 51, Springer, Berlin, 2009.

[15] World Health Organization, *Programme of acute respiratory infections*, Technical Bases for the WHO Recommendations on the Management of Pneumonia in Children at First-Level Health Facilities, World Health Organization, Geneva, Switzerland, 1991, https://apps.who.int/iris/handle/10665/61199.

[16] M. J. F. Martínez, E. G. Merino, E. G. Sánchez, J. E. G. Sánchez, A. M. d. Rey, and G. R. Sánchez, "A mathematical model to study the meningococcal meningitis," *Procedia Computer Science*, vol. 18, pp. 2492–2495, 2013.

[17] E. Joseph, *Mathematical Analysis of Prevention and Control Strategies of Pneumonia in- Adults and Children*, Unpublished MSc Dissertation. University of DareSalaam, Tanzania, 2012.

[18] G. T. Tilahun, O. D. Makinde, and D. Malonza, "Modelling and optimal control of typhoid fever disease with cost-effective strategies," *Computational and Mathematical Methods in Medicine*, vol. 2017, Article ID 2324518, 16 pages, 2017.

[19] D. Pessoa, *Modelling the Dynamics of streptococcus Pneumonia Transmission in Children*, Master's thesis, University of De Lisboa, Lisbon, Portugal, 2010.

[20] G. T. Tilahun, O. D. Makinde, and D. Malonza, "Modelling and optimal control of pneumonia disease with cost-effective strategies," *Journal of Biological Dynamics*, vol. 11, Article ID 28613986, 2017.

[21] J. K. K. Asamoah, F. Nyabadza, B. Seidu, M. Chand, H. Dutta, and H. Dutta, "Mathematical modelling of bacterial meningitis transmission dynamics with control measures," *Computational and Mathematical Methods in Medicine*, vol. 2018, Article ID 2657461, 21 pages, 2018.

[22] G. T. Tilahun, O. D. Makinde, and D. Malonza, "Co-dynamics of pneumonia and typhoid fever diseases with cost effective optimal control analysis," *Applied Mathematics and Computation*, vol. 316, pp. 438–459, 2018.

[23] D. O. Onyinge, N. O. Ongati, and F. Odundo, "Mathematical model for co-infection of pneumonia and HIV/AIDS with treatment," *Int. J. Sci. Eng. Appl. Sci.*vol. 2, 2016.

[24] O. C. Akinyi, J. Y. Mugisha, A. Manyonge, and C. Ouma, "Modelling the impact of misdiagnosis and treatment on the dynamics of malaria concurrent and co-infection with pneumonia," *Applied Mathematical Sciences*, 2013.

[25] S. Rashid, E. I. Abouelmagd, A. Khalid, F. B. Farooq, and Y.-M. Chu, "Some recent developments on dynamical $\hbar$--discrete fractional type inequalities in the frame of non-singular and nonlocal kernels," *Fractals*, vol. 30, Article ID 2240110, 2022.

[26] S. Rashid, S. Sultana, Y. Karaca, A. Khalid, and Y.-M. Chu, "Some further extensions considering discrete proportional fractional operators," *Fractals*, vol. 30, Article ID 2240026, 2022.

[27] K. Karthikeyan, P. Karthikeyan, H. M. Baskonus, K. Venkatachalam, and Y. M. Chu, "Almost sectorial operators on Ψ-Hilfer derivative fractional impulsive integro-differential equations ψ-Hilfer derivative fractional impulsive integro-differential equations," *Mathematical Methods in the Applied Sciences*, 2021.

[28] S. N. Hajiseyedazizi, M. E. Samei, J. Alzabut, and Y.-M. Chu, "On multi-step methods for singular fractional q-integro-differential equations," *Open Mathematics*, vol. 19, no. 1, pp. 1378–1405, 2021.

[29] F. Jin, Z.-S. Qian, Z.-S. Qian, Y.-M. Chu, and M. u. Rahman, "On nonlinear evolution model for drinking behavior under Caputo-Fabrizio derivative," *Journal of Applied Analysis & Computation*, vol. 12, no. 2, pp. 790–806, 2022.

[30] A. Atangana, "Extension of rate of change concept: from local to nonlocal operators with applications," *Results in Physics*, vol. 19, Article ID 103515, 2020.

[31] D. Baleanu, A. Jajarmi, S. S. Sajjadi, and D. Mozyrska, "A new fractional model and optimal control of a tumor-immune surveillance with non-singular derivative operator," *Chaos: An Interdisciplinary Journal of Nonlinear Science*, vol. 29, no. 8, Article ID 083127, 2019.

[32] N. Sene, "Fractional diffusion equation with new fractional operator," *Alexandria Engineering Journal*, vol. 59, no. 5, pp. 2921–2926, 2020.

[33] T.-H. Zhao, O. Castillo, H. Jahanshahi et al., "A fuzzy-based strategy to suppress the novel coronavirus (2019-NCOV) massive outbreak," *Applied and Computational Mathematics*, vol. 20, pp. 160–176, 2021.

[34] K. M. Owolabi, "Analysis and numerical simulation of multicomponent system with Atangana-Baleanu fractional derivative," *Chaos, Solitons & Fractals*, vol. 115, pp. 127–134, 2018.

[35] E. Demirci, A. Unal, and N. Ozalp, "A fractional order SEIR model with density dependent death rate," *Hacet. J. Math. Stat.*vol. 40, pp. 287–295, 2011.

[36] S. Uçar, "Analysis of a basic SEIRA model with Atangana-Baleanu derivative," *AIMS Mathematics*, vol. 5, no. 2, pp. 1411–1424, 2020.

[37] M. Toufik and A. Atangana, "New numerical approximation of fractional derivative with non-local and non-singular kernel: application to chaotic models," *European Physical Journal A: Hadrons and Nuclei*, vol. 132, p. 144, 2017.

[38] T. Abdeljawad and D. Baleanu, "Integration by parts and its applications of a new nonlocal fractional derivative with Mittag-Leffler nonsingular kernel," *The Journal of Nonlinear Science and Applications*, vol. 10, no. 03, pp. 1098–1107, 2017.

[39] J. Singh, D. Kumar, and D. Baleanu, "On the analysis of fractional diabetes model with exponential law," *Advances in Difference Equations*, vol. 2018, no. 1, p. 2018, 2018.

[40] Z. M. Odibat and N. T. Shawagfeh, "Generalized Taylor's formula," *Applied Mathematics and Computation*, vol. 186, no. 1, pp. 286–293, 2007.

[41] S. K. Panda, "Applying fixed point methods and fractional operators in the modelling of novel coronavirus 2019-nCoV/SARS-CoV-2," *Results in Physics*, vol. 19, Article ID 103433, 2020.

[42] S. M. Lenhart and J. T. Workman, *Optimal Control Applied to Biological Models*, CRC Press, Boca Raton, 2007.

[43] J. P. LaSalle, *The Stability of Dynamical Systems*, SIAM, Philadelphia, 1976.

Hindawi
Complexity
Volume 2022, Article ID 3878321, 14 pages
https://doi.org/10.1155/2022/3878321

Research Article

A Sampling Load Frequency Control Scheme for Power Systems with Time Delays

R. Sriraman,[1] **Jihad A. Younis**,[2] **C. P. Lim**,[3] **P. Hammachukiattikul**,[4] **G. Rajchakit**,[5] **and N. Boonsatit**[6]

[1]*Department of Mathematics, Kalasalingam Academy of Research and Education, Virudhunagar, Tamil Nadu 626126, India*
[2]*Department of Mathematics, Aden University, Khormaksar, P.O. Box 6014, Aden, Yemen*
[3]*Institute for Intelligent Systems Research and Innovation, Deakin University, Waurn Ponds, Geelong, Victoria 3216, Australia*
[4]*Department of Mathematics, Faculty of Science, Phuket Rajabhat University (PKRU), 6 Thepkasattree Road, Raddasa, Phuket 83000, Thailand*
[5]*Department of Mathematics, Faculty of Science, Maejo University, Chiang Mai 50290, Thailand*
[6]*Department of Mathematics, Faculty of Science and Technology, Rajamangala University of Technology Suvarnabhumi, Nonthaburi 11000, Thailand*

Correspondence should be addressed to Jihad A. Younis; jihadalsaqqaf@gmail.com

Received 14 February 2022; Accepted 11 May 2022; Published 29 June 2022

Academic Editor: Shanmugam Lakshmanan

In this study, we investigate the effectiveness of a robust sampled-data H_∞ load frequency control (LFC) scheme for power systems with randomly occurring time-varying delays. By using the input-delay technique, the sampled-data LFC model is reformulated as a continuous time-delay representation. Then, Bernoulli-distributed white noise sequences are used to describe randomly occurring time-varying delays in the sampled-data LFC model. Some less conservative conditions are achieved by utilizing the Lyapunov–Krasovskii functional (LKF) and employing Jensen inequality and reciprocal convex combination lemma to ensure the considered power system has mean-square asymptotic stability under the designed control scheme. The derived results are based on linear matrix inequalities (LMIs) that can readily be solved using the MATLAB LMI toolbox. The criteria obtained are used to analyze the upper bounds for time delays, and a comparison study to validate the efficacy of the presented method is presented.

1. Introduction

In recent years, research on power systems has advanced tremendously due to increased public demands for electricity, which promotes the incorporation of renewable energy into power systems [1, 2]. When a power system suffers from load disturbance or fluctuation, the system operating point can change, and deviations in the frequency of the system and the planned power exchanges can influence system performance in multiple contexts. Therefore, LFC has been proposed to ensure successful power system operations by maintaining an equilibrium among power supply and demand, thereby restoring the frequency of power systems to a proper range. Recently, a number of research studies have concentrated on the development of suitable controllers based on LFC for power systems [3–5]. In this respect, LFC schemes including proportional-integral (PI) control [2, 3], sliding mode control [6, 7], adaptive control [8], robust control [9, 10], sampled-data control [11], event-triggered control [12–14], and H_∞ control [15] have been well defined in the literature.

However, most LFC controllers operate in the continuous case, while practical controllers are often operated using a sampling period in the discrete case. In this context, the above-mentioned controllers do not always perform optimally in practice [16]. In power systems, control error signals are first received by sensors and sent to controllers via zero-order holders (ZOHs), before being transmitted to actuators

through ZOHs [17]. This sensor-controller-actuator (SCA) technique has a discrete link design, implying that the power system can be considered a continuous-discrete sampled-data model. In recent years, many studies have introduced sampled-data control designs for LFC-based systems [18–20]. Based on the LMI theory, discrete-time multivariable PID controllers were discussed in reference [19]. The study in reference [20] devised an input-delay strategy to convert a sampled-data model to a continuous model, while the studies in references [21, 22] revealed useful additional results for LFC-based power systems.

In real-world applications, random abrupt events are a common issue in sampled-data models due to environmental changes. Furthermore, owing to the appearance of time delays in dynamic systems, data transmission is frequently affected by random delays from sensors and remote receivers, which can significantly slow down the transmission of information [23, 24]. Therefore, investigations into sampled-data control systems with random delays have recently increased [11, 25, 26]. As an example, random delays are important for the application of the H_∞ algorithm performance, as reported in reference [25]. In reference [26], type-2 fuzzy systems with probabilistic delays and actuator failures were explored under nonfragile sampled-data control. A novel method for the finite-time stability for sampled-data control systems with random delays was proposed in reference [11].

On the other hand, many physical systems, including power systems, are susceptible to uncertainty under various conditions. It is essential to investigate power systems with uncertain parameters. There have been a few studies on robust LFC schemes for power systems [27–31]. In reference [29], the study examined LFC design for delayed power systems integrating a robust decentralized PI control. Applying Riccati equation, the study in reference [30] introduced a robust LFC method for one-area power systems. In reference [31], the potential of a physical system comprehension for robust controller designs in power systems was examined. On the other hand, the classic H_∞ control theory defines a control rule that yields the minimal value of the measured performance under the assumption of zero initial values. In this regard, the delay-dependent H_∞ LFC scheme for power systems has recently received significant interest from researchers [32–35]. For instance, in references [36, 37], based on the Lyapunov functional theory, some sufficient conditions are attained for H_∞ performance of uncertain systems, which gives the minimum value of the measured performance. In reference [32], the issue of robust H_∞ LFC methods for delayed multiarea power systems was examined. In reference [33], decentralized H_∞ LFC strategy for multiarea power systems including communication uncertainties was studied. Some relevant studies have explored the issue of H_∞ LFC methods for power systems with communication delays [34, 35]. To the best of our knowledge, the robust sampled-data H_∞ LFC problem for power systems with randomly occurring time-varying delays has never been completely addressed. As such, there is still potential for further investigation and development in the stability and stabilization analysis of power systems by addressing the robust sampled-data H_∞ LFC scheme, which motivated the present study.

On the basis of the above discussions, our primary goal in this study is to address the problem of robust sampled-data LFC for stability and stabilization of power systems with randomly occurring time delays by tackling the robust sampled-data H_∞ LFC scheme. The following are the major contributions of our research:

(i) Different from the traditional analyses, this article presents the robust sampled-data H_∞ LFC for power systems with randomly occurring time-varying delays. By taking the probability distribution characteristic of communication delays into consideration for LFC design, the power systems with PI controllers are modelled as stochastic time-delay systems. Moreover, the input-delay strategy converts the sampled-data model into a continuous time-delay representation.

(ii) The LMI-based mean-square asymptotic stability and stabilization criteria for power systems are established under the designed sampled-data H_∞ LFC scheme by constructing an appropriate LKF and employing Jensen inequality and the reciprocal convex combination inequality.

(iii) Two examples are offered to demonstrate that the presence of maximum allowable upper bounds of time delays by our approach is much better than the most recent results. A comparison study is also performed, demonstrating the low computational efficiency of the obtained criteria.

This study is organized as follows: the designed sampled-data LFC scheme for power systems is formally specified in Section 2. In Section 3, the sufficient criteria for stability and stabilization of the considered model are presented. In Section 4, the application of the robust sampled-data H_∞ LFC scheme to power systems with uncertainties is discussed. The case studies in Section 5 show the potential of the criteria presented. Conclusions are given in Section 6.

Notations. In the following sections, the superscripts $''T''$ and $''-1''$ indicate matrix transposition and inverse, respectively. I is any matrix with identity. Any matrix $Q > 0$ ($Q < 0$) denotes the positive definite (negative definite) matrix. The block diagonal matrix is represented by diag{...}, while $\mathbb{R}^n$ and $\mathbb{R}^{n\times n}$ denote the Euclidian n space and $n \times n$ real matrices, respectively. In a symmetric matrix, $*$ denotes symmetric terms.

2. Dynamic Model of Sampled-Data-Based LFC for Power System

In this section, the LFC scheme using sampled-data control and randomly occurring time-varying delays is detailed.

2.1. One-Area LFC Model. A block structure for a one-area LFC-based model with communication delays is shown in Figure 1, which can be represented in the following formula:

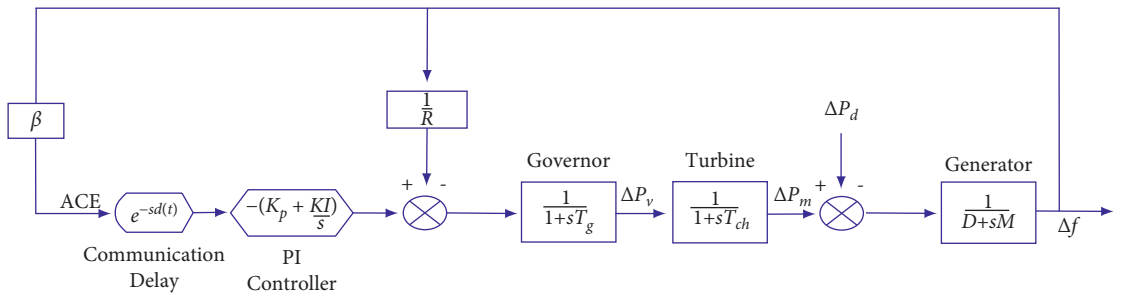

Figure 1: Dynamic model of one-area LFC scheme.

$$\begin{cases} \dot{\check{x}}(t) = \check{\mathscr{A}}\check{x}(t) + \check{\mathscr{B}}u(t) + \check{\mathscr{D}}w(t), \\ \check{y}(t) = \check{\mathscr{C}}\check{x}(t). \end{cases} \tag{1}$$

The notations of model (1) are standard and they are available in Appendix.

The area control error (ACE) is clearly illustrated in Figure 1 as the model output with no net tie-line power exchange. It follows that $\check{y}(t) = ACE = \beta\triangle f$, where $\beta > 0$ is the frequency bias factor. Furthermore, ACE is utilized as a control input to develop the PI-based controller that follows

$$u(t) = -\mathscr{K}_P ACE - \mathscr{K}_I \int ACE, \tag{2}$$

where $\int ACE$ is the integration of ACE, while bot integral and proportional gains are denoted as $\mathscr{K}_I$ and $\mathscr{K}_P$, respectively.

2.2. Sampled-Data LFC Scheme. In the continuous-time mode, state vectors are employed directly to generate the control signal. However, the sampled-data LFC scheme can only handle discrete measurements of state vectors in discrete time. Meanwhile, sampled output measurements $\check{y}(t)$ can only be used in the sampled-data control loop in the LFC scheme. As a result, we only use the measurement $\check{y}(t_k)$ at sampling instant t_k. It is obvious that in Figure 2, network-induced delays affect the communication network, which is defined as $d_{t_k} = d_{t_k}^{sc} + d_{t_k}^{ca} \le d_M < +\infty$, where d_M is constant. The sampling instants $t_k (k = 0, 1, 2, \ldots)$ are supposed to satisfy

$$0 = t_0 < t_1 < t_2 < \cdots < t_k < \cdots < \lim_{k\longrightarrow\infty} t_k = +\infty. \tag{3}$$

The sampling interval $d_k = t_{k+1} - t_k$ is set to satisfy $0 < d_k = t_{k+1} - t_k = d_M$, where d_M denotes the largest upper bound of d_k. Then, taking account of the influence of sampling and communication network delays, the possible LFC control signal $\check{y}(t)$ can be articulated as follows:

$$\check{y}(t) = \check{y}(t_k),\ t \in [t_k, t_{k+1}). \tag{4}$$

Then, the sampled-data LFC scheme in the network system is drawn out according to equations (2) and (4) as follows:

$$u(t) = u(t_k) = -\mathscr{K}_P \check{y}(t_k) - \mathscr{K}_I \int \check{y}(t_k)\mathrm{d}t. \tag{5}$$

By setting the following new vectors of virtual state and output measurement $x(t) = [\triangle f \triangle P_m \triangle P_v \int ACE]^T$ and $y(t) = [ACE \int ACE]^T$ and incorporating equations (1) and (5), the sampled-data LFC model can be obtained for $t \in [t_k, t_{k+1})$ as follows:

$$\begin{cases} \dot{x}(t) = \mathscr{A}x(t) - \mathscr{B}x(t_k) + \mathscr{D}w(t), \\ y(t) = \mathscr{C}x(t). \end{cases} \tag{6}$$

The expression of model (6) is given in Appendix. Then, we define $d(t) = t - t_k$ for $t \in [t_k, t_{k+1})$. As such, we can denote the sampling instant as $t_k = t - (t - t_k) = t - \mathrm{d}(t)$. It is supposed that $\mathrm{d}(t) \le t_{k+1} - t_k = d_k \le d_M$ for all t_k. Based on the technique of input delay [20], we can further define the sampled-data control in equation (6) as follows:

$$u(t) = -\mathscr{K}x(t - d(t)). \tag{7}$$

It is noteworthy that time delays often occur in a probabilistic form in many practical control systems. Thus, the impact of random delays in this study is important. Therefore, $d(t)$ is expected to satisfy the following two assumptions:

A1. Consider the probability distribution of the time-varying delay $d(t)$ that takes values in the range $[0, d_1]$ or $(d_1, d_2]$ and define the two sets as follows:

$$\begin{aligned} \Pi_1 &= \{t\colon d(t) \in [0, d_1]\}, \\ \Pi_2 &= \{t\colon d(t) \in (d_1, d_2]\}. \end{aligned} \tag{8}$$

We also consider the mapping functions as follows:

$$\begin{aligned} d_1(t) &= \begin{cases} d(t), & \text{for } t \in \Pi_1, \\ 0, & \text{forelse}, \end{cases} \\ d_2(t) &= \begin{cases} d(t), & \text{for } t \in \Pi_2, \\ d_1, & \text{forelse}. \end{cases} \end{aligned} \tag{9}$$

It has been inferred that if $t \in \Pi_1$ appears in the case of $d(t) \in [0, d_1]$, that is, $d(t) = d_1(t)$, and $t \in \Pi_2$ appears in the case of $d(t) \in (d_1, d_2]$, that is, $d(t) = d_2(t)$. New time-varying delays are $d_1(t)$ and $d_2(t)$, such that $0 \le d_1(t) \le d_1$ and $d_1 < d_2(t) \le d_2$. A stochastic variable $\sigma(t)$ is defined as follows:

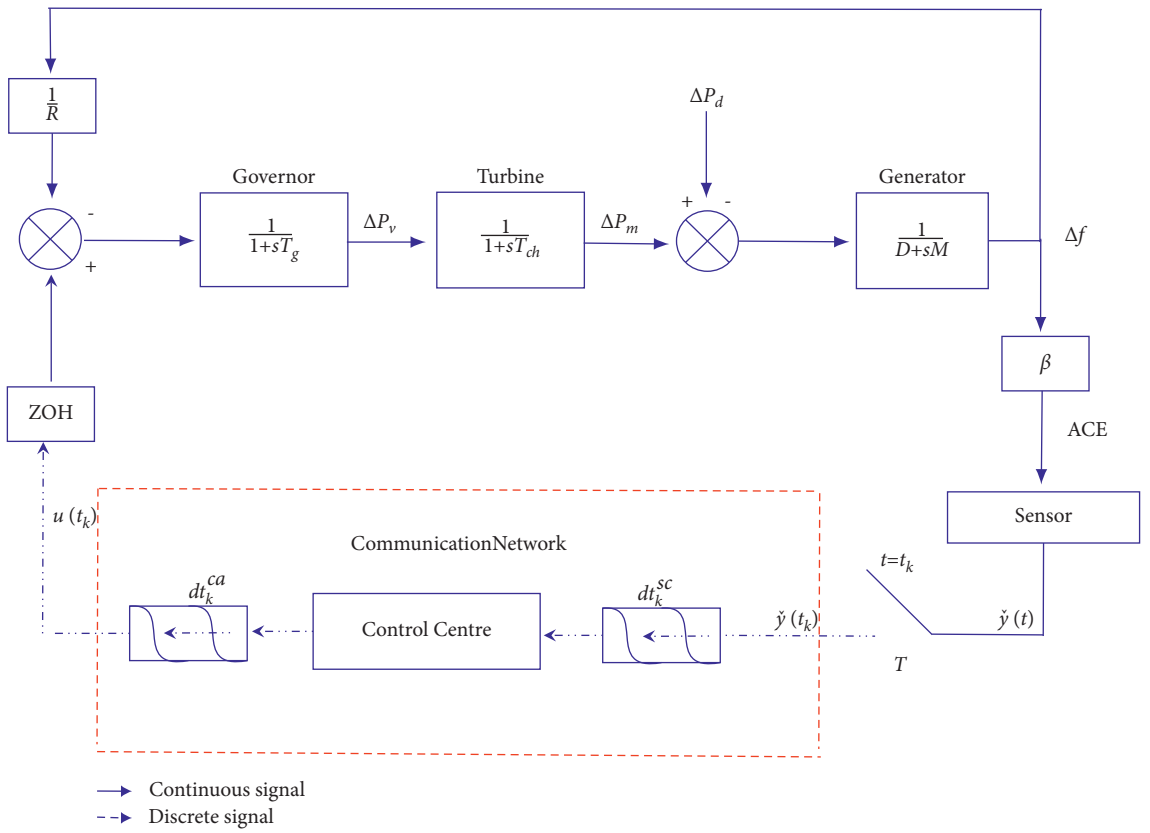

Figure 2: Dynamic model of one-area LFC scheme over the communication network and the transmission delay from SCA.

$$\sigma(t) = \begin{cases} 1, \text{for } t \in \Pi_1, \\ 0, \text{for } t \in \Pi_2. \end{cases} \tag{10}$$

A2. The variable $\sigma(t)$ is a Bernoulli-distributed sequence with the following properties: $\text{Prob}\{\sigma(t) = 1\} = \mathbb{E}\{\sigma(t)\} = \sigma_0$ and $\text{Prob}\{\sigma(t) = 0\} = 1 - \mathbb{E}\{\sigma(t)\} = 1 - \sigma_0$, where $0 \le \sigma_0 \le 1$ and $\mathbb{E}\{\sigma(t)\}$ is the expectation of $\sigma(t)$.

Remark 1. In practice, power systems often need broad open communication networks to supply relevant information. The operations of these networks are subject to undesirable events, including latent faults, packet loss, time delays, and others. Such nonlinear disturbances can appear in random ways as a result of different environmental conditions. As a result, the stochastic variable $\sigma(t)$ is used to represent this randomly occurring phenomenon.

By incorporating $d_1(t), d_2(t), \sigma(t)$, and equation (7) into model (6), we have

$$\begin{cases} \dot{x}(t) = & \mathscr{A}x(t) - \sigma(t)\mathscr{B}\mathscr{K}\mathscr{C}x(t - d_1(t)) \\ -(1 - \sigma(t)) & \mathscr{B}\mathscr{K}\mathscr{C}x(t - d_2(t)) + \mathscr{D}w(t), \\ y(t) = & \mathscr{C}x(t). \end{cases} \tag{11}$$

The initial condition of model (11) is given by $x(t) = \psi(t), t \in [-d_2, 0]$, where $\psi(t)$ is continuous on $[-d_2, 0]$.

The results presented below need the following definition and lemmas.

Definition 1. Given a prescribed scalar $\eta > 0$, model (11) is considered asymptotically stable with H_∞ performance if the conditions below hold [38]:

(i) Closed-loop model (11) with $w(t) = 0$ is asymptotically stable.

(ii) For every nonzero $w(t) \in \mathscr{L}_2[0, \infty)$ with a prescribed $\eta > 0$, the following inequality is true under the zero initial condition: $\mathbb{E}\{\|y(t)\|_2\} \le \eta\mathbb{E}\{\|w(t)\|_2\}$.

Lemma 1. *Given matrix $\mathscr{O} = \mathscr{O}^T > 0$, two matrices $\mathscr{X}_1, \mathscr{X}_2 \in \mathbb{R}^{n\times m}$, positive integers n and m, scalar $\theta \in (0, 1)$, and any vector $\zeta \in \mathbb{R}^m$ denote the function $\Xi(\theta, \mathscr{O})$ with the following form [39]:*

$$\Xi(\theta, \mathscr{O}) = \frac{1}{\theta}\zeta^T\mathscr{X}_1^T\mathscr{O}\mathscr{X}_1\zeta + \frac{1}{1-\theta}\zeta^T\mathscr{X}_2^T\mathscr{O}\mathscr{X}_2\zeta. \tag{12}$$

There exists a matrix $\mathscr{Y} \in \mathbb{R}^{n\times m}$ satisfying $\begin{bmatrix} \mathscr{O} & \mathscr{Y} \\ \mathscr{Y}^T & \mathscr{O} \end{bmatrix} > 0$, then

$$\min_{\theta\in(0,1)}\Xi(\theta, \mathscr{O}) \ge \begin{bmatrix} \mathscr{X}_1\zeta \\ \mathscr{X}_2\zeta \end{bmatrix}^T \begin{bmatrix} \mathscr{O} & \mathscr{Y} \\ \mathscr{Y}^T & \mathscr{O} \end{bmatrix} \begin{bmatrix} \mathscr{X}_1\zeta \\ \mathscr{X}_2\zeta \end{bmatrix}. \tag{13}$$

Lemma 2. *Given matrix $\mathcal{O} = \mathcal{O}^T > 0$, the following inequality is true for all continuously differentiable function $x(t)$ in $[\xi_1, \xi_2] \in \mathbb{R}^n$ as follows [40]:*

$$\begin{aligned} &-(\xi_2 - \xi_1)\int_{t-\xi_2}^{t-\xi_1} x^T(\alpha)\mathcal{O}x(\alpha)\mathrm{d}\alpha \\ &\le -\left[\int_{t-\xi_2}^{t-\xi_1} x(\alpha)d\alpha\right]^T \mathcal{O}\left[\int_{t-\xi_2}^{t-\xi_1} x(\alpha)\mathrm{d}\alpha\right]. \end{aligned} \tag{14}$$

Lemma 3. *Let $\Xi = \Xi^T$, $\mathcal{H}$ and $\mathcal{E}$ be real matrices, $\mathcal{F}(t)$ satisfies $\mathcal{F}^T(t)\mathcal{F}(t) \le I$. Then, $\Xi + \mathcal{H}\mathcal{F}(t)\mathcal{E} + (\mathcal{H}\mathcal{F}(t)\mathcal{E})^T < 0$, iff there exists a scalar $\varepsilon > 0$ such that $\Xi + \varepsilon^{-1}\mathcal{H}\mathcal{H}^T + \varepsilon\mathcal{E}^T\mathcal{E} < 0$ or equivalently [41]:*

$$\begin{bmatrix} \Xi & \mathcal{H} & \varepsilon \mathrm{E} \\ * & -\varepsilon I & 0 \\ * & * & -\varepsilon I \end{bmatrix} < 0. \tag{15}$$

In this study, the main aim is to obtain LMI-based sufficient criteria and ensure model (11) has mean-square stability and stabilization under the designed sampled-data robust H_∞ LFC scheme.

Problem 1. The following conditions are derived, in order to attain the aim of this study:

(i) Delay-dependent LKF with full model information is constructed to obtain the stability and stabilization criteria of model (11) based on Definition 1.

(ii) Sufficient gain matrices for control $\mathcal{K} = [\mathcal{K}_P\ \mathcal{K}_I]$ are calculated from the solution of LMIs to ensure stabilization of model (11) via the robust sampled-data H_∞ LFC scheme.

3. Design of Sampled-Data H_∞ LFC Scheme

We present a delay-dependent stability analysis in Section 3.1 and a stabilization analysis in Section 3.2 for model (11) using Jensen integral inequality, reciprocally convex combination lemma, and LMI methodology. The following notations simplify the remaining presentation:

$$\begin{aligned} \zeta(t) = col\{&x(t),\ x(t-d_1(t)),\ x(t-d_1),\ x(t-d_2(t)), \\ &x(t-d_2),\ \int_{t-d_1}^{t-d_1(t)} x(\alpha)\mathrm{d}\alpha,\ \int_{t-d_1(t)}^{t} x(\alpha)\mathrm{d}\alpha, \\ &\int_{t-d_2}^{t-d_2(t)} x(\alpha)\mathrm{d}\alpha,\ \int_{t-d_2(t)}^{t} x(\alpha)\mathrm{d}\alpha,\ \dot{x}(t),\ w(t)\}, \\ \int_{t-d_1(t)}^{t} \dot{x}(\alpha)\mathrm{d}\alpha &= [x(t) - x(t-d_1(t))], \\ \int_{t-d_1}^{t-d_1(t)} \dot{x}(\alpha)\mathrm{d}\alpha &= [x(t-d_1(t)) - x(t-d_1)], \\ \int_{t-d_2(t)}^{t} \dot{x}(\alpha)\mathrm{d}\alpha &= [x(t) - x(t-d_2(t))], \\ \int_{t-d_2}^{t-d_2(t)} \dot{x}(\alpha)\mathrm{d}\alpha &= [x(t-d_2(t)) - x(t-d_2)]. \end{aligned} \tag{16}$$

3.1. Sampled-Data LFC-Based H_∞ Stability Analysis. This subsection focuses on obtaining the sufficient criteria for establishing mean-square asymptotic stability of model (11), which is stated in Theorem 1.

Theorem 1. *Under given control gain $\mathcal{K}$ with H_∞ performance index η, model (11) is mean-square asymptotically stable for given positive scalars d_1, d_2, and η, if there exist matrices $\mathcal{P}$, $\mathcal{Q}_i$, $\mathcal{R}_i$, $\mathcal{S}_i$, $\mathcal{Y}_i$ $(i = 1, 2)$, and $\mathcal{M}$, which satisfy the following criteria:*

$$\mathcal{P} > 0, \mathcal{Q}_i > 0, \mathcal{R}_i > 0, \mathcal{S}_i > 0, i = 1, 2, \tag{17}$$

$$\begin{bmatrix} \mathcal{S}_i & \mathcal{Y}_i \\ \mathcal{Y}_i^T & \mathcal{S}_i \end{bmatrix} \ge 0, i = 1, 2, \tag{18}$$

$$[\Xi]_{11\times 11} < 0, \tag{19}$$

where $\Xi_{1,1} = \mathcal{Q}_1 + \mathcal{Q}_2 + d_1^2\mathcal{R}_1 + d_2^2\mathcal{R}_2 - \mathcal{S}_1 - \mathcal{S}_2 + \mathcal{M}\mathcal{A} + (\mathcal{M}\mathcal{A})^T + \mathcal{C}^T\mathcal{C}$, $\Xi_{1,2} = \mathcal{S}_1 - \mathcal{Y}_1 - \sigma_0\mathcal{M}\mathcal{B}\mathcal{K}\mathcal{K}$, $\Xi_{1,3} = \mathcal{Y}_1$, $\Xi_{1,4} = \mathcal{S}_2 - \mathcal{Y}_2 - (1-\sigma_0)\mathcal{M}\mathcal{B}\mathcal{K}\mathcal{K}$, $\Xi_{1,5} = \mathcal{Y}_2$, $\Xi_{1,10} = \mathrm{C} - \mathcal{M} + (\mathcal{M})^T$, $\Xi_{1,11} = \mathcal{M}\mathcal{A}$, $\Xi_{2,2} = -\mathcal{S}_1 - \mathcal{S}_1 + \mathcal{Y}_1^T + \mathcal{Y}_1$, $\Xi_{2,3} = \mathcal{S}_1 - \mathcal{Y}_1$, $\Xi_{2,10} = -\sigma_0(\mathcal{M}\mathcal{B}\mathcal{K}\mathcal{K})^T$, $\Xi_{3,3} = -\mathcal{Q}_1 - \mathcal{S}_1$, $\Xi_{4,4} = -\mathcal{S}_2 - \mathcal{S}_2 + \mathcal{Y}_2^T + \mathcal{Y}_2$, $\Xi_{4,5} = \mathcal{S}_2 - \mathcal{Y}_2$, $\Xi_{4,10} = -(1-\sigma_0)(\mathcal{M}\mathcal{B}\mathcal{K}\mathcal{K})^T$, $\Xi_{5,5} = -\mathcal{Q}_2 - \mathcal{S}_2$, $\Xi_{6,6} = -\mathcal{R}_1$, $\Xi_{7,7} = -\mathcal{R}_1$, $\Xi_{8,8} = -\mathcal{R}_2$, $\Xi_{9,9} = -\mathcal{R}_2$, $\Xi_{10,10} = d_1^2\mathcal{S}_1 + d_2^2\mathcal{S}_2 - \mathcal{M} - \mathcal{M}^T$, $\Xi_{10,11} = \mathcal{M}\mathcal{A}$, and $\Xi_{11,11} = -\eta^2 I$.

Proof. Construct the LKF candidate as follows: $\mathcal{V}(x(t)) = \mathcal{V}_1(x(t)) + \mathcal{V}_2(x(t)) + \mathcal{V}_3(x(t)) + \mathcal{V}_4(x(t))$, where

$$\begin{aligned}
\mathscr{V}_1(x(t)) &= x^T(t)\mathrm{C}x(t),\\
\mathscr{V}_2(x(t)) &= \sum_{i=1}^{2}\int_{t-d_i}^{t} x^T(\alpha)\mathscr{Q}_i x(\alpha)\mathrm{d}\alpha,\\
\mathscr{V}_3(x((t)) &= \sum_{i=1}^{2} d_i\int_{t-d_i}^{t}\int_{\alpha}^{t} x^T(\beta)\mathscr{R}_i x(\beta)d\beta\mathrm{d}\alpha,\\
\mathscr{V}_4(x(t)) &= \sum_{i=1}^{2} d_i\int_{t-d_i}^{t}\int_{\alpha}^{t} \dot{x}^T(\beta)\mathscr{S}_i\dot{x}(\beta)d\beta\mathrm{d}\alpha.
\end{aligned} \tag{20}$$

Obtaining the derivatives of $\mathscr{V}(x(t))$ and taking the mathematical expectation, we have

$$\mathbb{E}\left\{\dot{\mathscr{V}}_1(x(t))\right\} = \mathbb{E}\left\{2x^T(t)\mathscr{P}\dot{x}(t)\right\}, \tag{21}$$

$$\mathbb{E}\left\{\dot{\mathscr{V}}_2(x(t))\right\} = \mathbb{E}\left\{\sum_{i=1}^{2}\left[x^T(t)\mathscr{Q}_i x(t) - x^T(t-d_i)\mathscr{Q}_i x(t-d_i)\right]\right\}, \tag{22}$$

$$\mathbb{E}\left\{\dot{\mathscr{V}}_3(x(t))\right\} = \mathbb{E}\left\{\sum_{i=1}^{2} x^T(t)d_i^2\mathscr{R}_i x(t) - \sum_{i=1}^{2} d_i\int_{t-d_i}^{t} x^T(\alpha)\mathscr{R}_i x(\alpha)\mathrm{d}\alpha\right\}, \tag{23}$$

$$\mathbb{E}\left\{\dot{\mathscr{V}}_4(x(t))\right\} = \mathbb{E}\left\{\sum_{i=1}^{2} \dot{x}^T(t)d_i^2\mathscr{S}_i\dot{x}(t) - \sum_{i=1}^{2} d_i\int_{t-d_i}^{t} \dot{x}^T(\alpha)\mathscr{S}_i\dot{x}(\alpha)\mathrm{d}\alpha\right\}. \tag{24}$$

According to A1, the integral term in equation (23) can be employed by utilizing Lemma 2 in the form of

$$\begin{aligned}
&-\sum_{i=1}^{2} d_i\int_{t-d_i}^{t-d_i(t)} x^T(\alpha)\mathscr{R}_i x(\alpha)\mathrm{d}\alpha\\
&\quad\le -\sum_{i=1}^{2}\left(\left[\int_{t-d_i}^{t-d_i(t)} x(\alpha)\mathrm{d}\alpha\right]^T\mathscr{R}_i\left[\int_{t-d_i}^{t-d_i(t)} x(\alpha)\mathrm{d}\alpha\right]\right),
\end{aligned} \tag{25}$$

$$\begin{aligned}
&-\sum_{i=1}^{2} d_i\int_{t-d_i(t)}^{t} x^T(\alpha)\mathscr{R}_i x(\alpha)\mathrm{d}\alpha\\
&\quad\le -\sum_{i=1}^{2}\left(\left[\int_{t-d_i(t)}^{t} x(\alpha)\mathrm{d}\alpha\right]^T\mathscr{R}_i\left[\int_{t-d_i(t)}^{t} x(\alpha)\mathrm{d}\alpha\right]\right).
\end{aligned} \tag{26}$$

According to A1, the integral term in equation (24) can be employed by utilizing Lemma 2 in the form of

$$
\begin{aligned}
&-\sum_{i=1}^{2} d_i \int_{t-d_i}^{t} \dot{x}^T(\alpha)\mathcal{S}_i\dot{x}(\alpha)\mathrm{d}\alpha \\
&= -\sum_{i=1}^{2}\left(\frac{d_i}{d_i - d_i(t)}\left[\int_{t-d_i}^{t-d_i(t)} \dot{x}(\alpha)\mathrm{d}\alpha\right]^T \mathcal{S}_i\left[\int_{t-d_i}^{t-d_i(t)} \dot{x}(\alpha)\mathrm{d}\alpha\right]\right) \\
&\quad -\sum_{i=1}^{2}\left(\frac{d_i}{d_i(t)}\left[\int_{t-d_i(t)}^{t} \dot{x}(\alpha)\mathrm{d}\alpha\right]^T \mathcal{S}_i\left[\int_{t-d_i(t)}^{t} \dot{x}(\alpha)\mathrm{d}\alpha\right]\right) \\
&= -\sum_{i=1}^{2}\left(\left[\int_{t-d_i}^{t-d_i(t)} \dot{x}(\alpha)\mathrm{d}\alpha\right]^T \mathcal{S}_i\left[\int_{t-d_i}^{t-d_i(t)} \dot{x}(\alpha)\mathrm{d}\alpha\right]\right) \\
&\quad -\sum_{i=1}^{2}\left(\frac{d_i(t)}{d_i - d_i(t)}\left[\int_{t-d_i}^{t-d_i(t)} \dot{x}(\alpha)\mathrm{d}\alpha\right]^T \mathcal{S}_i\left[\int_{t-d_i}^{t-d_i(t)} \dot{x}(\alpha)\mathrm{d}\alpha\right]\right) \\
&\quad -\sum_{i=1}^{2}\left(\left[\int_{t-d_i(t)}^{t} \dot{x}(\alpha)\mathrm{d}\alpha\right]^T \mathcal{S}_i\left[\int_{t-d_i(t)}^{t} \dot{x}(\alpha)\mathrm{d}\alpha\right]\right) \\
&\quad -\sum_{i=1}^{2}\left(\frac{d_i - d_i(t)}{d_i(t)}\left[\int_{t-d_i(t)}^{t} \dot{x}(\alpha)d\alpha\right]^T \mathcal{S}_i\left[\int_{t-d_i(t)}^{t} \dot{x}(\alpha)\mathrm{d}\alpha\right]\right).
\end{aligned} \tag{27}
$$

If $\begin{bmatrix} \mathcal{S}_i & \mathcal{Y}_i \\ \mathcal{Y}_i^T & \mathcal{S}_i \end{bmatrix} \geq 0, i = 1, 2$ by Lemma 1, the following inequality is true:

$$
\sum_{i=1}^{2}\begin{bmatrix} \sqrt{\dfrac{d_i(t)}{d_i - d_i(t)}}\left[\displaystyle\int_{t-d_i}^{t-d_i(t)} \dot{x}(\alpha)\mathrm{d}\alpha\right] \\ \sqrt{\dfrac{d_i - d_i(t)}{d_i(t)}}\left[\displaystyle\int_{t-d_i(t)}^{t} \dot{x}(\alpha)\mathrm{d}\alpha\right] \end{bmatrix}^T \begin{bmatrix} \mathcal{S}_i & \mathcal{Y}_i \\ \mathcal{Y}_i^T & \mathcal{S}_i \end{bmatrix} \times \sum_{i=1}^{2}\begin{bmatrix} \sqrt{\dfrac{d_i(t)}{d_i - d_i(t)}}\left[\displaystyle\int_{t-d_i}^{t-d_i(t)} \dot{x}(\alpha)\mathrm{d}\alpha\right] \\ \sqrt{\dfrac{d_i - d_i(t)}{d_i(t)}}\left[\displaystyle\int_{t-d_i(t)}^{t} \dot{x}(\alpha)\mathrm{d}\alpha\right] \end{bmatrix} \geq 0, \tag{28}
$$

which implies

$$
\begin{aligned}
&-\sum_{i=1}^{2}\left(\frac{d_i(t)}{d_i - d_i(t)}\left[\int_{t-d_i}^{t-d_i(t)} \dot{x}(\alpha)\mathrm{d}\alpha\right]^T \mathcal{S}_i\left[\int_{t-d_i}^{t-d_i(t)} \dot{x}(\alpha)\mathrm{d}\alpha\right]\right) \\
&\quad -\sum_{i=1}^{2}\left(\frac{d_i - d_i(t)}{d_i(t)}\left[\int_{t-d_i(t)}^{t} \dot{x}(\alpha)\mathrm{d}\alpha\right]^T \mathcal{S}_i\left[\int_{t-d_i(t)}^{t} \dot{x}(\alpha)\mathrm{d}\alpha\right]\right) \\
&\leq -\sum_{i=1}^{2}\left(\left[\int_{t-d_i}^{t-d_i(t)} \dot{x}(\alpha)\mathrm{d}\alpha\right]^T \mathcal{Y}_i\left[\int_{t-d_i(t)}^{t} \dot{x}(\alpha)\mathrm{d}\alpha\right]\right) \\
&\quad -\sum_{i=1}^{2}\left(\left[\int_{t-d_i(t)}^{t} \dot{x}(\alpha)\mathrm{d}\alpha\right]^T \mathcal{Y}_i^T\left[\int_{t-d_i}^{t-d_i(t)} \dot{x}(\alpha)\mathrm{d}\alpha\right]\right).
\end{aligned} \tag{29}
$$

From equations (27) and (29), we can obtain that

$$
\begin{aligned}
&-\sum_{i=1}^{2} d_i \int_{t-d_i}^{t} \dot{x}^T(\alpha)\mathcal{S}_i\dot{x}(\alpha)\mathrm{d}\alpha \\
&\leq -\sum_{i=1}^{2}\left(\left[\int_{t-d_i}^{t-d_i(t)} \dot{x}(\alpha)\mathrm{d}\alpha\right]^T \mathcal{S}_i\left[\int_{t-d_i}^{t-d_i(t)} \dot{x}(\alpha)\mathrm{d}\alpha\right]\right) \\
&\quad -\sum_{i=1}^{2}\left(\left[\int_{t-d_i(t)}^{t} \dot{x}(\alpha)\mathrm{d}\alpha\right]^T \mathcal{S}_i\left[\int_{t-d_i(t)}^{t} \dot{x}(\alpha)\mathrm{d}\alpha\right]\right) \\
&\quad -\sum_{i=1}^{2}\left(\left[\int_{t-d_i}^{t-d_i(t)} \dot{x}(\alpha)\mathrm{d}\alpha\right]^T \mathcal{Y}_i\left[\int_{t-d_i(t)}^{t} \dot{x}(\alpha)\mathrm{d}\alpha\right]\right) \\
&\quad -\sum_{i=1}^{2}\left(\left[\int_{t-d_i(t)}^{t} \dot{x}(\alpha)\mathrm{d}\alpha\right]^T \mathcal{Y}_i^T\left[\int_{t-d_i}^{t-d_i(t)} \dot{x}(\alpha)\mathrm{d}\alpha\right]\right).
\end{aligned} \tag{30}
$$

In addition, for any matrix $\mathscr{M}$ with a suitable size, the following inequalities are valid:

$$0 = 2[x(t) + \dot{x}(t)]\mathscr{M}\big[-\dot{x}(t) + \mathscr{A}x(t) - \sigma_0\mathscr{B}\mathscr{K}\mathscr{C}x \cdot (t - d_1(t)) - (1-\sigma_0)\mathscr{B}\mathscr{K}\mathscr{C}x(t - d_2(t)) + \mathscr{D}w(t)\big]. \tag{31}$$

From equations (21)–(31), we can deduce that for all nonzero $w(t) \in \mathscr{L}_2[0,\infty)$,

$$\mathbb{E}\Big\{\dot{\mathscr{V}}(x((t)) + y^T(t)y(t) - \eta^2 w^T(t)w(t)\Big\} \le \mathbb{E}\Big\{\zeta^T(t)\big([\Xi]_{11\times 11}\big)\zeta(t)\Big\}. \tag{32}$$

Under zero conditions, we have $\mathscr{V}(0) = 0$ and $\mathscr{V}(\infty) \ge 0$. Integrating both sides of equation (30) yields $\mathbb{E}\{\|y(t)\|_2\} \le \eta\mathbb{E}\{\|w(t)\|_2\}$ for every $w(t) \in \mathscr{L}_2[0,+\infty)$. As such, model (11) is mean-square asymptotically stable under Definition 1. The proof is completed. □

3.2. Sampled-Data LFC-Based H_∞ Stabilization Analysis. According to the stability results developed in Section 3.1, we focus on obtaining stabilization results through the use of sampled-data LFC scheme for model (11), which is stated in Theorem 2.

Theorem 2. *Under sampled-data LFC with H_∞ performance index η, model (11) is mean-square asymptotically stable for given positive scalars d_1, d_2, η, and $\varsigma \longrightarrow 0$, if there exist matrices $\check{\mathscr{P}}$, $\check{\mathbb{Q}}_i$, $\check{\mathscr{R}}_i$, $\check{\mathscr{S}}_i$, $\check{\mathscr{Y}}_i (i = 1,2)$, $\mathscr{L}$, $\mathscr{W}$, and $\mathscr{Z}$, which satisfy the following criteria:*

$$\check{\mathscr{P}} > 0, \check{\mathbb{Q}}_i > 0, \check{\mathscr{R}}_i > 0, \check{\mathscr{S}}_i > 0, (i = 1,2), \tag{33}$$

$$\begin{bmatrix} \check{\mathscr{S}}_i & \check{\mathscr{Y}}_i \\ \check{\mathscr{Y}}_i^T & \check{\mathscr{S}}_i \end{bmatrix} \ge 0, \quad i = 1,2, \tag{34}$$

$$\begin{bmatrix} [\widetilde{\Xi}]_{11\times 11} & \overline{\Upsilon} \\ * & -I \end{bmatrix} < 0, \tag{35}$$

$$\begin{bmatrix} -\varsigma I & (\mathscr{W}\mathscr{C} - \mathscr{C}\mathscr{L})^T \\ * & -I \end{bmatrix} < 0, \tag{36}$$

where $\widetilde{\Xi}_{1,1} = \check{\mathbb{Q}}_1 + \check{\mathbb{Q}}_2 + d_1\check{\mathscr{R}}_1 + d_2\check{\mathscr{R}}_2 - \check{\mathscr{S}}_1 - \check{\mathscr{S}}_2 + \mathscr{A}\mathscr{L} + (\mathscr{A}\mathscr{L})^T$, $\widetilde{\Xi}_{1,2} = \check{\mathscr{S}}_1 - \check{\mathscr{Y}}_1 - \sigma_0\mathscr{B}\mathscr{Z}\mathscr{C}$, $\widetilde{\Xi}_{1,3} = \check{\mathscr{Y}}_1$, $\widetilde{\Xi}_{1,4} = \check{\mathscr{S}}_2 - \check{\mathscr{Y}}_2 - (1-\sigma_0)\mathscr{B}\mathscr{Z}\mathscr{C}$, $\widetilde{\Xi}_{1,5} = \check{\mathscr{Y}}_2$, $\widetilde{\Xi}_{1,10} = \check{\mathscr{P}} - \mathscr{L} + (\mathscr{L}\mathscr{A})^T$, $\widetilde{\Xi}_{1,11} = \mathscr{D}$, $\widetilde{\Xi}_{2,2} = -\check{\mathscr{S}}_1 - \check{\mathscr{S}}_1 + \check{\mathscr{Y}}_1 + \check{\mathscr{Y}}_1^T$, $\widetilde{\Xi}_{2,3} = \check{\mathscr{S}}_1 - \check{\mathscr{Y}}_1$, $\widetilde{\Xi}_{2,10} = -\sigma_0(\mathscr{B}\mathscr{Z}\mathscr{C})^T$, $\widetilde{\Xi}_{3,3} = -\check{\mathbb{Q}}_1 - \check{\mathscr{S}}_1$, $\widetilde{\Xi}_{4,4} = -\check{\mathscr{S}}_2 - \check{\mathscr{S}}_2 + \check{\mathscr{Y}}_2 + \check{\mathscr{Y}}_2^T$, $\widetilde{\Xi}_{4,5} = \check{\mathscr{S}}_2 - \check{\mathscr{Y}}_2$, $\widetilde{\Xi}_{4,10} = -(1-\sigma_0)(\mathscr{B}\mathscr{Z}\mathscr{C})^T$, $\widetilde{\Xi}_{5,5} = -\check{\mathbb{Q}}_2 - \check{\mathscr{S}}_2$, $\widetilde{\Xi}_{6,6} = -\check{\mathscr{R}}_1$, $\widetilde{\Xi}_{7,7} = -\check{\mathscr{R}}_1$, $\widetilde{\Xi}_{8,8} = -\check{\mathscr{R}}_2$, $\widetilde{\Xi}_{9,9} = -\check{\mathscr{R}}_2$, $\widetilde{\Xi}_{10,10} = d_1^2\check{\mathscr{S}}_1 + d_2^2\check{\mathscr{S}}_2 - \mathscr{L} - \mathscr{L}^T$, $\widetilde{\Xi}_{10,11} = \mathscr{D}$, $\widetilde{\Xi}_{11,11} = -\eta^2 I$, $\widetilde{\Upsilon} = [\mathscr{A}\mathscr{L}\ 0_{1\times 10}]^T$, *and* $\mathscr{K} = \mathscr{Z}\mathscr{W}^{-1}$.

Proof. We can define the change of variables in order to achieve the controller gain as follows: $\mathscr{L} = \mathscr{M}^{-1}$, $\check{\mathscr{P}} = \mathscr{L}\mathscr{L}$, $\check{\mathbb{Q}}_1 = \mathscr{L}\mathbb{Q}_1\mathscr{L}$, $\check{\mathbb{Q}}_2 = \mathscr{L}\mathbb{Q}_2\mathscr{L}$, $\check{\mathscr{R}}_1 = \mathscr{L}\mathscr{R}_1\mathscr{L}$, $\check{\mathscr{R}}_2 = \mathscr{L}\mathscr{R}_2\mathscr{L}$, $\check{\mathscr{S}}_1 = \mathscr{L}\mathscr{S}_1\mathscr{L}$, $\check{\mathscr{S}}_2 = \mathscr{L}\mathscr{S}_2\mathscr{L}$, $\check{\mathscr{Y}}_1 = \mathscr{L}\mathscr{Y}_1\mathscr{L}$, and $\check{\mathscr{Y}}_2 = \mathscr{L}\mathscr{Y}_2\mathscr{L}$. Post and premultiplying equations (18) and (19) by $\mathrm{diag}\{\mathscr{L},\mathscr{L}\}$ and $\mathrm{diag}\{\mathscr{L},\mathscr{L},\mathscr{L},\mathscr{L},\mathscr{L},\mathscr{L},\mathscr{L},\mathscr{L},\mathscr{L},\mathscr{L},I\}$, we can obtain that

$$[\overline{\Xi}]_{11\times 11} < 0, \tag{37}$$

where $\overline{\Xi}_{1,1} = \check{\mathbb{Q}}_1 + \check{\mathbb{Q}}_2 + d_1\check{\mathscr{R}}_1 + d_2\check{\mathscr{R}}_2 - \check{\mathscr{S}}_1 - \check{\mathscr{S}}_2 + \mathscr{A}\mathscr{L} + (\mathscr{A}\mathscr{L})^T + \mathscr{L}\mathscr{C}^T\mathscr{C}\mathscr{L}$, $\overline{\Xi}_{1,2} = \check{\mathscr{S}}_1 - \check{\mathscr{Y}}_1 - \sigma_0\mathscr{L}\mathscr{K}\mathscr{C}$, $\overline{\Xi}_{1,3} = \check{\mathscr{Y}}_1$, $\overline{\Xi}_{1,4} = \check{\mathscr{S}}_2 - \check{\mathscr{Y}}_2 - (1-\sigma_0)\mathscr{L}\mathscr{B}\mathscr{K}\mathscr{C}$, $\overline{\Xi}_{1,5} = \check{\mathscr{Y}}_2$, $\overline{\Xi}_{1,10} = \check{\mathscr{P}} - \mathscr{L} + (\mathscr{L}\mathscr{C})^T$, $\overline{\Xi}_{1,11} = \mathscr{D}$, $\overline{\Xi}_{2,2} = -\check{\mathscr{S}}_1 - \check{\mathscr{S}}_1 + \check{\mathscr{Y}}_1 + \check{\mathscr{Y}}_1^T$, $\overline{\Xi}_{2,3} = \check{\mathscr{S}}_1 - \check{\mathscr{Y}}_1$, $\overline{\Xi}_{2,10} = -\sigma_0(\mathscr{L}\mathscr{B}\mathscr{K}\mathscr{C})^T$, $\overline{\Xi}_{3,3} = -\check{\mathbb{Q}}_1 - \check{\mathscr{S}}_1$, $\overline{\Xi}_{4,4} = -\check{\mathscr{S}}_2 - \check{\mathscr{S}}_2 + \check{\mathscr{Y}}_2 + \check{\mathscr{Y}}_2^T$, $\overline{\Xi}_{4,5} = \check{\mathscr{S}}_2 - \check{\mathscr{Y}}_2$, $\overline{\Xi}_{4,10} = -(1-\sigma_0)(\mathscr{L}\mathscr{B}\mathscr{K}\mathscr{C})^T$, $\overline{\Xi}_{5,5} = -\check{\mathbb{Q}}_2 - \check{\mathscr{S}}_2$, $\overline{\Xi}_{6,6} = -\check{\mathscr{R}}_1$, $\overline{\Xi}_{7,7} = -\check{\mathscr{R}}_1$, $\overline{\Xi}_{8,8} = -\check{\mathscr{R}}_2$, $\overline{\Xi}_{9,9} = -\check{\mathscr{R}}_2$, $\overline{\Xi}_{10,10} = d_1^2\check{\mathscr{S}}_1 + d_2^2\check{\mathscr{S}}_2 - \mathscr{L} - \mathscr{L}^T$, $\overline{\Xi}_{10,11} = \mathscr{D}$, and $\overline{\Xi}_{11,11} = -\eta^2 I$, Because of the existence of nonlinear terms in equation (37) and $\mathscr{C}$ is not invertible, let $\mathscr{Y} = \mathscr{K}\mathscr{C}\mathscr{L}$, then $\mathscr{Y}\mathscr{C}^{-1}\mathscr{L}^{-1} = \mathscr{K}$ is not applicable to directly find $\mathscr{K}$. Therefore, by defining $\mathscr{Z}\mathscr{C} = \mathscr{K}\mathscr{C}\mathscr{L}$, $\mathscr{W}\mathscr{C} = \mathscr{C}\mathscr{L}$ and $\mathscr{Z}\mathscr{W}^{-1} = \mathscr{K}$.

By using Schur complement, equation (37) is equivalent to equation (35) and the nonlinear functions are changed to W problem as in reference [42]. Moreover, we can formulate inequality (36) for every small scalar ς and use Schur complement in $(\mathscr{W}\mathscr{C} - \mathscr{C}\mathscr{L})^T(\mathscr{W}\mathscr{C} - \mathscr{C}\mathscr{L}) = 0$. Here, $\mathscr{L} > 0$ and $\mathscr{W}$ is an invertible matrix. The proof is completed. □

4. Design of Robust Sampled-Data H_∞ LFC Scheme

In practical, uncertainties are commonly encountered in modelling of practical systems due to environmental imperfections and changes. As such, this study takes into account norm-bounded uncertainty, and we can describe the power system as follows:

$$\begin{cases} \dot{x}(t) = & (\mathscr{A} + \triangle\mathscr{A}(t))x(t) - \sigma(t)\mathscr{B}\mathscr{K}\mathscr{C}x(t - d_1(t)) \\ -(1-\sigma(t)) & \mathscr{B}\mathscr{K}\mathscr{C}x(t - d_2(t)) + \mathscr{D}w(t), \\ y(t) = & \mathscr{C}x(t), \end{cases} \tag{38}$$

where $\triangle\mathscr{A}(t)$ is the parametric uncertainty satisfying $\triangle\mathscr{A}(t) = \mathscr{H}\mathscr{F}(t)\mathscr{E}$, where $\mathscr{H}$ and $\mathscr{E}$ are known matrices, and $\mathscr{F}(t)$ is time-varying unknown matrix that satisfies $\mathscr{F}(t)^T\mathscr{F}(t) \le I$.

Theorem 3. *Under sampled-data LFC with H_∞ performance index η, model (38) is mean-square robust asymptotically stable for given positive scalars d_1, d_2, η, and $\varsigma \longrightarrow 0$, if there exist matrices $\check{\mathscr{P}}$, $\check{\mathbb{Q}}_i$, $\check{\mathscr{R}}_i$, $\check{\mathscr{S}}_i$, $\check{\mathscr{Y}}_i (i = 1,2)$, $\mathscr{L}$, $\mathscr{W}$, and $\mathscr{Z}$, which satisfy the following criteria:*

$$\check{\mathscr{P}} > 0, \check{\mathbb{Q}}_i > 0, \check{\mathscr{R}}_i > 0, \check{\mathscr{S}}_i > 0, \quad (i = 1,2), \tag{39}$$

$$\begin{bmatrix} \check{\mathscr{S}}_i & \check{\mathscr{Y}}_i \\ \check{\mathscr{Y}}_i^T & \check{\mathscr{S}}_i \end{bmatrix} \ge 0, \quad (i = 1,2), \tag{40}$$

$$\begin{bmatrix} [\tilde{\Xi}]_{11\times 11} & \bar{\varepsilon}\overline{\Lambda}_1 & \overline{\Lambda}_2 & \overline{\Upsilon} \\ * & -\bar{\varepsilon}I & 0 & 0 \\ * & * & -\bar{\varepsilon}I & 0 \\ 0 & 0 & 0 & -I \end{bmatrix} < 0, \tag{41}$$

$$\begin{bmatrix} -\varsigma I(\mathscr{W}\mathscr{C} - \mathscr{C}\mathscr{L})^T \\ * \quad -I \end{bmatrix} < 0, \tag{42}$$

where $[\tilde{\Xi}]_{11\times 11}$ *and* $\overline{\Upsilon}$ *are given in Theorem 2, and* $\overline{\Lambda}_1 = [\mathscr{H}^T 0_{1\times 8} \mathscr{H}^T 0]^T$, $\Lambda_2 = [\mathscr{E}\mathscr{L}^T 0_{1\times 10}]$, $\bar{\varepsilon} = \varepsilon^{-1}$, *and* $\mathscr{K} = \mathscr{Z}\mathscr{W}^{-1}$.

Proof. First, replacing $\mathscr{A}$ by $\mathscr{A} + \triangle\mathscr{A}(t)$ in equation (19), we have

$$[\Xi]_{11\times 11} + \Lambda_1 \mathscr{F}(t)\Lambda_2 + (\Lambda_1 \mathscr{F}(t)\Lambda_2)^T, \tag{43}$$

It follows from Lemma 3, there exists a scalar $\varepsilon > 0$, such that

$$[\Xi]_{11\times 11} + \frac{1}{\varepsilon}\Lambda_1\Lambda_1^T + \varepsilon\Lambda_2^T\Lambda_2 < 0, \tag{44}$$

where $\Lambda_1 = [(\mathscr{M}\mathscr{H})^T 0_{1\times 8}\ (\mathscr{M}\mathscr{H})^T 0]^T$ and $\Lambda_2 = [\mathscr{E} 0_{1\times 10}]$, and applying Lemma 3, it is easy to obtain

$$\begin{bmatrix} [\Xi]_{11\times 11} & \Lambda_1 & \varepsilon\Lambda_2 \\ * & -\varepsilon I & 0 \\ * & * & -\varepsilon I \end{bmatrix} < 0. \tag{45}$$

Post- and premultiplying equation (45) by $\mathrm{diag}\{\mathscr{L}, \mathscr{L}, \mathscr{L}, \mathscr{L}, \mathscr{L}, \mathscr{L}, \mathscr{L}, \mathscr{L}, \mathscr{L}, \mathscr{L}, I, \varepsilon^{-1}I, \varepsilon^{-1}I\}$ and by applying a similar procedure of Theorem 2 through the use of Schur complement lemma, equation (41) can be obtained. The proof is completed. □

Remark 2. In comparison with prior publications [21, 22], the proposed method is novel for model (1), which not only covers the model with sampled-data control but also considers random time-varying delays in the controller implementation that is characterized by Bernoulli-distributed sequences. It has many advantages over regular power system analysis.

For $\sigma(t) = 1$, since only one delay interval with $0 \le d_1(t) \le d_1$ exists, model (11) reduces to

$$\begin{cases} \dot{x}(t) = & \mathscr{A}x(t) + \mathscr{A}_d x(t - d_1(t)) + \mathscr{D}w(t), \\ y(t) = & \mathscr{C}x(t). \end{cases} \tag{46}$$

Corollary 1. *Model (46) with* $w(t) = 0$ *is asymptotically stable for given positive scalars* d_1, *if there exist matrices* $\mathscr{P}$, $\mathscr{Q}_1$, $\mathscr{R}_1$, $\mathscr{S}_1$, $\mathscr{Y}_1$, *which satisfy the following criteria:*

$$\mathscr{P} > 0, \mathscr{Q}_1 > 0, \mathscr{R}_1 > 0, \mathscr{S}_1 > 0,$$

$$\begin{bmatrix} \mathscr{S}_1 & \mathscr{Y}_1 \\ \mathscr{Y}_1^T & \mathscr{S}_1 \end{bmatrix} \ge 0,$$

$$\Gamma = \begin{bmatrix} \Gamma_{1,1} & * & * & * & * & * \\ \Gamma_{2,1} & \Gamma_{2,2} & * & * & * & * \\ \mathscr{Y}_1^T & \Gamma_{3,2} & \Gamma_{3,3} & * & * & * \\ 0 & 0 & 0 & -\mathscr{R}_1 & * & * \\ 0 & 0 & 0 & 0 & -\mathscr{R}_1 & * \\ d_1\mathscr{A}^T\mathscr{S}_1 & d_1\mathscr{A}_d^T\mathscr{S}_1 & 0 & 0 & 0 & -\mathscr{S}_1 \end{bmatrix} < 0, \tag{47}$$

where $\Gamma_{1,1} = \mathscr{Q}_1 + d_1^2\mathscr{R}_1 - \mathscr{S}_1 + \mathscr{P}\mathscr{A} + (\mathscr{P}\mathscr{P})^T$, $\Gamma_{2,1} = \mathscr{S}_1^T - \mathscr{Y}_1^T + \mathscr{A}_d^T\mathscr{P}^T$, $\Xi_{2,2} = -\mathscr{S}_1 - \mathscr{S}_1 + \mathscr{Y}_1 + \mathscr{Y}_1^T$, $\Xi_{3,2} = \mathscr{S}_1^T - \mathscr{Y}_1^T$, *and* $\Xi_{3,3} = -\mathscr{Q}_1 - \mathscr{S}_1$.

Proof. Choosing the same LKF as in Theorem 1 with $i = 1$ and computing the derivative of $\mathscr{V}(x(t))$, we have

$$\begin{aligned} \dot{\mathscr{V}}(x(t)) = {} & 2x^T(t)\mathscr{P}(\mathscr{A}x(t) + \mathscr{A}_d x(t - d(t))) + x^T(t)\mathscr{Q}_1 x(t) \\ & - x^T(t - d_1)\mathscr{Q}_1 x(t - d_1) + d_1^2 x^T(t)\mathscr{R}_1 x(t) - d_1\int_{t-d_1}^{t} x^T(\alpha)\mathscr{R}_1 x(\alpha)\mathrm{d}\alpha + d_1^2 \\ & ((\mathscr{A}x(t)) + \mathscr{A}_d x(t - d(t)))^T \mathscr{S}_1 (\mathscr{A}x(t) + \mathscr{A}_d x(t - d(t))) \\ & - d_1\int_{t-d_1}^{t} \dot{x}^T(\alpha)\mathscr{S}_1\dot{x}(\alpha)\mathrm{d}\alpha. \end{aligned} \tag{48}$$

By applying Lemma 2 and using Theorem 1, the remaining proof can be easily obtained. □

Remark 3. The following constraint optimization issue is presented to solve the stability criterion in Corollary 1:

Optimization problem is

$$\min_{\mathscr{P},\mathscr{Q}_1,\mathscr{R}_1,\mathscr{S}_1} d_1, \tag{49}$$

s.t

$$\begin{bmatrix} \mathscr{S}_1 & \mathscr{Y}_1 \\ \mathscr{Y}_1^T & \mathscr{S}_1 \end{bmatrix} \ge 0, \mathscr{P} = \mathscr{P}^T > 0, \mathscr{Q}_1 = \mathscr{Q}_1^T > 0, \\ \mathscr{R}_1 = \mathscr{R}_1^T > 0, \mathscr{S}_1 = \mathscr{S}_1^T > 0, \Gamma < 0. \tag{50}$$

The convex optimization issues are be easily solved by using certain numerical packages [39–43].

Remark 4. There have been a number of recent studies concentrating on developing suitable LFC-based

controllers for power systems. For example, the sliding mode LFC for hybrid power system is based on disturbance observer [8], an adaptive control scheme for LFC of multiarea power systems [9], robust H_∞ LFC of delayed multi-area power systems with stochastic disturbances [10, 37, 41], decentralized H_∞ LFC for multi area power systems with communication uncertainties [11, 42], and resilient reliable H_∞ LFC of power system with random gain fluctuations [44]. However, no work has yet been reported regarding the topic of robust sampled-data LFC schemes for power systems with randomly occurring time-varying delays. So, in order to fill these gaps, we introduced new sufficient conditions for ensuring mean-square asymptotic stability and stabilization criteria for power systems by addressing robust sampling of data H_∞ LFC schemes. Thus, the main results of this study are novel and distinct from those of the existing literature.

5. Case Studies

This section presents case studies including the MAUBs of time delays, H_∞ performance index, and efficiency of proposed sampled-data LFC scheme. In addition, the simulation results are given to demonstrate how the control scheme supports the achievement of system performance.

5.1. The Case of a One-Area LFC-Based Power System. Table 1 lists the parameters of one-area LFC-based power system taken from references [35, 45]. Correlations between gain of the sampled-data LFC scheme and effects of time delays on stability margins and H_∞ performance based on the proposed results are discussed in this subsection.

Case 1. MAUBs: based on Theorem 1, an MAUB of d_2 is calculated for model (11) without load disturbance. For different settings of σ_0 and fixed $\mathscr{K}_P = 0$, $\mathscr{K}_I = 0.05$, $d_1 = 0.1$, and $\eta = 6.0512$, the MAUB values of d_2 are given in Table 2.

Following that, the MAUB of d_1 is calculated and displayed in Table 3 for various gains of $\mathscr{K}_P$ and $\mathscr{K}_I$, in order to demonstrate the merit of the results obtained. Furthermore, the results presented in reference [45] are provided for comparison, in order to account for the advantage of the method presented in Corollary 1. According to Tables 3 and 4, our proposed method in Corollary 1 can achieve better MAUBs than those in reference [45] with respect to identical control gain.

The results presented in Tables 3 and 4 demonstrate that d_1 can significantly larger when $\mathscr{K}_P$ and $\mathscr{K}_I$ are smaller, and that d_1 is significantly lower for larger $\mathscr{K}_P$ and $\mathscr{K}_I$. With a lower $\mathscr{K}_I \leq 0.05$, d_1 drops as $\mathscr{K}_P$ increases. With the growth of $\mathscr{K}_I \geq 0.1$, d_1 initially increases and then decreases with the increase of $\mathscr{K}_P$. As such, there is a range of $\mathscr{K}_P$ that can achieve the MAUBs of d_1 for a given $\mathscr{K}_I$.

Case 2. MinimumH_∞Performance Index: the acceptable minimum H_∞ performance index $\eta_{\min}$ that uses Theorem 1 in this study is noted in Table 5 for various σ_0, fixed maximum delay bounds $d_1 = 0.2$ and $d_2 = 0.8$, and given gains $\mathscr{K}_P = 0.05$ and $\mathscr{K}_I = 0.1$. It is found that the designed control strategy in the power system is effective for managing load disturbances.

Table 1: Parameter values of one-area LFC-based model (1).

$\mathscr{T}_g$	$\mathscr{T}_{ch}$	β	$\mathscr{R}$	$\mathscr{D}$	$\mathscr{M}$
0.1	0.3	21.0	0.05	1.0	10

Table 2: The MAUBs of d_2 for various settings of σ_0 and fixed $\mathscr{K}_P$, $\mathscr{K}_I$, d_1, and η.

Methods	σ_0			
	0.2	0.4	0.6	0.8
Theorem 1	4.2874	4.0964	3.1925	3.0028

Table 3: The MAUB of d_1 for various control gains in reference [45].

d_1	$\mathscr{K}_I$						
$\mathscr{K}_P$	0.05	0.1	0.15	0.2	0.4	0.6	1.0
0	27.92	13.77	9.05	6.69	3.12	1.91	0.88
0.05	27.87	14.06	9.28	6.86	3.21	1.97	0.92
0.10	27.03	13.68	9.22	6.94	3.29	2.02	0.96
0.20	25.11	12.76	8.61	6.53	3.32	2.10	1.01
0.40	20.36	10.42	7.06	5.38	2.83	1.91	1.01
0.60	14.61	7.47	5.15	3.95	2.13	1.47	0.82
1.0	0.54	0.53	0.53	0.52	0.48	0.43	0.34

Table 4: The MAUB of d_1 for various control gains in Corollary 1.

d_1	$\mathscr{K}_I$						
$\mathscr{K}_P$	0.05	0.1	0.15	0.2	0.4	0.6	1.0
0	33.92	15.77	12.05	8.69	4.12	2.91	1.88
0.05	31.87	16.06	9.28	6.86	3.21	1.97	0.92
0.10	28.03	15.68	10.22	7.94	4.29	2.82	1.16
0.20	25.11	14.76	8.61	6.53	3.32	2.10	1.10
0.40	23.36	12.42	8.06	6.38	3.83	2.91	1.08
0.60	15.61	10.47	6.15	4.95	4.13	3.47	1.02
1.0	0.84	0.72	0.64	0.61	0.57	0.55	0.52

Table 5: The allowable minimum $\eta_{\min}$ for given values of d_1, d_2, $\mathscr{K}_P$, and $\mathscr{K}_I$ and different σ_0.

Methods	σ_0			
	0.2	0.4	0.6	0.8
Theorem 1	4.2013	4.5108	6.0512	6.9512

5.2. Sampled-Data H_∞ LFC Controller Design. To compute the control gain in this example, first let $d_1 = 0.1$, $d_2 = 0.3$, $\eta = 8.5$, $\sigma = 0.8$, and $\varsigma = 0.01$, then the inequalities (33)–(36) in Theorem 2 are solved, and the control gain is obtained, as presented in Table 6.

Let us use the disturbance to graphically verify the given results:

Table 6: The control gain $\mathscr{K}$ for fixed d_1, d_2, η, σ_0, and ς in Theorem 2.

d_1	d_2	σ_0	ς	η	$\mathscr{K}$
0.1	0.3	0.8	0.01	8.5	$[0.0309 \ \ 0.1343]$

$$w(t) = \begin{cases} 0.1\text{pu}, \text{if} t = 10s, 20s, 30s \\ 0, \text{otherwise.} \end{cases} \quad (51)$$

The time-varying delays for the simulation results are chosen as $d_1(t) = 0.05 \sin(t) + 0.05$ and $d_1(t) = 0.10 \sin(t) + 0.20$ satisfying $d_1 = 0.1$ and $d_2 = 0.3$. State trajectories of model (11) are displayed in Figures 3 and 4. These simulation results indicate that model (11) is stabilized with load disturbance and the presence of a stochastic variable and the control gain is listed in Table 6.

5.3. Sampled-Data Robust H_∞ LFC Controller Design. For this scenario, model (38) is considered with $\mathscr{H} = [0.20.20.20.2]^T$, $\mathscr{E} = \text{diag}[0.10.10.10.1]$, and $\mathscr{F}(t) = \text{diag}[\cos(t)\cos(t)\cos(t)\cos(t)]$. In addition, we assume that $d_1 = 0.1$, $d_2 = 0.3$, $\eta = 6.5$, $\sigma_0 = 0.4$, and $\varsigma = 0.01$. Then, inequalities (39)–(42) in Theorem 3 are solved, and the control gain is obtained, as given in Table 7.

Delays $d_1(t)$ and $d_2(t)$ and disturbance signal $w(t)$ are selected to be the same as in above case. To show the effect of the established control design scheme, state trajectories of model (38) are depicted in Figures 5 and 6 under the proposed sampled-data robust LFC control gain in Table 7.

5.4. Comparative Analysis

Case 3. Calculation of MAUBd_1: the benefit of the proposed criterion in Corollary 1 is proven numerically in the following example. Model (44) is considered to obtain the following equation:

$$\mathscr{A} = \begin{bmatrix} -2.0 & 0 \\ 0 & -0.9 \end{bmatrix}, \quad \mathscr{A}_d = \begin{bmatrix} -1.0 & 0 \\ -1.0 & -1 \end{bmatrix}. \quad (52)$$

With the above example, the comparison results are analyzed in detail. The MAUB values of d_1 are shown in Figure 7. They are compared with those published in references [39, 43, 44, 46, 47] for the case of $\mu = 0$. The results in Figure 7 clearly reveal the advantages of the proposed method.

Case 4. Computational Efficiency: the results presented in this study have been achieved on the basis of the LMI methodology. The total number of decision variables in LMI leads to computational issues of the main results. Consequently, the goal of this study is to establish new stability criteria that are less conservative and have a small number of decision variables. To do this, we have leveraged the Jensen-based integral inequality and reciprocal convex combination methods to reduce conservatism without adding new variables to the derivation of the main results. In addition, we have calculated the number of decision variables and compared them with those in prior studies [39, 43, 44, 46, 47], as listed in Table 8. In reference [43], enhanced stability criteria based on novel LKFs were discussed, which required $79.5n^2 + 4.5n$ in decision variables. With the derived results in Corollary 1, only a limited

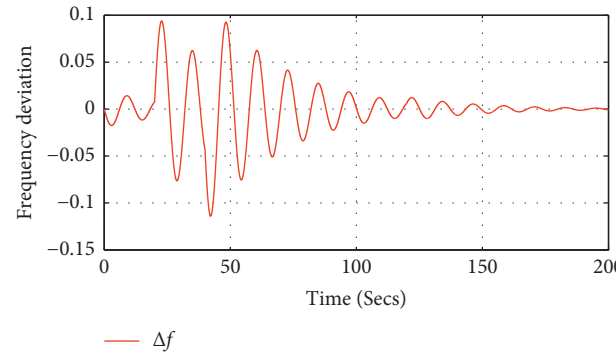

Figure 3: Evaluation of $\triangle f$ in equation (11) in Theorem 2.

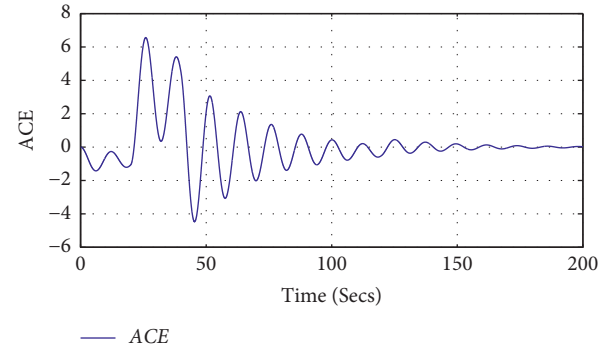

Figure 4: Evaluation of *ACE* in equation (11) in Theorem 2.

Table 7: The control gain $\mathscr{K}$ for fixed d_1, d_2, η, ς, and σ_0 in Theorem 3.

d_1	d_2	σ_0	ς	η	$\mathscr{K}$
0.1	0.3	0.4	0.01	8.5	$[0.0330 \ \ 0.0275]$

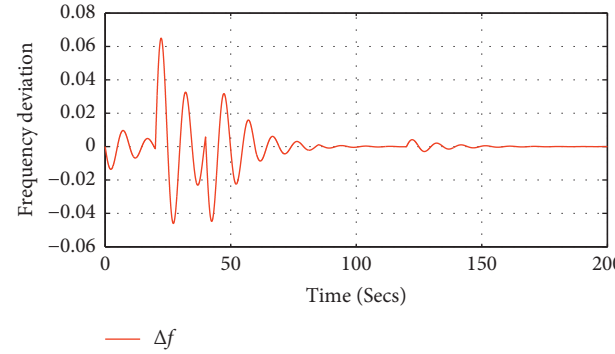

Figure 5: Evaluation of $\triangle f$ in equation (38) in Theorem 3.

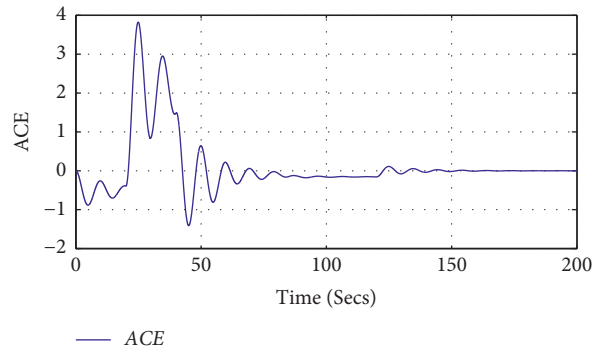

Figure 6: Evaluation of *ACE* in equation (38) in Theorem 3.

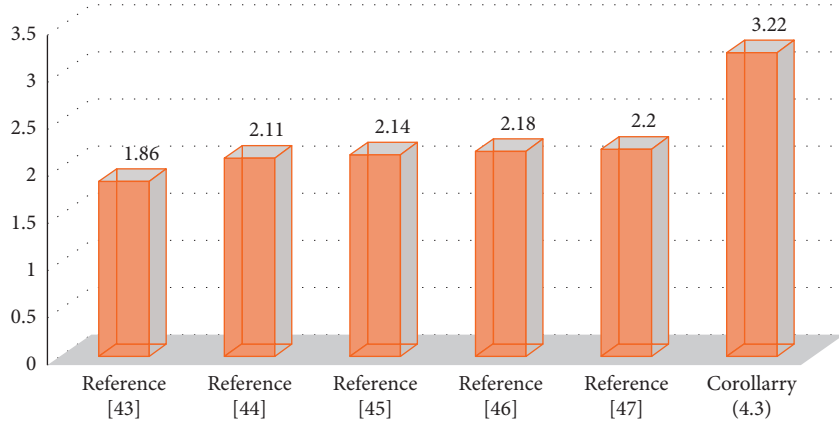

Figure 7: Comparative analysis of MAUB d_1 of Corollary 1 with references [39, 43, 44, 44, 46].

Table 8: Comparative analysis of number of decision variables in Corollary 1.

Methods	Number of decision variables
[39]	$3.5n^2 + 2.5n$
[44]	$10.5n^2 + 3.5n$
[47]	$21n^2 + 6n$
[46]	$54.5n^2 + 9.5n$
[43]	$79.5n^2 + 4.5n$
Corollary 1	$3n^2 + 2n$

number of decision variables $3n^2 + 2n$ are required. Therefore, it is evident that the stability criteria formulated in this study yields less conservatism with a smaller computational burden.

6. Conclusion

In this article, robust sampled-data H_∞ LFC scheme for power systems with randomly occurring time-varying delays has been considered. To better reflect the actual demands of practical dynamics, a generalized framework of the robust sampled-data H_∞ LFC scheme has been studied. By leveraging the input-delay technique, the sampled-data model is converted into a continuous representation. Bernoulli-distributed sequences are used to characterize random time-varying delays in the sampled-data LFC scheme. Less conservative conditions are achieved by utilizing the LKF and employing Jensen inequality and reciprocal convex combination lemma to ensure the considered power system is mean-square asymptotic stability under the designed control strategy. The results derived in this study are based on LMIs that can be easily solved using the MATLAB LMI toolbox. The criteria obtained have been used to analyze the upper bounds of time delays, and a comparison study has been presented to validate the efficacy of the designed control method.

It is worth noting that Markov processes are widely used for modelling complex systems that undergo unpredictable changes. Therefore, LFC for power systems with Markov processes is essential. As a result, we intend to analyze observer-based sliding mode LFC of power systems under deception attacks using the proposed Markovian jump approaches in references [48, 49]. The corresponding results will be carried out in the near future.

Appendix

In equation (1), the following matrices are defined:

$$\check{x}(t) = \left[\triangle f \triangle P_m \triangle P_v\right]^T, w(t) = \triangle P_d, \check{y}(t) = ACE,$$

$$\check{\mathscr{A}} = \begin{bmatrix} -\frac{\mathscr{D}}{\mathscr{M}} & \frac{1}{\mathscr{M}} & 0 \\ 0 & -\frac{1}{\mathscr{T}_{ch}} & \frac{1}{\mathscr{T}_{ch}} \\ -\frac{1}{\mathscr{R}\mathscr{T}_g} & 0 & -\frac{1}{\mathscr{T}_g} \end{bmatrix}, \check{\mathscr{B}} = \begin{bmatrix} 0_{2\times 1} \\ \frac{1}{\mathscr{T}_g} \end{bmatrix}, \tag{A.1}$$

$$\check{\mathscr{D}} = \begin{bmatrix} -\frac{1}{\mathscr{M}} \\ 0_{2\times 1} \end{bmatrix}, \check{\mathscr{C}} = \begin{bmatrix} \beta & 0_{1\times 2} \end{bmatrix},$$

where $\mathscr{R}$, speed droop; $\mathscr{T}_g$, time constant of the governor; $\triangle \mathscr{P}_m$, mechanical output from generator; $\mathscr{D}$, generator damping coefficient; $\mathscr{T}_{ch}$, time constant of the turbine; $\triangle f$, frequency deviation; $\triangle \mathscr{P}_d$, load disturbance; β, frequency bias factor; $\triangle \mathscr{P}_v$, deviation of the position valve; $\mathscr{M}$, moment of inertia of the generator.

In equation (6), the following matrices are defined:

$$\mathscr{A} = \begin{bmatrix} -\frac{\mathscr{D}}{\mathscr{M}} & \frac{1}{\mathscr{M}} & 0 & 0 \\ 0 & -\frac{1}{\mathscr{T}_{ch}} & \frac{1}{\mathscr{T}_{ch}} & 0 \\ -\frac{1}{\mathscr{R}\mathscr{T}_g} & 0 & -\frac{1}{\mathscr{T}_g} & 0 \\ \beta & 0 & 0 & 0 \end{bmatrix}, \mathscr{B} = \begin{bmatrix} 0_{2\times 1} \\ \frac{1}{\mathscr{T}_g} \\ 0 \end{bmatrix}, \tag{A.2}$$

$$\mathscr{C} = \begin{bmatrix} \beta & 0_{1\times 3} \\ 0_{1\times 3} & 1 \end{bmatrix}, \mathscr{D} = \begin{bmatrix} -\frac{1}{\mathscr{M}} \\ 0_{3\times 1} \end{bmatrix}. \mathscr{K} = \begin{bmatrix} \mathscr{K}_P \mathscr{K}_I \end{bmatrix}.$$

Data Availability

No data were used to support this study.

Conflicts of Interest

The authors declare that they have no conflicts of interest.

Authors' Contributions

All authors contributed equally and significantly in writing this article. All authors read and approved the final manuscript.

Acknowledgments

This work was supported by the Aden University, Yemen.

References

[1] J. Momoh, *Smart Grid: Fundamentals of Design and Analysis"*, Wiley, Hoboken, NY, USA, 2012.

[2] L. K. Kirchmayer, "Tie-line power and frequency control of electric power systems," *IEEE Transactions on Power Apparatus and Systems*, vol. 72, no. 2, pp. 562–572, 1953.

[3] J. J. Grainger, W. D. Stevenson, and G. W. Chang, *Power System Analysis*, McGraw-Hill, New York, NY, USA, 1994.

[4] P. Kundur, N. J. Balu, and M. G. Lauby, *Power System Stability and Control*, McGraw-Hill, New York, NY, USA, 1994.

[5] A. Petersson, L. Harnefors, and T. Thiringer, "Evaluation of current control methods for wind turbines using doubly-fed induction machines," *IEEE Transactions on Power Electronics*, vol. 20, no. 1, pp. 227–235, 2005.

[6] Y. Mi, Y. Fu, D. Li, C. Wang, P. C. Loh, and P. Wang, "The sliding mode load frequency control for hybrid power system based on disturbance observer," *International Journal of Electrical Power & Energy Systems*, vol. 74, pp. 446–452, 2016.

[7] G. Nagamani, C. Karthik, and Y. H. Joo, "Event-triggered observer-based sliding mode control for T-S fuzzy systems via improved relaxed-based integral inequality," *Journal of the Franklin Institute*, vol. 357, no. 14, pp. 9543–9567, 2020.

[8] A. Rubaai and V. Udo, "An adaptive control scheme for load-frequency control of multiarea power systems Part II. Implementation and test results by simulation," *Electric Power Systems Research*, vol. 24, no. 3, pp. 189–197, 1992.

[9] W. Tan and Z. Xu, "Robust analysis and design of load frequency controller for power systems," *Electric Power Systems Research*, vol. 79, no. 5, pp. 846–853, 2009.

[10] C. Karthik, G. Nagamani, and R. Subramaniyam, "Robust stabilization of T-S fuzzy systems via improved integral inequality," *Soft Computing*, vol. 26, no. 1, pp. 349–360, 2022.

[11] J. Cheng, S. Chen, Z. Liu, H. Wang, and J. Li, "Robust finite-time sampled-data control of linear systems subject to random occurring delays and its application to Four-Tank system," *Applied Mathematics and Computation*, vol. 281, pp. 55–76, 2016.

[12] N. Gnaneswaran and Y. H. Joo, "Event-triggered stabilisation for T-S fuzzy systems with asynchronous premise constraints and its application to wind turbine system," *IET Control Theory & Applications*, vol. 13, no. 10, pp. 1532–1542, 2019.

[13] G. Nagamani, Y. H. Joo, G. Soundararajan, and R. Mohajerpoor, "Robust event-triggered reliable control for T-S fuzzy uncertain systems via weighted based inequality," *Information Sciences*, vol. 512, pp. 31–49, 2020.

[14] J. Cheng, L. Liang, J. H. Park, H. Yan, and K. Li, "A dynamic event-triggered approach to state estimation for switched memristive neural networks with nonhomogeneous sojourn probabilities," *IEEE Transactions on Circuits and Systems I: Regular Papers*, vol. 68, no. 12, pp. 4924–4934, 2021.

[15] S. Kumar Pradhan and D. Kumar Das, "H∞ load frequency control design based on delay discretization approach for interconnected power systems with time delay," *Journal of Modern Power Systems and Clean Energy*, vol. 9, no. 6, pp. 1468–1477, 2021.

[16] J. Nanda, A. Mangla, and S. Suri, "Some new findings on automatic generation control of an interconnected hydrothermal system with conventional controllers," *IEEE Transactions on Energy Conversion*, vol. 21, no. 1, pp. 187–194, 2006.

[17] Y. Zhang, D. Yue, and S. Hu, "Digital PID Based Load Frequency Control through Open Communication Networks," in *Proceedings of the The 27th Chinese Control and Decision Conference (2015 CCDC)*, pp. 6243–6248, Qingdao, China, July 2015.

[18] T. Hiyama, "Optimisation of discrete-type load-frequency regulators considering generation-rate constraints," *IEE Proceedings C Generation, Transmission and Distribution*, vol. 129, no. 6, p. 285, 1982.

[19] J. S. Lim and Y. I. Lee, "Design of discrete-time multivariable PID controllers via LMI approach," *Int. Conf. Control, Autom. Syst*, vol. 38, no. 3, pp. 1867–1871, 2008.

[20] E. Fridman, "A refined input delay approach to sampled-data control," *Automatica*, vol. 46, no. 2, pp. 421–427, 2010.

[21] X.-C. Shangguan, C.-K. Zhang, Y. He et al., "Robust load frequency control for power system considering transmission delay and sampling period," *IEEE Transactions on Industrial Informatics*, vol. 17, no. 8, pp. 5292–5303, 2021.

[22] X. Shang-Guan, Y. He, C. Zhang, L. Jiang, J. W. Spencer, and M. Wu, "Sampled-data based discrete and fast load frequency control for power systems with wind power," *Applied Energy*, vol. 259, Article ID 114202, 2020.

[23] C. C. Chen, S. Hirche, and M. Buss, "Sampled-data networked control systems with random time delay," *IFAC Proceedings Volumes*, vol. 41, no. 2, Article ID 11594, 2008.

[24] S. Sun and G. Wang, "Modeling and estimation for networked systems with multiple random transmission delays and packet losses," *Systems & Control Letters*, vol. 73, pp. 6–16, 2014.

[25] N. Wang, W. Qian, and X. Xu, "H∞ performance for load frequency control systems with random delays," *Systems Science & Control Engineering*, vol. 9, no. 1, pp. 243–259, 2021.

[26] R. Sakthivel, S. A. Karthick, B. Kaviarasan, and F. Alzahrani, "Dissipativity-based non-fragile sampled-data control design of interval type-2 fuzzy systems subject to random delays," *ISA Transactions*, vol. 83, pp. 154–164, 2018.

[27] M. Wu, Y. He, and J. H. She, *Stability Analysis and Robust Control of Time-Delay Systems*, Springer-Verlag, New York, NY, USA, 2010.

[28] H. Bevrani, *Robust Power System Frequency Control*, Springer, New York, NY, USA, 2009.

[29] H. Bevrani and T. Hiyama, "Robust decentralised PI based LFC design for time delay power systems," *Energy Conversion and Management*, vol. 49, no. 2, pp. 193–204, 2008.

[30] Y. Wang, R. Zhou, and C. Wen, "Robust load-frequency controller design for power systems," *IEE Proceedings C Generation, Transmission and Distribution*, vol. 140, no. 1, p. 11, 1993.

[31] A. M. Stankovic, G. Tadmor, and T. A. Sakharuk, "On robust control analysis and design for load frequency regulation," *IEEE Transactions on Power Systems*, vol. 13, no. 2, pp. 449–455, 1998.

[32] Y. Sun, N. Li, X. Zhao, Z. Wei, G. Sun, and C. Huang, "Robust H_∞ load frequency control of delayed multi-area power system with stochastic disturbances," *Neurocomputing*, vol. 193, no. C, pp. 58–67, 2016.

[33] Y. Cui, G. Shi, L. Xu, X. Zhang, and X. Li, "Decentralized H_∞ load frequency control for multi-area power systems with communication uncertainties," *Adv. Comput. Meth. Energy, Power, Electric Vehicles, Their Integration*, Springer, vol. 4, pp. 429–438, 2017.

[34] R. Dey, S. Ghosh, and G. Ray, "H_∞load frequency control of interconnected power systems with communication delays," *International Journal of Electrical Power & Energy Systems*, vol. 42, no. 1, pp. 672–684, 2012.

[35] S. Kuppusamy and Y. H. Joo, "Resilient Reliable H_∞ load frequency control of power system with random gain fluctuations," *IEEE Trans. Syst., Man, Cyber.: Office Systems*, vol. 52, pp. 1–9, 2021.

[36] C. Karthik and G. Nagamani, "H_∞performance analysis for uncertain systems with actuator fault control via relaxed integral inequalities," *International Journal of Dynamical Systems and Differential Equations*, vol. 11, no. 5-6, pp. 630–646, 2021.

[37] M. Syed Ali and R. Saravanakumar, "Robust H_∞ control of uncertain systems with two additive time-varying delays," *Chinese Physics B*, vol. 24, no. 9, 2015.

[38] H. Huang, G. Feng, and J. Cao, "Guaranteed performance state estimation of static neural networks with time-varying delay," *Neurocomputing*, vol. 74, no. 4, pp. 606–616, 2011.

[39] P. G. Park, J. W. Ko, and C. Jeong, "Reciprocally convex approach to stability of systems with time-varying delays," *Automatica*, vol. 47, no. 1, pp. 235–238, 2011.

[40] K. Gu, V. Kharitonov, and J. Chen, *Stability of Time-Delay Systems*, Birkhauser, Boston, MA, USA, 2003.

[41] L. H. Xie, "Output feedback H_∞ control of systems with parameter uncertainty," *International Journal of Control*, vol. 63, pp. 741–750, 1996.

[42] C. A. R. Crusius and A. Trofino, "Sufficient LMI conditions for output feedback control problems," *IEEE Transactions on Automatic Control*, vol. 44, no. 5, pp. 1053–1057, 1999.

[43] K. Liu, A. Seuret, and Y. Xia, "Stability analysis of systems with time-varying delays via the second-order Bessel-Legendre inequality," *Automatica*, vol. 76, pp. 138–142, 2017.

[44] A. Seuret, F. Gouaisbaut, and E. Fridman, "Stability of systems with fast-varying delay using improved wirtinger's inequality," in *Proceedings of the 52nd IEEE Conf. Decision Control*, Firenze, Italy, December 2013.

[45] L. Jiang, W. Yao, Q. H. Wu, J. Y. Wen, and S. J. Cheng, "Delay dependent stability for load frequency control with constant and time-varying delays," *IEEE Transactions on Power Systems*, vol. 27, no. 2, pp. 932–941, 2012.

[46] H. B. Zeng, Y. He, M. Wu, and J. H. She, "Free-matrix-based integral inequality for stability analysis of systems with time-varying delay," *IEEE Transactions on Automatic Control*, vol. 60, no. 10, pp. 2768–2772, 2015.

[47] P. G. Park, W. I. Lee, and S. Y. Lee, "Auxiliary function-based integral inequalities for quadratic functions and their applications to time-delay systems," *Journal of the Franklin Institute*, vol. 352, no. 4, pp. 1378–1396, 2015.

[48] J. Cheng, Y. Wang, J. H. Park, J. Cao, and K. Shi, "Static output feedback quantized control for fuzzy Markovian switching singularly perturbed systems with deception attacks," *IEEE Transactions on Fuzzy Systems*, vol. 30, no. 4, pp. 1036–1047, 2022.

[49] J. Cheng, J. H. Park, and Z. G. Wu, "A hidden Markov model based control for periodic systems subject to singular perturbations," *Systems & Control Letters*, vol. 157, Article ID 105059, 2021.

Hindawi
Complexity
Volume 2022, Article ID 7093749, 7 pages
https://doi.org/10.1155/2022/7093749

Research Article

Single Phytoplankton Species Growth with Nonlocal Crowding Effect Caused by Chemosensory Aggregation in a Water Column

Yan Wang,[1] **Jinxiang Wang**,[2] **and Xiaobin Yao**[3]

[1]*School of Civil Engineering, Lanzhou University of Technology, Lanzhou 730050, China*
[2]*Department of Applied Mathematics, Lanzhou University of Technology, Lanzhou, China*
[3]*School of Mathematics and Statistics, Qinghai Nationalities University, Xining, China*

Correspondence should be addressed to Jinxiang Wang; wjx19860420@163.com

Received 9 May 2022; Accepted 6 June 2022; Published 28 June 2022

Academic Editor: C. Rajivganthi

In this paper, we study the existence of positive steady states for a nonlocal reaction-diffusion model which describes the growth of a single phytoplankton species with nonlocal crowding effect caused by chemosensory aggregation in a water column. Our result shows that under some conditions, the nonlocal crowding effect is effective to the existence of steady states of phytoplankton populations. Based on a key boundedness Lemma, the main result is proved by fixed point index theory and some analytical techniques.

1. Introduction

In this paper, we study the existence of positive solution for the following nonlocal problem:

$$-u''(x) = u(x)g\left(I_0 e^{-k_0 x}\exp\left(-k_1\int_0^x u(s)\mathrm{d}s\right)\right) - u(x)\int_0^L K(x,s)u(s)\mathrm{d}s, x \in (0,L), \tag{1}$$

$$u'(0) = u'(L) = 0, \tag{2}$$

which arises from the modeling of the growth of phytoplankton species with light and nonlocal crowding effect in a water column. In (1), $u = u(x)$ is the population density of the phytoplankton species, and $L > 0$ is the depth of the water column. The first nonlocal nonlinearity on the right-hand side of (1) describes the growth of the phytoplankton species depending on light intensity at different depths, and the second nonlocal nonlinearity corresponds to the total death due to the combination of intrinsic death rate and nonlocal crowding effect caused by chemosensory aggregation. The Neumann boundary condition (2) means that the water column is closed, with no phytoplankton entering or leaving the column at the top $x = 0$ or the bottom $x = L$. A more detailed explanation of the model and notations in it will be given as follows.

Our motivations to investigate above problem on the one hand stem from a kind of existing mathematical model of phytoplankton growth with light and, on the other hand, from the chemosensory aggregation behavior of phytoplankton which has never been considered in previous models. We will focus on the necessity of incorporating aggregation-crowding effect in phytoplankton individuals and its influence on the positive steady states of phytoplankton population.

Phytoplankton is microscopic plants that float in lakes and ocean waters, which form the foundation of the aquatic food chain. Most phytoplankton depend primarily on nutrients and light for growth, while a few rely entirely on light for metabolism. In eutrophic waters, where nutrients are plentiful, phytoplankton usually competes primarily for light. In [1], in order to understand the growth of phytoplankton species in eutrophication water, Huisman et al. introduced and discussed the following reaction-diffusion model for the growth of single species through numerical simulation.

$$u_t = \mathrm{D}u_{xx} + u\left[g\left(I_0 e^{-k_0 x}\exp\left(-k_1\int_0^x u(s,t)\mathrm{d}s\right)\right) - \mathrm{d}\right],$$
$$x \in (0,L), t>0, \tag{3}$$

where $u = u(x,t)$ is the population density of phytoplankton, $\mathrm{D}>0$ is the vertical diffusion coefficient, and $\mathrm{d}>0$ is the death rate; $I_0 e^{-k_0 x}\exp(-k_1\int_0^x u(s,t)\mathrm{d}s) = I(x,t)$ is the light intensity in accordance with Lambert–Beer law, where I_0 is incident light intensity, k_0 is background turbidity, and k_1 is the absorption coefficient of phytoplankton. $g(I)$ is the growth rate of phytoplankton as a function of light intensity $I = I(x,t)$. The growth rate $g(I)$ generally satisfies

$$g(0) = 0, g'(I) > 0 \text{ for } I \geq 0. \tag{4}$$

A typical example of $g(I)$ is the Michaelis–Menten form, and $g(I) = mI/a + I$, where m is the maximum growth rate, and a is the half saturation constant.

The model in [1] is one of the phytoplankton mathematical models proposed and studied in recent years, and related studies on the formation of phytoplankton blooms from mathematical, experimental, and numerical perspectives can be found in [2–9] and its references. In [10], to get a comprehensive mathematical treatment of the model in [1], Du and Hsu discussed the following steady-state problem of (3) with suitable scaling:

$$-Du'' = u\left[g\left(e^{-k_0 x}\exp\left(-k_1\int_0^x u(s)ds\right)\right) - d\right], x \in (0,1). \tag{5}$$

By using global bifurcation arguments, Du and Hsu proved that there exists a critical death rate d^* such that equation (5) with Neumann boundary condition (2) has a positive solution if and only if $0<d<d^*$, and then, they obtained a description of the long-time dynamical behavior of the model in [1] based upon the positive steady state ([10] also considered the case of two competing species). In [11], Hsu and Lou studied the following model which is an extension of (3)

$$u_t = Du_{xx} - vu_x + u\left[g\left(I_0 e^{-k_0 x}\exp\left(-k_1\int_0^x u(s,t)ds\right)\right) - d\right],$$
$$x \in (0,L), t>0, \tag{6}$$

where v is the sinking velocity ($v>0$) or the buoyant velocity (if $v<0$). In addition to getting similar results as [10] for corresponding steady state problem with zero flux boundary conditions, Hsu and Lou also studied in detail how the critical death rate varies with other parameters L, v, and D, and then, the comprehensive effect of the parameters on the persistence of a single phytoplankton species is studied. Du and Mei in [12] extended the results of [10, 11] to the model which has variable diffusion and sinking rate. In [13], the effect of photo-inhibition on the growth of phytoplankton in a single population was studied, and the results show that the model with photo-inhibition has at least two positive steady-state solutions in certain parameter ranges. In [14], by assuming that the incident light intensity and the death rate are time-periodic for single phytoplankton, Peng and Zhao established a threshold type result on the global dynamics of the model based on the basic reproduction number. In [15], Pang, Nie, and Wu introduced a local crowding effect into model (6), and they first proved the steady states in terms of the intrinsic death rate of the phytoplankton species and next investigated the asymptotic profiles of positive equilibria for small crowding effect and large advection rate. We notice that, in [15], the crowding effect of the population u at position x is assumed to only depend on the value of the population in the same point x, and the interaction and competition between phytoplankton individuals at different positions are not considered.

However, according to related studies on phytoplankton population [16–19], it seems more reasonable to consider that the crowding effect depends not only on their own point in space but also depends on the population around them. Indeed, many phytoplankton (such as the dinoflagellates and more generally algae) are known to leak organic matter into the solution which forms a zone around individual cells, the "phycosphere," in which the concentration of extracellular products is higher than the surrounding concentration, see [16, 17]. On the other hand, many species of phytoplankton (algae, bacteria, and dinoflagellates) have been found to have chemosensory abilities: they can sense the chemical field generated by the presence of other particles, see [18, 19]. Thus, the released products of individual phytoplankton will attract other individuals within a certain neighborhood and finally induce aggregation behavior of phytoplankton at small scales, see [20, 21]. A corollary of this aggregation behavior is increased nonlocal competition for light and nutrients between individuals within a certain space.

Motivated by the above-described works, in this paper, we take into account the more realistic nonlocal crowding effect in the phytoplankton model and study its influence on the steady states of phytoplankton populations. To avoid some technical details, we drop the advection term and then investigate the scaled models (1) and (2).

Models (1) and (2) are an extension of the previous steady-state model discussed in [1, 10–15], and it has important significance in planktology. In (1), the first nonlocal nonlinearity is the same as in the previous model, the second new nonlocal nonlinearity corresponds to the total death due to the combination of intrinsic death and nonlocal crowding effect caused by chemosensory aggregation, and the kernel $K(x,y)$ stands for the competition rate between individuals at position x and individuals at position y. According to the previous statement on phytoplankton, the extracellular products released by a phytoplankton particle located in x may attract nearby particles located in the centered ball at x of radius $\delta>0$ and then deduce a nonlocal crowding effect. Beyond the radius δ, particles cannot be usually attracted, because they are sensory-limited [21]. So, a typical form of K maybe $K(x,y) = K_\delta(|x,y|)$ which has the following characteristics:

(H1) $K_\delta(|x, y|)$ is continuous and monotone decreasing

(H2) $K_\delta(|x, y|) = 0$ if $|x, y| \geq \delta$

However, in this paper, we will study (1) and (2) with more general competition kernel $K(x, y)$ that will be detailed as follows.

From a mathematical point of view, models (1) and (2) also have some new interesting features that differ from previous models. Compared to the previous steady-state problems in [1, 10–15] and other related logistic population models with one nonlocal term (see e.g., [22–31]), the appearance of two nonlocal nonlinear terms in equation (1) will cause more mathematical difficulties and make the analysis of the model particularly interesting. Under certain new assumptions on g and K, our main result will be proved by using the fixed point index theory on cone. Although the idea is motivated by [15], significant changes are needed in the arguments due to the appearance of a new nonlocal nonlinearity, see the key boundedness Lemma 1 below which is ingeniously proved in terms of Taylor–Lagrange's formula. Our proof will provide a new idea for studying steady-state solutions of models with multiple nonlocal terms.

The rest paper is arranged as follows: in Section 2, we give some preliminaries and prove the key boundedness result; In Section 3, we give out the main result of this paper and its proof; finally, Section 4 contains our conclusions and some problems worthy of further study.

2. Preliminaries and a Boundedness Lemma

Let $h \in C[0, L]$, we define $\psi_\tau(h) = h[\tau g(I_0 e^{-k_0 x} \exp(-k_1 \int_0^x h(s)\mathrm{d}s)) - \int_0^L K(x, s)h(s)\mathrm{d}s + M]$ where M is large enough such that $\tau g(I_0 e^{-k_0 x} \exp - (-k_1 \int_0^x h(s)\mathrm{d}s)) - \int_0^L K(x, s)h(s)\mathrm{d}s + M > 0$ for all $x \in [0, L]$ and $\tau \in [0, L]$. Then, we define an operator Ψ_τ: $[0, 1] \times C[0, L] \longrightarrow C[0, L]$ by $\Psi_\tau(h)$: $= \Phi(\psi_\tau(h))$, where Φ is the solution operator $u = \Phi(m(x))$ for the problem

$$\begin{cases} -u'' + Mu(x) = m(x), x \in (0, L), \\ u'(0) = u'(L) = 0. \end{cases} \tag{7}$$

Obviously, Ψ_τ: $[0, 1] \times C[0, L] \longrightarrow C[0, L]$ is compact and continuously differentiable. Let $\Psi = \Psi_1$, then (1) and (2) have a solution if and only if Ψ has a fixed point.

Now, we prove a boundedness result for Ψ_τ which will play a key role in the proof of the main results.

Lemma 1. *Assume that (4) holds and*

$$g(I_0) \leq \frac{2}{L^2}. \tag{8}$$

The function K satisfies

(i) $K \in C([0, L] \times [0, L])$ and $K(x, y) \geq 0$ for all $x, y \in [0, L]$

(ii) There exist a constant $k > 0$ such that $K(x, x) \geq k$ for all $x \in [0, L]$

Then, there exists $R > 0$ such that for all $u \in C[0, L]$ positive and $\tau \in [0, 1]$ satisfying $u = \Psi_\tau(u)$, and we have $\|u\|_\infty < R$.

Proof. Let $u \in C[0, L]$, positive and $\tau \in [0, 1]$ such that $u = \Psi_\tau(u)$. u attain its maximum value at a point $x_0 \in [0, L]$. As u satisfies Neumann boundary conditions, for $x_0 \in [0, L]$, we have $u'(x_0) = 0$ and $u''(x_0) \leq 0$. Using (7) at the point x_0 and since $\tau \leq 1$, we get

$$-u''(x_0) + Mu(x_0) \leq u(x_0)\left[g\left(I_0 e^{-k_0 x} \exp\left(-k_1 \int_0^x u(s, t)\mathrm{d}s\right)\right) - \int_0^L K(x, s)h(s)\mathrm{d}s + M\right], \tag{9}$$

and consequently,

$$\left[g\left(I_0 e^{-k_0 x} \exp\left(-k_1 \int_0^x u(s, t)\mathrm{d}s\right)\right) - \int_0^L K(x, s)h(s)\mathrm{d}s \geq 0\right]. \tag{10}$$

Combining (10) with (4), we have

$$g(I_0) \geq g\left(I_0 e^{-k_0 x} \exp\left(-k_1 \int_0^x u(s, t)\mathrm{d}s\right)\right) - \int_0^L K(x, s)h(s)\mathrm{d}s. \tag{11}$$

We then use Taylor–Lagrange's formula for the function u at point x_0. For all $y \in [0, L]$, there exists $\xi \in (x_0, y)$ or (y, x_0) such that

$$u(y) = \|u\|_\infty + \frac{(y - x_0)^2}{2} u''(\xi). \tag{12}$$

Additionally, by using again (7), we obtain, for all $\xi \in [0, L]$

$$-u''(\xi) \leq u(\xi)\left[g\left(I_0 e^{-k_0 x} \exp\left(-k_1 \int_0^x u(s, t)\mathrm{d}s\right)\right) - \int_0^L K(x, s)h(s)\mathrm{d}s \geq 0\right], \tag{13}$$

and then,

$$-u''(\xi) \le u(\xi)\left[g\left(I_0 e^{-k_0 x}\exp\left(-k_1\int_0^x u(s,t)\mathrm{d}s\right)\right) - \int_0^L K(x,s)h(s)\mathrm{d}s \ge 0\right], \tag{14}$$

which implies that

$$u''(\xi) \le u(\xi)g\left(I_0 e^{-k_0 x}\exp\left(-k_1\int_0^x u(s,t)\mathrm{d}s\right)\right) \ge -\|u\|_\infty g(I_0). \tag{15}$$

Combining above inequality with (12), we have

$$u(y) \ge \|u\|_\infty\left[1 - \frac{(y-x_0)^2}{2}g(I_0)\right]. \tag{16}$$

Substituting (16) into (11), we have

$$\begin{aligned} g(I_0) &\ge \int_0^L K(x_0,s)u(s)\mathrm{d}s \\ &\ge \int_0^L K(x_0,y)\|u\|_\infty\left[1 - \frac{(y-x_0)^2}{2}g(I_0)\right]\mathrm{d}y. \end{aligned} \tag{17}$$

Since $1 - (y-x_0)^2/2g(I_0) \ge 0$ for all $y \in [0,L]$ according to condition (G), then (17) implies that

$$\|u\|_\infty \le g(I_0)\left[\int_0^L K(x_0,y)\left[1 - \frac{(y-x_0)^2}{2}g(I_0)\right]\mathrm{d}y\right]. \tag{18}$$

Since $K(x_0,\cdot)$ is positive in a neighborhood of x_0 by the condition (ii), we deduce that

$$g(I_0)\left[\int_0^L K(x_0,y)\left[1 - \frac{(y-x_0)^2}{2}g(I_0)\right]\mathrm{d}y\right]^{-1} < +\infty. \tag{19}$$

Then, there exists $R > 0$ such that for all $u \in C[0,L]$ positive and $\tau \in [0,L]$ satisfying $u = \Psi_\tau(u)$, and we have $\|u\|_\infty < R$.

Our main tool is the following fixed point index theorem. □

Lemma 2. ([32], Proposition 2 and [33], Theorem 2.1). *Let F: $W \longrightarrow W$ be a compact, continuously differentiable operator, W be a cone in the Banach space E with zero Θ. Suppose that $W - W$ is dense in E and the $\Theta \in W$ is a fixed point of F and $A_0 = F\prime(\Theta)$. Then, the following results hold:*

(i) $index_W(F,\Theta) = 1$ if the spectral radius $r\ (A_0) < 1$

(ii) $index_W(F,\Theta) = 0$ if A_0 has an eigenvalue greater, then 1 and Θ are an isolated solution of $x = F(x)$; that is, $h \ne A_0 h$ if $h \in \overline{W} - \Theta$

At last, we give a principal eigenvalue result to be used in the proof of the main result.

Lemma 3. *([34]) Let $q(x) \in C(\overline{\Omega})$ and $q(x) + p > 0$ on $\overline{\Omega}$ with $p > 0$, and let σ_1 be the first eigenvalue of the eigenvalue problem*

$$-\triangle\varphi - q(x)\varphi = \sigma\varphi, x \in \Omega, \frac{\partial\varphi}{\partial n} = 0, x \in \partial\Omega. \tag{20}$$

If $\sigma_1 > 0$ (or $\sigma_1 < 0$), then the eigenvalue problem

$$-\triangle\varphi + p\varphi = t(q(x)+p)\varphi, x \in \Omega, \frac{\partial\varphi}{\partial n} = 0, x \in \partial\Omega, \tag{21}$$

has no eigenvalue less than or equal to 1 (or has eigenvalue less than 1).

3. The Main Result and the Proof

Our main result is as follows.

Theorem 1. *Assume that conditions (4), (G), (i) and (ii) in Lemma 1 hold, and moreover, the function K satisfies*

(i) If $w \in C[0,L]$ is nonnegative and $\int_0^L\int_0^L K(x,y)w(y)w(x)dxdy = 0$, then $w \equiv 0$,

Then, problem (1) and (2) have a positive solution.

Proof. Denote $E = C^1[0,L]$, $W = \{u \in E: u(x) \ge 0, \forall x \in [0,L]\}$, then it is easy to see that W be a cone in the Banach space E with zero Θ. By Lemma 1, we can conclude that there exists $\widetilde{R} > 0$ such that for all $u \in W$ and $\tau \in [0,L]$ satisfying $u = \Psi_\tau(u)$, and we have $\|u\|_E < \widetilde{R}$. We then define $\Omega = \{u \in E: u(x) \ge 0, \forall x \in [0,L]\}$.

Obviously, Ψ_τ: $[0,1] \times \Omega \longrightarrow W$ is compact and continuously differentiable. Let $\Psi = \Psi_1$, then (1) and (2) have a nonnegative solution if and only if Ψ has a fixed point in Ω.

Following from the boundedness result, for $\tau \in [0,1]$, Ψ_τ has no fixed point on $\partial\Omega$, then, by the homotopic invariance of the degree, we conclude that

$$\begin{aligned} \mathrm{index}(\Psi,\Omega,W) &= \mathrm{index}(\Psi_\tau,\Omega,W), \\ &= \mathrm{index}(\Psi_0,\Omega,W). \end{aligned} \tag{22}$$

We claim that Ψ_0 has a unique fixed point 0 in Ω. Indeed, let $\Psi_0(u) = u$, then

$$\begin{cases} -u''(x) = -u(x)\displaystyle\int_0^L K(x,s)u(s)\mathrm{d}s, x \in (0,L), \\ u'(0) = u\prime(L) = 0. \end{cases} \tag{23}$$

Integrating the equation in (23) from 0 to L and by using the boundary value conditions, we can obtain that

$$\int_0^L \left[u(x) \int_0^L K(x,s)u(s)\mathrm{d}s \right] \mathrm{d}x = 0. \tag{24}$$

Then, by condition (iii), we get that $u(x) \equiv 0$. Thus, 0 is the unique fixed point of Ψ_0 in Ω, and

$$\mathrm{index}(\Psi_0, \Omega, W) = \mathrm{index}(\Psi_0, 0, W). \tag{25}$$

Now, we show that $\mathrm{index}(\Psi_0, 0, W) = 1$ by using Lemma 2. Let $\Psi_0'(0)$ be the Fréchet derivative of Ψ_0 with respect to u at 0. For $\varphi \in W$, let $\Psi_0'(0)\varphi = \lambda\varphi$ and $\varphi \equiv 0$. Then,

$$\begin{cases} -\varphi''(x) = \left(\dfrac{1}{\lambda} - 1\right) M\varphi(x), x \in (0, L), \\ \varphi'(0) = \varphi'(L) = 0. \end{cases} \tag{26}$$

Multiplying the above equation by φ and integrating from 0 to L by parts, we get that

$$\frac{1}{\lambda} - 1 = \frac{\int_0^L (\varphi'(x))^2 \mathrm{d}x}{M \int_0^L (\varphi'(x))^2 \mathrm{d}x} > 0. \tag{27}$$

Thus, $\lambda < 1$ and the spectral radius $r(\Psi_0'(0)) < 1$. By Lemma 2, we have $\mathrm{index}(\Psi_0, 0, W) = 1$, and then,

$$\begin{aligned} \mathrm{index}(\Psi_0, \Omega, W) &= \mathrm{index}(\Psi_0, 0, W), \\ &= \mathrm{index}(\Psi_0, 0, W) = 1. \end{aligned} \tag{28}$$

Next, we show that $\mathrm{index}(\Psi, 0, W) = 0$ by Lemma 2 again. Let $\Psi'(0)$ be the Fréchet derivative of Ψ with respect to u at 0. For $u \in W$, $\Psi'(0)u = u$ is equivalent to

$$\begin{cases} -u''(x) + Mu(x) = u(x)g\left(I_0 e^{-k_0 x}\right) + m(x), x \in (0, L), \\ u'(0) = u'(L) = 0. \end{cases} \tag{29}$$

We can see that $u \equiv 0$, that is, 1 is not an eigenvalue of $\Psi'(0)$ in W. Thus, 0 is an isolated fixed point of Ψ in W. Let $\Psi'(0)u = \lambda u$ and $u \equiv 0$. Then,

$$\begin{cases} -u''(x) + Mu(x) \\ = \dfrac{1}{\lambda}\left[u(x)g\left(I_0 e^{-k_0 x}\right) + Mu(x)\right], m(x), x \in (0, L), \\ u'(0) = u'(L) = 0. \end{cases} \tag{30}$$

Considering the following eigenvalue problem:

$$\begin{cases} -\eta''(x) - \eta(x)g\left(I_0 e^{-k_0 x}\right) = \mu\eta(x), \quad x \in (0, L), \\ \eta'(0) = \eta'(L) = 0. \end{cases} \tag{31}$$

Let $\mu_1(-g(I_0 e^{-k_0 x}))$ be the smallest eigenvalue of (31), and let $\mu_1(0)$ be the smallest eigenvalue of

$$\begin{cases} -\eta''(x) = \mu\eta(x), x \in (0, L), \\ \eta'(0) = \eta'(L) = 0. \end{cases} \tag{32}$$

It is easy to see that $\mu_1(0) = 0$. Since $g(I_0 e^{-k_0 x}) > 0$, it follows from monotonicity of the smallest eigenvalue with respect to the weight function that

$$\mu_1\left(-g\left(I_0 e^{-k_0 x}\right)\right) < \mu_1(0) = 0. \tag{33}$$

Then, by Lemma 3, the eigenvalue problem is as follows:

$$\begin{cases} -u''(x) + Mu(x) \\ = \rho\left[u(x)g\left(I_0 e^{-k_0 x}\right) + Mu(x)\right], m(x), x \in (0, L), \\ u'(0) = u'(L) = 0. \end{cases} \tag{34}$$

It has an eigenvalue ρ_1 less than 1. Thus, it is easy to see that $1/\rho_1 > 1$ is an eigenvalue of $\Psi'(0)$. That is, $\Psi'(0)$ has an eigenvalue greater than 1. It follows from Lemma 2 that $\mathrm{index}(\Psi, 0, W) = 0$.

Since $\mathrm{index}(\Psi_0, \Omega, W) \neq \mathrm{index}(\Psi_0, 0, W)$, it follows from Leray-Schauder degree theory that Ψ has at least one nonzero fixed point in Ω. That is, (1) and (2) have at least one nontrivial nonnegative solution. Moreover, by the strong maximum principle and Hopf boundary Lemma, we can show that the nontrivial nonnegative solution of (1) and (2) is a positive solution. □

4. Conclusion

In this paper, we proved the existence of positive steady states for a nonlocal reaction-diffusion model which describes the growth of a single phytoplankton species with nonlocal crowding effect caused by chemosensory aggregation in a water column. The main feature of our model is that it captures the idea of the attraction interaction between phytoplanktons due to the chemosensory behavior. This clustering characteristic in conjunction with the competition for light makes the problem become more complicated, which is manifested in the appearance of two nonlocal nonlinear terms in the model (1) and (2).

In contrast to the steady-state problem that does not account for nonlocal crowding effect such as (5) in [10], our results show that under a certain range of the growth rate depending on incident light intensity, problems (1) and (2) always have a positive solution for some positive nonlocal competitive mortality K. This shows that the nonlocal crowding effect is effective to the existence of steady states of phytoplankton populations.

Note that although the existence of positive solution for steady state problem (1) and (2) has been provided in Theorem 1, the uniqueness is not known, and this also prevents us from obtaining the asymptotic profiles of the positive steady states and the longtime dynamical behavior of the model. These problems remain to be resolved in the future.

Data Availability

No data were used to support this study.

Conflicts of Interest

All authors declare no conflicts of interest in this paper.

Authors' Contributions

YW and JW completed the main study together. YW wrote the manuscript, and XY checked the proofs process and verified the calculation. Moreover, all the authors read and approved the last version of the manuscript.

Acknowledgments

This work was supported by the NSFC (No. 12161071) and the Natural Science Foundation of Gansu Province, China (Grant no.: 21JR7RA274).

References

[1] J. Huisman, P. van Oostveen, and F. J. Weissing, "Species dynamics in phytoplankton blooms: incomplete mixing and competition for light," *The American Naturalist*, vol. 154, no. 1, pp. 46–68, 1999.

[2] N. Shigesada and A. Okubo, "Analysis of the self-shading effect on algal vertical distribution in natural waters," *Journal of Mathematical Biology*, vol. 12, no. 3, pp. 311–326, 1981.

[3] U. Ebert, M. Arrayas, N. Temme, B. Sommeijer, and J. Huisman, "Critical conditions for phytoplankton blooms," *Bulletin of Mathematical Biology*, vol. 63, no. 6, pp. 1095–1124, 2001.

[4] J. Huisman, N. N. Pham Thi, D. M. Karl, and B. Sommeijer, "Reduced mixing generates oscillations and chaos in the oceanic deep chlorophyll maximum," *Nature*, vol. 439, no. 7074, pp. 322–325, 2006.

[5] C. A. Klausmeier and E. Litchman, "Algal games: the vertical distribution of phytoplankton in poorly mixed water columns," *Limnology & Oceanography*, vol. 46, no. 8, pp. 1998–2007, 2001.

[6] Y. Du and S.-B. Hsu, "Concentration phenomena in a nonlocal quasi-linear problem modelling phytoplankton I: existence," *SIAM Journal on Mathematical Analysis*, vol. 40, no. 4, pp. 1419–1440, 2008.

[7] K. Yoshiyama, J. P. Mellard, E. Litchman, and C. A. Klausmeier, "Phytoplankton competition for nutrients and light in a stratified water column," *The American Naturalist*, vol. 174, no. 2, pp. 190–203, 2009.

[8] A. Zagaris, A. Doelman, N. N. P. Thi, and B. P. Sommeijer, "Blooming in a nonlocal, coupled phytoplankton-nutrient model," *SIAM Journal on Applied Mathematics*, vol. 69, no. 4, pp. 1174–1204, 2009.

[9] T. Kolokolnikov, C. Ou, and Y. Yuan, "Phytoplankton depth profiles and their transitions near the critical sinking velocity," *Journal of Mathematical Biology*, vol. 59, no. 1, pp. 105–122, 2009.

[10] Y. Du and S.-B. Hsu, "On a nonlocal reaction-diffusion problem arising from the modeling of phytoplankton growth," *SIAM Journal on Mathematical Analysis*, vol. 42, no. 3, pp. 1305–1333, 2010.

[11] S.-B. Hsu and Y. Lou, "Single phytoplankton species growth with light and advection in a water column," *SIAM Journal on Applied Mathematics*, vol. 70, no. 8, pp. 2942–2974, 2010.

[12] Y. Du and L. Mei, "On a nonlocal reaction-diffusion-advection equation modelling phytoplankton dynamics," *Nonlinearity*, vol. 24, no. 1, pp. 319–349, 2011.

[13] Y. Du, S. B. Hsu, and Y. Lou, "Multiple steady-states in phytoplankton population induced by photoinhibition," *Journal of Differential Equations*, vol. 258, no. 7, pp. 2408–2434, 2015.

[14] R. Peng and X.-Q. Zhao, "A nonlocal and periodic reaction-diffusion-advection model of a single phytoplankton species," *Journal of Mathematical Biology*, vol. 72, no. 3, pp. 755–791, 2016.

[15] D. Pang, H. Nie, H. Nie, and J. Wu, "Single phytoplankton species growth with light and crowding effect in a water column," *Discrete & Continuous Dynamical Systems - A*, vol. 39, no. 1, pp. 41–74, 2019.

[16] T. H. Mague, E. Friberg, D. J. Hughes, and I. Morris, "Extracellular release of carbon by marine phytoplankton; a physiological approach1," *Limnology & Oceanography*, vol. 25, no. 2, pp. 262–279, 1980.

[17] W. Bell and R. Mitchell, "Chemotactic and growth responses of marine bacteria to algal extracellular products," *The Biological Bulletin*, vol. 143, no. 2, pp. 265–277, 1972.

[18] W. K. Fitt, "Chemosensory responses of the symbiotic dinoflagellate Symbiodinium microadriatica (Dinophycae)," *Journal of Phycology*, vol. 21, pp. 62–67, 1985.

[19] H. J. Spero, "Chemosensory capabilities in the phagotrophic dinoflagellate Gymnodinium fungiforme," *Journal of Phycology*, vol. 21, pp. 181–184, 1985.

[20] P. S. Hill, "Reconciling aggregation theory with observed vertical fluxes following phytoplankton blooms," *Journal of Geophysical Research*, vol. 97, no. C2, p. 2295, 1992.

[21] T. Kiørboe, C. Lundsgaard, M. Olesen, and J. L. S. Hansen, "Aggregation and sedimentation processes during a spring phytoplankton bloom: a field experiment to test coagulation theory," *Journal of Marine Research*, vol. 52, no. 2, pp. 297–323, 1994.

[22] W. Allegretto and P. Nistri, "On a class of nonlocal problems with applications to mathematical biology. Differential equations with applications to biology," *Fields Institute Communications*, vol. 21, pp. 1–14, 1999.

[23] M. Chipot, *Remarks on Some Class of Nonlocal Elliptic Problems, Recent Advances on Elliptic and Parabolic Issues*, vol. 1, pp. 79–102, World Scientific, Singapore, 2006.

[24] B. Perthame, "Transport equations in biology, transport equations in biology," *Frontiers in Mathematics*, vol. 12, p. 126, 2007.

[25] S. Chen and J. Shi, "Stability and Hopf bifurcation in a diffusive logistic population model with nonlocal delay effect," *Journal of Differential Equations*, vol. 253, no. 12, pp. 3440–3470, 2012.

[26] J. Coville, "Convergence to equilibrium for positive solutions of some mutation-selection model," *arXiv*, vol. 1308, p. 647, 2013.

[27] L. Sun, J. Shi, and Y. Wang, "Existence and uniqueness of steady state solutions of a nonlocal diffusive logistic equation," *Zeitschrift für Angewandte Mathematik und Physik*, vol. 64, no. 4, pp. 1267–1278, 2013.

[28] C. O. Alves, M. Delgado, M. A. S. Souto, and A. Suárez, "Existence of positive solution of a nonlocal logistic population model," *Zeitschrift für Angewandte Mathematik und Physik*, vol. 66, no. 3, pp. 943–953, 2015.

[29] H. Leman, S. Méléard, S. Méléard, and S. Mirrahimi, "Influence of a spatial structure on the long time behavior of a competitive Lotka-Volterra type system," *Discrete &*

Continuous Dynamical Systems - B, vol. 20, no. 2, pp. 469–493, 2015.

[30] H. J. Alsakaji, S. Kundu, and F. A. Rihan, "Delay differential model of one-predator two-prey system with Monod-Haldane and holling type II functional responses," *Applied Mathematics and Computation*, vol. 397, 2021.

[31] F. A. Rihan and H. J. Alsakaji, "Stochastic delay differential equations of three-species prey-predator system with cooperation among prey species," *Discrete & Continuous Dynamical Systems - S*, vol. 15, no. 2, p. 245, 2022.

[32] E. N. Dancer, "On positive solutions of some pairs of differential equations," *Transactions of the American Mathematical Society*, vol. 284, no. 2, pp. 729–743, 1984.

[33] E. N. Dancer and Y. Du, "Positive solutions for a three-species competition system with diffusion-I. General existence results," *Nonlinear Analysis: Theory, Methods & Applications*, vol. 24, no. 3, pp. 337–357, 1995.

[34] M. X. Wang, *Nonlinear Elliptic Equations*, Science Press, Beijing, China, 2010.

Hindawi
Complexity
Volume 2023, Article ID 9852348, 1 page
https://doi.org/10.1155/2023/9852348

Retraction

Retracted: A Comparison of Finite Difference and Finite Volume Methods with Numerical Simulations: Burgers Equation Model

Complexity

Received 15 August 2023; Accepted 15 August 2023; Published 16 August 2023

This article has been retracted by Hindawi following an investigation undertaken by the publisher [1]. This investigation has uncovered evidence of one or more of the following indicators of systematic manipulation of the publication process:

(1) Discrepancies in scope
(2) Discrepancies in the description of the research reported
(3) Discrepancies between the availability of data and the research described
(4) Inappropriate citations
(5) Incoherent, meaningless and/or irrelevant content included in the article
(6) Peer-review manipulation

The presence of these indicators undermines our confidence in the integrity of the article's content and we cannot, therefore, vouch for its reliability. Please note that this notice is intended solely to alert readers that the content of this article is unreliable. We have not investigated whether authors were aware of or involved in the systematic manipulation of the publication process.

Wiley and Hindawi regrets that the usual quality checks did not identify these issues before publication and have since put additional measures in place to safeguard research integrity.

We wish to credit our own Research Integrity and Research Publishing teams and anonymous and named external researchers and research integrity experts for contributing to this investigation.

The corresponding author, as the representative of all authors, has been given the opportunity to register their agreement or disagreement to this retraction. We have kept a record of any response received.

References

[1] A. H. Ali, A. S. Jaber, M. T. Yaseen, M. Rasheed, O. Bazighifan, and T. A. Nofal, "A Comparison of Finite Difference and Finite Volume Methods with Numerical Simulations: Burgers Equation Model," *Complexity*, vol. 2022, Article ID 9367638, 9 pages, 2022.

Hindawi
Complexity
Volume 2022, Article ID 9367638, 9 pages
https://doi.org/10.1155/2022/9367638

Research Article

A Comparison of Finite Difference and Finite Volume Methods with Numerical Simulations: Burgers Equation Model

Ali Hasan Ali,[1,2] **Ahmed Shawki Jaber**,[3] **Mustafa T. Yaseen**,[4] **Mohammed Rasheed**,[5] **Omer Bazighifan**,[6,7] **and Taher A. Nofal**[8]

[1]*Department of Mathematics, College of Education for Pure Sciences, University of Basrah, Basrah, Iraq*
[2]*Doctoral School of Mathematical and Computational Sciences, University of Debrecen, H-4002 Debrecen, Pf 400, Hungary*
[3]*Department of Mechanical and Materials Engineering, Wright State University, 3640 Colonel Glenn Hwy, Dayton, OH 45435, USA*
[4]*Department of Business Administration, Shatt Al-Arab University College, Basrah, Iraq*
[5]*Applied Sciences Department, University of Technology, Baghdad, Iraq*
[6]*Department of Mathematics, Faculty of Science, Hadhramout University, Hadhramout 50512, Yemen*
[7]*Department of Mathematics, Faculty of Education, Seiyun University, Hadhramout 50512, Yemen*
[8]*Department of Mathematic, College of Science, Taif University, P.O Box 11099, Taif 21944, Saudi Arabia*

Correspondence should be addressed to Omer Bazighifan; o.bazighifan@gmail.com

Received 5 May 2022; Accepted 1 June 2022; Published 27 June 2022

Academic Editor: Fathalla A. Rihan

In this paper, we present an intensive investigation of the finite volume method (FVM) compared to the finite difference methods (FDMs). In order to show the main difference in the way of approaching the solution, we take the Burgers equation and the Buckley–Leverett equation as examples to simulate the previously mentioned methods. On the one hand, we simulate the results of the finite difference methods using the schemes of Lax–Friedrichs and Lax–Wendroff. On the other hand, we apply Godunov's scheme to simulate the results of the finite volume method. Moreover, we show how starting with a variational formulation of the problem, the finite element technique provides piecewise formulations of functions defined by a collection of grid data points, while the finite difference technique begins with a differential formulation of the problem and continues to discretize the derivatives. Finally, some graphical and numerical comparisons are provided to illustrate and corroborate the differences between these two main methods.

1. Introduction

In finite difference methods (FDMs), the differential equation is approximated by a set of algebraic equations (see [1, 11, 12]). These approximations are usually improved with the use of more terms and the use of smaller grid spacing (also known as more nodes). Starting with a variational formulation of the problem, the finite element technique provides piecewise formulations of functions defined by a collection of grid data points. The finite difference technique begins with a differential formulation of the problem and continues to discretize the derivatives [15]. Like any approximation, finite difference schemes have their limitations such as oscillations and diffusion especially at points of discontinuity. Another issue that FDM runs into is that mass is only conserved when the grid spacing goes to zero and they struggle with irregular geometry [2, 10]. Usually, a FDM's grid looks like the following (Figure 1).

However, in some geometries, it may not be possible to align the grid with perpendicular grid lines which means one might not be able to approximate some derivatives in terms of the values along a constant "i" line. Because of these shortcomings, some have turned to using control volume formulation or finite volume methods (FVMs). This started back in 1960 when it was called the integration method, and it turned out to have many applications in oscillation theory and diffusive convection [4–8]. Most recently, FVMs have been used in computational fluid dynamics because of their

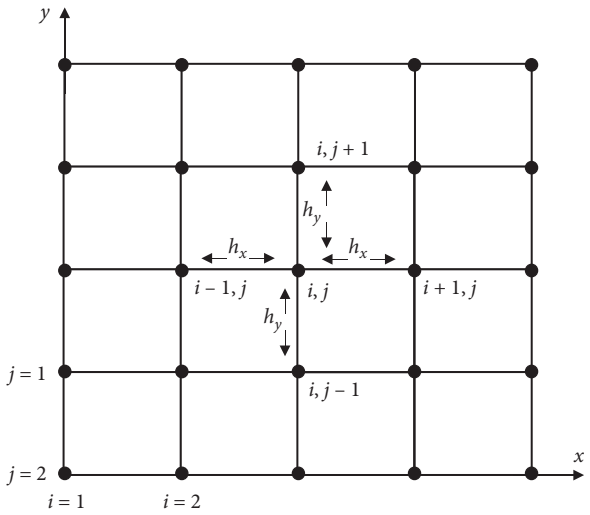

Figure 1: An FDM's grid.

ability to be used on unstructured meshes [3]. In general, in the FVM, the differential equation is integrated over a control volume and then discretized using some approximations. Another aspect of the huge advantages of using the FVM is that material (like mass or energy) is conserved because it uses integration over small volumes, and since the flux, which is the flow of material in space with time, of the material at the common side is represented by the same expression, this implies that global conservation is also ensured. In fact, both FDM and FVM have a huge number of applications in many engineering and natural science fields. Several important applications of the FDM can be found in computer vision, image processing, solving diffusion convection, and thermal problems (see [9, 13, 14]). On the other hand, the applications of FVM appear in many fields, and its software can be used in several branches, such as solid mechanics, thermal and electrical analysis, structural analysis, oscillation theory, and mechanical engineering design (see [16–21]). The structure of this paper is organized as follows. In Section 2, we provide the definition and the mechanism of the finite volume method (FVM). In Section 3, we consider a one-dimensional application of the FVM. In Section 4, we use an inviscid Burgers equation to apply the proposed comparison of the mentioned numerical methods. Finally, several simulations for the Burgers equation and one simulation for the Buckley–Leverett equation with the main results are presented in Section 5.

2. Finite Volume Method (FVM)

To understand the finite volume method, we need to start with the conservation form of the transport equation, which is given as

$$\frac{\partial T}{\partial t} + \nabla \cdot (\vec{u}T) = \nabla \cdot (\alpha \nabla T). \tag{1}$$

This partial differential equation is used on the infinitesimal volumes described in Figure 2.

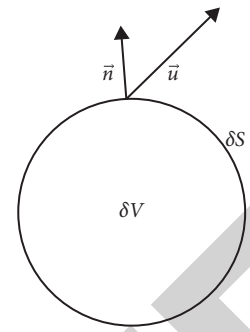

Figure 2: A PDE on an infinitesimal volume.

Knowing that the infinitesimal discrete volumes are unaffordable, they would need to be of some larger finite size. Now we derive the conservation form for a finite volume δV bounded by a surface, which we will denote as δS. Applying the integral gives us the following:

$$\int_{\delta V} \frac{\partial T}{\partial t} \mathrm{d}V + \int_{\delta V} \nabla \cdot (\vec{u}T)\mathrm{d}V = \int_{\delta V} \nabla \cdot (\alpha \nabla T)\mathrm{d}V. \tag{2}$$

If we assume the volume to be fixed in space, we can interchange the order of integration in space and differentiation in time:

$$\frac{\mathrm{d}}{\mathrm{d}t}\left(\int_{\delta V} T\mathrm{d}V\right) + \int_{\delta V} \nabla \cdot (\vec{u}T)\mathrm{d}V = \int_{\delta V} \nabla \cdot (\alpha \nabla T)\mathrm{d}V. \tag{3}$$

The understanding of the first integral on the left is the time rate of change of the T inside volume δV. The Gauss divergence theorem is necessary for the next step. The theorem says that the outward flux of a vector field through some closed surface is equal to the volume integral of the divergence over the region inside the surface. So, basically, we are going to change our equation from volume integrals to surface integrals.

$$\frac{\mathrm{d}}{\mathrm{d}t}\left(\int_{\delta V} T\mathrm{d}V\right) + \int_{\delta S} \vec{n} \cdot \vec{u}T\mathrm{d}V = \int_{\delta S} \vec{n} \cdot \alpha \nabla T\mathrm{d}V, \tag{4}$$

where $\vec{n}$ represents the outward part that is normal to the surface. The surface integral on the left describes the "in and out" advection flux across the surface of the volume. The one on the other side describes the diffusive transport of T across the surface. The equation can be summarized as the rate of change of the T value in δV which is equal to the rate of transport T through the surface by advection and diffusive fluxes. Notice that we have not given the surface a definite size or shape, so this equation could be applied to whatever we would like. Note the order of the derivatives as they appear in the differential equation (1) versus those of the integral form (4). In the differential equation, we have a first-order advection term and a second-order diffusion term, but in the integral form, there is a 0-th order advection term and a first-order diffusion term. This is an important change because it helps with problems that have discontinuities of the spatial derivative. Examples of those types are the problems that have shock or hydraulic jump.

Now we introduce the average T in δV which we will refer to as

$$\overline{T} = \frac{1}{\delta V}\int_{\delta V} T\mathrm{d}V. \tag{5}$$

The integral conservation law can now be written as a time evolution equation:

$$\delta V\frac{\mathrm{d}\overline{T}}{\mathrm{d}t} + \int_{\delta S}\vec{n}\cdot\vec{u}T\mathrm{d}V = \int_{\delta S}\vec{n}\cdot\alpha\nabla T\mathrm{d}V. \tag{6}$$

It is important to note that equations (4) and (6) are exact solutions and no approximation has yet been introduced. The approximation will come from

(1) Temporal integration of the equations.

(2) Calculation of the fluxes in space and time.

However, the first step is to divide the domain into a discrete number of cells which we will denote as δV_j where the cell average is known. After that, we calculate the advection and diffusion fluxes through function reconstruction, followed by evaluation of the integrals, and finally the temporal integration with a forward marching time step.

3. Application of the FVM

We consider here only the 1-D case. Therefore, we first break up the domain as shown in Figure 3.

The cell centres are denoted by the integer numbers and the cell edges are denoted by the fractions. In this case, the cells are line segments, and the cell "volumes" are reduced to just cell widths δx (which we will assume as uniform throughout). This means that the flux integrals reduce to the evaluation of the term at the cell edges, which means the conservation law can be rewritten as

$$\frac{\mathrm{d}\overline{T_j}}{\mathrm{d}t} = -\frac{F_{j+(1/2)} - F_{j-(1/2)}}{\delta x} + \frac{D_{j+(1/2)} - D_{j-(1/2)}}{\delta x}, \tag{7}$$

where F is the advection flux and D is the diffusive flux at the cell edge $x_{j+(1/2)}$.

The other assumption that we will make is that we are using a piecewise constant approximation as shown in Figure 4.

This means that we have the following approximation: $T = a_0$.

We can now write

$$\int_{x_{j+(1/2)}}^{x_{j+(1/2)}} a_0\mathrm{d}x = \delta x_j\overline{T_j}, \tag{8}$$

because we only have one unknown coefficient. Basically, the integral of T over a cell gives us $\delta x_j\overline{T_j}$. This means that the solution is $a_0 = \overline{T_j}$, which finishes our function reconstruction. Note that at each cell edge, there are two different values. For the advection term, we should use the upstream edge (what goes into the next term has to come from the previous term). This leads to

$$T_{j+(1/2)} = \begin{cases} \overline{T}_j, & u_{j+(1/2)} \geq 0, \\ \overline{T}_{j+1}, & u_{j+(1/2)} < 0. \end{cases} \tag{9}$$

The other implication of this is that piecewise constant functions cannot be used to compute the diffusive term because they have a zero derivative in space. This will not pose a problem for us later because we will be considering Burgers and the Buckley–Leverett equations which do not have a diffusive term.

4. Numerical Methods

Take a look at the inviscid Burgers equation

$$u_t + u\cdot u_x = 0. \tag{10}$$

Applying the Euler forward in time and backward in space discretization, one would come up with

$$U_j^{n+1} = U_j^n - \frac{k}{h}U_j^n\left(U_j^n - U_{j-1}^n\right). \tag{11}$$

This is sometimes referred to as the nonconservative upwind scheme. This method works well on nice smooth solutions but will not converge at discontinuous points as the grid is refined (see Figure 5).

To avoid this issue, we apply the conservation form

$$U_j^{n+1} = U_j^n - \frac{k}{h}\left[F\left(U_{j-p}^n, U_{j-p+1}^n, \ldots, U_{j+q}^n\right) - F\left(U_{j-p-1}^n, U_{j-p}^n, \ldots, U_{j+q-1}^n\right)\right], \tag{12}$$

where F is the numerical flux function. In general, methods that follow this type of scheme are called conservative methods. So, all the methods to follow were implemented using this type of scheme.

For the comparisons, we used the general conservation law:

$$u_t + \left[f(u)\right]_x = 0, \tag{13}$$

where for the Burgers equation, we use

$$f(u) = \frac{1}{2}u^2, \tag{14}$$

and for the Buckley–Leverett equation, we use

$$f(u) = \frac{u^2}{u^2 + 1/4(1-u)^2}. \tag{15}$$

The basic setup for the two different kinds of methods is as follows.

4.1. Finite Difference Methods

(1) Set up grid (or nodes).

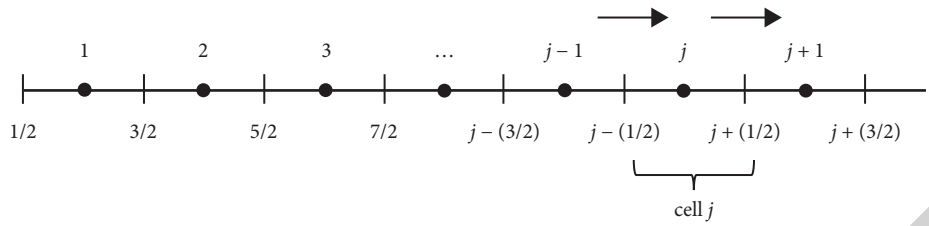

Figure 3: A sample domain of a 1-D case.

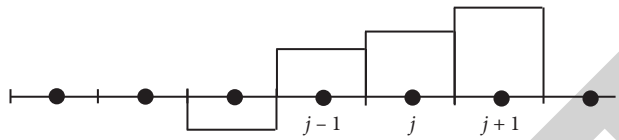

Figure 4: A piecewise constant approximation.

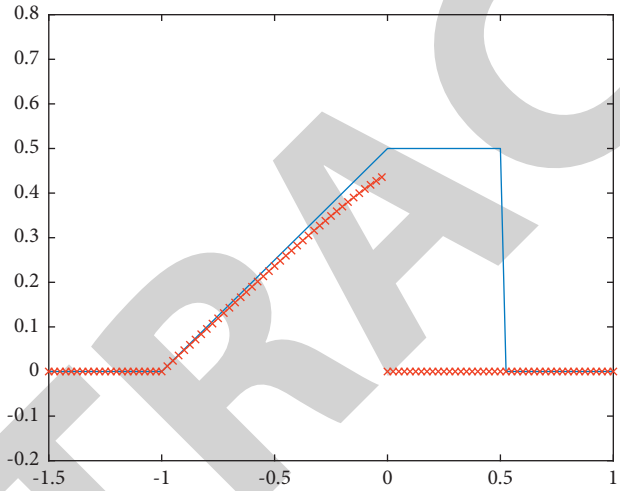

Figure 5: A nonconservative upwind method.

(2) Approximate and replace all the derivatives by their corresponding finite difference approximations.

(3) Solve the resulting algebraic system of equations.

4.2. Finite Volume Methods

(1) Grid generation.

(2) Discretize the integral conservation equation on control volumes.

(3) Solve the resultant discrete integral/flux equations.

4.3. Upwind Conservative Method. In fact, this method is first-order accurate in both time and space; however, it is only stable in the interval $0 \le a\,(k/h) \le 1$, where k is the size of the time step and h is the size of the space step.

Then, applying the standard finite difference upwind definition, we would get

$$U_j^{n+1} = U_j^n - \frac{k}{h}\left[f\left(U_j^n\right) - f\left(U_{j-1}^n\right)\right]. \tag{16}$$

Then, applying this to the Burgers equation, we get

$$U_j^{n+1} = U_j^n - \frac{k}{h}\left[\frac{1}{2}\left(U_j^n\right)^2 - \frac{1}{2}\left(U_{j-1}^n\right)^2\right]. \tag{17}$$

Moreover, we apply this method to the Buckley–Leverett equations to get

$$U_j^{n+1} = U_j^n - \frac{k}{h}\left[\frac{\left(U_j^n\right)^2}{\left(U_j^n\right)^2 + 1/4\left(1 - U_j^n\right)^2} - \frac{\left(U_{j-1}^n\right)^2}{\left(U_{j-1}^n\right)^2 + 1/4\left(1 - U_{j-1}^n\right)^2}\right]. \tag{18}$$

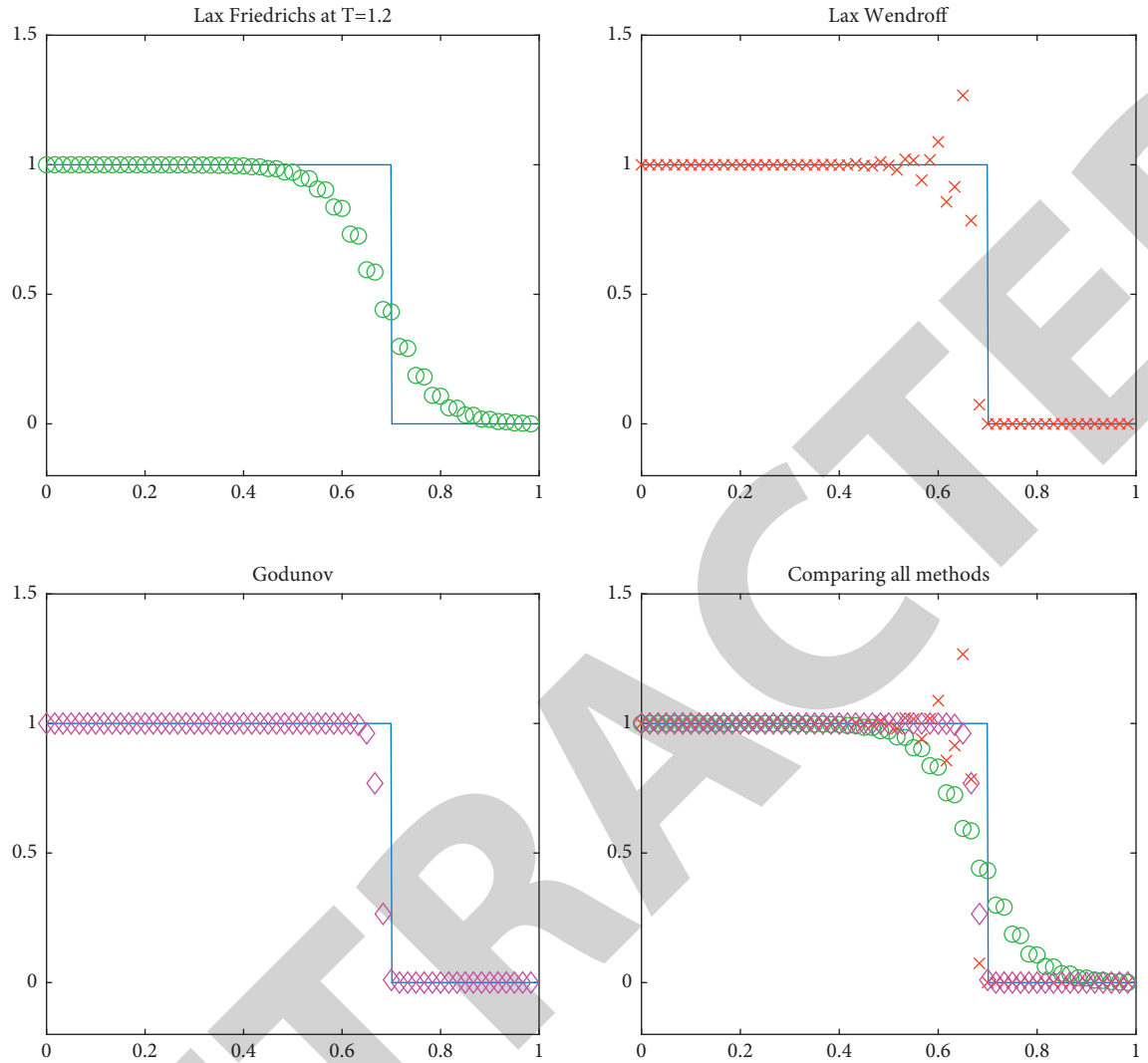

Figure 6: Graphs for the single shock simulation.

4.4. Lax–Friedrichs Method. Like the upwind conservative method, the Lax–Friedrichs method is first-order accurate in time and space. In addition, it has a stability requirement of $|ak/h| \leq 1$. The Lax–Friedrichs method takes the form

$$U_j^{n+1} = \frac{1}{2}\left(U_{j-1}^n + U_{j+1}^n\right) - \frac{k}{2h}\left[f\left(U_{j+1}^n\right) - f\left(U_{j-1}^n\right)\right]. \quad (19)$$

Then, applying this to the Burgers equation, we get

$$U_j^{n+1} = \frac{1}{2}\left(U_{j-1}^n + U_{j+1}^n\right) - \frac{k}{h}\left[\frac{1}{2}\left(U_{j+1}^n\right)^2 - \frac{1}{2}\left(U_{j-1}^n\right)^2\right]. \quad (20)$$

For the Buckley–Leverett equation, we would have

$$U_j^{n+1} = \frac{1}{2}\left(U_{j-1}^n + U_{j+1}^n\right) - \frac{k}{2h}\left[\frac{\left(U_{j+1}^n\right)^2}{\left(U_{j+1}^n\right)^2 + 1/4\left(1 - U_{j+1}^n\right)^2} - \frac{\left(U_{j-1}^n\right)^2}{\left(U_{j-1}^n\right)^2 + 1/4\left(1 - U_{j-1}^n\right)^2}\right]. \quad (21)$$

4.5. Lax–Wendroff Method. The Lax–Wendroff method is second-order accurate in both time and space, and it has a known stability of $|ak/h| \leq 1$. For the nonlinear conservation laws, it takes the form

$$U_j^{n+1} = U_{j+1}^n - \frac{k}{2h}\left(f\left(U_{j+1}^n\right) - f\left(U_{j-1}^n\right)\right) + \frac{k^2}{2h^2}\left[A_{j+1/2}\left(f\left(U_{j+1}^n\right) - f\left(U_j^n\right)\right) - A_{j-1/2}\left(f\left(U_j^n\right) - f\left(U_{j-1}^n\right)\right)\right]. \quad (22)$$

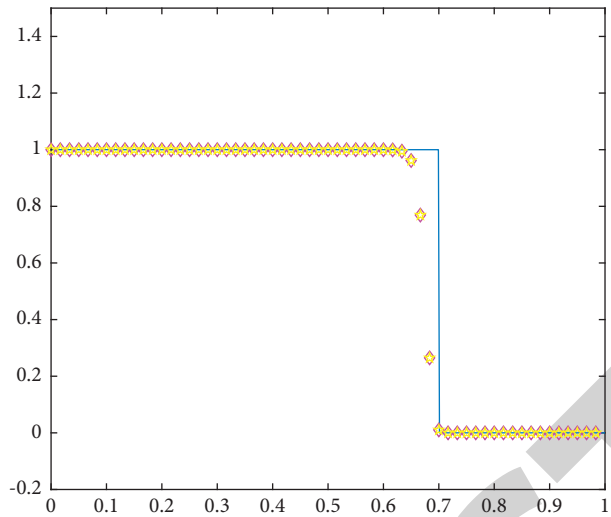

Figure 7: Comparing the Godunov method to the upwind method.

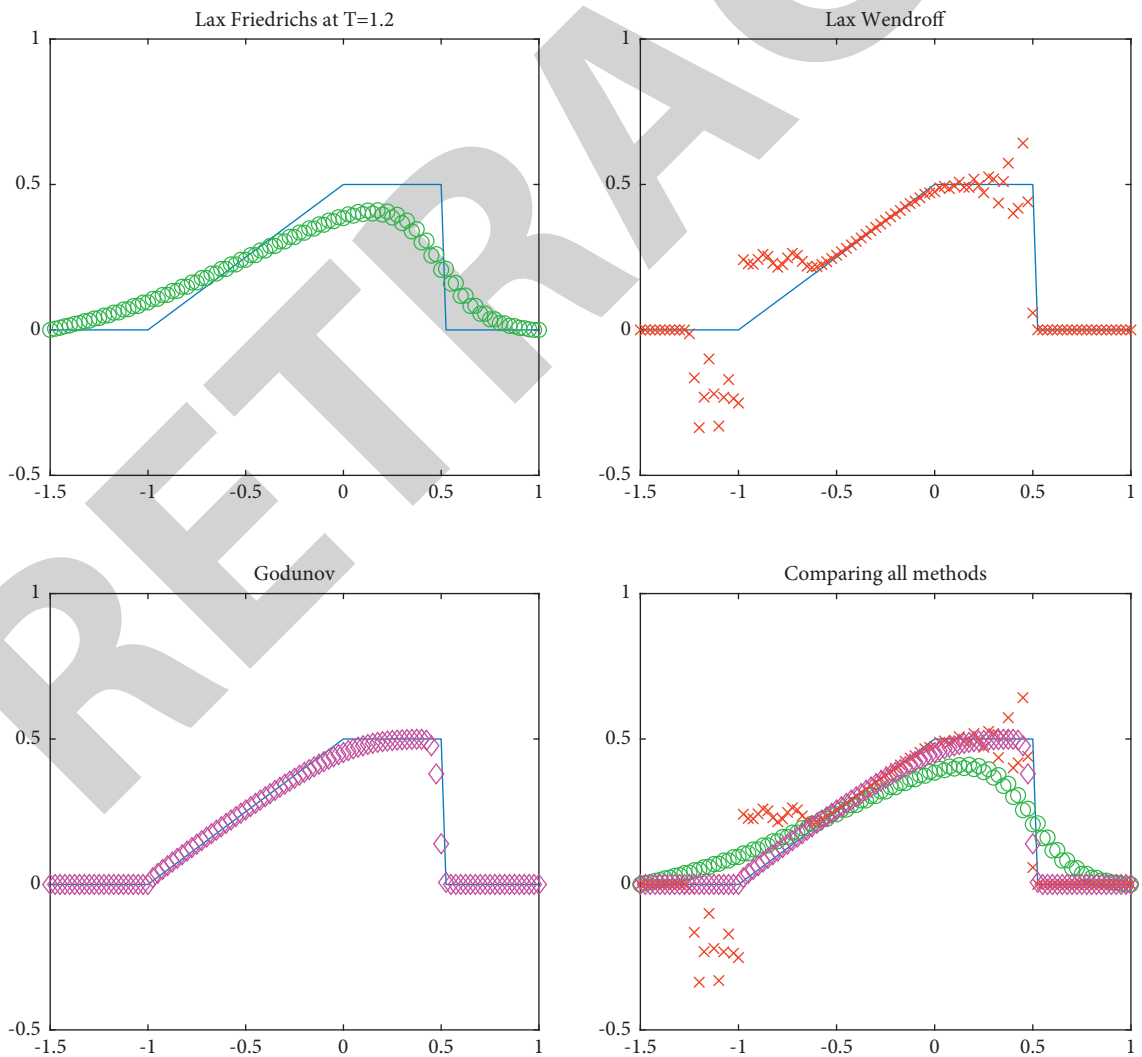

Figure 8: Graphs for the traveling pulse simulation.

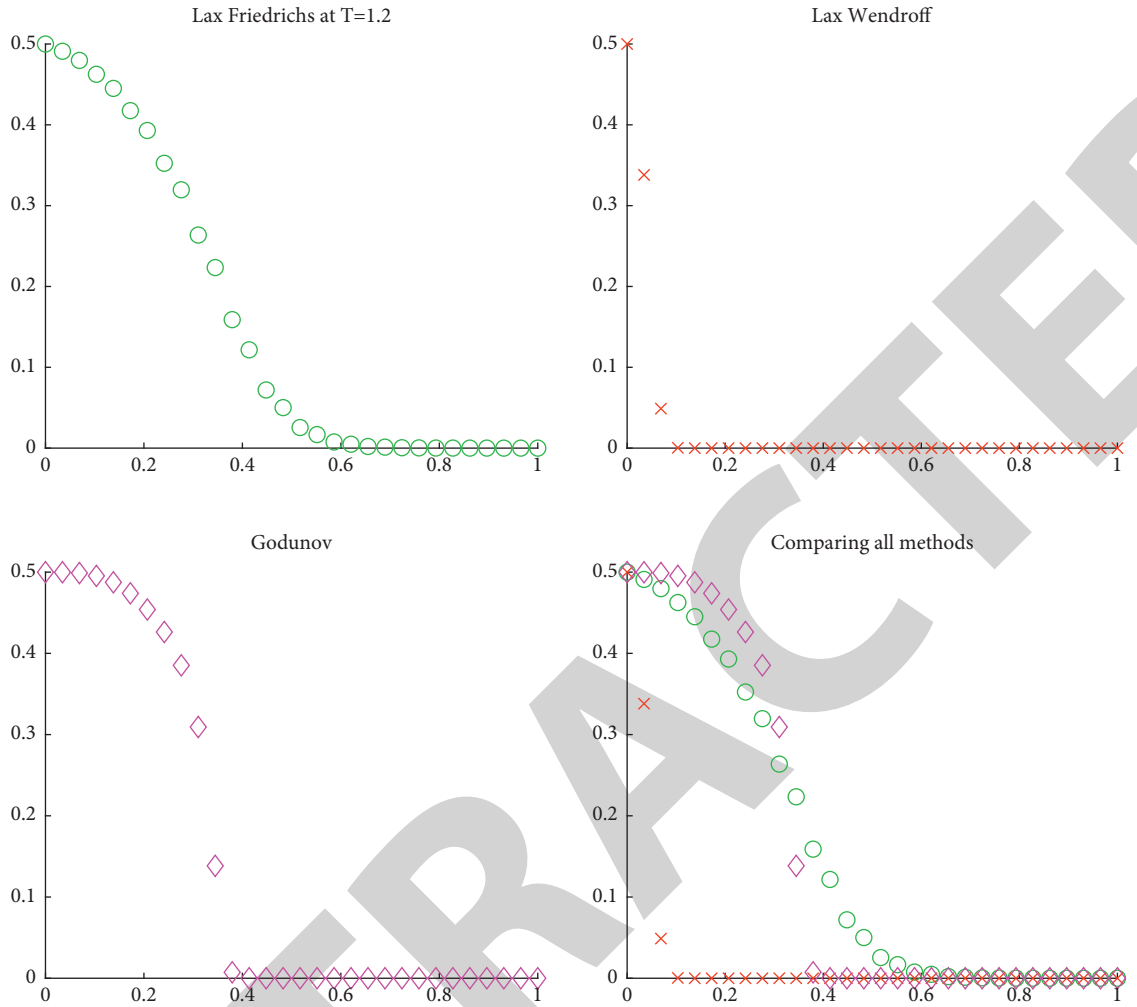

Figure 9: Graphs for the Buckley–Leverett simulation.

4.6. Godunov's Scheme. To compare the previous finite difference schemes with a finite volume scheme, we choose to use Godunov's scheme. Although this method is only first-order accurate, it is the basis of other high-order finite volume schemes. To get Godunov's method, we start by letting U_j^n be a numerical solution on the n-th layer. After that, we need to define a function $\widehat{U}^n(x,t)$ for the time interval $t_n < t < t_{n+1}$. At $t = t_n$, we have the following:

$$\widehat{U}^n(x,t) = U_j^n, \quad x_j - \frac{h}{2} < x < x_j + \frac{h}{2}, \quad \text{for } j = 2,\ldots,n-1. \tag{23}$$

We also need to define $\widehat{U}(x,t)$ to be the solution of the collection of Riemann problems on that interval. Then, the solution to the next value, U_j^{n+1}, is simply defined by averaging $\widehat{U}(x,t_{n+1})$ over the interval $x_j - (h/2) < x < x_j + (h/2)$. When everything is said and done, this idea reduces to the following:

$$U_j^{n+1} = U_j^n - \frac{k}{h}\left[F\left(U_j^n, U_{j+1}^n\right) - F\left(U_{j-1}^n, U_j^n\right)\right]. \tag{24}$$

When we apply this to the Burgers equation, the numerical flux F is

$$F(U,V) = \frac{\left(u^*\right)^2}{2}, \tag{25}$$

and when we apply this to the Buckley–Leverett equation,

$$F(U,V) = \frac{\left(u^*\right)^2}{\left(u^*\right)^2 + 1/4\left(1-u^*\right)^2}, \tag{26}$$

where u^* is defined as follows.

If $U \geq V$, then

$$u^* = \begin{cases} U, & \dfrac{U+V}{2} > 0, \\ V, & \text{else.} \end{cases} \tag{27}$$

If $U < V$, then

$$u^* = \begin{cases} U, & U > 0, \\ V, & V < 0, \\ 0, & U \leq 0 \leq V. \end{cases} \tag{28}$$

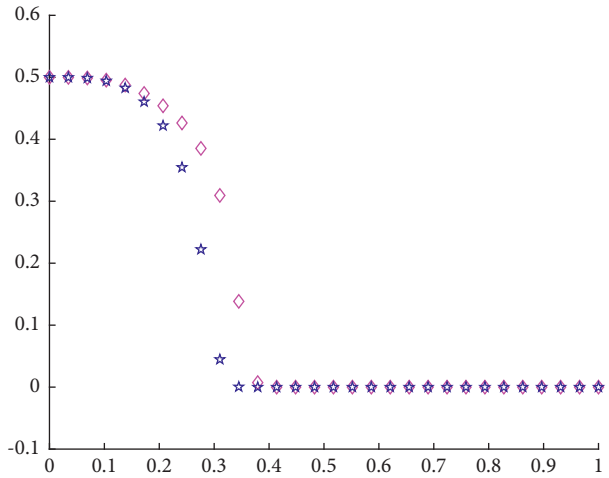

Figure 10: Comparing Godunov and upwind methods.

5. Results

In this section, several simulations for the Burgers equation and one simulation for the Buckley–Leverett equation are carried out. After we ran each simulation, we compared the results from the finite difference methods and the finite volume method.

5.1. Simulation 1: Single Shock. The equation and the solutions of the single shock simulation are given by equation (29) and shown in Figure 6 using the methods mentioned in Section 4.

$$u(x,0) = \begin{cases} 1, & x < 0.1, \\ 0, & x > 0.1. \end{cases} \tag{29}$$

To satisfy the stability condition for the finite schemes, we used $h = (1/60)$ and $k = 0.005$.

We can see from the results that the finite difference methods had issues at the sharp turns (the derivative does not exist). Notice that the Lax–Friedrichs method shows diffusion at the corners while the Lax–Wendroff method produces oscillations. The Godunov method handles the shock much better, but still it is not accurate. In fact, we also wanted to point out that for the Burgers equation, the classical upwind scheme and the Godunov scheme produce the same result (see Figure 7). This is basically because $f\prime(u) > 0$.

5.2. Simulation 2: Traveling Pulse. The equation and the solutions of the traveling pulse simulation are given by equation (30) and shown in Figure 8 using the methods mentioned in Section 4.

$$u(x,0) = \begin{cases} 0, & x < -1, \\ \dfrac{1}{2}, & -1 < x < 0, \\ 0, & x > 0. \end{cases} \tag{30}$$

In the simulation above, we used a smaller h value so that we could better see what happens at the corners; $h = 0.025$ and $k = 0.01$. We obtain the same results that we saw before with the single shock. It is interesting to note that the Lax–Wendroff method does not have oscillations at the top left corner $(x = 0)$, but it does have oscillations at the other places where the derivative does not exist. Note that we did not include the upwind scheme because we knew that it would produce the same results as the Godunov scheme.

5.3. Simulation 3: Buckley–Leverett Equations. The equation and the solutions of Buckley–Leverett simulation are given by equation (31) and shown in Figure 9 using the methods mentioned in Section 4.

$$u(x,0) = \begin{cases} \dfrac{1}{2}, & x = 0, \\ 0, & x > 0. \end{cases} \tag{31}$$

This produced the same results that we saw in the Burgers equation simulations. The Lax–Wendroff method does not have an oscillation by itself, but it definitely has its issues. To see the difference between the Godunov scheme and the upwind scheme, we had to use a different flux (the Buckley–Leverett flux) as shown in Figure 10.

6. Conclusion

Although we used the conservation equations to explain and illustrate the finite volume method, it can be used on any type of differential equation. We choose the conservation equations since usually finite volume methods are used on fluid flow, which is conservative. We can conclude by our comparison that the main difference of these methods can be seen in the way of approaching the solutions, as starting with a variational formulation of the problem, the finite element technique provides piecewise formulations of functions defined by a collection of grid data points, while the finite difference technique begins with a differential formulation of the problem and continues to discretize the derivatives. Moreover, the finite volume method even with the simplifications that we gave produced very good results for the simulations. In fact, it did not appear to have any difficulty handling the shocks and discontinuous derivatives, which is why FVMs are used in modelling fluid flow.

Data Availability

No data were used to support this study.

Conflicts of Interest

The authors declare that they have no conflicts of interest.

Acknowledgments

The sixth author received financial support from Taif University Researches Supporting Project number (TURSP-2020/031), Taif University, Taif, Saudi Arabia.

Hindawi
Complexity
Volume 2022, Article ID 1049561, 6 pages
https://doi.org/10.1155/2022/1049561

Research Article

Semianalytical Approach for the Approximate Solution of Delay Differential Equations

Xiankang Luo,[1] **Mustafa Habib**,[2] **Shazia Karim**,[3] **and Hanan A. Wahash**[4]

[1]*Faculty of Science, Yibin University, Yibin 644000, China*
[2]*Department of Mathematics, University of Engineering and Technology, Lahore 54890, Pakistan*
[3]*Department of Basic Sciences, UET Lahore, FSD Campus 54800, Lahore, Pakistan*
[4]*Department of Mathematics, Albaydaa University, Al Bayda, Yemen*

Correspondence should be addressed to Xiankang Luo; xkluo1978@163.com and Hanan A. Wahash; hawahash@baydaauniv.net

Received 17 May 2022; Accepted 8 June 2022; Published 25 June 2022

Academic Editor: Fathalla A. Rihan

In this analysis, we develop a new approach to investigate the semianalytical solution of the delay differential equations. Mohand transform coupled with the homotopy perturbation method is called Mohand homotopy perturbation transform method (MHPTM) and performs the solution results in the form of series. The beauty of this approach is that it does not need to compute the values of the Lagrange multiplier as in the variational iteration method, and also, there is no need to implement the convolution theorem as in the Laplace transform. The main purpose of this scheme is to reduce the less computational work and the error analysis of the problems than others studied in the literature. Some illustrated examples are interpreted to confirm the accuracy of the newly developed scheme.

1. Introduction

Many physical phenomena of differential equations play an important role in various branches of science and engineering such as physics, chemical energy, biology, and medicine involving time delay [1–4]. In most cases, time delay appears in everywhere of physical study of the reality. A delay differential equation is one of the most famous equations where the derivative of an unknown function is given at a specific time as far as the results of the function at the pas time. Numerous authors have demonstrated various approaches to find the approximate solution of delay differential equations in different fields of science; Rihan and Velmurugan [5] suggested a delay differential model with fractional order for the tumor-immune system with external treatments. Luis et al. [6] and Ogunfiditimi [7] used the Adomian decomposition method for the numerical solution of delay differential equations. Shakeri and Dehghan [4] obtained the solution of delay differential equations via a homotopy perturbation method. Evans and Raslan [8] applied the Adomian method to solve particular ordinary delay differential equations in which the delay is located in the linear or nonlinear part. Jane and Robert [9] used a computer algebra system to solve some very simple linear delay differential equations by combining Laplace transform method and a novel least-squares method. Barati and Ivaz [10] used the variational iteration method for delay differential equations whereas Mohyud-Din and Yildirim [11] combined the variational iteration method with He's polynomials to obtain the solution of delay differential equations. We recommend the readers to study the new developments in time-delay differential equations [12–14].

Recently, many integral transformations and strategies have been introduced to find the approximate solution of ordinary and partial differential equations such as Elzaki transform [15, 16], Sumudu transform [17], Aboodh transformation [18], spline methods [19], finite difference method [20], but it is still quite difficult to get the exact solutions for these problems. The homotopy perturbation method was developed by He [21–23] to obtain the solution of ordinary and partial differential equations involving nonlinear terms. Mishra and Tripathi [24] used the

homotopy perturbation method of delay differential equation using He's polynomial with Laplace transform. HPM gives the solution in the form of a rapid and consecutive series toward the exact solution.

In this paper, we develop a hybridization scheme where the Mohand transform is coupled with the homotopy perturbation method for obtaining the approximate solution of linear and nonlinear delay differential equations. This scheme derives the results in the aspect of series without any linearization, variation, and limiting expectations. In addition, this study is organized as follows: in Section 2, we present some basic definitions of the Mohand transform which help us to construct the idea of the semianalytical approach. In Section 3, we formulate the idea of MHPTM for obtaining the solution of delay differential equations. We illustrate two examples to show the accuracy and validity of this approach in Section 4. We demonstrate the results and discussion in Section 5, and finally, the conclusion is presented in Section 6.

2. Fundamental Concepts of Mohand Transform

In this section, we introduce some basic definitions and preliminary concepts of the Mohand transform which reveals the idea of its implementations to functions.

Definition 1. Mohand and Mahgoub [25] presented a new scheme Mohand transform $M(\cdot)$ in order to gain the results of ordinary differential equations and are defined as

$$\begin{aligned} M\{\vartheta(t)\} &= R(w) \\ &= w^2 \int_0^{\infty} \vartheta(t) e^{-wt} \mathrm{d}t, \quad k_1 \le w \le k_2. \end{aligned} \tag{1}$$

On the other hand, if $R(w)$ is the Mohand transform of a function $\vartheta(t)$, then $\vartheta(t)$ is the inverse of $R(w)$, such as

$$M^{-1}\{R(w)\} = \vartheta(t), \quad M^{-1} \text{ is inverse Mohand operator.} \tag{2}$$

Definition 2. If $\vartheta(t) = t^n$,

$$R(w) = \frac{n!}{w^{n-1}}. \tag{3}$$

Definition 3. If $M\{\vartheta(t)\} = R(w)$, then it has the following differential properties [26]:

(i) $M\{\vartheta'(t)\} = wR(w) - w^2F(0)$

(ii) $M\{\vartheta''(t)\} = w^2R(w) - w^3F(0) - w^2F'(0)$

(iii) $M\{F\vartheta^n(t)\} = w^nR(w) - w^{n+1}F(0) - w^nF'(0) - \cdots - w^nF^{n-1}(0)$

3. Formulation of MHPTM for Delay Differential Equations

This segment presents the construction of the Mohand homotopy perturbation transform method (MHPTM) for obtaining the approximate solution of linear and nonlinear delay differential equations. Let's consider a nonlinear second-order differential equation of the form [24]

$$\vartheta''(t) + \vartheta'(t) + \vartheta(t) + g(\vartheta) = g(t) \tag{4}$$

with the following conditions:

$$\begin{aligned} \vartheta(0) &= a, \\ \vartheta'(0) &= b, \end{aligned} \tag{5}$$

where ϑ is a function in the time domain t, $g(\vartheta)$ represents a nonlinear term, g(t) is a source term whereas a and b are constants. Rewrite (4) again

$$\vartheta''(t) + \vartheta'(t) = -\vartheta(t) - g(\vartheta) + g(t). \tag{6}$$

Now, taking MT on both sides of (6), we obtain

$$M[\vartheta''(t) + \vartheta'(t)] = M[-\vartheta(t) - g(\vartheta) + g(t)]. \tag{7}$$

Applying the differential properties of MT, we get

$$\begin{aligned} &w^2R[w] - w^3\vartheta(0) - w^2\vartheta'(0) + vR[w] - w^2\vartheta(0) \\ &= M[-\vartheta(t) - g(\vartheta) + g(t)]. \end{aligned} \tag{8}$$

Thus, $R(w)$ can be obtained from (8) such as

$$R[w] = \frac{w^3a + w^2b + w^2a}{\left(w + w^2\right)} - \frac{M[\vartheta(t) + g(\vartheta) - g(t)]}{\left(w + w^2\right)}. \tag{9}$$

Operating inverse Mohand transform, on (9), we get

$$\vartheta[t] = G(t) - M^{-1}\left[\frac{M[\vartheta]}{\left(w + w^2\right)} + \frac{M[g(\vartheta)]}{\left(w + w^2\right)}\right], \tag{10}$$

where

$$G(t) = M^{-1}\left[\frac{w^3a + w^2b + w^2a}{\left(w + w^2\right)} + M\left\{\frac{g(t)}{\left(w + w^2\right)}\right\}\right]. \tag{11}$$

Now, we apply HPM on (10). Let

$$\begin{aligned} \vartheta(t) &= \sum_{i=0}^{\infty} p^i \vartheta_i(n) \\ &= \vartheta_0 + p^1\vartheta_1 + p^2\vartheta_2 + \cdots, \end{aligned} \tag{12}$$

where p is the homotopy parameter, and thus, the nonlinear term $g(\vartheta)$ in (10) can be calculated by using the formula

$$\begin{aligned} g(\vartheta) &= \sum_{i=0}^{\infty} p^i H_i(\vartheta) \\ &= H_0 + p^1H_1 + p^2H_2 + \cdots, \end{aligned} \tag{13}$$

where $Hn\imath s$ is the He's polynomial, which may be computed using the following procedure.

$$H_n(u_0 + u_1 + \cdots + u_n) = \frac{1}{n!}\frac{\partial^n}{\partial p^n}\left(g\left(\sum_{i=0}^{\infty} p^i\vartheta_i\right)\right)_{p=0}, \quad n = 0, 1, 2, \ldots. \tag{14}$$

Put (12), (13), and (14) in (10) and comparing the similar factors of p, we get the following consecutive elements

$$\begin{aligned}
p^0&: \vartheta_0(t) = G(t),\\
p^1&: \vartheta_1(t) = -M^{-1}\left[\frac{1}{(w+w^2)}M\{\vartheta_0 + H_0(\vartheta)\}\right],\\
p^2&: \vartheta_2(t) = -M^{-1}\left[\frac{1}{(w+w^2)}M\{\vartheta_1 + H_1(\vartheta)\}\right],\\
p^3&: \vartheta_3(t) = -M^{-1}\left[\frac{1}{(w+w^2)}M\{\vartheta_2 + H_2(\vartheta)\}\right],\\
&\vdots .
\end{aligned} \tag{15}$$

On continuing the similar process, we can summarize this series to get the approximate solution such as

$$\begin{aligned}
\vartheta(t) &= \vartheta_0 + \vartheta_1 + \vartheta_2 + \cdots\\
&= \sum_{i=0}^{\infty}\vartheta_i.
\end{aligned} \tag{16}$$

Thus, (16) is to be considered as an approximate solution to delay differential equations of (4).

4. Numerical Examples

In this part, we test two examples for the authenticity and validity of MHPTM. We also demonstrate 2D plots for a better understanding of this strategy where we see that the solution graphs of the approximate solution and the exact solution coincide with each other only after few iterations.

4.1. Example 1. Consider a nonlinear delay differential equation of order first

$$\vartheta'(t) = 1 - 2\vartheta^2\left(\frac{t}{2}\right), \tag{17}$$

with the initial condition

$$\vartheta(0) = 0. \tag{18}$$

Applying MT on (17) together with the differential property as defined in (3), we get

$$wR(w) - w^2(0) = w - M\left[2\vartheta^2\left(\frac{t}{2}\right)\right]. \tag{19}$$

Using (18) into (19) for solving $R(w)$, it yields

$$R(w) = 1 - \frac{1}{w}M\left[2\vartheta^2\left(\frac{t}{2}\right)\right]. \tag{20}$$

Using inverse Mohand transform on (17), we get

$$\vartheta(t) = t - M^{-1}\left[\frac{1}{w}M\left\{2\vartheta^2\left(\frac{t}{2}\right)\right\}\right]. \tag{21}$$

Applying MHPTM to get the He's polynomials

$$\sum_{i=0}^{\infty}p^i\vartheta_i(n) = t - M^{-1}\left[\frac{2}{w}M\left\{\sum_{i=0}^{\infty}p^i\vartheta_i^2\left(\frac{t}{2}\right)\right\}\right]. \tag{22}$$

Observing the similar powers of p, we get

$$\begin{aligned}
p^0&: \vartheta_0(t) = t,\\
p^1&: \vartheta_1(t) = -M^{-1}\left[\frac{2}{w}M\left\{\vartheta_0^2\left(\frac{t}{2}\right)\right\}\right]\\
&\quad = -\frac{t^3}{6},\\
p^2&: \vartheta_2(t) = -M^{-1}\left[\frac{2}{w}M\left\{2\vartheta_0\left(\frac{t}{2}\right)\vartheta_1\left(\frac{t}{2}\right)\right\}\right]\\
&\quad = \frac{t^5}{120},\\
p^3&: \vartheta_3(t) = -M^{-1}\left[\frac{2}{w}M\left\{2\vartheta_2\left(\frac{t}{2}\right)\vartheta_0\left(\frac{t}{2}\right) + \vartheta_1^2\left(\frac{t}{2}\right)\right\}\right]\\
&\quad = -\frac{t^7}{5040},\\
p^4&: \vartheta_4(t) = -M^{-1}\left[\frac{2}{w}M\left\{2\vartheta_3\left(\frac{t}{2}\right)\vartheta_0\left(\frac{t}{2}\right) + 2\vartheta_1\left(\frac{t}{2}\right)\vartheta_2\left(\frac{t}{2}\right)\right\}\right]\\
&\quad = \frac{t^9}{362880},\\
&\vdots .
\end{aligned} \tag{23}$$

On continuing this process, the results of obtained series can be summarized as

$$\begin{aligned}
\vartheta(t) &= \vartheta_0(t) + \vartheta_1(t) + \vartheta_2(t) + \vartheta_3(t) + \vartheta_4(t) + \cdots\\
&= t - \frac{t^3}{3!} + \frac{t^5}{5!} - \frac{t^7}{7!} + \frac{t^9}{9!} + \cdots .
\end{aligned} \tag{24}$$

This series converges to the exact solution

$$\vartheta(t) = \sin(t). \tag{25}$$

4.2. Example 2. Consider a linear delay differential equation of 2nd order

$$\vartheta''(t) = \frac{3}{4}\vartheta(t) + \vartheta\left(\frac{t}{2}\right) - t^2 + 2, \tag{26}$$

with the initial condition

$$\vartheta(0) = 0, \quad \vartheta'(0) = 0. \tag{27}$$

Applying MT on (26) together with the differential property as defined in (3), we get

$$w^2R(w) - w^3\vartheta(0) - w^2\vartheta'(0) = M\left[\frac{3}{4}\vartheta(t) + \vartheta\left(\frac{t}{2}\right) - t^2 + 2\right]. \tag{28}$$

Using (27) into (28) for solving $R(w)$, it yields

$$\overline{R}(w) = -\frac{2}{w^3} + \frac{2}{w} + \frac{1}{w^2}M\left[\frac{3}{4}\vartheta(t) + \vartheta\left(\frac{t}{2}\right)\right]. \tag{29}$$

Using inverse Mohand transform on (29), we get

$$\vartheta(t) = -\frac{t^4}{12} + t^2 + M^{-1}\left[\frac{1}{w^2}M\left\{\frac{3}{4}\vartheta(t) + \vartheta\left(\frac{t}{2}\right)\right\}\right]. \tag{30}$$

Applying MHPTM to get the He's polynomials

$$\sum_{i=0}^{\infty} p^i\vartheta_i(n) = t^2 - \frac{t^4}{12} + M^{-1}\left[\frac{1}{w^2}M\left\{\frac{3}{4}\sum_{i=0}^{\infty}p^i\vartheta_i(t) + \sum_{i=0}^{\infty}p^i\vartheta_i\frac{t}{2}\right\}\right]. \tag{31}$$

Observing the similar powers of p, we get

$$\begin{aligned}
p^0\colon \vartheta_1(t) &= M^{-1}\left[\frac{1}{w^2}M\left\{\frac{3}{4}\vartheta_0(t) + \vartheta_0\left(\frac{t}{2}\right)\right\}\right] \\
&= t^2 - \frac{t^4}{12}, \\
p^1\colon \vartheta_2(t) &= M^{-1}\left[\frac{1}{w^2}M\left\{\frac{3}{4}\vartheta_1(t) + \vartheta_1\left(\frac{t}{2}\right)\right\}\right] \\
&= \frac{t^4}{12} - \frac{13t^6}{5760}, \\
p^2\colon \vartheta_3(t) &= M^{-1}\left[\frac{1}{w^2}M\left\{\frac{3}{4}\vartheta_2(t) + \vartheta_2\left(\frac{t}{2}\right)\right\}\right] \\
&= \frac{13t^6}{5760} - \frac{91t^8}{2949120}, \\
p^3\colon \vartheta_4(t) &= M^{-1}\left[\frac{1}{w^2}M\left\{\frac{3}{4}\vartheta_3(t) + \vartheta_3\left(\frac{t}{2}\right)\right\}\right] \\
&= \frac{91t^8}{2949120} - \frac{17563t^8}{67947724800}, \\
&\vdots .
\end{aligned} \tag{32}$$

On continuing this process, the results of obtained series can be summarized as

$$\begin{aligned}
\vartheta(t) &= \vartheta(t) + \vartheta_0(t) + \vartheta_1(t) + \vartheta_2(t) + \vartheta_3(t) + \vartheta_4(t) + \cdots \\
&= t^2 - \frac{17563t^8}{67947724800} + \cdots .
\end{aligned} \tag{33}$$

This series converges to the exact solution

$$\vartheta(t) = t^2. \tag{34}$$

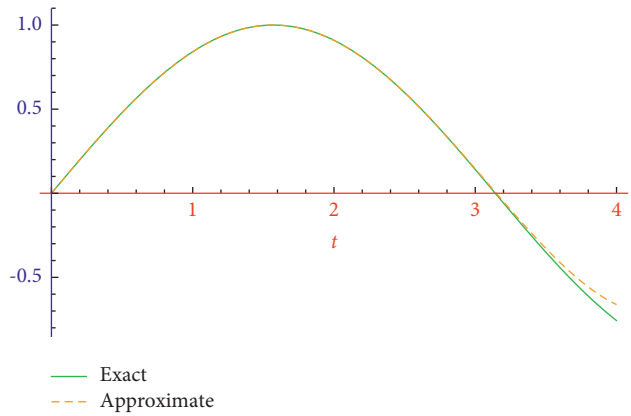

Figure 1: 2D Plot for $\vartheta(t)$ with various parameters of α.

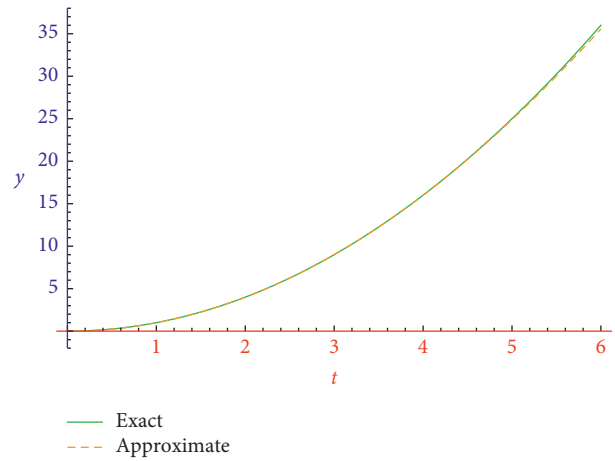

Figure 2: 2D plot for $\vartheta(t)$ with various parameters of α.

Table 1: The absolute error of $\vartheta(t)$ for different values of t.

t	Exact solution	Approximate solution	Absolute error
0.5	0.479426	0.47924	0.000
1	0.841471	0.841471	0.000
1.5	0.997495	0.997497	2×10^{-6}
2	0.909297	0.909347	0.00005
2.5	0.598472	0.599046	0.000574
3	0.14112	0.145313	0.004193
3.5	−0.350783	−0.328389	0.022394
4	−0.756802	−0.661728	0.095074
4.5	−0.97753	−0.639024	0.338506
5	−0.958924	0.089632	0.869292

5. Results and Discussion

In this section, we discuss some results obtained by MHPTM for linear and nonlinear delay differential equations. We calculate only four iterations to test the validity and accuracy of this new strategy in both examples. It can be seen that we need only few iterations to show the exact solution. We may extend the series of (22) and (31) for better performance and rapid convergence. Figures 1 and 2 show the error solution between the approximate solution and the exact solution for $0 \le t \le 4$ and $0 \le t \le 6$, respectively. We also present the

Table 2: The absolute error of $\vartheta(t)$ for different values of t.

t	Exact solution	Approximate solution	Absolute error
0.5	0.25	0.25	0.000
1	1	1	0.000
1.5	2.25	2.24999	0.00001
2	4	3.99993	0.00007
2.5	6.25	6.24961	0.00039
3	9	8.9983	0.0017
3.5	12.25	12.2442	0.0058
4	16	15.9831	0.0169
4.5	20.25	20.2065	0.0435
5	25	24.899	0.0101

absolute error of $\vartheta(t)$ between the exact solution and the approximate solution obtained by MHPTM in Tables 1 and 2, respectively. Moreover, this absolute error declares that MHPTM is a valid and authentic tool that does not require any heavy calculation for the computation of the approximate solution of linear and nonlinear delay differential equations. The obtained results are in full agreement with [11, 24].

6. Conclusion

In this analysis, we have employed an innovative scheme Mohand homotopy perturbation transform method (MHPTM) to achieve an approximate solution of linear and nonlinear delay differential equations. Since MT is limited to deal with nonlinear terms, so we introduced HPM to overcome this drawback and presented the results in the form of series solutions. The solution plots demonstrated the accuracy and validity of MHPTM and showed the error distribution between the approximate solution and the exact solution. We propose that MHPTM is applicable for future work both in the linear and nonlinear partial differential equation in science and engineering applications.

Data Availability

All the data are available within the article.

Conflicts of Interest

The authors declare that they have no conflicts of interest.

Acknowledgments

This work was supported by the Foundation of Yibin University, China (Grant no. 2019QD07).

References

[1] H. Khan, S.-J. Liao, R. Mohapatra, and K. Vajravelu, "An analytical solution for a nonlinear time-delay model in biology," *Communications in Nonlinear Science and Numerical Simulation*, vol. 14, no. 7, pp. 3141–3148, 2009.

[2] I. R. Epstein, "Delay effects and differential delay equations in chemical kinetics," *International Reviews in Physical Chemistry*, vol. 11, no. 1, pp. 135–160, 1992.

[3] K.-J. Wang, H.-C. Sun, C.-L. Li, G.-D. Wang, and H. W. Zhu, "Thermal management of the hotspots in 3-d integrated circuits," *Thermal Science*, vol. 22, no. 4, pp. 1685–1690, 2018.

[4] F. Shakeri and M. Dehghan, "Solution of delay differential equations via a homotopy perturbation method," *Mathematical and Computer Modelling*, vol. 48, no. 3-4, pp. 486–498, 2008.

[5] F. Rihan and G. Velmurugan, "Dynamics of fractional-order delay differential model for tumor-immune system," *Chaos, Solitons & Fractals*, vol. 132, Article ID 109592, 2020.

[6] L. B. Cocom, A. G. Estrella, and E. A. Vales, "Solving delay differential systems with history functions by the adomian decomposition method," *Applied Mathematics and Computation*, vol. 218, no. 10, pp. 5994–6011, 2012.

[7] F. Ogunfiditimi, "Numerical solution of delay differential equations using the adomian decomposition method (adm)," *International Journal of Engineering Science*, vol. 4, no. 5, pp. 18–23, 2015.

[8] D. J. Evans and K. R. Raslan, "The adomian decomposition method for solving delay differential equation," *International Journal of Computer Mathematics*, vol. 82, no. 1, pp. 49–54, 2005.

[9] J. M. Heffernan and R. M. Corless, "Solving some delay differential equations with computer algebra," *The Mathematical Scientist*, vol. 31, no. 1, pp. 21–34, 2006.

[10] S. Barati and K. Ivaz, "Variational iteration method for solving systems of linear delay differential equations," *International Journal of Computational and Mathematical Sciences*, vol. 6, pp. 132–135, 2012.

[11] S. T. Mohyud-Din and A. Yildirim, "Variational iteration method for delay differential equations using he's polynomials," *Zeitschrift für Naturforschung A*, vol. 65, no. 12, pp. 1045–1048, 2010.

[12] R. Shah, H. Khan, P. Kumam, M. Arif, and D. Baleanu, "Natural transform decomposition method for solving fractional-order partial differential equations with proportional delay," *Mathematics*, vol. 7, no. 6, p. 532, 2019.

[13] F. A. Rihan, *Delay Differential Equations and Applications to Biology*, Springer, Berlin, Germany, 2021.

[14] L. Dugard and E. I. Verriest, *Stability and control of time-delay systems*, Springer, Berlin, Germany, 1998.

[15] T. M. Elzaki, "The new integral transform elzaki transform," *Global Journal of Pure and Applied Mathematics*, vol. 7, no. 1, pp. 57–64, 2011.

[16] N. Anjum, M. Suleman, D. Lu, J.-H. He, and M. Ramzan, "Numerical iteration for nonlinear oscillators by elzaki transform," *Journal of Low Frequency Noise, Vibration and Active Control*, vol. 39, no. 4, pp. 879–884, 2020.

[17] M. Rana, A. Siddiqui, Q. Ghori, and R. Qamar, "Application of he's homotopy perturbation method to sumudu transform," *International Journal of Nonlinear Sciences and Numerical Stimulation*, vol. 8, no. 2, pp. 185–190, 2007.

[18] K. Aboodh, R. Farah, I. Almardy, and A. Osman, "Solving delay differential equations by aboodh transformation method," *International Journal of Applied Mathematics & Statistical Sciences*, vol. 7, no. 2, pp. 55–64, 2018.

[19] T. Aziz, A. Khan, and J. Rashidinia, "Spline methods for the solution of fourth-order parabolic partial differential equations," *Applied Mathematics and Computation*, vol. 167, no. 1, pp. 153–166, 2005.

[20] M. Dehghan, "Finite difference procedures for solving a problem arising in modeling and design of certain optoelectronic devices," *Mathematics and Computers in Simulation*, vol. 71, no. 1, pp. 16–30, 2006.

[21] J.-H. He, "Homotopy perturbation technique," *Computer Methods in Applied Mechanics and Engineering*, vol. 178, no. 3-4, pp. 257–262, 1999.

[22] J.-H. He, "Homotopy perturbation method: a new nonlinear analytical technique," *Applied Mathematics and Computation*, vol. 135, no. 1, pp. 73–79, 2003.

[23] J.-H. He, "Comparison of homotopy perturbation method and homotopy analysis method," *Applied Mathematics and Computation*, vol. 156, no. 2, pp. 527–539, 2004.

[24] H. K. Mishra and R. Tripathi, "Homotopy perturbation method of delay differential equation using he's polynomial with laplace transform," *Proceedings of the National Academy of Sciences, India, Section A: Physical Sciences*, vol. 90, no. 2, pp. 289–298, 2020.

[25] M. Mohand and A. Mahgoub, "The new integral transform mohand transform," *Applied Mathematical Sciences*, vol. 12, no. 2, pp. 113–120, 2017.

[26] S. Aggarwal and R. Chaudhary, "A comparative study of mohand and laplace transforms," *Journal of Emerging Technologies and Innovative Research*, vol. 6, no. 2, pp. 230–240, 2019.

Hindawi
Complexity
Volume 2022, Article ID 4935809, 24 pages
https://doi.org/10.1155/2022/4935809

WILEY | Hindawi

Research Article

The Analysis of Fractional-Order Nonlinear Systems of Third Order KdV and Burgers Equations via a Novel Transform

A. A. Alderremy,[1] Shaban Aly,[2] Rabia Fayyaz,[3] Adnan Khan,[4] Rasool Shah,[4] and Noorolhuda Wyal[5]

[1]*Department of Mathematics, Faculty of Science, King Khalid University, Abha 61413, Saudi Arabia*
[2]*Department of Mathematics, Faculty of Science, AL-Azhar University, Assiut, Egypt*
[3]*Department of Mathematics, COMSATS University Islamabad, Islamabad, Pakistan*
[4]*Department of Mathematics, Abdul Wali Khan University, Mardan, Pakistan*
[5]*Department of Mathematics, Kabul Polytechnic University, Kabul, Afghanistan*

Correspondence should be addressed to Rabia Fayyaz; rabia_fayyaz@comsats.edu.pk and Noorolhuda Wyal; noorolhuda.wyal@kpu.edu.af

Received 24 February 2022; Revised 19 April 2022; Accepted 6 May 2022; Published 22 June 2022

Academic Editor: C. Rajivganthi

In this article, we solve nonlinear systems of third order KdV Equations and the systems of coupled Burgers equations in one and two dimensions with the help of two different methods. The suggested techniques in addition with Laplace transform and Atangana–Baleanu fractional derivative operator are implemented to solve four systems. The obtained results by implementing the proposed methods are compared with exact solution. The convergence of the method is successfully presented and mathematically proved. The results we get are compared with exact solution through graphs and tables which confirms the effectiveness of the suggested techniques. In addition, the results obtained by employing the proposed approaches at different fractional orders are compared, confirming that as the value goes from fractional order to integer order, the result gets closer to the exact solution. Moreover, suggested techniques are interesting, easy, and highly accurate which confirm that these methods are suitable methods for solving any partial differential equations or systems of partial differential equations as well.

1. Introduction

In recent years, fractional calculus has surpassed ordinary calculus in popularity. The standard calculus has reached its pinnacle in terms of discovery. Mathematicians and engineers require fractional calculus as a solution. This permits a more accurate description of real-world phenomena than the traditional "integer" order. Numerous mathematicians, including Fourier, Laplace, Riesz, and others, were engaged and made substantial contribution to the subject. Modern definitions of fractional order derivatives and integrals, such as the Atangana–Baleanu fractional integral [1], the Caputo fractional derivative [2], and the Caputo–Fabrizio fractional derivative [3], have ushered in a new era in the literature of fractional derivatives. Models based on fractional calculus can accurately depict numerous engineering, physics, and chemistry processes, among others [4]. In addition, fractional calculus is used to simulate the frequency-dependent damping behavior of a variety of viscoelastic materials [5], the dynamics of interfaces between nanoparticles and substrates [6], economics [7], and numerous other applications [8–11].

Finding the actual or approximate solutions of FDEs is crucial in all of these areas of study, but because we lack a method for obtaining the precise solution of these sorts of FDEs, we must focus on approximating the exact solution. Determining the exact answer to such FDEs and other scientific applications is a difficult task in mathematics. Unlike the approximate answer [12], the exact solution enables us to comprehend the problem's mechanism and

complexity. Obtaining exact analytical expressions to FDEs is exceedingly difficult, if not impossible, due to the complexity of computation involved in these equations. As a result, it is necessary to seek out some useful approximations and numerical techniques, such as the homotopy perturbation method [13], variation iteration method [14], residual power series method [15], approximate-analytical method [16], Elzaki transform decomposition method [17], Iterative Laplace transform method [18], Adomian decomposition method [19], reduced differential transform method, and others [20–23].

In this paper, we provided two analytic approaches in conjunction with the Laplace transformation and fractional derivatives in Antagana–Baleanu solution to satisfy fractional-order problems [24]. The first method is the mixing of Laplace transform (LT) and variational iteration method known as variational iteration transform method (VITM) which was first developed by He [25] and is an effective solution for a broad variety of problems in scientific fields [26, 27]. The second significant methodology for solving nonlinear functional equations is the combination of the Adomian decomposition method and Laplace transform, which was first developed by George Adomian (1923–1996) in the 1980s. The technique depends on the decomposition of a nonlinear equation result into a series of functions. A polynomial produced by a power series expansion of an analytic function returns each series term. This method for solving several nonlinear fractional-order differential equations is interesting, straightforward, and accurate.

Harry Bateman introduced the Burgers equation in 1915 [28], and it was subsequently dubbed by the Burgers equation. The Burgers equation has many applications in science and engineering, especially when dealing with nonlinear problems. Burgers equation applications have grown in prominence and attention among mathematical scientists and researchers. This equation is acknowledged to represent a range of phenomena, such as dynamic modeling, heat conduction, acoustic waves, and turbulence [29–31]. In 1895, Korteweg and Vries initially derived the Korteweg-De Vries (KDV) equation. The KDV equation is used to predict long waves, tides, solitary waves, and wave propagation in a shallow canal. The KDV equation is utilized in several disciplines, including fluid mechanics, signal processing, hydrology, viscoelasticity, and fractional kinetics.

2. Preleminaries

In this section, we presented some basic definitions of fractional calculus related to our present work.

Definition 1. The derivative by Caputo having order fraction is defined as

$$ {}^{c}D_{\mathfrak{J}}^{\sigma}\{h(\mathfrak{J})\} = \frac{1}{(n-\sigma)}\int_{0}^{\mathfrak{J}}(\mathfrak{J}-k)^{n-\sigma-1}h^{n}(k)\mathrm{d}k, \text{ where } n<\sigma\le n+1. \tag{1} $$

Definition 2. The derivative by Caputo having order fraction with the aid of Laplace transform ${}^{LC}D_{\mathfrak{J}}^{\sigma}\{h(\mathfrak{J})\}$ is defined as

$$ \mathbb{L}\left\{{}^{LC}D_{\mathfrak{J}}^{\sigma}\{h(\mathfrak{J})\}\right\}(\omega) = \frac{1}{\omega^{n-\sigma}}\left[\omega^{n}\mathbb{L}\{h(\xi,\mathfrak{J})\}(\omega) - \omega^{n-1}h(\xi,0) - \cdots - h^{n-1}(\xi,0)\right]. \tag{2} $$

Definition 3. The fractional Atangana–Baleanu derivative in terms of Caputo manner is defined as

$$ {}^{ABC}D_{\mathfrak{J}}^{\sigma}\{h(\mathfrak{J})\} = \frac{B(\sigma)}{1-\sigma}\int_{a}^{\mathfrak{J}}h'(k)E_{\sigma}\left[-\frac{\sigma}{1-\sigma}(1-k)^{\sigma}\right]dk. \tag{3} $$

where normalization function is denoted by $B(\sigma)$ with $B(0)=B(1)=1, h\in H^{1}(a,b), b>a, \sigma\in[0,1]$ and E_{σ} is the Mittag–Leffler function.

Definition 4. In terms of Riemann–Liouville, the Atangana–Baleanu fractional derivative is defined as

$$ {}^{ABC}D_{\mathfrak{J}}^{\sigma}\{h(\mathfrak{J})\} = \frac{B(\sigma)}{1-\sigma}\frac{d}{d\mathfrak{J}}\int_{a}^{\mathfrak{J}}h(k)E_{\sigma}\left[-\frac{\gamma}{1-\sigma}(1-k)^{\sigma}\right]dk. \tag{4} $$

Definition 5. The Atangana–Baleanu operator in connection with Laplace transform is given by

$$ {}^{AB}D_{\mathfrak{F}}^{\sigma}\{h(\mathfrak{F})\}(\omega) = \frac{B(\sigma)\omega^{\sigma}\mathbb{L}\{h(\mathfrak{F})\}(\omega) - \omega^{\sigma-1}h(0)}{(1-\sigma)(\omega^{\sigma}+\sigma/1-\gamma)}. \tag{5} $$

Definition 6. Consider $0 < \sigma < 1$, and h is a function of order σ, then the fractional integral operator for σ is defined as

$$ {}^{ABC}I_{\mathfrak{F}}^{\sigma}\{h(\mathfrak{F})\} = \frac{1-\sigma}{B(\sigma)}h(\mathfrak{F}) + \frac{\sigma}{B(\sigma)\Gamma(\sigma)}\int_{a}^{\mathfrak{F}} h(k)(\mathfrak{F}-k)^{\sigma-1}\mathrm{d}k. \tag{6} $$

3. Idea of LTDM

Here, we discuss the methodology of LTDM for solving fractional-order partial differential equations.

$$ {}^{ABC}D_{\mathfrak{F}}^{\sigma}\varphi(\xi,\mathfrak{F}) + \overline{\mathscr{G}}_1(\xi,\mathfrak{F}) + \mathscr{N}_1(\xi,\mathfrak{F}) = \mathscr{F}(\xi,\mathfrak{F}), 0 < \sigma \le 1, \tag{7} $$

having initial terms

$$ \varphi(\xi,0) = \xi(\xi), \frac{\partial}{\partial\mathfrak{F}}\varphi(\xi,0) = \zeta(\xi). \tag{8} $$

Here, the fractional-order AB operator is indicated from ${}^{ABC}D_{\mathfrak{F}}^{\sigma} = \partial^{\sigma}/\partial\mathfrak{F}^{\sigma}$ having order σ, $\overline{\mathscr{G}}_1, \mathscr{N}_1$ are linear and nonlinear operator, and $\mathscr{F}(\xi,\mathfrak{F})$ represent the source term.

On taking the Laplace transform of (7), we get

$$ L\left[{}^{ABC}D_{\mathfrak{F}}^{\sigma}\varphi(\xi,\mathfrak{F}) + \overline{\mathscr{G}}_1(\xi,\mathfrak{F}) + \mathscr{N}_1(\xi,\mathfrak{F})\right] = L[\mathscr{F}(\xi,\mathfrak{F})]. \tag{9} $$

Using the differentiation property of LT, we obtain

$$ L[\varphi(\xi,\mathfrak{F})] = \Theta(\xi,\omega) - \frac{\omega^{\sigma}+\sigma(1-\sigma)}{\omega^{\sigma}}L\left[\overline{\mathscr{G}}_1(\xi,\mathfrak{F}) + \mathscr{N}_1(\xi,\mathfrak{F})\right], \tag{10} $$

where $\Theta(\xi,\omega) = 1/\omega^{\sigma+1}[\omega^{\sigma}h_0(\xi) + \omega^{\sigma-1} \quad h_1(\xi) + \cdots \quad + g_1(\xi)] + \omega^{\sigma} + \sigma(1-\sigma)/\omega^{\sigma}\mathscr{F}(\xi,\mathfrak{F})$.

Now, using the inverse Laplace transform, we get

$$ \varphi(\xi,\mathfrak{F}) = \Theta(\xi,\omega) - L^{-1}\left\{\frac{\omega^{\sigma}+\sigma(1-\sigma)}{\omega^{\sigma}}L\left[\overline{\mathscr{G}}_1(\xi,\mathfrak{F}) + \mathscr{N}_1(\xi,\mathfrak{F})\right]\right\}, \tag{11} $$

where $\Theta(\xi,\omega)$ shows the term that come from the source term. LTDM generates the result of the infinite series of $\varphi(\xi,\mathfrak{F})$

$$ \varphi(\xi,\mathfrak{F}) = \sum_{m=0}^{\infty}\varphi_m(\xi,\mathfrak{F}), \tag{12} $$

and decomposing the nonlinear operator $\mathscr{N}_1$ as

$$ \mathscr{N}_1(\xi,\mathfrak{F}) = \sum_{m=0}^{\infty}\mathscr{A}_m, \tag{13} $$

where the Adomian polynomials are represented by $\mathscr{A}_m$

$$ \mathscr{A}_m = \frac{1}{m!}\left[\frac{\partial^m}{\partial\ell^m}\left\{\mathscr{N}_1\left(\sum_{k=0}^{\infty}\ell^k\xi_k, \sum_{k=0}^{\infty}\ell^{k\mathfrak{F}_k}\right)\right\}\right]_{\ell=0}, \tag{14} $$

and putting equations (12) and (14) into (11), we get

$$ \sum_{m=0}^{\infty}\varphi_m(\xi,\mathfrak{F}) = \Theta(\xi,\omega) - L^{-1}\left\{\frac{\omega^{\sigma}+\sigma(1-\sigma)}{\omega^{\sigma}}L\left[\overline{\mathscr{G}}_1\left(\sum_{m=0}^{\infty}\xi_m, \sum_{m=0}^{\infty}\mathfrak{F}_m\right) + \sum_{m=0}^{\infty}\mathscr{A}_m\right]\right\}. \tag{15} $$

The terms listed below are defined as

$$ \begin{aligned} \varphi_0(\xi,\mathfrak{F}) &= \Theta(\xi,\omega), \\ \varphi_1(\xi,\mathfrak{F}) &= L^{-1}\left\{\frac{\omega^{\sigma}+\sigma(1-\sigma)}{\omega^{\sigma}}L\left[\overline{\mathscr{G}}_1(\xi_0,\mathfrak{F}_0) + \mathscr{A}_0\right]\right\}. \end{aligned} \tag{16} $$

As a result, all of the components for $m \ge 1$ are determined as

$$ \varphi_{m+1}(\xi,\mathfrak{F}) = L^{-1}\left\{\frac{\omega^{\sigma}+\sigma(1-\sigma)}{\omega^{\sigma}}L\left[\overline{\mathscr{G}}_1(\xi_m,\mathfrak{F}_m) + \mathscr{A}_m\right]\right\}. \tag{17} $$

4. VITM Formulation

Here, we discuss the methodology of VITM for solving fractional-order partial differential equations.

$$^{ABC}D^{\sigma}_{\mathfrak{F}}\varphi(\xi,\mathfrak{F})+\mathscr{M}\varphi(\xi,\mathfrak{F})+\mathscr{N}\varphi(\xi,\mathfrak{F})-\mathscr{F}(\xi,\mathfrak{F})=0,\quad m-1<\sigma\le m, \tag{18}$$

having initial term

$$\varphi(\xi,0)=g_1(\xi). \tag{19}$$

Here, the fractional-order AB operator is indicated from $^{ABC}D^{\sigma}_{\mathfrak{F}}=\partial^{\sigma}/\partial\mathfrak{F}^{\sigma}$. $\mathscr{M},\mathscr{N}$ are linear and non,linear operator and $\mathscr{F}$ represent the source term.

On taking the Laplace transform of (18), we get

$$L\left[D^{\sigma}_{\mathfrak{F}}\varphi(\xi,\mathfrak{F})\right]+L[\mathscr{M}\varphi(\xi,\mathfrak{F})+\mathscr{N}\varphi(\xi,\mathfrak{F})-\mathscr{F}(\xi,\mathfrak{F})]=0. \tag{20}$$

Using the differentiation property of LT, we obtain

$$L[\varphi(\xi,\mathfrak{F})]=\frac{\omega^{\sigma}}{\omega^{\sigma}+\sigma(1-\sigma)}L[\mathscr{M}\varphi(\xi,\mathfrak{F})+\mathscr{N}\varphi(\xi,\mathfrak{F})-\mathscr{F}(\xi,\mathfrak{F})]. \tag{21}$$

The method of iteration for the equation (21)

$$\varphi_{m+1}(\xi,\mathfrak{F})=\varphi_m(\xi,\mathfrak{F})+\sigma(s)\left[\frac{\omega^{\sigma}}{\omega^{\sigma}+\sigma(1-\sigma)}L[\mathscr{M}\varphi(\xi,\mathfrak{F})+\mathscr{N}\varphi(\xi,\mathfrak{F})-\mathscr{F}(\xi,\mathfrak{F})]\right]. \tag{22}$$

$\sigma(s)$ is Lagrange multiplier and

$$\sigma(s)=-\frac{\omega^{\sigma}+\sigma(1-\sigma)}{\omega^{\sigma}}, \tag{23}$$

Equation (22) series form solution is obtained by using the inverse Laplace transform.

$$\begin{aligned}
\varphi_0(\xi,\mathfrak{F})&=\varphi(0)+L^{-1}[\sigma(s)L[-\mathscr{F}(\xi,\mathfrak{F})]],\\
\varphi_1(\xi,\mathfrak{F})&=L^{-1}[\sigma(s)L[\mathscr{M}\varphi(\xi,\mathfrak{F})+\mathscr{N}\varphi(\xi,\mathfrak{F})]],\\
&\vdots\\
\varphi_{n+1}(\xi,\mathfrak{F})&=L^{-1}\big[\sigma(s)L\big[\mathscr{M}\big[\varphi_0(\xi,\mathfrak{F})+\varphi_1(\xi,\mathfrak{F})\\
&\quad+\cdots,\varphi_n(\xi,\mathfrak{F})\big]\big]+\mathscr{N}\big[\varphi_0(\xi,\mathfrak{F})+\varphi_1(\xi,\mathfrak{F}),\ldots,\varphi_n(\xi,\mathfrak{F})\big]\big].
\end{aligned} \tag{24}$$

5. Applications

To show the validity and capability of the suggested techniques, we implemented proposed methods for solving four nonlinear systems.

5.1. Problem 1. Consider system of homogeneous KdV equation having order three

$$\begin{aligned}
\frac{\partial^{\sigma}\varphi}{\partial\mathfrak{F}^{\sigma}}&=\frac{\partial^3\varphi}{\partial\xi^3}+\varphi\frac{\partial\varphi}{\partial\xi}+\nu\frac{\partial\nu}{\partial\xi},\\
\frac{\partial^{\sigma}\nu}{\partial\mathfrak{F}^{\sigma}}&=-2\frac{\partial^3\nu}{\partial\xi^3}+\varphi\frac{\partial\nu}{\partial\xi}\ 0<\sigma\le1,
\end{aligned} \tag{25}$$

with initial source

$$\varphi(\xi,0)=\left(3-6\tanh^2\frac{\xi}{2}\right),\quad \nu(\xi,0)=-\left(3l\sqrt{2}\tanh^2\frac{\xi}{2}\right). \tag{26}$$

On taking the Laplace transform of (25), we get

$$\begin{aligned}
\frac{\omega^{\sigma}L[\varphi(\xi,\mathfrak{F})]-\omega^{-1}\varphi(\xi,0)}{\omega^{\sigma}+\sigma(1-\omega^{\sigma})}&=L\left[\frac{\partial^3\varphi}{\partial\xi^3}+\varphi\frac{\partial\varphi}{\partial\xi}+\nu\frac{\partial\nu}{\partial\xi}\right].\\
\frac{\omega^{\sigma}L[\nu(\xi,\mathfrak{F})]-\omega^{-1}\nu(\xi,0)}{\omega^{\sigma}+\sigma(1-\omega^{\sigma})}&=L\left[-2\frac{\partial^3\nu}{\partial\xi^3}+\varphi\frac{\partial\nu}{\partial\xi}\right].
\end{aligned} \tag{27}$$

We obtain when we use the Laplace inverse transform

$$\varphi(\xi,\mathfrak{F}) = \left(3 - 6\tanh^2\frac{\xi}{2}\right) + L^{-1}\left[\frac{\omega^\sigma + \sigma(1-\omega^\sigma)}{\omega^\sigma} L\left[\frac{\partial^3\varphi}{\partial\xi^3} + \varphi\frac{\partial\varphi}{\partial\xi} + \nu\frac{\partial\nu}{\partial\xi}\right]\right].$$
$$\nu(\xi,\mathfrak{F}) = -\left(3l\sqrt{2}\tanh^2\frac{\xi}{2}\right) + L^{-1}\left[\frac{\omega^\sigma + \sigma(1-\omega^\sigma)}{\omega^\sigma} L\left[-2\frac{\partial^3\nu}{\partial\xi^3} + \varphi\frac{\partial\nu}{\partial\xi}\right]\right]. \tag{28}$$

Assume that the solution, $\varphi(\xi,\mathfrak{F})$ and $\nu(\xi,\mathfrak{F})$ in series form as

$$\varphi(\xi,\mathfrak{F}) = \sum_{m=0}^{\infty}\varphi_m(\xi,\mathfrak{F}), \quad \nu(\xi,\mathfrak{F}) = \sum_{m=0}^{\infty}\nu_m(\xi,\mathfrak{F}), \tag{29}$$

where $\varphi\varphi_\xi = \sum_{m=0}^{\infty}\mathscr{A}_m$, $\nu\nu_\xi = \sum_{m=0}^{\infty}\mathscr{B}_m$, and $\nu\nu_\xi = \sum_{m=0}^{\infty}\mathscr{B}_m$ are Adomian polynomials that characterize the nonlinear terms, and so equation (28) is rewritten as

$$\sum_{m=0}^{\infty}\varphi_m(\xi,\mathfrak{F}) = \left(3 - 6\tanh^2\frac{\xi}{2}\right) + L^{-1}\left[\frac{\omega^\sigma + \sigma(1-\omega^\sigma)}{\omega^\sigma} L\left[\frac{\partial^3\varphi}{\partial\xi^3} + \sum_{m=0}^{\infty}\mathscr{A}_m + \sum_{m=0}^{\infty}\mathscr{B}_m\right]\right].$$
$$\sum_{m=0}^{\infty}\nu_m(\xi,\mathfrak{F}) = -\left(3l\sqrt{2}\tanh^2\frac{\xi}{2}\right) + L^{-1}\left[\frac{\omega^\sigma + \sigma(1-\omega^\sigma)}{\omega^\sigma} L\left[-2\frac{\partial^3\nu}{\partial\xi^3} + \sum_{m=0}^{\infty}\mathscr{C}_m\right]\right]. \tag{30}$$

The decomposition of nonlinear terms by Adomian polynomials is defined as in equation (14),

$$\begin{aligned}
&\mathscr{A}_0 = \varphi_0\varphi_{0\xi}, \quad \mathscr{A}_1 = \varphi_1\varphi_{0\xi} + \varphi_0\varphi_{1\xi}, \quad \mathscr{A}_2 = \varphi_2\varphi_{0\xi} + \varphi_1\varphi_{1\xi} + \varphi_0\varphi_{2\xi},\\
&\mathscr{B}_0 = \nu_0\nu_{0\xi}, \quad \mathscr{B}_1 = \nu_1\nu_{0\xi} + \nu_0\nu_{1\xi}, \quad \mathscr{B}_2 = \nu_2\nu_{0\xi} + \nu_1\nu_{1\xi} + \nu_0\nu_{2\xi},\\
&\mathscr{C}_0 = \varphi_0\nu_{0\xi}, \quad \mathscr{C}_1 = \varphi_1\nu_{0\xi} + \varphi_0\nu_{1\xi}, \quad \mathscr{C}_2 = \varphi_2\nu_{0\xi} + \varphi_1\nu_{1\xi} + \varphi_0\nu_{2\xi},
\end{aligned} \tag{31}$$

As a result, when comparing the two sides of equation (30)

$$\varphi_0(\xi,\mathfrak{F}) = \left(3 - 6\tanh^2\frac{\xi}{2}\right),$$
$$\nu_0(\xi,\mathfrak{F}) = -\left(3l\sqrt{2}\tanh^2\frac{\xi}{2}\right). \tag{32}$$

For $m = 0$,

$$\varphi_1(\xi,\mathfrak{F}) = -6\operatorname{sech}^2\frac{\xi}{2}\tanh\frac{\xi}{2}\left[\frac{\sigma\mathfrak{F}^\sigma}{\Gamma(\sigma+1)} + (1-\sigma)\right],$$
$$\nu_1(\xi,\mathfrak{F}) = 3l\sqrt{2}\operatorname{sech}^2\frac{\xi}{2}\tanh\frac{\xi}{2}\left[\frac{\sigma\mathfrak{F}^\sigma}{\Gamma(\sigma+1)} + (1-\sigma)\right]. \tag{33}$$

For $m = 1$,

$$\varphi_2(\xi,\mathfrak{F}) = \frac{3}{2}\left(2\operatorname{sech}^2\frac{\xi}{2} + 7\operatorname{sech}^4\frac{\xi}{2} - 15\operatorname{sech}^6\frac{\xi}{2}\right)\left[\frac{\sigma^2\mathfrak{F}^{2\sigma}}{\Gamma(2\sigma+1)} + 2\sigma(1-\sigma)\frac{\mathfrak{F}^\sigma}{\Gamma(\sigma+1)} + (1-\sigma)^2\right],$$
$$\nu_2(\xi,\mathfrak{F}) = \frac{3l\sqrt{2}}{4}\left(2\operatorname{sech}^2\frac{\xi}{2} + 21\operatorname{sech}^4\frac{\xi}{2} - 24\operatorname{sech}^6\frac{\xi}{2}\right)\left[\frac{\sigma^2\mathfrak{F}^{2\sigma}}{\Gamma(2\sigma+1)} + 2\sigma(1-\sigma)\frac{\mathfrak{F}^\sigma}{\Gamma(\sigma+1)} + (1-\sigma)^2\right], \tag{34}$$

The approximate solution to the series is written as

$$\varphi(\xi,\mathfrak{F}) = \sum_{m=0}^{\infty} \varphi_m(\xi,\mathfrak{F}) = \varphi_0(\xi,\mathfrak{F}) + \varphi_1(\xi,\mathfrak{F}) + \varphi_2(\xi,\mathfrak{F}) + \cdots$$

$$\nu(\xi,\mathfrak{F}) = \sum_{m=0}^{\infty} \nu_m(\xi,\mathfrak{F}) = \nu_0(\xi,\mathfrak{F}) + \nu_1(\xi,\mathfrak{F}) + \nu_2(\xi,\mathfrak{F}) + \cdots$$

$$\begin{aligned}\varphi(\xi,\mathfrak{F}) &= \left(3 - 6\tanh^2\frac{\xi}{2}\right) - 6\mathrm{sec}h^2\frac{\xi}{2}\tanh\frac{\xi}{2}\left[\frac{\sigma\mathfrak{F}^{\sigma}}{\Gamma(\sigma+1)} + (1-\sigma)\right] + \frac{3}{2}\left(2\mathrm{sec}h^2\frac{\xi}{2} + 7\mathrm{sec}h^4\frac{\xi}{2} - 15\mathrm{sec}h^6\frac{\xi}{2}\right)\\ &\cdot\left[\frac{\sigma^2\mathfrak{F}^{2\sigma}}{\Gamma(2\sigma+1)} + 2\sigma(1-\sigma)\frac{\mathfrak{F}^{\sigma}}{\Gamma(\sigma+1)} + (1-\sigma)^2\right] + \cdots\\ \nu(\xi,\mathfrak{F}) &= -\left(3l\sqrt{2}\tanh^2\frac{\xi}{2}\right) + 3l\sqrt{2}\mathrm{sec}h^2\frac{\xi}{2}\tanh\frac{\xi}{2}\left[\frac{\sigma\mathfrak{F}^{\sigma}}{\Gamma(\sigma+1)} + (1-\sigma)\right] + \frac{3l\sqrt{2}}{4}\left(2\mathrm{sec}h^2\frac{\xi}{2} + 21\mathrm{sec}h^4\frac{\xi}{2} -\right.\\ &\left.\cdot\,24\mathrm{sec}h^6\frac{\xi}{2}\right)\left[\frac{\sigma^2\mathfrak{F}^{2\sigma}}{\Gamma(2\sigma+1)} + 2\sigma(1-\sigma)\frac{\mathfrak{F}^{\sigma}}{\Gamma(\sigma+1)} + (1-\sigma)^2\right] + \cdots\end{aligned} \tag{35}$$

We achieve the exact solution by putting $\sigma = 1$

$$\begin{aligned}\varphi(\xi,\mathfrak{F}) &= 3 - 6\tanh^2\left(\frac{\mathfrak{F}+\xi}{2}\right),\\ \nu(\xi,\mathfrak{F}) &= -3l\sqrt{2}\tanh^2\left(\frac{\mathfrak{F}+\xi}{2}\right).\end{aligned} \tag{36}$$

5.1.1. VITM Analytical Results. For Equation (25), we have the iteration formula:

$$\begin{aligned}\varphi_{m+1}(\xi,\mathfrak{F}) &= \varphi_m(\xi,\mathfrak{F}) - L^{-1}\left[\frac{\omega^{\sigma} + \sigma(1-\omega^{\sigma})}{\omega^{\sigma}} L\left\{\frac{\omega^{\sigma}}{\omega^{\sigma} + \sigma(1-\omega^{\sigma})}\frac{\partial^3\varphi_m}{\partial\xi^3} + \varphi_m\frac{\partial\varphi_m}{\partial\xi} + \nu_m\frac{\partial\nu_m}{\partial\xi}\right\}\right],\\ \nu_{m+1}(\xi,\mathfrak{F}) &= \nu_m(\xi,\mathfrak{F}) - L^{-1}\left[\frac{\omega^{\sigma} + \sigma(1-\omega^{\sigma})}{\omega^{\sigma}} L\left\{\frac{\omega^{\sigma}}{\omega^{\sigma} + \sigma(1-\omega^{\sigma})} - 2\frac{\partial^3\nu_m}{\partial\xi^3}\varphi_m\frac{\partial\nu_m}{\partial\xi}\right\}\right],\end{aligned} \tag{37}$$

where

For $m = 0, 1, 2, \cdots,$

$$\begin{aligned}\varphi_0(\xi,\mathfrak{F}) &= \left(3 - 6\tanh^2\frac{\xi}{2}\right),\\ \nu_0(\xi,\mathfrak{F}) &= -\left(3l\sqrt{2}\tanh^2\frac{\xi}{2}\right).\end{aligned} \tag{38}$$

$$\varphi_1(\xi,\mathfrak{F}) = \varphi_0(\xi,t\mathfrak{F}) - L^{-1}\left[\frac{\omega^{\sigma} + \sigma(1-\omega^{\sigma})}{\omega^{\sigma}} L\left\{\frac{\omega^{\sigma}}{\omega^{\sigma} + \sigma(1-\omega^{\sigma})}\frac{\partial^3\varphi_0}{\partial\xi^3} + \varphi_0\frac{\partial\varphi_0}{\partial\xi} + \nu_0\frac{\partial\nu_0}{\partial\xi}\right\}\right],$$

$$\varphi_1(\xi,\mathfrak{F}) = -6\mathrm{sec}h^2\frac{\xi}{2}\tanh\frac{\xi}{2}\left[\frac{\sigma\mathfrak{F}^{\sigma}}{\Gamma(\sigma+1)} + (1-\sigma)\right],$$

$$
\begin{aligned}
\nu_1(\xi,\mathfrak{F}) &= \nu_0(\xi,\mathfrak{F}) - L^{-1}\left[\frac{\omega^\sigma+\sigma(1-\omega^\sigma)}{\omega^\sigma} L\left\{\frac{\omega^\sigma}{\omega^\sigma+\sigma(1-\omega^\sigma)} -2\frac{\partial^3\nu_0}{\partial\xi^3}\varphi_0\frac{\partial\nu_0}{\partial\xi}\right\}\right],\\
\nu_1(\xi,\mathfrak{F}) &= 3l\sqrt{2}\mathrm{sech}^2\frac{\xi}{2}\tanh\frac{\xi}{2}\left[\frac{\sigma\mathfrak{F}^\sigma}{\Gamma(\sigma+1)}+(1-\sigma)\right],\\
\varphi_2(\xi,\mathfrak{F}) &= \varphi_1(\xi,\mathfrak{F}) - L^{-1}\left[\frac{\omega^\sigma+\sigma(1-\omega^\sigma)}{\omega^\sigma} L\left\{\frac{\omega^\sigma}{\omega^\sigma+\sigma(1-\omega^\sigma)}\frac{\partial^3\varphi_1}{\partial\xi^3}+\varphi_1\frac{\partial\varphi_1}{\partial\xi}+\nu_1\frac{\partial\nu_1}{\partial\xi}\right\}\right],\\
\varphi_2(\xi,\mathfrak{F}) &= \frac{3}{2}\left(2\mathrm{sech}^2\frac{\xi}{2}+7\mathrm{sech}^4\frac{\xi}{2}-15\mathrm{sech}^6\frac{\xi}{2}\right)\left[\frac{\sigma^2\mathfrak{F}^{2\sigma}}{\Gamma(2\sigma+1)}+2\sigma(1-\sigma)\frac{\mathfrak{F}^\sigma}{\Gamma(\sigma+1)}+(1-\sigma)^2\right],\\
\nu_2(\xi,\mathfrak{F}) &= \nu_1(\xi,\mathfrak{F}) - L^{-1}\left[\frac{\omega^\sigma+\sigma(1-\omega^\sigma)}{\omega^\sigma} L\left\{\frac{\omega^\sigma}{\omega^\sigma+\sigma(1-\omega^\sigma)} -2\frac{\partial^3\nu_1}{\partial\xi^3}\varphi_1\frac{\partial\nu_1}{\partial\xi}\right\}\right],\\
\nu_1(\xi,\mathfrak{F}) &= \frac{3l\sqrt{2}}{4}\left(2\mathrm{sech}^2\frac{\xi}{2}+21\mathrm{sech}^4\frac{\xi}{2}-24\mathrm{sech}^6\frac{\xi}{2}\right)\left[\frac{\sigma^2\mathfrak{F}^{2\sigma}}{\Gamma(2\sigma+1)}+2\sigma(1-\sigma)\frac{\mathfrak{F}^\sigma}{\Gamma(\sigma+1)}+(1-\sigma)^2\right],\\
\varphi(\xi,\mathfrak{F}) &= \sum_{m=0}^{\infty}\varphi_m(\xi,\mathfrak{F}) = \left(3-6\tanh^2\frac{\xi}{2}\right) - 6\mathrm{sech}^2\frac{\xi}{2}\tanh\frac{\xi}{2}\left[\frac{\sigma\mathfrak{F}^\sigma}{\Gamma(\sigma+1=)}+(1-\sigma)\right]\\
&\quad+\frac{3}{2}\left(2\mathrm{sech}^2\frac{\xi}{2}+7\mathrm{sech}^4\frac{\xi}{2}-15\mathrm{sech}^6\frac{\xi}{2}\right)\left[\frac{\sigma^2\mathfrak{F}^{2\sigma}}{\Gamma(2\sigma+1)}+2\sigma(1-\sigma)\frac{\mathfrak{F}^\sigma}{\Gamma(\sigma+1)}+(1-\sigma)^2\right]+\cdots\\
\nu(\xi,\mathfrak{F}) &= \sum_{m=0}^{\infty}\nu_m(\xi,\mathfrak{F}) = -\left(3l\sqrt{2}\tanh^2\frac{\xi}{2}\right) + 3l\sqrt{2}\mathrm{sech}^2\frac{\xi}{2}\tanh\frac{\xi}{2}\left[\frac{\sigma\mathfrak{F}^\sigma}{\Gamma(\sigma+1)}+(1-\sigma)\right]\\
&\quad+\frac{3l\sqrt{2}}{4}\left(2\mathrm{sech}^2\frac{\xi}{2}+21\mathrm{sech}^4\frac{\xi}{2}-24\mathrm{sech}^6\frac{\xi}{2}\right)\left[\frac{\sigma^2\mathfrak{F}^{2\sigma}}{\Gamma(2\sigma+1)}+2\sigma(1-\sigma)\frac{\mathfrak{F}^\sigma}{\Gamma(\sigma+1)}+(1-\sigma)^2\right]+\cdots
\end{aligned}
\tag{39}
$$

We achieve the exact solution by putting $\sigma = 1$

$$
\begin{aligned}
\varphi(\xi,\mathfrak{F}) &= 3-6\tanh^2\left(\frac{\mathfrak{F}+\xi}{2}\right),\\
\nu(\xi,\mathfrak{F}) &= -3l\sqrt{2}\tanh^2\left(\frac{\mathfrak{F}+\xi}{2}\right).
\end{aligned}
\tag{40}
$$

The analytical solution and exact solution is shown in Figures 1(a) and 1(b) at $\sigma = 1$ and $-5 \le \psi \ge 5$. Figure 1(c) shows the absolute error, and Figure 1(d) gives the solution at various fractional-order graph for $\varphi(\xi,\mathfrak{F})$. The behavior of the exact solution and analytical solution for $\nu(\xi,\mathfrak{F})$ is seen in Figures 2(a) and 2(b). Tables 1 and 2 show the comparison of the exact and our methods solution in addition with the absolute error at different fractional-order. From the figure and tables, it is clear that our methods solution is in good agreement with the exact solution.

5.2. Problem 2. Consider the generalized coupled Hirota Satsuma KdV system

$$
\begin{aligned}
\frac{\partial^\sigma\varphi}{\partial\mathfrak{F}^\sigma} &= \frac{1}{2}\frac{\partial^3\varphi}{\partial\xi^3} - 3\varphi\frac{\partial\varphi}{\partial\xi} + 3\frac{\partial}{\partial\xi}(\nu\ell),\\
\frac{\partial^\sigma\nu}{\partial\mathfrak{F}^\sigma} &= 3\varphi\frac{\partial\nu}{\partial\xi} - \frac{\partial^3\nu}{\partial\xi^3},\\
\frac{\partial^\sigma\ell}{\partial\mathfrak{F}^\sigma} &= 3\varphi\frac{\partial\ell}{\partial\xi} - \frac{\partial^3\ell}{\partial\xi^3}\ 0<\sigma\le 1,
\end{aligned}
\tag{41}
$$

with initial source

$$
\begin{aligned}
\varphi(\xi,0) &= -\frac{1}{3}+2\tanh^3\xi, \quad \nu(\xi,0)\\
&= \tanh\xi, \quad \ell(\xi,0) = \frac{8}{3}\tanh\xi.
\end{aligned}
\tag{42}
$$

On taking the Laplace transform of (41), we get

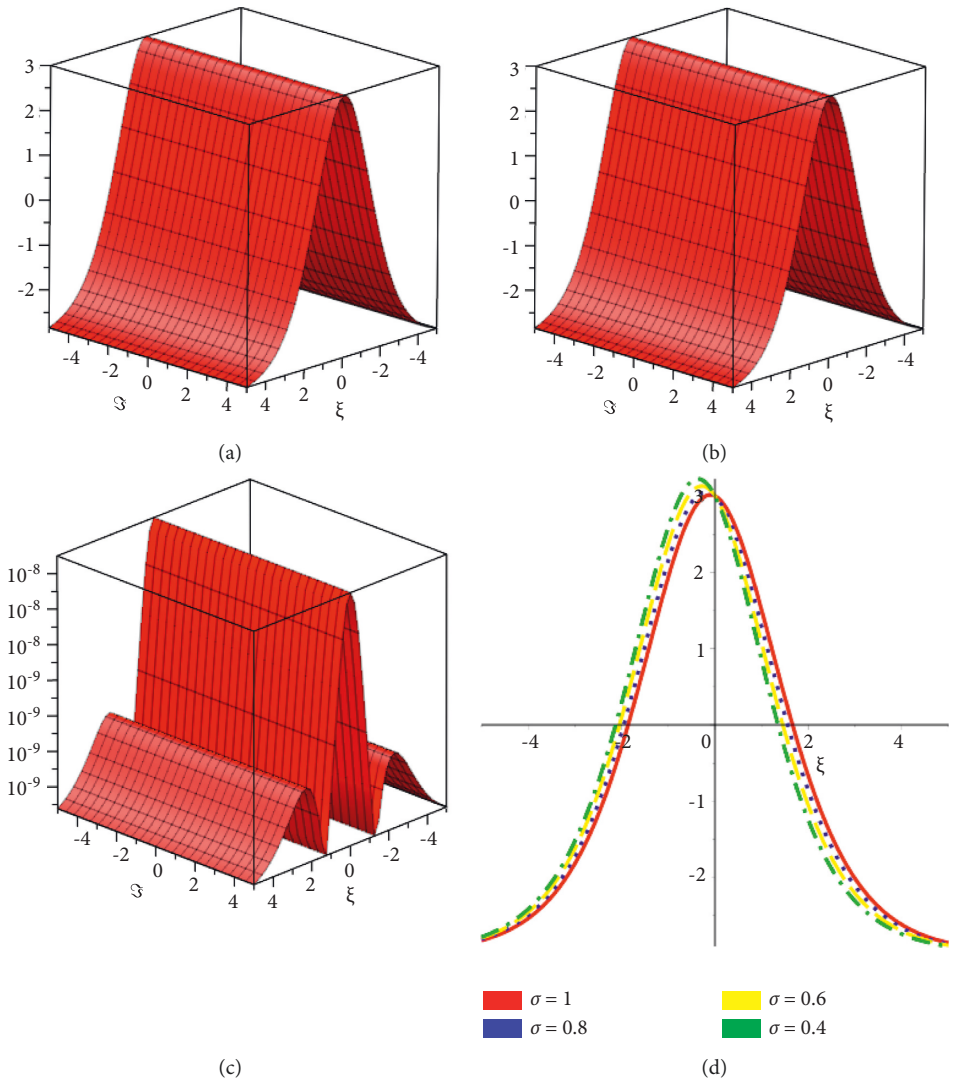

Figure 1: Exact solution, analytical solution, absolute error, and various fractional order solution for $\varphi(\xi, \mathfrak{F})$ of problem 1.

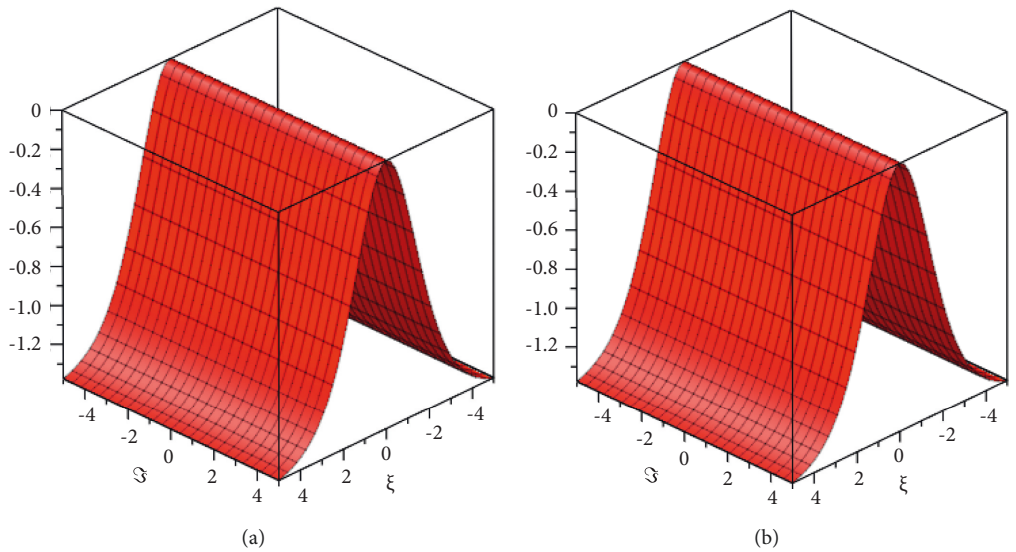

Figure 2: Exact solution and analytical solution for $\nu(\xi, \mathfrak{F})$ problem 1.

Table 1: Comparison of the proposed method and exact results with absolute error (AE) at various fractional order for $\varphi(\xi, \mathfrak{I})$ of problem 1.

$\mathfrak{I}$ = 0.0001	Exact solution	Proposed techniques solution	AE of proposed techniques	AE of proposed techniques	AE of proposed techniques
Υ	$\sigma = 1$	$\sigma = 1$	$\sigma = 1$	$\sigma = 0.9$	$\sigma = 0.8$
0	2.999999985000000	3.000000000000000	1.5000000000E-08	1.5000000000E-08	1.5000000000E-08
0.1	2.984995050000000	2.984995065000000	1.5000000000E-08	4.8177000000E-05	1.7264100000E-04
0.2	2.940338524000000	2.940338538000000	1.4000000000E-08	9.5412000000E-05	3.4187000000E-04
0.3	2.866912116000000	2.866912130000000	1.4000000000E-08	1.4077300000E-04	5.0438500000E-04
0.4	2.766144073000000	2.766144086000000	1.3000000000E-08	1.8342200000E-04	6.5718200000E-04
0.5	2.639950945000000	2.639950957000000	1.2000000000E-08	2.2262900000E-04	7.9764400000E-04
0.6	2.490661806000000	2.490661816000000	1.0000000000E-08	2.5779500000E-04	9.2363200000E-04
0.7	2.320929961000000	2.320929970000000	9.0000000000E-09	2.8847600000E-04	1.0335470000E-03
0.8	2.133637649000000	2.133637657000000	8.0000000000E-09	3.1437800000E-04	1.1263450000E-03
0.9	1.931799290000000	1.931799295000000	5.0000000000E-09	3.3536800000E-04	1.2015390000E-03
1.0	1.718468335000000	1.718468338000000	3.0000000000E-09	3.5145100000E-04	1.2591560000E-03

Table 2: Comparison of the proposed method and exact results with Absolute Error (AE) at various fractional order for $\nu(\xi, \mathfrak{I})$ of problem 1.

$\mathfrak{I}$ = 0.0001	Exact solution	Proposed techniques solution	AE of proposed techniques	AE of proposed techniques	AE of proposed techniques
Υ	$\sigma = 1$	$\sigma = 1$	$\sigma = 1$	$\sigma = 0.9$	$\sigma = 0.8$
0	−0.000000000010607	0.000000000000000	1.0606601700E-11	1.0606601700E-11	1.0606601700E-11
0.1	−0.000010610102200	−0.000010567806420	4.2295783020E-08	1.6438202410E-07	9.6316691610E-07
0.2	−0.000042187034300	−0.000042103293120	8.3741185290E-08	3.2548962340E-07	1.9071994720E-06
0.3	−0.000094107345200	−0.000093983802760	1.2354244410E-07	4.8020666600E-07	2.8137865210E-06
0.4	−0.000165361111500	−0.000165200148500	1.6096295920E-07	6.2567014160E-07	3.6661525080E-06
0.5	−0.000254593128400	−0.000254397765900	1.9536257270E-07	7.5938997350E-07	4.4497048860E-06
0.6	−0.000360156490500	−0.000359930273600	2.2621689430E-07	8.7933098140E-07	5.1525210840E-06
0.7	−0.000480175029200	−0.000479921894200	2.5313503520E-07	9.8396949140E-07	5.7656675160E-06
0.8	−0.000612610692900	−0.000612334832200	2.7586074000E-07	1.0723124430E-06	6.2833302080E-06
0.9	−0.000755331965700	−0.000755037691100	2.9427450770E-07	1.1438942760E-06	6.7027805770E-06
1.0	−0.000906179730200	−0.000905871346300	3.0838397500E-07	1.1987439840E-06	7.0241846510E-06

$$\begin{aligned}
\frac{\omega^{\sigma} L[\varphi(\xi,\mathfrak{I})] - \omega^{-1}\varphi(\xi,0)}{\omega^{\sigma} + \sigma(1-\omega^{\sigma})} &= L\left[\frac{1}{2}\frac{\partial^3\varphi}{\partial\xi^3} - 3\varphi\frac{\partial\varphi}{\partial\xi} + 3\frac{\partial}{\partial\xi}(\nu\ell)\right],\\
\frac{\omega^{\sigma} L[\nu(\xi,\mathfrak{I})] - \omega^{-1}\nu(\xi,0)}{\omega^{\sigma} + \sigma(1-\omega^{\sigma})} &= L\left[3\varphi\frac{\partial\nu}{\partial\xi} - \frac{\partial^3\nu}{\partial\xi^3}\right],\\
\frac{\omega^{\sigma} L[\ell(\xi,\mathfrak{I})] - \omega^{-1}\ell(\xi,0)}{\omega^{\sigma} + \sigma(1-\omega^{\sigma})} &= L\left[3\varphi\frac{\partial\ell}{\partial\xi} - \frac{\partial^3\ell}{\partial\xi^3}\right].
\end{aligned} \tag{43}$$

We obtain when we use the Laplace inverse transform

$$\begin{aligned}
\varphi(\xi,\mathfrak{I}) &= -\frac{1}{3} + 2\tanh^3\xi + L^{-1}\left[\frac{\omega^{\sigma} + \sigma(1-\omega^{\sigma})}{\omega^{\sigma}} L\left[\frac{1}{2}\frac{\partial^3\varphi}{\partial\xi^3} - 3\varphi\frac{\partial\varphi}{\partial\xi} + 3\frac{\partial}{\partial\xi}(\nu\ell)\right]\right],\\
\nu(\xi,\mathfrak{I}) &= \tanh\xi + L^{-1}\left[\frac{\omega^{\sigma} + \sigma(1-\omega^{\sigma})}{\omega^{\sigma}} L\left[3\varphi\frac{\partial\nu}{\partial\xi} - \frac{\partial^3\nu}{\partial\xi^3}\right]\right],\\
\ell(\xi,\mathfrak{I}) &= \frac{8}{3}\tanh\xi + L^{-1}\left[\frac{\omega^{\sigma} + \sigma(1-\omega^{\sigma})}{\omega^{\sigma}} L\left[3\varphi\frac{\partial\ell}{\partial\xi} - \frac{\partial^3\ell}{\partial\xi^3}\right]\right].
\end{aligned} \tag{44}$$

Assume that the solution, $\varphi(\xi,\mathfrak{T})$, $\nu(\xi,\mathfrak{T})$, and $\ell(\xi,\mathfrak{T})$ in series form as

$$\varphi(\xi,\mathfrak{T})=\sum_{m=0}^{\infty}\varphi_m(\xi,\mathfrak{T}),\quad \nu(\xi,\mathfrak{T})=\sum_{m=0}^{\infty}\nu_m(\xi,\mathfrak{T}),\quad \ell(\xi,\mathfrak{T})=\sum_{m=0}^{\infty}\ell_m(\xi,\mathfrak{T}),\tag{45}$$

where $\varphi\varphi_\xi=\sum_{m=0}^{\infty}\mathscr{A}_m$, $(\nu\ell)_\xi=\sum_{m=0}^{\infty}\mathscr{B}_m$, $\varphi\nu_\xi=\sum_{m=0}^{\infty}\mathscr{C}_m$, and $\varphi\ell_\xi=\sum_{m=0}^{\infty}\mathscr{D}_m$ are Adomian polynomials that characterize the nonlinear terms, and so equation (30) is rewritten as

$$\begin{aligned}
\sum_{m=0}^{\infty}\varphi_m(\xi,\mathfrak{T})&=-\frac{1}{3}+2\tanh^3\xi+L^{-1}\left[\frac{\omega^\sigma+\sigma(1-\omega^\sigma)}{\omega^\sigma}L\left[\frac{\partial^3\varphi}{\partial\xi^3}-3\sum_{m=0}^{\infty}\mathscr{A}_m+3\sum_{m=0}^{\infty}\mathscr{B}_m\right]\right].\\
\sum_{m=0}^{\infty}\nu_m(\xi,\mathfrak{T})&=\tanh\xi+L^{-1}\left[\frac{\omega^\sigma+\sigma(1-\omega^\sigma)}{\omega^\sigma}L\left[3\sum_{m=0}^{\infty}\mathscr{C}_m-\frac{\partial^3\nu}{\partial\xi^3}\right]\right],\\
\sum_{m=0}^{\infty}\ell_m(\xi,\mathfrak{T})&=\frac{8}{3}\tanh\xi+L^{-1}\left[\frac{\omega^\sigma+\sigma(1-\omega^\sigma)}{\omega^\sigma}L\left[3\sum_{m=0}^{\infty}\mathscr{D}_m-\frac{\partial^3\ell}{\partial\xi^3}\right]\right].
\end{aligned}\tag{46}$$

The decomposition of nonlinear terms by Adomian polynomials is defined as in equation (7),

$$\begin{aligned}
&\mathscr{A}_0=\varphi_0\varphi_{0\xi},\quad \mathscr{A}_1=\varphi_1\varphi_{0\xi}+\varphi_0\varphi_{1\xi},\quad \mathscr{A}_2=\varphi_2\varphi_{0\xi}+\varphi_1\varphi_{1\xi}+\varphi_0\varphi_{2\xi},\\
&\mathscr{B}_0=\nu_0\ell_{0\xi}+\ell_0\nu_{0\xi},\quad \mathscr{B}_1=\left(\nu_0\ell_{0\xi}+\nu_1\ell_{0\xi}\right)+\left(\ell_1\nu_{0\xi}+\ell_0\nu_{1\xi}\right),\\
&\mathscr{B}_2=\left(\nu_2\ell_{0\xi}+\nu_1\ell_{1\xi}+\nu_0\ell_{2\xi}\right)+\left(\ell_2\nu_{0\xi}+\ell_1\nu_{1\xi}+\ell_0\nu_{2\xi}\right),\\
&\mathscr{C}_0=\varphi_0\nu_{0\xi},\quad \mathscr{C}_1=\varphi_1\nu_{0\xi}+\varphi_0\nu_{1\xi},\quad \mathscr{C}_2=\varphi_2\nu_{0\xi}+\varphi_1\nu_{1\xi}+\varphi_0\nu_{2\xi},\\
&\mathscr{D}_0=\varphi_0\ell_{0\xi},\quad \mathscr{D}_1=\varphi_1\ell_{0\xi}+\varphi_0\ell_{1\xi},\quad \mathscr{D}_2=\varphi_2\ell_{0\xi}+\varphi_1\ell_{1\xi}+\varphi_0\ell_{2\xi},
\end{aligned}\tag{47}$$

As a result, when comparing the two sides of (46),

$$\begin{aligned}
\varphi_0(\xi,\mathfrak{T})&=-\frac{1}{3}+2\tanh^2\xi,\\
\nu_0(\xi,\mathfrak{T})&=\tanh\xi,\\
\ell_0(\xi,\mathfrak{T})&=\frac{8}{3}\tanh\xi.
\end{aligned}\tag{48}$$

For $m=0$,

$$\begin{aligned}
\varphi_1(\xi,\mathfrak{T})&=4\mathrm{sech}^2\xi\tanh\xi\left[\frac{\sigma\mathfrak{T}^\sigma}{\Gamma(\sigma+1)}+(1-\sigma)\right],\\
\nu_1(\xi,\mathfrak{T})&=\mathrm{sech}^2\xi\left[\frac{\sigma\mathfrak{T}^\sigma}{\Gamma(\sigma+1)}+(1-\sigma)\right],\\
\ell_1(\xi,\mathfrak{T})&=\frac{8}{3}\mathrm{sech}^2\xi\left[\frac{\sigma\mathfrak{T}^\sigma}{\Gamma(\sigma+1)}+(1-\sigma)\right].
\end{aligned}\tag{49}$$

For $m=1$,

$$\begin{aligned}
\varphi_2(\xi,\mathfrak{T})&=4\mathrm{sech}^2\xi\left(1-3\tanh^2\xi\right)\left[\frac{\sigma^2\mathfrak{T}^{2\sigma}}{\Gamma(2\sigma+1)}+2\sigma(1-\sigma)\frac{\mathfrak{T}^\sigma}{\Gamma(\sigma+1)}+(1-\sigma)^2\right],\\
\nu_2(\xi,\mathfrak{T})&=-\mathrm{sech}^2\xi\tanh\xi\left[\frac{\sigma^2\mathfrak{T}^{2\sigma}}{\Gamma(2\sigma+1)}+2\sigma(1-\sigma)\frac{\mathfrak{T}^\sigma}{\Gamma(\sigma+1)}+(1-\sigma)^2\right],\\
\ell_2(\xi,\mathfrak{T})&=-\frac{8}{3}\mathrm{sech}^2\xi\tanh\xi\left[\frac{\sigma^2\mathfrak{T}^{2\sigma}}{\Gamma(2\sigma+1)}+2\sigma(1-\sigma)\frac{\mathfrak{T}^\sigma}{\Gamma(\sigma+1)}+(1-\sigma)^2\right].
\end{aligned}\tag{50}$$

The approximate solution to the series is written as

$$\varphi(\xi,\mathfrak{F}) = \sum_{m=0}^{\infty} \varphi_m(\xi,\mathfrak{F}) = \varphi_0(\xi,\mathfrak{F}) + \varphi_1(\xi,\mathfrak{F}) + \varphi_2(\xi,\mathfrak{F}) + \cdots$$

$$\nu(\xi,\mathfrak{F}) = \sum_{m=0}^{\infty} \nu_m(\xi,\mathfrak{F}) = \nu_0(\xi,\mathfrak{F}) + \nu_1(\xi,\mathfrak{F}) + \nu_2(\xi,\mathfrak{F}) + \cdots$$

$$\ell(\xi,\mathfrak{F}) = \sum_{m=0}^{\infty} \ell_m(\xi,\mathfrak{F}) = \ell_0(\xi,\mathfrak{F}) + \ell_1(\xi,\mathfrak{F}) + \ell_2(\xi,\mathfrak{F}) + \cdots$$

$$\begin{aligned}\varphi(\xi,\mathfrak{F}) &= -\frac{1}{3} + 2\tanh^2\xi + 4\mathrm{sec}h^2\xi\tanh\xi\left[\frac{\sigma\mathfrak{F}^{\sigma}}{\Gamma(\sigma+1)} + (1-\sigma)\right] \\ &\quad + 4\mathrm{sec}h^2\xi\left(1 - 3\tanh^2\xi\right)\left[\frac{\sigma^2\mathfrak{F}^{2\sigma}}{\Gamma(2\sigma+1)} + 2\sigma(1-\sigma)\frac{\mathfrak{F}^{\sigma}}{\Gamma(\sigma+1)} + (1-\sigma)^2\right] + \cdots \\ \nu(\xi,\mathfrak{F}) &= \tanh\xi + \mathrm{sec}h^2\xi\left[\frac{\sigma\mathfrak{F}^{\sigma}}{\Gamma(\sigma+1)} + (1-\sigma)\right] - \mathrm{sec}h^2\xi\tanh\xi\left[\frac{\sigma^2\mathfrak{F}^{2\sigma}}{\Gamma(2\sigma+1)} + 2\sigma(1-\sigma)\frac{\mathfrak{F}^{\sigma}}{\Gamma(\sigma+1)} + (1-\sigma)^2\right] + \cdots \\ \ell(\xi,\mathfrak{F}) &= \frac{8}{3}\tanh\xi + \frac{8}{3}\mathrm{sec}h^2\xi\left[\frac{\sigma\mathfrak{F}^{\sigma}}{\Gamma(\sigma+1)} + (1-\sigma)\right] - \frac{8}{3}\mathrm{sec}h^2\xi\tanh\xi\left[\frac{\sigma^2\mathfrak{F}^{2\sigma}}{\Gamma(2\sigma+1)} + 2\sigma(1-\sigma)\frac{\mathfrak{F}^{\sigma}}{\Gamma(\sigma+1)} + (1-\sigma)^2\right] + \cdots\end{aligned} \tag{51}$$

We achieve the exact solution by putting $\sigma = 1$,

$$\begin{aligned}\varphi(\xi,\mathfrak{F}) &= -\frac{1}{3} + 2\tanh^2(\mathfrak{F}+\xi), \\ \nu(\xi,\mathfrak{F}) &= \tanh(\mathfrak{F}+\xi), \\ \ell(\xi,\mathfrak{F}) &= \frac{8}{3}\tanh(\mathfrak{F}+\xi).\end{aligned} \tag{52}$$

5.2.1. VITM Analytical Results. For equation (41), we have the iteration formula

$$\begin{aligned}\varphi_{m+1}(\xi,\mathfrak{F}) &= \varphi_m(\xi,\mathfrak{F}) - L^{-1}\left[\frac{\omega^{\sigma} + \sigma(1-\omega^{\sigma})}{\omega^{\sigma}} L\left\{\frac{\omega^{\sigma}}{\omega^{\sigma} + \sigma(1-\omega^{\sigma})}\left(\frac{1}{2}\frac{\partial^3\varphi_m}{\partial\xi^3} - 3\varphi_m\frac{\partial\varphi_m}{\partial\xi} + 3\frac{\partial}{\partial\xi}(\nu_m\ell_m)\right)\right\}\right], \\ \nu_{m+1}(\xi,\mathfrak{F}) &= \nu_m(\xi,\mathfrak{F}) - L^{-1}\left[\frac{\omega^{\sigma} + \sigma(1-\omega^{\sigma})}{\omega^{\sigma}} L\left\{\frac{\omega^{\sigma}}{\omega^{\sigma} + \sigma(1-\omega^{\sigma})}\left(3\varphi_m\frac{\partial\nu_m}{\partial\xi} - \frac{\partial^3\nu_m}{\partial\xi^3}\right)\right\}\right], \\ \ell_{m+1}(\xi,\mathfrak{F}) &= \ell_m(\xi,\mathfrak{F}) - L^{-1}\left[\frac{\omega^{\sigma} + \sigma(1-\omega^{\sigma})}{\omega^{\sigma}} L\left\{\frac{\omega^{\sigma}}{\omega^{\sigma} + \sigma(1-\omega^{\sigma})}\left(3\varphi_m\frac{\partial\ell_m}{\partial\xi} - \frac{\partial^3\ell_m}{\partial\xi^3}\right)\right\}\right],\end{aligned} \tag{53}$$

where

$$\begin{aligned}\varphi_0(\xi,\mathfrak{F}) &= -\frac{1}{3}+2\tanh^2\xi,\\ \nu_0(\xi,\mathfrak{F}) &= \tanh\xi,\\ \ell_0(\xi,\mathfrak{F}) &= \frac{8}{3}\tanh\xi.\end{aligned} \tag{54}$$

For $m = 0, 1, 2, \cdots,$

$$\begin{aligned}
\varphi_1(\xi,\mathfrak{F}) &== \varphi_0(\xi,\mathfrak{F}) - L^{-1}\left[\frac{\omega^\sigma+\sigma(1-\omega^\sigma)}{\omega^\sigma}L\left\{\frac{\omega^\sigma}{\omega^\sigma+\sigma(1-\omega^\sigma)}\frac{1}{2}\frac{\partial^3\varphi_0}{\partial\xi^3}-3\varphi_0\frac{\partial\varphi_0}{\partial\xi}+3\frac{\partial}{\partial\xi}(\nu_0\ell_0)\right\}\right],\\
\varphi_1(\xi,\mathfrak{F}) &= 4\mathrm{sec}h^2\xi\tanh\xi\left[\frac{\sigma\mathfrak{F}^\sigma}{\Gamma(\sigma+1)}+(1-\sigma)\right],\\
\nu_1(\xi,\mathfrak{F}) &= \nu_0(\xi,\mathfrak{F}) - L^{-1}\left[\frac{\omega^\sigma+\sigma(1-\omega^\sigma)}{\omega^\sigma}L\left\{\frac{\omega^\sigma}{\omega^\sigma+\sigma(1-\omega^\sigma)}3\varphi_m\frac{\partial\nu_0}{\partial\xi}-\frac{\partial^3\nu_0}{\partial\xi^3}\right\}\right],\\
\nu_1(\xi,\mathfrak{F}) &= \mathrm{sec}h^2\xi\left[\frac{\sigma\mathfrak{F}^\sigma}{\Gamma(\sigma+1)}+(1-\sigma)\right],\\
\ell_1(\xi,\mathfrak{F}) &= \ell_0(\xi,\mathfrak{F}) - L^{-1}\left[\frac{\omega^\sigma+\sigma(1-\omega^\sigma)}{\omega^\sigma}L\left\{\frac{\omega^\sigma}{\omega^\sigma+\sigma(1-\omega^\sigma)}3\varphi_0\frac{\partial\nu_0}{\partial\xi}-\frac{\partial^3\nu_0}{\partial\xi^3}\right\}\right],\\
\ell_1(\xi,\mathfrak{F}) &= \frac{8}{3}\mathrm{sec}h^2\xi\left[\frac{\sigma\mathfrak{F}^\sigma}{\Gamma(\sigma+1)}+(1-\sigma)\right],\\
\varphi_2(\xi,\mathfrak{F}) &== \varphi_1(\xi,\mathfrak{F}) - L^{-1}\left[\frac{\omega^\sigma+\sigma(1-\omega^\sigma)}{\omega^\sigma}L\left\{\frac{\omega^\sigma}{\omega^\sigma+\sigma(1-\omega^\sigma)}\frac{1}{2}\frac{\partial^3\varphi_1}{\partial\xi^3}-3\varphi_1\frac{\partial\varphi_1}{\partial\xi}+3\frac{\partial}{\partial\xi}(\nu_1\ell_1)\right\}\right],\\
\varphi_2(\xi,\mathfrak{F}) &= 4\mathrm{sec}h^2\xi\left(1-3\tanh^2\xi\right)\left[\frac{\sigma^2\mathfrak{F}^{2\sigma}}{\Gamma(2\sigma+1)}+2\sigma(1-\sigma)\frac{\mathfrak{F}^\sigma}{\Gamma(\sigma+1)}+(1-\sigma)^2\right],\\
\nu_2(\xi,\mathfrak{F}) &= \nu_1(\xi,\mathfrak{F}) - L^{-1}\left[\frac{\omega^\sigma+\sigma(1-\omega^\sigma)}{\omega^\sigma}L\left\{\frac{\omega^\sigma}{\omega^\sigma+\sigma(1-\omega^\sigma)}3\varphi_1\frac{\partial\nu_1}{\partial\xi}-\frac{\partial^3\nu_1}{\partial\xi^3}\right\}\right]\\
\nu_2(\xi,\mathfrak{F}) &= -\mathrm{sec}h^2\xi\tanh\xi\left[\frac{\sigma^2\mathfrak{F}^{2\sigma}}{\Gamma(2\sigma+1)}+2\sigma(1-\sigma)\frac{\mathfrak{F}^\sigma}{\Gamma(\sigma+1)}+(1-\sigma)^2\right],\\
\ell_2(\xi,\mathfrak{F}) &= \ell_1(\xi,\mathfrak{F}) - L^{-1}\left[\frac{\omega^\sigma+\sigma(1-\omega^\sigma)}{\omega^\sigma}L\left\{\frac{\omega^\sigma}{\omega^\sigma+\sigma(1-\omega^\sigma)}3\varphi_1\frac{\partial\nu_1}{\partial\xi}-\frac{\partial^3\nu_1}{\partial\xi^3}\right\}\right]\\
\ell_2(\xi,\mathfrak{F}) &= -\frac{8}{3}\mathrm{sec}h^2\xi\tanh\xi\left[\frac{\sigma^2\mathfrak{F}^{2\sigma}}{\Gamma(2\sigma+1)}+2\sigma(1-\sigma)\frac{\mathfrak{F}^\sigma}{\Gamma(\sigma+1)}+(1-\sigma)^2\right],\\
\varphi(\xi,\mathfrak{F}) &= -\frac{1}{3}+2\tanh^2\xi+4\mathrm{sec}h^2\xi\tanh\xi\left[\frac{\sigma\mathfrak{F}^\sigma}{\Gamma(\sigma+1)}+(1-\sigma)\right]\\
&\quad+4\mathrm{sec}h^2\xi\left(1-3\tanh^2\xi\right)\left[\frac{\sigma^2\mathfrak{F}^{2\sigma}}{\Gamma(2\sigma+1)}+2\sigma(1-\sigma)\frac{\mathfrak{F}^\sigma}{\Gamma(\sigma+1)}+(1-\sigma)^2\right]+\cdots\\
\nu(\xi,\mathfrak{F}) &= \tanh\xi+\mathrm{sec}h^2\xi\left[\frac{\sigma\mathfrak{F}^\sigma}{\Gamma(\sigma+1)}+(1-\sigma)\right]-\mathrm{sec}h^2\xi\tanh\xi\left[\frac{\sigma^2\mathfrak{F}^{2\sigma}}{\Gamma(2\sigma+1)}+2\sigma(1-\sigma)\frac{\mathfrak{F}^\sigma}{\Gamma(\sigma+1)}+(1-\sigma)^2\right]+\cdots\\
\ell(\xi,\mathfrak{F}) &= \frac{8}{3}\tanh\xi+\frac{8}{3}\mathrm{sec}h^2\xi\left[\frac{\sigma\mathfrak{F}^\sigma}{\Gamma(\sigma+1)}+(1-\sigma)\right]-\frac{8}{3}\mathrm{sec}h^2\xi\tanh\xi\left[\frac{\sigma^2\mathfrak{F}^{2\sigma}}{\Gamma(2\sigma+1)}+2\sigma(1-\sigma)\frac{\mathfrak{F}^\sigma}{\Gamma(\sigma+1)}+(1-\sigma)^2\right]+\cdots
\end{aligned} \tag{55}$$

We achieve the exact solution by putting $\sigma = 1$

$$\varphi(\xi, \mathfrak{F}) = -\frac{1}{3} + 2\tanh^2(\mathfrak{F} + \xi),$$
$$\nu(\xi, \mathfrak{F}) = \tanh(\mathfrak{F} + \xi) \tag{56}$$
$$\ell(\xi, \mathfrak{F}) = \frac{8}{3}\tanh(\mathfrak{F} + \xi)$$

The analytical solution and exact solution for $\varphi(\xi, \mathfrak{F})$ of example 2 at $\sigma = 1$ and $-5 \le \psi \ge 5$ are shown in Figures 3(a) and 3(b), whereas Figures 3(c) and 3(d) show the absolute error and the solution at various fractional-order. The graphical behavior of exact solution and analytical solution for $\nu(\xi, \mathfrak{F})$ are shown in Figures 4(a) and 4(b), while Figures 4(c) and 4(d) show the absolute error and the solution at different fractional-order. Figures 5(a) and 5(b) give the solution graph for $\ell(\xi, \mathfrak{F})$. Tables 3–5 show the comparison of the exact and suggested methods solution in addition with the absolute error at various fractional order. From the results of the figures and Tables, it is confirmed that our method solution converges quickly towards exact solution.

5.3. Problem 3. Consider the coupled Burgers equation in one dimension

$$\frac{\partial^\sigma \varphi}{\partial \mathfrak{F}^\sigma} = \frac{\partial^2 \varphi}{\partial \xi^2} + 2\varphi\frac{\partial \varphi}{\partial \xi} - \frac{\partial}{\partial \xi}(\varphi\nu),$$
$$\frac{\partial^\sigma \nu}{\partial \mathfrak{F}^\sigma} = \frac{\partial^2 \nu}{\partial \xi^2} + 2\nu\frac{\partial \nu}{\partial \xi} - \frac{\partial}{\partial \xi}(\varphi\nu)\ 0 < \sigma \le 1, \tag{57}$$

with initial source

$$\varphi(\xi, 0) = \cos\xi, \quad \nu(\xi, 0) = \cos\xi. \tag{58}$$

On taking the Laplace transform of (57), we get

$$\frac{\omega^\sigma L[\varphi(\xi, \mathfrak{F})] - \omega^{-1}\varphi(\xi, 0)}{\omega^\sigma + \sigma(1 - \omega^\sigma)} = L\left[\frac{\partial^2 \varphi}{\partial \xi^2} + 2\varphi\frac{\partial \varphi}{\partial \xi} - \frac{\partial}{\partial \xi}(\varphi\nu)\right].$$
$$\frac{\omega^\sigma L[\nu(\xi, \mathfrak{F})] - \omega^{-1}\nu(\xi, 0)}{\omega^\sigma + \sigma(1 - \omega^\sigma)} = L\left[\frac{\partial^2 \nu}{\partial \xi^2} + 2\nu\frac{\partial \nu}{\partial \xi} - \frac{\partial}{\partial \xi}(\varphi\nu)\right]. \tag{59}$$

We obtain when we use the Laplace inverse transform

$$\varphi(\xi, \mathfrak{F}) = \cos\xi + L^{-1}\left[\frac{\omega^\sigma + \sigma(1 - \omega^\sigma)}{\omega^\sigma} L\left[\frac{\partial^2 \varphi}{\partial \xi^2} + 2\varphi\frac{\partial \varphi}{\partial \xi} - \frac{\partial}{\partial \xi}(\varphi\nu)\right]\right].$$
$$\nu(\xi, \mathfrak{F}) = \cos\xi + L^{-1}\left[\frac{\omega^\sigma + \sigma(1 - \omega^\sigma)}{\omega^\sigma} L\left[\frac{\partial^2 \nu}{\partial \xi^2} + 2\nu\frac{\partial \nu}{\partial \xi} - \frac{\partial}{\partial \xi}(\varphi\nu)\right]\right]. \tag{60}$$

Assume that the solution, $\varphi(\xi, \mathfrak{F})$ and $\nu(\xi, \mathfrak{F})$, in series form as

$$\varphi(\xi, \mathfrak{F}) = \sum_{m=0}^{\infty} \varphi_m(\xi, \mathfrak{F}), \quad \nu(\xi, \mathfrak{F}) = \sum_{m=0}^{\infty} \nu_m(\xi, \mathfrak{F}), \tag{61}$$

where $\varphi\varphi_\xi = \sum_{m=0}^{\infty} \mathscr{A}_m$, $(\varphi\nu)_\xi = \sum_{m=0}^{\infty} \mathscr{B}_m$, and $\nu\nu_\xi = \sum_{m=0}^{\infty} \mathscr{C}_m$ are Adomian polynomials that characterize the nonlinear terms, and so (60) is rewritten as

$$\sum_{m=0}^{\infty} \varphi_m(\xi, \mathfrak{F}) = \cos\xi + L^{-1}\left[\frac{\omega^\sigma + \sigma(1 - \omega^\sigma)}{\omega^\sigma} L\left[\frac{\partial^2 \varphi}{\partial \xi^2} + 2\sum_{m=0}^{\infty} \mathscr{A}_m - \sum_{m=0}^{\infty} \mathscr{B}_m\right]\right].$$
$$\sum_{m=0}^{\infty} \nu_m(\xi, \mathfrak{F}) = \cos\xi + L^{-1}\left[\frac{\omega^\sigma + \sigma(1 - \omega^\sigma)}{\omega^\sigma} L\left[\frac{\partial^2 \nu}{\partial \xi^2} + \sum_{m=0}^{\infty} \mathscr{C}_m - \sum_{m=0}^{\infty} \mathscr{B}_m\right]\right]. \tag{62}$$

The decomposition of nonlinear terms by Adomian polynomials is defined as in equation (14),

$$\frac{\partial^\sigma \varphi}{\partial \mathfrak{F}^\sigma} = \frac{\partial^2 \varphi}{\partial \xi^2} + 2\varphi\frac{\partial \varphi}{\partial \xi} - \frac{\partial}{\partial \xi}(\varphi\nu),$$
$$\frac{\partial^\sigma \nu}{\partial \mathfrak{F}^\sigma} = \frac{\partial^2 \nu}{\partial \xi^2} + 2\nu\frac{\partial \nu}{\partial \xi} - \frac{\partial}{\partial \xi}(\varphi\nu)\ 0 < \sigma \le 1. \tag{63}$$

As a result, when comparing the two sides of (62),

$$\varphi(\xi, 0) = \cos\xi, \quad \nu(\xi, 0) = \cos\xi. \tag{64}$$

For $m = 0$,

$$\frac{\partial^\sigma \varphi}{\partial \mathfrak{F}^\sigma} = \frac{\partial^2 \varphi}{\partial \xi^2} + 2\varphi\frac{\partial \varphi}{\partial \xi} - \frac{\partial}{\partial \xi}(\varphi\nu),$$
$$\frac{\partial^\sigma \nu}{\partial \mathfrak{F}^\sigma} = \frac{\partial^2 \nu}{\partial \xi^2} + 2\nu\frac{\partial \nu}{\partial \xi} - \frac{\partial}{\partial \xi}(\varphi\nu)\ 0 < \sigma \le 1. \tag{65}$$

For $m = 1$,

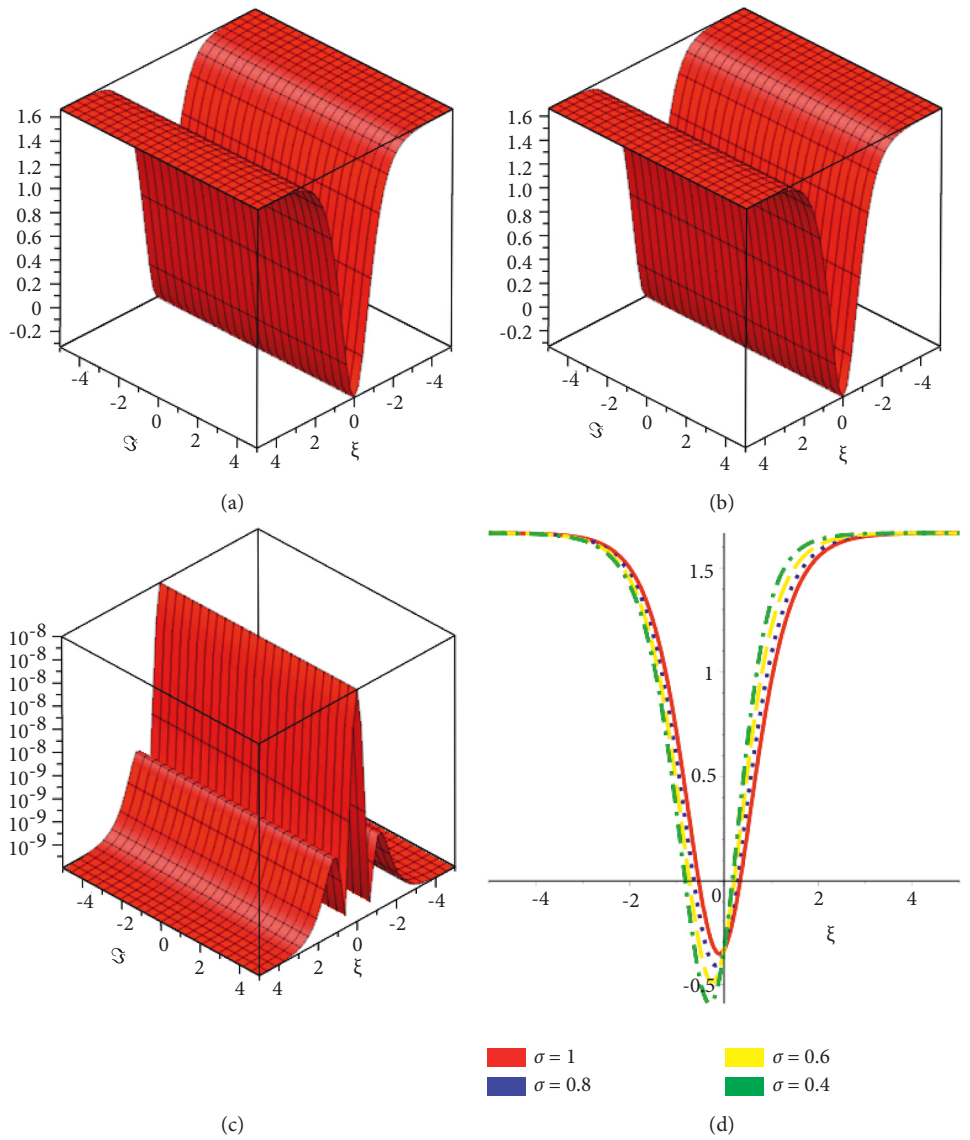

Figure 3: Exact solution, analytical solution, absolute error, and various fractional order solutions for $\varphi(\xi, \Im)$ of problem 2.

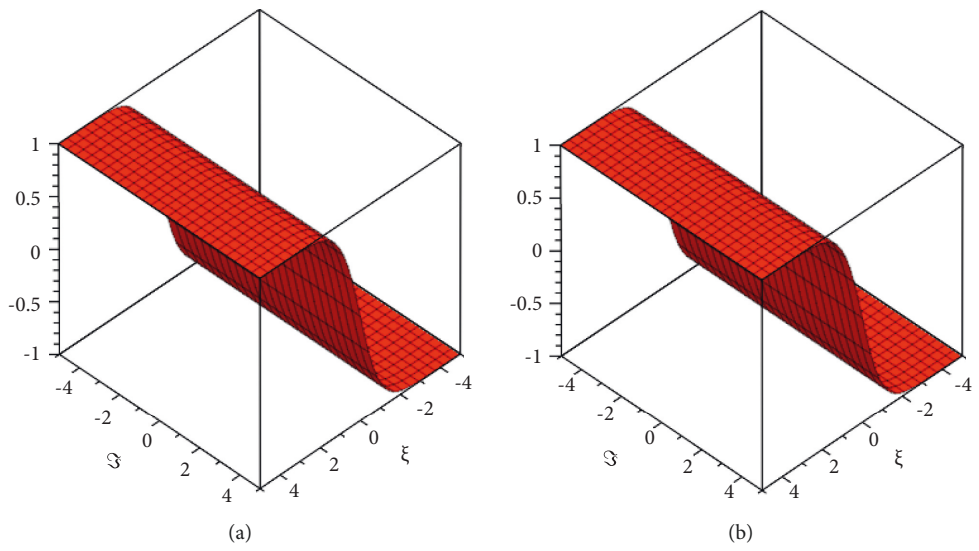

Figure 4: Continued.

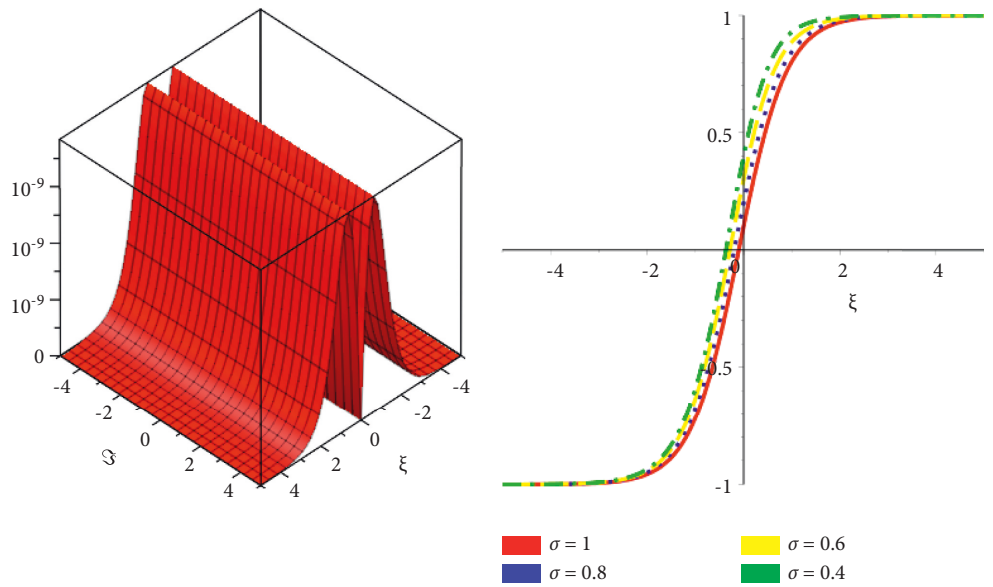

Figure 4: Exact solution, analytical solution, absolute error, and various fractional order solutions for $\nu(\xi, \mathfrak{I})$ of problem 2.

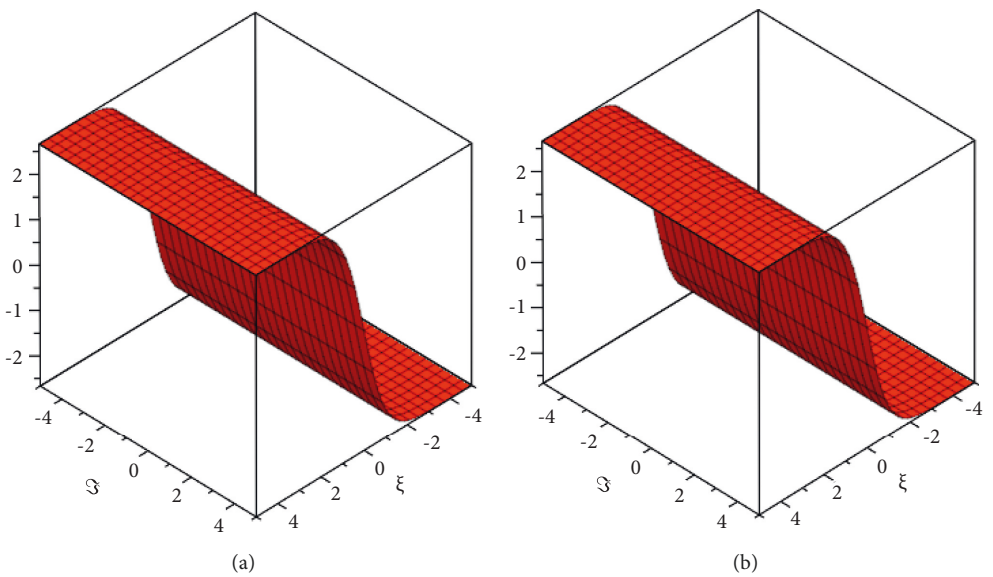

Figure 5: Exact solution and analytical solution for $\ell(\xi, \mathfrak{I})$ problem 2.

Table 3: Comparison of the proposed method and exact results with absolute error (AE) at various fractional order for $\varphi(\xi, \mathfrak{I})$ of problem 2.

$\mathfrak{I} = 0.0001$	Exact solution	Proposed techniques solution	AE of proposed techniques	AE of proposed techniques	AE of proposed techniques
Υ	$\sigma = 1$	$\sigma = 1$	$\sigma = 1$	$\sigma = 0.9$	$\sigma = 0.8$
0	−0.333333313300000	−0.333333333300000	2.0000000000E-08	2.0000000000E-08	2.0000000000E-08
0.1	−0.313426424600000	−0.313426443800000	1.9200000000E-08	6.3598200000E-05	6.4898550000E-04
0.2	−0.255343407800000	−0.255343424800000	1.7000000000E-08	1.2227320000E-04	1.2475490000E-03
0.3	−0.163500606900000	−0.163500620500000	1.3600000000E-08	1.7185690000E-04	1.7533551000E-03
0.4	−0.044480856100000	−0.044480865670000	9.5700000000E-09	2.0958106000E-04	2.1381671200E-03
0.5	0.093916578900000	0.093916573300000	5.6000000000E-09	2.3429753000E-04	2.3902801500E-03
0.6	0.243664004500000	0.243664002500000	2.0000000000E-09	2.4637090000E-04	2.5134153000E-03
0.7	0.397340931900000	0.397340933200000	1.3000000000E-09	2.4731770000E-04	2.5230449000E-03
0.8	0.548704820900000	0.548704824600000	3.7000000000E-09	2.3933690000E-04	2.4416045000E-03
0.9	0.692971449700000	0.692971455800000	6.1000000000E-09	2.2486240000E-04	2.2939183000E-03
1.0	0.826845917700000	0.826845923700000	6.0000000000E-09	2.0621260000E-04	2.1036596000E-03

Table 4: Comparison of the proposed method and exact results with absolute error (AE) at various fractional order for $\nu(\xi, \mathfrak{F})$ of problem 2.

$\mathfrak{F} = 0.0001$	Exact solution	Proposed techniques solution	AE of techniques methods	AE of proposed techniques	AE of proposed techniques
Υ	$\sigma = 1$	$\sigma = 1$	$\sigma = 1$	$\sigma = 0.9$	$\sigma = 0.8$
0	0.000099999999670	0.000100000000000	3.3000000000E-13	1.6117443060E-04	1.6442500900E-03
0.1	0.099767000270000	0.099767001250000	9.8000000000E-10	1.5957435000E-04	1.6279175300E-03
0.2	0.197471422600000	0.197471424500000	1.9000000000E-09	1.5489750000E-04	1.5801969000E-03
0.3	0.291404123500000	0.291404126200000	2.7000000000E-09	1.4749940000E-04	1.5047167000E-03
0.4	0.380034522900000	0.380034526200000	3.3000000000E-09	1.3791040000E-04	1.4068874000E-03
0.5	0.462195798400000	0.462195802100000	3.7000000000E-09	1.2675890000E-04	1.2931204000E-03
0.6	0.537120721000000	0.537120724800000	3.8000000000E-09	1.1469190000E-04	1.1700156000E-03
0.7	0.604431247200000	0.604431251100000	3.9000000000E-09	1.0230770000E-04	1.0436745000E-03
0.8	0.664092672100000	0.664092675800000	3.7000000000E-09	9.0109100000E-05	9.1923020000E-04
0.9	0.716346558400000	0.716346561900000	3.5000000000E-09	7.8482200000E-05	8.0061750000E-04
1.0	0.761636150200000	0.761636153400000	3.2000000000E-09	6.7692400000E-05	6.9054610000E-04

Table 5: Comparison of the proposed method and exact results with absolute error (AE) at various fractional order for $\ell(\xi, \mathfrak{F})$ of problem 2.

$\mathfrak{F} = 0.0001$	Exact solution	Proposed techniques solution	AE of proposed techniques	AE of proposed techniques	AE of proposed techniques
Υ	$\sigma = 1$	$\sigma = 1$	$\sigma = 1$	$\sigma = 0.9$	$\sigma = 0.8$
0	0.000266666665800	0.000266666666700	9.0000000000E-13	4.2979848170E-04	1.5398420700E-03
0.1	0.266045334100000	0.266045336700000	2.6000000000E-09	4.2553160000E-04	1.5245483000E-03
0.2	0.526590460300000	0.526590465300000	5.0000000000E-09	4.1305980000E-04	1.4798594000E-03
0.3	0.777077662700000	0.777077669800000	7.1000000000E-09	3.9333160000E-04	1.4091735000E-03
0.4	1.013425394000000	1.013425403000000	9.0000000000E-09	3.6776200000E-04	1.3175580000E-03
0.5	1.232522129000000	1.232522138000000	9.0000000000E-09	3.3802300000E-04	1.2110150000E-03
0.6	1.432321923000000	1.432321933000000	1.0000000000E-08	3.0584500000E-04	1.0957270000E-03
0.7	1.611816659000000	1.611816670000000	1.1000000000E-08	2.7282100000E-04	9.7741000000E-04
0.8	1.770913792000000	1.770913802000000	1.0000000000E-08	2.4029100000E-04	8.6086700000E-04
0.9	1.910257489000000	1.910257499000000	1.0000000000E-08	2.0928600000E-04	7.4978500000E-04
1.0	2.031029734000000	2.031029742000000	8.0000000000E-09	1.8051200000E-04	6.4670200000E-04

$$\varphi_2(\xi, \mathfrak{F}) = \cos\xi\left[\frac{\sigma^2\mathfrak{F}^{2\sigma}}{\Gamma(2\sigma+1)} + 2\sigma(1-\sigma)\frac{\mathfrak{F}^{\sigma}}{\Gamma(\sigma+1)} + (1-\sigma)^2\right],$$
$$\nu_2(\xi, \mathfrak{F}) = \cos\xi\left[\frac{\sigma^2\mathfrak{F}^{2\sigma}}{\Gamma(2\sigma+1)} + 2\sigma(1-\sigma)\frac{\mathfrak{F}^{\sigma}}{\Gamma(\sigma+1)} + (1-\sigma)^2\right]. \tag{66}$$

The approximate solution to the series is written as

$$\varphi(\xi, \mathfrak{F}) = \sum_{m=0}^{\infty}\varphi_m(\xi, \mathfrak{F}) = \varphi_0(\xi, \mathfrak{F}) + \varphi_1(\xi, \mathfrak{F}) + \varphi_2(\xi, \mathfrak{F}) + \cdots$$
$$\nu(\xi, \mathfrak{F}) = \sum_{m=0}^{\infty}\nu_m(\xi, \mathfrak{F}) = \nu_0(\xi, \mathfrak{F}) + \nu_1(\xi, \mathfrak{F}) + \nu_2(\xi, \mathfrak{F}) + \cdots$$
$$\varphi(\xi, \mathfrak{F}) = \cos\xi - \cos\xi\left[\frac{\sigma\mathfrak{F}^{\sigma}}{\Gamma(\sigma+1)} + (1-\sigma)\right] + \cos\xi\left[\frac{\sigma^2\mathfrak{F}^{2\sigma}}{\Gamma(2\sigma+1)} + 2\sigma(1-\sigma)\frac{\mathfrak{F}^{\sigma}}{\Gamma(\sigma+1)} + (1-\sigma)^2\right] + \cdots \tag{67}$$
$$\nu(\xi, \mathfrak{F}) = \cos\xi - \cos\xi\left[\frac{\sigma\mathfrak{F}^{\sigma}}{\Gamma(\sigma+1)} + (1-\sigma)\right] + \cos\xi\left[\frac{\sigma^2\mathfrak{F}^{2\sigma}}{\Gamma(2\sigma+1)} + 2\sigma(1-\sigma)\frac{\mathfrak{F}^{\sigma}}{\Gamma(\sigma+1)} + (1-\sigma)^2\right] + \cdots$$

We achieve the exact solution by putting $\sigma = 1$,

$$\varphi(\xi,\mathfrak{F}) = \cos\xi\left(1-\mathfrak{F}+\frac{\mathfrak{F}^2}{2}-\cdots\right),$$
$$\nu(\xi,\mathfrak{F}) = \cos\xi\left(1-\mathfrak{F}+\frac{\mathfrak{F}^2}{2}-\cdots\right). \tag{68}$$

In closed form, $\varphi(\xi,\mathfrak{F}) = \cos(\xi)\exp^{-\mathfrak{F}}$ and $\nu(\xi,\mathfrak{F}) = \cos(\xi)\exp^{-\mathfrak{F}}$.

5.3.1. VITM Analytical Results. For (57), we have the iteration formula:

$$\varphi_{m+1}(\xi,\mathfrak{F}) = \varphi_m(\xi,\mathfrak{F}) - L^{-1}\left[\frac{\omega^\sigma+\sigma(1-\omega^\sigma)}{\omega^\sigma}L\left\{\frac{\omega^\sigma}{\omega^\sigma+\sigma(1-\omega^\sigma)}\frac{\partial^2\varphi_m}{\partial\xi^2}+2\varphi_m\frac{\partial\varphi_m}{\partial\xi}-\frac{\partial}{\partial\xi}(\varphi_m\nu_m)\right\}\right],$$
$$\nu_{m+1}(\xi,\mathfrak{F}) = \nu_m(\xi,\mathfrak{F}) - L^{-1}\left[\frac{\omega^\sigma+\sigma(1-\omega^\sigma)}{\omega^\sigma}L\left\{\frac{\omega^\sigma}{\omega^\sigma+\sigma(1-\omega^\sigma)}\frac{\partial^2\nu_m}{\partial\xi^2}+2\nu_m\frac{\partial\nu}{\partial\xi}-\frac{\partial}{\partial\xi}(\varphi_m\nu_m)\right\}\right], \tag{69}$$

where

$$\varphi(\xi,0) = \cos\xi, \quad \nu(\xi,0) = \cos\xi. \tag{70}$$

For $m = 0, 1, 2, \cdots$,

$$\varphi_1(\xi,\mathfrak{F}) = \varphi_0(\xi,\mathfrak{F}) - L^{-1}\left[\frac{\omega^\sigma+\sigma(1-\omega^\sigma)}{\omega^\sigma}L\left\{\frac{\omega^\sigma}{\omega^\sigma+\sigma(1-\omega^\sigma)}\frac{\partial^2\varphi_0}{\partial\xi^2}+2\varphi_0\frac{\partial\varphi_0}{\partial\xi}-\frac{\partial}{\partial\xi}(\varphi_0\nu_0)\right\}\right],$$
$$\varphi_1(\xi,\mathfrak{F}) = -\cos\xi\left[\frac{\sigma\mathfrak{F}^\sigma}{\Gamma(1-\sigma)}+(1-\sigma)\right],$$
$$\nu_1(\xi,\mathfrak{F}) = \nu_0(\xi,\mathfrak{F}) - L^{-1}\left[\frac{\omega^\sigma+\sigma(1-\omega^\sigma)}{\omega^\sigma}L\left\{\frac{\omega^\sigma}{\omega^\sigma+\sigma(1-\omega^\sigma)}\frac{\partial^2\nu_0}{\partial\xi^2}+2\nu_0\frac{\partial\nu}{\partial\xi}-\frac{\partial}{\partial\xi}(\varphi_0\nu_0)\right\}\right],$$
$$\nu_1(\xi,\mathfrak{F}) = -\cos\xi\left[\frac{\sigma\mathfrak{F}^\sigma}{\Gamma(\sigma+1)}+(1-\sigma)\right],$$
$$\varphi_2(\xi,\mathfrak{F}) = \varphi_1(\xi,\mathfrak{F}) - L^{-1}\left[\frac{\omega^\sigma+\sigma(1-\omega^\sigma)}{\omega^\sigma}L\left\{\frac{\omega^\sigma}{\omega^\sigma+\sigma(1-\omega^\sigma)}\frac{\partial^2\varphi_1}{\partial\xi^2}+2\varphi_1\frac{\partial\varphi_1}{\partial\xi}-\frac{\partial}{\partial\xi}(\varphi_0\nu_0)\right\}\right],$$
$$\varphi_2(\xi,\mathfrak{F}) = \cos\xi\left[\frac{\sigma^2\mathfrak{F}^{2\sigma}}{\Gamma(2\sigma+1)}+2\sigma(1-\sigma)\frac{\mathfrak{F}^\sigma}{\Gamma(\sigma+1)}+(1-\sigma)^2\right], \tag{71}$$
$$\nu_2(\xi,\mathfrak{F}) = \nu_1(\xi,\mathfrak{F}) - L^{-1}\left[\frac{\omega^\sigma+\sigma(1-\omega^\sigma)}{\omega^\sigma}L\left\{\frac{\omega^\sigma}{\omega^\sigma+\sigma(1-\omega^\sigma)}\frac{\partial^2\nu_1}{\partial\xi^2}+2\nu_1\frac{\partial\nu}{\partial\xi}-\frac{\partial}{\partial\xi}(\varphi_0\nu_0)\right\}\right],$$
$$\nu_1(\xi,\mathfrak{F}) = \cos\xi\left[\frac{\sigma^2\mathfrak{F}^{2\sigma}}{\Gamma(2\sigma+1)}+2\sigma(1-\sigma)\frac{\mathfrak{F}^\sigma}{\Gamma(\sigma+1)}+(1-\sigma)^2\right],$$
$$\varphi(\xi,\mathfrak{F}) = \cos\xi - \cos\xi\left[\frac{\sigma\mathfrak{F}^\sigma}{\Gamma(\sigma+1)}+(1-\sigma)\right] + \cos\xi\left[\frac{\sigma^2\mathfrak{F}^{2\sigma}}{\Gamma(2\sigma+1)}+2\sigma(1-\sigma)\frac{\mathfrak{F}^\sigma}{\Gamma(1-\sigma)}+(1-\sigma)^2\right]+\cdots$$
$$\nu(\xi,\mathfrak{F}) = \cos\xi - \cos\xi\left[\frac{\sigma\mathfrak{F}^\sigma}{\Gamma(\sigma+1)}+(1-\sigma)\right] + \cos\xi\left[\frac{\sigma^2\mathfrak{F}^{2\sigma}}{\Gamma(2\sigma+1)}+2\sigma(1-\sigma)\frac{\mathfrak{F}^\sigma}{\Gamma(1-\sigma)}+(1-\sigma)^2\right]+\cdots$$

We achieve the exact solution by putting $\sigma = 1$,

$$\varphi(\xi, \mathfrak{F}) = \cos\xi\left(1 - \mathfrak{F} + \frac{\mathfrak{F}^2}{2} - \cdots\right),$$
$$\nu(\xi, \mathfrak{F}) = \cos\xi\left(1 - \mathfrak{F} + \frac{\mathfrak{F}^2}{2} - \cdots\right). \tag{72}$$

In closed form, $\varphi(\xi, \mathfrak{F}) = \cos(\xi)\exp^{-\mathfrak{F}}$ and $\nu(\xi, \mathfrak{F}) = \cos(\xi)\exp^{-\mathfrak{F}}$.

In Figures 6(a) and 6(b), we display the solution graph at $\sigma = 1$ for $\varphi(\xi, \mathfrak{F}), \phi(\xi, \mathfrak{F})$ in the domain $-5 \le \psi, \phi \ge 5$, and Figures 6(c) and 6(d) show solution graph of absolute error and various fractional order solution. Also Table 6 demonstrates the error comparison of the exact and suggested methods solution at various orders. It is verified from the figures and table that our solution is closely related with the exact solution.

5.4. Problem 4. Consider the coupled Burgers equation two dimension

$$\frac{\partial^\sigma \varphi}{\partial \mathfrak{F}^\sigma} = \frac{\partial^2 \varphi}{\partial \xi^2} + 2\varphi\frac{\partial \varphi}{\partial \xi} - \frac{\partial}{\partial \xi}(\varphi\nu),$$
$$\frac{\partial^\sigma \nu}{\partial \mathfrak{F}^\sigma} = \frac{\partial^2 \nu}{\partial \xi^2} + 2\nu\frac{\partial \nu}{\partial \xi} - \frac{\partial}{\partial \xi}(\varphi\nu)\ 0 < \sigma \le 1, \tag{73}$$

with initial source

$$\varphi(\xi, 0) = \cos\xi, \quad \nu(\xi, 0) = \cos\xi. \tag{74}$$

On taking the Laplace transform of (73), we get

$$\frac{\omega^\sigma L[\varphi(\xi, \varpi, \mathfrak{F})] - \omega^{-1}\varphi(\xi, \varpi, 0)}{\omega^\sigma + \sigma(1 - \omega^\sigma)} = L\left[\frac{\partial^2 \varphi}{\partial \xi^2} + \frac{\partial^2 \varphi}{\partial \varpi^2} + 2\varphi\frac{\partial \varphi}{\partial \xi} - \frac{\partial}{\partial \xi}(\varphi\nu)\right].$$
$$\frac{\omega^\sigma L[\nu(\xi, \varpi, \mathfrak{F})] - \omega^{-1}\nu(\xi, \varpi, 0)}{\omega^\sigma + \sigma(1 - \omega^\sigma)} = L\left[\frac{\partial^2 \nu}{\partial \xi^2} + \frac{\partial^2 \nu}{\partial \varpi^2} + 2\nu\frac{\partial \nu}{\partial \xi} - \frac{\partial}{\partial \xi}(\varphi\nu)\right]. \tag{75}$$

We obtain when we use the Laplace inverse transform

$$\varphi(\xi, \varpi, \mathfrak{F}) = \cos(\xi + \varpi) + L^{-1}\left[\frac{\omega^\sigma + \sigma(1 - \omega^\sigma)}{\omega^\sigma} L\left[\frac{\partial^2 \varphi}{\partial \xi^2} + \frac{\partial^2 \varphi}{\partial \varpi^2} + 2\varphi\frac{\partial \varphi}{\partial \xi} - \frac{\partial}{\partial \xi}(\varphi\nu)\right]\right].$$
$$\nu(\xi, \varpi, \mathfrak{F}) = \cos(\xi + \varpi) + L^{-1}\left[\frac{\omega^\sigma + \sigma(1 - \omega^\sigma)}{\omega^\sigma} L\left[\frac{\partial^2 \nu}{\partial \xi^2} + \frac{\partial^2 \nu}{\partial \varpi^2} + 2\nu\frac{\partial \nu}{\partial \xi} - \frac{\partial}{\partial \xi}(\varphi\nu)\right]\right]. \tag{76}$$

Assume that the solution, $\varphi(\xi, \varpi, \mathfrak{F})$ and $\nu(\xi, \varpi, \mathfrak{F})$ in series form as

$$\varphi(\xi, \varpi, \mathfrak{F}) = \sum_{m=0}^{\infty} \varphi_m(\xi, \varpi, \mathfrak{F}), \quad \nu(\xi, \varpi, \mathfrak{F}) = \sum_{m=0}^{\infty} \nu_m(\xi, \varpi, \mathfrak{F}), \tag{77}$$

where $\varphi\varphi_\xi = \sum_{m=0}^{\infty} \mathscr{A}_m$, $(\varphi\nu)_\xi = \sum_{m=0}^{\infty} \mathscr{B}_m$, and $\nu\nu_\xi = \sum_{m=0}^{\infty} \mathscr{C}_m$ are Adomian polynomials that characterize the nonlinear terms, and so (76) is rewritten as

$$\sum_{m=0}^{\infty} \varphi_m(\xi, \varpi, \mathfrak{F}) = \cos(\xi + \varpi) + L^{-1}\left[\frac{\omega^\sigma + \sigma(1 - \omega^\sigma)}{\omega^\sigma} L\left[\frac{\partial^2 \varphi}{\partial \xi^2} + \frac{\partial^2 \varphi}{\partial \varpi^2} + 2\sum_{m=0}^{\infty} \mathscr{A}_m - \sum_{m=0}^{\infty} \mathscr{B}_m\right]\right].$$
$$\sum_{m=0}^{\infty} \nu_m(\xi, \varpi, \mathfrak{F}) = \cos(\xi + \varpi) + L^{-1}\left[\frac{\omega^\sigma + \sigma(1 - \omega^\sigma)}{\omega^\sigma} L\left[\frac{\partial^2 \nu}{\partial \xi^2} + \frac{\partial^2 \varphi}{\partial \varpi^2} + \sum_{m=0}^{\infty} \mathscr{C}_m - \sum_{m=0}^{\infty} \mathscr{B}_m\right]\right]. \tag{78}$$

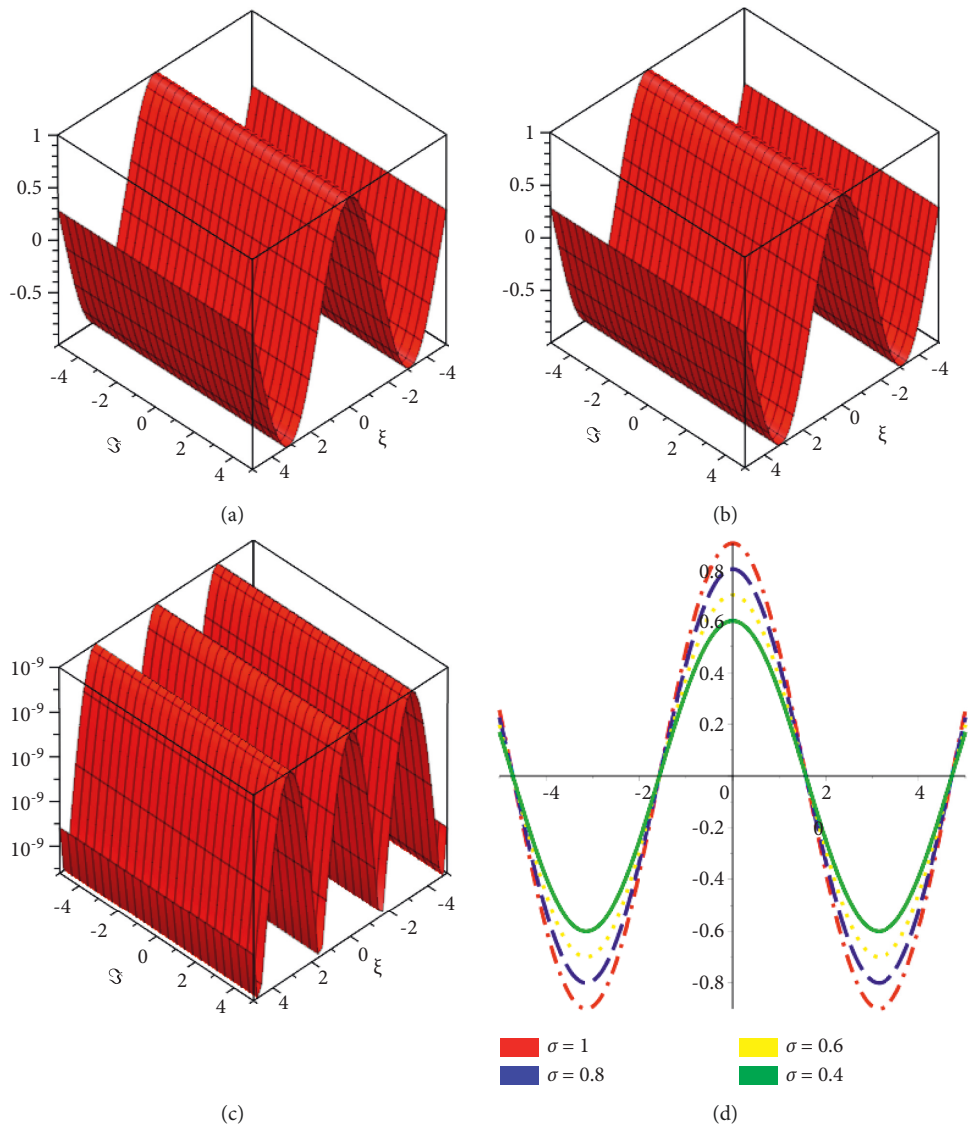

Figure 6: Exact solution, analytical solution, absolute error. and various fractional order solution for $\varphi(\xi, \mathfrak{I})$ and $\nu(\xi, \mathfrak{I})$ of problem 3.

Table 6: Comparison of the proposed method and exact results with absolute error (AE) at various fractional order for $\varphi(\xi, \mathfrak{I})$ and $\nu(\xi, \mathfrak{I})$ of problem 3.

$\mathfrak{I}$ = 0.0001	Exact solution	Proposed techniques solution	AE of proposed techniques	AE of proposed techniques	AE of proposed techniques
Υ	$\sigma = 1$	$\sigma = 1$	$\sigma = 1$	$\sigma = 0.9$	$\sigma = 0.8$
0	0.999900005000000	0.999900000000000	5.0000000000E-09	9.5960000000E-05	5.7744580000E-04
0.1	0.994904669900000	0.994904664900000	5.0000000000E-09	9.5480600000E-05	5.7456100000E-04
0.2	0.979968576000000	0.979968571100000	4.9000000000E-09	9.4047100000E-05	5.6593530000E-04
0.3	0.955240960200000	0.955240955500000	4.7000000000E-09	9.1674100000E-05	5.5165500000E-04
0.4	0.920968892500000	0.920968887900000	4.6000000000E-09	8.8385000000E-05	5.3186280000E-04
0.5	0.877494808000000	0.877494803600000	4.4000000000E-09	8.4212800000E-05	5.0675630000E-04
0.6	0.825253085500000	0.825253081300000	4.2000000000E-09	7.9199200000E-05	4.7658660000E-04
0.7	0.764765706900000	0.764765703100000	3.8000000000E-09	7.3394300000E-05	4.4165490000E-04
0.8	0.696637042100000	0.696637038600000	3.5000000000E-09	6.6856000000E-05	4.0231040000E-04
0.9	0.621547810400000	0.621547807300000	3.1000000000E-09	5.9649700000E-05	3.5894610000E-04
1.0	0.540248278400000	0.540248275700000	2.7000000000E-09	5.1847400000E-05	3.1199530000E-04

The decomposition of nonlinear terms by Adomian polynomials is defined as in equation (14),

$$\begin{aligned}
&\mathscr{A}_0 = \varphi_0\varphi_{0\xi}, \quad \mathscr{A}_1 = \varphi_1\varphi_{0\xi} + \varphi_0\varphi_{1\xi}, \quad \mathscr{A}_2 = \varphi_2\varphi_{0\xi} + \varphi_1\varphi_{1\xi} + \varphi_0\varphi_{2\xi},\\
&\mathscr{B}_0 = \varphi_0\nu_{0\xi} + \nu_0\varphi_{0\xi}, \quad \mathscr{B}_1 = \left(\varphi_0\nu_{0\xi} + \varphi_1\nu_{0\xi}\right) + \left(\nu_1\varphi_{0\xi} + \nu_0\varphi_{1\xi}\right),\\
&\mathscr{B}_2 = \left(\varphi_2\nu_{0\xi} + \varphi_1\nu_{1\xi} + \varphi_0\nu_{2\xi}\right) + \left(\nu_2\varphi_{0\xi} + \nu_1\varphi_{1\xi} + \nu_0\varphi_{2\xi}\right),\\
&\mathscr{C}_0 = \nu_0\nu_{0\xi}, \quad \mathscr{C}_1 = \nu_1\nu_{0\xi} + \nu_0\nu_{1\xi}, \quad \mathscr{C}_2 = \nu_2\nu_{0\xi} + \nu_1\nu_{1\xi} + \nu_0\nu_{2\xi}.
\end{aligned} \tag{79}$$

As a result, when comparing the two sides of (78),

$$\varphi(\xi, 0) = \cos\xi, \quad \nu(\xi, 0) = \cos\xi. \tag{80}$$

For $m = 0$,

$$\begin{aligned}
\varphi(\xi, \mathfrak{F}) &= \cos\xi\left(1 - \mathfrak{F} + \frac{\mathfrak{F}^2}{2} - \cdots\right),\\
\nu(\xi, \mathfrak{F}) &= \cos\xi\left(1 - \mathfrak{F} + \frac{\mathfrak{F}^2}{2} - \cdots\right).
\end{aligned} \tag{81}$$

For $m = 1$,

$$\begin{aligned}
\varphi_2(\xi, \varpi, \mathfrak{F}) &= 2\cos(\xi + \varpi)\left[\frac{\sigma^2\mathfrak{F}^{2\sigma}}{\Gamma(2\sigma+1)} + 2\sigma(1-\sigma)\frac{\mathfrak{F}^{\sigma}}{\Gamma(\sigma+1)} + (1-\sigma)^2\right],\\
\nu_2(\xi, \varpi, \mathfrak{F}) &= 2\cos(\xi + \varpi)\left[\frac{\sigma^2\mathfrak{F}^{2\sigma}}{\Gamma(2\sigma+1)} + 2\sigma(1-\sigma)\frac{\mathfrak{F}^{\sigma}}{\Gamma(\sigma+1)} + (1-\sigma)^2\right].
\end{aligned} \tag{82}$$

The approximate solution to the series is written as

$$\begin{aligned}
\varphi(\xi, \varpi, \mathfrak{F}) &= \sum_{m=0}^{\infty}\varphi_m(\xi, \mathfrak{F})\\
\nu(\xi, \varpi, \mathfrak{F}) &= \sum_{m=0}^{\infty}\nu_m(\xi, \mathfrak{F})\\
\varphi(\xi, \varpi, \mathfrak{F}) &= \cos(\xi + \varpi) - 2\cos(\xi + \varpi)\left[\frac{\sigma\mathfrak{F}^{\sigma}}{\Gamma(\sigma+1)} + (1-\sigma)\right]\\
&\quad + 2\cos(\xi + \varpi)\left[\frac{\sigma^2\mathfrak{F}^{2\sigma}}{\Gamma(2\sigma+1)} + 2\sigma(1-\sigma)\frac{\mathfrak{F}^{\sigma}}{\Gamma(\sigma-1)} + (1-\sigma)^2\right] + \cdots\\
\nu(\xi, \varpi, \mathfrak{F}) &= \cos(\xi + \varpi) - 2\cos(\xi + \varpi)\left[\frac{\sigma\mathfrak{F}^{\sigma}}{\Gamma(\sigma+1)} + (\sigma+1)\right] +\\
&\quad \cdot 2\cos(\xi + \varpi)\left[\frac{\sigma^2\mathfrak{F}^{2\sigma}}{\Gamma(2\sigma+1)} + 2\sigma(1-\sigma)\frac{\mathfrak{F}^{\sigma}}{\Gamma(\sigma+1)} + (\sigma+1)^2\right] + \cdots
\end{aligned} \tag{83}$$

We achieve the exact solution by putting $\sigma = 1$,

$$\begin{aligned}\varphi(\xi,\varpi,\mathfrak{F}) &= \cos(\xi+\varpi)\left(1-2\mathfrak{F}+\frac{4\mathfrak{F}^2}{2!}-\cdots\right),\\ \nu(\xi,\varpi,\mathfrak{F}) &= \cos(\xi+\varpi)\left(1-2\mathfrak{F}+\frac{4\mathfrak{F}^2}{2!}-\cdots\right).\end{aligned} \tag{84}$$

In closed form, $\varphi(\xi,\varpi,\mathfrak{F}) = \cos(\xi+\varpi)\exp^{-2\mathfrak{F}}$ and $\nu(\xi,\varpi,\mathfrak{F}) = \cos(\xi+\varpi)\exp^{-2\mathfrak{F}}$.

5.4.1. VITM Analytical Results. For (73), we have the iteration formula:

$$\begin{aligned}\varphi_{m+1}(\xi,\varpi,\mathfrak{F}) &= \varphi_m(\xi,\mathfrak{F}) - L^{-1}\left[\frac{\omega^\sigma+\sigma(1-\omega^\sigma)}{\omega^\sigma}L\left\{\frac{\omega^\sigma}{\omega^\sigma+\sigma(1-\omega^\sigma)}\frac{\partial^2\varphi_m}{\partial\xi^2}+\frac{\partial^2\varphi_m}{\partial\varpi^2}+2\varphi_m\frac{\partial\varphi_m}{\partial\xi}-\frac{\partial}{\partial\xi}(\varphi_m\nu_m)\right\}\right],\\ \nu_{m+1}(\xi,\varpi,\mathfrak{F}) &= \nu_m(\xi,\mathfrak{F}) - L^{-1}\left[\frac{\omega^\sigma+\sigma(1-\omega^\sigma)}{\omega^\sigma}L\left\{\frac{\omega^\sigma}{\omega^\sigma+\sigma(1-\omega^\sigma)}\frac{\partial^2\nu_m}{\partial\xi^2}+\frac{\partial^2\nu_m}{\partial\varpi^2}+2\nu_m\frac{\partial\nu_m}{\partial\xi}-\frac{\partial}{\partial\xi}(\varphi_m\nu_m)\right\}\right],\end{aligned} \tag{85}$$

where

$$\begin{aligned}\varphi_0(\xi,\varpi,\mathfrak{F}) &= \cos(\xi+\varpi),\\ \nu_0(\xi,\varpi,\mathfrak{F}) &= \cos(\xi+\varpi).\end{aligned} \tag{86}$$

For $m = 0, 1, 2, \cdots$,

$$\begin{aligned}\varphi_1(\xi,\varpi,\mathfrak{F}) &= \varphi_0(\xi,\mathfrak{F}) - L^{-1}\left[\frac{\omega^\sigma+\sigma(1-\omega^\sigma)}{\omega^\sigma}L\left\{\frac{\omega^\sigma}{\omega^\sigma+\sigma(1-\omega^\sigma)}\frac{\partial^2\varphi_0}{\partial\xi^2}+\frac{\partial^2\varphi_0}{\partial\varpi^2}+2\varphi_0\frac{\partial\varphi_0}{\partial\xi}-\frac{\partial}{\partial\xi}(\varphi_0\nu_0)\right\}\right],\\ \varphi_1(\xi,\varpi,\mathfrak{F}) &= -2\cos(\xi+\varpi)\left[\frac{\sigma\mathfrak{F}^\sigma}{\Gamma(\sigma+1)}+(1-\sigma)\right],\\ \nu_1(\xi,\varpi,\mathfrak{F}) &= \nu_0(\xi,\mathfrak{F}) - L^{-1}\left[\frac{\omega^\sigma+\sigma(1-\omega^\sigma)}{\omega^\sigma}L\left\{\frac{\omega^\sigma}{\omega^\sigma+\sigma(1-\omega^\sigma)}\frac{\partial^2\nu_0}{\partial\xi^2}+\frac{\partial^2\nu_0}{\partial\varpi^2}+2\nu_0\frac{\partial\nu_0}{\partial\xi}-\frac{\partial}{\partial\xi}(\varphi_0\nu_0)\right\}\right],\\ \nu_1(\xi,\varpi,\mathfrak{F}) &= -2\cos(\xi,\mathfrak{F})\left[\frac{\sigma\mathfrak{F}^\sigma}{\Gamma(\sigma+1)}+(1-\sigma)\right],\\ \varphi_2(\xi,\varpi,\mathfrak{F}) &= \varphi_1(\xi,\mathfrak{F}) - L^{-1}\left[\frac{\omega^\sigma+\sigma(1-\omega^\sigma)}{\omega^\sigma}L\left\{\frac{\omega^\sigma}{\omega^\sigma+\sigma(1-\omega^\sigma)}\frac{\partial^2\varphi_1}{\partial\xi^2}+\frac{\partial^2\varphi_1}{\partial\varpi^2}+2\varphi_1\frac{\partial\varphi_1}{\partial\xi}-\frac{\partial}{\partial\xi}(\varphi_0\nu_0)\right\}\right],\\ \varphi_2(\xi,\varpi,\mathfrak{F}) &= 2\cos(\xi,\mathfrak{F})\left[\frac{\sigma^2\mathfrak{F}^{2\sigma}}{\Gamma(2\sigma+1)}+2\sigma(1-\sigma)\frac{\mathfrak{F}^\sigma}{\Gamma(\sigma+1)}+(1-\sigma)^2\right],\\ \nu_2(\xi,\varpi,\mathfrak{F}) &= \nu_1(\xi,\mathfrak{F}) - L^{-1}\left[\frac{\omega^\sigma+\sigma(1-\omega^\sigma)}{\omega^\sigma}L\left\{\frac{\omega^\sigma}{\omega^\sigma+\sigma(1-\omega^\sigma)}\frac{\partial^2\nu_1}{\partial\xi^2}+\frac{\partial^2\nu_1}{\partial\varpi^2}+2\nu_1\frac{\partial\nu_1}{\partial\xi}-\frac{\partial}{\partial\xi}(\varphi_0\nu_0)\right\}\right],\\ \nu_2(\xi,\varpi,\mathfrak{F}) &= 2\cos(\xi,\mathfrak{F})\left[\frac{\sigma^2\mathfrak{F}^{2\sigma}}{\Gamma(2\sigma+1)}+2\sigma(1-\sigma)\frac{\mathfrak{F}^\sigma}{\Gamma(\sigma+1)}+(1-\sigma)^2\right],\\ \varphi(\xi,\varpi,\mathfrak{F}) &= \cos(\xi,\mathfrak{F})-2\cos(\xi+\varpi)\left[\frac{\sigma\mathfrak{F}^\sigma}{\Gamma(\sigma+1)}+(1-\sigma)\right]+2\cos(\xi+\varpi)\left[\frac{\sigma^2\mathfrak{F}^{2\sigma}}{\Gamma(2\sigma+1)}+2\sigma(1-\sigma)\frac{\mathfrak{F}^\sigma}{\Gamma(\sigma+1)}+(1-\sigma)^2\right],\\ \nu(\xi,\varpi,\mathfrak{F}) &= \cos(\xi,\mathfrak{F})-2\cos(\xi+\varpi)\left[\frac{\sigma\mathfrak{F}^\sigma}{\Gamma(\sigma+1)}+(1-\sigma)\right]+2\cos(\xi+\varpi)\left[\frac{\sigma^2\mathfrak{F}^{2\sigma}}{\Gamma(2\sigma+1)}+2\sigma(1-\sigma)\frac{\mathfrak{F}^\sigma}{\Gamma(\sigma+1)}+(1-\sigma)^2\right]\end{aligned} \tag{87}$$

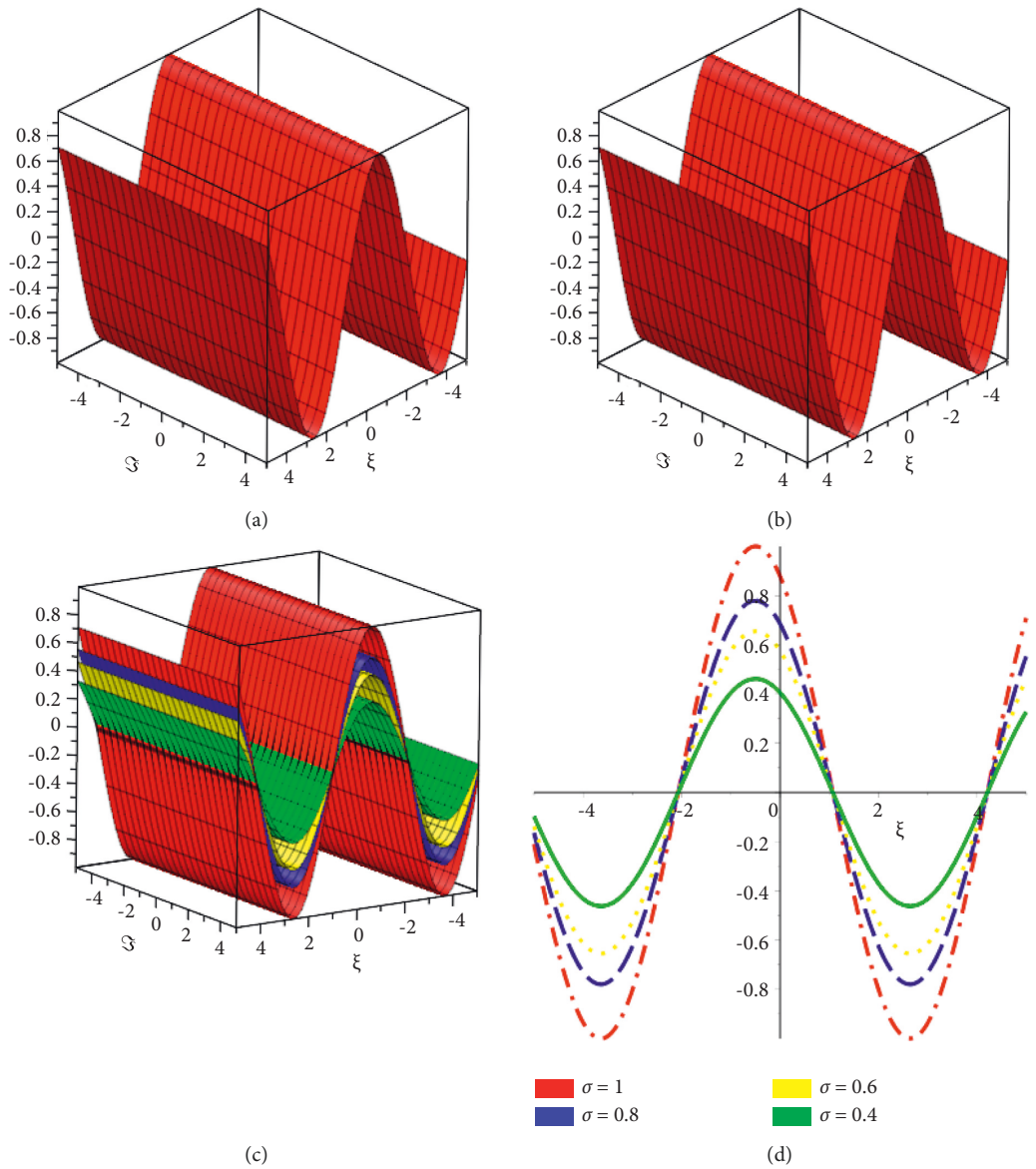

Figure 7: Exact solution, analytical solution, absolute error, and various fractional order solution for $\varphi(\xi, \mathfrak{T})$ and $\nu(\xi, \mathfrak{T})$ of problem 4.

Table 7: Comparison of the proposed method and exact results with absolute error (AE) at various fractional order for $\varphi(\xi, \mathfrak{T})$ and $\nu(\xi, \mathfrak{T})$ of problem 4.

$\mathfrak{T}$ = 0.0001	Exact solution	Proposed techniques solution	AE of proposed techniques	AE of proposed techniques	AE of proposed techniques
Υ	$\sigma = 1$	$\sigma = 1$	$\sigma = 1$	$\sigma = 0.9$	$\sigma = 0.8$
0	0.877407062900000	0.877407045400000	1.7500000000E-08	2.8290530000E-04	1.0135215000E-03
0.1	0.825170564300000	0.825170547800000	1.6500000000E-08	2.6606260000E-04	9.5318140000E-04
0.2	0.764689234200000	0.764689218900000	1.5300000000E-08	2.4656140000E-04	8.8331750000E-04
0.3	0.696567381900000	0.696567368000000	1.3900000000E-08	2.2459660000E-04	8.0462770000E-04
0.4	0.621485658700000	0.621485646300000	1.2400000000E-08	2.0038770000E-04	7.1789830000E-04
0.5	0.540194256200000	0.540194245400000	1.0800000000E-08	1.7417660000E-04	6.2399600000E-04
0.6	0.453505411200000	0.453505402200000	9.0000000000E-09	1.4622520000E-04	5.2385880000E-04
0.7	0.362285290200000	0.362285282900000	7.3000000000E-09	1.1681290000E-04	4.1848760000E-04
0.8	0.267445334200000	0.267445328800000	5.4000000000E-09	8.6233300000E-05	3.0893480000E-04
0.9	0.169933152900000	0.169933149500000	3.4000000000E-09	5.4792200000E-05	1.9629540000E-04
1.0	0.070723055640000	0.070723054230000	1.4100000000E-09	2.2803470000E-05	8.1694500000E-05

We achieve the exact solution by putting $\sigma = 1$,

$$\varphi(\xi, \varpi, \mathfrak{F}) = \cos(\xi + \varpi)\left(1 - 2\mathfrak{F} + \frac{4\mathfrak{F}^2}{2!} - \cdots\right),$$
$$\nu(\xi, \varpi, \mathfrak{F}) = \cos(\xi + \varpi)\left(1 - 2\mathfrak{F} + \frac{4\mathfrak{F}^2}{2!} - \cdots\right). \tag{88}$$

In closed form, $\varphi(\xi, \varpi, \mathfrak{F}) = \cos(\xi + \varpi)\exp^{-2\mathfrak{F}}$, and $\nu(\xi, \varpi, \mathfrak{F}) = \cos(\xi + \varpi)\exp^{-2\mathfrak{F}}$.

Figures 7(a) and 7(b) show the behavior of the exact and analytical solutions, respectively, whereas Figures 7(c) and 7(d) show the graphical perspective for various fractional orders. Table 7 also shows the behaviour of the exact and suggested method solutions in addition with absolute error at various orders of σ. Finally, the figures and tables show that the suggested techniques have higher degree of accuracy and rapid convergence towards the exact results.

6. Conclusion

The LTDM and VITM were used for solving of coupled nonlinear partial differential equations. On comparing the results of these methods with the exact solution, it is observed that proposed methods are extremely simple and easy to handle the nonlinear terms. The obtained results converge quickly in the form of series towards the exact solution. Four nonlinear systems are solved which shows that the suggested techniques solution are in strong agreement with the exact solution. It is confirmed that the proposed methods need much less computational work which shows fast convergence. Furthermore, LTDM and VITM are very effective and efficient for finding out the approximate analytic solutions for a wide range of real world problems arising in engineering and science.

Data Availability

The numerical data used to support the findings of this study are included within the article.

Conflicts of Interest

The authors declare that they have no conflicts of interest.

Acknowledgments

The authors extend their appreciation to the Deanship of Scientific Research at King Khalid University for funding this work through Larg Groups (R.G.P2./41/43).

References

[1] A. Atangana and D. Baleanu, "New fractional derivatives with nonlocal and non-singular kernel: theory and application to heat transfer model," *Thermal Science*, vol. 20, no. 2, pp. 763–769, 2016, arXiv preprint arXiv:1602.03408.

[2] M. Caputo, "Linear models of dissipation whose Q is almost frequency independent-II," *Geophysical Journal International*, vol. 13, no. 5, pp. 529–539, 1967.

[3] M. Caputo and M. Fabrizio, "A new definition of fractional derivative without singular kernel," *Progr. Fract. Differ. Appl*, vol. 1, no. 2, pp. 1–13, 2015.

[4] M. Areshi, A. Khan, R. Shah, and K. Nonlaopon, "Analytical investigation of fractional-order Newell-Whitehead-Segel equations via a novel transform," *AIMS Mathematics*, vol. 7, no. 4, pp. 6936–6958, 2022.

[5] R. L. Bagley and P. J. Torvik, "A theoretical basis for the application of fractional calculus to viscoelasticity," *Journal of Rheology*, vol. 27, no. 3, pp. 201–210, 1983.

[6] T. S. Chow, "Fractional dynamics of interfaces between soft-nanoparticles and rough substrates," *Physics Letters A*, vol. 342, no. 1-2, pp. 148–155, 2005.

[7] R. T. Baillie, "Long memory processes and fractional integration in econometrics," *Journal of Econometrics*, vol. 73, no. 1, pp. 5–59, 1996.

[8] M. Feckan, T. Sathiyaraj, and J. Wang, "Synchronization of butterfly fractional order chaotic system," *Mathematics*, vol. 8, no. 3, p. 446, 2020.

[9] T. Sathiyaraj, J. Wang, and D. O'Regan, "Controllability of stochastic nonlinear oscillating delay systems driven by the Rosenblatt distribution," *Proceedings of the Royal Society of Edinburgh Section A: Mathematics*, vol. 151, no. 1, pp. 217–239, 2021.

[10] T. Sathiyaraj and P. Balasubramaniam, "Controllability of Hilfer fractional stochastic system with multiple delays and Poisson jumps," *The European Physical Journal - Special Topics*, vol. 228, no. 1, pp. 245–260, 2019.

[11] T. Sathiyaraj and P. Balasubramaniam, "Controllability of fractional order stochastic differential inclusions with fractional Brownian motion in finite dimensional space," *IEEE/CAA Journal of Automatica Sinica*, vol. 3, no. 4, pp. 400–410, 2016.

[12] J. Wu, "Theory and applications of partial functional differential equations," *Applied Mathematical Sciences*, vol. 119, 1996.

[13] Y. Qin, A. Khan, I. Ali et al., "An efficient analytical approach for the solution of certain fractional-order dynamical systems," *Energies*, vol. 13, no. 11, p. 2725, 2020.

[14] X. J. Yang and D. Baleanu, "Numerical investigation of the time-fractional whitham-broer-kaup equation involving without singular kernel operators," *Complexity*, vol. 17, no. 2, pp. 625–628.

[15] A. Kumar, N. Kumar, G. Kumar, M. Patel, and P. Gupta, "Laparoscopic transperitoneal partial nephrectomy for clinical T1b renal tumors: a prospective evaluation," *Central European journal of urology*, vol. 70, no. 2, pp. 213–230, 2017.

[16] S. H. Mirmoradia, I. Hosseinpoura, S. Ghanbarpour, and A. Barari, "Application of an approximate analytical method to nonlinear Troesch's problem," *Applied Mathematical Sciences*, vol. 3, no. 32, pp. 1579–1585, 2009.

[17] H. Khan, A. Khan, P. Kumam, D. Baleanu, and M. Arif, "An approximate analytical solution of the Navier-Stokes equations within Caputo operator and Elzaki transform decomposition method," *Advances in Difference Equations*, vol. 2020, no. 1, pp. 1–23, 2020.

[18] H. Khan, A. Khan, M. Al-Qurashi, R. Shah, and D. Baleanu, "Modified modelling for heat like equations within Caputo operator," *Energies*, vol. 13, no. 8, p. 2002, 2020.

[19] D. J. Evans and K. R. Raslan, "The Adomian decomposition method for solving delay differential equation," *International Journal of Computer Mathematics*, vol. 82, no. 1, pp. 49–54, 2005.

[20] N. Iqbal, A. Akgul, R. Shah, A. Bariq, M. Mossa Al-Sawalha, and A. Ali, "On solutions of fractional-order gas dynamics equation by effective techniques," *Journal of Function Spaces*, vol. 2022, pp. 1–14, 2022.

[21] H. Khan, U. Farooq, R. Shah, D. Baleanu, P. Kumam, and M. Arif, "Analytical solutions of (2+ time fractional order) dimensional physical models, using modified decomposition method," *Applied Sciences*, vol. 10, no. 1, p. 122, 2019.

[22] R. P. Agarwal, F. Mofarreh, R. Shah, W. Luangboon, and K. Nonlaopon, "An analytical technique, based on natural transform to solve fractional-order parabolic equations," *Entropy*, vol. 23, no. 8, p. 1086, 2021.

[23] R. Shah, U. Farooq, H. Khan, D. Baleanu, P. Kumam, and M. Arif, "Fractional view analysis of third order Kortewege-De Vries equations, using a new analytical technique," *Frontiers in Physics*, vol. 7, p. 244, 2020.

[24] Y. Keskin and G. Oturanc, "Reduced differential transform method for partial differential equations," *International Journal of Nonlinear Sciences and Numerical Stimulation*, vol. 10, no. 6, pp. 741–750, 2009.

[25] Z. J. Liu, M. Y. Adamu, E. Suleiman, and J. H. He, "Hybridization of homotopy perturbation method and Laplace transformation for the partial differential equations," *Thermal Science*, vol. 21, no. 4, pp. 1843–1846, 2017.

[26] J. Hristov, "An exercise with the He's variation iteration method to a fractional Bernoulli equation arising in transient conduction with non-linear heat flux at the boundary," *Int. Rev. Chem. Eng*, vol. 4, no. 5, pp. 489–497, 2012.

[27] C. F. Liu, S. S. Kong, and S. J. Yuan, "Reconstructive schemes for variational iteration method within Yang-Laplace transform with application to fractal heat conduction problem," *Thermal Science*, vol. 17, no. 3, pp. 715–721, 2013.

[28] H. Bateman, "Some recent researches on the motion of fluids," *Monthly Weather Review*, vol. 43, no. 4, pp. 163–170, 1915.

[29] A. Naghipour and J. Manafian, "Application of the Laplace Adomian decomposition and implicit methods for solving Burgers equation," *TWMS Journal of Pure and Applied Mathematics*, vol. 6, no. 1, pp. 68–77, 2015.

[30] M. M. Rashidi and E. Erfani, "Laplace decomposition for solving nonlinear system of fractional order partial differential equations," *Advance in difference equations*, vol. 180, no. 9, pp. 1539–1544, 2020.

[31] W. M. Moslem and R. Sabry, "Zakharov-Kuznetsov-Burgers equation for dust ion acoustic waves," *Chaos, Solitons & Fractals*, vol. 36, no. 3, pp. 628–634, 2008.

Hindawi
Complexity
Volume 2022, Article ID 8321848, 13 pages
https://doi.org/10.1155/2022/8321848

Research Article

Immunokinetic Model for COVID-19 Patients

Y. Fadaei,[1] **F. A. Rihan**,[2] **and C. Rajivganthi**[3]

[1]*Modeling in Health Research Center, Shahrekord University of Medical Sciences, Shahrekord, Iran*
[2]*Department of Mathematical Sciences, College of Science, United Arab Emirates University, Al-Ain 15551, UAE*
[3]*Department of Mathematics, Vellore Institute of Technology, Vandalur, Kelambakkam Road, Chennai 600127, India*

Correspondence should be addressed to Y. Fadaei; fadaei.yasin@gmail.com and F. A. Rihan; frihan@uaeu.ac.ae

Received 19 November 2021; Revised 24 December 2021; Accepted 8 April 2022; Published 7 June 2022

Academic Editor: Ning Cai

In this paper, we develop a fractional-order differential model for the dynamics of immune responses to SARS-CoV-2 viral load in one host. In the model, a fractional-order derivative is incorporated to represent the effects of temporal long-run memory on immune cells and tissues for any age group of patients. The population of cytotoxic T cells ($CD8^+$), natural killer (NK) cells, and infected viruses is unknown in this model. Some interesting sufficient conditions that ensure the asymptotic stability of the steady states are obtained. This model indicates some complex phenomena in COVID-19 such as "immune exhaustion" and "long COVID." Sensitivity analysis is also investigated for model parameters to determine the parameters that are effective in disease control and future treatment as well as vaccine design. The model is verified with clinical and experimental data of 5 patients with COVID-19.

1. Introduction

The ongoing pandemic coronavirus pandemic (COVID-19), caused by the SARS-CoV-2 virus, started in Wuhan, China, in December 2019 and has spread to more than 197 countries. The rapid spread of this disease threatens the health of a large number of people. As a result, immediate measures must be taken to prevent the disease in the community. It is the seventh member of the coronavirus (CoV) family, along with MERS-CoV and SARS-CoV [1]. The virus is very serious and spread through respiratory droplets and close contact [2]. Scientists and researchers are therefore interested in how to develop treatment methods for such infectious diseases. Those methods are useful in understanding the dynamics/interactions between pathogens and their hosts. For years, mathematical modelers have been addressing specific aspects of infectious diseases [3, 4]. The majority of these efforts have been focused on multilevel diseases and have adopted quite different computational approaches [5–9].

Humans may develop upper respiratory tract infections as a result of COVID-19 transmission at the cellular level. Human cells have healthy, infected, virus cells, and antibodies that are input parameters, and the output will be infected lung cells. The transmission of CoV among groups has been discussed in many research papers [10–12]. Despite this, the dynamics of CoV infection in an individual (organism) [22] are not extensively explored in the literature, which we analyze in the present paper.

In epidemiology and immunology, mathematical models are used to understand the dynamics of infectious diseases. In general, the coronavirus model depends on the initial conditions, and the classical order model cannot explain the virus perfectly because of its local nature.

Fractional-order derivatives are nonlocal in nature and are also dependent on the initial values. Furthermore, the fractional-order model has more advantages in terms of best fitting data, information about its memory, and hereditary properties. Furthermore, the hereditary properties increase the utility of the models constructed in fractional-order derivatives to describe the real phenomenon (see [13, 14]). In [15], the authors studied the transmission dynamics of fractional-order coronavirus models and compared our results with some real data against confirmed infection and death cases per day for the first 67 days in Wuhan. According to [16], the authors compared the results of integer and fractional-order coronavirus (SEIRD) models, using real

data from Italy, reported by the WHO. The results proved that the fractional-order case has a less root-mean-square error of fitting the model to the real data than the classical one, and the fractional model has a closer estimation of the reality. Singh et al. [17] discussed the discretization computational techniques to solve numerically a fractional-order coronavirus model, and this technique is effective to show the behavior of the solution in a very long time period which is helpful to predict the coronavirus model accurately. Most of the authors studied the coronavirus dynamics in the sense of fractional-order derivatives ([18–21]). At the level of cells, the authors in [22] studied the dynamics of a fractional-order delay differential model for coronavirus (CoV) infection to give us the best understanding of what causes the intensity of symptoms and illness of contaminated lung and respiratory system; see also [23–25].

As a result of the above motivation, in this paper, we propose a fractional-order model for coronaviruses with three compartments, such as SARS-CoV-2 density, cytotoxic T cells, and natural killer cells. The Caputo fractional derivative has a power-law kernel, where its decaying rate depends directly on the fractional orders. For the considered model, we derive the positiveness of the solution and examine the local stability of existing equilibrium points. By using the important sensitive parameters, we study the model qualitatively to demonstrate the eradication of the disease. As graphs, we can show more interesting results and their theoretical and numerical justifications.

This paper is organized as follows: in Section 2, we propose a virus infection model and study the positivity solution and local stability results. In Section 3, we discuss parameter estimation. Section 4 provides numerical simulations to validate the obtained theoretical results. Section 5 provides sensitivity analyses. The conclusion is in Section 6.

2. The Mathematical Model

Herein, we develop a fractional-order mathematical model for the immune system response to the SARS-CoV-2 virus in COVID-19 patients. We consider the RNA SARS-CoV-2 viral load (S), a cell population of the innate immune system: natural killer (NK) cells, and a cell population of the adaptive immune system: cytotoxic ($CD8^+$) T cells (T). Also, we assume that t represents the variable time (day). The assumptions of the model are as follows:

(i) The population of infected cells and the SARS CoV 2 virus concentration are assumed same

(ii) The SARS-CoV-2 virus in the absence of an immune response grows logistically that is based on the fitting of the data [26]

(iii) The infected virus can be cleared by both NK and $CD8^+$ cells [26, 27]

(iv) The virus promotes an initial activation of NK and $CD8^+$ cells at the beginning of the disease [28, 30]

(v) The total number of NK cells was decreased in patients after some number of encounters with SARS-CoV-2 infection [30]

Based on the above assumptions, the system of fractional differential equations for representing interactions of the SARS-CoV-2 virus and the immune system is given by

$$\begin{aligned} D^{\alpha}S(t) &= a_1 S(t)(1 - bS(t)) - d_{st}S(t)\mathcal{F}(S,T) - d_{sn}S(t)N(t) - d_1 S(t),\\ D^{\alpha}T(t) &= b_t + r\mathcal{G}(S)T(t) + e_1 N(t)S(t) - qT(t)S(t) - d_t T(t),\\ D^{\alpha}N(t) &= b_n + k\mathcal{G}(S)N(t) - d_{ns}N(t)S(t) - d_n N(t), \end{aligned} \tag{1}$$

where $D^{\alpha} = \mathrm{d}^{\alpha}/\mathrm{d}t^{\alpha}$ defined in Caputo sense. In the equations, three cell populations are denoted by $S(t)$ = density of SARS-CoV-2 (copies/ml), $T(t)$ = total cytotoxic T cells population (cell/ ml), and $N(t)$ = total natural killer cells (cell/ml).

The term $\mathcal{F}(S,T) = (T/S)^{\alpha}/z + (T/S)^{\alpha}$ is fractional viral clearance rate of rational form by activated cytotoxic T cells which is based on de Pillis–Radunskaya Law [36]. However, $\mathcal{G}(S) = S^n/c_1^n + S^n$ is a modified Michaelis-Menten term for T cells activation and NK cell recruitment by SARS-CoV-2. $S(0) = S_0 > 0, T(0) = T_0 > 0, N(0) = N_0 > 0$ are initial conditions of the system (1), and $0 < \alpha \leq 1$ is derivative order.

The dynamics of the SARS-CoV-2 is represented by the first equation of the system (1). Infected virus growth is logistical with replication rate a_1 and carrying capacity b. Virus lysis by $CD8^+$ T cells is shown by $d_{st}S\mathcal{F}$, and the term $d_{sn}SN$ represents the virus death by NK cells. The viral clearance rate is presented by d_1.

The second equation shows the dynamic of the $CD8^+$ T cells against infected virus. Birth and death of $CD8^+$ T cells are represented by b_t and $d_t T$ terms [31]. The term $r\mathcal{R}T$ shows amount of $CD8^+$ T cells activation by infected virus. The term $e_1 NS$ represents recruitment of $CD8^+$ T cells by the debris from virus lysed by NK cells [32]. Inactivation of $CD8^+$ T cells by infected virus is shown by qTS term. Behavior of NK cells is represented by third equation. NK cells activation by SARS-CoV-2 is shown by $k\mathcal{R}N$. The term $d_{ns}NS$ is inactivation terms of NK cells by infected cells. Natural death of NK cells is represented by $d_n N$ term.

Definition 1. [14] Caputo derivative of fractional-order α for a function $f(t)$ is described as

$$D^{\alpha}f(t) = \frac{1}{\Gamma(n-\alpha)}\int_0^t (t-\tau)^{n-\alpha-1} f^n(\tau)\mathrm{d}\tau, \tag{2}$$

where $n - 1 < \alpha < n \in \mathbb{Z}^+$, $\Gamma(\cdot)$ is the Gamma function.

The Laplace transform of the Caputo derivative is described as

$$L\{D^{\alpha} f(t); s\} = s^{\alpha} F(s) - \sum_{i=1}^{n-1} s^{\alpha - i - 1} f^{(i)}(0), \tag{3}$$

where $F(s) = L\{f(t)\}$. In particular, when $f^{(i)}(0) = 0$, $i = 1, 2, \ldots, n-1$, then $L\{D^{\alpha} f(t); s\} = s^{\alpha} F(s)$.

The basic reproductive rate/ratio $\mathscr{R}_0$ is defined as the expected number of secondary infections arising from a single individual during his or her entire infectious period, in a population of susceptible. Epidemiology and pathogen dynamics within hosts are both based on this concept. Furthermore, $\mathscr{R}_0$ is used as a threshold parameter that predicts whether an infection will spread. However, related parameters that share this threshold behavior may or may not give the true value of $\mathscr{R}_0$. It also denotes as the number of secondary infection due to a single infection in a completely susceptible population. We derive the expression of $\mathscr{R}_0$, allied to the disease-free equilibrium $\mathscr{E}_0(S_0 = 0, T_0 = 0, N_0 = 0)$. The recovery rate from the virus and transmission rate of the virus from infected individuals to susceptible individuals are described by the following matrices:

$$\mathbb{D} = \begin{pmatrix} d_1 & 0 & 0 \\ 0 & 0 & 0 \\ 0 & 0 & 0 \end{pmatrix}, \qquad \mathbb{B} = \begin{pmatrix} a_1 & 0 & 0 \\ 0 & -d_t & 0 \\ 0 & 0 & -d_n \end{pmatrix}. \tag{4}$$

Thus, the basic reproduction number $\mathscr{R}_0 = \rho(\mathbb{D}^{-1}\mathbb{B})$, calculated as the spectral radius of the next generation matrix [33], is then defined by

$$\mathscr{R}_0 = \frac{a_1 d_t d_n}{d_1}. \tag{5}$$

The disease is eradicated if $\mathscr{R}_0 \le 1$ and will persist as t goes to infinity if $\mathscr{R}_0 > 1$; see [34].

2.1. Nonnegativity of the Model Solutions. Herein, we investigate the nonnegativity of the model solutions.

Lemma 1 (Generalized Mean Value Theorem [35]). *Let the function $f(t) \in \mathscr{C}[a, b]$ and its fractional derivative $D^{\alpha} f(t) \in \mathscr{C}(a, b]$ for $0 < \alpha \le 1$ and $a, b \in \mathbb{R}$, then we have*

$$f(t) = f(a) + \frac{1}{\Gamma(\alpha)} D^{\alpha} f(\xi)(t-a)^{\alpha}, \quad 0 \le \xi \le t, \text{ for every } t \in (a, b]. \tag{6}$$

Remark 1. Assume that the function $f(t)$ is α-differentiable on (a, b), then we have the following results [14]:

(i) If $D^{\alpha} f(t) < 0$ for all $t \in (a, b)$, then $f(t)$ is decreasing on (a, b)

(ii) If $D^{\alpha} f(t) > 0$ for all $t \in (a, b)$, then $f(t)$ is increasing on (a, b)

(iii) If $D^{\alpha} f(t) = 0$ for all $t \in (a, b)$, then $f(t)$ is constant on (a, b)

Lemma 2. *The solutions of model (1) with nonnegative initial values are nonnegative.*

Proof. To show this Lemma, we ought to consider that the domain $\Omega = \{(S, T, N) \in \mathbb{R}^3 : S \ge 0, T \ge 0, N \ge 0\}$ is a positively invariant region. Then, on the hyperplanes of the region Ω, we have

$$\begin{aligned} D^{\alpha} S(t)_{S=0} &= 0, \\ D^{\alpha} T(t)_{T=0} &= b_t + e_1 NS \ge 0, \\ D^{\alpha} N(t)_{N=0} &= b_n \ge 0. \end{aligned} \tag{7}$$

If $\{S(0), T(0), N(0)\} \in \Omega$ according to Lemma 1 and Remark 1, the solution $(S(t), T(t), N(t))$ cannot escape from the hyperplanes Ω. Thus, the solutions of the fractional-order model (1) are nonnegative if the initial conditions are nonnegative for all $t > 0$. □ □

2.2. Stability of the Steady States. The underlying model (1) has the following equilibrium points: (i) disease-free with immunity equilibrium $\mathscr{E}_1(S_1, T_1, N_1) = (0, b_t/d_t, b_n/d_n)$, (ii) endemic equilibrium point $\mathscr{E}_2(S_2, T_2, N_2)$, if they exist, satisfy the following equalities:

$$\begin{aligned} \mathscr{F}(S_2, T_2) &= \frac{a_1(1 - bS_2) - d_{sn} N_2 - d_1}{d_{st}}, \\ kN_2 T_2 (qS_2 + d_t) + b_n r T_2 &= r T_2 N_2 (d_{ns} S_2 + d_n) + kN_2 (e_1 N_2 S_2 + b_t). \end{aligned} \tag{8}$$

The corresponding linearized system of the model (1) at any steady-state (S^*, T^*, N^*) is calculated as follows:

$$\begin{aligned} D^{\alpha}S(t) &= \left(a_1 - 2a_1bS^* - d_1 - d_{sn}N^* - d_{st}\left(\mathcal{F}(S^*,T^*) + S^*\frac{\partial \mathcal{F}}{\partial S}(S^*,T^*)\right)\right)S(t) \\ &\quad -\left(d_{st}S^*\frac{\partial \mathcal{F}}{\partial T}(S^*,T^*)\right)T(t) - d_{sn}S^*N(t), \\ D^{\alpha}T(t) &= \left(rT^*\frac{\partial \mathcal{G}}{\partial S}(S^*) + e_1N^* - qT^*\right)S(t) + \left(r\mathcal{G}(S^*) - qS^* - d_t\right)T(t) + e_1S^*N(t), \\ D^{\alpha}N(t) &= \left(kN^*\frac{\partial \mathcal{G}}{\partial S}(S^*) - d_{ns}N^*\right)S(t) + \left(k\mathcal{G}(S^*) - d_{ns}S^* - d_n\right)N(t). \end{aligned} \tag{9}$$

Applying Laplace transform on both sides of (9), we can get

$$\begin{aligned} s^{\alpha}\mathcal{S}(s) - s^{\alpha-1}S(0) &= \left(a_1 - 2a_1bS^* - d_1 - d_{sn}N^* - d_{st}\left(\mathcal{F}(S^*,T^*) + S^*\frac{\partial \mathcal{F}}{\partial S}(S^*,T^*)\right)\right)\mathcal{S}(s) \\ &\quad -\left(d_{st}S^*\frac{\partial \mathcal{F}}{\partial T}(S^*,T^*)\right)\mathcal{T}(s) - d_{sn}S^*\mathcal{N}(s), \\ s^{\alpha}\mathcal{T}(s) - s^{\alpha-1}T(0) &= \left(rT^*\frac{\partial \mathcal{G}}{\partial S}(S^*) + e_1N^* - qT^*\right)\mathcal{S}(s) + \left(r\mathcal{G}(S^*) - qS^* - d_t\right)\mathcal{T}(s) + e_1S^*\mathcal{N}(s), \\ s^{\alpha}\mathcal{N}(s) - s^{\alpha-1}N(0) &= \left(kN^*\frac{\partial \mathcal{G}}{\partial S}(S^*) - d_{ns}N^*\right)\mathcal{S}(s) + \left(k\mathcal{G}(S^*) - d_{ns}S^* - d_n\right)\mathcal{N}(s). \end{aligned} \tag{10}$$

Here, $\mathcal{S}(s), \mathcal{T}(s), \mathcal{N}(s)$ are Laplace transform of $S(t), T(t)$, and $N(t)$ with $\mathcal{S}(s) = L(S(t)), \mathcal{T}(s) = L(T(t))$, and $\mathcal{N}(s) = L(N(t))$. The above (10) can be written as

$$\Delta(s) \star \begin{pmatrix} \mathcal{S}(s) \\ \mathcal{T}(s) \\ \mathcal{N}(s) \end{pmatrix} = \begin{pmatrix} h_1(s) \\ h_2(s) \\ h_3(s) \end{pmatrix}, \tag{11}$$

where

$$\begin{aligned} h_1(s) &= s^{\alpha-1}S(0), \\ h_2(s) &= s^{\alpha-1}T(0), \\ h_3(s) &= s^{\alpha-1}N(0), \\ \Delta(s) &= \begin{pmatrix} s^{\alpha} + a_2 & a_3 & a_4 \\ a_5 & s^{\alpha} + a_6 & a_7 \\ a_8 & 0 & s^{\alpha} + a_9 \end{pmatrix}, \end{aligned} \tag{12}$$

$\Delta(s)$ is the characteristic matrix for system (3) at (S^*, T^*, N^*), and

$$a_2 = 2a_1bS^* + d_1 + d_{sn}N^* + d_{st}\left(\mathcal{F}(S^*, T^*) + S^*\frac{\partial \mathcal{F}}{\partial S}(S^*, T^*)\right) - a_1, a_3 = d_{st}S^*\frac{\partial \mathcal{F}}{\partial T}(S^*, T^*), a_4 = d_{sn}S^*,$$

$$a_5 = qT^* - rT^*\frac{\partial \mathcal{G}}{\partial S}(S^*) - e_1N^*, a_6 = qS^* + d_t - r\mathcal{G}(S^*), a_7 = -e_1S^*, \tag{13}$$

$$a_8 = d_{ns}N^* - kN^*\frac{\partial \mathcal{G}}{\partial S}(S^*), a_9 = d_{ns}S^* + d_n - k\mathcal{G}(S^*).$$

Clearly, the eigenvalues of $\Delta(s)$ at $\mathscr{E}_0$ and $\mathscr{E}_1$ are $-d_t, -d_n, d_1 - a_1$ and $-d_t, -d_n, d_1 + d_{sn}N_1 - a_1$, respectively, and assume that $d_1 < a_1, d_1 + d_{sn}N_1 < a_1$, which confirms that the model (1) around the equilibrium points $\mathscr{E}_0$ and $\mathscr{E}_1$ is stable.

Lemma 3. *The endemic equilibrium point $\mathscr{E}_2$ is locally asymptotically stable if $p_1 > 0, p_3 > 0, p_1p_2 > p_3$.*

Proof. The characteristic equation at $\mathscr{E}_2$ is described by

$$s^{3\alpha} + p_1s^{2\alpha} + p_2s^{\alpha} + p_3 = 0, \tag{14}$$

where $p_1 = a_2 + a_6 + a_9, p_2 = a_6a_9 + a_2(a_6 + a_9) - a_3a_5 - a_4a_8, p_3 = a_8(a_3a_7 - a_4a_6) + a_9(a_2a_6 - a_3a_5)$.

By using the Routh-Hurwitz criterion, the endemic equilibrium $\mathscr{E}_2$ is locally asymptotically stable if $p_1 > 0, p_3 > 0, p_1p_2 > p_3$. □ □

3. Parameter Estimation

The study by Wölfel et al. [26] was done a virological analysis on nine patients with COVID-19 for examining the kinetics of viral load and measuring the virus replication in tissues of the upper respiratory tract. Infection of all patients was known because they had near contact with an index case. The patients were admitted to a hospital in Munich, Germany, and underwent virological tests in collaboration with two reputable laboratories. Both laboratories were equipped with the same technology in PCR-PT and the same standards for virus isolation. Authors measured and analyzed viral loads were projected to RNA copies per ml, per swab, and per g for sputum, throat swab, and stool samples, respectively. All samples were taken between 2 and 4 days after the onset of symptoms. In [29], swab samples are used for some mathematical models.

Here, data fitting is used to estimate the values of the parameters of the model (1). The parameters are fitted by measured RNA viral load in sputum samples of five patients from [26] by implementing a least-squares algorithm, `fminsearch`, which is a MATLAB function. The measured viral load was done daily. The results for parameter estimation are presented in Table 1. Data fitting is made for different values of $\alpha \in (0, 1]$. In Figures 1–5, the result of the fitting for values $\alpha = 1$ and $\alpha = 0.98$ is presented. Due to the arbitrary derivative order of the model and nonlocality properties of these derivatives, different curves may be obtained in data fitting. This advantage will help to find the best fitting to the parameters of the model.

4. Simulations and Model Validation

In order to numerically solve system (1), the Adams–Bashforth–Moulton method of fractional version (FABM) will be used. This method was introduced in [37]. Consider the following fractional-order differential equation:

$$D^{\alpha}y(t) = K(t, y(t)). \tag{15}$$

The fractional Adams–Bashforth–Moulton method included a two-step first step as a predictor.

$$y_h^{pr}(t_{n+1}) = \sum_{j=0}^{\lceil\alpha\rceil-1}\frac{t_{n+1}^j}{j!}y_0^{(j)} + \frac{1}{\Gamma(\alpha)}\sum_{i=0}^{n}p_{i,n+1}K(t_i, y_h(t_i)). \tag{16}$$

After computing, the predictor step in the second step modifier is calculated by

$$y_h^{m}(t_{n+1}) = \sum_{j=0}^{\lceil\alpha\rceil-1}\frac{t_{n+1}^j}{j!}y_0^{(j)} + \frac{h^{\alpha}}{\Gamma(\alpha+1)}\sum_{i=0}^{n}q_{i,n+1}K(t_i, y_h(t_i)), \tag{17}$$

where the $p_{i,n+1}$ and $q_{i,n+1}$ are

$$p_{i,n+1} = \frac{h^{\alpha}}{\alpha}((n+1-i)^{\alpha} - (n-i)^{\alpha}),$$

$$q_{i,n+1} = (n-i+2)^{\alpha+1} + (n-i)^{\alpha+1} - 2(n-i+1)^{\alpha+1}, \quad 1 \le i \le n,$$

$$q_{0,n+1} = n^{\alpha+1} - (n-\alpha)(n+1)^{\alpha},$$

$$q_{n+1,n+1} = 1, \tag{18}$$

in which $t_i \quad i = 0, 1, \ldots, n$ are equally selected points with fixed step length h.

Garrappa has written a MATLAB function for FABM, FDE12, which is available at the MathWorks [48]. The FDE12 algorithms are used for numerically solving the

Table 1: Information of the parameters.

Par.	Description	Units	Value range	Source
a_1	S replication rate	1/day	[2.86, 7.07]	[29]
b	Maximum S	ml/(RNA copies)	[1e − 010, 1e − 09]	[29]
d_{st}	Virus lysis by CD8$^+$ T cells rate	1/day	[0.01, 0.4]	Estimated
d_{sn}	Virus death rate by NK cells	ml/cell(day)	[1.2e − 11, 2e − 010]	Estimated
d_1	Natural death rate of virus	1/day	[0.0001, 0.1]	Estimated
b_t	CD8$^+$ T cells proliferation	cell/ml (day)	[50 1500]	[46]
r	CD8$^+$ T cell activation	1/day	[0.001, 0.032]	Estimated
e_1	CD8$^+$ T recruitment rate by virus lysed by NK	ml/(RNA copies) (day)	[2.1e − 06, 8.4e − 005]	Estimated
q	CD8$^+$ T inactivation rate by virus	ml/(RNA copies) (day)	[1.1e − 10, 9.5e − 10]	Estimated
d_t	Natural death rate of T cells	1/day	[0.001, 0.08]	[47]
b_n	NK cells proliferation	cell/ml (day)	[7, 200]	[43]
k	NK cells activation	1/day	[0.001, 0.02]	Estimated
d_{ns}	Inactivation NK cells rate	ml/(RNA copy) (day)	[1.1e − 06, 9.09e − 05]	Estimated
d_n	NK cells death rate	1/day	[4.2e − 02, 0.15]	[44, 45]
z	Steepness coefficient of virus lysis by T cells	—	[0.01, 1]	[43]
c_1	Steepness coefficient of NK recruitment	—	[1e + 03, 1e + 06]	Estimated
α	Fractional virus kill power	—	[9.1e − 01, 9.9e − 01]	Estimated
n	Michaelis-Menten order	—	2	[47]

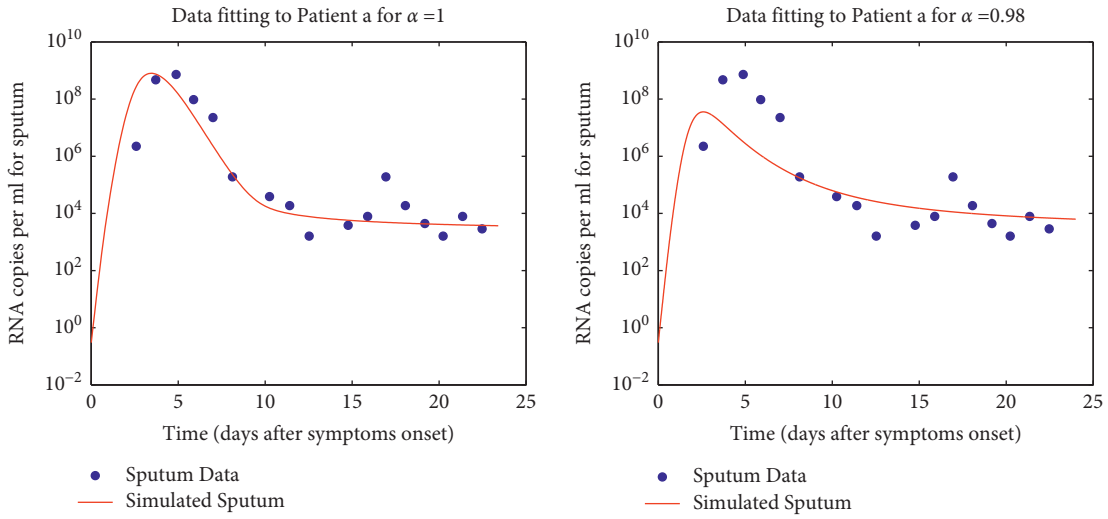

Figure 1: Data fitting for patient **a**.

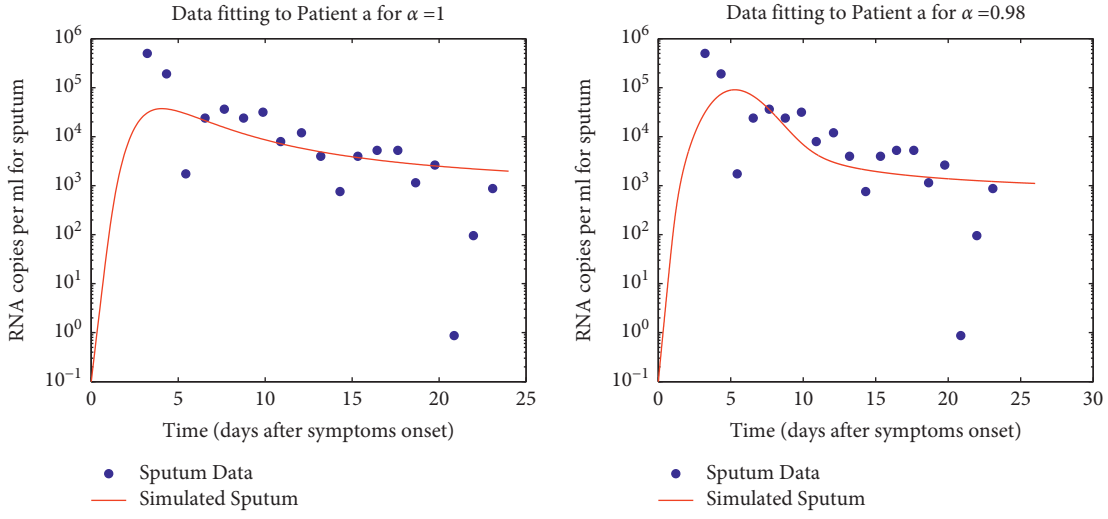

Figure 2: Data fitting for patient **c**.

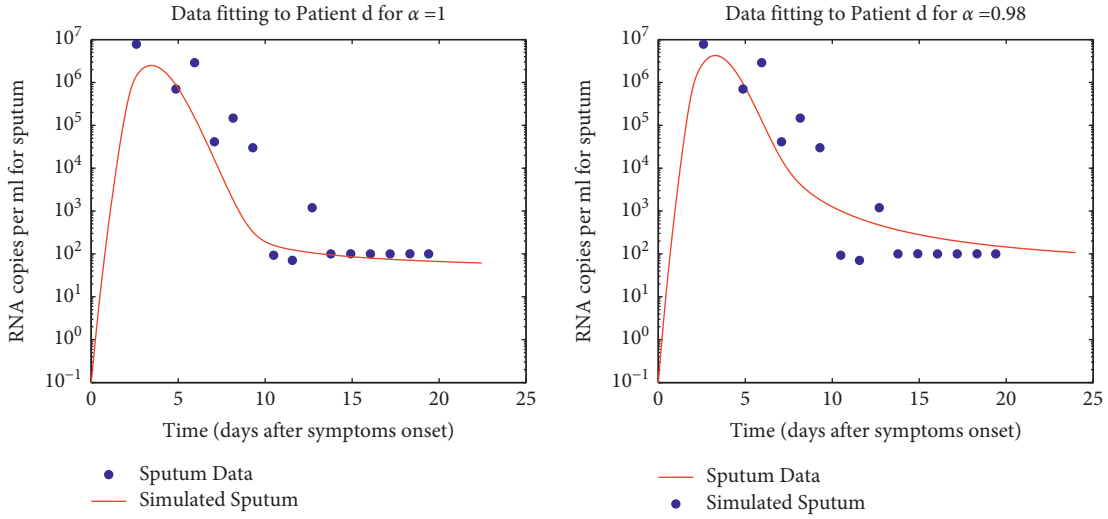

Figure 3: Data fitting for patient **d**.

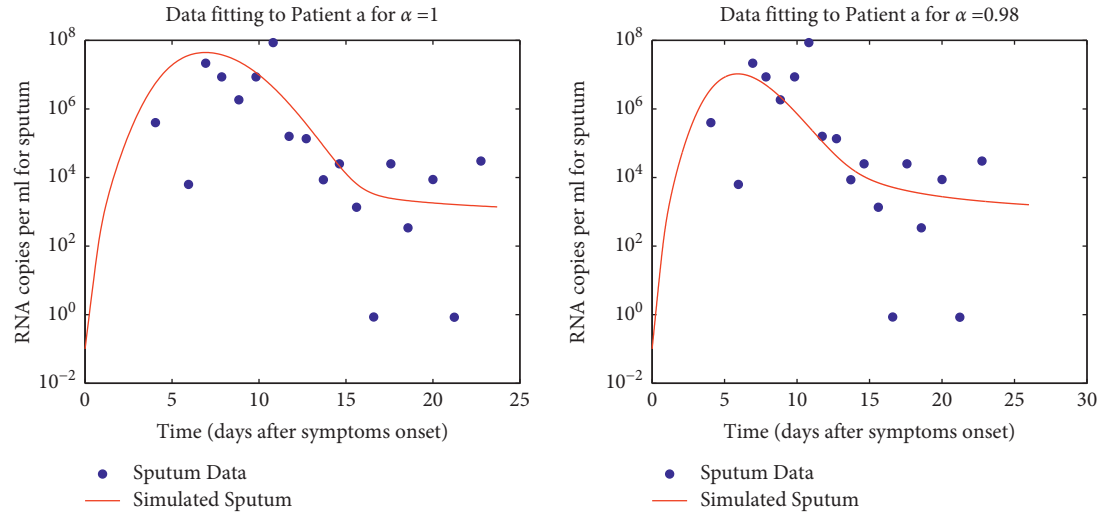

Figure 4: Data fitting for patient **e**.

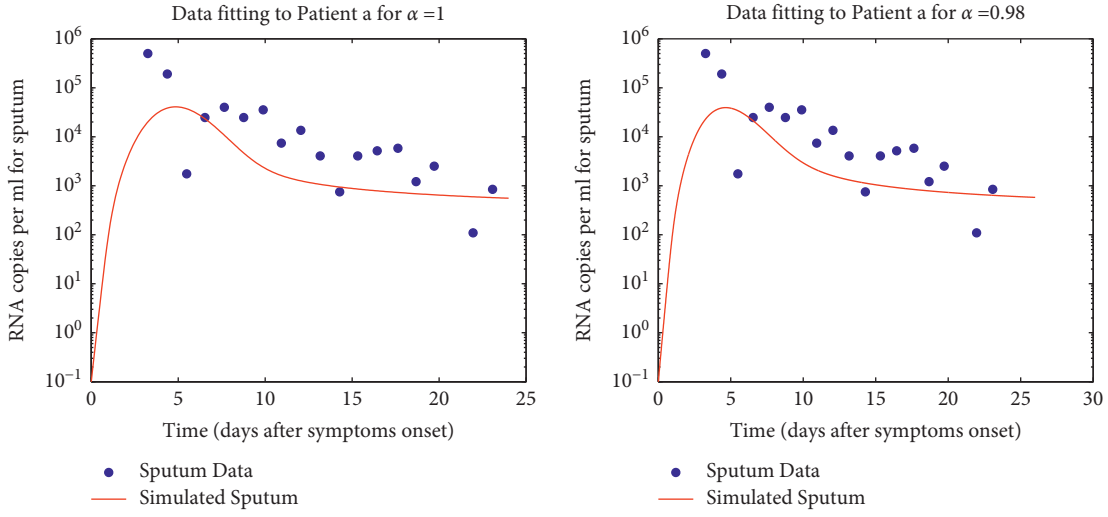

Figure 5: Data fitting for patient **g**.

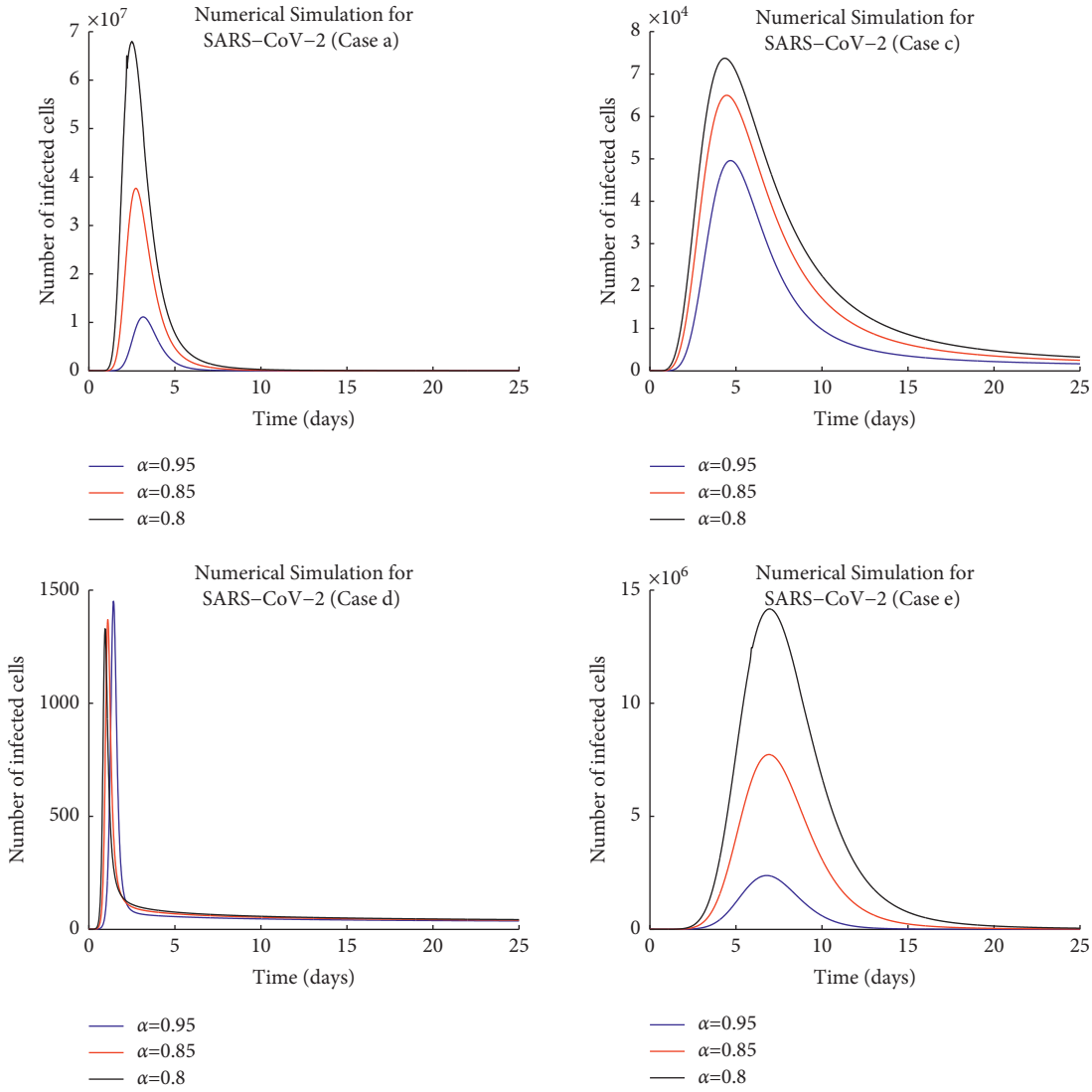

Figure 6: Numerical simulation results of SARS-CoV-2 behavior in patients **a**, **c**, **d**, **e**.

model (1). This numerical simulation is done for five patients **a**, **c**, **d**, **e**, **g** in [26] with their associated parameter values.

All simulations were performed to evaluate the behavior of the SARS-CoV-2 virus against immune cells 28 days after the onset of symptoms. In these simulations, three values $\alpha = 0.95, 0.85, 0.80$ are considered as the fractional-order derivatives of the equations in the model (1). The results are shown in Figures 6–8.

As can be seen in the graphs, the virus concentration is not accurate for each patient. Simulations show that for smaller amounts of α, the virus load is higher. It will also reduce the virus load with less speed and longer time.

In three patients **a**, **c**, and **d**, the maximum load of the virus is before the fifth day. This may depend on the amount of contact and the amount of primary virus that has been transmitted to the patient. Of course, the initial behavior of the patient's immune system against the virus should not be ignored.

Unlike patients **a**, **d**, in patient **c**, the decrease in the RNA viral concentration to its lowest level is about 30 days after the onset of symptoms. As the immune system and, in particular, the NK cells exhaust themselves, viral RNA concentrations slowly decrease. High infections usually lead to NK cells exhaustion, so limiting the infection potential of NK cells [27, 28]. In SARS-CoV-2 infections, exhaustion of the NK cell was confirmed by increased frequencies of programmed cell death protein 1 (PD-1) positive cells and reduced frequencies of natural killer group 2 member D (NKG2D)-, sialic acid-binding Ig-like lectin 7 (Siglec-7)-, and DNAX ancillary molecule-1 (DNAM-1)-expressing NK cells related to a reduced ability to spatter interferon IFN γ (see Figure 9) [27]. Furthermore, it was shown that in sera of COVID-19 patients, IL-6 is present in large surplus. It may downregulate NKG2D on NK cells, leading to disorder of NK cells activity [27].

In middle-aged patient **g**, due to the increased load of the virus, it leads to the NK cells exhaustion and reduces the infection potential. Decreased immune system function prolongs the course of the disease, so these patients need long-term treatment and a longer quarantine period than

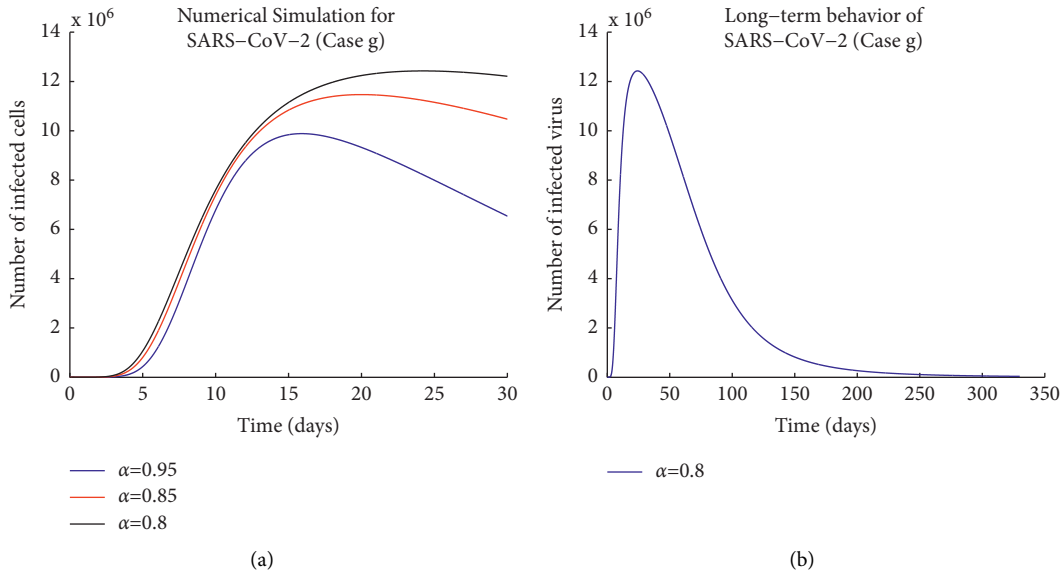

FIGURE 7: Numerical simulation results of SARS-CoV-2 behavior in patient **g** (a). Schematic of SARS-CoV-2 long-term behavior in patient **g** (b).

other patients. In addition, patients who show high viral loads 10 to 11 days after the first symptoms, due to immune exhaustion, will have symptoms of lung infection [27]. If the limit of quantification of RNA viral load be 200 RNA copies per ml, the concentration of the virus in the patient's body will reach this limit after 330 days for $\alpha = 0.8$ (see Figure 7(b)). In this case, it is said that the patient is involved in *long COVID* or *Post COVID* phenomenon. Chronic COVID, known in English as long COVID, is a long-term symptoms of acute COVID disease. The disease, which is characterized by long-term complications, persists after a normal recovery period. The diagnosis of the duration or how long these conditions last is not yet fully understood [38]. Based on our model, duration of long COVID for patient **g** is 330 days. Of note, it seems that delay in vaccination of immune exhaustion and long COVID individuals may be necessary. In the next section, we will discuss the process of the disease profile in the patient **g**.

In patient **e**, an increase in viral load occurs after the first week, potentially indicating an exacerbation of symptoms [26]. The immune system function of these patients needs further investigation, and more studies should be done in future studies.

The diagrams in Figure 8 show the behavior of infected virus versus the behavior of NK and $CD8^+$ cells one month after the first symptom in **a**, **c** patients. Order derivative values $\alpha = 0.95, 0.85$ are considered for both cases. System (1) solutions with $\alpha = 0.85$ indicate that in patient **a** because of severe NK cells depletion as the first defense factor, SARS-CoV-2 virus growth reaches more than 10^7. Two weeks after the peak viral load and with more $CD8^+$ T cells activation, the NK cells population increases and dominates the SARS-CoV-2 virus population. The solutions of model (1) for $\alpha = 0.95$ show that after approximately 10 days from the peak of infected virus concentration, the population of NK cells increases and overcomes viruses. Therefore, it can be said that it takes two to three weeks for the immune system to completely overcome the disease, in the patient **a**.

For the patient **c**, the solutions of (1) with $\alpha = 0.95, 0.85$ indicate that due to the greater resistance of NK cells to increased virus load and activated T cells, the virus concentration is a maximum of 10^5. Compared to the patient **a**, RNA viral had a lower burden, but due to NK cell exhaustion, NK cells were able to dominate SARS-CoV-2 infection with greater delay. About 25–30 days after the onset of symptoms, NK cells can return to their original value and completely dominate the infected virus.

The results of [42] show that despite the same initial viral load, innate immunity, such as NK cells and INF γ, is stronger in younger patients and is more active than in adults in exposure to SARS-CoV-2 and quickly return to homeostasis. This may be seen in the solutions of model (1) as shown in Figure 8, when the α value is closer to one, the NK cells proliferate and become active faster. Also, the model with smaller α values is suitable for older patients. Here, we can call α as the *age parameter*.

The response of $CD8^+$ T cells to the COVID virus is slow and at a constant rate. It seems that in order to reduce the peak load of the virus, T cells need to respond more quickly to the virus attack. Therefore, it is recommended that in the first days of the disease, drugs that lead to faster activation of T cells be prescribed. Rapid production of neutralizing antibodies is effective in treating the disease. In patients who made the neutralizing antibody before day 14, they eventually recovered, but in patients who started making the neutralizing antibody after 14 days, the antibodies lost their protective role [41].

5. Sensitivity Analysis

Sensitivity analysis is an important tool for assessing the dynamic behavior of the underlying biological system. Herein, we evaluate the sensitivity of state variables to small

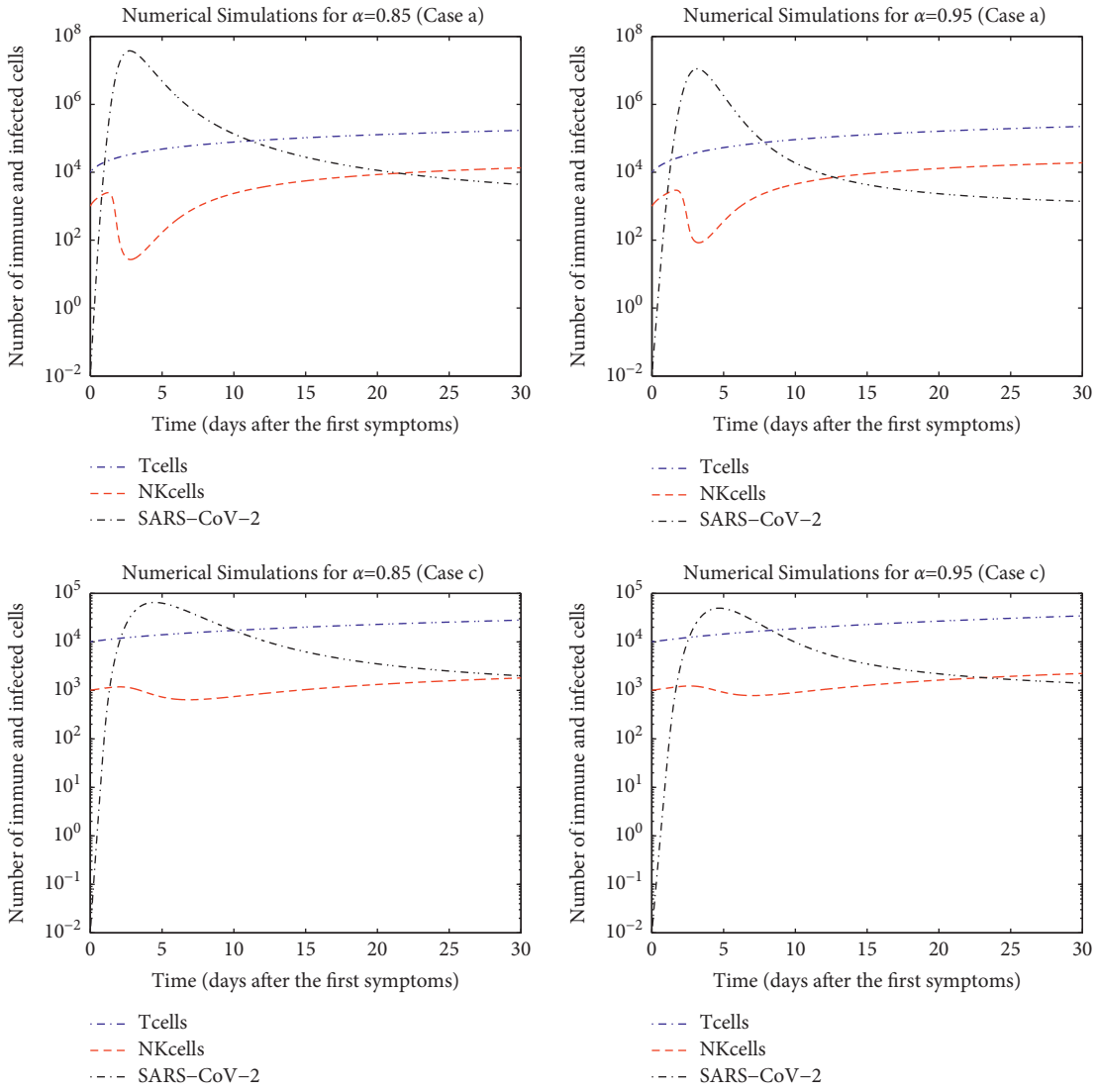

Figure 8: Numerical solutions of the model (1) for patient **a**, **c**.

variations in model parameters to enable us to (i) display how the robustness of the underlying infection model is too small changes in the parameter values, (ii) discover in which subinterval the model sensitive to a particular parameter to understand significant processes and immune system mechanisms. We evaluate the sensitivity functional throughout studying the effect of changes in the parameters on the period to estimate the severity of the diseases [22].

Some model parameters are very effective in determining the progression and decline of SARS-CoV-2 load. To determine the relationship between the parameters and model outcomes, we use sensitivity analysis. Here, we use partially ranked correlation coefficients (PRCC) to quantify the sensitivity and the relationships. The PRCC will be calculated for 1000 values of each parameter which is drawn by running the Latin hypercube sampling method (LSH). The LSH technique is a type of Monte Carlo sampling described in [39]. The LHS scheme allows the values of all input parameters to be changed simultaneously. This sampling method will be efficient if the outcome is a monotonic function of each of the input parameters. Here, we only use the parameters $a_1, d_{sn}, d_t, b_t, d_n, b_n, T_0$, and N_0 that are monotonically associated with the outcomes of the model in the sensitivity analysis.

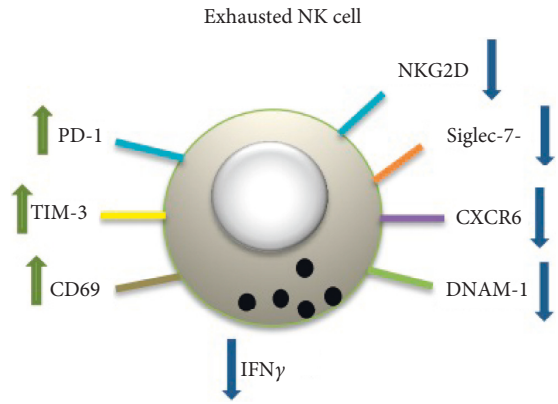

Figure 9: Schematic of exhausted NK cell.

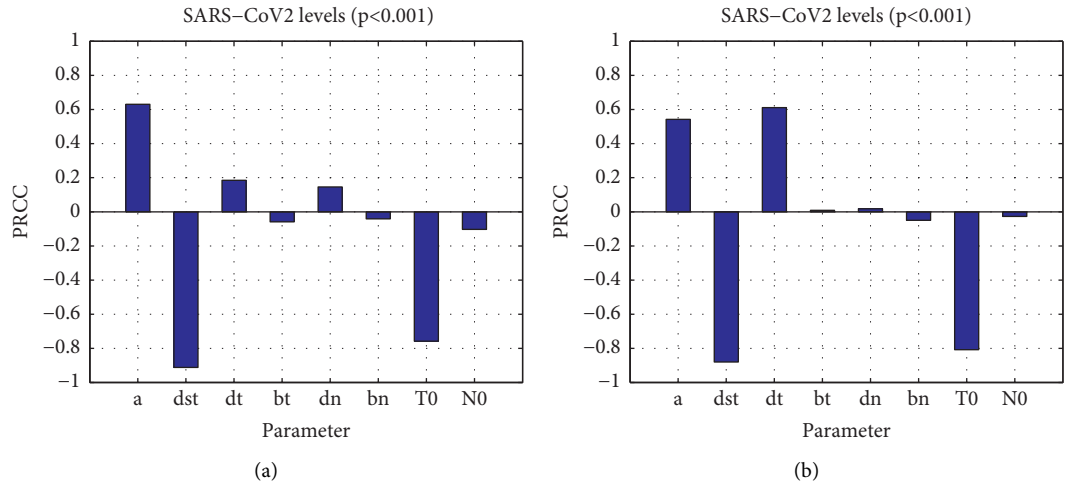

Figure 10: Sensitivity analysis for 4 (a) and 23 (b) days postonset of symptoms.

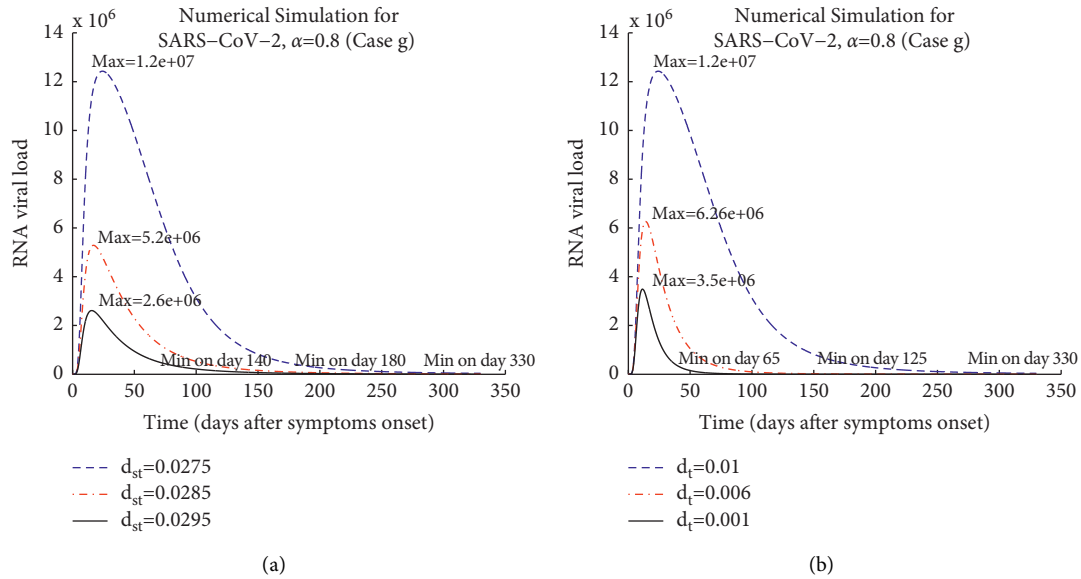

Figure 11: RNA viral load based on changing of d_{st} (a) and d_t (b) parameters for long COVID case **g**.

Sensitivity analysis of the selected parameters was performed for 4 and 23 days postonset of symptoms. The results for SARS-CoV-2 load are presented in Figure 10. On day 4 after the first symptom, the parameter a_1, which is the replication rate of the virus, had a significant positive relationship with virus load. The PRCC value for the parameter a_1 at a significance level of 0.001 was 0.62. The virus lysis by $CD8^+$ T cells rate parameter d_{st} had a high negative correlation with viral load. The correlation coefficient for this parameter was 0.87. This negative correlation with viral loading indicates that increasing the SARS-CoV-2 lysis by $CD8^+$ T cells may play an important role in controlling and reducing the virus load in the first days of the disease.

On day 23 postonset of symptoms, in addition to d_{st} and a_1 parameters, the d_t parameter, which indicates the natural death rate of $CD8^+$ T cells, had a significant correlation with SARS-CoV-2. This correlation is positive with PRCC value 0.62, which indicates that in the fourth week of the disease, death and consequently a decrease in the volume of cytotoxic T cells have great impact on the persistence of the virus, and the disease is exacerbated.

Furthermore, to show the effect of d_{st} and d_t parameters on SARS-CoV-2 behavior in long COVID patients, we solved the model (1) with $\alpha = 0.8$ for patient **g**, separately. According to Figure 11(a), the maximum RNA viral for $d_{st} = 0.0275$ is 1.2×10^7 copies per ml, and the time for complete clearance of the virus is 330 days after the onset of symptoms. For $d_{st} = 0.0285$, the maximum RNA viral is 5.2×10^6 copies per ml, and the clearance time of the virus is 180 days after the onset of symptoms, and for $d_{st} = 0.0295$, maximum RNA viral and clearance time are 2.6×10^6 copies per ml and 140 days after the onset of symptoms, respectively. As shown in Figure 11(b), the maximum RNA viral for $d_t = 0.01$ is 1.2×10^7 copies per ml, and the time for complete clearance of the virus is 330 days after the onset of symptoms. So if we assume that

vaccination increases the virus removal rate by $CD8^+$ T cells d_{st} by 0.002, then vaccination of COVID-19 reduces the severity and effect of long COVID for 140 days. This is due to the induction of T cells with the vaccine.

For $d_t = 0.006$, the maximum RNA viral is 6.26×10^6 copies per ml, and the clearance time of the virus is 120 days after the onset of symptoms, and for $d_t = 0.001$, maximum RNA viral and clearance time are 3.5×10^6 copies per ml and 65 days after the onset of symptoms, respectively.

Thus, by increasing the lifespan of $CD8^+$ T cells by 0.005 and inducing long-term responses of these cells by vaccination, the long COVID period can be reduced to 65 days. Of note, this feature will be challenging for vaccine technology.

The findings published in [40] confirm the results of our model. In [40], it is shown that the symptoms and severity of long COVID among patients with persistent symptoms are significantly reduced 120 days after vaccination.

6. Conclusion

The coronavirus associated with severe acute respiratory syndrome-2 (SARS-CoV-2) interacts dynamically with many components of the immune system. These interactions are poorly understood because of their complexity. Using reliable mathematical models is one way to understand the mechanism of SARS-CoV-2 viral behavior. This paper presents a fractional-order mathematical model of the immune system responses to SARS-CoV-2 viral load in 5 patients with COVID-19. In this model, the population of cytotoxic T cells ($CD8^+$) and natural killer cells is taken into account.

By sufficient conditions, nonnegativity of the solution and asymptotic stability of the steady states are guaranteed. Simulation results shed light on the dynamics of SARS-CoV-2 and the immune system of the patients. Depending on the immune system, the dynamics of SARS-CoV-2 differ from person to person. It is possible for patients to develop so-called long COVID due to immuno-exhaustion. In Model 1, innate immunity, including NK cells, was well demonstrated. It is possible to achieve more results by developing the model and adding other parts of the immune system, such as helper T cells ($CD4^+$).

A major advantage of the model was the fractional-order, which illustrated how age affects disease. In this case, the fractional-order value was $0 < \alpha \leq 1$. Model (1) with α values closer to one is suitable for younger people and with smaller values is suitable for older people.

We performed a sensitivity analysis on some parameters to determine their effect on the model. SARS-CoV-2 load was closely correlated with some model parameters, such as the replication rate, virus removal rate by CD8+ T cells, and death rate of T cells. In addition to vaccine design, these parameters are useful in disease control and future treatments.

In the future, vaccine-related variables and parameters could be added to the model to prevent SARS-CoV-2 from spreading.

Data Availability

The data used to support the findings of this study are available from the corresponding author upon request.

Conflicts of Interest

The authors declare that they have no conflicts of interest.

Acknowledgments

This research was funded by the UAE University, fund # 12S005-UPAR 2020.

References

[1] O. Diekmann, H. Heesterbeek, and T. Britton, *Mathematical Tools for Understanding Infectious Disease Dynamics*, Princeton University Press, Princeton, New Jersey, USA, 2012.

[2] WHO, *Report of the WHO-China Joint mission on Coronavirus Disease 2019 (COVID-19)*, World Health Organization, Geneva, Switzerland, 2020.

[3] R. M. Anderson and R. May, *Infectious Diseases of Humans: Dynamics and Control*, OUP, Oxford, England, 1991.

[4] G. Marchuk, *Mathematical Modelling of Immune Response in Infectious Diseases*, Kluwer Academic Publishers, Dordrecht, Netherlands, 1997.

[5] C. I. Siettos and L. Russo, "Mathematical modeling of infectious disease dynamics," *Virulence*, vol. 4, no. 4, pp. 295–306, 2013.

[6] W. M Liu, H. W. Hethcote, and S. A. Levin, "Dynamical behavior of epidemiological models with nonlinear incidence rates," *Journal of Mathematical Biology*, vol. 25, no. 4, pp. 359–380, 1987.

[7] S. A. Levin, B. Grenfell, A. Hastings, and A. S. Perelson, "Mathematical and computational challenges in population biology and ecosystems science," *Science*, vol. 275, no. 5298, pp. 334–343, 1997.

[8] A. S. Perelson, "Modelling viral and immune system dynamics," *Nature Reviews Immunology*, vol. 2, no. 1, pp. 28–36, 2002.

[9] A. S. Perelson and P. W. Nelson, "Mathematical analysis of HIV-1 dynamics in vivo," *SIAM Review*, vol. 41, no. 1, pp. 3–44, 1999.

[10] E. M. Ahmed and H. A. El-Saka, "On a fractional-order study of middle east respiratory syndrome coronalvirus (mers-cov)," *J. Fract. Calc. Appl.*, vol. 8, no. 1, pp. 118–126, 2017.

[11] B. Yong and L. Owen, "Dynamical transmission model of MERS-CoV in two areas," *P AIP Conference*, vol. 1716, no. 1, Article ID 020010, 2016.

[12] J. Lee, G. Chowell, and E. Jung, "A dynamic compartmental model for the Middle East respiratory syndrome outbreak in the Republic of Korea: a retrospective analysis on control interventions and superspreading events," *Journal of Theoretical Biology*, vol. 408, pp. 118–126, 2016.

[13] A. A. Kilbas, H. M. Srivastava, and J. J. Trujillo, *Theory and Applications of Fractional Differential Equations in: North-Holland Mathematics Studies, 204*, Elsevier Science B.V, Amsterdam, Netherlands, 2006.

[14] I. Podlubny, *Fractional Differential Equations*, Academic Press, Boca Raton, FL, USA, 1999.

[15] S. Ahmad, A. Ullah, Q. M. Al-Mdallal, H. Khan, K. Shah, and A. Khan, "Fractional order mathematical modeling of COVID-19 transmission," *Chaos, Solitons & Fractals*, vol. 139, Article ID 110256, 2020.

[16] K. Rajagopal, N. Hasanzadeh, F. Parastesh, I. I. Hamarash, S. Jafari, and I. Hussain, "A fractional-order model for the novel coronavirus (COVID-19) outbreak," *Nonlinear Dynamics*, vol. 101, no. 1, pp. 711–718, 2020.

[17] H. Singh, H. M. Srivastava, Z. Hammouch, and K. Sooppy Nisar, "Numerical simulation and stability analysis for the fractional-order dynamics of COVID-19," *Results in Physics*, vol. 20, Article ID 103722, 2021.

[18] I. A. Baba and B. A. Nasidi, "Fractional order epidemic model for the dynamics of novel COVID-19," *Alexandria Engineering Journal*, vol. 60, no. 1, pp. 537–548, 2021.

[19] R. P. Yadav and R. Renu Verma, "A numerical simulation of fractional order mathematical modeling of COVID-19 disease in case of Wuhan China," *Chaos, Solitons & Fractals*, vol. 140, Article ID 110124, 2020.

[20] A. N. Chatterjee and B. Ahmad, "A fractional-order differential equation model of COVID-19 infection of epithelial cells," *Chaos, Solitons & Fractals*, vol. 147, Article ID 110952, 2021.

[21] A. N. Chatterjee, F Basir, A. Almuqrin, M. A. Almuqrin, J. Mondal, and I. Khan, "SARS-CoV-2 infection with lytic and non-lytic immune responses: a fractional order optimal control theoretical study," *Results in Physics*, vol. 26, Article ID 104260, 2021.

[22] F. A. Rihan and G. Velmurugan, "Dynamics and sensitivity analysis of fractional-order delay differential model for coronavirus infection," *Progress in Fractional Differentiation and Applications*, vol. 7, pp. 43–61, 2021.

[23] J. Mondal, P. Samui, and A. N. Chatterjee, "Optimal control strategies of non-pharmaceutical and pharmaceutical interventions for COVID-19 control," *Journal of Interdisciplinary Mathematics*, vol. 24, no. 1, pp. 125–153, 2020.

[24] A. N. Chatterjee and F. Al Basir, "A model for SARS-CoV-2 infection with treatment," *Computational and Mathematical Methods in Medicine*, vol. 2020, Article ID 1352982, 11 pages, 2020.

[25] F. A. Rihan and H. J. Alsakaji, "Dynamics of a stochastic delay differential model for COVID-19 infection with asymptomatic infected and interacting people: case study in the UAE," *Results in Physics*, vol. 28, Article ID 104658, 2021.

[26] R. Wölfel, V. M. Corman, W. Guggemos et al., "Virological assessment of hospitalized patients with COVID-2019," *Nature*, vol. 581, no. 7809, pp. 465–469, 2020, mpldquosemicolon469.

[27] S. Varchetta, D. Mele, B. Oliviero et al., "Unique immunological profile in patients with COVID-19," *Cellular and Molecular Immunology*, vol. 18, no. 3, pp. 604–612, 2021.

[28] M. Li, W. Guo, Y. Dong et al., "Elevated exhaustion levels of NK and CD8+ T cells as indicators for progression and prognosis of COVID-19 disease. Front. Immunol," *Frontiers in Immunology*, vol. 11, Article ID 580237, 2020, eCollection.

[29] A. H. V. Esteban, "In-host mathematical modelling of COVID-19 in humans. Annu. Rev," *Con.*, vol. 50, pp. 448–456, 2020.

[30] C. v Eeden, L. Khan, M. S. Cohen, and J. W. Tervaert, "Natural killer cell dysfunction and its role in COVID-19," *International Journal of Molecular Sciences*, vol. 21, no. 17, p. 6351, 2020.

[31] H. Mellstedt and A. Choudhury, "T and B cells in B-chronic lymphocytic leukaemia: faust, Mephistopheles and the pact with the Devil," *Cancer Immunology, Immunotherapy*, vol. 55, no. 2, pp. 210–220, 2006.

[32] A. Y. C. Huang, P. Golumbek, M. Ahmadzadeh, E. Jaffee, D. Pardoll, and H. Levitsky, "Role of bone marrow-derived cells in presenting MHC class I-restricted tumor antigens," *Science*, vol. 264, no. 5161, pp. 961–965, 1994.

[33] O. Diekmann and J. A. Heesterbeek, "Metz, On the definition and the computation of the basic reproduction ratio R0 in models for infectious diseases," *J Math. The Biologist*, vol. 35, pp. 503–522, 1990.

[34] M. Ye, J. Liu, C. Cenedese, Z. Sun, and M. Cao, "A network SIS meta-population model with transportation flow," *IFAC-PapersOnLine*, vol. 53, no. 2, pp. 2562–2567, 2020.

[35] Z. M. Odibat and N. T. Shawagfeh, "Generalized Taylor's formula," *Applied Mathematics and Computation*, vol. 186, no. 1, pp. 286–293, 2007.

[36] L. G. D Pillis, A. E Radunskaya, and C. L Wiseman, "A validated mathematical model of cell-mediated immune response to tumor growth," *Cancer Research*, vol. 65, no. 17, pp. 7950–7958, 2005.

[37] K. Diethelm, N. J Ford and A. D Freed, A predictor–corrector approach for the numerical solution of fractional differential equations," *Nonlinear Dynamics*, vol. 29, pp. 3–22, 2002.

[38] A. M. Baig, "Chronic COVID syndrome," *need for an appropriate medical terminology for long-COVID and COVID long-haulers Journal of Medical Virology*, vol. 93, no. 5, pp. 2555-2556, 2021.

[39] S. M. Blower and H. Dowlatabadi, "Sensitivity and uncertainty analysis of complex models of disease transmission: an HIV model, as an example," *International Statistical Review/Revue Internationale de Statistique*, vol. 62, no. 2, pp. 229–243, 1994.

[40] V-T. Tran, "Efficacy of COVID-19 vaccination on the symptoms of patients with long COVID: a target trial emulation using data from the ComPaRe e-cohort in France," Preprints with The Lancet, 2021, https://papers.ssrn.com/sol3/papers.cfmabstract-id=3932953.

[41] L. Carolina, "Kinetics of antibody responses dictate COVID-19 outcome," *MedRxiv*, 2020.

[42] M. Vono, A. Huttner, S. Lemeille et al., "Robust innate responses to SARS-CoV-2 in children resolve faster than in adults without compromising adaptive immunity," *Cell Reports*, vol. 37, no. 1, Article ID 109773, 2021.

[43] S. Nanda, L. dePillis, L. dePillis, and A. Radunskaya, "B cell chronic lymphocytic leukemia - a model with immune response," *Discrete & Continuous Dynamical Systems - B*, vol. 18, no. 4, pp. 1053–1076, 2013.

[44] R. J. D Boer, H Mohri, D. H David, and A. S Perelson, "Turnover rates of B cells, T cells, and NK cells in simian immunodeficiency virus-infected and uninfected rhesus macaques," *The Journal of Immunology*, vol. 170, no. 5, pp. 2479–2487, 2003.

[45] A. M. Jamieson, P. Isnard, J. R. Dorfman, M. C. Coles, and D. H. Raulet, "Turnover and proliferation of NK cells in steady state and lymphopenic conditions," *The Journal of Immunology*, vol. 172, no. 2, pp. 864–870, 2004.

[46] Y. Fadaei, A. Ahmadi, K. Fekri, R. Masoumi, and A. Radunskaya, "A fractional order model for chronic lymphocytic leukemia and immune system interactions," *Mathematical Methods in the Applied Sciences*, vol. 44, no. 1, pp. 391–406, 2020.

[47] M. Hellerstein, M. B. Hanley, D. Cesar et al., "Directly measured kinetics of circulating T lymphocytes in normal and HIV-1-infected humans," *Nature Medicine*, vol. 5, no. 1, pp. 83–89, 1999.

[48] R. Garrappa, "Predictor-corrector PECE method for fractional differential equations," December 17, 2021, https://www.google.com/search?q=(https%3A%2F%2Fwww.mathworks.com%2Fmatlabcentral%2Ffileexchange%2F32918-predictor-corrector-pece-method-for-fractional-differential-equations)&rlz=1C1GCEB_enIN1002IN1002&oq=(https%3A%2F%2Fwww.mathworks.com%2Fmatlabcentral%2Ffile.

Hindawi
Complexity
Volume 2022, Article ID 8531858, 11 pages
https://doi.org/10.1155/2022/8531858

Research Article

ABC Fractional Derivative for the Alcohol Drinking Model using Two-Scale Fractal Dimension

Qura Tul Ain,[1] T. Sathiyaraj,[2] Shazia Karim,[3] Muhammad Nadeem,[4] and Patrick Kandege Mwanakatwe[5]

[1]*Department of Mathematics, Guizhou University, Guiyang 550025, China*
[2]*Institute of Actuarial Science and Data Analytics, UCSI University, Cheers 56000, Malaysia*
[3]*Department of Basic Sciences, FSD Campus, UET Lahore, Lahore, Pakistan*
[4]*Faculty of Science, Yibin University, Yibin 644000, China*
[5]*Eastern Africa Statistical Training Center, Dar es Salaam, Tanzania*

Correspondence should be addressed to Patrick Kandege Mwanakatwe; patrick26573@yahoo.co.uk

Received 22 March 2022; Revised 4 May 2022; Accepted 13 May 2022; Published 6 June 2022

Academic Editor: C. Rajivganthi

Drinking kills a significant proportion of individuals every year, particularly in low-income communities. An impulsive differential equation system is used to explore the effectiveness of activated charcoal in detoxifying the body after methanol poisoning. Our impression of activated charcoal is shaped by the fractional dynamics of the problem, which leads to speedy and low-cost first aid. The adsorption capacity of activated charcoal is investigated using impulsive differential equations. The ABC fractional operator's findings paint a more realistic image of first aid in public and primary health centers, which can assist to reduce methanol poisoning deaths. Numerical simulations are provided using generalized Adams–Bashforth–Moulton method (GABMM).

1. Introduction

Drinking is responsible for around 3.3 million deaths per year, with the majority of these deaths occurring without primary therapy [1]. The lack of good health-care facilities is a primary cause of untreated mortality. It is critical because of its impact on backward social and economic classes. The mortality rate caused by methanol poisoning can be lowered by using activated charcoal. Activated charcoal's adsorption action ensures that it has healing and cleansing properties. The negatively charged porous structure of activated charcoal attracts positive molecules, accumulating toxins from the stomach and finally removing them from the body [2–4]. Fractional derivative models are used for precise modeling of those systems which require precise damping modeling. In recent years, different analytical and numerical approaches have been proposed in these areas, including their applications to new problems [5, 6]. Mathematical simulation of real life problems typically leads to fractional differential equations and other problems; in one or more variables, essential functions of mathematical physics, as well as their extensions and generalizations, are included. Furthermore, most physical fluid dynamics phenomena, quantum mechanics, electricity, ecological structures, and many other models are regulated by fractional-order PDEs within their scope of validity [7–9]. Modern advances in theoretical and applied science have primarily relied on understanding of the positive integer-order derivatives and integrals. The features of mathematical functions, ranging from gamma and beta functions through special functions, as well as integral differential operators with convolutional integrals and singularities, exists. The solution of many relevant problems leads to integral equations, which have little in common with the integral equation of Abel at first glance, and additional efforts are made for the development of tiles of analytical or computational methods to solve these equations due to this impression. However, their conversion to the form of the integral equation of Abel can also be convenient.

The growth of fractional calculus theory was slow in the beginning due to a lack of context in practical applications. Mandelbrot proposed the "fractal" idea first, pointing out that there are multiple fractal dimensions in nature as well as several challenges in science and technology and implying that there is a self-similar phenomenon. Fractional calculus theory and FDE theory have swiftly emerged as the dynamic foundation of fractal geometry and fractal dimension and have become a popular academic topic around the world. Fractional calculus is an excellent way to define physical memory and heredity. Fractional differential equations have increased in popularity as the response of the fractional-order system and eventually converge with the equations of the integer-order [10]. Many different types of physical systems use special functions, elliptic functions, and elliptic integrals. Their presence is well-known in the solution of nonlinear differential equations. These functions and integrals can be studied in [11–15]. Over the last few decades, fractional differential equations and fractional operators have emerged as reliable and well-organized mathematical tools for analyzing a wide range of scientific and engineering events [16, 17]. Unlike the differential equation with integer orders, the differential equation of fractional orders can display nonlocal relations with memory kernels in time and space.

Mathematical modeling of physical systems has many successful applications in engineering and sciences such as medical science, nanotechnology, biological processes, space sciences, and artificial intelligence [18–20]. Mathematical modeling is a wide field that draws the attention of scientists, engineers, and mathematicians to solve the many problems facing humankind [21–24]. We will use the Atangana–Baleanu fractional operator in Caputo sense to examine the fractional dynamics of given model. The reason for using Atangana–Baleanu fractional derivatives is its nonlocal properties. This operator can also capture complex behavior more effectively than other operators:

$$
\begin{aligned}
{}_0^{ABC}D_t^{\alpha}E_1^{\bullet} &= -k_1^{\bullet}E_1^{\bullet}M^{\bullet} + k_{-1}^{\bullet}C_1^{\bullet} + k_2^{\bullet}C_1^{\bullet} - k_5^{\bullet}E_1^{\bullet}I^{\bullet} + k_{-5}^{\bullet}C_3^{\bullet} + k_6^{\bullet}C_3^{\bullet},\\
{}_0^{ABC}D_t^{\alpha}M^{\bullet} &= -k_1^{\bullet}E_1^{\bullet}M^{\bullet} + k_{-1}^{\bullet}C_1^{\bullet},\\
{}_0^{ABC}D_t^{\alpha}C_1^{\bullet} &= k_1^{\bullet}E_1^{\bullet}M^{\bullet} - k_{-1}^{\bullet}C_1^{\bullet} - k_2^{\bullet}C_2^{\bullet},\\
{}_0^{ABC}D_t^{\alpha}P_1^{\bullet} &= k_2^{\bullet}C_1^{\bullet} - k_3^{\bullet}P_1^{\bullet}E_2^{\bullet} + k_{-3}^{\bullet}C_2^{\bullet},\\
{}_0^{ABC}D_t^{\alpha}E_2^{\bullet} &= -k_3^{\bullet}P_1^{\bullet}E_2^{\bullet} + k_{-3}^{\bullet}C_2^{\bullet} + k_4^{\bullet}C_2^{\bullet},\\
{}_0^{ABC}D_t^{\alpha}C_2^{\bullet} &= k_3^{\bullet}P_1^{\bullet}E_2^{\bullet} - k_{-3}^{\bullet}C_2^{\bullet} - k_4^{\bullet}C_2^{\bullet},\\
{}_0^{ABC}D_t^{\alpha}P_2^{\bullet} &= k_4^{\bullet}C_2^{\bullet},\\
{}_0^{ABC}D_t^{\alpha}I^{\bullet} &= -k_5^{\bullet}E_1^{\bullet}I^{\bullet} + k_{-5}^{\bullet}C_3^{\bullet},\\
{}_0^{ABC}D_t^{\alpha}C_3^{\bullet} &= k_5^{\bullet}E_1^{\bullet}I^{\bullet} - k_{-5}^{\bullet}C_3^{\bullet} - k_6^{\bullet}C_3^{\bullet},\\
{}_0^{ABC}D_t^{\alpha}P_3^{\bullet} &= k_6^{\bullet}C_3^{\bullet} - k_7^{\bullet}P_3^{\bullet}e_3^{\bullet} + k_{-7}^{\bullet}C_4^{\bullet},\\
{}_0^{ABC}D_t^{\alpha}E_3^{\bullet} &= -k_{-7}^{\bullet}P_3^{\bullet}E_3^{\bullet} + k_{-7}^{\bullet}C_4^{\bullet} + k_8^{\bullet}C_4^{\bullet},\\
{}_0^{ABC}D_t^{\alpha}C_4^{\bullet} &= k_7^{\bullet}P_3^{\bullet}E_3^{\bullet} - k_{-7}^{\bullet}C_4^{\bullet} - k_8^{\bullet}C_4^{\bullet},\\
{}_0^{ABC}D_t^{\alpha}P_4^{\bullet} &= k_8^{\bullet}C_4^{\bullet}.
\end{aligned}
\tag{1}
$$

Table 1 demonstrates the variables used in the model. The model is followed by two reactions, which can be explained by the following mechanism.

1.1. Reaction 1

(1) Binding of methanol $M^{\bullet}$ and alcohol dehydrogenase enzyme (ADH) $E_1^{\bullet}$ takes place in the liver, which results in formaldehyde $P_1^{\bullet}$ and an enzyme-methanol complex $C_1^{\bullet}$. This reaction releases the free alcohol dehydrogenase enzyme (ADH) at the end of this process.

(2) The formaldehyde $P_2^{\bullet}$ starts binding with the formaldehyde dehydrogenase $E_{\bullet}^2$ enzyme at the spot, resulting in the enzyme formaldehyde complex $C_2^{\bullet}$, which then converts into formic acid $P_2^{\bullet}$. This reaction releases $E_2^{\bullet}$.

1.2. Reaction 2

(1) Replacing methanol $M^{\bullet}$, ethanol $I^{\bullet}$ behaves as the substrate and reacts with $E_1^{\bullet}$ to form acetaldehyde $P_3^{\bullet}$. Ethanol complex $C_3^{\bullet}$ is formed as results. This reaction releases the alcohol dehydrogenase enzyme (ADH) $E_1^{\bullet}$.

(2) Acetaldehyde binds with the enzyme acetaldehyde dehydrogenase (ALDH) $E_3^{\bullet}$ and the enzyme acetaldehyde complex $C_4^{\bullet}$ is formed. As a result, acetic acid $P_4^{\bullet}$ is formed and free enzyme $E_3^{\bullet}$ is released.

Table 1: Variables' definitions.

Parameters	Interpretation
$E_1^*(t)$	Alcohol dehydrogenase enzyme
$E_2^*(t)$	Formaldehyde dehydrogenase enzyme
$E_3^*(t)$	Acetaldehyde dehydrogenase enzyme
$M^*(t)$	Methanol
$P_1^*(t)$	Formaldehyde
$P_2^*(t)$	Formic acid
$P_3^*(t)$	Acetaldehyde
$C_1^*, C_2^*, C_3^*, C_4^*(t)$	Substrate-enzyme complexes
$E_4^*(t)$	Free enzyme

Here, $k_1^\bullet, k_2^\bullet, k_3^\bullet, k_4^\bullet, k_5^\bullet, k_6^\bullet, k_7^\bullet$, and $k_8^\bullet$ are the forward rate constants of the problem and $k_{-1}^\bullet, k_{-3}^\bullet, k_{-5}^\bullet$, and $k_{-7}^\bullet$ are the reverse rate constants.

In this work, we will use the drinking model of impulsive differential equations recently published by researchers [25]. Different fractional approaches has been done on drinking; relevant studies on drinking can be seen in [26–28]. To the best of our knowledge, two-scale approach has not been applied to the drinking model along with ABC derivative. So, this work is unique in its nature. The rest of the study is divided in the following sections. At the end of Section 1, basic definitions are provided to be used in coming framework of problem. Section 2 gives an overview of fractional-order drinking model. Section 3 discusses the two-scale transform in detail and subsequent theoretical work. Sections 4 and 5 consist of problem formulation and numerical simulation, respectively. In Section 6, we provide the main results, and we conclude our work in Section 7.

Definition 1. Let σ be a continuous function in (a, b) with $0 < \alpha \le 1$. The fractional-order derivative in ABC sense is defined as [29, 30]

$$ {}_0^{ABC}D_t^\alpha \sigma(t) = \frac{M(\alpha)}{1-\alpha}\frac{\mathrm{d}}{\mathrm{d}t}\int_0^t \sigma(\theta)E_\alpha\left[\frac{-\alpha}{1-\alpha}(t-\theta)^\alpha\right]\mathrm{d}\theta, \quad (2)$$

where $M(\alpha)$ is called normalization constant such that $M(0) = M(1) = 1$.

Definition 2. The fractional integral associated with the fractional derivative can be defined as [29, 30]

$$ {}_0^{ABC}I_t^\alpha \sigma(t) = \frac{1-\alpha}{M(\alpha)}\sigma(t) + \frac{\alpha}{M(\alpha)\Gamma(\alpha)}\int_0^t \left[(t-\theta)^{\alpha-1}\right]\sigma(\theta)\mathrm{d}\theta. \quad (3)$$

2. ABC Fractional-Order Model for Methanol Poisoning

Several researchers and scientists have emphasized fractional calculus in recent decades, demonstrating that fractional calculus better explains natural events than integer order. Fractional calculus has embraced the benefits and popularity of fractal modeling. In this area, we drew inspiration from a fractional mathematical model discussed in a recent research [25]. For the Atangana–Baleanu fractional derivative operator, we adopted a numerical technique. We find the following iterative formula by using the ABC fractional model to (1):

$$\begin{aligned} E_1^\bullet(t) - E_1^\bullet(0) &= \frac{1-\alpha}{M(\alpha)}\left[-k_1^\bullet E_1^\bullet M^\bullet + k_{-1}^\bullet C_1^\bullet + k_2^\bullet C_1^\bullet - k_5^\bullet E_1^\bullet I^\bullet + k_{-5}^\bullet C_3^\bullet + k_6^\bullet C_3^\bullet\right] \\ &+ \frac{\alpha}{M(\alpha)\Gamma(\alpha)}\int_0^t \left[(t-\theta)^{\alpha-1}\right]\left[-k_1^\bullet E_1^\bullet M^\bullet + k_{-1}^\bullet C_1^\bullet + k_2^\bullet C_1^\bullet - k_5^\bullet E_1^\bullet I^\bullet + k_{-5}^\bullet C_3^\bullet + k_6^\bullet C_3^\bullet\right]\mathrm{d}\theta. \end{aligned} \quad (4)$$

To simplify, we take

$$\Omega_1\left(t, E_1^\bullet\right) = -k_1^\bullet E_1^\bullet M^\bullet + k_{-1}^\bullet C_1^\bullet + k_2^\bullet C_1^\bullet - k_5^\bullet E_1^\bullet I^\bullet + k_{-5}^\bullet C_3^\bullet + k_6^\bullet C_3^\bullet. \quad (5)$$

Now, we show that the kernels Ω_i for $i = 1, 2, 3, \ldots, 9$ satisfy the Lipschitz condition and contraction.

3. Two-Scale Transform

There is a famous mathematical conceptual proverb: "If you cannot measure it you cannot manage it." In fact, mathematics is an abstract science of measurements. How about the measurement of a coastline? This example makes the notion of length inapplicable. Length of any coastline is variable and dependent on the scale of measurement. The problem of the coastline is the counterintuitive phenomenon that because the length of the coastline of a landmass is not well described. This stems from the coastlines' fractal curve-like features, i.e., the fact that a coastline usually has a fractal dimension (which literally renders the notion of longitude inapplicable). Benoit Mandelbrot documented the discovery of that phenomenon. The estimated length of the coastline relies on the scheme and the degree of cartographic generalization used to measure it. While there are characteristics of a land mass on all scales, from hundreds of kilometers in size to tiny fractions of one millimeter and below, there is no clear scale of the smallest feature to take into account when measured. The length of a smooth, idealized metal bar can be accurately measured using a measuring instrument to assess that the length is less than a certain amount and greater than

the other. The more accurate the measuring device is, the closer the measurements are to the true value of the metal strip. However, the enhancing measurement instrument does not result in a rise in precision when measuring a coastline. As with the metal pole, for the length of the coastline, there is no way to obtain a definite value; the value simply increases in length. The coastline problem is applied to the idea of fractal surfaces in 3 D space, whereby the area of a surface varies according to the scale of measurement. There are many physical laws that depend on scale and also have scale dependent consequences. In these systems, we can assume that the behavior is "scale" dependent with intense behavioral modifications accompanying the exclusive regimes. After the emergence of Einstein's theory of relativity, scientists believe in relative observation. Implementing the relativity of scale in the same manner, one may conclude the importance of scale dependence in every scientific law. Uncertainty is obvious if the application is taken on the wrong scale. To explain this important fact, two-scale transform is given [31]:

$$\Delta S = \frac{\Delta t^{\alpha}}{\Gamma(1+\alpha)}, \tag{6}$$

where ΔS is the smaller scale and Δt is the larger scale. In existing fractal calculus concepts, two-scale gives reasonable explanation [32]. It is a newly developed idea. It focuses on the importance of scale while analyzing any practical problem. We have been motivated by the researchers. In [33], the presented work became the source of our motivation. We are going to present our work as an example of ideas provided in the mentioned manuscript.

Theorem 1. *The kernel Ω_1 satisfy the Lipchitz condition and contraction if the inequality given below holds*

$$0 \le k_l^{\bullet} l_2 + k_5^{\bullet} l_8 < 1. \tag{7}$$

Proof. Let $a = k_l^{\bullet} l_2 + k_5^{\bullet} l_8$. For $E_1^{\bullet}$, we have

$$\begin{aligned}
\left\|\Omega_1(t, E^{\bullet}) - \Omega_1(t, E_1^{\bullet})\right\| &= -k_1^{\bullet} M^{\bullet}\left(E^{\bullet}(t) - E_1^{\bullet}(t)\right) - k_5^{\bullet} I^{\bullet}\left(E^{\bullet}(t) - E_1^{\bullet}(t)\right) \\
&\le k_1^{\bullet}\left\|M^{\bullet}\right\| \cdot \left\|\left(E^{\bullet}(t) - E_1^{\bullet}(t)\right)\right\| + k_5^{\bullet}\left\|I^{\bullet}\right\| \cdot \left\|\left(E^{\bullet}(t) - E_1^{\bullet}(t)\right)\right\| \\
&= \left(k_1^{\bullet}\left\|M^{\bullet}\right\| + k_5^{\bullet}\left\|I^{\bullet}\right\|\right)\left\|\left(E^{\bullet}(t) - E_1^{\bullet}(t)\right)\right\| \\
&\le \left(k_l^{\bullet} l_2 + k_5^{\bullet} l_8\right)\left\|\left(E^{\bullet}(t) - E_1^{\bullet}(t)\right)\right\|,
\end{aligned} \tag{8}$$

where $\|M^{\bullet}(t)\| \le l_2$ and $\|I^{\bullet}(t)\| \le l_8$ are bounded functions. So, we obtain the following result:

$$\left\|\Omega_1(t, E^{\bullet}) - \Omega_1(t, E_1^{\bullet})\right\| \le a\left\|\left(E^{\bullet}(t) - E_1^{\bullet}(t)\right)\right\|. \tag{9}$$

Thus, for Ω_1, the Lipchitz condition is obtained. Similarly, the Lipschitz condition for Ω_i for $i = 2, 3, 4, \ldots, 13$, also holds. Using this notation, we can write

$$\begin{aligned}
E_1^{\bullet}(t) = E_1^{\bullet}(0) &+ \frac{1-\alpha}{M(\alpha)}\Omega_1(t, E_1^{\bullet}) \\
&+ \frac{\alpha}{M(\alpha)\Gamma(\alpha)}\int_0^t \left[(t-\theta)^{\alpha-1}\right]\Omega_1(t, E_1^{\bullet})\mathrm{d}\theta.
\end{aligned} \tag{10}$$

The recursive formula can be written as

$$\begin{aligned}
E_{1n}^{\bullet}(t) = E_1^{\bullet}(0) &+ \frac{1-\alpha}{M(\alpha)}\Omega_1(t, E_{1n-1}^{\bullet}) \\
&+ \frac{\alpha}{M(\alpha)\Gamma(\alpha)}\int_0^t \left[(t-\theta)^{\alpha-1}\right]\Omega_1(t, E_{1n-1}^{\bullet})\mathrm{d}\theta.
\end{aligned} \tag{11}$$

With initial condition as $E_1^{\bullet}(0) = E_{1_0}^{\bullet}$, the successive terms of difference are defined as follows:

$$\begin{aligned}
\lambda_{1n} = E_{1n}^{\bullet}(t) - E_{1n-1}^{\bullet}(t) = & \\
&\cdot \frac{1-\alpha}{M(\alpha)}\left(\Omega_1(t, E_{1n-1}^{\bullet}) - \Omega_1(t, E_{1n-2}^{\bullet})\right) \\
&+ \frac{\alpha}{M(\alpha)\Gamma(\alpha)}\int_0^t \left[(t-\theta)^{\alpha-1}\right]\left(\Omega_1(t, E_{1n-1}^{\bullet}) - \Omega_1(t, E_{1n-2}^{\bullet})\right)\mathrm{d}\theta.
\end{aligned} \tag{12}$$

Obviously, we obtain

$$E_{1n}^{\bullet}(t) = \sum_{i=0}^{n} \lambda_{1i}(t). \tag{13}$$

We also define

$$E_{1_{-1}}^{\bullet}(0) = 0. \tag{14}$$

Consequently, we obtain the following results:

$$\left\|\lambda_{1n}\right\| \leq \frac{1-\alpha}{M(\alpha)}\gamma_1\left\|\lambda_{1n}\right\| + \frac{\gamma_1\alpha}{M(\alpha)\Gamma(\alpha)}\int_0^t \lambda_{1_{n-1}}(\theta)(t-\theta)^{\alpha-1}\mathrm{d}\theta, \tag{15}$$

where $(\gamma_1, \gamma_2, \gamma_3, \ldots, \gamma_{13}) \in (0,1)^{13}$. By using these results, the existence of the solution is guaranteed. □

Theorem 2. *The model under consideration has a solution if there is a τ_0 such that*

$$\frac{1-\alpha}{M(\alpha)}\gamma_1 + \frac{\tau_0^{\alpha}\gamma_1}{M(\alpha)\Gamma(\alpha)} < 1. \tag{16}$$

Proof. We assume that the model system is consisted of bounded functions. So, we can obtain

$$\left\|\lambda_{1n}\right\| \leq \left\|E_1(0)\right\|\left[\frac{1-\alpha}{M(\alpha)}\gamma_1 + \frac{\tau_0^{\alpha}\gamma_1}{M(\alpha)\Gamma(\alpha)}\right]^n. \tag{17}$$

In order to express (12) as the solution of (1), we suppose that $E_1(t) - E_1(0) = E_n(t) - G_{1_n}(0)$.

Next, we can conclude that

$$\left\|G_{1_n}\right\| \leq \left[\left(\frac{1-\alpha}{M(\alpha)}\right) + \left(\frac{\tau^{\alpha}}{(M(\alpha)\Gamma(\alpha))}\right)\right]^{n-1}\gamma_1^{n-1}, \tag{18}$$

for $\tau = \tau_0$,

$$\left\|G_{1_n}\right\| \leq \left[\frac{1-\alpha}{M(\alpha)} + \frac{\tau_0^{\alpha}}{M(\alpha)\Gamma(\alpha)}\right]^{n-1}\gamma_1^{n-1}. \tag{19}$$

By taking the limit $n \longrightarrow \infty$, we obtain

$$\left\|G_{1_n}(t)\right\| \longrightarrow \infty. \tag{20}$$

With the similar process, we have

$$\left\|G_{i_n}(t)\right\| \longrightarrow \infty, \tag{21}$$

for $i = 1, 2, 3, \ldots, 13$. □

Theorem 3. *model under consideration has a unique solution if*

$$\left[1 - \frac{1-\alpha}{M(\alpha)}\gamma_1 + \frac{\tau^{\alpha}\gamma_1}{M(\alpha)\Gamma(\alpha)}\right] > 0. \tag{22}$$

Proof. First, we assume that the model has another solution, that is, $E_1^{\bullet}$:

$$E_1(t) - E_1^{\bullet}(t) = \frac{1-\alpha}{M(\alpha)}\left(\Omega_1\left(t, E_1 - \Omega_1\left(t, E_1^{\bullet}\right)\right)\right) + \frac{\alpha}{M(\alpha)\Gamma(\alpha)}\int_0^t \left[(t-\theta)^{\alpha-1}\right]\left(\Omega_1\left(t, E_1\right) - \Omega_1\left(t, E_1^{\bullet}\right)\right)\mathrm{d}\theta. \tag{23}$$

By using the properties of norm, we obtain the following inequality:

$$\left\|E_1(t) - E_1^{\bullet}(t)\right\|\left[1 - \frac{1-\alpha}{M(\alpha)}\gamma_1 + \frac{\tau^{\alpha}\gamma_1}{M(\alpha)\Gamma(\alpha)}\right] \leq 0. \tag{24}$$

If condition of (18) is satisfied, then

$$\left\|E_1(t) - E_1^{\bullet}(t)\right\| = 0. \tag{25}$$

Clearly, it is shown that

$$E_1(t) = E_1^{\bullet}(t). \tag{26}$$

Through similar process, we can prove for other components of the model. □

4. Problem Formulation

We suppose the initial-value problem with the ABC fractional derivative:

$${}_0^{ABC}D_{\tau}^{\beta}g(\tau) = f(\tau, g(\tau)). \tag{27}$$

Recently, ABC fractional product integral rule (ABC-PIR) is defined as follows [17]:

$$g_m = g_0 + \frac{\beta h^{\beta}}{M(\beta)}\left(\beta_m f(\tau_0, g_0) + \sum_{i=1}^{n}\zeta_{m-i}f(\tau_i, g_i)\right), \tag{28}$$

where

$$\beta_m = \left(\frac{(m-1)^{\beta+1} - m^{\beta}(m-\beta-1)}{\Gamma(\beta+2)}\right), \tag{29}$$

and ζ_k is

$$\zeta_k = \left(\frac{1}{\Gamma(\beta+2)}\right) + \left(\frac{1-\beta}{\beta h h^{\beta}}\right), \quad \text{for } k = 0,$$

$$\zeta_k = \left(\frac{\left((k-1)^{\beta+1} - 2k^{\beta+1} + (k+1)^{\beta+1}\right)}{\Gamma(\beta+2)}\right), \tag{30}$$

$$\text{for } k = 1, 2, \ldots, m-1.$$

By using (23), our model can be transformed in the following form:

$$E^{\bullet}_{1_n} = E^{\bullet}_0 + \frac{\alpha h^{\alpha}}{M(\alpha)}\left[a_m y_1\left(t_0, M^{\bullet}_0, I^{\bullet}_0, E^{\bullet}_{1_0}, E^{\bullet}_{2_0}, E^{\bullet}_{3_0}, C^{\bullet}_{1_0}, C^{\bullet}_{2_0}, C^{\bullet}_{3_0}, C^{\bullet}_{4_0}, P^{\bullet}_{1_0}, P^{\bullet}_{2_0}, P^{\bullet}_{3_0}, P^{\bullet}_{4_0}\right)\right] + \sum_{i=1}^{m} \zeta_{m-i} y_1\left(t_i, M^{\bullet}_i, I^{\bullet}_i, E^{\bullet}_{1_i}, E^{\bullet}_{2_i}, E^{\bullet}_{3_i}, C^{\bullet}_{1_i}, C^{\bullet}_{2_i}, C^{\bullet}_{3_i}, C^{\bullet}_{4_i}, P^{\bullet}_{1_i}, P^{\bullet}_{2_i}, P^{\bullet}_{3_i}, P^{\bullet}_{4_i}\right). \tag{31}$$

Deriving other equations of model in the same manner, we obtain

$$M^{\bullet}_{1_n} = M^{\bullet}_0 + \frac{\alpha h^{\alpha}}{M(\alpha)}\left[a_m y_2\left(t_0, M^{\bullet}_0, I^{\bullet}_0, E^{\bullet}_{1_0}, E^{\bullet}_{2_0}, E^{\bullet}_{3_0}, C^{\bullet}_{1_0}, C^{\bullet}_{2_0}, C^{\bullet}_{3_0}, C^{\bullet}_{4_0}, P^{\bullet}_{1_0}, P^{\bullet}_{2_0}, P^{\bullet}_{3_0}, P^{\bullet}_{4_0}\right)\right] + \sum_{i=1}^{m} \zeta_{m-i} y_2\left(t_i, M^{\bullet}_i, I^{\bullet}_i, E^{\bullet}_{1_i}, E^{\bullet}_{2_i}, E^{\bullet}_{3_i}, C^{\bullet}_{1_i}, C^{\bullet}_{2_i}, C^{\bullet}_{3_i}, C^{\bullet}_{4_i}, P^{\bullet}_{1_i}, P^{\bullet}_{2_i}, P^{\bullet}_{3_i}, P^{\bullet}_{4_i}\right),$$

$$C^{\bullet}_{1_n} = C^{\bullet}_0 + \frac{\alpha h^{\alpha}}{M(\alpha)}\left[a_m y_3\left(t_0, M^{\bullet}_0, I^{\bullet}_0, E^{\bullet}_{1_0}, E^{\bullet}_{2_0}, E^{\bullet}_{3_0}, C^{\bullet}_{1_0}, C^{\bullet}_{2_0}, C^{\bullet}_{3_0}, C^{\bullet}_{4_0}, P^{\bullet}_{1_0}, P^{\bullet}_{2_0}, P^{\bullet}_{3_0}, P^{\bullet}_{4_0}\right)\right] + \sum_{i=1}^{m} \zeta_{m-i} y_3\left(t_i, M^{\bullet}_i, I^{\bullet}_i, E^{\bullet}_{1_i}, E^{\bullet}_{2_i}, E^{\bullet}_{3_i}, C^{\bullet}_{1_i}, C^{\bullet}_{2_i}, C^{\bullet}_{3_i}, C^{\bullet}_{4_i}, P^{\bullet}_{1_i}, P^{\bullet}_{2_i}, P^{\bullet}_{3_i}, P^{\bullet}_{4_i}\right),$$

$$E^{\bullet}_{2_n} = E^{\bullet}_{2_0} + \frac{\alpha h^{\alpha}}{M(\alpha)}\left[a_m y_5\left(t_0, M^{\bullet}_0, I^{\bullet}_0, E^{\bullet}_{1_0}, E^{\bullet}_{2_0}, E^{\bullet}_{3_0}, C^{\bullet}_{1_0}, C^{\bullet}_{2_0}, C^{\bullet}_{3_0}, C^{\bullet}_{4_0}, P^{\bullet}_{1_0}, P^{\bullet}_{2_0}, P^{\bullet}_{3_0}, P^{\bullet}_{4_0}\right)\right] + \sum_{i=1}^{m} \zeta_{m-i} y_5\left(t_i, M^{\bullet}_i, I^{\bullet}_i, E^{\bullet}_{1_i}, E^{\bullet}_{2_i}, E^{\bullet}_{3_i}, C^{\bullet}_{1_i}, C^{\bullet}_{2_i}, C^{\bullet}_{3_i}, C^{\bullet}_{4_i}, P^{\bullet}_{1_i}, P^{\bullet}_{2_i}, P^{\bullet}_{3_i}, P^{\bullet}_{4_i}\right),$$

$$P^{\bullet}_{1_n} = P^{\bullet}_0 + \frac{\alpha h^{\alpha}}{M(\alpha)}\left[a_m y_4\left(t_0, M^{\bullet}_0, I^{\bullet}_0, E^{\bullet}_{1_0}, E^{\bullet}_{2_0}, E^{\bullet}_{3_0}, C^{\bullet}_{1_0}, C^{\bullet}_{2_0}, C^{\bullet}_{3_0}, C^{\bullet}_{4_0}, P^{\bullet}_{1_0}, P^{\bullet}_{2_0}, P^{\bullet}_{3_0}, P^{\bullet}_{4_0}\right)\right] + \sum_{i=1}^{m} \zeta_{m-i} y_4\left(t_i, M^{\bullet}_i, I^{\bullet}_i, E^{\bullet}_{1_i}, E^{\bullet}_{2_i}, E^{\bullet}_{3_i}, C^{\bullet}_{1_i}, C^{\bullet}_{2_i}, C^{\bullet}_{3_i}, C^{\bullet}_{4_i}, P^{\bullet}_{1_i}, P^{\bullet}_{2_i}, P^{\bullet}_{3_i}, P^{\bullet}_{4_i}\right),$$

$$C^{\bullet}_{2_n} = C^{\bullet}_{2_0} + \frac{\alpha h^{\alpha}}{M(\alpha)}\left[\left(a_m y_6 t_0, M^{\bullet}_0, I^{\bullet}_0, E^{\bullet}_{1_0}, E^{\bullet}_{2_0}, E^{\bullet}_{3_0}, C^{\bullet}_{1_0}, C^{\bullet}_{2_0}, C^{\bullet}_{3_0}, C^{\bullet}_{4_0}, P^{\bullet}_{1_0}, P^{\bullet}_{2_0}, P^{\bullet}_{3_0}, P^{\bullet}_{4_0}\right)\right] + \sum_{i=1}^{m} \zeta_{m-i} y_6\left(t_i, M^{\bullet}_i, I^{\bullet}_i, E^{\bullet}_{1_i}, E^{\bullet}_{2_i}, E^{\bullet}_{3_i}, C^{\bullet}_{1_i}, C^{\bullet}_{2_i}, C^{\bullet}_{3_i}, C^{\bullet}_{4_i}, P^{\bullet}_{1_i}, P^{\bullet}_{2_i}, P^{\bullet}_{3_i}, P^{\bullet}_{4_i}\right),$$

$$P^{\bullet}_{2_n} = P^{\bullet}_{2_0} + \frac{\alpha h^{\alpha}}{M(\alpha)}\left[\left(a_m y_7 t_0, M^{\bullet}_0, I^{\bullet}_0, E^{\bullet}_{1_0}, E^{\bullet}_{2_0}, E^{\bullet}_{3_0}, C^{\bullet}_{1_0}, C^{\bullet}_{2_0}, C^{\bullet}_{3_0}, C^{\bullet}_{4_0}, P^{\bullet}_{1_0}, P^{\bullet}_{2_0}, P^{\bullet}_{3_0}, P^{\bullet}_{4_0}\right)\right] + \sum_{i=1}^{m} \zeta_{m-i} y_7\left(t_i, M^{\bullet}_i, I^{\bullet}_i, E^{\bullet}_{1_i}, E^{\bullet}_{2_i}, E^{\bullet}_{3_i}, C^{\bullet}_{1_i}, C^{\bullet}_{2_i}, C^{\bullet}_{3_i}, C^{\bullet}_{4_i}, P^{\bullet}_{1_i}, P^{\bullet}_{2_i}, P^{\bullet}_{3_i}, P^{\bullet}_{4_i}\right),$$

$$I^{\bullet}_n = I^{\bullet}_0 + \frac{\alpha h^{\alpha}}{M(\alpha)}\left[\left(a_m y_8 t_0, M^{\bullet}_0, I^{\bullet}_0, E^{\bullet}_{1_0}, E^{\bullet}_{2_0}, E^{\bullet}_{3_0}, C^{\bullet}_{1_0}, C^{\bullet}_{2_0}, C^{\bullet}_{3_0}, C^{\bullet}_{4_0}, P^{\bullet}_{1_0}, P^{\bullet}_{2_0}, P^{\bullet}_{3_0}, P^{\bullet}_{4_0}\right)\right] + \sum_{i=1}^{m} \zeta_{m-i} y_8\left(t_i, M^{\bullet}_i, I^{\bullet}_i, E^{\bullet}_{1_i}, E^{\bullet}_{2_i}, E^{\bullet}_{3_i}, C^{\bullet}_{1_i}, C^{\bullet}_{2_i}, C^{\bullet}_{3_i}, C^{\bullet}_{4_i}, P^{\bullet}_{1_i}, P^{\bullet}_{2_i}, P^{\bullet}_{3_i}, P^{\bullet}_{4_i}\right),$$

$$E^{\bullet}_{3_n} = E^{\bullet}_{3_0} + \frac{\alpha h^{\alpha}}{M(\alpha)}\left[a_m y_9\left(t_0, M^{\bullet}_0, I^{\bullet}_0, E^{\bullet}_{1_0}, E^{\bullet}_{2_0}, E^{\bullet}_{3_0}, C^{\bullet}_{1_0}, C^{\bullet}_{2_0}, C^{\bullet}_{3_0}, C^{\bullet}_{4_0}, P^{\bullet}_{1_0}, P^{\bullet}_{2_0}, P^{\bullet}_{3_0}, P^{\bullet}_{4_0}\right)\right] + \sum_{i=1}^{m} \zeta_{m-i} y_9\left(t_i, M^{\bullet}_i, I^{\bullet}_i, E^{\bullet}_{1_i}, E^{\bullet}_{2_i}, E^{\bullet}_{3_i}, C^{\bullet}_{1_i}, C^{\bullet}_{2_i}, C^{\bullet}_{3_i}, C^{\bullet}_{4_i}, P^{\bullet}_{1_i}, P^{\bullet}_{2_i}, P^{\bullet}_{3_i}, P^{\bullet}_{4_i}\right),$$

$$C^{\bullet}_{3_n} = C^{\bullet}_{3_0} + \frac{\alpha h^{\alpha}}{M(\alpha)}\left[a_m y_{10}\left(t_0, M^{\bullet}_0, I^{\bullet}_0, E^{\bullet}_{1_0}, E^{\bullet}_{2_0}, E^{\bullet}_{3_0}, C^{\bullet}_{1_0}, C^{\bullet}_{2_0}, C^{\bullet}_{3_0}, C^{\bullet}_{4_0}, P^{\bullet}_{1_0}, P^{\bullet}_{2_0}, P^{\bullet}_{3_0}, P^{\bullet}_{4_0}\right)\right]$$

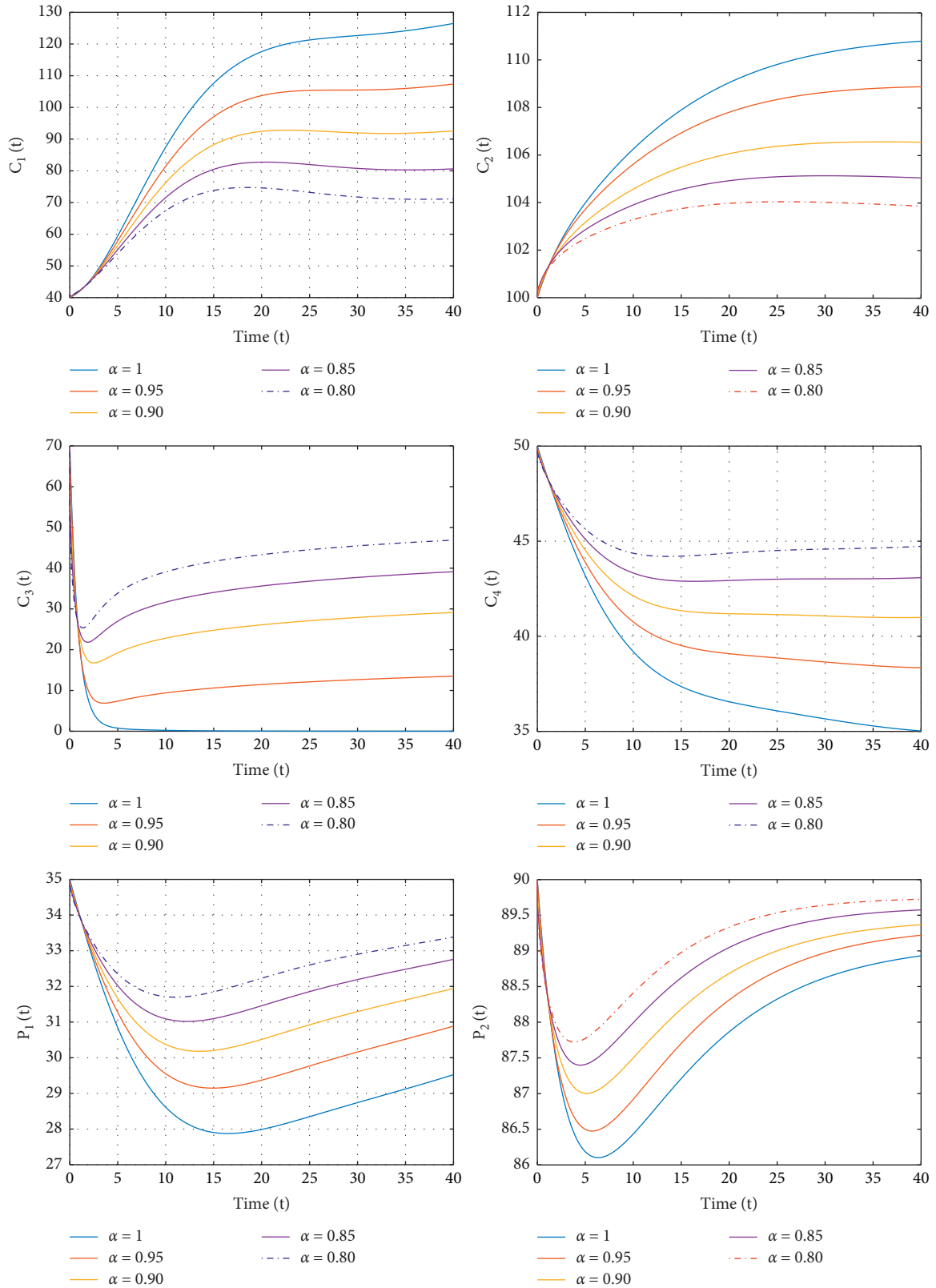

FIGURE 1: Fractional dynamics of reactants C_1, C_2, C_3, C_4, P_1, and P_2 in the enzymatic reaction of drinking model, respectively.

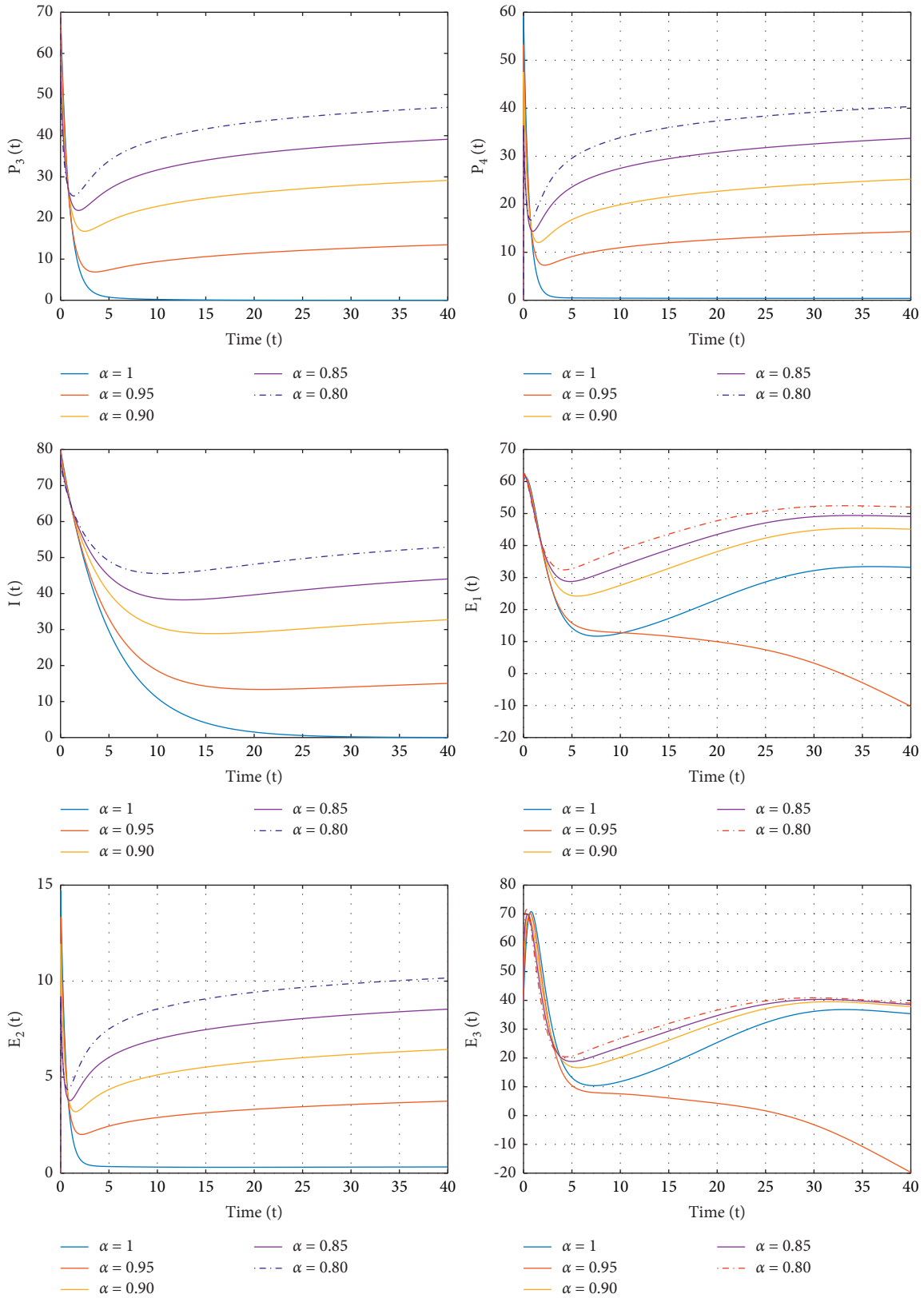

Figure 2: Fractional dynamics of reactants P_3, P_4, I, E_1, E_2, and E_3 in the enzymatic reaction of drinking model, respectively.

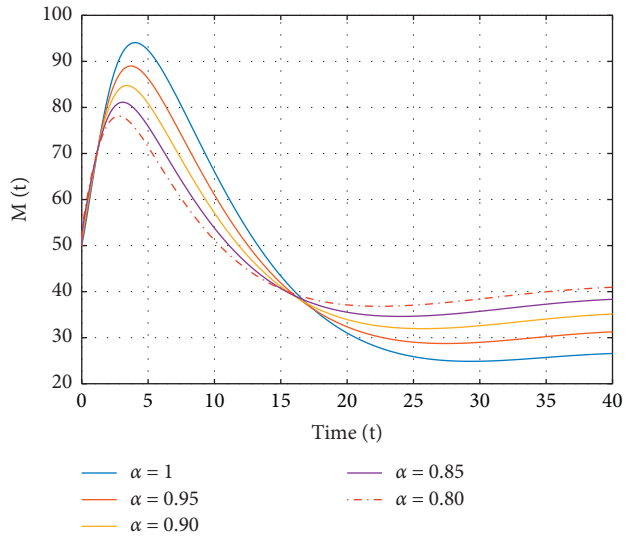

Figure 3: Schematic diagram for reaction process of methanol in the human body.

$$+\sum_{i=1}^{m}\zeta_{m-i}y_{10}\left(t_i,M_i^{\bullet},I_i^{\bullet},E_{1_i}^{\bullet},E_{2_i}^{\bullet},E_{3_i}^{\bullet},C_{1_i}^{\bullet},C_{2_i}^{\bullet},C_{3_i}^{\bullet},C_{4_i}^{\bullet},P_{1_i}^{\bullet},P_{2_i}^{\bullet},P_{3_i}^{\bullet},P_{4_i}^{\bullet}\right),$$

$$P_{3_n}^{\bullet}=P_{3_0}^{\bullet}+\frac{\alpha h^{\alpha}}{M(\alpha)}\left[a_m y_{11}\left(t_0,M_0^{\bullet},I_0^{\bullet},E_{1_0}^{\bullet},E_{2_0}^{\bullet},E_{3_0}^{\bullet},C_{1_0}^{\bullet},C_{2_0}^{\bullet},C_{3_0}^{\bullet},C_{4_0}^{\bullet},P_{1_0}^{\bullet},P_{2_0}^{\bullet},P_{3_0}^{\bullet},P_{4_0}^{\bullet}\right)\right]$$

$$+\sum_{i=1}^{m}\zeta_{m-i}y_{11}\left(t_i,M_i^{\bullet},I_i^{\bullet},E_{1_i}^{\bullet},E_{2_i}^{\bullet},E_{3_i}^{\bullet},C_{1_i}^{\bullet},C_{2_i}^{\bullet},C_{3_i}^{\bullet},C_{4_i}^{\bullet},P_{1_i}^{\bullet},P_{2_i}^{\bullet},P_{3_i}^{\bullet},P_{4_i}^{\bullet}\right),$$

$$C_{4_n}^{\bullet}=C_{4_0}^{\bullet}+\frac{\alpha h^{\alpha}}{M(\alpha)}\left[a_m y_{12}\left(t_0,M_0^{\bullet},I_0^{\bullet},E_{1_0}^{\bullet},E_{2_0}^{\bullet},E_{3_0}^{\bullet},C_{1_0}^{\bullet},C_{2_0}^{\bullet},C_{3_0}^{\bullet},C_{4_0}^{\bullet},P_{1_0}^{\bullet},P_{2_0}^{\bullet},P_{3_0}^{\bullet},P_{4_0}^{\bullet}\right)\right]$$

$$+\sum_{i=1}^{m}\zeta_{m-i}y_{12}\left(t_i,M_i^{\bullet},I_i^{\bullet},E_{1_i}^{\bullet},E_{2_i}^{\bullet},E_{3_i}^{\bullet},C_{1_i}^{\bullet},C_{2_i}^{\bullet},C_{3_i}^{\bullet},C_{4_i}^{\bullet},P_{1_i}^{\bullet},P_{2_i}^{\bullet},P_{3_i}^{\bullet},P_{4_i}^{\bullet}\right),$$

$$P_{4_n}^{\bullet}=P_{4_0}^{\bullet}+\frac{\alpha h^{\alpha}}{M(\alpha)}\left[a_m y_{13}\left(t_0,M_0^{\bullet},I_0^{\bullet},E_{1_0}^{\bullet},E_{2_0}^{\bullet},E_{3_0}^{\bullet},C_{1_0}^{\bullet},C_{2_0}^{\bullet},C_{3_0}^{\bullet},C_{4_0}^{\bullet},P_{1_0}^{\bullet},P_{2_0}^{\bullet},P_{3_0}^{\bullet},P_{4_0}^{\bullet}\right)\right]$$

$$+\sum_{i=1}^{m}\zeta_{m-i}y_{13}\left(t_i,M_i^{\bullet},I_i^{\bullet},E_{1_i}^{\bullet},E_{2_i}^{\bullet},E_{3_i}^{\bullet},C_{1_i}^{\bullet},C_{2_i}^{\bullet},C_{3_i}^{\bullet},C_{4_i}^{\bullet},P_{1_i}^{\bullet},P_{2_i}^{\bullet},P_{3_i}^{\bullet},P_{4_i}^{\bullet}\right). \tag{32}$$

5. Numerical Simulation

We introduce activated charcoal and ethanol to adsorb methanol and suppress the synthesis of hazardous metabolites, based on ABC fractional dynamics of methanol metabolism under the action of the ADH released by the liver.

Dropping • for simplification, we take the $k_1 = 0.1 - 0.3$, $k_{-1} = 0.01 - 0.3, k_2 = 0.2 - 3.5, k_3 = 0.05 - 2.5, k_{-3} = 0.01 - 0.15, k_4 = 0.2 - 2.9, k_5 = 2.5 - 8.0, k_{-5} = 0.2 - 1.85, k_6 = 3.0 - 10.0, k_7 = 1.5 - 5.0, k_{-7} = 0.1 - 1.0, k_8 = 3.5 - 10.0$, $E_{1_0} = 100$, $M_0 = 10, C_{1_0} = 70, P_{1_0} = 60, E_{2_0} = 50, C_{2_0} = 10, P_{2_0} = 30, I_0 = 10, C_{3_0} = 90, P_{3_0} = 80, E_{4_0} = 70, C_{4_0} = 70$, and $P_{4_0} = 100$ for numerical simulation.

Methanol level is lower in patients who get charcoal therapy for the first two hours than in those who do not. As a result, activated charcoal helps preventing toxicity from spreading in the first place.

6. Results and Discussion

From Figures 1 and 2, it is clear that the values of harmful reactants fluctuate when the fractal values for α changes. The value of methanol, which is the model's primary concern, drops rapidly, as shown in Figure 3, and several curves depict the impact of various two-scale dimension on the methanol level in the human body. The lower the fractional parameter is, the less methanol remains in the human body after

activated charcoal is introduced. Because this type of incident is more likely to occur in remote locations, we consider the worst-case scenario, in which travel to the medical center is too long.

Many researchers have employed the ABC fractional operator to represent various illness models, and the findings show that the methodology is accurate. To find a suitable solution, we used the same approach to investigate methanol toxicity, methanol adsorption by activated charcoal, and enzyme-substrate inhibitor dynamics. When activated charcoal is added to the system as soon as possible, the harmful formic acid production slows down. The absorption of methanol by activated charcoal and the enzymatic reaction of methanol in the liver cause methanol concentrations to decline faster. The quick drop in methanol has an impact on the additional reactants in the enzymatic process. Matlab 2020 has been used to get the graphical results. We conclude from these graphical results that, by employing this new concept of the two-sale and ABC fractional operator, one can obtain more accurate results and gain a better knowledge not only of an enzymatic reaction equation system but also of real-world problems in science and engineering.

7. Conclusion

The numerous negative effects of alcohol have been proven. We employed the new ABC fractional derivative to take the alcoholism model into fractional order in this work. The concept of a two-scale fractal dimension has been utilized to elaborate the scale effect in the topic under discussion. Simulations have been used to demonstrate the impact of fractional order. The results demonstrate the effectiveness of the ABC fractional derivative, integral operators, and two-scale transform. Thus, we can claim that the suggested approach is extremely efficient and can be employed to understand the nature of a wide class of nonlinear fractional-order mathematical models in science and engineering.

Data Availability

All the data used to support the findings of the study are available within the article.

Conflicts of Interest

The authors declare that they have no conflicts of interest.

References

[1] W. H. Organization, *Global Status Report on Alcohol and Health 2018*, World Health Organization, Geneva, Switzerland, 2019.

[2] T. Zhao, M. Wang, and Y. Chu, "On the bounds of the perimeter of an ellipse," *Acta Mathematica Scientia*, vol. 42, no. 2, pp. 491–501, 2022.

[3] T.-H. Zhao, M.-K. Wang, G.-J. Hai, and Y.-M. Chu, "Landen inequalities for Gaussian hypergeometric function, revista de la Real academia de Ciencias exactas, físicas y naturales," *Serie A. Matemáticas*, vol. 116, no. 1, pp. 1–23, 2022.

[4] T.-H. Zhao, M.-K. Wang, and Y. Chu, "Concavity and bounds involving generalized elliptic integral of the first kind," *Journal of Mathematical Inequalities*, vol. 15, no. 2, pp. 701–724, 2021.

[5] M. Nadeem and S.-W. Yao, "Solving system of partial differential equations using variational iteration method with He's polynomials," *Journal of Mathematics and Computer Science*, vol. 19, no. 3, pp. 203–211, 2019.

[6] S. N. Hajiseyedazizi, M. E. Samei, J. Alzabut, and Y. M. Chu, "On multi-step methods for singular fractional q-integro-differential equations," *Open Mathematics*, vol. 19, no. 1, pp. 1378–1405, 2021.

[7] H.-Z. Xu, W.-M. Qian, and Y.-M. Chu, "Sharp bounds for the lemniscatic mean by the one-parameter geometric and quadratic means," *Revista de la Real Academia de Ciencias Exactas, Físicas y Naturales. Serie A. Matemáticas*, vol. 116, no. 1, pp. 1–15, 2022.

[8] T.-H. Zhao, B. A. Bhayo, and Y.-M. Chu, "Inequalities for generalized grötzsch ring function," *Computational Methods and Function Theory*, 2021.

[9] M. Nadeem and S.-W. Yao, "Solving the fractional heat-like and wave-like equations with variable coefficients utilizing the Laplace homotopy method," *International Journal of Numerical Methods for Heat & Fluid Flow*, vol. 31, no. 1, pp. 273–292, 2020.

[10] Z.-B. Li and J.-H. He, "Fractional complex transform for fractional differential equations," *Mathematical and Computational Applications*, vol. 15, no. 5, pp. 970–973, 2010.

[11] H.-H. Chu, T.-H. Zhao, and Y.-M. Chu, "Sharp bounds for the toader mean of order 3 in terms of arithmetic, quadratic and contraharmonic means," *Mathematica Slovaca*, vol. 70, no. 5, pp. 1097–1112, 2020.

[12] Y. Chu and T.-H. Zhao, "Concavity of the error function with respect to Hölder means," *Mathematical Inequalities & Applications*, vol. 19, no. 2, pp. 589–595, 2016.

[13] T.-H. Zhao, Z.-H. Shen, and Y.-M. Chu, "Sharp power mean bounds for the lemniscate type means," *Revista de la Real Academia de Ciencias Exactas, Físicas y Naturales. Serie A. Matemáticas*, vol. 115, no. 4, pp. 1–16, 2021.

[14] Y.-Q. Song, T.-H. Zhao, Y.-M. Chu, and X.-H. Zhang, "Optimal evaluation of a toader-type mean by power mean," *Journal of Inequalities and Applications*, vol. 2015, no. 1, pp. 1–12, 2015.

[15] M.-K. Wang, M.-Y. Hong, Y.-F. Xu, Z.-H. Shen, and Y. Chu, "Inequalities for generalized trigonometric and hyperbolic functions with one parameter," *Journal of Mathematical Inequalities*, vol. 14, no. 1, pp. 1–21, 2020.

[16] Y.-M. Chu, U. Nazir, M. Sohail, M. M. Selim, and J.-R. Lee, "Enhancement in thermal energy and solute particles using hybrid nanoparticles by engaging activation energy and chemical reaction over a parabolic surface via finite element approach," *Fractal and Fractional*, vol. 5, no. 3, p. 119, 2021.

[17] S. Rashid, S. Sultana, Y. Karaca, A. Khalid, and Y.-M. Chu, "Some further extensions considering discrete proportional fractional operators," *Fractals*, vol. 30, no. 1, 2022.

[18] T.-H. Zha, O. Castillo, H. Jahanshahi et al., "A fuzzy-based strategy to suppress the novel coronavirus (2019-ncov) massive outbreak," *Applied and Computational Mathematics*, vol. 20, no. 1, pp. 160–176, 2021.

[19] Z.-Y. He, A. Abbes, H. Jahanshahi, N. D. Alotaibi, and Y. Wang, "Fractional-order discrete-time sir epidemic model with vaccination: chaos and complexity," *Mathematics*, vol. 10, no. 2, p. 165, 2022.

[20] F. Jin, Z.-S. Qian, Z.-S. Qian, Y.-M. Chu, and M. U. Rahman, "On nonlinear evolution model for drinking behavior under caputo-fabrizio derivative," *Journal of Applied Analysis & Computation*, vol. 12, no. 2, pp. 790–806, 2022.

[21] M. Nazeer, F. Hussain, M. I. Khan et al., "Theoretical study of mhd electro-osmotically flow of third-grade fluid in micro channel," *Applied Mathematics and Computation*, vol. 420, Article ID 126868, 2022.

[22] Y.-M. Chu, B. M. Shankaralingappa, B. J. Gireesha, F. Alzahrani, M. I. Khan, and S. U. Khan, "Combined impact of cattaneo-christov double diffusion and radiative heat flux on bio-convective flow of Maxwell liquid configured by a stretched nano-material surface," *Applied Mathematics and Computation*, vol. 419, Article ID 126883, 2022.

[23] T. H. Zhao, M. I. Khan, and Y. M. Chu, "Artificial neural networking (ANN) analysis for heat and entropy generation in flow of non-Newtonian fluid between two rotating disks," *Mathematical Methods in the Applied Sciences*, 2021.

[24] M. A. Iqbal, Y. Wang, M. M. Miah, and M. S. Osman, "Study on Date-Jimbo-Kashiwara-Miwa Equation with Conformable Derivative Dependent on Time Parameter to Find the Exact Dynamic Wave Solutions," *Fractal and Fractional*, vol. 6, no. 1, p. 4, 2021.

[25] P. Ghosh and J. F. Peters, "Impulsive differential equation model in methanol poisoning detoxification," *Journal of Mathematical Chemistry*, vol. 58, no. 1, pp. 126–145, 2020.

[26] S. Lee, E. Jung, and C. Castillo-Chavez, "Optimal control intervention strategies in low- and high-risk problem drinking populations," *Socio-Economic Planning Sciences*, vol. 44, pp. 258–265, 2010.

[27] H. F. Huo, Y. L. Chen, and H. Xiang, "Stability of a binge drinking model with delay," *Journal of biological dynamics*, vol. 11, pp. 210–225, 2017.

[28] Q. T. Ain, N. Anjum, A. Din, A. Zeb, S. Djilali, and Z. A. Khan, "On the analysis of Caputo fractional order dynamics of middle east lungs coronavirus (MERS-CoV) model," *Alexandria Engineering Journal*, vol. 61, no. 7, pp. 5123–5131, 2022.

[29] A. Atangana, "Fractal-fractional differentiation and integration: Connecting fractal calculus and fractional calculus to predict complex system," *Chaos, Solitons & Fractals*, vol. 102, pp. 396–406, 2017.

[30] A. Atangana and S. Qureshi, "Modeling attractors of chaotic dynamical systems with fractal-fractional operators," *Chaos, Solitons & Fractals*, vol. 123, pp. 320–337, 2019.

[31] Q. T. Ain and J.-H. He, "On two-scale dimension and its applications," *Thermal Science*, vol. 23, no. 3, pp. 1707–1712, 2019.

[32] J.-H. He and Q.-T. Ain, "New promises and future challenges of fractal calculus: from two-scale thermodynamics to fractal variational principle," *Thermal Science*, vol. 24, no. 2, pp. 659–681, 2020.

[33] J.-H. He, G. M. Moatimid, and M. H. Zekry, "Forced Nonlinear Oscillator in a Fractal Space," *Facta Universitatis, Series: Mechanical Engineering 20*, no. 1, p. 1, 2022.

Hindawi
Complexity
Volume 2022, Article ID 3570667, 9 pages
https://doi.org/10.1155/2022/3570667

Research Article

The Analysis of Fractional-Order System Delay Differential Equations Using a Numerical Method

Pongsakorn Sunthrayuth,[1] **Hina M. Dutt**,[2] **Fazal Ghani**,[3] **and Mohammad Asif Arefin**[4]

[1]*Department of Mathematics and Computer Science, Faculty of Science and Technology, Rajamangala University of Technology Thanyaburi (RMUTT), Thanyaburi, Pathumthani, Thailand*
[2]*Department of Humanities and Sciences, School of Electrical Engineering and Computer Science (SEECS), National University of Sciences and Technology (NUST), Islamabad, Pakistan*
[3]*Department of Mathematics, Abdul Wali Khan University, Mardan 23200, Pakistan*
[4]*Department of Mathematics, Jashore University of Science and Technology, Jashore-7408, Bangladesh*

Correspondence should be addressed to Mohammad Asif Arefin; asif.math@just.edu.bd

Received 25 February 2022; Accepted 5 May 2022; Published 28 May 2022

Academic Editor: Fathalla A. Rihan

To solve fractional delay differential equation systems, the Laguerre Wavelets Method (LWM) is presented and coupled with the steps method in this article. Caputo fractional derivative is used in the proposed technique. The results show that the current procedure is accurate and reliable. Different nonlinear systems have been solved, and the results have been compared to the exact solution and different methods. Furthermore, it is clear from the figures that the LWM error converges quickly when compared to other approaches. When compared with the exact solution to other approaches, it is clear that LWM is more accurate and gets closer to the exact solution faster. Moreover, on the basis of the novelty and scientific importance, the present method can be extended to solve other nonlinear fractional-order delay differential equations.

1. Introduction

In 1965, a mathematician named L'Hopital asked Leibniz what would be the solution to the problem if the derivatives and integrals were fractional order. This L'Hopital question has resulted in the creation of new mathematical knowledge, but no one has been able to deal with it for a long time [1]. Mathematicians began to conduct study in the field of fractional derivatives, integration, and the development of a new field of fractional calculus after a period of time. In mathematics, this domain is known as fractional calculus, and it is a significant branch of mathematics that deals with the study of fractional derivatives and integration. Mathematicians have recently started working on fractional calculus because of its wide applications in all fields of research such as economics [2], viscoelastic materials [3], dynamics of interfaces between soft nanoparticles and rough substrates [4], continuum and statistical mechanics [5], solid mechanics [6], and many other topics.

Many natural problems can be solved using mathematical formulations by transforming physical facts into equation form. Differential equations (DEs) are a type of equation that is used to model a variety of phenomena. However, certain cases are too complicated to be solved using a differential equation. In this case, the researchers used fractional differential equations (FDEs), which are more accurate than differential equations with order integers in modelling the phenomenon. FDEs have realised the importance of real-world modelling challenges in recent years. Such as electrochemistry of corrosion [7], electrode-electrolyte polarization [8], heat conduction [9], optics and signal processing [10], diffusion wave [11], circuit systems [12], control theory of dynamical systems [6], probability and statistics [14, 15], fluid flow [16], and so on.

Equations with delayed arguments are known as fractional delay differential equations (FDDEs). Time delay, spatial delay, step size delay, constant delay, and so on are examples of delayed arguments. Due to various delay arguments found in nature, FDDEs are classified into distinct types. FDDEs are time delay DDEs, which are equations in which the current time derivatives are dependent on the solution and possibly its derivatives at a previous time. In the last few decades, mathematicians have paid more attention to FDDEs for modelling than simple ODEs, because a small delay has a big impact. FDDEs are employed in a variety of domains of mathematics, including infection diseases, navigation control, population dynamics, circulating blood, and the body's reaction to carbon dioxide [17–19], as well as some additional applications in advanced research studies.

It is necessary to develop accurate, time-efficient, and computationally efficient numerical algorithms for solving FDDEs. Xu and Ma [20] investigated the SEIRS epidemic model with a saturation incidence rate and a time delay that defined the latent period. Rihan et al. [21] investigated a delay differential model, numerically analysed it, and established an effective method of combining chemotherapy with therapeutic immunotherapy in 2014. The global stability of the Lotka–Volterra autonomous model with diffusion and time delay was studied by Beretta and Takeuchi [22]. Lv and Gao [23] used the well-known reproducing kernel Hilbert space approach to solve neutral functional proportional delay differential equations (RKHSM). Galach [24] investigated the time delay in the model presented by Kuznetsov and Taylor, where the time delay was included to gain better compatibility with reality. Furthermore, some researchers discussed the behaviour of delay fractional differential equations or a system of delay fractional differential equations, as well as their stability and analysis. Some works, such as in [25, 26], demonstrate this style of research.

In a number of situations, exact FDDEs solutions are difficult to get. As a result, the researchers' key goal is to develop a numerical or analytical solution to FDDEs. As a result, many strategies have been employed such as the New Predictor Corrector Method (NPCM) [27], New Iterative Method (NIM) [28], Adomian Decomposition Method (ADM) [29], Backward Differentiation Formula (BDF) [30], Chebyshev Pseudospectral Method (CPM) [31], Legendre–Gauss Collocation Method (LGCM) [32], Adams–Bashforth–Moulton Algorithm (ABMA) [33], operational matrix based on poly-Bernoulli polynomials (OMM) [34], and Runge Kutta-type Method (RKM) [35]. Overall, some of the approaches used to obtain numerical or analytical solutions to FDDEs have low accuracy of convergence, while others have great accuracy. Among all of these approaches, the wavelet approximation family is one of the more recent methods for locating FDDE solutions. For the approximate solution of FDDEs systems in the current study, we implement Laguerre Wavelets Method (LWM) in combination with the steps method. The proposed solution is shown to be entirely compatible with the complexity of such problems and to be extremely user-friendly. The error comparison shows that the suggested technique has a very high level of accuracy.

The structure of remaining paper is summarized as follows. Section 2 defines some basic definitions related to our present work. The general methodology for solving FDDEs is provided in Section 3. Section 4 presents the main results, numerical simulations, and graphical representations. The conclusion along with future research directions is drawn in Section 5.

2. Preliminaries Concept

This section introduces the basic concept and several important definitions from fractional calculus, which we will apply in our current research.

2.1. Definition. The following mathematical statement demonstrates Caputo's definition for fractional derivatives of order δ [36, 37].

$$D^{\delta}\xi(\psi) = \frac{1}{\Gamma(m-\delta)}\int_0^{\psi}(\psi-\tau)^{m-\delta-1}\xi^{(m)}(\tau)\mathrm{d}\tau, \tag{1}$$

for $n-1<\delta\le m$, $m\in\mathbb{N}$, $\psi>0$, $\xi\in\mathbb{C}_{-1}^{n}$.

2.2. Definition. The Riemann–Liouville integral operator for order δ is given as [36, 37].

$$I^{\delta}\xi(\psi) = \frac{1}{\Gamma(\delta)}\int_0^{\psi}(\psi-\tau)^{\delta-1}\xi(\tau)\mathrm{d}\tau. \tag{2}$$

The following are the properties of the Caputo derivative and Riemann–Liouville integral operators.

$$D^{\delta}I^{\delta}\xi(\psi) = \xi(\psi),$$

$$I^{\delta}D^{\delta}\xi(\psi) = \xi(\psi) - \sum_{k=0}^{n-1}\frac{\xi^{(k)}(0^{+})}{k!}\psi^{k}, \quad \psi\ge 0\, n-1<\delta<n. \tag{3}$$

3. Laguerre Wavelets

Wavelets [38–40] are a family of functions made up of dilation and translation of a single function called the mother wavelet, $\varphi(\psi)$. The family of continuous wavelets [41] is formed when the dilation parameter a and the translation parameter b vary continuously.

$$\varphi_{a,b}(\psi) = |a|^{-1/2}\varphi\left(\frac{\psi-b}{a}\right), \quad a,b\in\mathbf{R}, a\neq 0. \tag{4}$$

The following family of discrete wavelets results from restricting the parameters a and b to discrete values as $a=a_0^{-p}, a=nb_0a_0^{-p}, a_0>1, b_0>0$,

$$\varphi_{p,n}(\psi) = |a|^{-p/2}\varphi\left(a_0^{p}(\psi)-nb_0\right), \quad p,n\in\mathbb{Z}, \tag{5}$$

Table 1: Comparison of the exact and MLWM solution for example 1 at $m = 9$.

ψ	Exact $\xi(\psi)$	Exact $\zeta(\psi)$	MLWM solution $\xi(\psi)$	MLWM solution $\zeta(\psi)$
0	1.000000000000000	0.000000000000000	1.000000000000000	0.000000000000000
0.1	0.900316999845194	0.998334166468281	0.900316999845194	0.998334166468281
0.2	0.802410647342520	0.198669330795061	0.802410647342527	0.198669330795061
0.3	0.707730678026351	0.295520206661339	0.707730678025662	0.295520206661339
0.4	0.617405647901646	0.389418342308650	0.617405647901653	0.389418342308637
0.5	0.532280730215671	0.479425538604203	0.532280730215273	0.479425538604203
0.6	0.452953789145250	.5646424733950353	0.452953789145497	.5646424733947035
0.7	0.379809389925154	0.644217687237691	0.37980938992536	0.644217687236876
0.8	0.313050504004480	0.717356090899522	0.313050504004346	0.717356090898501
0.9	0.252727753291169	0.783326909627483	0.252727753291868	0.783326909628249
1.0	0.198766110346413	0.841470984807896	0.198766110346480	0.841470984813237

Table 2: Error estimation of proposed method with FBPs for example 1 at $m = 9$.

ψ	Error (ξ_{MLWM})	Error (ζ_{MLWM})	Error (ξ_{FBPs})	Error (ζ_{FBPs})
0.2	7.1240361137E-15	2.1190342156276E-17	1.22E-11	3.55E-12
0.4	3.1090504913E-13	1.2920241091118E-14	9.91E-12	1.04E-11
0.6	4.0077803050E-12	3.3177676221433E-13	7.20E-12	1.59E-11
0.8	2.5602591191E-12	1.0209754593019E-12	6.56E-12	2.06E-11
1.0	4.9538867166E-11	5.3406078485367E-12	7.58E-10	1.47E-11

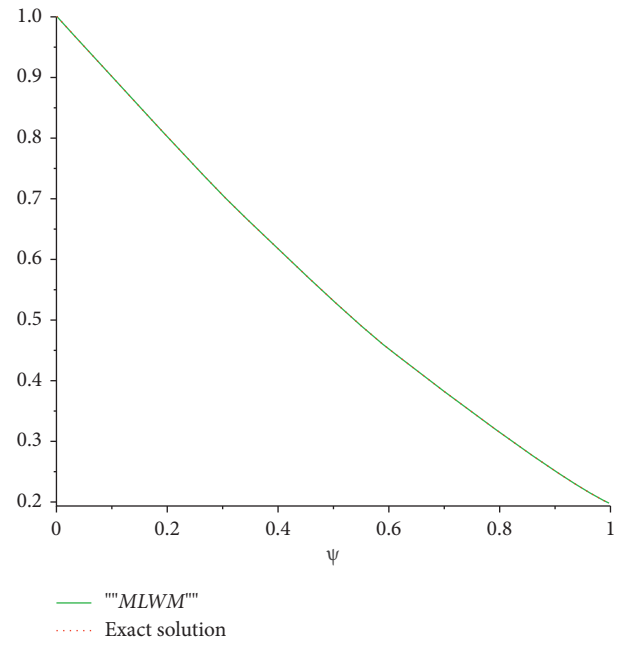

Figure 1: Behaviour of the exact solution and proposed method solution for $\xi(\psi)$ of problem 1.

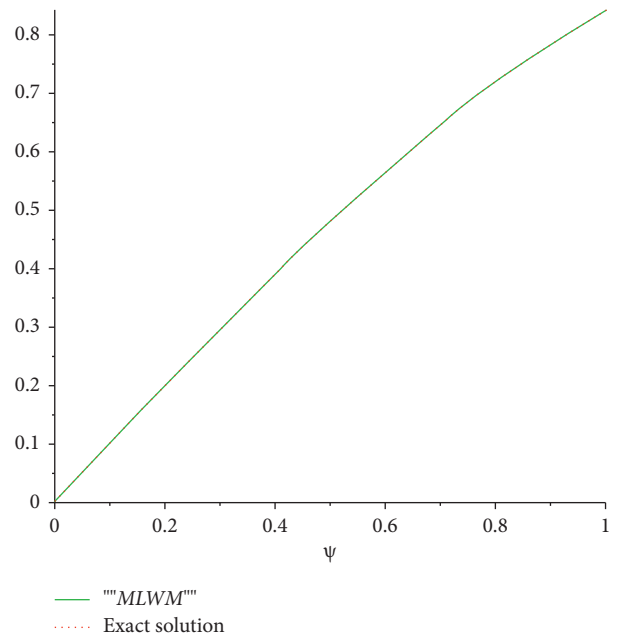

Figure 2: Behaviour of the exact solution and proposed method solution for $\zeta(\psi)$ of problem 1.

where the wavelet basis for $L^2(\mathbf{R})$ is $\varphi_{p,n}$. When $a_0 = 2$ and $b_0 = 1$, for instance, $\varphi_{p,n}(\psi)$ forms an orthonormal basis. There are four arguments in the Laguerre wavelets $\Phi_{n,m}(\psi) = \varphi(k, n, m, \psi)$, $n = 1, 2, \ldots, 2^{k-1}$, where k is non-negative integer, m represents the Laguerre polynomials degree, and represents normalized time. Over the interval $[0, 1)$, they are defined as

$$\varphi_{n,m} = \begin{cases} 2^{p/2}\widetilde{\mathscr{L}}_m\left(2^p\psi - 2n + 1\right), & \dfrac{n-1}{2^{p-1}} \le \psi < \dfrac{n}{2^{p-1}}, \\ 0, & \text{Otherwise}, \end{cases} \tag{6}$$

where

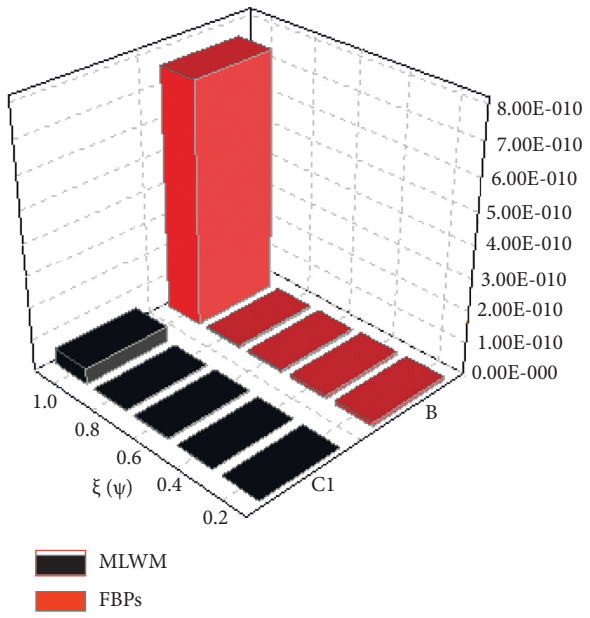

Figure 3: FBPs and proposed method error analysis for $\xi(\psi)$ of example 1.

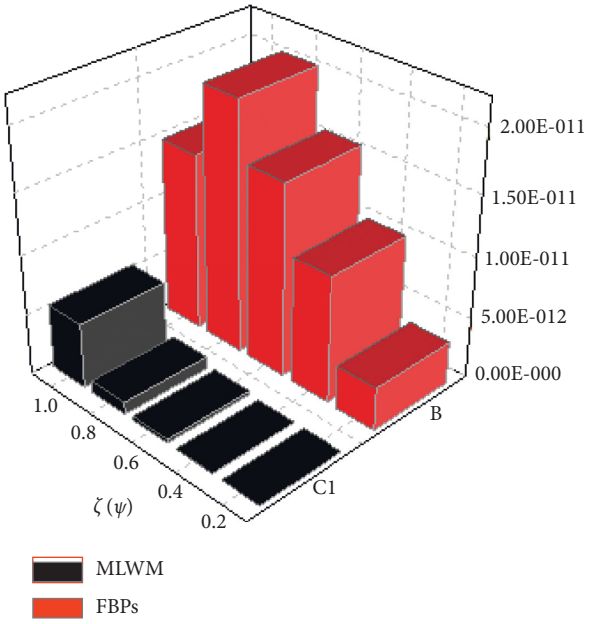

Figure 4: FBPs and proposed method error analysis for $\zeta(\psi)$ of example 1.

$$\tilde{\mathscr{L}}_m = \frac{1}{m!}\mathscr{L}_m(\psi) \quad m = 0, 1, 2, \ldots A - 1. \tag{7}$$

$m = 0, 1, 2, \ldots, M - 1$. The coefficients are utilised in (10) to determine orthonormality. The Laguerre polynomials having degree m with regard to $w(\psi) = 1$ weight function on the interval $[0, \infty]$ are $L_m(\psi)$ and satisfy the recursive formula:

$$\mathscr{L}_0(\psi) = 1, \ \mathscr{L}_1(\psi) = 1 - \psi,$$

$$\mathscr{L}_{m+2} = \frac{((2m + 3 - x)\mathscr{L}_{m+1}(\psi) - (m + 1)\mathscr{L}_m)}{m + 2} \quad m = 0, 1, 2, 3, 4, \ldots. \tag{8}$$

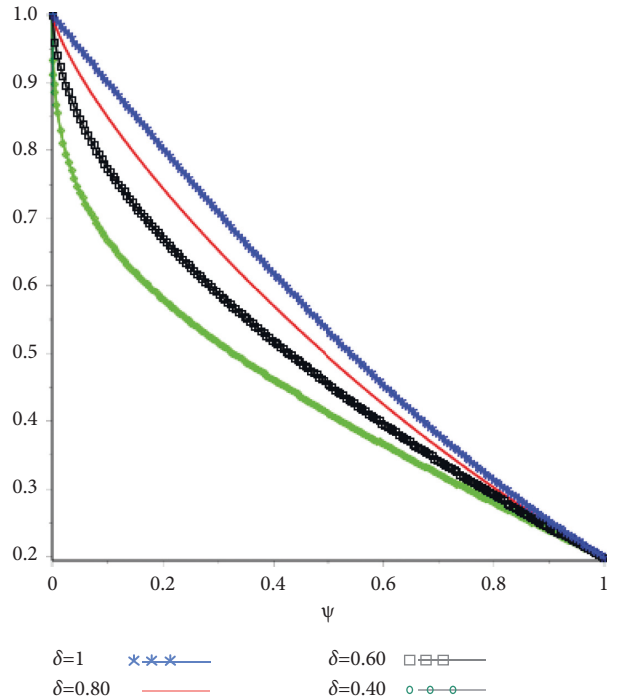

Figure 5: The error comparison at various fractional-orders of for $\xi(\psi)$ example 1.

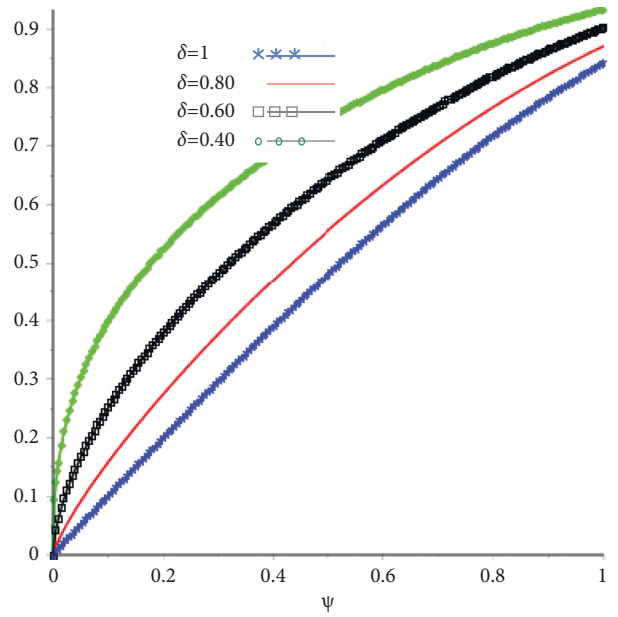

Figure 6: The error comparison at various fractional-orders of for $\zeta(\psi)$ example 1.

where

Modified Laguerre wavelets method (MLWM): Here, we consider the delay differential equation of the form:

$$y^{\alpha}(\psi) = f(\psi) + g(\psi)y\left(\frac{\psi}{a} - c\right), \quad 0 < \psi < b, 0 < \alpha \leq 1,$$
$$y(\psi) = p(\psi), \quad -b \leq \psi \leq 0, \tag{9}$$

Table 3: Comparison at different fractional-order of δ on the basis of error for example 2.

δ	ψ	Exact	$MLWM$ solution	$MLWM$ error	Spline functions
	0.01	0.0001	0.00009999986375	1.3625E-10	8.2E-4
	0.02	0.0004	0.0003999998553	1.447E-10	2.5E-3
0.1	0.03	0.0009	0.0008999998624	1.376E-10	4.7E-3
	0.04	0.0016	0.001599999883	1.17E-10	7.3E-3
	0.05	0.0025	0.002499999813	1.87E-10	1.0E-2
	0.01	0.0001	0.0001000000111	1.11E-11	4.4E-4
	0.02	0.0004	0.0004000001035	1.035E-10	1.4E-3
0.2	0.03	0.0009	0.0008999999845	1.55E-11	2.7E-3
	0.04	0.0016	0.001600000057	5.7E-11	4.4E-3
	0.05	0.0025	0.002500000022	2.2E-11	6.1E-3
	0.01	0.0001	0.0001000001798	1.798E-10	2.1E-4
	0.02	0.0004	0.0004000002303	2.303E-10	7.1E-4
0.3	0.03	0.0009	0.0009000001717	1.717E-10	1.4E-3
	0.04	0.0016	0.001600000106	1.06E-10	2.4E-3
	0.05	0.0025	0.002500000136	1.36E-10	3.5E-3
	0.01	0.0001	0.0001000000189	1.89E-11	8.1E-5
	0.02	0.0004	0.0003999999502	4.98E-11	2.9E-4
0.4	0.03	0.0009	0.0008999998916	1.084E-10	6.1E-4
	0.04	0.0016	0.001599999941	5.9E-11	1.0E-3
	0.05	0.0025	0.002499999997	3.000E-12	1.0E-3
	0.01	0.0001	0.00009999988074	1.1926E-10	4.5E-6
	0.02	0.0004	0.0003999997780	2.220E-10	2.6E-5
0.5	0.03	0.0009	0.0008999996906	3.094E-10	7.0E-5
	0.04	0.0016	0.001599999717	3.83E-10	1.4E-4
	0.05	0.0025	0.002499999657	3.43E-10	2.5E-4

Table 4: Comparison at different fractional-orders of δ on the basis of error for example 2.

δ	ψ	Exact	$MLWM$ solution	$MLWM$ error	Spline functions
	0.01	0.0001	0.00009999986375	1.3625E-10	8.2E-4
	0.02	0.0004	0.0003999998553	1.447E-10	2.5E-3
	0.03	0.0009	0.0008999998624	1.376E-10	4.7E-3
	0.04	0.0016	0.001599999883	1.17E-10	7.3E-3
0.1	0.05	0.0025	0.002499999813	1.87E-10	1.0E-2
	0.01	0.0001	0.0001000000111	1.11E-11	4.4E-4
	0.02	0.0004	0.0004000001035	1.035E-10	1.4E-3
	0.03	0.0009	0.0008999999845	1.55E-11	2.7E-3
	0.04	0.0016	0.001600000057	5.7E-11	4.4E-3
0.2	0.05	0.0025	0.002500000022	2.2E-11	6.1E-3
	0.01	0.0001	0.0001000001798	1.798E-10	2.1E-4
	0.02	0.0004	0.0004000002303	2.303E-10	7.1E-4
	0.03	0.0009	0.0009000001717	1.717E-10	1.4E-3
	0.04	0.0016	0.001600000106	1.06E-10	2.4E-3
0.3	0.05	0.0025	0.002500000136	1.36E-10	3.5E-3
	0.01	0.0001	0.0001000000189	1.89E-11	8.1E-5
	0.02	0.0004	0.0003999999502	4.98E-11	2.9E-4
	0.03	0.0009	0.0008999998916	1.084E-10	6.1E-4
	0.04	0.0016	0.001599999941	5.9E-11	1.0E-3
0.4	0.05	0.0025	0.002499999997	3.000E-12	1.0E-3
	0.01	0.0001	0.00009999988074	1.1926E-10	4.5E-6
	0.02	0.0004	0.0003999997780	2.220E-10	2.6E-5
	0.03	0.0009	0.0008999996906	3.094E-10	7.0E-5
0.5	0.04	0.0016	0.001599999717	2.83E-10	1.4E-4
	0.05	0.0025	0.002499999657	3.43E-10	2.5E-4

where $f(\psi)$ is a provided continuous linear or nonlinear function and $g(\psi)$ is a source term function. Using the proposed method, transform the delay differential equation (12) to an inhomogeneous ordinary differential equation by using the initial source, $p(\psi)$, as shown in (12):

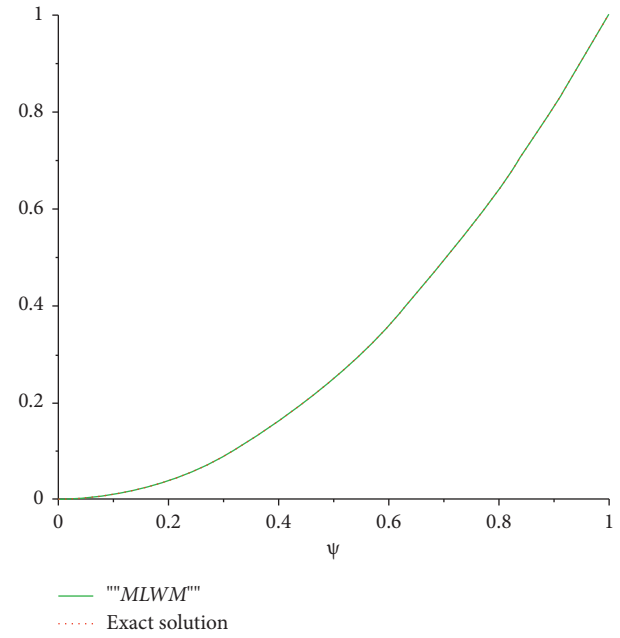

Figure 7: Analysis of the exact and proposed method solution for $\xi(\psi)$ of problem 2.

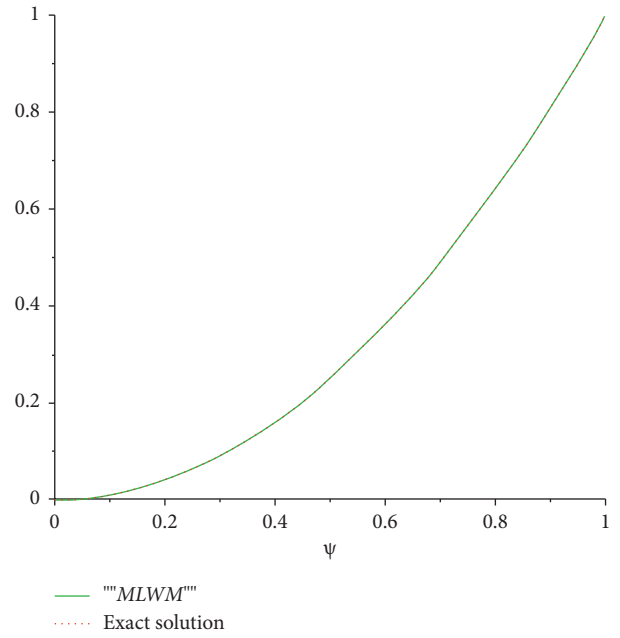

Figure 8: Analysis of the exact and proposed method solution for $\zeta(\psi)$ of problem 2.

$$y^{\alpha}(\psi) = f(\psi) + g(\psi)p\left(\frac{\psi}{a} - c\right), \quad 0 < \psi < b, 1 < \alpha \leq 2. \tag{10}$$

Equation (14) can be expanded as a Laguerre wavelets series as follows:

$$y(\psi) = \sum_{n=0}^{\infty} \sum_{m=0}^{\infty} d_{n,m}\varphi_{n,m}(\psi), \tag{11}$$

where $\varphi_{n,m}(\psi)$ is determined by (9). The truncated series is used to approximate $y(\psi)$.

$$y_p, A = \sum_{n=0}^{\infty} \sum_{m=0}^{\infty} d_{n,m}\varphi_{n,m}(\psi), \tag{12}$$

Then, there should be a total of $2^{p-1}A$ conditions for determining the $2^{p-1}A$ coefficient:

$$c_{10}, c_{11} \ldots c_{A-1} \ldots c_{20}, c_{2A-1} \ldots c_{2^{p-1}1} \ldots c_{2^{p-1}A-1}. \tag{13}$$

Since the initial and boundary conditions, respectively, provide the conditions.

$$y_p, A(0) = \sum_{n=1}^{2^{p-1}} \sum_{m=0}^{A-1} d_{n,m}\varphi_{n,m}(0) = q(0). \tag{14}$$

$$\frac{d}{d\psi} y_p, A(1) = \frac{d}{d\psi} \sum_{n=1}^{2^{p-1}} \sum_{m=0}^{A-1} d_{n,m}\varphi_{n,m}(1) = \acute{q}(1). \tag{15}$$

We see that there should be $2^{p-1}A - 2$ extra condition to recover the unknown coefficient $d_{n,m}$. These conditions can be obtained by substituting (14) in (12):

$$\frac{d^{\alpha}}{d\psi^{\alpha}} \sum_{n=1}^{2^{p-1}} \sum_{m=0}^{A-3} d_{n,m}\varphi_{n,m}(\psi) = f\left(\sum_{n=1}^{2^{p-1}} \sum_{m=0}^{A-3} d_{n,m}\varphi_{n,m}(\psi)\right) + g(\psi)p\left(\frac{\psi}{a} - c\right). \tag{16}$$

We, now assume equation (18) is exact at $2^{p-1}A - 3$ points ψ_i as follows:

$$\frac{d^{\alpha}}{d\psi^{\alpha}} \sum_{n=1}^{2^{p-1}} \sum_{m=0}^{A-3} d_{n,m}\varphi_{n,m}(\psi_i) = f\left(\sum_{n=1}^{2^{p-1}} \sum_{m=0}^{A-3} d_{n,m}\varphi_{n,m}(\psi_i)\right) + g(\psi_i)p\left(\frac{\psi_i}{a} - c\right). \tag{17}$$

The best choice of the ψ_i points are the zeros of the shifted Laguerre polynomials of degree $2^{p-1}A - 2$ in the interval [0, 1] that is $\psi_i = s_i - 1/2$, where $s_i = \cos((2_i - 1)\pi/2^{p-1}A - 1), i = 1, 2, 3, \ldots 2^{p-1}A - 2$. Since the initial and boundary conditions, respectively, provide the conditions. Combining equations (9) and (12) yields $2^{p-1}A$ linear equations from which the unknown coefficients, $d_{n,m}$, can be computed. The same technique is followed for first- and second-order delay differential equations.

4. Numerical Representation

4.1. Example. Consider the system of fractional ordinary delay differential equations [42],

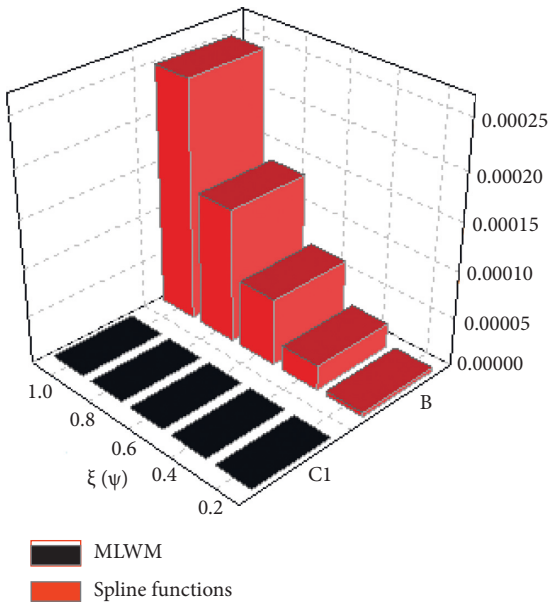

Figure 9: Spline functions and proposed method error analysis for $\xi(\psi)$ of example 2.

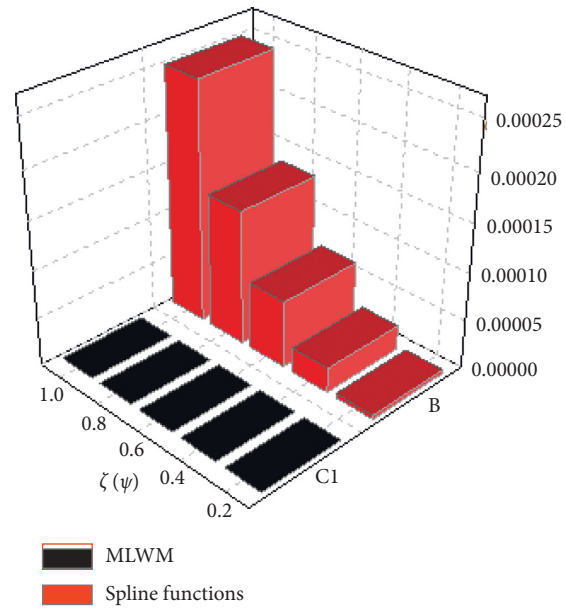

Figure 10: Spline functions and proposed method error analysis for $\zeta(\psi)$ of example 2.

$$D^{\delta}\xi(\psi) = -\zeta(\psi) - 2e^{-\frac{3}{4}\psi}\cos\left(\frac{1}{2}\psi\right)\sin\left(\frac{1}{4}\psi\right)\xi(0.25\psi) - e^{-\psi}\cos\left(\frac{1}{2}\psi\right)\zeta(0.5\psi),$$
$$D^{\delta}\zeta(\psi) = e^{\psi}\xi^{2}(0.5\psi) - \zeta^{2}(0.5\psi), \tag{18}$$

with the initial sources $\xi(0) = 1$, $\zeta(0) = 0$, and having exact solution at $\delta = 1$ as $\xi(\psi) = e^{-\psi}\cos(\psi)$, $\zeta(\psi) = \sin(\psi)$.

Table 1 shows the exact solution and numerical results achieved using the proposed method. Table 2 shows the comparison on the basis of absolute error between our technique and those derived from FBPs. When $\delta = 1$, the behaviour of the exact solution and proposed method solution of this problem is shown in Figures 1 and 2, respectively, whereas the error comparison of CPM and FBPs is shown in Figures 3 and 4. Figures 5 and 6 show graphical representations for different fractional orders of δ, confirming that the proposed method solution converges to the exact solution as the value of δ approaches from fractional-order towards integer-order.

4.2. Example. Consider the system of fractional ordinary delay differential equations [43].

$$D^{\delta}\xi(\psi) = -\xi(\psi) + \zeta\left(\frac{\psi}{2}\right) + \frac{3}{4}\psi^{2} + \frac{2}{\Gamma(3-\delta)}\psi^{2-\delta},$$
$$D^{\delta}\zeta(\psi) = \zeta(\psi) - \xi\left(\frac{\psi}{2}\right) - \frac{3}{4}\psi^{2} + \frac{2}{\Gamma(3-\delta)}\psi^{2-\delta}. \tag{19}$$

The exact solution is given by $\xi(\psi) = \psi^{2}$ and $\zeta(\psi) = \psi^{2}$.

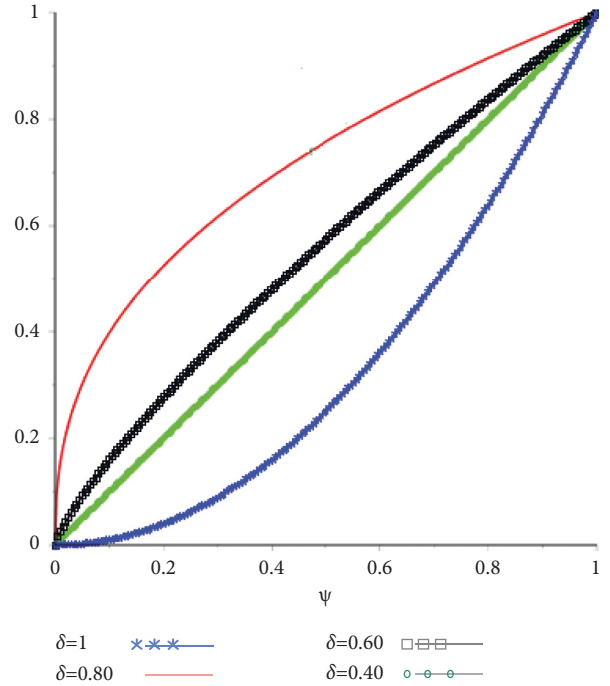

Figure 11: The error comparison at various fractional-orders for $\xi(\psi)$ of example 2.

The comparison among the exact solution and the Spline function polynomial technique solution are shown in Table 3. In Table 4, the errors acquired by the current technique are compared to those obtained by the Spline function polynomial method. In Figures 7 and 8, we compare the exact and approximated solutions, which shows that they are very close to each other. In addition, Figures 9 and 10 show the MLWM and Spline function error comparisons,

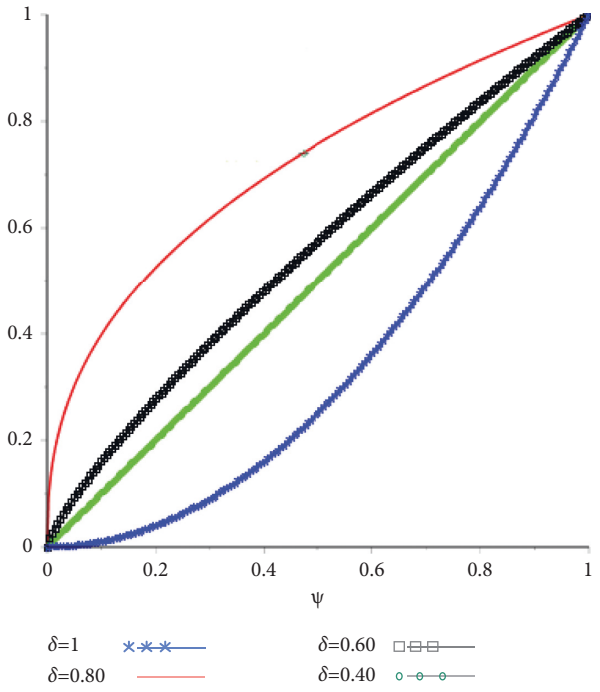

FIGURE 12: The error comparison at various fractional-orders for $\zeta(\psi)$ of example 2.

demonstrating that suggested approach is in best agreement with the exact solution.

5. Conclusion

We used the MLWM to solve fractional delay differential equations systems in this research. The proposed method's convergence is given special consideration. As demonstrated in Figures 1–12, the fractional-order delay differential equation solution approaches towards the solution of the integer-order delay differential equation. The results obtained by implementing the proposed method are in great agreement with the exact solution and are more accurate than those obtained by implementing other techniques. The proposed method (MLWM) is extremely user-friendly but extremely accurate, according to computational effort and numerical results. The computations work in this article are done using Maple.

Data Availability

The numerical data used to support the findings of this study are included within the article.

Conflicts of Interest

The authors declare that they have no conflicts of interest.

Authors' Contributions

All the authors jointly worked on the results, and they read and approved the final manuscript.

References

[1] L. Adam, "Fractional Calculus: History, Definitions and Applications for the Engineer," *Rapport technique*, pp. 1–28, Univeristy of Notre Dame: Department of Aerospace and Mechanical Engineering, Notre Dame, In, USA, 2004.

[2] R. T. Baillie, "Long memory processes and fractional integration in econometrics," *Journal of Econometrics*, vol. 73, no. 1, pp. 5–59, 1996.

[3] R. L. Bagley and P. J. Torvik, "Fractional calculus in the transient analysis of viscoelastically damped structures," *AIAA Journal*, vol. 23, no. 6, pp. 918–925, 1985.

[4] T. S. Chow, "Fractional dynamics of interfaces between soft-nanoparticles and rough substrates," *Physics Letters A*, vol. 342, no. 1-2, pp. 148–155, 2005.

[5] F. Mainardi, "Fractional calculus," in *Fractals and Fractional Calculus in Contin- Uum Mechanics*, A. Carpinteri and F. Mainardi, Eds., Springer-Verlag, New York, NY, USA, pp. 291–348, 1997.

[6] Y. A. Rossikhin and M. V. Shitikova, "Applications of fractional calculus to dynamic problems of linear and nonlinear hereditary mechanics of solids," *Applied Mechanics Reviews*, vol. 50, no. 1, pp. 15–67, 1997.

[7] K. B. Oldham, "The reformulation of an infinite sum via semiintegration," *SIAM Journal on Mathematical Analysis*, vol. 14, no. 5, pp. 974–981, 1983.

[8] W. H. Deng and C. P. Li, "Chaos synchronization of the fractional Lü system," *Physica A: Statistical Mechanics and Its Applications*, vol. 353, pp. 61–72, 2005.

[9] Y. Z. Povstenko, "Thermoelasticity that uses fractional heat conduction equation," *Journal of Mathematical Sciences*, vol. 162, no. 2, pp. 296–305, 2009.

[10] E. Baskin and A. Iomin, "Electro-chemical manifestation of nanoplasmonics in fractal media," *Open Physics*, vol. 11, no. 6, pp. 676–684, 2013.

[11] H. M. Srivastava, R. Shah, H. Khan, and M. Arif, "Some analytical and numerical investigation of a family of fractional–order Helmholtz equations in two space dimensions," *Mathematical Methods in the Applied Sciences*, vol. 43, no. 1, pp. 199–212, 2020.

[12] T. T. Hartley, C. F. Lorenzo, and H. Killory Qammer, "Chaos in a fractional order Chua's system," *IEEE Transactions on Circuits and Systems I: Fundamental Theory and Applications*, vol. 42, no. 8, pp. 485–490, 1995.

[13] H. Khan, U. Farooq, R. Shah, D. Baleanu, P. Kumam, and M. Arif, "Analytical solutions of (2+ time fractional order) dimensional physical models, using modified decomposition method," *Applied Sciences*, vol. 10, no. 1, p. 122, 2019.

[14] A. A. A. Kilbas, H. M. Srivastava, and J. J. Trujillo, . *Theory and applications of frac- tional differential equations*, Vol. 204, Elsevier Science Limited, Netherlands, 2006.

[15] I. B. Bapna and N. Mathur, "Application of fractional calculus in statistics," *Int. J. Contemp. Math. Sciences*, vol. 7, no. 18, pp. 849–856, 2012.

[16] V. V. Kulish and J. L. Lage, "Application of fractional calculus to fluid mechanics," *Journal of Fluids Engineering*, vol. 124, no. 3, pp. 803–806, 2002.

[17] F. A. Rihan, C. Tunc, S. H. Saker, S. Lakshmanan, and R. Rakkiyappan, "Applications of Delay Differential Equations in Biological Systems," *Complexity*, vol. 2018, Article ID 4584389, 3 pages, 2018.

[18] Y. Ding and H. Ye, "A fractional-order differential equation model of hiv infection of cd4+ t-cells," *Mathematical and Computer Modelling*, vol. 50, no. 3-4, pp. 386–392, 2009.

[19] V. Daftardar-Gejji, S. Bhalekar, and P. Gade, "The comparative study for solving fractional-order fornberg-whitham equation via ρ-laplace transform," *Symmtery*, vol. 79, no. 1, pp. 61–69.

[20] R. Xu and Z. Ma, "Numerical investigation of fractional-order Swift-Hohenberg equations via a Novel transform," *Symmtery*, vol. 61, pp. 229–239.

[21] F. A. Rihan, D. H. Abdelrahman, F. Al-Maskari, F. Ibrahim, and M. A. Abdeen, "Delay differential model for tumour-immune response with chemoimmunotherapy and optimal control," *Computational and Mathematical Methods in Medicine*, vol. 2014, Article ID 982978, 15 pages, 2014.

[22] E. Beretta and Y. Takeuchi, "Global stability of single-species diffusion Volterra models with continuous time delays," *Bulletin of Mathematical Biology*, vol. 49, no. 4, pp. 431–448, 1987.

[23] X. Lv and Y. Gao, "The RKHSM for solving neutral functional-differential equations with proportional delays," *Mathematical Methods in the Applied Sciences*, vol. 36, no. 6, pp. 642–649, 2013.

[24] M. Galach, "An analytical technique, based on natural transform to solve fractional-order parabolic equations," *Entropy*, vol. 13, pp. 395–406.

[25] D. Baleanu, R. L. Magin, S. Bhalekar, and V. Daftardar-Gejji, "Chaos in the fractional order nonlinear Bloch equation with delay," *Communications in Nonlinear Science and Numerical Simulation*, vol. 25, no. 1-3, pp. 41–49, 2015.

[26] B. Parsa Moghaddam, S. Yaghoobi, and J. A. Tenreiro Machado, "An extended predictor-corrector algorithm for variable-order fractional delay differential equations," *Journal of Computational and Nonlinear Dynamics*, vol. 11, no. 6, 2016.

[27] V. Daftardar-Gejji, Y. Sukale, and S. Bhalekar, "A new predictor-corrector method for fractional differential equations," *Applied Mathematics and Computation*, vol. 244, pp. 158–182, 2014.

[28] F. Awawdeh, "On new iterative method for solving systems of nonlinear equations," *Numerical Algorithms*, vol. 54, no. 3, pp. 395–409, 2010.

[29] D. J. Evans and K. R. Raslan, "The Adomian decomposition method for solving delay differential equation," *International Journal of Computer Mathematics*, vol. 82, no. 1, pp. 49–54, 2005.

[30] Z. B. Ibrahim, K. I. Othman, and M. Suleiman, "Implicit r-point block backward differentiation formula for solving first-order stiff ODEs," *Applied Mathematics and Computation*, vol. 186, no. 1, pp. 558–565, 2007.

[31] P. Sunthrayuth, R. Ullah, A. Khan et al., "Numerical analysis of the fractional-order nonlinear system of Volterra integro-differential equations," *Journal of Function Spaces*, vol. 2021, Article ID 1537958, 10 pages, 2021.

[32] S. A. Rakhshan and S. Effati, "A generalized Legendre-Gauss collocation method for solving nonlinear fractional differential equations with time varying delays," *Applied Numerical Mathematics*, vol. 146, pp. 342–360, 2019.

[33] D. Aksim and D. Pavlov, "On the extension of adams-bashforth-moulton methods for numerical integration of delay differential equations and application to the moon's orbit," *Mathematics in Computer Science*, vol. 14, no. 1, pp. 103–109, 2020.

[34] C. Phang, Y. T. Toh, and F. S. Md Nasrudin, "An operational matrix method based on poly-Bernoulli polynomials for solving fractional delay differential equations," *Computation*, vol. 8, no. 3, p. 82, 2020.

[35] N. Senu, K. C. Lee, A. Ahmadian, and S. N. I. Ibrahim, "Numerical solution of delay differential equation using two-derivative Runge-Kutta type method with Newton interpolation," *Alexandria Engineering Journal*, vol. 61, no. 8, pp. 5819–5835, 2022.

[36] M. Yi, L. Wang, and J. Huang, "Legendre wavelets method for the numerical solution of fractional integro-differential equations with weakly singular kernel," *Applied Mathematical Modelling*, vol. 40, no. 4, pp. 3422–3437, 2016.

[37] J.-H. He, Z.-B. Li, and Q.-l. Wang, "A new fractional derivative and its application to explanation of polar bear hairs," *Journal of King Saud University Science*, vol. 28, no. 2, pp. 190–192, 2016.

[38] J. H. He, "Some applications of nonlinear fractional differentialequations and their approximations," *Bulletin of Science and Technology*, vol. 15, no. 2, p. 86e90, 1999.

[39] R. L. Bagley, P. J. Torvik, N. H. Aljahdaly, R. P. Agarwal, R. Shah, and T. Botmart, "Analysis of the time fractional-order coupled burgers equations with non-singular kernel operators," *Mathematics*, vol. 9, no. 18, p. 2326, 2021.

[40] R. Panda and M. Dash, "On solutions of fractional-order gas dynamics equation by effective techniques," *Journal of function space*, vol. 8.

[41] T. Insperger and G. Stepan, "Remote control of periodic robotic motion," in *Proceedings of the Thirt Symp Theory and Practice of Robots and Manipulators*, Zakopane, Poland, Article ID 197e203, 2000.

[42] S. Davaeifar and J. Rashidinia, "Solution of a system of delay differential equations of multi pantograph type," *Journal of Taibah University for Science*, vol. 11, no. 6, pp. 1141–1157, 2017.

[43] M. N. Sherif, "Numerical solution of system of fractional delay differential equations using polynomial spline functions," *Applied Mathematics*, vol. 7, no. 6, pp. 518–526, 2016.

Hindawi
Complexity
Volume 2022, Article ID 9712388, 14 pages
https://doi.org/10.1155/2022/9712388

WILEY | Hindawi

Research Article

Novel Evaluation of the Fractional Acoustic Wave Model with the Exponential-Decay Kernel

Rabab Alyusof,[1] Shams Alyusof,[2] Naveed Iqbal,[3] and Mohammad Asif Arefin[4]

[1]*Department of Mathematics, Faculty of Science, King Saud University, Riyadh, Saudi Arabia*
[2]*Department of Mathematics, Faculty of Science, Imam Muhammad Ibn Saud Islamic University (IMSIU), Riyadh, Saudi Arabia*
[3]*Department of Mathematics, College of Science, University of Ha'il, Ha'il 2440, Saudi Arabia*
[4]*Department of Mathematics, Jashore University of Science and Technology, Jashore-7408, Bangladesh*

Correspondence should be addressed to Naveed Iqbal; n.iqbal@uoh.edu.sa and Mohammad Asif Arefin; asif.math@just.edu.bd

Received 10 April 2022; Accepted 9 May 2022; Published 28 May 2022

Academic Editor: Fathalla A. Rihan

This study employs a newly developed methodology called the variational homotopy perturbation transformation method to study fractional acoustic wave equations. The motivation for this study is to extend the variational homotopy perturbation technique to the variational homotopy perturbation transformation technique in the sense of the Yang–Caputo–Fabrizio operator. The suggested method demonstrated a straightforward and accurate technique for investigating fractional-order partial differential equations. The technique's validity is demonstrated through the use of several illustrative instances. The obtained answers were found to be extremely near to the precise solutions. Additionally, the proposed strategy achieves the best degree of accuracy. Indeed, the current technique can be seen as one of the analytic strategies for solving nonlinear fractional partial differential equations compared to other analytical techniques.

1. Introduction

Scientists, mathematicians, and engineers have recently been interested in fractional differential equations (FDEs) and fractional calculus. Many significant implementations were assessed in a variety of science and engineering disciplines, including viscoelasticity, material engineering, dynamics physics, electrochemistry, and electromagnetics; fractional partial differential equations (FPDEs) [1] are used to explain all of them. Analytical ways to solve FDEs are gaining traction. FDEs cannot be accurately answered using any method. Approximate methods must be developed utilising series solution or linearization techniques [2], followed by adequate system solvers [3–5] and numerical discretization [6–8].

Nonlinear phenomena may be found in various engineering and scientific domains, including chemical kinetics, solid-state physics, fluid physics, nonlinear spectroscopy, computational biology, thermodynamics, quantum mechanics, etc. Many nonlinear higher-order PDEs define the idea of nonlinearity [9, 10].

The following fractional long-wave equation is investigated with the variational homotopy perturbation transform method.

$$\frac{\partial^{\sigma} v}{\partial \eta^{\sigma}} + \frac{1}{2}\frac{\partial v^2}{\partial \wp} - \frac{\partial}{\partial \eta}\left(\frac{\partial^2 v}{\partial \wp^2}\right) = 0, \quad 0 < \wp \le 1, 0 < \sigma \le 1, \eta > 0, \tag{1}$$

with initial condition

$$v(\wp, 0) = \wp,$$

$$\frac{\partial^{\sigma} v}{\partial \eta^{\sigma}} + \frac{\partial v}{\partial \wp} + v\frac{\partial v}{\partial \eta} - \frac{\partial}{\partial \eta}\left(\frac{\partial^2 v}{\partial \wp^2}\right) = 0, \quad 0 < \wp \le 1, 0 < \sigma \le 1, \eta > 0, \tag{2}$$

with initial condition

$$v(\wp,0)=3\alpha\ \sec h^2(\sigma\wp),\quad \alpha>0,\sigma=\frac{1}{2}\sqrt{\frac{\alpha}{1+\alpha}},$$

$$\frac{\partial^\sigma v}{\partial\eta^\sigma}+\frac{\partial v}{\partial\wp}-2\frac{\partial}{\partial\eta}\left(\frac{\partial^2 v}{\partial\wp^2}\right)=0,\quad 0<\wp\le 1,0<\sigma\le 1,\eta>0, \tag{3}$$

with initial condition

$$v(\wp,0)=e^{-\wp}, \tag{4}$$

and

$$\frac{\partial^\sigma v(\wp.\eta)}{\partial\eta^\sigma}+\frac{\partial^4 v(\wp.\eta)}{\partial\wp^4}=0,\quad 0<\wp\le 1,0<\sigma\le 1,\eta>0, \tag{5}$$

with initial condition

$$v(\wp,0)=\sin\wp. \tag{6}$$

The nonlinear fractional-order regularised long-wave equation (RLWE) is called equation (1); equation (2) is called the nonlinear fractional general RLWE; and equations (3) and (5) are called linear fractional RLWEs [11].

The regularised long-wave (RLW) equation was also recognized by the Benjamin–Bona–Mahony equation (BBME). This is an upgraded form of the Korteweg–de Vries equation (KdV), representing low amplitude long surface gravity waves propagating unidirectionally in two dimensions. Wave propagation in elastic rods with longitudinal dispersion, stress waves in compressed gas bubble mixtures, ion-acoustic plasma waves, rotational tube flows, and plasma magneto-hydrodynamic waves are examples of RLW equations in action. The RLW equations are suitable models for many major physical structures in applied engineering and physics. It also creates a lot of liquid flow concerns where diffusion is a big deal, regardless of shocks or viscosity. Any dissipation-related nonlinear wave diffusion issue may be modelled using it. Depending on the issue modelling [12, 13], this dissipation might arise in heat conduction, chemical reaction, viscosity, thermal radiation, mass diffusion, or other causes.

The RLW equation is a collection of nonlinear growth models that provide great models for anticipating natural occurrences. The method was first used to describe the undular bore behaviour [14]. It was also discovered via the study of water and ion-acoustic plasma waves. In [15], under boundary circumstances and constrained beginning, an analytic result for the RLW equations was discovered. Many important engineering phenomena and ocean research, for example, long-wave and tiny frequency shallow-water waves, are defined by fractional RLW equations. Several researchers in the field of shallow liquid sea waves are interested in the nonlinear wave described by the fractional equations of RLW. The fractional RLW equations were used to represent nonlinear waves in the sea. Indeed, the tsunami's massive surface waves are characterized by fractional RLW equations. Large internal waves in the core of the ocean generated by temperature differences that might destroy marine ships can be expressed as fractional RLW equations using the present incredibly effective approach [16–18].

In recent years, numerous scientists and researchers have employed analytic approaches to handle issues like homotopy perturbation. The Adomian decomposition method (ADM) [19, 20], Sumudu transform method [11], optimal homotopy perturbation method [21], least-squares method [22], He's homotopy perturbation technique [23], and homotopy perturbation method and variational iteration method [24] have flaws such as the determination of the Lagrange multiplier, the calculation of Adomian polynomials, a large number of calculations, and divergent results. Consequently, VHPTM, a revised analytical technique for solving fractional-order differential equations, was created. VHPTM results from three well-known approaches being combined: variational iteration, homotopy perturbation, and Laplace transform [25–30]. The Lagrange multiplier is used to restrict the number of times an integral operator is implemented in a row and the computing cost. It continues to retain a better level of precision. VHPTM [31–34] has an outstanding scheme and incorporates all of the positive aspects of HPM and VIM.

At last, to construct the homotopy perturbation technique, He's polynomials were employed in the corrective fractional formula. The suggested approach is applied without discretization or transformation, and it is shown to be free of rounding errors. Normally, the variable separable technique requires both starting and boundary points; however, the current approach requires initial circumstances to produce an analytical solution. The proposed technique has the distinct benefit of not requiring the usage of Adomian polynomials, which are needed by the Adomian decomposition method. The proposed approach is shown to yield a solution in a sequence of quick convergence that may lead to a closed solution [35].

2. Basic Definitions

Definition 1. The fractional Caputo–Fabrizio derivative is defined as [36]

$${}^{\mathrm{CF}}D_\eta^\sigma[g(\eta)]=\frac{N(\sigma)}{1-\sigma}\int_0^\eta g'(\varrho)K(\eta,\varrho)\mathrm{d}\varrho,\quad n-1<\sigma\le n. \tag{7}$$

$N(\sigma)$ is the function of normalisation with $N(0)=N(1)=1$.

$${}^{\mathrm{CF}}D_\eta^\sigma[g(\eta)]=\frac{N(\sigma)}{1-\sigma}\int_0^\eta[g(\eta)-g(\varrho)]K(\eta,\varrho)\mathrm{d}\varrho. \tag{8}$$

Definition 2. For $N(\sigma)=1$, the following solution represents the Laplace transformation of the Caputo–Fabrizio operator [36]:

$$L\left[{}^{\mathrm{CF}}D_\eta^\sigma[g(\eta)]\right]=\frac{sL[g(\eta)-g(0)]}{s+\sigma(1-s)}. \tag{9}$$

Definition 3. The Caputo–Fabrizio fractional integral is defined as [36]

$$^{CF}I_{\eta}^{\sigma}[g(\eta)]t = n\frac{1-\sigma}{N(\sigma)}q\,gh(\eta)_{+}x\frac{\sigma}{N(\sigma)}7\int_{0}^{\eta}g(\varrho)\mathrm{d}\varrho,;\quad \eta\geq 0,\sigma\in(0,1\Big]. \tag{10}$$

Definition 4. The Yang transformation of $g(\eta)$ is given as [37]

$$\mathscr{Y}[g(\eta)] = \chi(s) = \int_{0}^{\infty} g(\eta)e^{-\eta/s}\mathrm{d}\eta,\quad \eta>0. \tag{11}$$

2.1. Remarks. The Yang transforms of many relevant terms are listed below.

$$\begin{aligned} Y[1] &= s,\\ Y[\eta] &= s^{2},\\ Y\left[\eta^{i}\right] &= \Gamma(i+1)s^{i+1}. \end{aligned} \tag{12}$$

Lemma 1. *(Yang–Laplace duality).*

Let the Laplace transformation of $g(\eta)$ be $F(s)$; then, $\chi(s) = F(1/s)$ [38].

Proof. From equation (11), we can achieve another type of the Yang transformation by putting $\eta/s = \zeta$ as

$$L[g(\eta)] = \chi(s) = s\int_{0}^{\infty} g(s\zeta)e^{\zeta}\mathrm{d}\zeta,\quad \zeta>0. \tag{13}$$

Since $L[g(\eta)] = F(s)$,

$$F(s) = L[g(\eta)] = \int_{0}^{\infty} g(\eta)e^{-s\eta}\mathrm{d}\eta. \tag{14}$$

Put $\eta = \zeta/s$ in (14), and we have

$$F(s) = \frac{1}{s}\int_{0}^{\infty} g\left(\frac{\zeta}{s}\right)e^{\zeta}\mathrm{d}\zeta. \tag{15}$$

Thus, from (13), we obtain

$$F(s) = \chi\left(\frac{1}{s}\right). \tag{16}$$

Also, from (11) and (14), we get

$$F\left(\frac{1}{s}\right) = \chi(s). \tag{17}$$

The connections (16) and (17) show the duality link among the Yang and Laplace transformation. □

Lemma 2. *Let $g(\eta)$ be a continuous function; then, the Caputo–Fabrizio–Yang transform derivative of $g(\eta)$ is given as [38]*

$$Y[g(\eta)] = \frac{Y[g(\eta) - sg(0)]}{1+\sigma(s-1)}. \tag{18}$$

Proof. The Laplace transform of fractional Caputo–Fabrizio operator is defined as

$$L[g(\eta)] = \frac{L[sg(\eta) - g(0)]}{s+\sigma(1-s)}. \tag{19}$$

Also, we have the link among Laplace and Yang properties, i.e., $\chi(s) = F(1/s)$. To achieve the necessaries solution, we put s by $1/s$ in (19), and we have

$$\begin{aligned} Y[g(\eta)] &= \frac{1/sY[g(\eta) - g(0)]}{1/s+\sigma(1-1/s)},\\ Y[g(\eta)] &= \frac{Y[g(\eta) - sg(0)]}{1+\sigma(s-1)}. \end{aligned} \tag{20}$$

The proof is completed. □

3. The General Implementation of the Technique

To show the basic idea of the current technique [31, 32], we are suggesting

$$D_{\eta}^{\sigma}\upsilon(\wp,\eta) + \overline{L}\upsilon(\wp,\eta) + \mathrm{N}\upsilon(\wp,\eta) = h(\wp,\eta), \tag{21}$$

with initial condition

$$\upsilon(\wp,0) = g(\wp). \tag{22}$$

Using Yang transformation of (21), we have

$$Y\{\upsilon(\wp,\eta)\} - s\upsilon(\wp,0) = -Y\{\overline{L}\upsilon(\wp,\eta) + \mathrm{N}\upsilon(\wp,\eta) - h(\wp,\eta)\}, \tag{23}$$

where $\upsilon(s) = Y(\upsilon(\wp,\eta)) = \int_{0}^{\infty} e^{-s\eta}\upsilon(\eta)\mathrm{d}\eta$.

Using the variation iteration method,

$$Y\left\{\upsilon_{j+1}(\wp,\eta)\right\} = Y\left\{\upsilon_{j}(\wp,\eta)\right\} + \lambda(s)\left[\frac{1}{(1+\sigma(s-1))}Y\left\{\upsilon_{\eta}(\wp,\eta) + Y\{\overline{L}\upsilon(\wp,\eta) + \mathrm{N}\upsilon(\wp,\eta) - h(\wp,\eta)\}\right\}\right]. \tag{24}$$

The Lagrange multiplier is $\lambda(s)$. Now we put $\lambda(s) = -(1+\sigma(s-1))$ [32].

Applying inverse Laplace of (24),

$$v_{j+1}(\wp,\eta) = v_j(\wp,\eta) - Y^{-1}\left[(1+\sigma(s-1))Y\left\{\frac{1}{(1+\sigma(s-1))}\frac{\partial v}{\partial \eta} + \overline{L}v_j(\wp,\eta) + \mathrm{N}v_j(\wp,\eta) - h(\wp,\eta)\right\}\right]. \tag{25}$$

The result may be expressed as a series in power of p, which is the underlying principle behind the homotopy perturbation approach:

$$v(\wp,\eta) = \sum_{j=0}^{\infty} p^j v_j(\wp,\eta) = v_0 + pv_1 + p^2 v_2 + p^3 v_3 + \cdots, \tag{26}$$

where the nonlinear equation is as follows:

$$\mathrm{N}v(\wp,\eta) = \sum_{j=0}^{\infty} p^j \overline{H_j}(v). \tag{27}$$

He's polynomials are $\overline{H_j}$:

$$\overline{H_j}\left(v_0 + v_1 + \cdots + u_j\right) = \frac{1}{j!}\frac{\partial^j}{\partial p^j}\left[\mathrm{N}\left(\sum_{i=0}^{\infty} p^i v_i\right)\right]. \tag{28}$$

The variational homotopy perturbation transform method is applied to (28):

$$\sum_{j=0}^{\infty} p^j v_j(\wp,\eta) = \sum_{j=0}^{\infty} p^j v_j(\wp,\eta) + Y^{-1}\left[\lambda(s)Y\left\{\sum_{j=0}^{\infty} p^j \frac{\partial^\sigma v_j}{\partial \eta^\sigma}(\wp,s) + \sum_{j=0}^{\infty} p^j \overline{L}v_j(\wp,\eta) + \sum_{j=0}^{\infty} p^j \overline{H_j}(v) - h(\wp,\eta)\right\}\right]. \tag{29}$$

We obtain the present technique solution to the given equation by evaluating the coefficient of like power of p (28).

4. Numerical Problems

Problem 1. Consider the fractional nonlinear regularised long-wave equation

$$\frac{\partial^\sigma v}{\partial \eta^\sigma} + \frac{1}{2}\frac{\partial v^2}{\partial \wp} - \frac{\partial \partial^2 v}{\partial \eta\, \partial \wp^2} = 0, \quad 0 < \wp \le 1, 0 < \sigma \le 1, \eta > 0, \tag{30}$$

with the initial condition

$$v(\wp,0) = \wp. \tag{31}$$

The fractional partial differential equation described in (30) can be expressed as

$$\sum_{j=0}^{\infty} p^j v_{j+1}(\wp,\eta) = \sum_{j=0}^{\infty} p^j v_j(\wp,\eta) + Y^{-1}\left[\lambda(s)Y\left\{\frac{1}{(1+\sigma(s-1))}\frac{\partial v_j(\wp,\eta)}{\partial \eta} + \frac{1}{2}\frac{\partial v_j^2(\wp,\eta)}{\partial \wp} - \frac{\partial \partial^2 v_j(\wp,\eta)}{\partial \eta\, \partial \wp^2}\right\}\right]. \tag{32}$$

The Lagrange multiplier $\lambda(s) = -(1 + \sigma(s-1))$. Applying variational homotopy perturbation transformation method and applying He's polynomials,

$$\sum_{j=0}^{\infty} p^j v_{j+1}(\wp,\eta) = \sum_{j=0}^{\infty} p^j v_j(\wp,\eta) - \sum_{j=0}^{\infty} p^j Y^{-1}\left[(1+\sigma(s-1))Y\left\{\frac{1}{(1+\sigma(s-1))}\left(\frac{\partial v_0}{\partial \eta} + p\frac{\partial v_1}{\partial \eta} + p^2\frac{\partial v_2}{\partial \eta} + \cdots\right)\right.\right.$$
$$\left.\left. + \frac{1}{2}\frac{\partial}{\partial \wp}\left\{v_0^2 + p\left(2v_0v_1\right) + p^2\left(2v_0v_2 + v_1^2\right) + \cdots\right\} - \left\{p^0\frac{\partial\partial^2 v_0}{\partial\eta\ \partial\wp^2} + p^1\frac{\partial\partial^2 v_1}{\partial\eta\ \partial\wp^2} + p^2\frac{\partial\partial^2 v_2}{\partial\eta\ \partial\wp^2} + \cdots\right\}\right\}\right]. \tag{33}$$

Evaluating p coefficient,

$$\begin{aligned}
v_0(\wp,\eta) &= \wp,\\
p^1v_1(\wp,\eta) &= p^1v_0(\wp,\eta) - p^1Y^{-1}\left[(1+\sigma(s-1))Y\left\{\frac{1}{(1+\sigma(s-1))}\frac{\partial v_0(\wp,\eta)}{\partial\eta} + \frac{1}{2}\frac{\partial}{\partial\wp}v_0^2(\wp,\eta) - \frac{\partial\partial^2 v_0(\wp,\eta)}{\partial\eta\ \partial\wp^2}\right\}\right],\\
v_1(\wp,\eta) &= \wp - \wp(1+\sigma\eta-\sigma),\\
p^2v_2(\wp,\eta) &= p^2v_1(\wp,\eta) - p^2Y^{-1}\left[(1+\sigma(s-1))Y\left\{\frac{1}{(1+\sigma(s-1))}\frac{\partial v_1(\wp,\eta)}{\partial\eta} + \frac{1}{2}\frac{\partial}{\partial\wp}\left(2v_0v_1\right) - \frac{\partial\partial^2 v_1}{\partial\eta\ \partial\wp^2}\right\}\right],\\
v_2(\wp,\eta) &= \wp - \wp(1+\sigma\eta-\sigma) + 2\wp\left((1-\sigma)2\sigma\eta + (1-\sigma)^2 + \frac{\sigma^2\eta^2}{2}\right),\\
p^3v_3(\wp,\eta) &= p^3v_2(\wp,\eta) - p^3Y^{-1}\left[(1+\sigma(s-1))Y\left\{\frac{1}{(1+\sigma(s-1))}\frac{\partial v_1}{\partial\eta} + \frac{1}{2}\left(2v_0v_2 + v_1^2\right) - \frac{\partial\partial^2 v_2}{\partial\eta\ \partial\wp^2}\right\}\right],\\
v_3(\wp,\eta) &= \wp - \wp(1+\sigma\eta-\sigma) + 2\wp\left((1-\sigma)2\sigma\eta + (1-\sigma)^2 + \frac{\sigma^2\eta^2}{2}\right)\\
&\quad - \wp(2\sigma-1)\left(3\sigma\left(-2\sigma+1+\sigma^2\right)\eta + \frac{\sigma^3\eta^3}{6} - \frac{3\sigma^2(\sigma-1)\eta^2}{2} + 3\sigma^2 - 3\sigma + 1 - \sigma^3\right)\\
&\quad - 4\wp\left(3\sigma\left(-2\sigma+1+\sigma^2\right)\eta + \frac{\sigma^3\eta^3}{6} - \frac{3\sigma^2(\sigma-1)\eta^2}{2} + 3\sigma^2 - 3\sigma + 1 - \sigma^3\right).\\
&\ \ \vdots
\end{aligned} \tag{34}$$

The analytic series solution can be achieved as

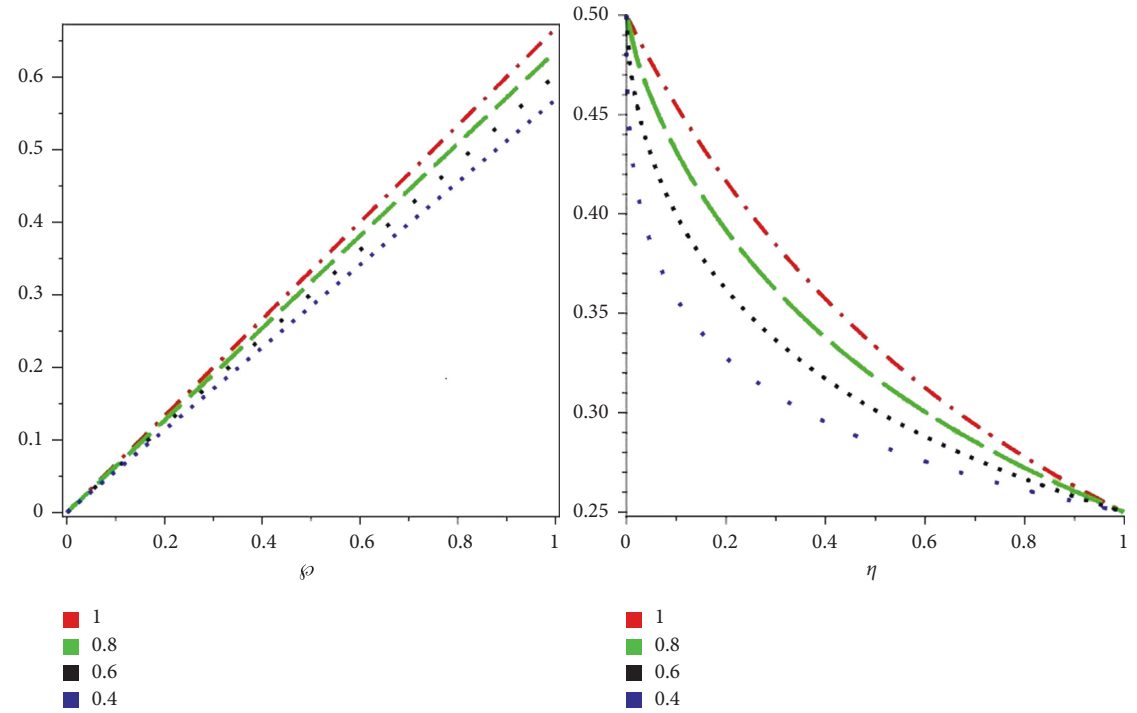

Figure 1: First figure show that the analytic result of various fractional-order of problem 1 and second graph with respect to time.

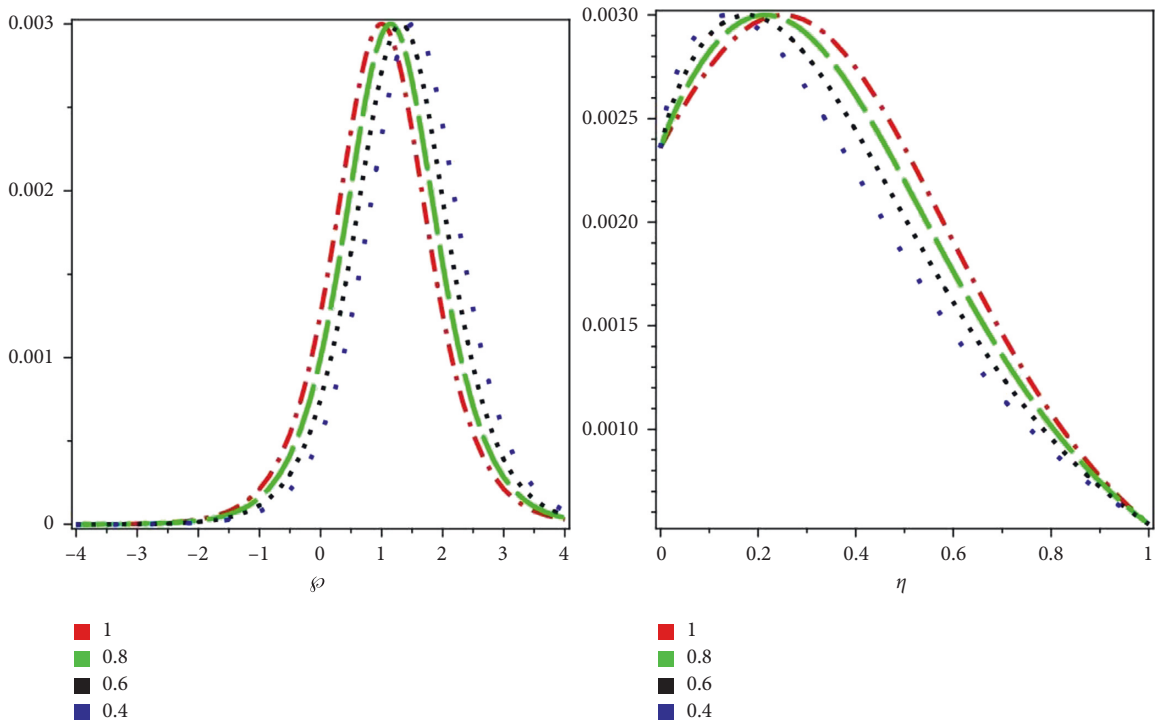

Figure 2: First figure show that the analytic result of various fractional-order of problem 2 and second graph with respect to time.

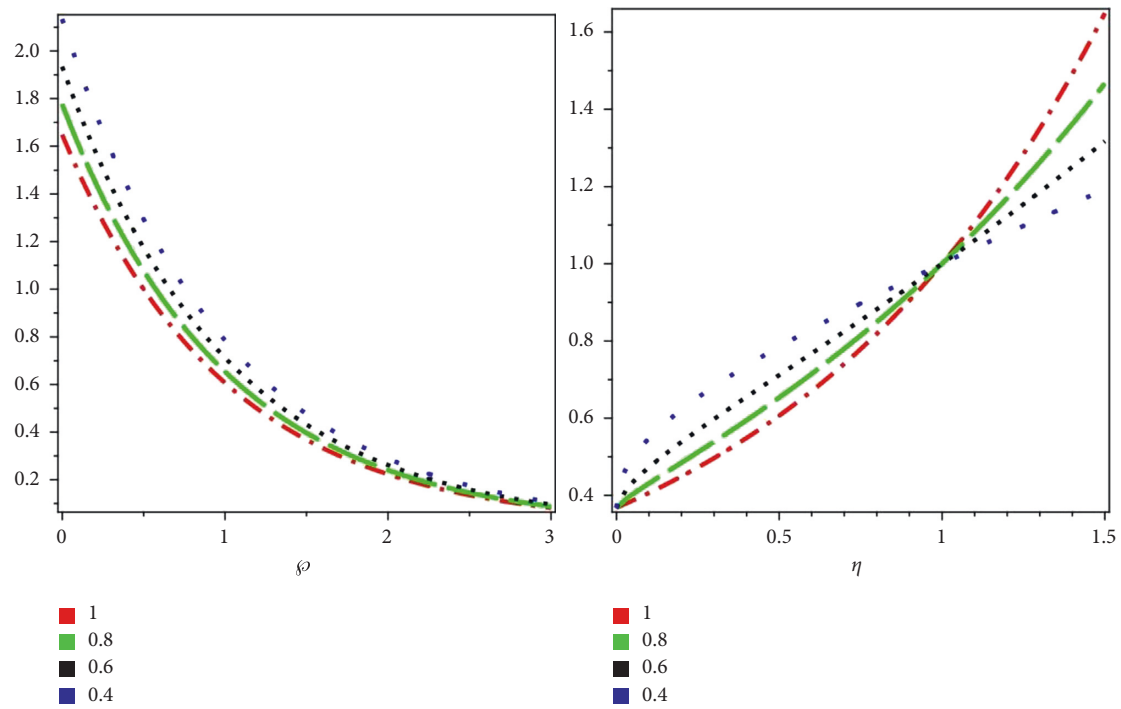

Figure 3: First figure show that the analytic result of various fractional-order of problem 3 and second graph with respect to time.

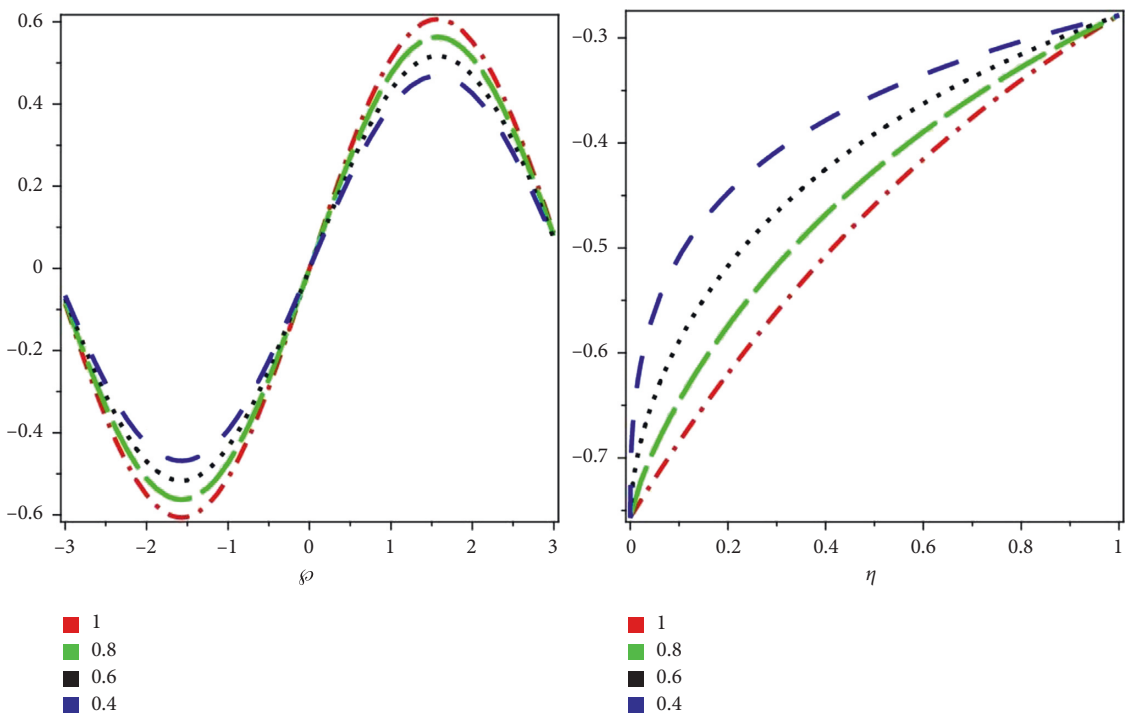

Figure 4: First figure show that the analytic result of various fractional-order of problem 4 and second graph with respect to time.

$$v(\wp,\eta)=\wp-\wp(1+\sigma\eta-\sigma)+2\wp\left((1-\sigma)2\sigma\eta+(1-\sigma)^2+\frac{\sigma^2\eta^2}{2}\right)$$
$$-\wp(2\sigma-1)\left(3\sigma\left(-2\sigma+1+\sigma^2\right)\eta+\frac{\sigma^3\eta^3}{6}-\frac{3\sigma^2(\sigma-1)\eta^2}{2}+3\sigma^2-3\sigma+1-\sigma^3\right)$$
$$-4\wp\left(3\sigma\left(-2\sigma+1+\sigma^2\right)\eta+\frac{\sigma^3\eta^3}{6}-\frac{3\sigma^2(\sigma-1)\eta^2}{2}+3\sigma^2-3\sigma+1-\sigma^3\right)+\cdots. \tag{35}$$

If $\sigma=1$, the series type solution is given as

$$v(\wp,\eta)=\wp\left(1-\eta+\eta^2-\eta^3+\cdots\right). \tag{36}$$

The exact result at $\sigma=1$ is

$$v(\wp,\eta)=\frac{\wp}{1+\eta}. \tag{37}$$

Problem 2. Consider the fractional nonlinear regularised long-wave equation

$$\frac{\partial^\sigma v}{\partial\eta^\sigma}+\frac{\partial v}{\partial\wp}+v\frac{\partial v}{\partial\wp}-\frac{\partial\partial^2 v}{\partial\eta\,\partial\wp^2}=0,\quad 0<\wp\le 1, 0<\sigma\le 1, \eta>0, \tag{38}$$

with the initial condition

$$v(\wp,0)=3\alpha\,\sec h^2(\sigma\wp),\quad \alpha>0, \sigma=\frac{1}{2}\sqrt{\frac{\alpha}{1+\alpha}}. \tag{39}$$

The fractional partial differential equation described in (38) can be expressed as

$$\sum_{j=0}^{\infty}p^j v_{j+1}(\wp,\eta)=\sum_{j=0}^{\infty}p^j v_j(\wp,\eta)+p^jY^{-1}$$
$$\left[\lambda(s)Y\left\{\frac{1}{(1+\sigma(s-1))}\frac{\partial v_j(\wp,\eta)}{\partial\eta}+\frac{\partial v_j(\wp,\eta)}{\partial\wp}+v_j(\wp,\eta)\frac{\partial v_j(\wp,\eta)}{\partial\wp}-\frac{\partial\partial^2 v_j(\wp,\eta)}{\partial\eta\,\partial\wp^2}\right\}\right]. \tag{40}$$

The Lagrange multiplier $\lambda(s)=-(1+\sigma(s-1))$. Applying variational homotopy perturbation transformation method and applying He's polynomials,

$$\sum_{j=0}^{\infty}p^j v_j(\wp,\eta)=\sum_{j=0}^{\infty}p^j v_j(\wp,\eta)-pY^{-1}\left[(1+\sigma(s-1))Y\left\{\frac{1}{(1+\sigma(s-1))}\left(\frac{\partial v_0}{\partial\eta}+p\frac{\partial v_1}{\partial\eta}+p^2\frac{\partial v_1}{\partial\eta}+\cdots\right)\right.\right.$$
$$+\left\{\frac{\partial v_0}{\partial\wp}+p^1\frac{\partial v_1}{\partial\wp}+p^2\frac{\partial v_2}{\partial\wp}+\cdots\right\}+\left\{v_0\frac{\partial v_0}{\partial\wp}+p\left(v_0\frac{\partial v_1}{\partial\wp}+v_1\frac{\partial v_0}{\partial\wp}\right)+p^2\left(v_0\frac{\partial v_2}{\partial\wp}+v_1\frac{\partial v_1}{\partial\wp}+v_2\frac{\partial v_0}{\partial\wp}\right)+\cdots\right\} \tag{41}$$
$$\left.\left.-\left\{\frac{\partial\partial^2 v_0}{\partial\eta\,\partial\wp^2}+p^1\frac{\partial\partial^2 v_1}{\partial\eta\,\partial\wp^2}+p^2\frac{\partial\partial^2 v_2}{\partial\eta\,\partial\wp^2}+\cdots\right\}\right\}\right].$$

Evaluating p coefficient,

$$
\begin{aligned}
v_0(\wp,\eta) &= 3\alpha\ \mathrm{sec}\ h^2(\sigma\wp),\\
p^1 v_1(\wp,\eta) &= p^1 v_0(\wp,\eta) - p^1 Y^{-1}\left[(1+\sigma(s-1))Y\left\{\frac{1}{(1+\sigma(s-1))}\frac{\partial v_0}{\partial \eta} + \frac{\partial v_0}{\partial \wp} + v_0\frac{\partial v_0}{\partial \wp} - \frac{\partial \partial^2 v_0}{\partial \eta\ \partial \wp^2}\right\}\right],\\
v_1(\wp,\eta) &= 3\alpha\ \mathrm{sec}\ h^2(\sigma\wp) + 3\alpha\sigma\{1+6\alpha\sigma+\cosh(2\sigma\wp)\}\mathrm{sec}\ h^4(\sigma\wp)\tanh(\sigma\wp)(1+\sigma\eta-\sigma),\\
p^2 v_2(\wp,\eta) &= p^2 v_1(\wp,\eta) - p^2 Y^{-1}\left[(1+\sigma(s-1))Y\left\{\frac{1}{(1+\sigma(s-1))}\frac{\partial v_1}{\partial \eta} + \frac{\partial v_1}{\partial \wp} + v_0\frac{\partial v_1}{\partial \wp} + v_1\frac{\partial v_0}{\partial \wp} - \frac{\partial \partial^2 v_1}{\partial \eta\ \partial \wp^2}\right\}\right],\\
v_2(\wp,\eta) &= 3\alpha\ \mathrm{sec}\ h^2(\sigma\wp) + 3\alpha\sigma\{1+6\alpha\sigma+\cosh(2\sigma\wp)\}\mathrm{sec}\ h^4(\sigma\wp)\tanh(\sigma\wp)(1+\sigma\eta-\sigma)\\
&\quad -\frac{3}{32}\alpha\sigma^2\left\{-8-96\alpha-576\alpha^2+3\left(-3-16\alpha+144\alpha^2\right)\cosh(2\sigma\wp)+48\alpha\cosh(4\sigma\wp)+\cosh(6\sigma\wp)\right\}\\
&\quad \mathrm{sec}\ h^8(\sigma\wp)\left((1-\sigma)2\sigma\eta+(1-\sigma)^2+\frac{\sigma^2\eta^2}{2}\right).\\
&\quad \vdots
\end{aligned}
\tag{42}
$$

The analytic series solution can be achieved as

$$
\begin{aligned}
v(\wp,\eta) &= 3\alpha\ \mathrm{sec}\ h^2(\sigma\wp) + 3\alpha\sigma\{1+6\alpha\sigma+\cosh(2\sigma\wp)\}\mathrm{sec}\ h^4(\sigma\wp)\tanh(\sigma\wp)(1+\sigma\eta-\sigma)\\
&-\frac{3}{32}\alpha\sigma^2\left\{-8-96\alpha-576\alpha^2+3\left(-3-16\alpha+144\alpha^2\right)\cosh(2\sigma\wp)+48\alpha\cosh(4\sigma\wp)+\cosh(6\sigma\wp)\right\}\\
&\mathrm{sec}\ h^8(\sigma\wp)\left((1-\sigma)2\sigma\eta+(1-\sigma)^2+\frac{\sigma^2\eta^2}{2}\right)+\frac{1}{32}\alpha\sigma^3\\
&\left\{-85-1416\alpha-8496\sigma^2-2937\sigma^3+4\left(-31-432\alpha-1584\alpha^2+3456\alpha^3\right)\right.\\
&\cosh(2\sigma\wp)-4\left(11+54\alpha-540\alpha^2\right)\cosh(4\sigma\wp)-4\cosh(6\sigma\wp)+96\alpha\cosh(6\sigma\wp)+\cosh(8\sigma\wp)\\
&\left.+\mathrm{sec}\ h^8(\sigma\wp)\tanh(\sigma\wp)\right\}\left(3\sigma\left(-2\sigma+1+\sigma^2\right)\eta+\frac{\sigma^3\eta^3}{6}-\frac{3\sigma^2(\sigma-1)\eta^2}{2}+3\sigma^2-3\sigma+1-\sigma^3\right)+\cdots.
\end{aligned}
\tag{43}
$$

The exact result at $\sigma = 1$ is

$$
v(\wp,\eta) = 3\alpha\ \mathrm{sec}\ h^2(\sigma(\wp-(1+\alpha)\eta)). \tag{44}
$$

Problem 3. Consider the fractional linear regularised long-wave equation

$$
\frac{\partial^\sigma v}{\partial \eta^\sigma} + \frac{\partial v}{\partial \wp} - 2\frac{\partial \partial^2 v}{\partial \eta\ \partial \wp^2} = 0, \quad 0 < \wp \le 1, 0 < \sigma \le 1, \eta > 0, \tag{45}
$$

with the initial condition

$$
v(\wp,0) = e^{-\wp}. \tag{46}
$$

The fractional partial differential equation described in (45) can be expressed as

$$\sum_{j=0}^{\infty} p^j v_{j+1}(\wp,\eta) = \sum_{j=0}^{\infty} p^j v_j(\wp,\eta) + p^j Y^{-1}\left[\lambda(s) Y\left\{\frac{1}{(1+\sigma(s-1))}\frac{\partial^\sigma v_j}{\partial \eta^\sigma}(\wp,\eta) + \frac{\partial v_j}{\partial \wp} - 2\frac{\partial \partial^2 v_j}{\partial \eta\, \partial \wp^2}\right\}\right]. \tag{47}$$

The Lagrange multiplier $\lambda(s) = -(1+\sigma(s-1))$. Applying variational homotopy perturbation transformation method and applying He's polynomials,

$$\begin{aligned}\sum_{j=0}^{\infty} p^j v_j(\wp,\eta) = \sum_{j=0}^{\infty} p^j v_j(\wp,\eta) - pY^{-1}\Bigg[(1+\sigma(s-1))Y\Bigg\{\frac{1}{(1+\sigma(s-1))}\left(\frac{\partial v_0}{\partial \eta} + p\frac{\partial v_1}{\partial \eta} + p^2\frac{\partial v_2}{\partial \eta} + \cdots\right)\\ +\frac{\partial}{\partial \wp}\left\{v_0 + pv_1 + p^2 v_2 + \cdots\right\} - 2\left\{\frac{\partial \partial^2 v_0}{\partial \eta\, \partial \wp^2} + p^1\frac{\partial \partial^2 v_1}{\partial \eta\, \partial \wp^2} + p^2\frac{\partial \partial^2 v_2}{\partial \eta\, \partial \wp^2} + \cdots\right\}\Bigg\}\Bigg].\end{aligned} \tag{48}$$

Evaluating p coefficient,

$$\begin{aligned}
v_0(\wp,\eta) &= e^{-\wp},\\
p^1 v_1(\wp,\eta) &= p^1 v_0(\wp,\eta) - p^1 Y^{-1}\left[(1+\sigma(s-1))Y\left\{\frac{1}{(1+\sigma(s-1))}\frac{\partial v_0}{\partial \eta}(\wp,\eta) + \frac{\partial v_0}{\partial \wp} - 2\frac{\partial \partial^2 v_0}{\partial \eta\, \partial \wp^2}\right\}\right],\\
v_1(\wp,\eta) &= e^{-\wp} + e^{-\wp}(1+\sigma\eta-\sigma),\\
p^2 v_2(\wp,\eta) &= p^2 v_1(\wp,\eta) - p^2 Y^{-1}\left[(1+\sigma(s-1))Y\left\{\frac{1}{(1+\sigma(s-1))}\frac{\partial v_1}{\partial \eta}(\wp,\eta) + \frac{\partial v_1}{\partial \wp} - 2\frac{\partial \partial^2 v_1}{\partial \eta\, \partial \wp^2}\right\}\right],\\
v_2(\wp,\eta) &= e^{-\wp} + e^{-\wp}(1+\sigma\eta-\sigma) + e^{-\wp}\left((1-\sigma)2\sigma\eta + (1-\sigma)^2 + \frac{\sigma^2\eta^2}{2}\right),\\
p^3 v_3(\wp,\eta) &= p^3 v_2(\wp,\eta) - p^3 Y^{-1}\left[-(1+\sigma(s-1))Y\left\{\frac{1}{(1+\sigma(s-1))}\frac{\partial v_2}{\partial \eta}(\wp,\eta) + \frac{\partial v_2}{\partial \wp} - 2\frac{\partial \partial^2 v_2}{\partial \eta\, \partial \wp^2}\right\}\right],\\
v_3(\wp,\eta) &= e^{-\wp} + e^{-\wp}(1+\sigma\eta-\sigma) + e^{-\wp}\left((1-\sigma)2\sigma\eta + (1-\sigma)^2 + \frac{\sigma^2\eta^2}{2}\right)\\
&\quad + e^{-\wp}\left(3\sigma\left(-2\sigma+1+\sigma^2\right)\eta + \frac{\sigma^3\eta^3}{6} - \frac{3\sigma^2(\sigma-1)\eta^2}{2} + 3\sigma^2 - 3\sigma + 1 - \sigma^3\right).
\end{aligned} \tag{49}$$

.

.

.

The analytic series solution can be achieved as

$$v(\wp,\eta) = e^{-\wp} + e^{-\wp}(1+\sigma\eta-\sigma) + e^{-\wp}\left((1-\sigma)2\sigma\eta + (1-\sigma)^2 + \frac{\sigma^2\eta^2}{2}\right) + e^{-\wp}\left(3\sigma\left(-2\sigma+1+\sigma^2\right)\eta + \frac{\sigma^3\eta^3}{6} - \frac{3\sigma^2(\sigma-1)\eta^2}{2} + 3\sigma^2 - 3\sigma + 1 - \sigma^3\right) + \cdots. \tag{50}$$

If $\sigma = 1$, the series type solution is given as

$$v(\wp,\eta) = e^{-\wp}\left(1+\eta+\frac{\eta^2}{2!}+\frac{\eta^3}{3!}+\cdots\right). \tag{51}$$

The exact result at $\sigma = 1$ is

$$v(\wp,\eta) = e^{\eta-\wp}. \tag{52}$$

Problem 4. Consider the fractional linear regularised long-wave equation

$$\frac{\partial^\sigma v(\wp.\eta)}{\partial\eta^\sigma} + \frac{\partial^4 v(\wp.\eta)}{\partial\wp^4} = 0, \quad 0 < \wp \le 1, 0 < \sigma \le 1, \eta > 0, \tag{53}$$

with the initial condition

$$v(\wp,0) = \sin\wp. \tag{54}$$

The fractional partial differential equation described in (53) can be expressed as

$$\sum_{j=0}^{\infty} p^j v_{j+1}(\wp,\eta) = \sum_{j=0}^{\infty} p^j v_j(\wp,\eta) + \sum_{j=0}^{\infty} p^j Y^{-1}\left[\lambda(s)Y\left\{\frac{1}{(1+\sigma(s-1))}\frac{\partial^\sigma v_j(\wp\cdot\eta)}{\partial\eta^\sigma}(\wp,\eta) + \frac{\partial^4 v_j(\wp\cdot\eta)}{\partial\wp^4}\right\}\right]. \tag{55}$$

The Lagrange multiplier $\lambda(s) = -(1+\sigma(s-1))$. Applying variational homotopy perturbation transformation method and applying He's polynomials,

$$\sum_{j=0}^{\infty} p^j v_j(\wp,\eta) = \sum_{j=0}^{\infty} p^j v_j(\wp,\eta) - pY^{-1}\left[(1+\sigma(s-1))Y\left\{\frac{1}{(1+\sigma(s-1))}\left(\frac{\partial v_0}{\partial\eta} + p\frac{\partial v_1}{\partial\eta} + p^2\frac{\partial v_2}{\partial\eta} + \cdots\right) + \frac{\partial^4}{\partial\wp^4}\left\{v_0 + pv_1 + p^2v_2 + \cdots\right\}\right\}\right]. \tag{56}$$

Evaluating p coefficient,

$$
\begin{aligned}
v_0(\wp,\eta) &= \sin\wp,\\
p^1 v_1(\wp,\eta) &= p^1 v_0(\wp,\eta) - p^1 Y^{-1}\left[(1+\sigma(s-1))Y\left\{\frac{1}{(1+\sigma(s-1))}\frac{\partial v_0(\wp.\eta)}{\partial\eta}(\wp,\eta)+\frac{\partial^4 v_0(\wp.\eta)}{\partial\wp^4}\right\}\right],\\
v_1(\wp,\eta) &= \sin\wp - \sin\wp(1+\sigma\eta-\sigma),\\
p^2 v_2(\wp,\eta) &= p^2 v_1(\wp,\eta) - p^2 Y^{-1}\left[(1+\sigma(s-1))Y\left\{\frac{1}{(1+\sigma(s-1))}\frac{\partial v_1(\wp.\eta)}{\partial\eta}(\wp,\eta)+\frac{\partial^4 v_1(\wp.\eta)}{\partial\wp^4}\right\}\right],\\
v_2(\wp,\eta) &= \sin\wp - \sin\wp(1+\sigma\eta-\sigma) + \sin\wp\left((1-\sigma)2\sigma\eta+(1-\sigma)^2+\frac{\sigma^2\eta^2}{2}\right),\\
p^3 v_3(\wp,\eta) &= p^3 v_2(\wp,\eta) - p^3 Y^{-1}\left[(1+\sigma(s-1))Y\left\{\frac{1}{(1+\sigma(s-1))}\frac{\partial v_2(\wp.\eta)}{\partial\eta}(\wp,\eta)+\frac{\partial^4 v_2(\wp.\eta)}{\partial\wp^4}\right\}\right],\\
v_3(\wp,\eta) &= \sin\wp - \sin\wp(1+\sigma\eta-\sigma) + \sin\wp\left((1-\sigma)2\sigma\eta+(1-\sigma)^2+\frac{\sigma^2\eta^2}{2}\right)\\
&\quad -\sin\wp\left(3\sigma\left(-2\sigma+1+\sigma^2\right)\eta+\frac{\sigma^3\eta^3}{6}-\frac{3\sigma^2(\sigma-1)\eta^2}{2}+3\sigma^2-3\sigma+1-\sigma^3\right).\\
&\ \ \vdots
\end{aligned}
\tag{57}
$$

The analytic series solution can be achieved as

$$
\begin{aligned}
v(\wp,\eta) &= \sin\wp - \sin\wp(1+\sigma\eta-\sigma) + \sin\wp\left((1-\sigma)2\sigma\eta+(1-\sigma)^2+\frac{\sigma^2\eta^2}{2}\right)\\
&\quad -\sin\wp\left(3\sigma\left(-2\sigma+1+\sigma^2\right)\eta+\frac{\sigma^3\eta^3}{6}-\frac{3\sigma^2(\sigma-1)\eta^2}{2}+3\sigma^2-3\sigma+1-\sigma^3\right)+\cdots.
\end{aligned}
\tag{58}
$$

If $\sigma = 1$, the series type solution is given as

$$
v(\wp,\eta) = \sin\wp\left(1-\eta+\frac{\eta^2}{2!}-\frac{\eta^3}{3!}+\cdots\right). \tag{59}
$$

The exact result at $\sigma = 1$ is

$$
v(\wp,\eta) = \sin\wp e^{-\eta}. \tag{60}
$$

5. Results and Discussion

The reliability and applicability of the suggested technique are tested using many numerical examples. The figure representation of the answers in examples 1 to 4 has supplied information regarding the proposed method's correctness and dependability. All of the findings from examples 1–4 revealed a high agreement between VHPTM solutions and the specific answers to the issues. Figures 1–4 show the analytical solution of the different fractional orders of example 1 to space and time. The graphs depicted the answers to each issue at various fractional orders of $\sigma = 1, 0.8, 0.6$, and 0.4. In the case of fractional-order solutions, the convergence of the suggested approach to integer-order solutions attests to the strategy's effectiveness. The solution of fractional-order issues is convergent with the solution of integer-order problems. Furthermore, the recommended method's implementation is basic and uncomplicated throughout the simulation. We hope that the current approach may be adapted to solve various fractional-order differential equations that arise in applied science based on the aforesaid qualities.

6. Conclusions

The fractional analysis of the acoustic wave equation is explored in this article by applying a modified analytic method. The result figure graphs are visualised and analysed to provide a visual representation of the acquired results. Compared to other analytical methods, the graphical representation showed the fastest convergence rate. The

fractional-order analysis of the acoustic wave equation is critical for examining the dynamics compared to the classic one. As a result, the proposed method has been important in describing sophisticated solutions to fractional-order partial differential equations that arise in various fields of science and engineering. Additionally, the proposed method uses variational parameters, which simplify the calculations. He's polynomials were employed to produce more precise solutions than Adomian polynomials. The proposed method is found to have a higher rate of convergence than other current methods. As a result, the proposed method can be expanded to solve various fractional nonlinear partial differential equations.

Data Availability

The numerical data used to support the findings of this study are included within the article.

Conflicts of Interest

The authors declare that there are no conflicts of interest regarding the publication of this article.

References

[1] K. B. Oldham and J. Spanier, "The fractional calculus," *Mathematics in Science and Engineering*, vol. 111, 1974.

[2] K. S. Miller and B. Ross, *An Introduction to the Fractional Calculus and Fractional Differential Equations*, Wiley, New York, NY, USA, 1993.

[3] M. Donatelli, M. Mazza, and S. Serra-Capizzano, "Spectral analysis and structure preserving preconditioners for fractional diffusion equations," *Journal of Computational Physics*, vol. 307, pp. 262–279, 2016.

[4] M. Donatelli, M. Mazza, and S. Serra-Capizzano, "Spectral analysis and multigrid methods for finite volume approximations of space-fractional diffusion equations," *SIAM Journal on Scientific Computing*, vol. 40, no. 6, Article ID A4007, 2018.

[5] X.-l. Lin, M. K. Ng, and H.-W. Sun, "A multigrid method for linear systems arising from time-dependent two-dimensional space-fractional diffusion equations," *Journal of Computational Physics*, vol. 336, pp. 69–86, 2017.

[6] M. M. Meerschaert and C. Tadjeran, "Finite difference approximations for two-sided space-fractional partial differential equations," *Applied Numerical Mathematics*, vol. 56, no. 1, pp. 80–90, 2006.

[7] M. Parvizi, M. R. Eslahchi, and M. Dehghan, "Numerical solution of fractional advection-diffusion equation with a nonlinear source term," *Numerical Algorithms*, vol. 68, no. 3, pp. 601–629, 2015.

[8] W. Bu, X. Liu, Y. Tang, and J. Yang, "Finite element multigrid method for multi-term time fractional advection diffusion equations," *International Journal of Modeling, Simulation, and Scientific Computing*, vol. 6, no. 1, Article ID 1540001, 2015.

[9] R. P. Agarwal, F. Mofarreh, R. Shah, W. Luangboon, and K. Nonlaopon, "An analytical technique, based on natural transform to solve fractional-order parabolic equations," *Entropy*, vol. 23, no. 8, p. 1086, 2021.

[10] N. H. Aljahdaly, R. P. Agarwal, and R. Shah, "Analysis of the time fractional-order coupled burgers equations with non-singular kernel operators," *Mathematics*, vol. 9, no. 18, 2021.

[11] A. Goswami, J. Singh, D. Kumar, and S. Gupta, "An efficient analytical technique for fractional partial differential equations occurring in ion acoustic waves in plasma," *Journal of Ocean Engineering and Science*, vol. 4, 2019.

[12] Y. Khan, R. Taghipour, M. Falahian, and A. Nikkar, "A new approach to modified regularized long wave equation," *Neural Computing & Applications*, vol. 23, pp. 1335–1341, 2013.

[13] C. Bota and B. Cruntu, "The solution of the absolute value equations using two generalized accelerated overrelaxation methods," *The Scientific World Journal*, vol. 2014, 2014.

[14] M. Naeem, A. M. Zidan, K. Nonlaopon, M. I. Syam, and Z. Al-Zhour, "A new analysis of fractional-order equal-width equations via novel techniques," *Symmetry*, vol. 13, no. 5, 2021.

[15] T. B. Brooke, J. L. Bona, and J. J. Mahony, "Model equations for long waves in nonlinear dispersive systems," *Philosophical Transactions of the Royal Society of London - Series A: Mathematical and Physical Sciences*, vol. 272, pp. 47–78, 1972.

[16] N. Iqbal, A. Akgul, A. Bariq, M. Mossa Al-Sawalha, and A. Ali, "On solutions of fractional-order gas dynamics equation by effective techniques," *Journal of Function Spaces*, vol. 2022, Article ID 3341754, 14 pages, 2022.

[17] M. Alesemi, N. Iqbal, and A. A. Hamoud, "The analysis of fractional-order proportional delay physical models via a novel transform," *Complexity*, vol. 2022, Article ID 2431533, 13 pages, 2022.

[18] M. Alesemi, N. Iqbal, and T. Botmart, "Novel analysis of the fractional-order system of non-linear partial differential equations with the exponential-decay kernel," *Mathematics*, vol. 10, no. 4, 2022.

[19] A. K. Khalifa, K. R. Raslan, and H. M. Alzubaidi, "Two new iteration methods with optimal parameters for solving absolute value equations," *International Journal of Algorithms, Computing and Mathematics*, vol. 8, pp. 2962–2972, 2022.

[20] T. Achouri and K. Omrani, "Numerical solutions for the damped generalized regularized long-wave equation with a variable coefficient by Adomian decomposition method," *Communications in Nonlinear Science and Numerical Simulation*, vol. 14, pp. 2025–2033, 2009.

[21] C. Bota and B. Caruntu, "Approximate analytical solutions of the regularized long wave equation using the optimal homotopy perturbation method," *The Scientific World Journal*, vol. 2014, Article ID 721865, 2014.

[22] D. dris, "Least-squares quadratic B-spline finite element method for the regularised long wave equation," *Computer Methods in Applied Mechanics and Engineering*, vol. 182, pp. 205–215, 2000.

[23] M. Inc and Y. Ugurlu, "Numerical simulation of the regularized long wave equation by He's homotopy perturbation method," *Physics Letters A*, vol. 369, no. 3, pp. 173–179, 2007.

[24] D. D. Ganji, H. Tari, and M. Bakhshi Jooybari, "Variational iteration method and homotopy perturbation method for nonlinear evolution equations," *Computers & Mathematics With Applications*, vol. 54, pp. 1018–1027, 2007.

[25] K. B. Oldham and J. Spanier, "The fractional calculus," *Mathematics in Science and Engineering*, vol. 111, 1974.

[26] A. A. A. Kilbas, H. M. Srivastava, and J. J. Trujillo, *Theory and Applications of Fractional Differential Equations*, Vol. 204, Elsevier Science Limited, , Amsterdam, Netherlands, 2006.

[27] R. Shah, H. Khan, M. Arif, and P. Kumam, "Application of laplace–adomian decomposition method for the analytical

solution of third-order dispersive fractional partial differential equations," *Entropy*, vol. 21, no. 4, p. 335, 2019.

[28] K. Nonlaopon, A. M. Alsharif, A. M. Zidan, A. Khan, and Y. S. Hamed, "Numerical investigation of fractional-order Swift-Hohenberg equations via a Novel transform," *Symmetry*, vol. 13, no. 7, p. 1263, 2021.

[29] P. Sunthrayuth, A. M. Zidan, S. W. Yao, and M. Inc, "The comparative study for solving fractional-order fornberg-whitham equation via ρ-Laplace transform," *Symmetry*, vol. 13, no. 5, p. 784, 2021.

[30] K. Shah, H. Khalil, and R. A. Khan, "Analytical solutions of fractional order diffusion equations by natural transform method," *Iranian Journal of Science and Technology Transaction A-Science*, vol. 42, no. 3, pp. 1479–1490, 2018.

[31] M. A. Noor and S. T. Mohyud-Din, "Modified variational iteration method for heat and wave-like equations," *Acta Applicandae Mathematica*, vol. 104, no. 3, pp. 257–269, 2008.

[32] M. A. Noor and S. T. Mohyud-Din, "Variational homotopy perturbation method for solving higher dimensional initial boundary value problems," *Mathematical Problems in Engineering*, vol. 2008, Article ID 696734, 18 pages, 2008.

[33] S. Mohammad Mehdi Hosseini, S. Tauseef Mohyud-Din, and H. Ghaneai, "Variational iteration method for Hirota-Satsuma coupled KdV equation using auxiliary parameter," *International Journal of Numerical Methods for Heat and Fluid Flow*, vol. 22, no. 3, pp. 277–286, 2012.

[34] S. T. Mohyud-Din, A. Yildirim, and M. M. Hosseini, "Variational iteration method for initial and boundary value problems using He's polynomials," *International Journal of Differential Equations*, vol. 2010, Article ID 426213, 28 pages, 2010.

[35] Y. Liu, "Variational homotopy perturbation method for solving fractional initial boundary value problems," in *Abstract and Applied Analysis*vol. 2012, Hindawi, Article ID 727031, 10 pages, Hindawi, 2012.

[36] M. Caputo and M. Fabrizio, "On the singular kernels for fractional derivatives. some applications to partial differential equations," *Progr Fract Differ Appl*, vol. 7, no. 2, pp. 1–4, 2021.

[37] X. J. Yang, "A new integral transform method for solving steady heat-transfer problem," *Thermal Science*, vol. 20, no. 3, pp. 639–642, 2016.

[38] S. Ahmad, A. Ullah, A. Akgul, and M. De la Sen, "A novel homotopy perturbation method with applications to nonlinear fractional order KdV and burger equation with exponential-decay kernel," *Journal of Function Spaces*, vol. 2021, Article ID 8770488, 11 pages, 2021.

Hindawi
Complexity
Volume 2022, Article ID 4475491, 12 pages
https://doi.org/10.1155/2022/4475491

Research Article

Euler's Numerical Method on Fractional DSEK Model under ABC Derivative

Fareeha Sami Khan,[1] M. Khalid,[1] Omar Bazighifan ,[2,3] and A. El-Mesady [4]

[1]*Department of Mathematical Sciences, Federal Urdu University of Arts, Science and Technology, University Road, Karachi 75300, Pakistan*
[2]*Department of Mathematics, Faculty of Science, Hadhramaut University, Hadhramaut, Al Mukalla 50512, Yemen*
[3]*Department of Mathematics, Faculty of Education, Seiyun University, Hadhramout 50512, Yemen*
[4]*Department of Physics and Engineering Mathematics, Faculty of Electronic Engineering, Menoufia University, Menouf 32952, Egypt*

Correspondence should be addressed to Omar Bazighifan; o.bazighifan@gmail.com

Received 28 March 2022; Accepted 30 April 2022; Published 26 May 2022

Academic Editor: Fathalla A. Rihan

In this paper, DSEK model with fractional derivatives of the Atangana-Baleanu Caputo (ABC) is proposed. This paper gives a brief overview of the ABC fractional derivative and its attributes. Fixed point theory has been used to establish the uniqueness and existence of solutions for the fractional DSEK model. According to this theory, we will define two operators based on Lipschitzian and prove that they are contraction mapping and relatively compact. Ulam-Hyers stability theorem is implemented to prove the fractional DSEK model's stability in Banach space. Also, fractional Euler's numerical method is derived for initial value problems with ABC fractional derivative and implemented on fractional DSEK model. The symmetric properties contribute to determining the appropriate method for finding the correct solution to fractional differential equations. The numerical solutions generated using fractional Euler's method have been plotted for different values of α where $\alpha \in (0, 1]$ and different step sizes h. Result discussion will be given, describing the changes that occur due to the step size h.

1. Introduction

Fractional calculus is as historic as integer calculus but not until 1819, it was properly introduced in the form of definitions and functions. Many scientists, researchers, and mathematicians played their role in developing its theory such as [1–5]. Since fractional calculus was developed theoretically at first and had no practical application at the time, it was not as well known as integer calculus among other areas of science. However, after the contribution of Professor Mandelbrot's fractal theory, fractional calculus theory developed rapidly and soon became the hot topic among all researchers around the globe.

The existing theory of nonlinear science is now seemed to be only focused on fractional order calculus theory and the theory of chaos and dissipative structure ([6, 7]). The fact that fractional calculus describes the heredity and memory of any physical phenomenon is fascinating [8, 9]. As a result, it is now used more than integer calculus in fluid dynamics, quantum mechanics, mathematical biology applications, chemistry, control and signal theory, economics, image processing, etc. Models developed in many areas of science and engineering are observed to be best explained by fractional differential equations. The symmetries can be found by solving a related set of partial fractional differential equations. Since integer-order models lack memory and heredity, they cannot adequately and sufficiently describe physical phenomena in many cases. These applications have also led to the rapid development of fractional calculus theory. The authors of [10–13] have a great deal of literature on the subject describing applications and types of fractional derivatives. It is critical to note that every one of those fractional derivative order definitions has its own advantages and disadvantages.

Aside from the mathematical satisfactions of the fractional-order Atangana-Baleanu derivative, the new derivative is being studied due to the necessity of implementing a model depicting the behavior of orthodox viscoelastic materials, thermal medium, and other materials. The proposed mechanism can depict material heterogeneities as well as some structure or media at multiple scales.

The new kernel's nonlocality enables the full description of memory inside of structure and media with multiple scales, which cannot be represented by classical fractional derivatives or those of the Caputo-Fabrizio type. Furthermore, we believe that Atangana-Baleanu derivatives can play an important role in the study of the microstructural behavior of some materials, particularly those involving nonlocal exchanges, which are important in defining the material's properties states [14]. Atangana-Baleanu derivatives are thus extremely useful in describing a wide range of scientific, engineering, and technological problems.

Descemet's stripping endothelial keratoplasty (DSEK) is the name given to eye surgery [15–17] in which a damaged corneal layer is replaced with a healthy corneal layer from a donor or synthetic cornea. Cornea is a clear layer of the eye that is very important in the anterior part of the eye; if it is scratched or damaged, it affects vision. It itself is made up of five layers, see Figure 1. Keeping this in mind, the authors of [18, 19] created the DSEK model, which predicts the behavior of ocular parameters posttreatment. Because this procedure has never been studied mathematically as an ordinary system of differential equations, this work is extremely important. Since fractional calculus has been said to be the generalization of integer calculus, the fractional DSEK model is developed and studied theoretically and numerically in this paper.

In this paper, the first section gives an overview of the literature background of fractional calculus and the DSEK model. The second section gives the preliminary concepts of fractional calculus that will be used in this work. Section three is based on the explanation of the fractional DSEK model. Section four shows the existence of a solution by the fixed point theory of the fractional DSEK model. Section five describes the Ulam-Hyers stability analysis of fractional DSEK. Section 6 describes the computation of fractional Euler's method for ABC fractional derivative and the application of fractional Euler's method to fractional DSEK. The last section is the discussion of the results obtained and the conclusion of this paper.

2. Preliminaries of Fractional Calculus

2.1. Atangana-Baleanu Caputo Fractional Derivative

Definition 1. The authors of [20] introduced a new Caputo fractional derivative as

$$D_t^{\alpha}(g(t)) = \frac{N(\alpha)}{1-\alpha}\int_c^t g'(y)e^{-\alpha/1-\alpha(t-y)}\mathrm{d}y, \tag{1}$$

where $g \in H^1(b,c), c > b, \alpha \in [0,1], N(\alpha)$ is the normalization function that follows the condition $N(0) = N(1) = 1$.

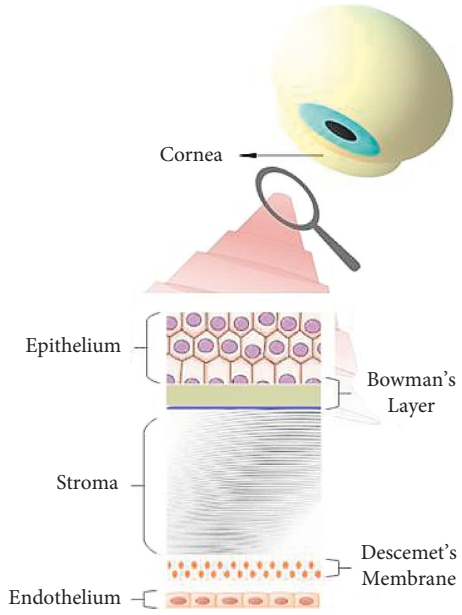

Figure 1: Five layers of the cornea.

Definition 2. If the function does not follow the condition $N(0) = N(1) = 1$, then it takes the form as

$$D_t^{\alpha}(g(t)) = \frac{\alpha N(\alpha)}{1-\alpha}\int_c^t (g(t)-g(y))e^{-\alpha/1-\alpha(t-y)}\mathrm{d}y. \tag{2}$$

This equation can also take the form of the condition $N(0) = N(\infty) = 1$

$$D_t^{\rho}(g(t)) = \frac{N(\rho)}{\rho}\int_c^t g'(y)e^{-(t-y)/\rho}\mathrm{d}y, \tag{3}$$

where $\rho = 1 - \alpha/\alpha \in [0,\infty)$, also $\alpha = 1/1+\rho \in [0,1]$.

This derivative was defined by [20] to involve an exponential kernel in fractional derivatives to represent the results of dynamic systems memory effects more accurately. With the passage of time, it occurred that this definition has a flaw in that it does not give the original function when $\alpha = 1$. To overcome this problem, the authors of [21] presented the accurate kernel and modified this definition accordingly.

Definition 3. Let the new fractional derivative be defined as

$${}_c^{\mathrm{ABC}}D_t^{\alpha}(g(t)) = \frac{N(\alpha)}{1-\alpha}\int_c^t g'(y)E_{\alpha}^{\alpha/\alpha-1(t-y)^{\alpha}}\mathrm{d}y, \tag{4}$$

where $g \in H^1(b,c), \quad c > b$ also $\alpha \in [0,1]$ and $N(\alpha)$ has the same properties defined in [20]. Here, E_{α} is the generalized Mittag-Leffler function defined as $E_{\alpha} = E_{\alpha}(-t^{\alpha}) = \sum_{k=0}^{\infty}(-t)^{\alpha k}/\Gamma(\alpha k+1)$.

For the above definition, the constant function has a fractional derivative of zero. The above description would be helpful when solving real-world issues and will also provide a great benefit in utilizing the Laplace transform to solve any initial state physical problem. Nevertheless, if alpha is 0, we will not recover the initial function except when the function vanishes at the origin. We suggest the following definition, in order to avoid this problem.

Definition 4. Let the new fractional derivative be defined as

$$ {}_{c}^{\mathrm{ABR}}D_t^{\alpha}(g(t)) = \frac{N(\alpha)}{1-\alpha}\frac{\mathrm{d}}{\mathrm{d}t}\int_c^t g(y)E_{\alpha}^{-\alpha/1-\alpha(t-y)^{\alpha}}\mathrm{d}y, \tag{5} $$

where $g \in H^1(b,c)$, $c > b$ also $\alpha \in [0,1]$ and $N(\alpha)$ has the same properties defined in [20]. Here, E_α is the generalized Mittag-Leffler function defined as $E_\alpha = E_\alpha(-t^\alpha) = \sum_{k=0}^{\infty}(-t)^{\alpha k}/\Gamma(\alpha k+1)$.

Both definitions have a nonlocal kernel. For calculations in this paper, we will use definitions in (4) and (5).

2.2. Properties of Atangana-Baleanu Caputo Fractional Derivative

(i) Laplace transformation on equation (4)is

$$ \mathscr{L}\left\{{}_{0}^{\mathrm{ABR}}D_t^{\alpha}(g(t))\right\}(s) = \frac{N(\alpha)}{1-\alpha}\frac{s^{\alpha}\mathscr{L}\{g(t)\}(s)}{s^{\alpha+}\alpha/1-\alpha}. \tag{6} $$

(ii) Laplace transformation on equation (5)is

$$ \mathscr{L}\left\{{}_{0}{}^{\mathrm{ABC}}D_t^{\alpha}(g(t))\right\}(s) = \frac{N(\alpha)}{1-\alpha}\frac{s^{\alpha}\mathscr{L}\{g(t)\}(s) - s^{\alpha-1}g(0)}{s^{\alpha+}\alpha/1-\alpha}. \tag{7} $$

(iii) Let $g \in H^1(b,c)$, $c > b$, $\alpha \in [0,1]$, then the following relation exists [20]:

$$ {}_{0}^{\mathrm{ABR}}D_t^{\alpha}(g(t)) = {}_{0}^{\mathrm{ABR}}D_t^{\alpha}(g(t)) + H(t). \tag{8} $$

(iv) If g is a continuous function on some closed interval $[a,b]$. Then, the following inequality can be written on $[a,b]$

$$ {}_{0}^{\mathrm{ABR}}D_t^{\alpha}(g(t))\| < \frac{N(\alpha)}{1-\alpha}K, \quad \|h(t)\| = \max_{b\le t\le c}\|h(t)\|. \tag{9} $$

(v) Lipschitz condition Atangana-Baleanu Caputo fractional derivative satisfies the Lipschitz condition in Riemann and Caputo sense, and the following inequality exists:

$$ {}_{0}^{\mathrm{ABC}}D_t^{\alpha}(g(t)) - {}_{0}^{\mathrm{ABC}}D_t^{\alpha}(f(t))\| \le H\|g(t)-f(t)\|. \tag{10} $$

Similarly, for (5), the Lipschitz condition exists as

$$ {}_{0}^{\mathrm{ABR}}D_t^{\alpha}(g(t)) - {}_{0}^{\mathrm{ABR}}D_t^{\alpha}(f(t))\| \le H\|g(t)-f(t)\|. \tag{11} $$

(vi) **AB fractional** integral for $\alpha \in (0,1]$ the AB fractional integral for $g(t) \in H^1(0,t)$ and nonlocal kernel is given as

$$ {}_{b}^{\mathrm{AB}}I_t^{\alpha}(g(t)) = \frac{1-\alpha}{N(\alpha)}g(t) + \frac{\alpha}{N(\alpha)\Gamma(\alpha)}\int_b^t (t-y)^{\alpha-1}g(y)\mathrm{d}y, \quad T>0. \tag{12} $$

When $\alpha = 1$, the ordinary integral is obtained, and for $\alpha = 0$, the initial function is obtained.

For proof of these, see [20].

Lemma 1. *[21] Suggests that the proposed problem for $\alpha \in (0,1]$ has a solution; that is,*

$$ {}^{\mathrm{ABC}}D_t^{\alpha}g(t) = \eta(t)g(0) = g_0, \tag{13} $$

its solution is given by $g(t) = g_0 + 1 - \alpha/N(\alpha)\eta(t) + \alpha/N(\alpha)\Gamma(\alpha)\int_0^t (t-y)^{\alpha-1}g(y)dy$.

3. Fractional DSEK Model

As mentioned in Section 2, the definitions in (4) and (5) have nonlocal kernels, and therefore, Atangana-Baleanu Caputo fractional derivative operator's performance in modeling eye surgery is better than any other definition. It inspired the valuable applications of several fractional operators in dynamic mathematical models; therefore, we are researching the dynamics of eye surgery derived in [18] by a system of nonlinear differential equations by involving ABC fractional derivative.

$$ \begin{aligned} {}^{\mathrm{ABC}}D_t^{\alpha}p(t) &= a\frac{r(t)}{s(t)} + \gamma q(t) + \delta, \\ {}^{\mathrm{ABC}}D_t^{\alpha}q(t) &= -\delta - \beta\frac{r(t)}{s(t)} - \gamma q(t) - s(t)q(t), \\ {}^{\mathrm{ABC}}D_t^{\alpha}r(t) &= -\beta\frac{r(t)}{s(t)} - q(t) - s(t)p(t), \\ {}^{\mathrm{ABC}}D_t^{\alpha}s(t) &= s(t)p(t) + s(t)q(t) + q(t), \end{aligned} \tag{14} $$

with initial conditions

$$ p(0) = p_0 \ge 0, q(0) = q_0 \ge 0, r(0) = r_0 \ge 0, s(0) = s_0 \ge 0, \tag{15} $$

where ${}^{\mathrm{ABC}}D_t^{\alpha}$ is the Atangana-Baleanu Caputo fractional derivative of order α. DSEK model is based on the same conditions given by [18]. Also, the defined parameters have the same description as given by [18]. Such as $p(t)$ is the refractive index, $q(t)$ is the axial length, $r(t)$ is the corneal curvature, and $s(t)$ is the central corneal thickness.

3.1. Preliminaries for Fractional DSEK Model.

For fractional analysis of the DSEK model, let us define $\xi = (p,q,r,s)$. To define the Banach space, let us say we have $B = [0,t]$ where $0 \le T \le t < \infty$. Then, the field can be written as $G = C(B, R^4)$ under the norm supremum as

$$ \|\xi\| = \sup_{T\in B}\{|\xi(T)|: \xi \in G\}, \tag{16} $$

where $|\xi| = |p| + |q| + |r| + |s|$. Also, $p,q,r,s,N \in C[0,t]$.

Definition 5. Let B be a Banach space. Then, ψ defined as $B \longrightarrow B$ will be a Lipschitzian if there exists a constant $l > 0$ for which the inequality exists such that

$$ \|\psi\xi_1 - \psi\xi_2\| \le l\|\xi_1 - \xi_2\|, \tag{17} $$

for all $\xi_1, \xi_2 \in B$. Where l is the Lipschitz constant for ψ. If $l < 1$, then ψ is a contraction.

Theorem 1. *Let B be a Banach space and ψ: $B \longrightarrow B$ be a contraction mapping. Then, there must exist a unique fixed point of ψ.*

Theorem 2. *A subset of Banach space B is supposed to be N. Let N be convex, closed, and nonempty. Suppose that F and G map N into G, and the following relations exist:*

(i) $Fu + Gv \in N \forall \xi_1, \xi_2 \in N$

(ii) F is continuous and compact

(iii) G is a contraction mapping

Then, there exists $\xi \in N$ such that $F\xi + G\xi = \xi$.

4. Existence of Solutions for Fractional DSEK Model

By using the fixed-point theory, let us prove the uniqueness and existence of the DSEK model. To prove its uniqueness and existence, let us reformulate the DSEK model of (14).

$$\begin{aligned} {}^{\mathrm{ABC}}D_t^{\alpha} p(t) &= G_1(t, p, q, r, s), \\ \mathrm{ABCD}_t^{\alpha} q(t) &= G_2(t, p, q, r, s), \\ \mathrm{ABCD}_t^{\alpha} r(t) &= G_3(t, p, q, r, s), \\ \mathrm{ABCD}_t^{\alpha} s(t) &= G_4(t, p, q, r, s), \end{aligned} \tag{18}$$

where

$$\begin{aligned} G_1(t, p, q, r, s) &= a\frac{r(t)}{s(t)} + \gamma q(t) + \delta, \\ G_2(t, p, q, r, s) &= -\delta - \beta\frac{r(t)}{s(t)} - \gamma q(t) - s(t)q(t), \\ G_3(t, p, q, r, s) &= -\beta\frac{r(t)}{s(t)} - q(t) - s(t)p(t), \\ G_4(t, p, q, r, s) &= s(t)p(t) + s(t)q(t) + q(t). \end{aligned} \tag{19}$$

Let us consider system (14) as

$${}^{\mathrm{ABC}}D_t^{\alpha} p(t)\xi(t) = G(t, \xi(t)), \tag{20}$$

with an initial condition $\xi(0) = \xi_0 \geq 0$ where

$$\begin{aligned} \xi(t) &= (p, q, r, s)^T, \\ \xi_0 &= (p_0, q_0, r_0, s_0)^T, \\ G(t, \xi(t)) &= (G_n(t, p, q, r, s))^T, \quad n = 1, 2, 3, 4. \end{aligned} \tag{21}$$

In (21), the superscript T represents the transpose. By using Lemma 1 and AB fractional integral, the (20) becomes the fractional integral equation as

$$\begin{aligned} \xi(t) = \xi_0 &+ \frac{1-\alpha}{N(\alpha)} G(t, \xi(t)) \\ &+ \frac{\alpha}{N(\alpha)\Gamma(\alpha)} \int_0^t (t-y)^{\alpha-1} G(y, \xi(y)) \mathrm{d}y. \end{aligned} \tag{22}$$

Now, to prove the existence uniqueness, we consider two hypotheses based on Lipschitzian and some growth condition assumptions.

Hypothesis 1. For two constants ϕ_E, θ_E, the inequality exists; that is,

$$|G(t, \xi(t))| \leq \phi_E |\xi| + \theta_E, \quad t \in [0, T]. \tag{23}$$

Hypothesis 2. For a constant $M_E > 0$ such that

$$\left|G(t, \xi_1) - G(t, \xi_2)\right| \leq M_E \left|\xi_1 - \xi_2\right|, \tag{24}$$

for each $\xi \in B$ and $T \in [0, t]$.

Let us define two operators ψ_1 and ψ_2 as

$$\begin{aligned} \psi_1 \xi(t) &= \xi_0 + \frac{1-\alpha}{N(\alpha)} G(T, \xi(T)), \\ \psi_2 \xi(t) &= \frac{\alpha}{N(\alpha)\Gamma(\alpha)} \int_0^T (T-y)^{\alpha-1} G(y, \xi(y)) \mathrm{d}y, \end{aligned} \tag{25}$$

where $B = \psi_1 + \psi_2$.

Theorem 3. *Consider a closed convex set $F_\epsilon = \{\xi \in B: \|\xi\| \leq \epsilon\}$ where $\epsilon = \beta_2/1 - \beta_1$ such that $\beta_1 = [1 - \alpha/N(\alpha) + t^\alpha/N(\alpha)\Gamma(\alpha)]\phi_E < 1$, $\beta_2 = |\xi_0| + [1 - \alpha/N(\alpha) + t^\alpha/N(\alpha)\Gamma(\alpha)]\theta_E$ and prove that*

$$\left\|\psi_1 \xi_1 + \psi_2 \xi_2\right\| \in F_\epsilon, \tag{26}$$

for $\xi_1, \xi_2 \in F_\epsilon$

$$\begin{aligned}\left\|\psi_1\xi_1+\psi_2\xi_2\right\| &\le \max_{T\in[0,t]}\left\{\left|\xi_0\right|+\frac{1-\alpha}{N(\alpha)}\left|G(T,\xi(T))\right|+\frac{\alpha}{N(\alpha)\Gamma(\alpha)}\int_0^T(T-y)^{\alpha-1}\left|G(y,\xi(y))\right|\mathrm{d}y\right\}\\ &\le\left\{\left|\xi_0\right|+\frac{1-\alpha}{N(\alpha)}\left[\phi_E\|\xi\|+\theta_E\right]+\frac{\alpha}{N(\alpha)\Gamma(\alpha)}\int_0^T(T-y)^{\alpha-1}\left[\phi_E\|\xi\|+\theta_E\right]\mathrm{d}y\right\}\\ &=\left|\xi_0\right|+\left[\frac{1-\alpha}{N(\alpha)}+\frac{t^\alpha}{N(\alpha)\Gamma(\alpha)}\right]\theta_E+\left[\frac{1-\alpha}{N(\alpha)}+\frac{t^\alpha}{N(\alpha)\Gamma(\alpha)}\right]\phi_E\epsilon\\ &=\beta_1+\beta_2\epsilon\le\epsilon.\end{aligned}\tag{27}$$

This confirms that $\psi_1\xi_1+\psi_2\xi_2\in F_\epsilon$.

Theorem 4. *Prove that* ψ_1 *is a contraction.*

To prove that ψ_1 *is a contraction suppose* $\xi,\xi^*\in F_\epsilon$. *Then, by using Hypothesis 2, we have*

$$\begin{aligned}\left\|\psi_1\xi-\psi_2\xi^*\right\| &\max_{T\in[0,t]}\frac{1-\alpha}{N(\alpha)}\left|G(T,\xi(T))-G(T,\xi^*(T))\right.\\ &\le\frac{1-\alpha}{N(\alpha)}M_E\max_{T\in[0,t]}\left|\xi(T)-\xi^*(T)\right|\\ &\le\frac{1-\alpha}{N(\alpha)}M_E\left|\xi-\xi^*\right|.\end{aligned}\tag{28}$$

As we know that $1-\alpha/N(\alpha)M_E<1$, ψ_1 *is a contraction mapping.*

Theorem 5. *Prove that* ψ_2 *is relatively compact.*

We can prove that ψ_2 *is relatively compact by showing that* ψ_2 *is continuous, uniformly bounded, and also equicontinuous.*

As we know that $\xi(T)$ *is continuous, then* $\psi_2\xi(T)$ *is also continuous.*

Let us assume that $\xi\in F_\epsilon$, *then*

$$\begin{aligned}\left\|\psi_2\xi\right\| &\le\max_{T\in[0,t]}\frac{\alpha}{N(\alpha)\Gamma(\alpha)}\int_0^T(T-y)^{\alpha-1}\left|G(y,\xi(y))\right|\mathrm{d}y\\ &\le\frac{\alpha}{N(\alpha)\Gamma(\alpha)}\int_0^T(T-y)^{\alpha-1}\left[\phi_E\max_{T\in[0,t]}|\xi|+\theta_E\right]\mathrm{d}y\\ &\le\frac{\alpha}{N(\alpha)\Gamma(\alpha)}\int_0^T(T-y)^{\alpha-1}\left[\phi_E\|\xi\|+\theta_E\right]\mathrm{d}y\\ &\le\frac{t^\alpha}{N(\alpha)\Gamma(\alpha)}\left[\phi_E\epsilon+\theta_E\right]\mathrm{d}y.\end{aligned}\tag{29}$$

Hence, proved that ψ_2 *is uniformly bounded on* F_ϵ. *Now, we have to show that* ψ_2 *is equicontinuous. Assume* $\xi\in F_\epsilon$ *and* $T_1,T_2\in[0,t]$ *where* $T_1<T_2$. *Then, we have*

$$\begin{aligned}\left\|\psi_2\xi(T_2)-\psi_2\xi(T_1)\right\| &\le\frac{\alpha}{N(\alpha)\Gamma(\alpha)}\int_{T_1}^{T_2}(T_2-y)^{\alpha-1}\left|G(y,\xi(y))\right|\mathrm{d}y\\ &\quad+\frac{\alpha}{N(\alpha)\Gamma(\alpha)}\int_0^{T_1}(T_1-y)^{\alpha-1}-(T_2-y)^{\alpha-1}\left|G(y,\xi(y))\right|\mathrm{d}y\\ &\le\frac{\left[\phi_E\epsilon+\theta_E\right]}{N(\alpha)\Gamma(\alpha)}\left[(T_2-T_1)^\alpha+(T_1^\alpha-T_2^\alpha)+(T_2-T_1)^\alpha\right]\\ &=\frac{2\left[\phi_E\epsilon+\theta_E\right]}{N(\alpha)\Gamma(\alpha)}(T_2-T_1)^\alpha=\lim_{T_1\longrightarrow T_2}\frac{2\left[\phi_E\epsilon+\theta_E\right]}{N(\alpha)\Gamma(\alpha)}(T_2-T_1)^\alpha\longrightarrow 0.\end{aligned}\tag{30}$$

Now, the Arzelá-Ascoli theorem suggests that ψ_2 *is relatively compact, and hence, it is completely continuous.*

Theorem 6. *If Hypothesis 1 and Hypothesis 2 hold, then the fractional integral equation that is equation (20) which is the solution of equation (12) has at least one solution only if* $1-\alpha/N(\alpha)M_E$ *where* β_1 *is*

$$\beta_1=\left[\frac{1-\alpha}{N(\alpha)}+\frac{t^\alpha}{N(\alpha)\Gamma(\alpha)}\right]\phi_E<1.\tag{31}$$

By using Theorems 2–5, it is proved that the integral equation given in (22) has at least one solution, and consequently, the DSEK model (14) under consideration also has at least one solution.

Theorem 7. *Prove that integral equation (20) has a unique solution if* $\beta_3 = (1-\alpha/N(\alpha) + t^\alpha/N(\alpha)\Gamma(\alpha))M_E < 1$ *under Hypothesis 2.*

As we have ψ: $B \longrightarrow B$ *defined as*

$$\psi\xi(t) = \xi_0 + \frac{1-\alpha}{N(\alpha)}G(T,\xi(T)) + \frac{\alpha}{N(\alpha)\Gamma(\alpha)}\int_0^T (T-y)^{\alpha-1}G(y,\xi(y))\mathrm{d}y. \tag{32}$$

Let $\xi, \xi^* \in B$ *and* $T \in [0,t]$. *Then, we have*

$$\begin{aligned}\left\|\psi\xi(t) - \psi\xi^*\right\| &\le \max_{T\in[0,T]}\frac{1-\alpha}{N(\alpha)}\left|G(T,\xi(T)) - G(T,\xi^*(T))\right| \\ &+ \max_{T\in[0,T]]}\frac{\alpha}{N(\alpha)\Gamma(\alpha)}\int_0^T (T-y)^{\alpha-1}\left|G(y,\xi(y)) - G(y,\xi^*(y))\right|\mathrm{d}y \\ &\le \left(\frac{1-\alpha}{N(\alpha)} + \frac{t^\alpha}{N(\alpha)\Gamma(\alpha)}\right)M_E\left\|\xi - \xi^*\right\|.\end{aligned} \tag{33}$$

Hence, β_3 *suggests* ψ *is a contraction. Hence, (22) has a unique solution which suggests that (14) also has a unique solution.*

5. Ulam-Hyers Stability for DSEK Model

Stability analysis of nonlinear dynamical models is a must. So, in this work, we use Ulam-Hyers stability for DSEK model12 with some nonlinear functional analysis concepts. Ulam-Hyers stability was introduced in 1940 by [22, 23] as a stability study for functional equations. This acted as a motivator for various researchers, and then, this stability was discussed in many forms. Using the fixed-point technique, the authors in [24] investigated the Hyers-Ulam-Rassias and Hyers-Ulam stability of the fractional Volterra integral-differential equation. In a Banach space, some results on generalized Hyers-Ulam stability of the linear differential equation were introduced in [25]. In [26], the authors investigated the Hyers-Ulam stability of first-order linear differential equations and extended previous results using the integral factor approach. In [27], the Hyers-Ulam-Rassias stability of a certain fractional differential equation was discussed, as well as the Hyers-Ulam stability of a certain fractional differential equation. For a particular family of fractional integrodifferential equations, the stability of Ulam-Hyers, Ulam-Hyers-Rassias, and semi-Ulam-Hyers-Rassias on some intervals was studied in [28]. The Ulam-Hyers and generalized Ulam-Hyers-Rassias stabilities for the solution of a fractional-order pseudoparabolic partial differential equation were investigated using the Gronwall inequality [29]. The existence and uniqueness of solutions, as well as Ulam-Hyers-Rassias stability, of an impulsive certain fractional differential equation were investigated in [30]. Sometimes, it is the stability analysis of differential equation ordinary or partial, integral equations, functional equations, etc. Various types have been formed of Ulam-Hyers stability theory, namely, Ulam-Hyers-Rassias, semi-Ulam-Hyers-Rassias [28, 31], and Ulam stability [32].

Definition 6. For some $\lambda > 0$, $\widetilde{\xi} \in B$ if

$$\left|{}^{\mathrm{ABC}}D_t^\alpha\widetilde{\xi}(T) - G(T,\widetilde{\xi}(T))\right| \le \lambda, \tag{34}$$

there must exist $\xi \in B$ that satisfies the DSEK model (14) having an initial condition

$$\xi(0) = \widetilde{\xi}(0), \tag{35}$$

where $\|\widetilde{\xi} - \xi\| \le \epsilon_\lambda$ such that

$$\begin{aligned}\xi(t) &= (\widetilde{p},\widetilde{q},\widetilde{r},\widetilde{s})^T, \\ \xi_0 &= (\widetilde{p_0},\widetilde{q_0},\widetilde{r_0},\widetilde{s_0})^T, \\ G(t,\widetilde{\xi}(t)) &= (G_n(t,\widetilde{p},\widetilde{q},\widetilde{r},\widetilde{s}))^T, \quad n = 1,2,3,4, \\ \lambda &= m(\lambda_1,\lambda_2,\lambda_3,\lambda_4)^T, \\ \epsilon &= m(\epsilon_1,\epsilon_2,\epsilon_3,\epsilon_4)^T,\end{aligned} \tag{36}$$

with this property, if there exists an $\epsilon > 0$, then it is said that the DSEK model (12) is UlamHyers stable.

Remark 1. Let f be a small perturbation such that $f \in C[0,t]$ where $f(0) = 0$ has the properties given as follows:

(i) $|f(T) \le \lambda|$, where $T \in [0,t]$ and $\lambda_1 > 0$

(ii) *For* $T \in [0,t]$ the model becomes

$${}^{\mathrm{ABC}}D_t^\alpha\widetilde{\xi}(T) = G(T,\widetilde{\xi}(T)) + f(T), \tag{37}$$

where $f(T) = (f_1(T), f_2(T), f_3(T), f_4(T))^T$ the superscript T represents the transpose.

Lemma 2. *Perturbed system (35)*

$$\begin{aligned}{}^{\mathrm{ABC}}D_t^\alpha\widetilde{\xi}(T) &= G(T,\widetilde{\xi}(T)) + f(T), \\ \widetilde{\xi}(0) &= \widetilde{\xi}_0,\end{aligned} \tag{38}$$

has a solution that satisfies the inequality

$$\left|\widetilde{\xi}_f(T) - \widetilde{\xi}(T)\right| \le l\lambda, \tag{39}$$

$\widetilde{\xi}_f(T)$ *represents the solution of the system (37),*

$$l = \left(\frac{\Gamma(\alpha)(1-\alpha) + t^\alpha}{N(\alpha\Gamma(\alpha))}\right). \tag{40}$$

By using Remark 1 and Lemma 2, the solution of system (37) is given as

$$\widetilde{\xi}_f(T) = \widetilde{\xi}_0 + \frac{1-\alpha}{N(\alpha)}G(T,\widetilde{\xi}(T)) + \frac{\alpha}{N(\alpha)\Gamma(\alpha)}\int_0^T (T-y)^{\alpha-1}G(y,\widetilde{\xi}(y))\mathrm{d}y + \frac{1-\alpha}{N(\alpha)}f(T) + \frac{\alpha}{N(\alpha)\Gamma(\alpha)}\int_0^T (T-y)^{\alpha-1}G(y)\mathrm{d}y. \tag{41}$$

Also, we know that

$$\widetilde{\xi}(T) = \widetilde{\xi}_0 + \frac{1-\alpha}{N(\alpha)}G(T,\widetilde{\xi}(T)) + \frac{\alpha}{N(\alpha)\Gamma(\alpha)}\int_0^T (T-y)^{\alpha-1}G(y,\widetilde{\xi}(y))\mathrm{d}y. \tag{42}$$

Now, Remark 1 suggests that

$$\begin{aligned}\left|\widetilde{\xi}_f(T) - \widetilde{\xi}(T)\right| &\le \frac{1-\alpha}{N(\alpha)}|f(T)| + \frac{\alpha}{N(\alpha)\Gamma(\alpha)}\int_0^T (T-y)^{\alpha-1}|f(y)|d \\ &\le \left(\frac{\Gamma(\alpha)(1-\alpha)+t^{\alpha}}{N(\alpha\Gamma(\alpha))}\right)\lambda = l\lambda.\end{aligned} \tag{43}$$

Theorem 8. *By using Theorem 4, it is proven that the DSEK system (35) is Ulam-Hyers stable in B. Let the DSEK system (12) with initial conditions*

$$\xi(0) = \widetilde{\xi}(0), \tag{44}$$

has a unique solution as $\xi \in B$ and $\widetilde{\xi} \in B$ is the solution of inequality (34), and then,

$$\xi(T) = \xi_0 + \frac{1-\alpha}{N(\alpha)}G(T,\xi(T)) + \frac{\alpha}{N(\alpha)\Gamma(\alpha)}\int_0^T (T-y)^{\alpha-1}G(y,\xi(y))\mathrm{d}y. \tag{45}$$

Since $\xi_0 = \widetilde{\xi}_0$ as suggested by an initial condition, hence, (45) becomes

$$\widetilde{\xi}(T) = \widetilde{\xi}_0 + \frac{1-\alpha}{N(\alpha)}G(T,\widetilde{\xi}(T)) + \frac{\alpha}{N(\alpha)\Gamma(\alpha)}\int_0^T (T-y)^{\alpha-1}G(y,\widetilde{\xi}(y))\mathrm{d}y. \tag{46}$$

Then, by Lemma 2 and the hypothesis above, we have

$$\begin{aligned}|\widetilde{\xi}(T) - \xi(T)| &\le \left|\widetilde{\xi}(T) - \widetilde{\xi}_f(T)\right| + \left|\widetilde{\xi}_f(T) - \xi(T)\right| \\ &\le l\lambda + \frac{1-\alpha}{N(\alpha)}|G(T,\widetilde{\xi}(T)) - G(T,\xi(T))| \\ &\quad + \frac{\alpha}{N(\alpha)\Gamma(\alpha)}\int_0^T (t-y)^{\alpha-1}|G(T,\widetilde{\xi}(T)) \\ &\quad - G(T,\xi(T))|\mathrm{d}y + l\lambda \\ &\le 2l\lambda + \left(\frac{1-\alpha}{N(\alpha)} + \frac{t^{\alpha}}{N(\alpha)\Gamma(\alpha)}\right)M_E\|\widetilde{\xi} - \xi\|,\end{aligned} \tag{47}$$

which implies that

$$\|\widetilde{\xi} - \xi\| \le \frac{2l\lambda}{1-\beta_3}. \tag{48}$$

Since $\beta_3 < 1$ hence from $\epsilon = 2l/1-\beta_3$, we obtain $\|\widetilde{\xi} - \xi\| \le \epsilon_\lambda$. Hence, proved that the DSEK system (35) is Ulam-Hyers stable.

6. Numerical Approximation of Fractional DSEK Model

In this section, the fractional DSEK model will be solved numerically by using fractional Euler's method. There are several numerical techniques to compute the numerical results of a fractional system of differential equations, but in this case, even Euler's method can analyze its solution. In order to do that, we first derive the fractional Euler's method for Atangana-Baleanu Caputo fractional derivative.

6.1. Fractional Euler's Method for Atangana-Baleanu Caputo Fractional Derivative. The authors of [33] proved that the generalized Taylor's formula of Atangana-Baleanu Caputo fractional derivative is given as

$$f(t) = \sum_{m=0}^{n}\left(\left({}^{\mathrm{ABC}}D_t^{\alpha}\right)^{n+1}\sum_{k=0}^{n+1}\frac{x^{\alpha k}(n+1)!\alpha^k(1-\alpha)^{-k+n+1}}{k!(-k+n+1)!B(\alpha)^{n+1}\Gamma(k\alpha+1)} + \left({}^{\mathrm{ABC}}D_t^{\alpha}\right)^{m}\sum_{k=0}^{m}\frac{x^{\alpha k}m!\alpha^k(1-\alpha)^{m-k}}{k!(m-k)!B(\alpha)^{m}\Gamma(k\alpha+1)}\right)(t-\alpha)f(a) \tag{49}$$

Suppose that we have an initial value problem

$${}^{\mathrm{ABC}}D_t^{\alpha}f(t) = G(t,f(t)),\ f(0) = f_0\ 0 < \alpha \le 1, t > 0. \tag{50}$$

Let $[0,a)$ be the interval on which we need to obtain the solution of our problem. For generalization instead of $[0,a)$, we consider $(t_i, f(t_i))$ and use this for our approximation.

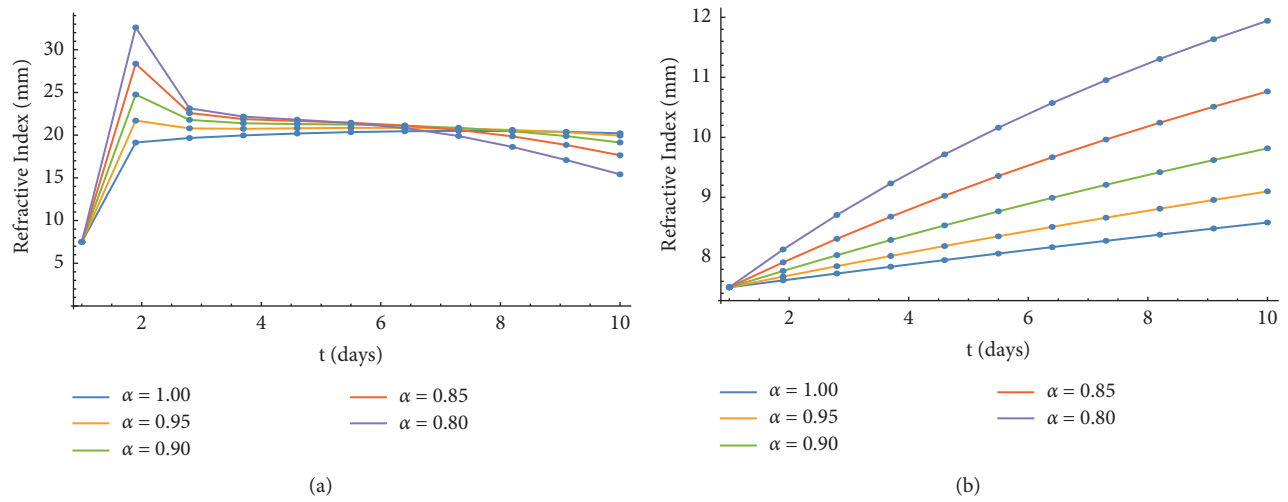

FIGURE 2: Numerical simulation of refractive index for different values of α and h implementing the fractional behavior. (a)$h = 0.01, 0 < \alpha \leq 1$ and $t \in (1, 10)$. (b)$h = 0.0001, 0 < \alpha \leq 1$ and $t \in (1, 10)$.

Let the k subintervals of equal width be $h = a/k$ by using nodes $t_i = ih$ for $i = 0, 1, \ldots, k$. Consider that $f(t)$, ${}^{ABC}D_t^{\alpha} f(t)$, etc. are continuous on $(t_i, f(t_i))$, then, by using (50), we expand $f(t)$ about $t = t_0$ as

$$f(t_1) = f(t_0) + {}^{ABC}D_t^{\alpha} f(t_0) \frac{\alpha (t_1 - a)^{\alpha}}{\Gamma(\alpha + 1) B(\alpha)} + \cdots. \tag{51}$$

Upon neglecting higher-order terms because step size h is considered as a smallest positive number and taking $h = t_1$, ${}^{ABC}D_t^{\alpha} f(t_0) = G(t_0, f(t_0))$, (51) becomes

$$f(t_1) = f(t_0) + G(t_0, f(t_0)) \frac{\alpha (h - a)^{\alpha}}{\Gamma(\alpha + 1) B(\alpha)}. \tag{52}$$

Equation (52) becomes the iterative equation for repeatedly calculating the points of t that approximates the solution of $f(t)$. Hence, the general form of fractional Euler's method for solving initial value problems with Atangana-Baleanu Caputo fractional derivative is

$$t_{i+1} = t_i + h. \tag{53}$$

$$f(t_{i+1}) = f(t_i) + G(t_i, f(t_i)) \frac{\alpha (h - a)^{\alpha}}{\Gamma(\alpha + 1) B(\alpha)}. \tag{54}$$

It can be observed easily that for $\alpha = 1$, this becomes the classical Euler method.

Now, to solve the fractional DSEK model numerically, we use the parameter values and initial conditions given in [18]. According to that table, $a = 100, \beta = 50, \gamma = 3.32mm$, $\delta = 0.015mm, p(0) = 7.50mm, q(0) = 24.39mm, r(0) = 5.63mm$, and $s(0) = 0.52mm$. Now, the fractional DSEK system in (14) with the iterative formula (54) becomes

$$\begin{aligned}
p(t_{i+1}) &= p_0 + \frac{\alpha (h - a)^{\alpha}}{\Gamma(\alpha + 1) B(\alpha)} \left(3.32 q(t_i) + \frac{100 r(t_i)}{s(t_i)} + 0.015 \right), \\
q(t_{i+1}) &= q_0 + \frac{\alpha (h - a)^{\alpha}}{\Gamma(\alpha + 1) B(\alpha)} \left(q(t_i)(-s(t_i)) - 3.32 q(t_i) - \frac{50 r(t_i)}{s(t_i)} - 0.015 \right), \\
r(t_{i+1}) &= r_0 + \frac{\alpha (h - a)^{\alpha}}{\Gamma(\alpha + 1) B(\alpha)} \left(-p(t_i) s(t_i) - q(t_i) - \frac{50 r(t_i)}{s(t_i)} \right), \\
s(t_{i+1}) &= s_0 + \frac{\alpha (h - a)^{\alpha}}{\Gamma(\alpha + 1) B(\alpha)} \left(p(t_i) s(t_i) + q(t_i) s(t_i) + q(t_i) \right).
\end{aligned} \tag{55}$$

By solving (55) with the help of software, we obtain the numerical solution for different values of α in the form of Figures 2–5 and 6. Figure 2(a) represents the fractional solution of refractive index $p(t)$ for different values of α between $0 < \alpha \leq 1$ and $h = 0.01$, whereas Figure 2(b) is obtained for the step size $h = 0.001$.

The only difference among the solutions presented in Figures 2(a) and 2(b) is the different values of h. If we

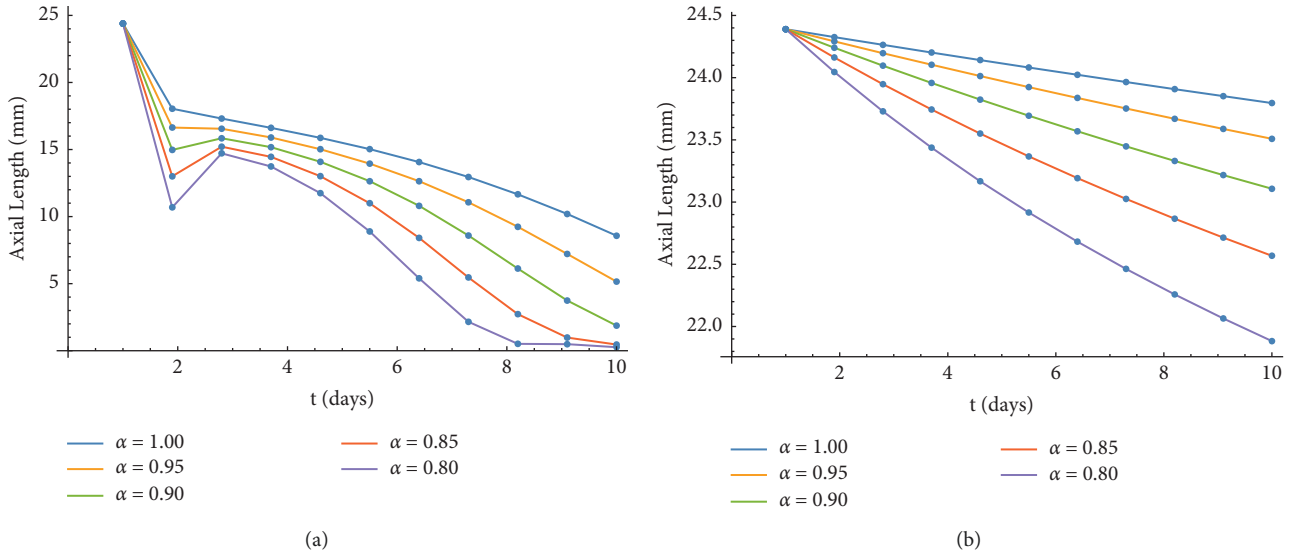

FIGURE 3: Numerical solution by fractional Euler's method of axial length at different values of α and h implementing the fractional behavior. (a)$h = 0.01, 0 < \alpha \leq 1$ and $t \in (1, 10)$. (b)$h = 0.0001, 0 < \alpha \leq 1$ and $t \in (1, 10)$.

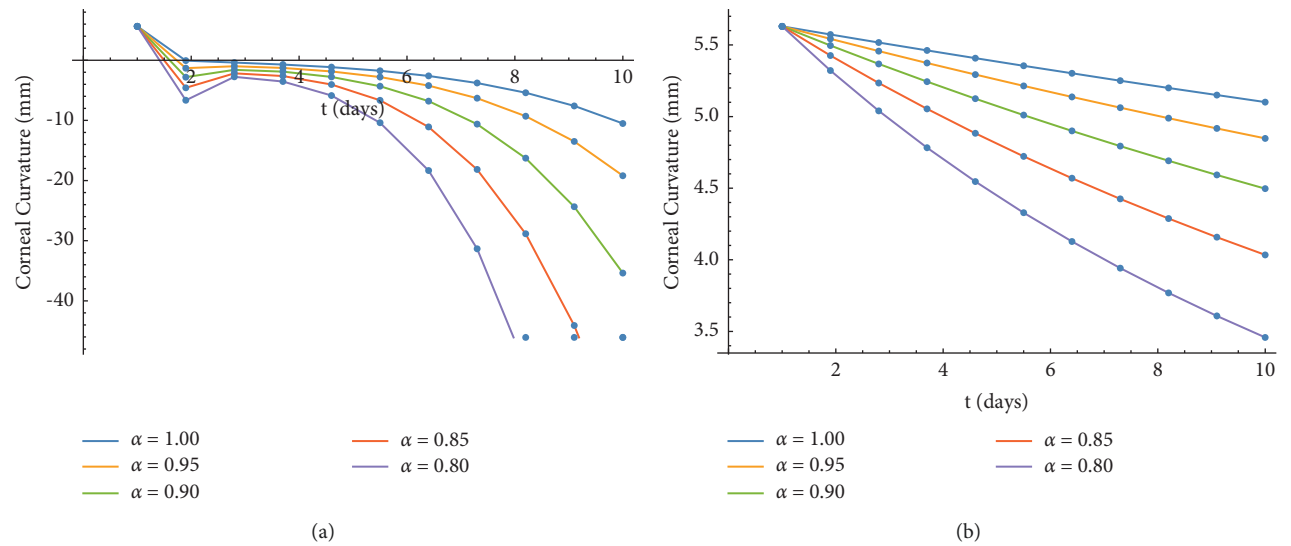

FIGURE 4: Numerical solution by fractional Euler's method of corneal curvature at different values of α and h implementing the fractional behavior. (a)$h = 0.01, 0 < \alpha \leq 1$ and $t \in (1, 10)$. (b)$h = 0.0001, 0 < \alpha \leq 1$ and $t \in (1, 10)$.

observe as $h \longrightarrow 0$, the fractional behavior is clearer to understand and gives us the accurate approximation for $\alpha = 1$, then $h \longrightarrow 1$.

Figures 3(a) and3(b) represent the numerical solution of axial length for different values of α where $0 < \alpha \leq 1$ and $h = 0.01, h = 0.0001$, respectively. By observing closely, the solutions depicted in Figure 3(a) show that $q(t) \longrightarrow 0$ as $t \longrightarrow \infty$. Since this model represents a real-life case of eye surgery, hence, this result is unacceptable. As for $h \longrightarrow 0$, the graphical results in Figure 3(b) are more accurate because it suggests the $q(t) \approx 24.0$ or lies closer to 24.0 as $t \longrightarrow \infty$.

Figures 4(a) and4(b) are the graphical illustration of corneal curvature for different values of $0 < \alpha \leq 1$ and step sizes as $h = 0.01$ and $h = 0.0001$, respectively. Similar to the refractive index and axial length, the corneal curvature also depicts more realistic behavior when $h \longrightarrow 0$.

Figures 5(a) and 5(b) represent the numerical solution of corneal thickness for different values of α where $0 < \alpha \leq 1$ and $h = 0.01, h = 0.0001$, respectively. By observing closely, the solutions depicted in Figure 5(a) show that $q(t) \longrightarrow 0$ as $t \longrightarrow \infty$. Since this model represents the real-life case of eye surgery, hence, this result is unacceptable.

As for $h \longrightarrow 0$, the graphical results in Figure 5(b) are more accurate because it suggests the $s(t) \approx 0.52mm$ or lies closer to $0.52mm$ as. $t \longrightarrow \infty$

Figures 6(a) and 6(b) show the numerical solution of fractional DSEK by fractional Euler's method. In Figure 6(a),

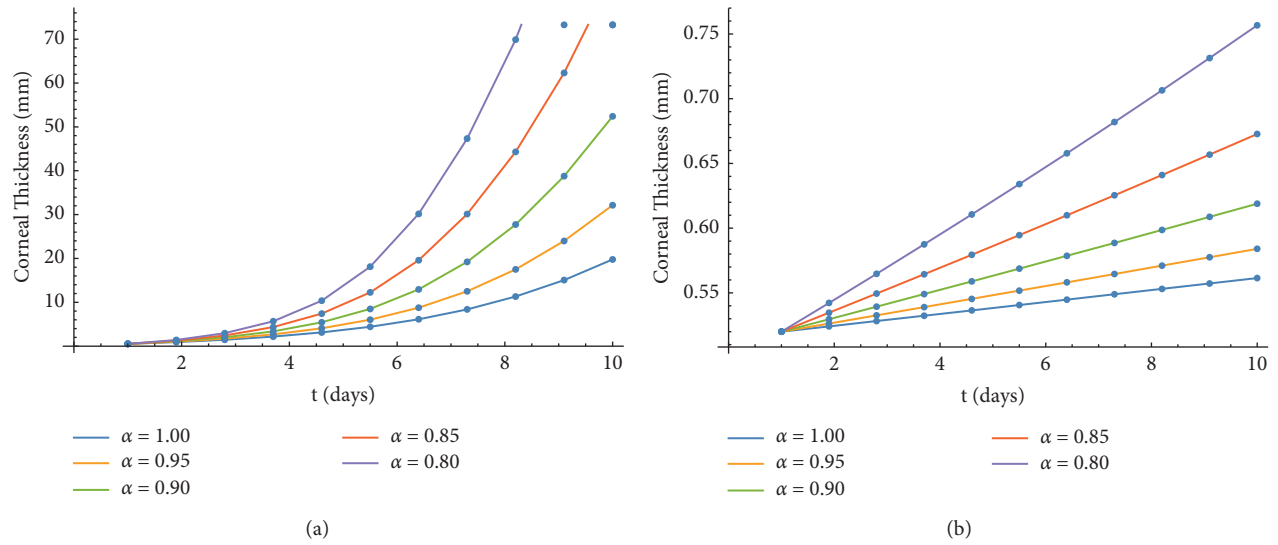

Figure 5: Numerical solution by fractional Euler's method of corneal thickness at different values of α and h implementing the fractional behavior. (a)$h = 0.01, 0 < \alpha \leq 1$ and $t \in (1, 10)$. (b)$h = 0.0001, 0 < \alpha \leq 1$ and $t \in (1, 10)$.

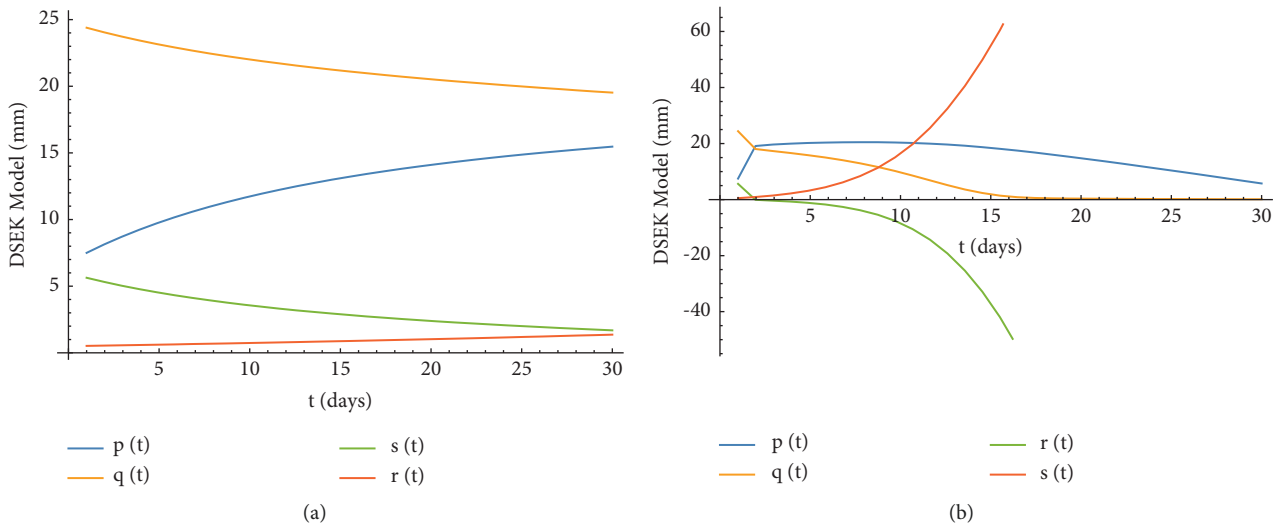

Figure 6: Numerical solution by fractional Euler's method of fractional DSEK system at different values of α and h implementing the fractional behavior. (a)$h = 0.0001, 0 < \alpha \leq 1$ and $t \in (1, 10)$. (b)$h = 0.01, 0 < \alpha \leq 1$ and $t \in (1, 10)$.

results have been presented for $h = 0.0001$ and different values of α between $(0, 1]$.

Graphical results are shown in Figures 2–5 and 6 described that as $h \longrightarrow 0$, the more accurate results we obtain. This is why the variables remain in $\Re_+^4$ for $h = 0.0001$ instead of $h = 0.001$.

Also, the fractional DSEK results have the hysteresis phenomenon, which means this system is influenced by the previous derivatives and values as well as the current conditions. The noninteger derivative given by different values of α introduces the memory effect in the fractional DSEK model. As we explained in definitions (4) and (5), the exponential kernel when applied to the fractional DSEK model calculates the memory effect. This is why we can see the smoothness in Figures 2–5 and 6 as compared to graphical results in [18]. Results of refractive index, axial length, corneal curvature, and central corneal thickness are shown graphically of the ordinary system of differential equation in [18] showed huge oscillation whereas, in real life after surgery, the effect on vision is not that blurry or oscillated. The fractional DSEK model shows more realistic results of ocular parameters after Descemet's stripping endothelial keratoplasty. It gives the same normal values but due to its fractal phenomenon, the oscillation among results is removed, and graphs are smoother giving the same normal values as the DSEK model in [18]. For more background about the numerical solutions of fractional-order differential equations, see [34–37].

7. Conclusion

In this paper, we investigated the fractional DSEK model presented by fractional derivatives of the Atangana-Baleanu Caputo type. We proved the uniqueness and existence of its solutions by using fixed point theory. For this, we defined a hypothesis based on Lipschitzian and two operators $\psi_i, i = 1, 2$. Then, we proved that ψ_1 and ψ_2 are contraction and relatively compact and hence proven the uniqueness and existence of those defined hypotheses. Furthermore, for the fractional DSEK model, proving its stability was a must so by UlamHyers stability in Banach space, we proved that fractional DSEK is Ulam-Hyers stable. Moreover, we have discussed the advantages of using the ABC fractional derivative instead of any other. In this paper, we presented and investigated the fractional behavior of the DSEK model and performed the numerical investigation using mathematical software. The numerical method "Euler" which is used to solve fractional DSEK is derived for initial value problems with ABC fractional derivatives, in this paper. Since eye surgery is a crucial process and with the passage of time, the results of surgery can be observed but with the help of the fractional DSEK model, a clearer picture of this surgery will be given.

Data Availability

The data used to support the findings of this study are available from the corresponding author on request.

Conflicts of Interest

The authors declare that they have no conflicts of interest.

References

[1] F. X. Chang Fu-Xuan, J. Huang Wei, and W. Huang, "Anomalous diffusion and fractional advection-diffusion equation," *Acta Physica Sinica*, vol. 54, no. 3, pp. 1113–1117, 2005.

[2] I. Podlubny, *Fractional Differential Equations*, Academic Press, San Diego-Boston-New York, 1990.

[3] Y. Z. Povstenko, "Fractional radial diffusion in a cylinder," *Journal of Molecular Liquids*, vol. 137, no. 1-3, pp. 46–50, 2008.

[4] Z. T. Wang, "Singular diffusion in fractal porous media," *Applied Mathematics and Mechanics*, vol. 21, no. 10, pp. 1033–1038, 2000.

[5] E. R. Weeks, J. S. Urbach, and H. L. Swinney, "Anomalous diffusion in asymmetric random walks with a quasi-geostrophic flow example," *Physica D: Nonlinear Phenomena*, vol. 97, no. 1-3, pp. 291–310, 1996.

[6] B. Li, Z. J. Chen, and H. W. Zhao, "Application and development of rheology," *Contemporary Chemical Industry*, vol. 37, no. 2, pp. 221–224, 2008.

[7] K. Q. Zhu, "Progress in the study of non-Newtonian fluid mechanics," *Mechanics and Practice*, vol. 28, no. 4, pp. 1–8, 2006.

[8] L. C. d. Barros, M. M. Lopes, F. S. Pedro, E. Esmi, J. P. C. dos Santos, and D. E. Sánchez, "The memory effect on fractional calculus: an application in the spread of COVID-19," *Computational and Applied Mathematics*, vol. 40, no. 3, pp. 72–21, 2021.

[9] V. E. Tarasov, "Generalized memory: fractional calculus approach," *Fractal and Fractional*, vol. 2, no. 4, pp. 23–17, 2018.

[10] A. A. M. Arafa, M. Khalil, and A. Sayed, "A non-integer variable order mathematical model of human immunodeficiency virus and malaria coinfection with time delay," *Complexity*, vol. 2019, Article ID 4291017, 13 pages, 2019.

[11] A. M. A. El-Sayed, A. A. M. Arafa, M. Khali, and A. Sayed, "Backward bifurcation in a fractional order epidemiological model," *Progress in Fractional Differentiation and Applications*, vol. 3, no. 4, pp. 281–287, 2017.

[12] A. A. M. Arafa, S. Z. Rida, and M. Khalil, "A fractional-order model of HIV infection: numerical solution and comparisons with data of patients," *International Journal of Biomathematics*, vol. 07, no. 04, Article ID 1450036, 2014.

[13] A. Atangana, "Derivative with a new parameter," *Theory, Methods and Applications*, Academic Press, Cambridge, Massachusetts, 2015.

[14] Z. Udo, *DAFX: Digital Audio Effects*, John Wiley & Sons, England, 2002.

[15] N. Bagheri, B. Wajda, C. Calvo, and A. Durrani, *The Wills Eye Manual*, Wolters Kluwer Health, New york, USA, 2016.

[16] E. D. Rosenberg, A. S. Nattis, and R. J. Nattis, *Operative Dictations in Ophthalmology*, Springer International Publishing, Switzerland, 2017.

[17] J. Kanski and B. Bowling, *Kanski's Clinical Ophthalmology*, Elsevier, Amsterdam, 2015.

[18] M. Khalid and S. K. Fareeha, "Nonlinear DSEK model: a novel mathematical model that predicts stability in ocular parameters after Descemet's stripping endothelial keratoplasty," *Punjab University Journal of Mathematics*, vol. 52, no. 4, pp. 1–14, 2020.

[19] S. K. Fareeha, *PhD Dissertation*, Federal Urdu University of Arts, Science and Technology, Karachi, Pakistan, 2021.

[20] M. Caputo and M. Fabrizio, "A new definition of fractional derivative without singular kernel," *Progress in Fractional Differentiation and Applications*, vol. 1, no. 2, pp. 73–85, 2015.

[21] A. Atangana and D. Baleanu, "New fractional derivatives with nonlocal and non-singular kernel: theory and application to heat transfer model," *Thermal Science*, vol. 20, no. 2, pp. 763–769, 2016.

[22] S. M. Ulam, *A Collection of Mathematical Problems*, Interscience Publishers, New york, USA, 1968.

[23] D. H. Hyers, "On the stability of the linear functional equation," *Proceedings of the National Academy of Sciences*, vol. 27, no. 4, pp. 222–224, 1941.

[24] C. Vanterler da, J. Sousa, and E. Capelas de Oliveira, "Ulam-Hyers stability of a nonlinear fractional Volterra integro-differential equation," *Applied Mathematics Letters*, vol. 81, pp. 50–56, 2018.

[25] D. Popa and I. Raşa, "On the Hyers-Ulam stability of the linear differential equation," *Journal of Mathematical Analysis and Applications*, vol. 381, no. 2, pp. 530–537, 2011.

[26] G. Wang, M. Zhou, and L. Sun, "Hyers-Ulam stability of linear differential equations of first order," *Applied Mathematics Letters*, vol. 21, no. 10, pp. 1024–1028, 2008.

[27] J. Wang, L. Lv, and Y. Zhou, "New concepts and results in stability of fractional differential equations," *Communications in Nonlinear Science and Numerical Simulation*, vol. 17, no. 6, pp. 2530–2538, 2012.

[28] E. C. de Oliveira and J. V. d. C. Sousa, "Ulam-Hyers-rassias stability for a class of fractional integro-differential equations," *Results in Mathematics*, vol. 73, no. 3, pp. 111–121, 2018.

[29] J. V. D. C. Sousa and E. C. D. Oliveira, "Fractional order pseudoparabolic partial differential equation: ulam-hyers stability," *Bulletin of the Brazilian Mathematical Society, New Series*, vol. 50, no. 2, pp. 481–496, 2019.

[30] J. V. da C Sousa, K. D. Kucche, and E. C. de Oliveira, "Stability of ψ-Hilfer impulsive fractional differential equations ψ-Hilfer impulsive fractional differential equations," *Applied Mathematics Letters*, vol. 88, pp. 73–80, 2019.

[31] S. Abbas and M. Benchohra, "On the generalized Ulam-Hyers-Rassias stability for Darboux problem for partial fractional implicit differential equations," *Applied Mathematics $_E$ Notes*, vol. 14, pp. 20–28, 2014.

[32] S. Abbas, M. Benchohra, and J. J. Nieto, "Ulam stabilities for partial impulsive fractional differential equations," *Facultas Rerum Naturalium Mathematics*, vol. 53, no. 1, pp. 5–17, 2014.

[33] A. Fernandez and D. Baleanu, "The mean value theorem and Taylor's theorem for fractional derivatives with Mittag-Leffler kernel," *Advances in Difference Equations*, vol. 2018, no. 1, 2018.

[34] F. A. Rihan, "Numerical modeling of fractional-order biological systems," *Abstract and Applied Analysis*, vol. 2013, Article ID 816803, 11 pages, 2013.

[35] F. A. Rihan, "Computational methods for delay parabolic and time-fractional partial differential equations," *Numerical Methods for Partial Differential Equations*, vol. 26, no. 6, pp. 1556–1571, 2010.

[36] M. Higazy, S. A. M. Alsallami, S. Abdel-Khalek, and A. El-Mesady, "Dynamical and structural study of a generalized Caputo fractional order Lotka-Volterra model," *Results in Physics*, vol. 37, Article ID 105478, 2022.

[37] M. Higazy, A. El-Mesady, A. M. S. Mahdy, S. Ullah, and A. Al-Ghamdi, "Numerical, approximate solutions, and optimal control on the deathly lassa hemorrhagic fever disease in pregnant women," *Journal of Function Spaces*, vol. 2021, Article ID 2444920, 15 pages, 2021.

Hindawi
Complexity
Volume 2022, Article ID 8761612, 12 pages
https://doi.org/10.1155/2022/8761612

Research Article

Adaptive Event-Triggered Control for Complex Dynamical Network with Random Coupling Delay under Stochastic Deception Attacks

M. Mubeen Tajudeen,[1] M. Syed Ali,[1] Syeda Asma Kauser,[2] Khanyaluck Subkrajang,[3] Anuwat Jirawattanapanit,[4] and Grienggrai Rajchakit[5]

[1]*Complex Systems and Networked Science Research Laboratory, Department of Mathematics, Thiruvalluvar University, Vellore-632115, Tamil Nadu, India*
[2]*Department of Mathematics, Prince Sattam Bin Abdulaziz University, Wadi al Dawaser, Riyadh, Saudi Arabia*
[3]*Faculty of Science and Technology, Rajamangala University of Technology Suvarnabhumi, 7/1 Village No. 1, Nonthaburi 1 Road, Suan Yai Sub-district, Muang District, Nonthaburi 11000, Thailand*
[4]*Department of Mathematics, Faculty of Science, Phuket Rajabhat University (PKRU), 6 Thepkasattree Road, Raddasa, Phuket 83000, Thailand*
[5]*Department of Mathematics, Faculty of Science, Maejo University, Chiang Mai 50290, Thailand*

Correspondence should be addressed to Khanyaluck Subkrajang; khanyaluck.s@rmutsb.ac.th

Received 21 March 2022; Accepted 16 April 2022; Published 11 May 2022

Academic Editor: Fathalla A. Rihan

This study concentrates on adaptive event-triggered control of complex dynamical networks with unpredictable coupling delays and stochastic deception attacks. The adaptive event-triggered mechanism is used to avoid the wasting of limited bandwidth. The probability of data communicated by the network is established by statistical properties and Bernoulli stochastic variables with an uncertain occurrence probability. Stability analysis based on Lyapunov–Krasovskii functional (LKF) and the stability of the closed-loop system is guaranteed. Using the LMI technique, we obtain triggered parameters. To demonstrate the feasibility and usefulness of the suggested methodology, two examples are shown.

1. Introduction

Complex dynamical network systems (CDNs) are typically made up of multiple nodes spread across a large area, with each node representing a dynamical system and control signals exchanged via a communication network [1]. CDNs have piqued the interest of many researchers in recent decades due to their wide range of applications in fields such as real-world networks, physics, telephone cell graphs, scientific citation webs, metabolic pathways, electrical power grids, biological networks, and food webs [2–5]. As a result, academics have spent considerable time studying the topological structure and dynamic behavior of CDNs [6–9].

As we all know, event-triggered mechanism has been demonstrated to be a good technique to reduce communication burden and preserve bandwidth resources when compared to implementing control systems that operate on a time-triggered scheme, which results in unneeded transmitted signals during the network process [10]. The event-triggered mechanism means that the control mission is only done when the system state meets specified criteria, which has a number of benefits, including reduced data transmission and improved resource [11–13]. It further reduces the limited bandwidth and optimizes the utilization of communication resources. As an aperiodic scheduling technique, the event-triggered mechanism (ETM) offers a way to avoid duplicate communication transmission

[14–18]. To deal with limited communication and processing resources, a learning-based ETM is presented, in which the triggering threshold can be adaptively changed via a vehicle communication network based on the states of the vehicle [19, 20].

The time delay is inevitable due to the amplifier's constrained switching speed and the nodes' inherent communication time. Its presence will have an impact on the stability of complex networks by causing oscillation and instability. In the models, the coupling delays of the huge complex systems are deterministic [10, 21]. Coupling delay is unavoidable in large-scale coupled nonlinear systems, such as CDNs, due to the limiting transmission speed of information between nodes [22]. Time-varying delays are more regular than constant time delays. The use of time-varying coupling delays in complex dynamical network stability has gained a lot of attention [23, 24]. In [25, 26], the synchronization of both continuous and discrete time complex dynamical networks are investigated. In [27], the problem of CDNs with sampled-data control and time-varying coupling delay was studied. To construct CDNs with time-varying coupling delay, the event-triggered mechanism and Jensen inequality were employed to estimate portions of the integral terms of the Lyapunov functional [28, 29].

Networked embedded signals in networked power systems are frequently transmitted through infrastructures, public networks, and devices that are susceptible to potential cyberattacks, and due to the inherent cyber vulnerability, the transmitted data could be exposed to malicious attacks by adversaries [30–32]. Cyberattacks are carried out by malicious attackers, according to several network control system researchers, and different cyberattacks attempt to compromise the data's security or availability [33, 34]. Deception attacks and denial-of service (DoS) attacks are two of the most popular forms of attacks [35, 36]. It is worth noting that DoS attacks can disrupt communication and cause data to become unavailable by interrupting the transmission medium [37, 38]. One of the really popular types of network security risks is deception attacks. Deception attacks, in particular, may undermine information integrity by modifying the content of sent data packets to prohibit the achievement of a predetermined performance index [39–44]. Some recent results about deception attacks are discussed in [36, 45, 46].

Based on the previous discussions, the purpose of this research is to build an adaptive event-triggered technique to address the complex dynamical network with random coupling delay and unknown probability under stochastic deception attacks. The following are the major contributions of this study:

(1) This study addresses the problem of adaptive event-triggered control for complex dynamical networks with time-varying coupling delays under stochastic deception attacks.

(2) Due to the threat of cyber security, the effect of deception attacks is considered. The independent Bernoulli variable is used to determine the probability of deception attacks.

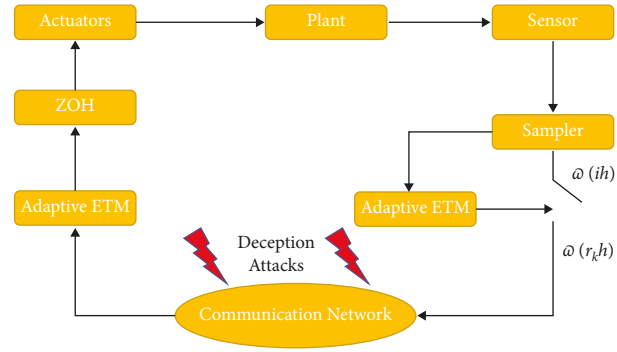

Figure 1: A framework of an adaptive event-triggered control (AETC) for CDNSs.

(3) By constructing Lyapunov–Krasvosikii functional, novel sufficient criteria are established for stochastic stability.

(4) The deception attacks damage the actuators and sensor signals, changing their value, delaying them, or doing both.

Notations: throughout the study, the symmetry-induced vector term is denoted by the symbol $*$. $\mathcal{Q} > 0$ denotes $\mathcal{Q}$ is a positive definite matrix. The superscript T is the transpose. $\mathbb{R}^m$ signifies the m-dimensional Euclidean space, and $\mathbb{R}^{m\times n}$ denotes the set of all $m \times n$ real matrices. Kronecker product is written in the form $\otimes$. The expectation operator is denoted by $\mathbf{E}$ and $\|\cdot\|$ refers to Euclidean norm. $\mathfrak{I}$ is an identity matrix with appropriate dimension.

2. Problem Formulation and Preliminaries

Consider the complex dynamical network system determined by the following equations:

$$\begin{aligned}\dot{\varpi}(r) &= (\mathfrak{I}\otimes\mathscr{A})\varpi(r) + (\mathfrak{I}\otimes\mathscr{B})h(\varpi(r)) + (\mathfrak{I}\otimes\mathscr{D})u(r)\\ &\quad + (1-\lambda(r))\sum_{q=1}^{N} o_{pq}\Lambda\varpi_q(r) + (\mathfrak{I}\otimes\mathscr{E})\omega(r)\\ &\quad + \lambda(r)\sum_{q=1}^{N}\widehat{o}_{pq}\widehat{\Lambda}\varpi_q(r-\alpha(r)),\\ z(r) &= (\mathfrak{I}\otimes\mathscr{C})\varpi(r),\\ \varpi(r) &= \varsigma(r), \quad r\in(-\infty,0],\end{aligned} \tag{1}$$

in which $z(r)\in\mathbb{R}^{n_z}$, $u(r)\in\mathbb{R}^{n_u}$, and $\varpi(r)\in\mathbb{R}^{n_\varpi}$ denote, respectively, the controlled output vector, the control input vector, and the state vector. The external disturbance vector $\omega(r)$, that is, $\omega(r)\in\mathscr{L}_2[0,\infty)$. $h(\varpi(r)) = [h_1(\varpi_1(r)), h_2(\varpi_2(r)),\ldots,h_n(\varpi_n(r))]^T$ represents the nonlinear vector-valued function. Delayed and nondelayed inner coupling matrices are $\widehat{\Lambda}$ and Λ, respectively. Delayed and nondelayed outer coupling matrices are $\widehat{O} = \widehat{o}_{pq}$ and $O = o_{pq}$, respectively. $\varsigma(r)$ denotes the initial condition of the state. $\alpha(r)$ is the time-varying coupling delay. Its satisfies $\alpha_1 \le \alpha(r) \le \alpha_2$, where $\alpha_1 > 0$ and $\alpha_2 > 0$, which represents minimum and maximum bounds of $\alpha(r)$ and $\dot{\alpha}(r) \le \varrho < 1$. Furthermore,

the given system matrices are $\mathscr{A}, \mathscr{B}, \mathscr{D}, \mathscr{E}$, and $\mathscr{C}$ with proper dimensions.

Remark 1. A coupling delay appears during the transmission of signals or information in many natural systems and also practical systems such as communication channels. The random variable $\lambda(r)$ satisfies the Bernoulli distributed white sequence, where $0 \le \lambda \le 1$. If $\lambda = 0$, the coupling delay does not happen. If $\lambda = 1$, the coupling delay happens, which obeys the following probability distribution laws: $\Pr\{\lambda(r) = 0\} = 1 - \overline{\lambda}$ and $\Pr\{\lambda(r) = 1\} = \overline{\lambda}$. $\mathbf{E}\{\lambda(r) - \overline{\lambda}\} = 0$ and $\mathbf{E}\{(\lambda(r) - \overline{\lambda})^2\} = \overline{\lambda}(1 - \overline{\lambda})$.

The configuration of AETC for the complex dynamical network system with deception attack is given in Figure 1. Adaptive event-triggered device is introduced between the sensor and the communication network in each subsystem. This device is responsible for selecting some necessary sampling packets for the control system to transmit over the network. It is assumed that the systems' state variables are periodically measured by a set of sensors with a constant sampling period. The measured state variables are transmitted to the AETM which is located near the sensor.

If the following condition is violated, the AETM transmits the instant to the controller via the communication network:

$$e^T(i\hbar)\Phi e(i\hbar) - \eta\varpi^T(i\hbar)\Phi\varpi(i\hbar) \le 0, \tag{2}$$

where $e(i\hbar) = \varpi(r_k\hbar) - \varpi(i\hbar)$. Here, $\varpi(r_k\hbar)$ and $\varpi(i\hbar)$ represent the released instant and initial instant, respectively. $\hbar$ is sampling period; $r_k\hbar, \{r_1, r_2, \ldots\} \subseteq \mathbb{N}$ represents the triggered instant. $0 < \Phi \in \mathbb{R}^{n_\varpi \times n_\varpi}$ is a matrix to be designed. The time-dependent function $0 < \eta(i\hbar) < 1$ is a triggering threshold function which is revised by the adaption law that follows:

$$\eta((i+1)\hbar) = Sat_{\left[\underline{\eta}, \overline{\eta}\right]}\left[\eta(i\hbar) + \zeta\left(\varpi^T(r_k\hbar)\Phi\varpi(r_k\hbar) - \varpi^T(i\hbar)\Phi\varpi(i\hbar)\right)\right], \quad \eta(0) \in \left[\underline{\eta}, \overline{\eta}\right], \tag{3}$$

where $\zeta > 0$ is a design parameter,

$$Sat_{\left[\underline{\eta}, \overline{\eta}\right]}[\varpi] = \begin{cases} \overline{\eta}, & \varpi \ge \overline{\eta}, \\ \varpi, & \underline{\eta} \le \varpi \le \overline{\eta}, \\ \underline{\eta}, & \varpi \le \underline{\eta}. \end{cases} \tag{4}$$

$\underline{\eta}$ and $\overline{\eta}$ are chosen as lower and upper bound of the triggering threshold function $\eta(i\hbar)$, respectively, and prescribed by the designer with considering the constraint $0 < \underline{\eta} \le \overline{\eta} < 1$.

Remark 2. It is worth noting that the presented event-triggered mechanism (2) and the adaptation law (3) are completely discrete unlike continuous-time adaptation laws presented in [16]. Hence, the proposed AETM is more practical for implementing on digital hardware. In the event of a disturbance, the value of $\rho_{i\hbar}$ should be decreased properly to improve performance. Some adaptation mechanisms, such as those described in [16, 18], keep the value of $\rho_{i\hbar}$ constant between two release instants, resulting in a delayed controller response to the disturbance. The suggested event-triggered mechanism (2), in contrast to them, uses an adaptive threshold $\rho_{i\hbar}$ that is modified at each sampling instant. As a result, the controller may respond quickly to external disturbances.

The control signal after the zero-order-hold (ZOH), while considering the effect of deception attacks, is regarded as

$$u(r) = \rho(r_k\hbar)K\varpi(r_k\hbar) + (1 - \rho(r_k\hbar))Kf\left(\varpi\left(r_q\hbar\right)\right), \quad r \in \Theta_k, \tag{5}$$

where $\Theta(k) = [r_k\hbar + \beta_k, r_{k+1}\hbar + \beta_k)$, $K \in \mathbb{R}^{n_u \times n_\varpi}$ is the state feedback gain matrix to be designed. The time-varying network-induced delay $\beta_k \ge 0$, which is satisfying

$$0 \le \beta_k \le \beta_a, \quad \forall k \in \mathbb{N}, \tag{6}$$

where $\beta_a \ge 0$ is known as a constant scalar, and

$$r_{k+1} = inf_{i > r_k}\left\{i \mid e^T(i\hbar)\Phi e(i\hbar) > \eta(i\hbar)\varpi^T(i\hbar)\Phi\varpi(i\hbar)\right\}. \tag{7}$$

Define $\beta(r) = r - (i\hbar)$ and $\gamma(r) = r - (r_j\hbar), \quad r \in \Theta_k$. It is easy to show that $0 \le \beta_c \le \beta(r) \le \hbar + \beta_a = \nu_a$ and $0 \le \gamma(r) \le M\hbar = \gamma_M$, where $M \in \mathbb{N}$ is a known constant.

To solve the problem under investigation with all the above challenges, we suggest that the adaptive controller (5) can be written as

$$u(r) = \rho(r_k\hbar)K\varpi(r - \beta(r)) + \rho(r_k\hbar)Ke(i\hbar) + (1 - \rho(r_k\hbar))Kf(\varpi(r - \gamma(r))), \quad r \in \Theta_k, \tag{8}$$

where $f: \mathbb{R}^{n_\varpi} \longrightarrow \mathbb{R}^{n_\varpi}$ is the function of deception attacks and $\gamma(r)$ is the time delay of the deception attacks.

Remark 3. The objective of a deception attack is to modify or inject data into communication channels. In contrast to the

attack method in [20], the data injection issue in the sensor-to-actuator controller channel is specifically examined in this study. The random variable $\rho(r_k\hbar)$ describes the occurrence of deception attacks on the communication network channel. If $\rho(r_k\hbar) = 0$, the communication network channel suffers from the deception attack, which means the real transmission data are replaced by the deception attack signal. Otherwise, $\rho(r_k\hbar) = 1$ means that there is no attack and the network is working normally. The sequence of data transmission is from the sampler to the controller. Here, $\rho(r_k\hbar)$ is a random variable with Bernoulli distribution which takes the value 1 with probability $\overline{\rho}$ and the value 0 with probability $1-\overline{\rho}$, that is, $\text{Prob}\{\rho(r_k\hbar) = 1\} = \overline{\rho}$ and $\text{Prob}\{\rho(r_k h) = 0\} = 1-\overline{\rho}$.

Abovementioned $\overline{\rho}$ is very difficult or impossible in practice. So, it is assumed that this value is accompanied by uncertainty and is described by

$$\begin{aligned}\mathbb{E}\{\rho(r_k\hbar)\} &= \overline{\rho} = \rho_1 + \rho_2 y(r_k\hbar),\\ \mathbb{E}\left\{\left(\rho(r_k\hbar) - \mathbb{E}\{\rho(r_k\hbar)\}\right)^2\right\} &= \overline{\delta} = \overline{\rho}(1-\overline{\rho}),\end{aligned} \tag{9}$$

where ρ_1 and ρ_2 are known nominal value and known constant scaling of the uncertainty, respectively, and $y(r_k\hbar)$ is an unknown function which satisfies the following condition:

$$y^2(r_k\hbar) \le 1, \quad \forall r_k \in \mathbb{N}. \tag{10}$$

Noticed that $\overline{\rho} \in [0,1]$. If $\rho_1 \in [0,1]$ and $\rho_2 \in [0,0.5]$; then, the closer $\overline{\rho}$ to zero, the greater the chances of an attack. The values of ρ_1 and ρ_2 indicate the uncertainty interval on this probability.

Assumption 1 (see [43]). The functions h: $\mathbb{R}^{n_\varpi} \longrightarrow \mathbb{R}^{n_h}$ and f: $\mathbb{R}^{n_\varpi} \longrightarrow \mathbb{R}^{n_\varpi}$ are assumed to satisfy the following conditions:

$$\begin{aligned}\|h(\varpi(r))\|_2 &\le \|H\varpi(r)\|_2,\\ \|f(\varpi(r))\|_2 &\le \|F\varpi(r)\|_2,\end{aligned} \tag{11}$$

where H and F are known constant matrices.

From (1) and (8), the closed-loop complex dynamical network system can be described by

$$\begin{aligned}\dot{\varpi}(r) = {} & (\mathfrak{I}\otimes A)\varpi(r) + (\mathfrak{I}\otimes B)h(\varpi(r)) + (\mathfrak{I}\otimes D)\overline{\rho}K\varpi(r-\beta(r)) + (\mathfrak{I}\otimes D)\overline{\rho}Ke(r) + (\mathfrak{I}\otimes D)\\ & (1-\overline{\rho})Kf(\varpi(r-\gamma(r))) + (\mathfrak{I}\otimes D)\left(\rho(r_k h) - \overline{\rho}\right)K[(\varpi(r-\beta(r)))\\ & + (\mathfrak{I}\otimes E)\omega(r) + (1-\lambda(r))(O\otimes\Lambda)\varpi(r) + \lambda(r)(\widehat{O}\otimes\widehat{\Lambda})\varpi(r-\alpha(r)), \quad r\in\Theta_k\\ z(r) = {} & (\mathfrak{I}\otimes C)\varpi(r), \quad r\in\Theta_k.\end{aligned} \tag{12}$$

Definition 1 (see [17]). The closed-loop system (12), under AETM and deception attacks, is stochastically stable and satisfies a prescribed $\mathscr{H}_\infty$ performance index $\breve{\gamma}$ if the following conditions hold:

$$\mathbb{E}\left\{\int_0^\infty z^T(r)z(r)\mathrm{d}r\right\} \le \breve{\gamma}^2\int_0^\infty \omega^T(r)\omega(r)\mathrm{d}r, \tag{13}$$

for any nonzero $\omega \in \mathscr{L}_2[0,\infty)$ under zero initial condition, where $\breve{\gamma}$ is prescribed performance level.

Lemma 1 (see [18],improved statement). *For any constant matrices U and V, the inequality,*

$$U + \eta(r)V < 0, \tag{14}$$

holds, for all $\underline{\eta} \le \eta(r) \le \overline{\eta}$, if and only if

$$\begin{aligned}U + \overline{\eta}V < 0,\\ U + \underline{\eta}V < 0.\end{aligned} \tag{15}$$

Lemma 2 (see [22]). *For $\beta(r) \in [0,\hbar]$ and any matrices $\mathcal{Q}$ and $\mathcal{S}$ with proper dimension, which satisfy $\begin{bmatrix}\mathcal{Q} & \mathcal{S}\\ * & \mathcal{Q}\end{bmatrix} \ge 0$, the following inequality holds:*

$$-\hbar\int_{r-\nu_a}^{r}\dot{\varpi}^T(t)(\mathfrak{I}\otimes\mathcal{Q})\dot{\varpi}(t)\mathrm{d}t \le \psi^T(r)\Gamma\psi(r), \tag{16}$$

where $\psi(r) = col\{\varpi(r)\varpi(r-\beta(r))\varpi(r-\nu_a)\}$ and

$$\Gamma = \begin{bmatrix}-(\mathfrak{I}\otimes\mathcal{Q}) & (\mathfrak{I}\otimes\mathcal{Q}) - (\mathfrak{I}\otimes\mathcal{S}) & (\mathfrak{I}\otimes\mathcal{S})\\ * & -2(\mathfrak{I}\otimes\mathcal{Q}) + (\mathfrak{I}\otimes\mathcal{S}) + \left(\mathfrak{I}\otimes\mathcal{S}^T\right) & (\mathfrak{I}\otimes\mathcal{Q}) - (\mathfrak{I}\otimes\mathcal{S})\\ * & * & -(\mathfrak{I}\otimes\mathcal{Q})\end{bmatrix}. \tag{17}$$

3. Main Results

In this section, a sufficient criterion will be established to verify that a complex networked control system with a deception attack is stochastically stable in controlling instants via an adaptive event-triggered mechanism.

Theorem 1. *For a given positive constants $\breve{\gamma}, \overline{\eta}, \mu, \varrho$ and $\overline{\rho}, \overline{\lambda} \in [0,1]$, the closed-loop system (12) is stochastically stable, presumed the existence of positive definite matrices $\mathscr{V}, \mathscr{T}, \mathscr{W}_1, \mathscr{W}_2, \mathcal{Q}_1, \mathcal{Q}_2, \mathscr{R}_1, \backslash\backslash\mathscr{R}_2, \mathscr{R}_3, J_1, \mathcal{S}_1$, and $\mathcal{S}_2$ are any proper dimension matrices and the event-triggered weighting matrix $\Phi > 0$, such that the following conditions hold:*

$$\mathcal{O}=\begin{bmatrix}
\mathcal{O}_{11} & \mathcal{O}_{12} & \mathcal{O}_{13} & \mathcal{O}_{14} & \mathcal{O}_{15} & \mathcal{O}_{16} & \mathcal{O}_{17} & \mathcal{O}_{18} & \mathcal{O}_{19} & 0 & \mathcal{O}_{1,11} & 0 & \mathcal{O}_{1,13}\\
* & \mathcal{O}_{22} & 0 & 0 & 0 & \mathcal{O}_{26} & 0 & 0 & 0 & 0 & 0 & 0 & 0\\
* & * & -(\mathfrak{I}\otimes\Phi) & 0 & 0 & 0 & 0 & 0 & 0 & 0 & 0 & 0 & 0\\
* & * & * & -\mathfrak{I} & 0 & 0 & 0 & 0 & 0 & 0 & 0 & 0 & 0\\
* & * & * & * & -\breve{\gamma}^2\mathfrak{I} & 0 & 0 & 0 & 0 & 0 & 0 & 0 & 0\\
* & * & * & * & * & \mathcal{O}_{6,6} & 0 & 0 & 0 & 0 & 0 & 0 & 0\\
* & * & * & * & * & * & \mathcal{O}_{77} & 0 & \mathcal{O}_{79} & 0 & 0 & 0 & 0\\
* & * & * & * & * & * & * & -\mu\mathfrak{I} & 0 & 0 & 0 & 0 & 0\\
* & * & * & * & * & * & * & * & \mathcal{O}_{99} & 0 & 0 & 0 & 0\\
* & * & * & * & * & * & * & * & * & \mathcal{O}_{10,10} & 0 & 0 & 0\\
* & * & * & * & * & * & * & * & * & 0 & \mathcal{O}_{11,11} & 0 & 0\\
* & * & * & * & * & * & * & * & * & 0 & * & \mathcal{O}_{12,12} & 0\\
* & * & * & * & * & * & * & * & * & 0 & * & * & \mathcal{O}_{13,13}
\end{bmatrix}<0, \tag{18}$$

$$\begin{bmatrix}\mathcal{Q}_\iota & \mathcal{S}_\iota\\ * & \mathcal{Q}_\iota\end{bmatrix}\geq 0,\quad \iota=1,2,$$

where

$$\begin{aligned}
\mathcal{O}_{11}&=(\mathfrak{I}\otimes\mathcal{A}\mathcal{T})+(\mathfrak{I}\otimes\mathcal{A}\mathcal{T})^T+(1-\lambda(r))\left(O\otimes\Lambda\mathcal{T}^T\right)\\
&\quad+(\mathfrak{I}\otimes\mathcal{W}_1)+(\mathfrak{I}\otimes\mathcal{W}_2)-(\mathfrak{I}\otimes\mathcal{Q}_1)-(\mathfrak{I}\otimes\mathcal{Q}_1)+(\mathfrak{I}\otimes\mathcal{V})\\
&\quad+(\mathfrak{I}\otimes\mathcal{R}_1)+\mu\left(\mathfrak{I}\otimes H^TH\right)+(\mathfrak{I}\otimes\mathcal{C})(\mathfrak{I}\otimes\mathcal{C})^T+2(\mathfrak{I}\otimes J_1\mathcal{A})+2(1-\lambda(r))(O\otimes J_1\Lambda),\\
\mathcal{O}_{12}&=\overline{\rho}(\mathfrak{I}\otimes\mathcal{T}\mathcal{D})+(\rho(r_kh)-\overline{\rho})(\mathfrak{I}\otimes\mathcal{T}\mathcal{D})K+(\mathfrak{I}\otimes\mathcal{Q}_1)-(\mathfrak{I}\otimes\mathcal{S}_1)\\
&\quad+2\overline{\rho}(\mathfrak{I}\otimes J_1\mathcal{D})K+2(\rho(r_kh)-\overline{\rho})(\mathfrak{I}\otimes J_1\mathcal{D})K,\\
\mathcal{O}_{13}&=\overline{\rho}(\mathfrak{I}\otimes\mathcal{T}\mathcal{D})+(\rho(r_kh)-\overline{\rho})(\mathfrak{I}\otimes\mathcal{T}\mathcal{D})K+2\overline{\rho}(\mathfrak{I}\otimes J_1\mathcal{D})K+2(\rho(r_kh)-\overline{\rho})(\mathfrak{I}\otimes J_1\mathcal{D})K,\\
\mathcal{O}_{14}&=(1-\overline{\rho})(\mathfrak{I}\otimes\mathcal{D}\mathcal{T})-(\rho(r_kh)-\overline{\rho})(\mathfrak{I}\otimes\mathcal{T}\mathcal{D})K+2(1-\overline{\rho})(\mathfrak{I}\otimes J_1\mathcal{D})K\\
&\quad-2(\rho(r_kh)-\overline{\rho})(\mathfrak{I}\otimes J_1\mathcal{D})K,\\
\mathcal{O}_{15}&=(\mathfrak{I}\otimes\mathcal{T}\mathcal{C})+2(\mathfrak{I}\otimes\mathcal{T}\mathcal{C}),\\
\mathcal{O}_{16}&=(\mathfrak{I}\otimes\mathcal{S}_1),\\
\mathcal{O}_{17}&=(\mathfrak{I}\otimes\mathcal{S}_1),\\
\mathcal{O}_{18}&=2(\mathfrak{I}\otimes J_1\mathcal{B})+(\mathfrak{I}\otimes\mathcal{T}\mathcal{B}),\\
\mathcal{O}_{19}&=(\mathfrak{I}\otimes\mathcal{Q}_2)-(\mathfrak{I}\otimes\mathcal{S}_2),\\
\mathcal{O}_{1,11}&=2\lambda(r)(O\otimes J_1\Lambda)+\lambda(r)(O\otimes\mathcal{T}\Lambda)+(\mathcal{I}\otimes\mathcal{T}\mathcal{B}),\\
\mathcal{O}_{1,13}&=-2(\mathfrak{I}\otimes J_1),\\
\mathcal{O}_{22}&=-2(\mathfrak{I}\otimes\mathcal{Q}_1)+(\mathfrak{I}\otimes\mathcal{S}_1)+\left(\mathfrak{I}\otimes\mathcal{S}_1^T\right)+\rho(\mathfrak{I}\otimes\Phi),\\
\mathcal{O}_{26}&=(\mathfrak{I}\otimes\mathcal{Q}_1)-(\mathfrak{I}\otimes\mathcal{S}_1),\\
\mathcal{O}_{66}&=-(\mathfrak{I}\otimes\mathcal{W}_1)-(\mathfrak{I}\otimes\mathcal{Q}_1),\\
\mathcal{O}_{77}&=-(\mathfrak{I}\otimes\mathcal{W}_2)-(\mathfrak{I}\otimes\mathcal{Q}_2),\\
\mathcal{O}_{79}&=(\mathfrak{I}\otimes\mathcal{Q}_2)-(\mathfrak{I}\otimes\mathcal{S}_2),\\
\mathcal{O}_{9,9}&=-2(\mathfrak{I}\otimes\mathcal{Q}_2)+(\mathfrak{I}\otimes\mathcal{S}_2)+\left(\mathfrak{I}\otimes\mathcal{S}_2^T\right)+\left(\mathfrak{I}\otimes F^TF\right),\\
\mathcal{O}_{10,10}&=(\mathfrak{I}\otimes\mathcal{V})-(\mathfrak{I}\otimes\mathcal{R}_2),\\
\mathcal{O}_{11,11}&=-(1-\varrho)(\mathfrak{I}\otimes\mathcal{V})-(1-\varrho)(\mathfrak{I}\otimes\mathcal{R}_2),\\
\mathcal{O}_{12,12}&=-(\mathfrak{I}\otimes\mathcal{R}_3),\\
\mathcal{O}_{13,13}&=\nu_a^2(\mathfrak{I}\otimes\mathcal{Q}_1)+\gamma_M^2(\mathfrak{I}\otimes\mathcal{Q}_2)-2(\mathfrak{I}\otimes J_1).
\end{aligned} \tag{19}$$

Proof. Choose the Lyapunov–Krasovskii functional candidate as follows:

$$\begin{aligned}
\mathbb{V}_1(\varpi(r)) &= \varpi^T(r)(\mathfrak{I}\otimes\mathscr{T})\varpi(r),\\
\mathbb{V}_2(\varpi(r)) &= \int_{r-\nu_a}^{r}\varpi^T(r)(\mathfrak{I}\otimes\mathscr{W}_1)\varpi(t)\mathrm{d}t + \int_{r-\gamma_M}^{r}\varpi^T(t)(\mathfrak{I}\otimes\mathscr{W}_2)\varpi(t)\mathrm{d}t,\\
\mathbb{V}_3(\varpi(r)) &= \nu_a\int_{-\nu_a}^{0}\int_{r+\theta}^{r}\dot{\varpi}^T(t)(\mathfrak{I}\otimes\mathscr{Q}_1)\dot{\varpi}(t)\mathrm{d}\theta\mathrm{d}t + \gamma_M\int_{-\gamma_M}^{0}\int_{r+\theta}^{r}\dot{\varpi}^T(t)(\mathfrak{I}\otimes\mathscr{Q}_2)\dot{\varpi}(t)\mathrm{d}\theta\mathrm{d}t,\\
\mathbb{V}_4(\varpi(r)) &= \int_{r-\alpha(r)}^{r}\varpi^T(t)(\mathfrak{I}\otimes\mathscr{V})\varpi(t)\mathrm{d}t,\\
\mathbb{V}_5(\varpi(r)) &= \int_{r-\alpha_1}^{r}\varpi^T(t)(\mathfrak{I}\otimes\mathscr{R}_1)\varpi(t)\mathrm{d}t + \int_{r-\alpha(r)}^{r-\alpha_1}\varpi^T(t)(\mathfrak{I}\otimes\mathscr{R}_2)\varpi(t)\mathrm{d}t + \int_{r-\alpha_2}^{r-\alpha_1}\varpi^T(t)(\mathfrak{I}\otimes\mathscr{R}_3)\varpi(t)\mathrm{d}t\Big].
\end{aligned} \tag{20}$$

Let $\mathfrak{L}$ be the infinitesimal generator of $\mathbb{V}(r)$:

$$\begin{aligned}
\mathfrak{L}\mathbb{V}_1(\varpi(r)) &= 2\varpi^T(r)(\mathfrak{I}\otimes\mathscr{T})\dot{\varpi}(r),\\
\mathfrak{L}\mathbb{V}_2(\varpi(r)) &= \varpi^T(r)(\mathfrak{I}\otimes\mathscr{W}_1+\mathfrak{I}\otimes\mathscr{W}_2)\varpi(r)\\
&\quad-\varpi^T(r-\nu_a)(\mathfrak{I}\otimes\mathscr{W}_1)\varpi(r-\nu_a),\\
&\quad-\varpi^T(r-\gamma_M)(\mathfrak{I}\otimes\mathscr{W}_2)\varpi(r-\gamma_M),\\
\mathfrak{L}\mathbb{V}_3(\varpi(r)) &= \dot{\varpi}^T(r)\left[\nu_a^2(\mathfrak{I}\otimes\mathscr{Q}_1)+\gamma_M^2(\mathfrak{I}\otimes\mathscr{Q}_2)\right]\dot{\varpi}(r)\\
&\quad-\nu_a\int_{r-\nu_a}^{r}\dot{\varpi}^T(t)(\mathfrak{I}\otimes\mathscr{Q}_1)\dot{\varpi}(t)\mathrm{d}t,
\end{aligned} \tag{21}$$

$$-\gamma_M\int_{r-\gamma_M}^{r}\dot{\varpi}^T(t)(\mathfrak{I}\otimes\mathscr{Q}_2)\dot{\varpi}(t)\mathrm{d}t. \tag{22}$$

According to Lemma (2), we have

$$-\nu_a\int_{r-\nu_a}^{r}\dot{\varpi}^T(t)(\mathfrak{I}\otimes\mathscr{Q}_1)\dot{\varpi}(t)\mathrm{d}t \le \psi_1^T(r)\Gamma_1\psi_1(r), \tag{23}$$

$$-\gamma_M\int_{r-\gamma_M}^{r}\dot{\varpi}^T(t)(\mathfrak{I}\otimes\mathscr{Q}_2)\dot{\varpi}(t)\mathrm{d}t \le \psi_2^T(r)\Gamma_2\psi_2(r), \tag{24}$$

where $\psi_1(r) = col\{\varpi(r)\ \ \varpi(r-\beta(r))\ \ \varpi(r-\nu_a)\}$, $\psi_2(r) = col\{\varpi(r)\ \ \varpi(r-\gamma(r))\ \ \varpi(r-\gamma_M)\}^T$, and

$$\Gamma_\iota = \begin{bmatrix} -(\mathfrak{I}\otimes\mathscr{Q}_\iota) & (\mathfrak{I}\otimes\mathscr{Q}\iota)-(\mathfrak{I}\otimes\mathscr{S}_\iota) & (\mathfrak{I}\otimes\mathscr{S}_\iota)\\ * & -2(\mathfrak{I}\otimes\mathscr{Q}_\iota)+(\mathfrak{I}\otimes\mathscr{S}_\iota)+(\mathfrak{I}\otimes\mathscr{S}_\iota^T) & (\mathfrak{I}\otimes\mathscr{Q}_\iota)-(\mathfrak{I}\otimes\mathscr{S}_\iota)\\ * & * & -(\mathfrak{I}\otimes\mathscr{Q}_\iota)\end{bmatrix}, \quad \iota = 1,2, \tag{25}$$

$$\mathfrak{L}\mathbb{V}_4(\varpi(r)) = \varpi^T(r)(\mathfrak{I}\otimes\mathscr{V})\varpi(r) - (1-\varrho)\varpi^T(r-\alpha(r))(\mathfrak{I}\otimes\mathscr{V})\varpi(r-\alpha(r)), \tag{26}$$

$$\begin{aligned}
\mathfrak{L}\mathbb{V}_5(\varpi(r)) &= \varpi^T(r)(\mathfrak{I}\otimes\mathscr{R}_1)\varpi(r) - \varpi^T(r-\alpha_1)(\mathfrak{I}\otimes\mathscr{R}_1)\varpi(r-\alpha_1) + \varpi^T(r-\alpha_1)(\mathfrak{I}\otimes\mathscr{R}_2)\varpi(r-\alpha_1)\\
&\quad-(1-\varrho)\varpi^T(r-\alpha(r))(\mathfrak{I}\otimes\mathscr{R}_2)\varpi(r-\alpha(r)) + \varpi^T(r-\alpha_1)(\mathfrak{I}\otimes\mathscr{R}_3)\varpi(r-\alpha_1) - \varpi^T(r-\alpha_2)\\
&\quad\times(\mathfrak{I}\otimes\mathscr{R}_3)\varpi(r-\alpha_2).
\end{aligned} \tag{27}$$

From Assumption (1),

$$\mu\varpi^T(r)H^TH\varpi(r) - \mu h^T(\varpi(r))h(\varpi(r)) \ge 0, \tag{28}$$

$$\begin{aligned}
&\varpi^T(r-\gamma(r))F^TF\varpi(r-\gamma(r))\\
&\quad-f^T(\varpi(r-\gamma(r)))f(\varpi(r-\gamma(r))) \ge 0.
\end{aligned} \tag{29}$$

For any appropriately dimensioned matrices J_1, the following equations hold:

$$0 = 2[(\mathfrak{J}\otimes A)\varpi(r) + (\mathfrak{J}\otimes B)h(\varpi(r)) + (\mathfrak{J}\otimes D)\overline{\rho}\times K\varpi(r-\beta(r)) + (\mathfrak{J}\otimes D)\overline{\rho}Ke(r) + (\mathfrak{J}\otimes D)$$
$$(1-\overline{\rho})Kf(\varpi(r-\gamma(r))) + (\mathfrak{J}\otimes D)\big(\rho(r_k h) - \overline{\rho}\big)K[(\varpi(r-\beta(r))) + e(r) - f(\varpi(r-\gamma(r)))] \tag{30}$$
$$+ (\mathfrak{J}\otimes E)\omega(r) + (1-\lambda(r))(O\otimes\Lambda)\varpi(r) + \lambda(r)(\widehat{O}\otimes\widehat{\Lambda})\varpi(r-\alpha(r)) - \dot{\varpi}(r)\big]\big[\varpi(r)J_1 + \dot{\varpi}(r)J_1\big].$$

Combining (21)–(30) and taking mathematical expectation, we obtain

$$\begin{aligned}
&\mathbf{E}\Big\{\mathscr{L}\mathbb{V}(\varpi(r)) + z^T(r)z(r) - \wp^2\omega^T(r)\omega(r)\Big\},\\
&\le 2\varpi^T(r)(\mathfrak{J}\otimes\mathscr{T})\dot{\varpi}(r) + \varpi^T(r)\big(\mathfrak{J}\otimes\mathscr{W}_1 + \mathfrak{J}\otimes\mathscr{W}_2\big)\varpi(r) - \varpi^T\big(r-\nu_a\big)\big(\mathfrak{J}\otimes\mathscr{W}_1\big)\varpi\big(r-\nu_a\big) - \varpi^T\big(r-\gamma_M\big)\\
&\quad(\mathfrak{J}\otimes\mathscr{W}_2)\varpi\big(r-\gamma_M\big) + \dot{\varpi}^T(r)\Big[\nu_a^2(\mathfrak{J}\otimes\mathscr{Q}_1) + \gamma_M^2\big(\mathfrak{J}\otimes\mathscr{Q}_2\big)\Big]\dot{\varpi}(r) + \psi_1^T(r)\Gamma_1\psi_1(r) + \psi_2^T(r)\Gamma_2\psi_2(r)\\
&\quad + \varpi^T(r)(\mathfrak{J}\otimes\mathscr{V})\varpi(r) - (1-\varrho)\varpi^T(r-\alpha(r))(\mathfrak{J}\otimes\mathscr{V})\varpi(r-\alpha(r)) + \varpi^T(r)\big(\mathfrak{J}\otimes\mathscr{R}_1\big)\varpi(r) - \varpi^T\big(r-\alpha_1\big)\big(\mathfrak{J}\otimes\mathscr{R}_1\big)\\
&\quad\times\varpi\big(r-\alpha_1\big) + \varpi^T\big(r-\alpha_1\big)\big(\mathfrak{J}\otimes\mathscr{R}_2\big)\varpi\big(r-\alpha_1\big) - (1-\varrho)\varpi^T(r-\alpha(r))\big(\mathfrak{J}\otimes\mathscr{R}_2\big)\varpi(r-\alpha(r)) + \varpi^T\big(r-\alpha_1\big)\\
&\quad\times\big(\mathfrak{J}\otimes\mathscr{R}_3\big)\varpi\big(r-\alpha_1\big) - \varpi^T\big(r-\alpha_2\big)\big(\mathfrak{J}\otimes\mathscr{R}_3\big) + \mu\varpi^T(r)H^TH\varpi(r) - \mu h^T(\varpi(r))h(\varpi(r)) + \varpi^T\big(r-\gamma_M\big)\\
&\quad\times F^TF\varpi\big(r-\gamma_M\big) - f^T\big(\varpi\big(r-\gamma_M\big)\big)f\big(\varpi\big(r-\gamma_M\big)\big) - e^T(r)\Phi e(r) + \eta(i\hbar)\varpi^T(r-\beta(r))\Phi\varpi(r-\beta(r))\\
&\quad + 2[(\mathfrak{J}\otimes A)\varpi(r) + (\mathfrak{J}\otimes B)h(\varpi(r)) + (\mathfrak{J}\otimes D)\overline{\rho}\times K\varpi(r-\beta(r)) + (\mathfrak{J}\otimes D)\overline{\rho}Ke(r) + (\mathfrak{J}\otimes D)(1-\overline{\rho})\\
&\quad\times Kf(\varpi(r-\gamma(r))) + (\mathfrak{J}\otimes D)\big(\rho(r_k h) - \overline{\rho}\big)K((\varpi(r-\beta(r))) + e(r) - f(\varpi(r-\gamma(r)))) + (\mathfrak{J}\otimes E)\omega(r)\\
&\quad + (1-\lambda(r))(O\otimes\Lambda)\varpi(r) + \lambda(r)(\widehat{O}\otimes\widehat{\Lambda})\varpi(r-\alpha(r)) - \dot{\varpi}(r)\big]\big[\varpi(r)J_1 + \dot{\varpi}(r)J_1\big] + z^T(r)z(r)\\
&\quad - \breve{\gamma}^2\omega^T(r)\omega(r)\\
&\le \mathbf{E}\big[\pi^T(r)\Upsilon\pi(r)\big],
\end{aligned} \tag{31}$$

where $\pi(r) = col\{\varpi(r)\quad\varpi(r-\beta\ (r))e(r)f(\varpi(r-\gamma(r)))\omega(r)\varpi(r-\nu_a)\varpi(r-\gamma_M)h(\varpi(r))\varpi(r-\gamma\quad(r))\varpi(r-\alpha_1)\varpi(r-\alpha(r))\varpi(r-\alpha_2)\varpi(r)\}$. By employing Schur complement [4], it can be implied that (18) is equivalent to (31), which means $\Upsilon<0$ then $\overline{\sigma}<0$.

Then, substituting $\overline{\eta}$ with $\eta(i\hbar)$. Based on Lemma (1), the sufficient condition for $\Upsilon = \Upsilon_1 + \eta\Upsilon_2 < 0$ holds for

$$\begin{aligned}
\Upsilon &= \Upsilon_1 + \underline{\eta}\,\Upsilon_2 < 0,\\
\Upsilon &= \Upsilon_1 + \overline{\eta}\Upsilon_2 < 0.
\end{aligned} \tag{32}$$

By the fact that $\Upsilon_2<0$, the following is always true:

$$\Upsilon_1 + \underline{\eta}\,\Upsilon_2 \le \Upsilon_1 + \overline{\eta}\Upsilon_2. \tag{33}$$

So, $\Upsilon<0$ is equivalent to $\Upsilon_1 + \overline{\eta}\Upsilon_2 < 0$ and (18) by Schur complements [4]. Therefore,

$$\mathbf{E}\Big\{\mathscr{L}\mathbb{V}(\varpi(r)) + z^T(r)z(r) - \breve{\gamma}^2\omega^T(r)\omega(r)\Big\} < 0. \tag{34}$$

By integrating both sides of the inequality from 0 to ∞ under zero initial conditions, one obtains (13). Note that, for $\omega(t)=0$, the above condition can be expressed as

$$\mathbf{E}\big\{\mathscr{L}\mathbb{V}(\varpi(r))\big\} + \mathbf{E}\big\{z^T(r)z(r)\big\} < 0. \tag{35}$$

It can be conclude that closed-loop system (12) with $\omega(r)=0$ is stochastically stable according to Definition 1. This completes the proof. □

Theorem 2. *For given positive constants $\breve{\gamma}, \overline{\eta}, \varrho$ and $\overline{\rho}, \overline{\lambda}\in[0,1]$, the closed-loop system (12) is stochastically stable, presumed the existence of positive definite matrices $\overline{\mathscr{V}}, \overline{\mathscr{T}}, \overline{\mathscr{W}_1}, \overline{\mathscr{W}_2}, \overline{\mathscr{Q}_1}, \overline{\mathscr{Q}_2}, \overline{\mathscr{R}_1}, \overline{\mathscr{R}_2}, \overline{\mathscr{R}_3}, J_1, \overline{\mathscr{S}_1}$, and $\overline{\mathscr{S}_2}$ are any proper dimension matrices. μ be positive scalars and the event-triggered weighting matrix $\overline{\Phi}>0$, such that the following conditions hold:*

$$\overline{\sigma} < 0, \tag{36}$$

where

$$\overline{\sigma}=\begin{bmatrix}
\overline{\sigma}_{11} & \overline{\sigma}_{12} & \overline{\sigma}_{13} & \overline{\sigma}_{14} & \overline{\sigma}_{15} & \overline{\sigma}_{16} & \overline{\sigma}_{17} & \overline{\sigma}_{18} & \overline{\sigma}_{19} & 0 & \overline{\sigma}_{1,11} & 0 & \overline{\sigma}_{1,13} & \overline{\sigma}_{1,14} & 0\\
* & \overline{\sigma}_{22} & 0 & 0 & 0 & \overline{\sigma}_{26} & 0 & 0 & 0 & 0 & 0 & 0 & 0 & 0 & 0\\
* & * & \overline{\sigma}_{33} & 0 & 0 & 0 & 0 & 0 & 0 & 0 & 0 & 0 & 0 & 0 & 0\\
* & * & * & -\mathfrak{I} & 0 & 0 & 0 & 0 & 0 & 0 & 0 & 0 & 0 & 0 & 0\\
* & * & * & * & -\breve{\gamma}^2\mathfrak{I} & 0 & 0 & 0 & 0 & 0 & 0 & 0 & 0 & 0 & 0\\
* & * & * & * & * & \overline{\sigma}_{66} & 0 & 0 & 0 & 0 & 0 & 0 & 0 & 0 & 0\\
* & * & * & * & * & * & \overline{\sigma}_{77} & 0 & \overline{\sigma}_{79} & 0 & 0 & 0 & 0 & 0 & 0\\
* & * & * & * & * & * & * & -\overline{\mu}\mathfrak{I} & 0 & 0 & 0 & 0 & 0 & 0 & 0\\
* & * & * & * & * & * & * & * & \overline{\sigma}_{99} & 0 & 0 & 0 & 0 & 0 & \overline{\sigma}_{9,15}\\
* & * & * & * & * & * & * & * & * & \overline{\sigma}_{10,10} & 0 & 0 & 0 & 0 & 0\\
* & * & * & * & * & * & * & * & * & 0 & \overline{\sigma}_{11,11} & 0 & 0 & 0 & 0\\
* & * & * & * & * & * & * & * & * & 0 & * & \overline{\sigma}_{12,12} & 0 & 0 & 0\\
* & * & * & * & * & * & * & * & * & 0 & * & * & \overline{\sigma}_{13,13} & -\mu\mathfrak{I} & -\mathfrak{I}
\end{bmatrix}<0,$$

$$\begin{bmatrix}\overline{\mathcal{Q}}_\iota & \overline{\mathcal{S}}_\iota\\ * & \overline{\mathcal{Q}}_\iota\end{bmatrix}\geq 0,\quad \iota=1,2,$$

$$\begin{aligned}
\text{where }\overline{\sigma}_{11}&=(\mathfrak{I}\otimes\mathscr{A}\overline{\mathscr{T}})+\left(\mathfrak{I}\otimes\overline{\mathscr{T}}^T\mathscr{A}\right)+(1-\overline{\lambda(r)})\overline{\mathscr{T}}(O\otimes\Lambda)+\left(\mathfrak{I}\otimes\overline{\mathscr{W}}_1\right)+\left(\mathfrak{I}\otimes\overline{\mathscr{W}}_2\right)-\left(\mathfrak{I}\otimes\overline{\mathcal{Q}}_1\right)-\left(\mathfrak{I}\otimes\overline{\mathcal{Q}}_1\right)\\
&+\left((\mathfrak{I}\otimes\overline{\mathscr{V}})+\mathfrak{I}\otimes\overline{\mathscr{R}}_1\right)+\left(\mathfrak{I}\otimes\overline{\mu}H^TH\right)+(\mathfrak{I}\otimes\mathscr{C})(\mathfrak{I}\otimes\mathscr{C})^T\\
&+2\epsilon\overline{T}(\mathfrak{I}\otimes\mathscr{A})+2\epsilon(1-\lambda(r))(O\otimes\overline{\mathscr{T}}\Lambda),\\
\overline{\sigma}_{12}&=\overline{\rho}(\mathfrak{I}\otimes X\mathscr{D})+(\rho(r_kh)-\overline{\rho})(\mathfrak{I}\otimes X\mathscr{D})+\left(\mathfrak{I}\otimes\overline{\mathcal{Q}}_1\right)-\left(\mathfrak{I}\otimes\overline{\mathcal{S}}_1\right)\\
&+2\epsilon\overline{\rho}(\mathfrak{I}\otimes X\mathscr{D})+2\epsilon(\rho(r_kh)-\overline{\rho})(\mathfrak{I}\otimes X\mathscr{D}),\\
\overline{\sigma}_{13}&=\overline{\rho}(\mathfrak{I}\otimes X\mathscr{D})+(\rho(r_kh)-\overline{\rho})(\mathfrak{I}\otimes X\mathscr{D})+2\epsilon\overline{\rho}(\mathfrak{I}\otimes X\mathscr{D})\\
&+2\epsilon(\rho(r_kh)-\overline{\rho})(\mathfrak{I}\otimes X\mathscr{D}),\overline{\sigma}_{14}=(1-\overline{\rho})(\mathfrak{I}\otimes X\mathscr{D})\\
&-(\rho(r_kh)-\overline{\rho})(\mathfrak{I}\otimes X\mathscr{D})+2\epsilon(1-\overline{\rho})(\mathfrak{I}\otimes X\mathscr{D})\\
&-2\epsilon(\rho(r_kh)-\overline{\rho})(\mathfrak{I}\otimes X\mathscr{D}),\overline{\sigma}_{15}=(\mathfrak{I}\otimes\overline{\mathscr{T}}\mathscr{E})+2\epsilon(\mathfrak{I}\otimes\overline{\mathscr{T}}\mathscr{E}),\\
\overline{\sigma}_{16}&=\left(\mathfrak{I}\otimes\overline{\mathcal{S}}_1\right),\overline{\sigma}_{17}=\left(\mathfrak{I}\otimes\overline{\mathcal{S}}_2\right),\overline{\sigma}_{18}=2\epsilon(\mathfrak{I}\otimes\overline{\mathscr{T}}\mathscr{B})\\
&+(\mathfrak{I}\otimes\overline{\mathscr{T}}\mathscr{B}),\overline{\sigma}_{19}=\left(\mathfrak{I}\otimes\overline{\mathcal{Q}}_2\right)-\left(\mathfrak{I}\otimes\overline{\mathcal{S}}_2\right),\overline{\sigma}_{1,11}=2\epsilon\lambda(r)(\hat{O}\otimes\overline{\mathscr{T}}\hat{\Lambda})+\lambda(r)(\hat{O}\otimes\overline{\mathscr{T}}\hat{\Lambda}),\\
\overline{\sigma}_{1,13}&=-2\epsilon(\mathfrak{I}\otimes\overline{\mathscr{T}}),\overline{\sigma}_{1,13}=(\mathfrak{I}\otimes\mathscr{T}H),\overline{\sigma}_{9,15}=(\mathfrak{I}\otimes\mathscr{T}F),\overline{\sigma}_{22}=-2\left(\mathfrak{I}\otimes\overline{\mathcal{Q}}_1\right)\\
&+\left(\mathfrak{I}\otimes\overline{\mathcal{S}}_1\right)+\left(\mathfrak{I}\otimes\overline{\mathcal{S}}_1^T\right)+\eta(\mathfrak{I}\otimes\overline{\Phi}),\\
\overline{\sigma}_{33}&=-(\mathfrak{I}\otimes\overline{\Phi}),\overline{\sigma}_{26}=\left(\mathfrak{I}\otimes\overline{\mathcal{Q}}_1\right)-\left(\mathfrak{I}\otimes\overline{\mathcal{S}}_1\right),\overline{\sigma}_{66}=-\left(\mathfrak{I}\otimes\overline{\mathscr{W}}_1\right)\\
&-\left(\mathfrak{I}\otimes\overline{\mathcal{Q}}_1\right),\overline{\sigma}_{77}=-\left(\mathfrak{I}\otimes\overline{\mathscr{W}}_2\right)-\left(\mathfrak{I}\otimes\overline{\mathcal{Q}}_2\right),\overline{\sigma}_{79}=\left(\mathfrak{I}\otimes\overline{\mathcal{Q}}_2\right)-\left(\mathfrak{I}\otimes\overline{\mathcal{S}}_2\right),\\
\overline{\sigma}_{99}&=-2\left(\mathfrak{I}\otimes\overline{\mathcal{Q}}_2\right)+\left(\mathfrak{I}\otimes\overline{\mathcal{S}}_2\right)+\left(\mathfrak{I}\otimes\overline{\mathcal{S}}_2^T\right)+\left(\mathfrak{I}\otimes F^T\overline{I}F\right),\overline{\sigma}_{10,10}=-\left(\mathfrak{I}\otimes\overline{\mathscr{R}}_1\right)\\
&+\left(\mathfrak{I}\otimes\overline{\mathscr{R}}_2\right)+\left(\mathfrak{I}\otimes\overline{\mathscr{R}}_3^T\right),\overline{\sigma}_{11,11}=-(1-\varrho)(\mathfrak{I}\otimes\overline{\mathscr{V}})-(1-\varrho)\left(\mathfrak{I}\otimes\overline{\mathscr{R}}_2\right),\\
\overline{\sigma}_{12,12}&=-\left(\mathfrak{I}\otimes\overline{\mathscr{R}}_3\right),\sigma_{13,13}=v_a^2\left(\mathfrak{I}\otimes\overline{\mathcal{Q}}_1\right)+\gamma_M^2\left(\mathfrak{I}\otimes\overline{\mathcal{Q}}_2\right)-2\epsilon(\mathfrak{I}\otimes\overline{\mathscr{T}}).
\end{aligned}\tag{37}$$

Moreover, the controller gain matrix K is given by

$$K=\overline{\mathscr{T}}^{-1}X.\tag{38}$$

Proof. We can calculate $\overline{\overline{\sigma}} = \aleph^T(r)\sigma_{i\times j}\aleph(r)(i,j = 1,2,\ldots,15)$ with

$$\aleph(r) = \operatorname{diag}\left\{\overline{\mathcal{T}},\overline{\mathcal{T}},\overline{\mathcal{T}},\overline{\mathcal{T}},\overline{\mathcal{T}},\overline{\mathcal{T}},\overline{\mathcal{T}},\overline{\mathcal{T}},\overline{\mathcal{T}},\overline{\mathcal{T}},\overline{\mathcal{T}},\overline{\mathcal{T}},\overline{\mathcal{T}},\overline{\mathcal{T}},\overline{\mathcal{T}}\right\}, \tag{39}$$

where $\overline{\overline{\mathcal{T}}} = \mathcal{T}^{-1}$. Defining $\overline{\overline{\mathcal{W}}_\diamond} = \overline{\overline{\mathcal{T}}}^T\mathcal{W}_\diamond\overline{\overline{\mathcal{T}}}$, $\overline{\overline{\mathcal{Q}_\diamond}} = \overline{\overline{\mathcal{T}}}^T\mathcal{Q}_\diamond\overline{\overline{\mathcal{T}}}$, $\overline{\overline{\mathcal{R}_*}} = \overline{\overline{\mathcal{T}}}^T\mathcal{R}_*\overline{\overline{\mathcal{T}}}$ $(* = 1,2,3)$, $\overline{\overline{\mathcal{V}_\diamond}} = \overline{\overline{\mathcal{T}}}^T\mathcal{V}_\diamond\overline{\overline{\mathcal{T}}}$, $\overline{\overline{\mathcal{S}_\diamond}} = \overline{\overline{\mathcal{T}}}^T\mathcal{S}_\diamond\overline{\overline{\mathcal{T}}}$ $(\diamond = 1,2)$, and $\overline{\overline{\Phi}} = \overline{\overline{\mathcal{T}}}^T\Phi\overline{\overline{\mathcal{T}}}$ and letting $J_1 = \epsilon\overline{\overline{\mathcal{T}}}$, we obtain (36). □

4. Numerical Example

In this section, we provide some numerical information to ensure the method's effectiveness and applicability.

Example 1. Consider the adaptive event-triggered control for complex dynamical network system (12) with time-varying coupling delays under stochastic deception attacks, with the following parameters:

$$\begin{aligned}
\dot{\varpi}(r) &= (\mathfrak{I}\otimes\mathscr{A})\varpi(r) + (\mathfrak{I}\otimes\mathscr{B})h(\varpi(r))\\
&\quad + (\mathfrak{I}\otimes\mathscr{D})\overline{\rho}\times K\varpi(r-\beta(r))\\
&\quad + (\mathfrak{I}\otimes\mathscr{D})\overline{\rho}Ke(r) + (\mathfrak{I}\otimes\mathscr{D})z\\
&\quad (1-\overline{\rho})Kf(\varpi(r-\gamma(r)))\\
&\quad + (\mathfrak{I}\otimes\mathscr{D})\left(\rho\left(r_k h\right) - \overline{\rho}\right)K[(\varpi(r-\beta(r))\\
&\quad + e(r) - f(\varpi(r-\gamma(r)))]\\
&\quad + (\mathfrak{I}\otimes\mathscr{E})\omega(r) + (1-\lambda(r))(O\otimes\Lambda)\varpi(r)\\
&\quad + \lambda(r)(\widehat{O}\otimes\widehat{\Lambda})\varpi(r-\alpha(r)),\\
z(r) &= (\mathfrak{I}\otimes\mathscr{C})\varpi(r),
\end{aligned}$$

$$\begin{aligned}
\mathscr{A} &= \begin{bmatrix} -2 & 0\\ 0 & -4\end{bmatrix},\\
\mathscr{B} &= \begin{bmatrix} 0.1 & -0.2\\ 0.1 & 0.1\end{bmatrix},\\
\mathscr{C} &= \begin{bmatrix} 0.2 & 0\\ 0 & 0.1\end{bmatrix},\\
\mathscr{D} &= \begin{bmatrix} 0.05 & 0.1\\ 0.2 & 0.1\end{bmatrix},\\
\mathscr{E} &= \begin{bmatrix} 0.1 & 0\\ 0 & 0.1\end{bmatrix},\\
\mathscr{F} &= \begin{bmatrix} -0.1 & 0.1\\ 0.1 & -0.1\end{bmatrix},\\
\mathscr{G} &= \begin{bmatrix} 0.2 & -0.2\\ 0.2 & -0.2\end{bmatrix},\\
\mathscr{J} &= \begin{bmatrix} 1 & 0\\ 0 & 1\end{bmatrix}.
\end{aligned} \tag{40}$$

The inner coupling matrices are $\Lambda = \operatorname{diag}\{0.7.0.7\}$ and $\widehat{\Lambda} = \operatorname{diag}\{0.6.0.6\}$. The outer coupling matrices are

$$\begin{aligned}
O &= \begin{bmatrix} -8.9 & 0.1 & 0.1\\ 0.1 & -8.9 & 0.1\\ 0.1 & 0.1 & -8.9\end{bmatrix},\\
\widehat{O} &= \begin{bmatrix} -4.4 & 0.1 & 0.1\\ 0.1 & -4.4 & 0.1\\ 0.1 & 0.1 & -4.4\end{bmatrix}.
\end{aligned} \tag{41}$$

Choose $\gamma_M = 0.8, \lambda(r) = 0.5, \mu = 2, \nu_a = 12.5, \overline{\rho} = 0.5$, $\eta = 0.4, \epsilon = 0.1, \varrho = 0.2$, and H_∞ performance $\breve{\gamma} = 1.4$. The following solutions are achieved by solving LMI in Theorem (2):

$$\begin{aligned}
\mathscr{W}_1 &= \begin{bmatrix} 85.0696 & 17.6977\\ 17.6977 & 126.4490\end{bmatrix},\\
\mathscr{W}_2 &= \begin{bmatrix} 99.3898 & 5.6280\\ 5.6280 & 133.1595\end{bmatrix},\\
\mathcal{Q}_1 &= \begin{bmatrix} 4.2512 & -0.0382\\ -0.0382 & 4.1737\end{bmatrix},\\
\mathcal{Q}_2 &= \begin{bmatrix} 369.6281 & -4.3094\\ -4.3094 & 327.1350\end{bmatrix},\\
\mathscr{V} &= \begin{bmatrix} 213.2716 & 28.8430\\ 28.8430 & 160.1214\end{bmatrix},\\
\mathscr{R}_1 &= \begin{bmatrix} 152.2082 & 25.0528\\ 25.0528 & 145.7121\end{bmatrix},\\
\mathscr{R}_2 &= \begin{bmatrix} 64.3787 & 4.0647\\ 4.0647 & 13.3491\end{bmatrix},\\
\mathscr{R}_3 &= \begin{bmatrix} 43.9148 & 10.4940\\ 10.4940 & 66.1815\end{bmatrix},\\
X &= \begin{bmatrix} 4.0192 & -3.7714\\ -3.7714 & 0.4453\end{bmatrix},\\
\mathcal{S}_1 &= \begin{bmatrix} 51.7924 & -9.4347\\ -9.4347 & 70.5017\end{bmatrix},\\
\mathcal{S}_2 &= \begin{bmatrix} 18.0418 & 6.4145\\ 6.4145 & 22.5261\end{bmatrix},\\
J_1 &= \begin{bmatrix} 16.59265 & 1.67527\\ 1.67527 & 8.33000\end{bmatrix},\\
\mathcal{T} &= \begin{bmatrix} 165.9265 & 16.7527\\ 16.7527 & 83.3000\end{bmatrix},\\
\Phi &= \begin{bmatrix} 72.4205 & 13.7013\\ 13.7013 & 103.9256\end{bmatrix},\\
K &= \begin{bmatrix} 0.0294 & -0.0512\\ -0.0238 & 0.0101\end{bmatrix}.
\end{aligned} \tag{42}$$

Then, it follows from Theorem (2), adaptive event-triggered mechanism for a complex dynamical network system subject to deception attack (12), is stochastically stable.

Example 2. Consider the adaptive event-triggered control for complex dynamical network system (12) with time-varying coupling delays under stochastic deception attacks, with the following parameters:

$$\begin{aligned}\dot{\varpi}(r) &= (\mathfrak{T}\otimes\mathscr{A})\varpi(r) + (\mathfrak{T}\otimes\mathscr{B})h(\varpi(r))\\ &\quad + (\mathfrak{T}\otimes\mathscr{D})\overline{\rho}\times K\varpi(r-\beta(r))\\ &\quad + (\mathfrak{T}\otimes\mathscr{D})\overline{\rho}Ke(r) + (\mathfrak{T}\otimes\mathscr{D})\\ &\quad (1-\overline{\rho})Kf(\varpi(r-\gamma(r)))\\ &\quad + (\mathfrak{T}\otimes\mathscr{D})\left(\rho\left(r_k h\right)-\overline{\rho}\right)K[(\varpi(r-\beta(r)))\\ &\quad + (\mathfrak{T}\otimes\mathscr{E})\omega(r) + (1-\lambda(r))(O\otimes\Lambda)\varpi(r)\\ &\quad + \lambda(r)(\widehat{O}\otimes\widehat{\Lambda})\varpi(r-\alpha(r)),\\ z(r) &= (\mathfrak{T}\otimes\mathscr{C})\varpi(r),\end{aligned}$$

$$\begin{aligned}\mathscr{A} &= \begin{bmatrix}-23 & 0.1 & 0\\ 0 & -23 & 0.1\\ 0 & 0.1 & -22\end{bmatrix},\\ \mathscr{B} &= \begin{bmatrix}-1.2 & -0.5 & 0.2\\ -0.5 & 0 & 0.5\\ 0.1 & 0.5 & -0.5\end{bmatrix},\\ \mathscr{C} &= \begin{bmatrix}0.1 & -0.8 & 0\\ -0.8 & 0.2 & 0\\ 0 & -1.4 & 0.6\end{bmatrix},\\ \mathscr{D} &= \begin{bmatrix}1.8 & 0 & -1.2\\ -1.5 & 0 & 1.8\\ 1.2 & -0.1 & 0\end{bmatrix},\\ \mathscr{E} &= \begin{bmatrix}-0.5 & 0 & 0\\ 0 & -0.5 & 0\\ 0 & 0 & -0.5\end{bmatrix},\\ \mathscr{F} &= \begin{bmatrix}-0.5 & 0 & 0\\ 0 & -0.5 & 0\\ 0 & 0 & -0.5\end{bmatrix},\\ \mathscr{G} &= \begin{bmatrix}1 & 0 & 0\\ 0 & 1 & 0\\ 0 & 0 & 1\end{bmatrix},\\ \mathscr{I} &= \begin{bmatrix}1 & 0 & 0\\ 0 & 1 & 0\\ 0 & 0 & 1\end{bmatrix}.\end{aligned} \tag{43}$$

The inner coupling matrices are $\Lambda = \mathrm{diag}\{1, 1, 1\}$ and $\widehat{\Lambda} = \mathrm{diag}\{1, 1, 1\}$. The outer coupling matrices are

$$\begin{aligned}O &= \begin{bmatrix}-2 & 1 & 1 & 0 & 0\\ 0 & -2 & 1 & 1 & 0\\ 0 & 0 & -2 & 1 & 1\\ 1 & 0 & 0 & -2 & 1\\ 1 & 1 & 0 & 0 & -2\end{bmatrix},\\ \widehat{O} &= \begin{bmatrix}-2 & 1 & 1 & 0 & 0\\ 0 & -2 & 1 & 1 & 0\\ 0 & 0 & -2 & 1 & 1\\ 1 & 0 & 0 & -2 & 1\\ 1 & 1 & 0 & 0 & -2\end{bmatrix}.\end{aligned} \tag{44}$$

Choose $\gamma_M = 0.82, \lambda(r) = 0.5, \mu = 2,\ \nu_a = 11.3, \overline{\rho} = 0.5$, $\eta = 0.4, \varrho = 0.2$, and $\epsilon = 0.1$ with H_∞ performance $\widetilde{\gamma} = 0.9$. The following solutions are achieved by solving LMI in Theorem (2):

$$\begin{aligned}\mathscr{W}_1 &= \begin{bmatrix}85.0696 & 17.6977\\ 17.6977 & 126.4490\end{bmatrix},\\ \mathscr{W}_2 &= \begin{bmatrix}99.3898 & 5.6280\\ 5.6280 & 133.1595\end{bmatrix},\\ \mathscr{Q}_1 &= \begin{bmatrix}4.2512 & -0.0382\\ -0.0382 & 4.1737\end{bmatrix},\\ \mathscr{Q}_2 &= \begin{bmatrix}369.6281 & -4.3094\\ -4.3094 & 327.1350\end{bmatrix},\\ \mathscr{V} &= \begin{bmatrix}213.2716 & 28.8430\\ 28.8430 & 160.1214\end{bmatrix},\\ \mathscr{R}_1 &= \begin{bmatrix}152.2082 & 25.0528\\ 25.0528 & 145.7121\end{bmatrix},\\ \mathscr{R}_2 &= \begin{bmatrix}64.3787 & 4.0647\\ 4.0647 & 13.3491\end{bmatrix},\\ \mathscr{R}_3 &= \begin{bmatrix}43.9148 & 10.4940\\ 10.4940 & 66.1815\end{bmatrix},\\ X &= \begin{bmatrix}4.0192 & -3.7714\\ -3.7714 & 0.4453\end{bmatrix},\\ \mathscr{S}_1 &= \begin{bmatrix}51.7924 & -9.4347\\ -9.4347 & 70.5017\end{bmatrix},\\ \mathscr{S}_2 &= \begin{bmatrix}18.0418 & 6.4145\\ 6.4145 & 22.5261\end{bmatrix},\\ J_1 &= \begin{bmatrix}16.59265 & 1.67527\\ 1.67527 & 8.33000\end{bmatrix},\\ \mathscr{T} &= \begin{bmatrix}165.9265 & 16.7527\\ 16.7527 & 83.3000\end{bmatrix},\\ \Phi &= \begin{bmatrix}72.4205 & 13.7013\\ 13.7013 & 103.9256\end{bmatrix},\\ K &= \begin{bmatrix}0.0294 & -0.0512\\ -0.0238 & 0.0101\end{bmatrix}.\end{aligned} \tag{45}$$

Then, it follows from Theorem (2) that adaptive event-triggered mechanism for a complex dynamical network system subject to deception attack (12) is stochastically stable.

5. Conclusion

The issue of adaptive event-triggered mechanism for a class of complex dynamical networks with random time-varying coupling delays under stochastic deception attacks has been investigated. We established two sets of random stochastic variables $\rho(i_k\hbar)$ and $\lambda(r)$, respectively, to represent the probability of data conveyed by the network being subjected to deception attacks and time-varying coupling delays. Based on the Lyapunov–Krasovskii functional theory some sufficient conditions derived for the closed-loop system that can ensure the system is stochastically stable. Two examples are presented to demonstrate the effectiveness of the presented approach.

Data Availability

No data were used to support this study.

Conflicts of Interest

The authors declare no conflicts of interest.

Authors' Contributions

All authors contributed equally and significantly in writing this article. All authors read and approved the final manuscript.

Acknowledgments

This work was supported by the Rajamangala University of Technology Suvarnabhumi, Thailand.

References

[1] Y. Wang, X. Hu, K. Shi, X. Song, and H. Shen, "Network-based passive estimation for switched complex dynamical networks under persistent dwell-time with limited signals," *Journal of the Franklin Institute*, vol. 357, no. 15, pp. 10921–10936, 2020.

[2] M. Syed Ali, L. Palanisamy, N. Gunasekaran, A. Alsaedi, and B. Ahmad, "Finite-time exponential synchronization of reaction-diffusion delayed complex-dynamical networks," *Discrete & Continuous Dynamical Systems - S*, vol. 14, no. 4, pp. 1465–1477, 2021.

[3] T. H. Lee, J. H. Park, H. Y. Jung, S. M. Lee, and O. M. Kwon, "Synchronization of a delayed complex dynamical network with free coupling matrix," *Nonlinear Dynamics*, vol. 69, no. 3, pp. 1081–1090, 2012.

[4] J. Yogambigai, M. Syed Ali, H. Alsulami, and M. S. Alhodaly, "Impulsive and pinning control synchronization of Markovian jumping complex dynamical networks with hybrid coupling and additive interval time-varying delays," *Communications in Nonlinear Science and Numerical Simulation*, vol. 85, Article ID 105215, 2020.

[5] M. S. Ali, M. Usha, O. M. Kwon, N. Gunasekaran, and G. K. Thakur, "/passive non-fragile synchronisation of Markovian jump stochastic complex dynamical networks with time-varying delays," *International Journal of Systems Science*, vol. 52, no. 7, pp. 1270–1283, 2021.

[6] B. Kaviarasan, O. M. Kwon, M. J. Park, and R. Sakthivel, "Composite synchronization control for delayed coupling complex dynamical networks via a disturbance observer-based method," *Nonlinear Dynamics*, vol. 99, no. 2, pp. 1601–1619, 2020.

[7] N. Gunasekaran, M. S. Ali, S. Arik, H. A. Ghaffar, and A. A. Z. Diab, "Finite-time and sampled-data synchronization of complex dynamical networks subject to average dwell-time switching signal," *Neural Networks*, vol. 149, pp. 137–145, 2022.

[8] J. Wang, X. Hu, Y. Wei, and Z. Wang, "Sampled-data synchronization of semi-Markov jump complex dynamical networks subject to generalized dissipativity property," *Applied Mathematics and Computation*, vol. 346, pp. 853–864, 2019.

[9] N. Gunasekaran, R. Saravanakumar, Y. H. Joo, and H. S. Kim, "Finite-time synchronization of sampled-data T-S fuzzy complex dynamical networks subject to average dwell-time approach," *Fuzzy Sets and Systems*, vol. 374, pp. 40–59, 2019.

[10] H. Lu, Y. Hu, C. Guo, and W. Zhou, "Cluster synchronization for a class of complex dynamical network system with randomly occurring coupling delays via an improved event-triggered pinning control approach," *Journal of the Franklin Institute*, vol. 357, no. 4, pp. 2167–2184, 2020.

[11] M. Gao, J. Liu, L. Zhang et al., "Security control for T-S fuzzy systems with multi-sensor saturations and distributed event-triggered mechanism," *Journal of the Franklin Institute*, vol. 357, no. 5, pp. 2851–2867, 2020.

[12] J. Wang, C. Yang, J. Xia, Z.-G. Wu, and H. Shen, "Observer-based sliding mode control for networked fuzzy singularly perturbed systems under weighted try-once-discard protocol," *IEEE Transactions on Fuzzy Systems*, .

[13] G. Nagamani, C. Karthik, and Y. H. Joo, "Event-triggered observer-based sliding mode control for T-S fuzzy systems via improved relaxed-based integral inequality," *Journal of the Franklin Institute*, vol. 357, no. 14, pp. 9543–9567, 2020.

[14] X. Li, D. Peng, and J. Cao, "Lyapunov stability for impulsive systems via event-triggered impulsive control," *IEEE Transactions on Automatic Control*, vol. 65, no. 11, pp. 4908–4913, 2020.

[15] G. Nagamani, Y. H. Joo, G. Soundararajan, and R. Mohajerpoor, "Robust event-triggered reliable control for T-S fuzzy uncertain systems via weighted based inequality," *Information Sciences*, vol. 512, pp. 31–49, 2020.

[16] J. Liu, Q. Liu, J. Cao, and Y. Zhang, "Adaptive event-triggered H∞ filtering for T-S fuzzy system with time delayfiltering for T-S fuzzy system with time delay," *Neurocomputing*, vol. 189, pp. 86–94, 2016.

[17] A. Kazemy, J. Lam, and Z. Chang, "Adaptive event-triggered mechanism for networked control systems under deception attacks with uncertain occurring probability," *International Journal of Systems Science*, vol. 52, no. 7, pp. 1426–1439, 2021.

[18] Z. Gu, D. Yue, and E. Tian, "On designing of an adaptive event-triggered communication scheme for nonlinear networked interconnected control systems," *Information Sciences*, vol. 422, pp. 257–270, 2018.

[19] Y. Wang, Z. Jia, and Z. Zuo, "Dynamic event-triggered and self-triggered output feedback control of networked switched linear systems," *Neurocomputing*, vol. 314, pp. 39–47, 2018.

[20] M. Rehan, M. Tufail, and S. Ahmed, "Leaderless consensus control of nonlinear multi-agent systems under directed topologies subject to input saturation using adaptive event-triggered mechanism," *Journal of the Franklin Institute*, vol. 358, no. 12, pp. 6217–6239, 2021.

[21] M. Syed Ali, M. Usha, J. Cao, and G. Lu, "Synchronisation analysis for stochastic TS fuzzy complex networks with coupling delay," *International Journal of Systems Science*, vol. 50, no. 3, pp. 585–598, 2019.

[22] Z. G. Wu, J. H. Park, H. Su, and J. Chu, "Stochastic stability analysis of piece wise homogeneous Markovian jump neural networks with mixed time-delays," *Journal of the Franklin Institute*, vol. 349, no. 6, pp. 2136–2150, 2012.

[23] H. Shen, X. Hu, J. Wang, J. Cao, and W. Qian, "Non-Fragile synchronization for markov jump singularly perturbed coupled neural networks subject to double-layer switching regulation," *IEEE Transactions on Neural Networks and Learning Systems*, .

[24] N. Padmaja and P. Balasubramaniam, "Mixed/passivity based stability analysis of fractional-order gene regulatory networks with variable delays," *Mathematics and Computers in Simulation*, vol. 192, pp. 167–181, 2022.

[25] P. Selvaraj, R. Sakthivel, and O. M. Kwon, "Synchronization of fractional-order complex dynamical network with random coupling delay, actuator faults and saturation," *Nonlinear Dynamics*, vol. 94, no. 4, pp. 3101–3116, 2018.

[26] N. Gunasekaran, G. Zhai, and Q. Yu, "Sampled-data synchronization of delayed multi-agent networks and its application to coupled circuit," *Neurocomputing*, vol. 413, pp. 499–511, 2020.

[27] R. Sakthivel, R. Sakthivel, O. M. Kwon, and B. Kaviarasan, "Fault estimation and synchronization control for complex dynamical networks with time-varying coupling delay," *International Journal of Robust and Nonlinear Control*, vol. 31, no. 6, pp. 2205–2221, 2021.

[28] J. Suo, Z. Wang, and B. Shen, "Pinning synchronization control for a class of discrete-time switched stochastic complex networks under event-triggered mechanism," *Nonlinear Analysis: Hybrid Systems*, vol. 37, Article ID 100886, 2020.

[29] H. Dong, N. Hou, and Z. Wang, "Fault estimation for complex networks with randomly varying topologies and stochastic inner couplings," *Automatica*, vol. 112, Article ID 108734, 2020.

[30] J. Liu, W. Suo, X. Xie, D. Yue, and J. Cao, "Quantized control for a class of neural networks with adaptive event-triggered scheme and complex cyber-attacks," *International Journal of Robust and Nonlinear Control*, vol. 31, no. 10, pp. 4705–4728, 2021.

[31] K. Shi, J. Wang, S. Zhong, Y. Tang, and J. Cheng, "Hybrid-driven finite-time H∞ sampling synchronization control for coupling memory complex networks with stochastic cyber attackssampling synchronization control for coupling memory complex networks with stochastic cyber attacks," *Neurocomputing*, vol. 387, pp. 241–254, 2020.

[32] R. Pan, Y. Tan, D. Du, and S. Fei, "Adaptive event-triggered synchronization control for complex networks with quantization and cyber-attacks," *Neurocomputing*, vol. 382, pp. 249–258, 2020.

[33] X. Zhou, Z. Gu, and F. Yang, "Resilient event-triggered output feedback control for load frequency control systems subject to cyber attacks," *IEEE Access*, vol. 7, pp. 58951–58958, 2019.

[34] T. Li, X. Tang, H. Zhang, and S. Fei, "Improved event-triggered control for networked control systems under stochastic cyber-attacks," *Neurocomputing*, vol. 350, pp. 33–43, 2019.

[35] M. Cong, X. Mu, and Z. Hu, "Sampled-data-based event-triggered secure bipartite tracking consensus of linear multi-agent systems under DoS attacks," *Journal of the Franklin Institute*, vol. 358, no. 13, pp. 6798–6817, 2021.

[36] D. Ding, Z. Tang, Y. Wang, and Z. Ji, "Secure synchronization of complex networks under deception attacks against vulnerable nodes," *Applied Mathematics and Computation*, vol. 399, p. 126017, 2021.

[37] D. Liu and D. Ye, "Pinning-observer-based secure synchronization control for complex dynamical networks subject to dos attacks," *IEEE Transactions on Circuits and Systems I: Regular Papers*, vol. 67, no. 12, pp. 5394–5404, 2020.

[38] L. Zhao and G. H. Yang, "Adaptive fault-tolerant control for nonlinear Multi-agent systems with DoS attacks," *Information Sciences*, vol. 526, pp. 39–53, 2020.

[39] J. Feng, J. Xie, J. Wang, and Y. Zhao, "Secure synchronization of stochastic complex networks subject to deception attack with nonidentical nodes and internal disturbance," *Information Sciences*, vol. 547, pp. 514–525, 2021.

[40] B. Shen, Z. Wang, D. Wang, and Q. Li, "State-saturated recursive filter design for stochastic time-varying nonlinear complex networks under deception attacks," *IEEE Transactions on Neural Networks and Learning Systems*, vol. 31, no. 10, pp. 3788–3800, 2020.

[41] D. Wang, F. Chen, B. Meng, X. Hu, and J. Wang, "Event-based secure load frequency control for delayed power systems subject to deception attacks," *Applied Mathematics and Computation*, vol. 394, p. 125788, 2021.

[42] H. Lu, Y. Deng, Y. Xu, and W. Zhou, "Event-Triggered H_∞ Filtering for Networked Systems under Hybrid Probability Deception Attacksfiltering for networked systems under hybrid probability deception attacks," *IEEE Access*, vol. 8, pp. 192030–192040, 2020.

[43] Y. Wang, F. Chen, G. Zhuang, and G. Song, "Event-based asynchronous and resilient filtering for Markov jump singularly perturbed systems against deception attacks," *ISA Transactions*, vol. 112, pp. 56–73, 2021.

[44] M. S. Mahmoud, M. M. Hamdan, and U. A. Baroudi, "Secure control of cyber physical systems subject to stochastic distributed DoS and deception attacks," *International Journal of Systems Science*, vol. 51, no. 9, pp. 1653–1668, 2020.

[45] J. Xie, S. Zhu, and D. Zhang, "A robust distributed secure interval observation approach for uncertain discrete-time positive systems under deception attacks," *Applied Mathematics and Computation*, vol. 413, Article ID 126638, 2022.

[46] W. Yang, X. K. Liu, Y. W. Wang, Z. W. Liu, and J. W. Xiao, "Secure stabilization of singularly perturbed switched systems under deception attacks," *Nonlinear Dynamics*, vol. 108, no. 1, pp. 683–695, 2022.

Hindawi
Complexity
Volume 2022, Article ID 4247800, 15 pages
https://doi.org/10.1155/2022/4247800

Research Article

Dynamics of a Stochastic Epidemic Model with Vaccination and Multiple Time-Delays for COVID-19 in the UAE

H. J. Alsakaji, F. A. Rihan, and A. Hashish

United Arab Emirates University, Al Ain, UAE

Correspondence should be addressed to H. J. Alsakaji; heba.sakaji@uaeu.ac.ae

Received 21 December 2021; Accepted 8 April 2022; Published 25 April 2022

Academic Editor: Georgi Georgiev

In this paper, we study the dynamics of COVID-19 in the UAE with an extended SEIR epidemic model with vaccination, time-delays, and random noise. The stationary ergodic distribution of positive solutions is examined, in which the solution fluctuates around the equilibrium of the deterministic case, causing the disease to persist stochastically. It is possible to attain infection-free status (extinction) in some situations, in which diseases die out exponentially and with a probability of one. The numerical simulations and fit to real observations prove the effectiveness of the theoretical results. Combining stochastic perturbations with time-delays enhances the dynamics of the model, and white noise intensity is an important part of the treatment of infectious diseases.

1. Introduction

COVID-19 is a disease caused by SARS-CoV-2 that can trigger a respiratory tract infection. It spreads likewise other coronaviruses do, basically through person-to-person contact. Infections range from mild to deadly [1, 2]. To combat the spreading of all infectious diseases, vaccination is one of the most important procedures [3, 4]. Vaccines generally expose the immune system to harmless parts of the pathogen so that the immune system learns to recognize it and may be able to tamp down the infection before any symptoms appear [5, 6]. COVID-19 vaccines, such as Pfizer, AstraZeneca, and Sinopharm, are now widely available for people aged five years and older, and all the currently authorized COVID-19 vaccines are effective and reduce the risk of severe illness [7]. It is normal for a virus to mutate as it infects people, and SARS-CoV-2 has mutated so [8–10]. There are various variants which are now spreading, such as Alpha, Beta, Gamma, Delta, and Omicron. An initial study showed Omicron variant reduced the antibody protection by some vaccines, but a booster shot is likely to protect people from severe disease, and research works are still in proceedings in this field [11].

Up to date, more than 4.41 billion people worldwide have received a dose of the COVID-19 vaccine, equal to about 57.4 percent of the world population [12]. A vaccinated person refers to someone who has received at least one dose of a vaccine, and a fully vaccinated person has completed receiving the vaccine, whether that is one dose or two, and two weeks have passed. A COVID-19 booster shot is an additional dose of a vaccine given after the protection provided by the original shot(s) has begun to decline [13]. The booster is recommended to help people keep up their level of immunity for longer. In the UAE, more than 99 percent of the population at least have one dose of the vaccine, 91 percent of the population are fully vaccinated, and 32.3 percent of the population are booster given [14]; therefore, the number of confirmed cases of COVID-19 in the UAE has decreased significantly.

Modeling infectious diseases provides a controlled environment in which complex relationships between environmental and biological factors can be examined. In public health science, mathematical models of infectious diseases can be used to analyze various scenarios, and the results can inform policy, programs, and practices [15, 16].

Researchers are working to develop mathematical models that can be used to predict vaccination strategies for controlling epidemic diseases [3, 4, 17, 18].

Human virus diseases are highly affected by stochastic perturbations. Because human contact can change from one person to another, epidemic growth and spread in human disease are normally random, and the population is subject to factors that are either not fully understood or difficult to model precisely. A model that ignores these phenomena will negatively affect the analysis of the studied biological systems. Stochastic differential equation models (SDEs) are more suitable for modeling epidemic dynamics under certain conditions [19–21]. Increasingly, deterministic models need to be extended to stochastic models that can account for more complex variations in dynamics [22]. Furthermore, delay differential equations (DDEs) are extensively used to describe the dynamics of infectious diseases. Due to the fact that time-delay is relevant to hidden mechanisms such as the incubation period and the recovery of infected individuals [23–25].

In this paper, we study the dynamics of the COVID-19 epidemic in the UAE, using a modified stochastic delayed SEIRV (Susceptible-Exposed-Infected-Recovered-Vaccinated) model. The model incorporates white noise and time-delays. This model assumes that individuals can become infected during vaccination, but then become healthy afterwards. A stochastic Lyapunov function and Ito's formula are used to determine the existing results of stationary distribution and extinction of the disease. Combining stochastic perturbations and time-delays can provide a more realistic view of disease dynamics. The rest of this paper is organized as follows: Section 2 presents the model formulation. In Sections 3 and 4, this model derives the stationary distribution and extinction results. In Section 5, numerical simulations are presented to verify the theory. In Section 6, conclusions are provided.

2. The Model

For the dynamics of COVID-19 in the UAE, we propose an extended SEIR epidemic model with vaccination, time-delays, and random noise [26, 27]. The basic model categorized people into four classes: susceptible (S): individuals not yet infected; exposed (E): individuals experiencing incubation duration; infectious (I): confirmed cases; and removed (R): recovered individuals. We assume that the recovered individuals will remain in the class $R(t)$. Therefore, the SEIR model has the following equations system:

$$\begin{aligned}
\frac{\mathrm{d}S}{\mathrm{d}t} &= \Lambda - \beta_1 SE - \alpha S,\\
\frac{\mathrm{d}E}{\mathrm{d}t} &= \beta_1 SE - \beta_2 EI - (\kappa + \alpha)E,\\
\frac{\mathrm{d}I}{\mathrm{d}t} &= \beta_2 EI - (\mathrm{d} + r + \alpha)I,\\
\frac{\mathrm{d}R}{\mathrm{d}t} &= rI + \kappa E - \alpha R.
\end{aligned} \tag{1}$$

Here, Λ is the recruitment rate; β_1 is the transmission rate of susceptible into exposed class; β_2 is the rate of transmission of exposed into infected class; α and d are natural and disease death rates; κ is the transmission rate of exposed into recovered class; and r is the transmission rate of infected into recovered class. Many researchers develop the above model to include vaccination strategies to control epidemic diseases realistically [17, 18]. There is evidence that individuals can become infected during vaccination and go on to be healthy afterward [28]. Incorporating time lags in epidemic models makes the systems much more realistic and enriches the dynamics of the model. Therefore, we include time-delays τ_1 and τ_2 to represent the incubation period; while τ_3 stands for the time required for the infected individuals to become recovered. Hence, the deterministic SEIR model with vaccination and time-delays takes the form (see Figure 1).

$$\begin{aligned}
\frac{\mathrm{d}S}{\mathrm{d}t} &= \Lambda - \beta_1 SE - (\beta_3 + \alpha)S,\\
\frac{\mathrm{d}E}{\mathrm{d}t} &= \beta_4 VE + \beta_1 SE - \beta_2 EI(t-\tau_1) - (\kappa + \alpha)E,\\
\frac{\mathrm{d}I}{\mathrm{d}t} &= \beta_5 VI(0) + \beta_2 EI(t-\tau_1) - (d + r + \alpha)I,\\
\frac{\mathrm{d}R}{\mathrm{d}t} &= \beta_6 V + rI(t-\tau_3) + \kappa E - \alpha R,\\
\frac{\mathrm{d}V}{\mathrm{d}t} &= \beta_3 S - (\beta_6 + \alpha)V - \beta_4 VE - \beta_5 VI(t-\tau_2).
\end{aligned} \tag{2}$$

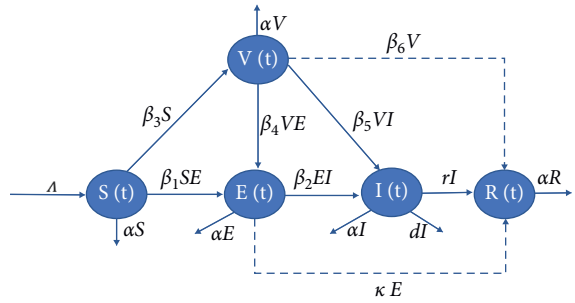

Figure 1: Flow chart of the model (2).

$\beta_3, \beta_4, \beta_5$, and β_6 are the transmission rates of susceptible into vaccinated class; vaccinated into exposed class; vaccinated into infected class; and β_6 vaccinated into recovered class, respectively.

The basic reproduction number,

$$\mathscr{R}_0 = \frac{\beta_1 \Lambda}{(\beta_3 + \alpha)(\kappa + \alpha)} + \frac{\Lambda \beta_3 \beta_4}{(\beta_3 + \alpha)(\kappa + \alpha)(\beta_6 + \alpha)}, \tag{3}$$

of model (2), has a significant impact in epidemiology since it decides whether an epidemic occurs or the disease dies out [29]. If $\mathscr{R}_0 < 1$, then model (2) has only a disease-free equilibrium $\mathscr{E}_0 = (S^+, 0, 0, R^+, V^+) = (\Lambda/\beta_3 + \alpha, 0, 0, \Lambda\beta_3 \beta_6/\alpha(\beta_6 + \alpha)(\beta_3 + \alpha), \Lambda\beta_3/(\beta_6 + \alpha)(\beta_3 + \alpha))$ and it is globally asymptotically stable; while if $\mathscr{R}_0 > 1$, then, $\mathscr{E}_0$ is unstable and there is a unique endemic equilibrium $\mathscr{E}^* = (S^*, E^*, I^*, R^*, V^*)$ which is globally asymptotically stable [28].

Because some factors cannot be measured precisely, stochastic models always provide an estimate of these uncertainties based on approximate estimates [1, 30–32]. Therefore, we introduce randomness into model (2) by adding white noise to the state of the SEIR model with vaccination and time-delays. The modified model takes the form:

$$\begin{aligned}
\mathrm{d}S &= [\Lambda - \beta_1 SE - (\beta_3 + \alpha)S]\mathrm{d}t + \nu_1 S\, dW_1,\\
dE &= [\beta_4 VE + \beta_1 SE - \beta_2 EI(t - \tau_1) - (\kappa + \alpha)E]\mathrm{d}t + \nu_2 E\, dW_2,\\
\mathrm{d}I &= [\beta_5 VI(t - \tau_2) + \beta_2 EI(t - \tau_1) - (d + r + \alpha)I]\mathrm{d}t + \nu_3 I\, dW_3,\\
\mathrm{d}R &= [\beta_6 V + rI(t - \tau_3) + \kappa E - \alpha R]\mathrm{d}t + \nu_4 R\, dW_4,\\
\mathrm{d}V &= [\beta_3 S - (\beta_6 + \alpha)V - \beta_4 VE - \beta_5 VI(t - \tau_2)]\mathrm{d}t + \nu_5 V\, dW_5,
\end{aligned} \tag{4}$$

with

$$\begin{aligned}
&S(\theta) = \phi_1(\theta), E(\theta) = \phi_2(\theta), I(\theta) = \phi_3(\theta), R(\theta)\\
&\quad = \phi_4(\theta), V(\theta) = \phi_5(\theta),\\
&\theta \in [-\tau, 0], \quad \tau = \max\{\tau_1, \tau_2, \tau_3\},
\end{aligned} \tag{5}$$

$\phi_i(0) > 0$ and $\phi_i(\theta)$, $i = 1, \ldots, 5$, are non-negative continuous initial functions on $[-\tau, 0]$. $W_i(t)$, $i = 1, \ldots, 5$, represent the independent Brownian motions defined on a complete probability space $(\Omega, \mathscr{U}, \{\mathscr{U}\}_{t\geq 0}, P)$ with a filtration $\{\mathscr{U}_t\}_{t\geq 0}$ satisfying the usual conditions (it is right continuous and $\mathscr{U}_0$ contains all $P-$ null sets), where ν_i, $i = 1, \ldots, 5$ are the intensities of white noise.

3. Stationary Distribution and Ergodicity

Among the most important and significant characteristics of the stochastic epidemic model (4) is its ergodic property. Under some conditions of white noise, the stochastic model fluctuates in the neighborhood of the infected equilibrium of the corresponding deterministic model for all time regardless of the starting conditions. First, we need to show that there is a global non-negative solution of model (4), which is as follows:

Theorem 1. *For any given initial value (5), system (4) has a unique solution $(S(t), E(t), I(t), R(t), V(t))$ on $t \geq -\tau$, and the solution will remain in $\mathbb{R}^5_+$ with probability one.*

Proof. Since the system coefficients (4) satisfy linear growth and Lipschitzian conditions and based Khasminskii Lyapunov functional approach, we can show that system (4) has a global positive solution. The main challenge is to establish a Lyapunov function, so we define

$$\begin{aligned}
\mathscr{G}(S, E, I, R, V) = \mathscr{G}(.) &= (S - 1 - \ln S) + (E - 1 - \ln E)\\
&+ (I - 1 - \ln I) + (R - 1 - \ln R)\\
&+ (V - 1 - \ln V) + \beta_2 \int_t^{t+\tau_1} I(s - \tau_1)\mathrm{d}s\\
&+ \beta_5 \int_t^{t+\tau_2} I(s - \tau_2)\mathrm{d}s\\
&+ r \int_t^{t+\tau_3} I(s - \tau_3)\mathrm{d}s.
\end{aligned} \tag{6}$$

By *Itô*'s formula on $\mathscr{G}$,

$$\begin{aligned} \mathrm{d}\mathscr{G}(.) &= \mathscr{L}\mathrm{G}\mathrm{d}t + \nu_1(S-1)\mathrm{d}W_1(t) + \nu_2(E-1)\mathrm{d}W_2(t) \\ &\quad + \nu_3(I-1)\mathrm{d}W_3(t) \\ &\quad + \nu_4(R-1)\mathrm{d}W_4(t) + \nu_5(V-1)\mathrm{d}W_5(t), \end{aligned} \tag{7}$$

where

$$\begin{aligned} \mathscr{L}\mathrm{G} &= \Lambda - \alpha S - \frac{\Lambda}{S} + \beta_1 E + (\beta_3 + \alpha) - (\kappa + \alpha)E - \beta_4 V - \beta_1 S + \beta_2 I + (\kappa + \alpha) \\ &\quad - (d + r + \alpha)I - \frac{\beta_5 V I(t-\tau_2)}{I} - \frac{\beta_2 E I(t-\tau_2)}{I} + (d + r + \alpha) + \beta_6 V + rI + \kappa E - \alpha R \\ &\quad - \frac{\beta_6 V}{R} - \frac{rI(t-\tau_3)}{R} - \frac{\kappa E}{R} + \alpha - (\beta_6 + \alpha)V - \frac{\beta_3 S}{V} + (\beta_6 + \alpha) + \beta_4 E + \beta_5 I \\ &\quad + \frac{\nu_1^2 + \nu_2^2 + \nu_3^2 + \nu_4^2 + \nu_5^2}{2} \\ &\le \Lambda + \beta_3 + \kappa + d + r + \beta_6 + 5\alpha - (\alpha + \beta_1)S + (\beta_1 + \beta_4 - \alpha)E + (\beta_2 + \beta_5 - \mathrm{d} - \alpha)I \\ &\quad - \alpha R - (\beta_4 + \alpha)V + \frac{\nu_1^2 + \nu_2^2 + \nu_3^2 + \nu_4^2 + \nu_5^2}{2} \\ &\le \mathscr{A}, \end{aligned} \tag{8}$$

where $\mathscr{A}$ is a positive constant. It follows that $\mathscr{L}\mathrm{G}$ is bounded. Hence, the rest of the proof is standard [33], so it is omitted. □

Theorem 2. *Define*

$$\widehat{\mathscr{R}}_0 = \frac{\beta_1 \Lambda}{\widehat{\nu}_1 \widehat{\nu}_2} + \frac{\Lambda \beta_3 \beta_4}{\widehat{\nu}_1 \widehat{\nu}_2 \widehat{\nu}_5}, \tag{9}$$

where $\widehat{\nu}_1 = \beta_3 + \alpha + \nu_1^2/2$, $\widehat{\nu}_2 = \kappa + \alpha + \nu_2^2/2$, $\widehat{\nu}_3 = d + r + \alpha + \nu_3^2/2$, $\widehat{\nu}_4 = \alpha + \nu_4^2/2$, *and* $\widehat{\nu}_5 = \beta_6 + \alpha + \nu_5^2/2$. *If* $\widehat{\mathscr{R}}_0 > 1$, *then, system (4) has a unique stationary distribution* $\pi(.)$ *and it admits the ergodic property.*

Proof. Let $Y(t)$ is a regular time-homogenous Markov process in $\mathbb{R}^n$, defined by the stochastic delay differential equation:

$$\mathrm{d}Y(t) = f(Y(t), Y(t-\tau), t)\mathrm{d}t + \sum_{r=1}^{n} g_r(Y(t), t)\mathrm{d}W_r(t). \tag{10}$$

The diffusion matrix of the process $Y(t)$ is

$$\begin{aligned} \Pi(y) &= \left(\varsigma_{ij}(y)\right), \\ \varsigma_{ij}(y) &= \sum_{r=1}^{n} g_r^i(y) g_r^j(y). \end{aligned} \tag{11}$$

□

Lemma 1 ([see 34]). *The Markov process* $Y(t)$ *has a unique ergodic stationary distribution* $\pi(.)$ *if there exists a bounded domain* $\mathscr{B} \subset \mathbb{R}^n$ *with regular boundary* Δ *and*

(i) there is a positive number $\mathscr{X}$ *such that* $\sum_{i,j=1}^{n} \varsigma_{ij}(y)\xi_i\xi_j \ge \mathscr{X}|\xi|^2$, $5y \in \mathscr{B}$, $\xi \in \mathbb{R}^n$.

(ii) there exists a non-negative $\mathscr{C}^2$*-function* V *such that* $\mathscr{L}V$ *is negative for any* $\mathbb{R}^n \setminus \mathscr{B}$.

With a view to prove Theorem 2, we need to guarantee the validity of conditions (i) and (ii) of Lemma 1. Clearly, condition (i) satisfies; we need to check condition (ii). Define $\mathscr{F}_5 = \mathscr{F}_3 + \mathscr{F}_4$, where

$$\begin{aligned} \mathscr{F}_1 &= -\ln E - \omega_1 \ln S + \beta_2 \int_t^{t+\tau_1} I(s-\tau_1)\mathrm{d}s, \\ \mathscr{F}_2 &= \mathscr{F}_1 - \omega_2 \ln S - \omega_3 \ln V + \omega_3 \beta_5 \int_t^{t+\tau_3} I(s-\tau_3)\mathrm{d}s, \\ \mathscr{F}_3 &= \mathscr{N}\mathscr{F}_2 + (-2\ln S - \ln R - \ln I), \\ \mathscr{F}_4 &= \frac{1}{\eta+1}(S + E + I + R + V)^{\eta+1}. \end{aligned} \tag{12}$$

$\omega_1 = \beta_1 \Lambda/\widehat{\nu}_1^2$, $\omega_2 = \beta_3\beta_4\Lambda/\widehat{\nu}_1^2\widehat{\nu}_5$, and $\omega_3 = \beta_3\beta_4\Lambda/\widehat{\nu}_1\widehat{\nu}_5^2$, $0 < \eta < 4\alpha/\nu_1^2 \vee \nu_2^2 \vee \nu_3^2 \vee \nu_4^2 \vee \nu_5^2$, where $\mathscr{N}$ is a positive constant so that

$$-\mathcal{N}\widehat{\nu}_2\left(\widehat{\mathcal{R}}_0-1\right)+D\leq -2, \tag{13}$$

where $D=\max\{D_1,D_2\}$ such that

$$\begin{aligned}
D_0&=\sup_{(S,E,I,R,V)\in\mathbb{R}_+^5}\left\{\Lambda(S+E+I+R+V)^{\eta}-\frac{\widehat{\alpha}}{2}(S+E+I+R+V)^{\eta+1}\right\},\\
D_1&=\sup_{(S,E,I,R,V)\in\mathbb{R}_+^5}\left\{\mathcal{N}\left(\beta_2+\omega_3\beta_5\right)I+2\beta_1E+2\widehat{\nu}_1+\widehat{\nu}_3+\widehat{\nu}-\frac{\widehat{\alpha}}{4}E^{\eta+1}+D_0\right\},\\
D_2&=\sup_{(S,E,I,R,V)\in\mathbb{R}_+^5}\left\{\mathcal{N}\left(\omega_1\beta_1+\omega_2\beta_1+\omega_3\beta_4\right)E+2\beta_1E+2\widehat{\nu}_1+\widehat{\nu}_3+\widehat{\nu}-\frac{\widehat{\alpha}}{4}I^{\eta+1}+D_0\right\},\\
D_3&=\sup_{(S,E,I,R,V)\in\mathbb{R}_+^5}\left\{\mathcal{N}\left(\omega_1\beta_1+\omega_2\beta_1+\omega_3\beta_4\right)E+\mathcal{N}\left(\beta_2+\omega_3\beta_5\right)I+2\beta_1E+2\widehat{\nu}_1+\widehat{\nu}_3+\widehat{\nu}-\frac{\widehat{\alpha}}{4}\left(E^{\eta+1}+I^{\eta+1}\right)+D_0\right\}.
\end{aligned} \tag{14}$$

In addition, $\mathcal{F}_5$ is continuous and tends to $+\infty$ as (S,E,I,R,V) approaches the boundary of $\mathbb{R}_+^5$ and $\|(S,E,I,R,V)\|\longrightarrow\infty$. Hence, $\mathcal{F}_5$ must have a minimum point in the interior of $\mathbb{R}_+^5$.

We define a $\mathcal{C}^2$-function $\mathcal{F}(.)\colon \mathbb{R}_+^5\longrightarrow\mathbb{R}_+$ as

$$\begin{aligned}
\mathcal{F}(S,E,I,R,V)=\mathcal{F}_5(S,E,I,R,V)\\
-\mathcal{F}_5(S(0),E(0),I(0),R(0),V(0)).
\end{aligned} \tag{15}$$

By *Itô*'s formula, we obtain

$$\begin{aligned}
\mathcal{L}\mathcal{F}_1&=-\beta_4V-\beta_1S+\beta_2I+\widehat{\nu}_2+\omega_1\left(-\frac{\Lambda}{S}+\beta_1E+\widehat{\nu}_1\right)\\
&\leq-\frac{\beta_1\Lambda}{\widehat{\nu}_1}+\widehat{\nu}_2-\beta_4V+\beta_2I+\omega_1\beta_1E,\\
\mathcal{L}\mathcal{F}_2&\leq-\frac{\beta_1\Lambda}{\widehat{\nu}_1}+\widehat{\nu}_2-\beta_4V+\beta_2I+\omega_1\beta_1E+\omega_2\left(-\frac{\Lambda}{S}+\beta_1E+\widehat{\nu}_1\right)+\omega_3\left(-\frac{\beta_3S}{V}+\widehat{\nu}_5+\beta_4E+\beta_5I\right)\\
&\leq-\frac{\beta_1\Lambda}{\widehat{\nu}_1}+\widehat{\nu}_2+(\omega_1\beta_1+\omega_2\beta_1+\omega_3\beta_4)E+(\beta_2+\omega_3\beta_5)I+\omega_2\widehat{\nu}_1+\omega_3\widehat{\nu}_5-3\sqrt[3]{\Lambda\beta_3\beta_4\omega_2\omega_3}\\
&\leq-\widehat{\nu}_2\left(\frac{\beta_1\Lambda}{\widehat{\nu}_1\widehat{\nu}_2}+\frac{\Lambda\beta_3\beta_4}{\widehat{\nu}_1\widehat{\nu}_2\widehat{\nu}_3}-1\right)+(\omega_1\beta_1+\omega_2\beta_1+\omega_3\beta_4)E+(\beta_2+\omega_3\beta_5)I\\
&\coloneqq-\widehat{\nu}_2\left(\widehat{\mathcal{R}}_0-1\right)+(\omega_1\beta_1+\omega_2\beta_1+\omega_3\beta_4)E+(\beta_2+\omega_3\beta_5)I\\
\mathcal{L}\mathcal{F}_3&\leq-\mathcal{N}\widehat{\nu}_2\left(\widehat{\mathcal{R}}_0-1\right)+\mathcal{N}(\omega_1\beta_1+\omega_2\beta_1+\omega_3\beta_4)E+\mathcal{N}(\beta_2+\omega_3\beta_5)I-\frac{2\Lambda}{S}+2\beta_1E+2\widehat{\nu}_1\\
&\quad-\frac{\beta_5VI(t-\tau_2)}{I}-\frac{\beta_2EI(t-\tau_1)}{I}+\widehat{\nu}_3-\frac{\beta_6V}{R}-\frac{rI(t-\tau_3)}{R}-\frac{\kappa E}{R}+\widehat{\nu}_4,\\
\mathcal{L}\mathcal{F}_4&=(S+E+I+R+V)^{\eta}[\Lambda-\alpha S-\alpha E-(d+\alpha)I-\alpha R-\alpha V]\\
&\quad+\frac{\eta}{2}(S+E+I+R+V)^{\eta-1}\left(\frac{1}{2}\nu_1^2S^2+\frac{1}{2}\nu_2^2E^2+\frac{1}{2}\nu_3^2I^2+\frac{1}{2}\nu_4^2R^2+\frac{1}{2}\nu_5^2V^2\right)\\
&\leq\Lambda(S+E+I+R+V)^{\eta}-\alpha(S+E+I+R+V)^{\eta+1}\\
&\quad+\frac{\eta}{4}\left(\nu_1^2\vee\nu_2^2\vee\nu_3^2\vee\nu_4^2\vee\nu_5^2\right)(S+E+I+R+V)^{\eta+1}\\
&=\Lambda(S+E+I+R+V)^{\eta}-\left[\alpha-\frac{\eta}{4}\left(\nu_1^2\vee\nu_2^2\vee\nu_3^2\vee\nu_4^2\vee\nu_5^2\right)\right](S+E+I+R+V)^{\eta+1}\\
&\coloneqq\Lambda(S+E+I+R+V)^{\eta}-\widehat{\alpha}(S+E+I+R+V)^{\eta+1},
\end{aligned} \tag{16}$$

such that $\widehat{\alpha} = \alpha - \eta/4\,(\nu_1^2 \vee \nu_2^2 \vee \nu_3^2 \vee \nu_4^2 \vee \nu_5^2)$. Hence,

$$\begin{aligned}\mathscr{L}\mathscr{F} = L\mathscr{F}_5 \leq & -\mathscr{N}\widehat{\nu}_2\left(\widehat{\mathscr{R}}_0 - 1\right) + \mathscr{N}\left(\omega_1\beta_1 + \omega_2\beta_1 + \omega_3\beta_4\right)E + \mathscr{N}\left(\beta_2 + \omega_3\beta_5\right)I - \frac{2\Lambda}{S} + 2\beta_1 E + 2\widehat{\nu}_1 \\ & + \widehat{\nu}_3 - \frac{\beta_6 V}{R} - \frac{rI}{R} - \frac{\kappa E}{R} + \widehat{\nu}_4 + \Lambda\,(S + E + I + R + V)^{\eta} - \widehat{\alpha}\,(S + E + I + R + V)^{\eta+1}.\end{aligned} \tag{17}$$

Define a closed bounded set.

$$\mathscr{B} = \left\{(S, E, I, R, V) \in \mathbb{R}_+^5 \colon \epsilon \leq S \leq \frac{1}{\epsilon}, \epsilon \leq E \leq \frac{1}{\epsilon}, \epsilon \leq I \leq \frac{1}{\epsilon}, \epsilon^2 \leq R \leq \frac{1}{\epsilon^2}, \epsilon \leq V \leq \frac{1}{\epsilon}\right\}. \tag{18}$$

By Lemma 1, we need to show that $\mathscr{L}\mathscr{F} \leq -1$ for $(S, E, I, R, V) \in \mathbb{R}_+^5 \setminus \mathscr{B}_\epsilon$. such that $\mathbb{R}_+^5 \setminus \mathscr{B}_\epsilon = \cup_{i=1}^{9} \mathscr{B}_i$, where

$$\begin{aligned}&\mathscr{B}_1 = \left\{(S, E, I, R, V) \in \mathbb{R}_+^5 \colon 0 < E < \epsilon\right\}, \ \mathscr{B}_2 = \left\{(S, E, I, R, V) \in \mathbb{R}_+^5 \colon 0 < I < \epsilon\right\}, \\ &\mathscr{B}_3 = \left\{(S, E, I, R, V) \in \mathbb{R}_+^5 \colon 0 < S < \epsilon\}\right\}, \ \mathscr{B}_4 = \left\{(S, E, I, R, V) \in \mathbb{R}_+^5 \colon 0 < V < \epsilon, R > \epsilon^2\right\}, \\ &\mathscr{B}_5 = \left\{(S, E, I, R, V) \in \mathbb{R}_+^5 \colon 0 < R < \epsilon^2, V \leq \frac{1}{\epsilon}\right\}, \ \mathscr{B}_6 = \left\{(S, E, I, R, V) \in \mathbb{R}_+^5 \colon R > \frac{1}{\epsilon^2}\right\}, \\ &\mathscr{B}_7 = \left\{(S, E, I, R, V) \in \mathbb{R}_+^5 \colon I > \frac{1}{\epsilon}\right\}, \ \mathscr{B}_8 = \left\{(S, E, I, R, V) \in \mathbb{R}_+^5 \colon S > \frac{1}{\epsilon}\right\}, \\ &\mathscr{B}_9 = \left\{(S, E, I, R, V) \in \mathbb{R}_+^5 \colon V > \frac{1}{\epsilon}\right\}, \ \mathscr{B}_{10} = \left\{(S, E, I, R, V) \in \mathbb{R}_+^5 \colon E > \frac{1}{\epsilon}\right\}.\end{aligned} \tag{19}$$

Case 1. If $(S, E, I, R, V) \in \mathscr{B}_1$, then

$$\begin{aligned}\mathscr{L}\mathscr{F} \leq & -\mathscr{N}\widehat{\nu}_2\left(\widehat{\mathscr{R}}_0 - 1\right) + \mathscr{N}\left(\omega_1\beta_1 + \omega_2\beta_1 + \omega_3\beta_4\right)E \\ & + \mathscr{N}\left(\beta_2 + \omega_3\beta_5\right)I + 2\beta_1 E + 2\widehat{\nu}_1 \\ & + \widehat{\nu}_3 + \widehat{\nu}_4 - \frac{\widehat{\alpha}}{4}E^{\eta+1} + D_0 \\ & \leq -\mathscr{N}\widehat{\nu}_2\left(\widehat{\mathscr{R}}_0 - 1\right) + \mathscr{N}\left(\omega_1\beta_1 + \omega_2\beta_1 + \omega_3\beta_4\right)E + D_1 \\ & \leq -\mathscr{N}\widehat{\nu}_2\left(\widehat{\mathscr{R}}_0 - 1\right) + \mathscr{N}\left(\omega_1\beta_1 + \omega_2\beta_1 + \omega_3\beta_4\right)\epsilon + D_1 \leq -1,\end{aligned} \tag{20}$$

from condition (10) and $-\mathscr{N}\widehat{\nu}_2\,(\widehat{\mathscr{R}}_0 - 1) + \mathscr{N}\left(\omega_1\beta_1 + \omega_2\beta_1 + \omega_3\beta_4\right)\epsilon + D_1 \leq -1$, we obtain $\mathscr{L}\mathscr{F} \leq -1$.

Case 2. If $(S, E, I, R, V) \in \mathscr{B}_2$, we have

$$\begin{aligned}\mathscr{L}\mathscr{F} \leq & -\mathscr{N}\widehat{\nu}_2\left(\widehat{\mathscr{R}}_0 - 1\right) + \mathscr{N}\left(\omega_1\beta_1 + \omega_2\beta_1 + \omega_3\beta_4\right)E \\ & + \mathscr{N}\left(\beta_2 + \omega_3\beta_5\right)I + 2\beta_1 E + 2\widehat{\nu}_1 \\ & + \widehat{\nu}_3 + \widehat{\nu}_4 - \frac{\widehat{\alpha}}{4}I^{\eta+1} + D_0 \\ & \leq -\mathscr{N}\widehat{\nu}_2\left(\widehat{\mathscr{R}}_0 - 1\right) + \mathscr{N}\left(\beta_2 + \omega_3\beta_5\right)I + D_2 \\ & \leq -\mathscr{N}\widehat{\nu}_2\left(\widehat{\mathscr{R}}_0 - 1\right) + \mathscr{N}\left(\beta_2 + \omega_3\beta_5\right)\epsilon + D_2 \leq -1,\end{aligned} \tag{21}$$

which is obtained from (13) and $-\mathcal{N}\widehat{\nu}_2(\widehat{\mathcal{R}}_0 - 1) + \mathcal{N}(\beta_2 + \omega_3\beta_5)\epsilon + D_2 \leq -1$.

Case 3. If $(S, E, I, R, V) \in \mathcal{B}_3$, we get

$$\begin{aligned}\mathcal{L}\mathcal{F} &\leq \mathcal{N}(\omega_1\beta_1 + \omega_2\beta_1 + \omega_3\beta_4)E + \mathcal{N}(\beta_2 + \omega_3\beta_5)I - \frac{2\Lambda}{S} \\ &+ 2\beta_1 E + 2\widehat{\nu}_1 \\ &+ \widehat{\nu}_3 + \widehat{\nu}_4 + D_0 - \frac{\widehat{\alpha}}{4}\left(I^{\eta+1} + E^{\eta+1}\right) \\ &\leq -\frac{2\Lambda}{S} + D_3 \\ &\leq -\frac{2\Lambda}{\epsilon} + D_3 \leq -1,\end{aligned} \tag{22}$$

such that $0 < \epsilon \leq 2\Lambda/D_3 + 1$.

Case 4. Let $(S, E, I, R, V) \in \mathcal{B}_4$, one may obtain

$$\begin{aligned}\mathcal{L}\mathcal{F} &\leq -\frac{\beta_6 V}{R} + \mathcal{N}(\omega_1\beta_1 + \omega_2\beta_1 + \omega_3\beta_4)E \\ &+ \mathcal{N}(\beta_2 + \omega_3\beta_5)I + 2\beta_1 E + 2\widehat{\nu}_1 \\ &+ \widehat{\nu}_3 + \widehat{\nu}_4 + D_0 - \frac{\widehat{\alpha}}{4}\left(I^{\eta+1} + E^{\eta+1}\right) \\ &\leq D_3 - \frac{\beta_6}{\epsilon} \leq -1,\end{aligned} \tag{23}$$

where $0 < \epsilon \leq \beta_6/D_3 + 1$.

Case 5. If $(S, E, I, R, V) \in \mathcal{B}_5$, we have

$$\begin{aligned}\mathcal{L}\mathcal{F} &\leq -\frac{\beta_6 V}{R} + \mathcal{N}(\omega_1\beta_1 + \omega_2\beta_1 + \omega_3\beta_4)E \\ &+ \mathcal{N}(\beta_2 + \omega_3\beta_5)I + 2\beta_1 E + 2\widehat{\nu}_1 \\ &+ \widehat{\nu}_3 + \widehat{\nu}_4 + D_0 - \frac{\widehat{\alpha}}{4}\left(I^{\eta+1} + E^{\eta+1}\right) \\ &\leq D_3 - \frac{\beta_6}{\epsilon^3} \leq -1,\end{aligned} \tag{24}$$

where $0 < \epsilon \leq \sqrt[3]{\beta_6/D_3 + 1}$.

Case 6. If $(S, E, I, R, V) \in \mathcal{B}_6$, we have

$$\begin{aligned}\mathcal{L}\mathcal{F} &\leq -\frac{\widehat{\alpha}}{4}R^{\eta+1} + D_3 \\ &\leq D_3 - \frac{\widehat{\alpha}}{4}\epsilon^{-2(\eta+1)} \leq -1,\end{aligned} \tag{25}$$

where $0 < \epsilon \leq [\widehat{\alpha}/4(D_3 + 1)]^{1/2(1+\eta)}$.

Case 7. If $(S, E, I, R, V) \in \mathcal{B}_7$, one may obtain

$$\begin{aligned}\mathcal{L}\mathcal{F} &\leq -\frac{\widehat{\alpha}}{4}I^{\eta+1} + D_3 \\ &\leq D_3 - \frac{\widehat{\alpha}}{4}\epsilon^{-(\eta+1)} \leq -1.\end{aligned} \tag{26}$$

where $0 < \epsilon \leq [\widehat{\alpha}/4(D_3 + 1)]^{1/(1+\eta)}$.

Cases 8, 9, and 10 are the same as Case 7.

Thus, condition (ii) of Lemma 1 holds; hence, system (4) identifies a unique stationary distribution $\pi(.)$.

4. Extinction of the Disease

In this section, we discuss conditions that predict the extinction of the disease. From the formula of the reproduction number, we can conclude that $\widehat{\mathcal{R}_0} < \mathcal{R}_0$. First, we go through the following Lemmas [21, 32]

Lemma 2. *Let $(S(t), E(t), I(t), R(t), V(t))$ be the solution of (4) with initial conditions (5), then*

$$\begin{aligned}\lim_{t\longrightarrow\infty}\frac{S(t)}{t} &= 0, \\ \lim_{t\longrightarrow\infty}\frac{E(t)}{t} &= 0, \\ \lim_{t\longrightarrow\infty}\frac{I(t)}{t} &= 0, \\ \lim_{t\longrightarrow\infty}\frac{R(t)}{t} &= 0, \\ \lim_{t\longrightarrow\infty}\frac{V(t)}{t} &= 0.\end{aligned} \tag{27}$$

Lemma 3. *Assume that $\alpha > 1/2(\nu_1^2 \vee \nu_2^2 \vee \nu_3^2 \vee \nu_4^2 \vee \nu_5^2)$. Let $(S(t), E(t), I(t), R(t), V(t))$ be the solution of (4) with initial conditions (4), we have*

$$\begin{aligned}&\lim_{t\longrightarrow\infty}\frac{\int_0^t S(r)\mathrm{d}W_1(r)}{t} = 0, \lim_{t\longrightarrow\infty}\frac{\int_0^t E(r)\mathrm{d}W_2(r)}{t} = 0, \lim_{t\longrightarrow\infty}\frac{\int_0^t I(r)\mathrm{d}W_3(r)}{t} = 0, \\ &\lim_{t\longrightarrow\infty}\frac{\int_0^t R(r)\mathrm{d}W_4(r)}{t} = 0, \lim_{t\longrightarrow\infty}\frac{\int_0^t V(r)\mathrm{d}W_5(r)}{t} = 0.\end{aligned} \tag{28}$$

Theorem 3. *Assume* $\alpha > 1/2(\nu_1^2 \vee \nu_2^2 \vee \nu_3^2 \vee \nu_4^2 \vee \nu_5^2)$. *Let* $(S(t), E(t), I(t), R(t), V(t))$ *be the solution of (4) with initial conditions (5). If* $\mathscr{R}_0 < 1$, *then*

$$\lim_{t\longrightarrow\infty}\left[\frac{\log E(t)}{t} + \beta_2\langle I(t)\rangle\right] \le (\kappa+\alpha)(\mathscr{R}_0 - 1) < 0 \quad \text{a.s.}, \tag{29}$$

which means $E(t)$ *and* $I(t)$ *tend to zero exponentially almost surely. In other words the disease dies out with probability one. Moreover,*

$$\lim_{t\longrightarrow\infty}(S(t) + R(t) + V(t)) = \frac{\Lambda}{\alpha} = S^+ + R^+ + V^+. \tag{30}$$

Proof. Taking integration of the first and fifth equations of (4), we obtain

$$\begin{aligned}\frac{S(t)-S(0)}{t} &= \Lambda - \beta_1\langle S(t)E(t)\rangle - (\beta_3+\alpha)\langle S(t)\rangle \\ &\quad + \nu_1\frac{\int_0^t S(r)\mathrm{d}W_1(r)}{t}, \\ \frac{V(t)-V(0)}{t} &= \beta_3\langle S(t)\rangle - (\beta_6+\alpha)\langle V(t)\rangle - \beta_4\langle V(t)E(t)\rangle \\ &\quad - \beta_5\langle V(t)I(t)\rangle + \nu_5\frac{\int_0^t V(r)\mathrm{d}W_5(r)}{t}.\end{aligned} \tag{31}$$

Therefore,

$$\begin{aligned}\langle S(t)\rangle &= \frac{1}{(\beta_3+\alpha)}\left[\Lambda - \beta_1\langle S(t)E(t)\rangle + \nu_1\frac{\int_0^t S(r)\mathrm{d}W_1(r)}{t} - \frac{S(t)-S(0)}{t}\right] \\ &\le \frac{\Lambda}{(\beta_3+\alpha)} + \frac{1}{(\beta_3+\alpha)}\left(\nu_1\frac{\int_0^t S(r)\mathrm{d}W_1(r)}{t} - \frac{S(t)-S(0)}{t}\right) \coloneqq \frac{\Lambda}{(\beta_3+\alpha)} + \varphi_1(t),\end{aligned} \tag{32}$$

so that $\lim_{t\longrightarrow\infty}\varphi_1(t) = 0$.

Additionally, we have

$$\begin{aligned}\langle V(t)\rangle &= \frac{1}{(\beta_6+\alpha)}\left[\beta_3\langle S(t)\rangle - \beta_4\langle V(t)E(t)\rangle - \beta_5\langle V(t)I(t)\rangle + \nu_5\frac{\int_0^t V(r)\mathrm{d}W_5(r)}{t} - \frac{V(t)-V(0)}{t}\right] \\ &\le \frac{\beta_3\langle S(t)\rangle}{(\beta_6+\alpha)} + \frac{1}{(\beta_6+\alpha)}\left(\nu_5\frac{\int_0^t V(r)\mathrm{d}W_5(r)}{t} - \frac{V(t)-V(0)}{t}\right) \\ &\le \frac{\beta_3\Lambda}{(\beta_6+\alpha)(\beta_3+\alpha)} + \frac{\beta_3}{(\beta_6+\alpha)}\varphi_1(t) + \frac{1}{(\beta_6+\alpha)}\left(\nu_5\frac{\int_0^t V(r)\mathrm{d}W_5(r)}{t} - \frac{V(t)-V(0)}{t}\right) \\ &\coloneqq \frac{\beta_3\Lambda}{(\beta_6+\alpha)(\beta_3+\alpha)} + \frac{\beta_3}{(\beta_6+\alpha)}\varphi_1(t) + \varphi_2(t),\end{aligned} \tag{33}$$

where $\lim_{t\longrightarrow\infty}\varphi_2(t) = 0$. Applying *Itô*'s formula to the second equation of system (4) yields

$$\begin{aligned}\mathrm{d}\log(E(t)) = &\left(\beta_4 V(t) + \beta_1 S(t) - \beta_2 I(t) - \left(\kappa+\alpha+\frac{\nu_2^2}{2}\right)\right)\mathrm{d}t \\ &+ \nu_2\mathrm{d}W_2(t).\end{aligned} \tag{34}$$

Integrating equation (34) from 0 to t results in

$$\frac{\log E(t) - \log E(0)}{t} = \beta_4\langle V(t)\rangle + \beta_1\langle S(t)\rangle - \beta_2\langle I(t)\rangle - \left(\kappa+\alpha+\frac{\nu_2^2}{2}\right) + \frac{\nu_2\mathrm{d}W_2(t)}{t}. \tag{35}$$

Then, from (32) and (33), we have

$$\begin{aligned}\frac{\log E(t)}{t}+\beta_2\langle I(t)\rangle &\le \beta_4\left[\frac{\beta_3\Lambda}{(\beta_6+\alpha)(\beta_3+\alpha)}+\frac{\beta_3}{(\beta_6+\alpha)}\varphi_1(t)+\varphi_2(t)\right]\\&+\beta_1\left[\frac{\Lambda}{(\beta_3+\alpha)}+\varphi_1(t)\right]-(\kappa+\alpha)+\frac{\nu_2 dW_2(t)}{t}+\frac{\log E(0)}{t}\\&=\frac{\beta_4\beta_3\Lambda}{(\beta_6+\alpha)(\beta_3+\alpha)}+\frac{\beta_1\Lambda}{(\beta_3+\alpha)}-(\kappa+\alpha)\\&+\left(\frac{\beta_3\beta_4}{\beta_6+\alpha}+\beta_1\right)\varphi_1(t)+\beta_4\varphi_2(t)+\frac{\nu_2 dW_2(t)}{t}+\frac{\log E(0)}{t}\\&:=\frac{\beta_4\beta_3\Lambda}{(\beta_6+\alpha)(\beta_3+\alpha)}+\frac{\beta_1\Lambda}{(\beta_3+\alpha)}-(\kappa+\alpha)+\varphi_3(t),\end{aligned}\tag{36}$$

and $\lim_{t\longrightarrow\infty}\varphi_3(t)=0$ a.s. If $\mathscr{R}_0<1$, from (36),

$$\lim_{t\longrightarrow\infty}\left[\frac{\log E(t)}{t}+\beta_2\langle I(t)\rangle\right]\le\frac{\beta_4\beta_3\Lambda}{(\beta_6+\alpha)(\beta_3+\alpha)}+\frac{\beta_1\Lambda}{(\beta_3+\alpha)}-(\kappa+\alpha)=(\kappa+\alpha)(\mathscr{R}_0-1)<0.\tag{37}$$

Therefore, $\lim_{t\longrightarrow\infty}E(t)=\lim_{t\longrightarrow\infty}I(t)=0$. From model (4), we get

$$\begin{aligned}\mathrm{d}(S(t)+E(t)+I(t)+R(t)+V(t))&=[\Lambda-\alpha(S(t)+E(t)+I(t)+R(t)+V(t))-\mathrm{d}I(t)]\mathrm{d}t\\&+\nu_1 S(t)\mathrm{d}W_1(t)+\nu_2 E(t)\mathrm{d}W_2(t)+\nu_3 I(t)\mathrm{d}W_3(t)+\nu_4 R(t)\mathrm{d}W_4(t)+\nu_5 V(t)\mathrm{d}W_5(t).\end{aligned}\tag{38}$$

Taking integration of (38) from 0 to t, one obtains where

$$\langle S(t)+E(t)+I(t)+R(t)+V(t)\rangle=\frac{\Lambda}{\alpha}+\varphi_4(t),\tag{39}$$

$$\begin{aligned}\varphi_4(t)=\frac{1}{\alpha}\Bigg[&\frac{1}{t}(S(0)+E(0)+I(0)+R(0)+V(0))-\frac{1}{t}(S(t)+E(t)+I(t)+R(t)+V(t))\\&-\mathrm{d}\langle I(t)\rangle+\frac{\nu_1\int_0^t S(r)dW_1(r)}{t}+\frac{\nu_2\int_0^t E(r)\mathrm{d}W_2(r)}{t}\\&+\frac{\nu_3\int_0^t I(r)\mathrm{d}W_3(r)}{t}+\frac{\nu_4\int_0^t R(r)\mathrm{d}W_4(r)}{t}+\frac{\nu_5\int_0^t V(r)\mathrm{d}W_5(r)}{t}\Bigg].\end{aligned}\tag{40}$$

One can easily obtain that $\lim_{t\longrightarrow\infty}\varphi_4(t) = 0$, and since $\lim_{t\longrightarrow\infty}E(t) = \lim_{t\longrightarrow\infty}I(t) = 0$, we have

$$\limsup_{t\longrightarrow\infty}\langle S(t) + E(t) + I(t) + R(t) + V(t)\rangle = \frac{\Lambda}{\alpha}, \tag{41}$$

which implies that $\lim_{t\longrightarrow\infty}(S(t) + R(t) + V(t)) = \Lambda/\alpha = S^+ + R^+ + V^+$, as required; hence, the proof is completed. □

5. Numerical Simulations

In this section, we numerically simulate the solution of the stochastic system (4) using Milstein's higher-order method [35]. The discretization transformation takes the form:

$$\begin{aligned}
S_{j+1} &= S_j + \left[\Lambda - \beta_1 S_j E_j - (\beta_3 + \alpha)S_j\right]h + \nu_1 S_j \xi_{1,j}\sqrt{h} + \frac{\nu_1^2}{2}S_j\left[\xi_{1,j}^2 - 1\right]h,\\
E_{j+1} &= E_j + \left[\beta_4 V_j E_j + \beta_1 S_j E_j - \beta_2 E_j I_{(j-n_1)} - (\kappa + \alpha)E_j\right]h + \nu_2 E_j \xi_{2,j}\sqrt{h} + \frac{\nu_2^2}{2}E_j\left[\xi_{2,j}^2 - 1\right]h,\\
I_{j+1} &= I_j + \left[\beta_5 V_j I_{(j-n_2)} + \beta_2 E_j I_{(j-n_1)} - (d + r + \alpha)I_j\right]h + \nu_3 I_j \xi_{3,j}\sqrt{h} + \frac{\nu_3^2}{2}I_j\left[\xi_{3,j}^2 - 1\right]h,\\
R_{j+1} &= R_j + \left[\beta_6 V_j + rI_{(j-n_3)} + \kappa E_j - \alpha R_j\right]h + \nu_4 R_j \xi_{4,j}\sqrt{h} + \frac{\nu_4^2}{2}R_j\left[\xi_{4,j}^2 - 1\right]h,\\
V_{j+1} &= V_j + \left[\beta_3 S_j - (\beta_6 + \alpha)V_j - \beta_4 V_j E_j - \beta_5 V_j I_{(j-n_2)}\right]h + \nu_5 V_j \xi_{5,j}\sqrt{h} + \frac{\nu_5^2}{2}V_j\left[\xi_{5,j}^2 - 1\right]h,
\end{aligned} \tag{42}$$

where $\xi_{i,j}$, $i = 1, \ldots, 5$ are mutually independent $N(0,1)$ random variables, n_1, n_2, and n_3 are integers such that the time-delays can be expressed in terms of the step-size as $\tau_1 = n_1 h$, $\tau_2 = n_2 h$, and $\tau_3 = n_3 h$. We choose a set of parameters $\Lambda = 0.5, \beta_1 = 0.9905, \beta_2 = 1.9, \beta_3 = 0.6, \beta_4 = 0.928$, $\beta_5 = 1.93$, $\beta_6 = 0.9092$, $\alpha = 0.5$, $\kappa = 0.003$, $d = 0.01$, and $r = 0.001$, with $\tau_1 = \tau_2 = 3$ and $\tau_3 = 4$.

Figure 2 indicates that the system has a unique stationary distribution and the disease is persistent by Theorem 2, such that the intensities of white noise are relatively small where $\widehat{\mathscr{R}}_0 > 1$ with $\nu_i = 0.01, i = 1, \ldots, 5$. In Figure 3, we increase slightly the intensities of white noise to $\nu_1 = 0.09$, $\nu_2 = 0.05$, $\nu_3 = 0.08$, $\nu_4 = 0.09$, and $\nu_5 = 0.1$ with the the same set of parameters as in Figure 2, that is the positive equilibrium is globally asymptotically stable such that the stochastic solution fluctuates around the deterministic steady state value and the disease still persistent. However, we increase the intensities of white noise $\nu_1 = 0.1$, $\nu_2 = 0.5$, and $\nu_3 = \nu_4 = \nu_5 = 0.2$ such that $\widehat{\mathscr{R}}_0 < 1$. Figure 4 implies that the disease will ultimately tend to extinction under the relatively strong white noises $\nu_1 = 0.1, \nu_2 = 0.5, \nu_3 = 0.3, \nu_4 = 0.4$, and $\nu_5 = 0.2$ confirmed by Theorem 3. In Figure 5, we investigate the impact of the transition rate from susceptible into vaccinated class with different values of β_3, which indicates that the number of susceptible, exposed, and infected individuals decrease as β_3 increases, while the recovered individuals increase as β_3 increases, other parameter values are the same as in Figure 2.

Remark 1. Under certain criteria with a large magnitude of white noises, the disease can be eradicated, whereas the small intensity of white noises can preserve a stationary distribution.

5.1. Fitting the DDEs Model to Real Data. To investigate the reality of the deterministic model (2), we fit real data for the number of the confirmed cases of COVID-19 in the UAE during June 22, 2021, to August 11, 2021 [36] with model (2) using least-square approach [37, 38].

Given a set of real data in Table 1 and a mathematical model (2), the objective function (weighted least squares function) is as follows:

$$\Phi_H(p) = \sum_{i=1}^{5}\sum_{j=1}^{M}\left[x^i(t_j, p) - X_j^i\right]^2 h_{ij}. \tag{43}$$

Here, $x^i, i = 1, \ldots, 5$ represents the variables S, E, I, R, V; p is the model parameter to be estimated. Thus, we then try to attain the optimum parameter $\widehat{p}$ that satisfies $\Phi(\widehat{p}) \leq \min_p \Phi(p) \equiv \max_p \mathscr{L}(p)$, where $\mathscr{L}(p)$ is the likelihood function [37, 38]. However, the estimation of the parameters that appear in the undisturbed model (2) is considered as an optimization problem. Herein, the data are scaled in ten thousands.

Parameters estimates are $\widehat{\beta}_2 = 1.99854$, $\widehat{\beta}_5 = 1.9813$, $\widehat{\beta}_6 = 0.219092$, $\widehat{\kappa} = 0.01099$, and $\widehat{r} = 0.047$; therefore, $\widehat{\mathscr{R}}_0 = 1.54 > 1$, see Figure 6; while Figure 7 illustrates the

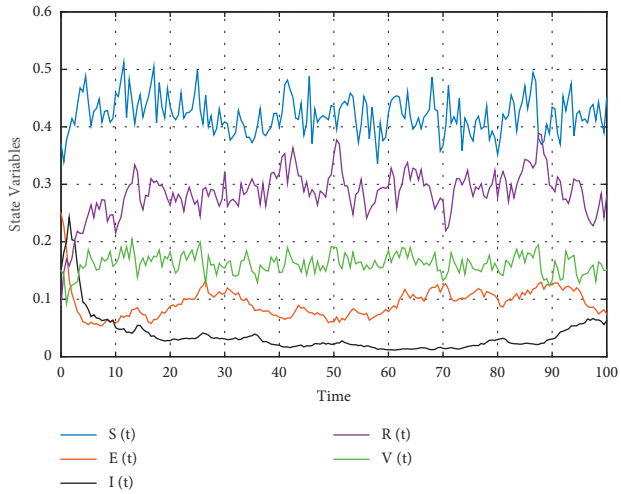

FIGURE 2: Numerical simulations of model (4), which shows that model (4) has a unique ergodic stationary distribution where the disease is persistent and $\widehat{\mathcal{R}}_0 > 1$ with $\nu_i = 0.01$, $i = 1, \ldots, 5$.

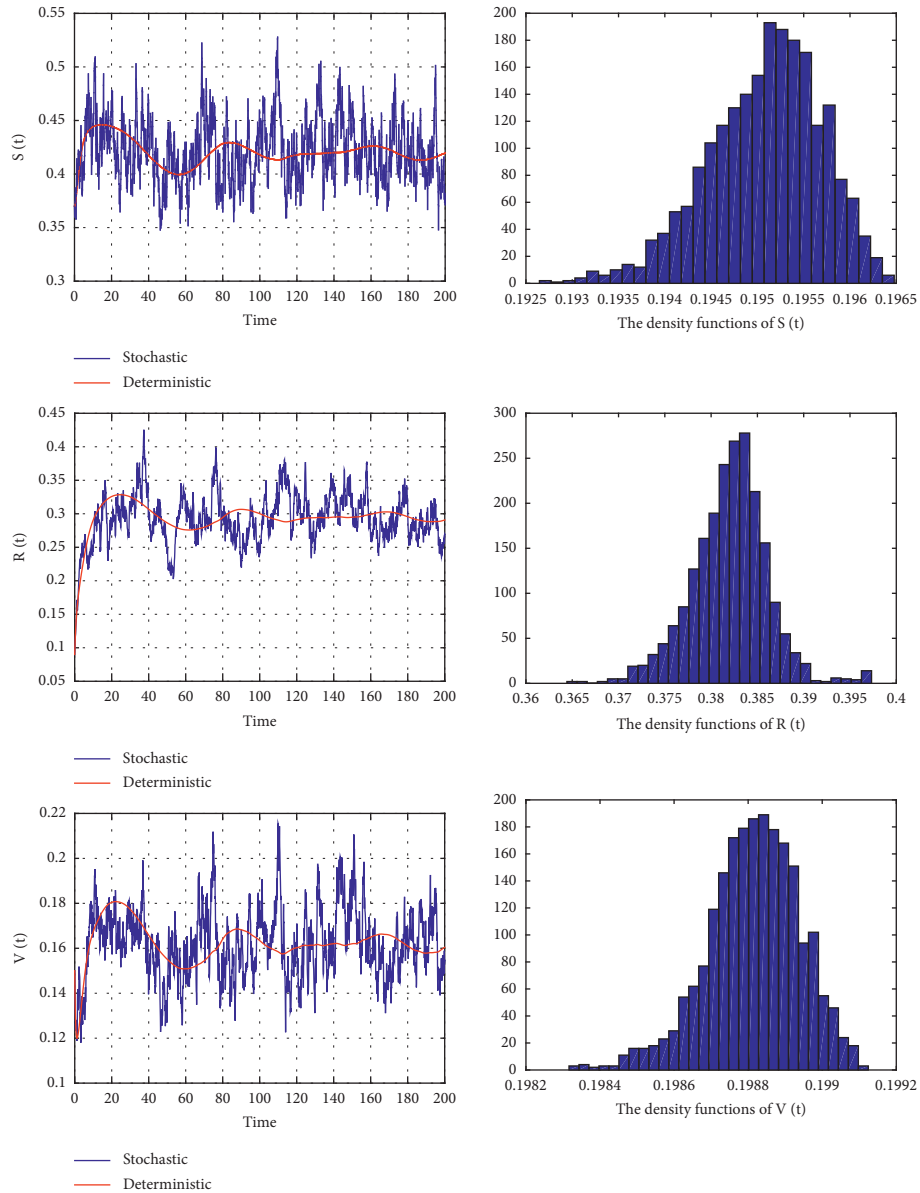

FIGURE 3: The solutions of the stochastic system (4) and the undisturbed system (2) left banners such that $\widehat{\mathcal{R}}_0 > 1$. While right banners show the density function diagram of $S(t)$, $R(t)$, and $V(t)$.

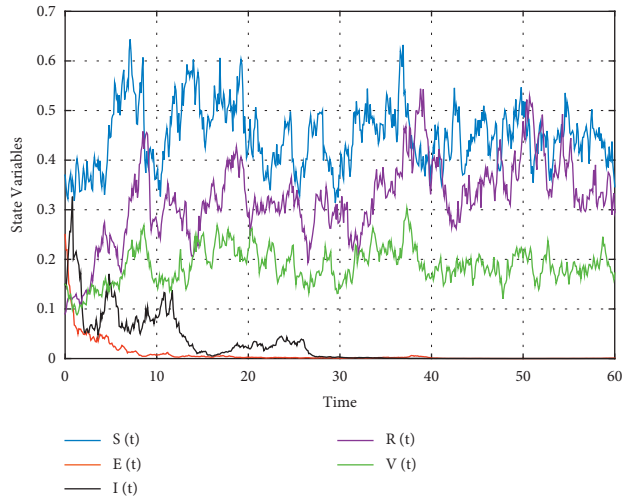

Figure 4: Numerical simulations of model (4) shows that the disease dies out when the white noise is relatively large such that $\widehat{\mathcal{R}}_0 < 1$.

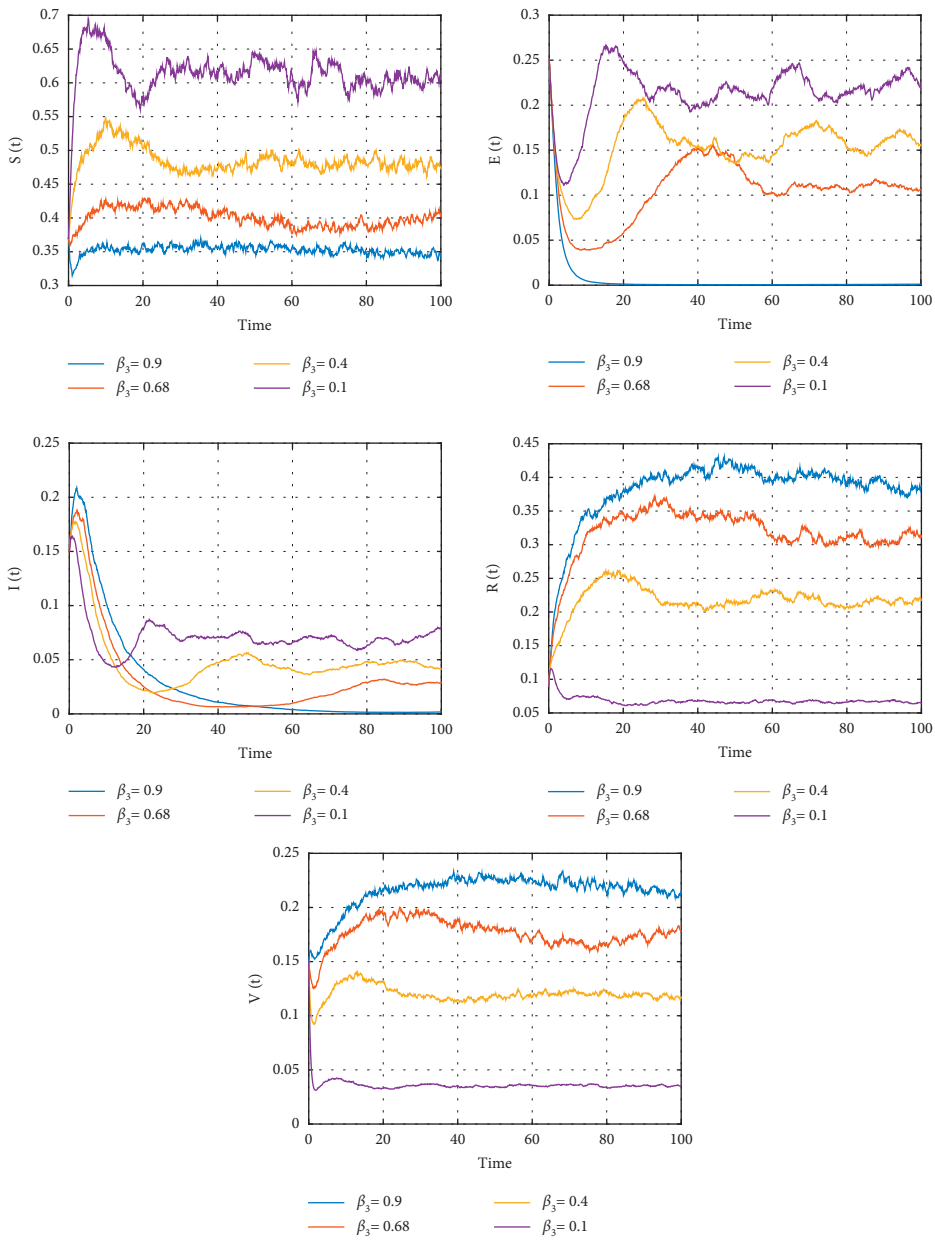

Figure 5: The impact of the transition rate from susceptible into vaccinated class with different values of β_3, which indicates that the number of susceptible, exposed, and infected individuals decrease as β_3 increases, while the recovered individuals increase as β_3 increases.

Table 1: Number of recorded COVID-19 cases in the UAE, from June 21, 2021, to August 11, 2021 [36].

Time (days)	June 21	June 22	June 23	June 24	June 25	June 26	June 27
Infected cases	1,850	1,964	2,167	1,988	2,161	2,223	2,282
Time (days)	June 28	June 29	June 30	July 1	July 2	July 3	July 4
Infected cases	2,122	1,747	1,675	1,663	1,632	1,599	1,573
Time (days)	July 5	July 6	July 7	July 8	July 9	July 10	July 11
Infected cases	1,552	1,513	2,04	2,184	1,539	1,529	1,52
Time (days)	July 12	July 13	July 14	July 15	July 16	July 17	July 18
Infected cases	1,518	1,542	1,522	1,529	1,508	1,541	1,506
Time (days)	July 19	July 20	July 21	July 22	July 23	July 24	July 25
Infected cases	1,547	1,521	1,507	1,529	1,549	1,539	1,55
Time (days)	July 26	July 27	July 28	July 29	July 30	July 31	August 1
Infected cases	1,52	1,537	1,519	1,537	1,548	1,52	1,537
Time (days)	August 2	August 3	August 4	August 5	August 6	August 7	August 8
Infected cases	1,519	1,537	1,548	1,519	1,508	1,52	1,545
Time (days)	August 9	August 10	August 11				
Infected cases	1,41	1,321	1,334				

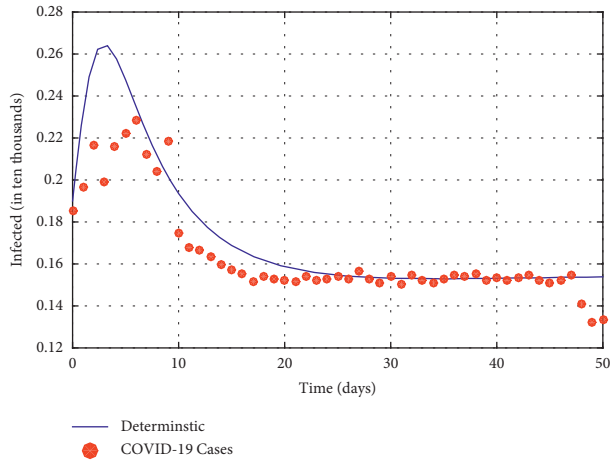

Figure 6: The fitted curve of DDEs model (2) and the confirmed COVID-19 cases in the UAE from June 22, 2021 to August 11, 2021. The estimated parameters are $\widehat{\beta}_2 = 1.99854$, $\widehat{\beta}_5 = 1.9813$, $\widehat{\beta}_6 = 0.219092$, $\widehat{\kappa} = 0.01099$, and $\widehat{r} = 0.047$.

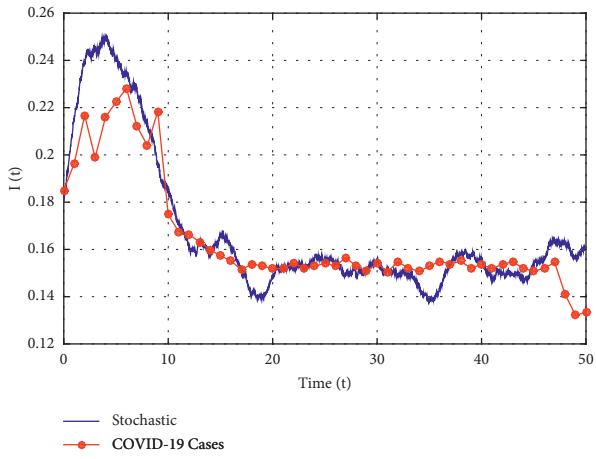

Figure 7: The response of the stochastic model (4) with the estimated parameters $\widehat{\beta}_2 = 1.99854$, $\widehat{\beta}_5 = 1.9813$, $\widehat{\beta}_6 = 0.219092$, $\widehat{\kappa} = 0.01099$, and $\widehat{r} = 0.047$, such that the intensities of white noises are $\nu_1 = 0.03$, $\nu_2 = 0.02$, $\nu_3 = 0.02$, $\nu_4 = 0.04$, and $\nu_5 = 0.04$.

response of the stochastic model (4) with the estimated parameters; therefore, the stochastic fluctuations enhance the consistency of the model with the real data.

The steps of parameter estimations are summarized as follows:

(1) Guess an initial parameter estimate p_0;

(2) We then solve the system using a deterministic model (2) using the current parameters;

(3) A minimization routine, such as OPTIMTOOL in Matlab, is then used to adjust the parameter values;

(4) When the value $\Phi(p)$ cannot be further reduced, the best fit parameter values have been determined;

(5) Determine if the chosen set of parameters is acceptable or not.

6. Concluding Remarks

In this paper, we extended the classical SEIR epidemic model to include vaccination and time-delays that incorporate randomness into the equations by including white noise perturbations on some parameters. The model has been examined by fitting to real observations in UAE, during June 22, 2021, to August 11, 2021. The study found that disease extinction is more likely if the noise intensity is high, and this

can be used to develop some effective control strategies. Biological systems models should include random influences as they deal with real-life subsystems, which cannot be adequately isolated from factors outside the system. The addition of white noise and time-delays adds complexity to the model and enriches its dynamics.

Our conclusions are as follows.

(i) When the intensity of white noise is relatively low, the disease will persist as long as $\widehat{\mathcal{R}}_0 > 1$ (see Figures 2 and 3) and will die out with greater white noise; see Figure 4.

(ii) The stochastic fluctuations improve the consistency of the model with the real data; see Figure 7.

(iii) It is shown that the disease can be controlled efficiently if the level of vaccination is increased. Therefore, as β_3 is increased, the solution of model (4) fluctuates around the disease-free equilibrium.

(iv) If the stochastic perturbations $\nu_i = 0$, $i = 1, \ldots, 5$, then, the threshold of the stochastic model (4) can be reduced to that of the deterministic counterpart. Therefore, $\widehat{\mathcal{R}}_0 > 1$ is a generalized result indicating the persistence of the disease.

(v) Using mathematical models to develop, manufacture, and deliver vaccines is more efficient and results in safer and more efficient vaccines.

Future research will focus on stochastic epidemic models with Markovian switching and time-delays.

Data Availability

The authors confirm that the data supporting the findings of this study are available within the article.

Conflicts of Interest

The authors declare no conflicts of interest.

Acknowledgments

This research was funded by the UAEU-ZU Joint Research, fund # 12S107- 2022.

References

[1] F. A. Rihan and H. J. Alsakaji, "Dynamics of a stochastic delay differential model for covid-19 infection with asymptomatic infected and interacting people: case study in the uae," *Results in Physics*, vol. 28, p. 104658, 2021.

[2] A. Din, Y. Li, T. Khan, and G. Zaman, "Mathematical analysis of spread and control of the novel corona virus (covid-19) in China," *Chaos, Solitons & Fractals*, vol. 141, p. 110286, 2020.

[3] J. Wang, G. Huang, Y. Takeuchi, and S. Liu, "SVEIR epidemiological model with varying infectivity and distributed delays," *Mathematical Biosciences and Engineering*, vol. 8, no. 3, p. 875, 2011.

[4] O. Chiekezi Zephaniah, U.-I. Ruth Nwaugonma, I. Simeon Chioma, and O. Adrew, "A mathematical model and analysis of an SVEIR model for streptococcus pneumonia with saturated incidence force of infection," *Mathematical Modelling and Applications*, vol. 5, no. 1, pp. 16–38, 2020.

[5] F. Andre, R. Booy, H. Bock et al., "Vaccination greatly reduces disease, disability, death and inequity worldwide," *Bulletin of the World Health Organization*, vol. 86, no. 2, pp. 140–146, 2008.

[6] R. M. Anderson, C. Vegvari, J. Truscott, and B. S. Collyer, "Challenges in creating herd immunity to sars-cov-2 infection by mass vaccination," *The Lancet*, vol. 396, no. 10263, pp. 1614–1616, 2020.

[7] National Center for Immunization and Respiratory Diseases, "COVID-19 vaccination clinical & professional resources," 2021, https://www.cdc.gov/coronavirus/2019-ncov/vaccines/different-vaccines.html.

[8] Who, "Tracking SARS-CoV-2 variants," 2021, https://www.who.int/en/activities/tracking-SARS-CoV-2-variants/.

[9] P. Wang, M. S. Nair, L. Liu et al., "Antibody resistance of sars-cov-2 variants b. 1.351 and b. 1.1. 7," *Nature*, vol. 593, pp. 1–6, 2021.

[10] A. S. Lauring and E. B. Hodcroft, "Genetic variants of SARS-CoV-2-what do they mean?" *JAMA*, 2021.

[11] UNICEF, "What we know about the Omicron variant," 2021, https://www.unicef.org/coronavirus/what-we-know-about-omicron-variant.

[12] The New York Times, "Tracking coronavirus vaccinations around the world," 2021, https://www.nytimes.com/interactive/2021/world/covid-vaccinations-tracker.html.

[13] A. Singanayagam, S. Hakki, J. Dunning et al., "Community Transmission and Viral Load Kinetics of the Sars-Cov-2 delta (B. 1.617. 2) Variant in Vaccinated and Unvaccinated Individuals in the uk: A Prospective, Longitudinal, Cohort Study," *The Lancet Infectious Diseases*, vol. 22, no. 2, pp. 183–195, 2021.

[14] Our World, "Data. Coronavirus (COVID-19) vaccinations," 2021, https://ourworldindata.org/covid-vaccinations?country= ARE.

[15] A. L. Costa, M. A. Pires, R. L. Resque, and S. Almeida, "Mathematical modeling of the infec-tious diseases: key concepts and applications," *Journal of Infectious Diseases and Epidemiology*, vol. 7, p. 209, 2021.

[16] O. Diekmann, H. Heesterbeek, and T. Britton, *Mathematical Tools for Understanding Infectious Disease Dynamics*, Princeton University Press, Princeton, New Jersey, 2012.

[17] A. Nabti and B. Ghanbari, "Global stability analysis of a fractional SVEIR epidemic model," *Mathematical Methods in the Applied Sciences*, vol. 44, no. 11, pp. 8577–8597, 2021.

[18] S. A. Rella, Y. A. Kulikova, E. T. Dermitzakis, and F. A. Kondrashov, "Rates of SARS-CoV-2 transmission and vaccination impact the fate of vaccine-resistant strains," *Scientific Reports*, vol. 11, no. 1, pp. 1–10, 2021.

[19] Q. Liu and D. Jiang, "Stationary distribution and extinction of a stochastic SIR model with nonlinear perturbation," *Applied Mathematics Letters*, vol. 73, pp. 8–15, 2017.

[20] C. Ji, "The stationary distribution of hepatitis B virus with stochastic perturbation," *Applied Mathematics Letters*, vol. 100, p. 106017, 2020.

[21] F. A. Rihan, H. J. Alsakaji, and C. Rajivganthi, "Stability and hopf bifurcation of three-species prey-predator system with time delays and allee effect," *Complexity*, vol. 2020, no. 1, pp. 1–15, Article ID 7306412, 2020.

[22] N. S. Goel and N. Richter-Dyn, *Stochastic Models in Biology*, Academic Press, Cambridge, Massachusetts, 1974.

[23] M. S. Ali, M. Usha, Q. Zhu, and S. Shanmugam, "Synchronization analysis for stochastic ts fuzzy complex networks

with Markovian jumping parameters and mixed time-varying delays via impulsive control," *Mathematical Problems in Engineering*, vol. 2020, Article ID 9739876, 27 pages, 2020.

[24] F. A. Rihan, *Delay Differential Equations and Applications to Biology*, Springer, Heidelberg, Germany, 2021.

[25] X. Luo, N. Shao, J. Cheng, and W. Chen, "Modeling the trend of outbreak of covid-19 in the diamond princess cruise ship based on a time-delay dynamic system," *Mathematical Modeling and Its Applications*, vol. 9, pp. 15–22, 2020.

[26] S. Feng, Z. Feng, C. Ling, C. Chang, and Z. Feng, "Prediction of the covid-19 epidemic trends based on seir and ai models," *PLoS One*, vol. 16, no. 1, p. e0245101, 2021.

[27] L. Lo'pez and X. Rodo, "A modified SEIR model to predict the COVID-19 outbreak in Spain and Italy: simulating control scenarios and multi-scale epidemics," *Results in Physics*, vol. 21, p. 103746, 2021.

[28] W. Ahmad, M. Abbas, M. Rafiq, and D. Baleanu, "Mathematical analysis for the effect of voluntary vaccination on the propagation of corona virus pandemic," *Results in Physics*, vol. 31, p. 104917, 2021.

[29] P. L. Delamater, E. J. Street, T. F. Leslie, Y. T. Yang, and K. H. Jacobsen, "Complexity of the basic reproduction number (R0)," *Emerging Infectious Diseases*, vol. 25, no. 1, pp. 1–4, 2019.

[30] K. Hattaf, M. Mahrouf, J. Adnani, and N. Yousfi, "Qualitative analysis of a stochastic epidemic model with specific functional response and temporary immunity," *Physica A: Statistical Mechanics and Its Applications*, vol. 490, pp. 591–600, 2018.

[31] X. Zhang and H. Peng, "Stationary distribution of a stochastic cholera epidemic model with vaccination under regime switching," *Applied Mathematics Letters*, vol. 102, p. 106095, 2020.

[32] Y. Zhao and D. Jiang, "The threshold of a stochastic SIS epidemic model with vaccination," *Applied Mathematics and Computation*, vol. 243, pp. 718–727, 2014.

[33] F. A. Rihan and H. J. Alsakaji, "Stochastic Delay Differential Equations of Three-Species Prey-Predator System with Cooperation Among Prey Species," *Discrete & Continuous Dynamical Systems-S*, vol. 15, p. 245, 2020.

[34] R. Z. Hasminskii, *Stochastic Stability of Differential Equations*, Springer, Heidelberg, Germany, 1980.

[35] E. Buckwar, "Introduction to the numerical analysis of stochastic delay differential equations," *Journal of Computational and Applied Mathematics*, vol. 125, no. 1-2, pp. 297–307, 2000.

[36] Who, "The current COVID-19 situation in the UAE," 2021, https://www.who.int/countries/are/.

[37] Y. Bard, *Nonlinear Parameter Estimation*, New York Academic Press, Cambridge, Massachusetts, 1974.

[38] F. A. Rihan, A. A. Azamov, and H. J. Al-Sakaji, "An inverse problem for delay differential equations: parameter estimation, nonlinearity, sensitivity," *Applied Mathematics & Information Sciences*, vol. 12, no. 1, pp. 63–74, 2018.

Hindawi
Complexity
Volume 2022, Article ID 8705388, 9 pages
https://doi.org/10.1155/2022/8705388

Research Article

Solitary Wave Solutions of Conformable Time Fractional Equations Using Modified Simplest Equation Method

Waseem Razzaq,[1] Mustafa Habib,[2] Muhammad Nadeem,[3] Asim Zafar,[4] Ilyas Khan,[5] and Patrick Kandege Mwanakatwea[6]

[1]*Math Center, House No 87 Rahmanyia Colony, Vehari, Pakistan*
[2]*Department of Mathematics, University of Engineering and Technology, Lahore, Pakistan*
[3]*Faculty of Science, Yibin University, Yibin 644000, China*
[4]*Department of Mathematics, Vehari Campus, Multan, Pakistan*
[5]*Department of Mathematics, Al-Zulfi, Majmmah University, Al-Majmmah 11952, Saudi Arabia*
[6]*Eastern Africa Statistical Training Center, Dar es Salaam, Tanzania*

Correspondence should be addressed to Patrick Kandege Mwanakatwea; patrick26573@yahoo.co.uk

Received 1 February 2022; Revised 2 March 2022; Accepted 9 March 2022; Published 22 April 2022

Academic Editor: C. Rajivganthi

This study presents a modified simplest equation method (MSEM) to investigate some real and exact solutions of conformable time fractional Benjamin-Bona-Mahony (BBM) equation and Chan-Hilliard (CH) equation. We use traveling wave transformation to obtain the results in the form of series solution. Some calculations are performed through Mathematica software to analyze the accuracy of this approach. Graphical representations are reported for more significant results at different fractional-order which demonstrates that this approach is very simple, adequate, and legitimate.

1. Introduction

Various applications of applied mathematics in the form of partial differential equations (PDEs) play important role with derivative and integral of arbitrary orders. Fractional differential equations (FDEs) are used for modeling in various fields of sciences such as physics, chemistry, mathematics, biology, engineering, fluid dynamics, and other physical phenomena [1–4]. So, they have gained much attention of many scholar. The exact/analytical solutions of these PDEs are ideal. Therefore, a lot of scholars have paid much attentions to acquire the solutions of these kinds of FDEs with the help of various numerical and analytical methods. Mainly, a wave transformation is used to transform the FDEs into a nonlinear ordinary differential equation, which leads for further exact solution. A lot of significant approaches have been generated and applied to search exact solutions in different research articles including Lie symmetry analysis method [5–8], the differential transform method [9], the iteration method [10, 11], the (G'/G)-expansion method [12], homotopy analysis method [13], Adomian decomposition method [14], homotopy perturbation method [15], the functional variable method [16], the first integral method [1], modified Kudryashov method [17], $(G'/G, 1/G)$-expansion [18], and improved G'/G-expansion method [19]. Very recently, Wang presented a new idea on the fractal theory of nonlinear system to find the solitary wave solutions which show the promising results [20–22]. A full detail of conformable time fractional equations has been explained in [23, 24].

In this work, we will go over the conformable time fractional BBM and nonlinear space-time fractional CH equation. Many inquirer quaere the exact solutions of these equations by applying different approaches in the past [25–27]. Some recent developments in time fractional equations developments can be studied through He's fractional derivative and the two-scale fractal derivative [28, 29]. We discussed some of their investigations here. They used fractional exp-function method to

construct the exact solutions for the conformable time fractional Benjamin-Bona-Mahony equation and conformable time fractional Chan-Hilliard equation. The scheme of this paper is as follows: in Section 2, we will briefly discuss some basic properties of conformable fractional derivative. In Section 3, we present the description of simplest equation method. Two examples of conformable time fractional BBM and CH have been tested in Section 4 to verify this approach and conclusion is discussed in Section 5.

2. Conformable Fractional Derivative

In this part, we shortly explain the definition and properties of conformable fractional derivatives [30–33].

Definition: let f: $(0,\infty) \longrightarrow \mathbb{R}$ be a function. Then, the conformable fractional derivative of f for order δ is defined as

$$T_\delta(f(t)) = \lim_{\varepsilon \longrightarrow 0} \frac{f\left(t + \varepsilon t^{1-\delta}\right) - f(t)}{\varepsilon}, \quad \forall t > 0, \delta \in (0,1). \tag{1}$$

Assuming the conformable fractional derivative on f regarding order δ, then we can say f is δ-differentiable.

Properties: let f and g be δ-differentiable at a value $t > 0$, then the conformable fractional derivative has some useful properties as follows:

(1) $T_\delta(af + bg) = aT_\delta(f) + bT_\delta(g)$, for all $a, b \in \mathbb{R}$
(2) $T_\delta(fg) = fT\delta(g) + gT_\delta(f)$
(3) $T_\delta(t^\mu) = \mu t^{\mu-\delta}$, for all $\mu \in \mathbb{R}$
(4) $T_\delta(\lambda) = 0$, where λ is constant
(5) $T_\delta(f/g) = gT_\delta(f) - fT_\delta(g)/g^2$
(6) If f is differentiable, then $T_\delta(f(t)) = t^{1-\delta}\mathrm{d}f(t)/\mathrm{d}t$

This definition also satisfies the chain rule as follows.

Let f, g: $[0,\infty) \longrightarrow \mathbb{R}$ be an δ-differentiable function and $\delta \in (0,1)$. Then, the following rule is defined.

$$T_\delta\left(f^\circ g(t)\right) = t^{1-\delta} g'(t) f'(g(t)). \tag{2}$$

3. Description of the Modified Simplest Equation Method (MSEM)

Consider the following nonlinear PDE in the form time fractional

$$F\left(u, D_t^\delta \vartheta, \vartheta_{x^i}, \vartheta_{x^i,x^j}, \vartheta_{x^i,x^j,x^k}, \ldots\right) = 0, \tag{3}$$

where D_t^δ is known as conformable fractional derivative and $\delta \in (0,1)$. (3) has $n+1$ independent variables $x = (x^1, x^2, \ldots, x^n)$ and dependent variable $\vartheta = \vartheta(x,t)$, where

$$\vartheta_{x^i} = \frac{\partial \vartheta}{\partial x^i}, \vartheta_{x^i,x^j} = \frac{\partial^2 \vartheta}{\partial x^i \partial x^j}, \vartheta_{x^i,x^j,x^k} = \frac{\partial^3 \vartheta}{\partial x^i \partial x^j \partial x^k}, \ldots \tag{4}$$

We will execute MSEM to provide particular results of (3). Over here, we summarize the fundamental points of MSEM.

Step 1. Employing the fractional traveling wave transform,

$$\vartheta(x,t) = V(\mathfrak{F}), \mathfrak{F} = \sum_{i=1}^{n} k_i \frac{x^\delta}{\delta} - l\frac{t^\delta}{\delta}, \tag{5}$$

where k, l are nonzero constants; we can rewrite (3) as the following nonlinear ODE:

$$N\left(V, lV_{\mathfrak{F}}, kV_{\mathfrak{F}\mathfrak{F}}, \ldots\right) = 0, \tag{6}$$

where $V = (\mathrm{d}V/\mathrm{d}\mathfrak{F}), V_{\mathfrak{F}\mathfrak{F}} = (\mathrm{d}V^2/\mathrm{d}\mathfrak{F}^2), \ldots$

Step 2. Consider the solution of equation (6) in the following form:

$$V(\mathfrak{F}) = \sum_{i=1}^{m} a_i \phi^i(\mathfrak{F}), \tag{7}$$

where $a_i (i = 1, 2, \ldots, m)$ are constants and $a_m \neq 0$, whereas $\phi(\mathfrak{F})$ conforms to some ordinary differential equations. Now, consider the Riccati equations such as

$$\phi'(\mathfrak{F}) = \phi^2(\mathfrak{F}) + \varrho, \tag{8}$$

where ϱ is an arbitrary constant and prime represents the differentiation according to $\mathfrak{F}$. We can dissolve the solution of (8) in the following possible ways:

If $\varrho < 0$, then

$$\phi(\mathfrak{F}) = -\sqrt{-\varrho}\tanh\sqrt{-\varrho}\mathfrak{F}, \tag{9}$$

$$\phi(\mathfrak{F}) = -\sqrt{-\varrho}\coth\sqrt{-\varrho}\mathfrak{F}, \tag{10}$$

$$\phi(\mathfrak{F}) = \sqrt{-\varrho}\left(-\tanh\left(2\sqrt{-\varrho}\,\mathfrak{F}\right) \pm i\,\mathrm{sech}\left(2\sqrt{-\varrho}\,\mathfrak{F}\right)\right), \tag{11}$$

$$\phi(\mathfrak{F}) = -\frac{\sqrt{-\varrho}}{2}\left(\tanh\left(\frac{\sqrt{-\varrho}}{2}\mathfrak{F}\right) + \coth\left(\frac{\sqrt{-\varrho}}{2}\mathfrak{F}\right)\right). \tag{12}$$

If $\varrho > 0$, then

$$\phi(\mathfrak{F}) = \sqrt{\varrho}\tan\sqrt{\varrho}\mathfrak{F}, \tag{13}$$

$$\phi(\mathfrak{F}) = -\sqrt{\varrho}\cot\sqrt{\varrho}\mathfrak{F}, \tag{14}$$

$$\phi(\mathfrak{F}) = \sqrt{\varrho}\left(\tan\left(2\sqrt{\varrho}\,\mathfrak{F}\right) \pm \sec\left(2\sqrt{\varrho}\,\mathfrak{F}\right)\right), \tag{15}$$

$$\phi(\mathfrak{F}) = \sqrt{\varrho}\left(-\cot\left(2\sqrt{\varrho}\,\mathfrak{F}\right) \pm \csc\left(2\sqrt{\varrho}\,\mathfrak{F}\right)\right), \tag{16}$$

$$\phi(\mathfrak{F}) = \frac{\sqrt{\varrho}}{2}\left(\tan\left(\frac{\sqrt{\varrho}}{2}\mathfrak{F}\right) - \cot\left(\frac{\sqrt{\varrho}}{2}\mathfrak{F}\right)\right), \tag{17}$$

If $\varrho = 0$, then

$$\phi(\mathfrak{F}) = -\frac{1}{\mathfrak{F}}. \tag{18}$$

Step 3. After substituting equations (7) and (8) into (6), and setting all the coefficients of ϕ^i to zero, we can get the system of algebraic equations in terms of a_i, k, l, which leads to a very simple solution.

Step 4. The obtained values of a_i, k, l from Step 2 can be used in equation (5) to achieve the traveling wave solutions of equation (3).

Remarks. The results in equation (9) or (10) are referred to as the solitary wave solutions and the results in equation (13) or (14) are considered to be periodic function solutions, whereas the result in equation (18) is termed as rational function solution.

4. Applications of MSEM

In this section, MSEM is applied to compute the solitary wave solutions of conformable time fractional differential BBM and CH equation.

4.1. Example 1. Consider the conformable time fractional differential BBM equation:

$$D_t^{\delta}\vartheta - \nu\vartheta^2\vartheta_x + \vartheta_x + \vartheta_{xxx} = 0, \tag{19}$$

where δ is a parameter representing the order of the fractional time derivative. When $\delta = 1$, equation (19) is called classical Benjamin-Bona-Mahony equation. We used a new proposed simplest equation method and applied it on the conformable time fractional differential Benjamin-Bona-Mahony equation for obtaining the exact solutions.

By using the transformation,

$$\vartheta(x,t) = V(\mathfrak{F}), \quad \mathfrak{F} = kx - l\frac{t^{\delta}}{\delta}. \tag{20}$$

Equation (19) can be reduced to the following nonlinear ODE:

$$(k-l)V' - \nu k V' V^2 + k^3 V''' = 0. \tag{21}$$

Balancing V''' and $V'V^2$ in equation (22), then we drive $m = 1$.

$$V(\mathfrak{F}) = a_1\phi(\mathfrak{F}) + a_0. \tag{22}$$

Putting equation (22) into (21) and using some mathematical operations, we obtained an algebraic system. Solving this system for different value of a_0, a_1, k, l results in the following.

Case 1.

$$\begin{aligned} a_0 &= 0, \\ a_1 &= -\frac{\sqrt{6}k}{\sqrt{\nu}}, \quad l = 2k^3\varrho + k, \end{aligned} \tag{23}$$

where $\varrho < 0$. Therefore, we obtain the following solitary wave solution for the equation:

$$\vartheta(x,t) = -\frac{(\sqrt{6}\,k)\left(-\sqrt{-\varrho}\tanh\left(\sqrt{-\varrho}\left(kx - \left(k - 2k^3\varrho\right)\left(t^{\delta}/\delta\right)\right)\right)\right)}{\sqrt{\nu}}, \tag{24}$$

$$\vartheta(x,t) = -\frac{(\sqrt{6}\,k)\left(-\sqrt{-\varrho}\coth\left(\sqrt{-\varrho}\left(kx - \left(k - 2k^3\varrho\right)\left(t^{\delta}/\delta\right)\right)\right)\right)}{\sqrt{\nu}}, \tag{25}$$

$$\vartheta(x,t) = -\frac{\sqrt{6}k}{\sqrt{\nu}}\left[\sqrt{-\varrho}\,\left(-\tanh\left(2\sqrt{-\varrho}\,\mathfrak{F}\right) \pm i\,\mathrm{sech}\left(2\sqrt{-\varrho}\,\mathfrak{F}\right)\right)\right], \tag{26}$$

$$\vartheta(x,t) = -\frac{\sqrt{6}k}{\sqrt{\nu}}\left[-\frac{\sqrt{-\varrho}}{2}\left(\tanh\left(\frac{\sqrt{-\varrho}}{2}\mathfrak{F}\right) + \coth\left(\frac{\sqrt{-\varrho}}{2}\mathfrak{F}\right)\right)\right], \tag{27}$$

where $\varrho > 0$. Therefore, we obtain the following periodic function solution for the equation:

$$\vartheta(x,t) = -\frac{(\sqrt{6}\,k)\left(\sqrt{\varrho}\,\tan\left(\sqrt{\varrho}\left(kx - \left(2k^3\varrho + k\right)\left(t^{\delta}/\delta\right)\right)\right)\right)}{\sqrt{\nu}}, \tag{28}$$

$$\vartheta(x,t) = -\frac{(\sqrt{6}\,k)\left(-\sqrt{\varrho}\,\cot\left(\sqrt{\varrho}\left(kx - \left(2k^3\varrho + k\right)\left(t^{\delta}/\delta\right)\right)\right)\right)}{\sqrt{\nu}}, \tag{29}$$

$$\vartheta(x,t) = -\frac{\sqrt{6}k}{\sqrt{\nu}}\left[\sqrt{\varrho}\,\left(\tan\left(2\sqrt{\varrho}\,\mathfrak{F}\right) \pm \sec\left(2\sqrt{\varrho}\,\mathfrak{F}\right)\right)\right], \tag{30}$$

$$\vartheta(x,t) = -\frac{\sqrt{6}k}{\sqrt{\nu}}\left[\sqrt{\varrho}\,\left(-\cot\left(2\sqrt{\varrho}\,\mathfrak{F}\right) \pm \csc\left(2\sqrt{\varrho}\,\mathfrak{F}\right)\right)\right], \tag{31}$$

$$\vartheta(x,t) = -\frac{\sqrt{6}k}{\sqrt{\nu}}\left[\frac{\sqrt{\varrho}}{2}\left(\tan\left(\frac{\sqrt{\varrho}}{2}\mathfrak{F}\right) - \cot\left(\frac{\sqrt{\varrho}}{2}\mathfrak{F}\right)\right)\right]. \tag{32}$$

If $\varrho = 0$,

$$\vartheta(x,t) = -\frac{\sqrt{6}k}{\sqrt{\nu}}\left(-\frac{1}{\mathfrak{F}}\right). \tag{33}$$

Case 2.

$$\begin{aligned} a_0 &= 0, \\ a_1 &= \frac{\sqrt{6}k}{\sqrt{\nu}}, \quad l = 2k^3\varrho + k, \end{aligned} \tag{34}$$

where $\varrho < 0$. Therefore, we obtain the following solitary wave solution for the equation:

$$\vartheta(x,t)=\frac{(\sqrt{6}\,k)\left(-\sqrt{-\varrho}\tanh\left(\sqrt{-\varrho}\left(kx-\left(k-2k^3\varrho\right)\left(t^\delta/\delta\right)\right)\right)\right)}{\sqrt{\nu}},$$

$$\vartheta(x,t)=\frac{(\sqrt{6}\,k)\left(-\sqrt{-\varrho}\coth\left(\sqrt{-\varrho}\left(kx-\left(k-2k^3\varrho\right)\left(t^\delta/\delta\right)\right)\right)\right)}{\sqrt{\nu}},$$

$$\vartheta(x,t)=\frac{\sqrt{6}k}{\sqrt{\nu}}\left[\sqrt{-\varrho}\left(-\tanh\left(2\sqrt{-\varrho}\,\mathfrak{F}\right)\pm i\operatorname{sech}\left(2\sqrt{-\varrho}\,\mathfrak{F}\right)\right)\right],$$

$$\vartheta(x,t)=\frac{\sqrt{6}k}{\sqrt{\nu}}\left[-\frac{\sqrt{-\varrho}}{2}\left(\tanh\left(\frac{\sqrt{-\varrho}}{2}\mathfrak{F}\right)+\coth\left(\frac{\sqrt{-\varrho}}{2}\mathfrak{F}\right)\right)\right].\tag{35}$$

Thus, we can obtain the following periodic function solution for the equation:

$$\vartheta(x,t)=\frac{(\sqrt{6}\,k)\left(\sqrt{\varrho}\tan\left(\sqrt{\varrho}\left(kx-\left(2k^3\varrho+k\right)\left(t^\delta/\delta\right)\right)\right)\right)}{\sqrt{\nu}},$$

$$\vartheta(x,t)=\frac{(\sqrt{6}\,k)\left(-\sqrt{\varrho}\cot\left(\sqrt{\varrho}\left(kx-\left(2k^3\varrho+k\right)\left(t^\delta/\delta\right)\right)\right)\right)}{\sqrt{\nu}},$$

$$\vartheta(x,t)=\frac{\sqrt{6}k}{\sqrt{\nu}}\left[\sqrt{\varrho}\left(\tan\left(2\sqrt{\varrho}\,\mathfrak{F}\right)\pm\sec\left(2\sqrt{\varrho}\,\mathfrak{F}\right)\right)\right],$$

$$\vartheta(x,t)=\frac{\sqrt{6}k}{\sqrt{\nu}}\left[\sqrt{\varrho}\left(-\cot\left(2\sqrt{\varrho}\,\mathfrak{F}\right)\pm\csc\left(2\sqrt{\varrho}\,\mathfrak{F}\right)\right)\right],$$

$$\vartheta(x,t)=\frac{\sqrt{6}k}{\sqrt{\nu}}\left[\frac{\sqrt{\varrho}}{2}\left(\tan\left(\frac{\sqrt{\varrho}}{2}\mathfrak{F}\right)-\cot\left(\frac{\sqrt{\varrho}}{2}\mathfrak{F}\right)\right)\right].\tag{36}$$

If $\varrho=0$,

$$\vartheta(x,t)=\frac{\sqrt{6}k}{\sqrt{\nu}}\left(-\frac{1}{\mathfrak{F}}\right).\tag{37}$$

4.2. Example 2. Let us consider the conformable time fractional CH equation

$$D_t^\delta\vartheta-\left(3\vartheta^2-1\right)\vartheta_{xx}-6\vartheta\left(\vartheta_x\right)^2-\vartheta_x+\vartheta_{xxxx}=0,\quad \text{where } t>0,\,0<\delta\le 1.\tag{38}$$

Applying the transformation,

$$\vartheta(x,t)=V(\mathfrak{F}),\qquad \mathfrak{F}=kx-l\frac{t^\delta}{\delta}.\tag{39}$$

Equation (38) is reduced to the following nonlinear ODE:

$$-(k+l)V'-6k^2\left(V'\right)^2V-k^2\left(3V^2-1\right)V''+k^4V''''=0.\tag{40}$$

Through balancing the terms V'''' and $(V')^2V$, we select $m=1$, then the nontrivial solution (40) reduces to

$$V(\mathfrak{F})=a_1\phi(\mathfrak{F})+a_0.\tag{41}$$

By setting the above solution in (40) and equating factors of each power of ϕ^i, we get nonlinear algebraic system, solving this system for different value of a_0, a_1, k, l.
Case 1:

$$a_0=0,\qquad a_1=\frac{i}{\sqrt{\varrho}},\qquad k=\pm\frac{i}{\sqrt{2}\sqrt{\varrho}},\qquad l=\pm\frac{i}{\sqrt{2}\sqrt{\varrho}}.\tag{42}$$

If $\varrho<0$,

$$\vartheta(x,t)=\frac{i}{\sqrt{\varrho}}\left[-\sqrt{-\varrho}\tanh\sqrt{-\varrho}\,\mathfrak{F}\right],\tag{43}$$

$$\vartheta(x,t)=\frac{i}{\sqrt{\varrho}}\left[-\sqrt{-\varrho}\coth\sqrt{-\varrho}\,\mathfrak{F}\right],\tag{44}$$

$$\vartheta(x,t)=\frac{i}{\sqrt{\varrho}}\left[\sqrt{-\varrho}\left(-\tanh\left(2\sqrt{-\varrho}\,\mathfrak{F}\right)\pm i\operatorname{sech}\left(2\sqrt{-\varrho}\,\mathfrak{F}\right)\right)\right],\tag{45}$$

$$\vartheta(x,t)=\frac{i}{\sqrt{\varrho}}\left[\sqrt{-\varrho}\left(-\coth\left(2\sqrt{-\varrho}\,\mathfrak{F}\right)\pm\operatorname{csch}\left(2\sqrt{-\varrho}\,\mathfrak{F}\right)\right)\right],\tag{46}$$

$$\vartheta(x,t)=\frac{i}{\sqrt{\varrho}}\left[-\frac{\sqrt{-\varrho}}{2}\left(\tanh\left(\frac{\sqrt{-\varrho}}{2}\mathfrak{F}\right)+\coth\left(\frac{\sqrt{-\varrho}}{2}\mathfrak{F}\right)\right)\right].\tag{47}$$

If $\varrho>0$,

$$\vartheta(x,t)=\frac{i}{\sqrt{\varrho}}\left[\sqrt{\varrho}\tan\sqrt{\varrho}\,\mathfrak{F}\right],\tag{48}$$

$$\vartheta(x,t)=\frac{i}{\sqrt{\varrho}}\left[-\sqrt{\varrho}\cot\sqrt{\varrho}\,\mathfrak{F}\right],\tag{49}$$

$$\vartheta(x,t)=\frac{i}{\sqrt{\varrho}}\left[\sqrt{\varrho}\left(\tan\left(2\sqrt{\varrho}\,\mathfrak{F}\right)\pm\sec\left(2\sqrt{\varrho}\,\mathfrak{F}\right)\right)\right],\tag{50}$$

$$\vartheta(x,t)=\frac{i}{\sqrt{\varrho}}\left[\sqrt{\varrho}\left(-\cot\left(2\sqrt{\varrho}\,\mathfrak{F}\right)\pm\csc\left(2\sqrt{\varrho}\,\mathfrak{F}\right)\right)\right],\tag{51}$$

$$\vartheta(x,t)=\frac{i}{\sqrt{\varrho}}\left[\frac{\sqrt{\varrho}}{2}\left(\tan\left(\frac{\sqrt{\varrho}}{2}\mathfrak{F}\right)-\cot\left(\frac{\sqrt{\varrho}}{2}\mathfrak{F}\right)\right)\right].\tag{52}$$

Case 3.

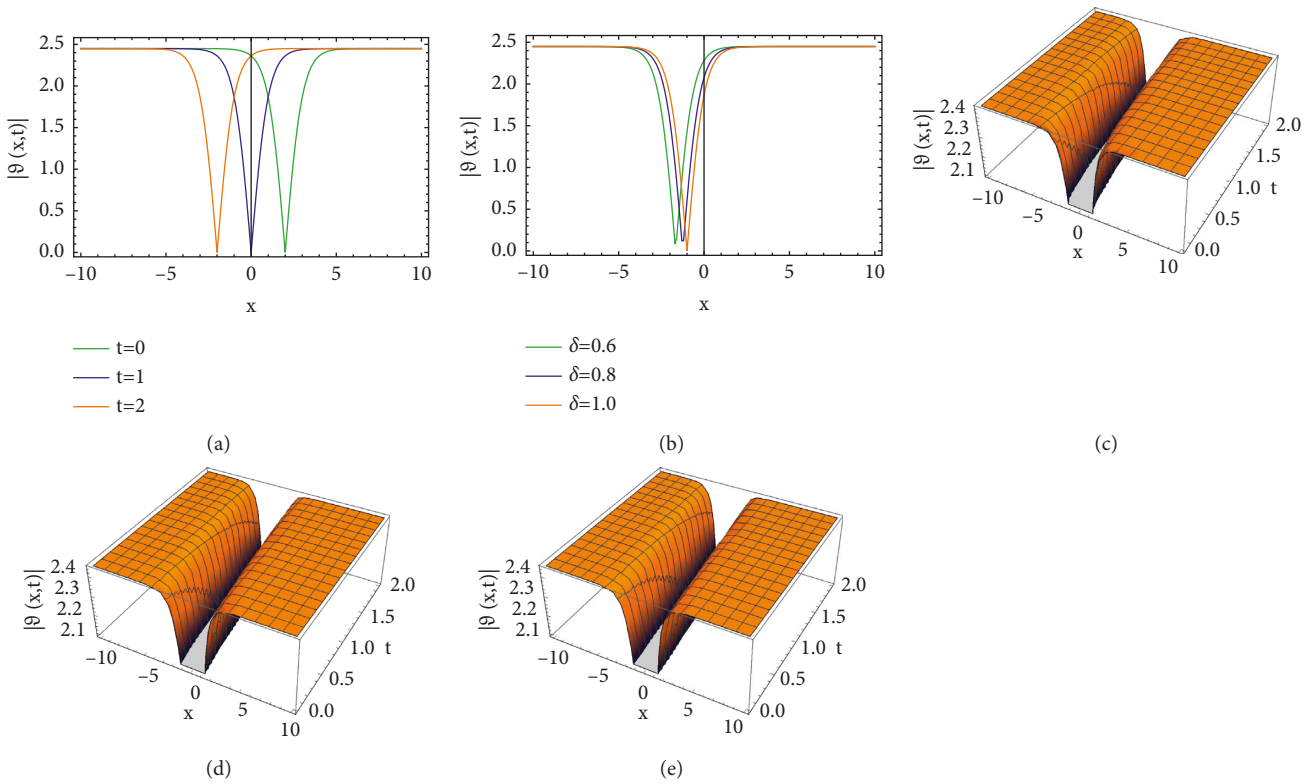

Figure 1: Solitary wave profile of $\vartheta_{(x,t)}$ appears in equation (24).

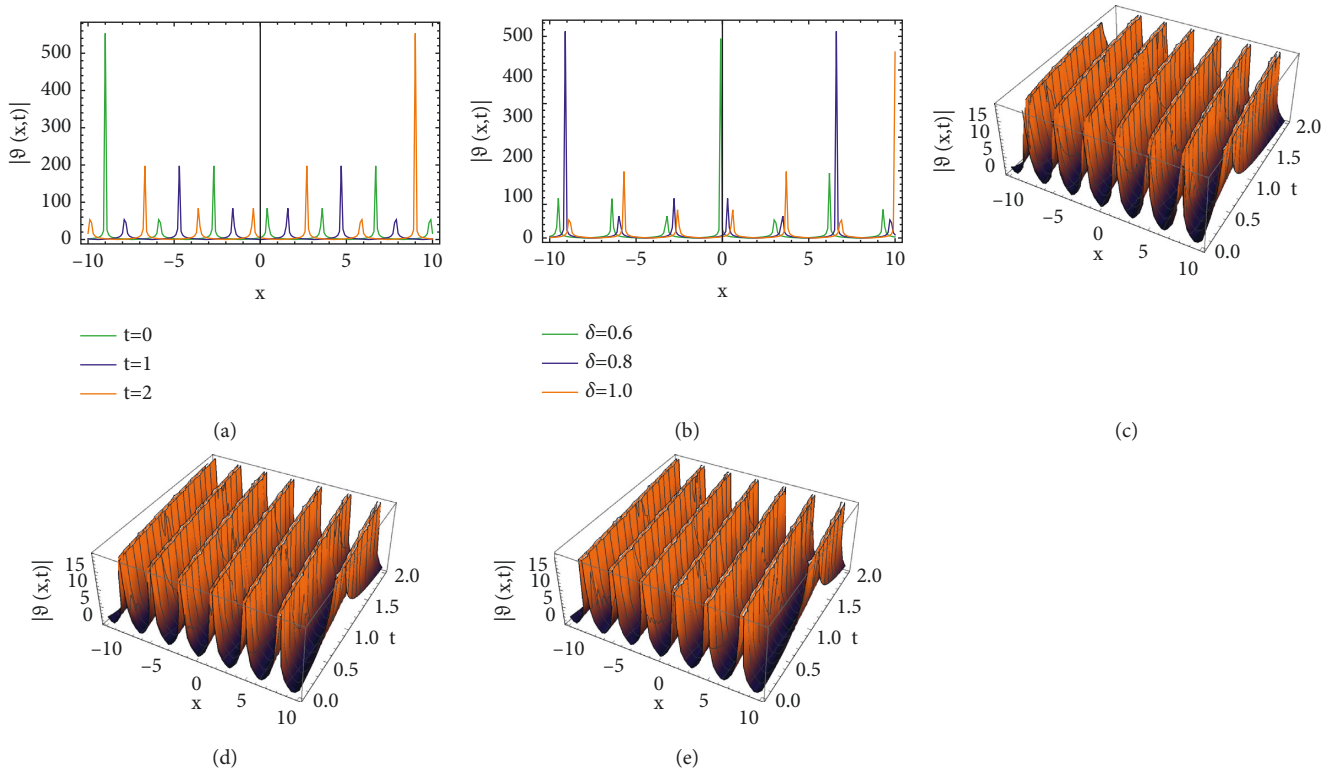

Figure 2: Periodic wave profile of $\vartheta_{(x,t)}$ appears in equation (28).

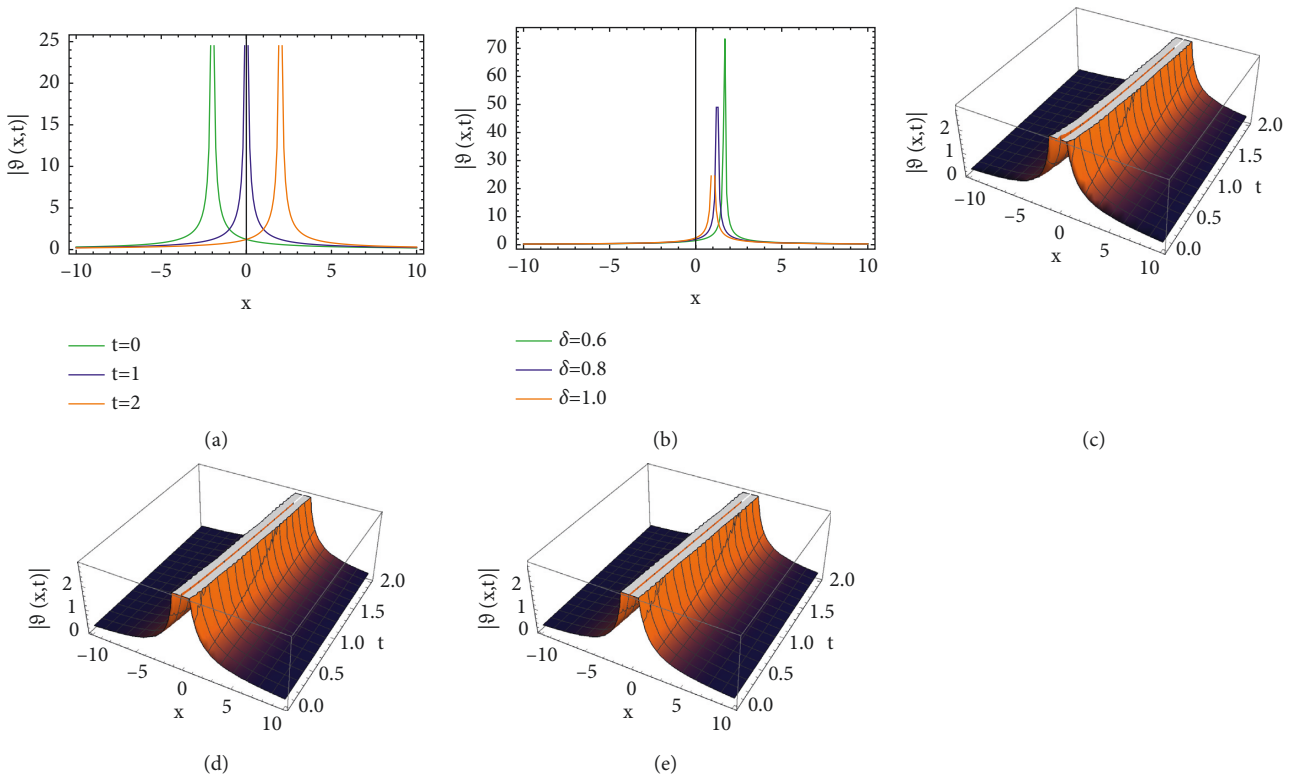

Figure 3: Wave profile of $\vartheta_{(x,t)}$ appears in equation (33).

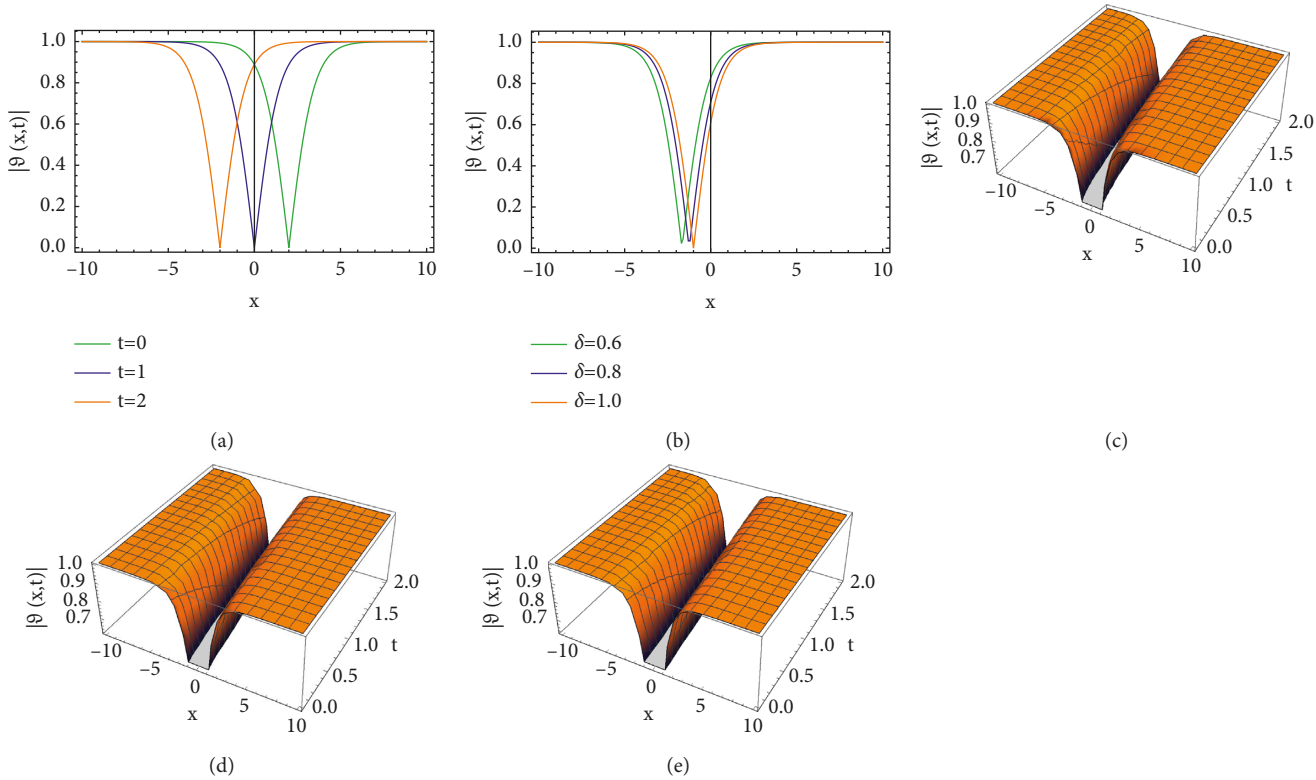

Figure 4: Solitary wave profile of $\vartheta_{(x,t)}$ appears in equation (43).

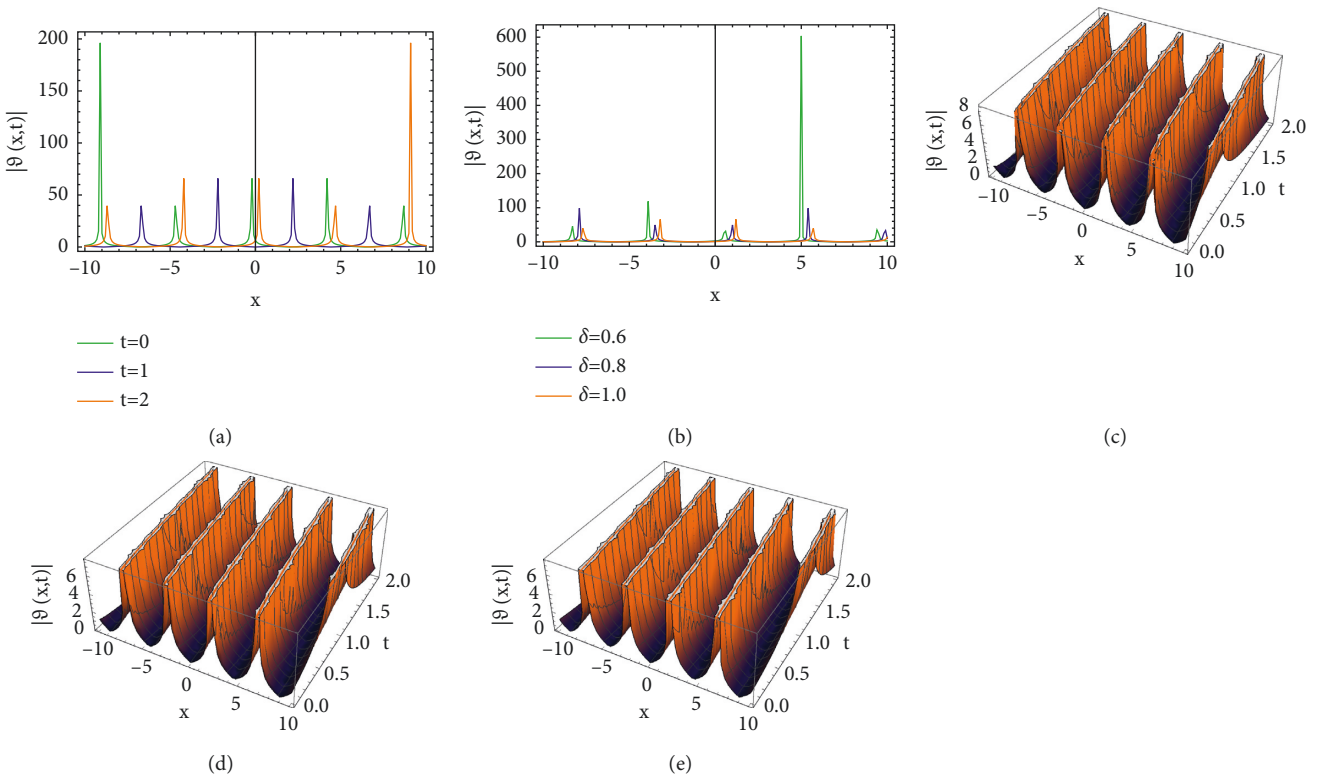

Figure 5: Solitary wave profile of $\vartheta_{(x,t)}$ appears in equation (48).

$$a_0 = 0,$$
$$a_1 = -\frac{i}{\sqrt{\varrho}},$$
$$k = \pm\frac{i}{\sqrt{2}\sqrt{\varrho}}, \tag{53}$$
$$l = \pm\frac{i}{\sqrt{2}\sqrt{\varrho}}.$$

If $\varrho < 0$,

$$\vartheta(x,t) = -\frac{i}{\sqrt{\varrho}}\left[-\sqrt{-\varrho}\tanh\sqrt{-\varrho}\,\mathfrak{F}\right],$$
$$\vartheta(x,t) = -\frac{i}{\sqrt{\varrho}}\left[-\sqrt{-\varrho}\coth\sqrt{-\varrho}\,\mathfrak{F}\right],$$
$$\vartheta(x,t) = -\frac{i}{\sqrt{\varrho}}\left[\sqrt{-\varrho}\left(-\tanh\left(2\sqrt{-\varrho}\,\mathfrak{F}\right) \pm i\,\mathrm{sech}\left(2\sqrt{-\varrho}\,\mathfrak{F}\right)\right)\right],$$
$$\vartheta(x,t) = -\frac{i}{\sqrt{\varrho}}\left[\sqrt{-\varrho}\left(-\coth\left(2\sqrt{-\varrho}\,\mathfrak{F}\right) \pm \mathrm{csch}\left(2\sqrt{-\varrho}\,\mathfrak{F}\right)\right)\right],$$
$$\vartheta(x,t) = -\frac{i}{\sqrt{\varrho}}\left[-\frac{\sqrt{-\varrho}}{2}\left(\tanh\left(\frac{\sqrt{-\varrho}}{2}\mathfrak{F}\right) + \coth\left(\frac{\sqrt{-\varrho}}{2}\mathfrak{F}\right)\right)\right]. \tag{54}$$

If $\varrho > 0$,

$$\vartheta(x,t) = -\frac{i}{\sqrt{\varrho}}\left[\sqrt{\varrho}\tan\sqrt{\varrho}\,\mathfrak{F}\right],$$
$$\vartheta(x,t) = -\frac{i}{\sqrt{\varrho}}\left[-\sqrt{\varrho}\cot\sqrt{\varrho}\,\mathfrak{F}\right],$$
$$\vartheta(x,t) = -\frac{i}{\sqrt{\varrho}}\left[\sqrt{\varrho}\left(\tan\left(2\sqrt{\varrho}\,\mathfrak{F}\right) \pm \sec\left(2\sqrt{\varrho}\,\mathfrak{F}\right)\right)\right], \tag{55}$$
$$\vartheta(x,t) = -\frac{i}{\sqrt{\varrho}}\left[\sqrt{\varrho}\left(-\cot\left(2\sqrt{\varrho}\,\mathfrak{F}\right) \pm \csc\left(2\sqrt{\varrho}\,\mathfrak{F}\right)\right)\right],$$
$$\vartheta(x,t) = -\frac{i}{\sqrt{\varrho}}\left[\frac{\sqrt{\varrho}}{2}\left(\tan\left(\frac{\sqrt{\varrho}}{2}\mathfrak{F}\right) - \cot\left(\frac{\sqrt{\varrho}}{2}\mathfrak{F}\right)\right)\right].$$

5. Conclusion

By using simplest equation method, we have succeeded to find out the solitary wave and periodic and rational solutions of conformable nonlinear space-time fractional differential BBM and CH equations. These solutions have also been demonstrated through graph. Figures 1–3 show the solitary wave profile of $\vartheta_{(x,t)}$ for conformable time fractional differential BBM equation, whereas Figures 4 and 5 represent the solitary wave profile of $\vartheta_{(x,t)}$ for conformable time fractional differential CH equation. All the results are obtained with the help of traveling wave transformation. At the end, it is concluded that the simplest equation method

suggests an innovative and powerful mathematical aid to deal with nonlinear partial differential equations of a wide class of nonlinear fractional-order of mathematical models in science and engineering. The performance of this method can also be used for fractal theory and microgravity space in our future research.

Data Availability

All the data are available within the article.

Conflicts of Interest

The authors declare that they have no conflicts of interest in this article.

References

[1] B. Lu, "The first integral method for some time fractional differential equations," *Journal of Mathematical Analysis and Applications*, vol. 395, no. 2, pp. 684–693, 2012.

[2] K. S. Miller and B. Ross, *An Introduction to the Fractional Calculus and Fractional Di!erential Equations*, Wiley, New York, NY, USA, 1993.

[3] G.-H. Gao, Z.-Z. Sun, and Y.-N. Zhang, "A finite difference scheme for fractional sub-diffusion equations on an unbounded domain using artificial boundary conditions," *Journal of Computational Physics*, vol. 231, no. 7, pp. 2865–2879, 2012.

[4] A. Kadem and A. Kılıçman, "Note on transport equation and fractional sumudu transform," *Computers & Mathematics with Applications*, vol. 62, no. 8, pp. 2995–3003, 2011.

[5] G.-W. Wang, X.-Q. Liu, and Y.-Y. Zhang, "Lie symmetry analysis to the time fractional generalized fifth-order kdv equation," *Communications in Nonlinear Science and Numerical Simulation*, vol. 18, no. 9, pp. 2321–2326, 2013.

[6] R. K. Gazizov, A. A. Kasatkin, and S. Y. Lukashchuk, "Symmetry properties of fractional diffusion equations," *Physica Scripta*, vol. T136, Article ID 014016, 2009.

[7] R. Sahadevan and T. Bakkyaraj, "Invariant analysis of time fractional generalized Burgers and Korteweg-de Vries equations," *Journal of Mathematical Analysis and Applications*, vol. 393, no. 2, pp. 341–347, 2012.

[8] C. Chen and Y.-L. Jiang, "Lie group analysis method for two classes of fractional partial differential equations," *Communications in Nonlinear Science and Numerical Simulation*, vol. 26, no. 1-3, pp. 24–35, 2015.

[9] Z. Odibat and S. Momani, "A generalized differential transform method for linear partial differential equations of fractional order," *Applied Mathematics Letters*, vol. 21, no. 2, pp. 194–199, 2008.

[10] G.-C. Wu and E. W. M. Lee, "Fractional variational iteration method and its application," *Physics Letters A*, vol. 374, no. 25, pp. 2506–2509, 2010.

[11] Y.-L. Jiang and X.-L. Ding, "Nonnegative solutions of fractional functional differential equations," *Computers & Mathematics with Applications*, vol. 63, no. 5, pp. 896–904, 2012.

[12] E. M. Zayed and Y. A. Amer, "Exact solutions for the nonlinear kpp equation by using the riccati equation method combined with the g/g-expansion method," *Scientific Research and Essays*, vol. 10, no. 3, pp. 86–96, 2015.

[13] G. Hariharan, "The homotopy analysis method applied to the Kolmogorov-Petrovskii-Piskunov (KPP) and fractional KPP equations," *Journal of Mathematical Chemistry*, vol. 51, no. 3, pp. 992–1000, 2013.

[14] V. Daftardar-Gejji and S. Bhalekar, "Solving multi-term linear and non-linear diffusion-wave equations of fractional order by Adomian decomposition method," *Applied Mathematics and Computation*, vol. 202, no. 1, pp. 113–120, 2008.

[15] K. A. Gepreel, "The homotopy perturbation method applied to the nonlinear fractional Kolmogorov-Petrovskii-Piskunov equations," *Applied Mathematics Letters*, vol. 24, no. 8, pp. 1428–1434, 2011.

[16] W. Liu and K. Chen, "The functional variable method for finding exact solutions of some nonlinear time-fractional differential equations," *Pramana*, vol. 81, no. 3, pp. 377–384, 2013.

[17] S. M. Ege and E. Misirli, "The modified kudryashov method for solving some fractional-order nonlinear equations," *Advances in Difference Equations*, vol. 2014, no. 1, p. 135, 2014.

[18] M. Topsakal, O. Guner, A. Bekir, and O. Unsal, "Exact solutions of some fractional differential equations by various expansion methods," *Journal of Physics: Conference Series*, vol. 766, Article ID 012035, 2016.

[19] D. Baleanu, Y. Uğurlu, and B. Kilic, "Improved (g'/g)-expansion method for the time-fractional biological population model and Cahn–Hilliard equation," *Journal of Computational and Nonlinear Dynamics*, vol. 10, no. 5, Article ID 051016, 2015.

[20] K.-L. Wang, "Exact solitary wave solution for fractal shallow water wave model by he's variational method," *Modern Physics Letters B*, vol. 36, Article ID 2150602, 2022.

[21] K. Wang, "Solitary wave solution of nonlinear bogoyavlenskii system by variational analysis method," *International Journal of Modern Physics B*, vol. 36, Article ID 2250015, 2021.

[22] K. Wang, "New variational theory for coupled nonlinear fractal Schrödinger system," *International Journal of Numerical Methods for Heat and Fluid Flow*, vol. 32, no. 2, pp. 589–597, 2021.

[23] A. Ali, A. R. Seadawy, and D. Baleanu, "Computational solutions of conformable space-time derivatives dynamical wave equations: analytical mathematical techniques," *Results in Physics*, vol. 19, Article ID 103419, 2020.

[24] N. H. M. Shahen, M. H. Bashar, T. Tahseen, and S. Hossain, "Solitary and rogue wave solutions to the conformable time fractional modified kawahara equation in mathematical physics," *Advances in Mathematical Physics*, vol. 2021, Article ID 6668092, 9 pages, 2021.

[25] P.-X. Wu, Q. Yang, and J.-H. He, "Solitary Waves of the Variant Boussinesq-Burgers Equation in a Fractal Dimensional Space," *Fractals*, 2021.

[26] K.-J. Wang and K.-L. Wang, "Variational principles for fractal whitham-broer-kaup equations in shallow water," *Fractals*, vol. 29, no. 02, Article ID 2150028, 2021.

[27] K.-L. Wang, "A novel perspective for the fractal schrödinger equation," *Fractals*, vol. 29, no. 04, Article ID 2150093, 2021.

[28] S. Habib, A. Islam, A. Batool, M. U. Sohail, and M. Nadeem, "Numerical solutions of the fractal foam drainage equation," *GEM-International Journal on Geomathematics*, vol. 12, no. 1, pp. 1–10, 2021.

[29] M. Nadeem and J.-H. He, "The homotopy perturbation method for fractional differential equations: part 2, two-scale transform," *International Journal of Numerical Methods for Heat and Fluid Flow*, vol. 32, no. 2, pp. 559–567, 2021.

[30] R. Khalil, M. Al Horani, A. Yousef, and M. Sababheh, "A new definition of fractional derivative," *Journal of Computational and Applied Mathematics*, vol. 264, pp. 65–70, 2014.
[31] T. Abdeljawad, "On conformable fractional calculus," *Journal of Computational and Applied Mathematics*, vol. 279, pp. 57–66, 2015.
[32] T. Abdeljawad, M. Al Horani, and R. Khalil, "Conformable fractional semigroups of operators," *Journal of Semigroup Theory and Applications 2015*, vol. 32, 2015.
[33] M. Eslami, "Exact traveling wave solutions to the fractional coupled nonlinear schrodinger equations," *Applied Mathematics and Computation*, vol. 285, pp. 141–148, 2016.

Hindawi
Complexity
Volume 2022, Article ID 6931354, 21 pages
https://doi.org/10.1155/2022/6931354

WILEY | Hindawi

Research Article

A Novel Discrete-Time Leslie–Gower Model with the Impact of Allee Effect in Predator Population

S. Vinoth,[1] **R. Sivasamy**,[2] **K. Sathiyanathan**,[1] **B. Unyong**,[3] **R. Vadivel**,[3] **and Nallappan Gunasekaran**[4]

[1]*Department of Mathematics, SRMV College of Arts and Science, Coimbatore, TN, India*
[2]*Department of Science and Humanities, M.Kumarasamy College of Engineering, Karur, TN, India*
[3]*Department of Mathematics, Faculty of Science and Technology, Phuket Rajabhat University, Phuket 83000, Thailand*
[4]*Department of Advanced Science and Technology, Computational Intelligence Laboratory, Toyota Technological Institute, Nagoya 468-8511, Japan*

Correspondence should be addressed to B. Unyong; bundit.u@pkru.ac.th

Received 11 October 2021; Revised 23 December 2021; Accepted 1 February 2022; Published 28 March 2022

Academic Editor: C. Rajivganthi

The discrete-time system has more complex and chaotic dynamical behaviors as compared to the continuous-time system. This paper extends a discrete Leslie–Gower predator-prey system with the Allee effect in the predator's population, whose dynamics are analyzed and explored. We have determined the equilibrium points and studied their local stability properties. We find that the system undergoes flip bifurcation and Neimark–Sacker bifurcation around the interior equilibrium point by choosing the Allee parameter as a bifurcation parameter. We discuss the stability and direction of both bifurcations with the help of the normal form theory and center manifold theorem. The flip bifurcation and Neimark–Sacker bifurcation are the most common routes to the chaotic orbit in the discrete system. Moreover, we utilize state feedback, pole placement, and hybrid control methods to control the chaos in the system. The work is complete with the numerical simulations to confirm the analytical findings.

1. Introduction

The study of interactions between prey and predator has particular interest for many mathematicians and ecologists. Many researchers investigated the dynamic behavior of the predator-prey system and contributed to the development of continuous-time systems. Another possible way to understand the complex problem of two interacting species is by discrete systems [1]. Moreover, it has been observed that the discrete-time systems are more appropriate than the continuous-time systems for the populations with nonoverlapping generations [2]. The discrete-time models are more appropriate and provide efficient results than continuous models for small-size populations [3]. For example, the discrete model is better for studying insect populations since there is only one generation per year and an annual plant population because there are no overlapping generations annually. Jing and Yang [4], Liu and Xiao [5], and Elabbasy et al. [6] showed that the discrete-time system showed richer and more complex dynamics compared to the continuous-time systems. Many researchers formulated and studied the discrete-time predator-prey system by implementing the forward Euler scheme [4, 5, 7], nonstandard finite difference scheme [8, 9], and piecewise constant arguments [10–12]. For instance, the authors in [13] obtained a discrete-time predator-prey system with a crowding effect and predator partially dependent on prey by applying the forward Euler's scheme from the continuous-time system. They also showed the existence of a cascade of period-doubling bifurcation and Hopf bifurcation in the considered system. On the other hand, Abbasi et al. [12] used the method of piecewise constant arguments and obtained the discrete system. Also, the authors investigated stability, bifurcations, and chaos control analysis. In [14], the authors investigated the discrete-time predator-prey system with hunting cooperation through numerical simulation and observed that the system

undergoes both types of bifurcations. In [15], the authors discussed the chaotic dynamics of a discrete prey-predator system with Holling-II type functional response. The other fruitful results on discrete-time models can be found in [16, 17].

The Allee effect is a biological phenomenon named after Allee [18], who was the first to write thoroughly about it. It denotes the presence of a positive relationship between population size and per capita growth rate. This effect usually saturates or vanishes as the population expands. There has been a great deal of literature on deriving continuous-time prey-predator models with the Allee effect [19–22]. The impact of the Allee effect in the discrete-time prey-predator models has also been studied in the literature [23–26]. For example, Celik and Duman [23] studied the impact of the Allee effect in the discrete-time predator-prey model with linear interaction. They showed that the Allee effect on prey population changes the unstable equilibrium into a stable state. In [25], the authors studied the discrete-time predator-prey model with strong and weak Allee effects. Also, they showed that the chaotic orbits appear for larger step size values through period-doubled orbits and invariant circle orbits. AlSharawi et al. [26] considered the Allee effect in the discrete-time prey-predator model with a nonmonotonic functional response. They performed the stability analysis and provided conditions for the occurrence of flip and Neimark–Sacker bifurcations by taking the Allee parameter as a bifurcation parameter. Also, they showed that the system has two types of bistability behaviors.

Several research works have been done for bifurcation and chaos control in nonlinear systems. It refers to the role of constructing a controller to alter the chaotic and bifurcating properties of a given nonlinear system to achieve some desired dynamical behaviors [27–30]. One can shift the chaotic attractor to any one of a large number of possible attracting periodic motions, as in [31]. Recently, the studies on bifurcation and chaos control in the discrete-time predator-prey models attained much more interest among researchers. For example, Din [32] showed that the model undergoes flip bifurcation (FB) and Neimark–Sacker bifurcation (NSB) for larger values of the growth rate of the prey population. Furthermore, the author implemented three different types of control strategies to control the chaos. Moreover, for some interesting results related to bifurcation and chaos control in the predator-prey models, we refer the readers to [33–35].

Motivated by the above-mentioned works, we consider the modified Leslie–Gower prey-predator system introduced by Alaoui and Okiye in [36] by assuming that the growth rate of the predator is affected by the presence of the Allee effect. Also, the prey and predator populations have nonoverlapping generations. The discrete-time model is obtained by the method of piecewise constant arguments for the differential equation [10–12] from its corresponding continuous-time system. We attempt to study the discrete-time system and observe some rich dynamics that the continuous-time system does not have. Feng and Kang [20] investigated the [36] continuous-time model with an Allee effect in both prey and predator. To the best of our knowledge, there has been less research done in discrete predator-prey systems with the Allee effect in the predator population. The main purpose of this paper is to show the rich dynamics of the discrete system in terms of bifurcations (FB and NSB) and chaos by taking the Allee parameter as a bifurcation parameter. Flip and Neimark–Sacker bifurcations are the common routes to chaos in discrete systems. Additionally, if the discrete system is chaotic under certain parametric conditions, we can use various control methods to stabilize the chaotic orbits near the unstable equilibrium point. It is worth mentioning here that the study on stability, bifurcation, and chaos control analysis for the prey-predator model with Allee effect in predator population is different from the whole of the existing works.

This paper is organized as follows: in Section 2, we describe the formation of a discrete-time system for populations with nonoverlapping generations from the continuous counterpart. In Section 3, we study the existence and local stability of the equilibrium points for the discrete-time system. In Section 4, we illustrate the existence of flip and Neimark–Sacker bifurcation by taking the Allee parameter as a bifurcation parameter. Section 5 is related to the implementation of state feedback, pole-placement, and hybrid control methods to delay the chaos in the system. Lastly, to ensure our analytical results, the various numerical simulations are performed in Section 6.

2. Model Formulation

Firstly, we describe the continuous-time predator-prey system of modified Leslie–Gower with Holling type II functional response. It was introduced by Alaoui and Okiye in [36], which is of the following form:

$$\begin{cases} \dfrac{\mathrm{d}x(t)}{\mathrm{d}t} = x(t)\left(r_1 - ax(t) - \dfrac{gy(t)}{x(t)+b}\right), \\ \dfrac{\mathrm{d}y(t)}{\mathrm{d}t} = y(t)\left(r_2 - \dfrac{hy(t)}{x(t)+c}\right). \end{cases} \tag{1}$$

$x(0) \geq 0$ and $y(0) \geq 0$, where $x(t)$ and $y(t)$ represent the population sizes of prey and predator at time t. r_1, a, g, b, r_2, h, and c are all positive constants. r_1 and r_2 are the growth rates of x and y. a measures the strength of competition among the individuals of species x. g is the maximum value a per capita reduction rate of x can attain. b (respectively, c) measures the extent to which the environment provides protection to prey x (respectively, to predator y), and h has a similar meaning to g. The assumption that the amount to which the environment provides protection to both the predator and the prey is the same (i.e., $b = c$) has been considered in [37, 38]. Singh et al. [39] extended system (1) with the death rate of predators, obtained a discrete system by Euler's method, and also considered step size as a bifurcation parameter. This fact violates the numerical method of discretization. To overcome this, Din in [32] applied the method of piecewise constant arguments to obtain the discrete system. Recently, the discrete version of system (1)

was derived using Euler's method with step size 1 by the authors in [40] and showed bifurcation behavior with other model parameters.

Now, we consider that system (1) is subject to the Allee effect in predator population, and it is given by

$$\begin{cases} \dfrac{\mathrm{d}x(t)}{\mathrm{d}t} = x(t)\left(r_1 - ax(t)\right) - \dfrac{gx(t)y(t)}{x(t)+b}, \\ \dfrac{\mathrm{d}y(t)}{\mathrm{d}t} = y(t)\left(\dfrac{r_2 y(t)}{y(t)+m} - \dfrac{hy(t)}{x(t)+c}\right), \end{cases} \tag{2}$$

where $y(t)/m + y(t)$ is the Allee effect term and $m > 0$ represents the severity of Allee effect in the predator population. The authors in [41] studied system (2) with ratio-dependent functional response and the fear in prey population.

Next, based on the appropriate modifications of overlapping generations, one can get the difference equation for modeling population with nonoverlapping generations. We aim to study the populations that have nonoverlapping generations for system (2). Moreover, it is necessary to obtain the discrete-time system from its continuous counterpart. In this way, the method of piecewise constant argument has been useful. The corresponding discrete-time system (2) is obtained by the method of piecewise constant arguments for the differential equations [10–12, 14], assuming that the populations have no overlap between successive generations and the population growth occurs in discrete steps $t \in [n, n+1)$, $n = 0, 1, 2, \cdots$. Let us consider that the variables and constants in (2) change in the regular time intervals and obtain the following modified system:

$$\begin{cases} \dfrac{1}{x(t)}\dfrac{\mathrm{d}x(t)}{\mathrm{d}t} = r_1 - ax(t) - \dfrac{gy(t)}{x(t)+b}, \\ \dfrac{1}{y(t)}\dfrac{\mathrm{d}y(t)}{\mathrm{d}t} = \dfrac{r_2 y(t)}{y(t)+m} - \dfrac{hy(t)}{x(t)+c}, \end{cases} \quad t \neq 0, 1, 2, \ldots, \tag{3}$$

where $[t]$ is the integer part of t, $t \in (0, +\infty)$. On any interval of the form $[n, n+1)$, $n = 0, 1, 2, \ldots$, we can integrate (3) and obtain the following:

$$\begin{cases} \ln\dfrac{x(t)}{x(n)} = \left[r_1 - ax(n) - \dfrac{gy(n)}{x(n)+b}\right](t-n), \\ \ln\dfrac{y(t)}{y(n)} = \left[\dfrac{r_2 y(t)}{y(t)+m} - \dfrac{hy(n)}{x(n)+c}\right](t-n), \quad n = 0, 1, 2, \ldots. \end{cases} \tag{4}$$

By simplification and letting $t \longrightarrow n+1$, the corresponding discrete-time system for (2) is obtained by the method of piecewise constant arguments for differential equations can be written as follows:

$$\begin{cases} x(n+1) = x(n)\exp\left[r_1 - ax(n) - \dfrac{gy(n)}{x(n)+b}\right], \\ y(n+1) = y(n)\exp\left[\dfrac{r_2 y(n)}{y(n)+m} - \dfrac{hy(n)}{x(n)+c}\right], \end{cases} \tag{5}$$

where $x(n+1)$ and $y(n+1)$ denote the populations in generation $n+1$, and they are related to the sizes $x(n)$ and $y(n)$ of the populations in the preceding generation n. Note that in the absence of a predator, system (5) reduces to the one-dimensional system, similar to the Ricker model [16]. Thus, this current article aims to analyze the local stability, bifurcation, and chaos control analyses for the discrete system (5) that models the interaction between populations that have nonoverlapping generations.

3. The Existence and Local Stability of the Equilibia

3.1. The Equilibria. To find the equilibrium points of system (5), we use direct substitution method to solve the following equations:

$$r_1 - ax - \frac{gy}{x+b} = 0, \quad \frac{r_2}{y+m} - \frac{h}{x+c} = 0. \tag{6}$$

Form the above equations, we have the following points of equilibria:

The origin $E_0 = (0, 0)$.

The predator-free equilibrium $E_1 = (\overline{x}, 0) = (r_1/a, 0)$.

The prey-free equilibrium $E_2 = (0, \overline{y}) = (0, r_2 c/h - m)$ exists if $r_2 c/h > m$.

The interior equilibrium point is $E^*(x^*, y^*)$, where $y^* = r_2 x^*/h + r_2 c - mh/h$ and x^* is the positive root of the following equation:

$$ahx^{*2} + (abh + gr_2 - r_1 h)x^* + g(r_2 c - mh) - r_1 hb = 0, \tag{7}$$

If $r_2 c - mh/h < r_1 b/g$ holds, then (6) has at least one positive real root x^*.

To guarantee the existence of interior equilibrium point $E^*(x^*, y^*)$, we need the following lemma.

Lemma 1. *Let us assume that $r_2 c - mh/h < r_1 b/g$ and $r_2(x^* + c) > mh$ always hold. Then, $E^*(x^*, y^*)$ is the unique positive interior equilibrium point of system (5).*

3.2. Local Stability Analysis. To analyze the local stability properties of the equilibria, we need the Jacobian matrix at an arbitrary equilibrium $E(x, y)$, which is given as follows:

$$J = \begin{pmatrix} \left(1 - ax + \frac{gxy}{(x+b)^2}\right)A_1 & \frac{-gx}{x+b}A_1 \\ \frac{hy^2}{(c+x)^2}A_2 & \left(1 - \frac{hy}{c+x} + \frac{r_2my}{(y+m)^2}\right)A_2 \end{pmatrix}, \tag{8}$$

where $A_1 = \exp[r_1 - ax - gy/x + b]$ and $A_2 = \exp[r_2y/y + m - hy/x + c]$.

Then, we have the subsequent lemmas for the local stability analysis of the equilibria.

Lemma 2. *For system (5), we have,*

(1) E_0, E_1 are nonhyperbolic points.

(2)

(a) $E_2(0, \overline{y})$ is a sink if $|\exp(r_1 - g\overline{y}/b)| < 1$ and $|(1 - h\overline{y}/c + r_2m\overline{y}/(\overline{y}+m)^2)A_3| < 1$.
(b) $E_2(0, \overline{y})$ is a source if $|\exp(r_1 - g\overline{y}/b)| > 1$ and $|(1 - h\overline{y}/c + r_2m\overline{y}/(\overline{y}+m)^2)A_3| < 1$.
(c) $E_2(0, \overline{y})$ is a saddle if $|\exp(r_1 - g\overline{y}/b)| < 1$, $|(1 - h\overline{y}/c + r_2m\overline{y}/(\overline{y}+m)^2)A_3| < 1$, $|\exp(r_1 - g\overline{y}/b)| < 1$, and $|(1 - h\overline{y}/c + r_2m\overline{y}/(\overline{y}+m)^2)A_3| > 1$.
(d) $E_2(0, \overline{y})$ is a nonhyperbolic if $|\exp(r_1 - g\overline{y}/b)| = 1 | (1 - h\overline{y}/c + r_2m\overline{y}/(\overline{y}+m)^2)A_3| = 1$.

Proof. The Jacobian matrix at $E_0(0,0)$ is as follows:

$$J_{E_0} = \begin{pmatrix} \exp(r_1) & 0 \\ 0 & 1 \end{pmatrix}, \tag{9}$$

with the eigenvalues $\lambda_{1,2} = \exp(r_1), 1$.

The Jacobian matrix at $E_1(\overline{x}, 0)$ is as follows:

$$J_{E_1} = \begin{pmatrix} 1 - r_1 & -\frac{gr_1}{ab + r_1} \\ 0 & 1 \end{pmatrix}, \tag{10}$$

with the eigenvalues $\lambda_{1,2} = \exp(1 - r_1), 1$.

The Jacobian matrix at $E_2(0, \overline{y})$ is as follows:

$$J_{E_2} = \begin{pmatrix} \exp\left(r_1 - \frac{g\overline{y}}{b}\right) & 0 \\ \frac{h\overline{y}^2}{c^2}A_3 & \left(1 - \frac{h\overline{y}}{c} + \frac{r_2m\overline{y}}{(\overline{y}+m)^2}\right)A_3 \end{pmatrix}, \tag{11}$$

with $A_3 = \exp[r_2\overline{y}/\overline{y} + m - h\overline{y}/c]$, and the eigenvalues are $\lambda_1 = \exp(r_1 - g\overline{y}/b)$ and $\lambda_2 = (1 - h\overline{y}/c + r_2m\overline{y}/(\overline{y}+m)^2)A_3$. □

Lemma 3. *The interior equilibrium point*

(a) $E^*(x^*, y^*)$ is a sink if $B_2 < 1$ and $|B_1| < B_2 + 1$.

(b) $E^*(x^*, y^*)$ is a source if $B_2 > 1$ and $|B_1| < B_2 + 1$ or $|B_1| > B_2 + 1$.

(c) $E^*(x^*, y^*)$ is a saddle if $0 < |B_1| + B_2 + 1 < 2|B_1|$.

(d) $E^*(x^*, y^*)$ is nonhyperbolic if $|B_1| = |B_2 + 1|$, or $B_2 = 1$, and $|B_1| \le 2$.

Proof. The Jacobian matrix at $E^*(x^*, y^*)$ is as follows:

$$J_{E^*} = \begin{pmatrix} 1 - ax^* + \frac{gx^*y^*}{(x^*+b)^2} & -\frac{gx^*}{x^*+b} \\ \frac{hy^{*2}}{(x^*+c)^2} & 1 - \frac{r_2y^{*2}}{(y^*+m)^2} \end{pmatrix}. \tag{12}$$

Then, the characteristic polynomial of J_{E^*} is as follows:

$$F(\lambda) := \lambda^2 - B_1\lambda + B_2 = 0, \tag{13}$$

where

$$\begin{aligned} B_1 &= 2 - ax^* + \frac{gx^*y^*}{(x^*+b)^2} - \frac{r_2y^{*2}}{(y^*+m)^2}, \\ B_2 &= \left(1 - ax^* + \frac{gx^*y^*}{(x^*+b)^2}\right)\left(1 - \frac{r_2y^{*2}}{(y^*+m)^2}\right) \\ &\quad + \frac{ghx^*y^{*2}}{(x^*+b)(x^*+c)^2}. \end{aligned} \tag{14}$$

□

3.3. Bistability. Since model (5) is with the Allee effect in predator population, it is possible for the occurrence of bistability criteria, which is for two positive equilibrium points to exist and for both to be stable. From Lemma 2, E_0 and E_1 are nonhyperbolic points. The only possibility is between E_2 and E^*. Also, from Lemma 1,E_2 exists if $r_2c/h > m$, and E^* exists if $r_2c - mh/h < r_1b/g$ and $r_2(x^* + c) > mh$ holds. If $r_2c - mh/h < r_1b/g$, then E_2 is unstable form Lemma 2 (a), since one of the eigenvalues of J_{E_2} is $|\exp(r_1 - \overline{y}/b)| > 1$. Then, we can say that if E^* exists, then E_2 is unstable. Hence, there is less possibility for the occurrence of bistability for model (5).

4. Bifurcation Analysis

We have studied the stability properties of $E^*(x^*, y^*)$ previously. In the subsequent section, we choose the Allee parameter m as a bifurcation parameter to analyze the bifurcation behaviour of system (5). We derive the conditions to obtain flip bifurcation (FB) and Neimark–Sacker bifurcation (NSB) at $E^*(x^*, y^*)$. Moreover, we utilize the center manifold theorem and the normal form theory [42, 43] to discuss the direction and stability property of the flip bifurcation and Neimark–Sacker bifurcation at $E^*(x^*, y^*)$.

4.1. Flip Bifurcation. System (5) undergoes flip bifurcation if one of the eigenvalues of J_{E^*} must be −1 and the other should not be 1 or −1. Using this, we assume one of the

eigenvalues of J_{E^*} as -1. Then, from (12), we have the following:

$$F(-1) := 4 - 2ax^* - \frac{2r_2y^{*2}}{(y^*+m)^2} + \frac{2gx^*y^*}{(x^*+b)^2} + \frac{ar_2x^*y^{*2}}{(y^*+m)^2} + \frac{ghx^*y^{*2}}{(x^*+b)(x^*+c)^2} - \frac{gr_2x^*y^{*3}}{(x^*+b)^2(y^*+m)^2} = 0. \tag{15}$$

Note that the left-hand side of expression (13) is in terms of parameter m in denominator with power. Hence, it is difficult to find the explicit value of m for which system (5) undergoes flip bifurcation. Hence, we denote $m = m_h$ as the critical parameter value that satisfies (13). Also, $E^*(x^*, y^*)$ is derived at the critical value $m = m_f$.

Next, if $a_2 > 0$, $a_3 < 0$, and $h(y^* + m)/r_2 > c$ holds, we define that the neighborhood Θ_f for system (5) undergoes flip bifurcation near the equilibrium point E^* at some critical value $m = m_f$ as follows:

$$\Theta_f = \{(r_1, r_2, a, b, c, g, h, m): m = m_f, r_1, r_2, a, b, c, g, h > 0\}. \tag{16}$$

Hence, we assume that system (5) undergoes flip bifurcation when $m = m_f$ changes in the neighborhood Θ_f.

Now, we investigate the direction and stability of the possible occurrence of flip bifurcation for system (5) at $E^*(x^*, y^*)$ with the steps followed in [32, 42]. Since, $(r_1, r_2, a, b, c, g, h, m) \in \Theta_f$ on giving a perturbation $|m_1| \ll 1$ of critical value $m = m_f$ for which system (5) undergoes flip bifurcation, then the perturbation system is given by the following:

$$\begin{cases} x_{n+1} = x_n \exp\left[r_1 - ax_n - \dfrac{gy_n}{x_n + b}\right], \\ y_{n+1} = y_n \exp\left[\dfrac{r_2y_n}{y_n + m_1 + m_f} - \dfrac{hy_n}{x_n + c}\right]. \end{cases} \tag{17}$$

Next, we transform the equilibrium point $E^*(x^*, y^*)$ into the origin by letting $p_n = x_n - x^*$ and $q_n = y_n - y^*$. Form (17), we obtain the following:

$$\begin{cases} p_{n+1} = (p_n + x^*)\exp\left[r_1 - a(p_n + x^*) - \dfrac{g(q_n + y^*)}{(p_n + x^*) + b}\right] - x^*, \\ q_{n+1} = (q_n + y^*)\exp\left[\dfrac{r_2(q_n + y^*)}{(q_n + y^*) + (m_1 + m_f)} - \dfrac{h(q_n + y^*)}{(p_n + x^*) + c}\right] - y^*. \end{cases} \tag{18}$$

By Taylor's series expansion, (16) becomes,

$$\begin{cases} p_{n+1} = \alpha_1p_n + \alpha_2q_n + \alpha_3m_1 + \alpha_4p_n^2 + \alpha_5q_n^2 + \alpha_6m_1^2 + \alpha_7p_nq_n \\ + \alpha_8p_nm_1 + \alpha_9q_nm_1 + o\left(\left(|p_n| + |q_n| + |m_1|\right)^2\right), \\ q_{n+1} = \beta_1p_n + \beta_2q_n + \beta_3m_1 + \beta_4p_n^2 + \beta_5q_n^2 + \beta_6m_1^2 + \beta_7p_nq_n \\ + \beta_8p_nm_1 + \beta_9q_nm_1 + o\left(\left(|p_n| + |q_n| + |m_1|\right)^2\right), \end{cases} \tag{19}$$

where

$$\alpha_1 = 1 + x*M_1, \alpha_2 = \frac{-gx*}{x* + b'}, \alpha_3 = 0, \alpha_4 = \frac{-gx*y*}{(x* + b)} + M_1\frac{x*}{2}M_1^2,$$

$$\alpha_5 = \frac{g^2x*}{2(x* + b)^2}, \alpha_6 = 0, \alpha_7\frac{-gb}{(x* + b)^2} - \frac{gM_1x*}{x* + b}, \alpha_8 = 0, \alpha_9 = 0,$$

$$\beta_1 = \frac{hy*^2}{(x* + c)^2}, \beta_2 = 1 + y*M_2, \beta_3 = -\frac{r_2y*^2}{\left(y* + m_f\right)^2},$$

$$\beta_4 = \frac{-hy*^2}{(x* + c)^3} + \frac{h^2y*^3}{2(x* + c)^4}, \beta_5 = \frac{-r_2m_fy*}{\left(y* + m_f\right)^3} + M_2 + \frac{y*M_2^2}{2}, \tag{20}$$

$$\beta_6 = \frac{r_2^2y*^3}{2\left(y* + m_f\right)^4} + \frac{r_2y*^2}{\left(y* + m_f\right)^3}, \beta_7 = \frac{2hy*}{(x* + c)^2} + \frac{hy*^2M_2}{(x* + c)^2},$$

$$\beta_8 = \frac{-hr_2y*^3}{(x* + c)^2(y* + b)^2}, \beta_9 = \frac{-2m_fr_2y*}{\left(y* + m_f\right)^3} - \frac{r_2M_2y*^2}{\left(y* + m_f\right)^2},$$

$$M_1 = -\alpha + \frac{gy*}{(x* + b)^2}, M_2 = \frac{-r_2y*}{\left(y* + m_f\right)^2}.$$

Consider

$$J_{E^*} = \begin{pmatrix} 1 - ax^* + \dfrac{gx^*y^*}{\left(x^* + b\right)^2} & -\dfrac{gx^*}{x^* + b} \\ \dfrac{hy^{*2}}{\left(x^* + c\right)^2} & 1 - \dfrac{r_2y^{*2}}{\left(y^* + m_f\right)^2} \end{pmatrix}. \tag{21}$$

Let us assume that the matrix J_{E^*} has eigenvalues.

$$\lambda_1 = -1, \lambda_2$$

$$= 1 - ax^* + \frac{gx^*y^*}{\left(x^* + b\right)^2} + \frac{ghx^*y^{*2}\left(y^* + m_f\right)^2}{\left(x^* + b\right)\left(x^* + c\right)^2\left(2\left(y^* + m_f\right)^2 - r_2y^*\right)}, \tag{22}$$

satisfies $|\lambda_1| = 1$ and $|\lambda_2| \neq 1$.
Next, we construct the nonsingular matrix L as follows:

$$L = \begin{pmatrix} \alpha_2 & \alpha_2 \\ -1 - \alpha_1 & \lambda_2 - \alpha_1 \end{pmatrix}. \tag{23}$$

Using translation $\begin{pmatrix} p_n \\ q_n \end{pmatrix} = L\begin{pmatrix} P_n \\ Q_n \end{pmatrix}$. Then, (17) can be written as

$$\begin{cases} P_{n+1} = -P_n + G_1(p_n, q_n, m_1) + o\left(\left(|p_n| + |q_n| + |m_1|\right)^2\right), \\ Q_{n+1} = \lambda_2 Q_n + G_2(p_n, q_n, m_1) + o\left(\left(|p_n| + |q_n| + |m_1|\right)^2\right), \end{cases} \tag{24}$$

where

$$\begin{aligned} G_1(p_n, q_n, m_1) &= \phi_1 m_1 + \phi_2 p_n^2 + \phi_3 q_n^2 + \phi_4 m_1^2 + \phi_5 p_n q_n + \phi_6 p_n m_1 + \phi_7 q_n m_1, \\ G_2(p_n, q_n, m_1) &= \theta_1 m_1 + \theta_2 p_n^2 + \theta_3 q_n^2 + \theta_4 m_1^2 + \theta_5 p_n q_n + \theta_6 p_n m_1 + \theta_7 q_n m_1, \end{aligned} \tag{25}$$

and

$$\begin{aligned} \phi_1 &= \frac{(\lambda_2 - \alpha_1)\alpha_3 - \alpha_2\beta_3}{\alpha_2(1+\lambda_2)}, \\ \phi_2 &= \frac{(\lambda_2 - \alpha_1)\alpha_4 - \alpha_2\beta_4}{\alpha_2(1+\lambda_2)}, \\ \phi_3 &= \frac{(\lambda_2 - \alpha_1)\alpha_5 - \alpha_2\beta_5}{\alpha_2(1+\lambda_2)}, \\ \phi_4 &= \frac{(\lambda_2 - \alpha_1)\alpha_6 - \alpha_2\beta_6}{\alpha_2(1+\lambda_2)}(1+\lambda_2), \\ \phi_5 &= \frac{(\lambda_2 - \alpha_1)\alpha_7 - \alpha_2\beta_7}{\alpha_2(1+\lambda_2)}, \\ \phi_6 &= \frac{(\lambda_2 - \alpha_1)\alpha_8 - \alpha_2\beta_8}{\alpha_2(1+\lambda_2)}, \\ \phi_7 &= \frac{(\lambda_2 - \alpha_1)\alpha_9 - \alpha_2\beta_9}{\alpha_2(1+\lambda_2)}, \\ \theta_1 &= \frac{(1+\alpha_1)\alpha_3 + \alpha_2\beta_3}{\alpha_2(1+\lambda_2)}, \\ \theta_2 &= \frac{(1+\alpha_1)\alpha_4 + \alpha_2\beta_4}{\alpha_2(1+\lambda_2)}, \\ \theta_3 &= \frac{(1+\alpha_1)\alpha_5 + \alpha_2\beta_5}{\alpha_2(1+\lambda_2)}, \\ \theta_4 &= \frac{(1+\alpha_1)\alpha_6 + \alpha_2\beta_6}{\alpha_2(1+\lambda_2)}, \\ \theta_5 &= \frac{(1+\alpha_1)\alpha_7 + \alpha_2\beta_7}{\alpha_2(1+\lambda_2)}, \\ \theta_6 &= \frac{(1+\alpha_1)\alpha_8 + \alpha_2\beta_8}{\alpha_2(1+\lambda_2)}, \\ \theta_7 &= \frac{(1+\alpha_1)\alpha_9 + \alpha_2\beta_9}{\alpha_2(1+\lambda_2)}. \end{aligned} \tag{26}$$

Now, by the center manifold theorem, we obtain the center manifold $G^c(0,0)$ of system (19) at $(0,0)$ in a small neighborhood of $m_1 = 0$ as follows:

$$\begin{aligned} G^c(0,0) &= \{(P_n, Q_n) : Q_n = h(P_n, m_1)\}, \\ &= \{(P_n, Q_n) : Q_n = e_1 m_1 + e_2 P_n^2 + e_3 m_1 P_n \\ &\quad + e_4 m_1^2 + o\left(\left(|P_n| + |m_1|\right)^2\right)\}. \end{aligned} \tag{27}$$

On applying map (19) on both sides of $Q_n = h(P_n, m_1)$, we have the following:

$$\begin{aligned} \lambda_2 Q_n + G_2(p_n, q_n, m_1) &= e_1 m_1 + e_2(-P_n + G_1(p_n, q_n, m_1))^2 \\ &\quad + e_3 m_1(-P_n + G_1(p_n, q_n, m_1)) \\ &\quad + e_4 m_1^2 + o\left(\left(|P_n| + |m_1|\right)^2\right), \end{aligned} \tag{28}$$

where

$$\begin{aligned} p_n &= \alpha_2(P_n + Q_n) = \alpha_2(P_n + h(P_n, m_1)), \\ q_n &= (-1-\alpha_1)P_n + (\lambda_2 - \alpha_1)Q_n \\ &= (-1-\alpha_1)P_n + (\lambda_2 - \alpha_1)h(P_n, m_1), \\ e_1 &= \frac{\theta_1}{1-\lambda_2}, \\ e_2 &= \frac{1}{1-\lambda_2}\left[\theta_2\alpha_2^2 + \theta_3(1+\alpha_1)^2 - \theta_5\alpha_2(-1-\alpha_1)\right], \\ e_3 &= \frac{1}{1+\lambda_2}\left[-2e_2\phi_1 - \theta_6\alpha_2 + \theta_7(-1-\alpha_1) - 2e_1\theta_2\alpha_2^2\right. \\ &\quad \left. + 2e_1\theta_3(-1-\alpha_1)(\lambda_2 - \alpha_1) - e_1\theta_5\alpha_2(\beta_2 - \alpha_1)\right], \\ e_4 &= \frac{1}{1-\lambda_2}\left[e_1^2\theta_2\alpha_2^2 + e_1^2\theta_3(\lambda_2 - \alpha_1)^2 + e_1^2\theta_5\alpha_2(\lambda_2 - \alpha_1)\right. \\ &\quad \left. + e_1\theta_6\alpha_2 + e_1\theta_7(\lambda_2 - \alpha_1) - e_2\phi_1^2 + \theta_4 - \phi_1 e_3\right]. \end{aligned} \tag{29}$$

Therefore, on the center manifold M^c at origin, we have the following:

$$\begin{aligned} p_n^2 &= \beta_2^2\left(P_n^2 + 2P_nQ_n + Q_n^2\right),\\ p_nq_n &= -\beta_2\left(1+\beta_1\right)P_n^2 + \beta_2\left(\delta_2 - \beta_1\right)P_nQ_n + \beta_2\left(\lambda_2 - \beta_1\right)Q_n^2,\\ q_n^2 &= \left(1+\beta_1\right)^2P_n^2 - 2\left(1+\beta_1\right)\left(\lambda_2 - \beta_1\right)P_nQ_n + \left(\lambda_2 - \beta_1\right)^2Q_n^2, \end{aligned} \tag{30}$$

where

$$\begin{aligned} P_nQ_n &= e_1m_1P_n + e_2P_n^3 + e_3m_1P_n^2 + e_4m_1^2P_n + o\left(\left(\left|P_n\right| + \left|m_1\right|\right)\right)^3,\\ Q_n^2 &= e_1^2m_1^2 + 2e_1e_2m_1P_n^2 + 2e_1e_3m_1^2P_n + 2e_1e_4m_1^3 + o\left(\left(\left|P_n\right| + \left|m_1\right|\right)\right)^3. \end{aligned} \tag{31}$$

Moreover, the map G^* restricted to CM $G^c(0,0)$ is as follows:

$$\begin{aligned} G^*\left(P_n\right) &= -P_n + G_1\left(p_n, q_n, m_1\right)\\ &= -P_n + g_1m_1 + g_2P_n^2 + g_3P_nm_1 + g_4m_1^2 + g_5P_n^2m_1\\ &\quad + g_6P_nm_1^2 + g_7P_n^3 + g_8m_1^3 + o\left(\left(\left|P_n\right| + \left|m_1\right|\right)^3\right), \end{aligned} \tag{32}$$

where

$$\begin{aligned} g_1 &= \phi_1,\\ g_2 &= \phi_2\beta_2^2 + \phi_3\left(1+\beta_1\right)^2 - \phi_5\beta_2\left(1+\beta_1\right),\\ g_3 &= 2e_1\phi_2\beta_2^2 - 2e_1\phi_3\left(1+\beta_1\right)\left(\lambda_2 - \beta_1\right) + e_1\phi_5\beta_2\left(\lambda_2 - \beta_1\right) + \phi_6\beta_2 - \phi_7\left(1+\beta_1\right),\\ g_4 &= e_1^2\phi_2\beta_2^2 + e_1^2\phi_3\left(\lambda_2 - \beta_1\right)^2 + \phi_4 + e_1^2\phi_5\beta_2\left(\lambda_2 - \beta_1\right) + e_1\phi_6\beta_2 + e_1\phi_7\left(\lambda_2 - \beta_1\right),\\ g_5 &= 2e_3\phi_2\beta_2^2 + 2e_1e_2\phi_2\beta_2^2 - 2e_3\phi_3\left(1+\beta_1\right)\left(\lambda_2 - \beta_1\right) + 2e_1e_2\phi_3\left(\lambda_2 - \beta_1\right)^2 + e_3\phi_5\beta_2\\ &\quad \left(\lambda_2 - \beta_1\right) + 2e_1e_2\phi_5\beta_2\left(\lambda_2 - \beta_1\right) + e_2\phi_6\beta_2 + e_2\phi_7\left(\lambda_2 - \beta_1\right),\\ g_6 &= 2e_4\phi_2\beta_2^2 + 2e_1e_3\phi_2\beta_2^2 - 2e_4\phi_3\left(1+\beta_1\right)\left(\lambda_2 - \beta_1\right) + 2e_1e_3\phi_3\left(\lambda_2 - \beta_1\right)^2 + e_4\phi_5\beta_2\\ &\quad \left(\lambda_2 - \beta_1\right) + 2e_1e_3\phi_5\beta_2\left(\lambda_2 - \beta_1\right) + e_3\phi_6\beta_2 + e_3\phi_7\left(\lambda_2 - \beta_1\right),\\ g_7 &= 2e_2\phi_2\beta_2^2 - 2e_2\phi_3\left(1+\beta_1\right)\left(\lambda_2 - \beta_1\right) + e_2\phi_5\beta_2\left(\lambda_2 - \beta_1\right),\\ g_8 &= 2e_1e_4\phi_2\beta_2^2 + 2e_1e_4\phi_3\left(\lambda_2 - \beta_1\right)^2 + 2e_1e_4\phi_5\beta_2\left(\lambda_2 - \beta_1\right) + e_4\phi_6\beta_2 + e_4\phi_7\left(\lambda_2 - \beta_1\right). \end{aligned} \tag{33}$$

From [43], we define ζ_1 and ζ_2 as follows:

$$\zeta_1 = \left(G^*_{P_nm_1} + \frac{1}{2}G^*_{m_1}G^*_{P_nP_n}\right)\Big|_{(P_n,m_1)=(0,0)} = g_3 + g_1g_2, \tag{34}$$

$$\zeta_2 = \left(\frac{1}{6}G^*_{P_nP_nP_n} + \left(\frac{1}{2}G^*_{P_nP_n}\right)^2\right)\Big|_{(P_n,m_1)=(0,0)} = g_7 + g_2^2. \tag{35}$$

Therefore, we have got the following findings of flip bifurcation from the aforementioned study.

Theorem 1. *If $\zeta_1 \neq 0$ and $\zeta_2 \neq 0$, then system (5) exhibits a flip bifurcation at $E^*(x^*, y^*)$ when m_1 changes in a small neighborhood of the origin. Moreover, if $\zeta_2 > 0$ (or $\zeta_2 < 0$), then the existing period-two orbits from $E^*(x^*, y^*)$ are stable (or unstable).*

4.2. Neimark–Sacker Bifurcation. In this subsection, we find the condition for the existence of Neimark–Sacker (NS) bifurcation and also its direction and stability properties for system (5) near $E^*(x^*, y^*)$ using the method followed in [32, 42]. For the existence of NS bifurcation of system (5), the complex conjugate eigenvalues of the characteristic equation at $E^*(x^*, y^*)$ should have absolute value one. For this, it is necessary to satisfy the following:

$$(B_1(x^*, y^*))^2 - 4B_2(x^*, y^*) < 0 \text{ and } B_2(x^*, y^*) = 1, \quad (36)$$

which provides

$$A(m) := \left(2 - ax^* + \frac{gx^*y^*}{(x^*+b)^2} - \frac{r_2y^{*2}}{(y^*+m)^2}\right)^2 - 4\left(1 - ax^* + \frac{gx^*y^*}{(x^*+b)^2}\right)$$
$$- \frac{r_2(1-ax^*)y^{*2}}{(y^*+m)^2} - \frac{gr_2x^*y^{*3}}{(x^*+b)^2(y^*+m)^2} + \frac{ghx^*y^{*2}}{(x^*+b)(x^*+c)^2} < 0, \quad (37)$$

$$B(m) := -ax^* + \frac{gx^*y^*}{(x^*+b)^2} - \frac{r_2(1-ax^*)y^{*2}}{(y^*+m)^2} - \frac{gr_2x^*y^{*3}}{(x^*+b)^2(y^*+m)^2} + \frac{ghx^*y^{*2}}{(x^*+b)^2(x^*+c)^2} = 0.$$

Note that the left-hand side of (37) is in terms of m since m is taken as a bifurcation parameter. It is difficult to find the explicit expression for the critical value m to satisfy (24) for the occurrence of NS bifurcation of system (5). Therefore, we assume that the critical value is $m = m_h$. Also, the interior equilibrium $E^*(x^*, y^*)$ is calculated at the critical value $m = m_h$.

Next, if $a_2 > 0$, $a_3 < 0$, and $h(y^* + m)/r_2 > c$ holds, we define the neighborhood as follows:

$$\Theta_h = \{(r_1, r_2, a, b, c, g, h, m) : m = m_h, r_1, r_2, a, b, c, g, h > 0\}. \quad (38)$$

Then, the equilibrium point $E^*(x^*, y^*)$ can arise NS bifurcation at $m = m_h$ when it changes in the neighborhood of Θ_h. Now, we analyze the properties of possible NS bifurcation at $E^*(x^*, y^*)$ for system (5) if (24) holds for some m_h. Given a perturbation $|m_2| \ll 1$ of critical value m_h, then the perturbation system is described as follows:

$$\begin{cases} x_{n+1} = x_n \exp\left[r_1 - ax_n - \dfrac{gy_n}{x_n + b}\right], \\ y_{n+1} = y_n \exp\left[\dfrac{r_2y_n}{y_n + (m_2 + m_h)} - \dfrac{hy_n}{x_n + c}\right]. \end{cases} \quad (39)$$

Let us use the transform $p_n = x_n - x^*$, $q_n = y_n - y^*$ and shift $E^*(x^*, y^*)$ to $(0, 0)$. Then, system (28) takes the following form:

$$\begin{cases} p_{n+1} = (p_n + x^*)\exp\left[r_1 - a(p_n + x^*) - \dfrac{g(q_n + y^*)}{E^*(x^*, y^*) + b}\right] - x^*, \\ q_{n+1} = (q_n + y^*)\exp\left[\dfrac{r_2(q_n + y^*)}{(q_n + y^*) + (m_2 + m_h)} - \dfrac{h(q_n + y^*)}{E^*(x^*, y^*) + c}\right] - y^*. \end{cases} \quad (40)$$

Therefore, by Taylor expansion of (40),

$$\begin{cases} p_{n+1} = \rho_1p_n + \rho_2q_n + \rho_3p_n^2 + \rho_4p_nq_n + \rho_5q_n^2 + \rho_6p_n^3 \\ \qquad + \rho_7p_n^2q_n + \rho_8p_nv_n^2 + \rho_9v_n^3 + o\left(\left(|p_n| + |q_n|\right)^3\right), \\ q_{n+1} = \eta_1p_n + \eta_2q_n + \eta_3p_n^2 + \eta_4p_nq_n + \eta_5q_n^2 + \eta_6p_n^3 + \eta_7p_n^2q_n \\ \qquad + \eta_8p_nv_n^2 + \eta_9v_n^3 + o\left(\left(|p_n| + |q_n|\right)^3\right), \end{cases} \quad (41)$$

where

$$\rho_1 = 1 + x^* N_1,$$
$$\rho_2 = \frac{-gx^*}{x^* + b},$$
$$\rho_3 = \frac{-gx^* y^*}{(x^* + b)^3} + N_1 + \frac{x^* N_1^2}{2},$$
$$\rho_4 = -\frac{gb}{(x^* + b)^2} - \frac{gN_1 x^*}{x^* + b},$$
$$\rho_5 = \frac{g^2 x^*}{2(x^* + b)^2},$$
$$\rho_6 = -\frac{bgy^*}{(x^* + b)^4} - \frac{gN_1 x^* y^*}{(x^* + b)^3} + \frac{N_1^2}{2} + \frac{x^* N_1^3}{6},$$
$$\rho_7 = \frac{g^2 x^* y^*}{(x^* + b)^4} + \frac{gb}{(x^* + b)^3} - \frac{gbN_1}{(x^* + b)^2} - \frac{gN_1^2 x^*}{2(x^* + b)},$$
$$\rho_8 = -\frac{g^2 x^*}{(x^* + b)^3} + \frac{g^2(1 + x^* N_1)}{2(x^* + b)^2},$$
$$\rho_9 = -\frac{g^3 x^*}{6(x^* + b)^3},$$
$$\eta_1 = \frac{hy^{*2}}{(x^* + c)^2},$$
$$\eta_2 = 1 + y^* N_2,$$
$$\eta_3 = \frac{-hy^{*2}}{(x^* + c)^3} + \frac{h^2 y^{*3}}{2(x^* + c)^4},$$
$$\eta_4 = \frac{2hy^*}{(x^* + c)^2} + \frac{hy^{*2} N_2}{(x^* + c)^2},$$
$$\eta_5 = \frac{-r_2 m_h y^*}{(y^* + m_h)^3} + N_2 + \frac{y^* N_2^2}{2},$$
$$\eta_6 = \frac{hy^{*2}}{(x^* + c)^4} - \frac{h^2 y^{*3}}{(x^* + c)^5} + \frac{h^3 y^{*4}}{6(x^* + c)^6},$$
$$\eta_7 = \frac{-hy^*(2 + y^* N_2)}{(x^* + c)^3} + \frac{h^2 y^{*2}(3 + y^* N_2)}{2(x^* + c)^4},$$
$$\eta_8 = \frac{h\left(1 + y^{*2} N_2^2\right)}{2(x^* + c)^2} + \frac{2hy^* N_2}{(x^* + c)^2} - \frac{r_2 m_h}{(y^* + m_h)^2},$$
$$\eta_9 = \frac{r_2 m_h y^*}{(y^* + m_h)^4} - \frac{r_2 m_h(1 + N_2 y^*)}{(y^* + m_h)^3} + \frac{N_2^2}{2} + \frac{N_2^3 y^*}{6},$$
$$N_1 = -a + \frac{gy^*}{(x^* + b)^2},$$
$$N_2 = \frac{-r_2 y^*}{(y^* + m_h)^2}. \tag{42}$$

The characteristic polynomial equation associated with the linearized system (30) at the origin can be given as follows:

$$\lambda^2 + q_1(m_2)\lambda + q_2(m_2) = 0, \tag{43}$$

where

$$q_1(m_2) = \left(-1 + ax^* - \frac{gx^* y^*}{(x^* + b)^2}\right)\Omega_1 - \left(1 - \frac{r_2 y^{*2}}{(y^* + (m_h + m_2))^2}\right)\Omega_2,$$
$$q_2(m_2) = \left[\left(1 - ax^* + \frac{gx^* y^*}{(x^* + b)^2}\right)\left(1 - \frac{r_2 y^{*2}}{(y^* + (m_h + m_2))^2}\right) + \frac{ghx^* y^{*2}}{(x^* + b)(x^* + c)^2}\right]\Omega_1\Omega_2, \tag{44}$$

With $\Omega_1 = \exp[r_1 - ax^* - gy^*/x^* + b]$ and $\Omega_2 = \exp[r_2 y^*/ y^* + (m_h + m_2) - hy^*/x^* + c]$. Now, the roots of (43) are the pair of complex conjugates.

$$\lambda_{1,2} = \frac{1}{2}\left[-q_1(m_2) \pm i\sqrt{4q_2(m_2) - (q_1(m_2))^2}\right]. \tag{45}$$

Since $(r_1, r_2, a, b, c, g, h, m) \in \Theta_h$, we have,
$|\lambda_{1,2}| = \sqrt{q_2(m_2)}$
and

$$\frac{d|\lambda_{1,2}|}{dm_2} = \frac{1}{2\sqrt{q_2(0)}}\left\{\left(1 - ax^* + \frac{gx^* y^*}{(x^* + b)^2}\right)\left(\frac{2r_2 y^{*2}}{(y^* + m_h)^3}\right) - \frac{r_2 y^*}{(y^* + m_h)^2}\left[\left(1 - ax^* + \frac{gx^* y^*}{(x^* + b)^2}\right) \times\left(1 - \frac{r_2 y^{*2}}{(y^* + m_h)^2}\right) + \frac{ghx^* y^{*2}}{(x^* + b)(x^* + c)^2}\right]\right\} \neq 0. \tag{46}$$

Furthermore, it is required $\lambda_1^k, \lambda_2^k \neq 1$ for $k = 1, 2, 3, 4$, when $m_2 = 0$, which implies $q_1(0) = \pm 2, 0, -1$. Therefore, $q_1(0) = -2 + ax^* - gx^* y^*/(x^* + b)^2 + r_2 y^{*2}/(y^* + m_h)^2 \neq \pm 2$. We only require $q_1(0) \neq 0, 1$, i.e.,

$$ax^* - \frac{gx^* y^*}{(x^* + b)^2} + \frac{r_2 y^{*2}}{(y^* + m_h)^2} \neq 2, 3. \tag{47}$$

Let $m_2 = 0$, $\sigma = -q_1(0)/2$, and $\theta = \sqrt{4q_2(0) - q_1^2(0)}/2$, and construct the nonsingular matrix.

$$L = \begin{pmatrix} \rho_2 & 0 \\ \sigma - \rho_1 & \theta \end{pmatrix}, \tag{48}$$

Use the translation $\begin{pmatrix} p_n \\ q_n \end{pmatrix} = L\begin{pmatrix} P_n \\ Q_n \end{pmatrix}$. Thus, system (30) takes the following form:

$$\begin{cases} P_{n+1} = \sigma P_n + \theta Q_n + R_1(P_n, Q_n) + o\left(\left(|p_n| + |q_n|\right)^3\right), \\ Q_{n+1} = -\theta P_n + \sigma Q_n + R_2(P_n, Q_n) + o\left(\left(|p_n| + |q_n|\right)^3\right), \end{cases} \tag{49}$$

where

$$R_1(P_n, Q_n) = \frac{1}{\rho_2}\begin{bmatrix} \left\{\rho_3\rho_2^2 + \rho_4\rho_2(\sigma-\rho_1) + \rho_5(\sigma-\rho_1)^2\right\}P_n^2 \\ +\left\{\rho_4\rho_2\theta + 2\theta\rho_5(\sigma-\rho_1)\right\}P_nQ_n + \rho_5\theta^2Q_n^2 \\ +\left\{\rho_6\rho_2^3 + \rho_7\rho_2^2(\sigma-\rho_1) + \rho_8\rho_2(\sigma-\rho_1)^2 + \rho_9(\sigma-\rho_1)^3\right\}P_n^3, \\ +\left\{\rho_7\rho_2^2 + 2\theta\rho_8\rho_2(\sigma-\rho_1) + 3\theta\rho_9(\sigma-\rho_1)(\sigma-\rho_1)^2\right\}P_n^2Q_n \\ +\left\{\theta^2\rho_8\rho_2 + 3\theta^2\rho_9(\sigma-\rho_1)\right\}P_nQ_n^2 + \theta^3\rho_9Q_n^3 \end{bmatrix},$$

$$R_2(P_n, Q_n) = \begin{bmatrix} \frac{1}{\rho_2\theta}\left\{\rho_2^2\rho_3(\rho_1-\sigma) + \rho_2\eta_3 + \rho_2(\sigma-\rho_1)(\rho_4(\rho_1-\sigma)\right. \\ \left.+\rho_2\eta_4) + (\sigma-\rho_1)^2(\rho_5(\rho_1-\sigma) + \rho_2\eta_5)\right\}P_n^2 + \{\theta\rho_2(\rho_4 \\ \times(\rho_1-\sigma) + \rho_2\eta_4) + 2\theta(\sigma-\rho_1)(\rho_5(\rho_1-\sigma) + \rho_2\eta_5)\}P_nQ_n \\ +\theta^2\{\rho_5(\rho_1-\sigma) + \rho_2\eta_5\}Q_n^2 + \left\{\rho_2^3\rho((\rho_1-\sigma) + \rho_2\eta_6)\right. \\ +\rho_2^2(\sigma-\rho_1)(\rho_7(\rho_1-\sigma) + \rho_2\eta_7) + \rho_2(\sigma-\rho_1)^2(\rho_8(\rho_1-\sigma) \\ \left.+\rho_2\eta_8)(\sigma-\rho_1)^3(\rho_9(\rho_1-\sigma) + \rho_2\eta_9)\right\}P_n^3 + \left\{\theta\rho_2^2(\rho_7(\rho_1-\sigma)\right. \\ \left.+\rho_2\eta_7) + 2\theta\rho_2(\sigma-\rho_1)(\rho_8(\rho_1-\sigma) + \rho_2\eta_8) + 3\theta(\sigma-\rho_1)^2\right. \\ \left.\times(\rho_9(\rho_1-\sigma) + \rho_2\eta_9)\right\}P_n^2Q_n + \left\{\theta^2\rho_2(\rho_8(\rho_1-\sigma) + \rho_2\eta_8)\right. \\ \left.+3\theta^2(\sigma-\rho_1)(\rho_9(\rho_1-\sigma) + \rho_2\eta_9)\right\}P_nQ_n^2 + \theta^3(\rho_9(\rho_1-\sigma) \\ +\rho_2\eta_9)Q_n^3. \end{bmatrix} \tag{50}$$

Next, we require the nonzero quantity χ^* to ensure that system (34) undergoes NS bifurcation.

$$\chi^* = -\mathrm{Re}\left[\frac{(1-2\lambda)\bar{\lambda}^2}{1-\lambda}\xi_{11}\xi_{20}\right] - \frac{1}{2}|\xi_{11}|^2 - |\xi_{02}|^2 + \mathrm{Re}\left(\bar{\lambda}\xi_{21}\right), \tag{51}$$

where

$$\xi_{20} = \frac{1}{8}\left[\left(R_{1P_nP_n} - R_{1Q_nQ_n} + 2R_{2P_nQ_n}\right) + i\left(R_{2P_nP_n} - R_{2Q_nQ_n} - 2R_{1P_nQ_n}\right)\right],$$

$$\xi_{11} = \frac{1}{4}\left[\left(R_{1P_nP_n} + R_{1Q_nQ_n}\right) + i\left(R_{2P_nP_n} + R_{2Q_nQ_n}\right)\right],$$

$$\xi_{02} = \frac{1}{8}\left[\left(R_{1P_nP_n} - R_{1Q_nQ_n} - 2R_{2P_nQ_n}\right) + i\left(R_{2P_nP_n} - R_{2Q_nQ_n} + 2R_{1P_nQ_n}\right)\right], \tag{52}$$

$$\xi_{21} = \frac{1}{16}\left[\begin{array}{l}\left(R_{1P_nP_nP_n} + R_{1P_nQ_nQ_n} + R_{2P_nP_nQ_n} + R_2Q_nQ_nQ_n\right)\\ +i\left(R_{2P_nP_nP_n} + R_{2P_nQ_nQ_n} - R_{1P_nP_nQ_n} - R_{1Q_nQ_nQ_n}\right)\end{array}\right].$$

Therefore, from [42], we can state the subsequent results.

Theorem 2. *If (32) and (33) hold and also the quantity χ^* is nonzero, then system (28) admits NS bifurcation at $E^*(x^*, y^*)$ when m_h changes in the neighborhood of Θ_h. Additionally, if the quantity $\chi^* < 0$ (or $\chi^* > 0$), then the stable (or unstable) invariant closed curve starts to bifurcate from $E^*(x^*, y^*)$.*

5. Chaos Control

In this section, we study the chaos control analyses for system (5). Firstly, we use the state feedback control method as in [27] to control the chaotic system. For system (5), we consider the following corresponding controlled system:

$$\begin{cases} x_{n+1} = x_n \exp\left[r_1 - ax_n - \dfrac{gy_n}{x_n + b} - u(x_n, y_n)\right], \\ y_{n+1} = y_n \exp\left[\dfrac{r_2 y_n}{y_n + m} - \dfrac{hy_n}{x_n + c}\right], \end{cases} \tag{53}$$

where $u(x_n, y_n) = h_1(x_n - x^*) + h_2(y_n - y^*)$ is the feedback controlling force with feedback gains h_1 and h_2, with equilibrium $E^*(x^*, y^*)$ of (53). For the controlled system (36), the Jacobian matrix at $E^*(x^*, y^*)$ is given as

$$J(x^*, y^*) = \begin{pmatrix} \kappa_{11} - h_1 & \kappa_{12} - h_2 \\ \kappa_{21} & \kappa_{22} \end{pmatrix}, \tag{54}$$

where

$$\begin{aligned} \kappa_{11} &= 1 - ax^* + \frac{gx^*y^*}{(x^* + b)^2}, \\ \kappa_{12} &= -\frac{gx^*}{x^* + b}, \\ \kappa_{21} &= \frac{hy^{*2}}{(x^* + b)^2}, \\ \kappa_{22} &= 1 - \frac{r_2 y^{*2}}{(y^* + m)^2}. \end{aligned} \tag{55}$$

Then, for $J(x^*, y^*)$, we have the characteristic equation as follows:

$$\overline{\lambda}^2 - (\kappa_{11} + \kappa_{22} - h_1)\overline{\lambda} + \kappa_{22}(\kappa_{11} - h_1) - \kappa_{21}(\kappa_{12} - h_2) = 0. \tag{56}$$

Let $\overline{\lambda}_1$ and $\overline{\lambda}_2$ be the eigenvalues of (54), which yields the following:

$$\overline{\lambda}_1 + \overline{\lambda}_2 = \kappa_{11} + \kappa_{22} - h_1, \tag{57}$$

$$\overline{\lambda}_1\overline{\lambda}_2 = \kappa_{22}(\kappa_{11} - h_1) - \kappa_{21}(\kappa_{12} - h_2). \tag{58}$$

Using (57) and (58), $\overline{\lambda}_1\overline{\lambda}_2 = 1$, $\overline{\lambda}_1 = 1$, and $\overline{\lambda}_1 = -1$. Also, ensure that $|\overline{\lambda}_{1,2}| < 1$. Then, we derive the marginal stability lines as follows:

$$\begin{aligned} &\overline{L}_1\colon \kappa_{11}\kappa_{22} - \kappa_{21}\kappa_{12} - 1 = h_1\kappa_{22} - h_2\kappa_{21}, \\ &\overline{L}_2\colon h_1(1 - \kappa_{22}) + h_2\kappa_{21} = \kappa_{11} + \kappa_{22} - 1 - \kappa_{11}\kappa_{22} + \kappa_{21}\kappa_{12}, \\ &\overline{L}_3\colon h_1(1 + \kappa_{22}) - h_2\kappa_{21} = \kappa_{11} + \kappa_{22} + 1 + \kappa_{11}\kappa_{22} - \kappa_{21}\kappa_{12}. \end{aligned} \tag{59}$$

Moreover, the triangular region enclosed by lines $\overline{L}_1$, $\overline{L}_2$, and $\overline{L}_3$ have stable eigenvalues for the Jacobian matrix (37).

Next, the pole-placement control method, as in [31], is utilized to control the unstable dynamics of system (5). By taking m as control parameter, we rewrite system (5) as follows:

$$\begin{cases} x_{n+1} = x_n \exp\left[r_1 - ax_n - \dfrac{gy_n}{x_n + b}\right] = f_1(x_n, y_n), \\ y_{n+1} = y_n \exp\left[\dfrac{r_2 y_n}{y_n + m} - \dfrac{hy_n}{x_n + c}\right] = f_2(x_n, y_n). \end{cases} \tag{60}$$

Furthermore, m is needed to lie in some interval $|m - m_0| < \delta$ with $\delta > 0$ and m_0 denotes the nominal value, for which system (5) has unstable dynamics. Now, we utilize the state feedback control method to shift the trajectory to the expected state. Let the equilibrium point $E^*(x^*, y^*)$ be unstable for system (5) because of NS bifurcation. Then,

system (5) can be approximated near $E^*(x^*, y^*)$ using the linear map, which is given by the following:

$$\begin{pmatrix} x_{n+1} - x^* \\ y_{n+1} - y^* \end{pmatrix} \approx A\begin{pmatrix} x_n - x^* \\ y_n - y^* \end{pmatrix} + tBn\left[m - m_0\right), \tag{61}$$

where

$$A = \begin{pmatrix} \dfrac{\partial f_1(x^*, y^*, m_0)}{\partial x_n} & \dfrac{\partial f_1(x^*, y^*, m_0)}{\partial y_n} \\ \dfrac{\partial f_2(x^*, y^*, m_0)}{\partial x_n} & \dfrac{\partial f_2(x^*, y^*, m_0)}{\partial y_n} \end{pmatrix},$$

$$B = \begin{pmatrix} \dfrac{\partial f_1(x^*, y^*, m_0)}{\partial m} \\ \dfrac{\partial f_2(x^*, y^*, m_0)}{\partial m} \end{pmatrix} = \begin{pmatrix} 0 \\ \dfrac{-r_2 y^*}{(y^* + m)^2} \end{pmatrix}. \tag{62}$$

It is clear to observe that system (44) is controllable, provided matrix C has rank 2, which is,

$$C = (B:\ AB) = \begin{pmatrix} 0 & \left(\dfrac{\partial f_1(x^*, y^*, m_0)}{\partial y_n}\right)\dfrac{-r_2 y^{*2}}{(y^* + m)^2} \\ \dfrac{-r_2 y^*}{(y^* + m)^2} & \left(\dfrac{\partial f_2(x^*, y^*, m_0)}{\partial y_n}\right)\dfrac{-r_2 y^*}{(y^* + m)^2} \end{pmatrix}. \tag{63}$$

Furthermore, $-r_2 y^{*2}/(y^* + m)^2 \neq 0$, and assume that $\partial f_2(x^*, y^*, m_0)/\partial y_n \neq 0$. Then, system (44) is controllable. Next, we assume that $[m - m_0] = -K\begin{bmatrix} x_n - x^* \\ y_n - y^* \end{bmatrix}$, where $K = \begin{bmatrix} s_1 & s_2 \end{bmatrix}$. Then, system (44) can be written as follows:

$$\begin{pmatrix} x_{n+1} - x^* \\ y_{n+1} - y^* \end{pmatrix} \approx (A - BK)\begin{pmatrix} x_n - x^* \\ y_n - y^* \end{pmatrix}. \tag{64}$$

Then, the controller system is given by the following:

$$\begin{cases} x_{n+1} = x_n \exp\left[r_1 - ax_n - \dfrac{gy_n}{x_n + b}\right] = f_1(x_n, y_n), \\ y_{n+1} = y_n \exp\left[\dfrac{r_2 y_n}{m_0 - S + y_n} - \dfrac{hy_n}{x_n + c}\right] = f_2(x_n, y_n). \end{cases} \tag{65}$$

where $S = s_1(x_n - x^*) + s_2(y_n - y^*)$. Furthermore, if the matrix $A - BK$ has eigenvalues $\overline{\lambda}_1$ and $\overline{\lambda}_2$ that lie in an open unit disk, then $E^*(x^*, y^*)$ is locally asymptotically stable. Thus, we have the following:

$$A - BK = \begin{pmatrix} \kappa_{11} & \kappa_{12} \\ \kappa_{21} - \theta s_1 & \kappa_{22} - \theta s_1 \end{pmatrix}, \tag{66}$$

where $\theta = -r_2 y^{*2}/(y^* + m)^2$, and κ_{11}, κ_{12}, κ_{21}, and κ_{22} are the same as in (54). Then, the characteristic polynomial of (66) can be written as follows:

$$\overline{\lambda}^2 - (\kappa_{11} + \kappa_{22} - \theta s_2)\overline{\lambda} + \kappa_{11}(\kappa_{22} - \theta s_2) + \kappa_{12}(\theta s_1 - \kappa_{21}) = 0. \tag{67}$$

The lines of marginal stability are obtained, which are as follows:

$$\begin{aligned} &\overline{L}_1\colon \kappa_{11}(\kappa_{22} - \theta s_2) + \kappa_{12}(\theta s_1 - \kappa_{21}) = 1, \\ &\overline{L}_2\colon \kappa_{11} + \kappa_{22} = 1 + \theta s_2 + \kappa_{11}(\kappa_{22} - \theta s_2) + \kappa_{12}(\theta s_1 - \kappa_{21}), \\ &\overline{L}_3\colon \theta s_2 = \kappa_{11} + \kappa_{22} + 1 + \kappa_{11}(\kappa_{22} - \theta s_2) + \kappa_{12}(\theta s_1 - \kappa_{21}). \end{aligned} \tag{68}$$

Therefore, matrix (49) has stable eigenvalues enclosed by the straight lines $\overline{L}_1$, $\overline{L}_2$, and $\overline{L}_3$ in s_1, s_2- plane.

Next, we apply the hybrid control feedback methodology [28, 29] for controlling the bifurcation behavior of the system near the equilibrium point $E^*(x^*, y^*)$. Then, the controlled system can be written as follows:

$$\begin{cases} x_{n+1} = \epsilon x_n \exp\left[r_1 - ax_n - \dfrac{gy_n}{x_n + b}\right] + (1 - \epsilon)x_n, \\ y_{n+1} = \epsilon y_n \exp\left[\dfrac{r_2 y_n}{y_n + m} - \dfrac{hy_n}{x_n + c}\right] + (1 - \epsilon)y_n, \end{cases} \tag{69}$$

where $0 < \epsilon < 1$ is the controlled strategy of the combination of both feedback control and parameter perturbation. The Jacobian matrix evaluated for system (54) at $E^*(x^*, y^*)$ is given by the following:

$$\begin{pmatrix} 1 - \epsilon a x^* + \dfrac{\epsilon g x^* y^*}{(x^* + b)^2} & -\dfrac{\epsilon g x^*}{x^* + b} \\ \dfrac{\epsilon h y^{*2}}{(x^* + C)^2} & 1 - \dfrac{\epsilon r_2 y^{*2}}{(y^* + m)^2} \end{pmatrix}. \tag{70}$$

Note that one can select the appropriate value for ϵ to ensure that all eigenvalues of the above matrix satisfy $|\overline{\lambda}_{1,2}| < 1$.

Remark 1. System (2) is the extension of a continuous-time system (1) with the Allee effect in the predator's growth term. It is worth mentioning here that the discrete form of system (2) is not studied elsewhere in the literature. Hence, we obtained discrete-time system (5) from (2) using methods similar to those in [11, 12]. Moreover, the influence of the Allee effect is shown in terms of flip and Neimark–Sacker

Table 1: The equilibrium point values of Case (i).

m	x^*	y^*
0.2	0.755 253	2.190 958
0.27	0.762 114	2.134 027
0.4	0.774 789	2.028 170
0.5	0.784 481	1.946 631
0.53	0.787 379	1.922 151
0.9	0.822 760	1.619 543

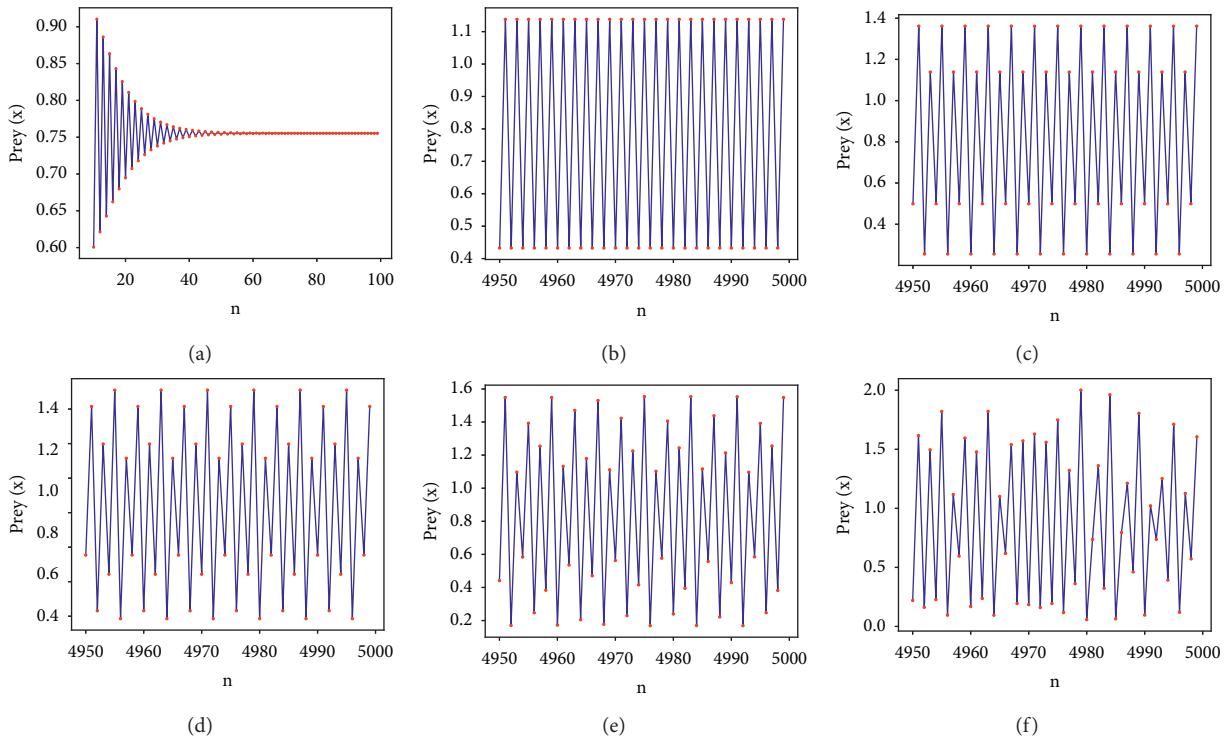

Figure 1: The time series plots for system (5) with $r_1 = 3.3$, $a = 3.3$, $g = 1.2$, $b = 2.5$, $r_2 = 1$, $h = 0.525$, and $c = 0.5$ (a) locally stable for $m = 0.2$, (b) period-2 for $m = 0.27$, (c) period-4 for $m = 0.4$, (d) period-8 for $m = 0.5$, (e) 8-chaotic like attractor for $m = 0.53$, and (f) chaotic attractor for $m = 0.9$.

bifurcations for system (5). Using the results in [42, 43], the direction and stability properties of both bifurcations can be discussed with the help of Theorem 1 and 2. Also, the bifurcation and chaos control analyses are carried out by utilizing the methods in [27–31].

6. Numerical Simulations

In the subsequent section, we perform some simulations for system (5) at $E^*(x^*, y^*)$ to ensure our mathematical results obtained in the previous sections.

Case (i): firstly, let us take the parameter values as $r_1 = 3.3$, $a = 3.3$, $g = 1.2$, $b = 2.5$, $r_2 = 1$, $h = 0.525$, and $c = 0.5$ and varying $m \in (0, 1]$ for system (5). Then, system (5) exhibits flip bifurcation when m reaches the critical value $m_f = 0.28805$, and the interior equilibrium point at m_f is $E^*(x^*, y^*) = (0.76387948, 2.11933949)$, which also satisfies (13). Also, the characteristic (12) is given by the following:

$$\lambda^2 + 1.11345044\lambda + 0.11345926 = 0, \tag{71}$$

where $\lambda_{1,2} = -0.11346, -1$ are the eigenvalues of the Jacobian matrix at $E^*(x^*, y^*)|_{m_f}$. Then, from (34) and (35), we obtain $\zeta_1 = 1.3842$ and $\zeta_2 = 5.17693$, and the properties of flip bifurcation are illustrated in Theorem 1.

The interior equilibrium point varies accordingly for various values of m, which is given in Table 1. The nature of system (5) near $E^*(x^*, y^*)$ is shown for different values of m, for $m = 0.2$ is stable, $m = 0.27$ is period-2, $m = 0.4$ is period-4, $m = 0.5$ is period-8, $m = 0.53$ is chaotic, and $m = 0.9$ is chaotic, which are shown by the time series plots in Figure 1 and the phase portraits in Figure 2. It shows that the system becomes chaotic from stable via period-doubling cascade for larger values of m. Also, the chaotic nature of the system is confirmed by one parameter bifurcation diagram and the maximum Lyapunov exponent in Figure 3.

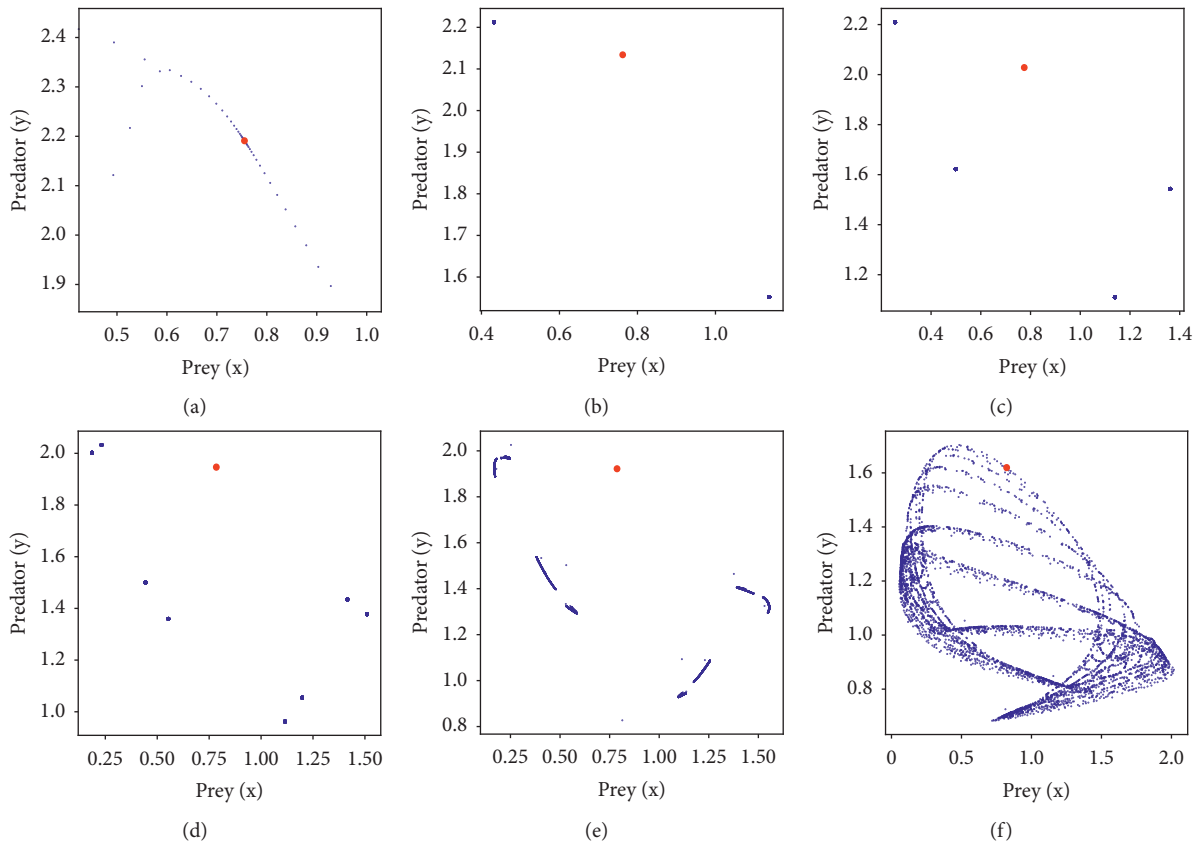

Figure 2: The phase portraits for system (5) with $r_1 = 3.3$, $a = 3.3$, $g = 1.2$, $b = 2.5$, $r_2 = 1$, $h = 0.525$, and $c = 0.5$ (a) locally stable for $m = 0.2$, (b) period-2 for $m = 0.27$, (c) period-4 for $m = 0.4$, (d) period-8 for $m = 0.5$, (e) 8-chaotic like attractor for $m = 0.53$, and (f) chaotic attractor for $m = 0.9$. The red points represent the interior equilibrium point $E^*(x^*, y^*)$, and its values are given in Table 1.

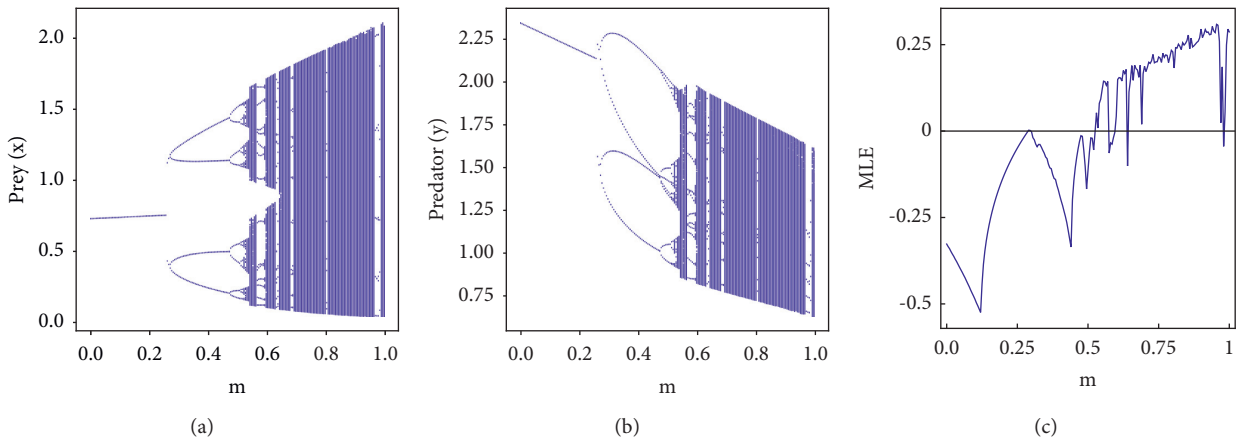

Figure 3: ((a), (b)). The flip bifurcation diagrams. (c) The maximum Lyapunov exponents for system (5) with $r_1 = 3.3$, $a = 3.3$, $g = 1.2$, $b = 2.5$, $r_2 = 1$, $h = 0.525$, $c = 0.5$, and $m \in [0, 1]$.

Table 2: The equilibrium point values of Case (ii).

m	x^*	y^*
0.18	0.655 489	2.230 839
0.2	0.692 054	2.245 334
0.5	1.099 589	2.329 801
0.58	1.184 178	2.329 602
0.88	1.457 370	2.287 330
0.9	1.513 887	2.270 648

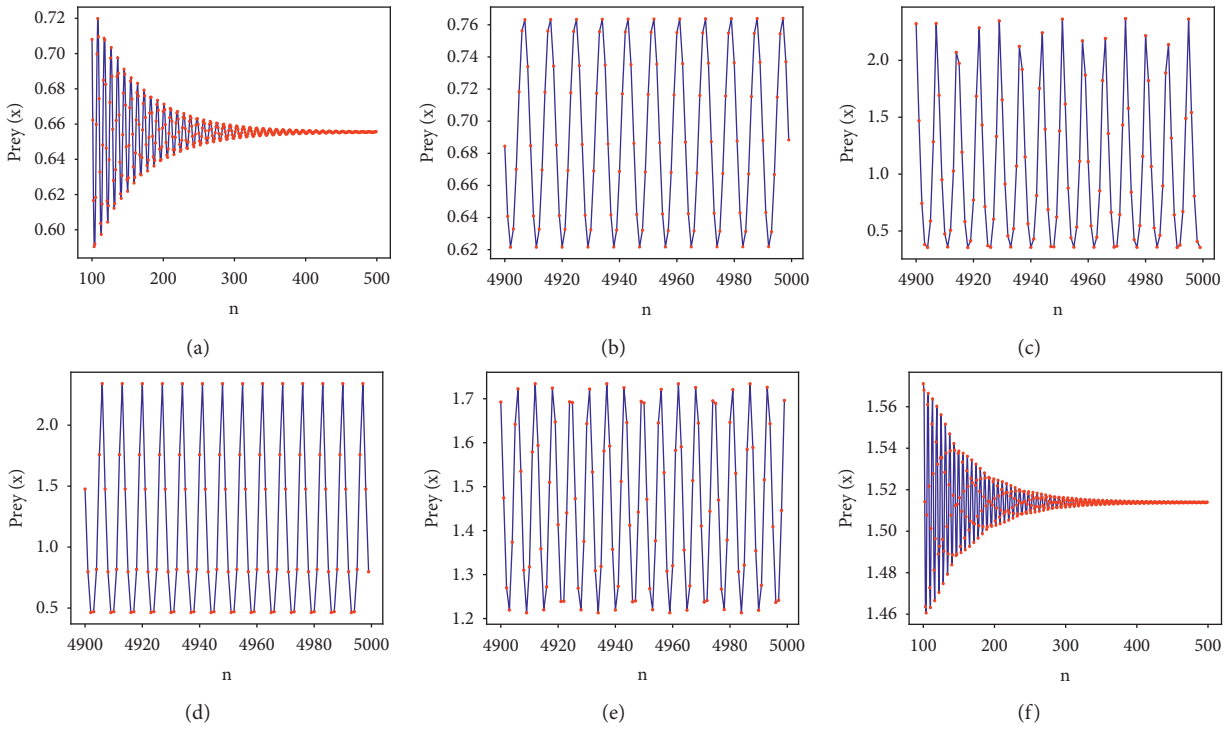

Figure 4: The time series plots for system (5) with $r_1 = 4$, $a = 1.15$, $g = 2.7$, $b = 1.2$, $r_2 = 1$, $h = 1.06$, and $c = 1.9$ (a) asymptotically stable for $m = 0.18$, ((b), (c)) invariant circles for $m = 0.2, 0.5$, (d) period-8 for $m = 0.58$, (e) invariant circle for $m = 0.88$, and (e) asymptotically stable for $m = 0.95$.

Case (ii): next, choose the system parameter values as $r_1 = 4$, $a = 1.15$, $g = 2.7$, $b = 1.2$, $r_2 = 1$, $h = 1.06$, $c = 1.9$, and varying $m \in (0, 1]$. Then, system (5) exhibits NK bifurcation at the critical value $m = m_h = 0.199023$ and has the equilibrium point $E^*(x^*, y^*) = (0.69031513, 2.24467052)$. Then, the characteristic (12) takes the following form:

$$\lambda^2 - 1.53322562\lambda + 1 = 0, \tag{72}$$

Then, the above characteristic polynomial has the eigenvalues $\lambda_{1,2} = 0.766613 \pm i0.64211$. From (51), we obtain $\chi^* = -0.0946108$. Then, the properties of NK bifurcation are illustrated in Theorem 2.

The interior equilibrium point varies for various values of m, which is given in Table 2. The nature of system (5) near $E^*(x^*, y^*)$ is shown for different values of m, for $m = 0.18$ is asymptotically stable, $m = 0.2, 0.5$ are invariant circles, $m = 0.58$ is period-8, $m = 0.88$ is invariant circle, and $m = 0.95$ is locally asymptotically stable, as shown by the time plots in Figure 4 and the phase portraits in Figure 5. It shows that system (5) undergoes NK bifurcation and again attains stability via NK bifurcation. Also, the one parameter bifurcation diagram and the maximum Lyapunov exponent are shown in Figure 6.

6.1. Chaos Control. Next, we apply the state feedback control method for existing chaos in the flip bifurcation. The system (5) is in chaotic state for the parameter values in case (i), $r_1 = 3.3$, $a = 3.3$, $g = 1.2$, $b = 2.5$, $r_2 = 1$, $h = 0.525$, $c = 0.5$ and $m = 0.53$. Then, $E^*(x^*, y^*) = (0.787379, 1.922151)$ is unstable, and its phase portrait is given in Figure 2(e). We need to shift the unstable equilibrium toward the stable state. For this, take $m = 0.53$, and the corresponding controlled system is given by the following:

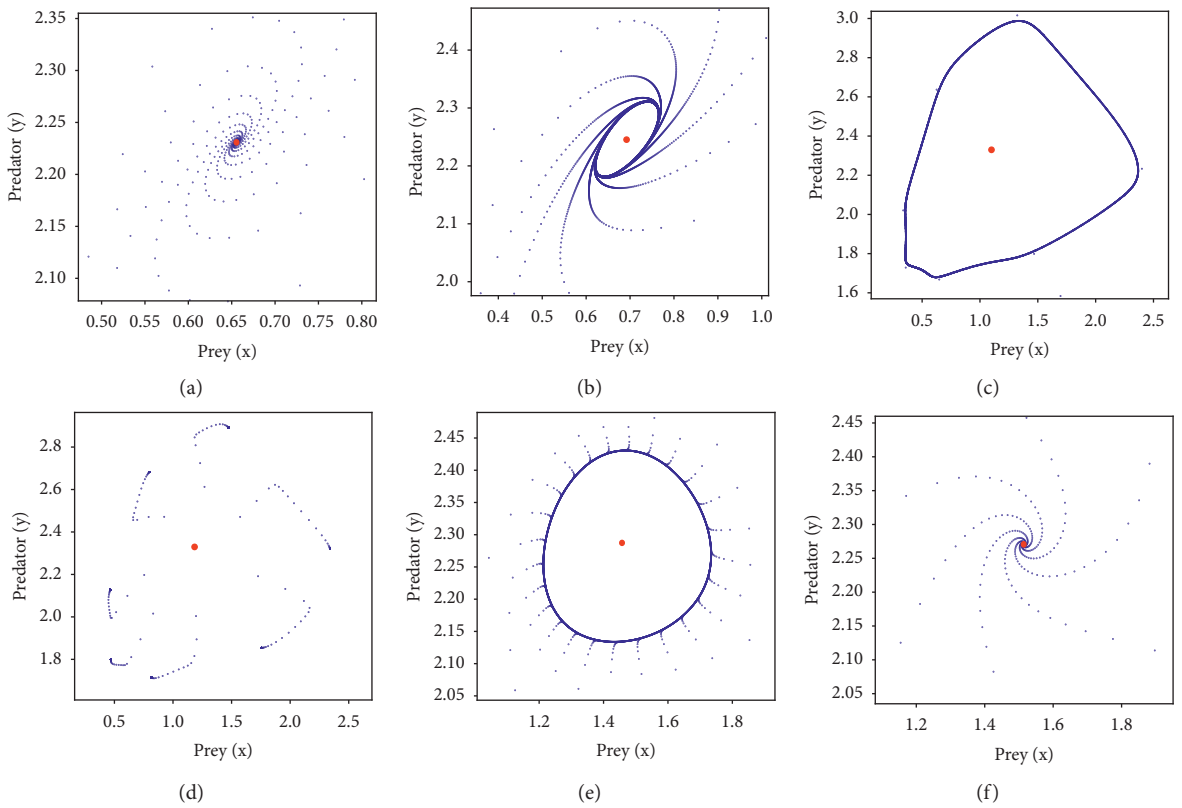

FIGURE 5: The phase portraits for system (5) with $r_1 = 4$, $a = 1.15$, $g = 2.7$, $b = 1.2$, $r_2 = 1$, $h = 1.06$, $c = 1.9$ (a) locally asymptotically stable for $m = 0.18$; ((b), (c)) invariant circles for $m = 0.2, 0.5$, (d) period-8 for $m = 0.58$, (e) invariant circle for $m = 0.88$, and (f) asymptotically stable for $m = 0.95$. The red points represent the interior equilibrium point $E^*(x^*, y^*)$, and its values are given in Table 2.

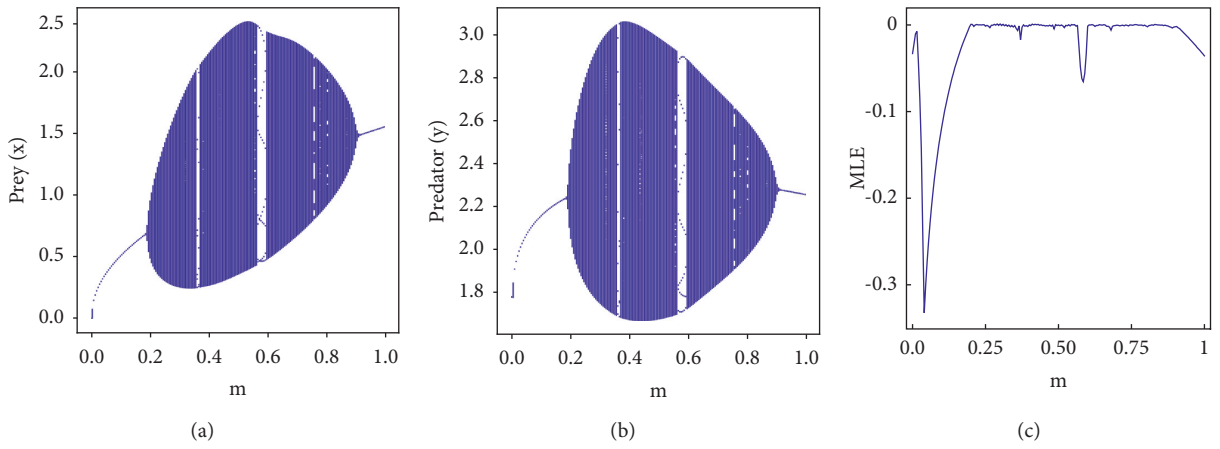

FIGURE 6: ((a), (b)).The Neimark–Sacker bifurcation diagram. (c) The maximum Lyapunov exponents for system (5) with $r_1 = 4$, $a = 1.15$, $g = 2.7$, $b = 1.2$, $r_2 = 1$, $h = 1.06$, $c = 1.9$, and $m \in [0, 1]$.

$$\begin{cases} x_{n+1} = x_n \exp\left[3.3 - 3.3x_n - \dfrac{1.2y_n}{x_n + 2.5} - u(x_n, y_n)\right], \\ y_{n+1} = y_n \exp\left[\dfrac{y_n}{y_n + 0.53} - \dfrac{0.525y_n}{x_n + 0.5}\right], \end{cases} \tag{73}$$

where $u(x_n, y_n) = h_1(x_n - x^*) + h_2(y_n - y^*)$, and h_1, h_2 are feedback gains. Furthermore, system (56) has the Jacobian matrix as follows:

$$J = \begin{pmatrix} -1.4303 - h_1 & -0.287419 - h_2 \\ 1.17037 & 0.385558 \end{pmatrix}. \tag{74}$$

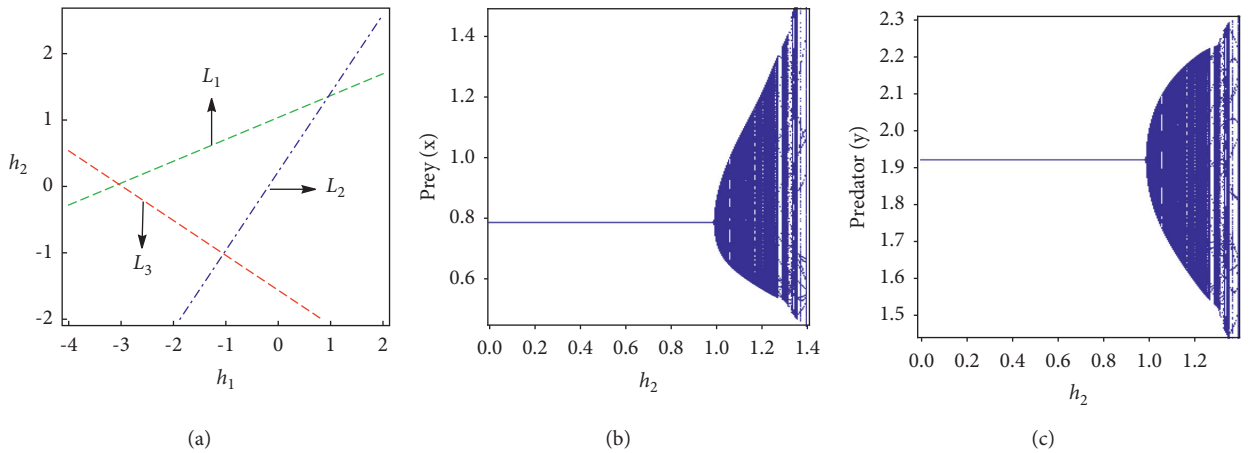

FIGURE 7: For the controlled system (36) with $r_1 = 3.3$, $a = 3.3$, $g = 1.2$, $b = 2.5$, $r_2 = 1$, $h = 0.525$, $c = 0.5$, $m = 0.53$, and $E^*(x^*, y^*) = (0.787379, 1.922151)$. (a) The stability triangle and ((b), (c) the bifurcation diagrams with $h_1 = -1$ and $h_2 = [0, 1.4]$.

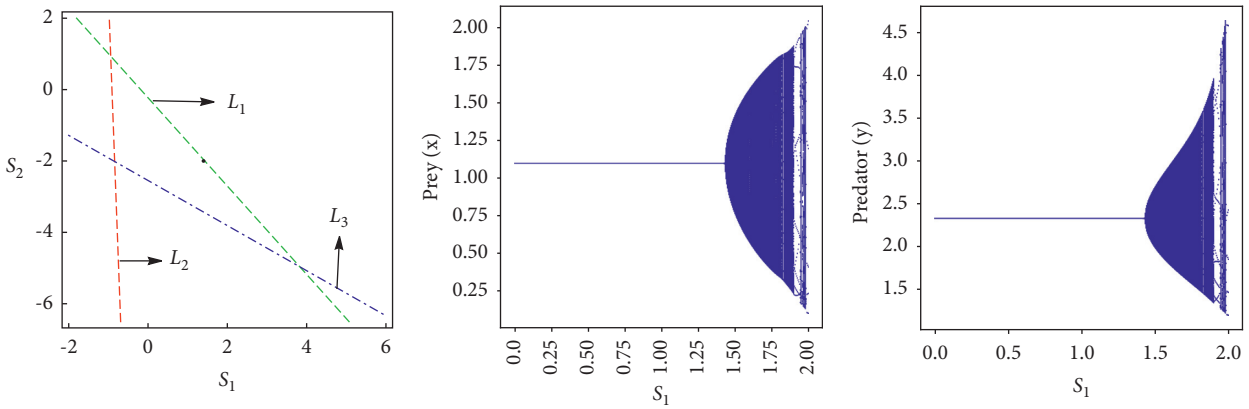

FIGURE 8: For the controlled system (48) with $r_1 = 4$, $a = 1.15$, $g = 2.7$, $b = 1.2$, $r_2 = 1$, $h = 1.06$, $c = 1.9$, $m = 0.5$, and $E^*(x^*, y^*) = (1.099589, 2.329801)$. (a) The stability triangle and ((b), (c) depict the bifurcation diagrams with $s_2 = -2$ and $s_1 = [0, 2]$.

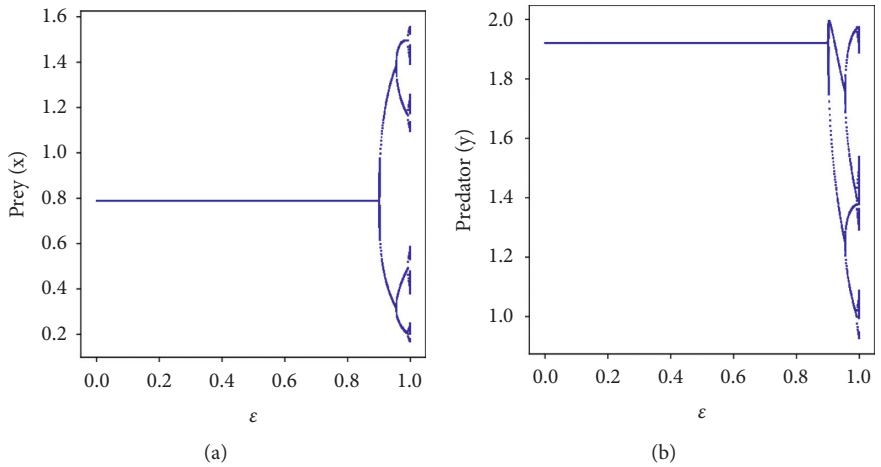

FIGURE 9: The bifurcation diagrams for the controlled system (54) with $r_1 = 3.3, a = 3.3, g = 1.2, b = 2.5, r_2 = 1, h = 0.525, c = 0.5, m = 0.53$, $E^*(x^*, y^*) = (0.787379, 1.922151)$, and $\epsilon \in (0, 1]$.

Then, we obtain the characteristic equation as follows:

$$\overline{\lambda}^2 + (1.04474 + h_1)\overline{\lambda} - 0.385558h_1 + 1.17037h_2 - 0.215078 = 0. \tag{75}$$

Furthermore, system (56) has the marginal stability lines, which are given by the following:

$$\begin{aligned} \overline{L}_1 &:= 0.38558h_1 - 1.17037h_2 = -1.21508, \\ \overline{L}_2 &:= 0.614442h_1 + 1.17037h_2 = -1.82966, \\ \overline{L}_3 &:= 1.38556h_1 - 1.17037h_2 = -0.259816. \end{aligned} \tag{76}$$

Then, the controlled system (56) has eigenvalues that may then be shown to be located within the triangular region defined by the straight lines $\overline{L}_1$, $\overline{L}_2$, and $\overline{L}_3$ (see Figure 7(a)). On choosing $k_1 = -1$, $E^*(x^*, y^*) = (0.787379, 1.922151)$ is locally stable if and only if $h_2 \in [-1, 0.8]$. Take $h_1 = -1$ and $h_2 \in [0, 1.4]$. Then, the bifurcation diagram for system (56) is plotted in Figures 7(b) and 7(c).

Secondly, we utilize the pole-placement control method by taking parameter values as in case (ii) $r_1 = 4$, $a = 1.15$, $g = 2.7$, $b = 1.2$, $r_2 = 1$, $h = 1.06$, $c = 1.9$, and $m = 0.5$. Then, system (5) is unstable near the equilibrium point $E^*(x^*, y^*) = (1.099589, 2.329801)$. To shift the unstable trajectory to the desired stable state, take $m = 0.5$, and system (48) is given by the following:

$$\begin{cases} x_{n+1} = x_n \exp\left[4 - 1.15x_n - \dfrac{2.7y_n}{x_n + 1.2}\right] = f_1(x_n, y_n), \\ y_{n+1} = y_n \exp\left[\dfrac{y_n}{0.5 - S + y_n} - \dfrac{1.06y_n}{x_n + 1.9}\right] = f_2(x_n, y_n), \end{cases} \tag{77}$$

where $S = s_1(x_n - x^*) + s_2(y_n - y^*)$, s_1 and s_2 are feedback gains. Then, we have the following:

$$\begin{aligned} A &= \begin{pmatrix} 1.04349 & -1.29105 \\ 0.63947 & 0.322162 \end{pmatrix}, \\ B &= \begin{pmatrix} 0 \\ -0.677838 \end{pmatrix}, \\ C &= \begin{pmatrix} 0 & 0.875124 \\ -0.677838 & -0.218374 \end{pmatrix}, \end{aligned} \tag{78}$$

and the above-controlled system has the Jacobian matrix, which is of the following form:

$$A - BK = \begin{pmatrix} 1.04349 & -1.29105 \\ 0.63947 + 0.677838s_1 & 0.322162 + 0.677838s_2 \end{pmatrix}, \tag{79}$$

and its characteristic polynomial is written as follows:

$$\begin{aligned} &\overline{\lambda}^2 - (1.36565 + 0.677838s_2)\overline{\lambda} + 0.875124s_1 \\ &\quad + 0.707315s_2 + 1.16176 = 0. \end{aligned} \tag{80}$$

Furthermore, the lines of marginal stability of (77) are computed as follows:

$$\begin{aligned} L_1 &:= 1.16176 + 0.875124s_1 - 0.707315s_2 = 1, \\ L_2 &:= 2.16176 + 0.875124s_1 + 0.0294771s_2 = 1.36565, \\ L_3 &:= 3.52741 + 0.875124s_1 + 0.707315s_2 = -0.677838s_2. \end{aligned} \tag{81}$$

The eigenvalues may then be shown to be located within the triangular region defined by the straight lines $\overline{L}_1$, $\overline{L}_2$, and $\overline{L}_3$ for system (57) (see Figure 8(a)). On choosing $s_2 = -2$, $E^*(x^*, y^*)$ is locally asymptotically stable if and only if $s_1 \in [-0.84, 1.43]$. Take s_1 and $s_2 \in [0, 2]$. Then, the bifurcation diagrams for the controlled system (57) are depicted in figures 8(b) and 8(c).

Finally, we choose the parameter values as in case (i) $r_1 = 3.3$, $a = 3.3$, $g = 1.2$, $b = 2.5$, $r_2 = 1$, $h = 0.525$, $c = 0.5$, and $m = 0.53$ to explore the hybrid control strategy. Now, the controlled system (54) takes the following form:

$$\begin{cases} x_{n+1} = \epsilon x_n \exp\left[3.3 - 3.3x_n - \dfrac{1.2y_n}{x_n + 2.5}\right] + (1 - \epsilon)x_n, \\ y_{n+1} = \epsilon y_n \exp\left[\dfrac{y_n}{y_n + 0.53} - \dfrac{0.525y_n}{x_n + 0.5}\right] + (1 - \epsilon)y_n. \end{cases} \tag{82}$$

Moreover, we have $E^*(x^*, y^*) = (0.787379, 1.922151)$ for system (58), and its Jacobian matrix is written as follows:

$$\begin{pmatrix} 1 - 2.4303\epsilon & -0.28419\epsilon \\ 1.17037\epsilon & 1 - 0.614442\epsilon \end{pmatrix}. \tag{83}$$

If $(0 < \varepsilon < 0.900535)$, then the above matrix has stable eigenvalues. Then, system (58) is stable near $E^*(x^*, y^*)$ for $(0 < \epsilon < 0.900535)$, which is depicted in the bifurcation diagram in Figure 9.

Remark 2. Allee effect could have a stabilizing or destabilizing effect or both, which depends on the parameters in the prey-predator model. For example, the growth of prey can cause chaotic dynamics in the discrete-time predator-prey model, and how the populations are changed from extinction to persistence because of the Allee effect in both prey and predator have been reported in [24]. The authors in [26] showed that without the Allee effect for a larger growth rate of prey, the system becomes chaotic near the boundary equilibrium point. In the presence of the Allee effect, the system becomes stable via reverse periodic doubling. Also, the considered system undergoes flip and Neimark–Sacker bifurcation near the interior equilibrium point at some critical Allee parameter value. System (5) considered in the present study has destabilizing effect for larger m, which is clearly shown in Figure 3. Also, with a different set of parameters, system (5) has both stabilizing and destabilizing effect because of m via Neimark–Sacker bifurcation, as shown in Figure 6.

Remark 3. Tassaddiq et al. [35] used a nonstandard finite difference scheme and obtained the discrete ratio-dependent prey-predator model. They showed that the considered system undergoes Neimark–Sacker bifurcation for larger values of the catchability coefficient. Moreover, they applied a pole-placement control strategy to obtain the controlled system and showed the controllable region in the feedback control space. Also, they applied the hybrid control strategy by choosing the catchability coefficient in the chaotic region and found the stability interval for the control parameter. Din [32] obtained the discrete system for (1) with a death rate of a predator by the method of piecewise constant arguments and showed that the considered system undergoes both types of bifurcations. Also, the author successfully implemented the state feedback control strategy to control FB and NSB and pole placement to control NSB. Hence, in the present study, we successfully implemented state feedback and hybrid control method to control FB, and the stable regions and bifurcation diagrams for feedback gains are shown in Figures 7 and 9 for system (5). Also, we implemented a pole-placement control method to control NSB, and it is depicted in Figure 8.

7. Conclusion

This article deals with a discrete-time modified Leslie–Gower system with the Allee effect in the predator population. The presence of the Allee effect in the prey-predator model can have a stabilizing or destabilizing effect. The existence criteria of biologically meaningful equilibrium points have been investigated, and their stability analysis has also been carried out. In system (1), even if the prey goes extinct, the predator can survive by changing its food habits and going for an alternative food source. Note that in system (5), the prey extinction equilibrium point $E_1 = (0, (r_2c/h) - m)$ exists only if $r_2c/h > m$, i.e., the Allee parameter m is certainly less than r_2c/h. Otherwise, the predator also goes to extension in the absence of prey. In the absence of the Allee effect $(m = 0)$, the prey extinction equilibrium point E_1 always exists. The existence and local stability of an interior equilibrium $E^*(x^*, y^*)$ can be achieved from Lemma 1 and Lemma 3. Figures 1(a), 4(a), and 4(f) show how the impact of m ensures the long-term survival of both species. We derived the conditions for the occurrence of flip and Neimark–Sacker bifurcations for system (5). Furthermore, we have discussed the direction and stability of both bifurcations with the help of the center manifold theorem and normal form theory. We showed that the size of the prey population increases and the predator population decreases when the Allee parameter m increases in Case (i), which is given in Table 1. Also, the sizes of both prey and predator populations increase when the Allee parameter m increases in Case (ii), which is given in Table 2. We showed that system (5) becomes chaotic from stable via flip bifurcation and also changes from stable to unstable via Neimark–Sacker bifurcation in numerical simulations for different sets of model parameters, varying the Allee parameter, see Figures 3 and 6. We verified the chaotic nature of the system with the help of a one-parameter bifurcation diagram and a maximum Lyapunov exponent, which show the stabilizing and destabilizing effect of the Allee parameter m. We observed that the proposed system exhibits complex behavior and is sensitive to the choice of parameter values and initial conditions. The presence of complex and chaotic behaviors in system (5) by varying the Allee parameter m can cause both prey and predator populations to have a higher risk of extinction. The presence of chaotic behavior in system (5) affects the prediction of the sizes of both populations in future generations. Also, we showed that the state feedback, pole-placement, and hybrid control methods help to shift the unstable equilibrium to a stable state for a suitable range of control parameters in Figures 7, 8, and 9.

In short, the presence of the Allee effect on the predator population has a high impact on the dynamics of the modified Leslie–Gower system with populations that have no overlap between generations, resulting in a new discrete system (5) with various dynamical behaviors. Thus, it could be interesting and meaningful to study the dynamics of the discrete predator-prey system (5) with the Allee effects in both prey and predator, also with other interaction functions. However, these terms will increase the complexity of system (5), and we will leave this as future research.

Data Availability

Data sharing is not applicable to this article as no datasets were generated or analyzed during the current study.

Conflicts of Interest

The authors declare that they have no competing interests.

Authors' Contributions

All authors contributed equally and significantly in writing this paper and typed, read, and approved the final manuscript.

References

[1] M. Danca, S. Codreanu, and B. Bakó, "Detailed analysis of a nonlinear prey-predator model," *Journal of Biological Physics*, vol. 23, no. 1, pp. 11–20, 1997.

[2] R. M. May, "Biological populations with nonoverlapping generations: stable points, stable cycles, and chaos," *Science*, vol. 186, no. 4164, pp. 645–647, 1974.

[3] H. I. Freedman, *Deterministic Mathematical Models in Population Ecology*, Wiley online library, Hoboken, New Jersey, USA, 1980.

[4] Z. Jing and J. Yang, "Bifurcation and chaos in discrete-time predator-prey system," *Chaos, Solitons & Fractals*, vol. 27, no. 1, pp. 259–277, 2006.

[5] X. Liu and D. Xiao, "Complex dynamic behaviors of a discrete-time predator-prey system," *Chaos, Solitons & Fractals*, vol. 32, no. 1, pp. 80–94, 2007.

[6] A. Elalim, A. Elsadany, H. A. El-Metwally, E. M. Elabbasy, and H. N. Agiza, "Chaos and bifurcation of a nonlinear discrete prey-predator system," *Computational Ecology and Software*, vol. 2, no. 3, p. 169, 2012.

[7] Z. He and X. Lai, "Bifurcation and chaotic behavior of a discrete-time predator-prey system," *Nonlinear Analysis: Real World Applications*, vol. 12, no. 1, pp. 403–417, 2011.

[8] M. S. Shabbir, Q. Din, M. Safeer, M. A. Khan, and K. Ahmad, "A dynamically consistent nonstandard finite difference scheme for a predator-prey model," *Advances in Difference Equations*, vol. 381, no. 1, pp. 1–17, 2019.

[9] R. E. Mickens, "A nonstandard finite-difference scheme for the Lotka-Volterra system," *Applied Numerical Mathematics*, vol. 45, no. 2-3, pp. 309–314, 2003.

[10] L. Dai, *Nonlinear Dynamics of Piecewise Constant Systems and Implementation of Piecewise Constant Arguments*, World scientific, Singapore, 2008.

[11] Q. Din, "Stability, bifurcation analysis and chaos control for a predator-prey system," *Journal of Vibration and Control*, vol. 25, no. 3, pp. 612–626, 2019.

[12] M. A. Abbasi and Q. Din, "Under the influence of crowding effects: stability, bifurcation and chaos control for a discrete-time predator-prey model," *International Journal of Biomathematics*, vol. 12, no. 04, Article ID 1950044, 2019.

[13] J. Dhar, H. Singh, and H. S. Bhatti, "Discrete-time dynamics of a system with crowding effect and predator partially dependent on prey," *Applied Mathematics and Computation*, vol. 252, pp. 324–335, 2015.

[14] S. Pal, N. Pal, and J. Chattopadhyay, "Hunting cooperation in a discrete-time predator-prey system," *International Journal of Bifurcation and Chaos*, vol. 28, no. 07, Article ID 1850083, 2018.

[15] H. N. Agiza, E. M. Elabbasy, H. El-Metwally, and A. A. Elsadany, "Chaotic dynamics of a discrete prey-predator model with Holling type II," *Nonlinear Analysis: Real World Applications*, vol. 10, no. 1, pp. 116–129, 2009.

[16] W. E. Ricker, "Stock and recruitment," *Journal of the Fisheries Research Board of Canada*, vol. 11, no. 5, pp. 559–623, 1954.

[17] J. D. Murray, *Mathematicalbiology I. An Introduction*, Springer Science & Business Media, 2007, Berlin/Heidelberg, Germany, 2002.

[18] W. C. Allee, *Animal Aggregations, a Study in General Sociology*, Univ. Press, Chicago, 1931.

[19] M. Sen, M. Banerjee, and A. Morozov, "Bifurcation analysis of a ratio-dependent prey-predator model with the Allee effect," *Ecological Complexity*, vol. 11, pp. 12–27, 2012.

[20] F. Peng and Y. Kang, "Dynamics of a modified Leslie-Gower model with double Allee effects," *Nonlinear Dynamics*, vol. 80, no. 1, pp. 1051–1062, 2015.

[21] M. Sen and M. Banerjee, "Rich global dynamics in a prey-predator model with Allee effect and density dependent death rate of predator," *International Journal of Bifurcation and Chaos*, vol. 25, no. 03, Article ID 1530007, 2015.

[22] S. Vinoth, R. Sivasamy, K. Sathiyanathan et al., "Dynamical analysis of a delayed food chain model with additive Allee effect," *Advances in Difference Equations*, vol. 54, no. 1, pp. 1–20, 2021.

[23] C. Çelik and O. Duman, "Allee effect in a discrete-time predator-prey system," *Chaos, Solitons & Fractals*, vol. 40, no. 4, pp. 1956–1962, 2009.

[24] W. X. Wang, Y. B. Zhang, and C. Z. Liu, "Analysis of a discrete-time predator-prey system with Allee effect," *Ecological Complexity*, vol. 8, no. 1, pp. 81–85, 2011.

[25] L. Cheng and H. Cao, "Bifurcation analysis of a discrete-time ratio-dependent predator-prey model with Allee effect," *Communications in Nonlinear Science and Numerical Simulation*, vol. 38, pp. 288–302, 2016.

[26] Z. AlSharawi, S. Pal, N. Pal, and J. Chattopadhyay, "A discrete-time model with non-monotonic functional response and strong Allee effect in prey," *Journal of Difference Equations and Applications*, vol. 26, no. 3, pp. 404–431, 2020.

[27] G. Chen and X. Dong, *From Chaos to Order: Methodologies, Perspectives and Applications*, World scientific, Singapore, 1998.

[28] Y. A. Kuznetsov, *Elements of Applied Bifurcation Theory*, Springer, Berlin, Heidelberg, Germany, 2013.

[29] L.-G. Yuan and Q.-G. Yang, "Bifurcation, invariant curve and hybrid control in a discrete-time predator-prey system," *Applied Mathematical Modelling*, vol. 39, no. 8, pp. 2345–2362, 2015.

[30] S. Lynch, *Dynamical Systems with Applications Using python*, 2018.

[31] E. Ott, C. Grebogi, and J. A. Yorke, "Controlling chaos," *Physical Review Letters*, vol. 64, no. 11, pp. 1196–1199, 1990.

[32] Q. Din, "Complexity and chaos control in a discrete-time prey-predator model," *Communications in Nonlinear Science and Numerical Simulation*, vol. 49, pp. 113–134, 2017.

[33] Q. Din, N. Saleem, and M. S. Shabbir, "A class of discrete predator-prey interaction with bifurcation analysis and chaos control," *Mathematical Modelling of Natural Phenomena*, vol. 15, p. 60, 2020.

[34] M. Bilal Ajaz, U. Saeed, Q. Din, I. Ali, and M. I. Siddiqui, "Bifurcation analysis and chaos control in discrete-time modified Leslie-Gower prey harvesting model," *Advances in Difference Equations*, vol. 45, no. 1, pp. 1–24, 2020.

[35] A. Tassaddiq, M. S. Shabbir, Q. Din, K. Ahmad, and S. Kazi, "A ratio-dependent nonlinear predator-prey model with certain dynamical results," *IEEE Access*, vol. 8, pp. 195074–195088, 2020.

[36] M. A. Aziz-Alaoui and M. Daher Okiye, "Boundedness and global stability for a predator-prey model with modified Leslie-Gower and Holling-type II schemes," *Applied Mathematics Letters*, vol. 16, no. 7, pp. 1069–1075, 2003.

[37] C. Ji, D. Jiang, and N. Shi, "Analysis of a predator-prey model with modified Leslie-Gower and Holling-type II schemes with stochastic perturbation," *Journal of Mathematical Analysis and Applications*, vol. 359, no. 2, pp. 482–498, 2009.

[38] C. Ji, D. Jiang, and N. Shi, "A note on a predator-prey model with modified Leslie-Gower and Holling-type II schemes with stochastic perturbation," *Journal of Mathematical Analysis and Applications*, vol. 377, no. 1, pp. 435–440, 2011.

[39] H. Singh, J. Dhar, and H. Singh Bhatti, "Discrete-time bifurcation behavior of a prey-predator system with generalized predator," *Advances in Difference Equations*, vol. 206, no. 1, pp. 1–15, 2015.

[40] W. Liu and D. Cai, "Bifurcation, chaos analysis and control in a discrete-time predator-prey system," *Advances in Difference Equations*, vol. 11, no. 1, pp. 1–22, 2019.

[41] S. Vinoth, R. Sivasamy, K. Sathiyanathan et al., "The dynamics of a leslie type predator-prey model with fear and Allee effect," *Advances in Difference Equations*, vol. 338, no. 1, pp. 1–22, 2021.

[42] J. Guckenheimer and P. Holmes, *Nonlinear Oscillations, Dynamical Systems, and Bifurcations of Vector fields*, Springer, Berlin, Heidelberg, Germany, 2013.

[43] C. Robinson, *Dynamical Systems: Stability, Symbolic Dynamics, and Chaos*, Routledge, Oxfordshire, England, UK, 1998.

Hindawi
Complexity
Volume 2022, Article ID 5121636, 9 pages
https://doi.org/10.1155/2022/5121636

Research Article

The Power of Delay on a Stochastic Epidemic Model in a Switching Environment

Amine El Koufi

Laboratory of Analysis, Modeling and Simulation (LAMS), Faculty of Sciences Ben M'sik, Hassan II University, P. O Box 7955, Sidi Othman, Casablanca, Morocco

Correspondence should be addressed to Amine El Koufi; elkoufiamine1@gmail.com

Received 26 January 2022; Revised 23 February 2022; Accepted 25 February 2022; Published 19 March 2022

Academic Editor: Fathalla A. Rihan

In recent years, the world knew many challenges concerning the propagation of infectious diseases such as avian influenza, Ebola, SARS-CoV-2, etc. These epidemics caused a change in the healthy balance of humanity. Also, the epidemics disrupt the economies and social activities of countries around the world. Mathematical modeling is a vital means to represent and control the propagation of infectious diseases. In this paper, we consider a stochastic epidemic model with a Markov process and delay, which generalizes many models existing in the literature. In addition, we show the stochastic threshold for the extinction of the disease. Furthermore, numerical examples are discussed to confirm the theoretical result.

1. Introduction and Preliminaries

For years, the development of more realistic mathematical models in epidemiology has attracted the attention of many researchers. Consequently, many deterministic models have been suggested to understand and control the propagation of infectious diseases.

The first mathematical model that describes the spread of an epidemic in a human population divided into three categories (susceptible (S), infected (I), and recovered (R)) was initially proposed by Kermack and Mackendrick [1]. Then, several generalizations of the SIR model of Kermack and Mackendrick were proposed. For example, in [2], a mathematical model called SEIR was proposed, which describes the propagation of an epidemic in a human population divided into four classes: susceptible, exposed, infected, and recovered. In [3], Cheng et al. investigated a network-based SIQS infectious disease model with a particular incidence rate. They proved that the disease-free equilibrium of the system is globally asymptotically stable, and the unique endemic equilibrium is globally attractive. Zhang et al. [4] constructed an epidemic model with a saturated treatment function described by the following ordinary differential equation system:

$$\begin{cases} \dfrac{dS(t)}{dt} = \Lambda - \rho S(t) - \dfrac{\beta S(t) I(t)}{1 + kI(t)}, \\ \dfrac{dI(t)}{dt} = \dfrac{\beta S(t) I(t)}{1 + kI(t)} - (\rho + \theta + \mu) I(t) - \dfrac{\overline{r} I(t)}{1 + \eta I(t)}, \\ \dfrac{dR(t)}{dt} = \mu I(t) + \dfrac{\overline{r} I(t)}{1 + \eta I(t)} - \rho R(t). \end{cases} \tag{1}$$

The parameters in system (1) have the following meaning: Λ represent the recruitment rate of the susceptible class, ρ specify the death rate of the population, and θ denotes the death rate due to the epidemic. Moreover, the parameter μ is the death rate due to the epidemic. $\beta SI/1 + kI$ is the saturated incidence rate of disease [5], β is the contact rate, and k is a parameter that measures the psychological or inhibitory effect of the population. There exist other types of incidence rates, and each one represents some advantages in modeling (for more detail, see Table 1). $\overline{r} I/1 + \eta I$ is saturated treatment function [4]; $\overline{r}$ designates the cure rate and η measure the extent of the effect of the infected being delayed for treatment (see, [4]).

However, the stochastic model represents some advantages compared with the deterministic one. In effect, the

propagation of transmissible diseases is naturally randomized. Thus, it is necessary to introduce an environmental noise into the system to present the fluctuation of the environment. Generally, there exist many types of environmental noise: white noise [11], colored noise [12], Lévy noise [13], etc., and every one represents some advantages in modeling. Rajasekar et al. [14] studied a stochastic epidemic model with a saturated incidence rate and saturated treatment function. While El Koufi et al. [12] proposed an epidemic model incorporating with the Lévy process. Other works have used two types of noise in their models. For example, Li and Guo [15] presented a stochastic SIS epidemic model in which they mixed three types of noise, namely, white noise, colored noise, and Lévy noise. In the works [16, 17], the authors proposed models with delay and Markovian switching for ecological populations. We can use the telegraph (or colored) noise to describe the mutation of the system from one state to another. Indeed, the propagation of an epidemic is affected by external factors such as nutrition, pandemics, climate, etc. For example, the transmission rate of the influenza epidemic in the spring is not the same as in the summer. Thus, the system frequently transitions from one regime to another. Many scholars studied the effect of telegraphic noise on the transmission of an epidemic (see, for example, [18–23]).

To develop the model (1) and the stochastic model proposed by Rajasekar et al. [14], we suppose that the transmission rate of disease β fluctuates randomly around an average value and that the system often switches between two or more environmental regimes.

We assume that the stochastic perturbations are of the white and telegraphic noises types, that is,

$$\beta \rightsquigarrow \beta(r(t)) + \sigma(r(t))dW(t), \tag{2}$$

where $W(t)$ is a Brownian motion and σ is the intensity of noise, $r(t)$ is a right-continuous Markov chain.

Then, we present a new stochastic epidemic model for a human population with a saturated incidence rate and saturated treatment function in regime-switching described by the following stochastic hybrid differential equations:

$$\begin{cases} dS(t) = \left[\Lambda(r(t)) - (\rho(r(t)) + m(r(t))S(t) - \dfrac{\beta(r(t))S(t)I(t)}{1 + k(r(t))I(t)} + m(r(t))S(t-\tau_1)e^{-\rho(r(t))\tau_1}\right. \\ \qquad \left. + \mu(r(t))I(t-\tau_2)e^{-\rho(r(t))\tau_2}\right]dt - \dfrac{\sigma(r(t))S(t)I(t)}{1 + k(r(t))I(t)}dW(t), \\ dI(t) = \left[\dfrac{\beta(r(t))S(t)I(t)}{1 + k(r(t))I(t)} - (\rho(r(t)) + \theta(r(t)) + \mu(r(t)))I(t) - \dfrac{\overline{r}(r(t))I(t)}{1 + \eta(r(t))I(t)}\right]dt \\ \qquad + \dfrac{\sigma(r(t))S(t)I(t)}{1 + k(r(t))I(t)}dW(t), \\ dR(t) = \left[\mu(r(t))I(t) + \dfrac{\overline{r}(r(t))I(t)}{1 + \eta(r(t))I(t)} - \rho(r(t))R(t) - m(r(t))S(t-\tau_1)e^{-\rho(r(t))\tau_1}\right. \\ \qquad \left. - \mu(r(t))I(t-\tau_2)e^{-\rho(r(t))\tau_2}\right]dt\ , \end{cases} \tag{3}$$

with the initial value

$$\begin{aligned} S(\theta) &= \varphi_1(\theta) \geq 0, \mathrm{I}(\theta) \\ &= \varphi_2(\theta) \geq 0, R(\theta) \\ &= \varphi_3(\theta) \geq 0, \theta \in [-\tau, 0], \varphi_{\mathrm{i}}(\theta) > 0, \ \mathrm{i} \\ &= 1, 2, 3, \end{aligned} \tag{4}$$

where $(\varphi_1(\theta), \varphi_2(\theta), \varphi_3(\theta)) \in (\mathscr{C}([-\tau, 0]; \mathbb{R}^3_+))^3$ with $\mathscr{C}([-\tau, 0]; \mathbb{R}^3_+)$ is the Banach space of continuous functions, mapping the interval $[-\tau, 0]$ into $\mathbb{R}^3_+$, and $\tau = \max\{\tau_1, \tau_2\}$.

The parameter m stands for the successful vaccination rate of susceptible individuals. The quantity $\mu I(t-\tau_2)e^{-\rho\tau_2}$ represents the case that an individual survives natural death before reverting to the susceptible class, τ_2 is the length of immunity period of the recovered. The quantity $S(t-\tau_1)$ indicates the period in which the vaccine has not yet given its effect, and τ_1 is the validity period of the vaccination.

Throughout this paper, $W(t)$ is a Brownian motion defined in a complete probability space $(\Omega, \mathscr{F}, \{\mathscr{F}_t\}_{t\geq 0}, \mathbb{P})$ with a filtration $\{\mathscr{F}_t\}_{t\geq 0}$ satisfying the usual conditions (i.e., it is increasing and right-continuous while $\mathscr{F}_0$ contains all $\mathbb{P}$-null sets), σ is the intensity of noise. $r(t)$ is a right-continuous Markov chain defined in the same space as the Brownian motion, and supposedly independent of the Brownian motion. The Markov chain $r(t)$ takes values in a finite-state space $\mathbb{V} = \{1, 2, \ldots, N\}$ with the generator $\Psi = (\varphi_{uv})_{1\leq u,v\leq N}$ defined for $T > 0$ by

Table 1: Some nonlinear incidence rates.

Incidence name	Expression	Reference
Standard incidence rate	$\beta SI/N$	[6]
Saturated incidence rate	$\beta SI/1+kI$	[5]
Beddington–DeAngelis functional response	$\beta SI/1+k_1S+k_2I$	[7]
Crowley–Martin functional response	$\beta SI/1+k_1S+k_2I+k_1k_2SI$	[8]
Incidence with media coverage effect	$\beta_1-\beta_2 I/I+m$	[9]
General functional response	$\beta SI/1+k_1S+k_2I+k_3SI$	[10]

$$\mathbb{P}\left(r\left(t+T\right)=v\,|\,r\left(t\right)=u\right)=\begin{cases}\phi_{uv}T+o\left(T\right)\phi, & \text{if } u\neq v,\\ 1+\phi_{uu}T+o\left(T\right), & \text{if } u=v,\end{cases} \tag{5}$$

where φ_{uv} is the transition rate from u to v and $\varphi_{uv}\geq 0$ if $u\neq v$, while (Tex translation failed). To ensure that the system goes switching from one regime to another regime. In the present paper, we suppose that the Markov chain is irreducible. Then, there exists a unique stationary distribution $\pi=(\pi_1,\ldots,\pi_m)$ of $r(t)$ such that $\pi\Psi=0$, with $\sum_{i=1}^{N}\pi_i=1$ and $\pi_i>0$, for each i in $\mathbb{V}$. Therefore, for any sequence $g=(g(1),\ldots,g(N))^T$, let $\widehat{g}=\min_{i\in\mathbb{V}}\{g(i)\}$ and $\check{g}=\max_{i\in\mathbb{V}}\{g(i)\}$.

The stochastic differential equations with Markovian switching [24] have the following form:

$$\begin{aligned}dx\left(t\right)&=f\left(x\left(t\right),r\left(t\right)\right)dt+h\left(x\left(t\right),r\left(t\right)\right)dW\left(t\right),t\geq 0,\text{with } x\left(0\right)\\&=x_0\in\mathbb{R}^n,\end{aligned} \tag{6}$$

where $f\colon \mathbb{R}^n\times\mathbb{V}\longrightarrow\mathbb{R}^n$, and $h\colon \mathbb{R}^n\times\mathbb{V}\longrightarrow\mathbb{R}^{n\times m}$. We present the operator $\mathscr{L}$ associated with equation (6) and for any function $M(x,e)$ twice continuously differentiable for x by

$$\mathscr{L}M\left(x,e\right)=M_t\left(x,e\right)+M_x\left(x,e\right)f\left(x,e\right)+\frac{1}{2}\text{trace}\left[h^T\left(x,e\right)M_{xx}\left(x,e\right)h\left(x,e\right)\right]_{ij}+\sum_{i\in\mathbb{V}}\varphi_{ei}M\left(x,e\right), \tag{7}$$

where

$$M_t=\frac{\partial M}{\partial t},M_x=\left(\frac{\partial M}{\partial x_1},\ldots,\frac{\partial M}{\partial x_n}\right),M_{xx}=\left(\frac{\partial^2 M}{\partial x_i\partial x_j}\right)_{n\times n}. \tag{8}$$

Then the generalized Itô's formula [25] is displayed by

$$dM\left(x\left(t\right),e\right)=\mathscr{L}M\left(x\left(t\right),e\right)dt+M_x\left(x\left(t\right),e\right)h\left(x\left(t\right),e\right)dW\left(t\right). \tag{9}$$

Theorem 1. *For any initial value defined in (4), the model (2) has a unique solution $(S(t),I(t),R(t))$ for all $t\geq-\tau$ and the solution will remain in $\mathbb{R}_+^3$ with probability one.*

With the same step in [11], we can prove the above theorem, and the following region is almost surely positively invariant [12].

$$Y=\left\{\left(S\left(t\right),I\left(t\right),R\left(t\right)\right)\in\mathbb{R}_+^3\colon K\leq S\left(t\right)+I\left(t\right)+R\left(t\right)\leq\frac{\check{\Lambda}}{\widehat{\rho}}\right\}. \tag{10}$$

Our model represents many effects compatible with the natural word as

(i) The memory effect represents an essential component of the natural population [26–28].

(ii) The regime-switching. In fact, the epidemic disease often switches between two or more different regimes of the environment [18, 19]. So, integrating the colored noise into the epidemic system allows the latter to switch between different environmental regimes. Often, the switching between environmental regimes is usually memoryless. In addition, the waiting time for the ensuing switch follows the exponential distribution [25]. Then, we model the regime-switching by a Markov chain $(r(t))_{t\geq 0}$ taking value in a finite-state space $\mathbb{V}=\{1,2,\ldots,N\}$.

(iii) The vaccination represents an intervention medical that plays a significant role in the reduction of the infected class [29].

This paper aims to study the extinction of disease. By proposing a threshold that includes the noise term of the stochastic system, we establish sufficient conditions for the extinction of disease. Moreover, our model (2) can be used to represent the switching between two or more regimes of environment, which differ by factors such as nutrition or socio-cultural factors. In addition, the model (2) represents a generalized form of many SIR epidemic models existing in the literature. The rest of this paper is as follows: in Section 2, we prove the sufficient conditions for the extinction of the disease. In Section 3, we make simulations to confirm our theoretical results.

2. Extinction

The main question in mathematical epidemiology is the determination of the conditions that ensure the

disappearance of an epidemic in a population. For the deterministic system, the answer to this question is made when the value of $\mathscr{R}_0$ (the basic reproduction number [30]) is less than or equal to one. In general, the value of $\mathscr{R}_0$ depends on the parameters of the deterministic system. So, for our stochastic delayed system, we have defined a threshold value that depends on the delay and the random effects defined by

$$\mathscr{R}_{swh} = \frac{\check{\lambda}\check{\Lambda}}{\left(\widehat{\rho} + \widehat{m}\left(1 - e^{-\widehat{\rho}\tau_2}\right)\right)\chi}, \tag{11}$$

where $\chi = \sum_{i=1}^{N} \pi_i(\rho(i) + \theta(i) + \mu(i) + \overline{r}(i)\kappa_1 + (\sigma^2(i)/2)\kappa_2)$. The following theorem presents a condition for the extinction of the disease in model (2) in the function of the threshold value $\mathscr{R}_{swh}$.

Theorem 2. *Let $(S(t), I(t), R((t))$ be a positive solution of system (2) with the initial value given in (4), if $\mathscr{R}_{swh} < 1$, then*

$$\limsup_{t\longrightarrow\infty} \frac{\ln I(t)}{t} \leq \sum_{i=1}^{N} \pi_i\left(\rho(i) + \theta(i) + \mu(i) + \overline{r}(i)\kappa_1 + \frac{\sigma^2(i)}{2}\kappa_2\right) \left[\mathscr{R}_{swh} - 1\right], \text{a.s.} \tag{12}$$

In other words, $I(t)$ will go to zero exponentially, namely, the disease dies out with probability one.

Proof. Applying Itô's formula to $\ln I(t)$ yields

$$d\ln\ I(t) = \left[\begin{array}{c} \frac{\lambda(r(t))S(t)}{1 + k(r(t))I(t)} - (\rho(r(t)) + \theta(r(t)) + \mu(r(t))) \\ \\ -\frac{\overline{r}(r(t))}{1 + \eta(r(t))I(t)} - \frac{\sigma^2(r(t))S^2(t)}{(1 + k(r(t))I(t))^2} \end{array}\right]\mathrm{d}t + \frac{\sigma(r(t))S(t)}{1 + k(r(t))I(t)}dW(t). \tag{13}$$

By (7), we get

$$d\ln\ I(t) \leq \left[\lambda(r(t))S(t) - \left(\begin{array}{c} \rho(r(t)) + \theta(r(t)) + \mu(r(t)) \\ \\ +\overline{r}(r(t))\kappa_1 + \frac{\sigma^2(r(t))}{2}\kappa_2 \end{array}\right)\right]\mathrm{d}t + \frac{\sigma(r(t))S(t)}{1 + k(r(t))I(t)}dW(t). \tag{14}$$

Integrating both sides of the above inequality from 0 to t and dividing by t, we have

$$\frac{\ln I(t)}{t} \leq \check{\lambda}\frac{1}{t}\int_0^t S(s)ds - \frac{1}{t}\int_0^t (\rho(r(s)) + \theta(r(s)), \tag{15}$$

$$+\mu(r(s)) + \overline{r}(r(s))\kappa_1 + \frac{\sigma^2(r(s))}{2}\kappa_2\Big)dt - \frac{\ln I(0)}{t} + \frac{\mathscr{M}(t)}{t}, \tag{16}$$

where $\mathscr{M}(t) = \int_0^t \sigma(r(s))S(s)/1 + k(r(s))I(s)\mathrm{d}W(s)$ is a local martingale with quadratic variation expressed as

$$\langle \mathscr{M}(t), \mathscr{M}(t) \rangle = \int_0^t \left(\frac{\sigma(r(s))S(s)}{1 + k(r(s))I}\right)^2 ds \leq \sigma_2^2 ct. \tag{17}$$

By the strong law of large numbers for local martingales (see, [31]), we result

$$\lim_{t\longrightarrow\infty} \frac{\mathscr{M}(t)}{t} = 0 \text{ a.s.} \tag{18}$$

On the other hand, in view of the system (2), we derive

$$d\left(S(t) + I(t) + \mu(r(t))e^{-\rho(r(t))\tau_2}\int_{t-\tau_2}^{t} I(s)ds + m(r(t))e^{-\rho(r(t))\tau_1}\int_{t-\tau_1}^{t} S(s)ds\right)$$
$$= \left\{\Lambda - \left[\rho(r(t)) + \theta(r(t)) + \mu(r(t))\left(1 - e^{-\rho(r(t))\tau_1}\right) + \frac{\overline{r}(r(t))}{1 + \eta(r(t))I(t)}\right]I(t) - \left[\rho(r(t)) + m(r(t))\left(1 - e^{-\rho(r(t))\tau_2}\right)\right]S(t)\right\}dt\ . \tag{19}$$

Thus, we have

$$\begin{aligned}
&\frac{S(t)+I(t)+\mu(r(t))e^{-\rho(r(t))\tau_2}\int_{t-\tau_2}^{t}I(s)ds}{t}+\frac{m(r(t))e^{-\rho(r(t))\tau_1}\int_{t-\tau_1}^{t}S(s)ds}{t}\\
&-\frac{S(0)+I(0)+\mu(r(0))e^{-\rho(r(0))\tau_2}\int_{-\tau_2}^{0}I(s)ds}{t}-\frac{m(r(0))e^{-\rho(r(0))\tau_1}\int_{-\tau_1}^{0}S(s)ds}{t}\\
&=\Lambda(r(t))-\left[\rho(r(t))+\theta(r(t))+\mu(r(t))\left(1-e^{-\rho(r(t))\tau_1}\right)+\frac{\overline{r}(r(t))}{1+\eta(r(t))I(t)}\right]\\
&\frac{1}{t}\int_0^t I(s)ds-\left[\rho(r(t))+m(r(t))\left(1-e^{-\rho(r(t))\tau_2}\right)\right]\frac{1}{t}\int_0^t S(s)ds\\
&\le\check{\Lambda}-\left[\widehat{\rho}+\widehat{\theta}+\widehat{\mu}\left(1-e^{-\widehat{\rho}\tau_1}\right)+\widehat{r}\kappa_1\right]\\
&\frac{1}{t}\int_0^t I(s)ds-\left[\widehat{\rho}+\widehat{m}\left(1-e^{-\widehat{\rho}\tau_2}\right)\right]\frac{1}{t}\int_0^t S(s)d.
\end{aligned}\tag{20}$$

Consequently, we have

$$\frac{1}{t}\int_0^t S(s)ds\ \le\frac{\check{\Lambda}}{\widehat{\rho}+\widehat{m}\left(1-e^{-\widehat{\rho}\tau_2}\right)}-\frac{\widehat{\rho}+\widehat{\theta}+\widehat{\mu}\left(1-e^{-\widehat{\rho}\tau_1}\right)+\widehat{\overline{r}}\kappa_1}{\widehat{\rho}+\widehat{m}\left(1-e^{-\widehat{\rho}\tau_2}\right)}\frac{1}{t}\int_0^t I(s)ds\ .\tag{21}$$

By substituting the inequality (10) in (16), we find

$$\begin{aligned}
\frac{\ln I(t)}{t}\le&\frac{\check{\lambda}\check{\Lambda}}{\widehat{\rho}+\widehat{m}\left(1-e^{-\widehat{\rho}\tau_2}\right)}-\frac{\check{\lambda}\left[\widehat{\rho}+\widehat{\theta}+\widehat{\mu}\left(1-e^{-\widehat{\rho}\tau_1}\right)+\widehat{\overline{r}}\kappa_1\right]}{\widehat{\rho}+\widehat{m}\left(1-e^{-\widehat{\rho}\tau_2}\right)}\frac{1}{t}\int_0^t I(s)ds\\
&-\frac{1}{t}\int_0^t\left(\rho(r(s))+\theta(r(s))+\mu(r(s))+\overline{r}(r(s))\kappa_1+\frac{\sigma^2(r(s))}{2}\kappa_2\right)dt\\
&-\frac{\ln I(0)}{t}+\frac{\mathscr{M}(t)}{t}\le\frac{\check{\lambda}\check{\Lambda}}{\widehat{\rho}+\widehat{m}\left(1-e^{-\widehat{\rho}\tau_2}\right)}\\
&-\frac{1}{t}\int_0^t\left(\rho(r(s))+\theta(r(s))+\mu(r(s))+\overline{r}(r(s))\kappa_1+\frac{\sigma^2(r(s))}{2}\kappa_2\right)dt\\
&-\frac{\ln I(0)}{t}+\frac{\mathscr{M}(t)}{t}.
\end{aligned}\tag{22}$$

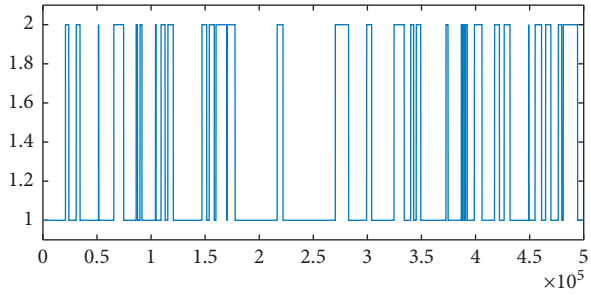

Figure 1: The trajectory of the Markov chain $r(t)$.

Taking the limit superior on both sides of (22) and combining with (18), using the ergodic theory of the Markov chain, we obtain

$$\begin{aligned}\limsup_{t\longrightarrow\infty}\frac{\ln I(t)}{t} &\leq \frac{\check{\lambda}\check{\Lambda}}{\widehat{\rho}+\widehat{m}\left(1-e^{-\widehat{\rho}\tau_2}\right)}-\sum_{i=1}^{N}\pi_i\left(\rho(i)+\theta(i)+\mu(i)+\overline{r}(i)\kappa_1+\frac{\sigma^2(i)}{2}\kappa_2\right)\\ &\triangleq \sum_{i=1}^{N}\pi_i\left(\rho(i)+\theta(i)+\mu(i)+\overline{r}(i)\kappa_1+\frac{\sigma^2(i)}{2}\kappa_2\right)[\mathscr{R}_{swh}-1]\text{a.s.}\end{aligned} \tag{23}$$

If $\mathscr{R}_{swh}<1$, we obtain that

$$\limsup_{t\longrightarrow\infty}\frac{\ln I(t)}{t}\leq 0,\ \text{a.s,} \tag{24}$$

which implies that

$$\lim_{t\longrightarrow\infty} I(t)=0\,\text{a.s.} \tag{25}$$

However, the diseases in the system (2) die out exponentially with probability one. □

Remark 1. Through Theorem 2, we find an impressive result, namely, when $\mathscr{R}_{swh}$ is less than one infective $I(t)$ go to extinction. Thus, the evanishment of the disease depends on the delay and the noise value.

3. Numerical Simulations

In this part, we present some numerical simulations in order to support our analytical results. For this, we use the approximate numerical resolution method for the stochastic differential equations of Euler and Maruyama. Many authors have chosen this method to give a numerical approximation of solutions for some stochastic differential equations. Then, we consider the Markov chain $\{r(t)\}_{t\geq 0}$ taking values on the state space $\mathbb{V}=1,2$, with a generator defined by

$$\Phi=\begin{pmatrix}-1 & 1\\ 2 & -2\end{pmatrix}. \tag{26}$$

and the stationary distribution $\pi=(2/3,1/3)$. Figure 1 demonstrates the path of the Markov chain $\{r(t)\}_{t\geq 0}$.

Therefore, to simulate, we take the parameter values presented in Table 2. Next, a simple computation gives

$$\mathscr{R}_{swh}=\frac{\check{\lambda}\check{\Lambda}}{\left(\widehat{\rho}+\widehat{m}\left(1-e^{-\widehat{\rho}\tau_2}\right)\right)\chi}=0.3515<1. \tag{27}$$

Then by Theorem 2, for any initial (3), the solution of (3) satisfies

$$\limsup_{t\longrightarrow\infty}\frac{\ln I(t)}{t}\leq 0,\ \text{a.s.} \tag{28}$$

Thus, the disease in model (2) is extinct, Figure 2 supports this result.

By choosing different noise values as Case 1: $\sigma(1)=0.1$, $\sigma(1)=0.1$, Case 2: $\sigma(1)=0.2$, $\sigma(1)=0.3$, and Case 3: $\sigma(1)=0.4$, $\sigma(1)=0.6$, according to Figure 3, we see that when the value of noises increases, $I(t)$ tends more rapidly to zero, then we conclude that a large value of noise leads to the disappearance of the epidemic from the population.

In order to examine the effect of vaccination immunity on the dynamics of an epidemic in the model (2), we keep the same parameter values in Table 1, and we vary the value of the period immunity τ_1. So, we see that when the period of validity of the vaccination is sufficiently large, the epidemic disease can be decreased in the population (see, Figure 4).

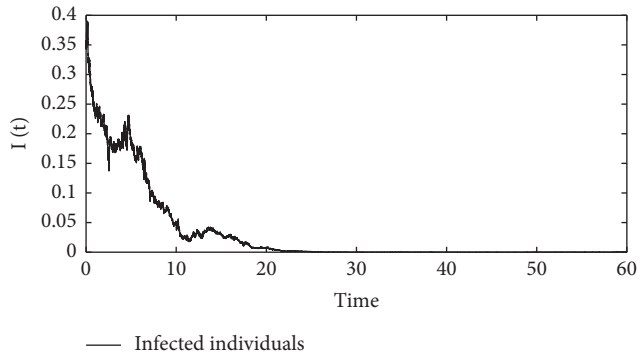

Figure 2: The stochastic trajectory of $I(t)$.

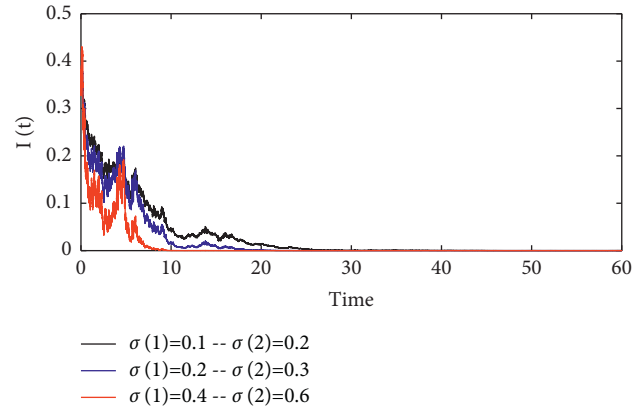

Figure 3: The stochastic trajectory of $I(t)$ with different noise values.

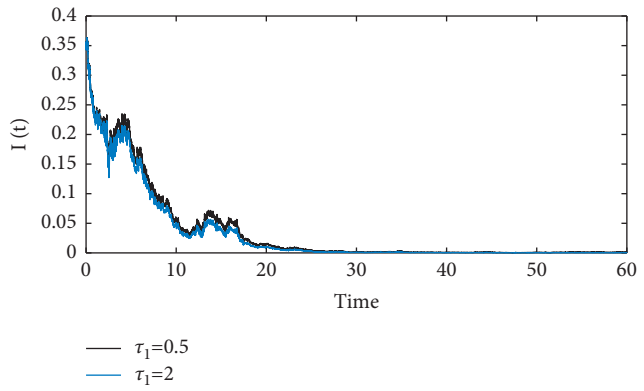

Figure 4: The effects of the validity period τ_1 to the system (2).

Table 2: Parameters value used in simulation of model (2).

Parameter	State 1	State 2
Λ	0.25	0.3
ρ	0.5	0.6
δ	0.6	0.5
η	0.6	0.4
k	0.5	0.4
m	0.4	0.2
θ	0.3 7	0.4
μ	0.2	0.12
τ_1	0.1	0.2
τ_2	0.5	0.6

4. Conclusion

In this paper, we have proposed a stochastic epidemic model with Markov switching. Our model represents a generalization of many models existing in the literature. For example, the stochastic model proposed by Rajasekar et al. in [14], when $m = 0$, the regime-switching and delay are not considered. Also, using the stochastic Lyapunov approach, sufficient conditions are established to guarantee the extinction of epidemic disease by introducing a suitable stochastic threshold value $\mathscr{R}_{swh}$, which depends on delay terms and stochastic noise. We have obtained exactly the following results:

(i) Let $(S(t), I(t), R(t))$ be a positive solution of system (2) with the initial value given in (4), if

$$\mathscr{R}_{swh} = \frac{\check{\lambda}\check{\Lambda}}{\left(\widehat{\rho} + \widehat{m}\left(1 - e^{-\widehat{\rho}\tau_2}\right)\right)\chi}, <1, \tag{29}$$

then epidemic infection dies out with probability one.

Then, from the expression of $\mathscr{R}_{swh}$, we remark that a large value of white noise is helpful to control the propagation of infectious diseases (see Figure 3). In addition, the long period of vaccination validation can reduce the number of infected people in the population (see Figure 4). In our future works, we can study the memory effect on the dynamics of model (2) by using the new generalized fractional derivative presented by Hattaf in [32].

Data Availability

The data used to support the findings of this study are included within the article.

Conflicts of Interest

The author declares that there are no conflicts of interest.

References

[1] W. O. Kermack and A. G. McKendrick, "A contribution to the mathematical theory of epidemics," *Proceedings of the Royal Society of London. Series A, Containing Papers of a Mathematical and Physical Character*, vol. 115, no. 772, pp. 700–721, 1927.

[2] S. J. Weinstein, M. S. Holland, K. E. Rogers, and N. S. Barlow, "Analytic solution of the SEIR epidemic model via asymptotic approximant," *Physica D: Nonlinear Phenomena*, vol. 411, Article ID 132633, 2020.

[3] X. Cheng, Y. Wang, and G. Huang, "Global dynamics of a network-based SIQS epidemic model with nonmonotone incidence rate," *Chaos, Solitons & Fractals*, vol. 153, Article ID 111502, 2021.

[4] X. Zhang and X. Liu, "Backward bifurcation of an epidemic model with saturated treatment function," *Journal of Mathematical Analysis and Applications*, vol. 348, no. 1, pp. 433–443, 2008.

[5] V. Capasso and G. Serio, "A generalization of the Kermack-McKendrick deterministic epidemic model," *Mathematical Biosciences*, vol. 42, no. 1-2, pp. 43–61, 1978.

[6] M. C. M. De Jong, O. Diekmann, and H. Heesterbeek, "How does transmission of infection depend on population size," in *Epidemic Models: Their Structure and Relation to Data*, D. Mollison, Ed., , 1995.

[7] J. R. Beddington, "Mutual interference between parasites or predators and its effect on searching efficiency," *Journal of Animal Ecology*, vol. 44, pp. 331–340, 1975.

[8] P. H. Crowley and E. K. Martin, "Functional responses and interference within and between year classes of a dragonfly population," *Journal of the North American Benthological Society*, vol. 8, no. 3, pp. 211–221, 1989.

[9] Y. Liu and J. A. Cui, "The impact of media coverage on the dynamics of infectious disease," *International Journal of Biomathematics*, vol. 1, no. 01, pp. 65–74, 2008.

[10] K. Hattaf, A. Lashari, Y. Louartassi, and N. Yousfi, "A delayed SIR epidemic model with a general incidence rate," *Electronic Journal of Qualitative Theory of Differential Equations*, vol. 3, pp. 1–9, 2013.

[11] X. Mao, G. Marion, and E. Renshaw, "Environmental Brownian noise suppresses explosions in population dynamics," *Stochastic Processes and Their Applications*, vol. 97, no. 1, pp. 95–110, 2002.

[12] A. El Koufi, J. Adnani, A. Bennar, and N. Yousfi, "Dynamics of a stochastic SIR epidemic model driven by Lévy jumps with saturated incidence rate and saturated treatment function," *Stochastic Analysis and Applications*, pp. 1–19, 2021.

[13] A. Settati and A. Lahrouz, "Stationary distribution of stochastic population systems under regime switching," *Applied Mathematics and Computation*, vol. 244, pp. 235–243, 2014.

[14] S. P. Rajasekar, M. Pitchaimani, and Q. Zhu, "Dynamic threshold probe of stochastic SIR model with saturated incidence rate and saturated treatment function," *Physica A: Statistical Mechanics and Its Applications*, vol. 535, Article ID 122300, 2019.

[15] S. Li and S. Guo, "Persistence and extinction of a stochastic SIS epidemic model with regime switching and Lévy jumps," *Discrete Continuous Dynamical Systems-B*, vol. 26, no. 9, p. 5101, 2021.

[16] H. Qi and H. Guo, "Dynamics Analysis of a Stochastic Hybrid Logistic Model with Delay and Two-Pulse Perturbations," *Complexity*, vol. 2020, Article ID 5024830, 24 pages, 2020.

[17] Y. Cai, S. Cai, and X. Mao, "Stochastic delay foraging arena predator-prey system with Markov switching," *Stochastic Analysis and Applications*, vol. 38, no. 2, pp. 191–212, 2020.

[18] Q. Luo and X. Mao, "Stochastic population dynamics under regime switching," *Journal of Mathematical Analysis and Applications*, vol. 334, no. 1, pp. 69–84, 2007.

[19] A. El Koufi, A. Bennar, N. Yousfi, and M. Pitchaimani, "Threshold dynamics for a class of stochastic SIRS epidemic models with nonlinear incidence and Markovian switching," *Mathematical Modelling of Natural Phenomena*, vol. 16, p. 55, 2021.

[20] A. E. Koufi, A. Bennar, and N. Yousfi, "Dynamics of a stochastic SIRS epidemic model with regime switching and specific functional response," *Discrete Dynamics in Nature and Society*, vol. 2020, Article ID 5898456, 13 pages, 2020.

[21] A. El Koufi, A. Bennar, and N. Yousfi, "A stochastic switched epidemic model with two epidemic diseases," *Complexity*, vol. 2021, Article ID 5560538, 13 pages, 2021.

[22] X. Guo and J. Luo, "Stationary distribution and extinction of SIR model with nonlinear incident rate under Markovian

switching," *Physica A: Statistical Mechanics and its Applications*, vol. 505, pp. 471–481, 2018.

[23] B. Zhou, B. Han, D. Jiang, T. Hayat, and A. Alsaedi, "Ergodic stationary distribution and extinction of a hybrid stochastic SEQIHR epidemic model with media coverage, quarantine strategies and pre-existing immunity under discrete Markov switching," *Applied Mathematics and Computation*, vol. 410, Article ID 126388, 2021.

[24] X. Mao, G. G. Yin, and C. Yuan, "Stabilization and destabilization of hybrid systems of stochastic differential equations," *Automatica*, vol. 43, no. 2, pp. 264–273, 2007.

[25] X. Mao and C. Yuan, *Stochastic Differential Equations with Markovian Switching*, Imperial college press, London , UK, 2006.

[26] S. Gao, L. Chen, J. J. Nieto, and A. Torres, "Analysis of a delayed epidemic model with pulse vaccination and saturation incidence," *Vaccine*, vol. 24, no. 35-36, pp. 6037–6045, 2006.

[27] F. A. Rihan, Q. M. Al-Mdallal, H. J. AlSakaji, and A. Hashish, "A fractional-order epidemic model with time-delay and nonlinear incidence rate," *Chaos, Solitons & Fractals*, vol. 126, pp. 97–105, 2019.

[28] F. A. Rihan, H. J. Alsakaji, and C. Rajivganthi, "Stochastic SIRC epidemic model with time-delay for COVID-19," *Advances in Difference Equations*, vol. 2020, no. 1, pp. 1–20, 2020.

[29] F. Andre, R. Booy, H. Bock et al., "Vaccination greatly reduces disease, disability, death and inequity worldwide," *Bulletin of the World Health Organization*, vol. 86, pp. 140–146, 2008.

[30] P. Van den Driessche and J. Watmough, "Reproduction numbers and sub-threshold endemic equilibria for compartmental models of disease transmission," *Mathematical Biosciences*, vol. 180, no. 1-2, pp. 29–48, 2002.

[31] X. Mao, *Stochastic Differential Equations and Applications*, Elsevier, Chennai, Tamil Nadu, 2007.

[32] K. Hattaf, "A new generalized definition of fractional derivative with non-singular kernel," *Computation*, vol. 8, no. 2, p. 49, 2020.

Hindawi
Complexity
Volume 2022, Article ID 3218213, 14 pages
https://doi.org/10.1155/2022/3218213

Research Article

Analysis of the Fractional-Order Delay Differential Equations by the Numerical Method

Saadia Masood,[1] **Muhammad Naeem**,[2] **Roman Ullah**,[3] **Saima Mustafa**,[1] **and Abdul Bariq**[4]

[1]*Department of Mathematics and Statistics, Pir Mehr Ali Shah Arid Agriculture University, Rawalpindi 46000, Pakistan*
[2]*Deanship of Joint First Year Umm Al-Qura University Makkah, Saudi Arabia*
[3]*Department of General Requirements, University of Technology and Applied Sciences, Sohar, Oman*
[4]*Department of Mathematics, Laghman University, Mehterlam, 2701, Laghman, Afghanistan*

Correspondence should be addressed to Muhammad Naeem; mfaridoon@uqu.edu.sa and Abdul Bariq; abdulbariq.maths@lu.edu.af

Received 10 January 2022; Revised 10 February 2022; Accepted 12 February 2022; Published 14 March 2022

Academic Editor: Fathalla A. Rihan

In this study, we implemented a new numerical method known as the Chebyshev Pseudospectral method for solving nonlinear delay differential equations having fractional order. The fractional derivative is defined in Caputo manner. The proposed method is simple, effective, and straightforward as compared to other numerical techniques. To check the validity and accuracy of the proposed method, some illustrative examples are solved by using the present scenario. The obtained results have confirmed the greater accuracy than the modified Laguerre wavelet method, the Chebyshev wavelet method, and the modified wavelet-based algorithm. Moreover, based on the novelty and scientific importance, the present method can be extended to solve other nonlinear fractional-order delay differential equations.

1. Introduction

Fractional calculus is used in various branches of mathematics due to its numerous applications in modeling different physical phenomena in engineering and science. The concept of fractional calculus has been derived from the fact $D^{\alpha}(f(x))$, where alpha is noninteger. Later on, different scientists such as Riemann–Liouville, Euler, Leibniz, L'Hospital, Bernoulli, and Wallis have devoted their work to this research area. Fractional calculus has numerous applications in different field of sciences. For example dynamic of viscoelastic materials [1], electromagnetism [2], fluid mechanics [3], propagation of spherical flames [4], and viscoelastic materials [5].

In our real life, DEs are used to develop a different number of physical problems. Some are more complex and cannot be modeled with the help of simple differential equations. For these complex problems, a new technique has been used by the researchers known as fractional differential equations (FDEs). In the mathematical modeling of real-world physical problems, FDEs have been widespread due to their numerous applications in engineering and real-life sciences problems [6–9], such as economics [10], solid mechanics [11], continuum and statistical mechanics [12], oscillation of earthquakes [13], dynamics of interfaces between soft-nanoparticles and rough substrates [14], fluid-dynamic traffic model [15], colored noise [16], solid mechanics [11], anomalous transport [17], and bioengineering [18–20].

Delay differential equations (DDEs) have a wide range of applications in engineering and science. Delay differential equation simplifies the ordinary differential equation, depends on the past data, and is suitable for physical systems. Nowadays, researchers pay more attention to FDDEs as compared to DEs because a slight delay has a large effect. In this regard, numerous papers have been dedicated to the study of the numerical solution of FDDEs. FDDs have been widespread in mathematical modelings, such as population

dynamics, epidemiology, immunology, physiology, and neural networks [21–25].

In literature, there is no precise technique for finding an exact or analytical solution for every FDDEs; the researcher's effort is to find the numerical solution of FDDEs. Various methods have been implemented for solving these problems numerically. The well-known among these methods are new predictor corrector method (NPCM) [26], adomian decomposition method (ADM) [27], Legendre pseudospectral method (LSM) [28], kernel method (KM) [29], LMS method (LMSM) [30], Adams–Bashforth–Moulton algorithm (ABMA) [31], extend predictor corrector method (EPCM) [32], simplified reproducing kernel method (SRKM) [29], variation iteration method (VIM) [33], homotopy perturbation method (HPM) [34], Galerkin method (GM) [35], Runge–Kutta-type methods (RKM) [36], Bernoulli wavelet method (BWM) [37], and modified Laguerre wavelet method [38] have been used for the analytical and numerical solution of FDDEs.

In the present work, CPM is extended for the solutions of FDDEs. The results we obtained are compared with other methods, which show that CPM has good convergence rate than other methods. We focus on FDDE of the form

$$D_u^{\gamma} f(u) = g(u, f(u), f(h(u))), \quad c \le u \le d,\ m < \gamma \le m+1,\ m = 1, 2, 3, \ldots, \tag{1}$$

with the following boundary conditions:

$$f(c) = \alpha_0, \quad f(d) = \alpha_1,\ f(u) = \zeta(u),\ u \in [c_0, c], \tag{2}$$

where h is the delay function which is to be assumed continues in the interval [c, d] and satisfies the inequality $c_0 \le h(u) \le u$ for some fix real constant c_0, for $u \in [c, d]$ and $\zeta \in C[c_0, c]$

The following is a summary of the paper's structure. In Section 2, we introduce some fundamental fractional calculus definitions and mathematical techniques that will be useful in our later study. The approximation of the fractional derivative $D_u^{\gamma} f(u)$ is obtained in Section 3. Section 4 describes the Chebyshev collocation method's application to the solution of eq. (1). As a result, a set of algebraic equations is created, and the solution to the problem in question is presented. Section 5 provides some numerical results to help clarify the method.

2. Basic Definitions of Fractional Derivatives

Definition 1. A real function, $g(u), u > 0$, is said to be in the space $C_{\mu}, \mu \in \mathbb{R}$, if there exists a real number $p > \mu$, such that $g(u) = u^p g_1(u)$, where $g_1(u) \in [0, \infty)$, and it is said to be in the space C_{μ}^m if and only if $g^{(m)} \in C_{\mu}$, $m \in \mathbb{N}$.

Definition 2. In Caputo manner, the derivative having fractional-order $D^{\gamma} g(u)$ is given as below:

$$D^{\gamma} g(u) = \frac{1}{\Gamma(j-\gamma)} \int_0^u (u-t)^{j-\gamma-1} g^{(n)}(t) \mathrm{d}t, \quad u > 0,\ j-1 < \gamma < j. \tag{3}$$

The order of the derivative is $\gamma > 0$, and the lowest integer greater than γ is $j \in \mathbb{N}$ and $g \in C_{-1}^n$.

We have the Caputo derivative [39]:

$$D^{\gamma} C = 0, \quad C \text{ is a constant}, \tag{4}$$

$$D^{\gamma} u^{\alpha} = \begin{cases} 0 \text{ for } \alpha \in \mathbb{N}_0 \text{ and } \alpha < \lceil \gamma \rceil \\ \dfrac{\Gamma(\alpha+1)}{\Gamma(\alpha+1-\gamma)} u^{\alpha-\gamma} \text{ for } \alpha \in \mathbb{N}_0 \text{ and } \alpha \ge \lceil \gamma \rceil \end{cases}, \tag{5}$$

where the lowest integer larger than or equal to γ is denoted by the ceiling function $\lceil \gamma \rceil$ and $\mathbb{N}_0 = 1, 2, \ldots$. Remember that the Caputo differential operator is the same as the normal differential operator of the integer order for $\gamma \in \mathbb{N}$. Fractional differentiation is a linear operation, just like integer-order differentiation:

$$D^{\gamma}(\phi g(u) + \mu h(u)) = \phi D^{\gamma} g(u) + \mu D^{\gamma} h(u), \tag{6}$$

where ϕ and μ are constants.

3. Chebyshev Series Expansion Is Used to Approximate a Caputo Derivative

On the interval $[-1, 1]$, Chebyshev polynomials are defined and, with the help of recurrence formulae, explained as [40, 41]

$$T_{j+1}(u) = 2uT_j(u) - T_{j-1}(u), \quad j = 1, 2, \ldots, \tag{7}$$

where $T_0(u) = 1$ and $T_1(u)u$. The Chebyshev polynomial analytical form for degree j is defined as [41]

$$T_j(u) = \frac{j}{2} \sum_{r=0}^{\lfloor j/2 \rfloor} (-1)^r \frac{(j-r-1)!}{r!(j-2r)!} (2u)^{j-2r}. \tag{8}$$

If we apply the Chebyshev polynomials over the $[0, 1]$ interval, we explain the Chebyshev shifted polynomials $\widehat{T}_j(u)$. These are described in the sense of Chebyshev polynomials $T_j(u)$ as [41]

$$\widehat{T}_j(u) = T_j(2u-1). \tag{9}$$

And recurrence formula is as follows:

$$\widehat{T}_{j+1}(u) = 2(2u-1)\widehat{T}_j(u) - \widehat{T}_{j-1}(u), \quad j = 1, 2, \ldots, \tag{10}$$

where $\widehat{T}_0(u) = 1$ and $\widehat{T}_1(u) = 2u - 1$. The orthogonality condition is [42]

$$\int_0^1 \frac{\widehat{T}_j(u)\widehat{T}_m(u)}{\sqrt{u-u^2}} \mathrm{d}u = \begin{cases} 0\, m \ne j, \\ \dfrac{\pi}{2}\, m = j \ne 0, \\ \pi\, m = j = 0. \end{cases} \tag{11}$$

Now, we can use the well-known relation,

$$\widehat{T}_j(u) = T_{2j}(\sqrt{u}), \tag{12}$$

and equation (8) to get shifted Chebyshev polynomials analytical form having order j as

$$\widehat{T}_j(u) = \sum_{r=0}^{j} (-1)^r 2^{2j-2r} \frac{j(2j-r-1)!}{r!(2j-2r)!}(x)^{j-2r}. \tag{13}$$

A function $f(u) \in L_2[0,1]$ may be described in terms of Chebyshev shifted polynomials as

$$f(u) = \sum_{j=1}^{\infty} c_j \widehat{T}_j(u), \tag{14}$$

where the coefficients c_j, $j = 1, 2, \ldots$, are given by

$$c_0 = \frac{1}{\pi}\int_0^1 \frac{g(u)\widehat{T}_0(u)}{\sqrt{u-u^2}}\mathrm{d}u \text{ and } c_n = \frac{2}{\pi}\int_0^1 \frac{g(u)\widehat{T}_j(u)}{\sqrt{u-u^2}}\mathrm{d}u. \tag{15}$$

Only Chebyshev shifted polynomials first $(m+1)$-terms are considered in practice. Thus,

$$f_m(u) = \sum_{j=0}^{m} c_j \widehat{T}_j(u). \tag{16}$$

3.1. Chebyshev Truncation Theorem [43]. The sum of the absolute values of all the disregarded coefficients limits the inaccuracy in approximating $f(u)$ by the sum of its first m terms. That is, assuming

$$f_m(u) = \sum_{k=0}^{m} c_k T_k(u), \tag{17}$$

then, for all $f(u)$, all m, and all $u \in [-1,1]$, we obtain

$$E_T(m) = \left|f(u) - f_m(u)\right| \le \sum_{k=m+1}^{\infty} |c_k|. \tag{18}$$

Proof. For any $u \in [-1,1]$ and all k, the Chebyshev polynomials are bounded by 1, $|T_k(u)| \le 1$. As a result, the kth term is restricted by $|c_k|$. By subtracting the reduced series from the infinite series, bounding each term in the difference, and then summing the bounds, the theorem can be derived.

The following theorem contains the main approximate formula for the fractional derivative of $f(u)$. □

3.2. Theorem [44]. Assume $\alpha > 0$ and that $f(u)$ is estimated by the shifted Chebyshev polynomials as in (16). Then,

$$D^{\alpha}\left(f_m(u)\right) = \sum_{j=\lceil\alpha\rceil}^{m}\sum_{r=0}^{n-\lceil\alpha\rceil} c_j b_{j,r}^{\alpha} u^{j-r-\alpha}, \tag{19}$$

where $b_{j,r}^{\alpha}$ is given by

$$b_{j,r}^{\alpha} = (-1)^r 2^{2j-2r} \frac{j(2j-r-1)!(j-r)!}{r!(2j-2r)!\Gamma(j-r+1-\alpha)}. \tag{20}$$

Proof. Since Caputo fractional differentiation is a linear operation, we have

$$D^{\alpha}\left(f_m(u)\right) = \sum_{j=0}^{m} c_n D^{\alpha}\left(\widehat{T}_j(u)\right). \tag{21}$$

Now, to evaluate $D^{\alpha}(\widehat{T}_j(u))$, applying to equations (4) and (5)–(13),

$$D^{\alpha}\left(\widehat{T}_j(u)\right) = \sum_{r=0}^{j} (-1)^r 2^{2j-2r} \frac{j(2j-r-1)!}{r!(2j-2r)!} D^{\alpha}(u)^{j-r}, \quad j = \lceil\alpha\rceil, \lceil\alpha\rceil+1, \ldots m. \tag{22}$$

Since $\widehat{T}_j(u)$ is a polynomial having degree j, we obtain

$$D^{\alpha}\left(\widehat{T}_j(u)\right) = 0 \text{ forall } \quad j = 0, 1, 2, \ldots, \lceil\alpha\rceil - 1,\ \alpha > 0. \tag{23}$$

The following is the result of combining (21)–(23):

$$D^{\alpha}\left(f_m(u)\right) = \sum_{j=\lceil\alpha\rceil}^{m}\sum_{r=0}^{n-\lceil\alpha\rceil} \frac{c_j(-1)^r 2^{2j-2r} j(2j-r-1)!(j-r)!}{r!(2j-2r)!\Gamma(j-r+1-\alpha)} u^{j-r-\alpha} = \sum_{j=\lceil\alpha\rceil}^{m}\sum_{r=0}^{n-\lceil\alpha\rceil} c_j b_{j,r}^{\alpha} u^{j-2r-\alpha}, \tag{24}$$

which is the desired result.

Test example: consider formula (19) with $f(u) = u^2, m = 2$. The shifted series of u^2 is

$$u^2 = c_0\widehat{T}_0(u) + c_1\widehat{T}_1(u) + c_2\widehat{T}_2(u) = \frac{3}{8}\widehat{T}_0(u) + \frac{1}{2}\widehat{T}_1(u) + \frac{1}{8}\widehat{T}_2(u) \tag{25}$$

and

$$D^{\frac{1}{2}}(u^2) = \sum_{j=1}^{2}\sum_{r=0}^{n-1} c_n b_{n,r}^{\left(\frac{1}{2}\right)} u^{j-r-\frac{1}{2}} = c_1 b_{1,0}^{\left(\frac{1}{2}\right)} u^{\frac{1}{2}} + c_2 b_{2,0}^{\left(\frac{1}{2}\right)} u^{\frac{3}{2}} + c_2 b_{2,1}^{\left(\frac{1}{2}\right)} u^{\frac{1}{2}} = \frac{2}{\sqrt{\pi}} u^{\frac{1}{2}} + \frac{8}{3\sqrt{\pi}} u^{\frac{3}{2}} - \frac{2}{\sqrt{\pi}} u^{\frac{1}{2}} = \frac{8}{3\sqrt{\pi}} u^{\frac{3}{2}}, \tag{26}$$

which yields the same result as evaluating $D^{1/2}(u^2)$ by relation (5). □

4. Chebyshev Collocation Method

We solve the FDDE (1) with the boundary conditions (2) stated in the next part using Chebyshev's collocation method in this section. Assume that the approximate solution $f(u)$ is defined in terms of a finite number m of shifted Chebyshev polynomials, i.e.,

$$f_m(u) = \sum_{j=0}^{m} c_j \widehat{T}_j(u). \tag{27}$$

We can use theorem (4.1) and equation (22) to solve equation (1):

$$\sum_{j=\lceil \alpha \rceil}^{m}\sum_{r=0}^{n-\lceil \alpha \rceil} c_j b_{j,r}^{\alpha} u^{j-2r-\alpha} = g\left(u, \sum_{j=0}^{m} c_j \widehat{T}_j(u), \sum_{j=0}^{m} c_j \widehat{T}_j(h(u))\right), \quad 0 < u < 1,\ m+1 < \alpha < m. \tag{28}$$

Now, we collocate (23) at points u_p, $p = 0, 1, 2, \ldots, m - \lceil \alpha \rceil$:

$$\sum_{j=\lceil \alpha \rceil}^{m}\sum_{r=0}^{n-\lceil \alpha \rceil} c_j b_{j,r}^{\alpha} u_p^{j-2r-\alpha} = g\left(u_p, \sum_{j=0}^{m} c_j \widehat{T}_j(u_p), \sum_{j=0}^{m} c_j \widehat{T}_j\left(h(u_p)\right)\right), \quad u_p,\ p = 0, 1, \ldots m - \lceil \alpha \rceil,\ m+1 < \alpha < m. \tag{29}$$

Using (22) in the boundary conditions (2), we may construct the following $\lceil \alpha \rceil$ equations:

$$\sum_{i=0}^{m} (-1)^i c_i = \alpha_0, \quad \sum_{i=0}^{m} c_i = \alpha_1. \tag{30}$$

We get $(m + 1 - \lceil \alpha \rceil)$ algebraic equations from (24) and $\lceil \alpha \rceil)$ algebraic equations from (26). As a result, we have total $(m+1)$ linear or nonlinear algebraic equations that can be easily solved using matrices for unknowns c_j, $j = 0, 1, 2, \ldots m$, to find out an estimated solution $\mu_m(\psi)$.

5. Numerical Representation

In this section, we solve some delay problems. The results we obtained are compared with other methods. All the numerical results are obtained using MAPLE.

Problem 1. Consider the FDDE:

$$\frac{d^{\alpha} f(u)}{du} = \frac{1}{2}\exp^{\frac{u}{2}} f\left(\frac{u}{2}\right) + \frac{1}{2} f(u), \quad 0 < \alpha \le 1, \tag{31}$$

subject to the initial conditions $f(0) = 1$, having accurate solution $f(u) = \exp^u$ at $\alpha = 1$.

The exact solution and CPM solution are given in Table 1. Table 2 shows CPM and CWM error comparison at $m = 4$ which confirm that CPM converges quickly as compared to CWM. We illustrate the accurate and estimated solutions for $m = 4$ in Figure 1, while Figure 2 shows the error comparison of both methods. Also, Figure 3 provides the graphical layout of the solution of example 1 at various fractional orders. It can be seen that the solutions of CPM are in good agreement to the actual solution than that of CWM.

Problem 2. Consider the nonlinear DDE,

$$\frac{d^{\alpha} f(u)}{du} = 1 - 2f^2\left(\frac{u}{2}\right), \quad 0 \le u \le 1,\ 1 < \alpha \le 2, \tag{32}$$

subjects to the initial condition $f(0) = 1$, $f'(0) = 0$.

The accurate solution of this equation for $\alpha = 2$ is $f(u) = \cos(u)$. The exact solution and CPM solution are shown in Table 3. Table 4 shows the error comparison of CPM at $m = 3$ and MWBA at $m = 20$ which confirm that CPM converges quickly as compare to MLWM. The estimated and accurate solutions are illustrated in Figure 4, whereas Figure 5 shows the error comparison of both methods. In addition, the convergence phenomena of the solutions at different fractional orders can be seen in Figure 6. The results of the presented method are better than those of the MWBA method for example 2.

Problem 3. Consider the fractional DDE of the form

$$\frac{d^{\alpha} f(u)}{du} = f\left(\frac{u}{2}\right) + \frac{3}{4} f(u) - u^2 + 2, \quad 0 \le u \le 1,\ 1 < \alpha \le 2, \tag{33}$$

with initial conditions $f(0) = f'(0) = 0$.

Table 1: Exact, CPM solution, and CPM A.E of problem 1 for $m = 4$.

u	Exact	CPM	CPM error
0	1.000 000 000 000 000	1.000 000 000 000 000	0.0 000 000 000$E+00$
0.01	1.010 050 167 084 170	1.010 050 167 197 000	1.1 283 000 000$E-10$
0.02	1.020 201 340 026 760	1.020 201 341 818 670	1.7 919 100 000$E-09$
0.03	1.030 454 533 953 520	1.030 454 542 957 020	9.0 035 000 000$E-09$
0.04	1.040 810 774 192 390	1.040 810 802 432 060	2.8 239 670 000$E-08$
0.05	1.051 271 096 376 020	1.051 271 164 791 820	6.8 415 800 000$E-08$
0.06	1.061 836 546 545 360	1.061 836 687 312 300	1.4 076 694 000$E-07$
0.07	1.072 508 181 254 220	1.072 508 439 997 560	2.5 874 334 000$E-07$
0.08	1.083 287 067 674 960	1.083 287 505 579 630	4.3 790 467 000$E-07$
0.09	1.094 174 283 705 210	1.094 174 979 518 540	6.9 581 333 000$E-07$
0.10	1.105 170 918 075 650	1.105 171 970 002 350	1.0 519 267 000$E-06$

Table 2: Absolute error (A.E) comparison of CPM and other different methods of problem 1 at $m = 4$.

u	CPM A.E	CWM A.E
0	0.0 000 000 000$E+00$	0.0 000 000 000$E+00$
0.01	1.1 283 000 000$E-10$	1.82 567$E-04$
0.02	1.7 919 100 000$E-09$	3.68 446$E-04$
0.03	9.0 035 000 000$E-09$	5.57 408$E-04$
0.04	2.8 239 670 000$E-08$	7.49 213$E-04$
0.05	6.8 415 800 000$E-08$	9.43 609$E-04$
0.06	1.4 076 694 000$E-07$	1.14 034$E-03$
0.07	2.5 874 334 000$E-07$	1.33 912$E-03$
0.08	4.3 790 467 000$E-07$	1.53 969$E-03$
0.09	6.9 581 333 000$E-07$	1.74 174$E-03$
0.10	1.0 519 267 000$E-06$	1.94 497$E-03$

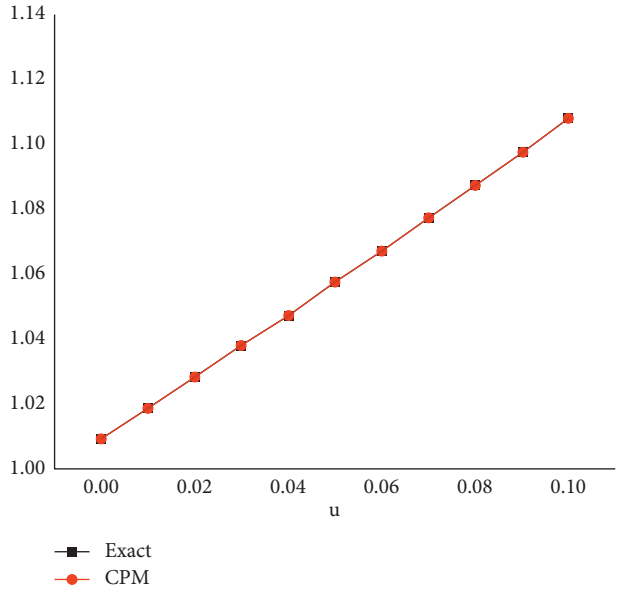

Figure 1: The exact and CPM solution graph for problem 1.

The exact solution of this equation for $\alpha = 2$ is $f(u) = u^2$. The exact solution and CPM solution are shown in Table 5. Table 6 shows the error comparison of CPM at $m = 3$ and MWLM at $m = 5$ which confirm that CPM converges quickly as compare to MLWM. We illustrate the accurate and estimated solutions for $m = 3$ in Figure 7, while Figure 8 shows the error comparison of both methods. The results of the presented method are better than those of the MWBA method for example 3.

Problem 4. Consider the following nonlinear delay differential equation with boundary conditions $f(0) = 1$ and $f(1) = 1$:

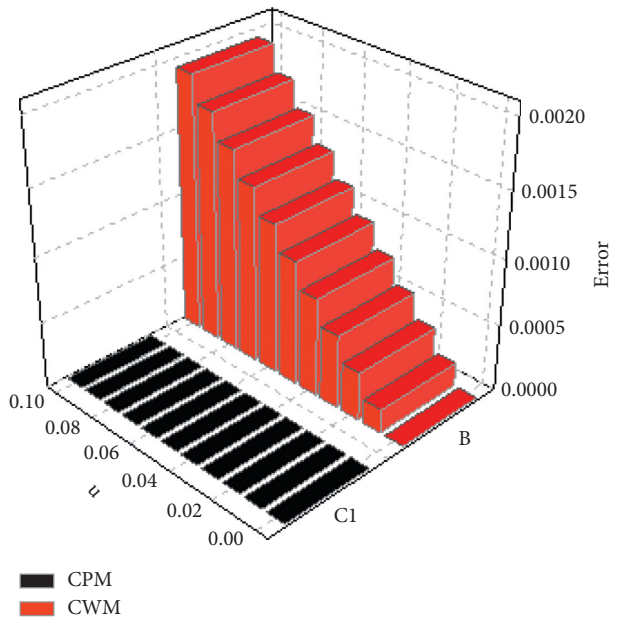

Figure 2: Error graph of CWM and CPM for problem 1.

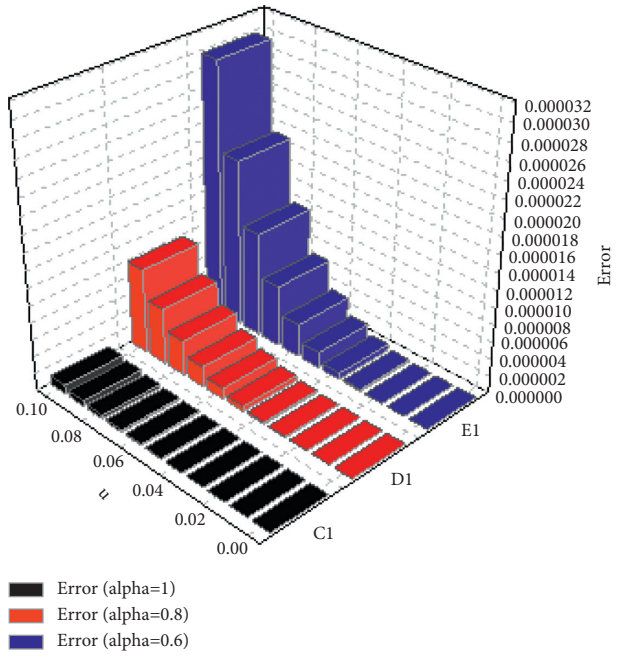

Figure 3: The graph of the absolute error at various fractional orders for problem 1.

$$\frac{d^{\alpha}}{du^{\alpha}} f(u) = \frac{8}{3}\frac{d}{du}\left(f\left(\frac{u}{2}\right)\right) f(u) + 8u^2 f\left(\frac{u}{2}\right) - \frac{4}{3} - \frac{22}{3}u - 7u^2 - \frac{5}{3}u^3, \quad 1 < \alpha \leq 2. \tag{34}$$

The accurate solution of this equation for $\alpha = 2$ is $f(u) = 1 + u - u^3$. The exact and CPM solution are shown in Table 7. Table 8 shows the error comparison of CPM at $m = 4$ and MWBA at $m = 8$ which confirm that CPM converges quickly as compare to MWBA. The estimated and accurate solutions are illustrated in Figure 9, while Figure 10 shows the error comparison of both methods. It can be seen that our method is more accurate.

Table 3: Exact, CPM solution, and CPM A.E of problem 2 at $m = 10$.

u	Exact	CPM	CPM error
0	1.000 000 000 000 000	1.000 000 000 000 000	0.0 000 000 000$E+00$
0.10	0.995 004 165 278 026	0.995 004 165 278 026	2.9 000 000 000$E-19$
0.20	0.980 066 577 841 242	0.980 066 577 841 242	2.7 250 000 000$E-16$
0.30	0.955 336 489 125 606	0.955 336 489 125 621	1.5 097 140 000$E-14$
0.40	0.921 060 994 002 885	0.921 060 994 003 138	2.5 278 786 000$E-13$
0.50	0.877 582 561 890 373	0.877 582 561 892 544	2.1 711 958 200$E-12$
0.60	0.825 335 614 909 678	0.825 335 614 921 738	1.2 059 545 750$E-11$
0.70	0.764 842 187 284 488	0.764 842 187 333 195	4.8 707 056 530$E-11$
0.80	0.696 706 709 347 165	0.696 706 709 498 894	1.5 172 838 626$E-10$
0.90	0.621 609 968 270 664	0.621 609 968 640 609	3.6 994 453 098$E-10$
1.0	0.540 302 305 868 140	0.540 302 306 536 394	6.6 825 465 360$E-10$

Table 4: Absolute error (A.E) comparison of CPM and other different methods for problem 2.

u	CPM A.E at $(m = 3)$	MLWM A.E at $(m = 20)$
0	0	2.10 000$E-08$
0.10	2.9 000 000 000$E-19$	2.11 000$E-08$
0.20	2.7 250 000 000$E-16$	2.09 000$E-08$
0.30	1.5 097 140 000$E-14$	2.09 000$E-08$
0.40	2.5 278 786 000$E-13$	2.08 000$E-08$
0.50	2.1 711 958 200$E-12$	2.06 000$E-08$
0.60	1.2 059 545 750$E-11$	2.04 000$E-08$
0.70	4.8 707 056 530$E-11$	2.03 000$E-08$
0.80	1.5 172 838 626$E-10$	2.00 000$E-08$
0.90	3.6 994 453 098$E-10$	1.99 000$E-08$
1.0	6.6 825 465 360$E-10$	1.97 000$E-08$

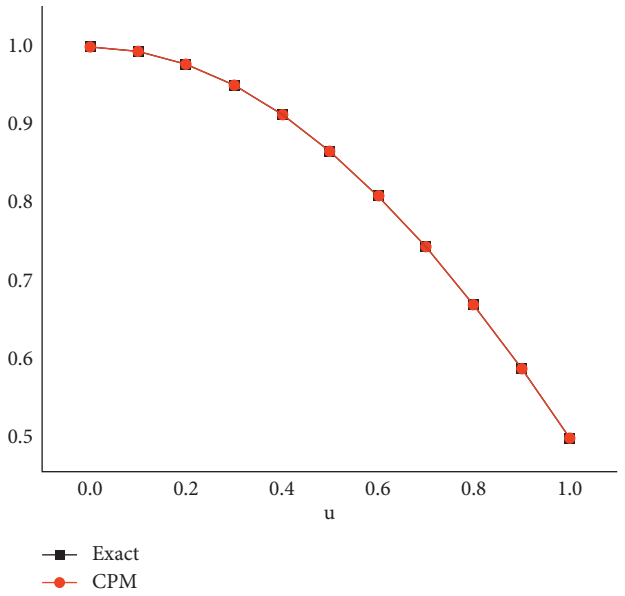

Figure 4: The graph of absolute error at various fractional orders for problem 2.

Problem 5. Consider the FDDE

$$\frac{d^{\alpha} f(u)}{du} + f(u) + f(u - 0.3) = \exp^{-u+0.3}, \quad 1 < \alpha < 2,\ 0 < \alpha < 1, \tag{35}$$

having initial conditions $f(0) = 1, f'(0) = -1$, and $f''(0) = 1$.

The accurate solution of this problem for $\alpha = 3$ is $f(u) = \exp^{-u}$. The exact and CPM solutions are shown in

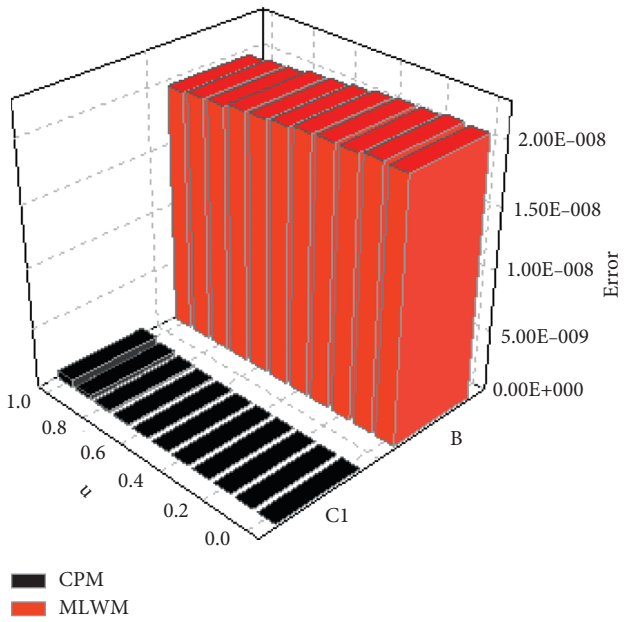

Figure 5: Exact and CPM solution graph for problem 2.

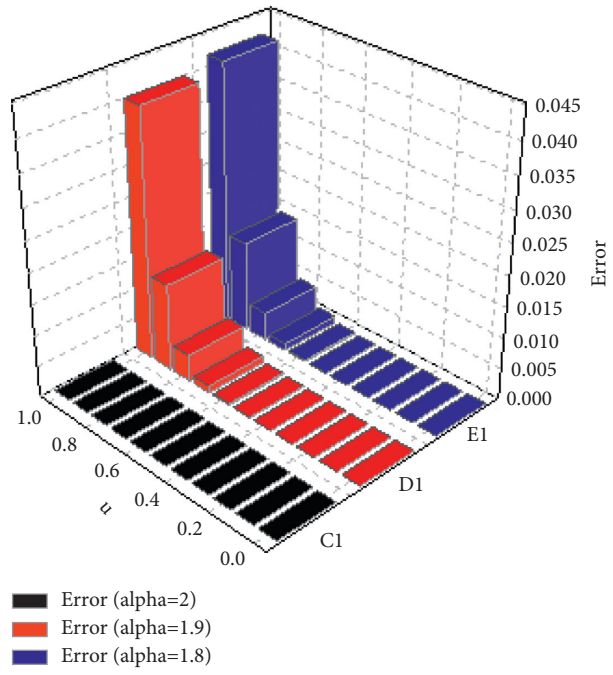

Figure 6: Error graph of MLWM and CPM for problem 2.

Table 9. Table 10 shows the error comparison of CPM and CWM at $m = 6$ which confirm that CPM converges quickly as compared to CWM. We illustrate the accurate and estimated solutions for $m = 6$ in Figure 11, while Figure 12 shows the error comparison of both methods. In Figure 13, the solution for example 4.5 at different fractional orders is calculated. It is confirmed that the solution at various fractional order approaches towards the integer-order solution. The results of the presented method are better than those of the CWM method for this problem.

Table 5: Exact, CPM solution, and CPM A.E of problem 3 at $m = 3$.

u	Exact	CPM	CPM error
0	0.000 000 000 000 00	0.000 000 000 000 00	4.0 000 000 000$E+00$
0.10	0.010 000 000 000 00	0.010 000 000 000 00	1.2 100 000 000$E-29$
0.20	0.040 000 000 000 00	0.040 000 000 000 00	2.4 800 000 000$E-29$
0.30	0.090 000 000 000 00	0.090 000 000 000 00	3.7 400 000 000$E-29$
0.40	0.160 000 000 000 00	0.160 000 000 000 00	5.0 000 000 000$E-29$
0.50	0.250 000 000 000 00	0.250 000 000 000 00	6.4 000 000 000$E-29$
0.60	0.360 000 000 000 00	0.360 000 000 000 00	7.8 000 000 000$E-29$
0.70	0.490 000 000 000 00	0.490 000 000 000 00	9.4 000 000 000$E-29$
0.80	0.640 000 000 000 00	0.640 000 000 000 00	1.1 100 000 000$E-28$
0.90	0.810 000 000 000 00	0.810 000 000 000 00	1.2 800 000 000$E-28$
1.0	1.000 000 000 000 00	1.000 000 000 000 00	1.4 000 000 000$E-28$

Table 6: Absolute error (A.E) comparison of CPM and other different methods of problem 3.

u	CPM A.E at ($m = 3$)	MLWM A.E at ($m = 5$)
0	4.0 000 000 000$E+00$	1.41 421$E-09$
0.10	1.2 100 000 000$E-29$	4.75 800$E-08$
0.20	2.4 800 000 000$E-29$	9.69 300$E-08$
0.30	3.7 400 000 000$E-29$	1.47 010$E-07$
0.40	5.0 000 000 000$E-29$	1.98 200$E-07$
0.50	6.4 000 000 000$E-29$	2.50 900$E-07$
0.60	7.8 000 000 000$E-29$	3.05 500$E-07$
0.70	9.4 000 000 000$E-29$	3.62 400$E-07$
0.80	1.1 100 000 000$E-28$	4.22 000$E-07$
0.90	1.2 800 000 000$E-28$	4.84 800$E-07$
1.0	1.4 000 000 000$E-28$	5.51 000$E-07$

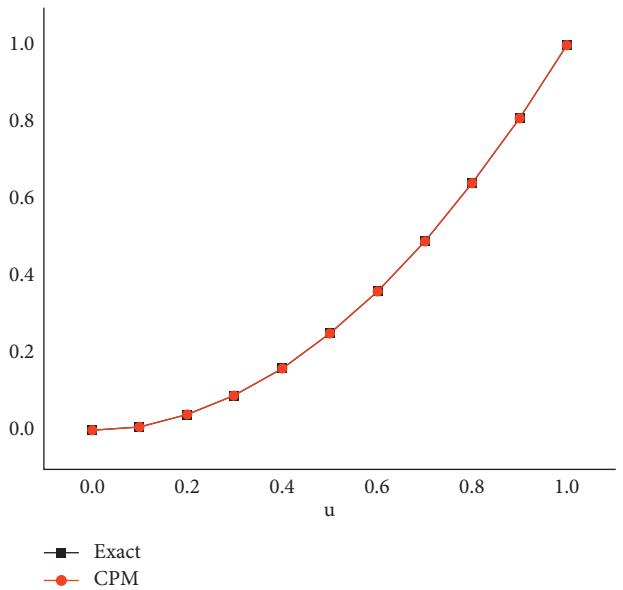

Figure 7: The exact and CPM solution graph for problem 3.

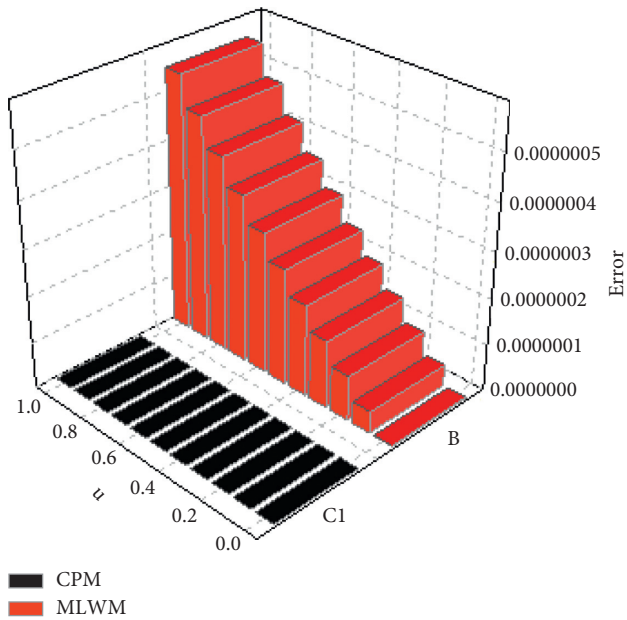

Figure 8: Error graph of MLWM and CPM for problem 3.

Table 7: Exact, CPM solution, and CPM A.E at $m = 4$ of problem 4.

u	Exact	CPM	CPM error
0	1.000 000 000 000 000	1.000 000 000 000 000	$2.0\,000\,000\,000E-40$
0.10	1.099 000 000 000 000	1.099 000 000 000 000	$3.0\,000\,000\,000E-39$
0.20	1.192 000 000 000 000	1.192 000 000 000 000	$6.0\,000\,000\,000E-39$
0.30	1.273 000 000 000 000	1.273 000 000 000 000	$7.0\,000\,000\,000E-39$
0.40	1.336 000 000 000 000	1.336 000 000 000 000	$1.0\,000\,000\,000E-38$
0.50	1.375 000 000 000 000	1.375 000 000 000 000	$1.3\,000\,000\,000E-38$
0.60	1.384 000 000 000 000	1.384 000 000 000 000	$1.6\,000\,000\,000E-38$
0.70	1.357 000 000 000 000	1.357 000 000 000 000	$1.9\,000\,000\,000E-38$
0.80	1.288 000 000 000 000	1.288 000 000 000 000	$2.3\,000\,000\,000E-38$
0.90	1.171 000 000 000 000	1.171 000 000 000 000	$2.5\,000\,000\,000E-38$
1.0	1.000 000 000 000 000	1.000 000 000 000 000	$2.9\,000\,000\,000E-38$

Table 8: Absolute error (A.E) comparison of CPM and other different methods for problem 4.

u	CPM error at $(m = 4)$	MWBA error at $(m = 8)$
0	$2.0\,000\,000\,000E-40$	$1.20\,000E-29$
0.10	$3.0\,000\,000\,000E-39$	$1.00\,000E-29$
0.20	$6.0\,000\,000\,000E-39$	$1.00\,000E-29$
0.30	$7.0\,000\,000\,000E-39$	$1.00\,000E-29$
0.40	$1.0\,000\,000\,000E-38$	$1.00\,000E-29$
0.50	$1.3\,000\,000\,000E-38$	$1.00\,000E-29$
0.60	$1.6\,000\,000\,000E-38$	$1.00\,000E-29$
0.70	$1.9\,000\,000\,000E-38$	$1.00\,000E-29$
0.80	$2.3\,000\,000\,000E-38$	$2.00\,000E-29$
0.90	$2.5\,000\,000\,000E-38$	$2.00\,000E-29$
1.0	$2.9\,000\,000\,000E-38$	$1.50\,000E-29$

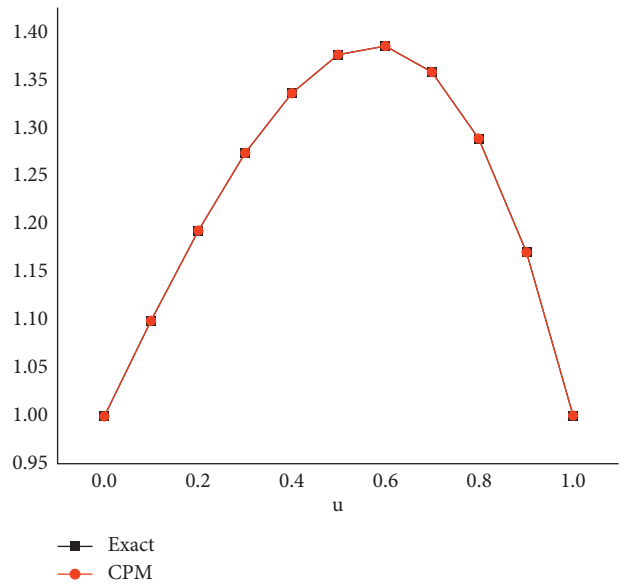

Figure 9: The exact and CPM solution graph for problem 4.

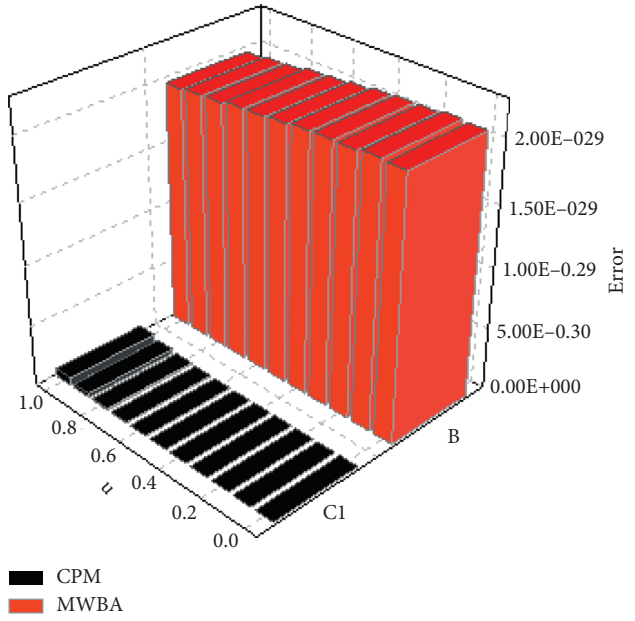

Figure 10: Error graph of MWBA and CPM for problem 4.

Table 9: Exact, CPM solution, and CPM error of problem 5 for $m = 6$.

u	Exact	CPM	CPM (A.E)
0	1.000 000 000 000 000	1.000 000 000 000 000	$0.0\,000\,000\,000E+00$
0.01	0.990 049 833 749 168	0.990 049 833 749 168	$2.6\,506\,231\,572E-16$
0.02	0.980 198 673 306 755	0.980 198 673 306 738	$1.6\,837\,479\,038E-14$
0.03	0.970 445 533 548 508	0.970 445 533 548 318	$1.9\,035\,198\,323E-13$
0.04	0.960 789 439 152 323	0.960 789 439 151 262	$1.0\,614\,659\,655E-12$
0.05	0.951 229 424 500 714	0.951 229 424 496 695	$4.0\,185\,154\,936E-12$
0.06	0.941 764 533 584 249	0.941 764 533 572 341	$1.1\,907\,912\,782E-11$
0.07	0.932 393 819 905 948	0.932 393 819 876 151	$2.9\,797\,628\,776E-11$
0.08	0.923 116 346 386 636	0.923 116 346 320 752	$6.5\,884\,200\,594E-11$
0.09	0.913 931 185 271 228	0.913 931 185 138 694	$1.3\,253\,379\,871E-10$
0.10	0.904 837 418 035 960	0.904 837 417 788 512	$2.4\,744\,798\,291E-10$

Table 10: Absolute error (A.E) comparison of CPM and other different methods of problem 5 at $m = 6$.

u	CPM A.E	CWM A.E
0	$0.0\,000\,000\,000E+00$	$0.0\,000\,000\,000E+00$
0.01	$2.6\,506\,231\,572E-16$	$8.20\,000E-09$
0.02	$1.6\,837\,479\,038E-14$	$6.68\,000E-08$
0.03	$1.9\,035\,198\,323E-13$	$2.28\,800E-07$
0.04	$1.0\,614\,659\,655E-12$	$5.50\,500E-07$
0.05	$4.0\,185\,154\,936E-12$	$1.09\,130E-06$
0.06	$1.1\,907\,912\,782E-11$	$1.91\,420E-06$
0.07	$2.9\,797\,628\,776E-11$	$3.08\,520E-06$
0.08	$6.5\,884\,200\,594E-11$	$4.67\,410E-06$
0.09	$1.3\,253\,379\,871E-10$	$6.75\,420E-06$
0.10	$2.4\,744\,798\,291E-10$	$9.40\,260E-06$

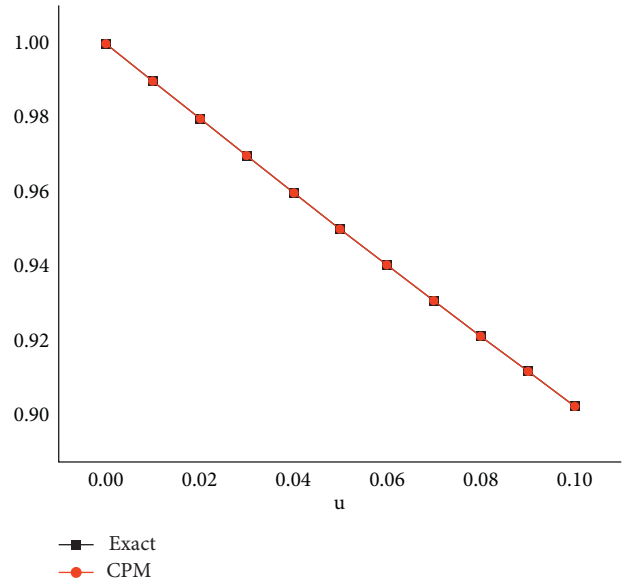

Figure 11: The exact and CPM solution graph for problem 5.

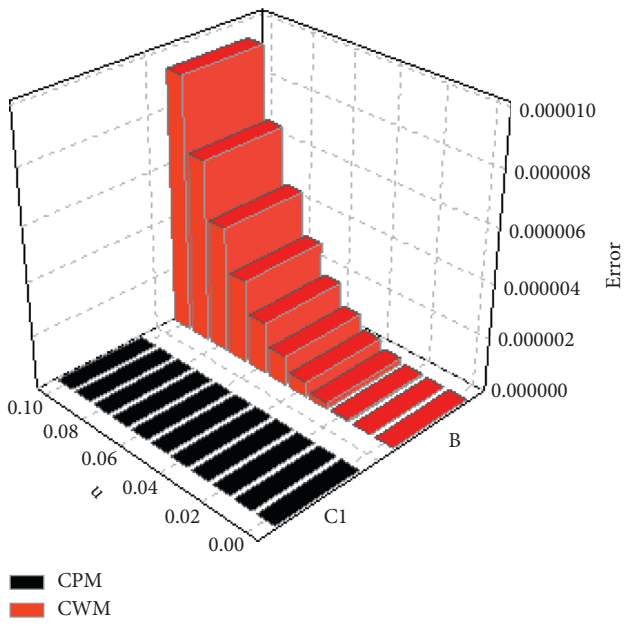

Figure 12: Error graph of CWM and CPM for problem 5.

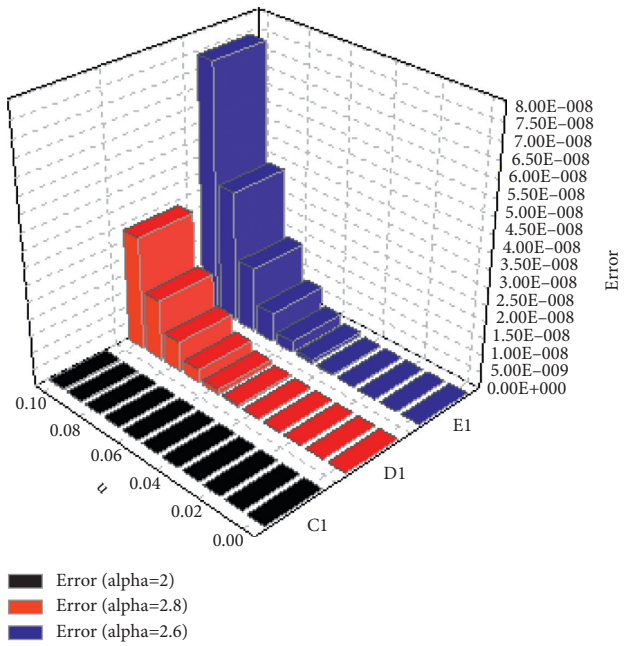

Figure 13: The graph of absolute error at various fractional orders for problem 5.

6. Conclusion

In this study, we applied the Chebyshev pseudospectral method for solving fractional delay differential equations. The technique is easy to implement and show good convergence rate than other methods. Some examples are solved which shows the effectiveness of the present method. The results we obtained are compared with other methods such as modified wavelet-based algorithm (MWBA), modified Laguerre wavelet method (MLWM), Chebyshev wavelet method (CWM). It is clear from comparison that CPM has higher accuracy than all these methods. Although, CPM can easily be extended to other fractional delay or nondelay models of physics and real-life sciences.

Data Availability

The numerical data used to support the findings of this study are included within the article.

Conflicts of Interest

The authors declare that there are no conflicts of interest regarding the publication of this article.

Acknowledgments

The authors would like to thank the Deanship of Scientific Research at Umm Al-Qura University for supporting this work by Grant CODE: 22UQU4310396DSR02.

References

[1] C. Lederman, J.-M. Roquejoffre, and N. Wolanski, "Mathematical justification of a nonlinear integro-differential equation for the propagation of spherical flames," *Annali di Matematica Pura ed Applicata*, vol. 183, no. 2, pp. 173–239, 2004.

[2] N. Engheta, "On fractional calculus and fractional multipoles in electromagnetism," *IEEE Transactions on Antennas and Propagation*, vol. 44, no. 4, pp. 554–566, 1996.

[3] V. V. Kulish and J. L. Lage, "Application of fractional calculus to fluid mechanics," *Journal of Fluids Engineering*, vol. 124, no. 3, pp. 803–806, 2002.

[4] M. Naeem, A. M. Zidan, K. Nonlaopon, M. I. Syam, Z. Al-Zhour, and R. Shah, "A new analysis of fractional-order equal-width equations via novel techniques," *Symmetry*, vol. 13, no. 5, p. 886, 2021.

[5] R. L. Bagley and P. J. Torvik, "Fractional calculus in the transient analysis of viscoelastically damped structures," *AIAA Journal*, vol. 23, no. 6, pp. 918–925, 1985.

[6] R. P. Agarwal, F. Mofarreh, R. Shah, W. Luangboon, and K. Nonlaopon, "An analytical technique, based on natural transform to solve fractional-order parabolic equations," *Entropy*, vol. 23, no. 8, p. 1086, 2021.

[7] P. Sunthrayuth, N. H. Aljahdaly, A. Ali, R. Shah, I. Mahariq, and A. M. Tchalla, "ψ-Haar wavelet operational matrix method for fractional relaxation-oscillation equations containing ψ-Caputo fractional derivative," *Journal of function spaces*, vol. 2021, Article ID 7117064, 14 pages, 2021.

[8] N. H. Aljahdaly, R. P. Agarwal, R. Shah, and T. Botmart, "Analysis of the time fractional-order coupled burgers equations with non-singular kernel operators," *Mathematics*, vol. 9, no. 18, p. 2326, 2021.

[9] P. Sunthrayuth, R. Ullah, A. Khan et al., "Numerical analysis of the fractional-order nonlinear system of Volterra integro-differential equations," *Journal of Function Spaces*, vol. 2021, Article ID 1537958, 10 pages, 2021.

[10] P. Sunthrayuth, A. M. Zidan, S.-W. Yao, R. Shah, and M. Inc, "The comparative study for solving fractional-order fornberg-whitham equation via ρ-laplace transform," *Symmetry*, vol. 13, no. 5, p. 784, 2021.

[11] Y. A. Rossikhin and M. V. Shitikova, "Applications of fractional calculus to dynamic problems of linear and nonlinear hereditary mechanics of solids," *Applied Mechanics Reviews*, vol. 50, no. 1, pp. 15–67, 1997.

[12] F. Mainardi, "Fractional calculus," in *Fractals and Fractional Calculus in Continuum Mechanics*, A. Carpinteri and F. Mainardi, Eds., Springer-Verlag, New York, NY, USA, pp. 291–348, 1997.

[13] J. H. He, "Nonlinear oscillation with fractional derivative and its applications," in *Proceedings of the International Conference on Vibrating Engineering, 98*, pp. 288–291, Dalian, China, August 1998.

[14] K. Nonlaopon, A. M. Alsharif, A. M. Zidan, A. Khan, Y. S. Hamed, and R. Shah, "Numerical investigation of fractional-order Swift-Hohenberg equations via a Novel transform," *Symmetry*, vol. 13, no. 7, p. 1263, 2021.

[15] J. H. He, "Some applications of nonlinear fractional differential equations and their approximations," *Bulletin of Science and Technology*, vol. 15, no. 2, pp. 86–90, 1999.

[16] B. Mandelbrot, "Some noises withI/fspectrum, a bridge between direct current and white noise," *IEEE Transactions on Information Theory*, vol. 13, no. 2, pp. 289–298, 1967.

[17] R. Metzler and J. Klafter, "The restaurant at the end of the random walk: recent developments in the description of anomalous transport by fractional dynamics," *Journal of Physics*, vol. A37, pp. 161–208, 2004.

[18] R. L. Magin, "Fractional calculus in bioengineering, Part 1," *Critical Reviews in Biomedical Engineering*, vol. 32, no. 1, pp. 1–104, 2004.

[19] R. L. Magin, "Fractional calculus in bioengineering, Part 2," *Critical Reviews in Biomedical Engineering*, vol. 32, no. 2, pp. 105–194, 2004.

[20] R. L. Magin, "Fractional calculus in bioengineering, part 3," *Critical Reviews in Biomedical Engineering*, vol. 32, no. 3/4, pp. 195–377, 2004.

[21] K. Nonlaopon, M. Naeem, A. M. Zidan, R. Shah, A. Alsanad, and A. Gumaei, "Numerical Investigation of the Tim*E* – Fractional Whitham-Broer-Kaup Equation Involving without Singular Kernel Operators," *Complexity*, vol. 2021, Article ID 7979365, 21 pages, 2021.

[22] F. A. Rihan, D. H. Abdelrahman, F. Al-Maskari, F. Ibrahim, and M. A. Abdeen, "Delay differential model for tumour-immune response with chemoimmunotherapy and optimal control," *Computational and mathematical methods in medicine*, vol. 2014, Article ID 982978, 15 pages, 2014.

[23] C. T. H. Baker, G. A. Bocharov, C. A. H. Paul, and F. A. Rihan, "Modelling and analysis of tim*E* – lags in some basic patterns of cell proliferation," *Journal of Mathematical Biology*, vol. 37, no. 4, pp. 341–371, 1998.

[24] S. Lakshmanan, F. A. Rihan, R. Rakkiyappan, and J. H. Park, "Stability analysis of the differential genetic regulatory networks model with tim*E* – varying delays and Markovian jumping parameters," *Nonlinear analysis: Hybrid systems*, vol. 14, pp. 1–15, 2014.

[25] R. Rakkiyappan, G. Velmurugan, F. A. Rihan, and S. Lakshmanan, "Stability analysis of memristor-based complex-valued recurrent neural networks with time delays," *Complexity*, vol. 21, no. 4, pp. 14–39, 2016.

[26] S. Bhalekar and V. Daftardar-Gejji, "Antisynchronization of nonidentical fractional-order chaotic systems using active control," *International Journal of Differential Equations*, vol. 2011, no. 5, pp. 1–13, 2011.

[27] O. H. Mohammed and A. I. Khlaif, "Adomian decomposition method for solving delay differential equations of fractional order," *Structure*, vol. 12, no. 13, pp. 14-15, 2014.

[28] M. M. Khader and A. S. Hendy, "The approximate and exact solutions of the fractional-order delay differential equations using Legendre seudospectral method," *International Journal of Pure and Applied Mathematics*, vol. 74, no. 3, pp. 287–297, 2012.

[29] M.-Q. Xu and Y.-Z. Lin, "Simplified reproducing kernel method for fractional differential equations with delay," *Applied Mathematics Letters*, vol. 52, pp. 156–161, 2016.

[30] K. Engelborghs and D. Roose, "On stability of LMS methods and characteristic roots of delay differential equations," *SIAM Journal on Numerical Analysis*, vol. 40, no. 2, pp. 629–650, 2002.

[31] Z. Wang, "A numerical method for delayed fractional-order differential equations," *Journal of Applied Mathematics*, vol. 2013, Article ID 256071, 7 pages, 2013.

[32] B. P. Moghaddam, S. Yaghoobi, and J. T. Machado, "An extended predictor-corrector algorithm for variabl*E* – order fractional delay differential equations," *Journal of Computational and Nonlinear Dynamics*, vol. 11, no. 6, Article ID 61001, 2016.

[33] X. Chen and L. Wang, "The variational iteration method for solving a neutral functional-differential equation with proportional delays," *Computers & Mathematics with Applications*, vol. 59, no. 8, pp. 2696–2702, 2010.

[34] F. Shakeri and M. Dehghan, "Solution of delay differential equations via a homotopy perturbation method," *Mathematical and Computer Modelling*, vol. 48, no. 3-4, pp. 486–498, 2008.

[35] E. Sokhanvar and A. Askari-Hemmat, "A numerical method for solving delay-fractional differential and integro-differential equations," *Journal of Mahani Mathematical Research Center*, vol. 4, no. 1, pp. 11–24, 2017.

[36] W. Wang, Y. Zhang, and S. Li, "Stability of continuous Rung*E* – Kutta-type methods for nonlinear neutral delay-differential equations," *Applied Mathematical Modelling*, vol. 33, no. 8, pp. 3319–3329, 2009.

[37] P. Rahimkhani, Y. Ordokhani, and E. Babolian, "Numerical solution of fractional pantograph differential equations by using generalized fractional-order Bernoulli wavelet," *Journal of Computational and Applied Mathematics*, vol. 309, pp. 493–510, 2017.

[38] M. A. Iqbal, U. Saeed, and S. T. Mohyud-Din, "Modified Laguerre wavelets method for delay differential equations of fractional-order," *Egyptian Journal of Basic and Applied Sciences*, vol. 2, no. 1, pp. 50–54, 2015.

[39] I. Podlubny, *Fractional Differential Equations*, Academic Press, San Diego, CA, USA, 1999.

[40] M. Y. Hussaini, A. Quarteroni, and T. A. Zang, *Spectral Methods in Fluid Dynamic*, PrenticE – Hall, Englewood Cliffs, NJ, USA, 1988.

[41] A. A. Kilbas, H. M. Srivastava, and J. J. Trujillo, *Theory and Applications of Fractional Differential Equations*, Elsevier, San Diego, CA, USA, 2006.

[42] A. Kadem and D. Baleanu, "Analytical method based on Walsh function combined with orthogonal polynomial for fractional transport equation," *Communications in Nonlinear Science and Numerical Simulation*, vol. 15, no. 3, pp. 491–501, 2010.

[43] M. A. Snyder, *Chebyshev Methods in Numerical Approximation*, PrenticE – Hall, Englewood Cliffs, NJ, USA, 1966.

[44] M. M. Khader, "On the numerical solutions for the fractional diffusion equation," *Communications in Nonlinear Science and Numerical Simulation*, vol. 16, no. 6, pp. 2535–2542, 2011.

Hindawi
Complexity
Volume 2022, Article ID 5147951, 13 pages
https://doi.org/10.1155/2022/5147951

Research Article

Analysis of the Epidemic Biological Model of Tuberculosis (TB) via Numerical Schemes

S. Kanwal,[1] **M.K. Siddiqui**,[2] **E. Bonyah**,[3] **K. Sarwar**,[1] **T.S. Shaikh**,[1] **and N. Ahmed**[4]

[1]*Department of Mathematics, Lahore College for Women University, Lahore, Pakistan*
[2]*Department of Mathematics, COMSATS University Islamabad, Lahore Campus, Lahore, Pakistan*
[3]*Department of Mathematics Education, Akenten Appiah-Menka University of Skills Training and Entrepreneurial Development, Kumasi 00233, Ghana*
[4]*Department of Mathematics and Statics, University of Lahore, Lahore, Pakistan*

Correspondence should be addressed to E. Bonyah; ebonyah@aamusted.edu.gh

Received 8 January 2022; Revised 7 February 2022; Accepted 16 February 2022; Published 11 March 2022

Academic Editor: C. Rajivganthi

Tuberculosis (TB) is caused by bacillus *Mycobacterium tuberculosis* (MTB). In this study, a mathematical model of tuberculosis (TB) is analyzed. The numerical behaviour of the considered model is analyzed including basic reproduction number and stability. We applied three numerical techniques to this model, i.e., nonstandard finite difference (NSFD) scheme, Runge–Kutta method of order 4(RK-4), and forward Euler (FD) scheme. NSFD scheme preserves all the essential properties of the model. Acquired results corroborate that NSFD scheme converges for each step size. While the other two schemes failed to preserve some properties of the model such as positivity and convergence. A graphical comparison presented in this study confirms the numerical stability of the NSFD technique shown here is maintained over a large area.

1. Introduction

Tuberculosis (TB) is a chronic, bacterial infectious disease. TB is one of the oldest diseases. In 1882, Robert Koch discovered the tubercle bacillus and *Mycobacterium tuberculosis* which is the contributing agent of tuberculosis. It attacks the lungs and other organs of body as well. Tuberculosis is an airborne infection. When TB active individuals (infectious) cough, sneeze, speak, or spit, the tubercle bacilli spread in the air. When susceptible people inhale that air, they might become infected. The people who are regularly in contact with TB active are at higher risk. The bacillus mycobacterium sets up in lungs and transmits to other organs of the body if immune system of that individual is not strong enough to suppress it.

The people who are infected have 10 percent risk to be infectious (active TB). Most of the infected individuals stay latently infected (noninfectious) for whole life, and this latent period may be from months to centuries. However, this period may depend on the co-infectious diseases that individual contains. With co-infectious diseases immunity decrease, the risk of infected to be infectious increases. The presence of HIV enhances faster the risk towards the active TB stage.

According to world health organization (WHO) report 2019, about 10.0 million fell ill with tuberculosis in 2018 [1]. Globally, an estimated 1.2 million people expired due to tuberculosis among HIV negative and about 251,000 among HIV positive, in 2018. Pakistan reports about 518,000 new TB cases per year, and among 30 high burden countries, Pakistan ranks 6th [2]. Annually, an estimated 44,000 people expire due to tuberculosis, in Pakistan. Four lakh sixty two thousand nine hundred and twenty cases were reported in Khyber Pakhtunkhwa, province of Pakistan, in the duration from 2002 to 2017, according to NTP [3]. Newly registered case statics will be analyzed in this research work. Now, there is no direct way to discover if MTB has been removed or not. In this situation, mathematical models help us to estimate the future trend.

To discover the parameters for infectious diseases, mathematical models use all collected data and statics and execute mathematical operations on them. These parameters are used to investigate the effects of various control strategies. Mathematical modeling determines which controls should be implemented and which should not. Modeling also aids in predicting the spread or contraction of infectious diseases in the future. Scientific experts have developed a large number of mathematical models for many communicable diseases throughout history. For a wide range of infectious diseases and epidemics, precise mathematical models are developed and implemented. The system of differential equations is often used in mathematical models. Different approaches can be used to control different contagious diseases. Vaccination and other control methods, as well as treatment, are used to combat some infectious diseases. To address the models' flaws, several numerical techniques are employed, and results are derived. Simulations corroborate these findings.

Waaler et al. [4] contributed significantly in the epidemiology of tuberculosis. They separated the population into three classes and proposed a model according to the characteristics of tuberculosis communication. The system of nonlinear ordinary differential equation was studied and a model for tuberculosis was constructed [5]. Carlos Castillo-Chavez and Feng [6, 7] worked a lot in the field of tuberculosis epidemiology. They analyzed the dynamics of tuberculosis and presented different models for detailed observations and provided results. Castillo and Song (2004) [8] presented a thorough analysis of the work on tuberculosis dynamics. They gathered different dynamical models of tuberculosis and provided a theoretical structure.

Heesterbeek et al. [9] worked to explore the basic reproduction number and the estimated number of resulting cases generated by a typical primary infected individual during its period of infection. In [10], analysis of a SEIR model was presented for infectious disease which includes exponential normal birth and death rate and deaths due to disease, so the size of population might be changed with time. In 1994, Mickens suggested that numerical methods are the only way to find out exact solution of differential equations.

Anguelov and Lubuma [11] presented their contributions to the construction of the nonstandard finite difference method and its application. Garba et al. [12] considered the problem of creating qualitative consistent finite difference schemes; they approximate with the innovative continuous-time model. To accomplish their goal, they considered a deterministic continuous-time model for the dynamics of transmission for any disease, for the presence of deficient vaccine. The model was thoroughly analyzed to investigate the dynamic features of the model.

Gurski [13] presented a general construction of simple NSFD schemes for simple nonlinear systems and for construction used approximation techniques of standard differential equations, for example, predictor-corrector method and artificial viscosity. Memarbashi et al. [14] presented NSFD technique with the help of Mickens discretization scheme. Authors proved that the proposed NSFD scheme conserves the equilibrium points of the related continuous system. They analyzed the qualitative properties of the proposed system, and it preserves stability of equilibrium points, positivity as well as Neimark–Sacker bifurcations. The results proved the dynamical consistency of the considered discretized SEI epidemic model through the continuous system. Ahmed et al. considered an SEIQV model of saturated incidence rate and presented its numerical modeling. They developed a NSFD technique to solve the continuous model [15]. Authors analyzed the convergence of developed NSFD technique as well as showed the unconditional stability of the NSFD scheme. They compared the results of the proposed scheme to the RK-4 finite difference scheme. Comparison showed that RK-4 scheme produces nonphysical oscillations, fails to conserve the positivity property, and diverges even for small step size, as well as it converges to false stable position. Results were verified of the NSFD technique by simulations. Fatima et al. [16] presented the mathematical modeling of computer virus dynamics (SLBQRS). Ahmed et al. presented two operator splitting nonstandard finite difference schemes (NSFD) for the reaction diffusion SEIR epidemic model to solve numerically [17]. In 2019, Ahmed et al. proposed a Brusselator reaction diffusion model and checked the stability of the model by Neumann criteria of stability. They examined the solution by presenting finite difference scheme (FD), forward Euler explicit FD scheme, and semi-implicit Crank–Nicolson FD scheme [18].

Ahmed et al. considered a model of autocatalytic glycolysis and investigated the numerical solution. Unknown variables showed the concentration of chemical elements, so the considered model established the positive results in [19]. Authors presented three different numerical techniques: the nonstandard finite (NSFD) method, the Runge–Kutta method (RK-4) method, and the forward Euler (FD) finite difference method.

Kim et al., in 2018, presented a fitted model of tuberculosis to analyze the dynamics of TB transmission. They fitted data of Philippines and examined various control strategies such as hidden case discoveries, presence of case, active cases discoveries, and distancing. The analysis suggests that most favorable control strategies can reduce the number of infectious cases with minimum cost of implementation [20]. For tuberculosis (TB) transmission, authors presented a fractional-order delay differential model that includes the impacts of endogenous reactivation and external reinfections. All through the local stability of the steady states and bifurcation studies, they analyzed the qualitative characteristics of the model. The framework incorporates a discrete time delay to account for the time it takes to evaluate the ailment [21]. In [22], authors presented a stochastic epidemic model with time delays for COVID-19 dynamics (SIAQR). In the model, there is only one global favorable response with expecting value one. They derived a generalized stochastic threshold as a requirement of permanence and availability of an ergodic stationary population.

In [1], to solve a SIR epidemic model, the authors provided two nonstandard finite difference (NFSD)

approaches. The proposed approaches have key qualities including positivity and boundedness, as well as conservation law preservation. Numerical comparisons show that our method outperforms other existing standard methods including the second-order Runge–Kutta (RK2) method, the Euler method, and several readymade MATLAB scripts in terms of accuracy. In [2], authors constructed a nonstandard finite difference scheme to solve numerically a mathematical model for obesity population dynamics. Numerical comparisons between the proposed nonstandard numerical scheme and Euler's method reveal that the suggested nonstandard numerical scheme is more effective. The nonstandard difference scheme methodology is a suitable alternative for solving numerically varied mathematical models where important properties of the populations must be achieved in order to represent the real world, as demonstrated by numerical examples. The creation of an NSFD scheme that is compatible with the aspects of a continuous dynamic model, such as positivity and population conservation, is thus the novel aspect of this work. In contrast to the smaller regions of other common numerical approaches, all of the numerical simulations with varying parameter values imply that the NSFD scheme described here keeps numerical stability in wide areas.

In this work, the mathematical model of tuberculosis is numerically analyzed. Three numerical techniques, nonstandard finite difference (NFSD), forward Euler (FD), and Runge–Kutta of 4th-order (RK-4) schemes, are used to analyze the tuberculosis model. Numerical schemes analyze the mathematical presentation of proposed model resolution, permanency property, stability analysis, and threshold criteria. As a result, this study is divided into the following sections. We begin with a generalized tuberculosis model and description of the suggested model in Section 2. Followed by a mathematical analysis, we compute the basic reproduction number and demonstrate the solution's positivity, as well as the derivation of equilibrium points (DFE and EE) and equilibrium point stability, existence, and uniqueness in Section 3. Before discussing the results, some simulations are shown in Section 4. We constructed the different numerical schemes for the mathematical model of tuberculosis and provided the convergence analysis of the NSFD scheme for the proposed model. In Section 5, we present the graphical comparison of these numerical schemes. The last remarks bring this study article to a conclusion.

The goal of this research is to build and analyze numerical schemes whose equilibrium points correspond with the continuous system's equilibrium points while preserving all of the continuous system's key attributes. The motivation of this study is to create consistent positivity-preserving numerical algorithms for the continuous model of tuberculosis (TB).

2. Materials and Methods

In this section, we present the generalized mathematical model of tuberculosis and describe its parameters.

2.1. Mathematical Model. The mathematical model for tuberculosis (TB) is given by [23]. We have a system of equations (1)–(5):

$$\frac{dS}{dt} = \Delta - \frac{\theta SI}{N} - \omega S, \tag{1}$$

$$\frac{dL}{dt} = \frac{\theta SI}{N} - (\omega + \xi)L + (1 - \Psi)\varphi T, \tag{2}$$

$$\frac{dI}{dt} = \xi L + \Psi\varphi T - (\omega + \Upsilon + \psi_1)I, \tag{3}$$

$$\frac{dT}{dt} = \Upsilon I - (\omega + \varphi + \psi_2 + \chi)T, \tag{4}$$

$$\frac{dR}{dt} = \chi T - \omega R, \tag{5}$$

where all the coefficients are positive and $N(t) = S(t) + L(t) + I(t) + T(t) + R(t)$. Here, we have the variables.

$S(t)$: suceptible class

$L(t)$: exposed class

$I(t)$: infected class

$T(t)$: under treatment class

$R(t)$: recovered class

At time t, initially, we have

$$S(0) > 0, L(0) \geq 0, I(0) \geq 0, T(0) \geq 0, R(0) \geq 0. \tag{6}$$

2.2. Description of Parameters. The model parameters are estimated and described below:

Δ: the recruitment rate of susceptible population

ω: the coefficient of the natural death rate of all epidemiological human classes

θ: the coefficient of transmission of TB infection from susceptible to infected

ξ: the progression rate from L to I

Υ: the rate at which infected individuals are treated

φ: the rate at which treated individuals leave the class T

Ψ: the parameter of treatment failure

$(1 - \Psi)\varphi T$: when $\Psi = 0$, it means that all the infected class under treatment become latent, and when $\Psi = 1$, it means the treatment failure and treatment failure and treated class will remain as a latent class due to the remainder of *Mycobacterium tuberculosis* or infected class I due to the failure of treatment at the rate in the infected class φ

ψ_1: the disease mortality rate in the infected class I

ψ_2: mortality ratio of treated people

χ: the coefficient of recovery of treated individuals

3. Analysis of the Model

The present section contains the mathematical analysis of basic properties of the epidemic tuberculosis model: threshold quantity, equilibria, and stability.

3.1. Basic Reproduction Number. Basic reproduction number is of central importance and usually denoted by $\mathfrak{R}_0$. It represents the number of resulting infections affected by primary when main infectious individuals are presented to host inhabitants where every individual is susceptible. It is the threshold quantity that predicts whether the infection will expire or not in a population. If $\mathfrak{R}_o > 1$, then infection will remain in population, and if $\mathfrak{R}_0 < 1$, then infection will vanish from the population. We calculated the basic reproduction number using the next generation method. Let $x = (S, L, I, T, R)^\tau$; then, we can write the system of equations (1)–(5) as

$$\frac{dx}{dt} = F(x) - \nu(x), \tag{7}$$

where

$$F(x) = \begin{bmatrix} \dfrac{\theta SI}{N} \\ 0 \\ 0 \end{bmatrix}, \tag{8}$$

and

$$\nu(x) = \begin{bmatrix} d_1 L - (1-\Psi)\varphi T \\ d_2 I - \xi L - \Psi\varphi T \\ d_3 T - \Upsilon I \end{bmatrix}. \tag{9}$$

Here, $F(x)$ and $\nu(x)$ are the Jacobian matrices at DFE. Hence, we have

$$\mathfrak{R}_0 = \frac{\theta\xi d_3}{d_1 d_2 d_3 - d_1\Upsilon\Psi\varphi - (1-\Psi)\varphi\xi\Upsilon}. \tag{10}$$

This is the spectral radius of next generation matrix $(F\nu^{-1})$.

3.2. Existence of Equilibria. Equilibrium points of the considered epidemic model exist and are as follows.

Disease-free equilibrium: disease-free equilibrium is a state when disease dies out of the system $F^0 = (S^0, 0, 0, 0, 0)$, where $S^0 = \Delta/\omega$ is a number of susceptible at DFE.

Endemic equilibrium: endemic equilibrium is a state when the disease remains in the system $F_1 = (S^*, L^*, I^*, T^*, R^*)$, where

$$\begin{aligned}
S^* &= \frac{N^*}{\mathfrak{R}_0}, \\
L^* &= \frac{((\omega+\psi_1) + \Upsilon(\omega+\psi_2+\chi) + \Upsilon\varphi(1-\Psi))N^*(\mathfrak{R}_0 - 1)}{\mathfrak{R}_0[(\omega+\psi_1) + \Upsilon(\omega+\psi_2+\chi) + \Upsilon\varphi(1-\Psi) + \xi(\Upsilon+d_3)]}, \\
I^* &= \frac{\xi d_3 N^*(\mathfrak{R}_0 - 1)}{\mathfrak{R}_0[(\omega+\psi_1) + \Upsilon(\omega+\psi_2+\chi) + \Upsilon\varphi(1-\Psi) + \xi(\Upsilon+d_3)]}, \\
T^* &= \frac{\xi\Upsilon N^*(\mathfrak{R}_0 - 1)}{\mathfrak{R}_0[(\omega+\psi_1) + \Upsilon(\omega+\psi_2+\chi) + \Upsilon\varphi(1-\Psi) + \xi(\Upsilon+d_3)]}, \\
R^* &= \frac{\chi T^*}{\omega}.
\end{aligned} \tag{11}$$

There exist a unique endemic equilibrium, for $\mathfrak{R}_0 > 1$.

3.3. Stability of the Model

3.3.1. Local Stability at DFE. For disease-free equilibrium, $F^0 = (S^0, 0, 0, 0, 0)$, the following is the variational matrix of the system of equations (1)–(5):

$$Z = \begin{bmatrix} z_{11} & z_{12} & z_{13} & z_{14} & z_{15} \\ z_{21} & z_{22} & z_{23} & z_{24} & z_{25} \\ z_{31} & z_{32} & z_{33} & z_{34} & z_{35} \\ z_{41} & z_{42} & z_{43} & z_{44} & z_{45} \\ z_{51} & z_{52} & z_{53} & z_{54} & z_{55} \end{bmatrix}, \tag{12}$$

where

$$
\begin{aligned}
&z_{11} = -\omega, z_{12} = 0, z_{13} = -\theta, z_{14} = 0, z_{15} = 0,\\
&z_{21} = 0, z_{22} = -d_1, z_{23} = \theta, z_{24} = (1-\Psi)\varphi, z_{25} = 0,\\
&z_{31} = 0, z_{32} = \xi, z_{33} = -d_2, z_{34} = \Psi\varphi, z_{35} = 0,\\
&z_{41} = 0, z_{42} = 0, z_{43} = \Upsilon, z_{44} = -d_3, z_{45} = 0,\\
&z_{51} = 0, z_{52} = 0, z_{53} = 0, z_{54} = \chi, z_{55} = -\omega.
\end{aligned} \tag{13}
$$

Thus, we have

$$
Z = \begin{bmatrix}
-\omega & 0 & -\theta & 0 & 0\\
0 & -d_1 & \theta & (1-\Psi)\varphi & 0\\
0 & \xi & -d_2 & \Psi\varphi & 0\\
0 & 0 & \Upsilon & -d_3 & 0\\
0 & 0 & 0 & \chi & -\omega
\end{bmatrix}. \tag{14}
$$

By finding the eigenvalues of the Jacobian matrix, disease-free equilibrium is locally asymptotically stable, for $\mathfrak{R}_0 < 1$. When $\mathfrak{R}_0 > 1$, the system becomes unstable at S^0.

3.3.2. Local Stability at EE.

$$
E = \begin{bmatrix}
-\frac{\theta I^*}{N^*} - \omega & 0 & -\frac{\theta S^*}{N^*} & 0 & 0\\
\frac{\theta I^*}{N^*} & -d_1 & \frac{\theta S^*}{N^*} & (1-\Psi)\varphi & 0\\
0 & \xi & -d_2 & \Psi\varphi & 0\\
0 & 0 & \Upsilon & -d_3 & 0\\
0 & 0 & 0 & \chi & -\omega
\end{bmatrix}. \tag{15}
$$

We have the characteristic equation of the Jacobian matrix of the form

$$
\lambda^4 + \lambda^3 c_1 + \lambda^2 c_2 + \lambda c_3 + c_4 = 0, \tag{16}
$$

where

$$
\begin{aligned}
c_1 &= \frac{\theta I^*}{N^*} + \omega + d_1 + d_2 + d_3,\\
c_2 &= \frac{\theta I^*}{N^*}(d_1 + d_2 + d_3) + \omega(d_1 + d_2 + d_3) + d_1 d_2 + d_2 d_3 + d_1 d_3 - \Upsilon\Psi\varphi - \frac{\theta S^*}{N^*}\xi,\\
c_3 &= \frac{\theta I^*}{N^*}(d_1 d_2 + d_2 d_3 + (d_1 d_3) + \omega(d_1 d_2 + d_2 d_3 + d_1 d_3) + d_1 d_2 d_3 - \frac{\theta I^*}{N^*}\Upsilon\Psi\varphi - \omega\Upsilon\Psi\varphi + \omega\frac{\theta S^*}{N^*}\\
&\quad \cdot \xi - d_1\Upsilon\Psi\varphi + \frac{\theta S^*}{N^*}\xi d_3 + (1-\Psi)\varphi\xi\Upsilon,\\
c_4 &= \frac{\theta I^*}{N^*} d_1 d_2 d_3 + \omega d_1 d_2 d_3 - \frac{\theta I^*}{N^*} d_1\Upsilon\Psi\varphi + \frac{\theta I^*}{N^*}(1-\Psi)\varphi\xi\Upsilon - \omega d_1\Upsilon\Psi\varphi + \omega\frac{\theta S^*}{N^*}\xi k^3 + (1-\Psi)\omega\varphi\xi\Upsilon.
\end{aligned} \tag{17}
$$

According to Routh–Hurwitz criteria, all the eigenvalues of the characteristic polynomial are negative and conditions are satisfied, i.e, $c_i > 0$, for $i = 1, 2, 3, 4$ and $c_1 c_2 c_3 > c_3^2 + c_1^2 c_4$. Endemic equilibrium (EE) of the system of equations (1)–(5) is locally asymptotically stable for $\mathfrak{R}_0 > 1$.

4. Numerical Schemes

In this section, three numerical schemes are developed according to systems (1)–(5), i.e., NSFD scheme, RK-4, and forward Euler (FD) scheme. NSFD scheme is used to solve systems (1)–(5) numerically and results will be compared with the other two schemes.

4.1. Runge–Kutta (RK-4) Scheme of Fourth Order. RK-4 is developed for the system of equations (1)–(5) as follows:

Step 1:

$$
\begin{aligned}
u_1 &= h\left[-\frac{\theta S^n I^n}{N} - \omega S^n\right],\\
v_1 &= h\left[\frac{\theta S^n I^n}{N} - (\omega + \xi)L^n + (1-\Psi)\varphi T^n\right],\\
w_1 &= h[\xi L^n + \Psi\varphi T^n - (\omega + \Upsilon + \psi_1)I^n],\\
x_1 &= h[\Upsilon I^n - (\omega + \varphi + \psi_2 + \chi)T^n],\\
y_1 &= h[\chi T^n - \omega R^n].
\end{aligned} \tag{18}
$$

Step 2:

$$u_2 = h\left[-\frac{\theta}{N}\left(S^n + \frac{u_1}{2}\right)\left(I^n + \frac{w_1}{2}\right) - \omega\left(S^n + \frac{u_1}{2}\right)\right],$$

$$v_2 = h\left[\frac{\theta}{N}\left(S^n + \frac{u_1}{2}\right)\left(I^n + \frac{w_1}{2}\right) - (\omega + \xi)\left(L^n + \frac{v_1}{2}\right) + (1 - \Psi)\varphi\left(T^n + \frac{x_1}{2}\right)\right],$$

$$w_2 = h\left[\xi\left(L^n + \frac{v_1}{2}\right) + \Psi\varphi\left(T^n + \frac{x_1}{2}\right) - (\omega + \Upsilon + \psi_1)\left(I^n + \frac{w_1}{2}\right)\right],$$

$$x_2 = h\left[\Upsilon\left(I^n + \frac{w_1}{2}\right) - (\omega + \varphi + \psi_2 + \chi)\left(T^n + \frac{x_1}{2}\right)\right],$$

$$y_2 = h\left[\chi\left(T^n + \frac{x_1}{2}\right) - \omega\left(R^n + \frac{y_1}{2}\right)\right]. \tag{19}$$

Step 3:

$$u_3 = h\left[-\frac{\theta}{N}\left(S^n + \frac{d_2}{2}\right)\left(I^n + \frac{w_2}{2}\right) - \omega\left(S^n + \frac{u_2}{2}\right)\right],$$

$$v_3 = h\left[\frac{\theta}{N}\left(S^n + \frac{u_2}{2}\right)\left(I^n + \frac{w_2}{2}\right) - (\omega + \xi)\left(L^n + \frac{v_2}{2}\right) + (1 - \Psi)\varphi\left(T^n + \frac{x_2}{2}\right)\right],$$

$$w_3 = h\left[\xi\left(L^n + \frac{v_2}{2}\right) + \Psi\varphi\left(T^n + \frac{x_2}{2}\right) - (\omega + \Upsilon + \psi_2)\left(I^n + \frac{w_2}{2}\right)\right],$$

$$x_3 = h\left[\Upsilon\left(I^n + \frac{w_2}{2}\right) - (\omega + \varphi + \psi_2 + \chi)\left(T^n + \frac{x_2}{2}\right)\right],$$

$$y_3 = h\left[\chi\left(T^n + \frac{x_2}{2}\right) - \omega\left(R^n + \frac{y_2}{2}\right)\right]. \tag{20}$$

Step 4:

$$u_4 = h\left[-\frac{\theta}{N}\left(S^n + \frac{u_3}{2}\right)\left(I^n + \frac{w_3}{2}\right) - \omega\left(S^n + \frac{u_3}{2}\right)\right],$$

$$v_4 = h\left[\frac{\theta}{N}\left(S^n + \frac{u_3}{2}\right)\left(I^n + \frac{w_3}{2}\right) - (\omega + \xi)\left(L^n + \frac{v_3}{2}\right) + (1 - \Psi)\varphi\left(T^n + \frac{x_3}{2}\right)\right],$$

$$w_4 = h\left[\xi\left(L^n + \frac{v_3}{2}\right) + \Psi\varphi\left(T^n + \frac{x_3}{2}\right) - (\omega + \Upsilon + \psi_3)\left(I^n + \frac{w_3}{2}\right)\right],$$

$$x_4 = h\left[\Upsilon\left(I^n + \frac{w_3}{2}\right) - (\omega + \varphi + \psi_3 + \chi)\left(T^n + \frac{x_3}{2}\right)\right],$$

$$y_4 = h\left[\chi\left(U^n + \frac{x_3}{2}\right) - \omega\left(R^n + \frac{y_3}{2}\right)\right]. \tag{21}$$

Step 5:

Table 1: Disease-free equilibrium, $R_0 < 1$.

Δ	450,862.200 862 6
θ	0.243 3
χ	0.396 8
Υ	0.287 3
ω	0.014 78
ψ_1	0.220 2
ψ_2	0.055 0
φ	1.199 6
Ψ	0.150 0
ξ	0.200 7

Table 2: Endemic equilibrium, $R_0 > 1$.

Δ	450,862.200 862 6
θ	0.543 3
χ	0.396 8
Υ	0.287 3
ω	0.014 78
ψ_1	0.220 2
ψ_2	0.055 0
φ	1.199 6
Ψ	0.150 0
ξ	0.200 7

$$S^{n+1} = S^n + \frac{1}{6}\left[u_1 + 2u_2 + 2u_3 + u_4\right],$$

$$L^{n+1} = L^n + \frac{1}{6}\left[v_1 + 2v_2 + 2v_3 + v_4\right],$$

$$I^{n+1} = I^n + \frac{1}{6}\left[w_1 + 2w_2 + 2w_3 + w_4\right], \tag{22}$$

$$T^{n+1} = T^n + \frac{1}{6}\left[x_1 + 2x_2 + 2x_3 + x_4\right],$$

$$R^{n+1} = R^n + \frac{1}{6}\left[y_1 + 2y_2 + 2y_3 + y_4\right].$$

4.2. Forward Euler (FD) Scheme. Forward Euler finite difference scheme developed for system of equations (1)–(5) is as follows:

$$S^{n+1} = S^n + h\left[-\frac{\theta S^n I^n}{N} - \omega S^n\right],$$

$$L^{n+1} = L^n + h\left[\frac{\theta S^n I^n}{N} - (\omega + \xi)L^n + (1 - \Psi)\varphi T^n\right],$$

$$I^{n+1} = I^n + h\left[\xi L^n + \Psi\varphi T^n - (\omega + \Upsilon + \psi_1)I^n\right], \tag{23}$$

$$T^{n+1} = T^n + h\left[\Upsilon I^n - (\omega + \varphi + \psi_2 + \chi)T^n\right],$$

$$R^{n+1} = R^n + h\left[\chi T^n - \omega R^n\right].$$

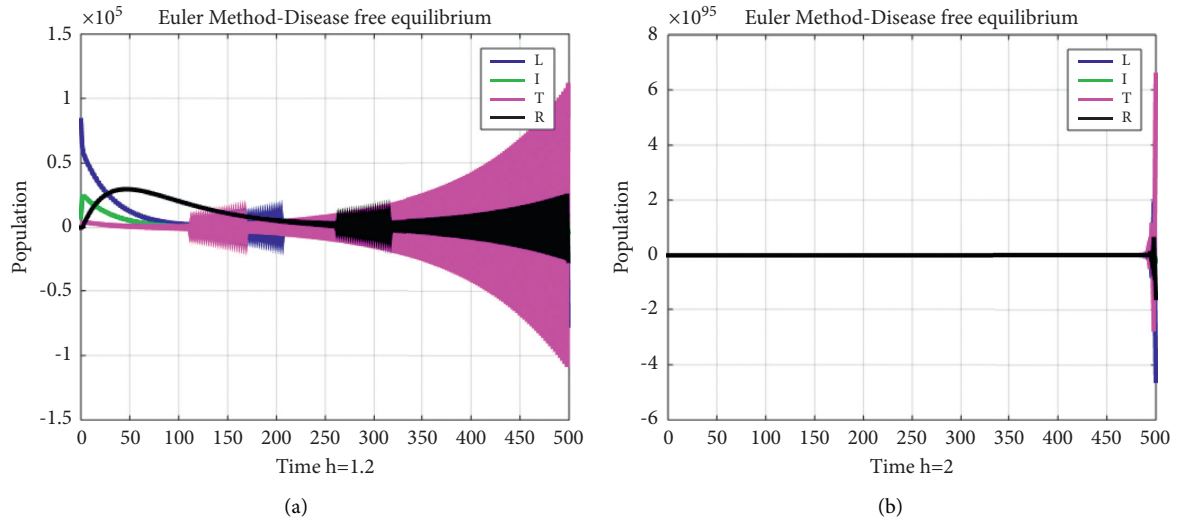

Figure 1: Simulations of forward Euler at disease-free equilibrium for step size $h = 1.2$ and $h = 2$. (a) Simulations of forward Euler. (b) Simulations of forward Euler.

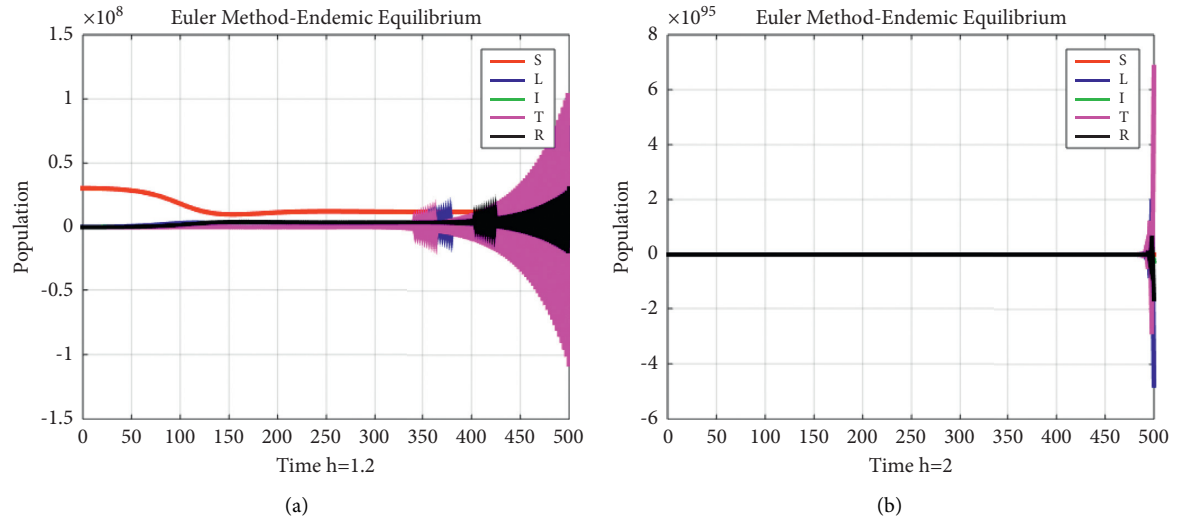

Figure 2: Simulations of forward Euler at endemic equilibrium for step size $h = 1.2$ and $h = 2$ (a) Simulations of forward Euler. (b) Simulations of forward Euler.

4.3. Nonstandard Finite Difference Scheme. Nonstandard finite difference scheme was proposed by Mickens in 1989. NFSD scheme maintains dynamic consistency as well as numerical stability in terms of initial restriction with irregular step length. The system of equations (1)–(5) is developed according to the laws given by Mickens:

$$\begin{aligned}
\frac{S^{n+1}-S^n}{h} &= -\frac{\theta S^{n+1}I^n}{N} - \omega S^{n+1},\\
S^{n+1} &= S^n + h - h\frac{\theta S^{n+1}I^n}{N} - h\omega S^{n+1},\\
S^{n+1}\left(1 + h\frac{\theta I^n}{N} + h\omega\right) &= S^n + h,\\
S^{n+1} &= \frac{S^n + h}{1 + h\theta I^n/N + h\omega}.
\end{aligned} \tag{24}$$

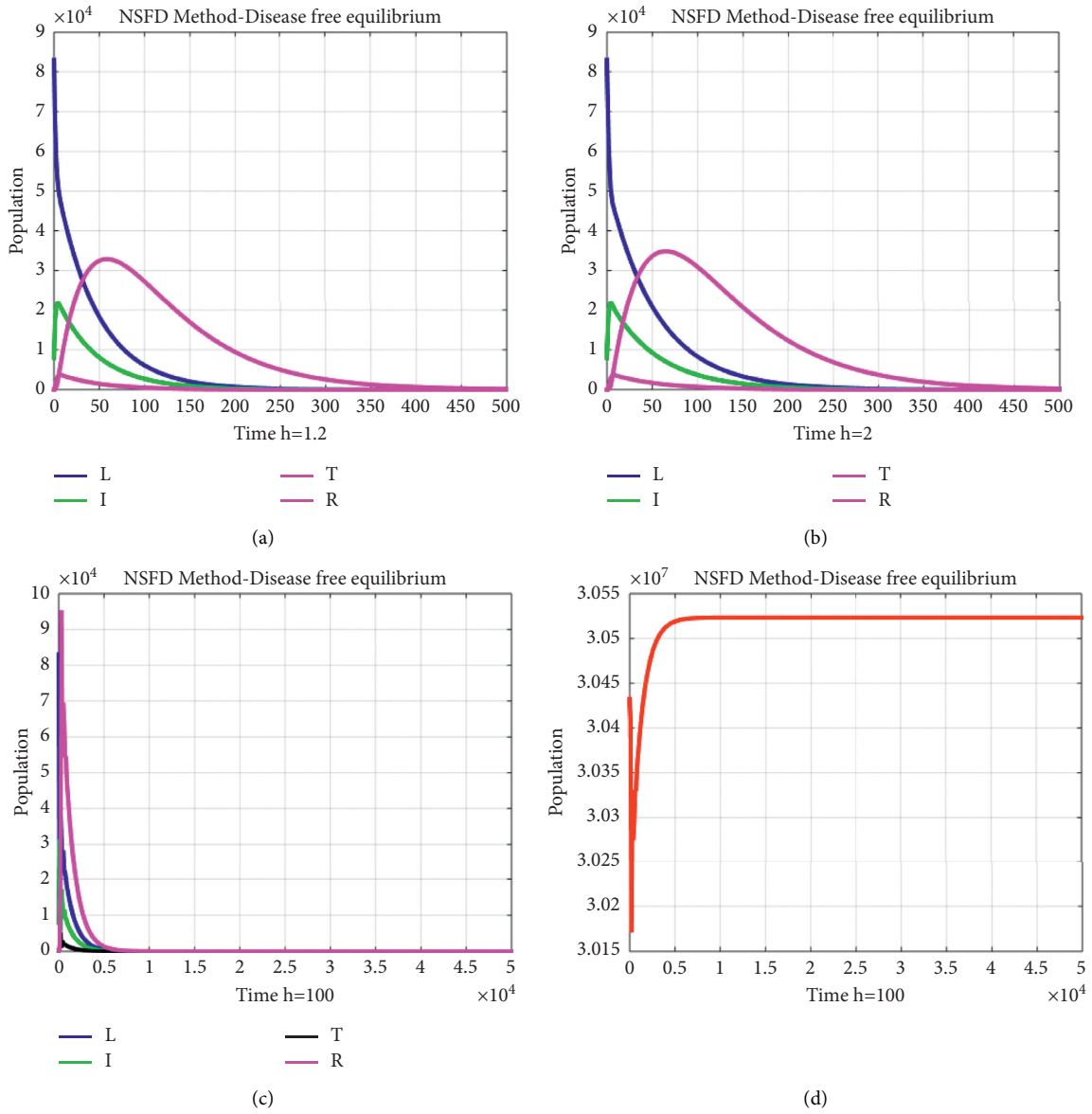

FIGURE 3: Simulations of forward Euler at endemic equilibrium for step size $h = 1.2$ and $h = 2$. (a) Simulations of NSFD. (b) Simulations of NSFD. (c) Simulations of NSFD. (d) Simulations of NSFD.

Similarly, we have

$$L^{n+1} = \frac{L^n + h\theta S^n I^n/N + h(1-\Psi)\varphi T^n}{1 + h(\omega + \xi)},$$

$$I^{n+1} = \frac{I^n + h\xi L^n + h\Psi\varphi U^n}{(1 + h(\omega + \Upsilon + \psi_1)},$$

$$T^{n+1} = \frac{T^n + h\Upsilon I^n}{1 + h(\omega + \varphi + \psi_2 + \chi)}, \tag{25}$$

$$R^{n+1} = \frac{R^n + h\chi T^n}{1 + h\omega}.$$

See more details in Tables 1 and 2.

4.4. Convergence Analysis of NSFD Scheme. Nonstandard finite difference scheme (NSFD) converges unconditionally at disease-free equilibrium (DFE) and endemic equilibrium (EE), see Appendix.

4.5. Positivity of NSFD Scheme. We have assumed that all the initial conditions are nonnegative. *i.e.*,

$$S(0) \geq 0, L(0) \geq 0, I(0) \geq 0, T(0) \geq 0, R(0) \geq 0. \tag{26}$$

These variables have approximate values which also are nonnegative due to the following supposition: $S^n \geq 0, L^n \geq 0, I^n \geq 0, T^n \geq 0,$ and $R^n \geq 0$.

Solution of NSFD scheme's formulas suggests the positivity of NSFD scheme, *i.e.*, $S^{n+1} \geq 0, L^{n+1} \geq 0, I^{n+1} \geq 0, T^{n+1} \geq 0,$ and $R^{n+1} \geq 0$.

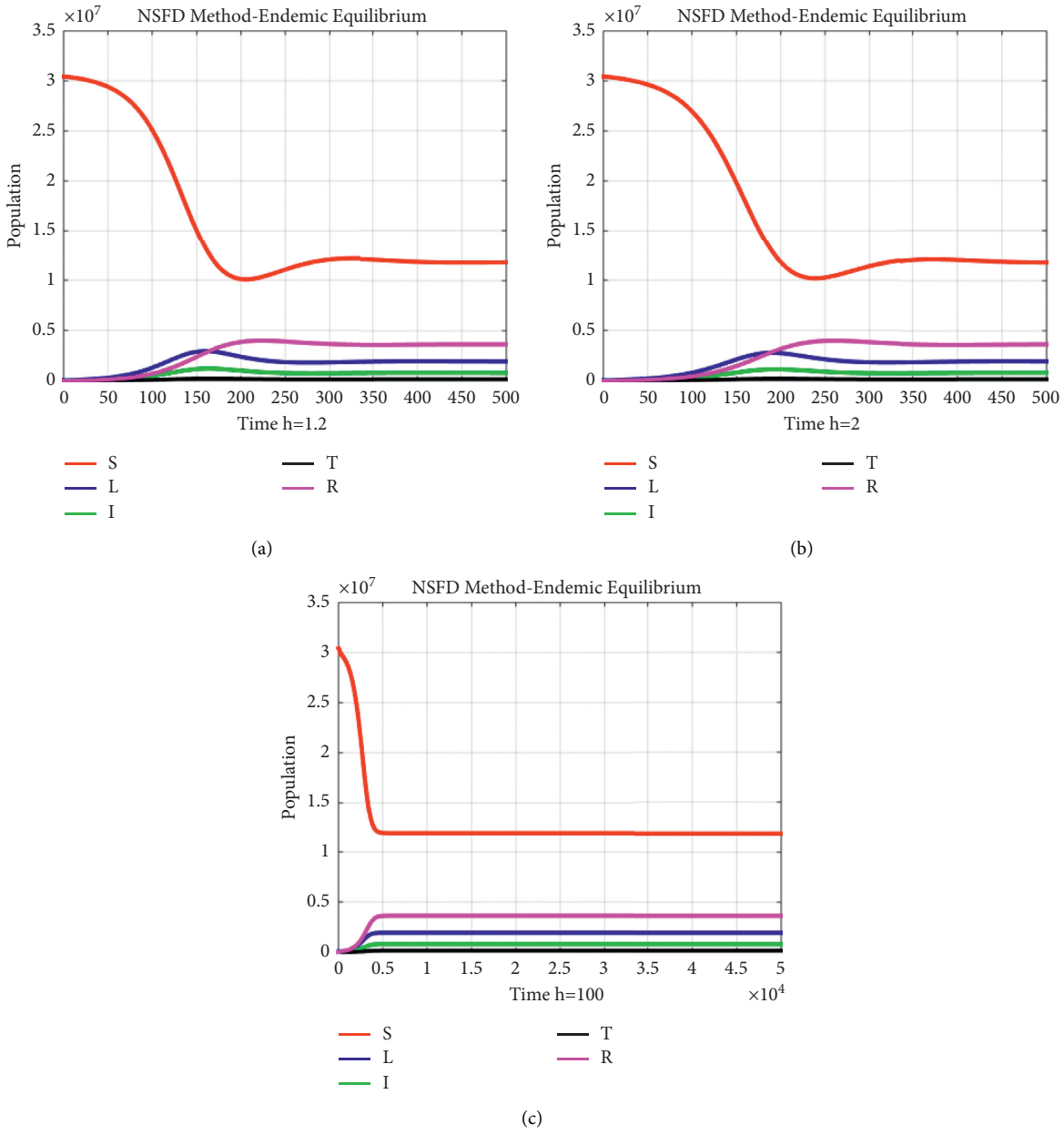

FIGURE 4: Simulations of forward Euler at endemic equilibrium for $h = 1.2$, $h = 2$, and $h = 100$. (a) Simulations of NSFD. (b) Simulations of NSFD (c) Simulations of NSFD.

5. Graphical Comparison of the Epidemic Model Using Numerical Methods

The graphical comparison of the epidemic model using numerical methods is shown in Figures 1–4.

Figures 1(a) and 1(b) show L (exposed), I (TB active), T (under treatment), and R (recovered) population using the Euler method at disease-free equilibrium for step size $h = 1.2$ and $h = 2$, respectively. Figures 1(a) and 1(b) show the behaviour of state variables obtained from forward Euler's method at disease-free equilibrium. It is shown in Figure 1(a) that the forward Euler's method gives the negative behaviour which is always meaningless in the population dynamics model. Also, by changing the step size in Figure 1(b), the forward Euler's scheme gives the divergence behaviour.

Similarly, Figures 2(a) and 2(b) depict the unusual behaviour of the state variables evaluated from forward Euler's method at endemic equilibrium point. On the same step sizes, Figures 2(a) and 2(b) give the negativity and divergence, respectively.

Figures 2(a) and 2(b) show L (exposed), I (TB active), T (under treatment), and R (recovered) population using the Euler Method at endemic equilibrium for step size $h = 1.2$ and $h = 2$, respectively.

Figures 3(a)–3(d) represent all population for the NSFD scheme for disease-free equilibrium. The NSFD method

converges at different step sizes $h = 1.2$, $h = 2$, and $h = 100$, respectively.

Figures 4(a)–4(c) represent the NSFD scheme for all population at endemic equilibrium. The NFSD scheme converges for even for large step sizes here the graphical representation for $h = 1.2$, $h = 2$, and $h = 100$ respectively.

6. Conclusion

This study is based on the numerical study of the epidemic model of tuberculosis (TB). Basic reproduction number and stability analysis for disease-free equilibrium and endemic equilibrium points are evaluated. Three numerical schemes are applied to this model. The nonstandard finite difference (NSFD) scheme is being used to find out the numerical solution of the model. The NSFD scheme preserves essential properties, e.g., positivity, unconditional convergence, and stability. Here, we analyzed the convergence of nonstandard finite difference scheme. Results prove the unconditional convergence of the NSFD scheme of the epidemic model of tuberculosis. Results of forward Euler (FD) and Runge–Kutta (RK-4) are presented and compared. The NSFD scheme converges unconditionally for each step size, while forward Euler (FD) and Runge–Kutta (RK-4) fail to converge even at small step size h. Results are presented graphically and confirm the numerical stability of the NSFD technique shown here which is maintained over a large area, and a comparison is presented here. [24].

Appendix

To examine the convergence of the nonstandard finite difference scheme (NSFD), let us suppose that

$$\begin{aligned} G &= \frac{S+h}{1+h\theta I/N+h\omega}, \\ H &= \frac{L+h\theta SI/N+h(1-\Psi)\varphi T}{1+h(\omega+\xi)}, \\ Q &= \frac{I+h\xi L+h\Psi\varphi T}{1+h(\omega+\Upsilon+\psi_1)}, \\ M &= \frac{T+h\Upsilon I}{1+h(\omega+\varphi+\psi_2+\chi)}, \\ O &= \frac{R+h\chi T}{1+h\omega}. \end{aligned} \tag{A.1}$$

Now,

$$\begin{aligned} G &= \frac{S+h}{1+h\theta I/N+h\omega}, \\ \frac{\partial G}{\partial S} &= \frac{1}{1+h\theta I/N+h\omega}, \\ \frac{\partial G}{\partial L} &= 0, \\ \frac{\partial G}{\partial I} &= -\frac{(S+h)(h\theta/N)}{(1+h\theta I/N+h\omega)^2}, \\ \frac{\partial G}{\partial T} &= 0, \\ \frac{\partial G}{\partial R} &= 0, \end{aligned} \tag{A.2}$$

$$\begin{aligned} H &= \frac{L+h\theta SI/N+h(1-\Psi)\varphi T}{1+h(\omega+\xi)}, \\ \frac{\partial H}{\partial S} &= \frac{h\theta I/N}{1+h(\omega+\xi)}, \\ \frac{\partial H}{\partial L} &= \frac{1}{1+h(\omega+\xi)}, \\ \frac{\partial H}{\partial I} &= \frac{h\theta S/N}{1+h(\omega+\xi)}, \\ \frac{\partial H}{\partial T} &= \frac{h(1-\Psi)\varphi}{1+h(\omega+\xi)}, \\ \frac{\partial H}{\partial R} &= 0, \end{aligned} \tag{A.3}$$

$$\begin{aligned} Q &= \frac{I+h\xi L+h\Psi\varphi T}{1+h(\omega+\Upsilon+\psi_1)}, \\ \frac{\partial Q}{\partial S} &= 0, \\ \frac{\partial Q}{\partial L} &= \frac{h\xi}{1+h(\omega+\Upsilon+\psi_1)}, \\ \frac{\partial Q}{\partial I} &= \frac{1}{1+h(\omega+\Upsilon+\psi_1)}, \\ \frac{\partial Q}{\partial T} &= \frac{h\Psi\varphi}{1+h(\omega+\Upsilon+\psi_1)}, \\ \frac{\partial Q}{\partial R} &= 0, \end{aligned} \tag{A.4}$$

$$
\begin{aligned}
M &= \frac{U + h\Upsilon I}{1 + h(\omega + \varphi + \psi_2 + \chi)},\\
\frac{\partial M}{\partial S} &= 0,\\
\frac{\partial M}{\partial L} &= 0,\\
\frac{\partial M}{\partial I} &= \frac{h\Upsilon}{1 + h(\omega + \varphi + \psi_2 + \chi)},\\
\frac{\partial M}{\partial T} &= \frac{1}{1 + h(\omega + \varphi + \psi_2 + \chi)},\\
\frac{\partial M}{\partial R} &= 0.
\end{aligned}
\tag{A.5}
$$

Similarly,

$$
\begin{aligned}
O &= \frac{R + h\chi U}{1 + h\omega},\\
\frac{\partial O}{\partial S} &= 0,\\
\frac{\partial O}{\partial L} &= 0,\\
\frac{\partial O}{\partial I} &= 0,\\
\frac{\partial O}{\partial T} &= \frac{h\chi}{1 + h\omega},\\
\frac{\partial O}{\partial R} &= \frac{1}{1 + h\omega}.
\end{aligned}
\tag{A.6}
$$

Now, we have the Jacobian matrix:

$$
J = \begin{bmatrix}
\frac{\partial G}{\partial S} & \frac{\partial G}{\partial L} & \frac{\partial G}{\partial I} & \frac{\partial G}{\partial T} & \frac{\partial G}{\partial R}\\
\frac{\partial H}{\partial S} & \frac{\partial H}{\partial L} & \frac{\partial H}{\partial I} & \frac{\partial H}{\partial T} & \frac{\partial H}{\partial R}\\
\frac{\partial Q}{\partial S} & \frac{\partial Q}{\partial L} & \frac{\partial Q}{\partial I} & \frac{\partial Q}{\partial T} & \frac{\partial Q}{\partial R}\\
\frac{\partial M}{\partial S} & \frac{\partial M}{\partial L} & \frac{\partial M}{\partial I} & \frac{\partial M}{\partial T} & \frac{\partial M}{\partial R}\\
\frac{\partial O}{\partial S} & \frac{\partial O}{\partial L} & \frac{\partial O}{\partial I} & \frac{\partial O}{\partial T} & \frac{\partial O}{\partial R}
\end{bmatrix}.
\tag{A.7}
$$

For endemic equilibrium points $F_1 = (S^*, L^*, I^*, T^*, R^*)$,

$$
J^*(F_1) = \begin{bmatrix}
\frac{1}{1 + h\theta I^*/N^* + h\omega} & 0 & -\frac{(S^* + h)(h\theta/N^*)}{(1 + h\theta I^*/N^* + h\omega)^2} & 0 & 0\\
\frac{h\theta I^*/N^*}{1 + h(\omega + \xi)} & \frac{1}{1 + h(\omega + \xi)} & \frac{h\theta S^*/N^*}{1 + h(\omega + \xi)} & \frac{h(1 - \Psi)\varphi}{1 + h(\omega + \xi)} & 0\\
0 & \frac{h\xi}{1 + h(\omega + \Upsilon + \psi_1)} & \frac{1}{1 + h(\omega + \Upsilon + \psi_1)} & \frac{h\Psi\varphi}{1 + h(\omega + \Upsilon + \psi_1)} & 0\\
0 & 0 & \frac{h\Upsilon}{1 + h(\omega + \varphi + \psi_2 + \chi)} & \frac{1}{1 + h(\omega + \varphi + \psi_2 + \chi)} & 0\\
0 & 0 & 0 & \frac{h\chi}{1 + h\omega} & \frac{1}{1 + h\omega}
\end{bmatrix}.
\tag{A.8}
$$

The eigenvalues of the Jacobian matrix for endemic equilibrium can be evaluated. Here, we have

$$
\lambda_1 = \frac{1}{1 + h\omega}.
\tag{A.9}
$$

The remaining matrix is as follows:

$$\begin{vmatrix} \frac{1}{1+h\theta I^*/N^*+h\omega}-\lambda & 0 & -\frac{(S^*+h)(h\theta/N^*)}{(1+h\theta I^*/N^*+h\omega)^2} & 0 \\ \frac{h\theta I^*/N^*}{1+h(\omega+\xi)} & \frac{1}{1+h(\omega+\xi)}-\lambda & \frac{h\theta S^*/N^*}{1+h(\omega+\xi)} & \frac{h(1-\Psi)\varphi}{1+h(\omega+\xi)} \\ 0 & \frac{h\xi}{1+h(\omega+\Upsilon+\psi_1)} & \frac{1}{1+h(\omega+\Upsilon+\psi_1)}-\lambda & \frac{h\Psi\varphi}{1+h(\omega+\Upsilon+\psi_1)} \\ 0 & 0 & \frac{h\Upsilon}{1+h(\omega+\varphi+\psi_2+\chi)} & \frac{1}{1+h(\omega+\varphi+\psi_2+\chi)}-\lambda \end{vmatrix}. \tag{A.10}$$

It is clear from the matrix that all the eigenvalues are less than one, which shows the convergence of the NSFD scheme at endemic equilibrium for each step size h.

Now, for disease-free equilibrium $F^0 = (S^0, 0, 0, 0, 0)$, we have

$$J(F_0) = \begin{bmatrix} \frac{1}{1+h\omega} & 0 & -\frac{(S^0+h)(h\theta/S^0)}{(1+h\omega)^2} & 0 & 0 \\ 0 & \frac{1}{1+h(\omega+\xi)} & \frac{h\theta}{1+h(\omega+\xi)} & \frac{h(1-\Psi)\varphi}{1+h(\omega+\xi)} & 0 \\ 0 & \frac{h\xi}{1+h(\omega+\Upsilon+\psi_1)} & \frac{1}{1+h(\omega+\Upsilon+\psi_1)} & \frac{h\Psi\varphi}{1+h(\omega+\Upsilon+\psi_1)} & 0 \\ 0 & 0 & \frac{h\Upsilon}{1+h(\omega+\varphi+\psi_2+\chi)} & \frac{1}{1+h(\omega+\varphi+\psi_2+\chi)} & 0 \\ 0 & 0 & 0 & \frac{h\chi}{1+h\omega} & \frac{1}{1+h\omega} \end{bmatrix}. \tag{A.11}$$

We can find out the eigenvalues from this matrix. Here, we have

$$\begin{aligned} \lambda_1 &= \frac{1}{1+h\omega}, \\ \lambda_2 &= \frac{1}{1+h\omega}, \end{aligned} \tag{A.12}$$

which are < 1. And, the remaining matrix we have is

$$\begin{vmatrix} \frac{1}{1+h(\omega+\xi)}-\lambda & \frac{h\theta}{1+h(\omega+\xi)} & \frac{h(1-\Psi)\varphi}{1+h(\omega+\xi)} \\ \frac{h\xi}{1+h(\omega+\Upsilon+\psi_1)} & \frac{1}{1+h(\omega+\Upsilon+\psi_1)}-\lambda & \frac{h\Psi\varphi}{1+h(\omega+\Upsilon+\psi_1)} \\ 0 & \frac{h\Upsilon}{1+h(\omega+\varphi+\psi_2+\chi)} & \frac{1}{1+h(\omega+\varphi+\psi_2+\chi)}-\lambda \end{vmatrix}. \tag{A.13}$$

Data Availability

The data used to support the findings of this study are cited at relevant places within the article as references.

Conflicts of Interest

The authors declare that they have no conflicts of interest.

Authors' Contributions

This work was equally contributed by all authors.

References

[1] WHO, "Global tuberculosis report," 2019, https://www.who.int/tb/country/data/profiles/en/.

[2] Pakistan Bureau of Statistics, "Pakistan's 6th census: population of major cities census," 2017, http://www.pbscensus.gov.pk/.

[3] National Institute of Health, "National tuberculosis Pakistan," 2021, http://www.ntp.gov.pk/webdatabase.php.

[4] H. Waaler, A. Geser, and S. Andersen, "The use of mathematical models in the study of the epidemiology of tuberculosis," *American Journal of Public Health and the Nation's Health*, vol. 52, no. 6, pp. 1002–1013, 1962.

[5] C. S. Revelle, W. R. Lynn, and F. Feldmann, "Mathematical models for the economic allocation of tuberculosis control activities in developing nations," *American Review of Respiratory Disease*, vol. 96, no. 5, pp. 893–909, 1967.

[6] C. Castillo-Chavez and Z. Feng, "To treat or not to treat: the case of tuberculosis," *Journal of Mathematical Biology*, vol. 35, no. 6, pp. 629–656, 1997.

[7] C. Castillo-Chavez and Z. Feng, *Mathematical Models for the Disease Dynamics of Tuberculosis*, 1996.

[8] C. Castillo-Chavez, B. Song, and B. Song, "Dynamical models of tuberculosis and their applications," *Mathematical Biosciences and Engineering*, vol. 1, no. 2, pp. 361–404, 2004.

[9] J. A. P. Heesterbeek, "On the definition and the computation of the basic reproduction ratio Ro in models for infectious diseases in heterogeneous populations," *Journal of Mathematical Biology*, vol. 28, pp. 365–382, 1990.

[10] M. Y. Li, J. R. Graef, L. Wang, and J. Karsai, "Global dynamics of a SEIR model with varying total population size," *Mathematical Biosciences*, vol. 160, no. 2, pp. 191–213, 1999.

[11] R. Anguelov and J. M.-S. Lubuma, "Contributions to the mathematics of the nonstandard finite difference method and applications," *Numerical Methods for Partial Differential Equations*, vol. 17, no. 5, pp. 518–543, 2001.

[12] S. M. Garba, A. B. Gumel, and J. S. Lubuma, "Dynamically-consistent non-standard finite difference method for an epidemic model," *Mathematical and Computer Modelling*, vol. 53, no. 1-2, pp. 131–150, 2011.

[13] K. F. Gurski, "A simple construction of nonstandard finite-difference schemes for small nonlinear systems applied to SIR models," *Computers & Mathematics with Applications*, vol. 66, no. 11, pp. 2165–2177, 2013.

[14] R. Memarbashi, F. Alipour, and A. Ghasemabadi, "A non-standard finite difference scheme for a SEI epidemic model," *Punjab University Journal of Mathematics*, vol. 49, no. 3, pp. 133–147, 2017.

[15] N. Ahmed, N. Shahid, Z. Iqbal et al., "Numerical modeling of SEIQV epidemic model with saturated incidence rate," *J. Appl. Environ. Biol. Sci.*vol. 8, no. 4, pp. 67–82, 2018.

[16] U. Fatima, M. Ali, N. Ahmed, and M. Rafiq, "Numerical modeling of susceptible latent breaking-out quarantine computer virus epidemic dynamics," *Heliyon*, vol. 4, no. 5, p. e00631, 2018.

[17] N. Ahmed, T. S.S., M. Rafiq, M. A. Rehman, M. Ali, and M. O. Ahmad, "Positivity preserving operator splitting nonstandard finite difference methods for SEIR reaction diffusion model," *Open Mathematics*, vol. 17, no. 1, pp. 313–330, 2019.

[18] N. Ahmed, M. Rafiq, D. Baleanu, and M. A. Rehman, "Spatio-temporal numerical modeling of auto-catalytic Brusselator model," *Romanian Journal of Physics*, vol. 64, pp. 1–14, 2019.

[19] N. Ahmed, S. S. Tahira, M. Imran, M. Rafiq, M. A. Rehman, and M. Younis, "Numerical analysis of auto-catalytic glycolysis model," *AIP Advances*, vol. 9, no. 8, p. 085213, 2019.

[20] S. Kim, A. A. de los Reyes, and E. Jung, "Mathematical model and intervention strategies for mitigating tuberculosis in the Philippines," *Journal of Theoretical Biology*, vol. 443, pp. 100–112, 2018.

[21] R. Chinnathambi, F. A. Rihan, and H. J. Alsakaji, "A fractional-order model with time delay for tuberculosis with endogenous reactivation and exogenous reinfections," *Mathematical Methods in the Applied Sciences*, vol. 44, no. 10, pp. 8011–8025, 2021.

[22] F. A. Rihan and H. J. Alsakaji, "Dynamics of a stochastic delay differential model for COVID-19 infection with asymptomatic infected and interacting people: case study in the UAE," *Results in Physics*, vol. 28, p. 104658, 2021.

[23] S. Ullah, M. A. Khan, M. Farooq, and T. Gul, "Modeling and analysis of tuberculosis (TB) in khyber Pakhtunkhwa, Pakistan," *Mathematics and Computers in Simulation*, vol. 165, pp. 181–199, 2019.

[24] TB country profiles, "TB country profiles," 2018, https://www.who.int/tb/country/data/profiles/en/.

Hindawi
Complexity
Volume 2022, Article ID 2431533, 13 pages
https://doi.org/10.1155/2022/2431533

Research Article

The Analysis of Fractional-Order Proportional Delay Physical Models via a Novel Transform

Meshari Alesemi,[1] Naveed Iqbal,[2] and Ahmed A. Hamoud[3]

[1]*Department of Mathematics, College of Science, University of Bisha, P. O. Box 511, Bisha 61922, Saudi Arabia*
[2]*Department of Mathematics, Faculty of Science, University of Ha'il, Ha'il 2440, Saudi Arabia*
[3]*Department of Mathematics, Taiz University, Taiz 96704, Yemen*

Correspondence should be addressed to Naveed Iqbal; n.iqbal@uoh.edu.sa and Ahmed A. Hamoud; ahmed.hamoud@taiz.edu.ye

Received 28 November 2021; Accepted 20 January 2022; Published 15 February 2022

Academic Editor: C. Rajivganthi

In this paper, we deal with an alternative analytical analysis of fractional-order partial differential equations with proportional delay, achieved by applying Yang decomposition method, where the fractional derivative is taken in Caputo sense. The suggested series results are discovered to quickly converge to an exact solution. The computation of three test problems of fractional-order with proportional delay partial differential equations was presented to confirm the validity and efficiency of suggested method. The system appears to be a very dependable, effective, and powerful method for solving a variety of physical problems that arise in engineering and science.

1. Introduction

Because of its numerous applications in modelling, $\mu(0,\eta) = \beta_0(\eta), \quad \mu(1,\eta) = \beta_1(\eta), \quad \eta \in (0,T]$, the study of fractional calculus has recently attracted a lot of attention of fluid dynamics, electrodynamics, biological mathematics, signal processing, and numerous different fields of science. The researchers have written a number of books on fractional calculus such as Ross and Miller [1], Zhou et al. [2], Kilbas et al. [3], Podlubny [4], and Agarwal et al. [5]. Furthermore, delay differential problems have various uses in transportation networks, biological and chemical, which can be identified in [6–11]. In this paper, we suggest with time delay coefficient variable partial differential equation (PDE), provided by

$$D_\eta^\delta \mu(\zeta,\eta) - \left(\nu(\zeta)\mu_\zeta(\zeta,\eta)\right)_\zeta + \mu^p(\zeta,\eta)\mu_\zeta(\zeta,\eta) = g(\zeta,\eta,\mu(\zeta,\eta-\eta)), \quad (\zeta,\eta) \in (0,1)\times(0,T], \tag{1}$$

the boundaries condition and initial condition

$$\mu(\zeta,\eta) = \varphi(\zeta,\eta), \quad (\zeta,\eta) \in [0,1]\times[-\eta,0], \tag{2}$$

where $\mu(\zeta,\eta) \in C^{2,1}([0,1]\times[-\eta,T])$ is the unknown term with ζ,η space and time variables. When $\nu(\zeta)$ is variable coefficient of space which provides $0 < c_0 \le \nu(\zeta) \le c_1$, p is any positive integer and $\varphi(\zeta,\eta)$ is sufficiently smooth prehistory function.

For $\delta = 1$, (1) becomes classical semilinear with time delay convection reaction diffusion equation (CRDE). Numerous numeric systems have been investigated at $\delta = 1$. For example, Zhang and Zhang [12] described a linearize splitting multicompact system to overcome nonlinear PDEs with delay time. Pao [13] suggested a monotone iterative algorithm for the numeric solution of a delay CRDE. For nonlinear CRDEs with time delay, Zhang et al. [14]

introduced explicit implicit multistep finite element technique. For variable coefficient time delay PDEs, Ran and He [15] suggested a linearized Crank–Nicolson method.

In the meantime, fractional with delay differential equations have attracted the interest of investigators due to its wide implementation in dynamics population, finance, automatic control, etc. [16–18]. Furthermore, by using variable coefficients, more complex natural phenomena can be introduced in [19–21]. It is not straightforward to solve fractional delay PDEs effectively and accurately. The evolution of the dependent variable of fractional delay partial differential equations is at time η, but also on all earlier findings, due to the nature of history dependence of a fractional derivative. In a few cases, analytical solutions to fractional differential equations with delay can be found. Ouyang [22], for example, investigated the uniqueness and existence of results for nonlinear fractional-order delay PDEs. To analyze time fractional delay PDEs, Rihan [23] suggest a different approach which is unconditionally implicit stable. For fractional nonlinear delay diffusion equations, Pimenov and Ahmed [24] suggested a numerical solution for a class of time fractional diffusion equations with delay. For semilinear fractional PDEs with time delay, Zang et al. [25] suggested a compact finite difference approach. For the numeric solution of semilinear fractional delay partial differential equations, Mohebbi [26] suggested a spectral collocation and finite difference methods. For the mathematical investigation of variable order delay Burgers equation, Sweilam et al. [27] presented a nonstandard weighted average finite difference approach. To explore the propagation of the population growth model, Jaradat et al. [28] suggested two numerical schemes based on fractional homotopy perturbation and power series methods.

Adomian decomposition method and Yang transform are two well-known techniques that have been applied to have introduced Yang decomposition method. Several physical phenomena which are modeled by partial differential equations and fractional partial differential equations are solved by applying Adomian transform decomposition method, such as the analytical investigation of fractional system partial differential equations are proposed in [29–31], the analysis of nonlinear ordinary differential equations is successfully shown in [32], nonlinear partial differential equations [33–35], fractional unsteady flow of fractional telegraph equations [36], polytropic gas model [37], fractional Schrodinger equation [38], and Fokker–Plank equation [39–41].

2. Basic Definitions

In this portion, we described a few basic concepts of fractional calculus along with properties of Laplace transformation.

2.1. Definition. The Caputo fractional derivative is define as

$$D_{\eta}^{\delta}\nu(\psi,\eta)=\frac{1}{\Gamma(k-\delta)}\int_{0}^{\eta}(\eta-\rho)^{k-\delta-1}\nu^{(k)}(\psi,\rho)d\rho,\quad k-1<\delta\le k,\quad k\in N. \tag{3}$$

2.2. Definition. Xiao Jun Yang introduced the Yang Laplace transform in 2018. The Yang transformation for a term $\nu(\eta)$ is determined by $Y\{\nu(\eta)\}$ or $M(u)$ and is given as

$$Y\{\nu(\eta)\}=M(u)=\int_{0}^{\infty}e^{-\eta/u}\nu(\eta)d\eta\ ,\quad \eta>0,u\in(-\eta_1,\eta_2). \tag{4}$$

The inverse Yang transformation is expressed as

$$Y^{-1}\{M(u)\}=\nu(\eta), \tag{5}$$

where Y^{-1} is the inverse Yang operator.

2.3. Definition. The nth derivatives of Yang transformation are given as

$$Y\{\nu^{n}(\eta)\}=\frac{M(u)}{u^{n}}-\sum_{k=0}^{n-1}\frac{\nu^{k}(0)}{u^{n-k-1}},\quad \forall n=1,2,3,\ldots. \tag{6}$$

2.4. Definition. The fractional-order derivatives of Yang transformation are define as

$$Y\left\{\nu^{\delta}(\eta)\right\}=\frac{M(u)}{u^{\gamma}}-\sum_{k=0}^{n-1}\frac{\nu^{k}(0)}{u^{\delta-(k+1)}},\quad 0<\delta\le n. \tag{7}$$

3. Idea of Yang Decomposition Technique

In this portion, the YDM to investigate the general solution of fractional delay partial differential equations:

$$D_{\eta}^{\delta}\mu(\zeta,\eta)+L\mu(\zeta,\eta)+N\mu\left(\frac{\zeta}{2},\frac{\eta}{2}\right)=q(\zeta,\eta),\quad \zeta,\eta\ge 0,\ell-1<\delta<\ell,$$
$$\mu(\zeta,\eta)=k(\zeta), \tag{8}$$

where $D^{\delta}=\partial^{\delta}/\partial\eta^{\delta}$ is the Caputo operator $\delta,\ell\in\mathbb{N}$, where L is linear and N is the nonlinear term, and q is the source term. Using the Yang transformation to (8), we have

$$\mathbb{Y}\left[D^{\delta}\mu(\zeta,\eta)\right]+\mathbb{Y}\left[L\mu(\zeta,\eta)+N\mu\left(\frac{\zeta}{2},\frac{\eta}{2}\right)\right]=\mathbb{Y}[q(\zeta,\eta)], \tag{9}$$

and applying the Yang transformation of differentiation property, we get

$$\frac{1}{s^{\delta}}\mathbb{Y}[\mu(\zeta,\eta)] - s\mu(\zeta,0) = \mathbb{Y}[q(\zeta,\eta)] - \mathbb{Y}\left[L\mu(\zeta,\eta) + N\mu\left(\frac{\zeta}{2},\frac{\eta}{2}\right)\right],$$
$$\mathbb{Y}[\mu(\zeta,\eta)] = sk(\zeta) + s^{\delta}\mathbb{Y}[q(\zeta,\eta)] - s^{\delta}\mathbb{Y}\left[L\mu(\zeta,\eta) + N\mu\left(\frac{\zeta}{2},\frac{\eta}{2}\right)\right]. \tag{10}$$

The YDM solution $\mu(\zeta,\eta)$ is represented by the following infinite series:

$$\mu(\zeta,\eta) = \sum_{\ell=0}^{\infty}\mu_{\ell}(\zeta,\eta), \tag{11}$$

and the nonlinear functions are expressed by the Adomian polynomials,

$$N\mu\left(\frac{\zeta}{2},\frac{\eta}{2}\right) = \sum_{\ell=0}^{\infty}A_{\ell},$$
$$A_{\ell} = \frac{1}{\ell!}\left[\frac{d^{\ell}}{d\lambda^{\ell}}\left[N\sum_{\ell=0}^{\infty}\left(\lambda^{\ell}\mu_{\ell}\right)\right]\right]_{\lambda=0}, \quad \ell = 0,1,2,\ldots, \tag{12}$$

and substituting equations (10) and (11) in (10), we get

$$\mathbb{Y}\left[\sum_{\ell=0}^{\infty}\mu(\zeta,\eta)\right] = sk(\zeta) + s^{\delta}\mathbb{Y}[q(\zeta,\eta)] - s^{\delta}\mathbb{Y}\left[L\sum_{\ell=0}^{\infty}\mu_{\ell}(\zeta,\eta) + \sum_{\ell=0}^{\infty}A_{\ell}\right],$$
$$\mathbb{Y}[\mu_0(\zeta,\eta)] = s\mu(\zeta,0) + s^{\delta}\mathbb{Y}[q(\zeta,\eta)], \tag{13}$$
$$\mathbb{Y}[\mu_1(\zeta,\eta)] = -s^{\delta}\mathbb{Y}[L\mu_0(\zeta,\eta) + A_0].$$

Generally, we can write

$$\mathbb{Y}[\mu_{\ell+1}(\zeta,\eta)] = -s^{\delta}\mathbb{Y}[L\mu_{\ell}(\zeta,\eta) + A_{\ell}], \quad \ell \geq 1. \tag{14}$$

Applying the inverse Yang transform in (14), we get

$$\mu_0(\zeta,\eta) = k(\zeta,\eta),$$
$$\mu_{\ell+1}(\zeta,\eta) = -\mathbb{Y}^{-1}\left[s^{\delta}\mathbb{Y}[L\mu_{\ell}(\zeta,\eta) + A_{\ell}]\right]. \tag{15}$$

4. Numerical Results

Example 1. Consider the generalized Burgers equation with proportional delay as defined by [42]:

$$\frac{\partial^{\delta}\mu}{\partial\eta^{\delta}} - \frac{\partial^2\mu(\zeta,\eta)}{\partial\zeta^2} - \mu\left(\frac{\zeta}{2},\frac{\eta}{2}\right)\frac{\partial\mu(\zeta,(\eta/2))}{\partial\zeta} - \frac{1}{2}\mu(\zeta,\eta) = 0, \tag{16}$$

with initial condition

$$\mu(\zeta,0) = \zeta. \tag{17}$$

Taking Yang transform of (16), we get

$$\frac{1}{s^{\delta}}\mathbb{Y}[\mu(\zeta,\eta)] - s\mu(\zeta,0) = \mathbb{Y}\left[\frac{\partial^2\mu(\zeta,\eta)}{\partial\zeta^2} + \mu\left(\frac{\zeta}{2},\frac{\eta}{2}\right)\frac{\partial\mu(\zeta,(\eta/2))}{\partial\zeta} + \frac{1}{2}\mu(\zeta,\eta)\right]. \tag{18}$$

Applying inverse Yang transform,

$$\mu(\zeta,\eta) = \mathbb{Y}^{-1}\left[s\mu(\zeta,0) - s^{\delta}\mathbb{Y}\left\{\frac{\partial^2\mu(\zeta,\eta)}{\partial\zeta^2} + \mu\left(\frac{\zeta}{2},\frac{\eta}{2}\right)\frac{\partial\mu(\zeta,(\eta/2))}{\partial\zeta} + \frac{1}{2}\mu(\zeta,\eta)\right\}\right]. \tag{19}$$

Using ADM procedure, we get

$$\begin{aligned}
\mu_0(\zeta,\eta) &= \mathbb{Y}^{-1}[s\mu(\zeta,0)] = \zeta,\\
\sum_{\ell=0}^{\infty}\mu_{\ell+1}(\zeta,\eta) &= \mathbb{Y}^{-1}\left[s^{\delta}\mathbb{Y}\left\{\sum_{\ell=0}^{\infty}\left(\mu_{\zeta\zeta}(\zeta,\eta)\right)_{\ell}+\sum_{\ell=0}^{\infty}A_{\ell}\left(\mu\mu_{\zeta}\right)+\frac{1}{2}\sum_{\ell=0}^{\infty}\mu_{\ell}(\zeta,\eta)\right\}\right], \quad \ell=0,1,2,\ldots,\\
A_0\left(\mu\mu_{\zeta}\right) &= \mu_0\frac{\partial\mu_0}{\partial\zeta},\\
A_1\left(\mu\mu_{\zeta}\right) &= \mu_0\frac{\partial\mu_1}{\partial\zeta}+\mu_1\frac{\partial\mu_0}{\partial\zeta},\\
A_2\left(\mu\mu_{\zeta}\right) &= \mu_0\frac{\partial\mu_2}{\partial\zeta}+\mu_1\frac{\partial\mu_1}{\partial\zeta}+\mu_2\frac{\partial\mu_0}{\partial\zeta},
\end{aligned} \tag{20}$$

for $\ell = 0$,

$$\begin{aligned}
\mu_1(\zeta,\eta) &= \mathbb{Y}^{-1}\left[s^{\delta}\mathbb{Y}\left\{\frac{\partial^2\mu_0(\zeta,\eta)}{\partial\zeta^2}+\mu_0\left(\frac{\zeta}{2},\frac{\eta}{2}\right)\frac{\partial\mu_0(\zeta,(\eta/2))}{\partial\zeta}+\frac{1}{2}\mu_0(\zeta,\eta)\right\}\right],\\
\mu_1(\zeta,\eta) &= \zeta\frac{\eta^{\delta}}{\Gamma(\delta+1)}.
\end{aligned} \tag{21}$$

The subsequent terms are

$$\begin{aligned}
\mu_2(\zeta,\eta) &= \mathbb{Y}^{-1}\left[s^{\delta}\mathbb{Y}\left\{\frac{\partial^2\mu_1(\zeta,\eta)}{\partial\zeta^2}+\mu_0\left(\frac{\zeta}{2},\frac{\eta}{2}\right)\frac{\partial\mu_1(\zeta,(\eta/2))}{\partial\zeta}+\mu_1\left(\frac{\zeta}{2},\frac{\eta}{2}\right)\frac{\partial\mu_0(\zeta,(\eta/2))}{\partial\zeta}+\frac{1}{2}\mu_1(\zeta,\eta)\right\}\right],\\
\mu_2(\zeta,\eta) &= \frac{\zeta\left(2+2^{\delta}\right)\eta^{2\delta}}{2^{\delta}2\Gamma(2\delta+1)},\\
\mu_3(\zeta,\eta) &= \mathbb{Y}^{-1}\left[s^{\delta}\mathbb{Y}\left\{\frac{\partial^2\mu_2(\zeta,\eta)}{\partial\zeta^2}+\mu_0\left(\frac{\zeta}{2},\frac{\eta}{2}\right)\frac{\partial\mu_2(\zeta,\eta/2)}{\partial\zeta}+\mu_1\left(\frac{\zeta}{2},\frac{\eta}{2}\right)\frac{\partial\mu_1(\zeta,\eta/2)}{\partial\zeta}+\mu_2\left(\frac{\zeta}{2},\frac{\eta}{2}\right)\frac{\partial\mu_0(\zeta,\eta/2)}{\partial\zeta}+\frac{1}{2}\mu_2(\zeta,\eta)\right\}\right],\\
\mu_3(\zeta,\eta) &= \frac{\zeta\eta^{3\delta}}{4\Gamma(3\delta+1)}\left(1+\frac{2}{2^{\delta}}+\frac{2}{2^{2\delta}}+\frac{2^2}{2^{3\delta}}+\frac{2\Gamma(1+2\delta)}{2^{\delta}\Gamma(1+\delta)^2}\right),\\
\mu_4(\zeta,\eta) &= \mathbb{Y}^{-1}\left[s^{\delta}\mathbb{Y}\left[\begin{array}{l}\dfrac{\partial^2\mu_3(\zeta,\eta)}{\partial\zeta^2}+\mu_0\left(\dfrac{\zeta}{2},\dfrac{\eta}{2}\right)\dfrac{\partial\mu_3(\zeta,(\eta/2))}{\partial\zeta}+\mu_1\left(\dfrac{\zeta}{2},\dfrac{\eta}{2}\right)\dfrac{\partial\mu_2(\zeta,(\eta/2))}{\partial\zeta}\\ \\ +\mu_2\left(\dfrac{\zeta}{2},\dfrac{\eta}{2}\right)\dfrac{\partial\mu_1(\zeta,(\eta/2))}{\partial\zeta}+\mu_3\left(\dfrac{\zeta}{2},\dfrac{\eta}{2}\right)\dfrac{\partial\mu_0(\zeta,(\eta/2))}{\partial\zeta}+\dfrac{1}{2}\mu_3(\zeta,\eta)\end{array}\right]\right],\\
\mu_4(\zeta,\eta) &= \frac{\zeta\eta^{4\delta}}{8\Gamma(4\delta+1)}\left[\begin{array}{c}1+\dfrac{2^9}{2^{6\delta}}+\dfrac{2^8}{2^{5\delta}}+\dfrac{3\times2^7}{2^{3\delta}}+\dfrac{2^7}{2^{2\delta}}+\dfrac{2^7}{2^{\delta}}+\dfrac{2^8}{2^{4\delta}}\\ \\ +\left(\dfrac{2^8}{2^{5\delta}}+\dfrac{2^7}{2^{2\delta}}\right)\dfrac{\Gamma(2\delta+1)}{\Gamma(\delta+1)^2}+\left(\dfrac{2^9}{2^{4\delta}}+\dfrac{2^8}{2^{3\delta}}\right)\dfrac{\Gamma(3\delta+1)}{\Gamma(\delta+1)\Gamma(2\delta+1)}\end{array}\right].
\end{aligned} \tag{22}$$

The YDM series form solution for Examples 1–3 is

$$\mu(\zeta,\eta)=\mu_0(\zeta,\eta)+\mu_1(\zeta,\eta)+\mu_2(\zeta,\eta)+\mu_3(\zeta,\eta)+\mu_4(\zeta,\eta)\ldots,$$

$$\mu(\zeta,\eta)=\zeta+\zeta\frac{\eta^{\delta}}{\Gamma(\delta+1)}+\frac{\zeta\left(2+2^{\delta}\right)\eta^{2\delta}}{2^{\delta}2\Gamma(2\delta+1)}+\frac{\zeta\eta^{3\delta}}{4\Gamma(3\delta+1)}\left(1+\frac{2}{2^{\delta}}+\frac{2}{2^{2\delta}}+\frac{2^2}{2^{3\delta}}+\frac{2\Gamma(1+2\delta)}{2^{\delta}\Gamma(1+\delta)^2}\right)$$
$$+\frac{\zeta\eta^{4\delta}}{8\Gamma(4\delta+1)}\left[1+\frac{2^9}{2^{6\delta}}+\frac{2^8}{2^{5\delta}}+\frac{3\times2^7}{2^{3\delta}}+\frac{2^7}{2^{2\delta}}+\frac{2^7}{2^{\delta}}+\frac{2^8}{2^{4\delta}}+\left(\frac{2^8}{2^{5\delta}}+\frac{2^7}{2^{2\delta}}\right)\frac{\Gamma(2\delta+1)}{\Gamma(\delta+1)^2}+\left(\frac{2^9}{2^{4\delta}}+\frac{2^8}{2^{3\delta}}\right)\frac{\Gamma(3\delta+1)}{\Gamma(\delta+1)\Gamma(2\delta+1)}\right]+\ldots,$$

$$\mu(\zeta,\eta)=\zeta+\zeta\frac{\eta^{\delta}}{\Gamma(\delta+1)}+\frac{\zeta\left(2+2^{\delta}\right)\eta^{2\delta}}{2^{\delta}2\Gamma(2\delta+1)}+\frac{\zeta\eta^{3\delta}}{4\Gamma(3\delta+1)}\left(1+\frac{2}{2^{\delta}}+\frac{2}{2^{2\delta}}+\frac{2^2}{2^{3\delta}}+\frac{2\Gamma(1+2\delta)}{2^{\delta}\Gamma(1+\delta)^2}\right)$$
$$+\frac{\zeta\eta^{4\delta}}{8\Gamma(4\delta+1)}\left[1+\frac{2^9}{2^{6\delta}}+\frac{2^8}{2^{5\delta}}+\frac{3\times2^7}{2^{3\delta}}+\frac{2^7}{2^{2\delta}}+\frac{2^7}{2^{\delta}}+\frac{2^8}{2^{4\delta}}+\left(\frac{2^8}{2^{5\delta}}+\frac{2^7}{2^{2\delta}}\right)\frac{\Gamma(2\delta+1)}{\Gamma(\delta+1)^2}+\left(\frac{2^9}{2^{4\delta}}+\frac{2^8}{2^{3\delta}}\right)\frac{\Gamma(3\delta+1)}{\Gamma(\delta+1)\Gamma(2\delta+1)}\right]+\ldots, \tag{23}$$

when $\delta=1$, then YDM series form result is

$$\mu(\zeta,\eta)=\zeta\left(1+\eta+\frac{\eta^2}{2!}+\frac{\eta^3}{3!}+\frac{\eta^4}{4!}+\ldots\right). \tag{24}$$

The exact result is

$$\mu(\zeta,\eta)=\zeta e^{\eta}. \tag{25}$$

In Figure 1, the approximate solution graph of problem 4.1, at $\delta=1$ and 0.8, which shows the close contact with each other. Figure 2 shows the approximate result graph of problem 4.1, at $\delta=0.6$ and 0.4. Figure 3 shows the analytical solution graph of different fractional-order of δ.

Example 2. Consider the fractional partial differential equation with proportional delay as defined in [42]:

$$\frac{\partial^{\delta}\mu(\zeta,t)}{\partial\eta^{\delta}}-\mu\left(\zeta,\frac{\eta}{2}\right)\frac{\partial^2\mu(\zeta,\eta/2)}{\partial\zeta^2}+\mu(\zeta,\eta)=0, \tag{26}$$

with the initial condition

$$\mu(\zeta,0)=\zeta^2. \tag{27}$$

Taking Yang transform of (26), we get

$$\frac{1}{s^{\delta}}\mathbb{Y}[\mu(\zeta,\eta)]-s\mu(\zeta,0)=\mathbb{Y}\left[\mu\left(\zeta,\frac{\eta}{2}\right)\frac{\partial^2\mu(\zeta,\eta/2)}{\partial\zeta^2}-\mu(\zeta,\eta)\right]. \tag{28}$$

Applying inverse Yang transform,

$$\mu(\zeta,\eta)=\mathbb{Y}^{-1}\left[s\mu(\zeta,0)=\mathbb{Y}\left[\mu\left(\zeta,\frac{\eta}{2}\right)\frac{\partial^2\mu(\zeta,\eta/2)}{\partial\zeta^2}-\mu(\zeta,\eta)\right]\right]. \tag{29}$$

Using ADM procedure, we get

$$\mu_0(\zeta,\eta)=\mathbb{Y}^{-1}[s\mu(\zeta,0)]=\zeta^2,$$
$$\sum_{\ell=0}^{\infty}\mu_{\ell+1}(\zeta,\eta)=\mathbb{Y}^{-1}\left[s^{\delta}\mathbb{Y}\left\{\sum_{\ell=0}^{\infty}B_{\ell}\left(\mu\mu_{\zeta\zeta}\right)-\sum_{\ell=0}^{\infty}\mu_{\ell}(\zeta,\eta)\right\}\right],\quad \ell=0,1,2,$$
$$B_0\left(\mu\mu_{\zeta\zeta}\right)=\mu_0\frac{\partial^2\mu_0}{\partial\zeta^2},$$
$$B_1\left(\mu\mu_{\zeta\zeta}\right)=\mu_0\frac{\partial^2\mu_1}{\partial\zeta^2}+\mu_1\frac{\partial^2\mu_0}{\partial\zeta^2}, \tag{30}$$
$$B_2\left(\mu\mu_{\zeta\zeta}\right)=\mu_0\frac{\partial^2\mu_2}{\partial\zeta^2}+\mu_1\frac{\partial^2\mu_1}{\partial\zeta^2}+\mu_2\frac{\partial^2\mu_0}{\partial\zeta^2},$$

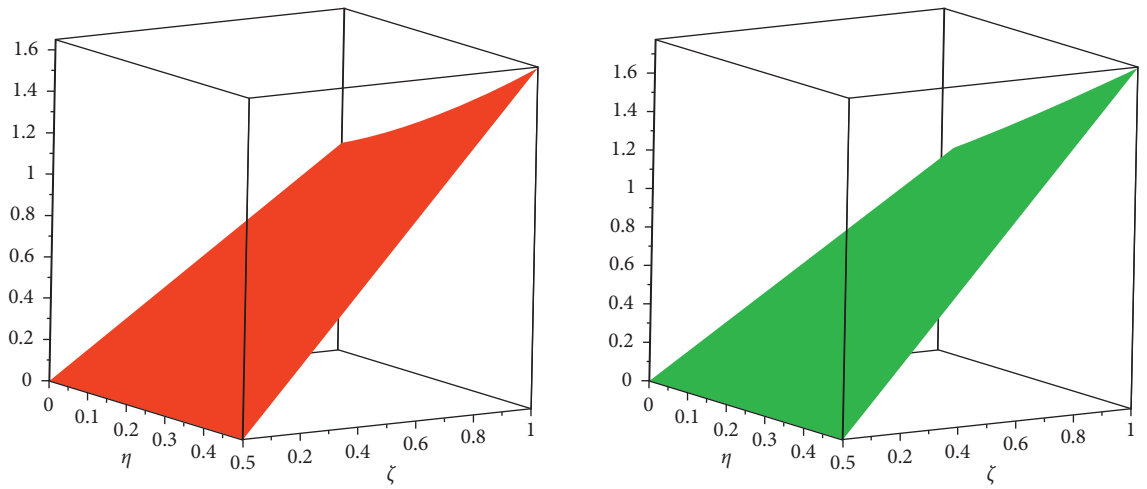

Figure 1: The approximate solution graph of problem 4.1, at $\delta = 1$ and 0.8.

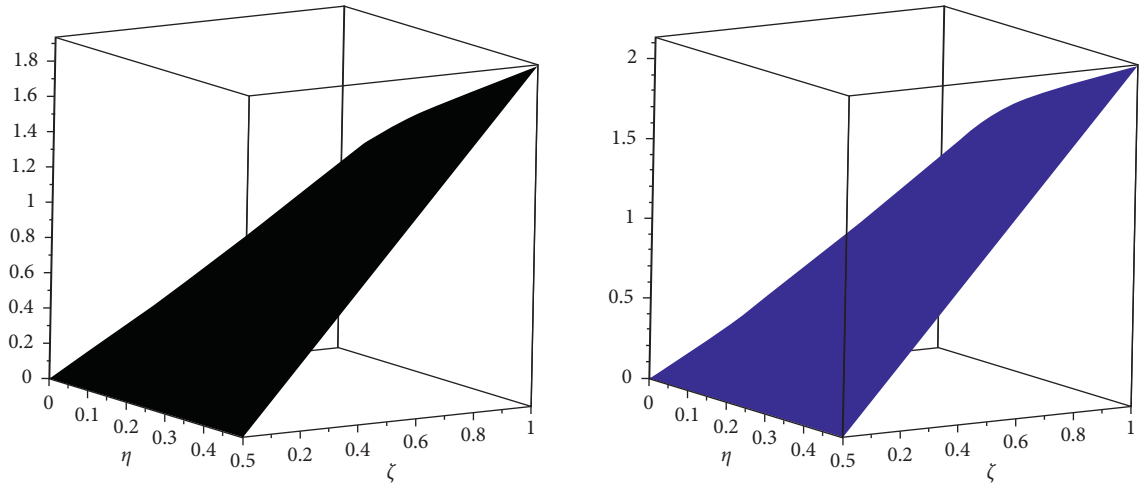

Figure 2: The approximate result graph of problem 4.1, at $\delta = 0.6$ and 0.4.

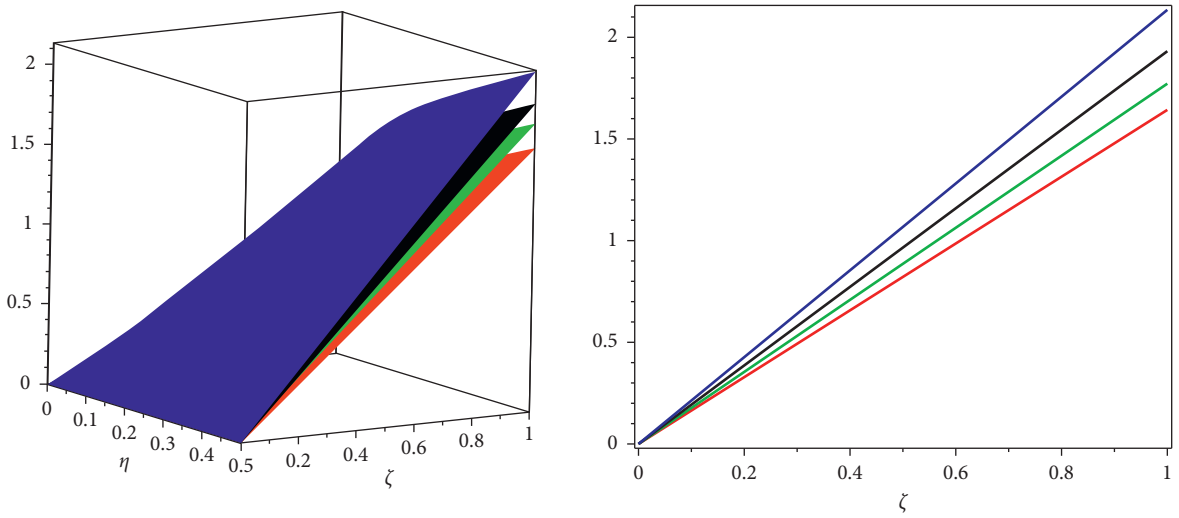

Figure 3: The approximate result graph of problem 4.1, at different fractional-order of δ.

for $\ell = 0$,

$$\mu_1(\zeta,\eta) = \mathbb{Y}^{-1}\left[s^{\delta}\mathbb{Y}\left\{\mu_0\left(\zeta,\frac{\eta}{2}\right)\frac{\partial^2\mu_0(\zeta,\eta/2)}{\partial\zeta^2} + \mu_0(\zeta,\eta)\right\}\right],$$
$$\mu_1(\zeta,\eta) = \zeta^2\frac{\eta^{\delta}}{\Gamma(\delta+1)}. \tag{31}$$

The subsequent terms are

$$\mu_2(\zeta,\eta) = \mathbb{Y}^{-1}\left[s^{\delta}\mathbb{Y}\left\{\mu_0\left(\zeta,\frac{\eta}{2}\right)\frac{\partial^2\mu_1(\zeta,\eta/2)}{\partial\zeta^2} + \mu_1\left(\zeta,\frac{\eta}{2}\right)\frac{\partial^2\mu_0(\zeta,\eta/2)}{\partial\zeta^2} - \mu_1(\zeta,\eta)\right\}\right],$$
$$\mu_2(\zeta,\eta) = \frac{\zeta^2\left(2-2^{\delta}\right)\eta^{2\delta}}{2^{\delta}\Gamma(2\delta+1)},$$
$$\mu_3(\zeta,\eta) = \mathbb{Y}^{-1}\left[s^{\delta}\mathbb{Y}\left\{\mu_0\left(\zeta,\frac{\eta}{2}\right)\frac{\partial\mu_2(\zeta,\eta/2)}{\partial\zeta} + \mu_1\left(\zeta,\frac{\eta}{2}\right)\frac{\partial\mu_1(\zeta,\eta/2)}{\partial\zeta} + \mu_2\left(\zeta,\frac{\eta}{2}\right)\frac{\partial\mu_0(\zeta,\eta/2)}{\partial\zeta} - \mu_2(\zeta,\eta)\right\}\right], \tag{32}$$
$$\mu_3(\zeta,\eta) = \frac{\zeta^2\eta^{3\delta}}{\Gamma(3\delta+1)}\left(1 - \frac{2}{2^{\delta}} - \frac{2^2}{2^{2\delta}} + \frac{2^4}{2^{3\delta}} + \frac{2\Gamma(2\delta+1)}{2^{\delta}\Gamma(\delta+1)^2}\right).$$

The YDM result for problem 4.2 is

$$\mu(\zeta,\eta) = \mu_0(\zeta,\eta) + \mu_1(\zeta,\eta) + \mu_2(\zeta,\eta) + \mu_3(\zeta,\eta) + \mu_4(\zeta,\eta)\ldots,$$
$$\mu(\zeta,\eta) = \zeta^2 + \zeta^2\frac{\eta^{\delta}}{\Gamma(\delta+1)} + \frac{\zeta^2\left(2-2^{\delta}\right)\eta^{2\delta}}{2^{\delta}\Gamma(2\delta+1)} + \frac{\zeta^2\eta^{3\delta}}{\Gamma(3\delta+1)}\left(1 - \frac{2}{2^{\delta}} - \frac{2^2}{2^{2\delta}} + \frac{2^4}{2^{3\delta}} + \frac{2\Gamma(2\delta+1)}{2^{\delta}\Gamma(\delta+1)^2}\right)\ldots, \tag{33}$$

when $\delta = 1$, then YDM series form result is

$$\mu(\zeta,\eta) = \zeta^2\left(1 + \eta + \frac{\eta^2}{2!} + \frac{\eta^3}{3!} + \frac{\eta^4}{4!} + \ldots\right). \tag{34}$$

The exact solution

$$\mu(\zeta,\eta) = \zeta^2 e^{\eta}. \tag{35}$$

In Figure 4, approximate and exact result graph of problem 4.2, at $\delta = 1$, which shows the close contact with each other. Figure 5 shows the approximate solution graph of problem 4.1, at different fractional order of $\delta = 1$ with respect to ζ and η. Figure 6 shows the different fractional-order graphs of problem 4.2, with respect to time.

Example 3. Consider the fractional partial differential equation with proportional delay as given by [42]:

$$\frac{\partial^{\delta}\mu(\zeta,\eta)}{\partial\eta^{\delta}} - \frac{\partial^2\mu(\zeta/2,\eta/2)}{\partial\zeta^2}\frac{\partial\mu(\zeta/2,\eta/2)}{\partial\zeta} + \frac{1}{8}\mu(\zeta,\eta) + \mu(\zeta,\eta) = 0, \tag{36}$$

with initial condition

$$\mu(\zeta,0) = \zeta^2. \tag{37}$$

Using Yang transformation of (36), we get

$$\frac{1}{s^{\delta}}\mathbb{Y}[\mu(\zeta,\eta)] - s\mu(\zeta,0) = \mathbb{Y}\left[\frac{\partial^2\mu(\zeta/2,\eta/2)}{\partial\zeta^2}\frac{\partial\mu(\zeta/2,\eta/2)}{\partial\zeta} + \frac{1}{8}\mu(\zeta,\eta) + \mu(\zeta,\eta)\right]. \tag{38}$$

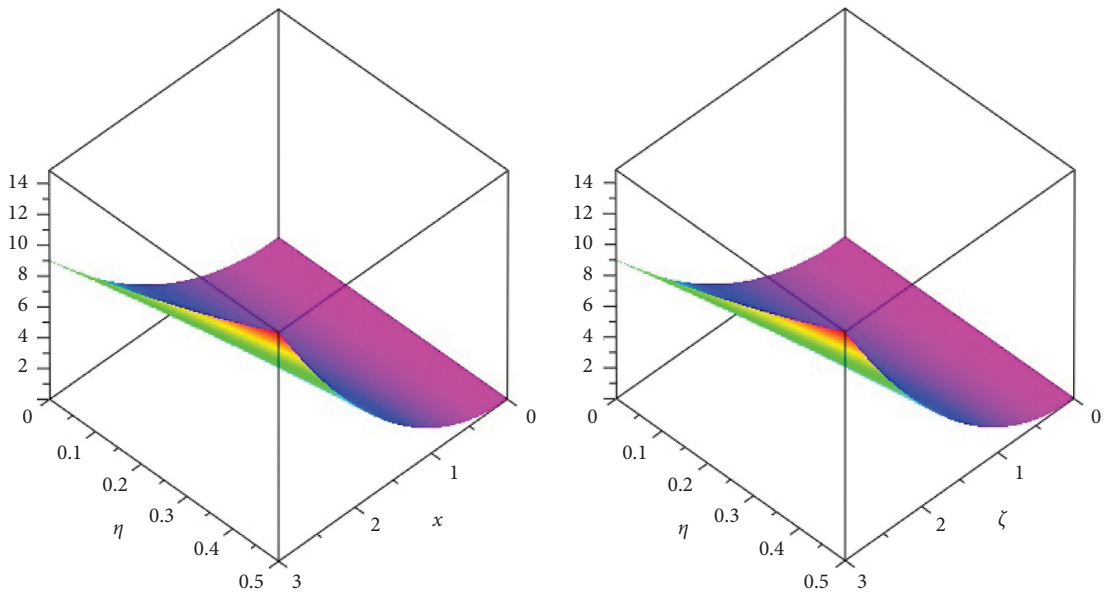

Figure 4: The approximate and exact result graph of problem 4.2, at $\delta = 1$.

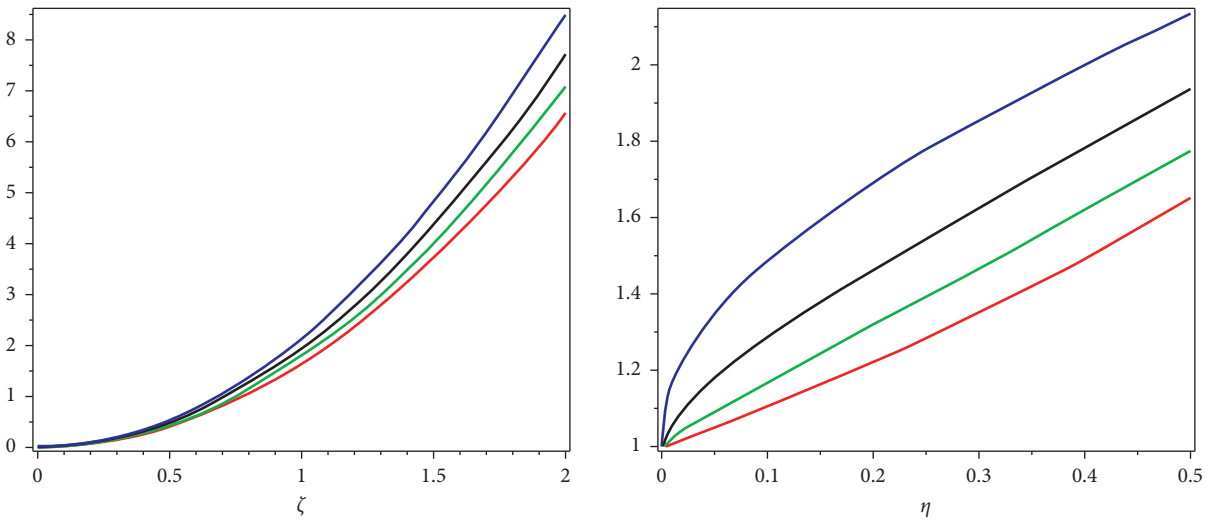

Figure 5: The approximate solution graph of problem 4.1, at different fractional order of $\delta = 1$ with respect to ζ and η.

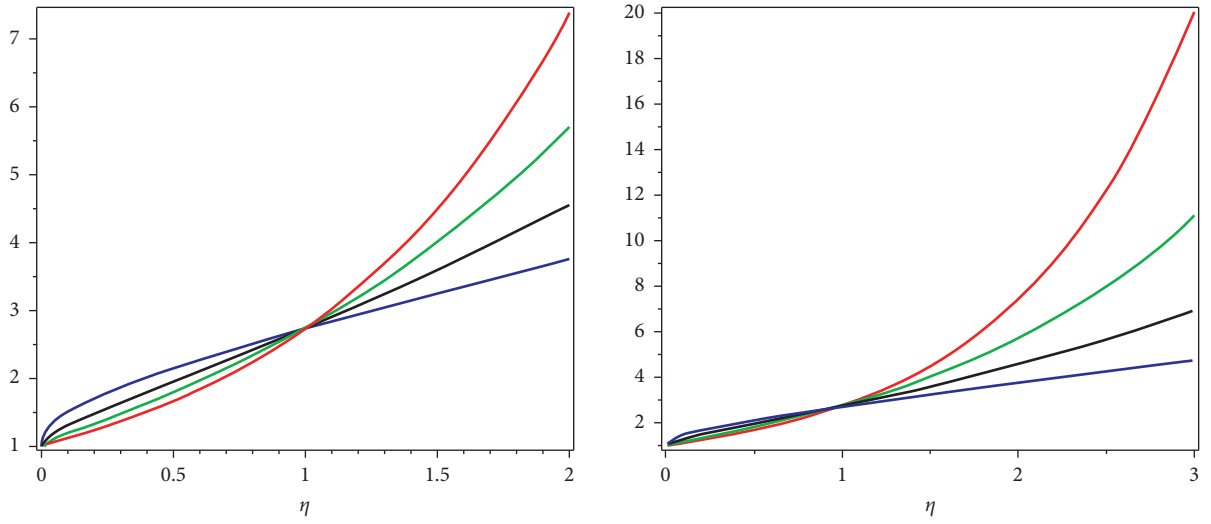

Figure 6: The different fractional-order graphs of problem 4.2, with respect to time.

Applying inverse Yang transform,

$$\mu(\zeta,\eta)=\mathbb{Y}^{-1}\left[s\mu(\zeta,0)-s^{\delta}\mathbb{Y}\left\{\frac{\partial^2\mu(\zeta/2,\eta/2)}{\partial\zeta^2}\frac{\partial\mu(\zeta/2,\eta/2)}{\partial\zeta}+\frac{1}{8}\mu(\zeta,\eta)+\mu(\zeta,\eta)\right\}\right]. \tag{39}$$

Using ADM procedure, we get

$$\begin{aligned}
\mu_0(\zeta,\eta)&=\mathbb{Y}^{-1}[s\mu(\zeta,0)]=\zeta^2,\\
\sum_{\ell=0}^{\infty}\mu_{\ell+1}(\zeta,\eta)&=\mathbb{Y}^{-1}\left[s^{\delta}\mathbb{Y}\left\{\sum_{\ell=0}^{\infty}C_{\ell}\left(\mu_{\zeta\zeta}\mu_{\zeta}\right)-\frac{1}{8}\sum_{\ell=0}^{\infty}\mu_{\ell}(\zeta,\eta)-\sum_{\ell=0}^{\infty}\mu_{\ell}(\zeta,\eta)\right\}\right],\quad \ell=0,1,2,\\
C_0\left(\mu_{\zeta\zeta}\mu_{\zeta}\right)&=\frac{\partial^2\mu_0}{\partial\zeta^2}\frac{\partial\mu_0}{\partial\zeta},\\
C_1\left(\mu_{\zeta\zeta}\mu_{\zeta}\right)&=\frac{\partial^2\mu_0}{\partial\zeta^2}\frac{\partial\mu_1}{\partial\zeta}+\frac{\partial^2\mu_1}{\partial\zeta^2}\frac{\partial\mu_0}{\partial\zeta},\\
C_2\left(\mu_{\zeta\zeta}\mu_{\zeta}\right)&=\frac{\partial^2\mu_0}{\partial\zeta^2}\frac{\partial\mu_2}{\partial\zeta}+\frac{\partial^2\mu_1}{\partial\zeta^2}\frac{\partial\mu_1}{\partial\zeta}+\frac{\partial^2\mu_2}{\partial\zeta^2}\frac{\partial\mu_0}{\partial\zeta},
\end{aligned} \tag{40}$$

for $\ell=0$,

|No Image for this Article

$$\begin{aligned}
\mu_1(\zeta,\eta)&=\mathbb{Y}^{-1}\left[s^{\delta}\mathbb{Y}\left\{\frac{\partial^2\mu(\zeta/2,\eta/2)}{\partial\zeta^2}\frac{\partial\mu(\zeta/2,\eta/2)}{\partial\zeta}+\frac{1}{8}\mu(\zeta,\eta)+\mu(\zeta,\eta)\right\}\right],\\
\mu_1(\zeta,\eta)&=-\zeta^2\frac{\eta^{\delta}}{\Gamma(\delta+1)},\\
\mu_2(\zeta,\eta)&=\mathbb{Y}^{-1}\left[s^{\delta}\mathbb{Y}\left\{\frac{\partial^2\mu(\zeta/2,\eta/2)}{\partial\zeta^2}\frac{\partial\mu(\zeta/2,\eta/2)}{\partial\zeta}+\frac{1}{8}\mu(\zeta,\eta)+\mu(\zeta,\eta)\right\}\right],\\
\mu_2(\zeta,\eta)&=\frac{\zeta\left(2^{1-\delta}+2^2\zeta+1\right)\eta^{2\delta}}{2\Gamma(2\delta+1)},\\
\mu_3(\zeta,\eta)&=\mathbb{Y}^{-1}\left[ss^{\delta}\mathbb{Y}\left\{\frac{\partial^2\mu(\zeta/2,\eta/2)}{\partial\zeta^2}\frac{\partial\mu(\zeta/2,\eta/2)}{\partial\zeta}+\frac{1}{8}\mu(\zeta,\eta)+\mu(\zeta,\eta)\right\}\right],\\
\mu_3(\zeta,\eta)&=\frac{\eta^{3\delta}}{2\Gamma(3\delta+1)}\left(-1-2\zeta^2-2^4+\frac{1}{2^{\delta}}+\frac{1}{2^{2\delta}}+\frac{2^{-3}}{2^{\delta}}+\frac{2^{-2}}{2^{3\delta}}+\zeta\frac{2^{-1}}{2^{2\delta}}\frac{2\Gamma(1+2\delta)}{2^{\delta}\Gamma(1+\delta)^2}\right).
\end{aligned} \tag{41}$$

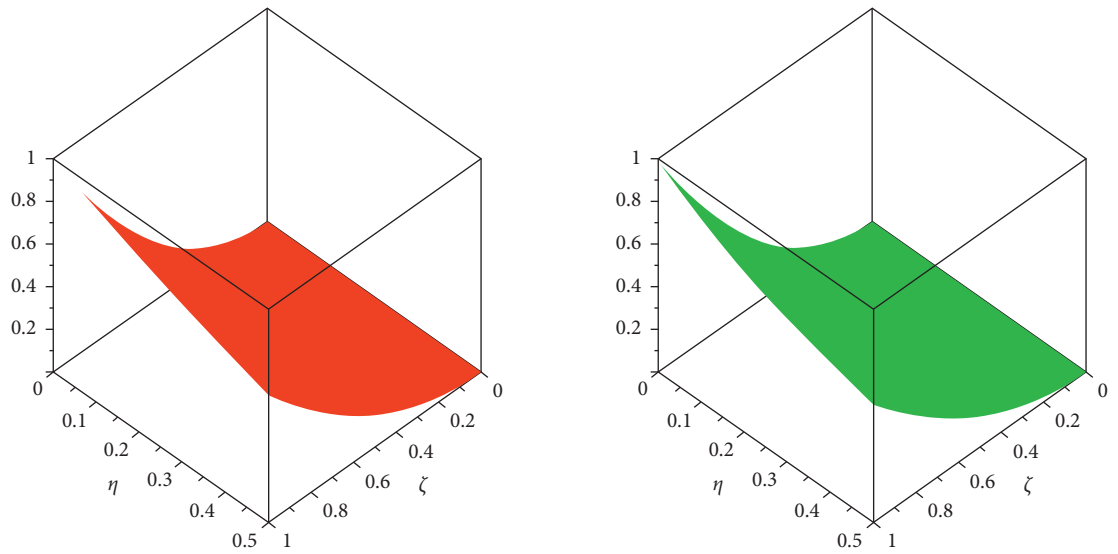

Figure 7: The approximate result graph of problem 4.3, at $\delta = 1$ and 0.8.

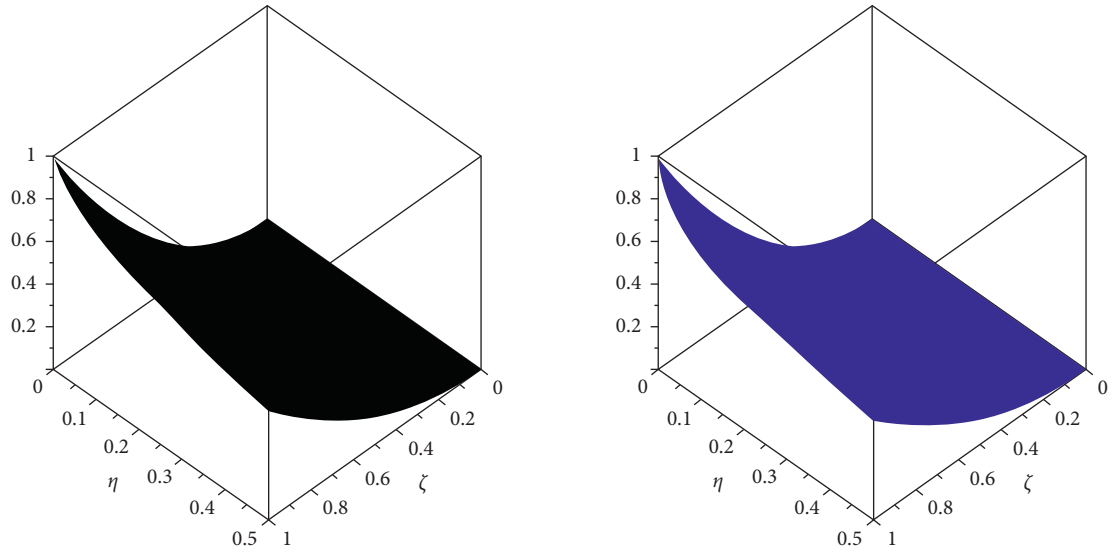

Figure 8: The approximate result graphs of problem 4.3, at $\delta = 0.6$ and 0.4.

The YDM result of problem 4.3 is

$$\begin{aligned}\mu(\zeta,\eta) &= \mu_0(\zeta,\eta) + \mu_1(\zeta,\eta) + \mu_2(\zeta,\eta) + \mu_3(\zeta,\eta) + \mu_4(\zeta,\eta)\ldots,\\ \mu(\zeta,\eta) &= \zeta^2 - \zeta^2\frac{\eta^{\delta}}{\Gamma(\delta+1)} + \frac{\zeta\left(2^{1-\delta}+2^2\zeta+1\right)\eta^{2\delta}}{2\Gamma(2\delta+1)}\\ &\quad + \frac{\eta^{3\delta}}{2\Gamma(3\delta+1)}\left(-1-2\zeta^2-2^4+\frac{1}{2^{\delta}}+\frac{1}{2^{2\delta}}+\frac{2^{-3}}{2^{\delta}}+\frac{2^{-2}}{2^{3\delta}}+\zeta\frac{2^{-1}}{2^{2\delta}}\frac{2\Gamma(1+2\delta)}{2^{\delta}\Gamma(1+\delta)^2}\right)+\ldots,\end{aligned} \tag{42}$$

when $\delta = 1$, then YDM result is

$$\mu(\zeta,\eta) = \zeta^2\left(1-\eta+\frac{\eta^2}{2!}-\frac{\eta^3}{3!}+\frac{\eta^4}{4!}-\frac{\eta^5}{5!}+\ldots\right). \tag{43}$$

The exact result is

$$\mu(\zeta,\eta) = \zeta^2 e^{-\eta}. \tag{44}$$

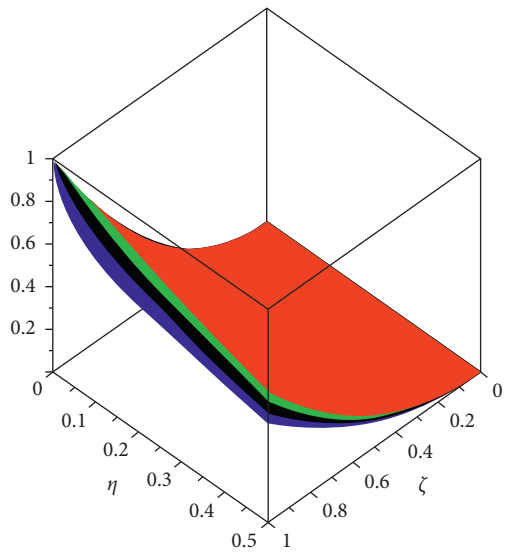

Figure 9: The approximate solution graph of problem 4.3, at different fractional-order of δ.

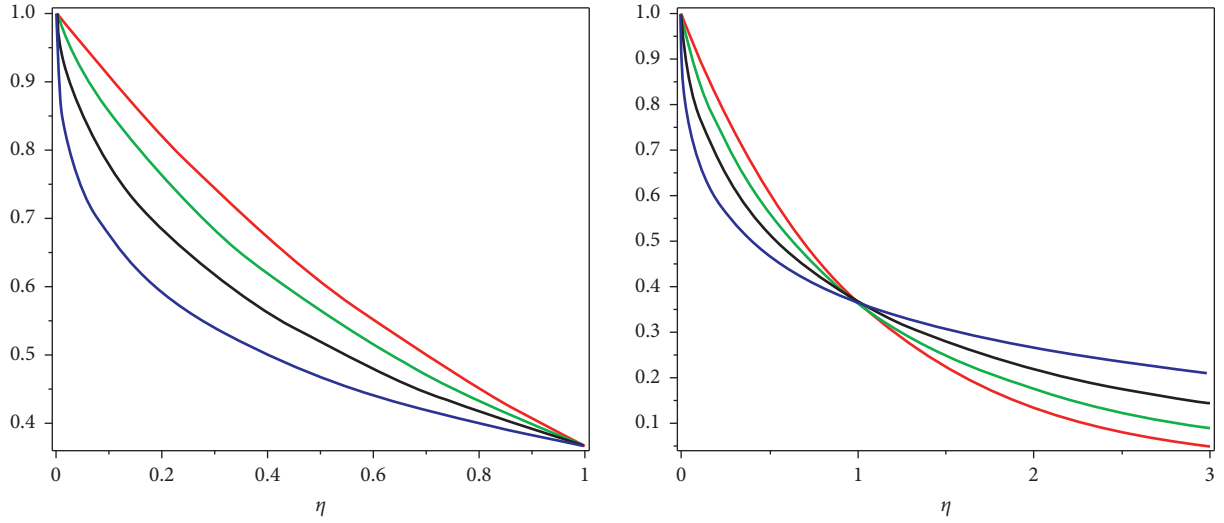

Figure 10: The approximate solution graph of problem 4.3, at different fractional-order of δ with respect to η.

Figure 7 shows the approximate result graph of problem 4.3, at $\delta = 1$ and 0.8. Figure 8 shows the approximate result graphs of problem 4.3, at $\delta = 0.6$ and 0.4. Figure 9 shows the approximate solution graph of problem 4.3, at different fractional-order of δ. Figure 10 shows the approximate solution graph of problem 4.3, at different fractional-order of δ with respect to η.

5. Conclusions

In this article, the approximate results of fractional-order delay partial differential equations are calculated, applying Yang decomposition method. The Yang decomposition method solutions are calculated for both fractional and integer order models. The suggested results are in close contact with homotopy perturbation technique [42], reduced differential transform technique [43], and homotopy perturbation transformation technique. The Yang decomposition method results have seen the highest concurrence with the actual results of the models. Moreover, the applicability and validity of the suggested technique confirm with the aid of three numeric problems. Yang decomposition method, results for fractional-order models, will prove the better understanding of the real world models represented by fractional partial differential equations.

Data Availability

The numerical data used to support the findings of this study are included within the article.

Conflicts of Interest

The authors declare that there are no conflicts of interest regarding the publication of this article.

References

[1] K. S. Miller and B. Ross, *An Introduction to the Fractional Calculus and Fractional Differential Equations*, Wiley, New Jersey, NY, USA, 1993.

[2] Y. Zhou, J. Wang, and L. Zhang, *Basic Theory of Fractional Differential Equations*, World Scientific, New Jersey, NY, USA, 2016.

[3] A. A. Kilbas, H. M. Srivastava, and J. J. Trujillo, *Theory and Applications of Fractional Differential Equations*, Elsevier, Amsterdam, Netherland, 2006.

[4] I. Podlubny, *Fractional Differential Equations: An Introduction to Fractional Derivatives, Fractional Differential Equations, to Methods of Their Solution and Some of Their Applications*, Elsevier, Amsterdam, Netherland, 1998.

[5] P. Agarwal, R. P. Agarwal, and M. Ruzhansky, *Special Functions and Analysis of Differential Equations*, CRC Press, Florida, USA, 2020.

[6] G. Adomian and R. Rach, "Nonlinear stochastic differential delay equations," *Journal of Mathematical Analysis and Applications*, vol. 91, no. 1, pp. 94–101, 1983.

[7] A. D. Polyanin, V. G. Sorokin, and A. V. Vyazmin, "Reaction-diffusion models with delay: some properties, equations, problems, and solutions," *Theoretical Foundations of Chemical Engineering*, vol. 52, no. 3, pp. 334–348, 2018.

[8] K. Nonlaopon, A. M. Alsharif, A. M. Zidan, A. Khan, Y. S. Hamed, and R. Shah, "Numerical investigation of fractional-order Swift-Hohenberg equations via a Novel transform," *Symmetry*, vol. 13, no. 7, p. 1263, 2021.

[9] R. P. Agarwal, F. Mofarreh, R. Shah, W. Luangboon, and K. Nonlaopon, "An analytical technique, based on natural transform to solve fractional-order parabolic equations," *Entropy*, vol. 23, no. 8, p. 1086, 2021.

[10] N. H. Aljahdaly, R. P. Agarwal, R. Shah, and T. Botmart, "Analysis of the time fractional-order coupled burgers equations with non-singular kernel operators," *Mathematics*, vol. 9, no. 18, p. 2326, 2021.

[11] P. Sunthrayuth, A. M. Zidan, S. W. Yao, R. Shah, and M. Inc, "The comparative study for solving fractional-order fw equation via ρ-laplace transform," *Symmetry*, vol. 13, no. 5, p. 784, 2021.

[12] Q. Zhang and C. Zhang, "A new linearized compact multisplitting scheme for the nonlinear convection-reaction-diffusion equations with delay," *Communications in Nonlinear Science and Numerical Simulation*, vol. 18, no. 12, pp. 3278–3288, 2013.

[13] C. V. Pao, "Monotone iterations for numerical solutions of reaction-diffusion-convection equations with time delay," *Numerical Methods for Partial Differential Equations*, vol. 14, no. 3, pp. 339–351, 1998.

[14] G. Zhang, A. Xiao, and J. Zhou, "Implicit-explicit multistep finite-element methods for nonlinear convection-diffusion-reaction equations with time delay," *International Journal of Computer Mathematics*, vol. 95, no. 12, pp. 2496–2510, 2018.

[15] M. Ran and Y. He, "Linearized Crank-Nicolson method for solving the nonlinear fractional diffusion equation with multi-delay," *International Journal of Computer Mathematics*, vol. 95, no. 12, pp. 2458–2470, 2018.

[16] Q. Zhang, M. Chen, Y. Xu, and D. Xu, "Compact θ-method for the generalized delay diffusion equation," *Applied Mathematics and Computation*, vol. 316, pp. 357–369, 2018.

[17] P. K. C. Wang and K. Chieh, *Asymptotic Stability of a Time-Delayed Diffusion System*, Elsevier, Amsterdam, Netherland, 1963.

[18] J. D. Murray, "Spatial structures in predator-prey communities a nonlinear time delay diffusional model," *Mathematical Biosciences*, vol. 31, no. 1–2, pp. 73–85, 1976.

[19] M. Cui, "Compact exponential scheme for the time fractional convection-diffusion reaction equation with variable coefficients," *Journal of Computational Physics*, vol. 280, pp. 143–163, 2015.

[20] M. Cui and F. Geng, "A computational method for solving one-dimensional variable-coefficient Burgers equation," *Applied Mathematics and Computation*, vol. 188, no. 2, pp. 1389–1401, 2007.

[21] W. W. Mohammed, S. Albosaily, N. Iqbal, and M. El-Morshedy, "The effect of multiplicative noise on the exact solutions of the stochastic Burgers' equation," *Waves in Random and Complex Media*, pp. 1–13, 2021.

[22] Z. Ouyang, "Existence and uniqueness of the solutions for a class of nonlinear fractional order partial differential equations with delay," *Computers & Mathematics with Applications*, vol. 61, no. 4, pp. 860–870, 2011.

[23] F. A. Rihan, "Computational methods for delay parabolic and time-fractional partial differential equations," *Numerical Methods for Partial Differential Equations*, vol. 26, no. 6, pp. 1556–1571, 2010.

[24] V. G. Pimenov and S. H. Ahmed, "A numerical solution for a class of time fractional diffusion equations with delay," *International Journal of Applied Mathematics and Computer Science*, vol. 27, p. 3, 2017.

[25] Q. Zhang, M. Ran, and D. Xu, "Analysis of the compact difference scheme for the semilinear fractional partial differential equation with time delay," *Applicable Analysis*, vol. 96, no. 11, pp. 1867–1884, 2017.

[26] A. Mohebbi, "Finite difference and spectral collocation methods for the solution of semilinear time fractional convection-reaction-diffusion equations with time delay," *Journal of Applied Mathematics and Computing*, vol. 61, no. 1, pp. 635–656, 2019.

[27] N. Sweilam, S. Al-Mekhlafi, S. Shatta, and D. Baleanu, "Numerical study for two types variable-order Burgers' equations with proportional delay," *Applied Numerical Mathematics*, vol. 156, pp. 364–376, 2020.

[28] I. Jaradat, M. Alquran, S. Momani, and D. Baleanu, "Numerical schemes for studying biomathematics model inherited with memory-time and delay-time," *Alexandria Engineering Journal*, vol. 59, no. 5, pp. 2969–2974, 2020.

[29] M. S. Rawashdeh and S. Maitama, "Solving coupled system of nonlinear PDE's using the natural decomposition method," *International Journal of Pure and Applied Mathematics*, vol. 92, pp. 757–776, 2014.

[30] N. Iqbal, R. Wu, and W. W. Mohammed, "Pattern formation induced by fractional cross-diffusion in a 3-species food chain model with harvesting," *Mathematics and Computers in Simulation*, vol. 188, pp. 102–119, 2021.

[31] N. Iqbal and R. Wu, "Pattern formation by fractional cross-diffusion in a predator-prey model with Beddington-DeAngelis type functional response," *International Journal of Modern Physics A*, vol. 33, Article ID 1950296, 2019.

[32] M. S. Rawashdeh and S. S. Maitama, "Solving nonlinear ordinary differential equations using the NDM," *Journal of Applied Analysis & Computation*, vol. 5, no. 1, pp. 77–88, 2015.

[33] M. Rawashdeh and S. Maitama, "Finding exact solutions of nonlinear PDEs using the natural decomposition method," *Mathematical Methods in the Applied Sciences*, vol. 40, no. 1, pp. 223–236, 2017.

[34] N. Iqbal, H. Yasmin, A. Ali, A. Bariq, M. M. Al-Sawalha, and W. W. Mohammed, "Numerical methods for fractional-order fornberg-whitham equations in the sense of atangana-baleanu derivative," *Journal of Function Spaces*, vol. 2021, pp. 1–10, Article ID 2197247, 2021.

[35] N. Iqbal, H. Yasmin, A. Rezaiguia, J. Kafle, A. O. Almatroud, and T. S. Hassan, "Analysis of the fractional-order kk equation via novel transforms," *Journal of Mathematics*, vol. 2021, pp. 1–13, Article ID 2567927, 2021.

[36] H. Eltayeb, Y. Abdalla, I. Bachar, and M. Khabir, "Fractional telegraph equation and its solution by natural transform decomposition method," *Symmetry*, vol. 11, no. 3, p. 334, 2019.

[37] M. H. Cherif, D. Ziane, and K. Belghaba, "Fractional natural decomposition method for solving fractional system of nonlinear equations of unsteady flow of a polytropic gas," *Nonlinear Studies*, vol. 25, pp. 753–764, 2018.

[38] A. S. Abdel-Rady, S. Z. Rida, A. A. M. Arafa, and H. R. Abedl-Rahim, "Natural transform for solving fractional models," *Journal of Applied Mathematics and Physics*, vol. 03, no. 12, pp. 1633–1644, 2015.

[39] J. Xu, H. Khan, H. Khan et al., "The analytical analysis of nonlinear fractional-order dynamical models," *AIMS Mathematics*, vol. 6, no. 6, pp. 6201–6219, 2021.

[40] H. Liu, H. Khan, R. Shah, A. A. Alderremy, S. Aly, and D. Baleanu, "On the fractional view analysis OF Keller-Segel equations with sensitivity functions," *Complexity*, vol. 2020, 2020.

[41] H. M. Srivastava, R. Shah, H. Khan, and M. Arif, "Some analytical and numerical investigation of a family of fractional-order Helmholtz equations in two space dimensions," *Mathematical Methods in the Applied Sciences*, vol. 43, no. 1, pp. 199–212, 2020.

[42] M. G. Sakar, F. Uludag, and F. Erdogan, "Numerical solution of time-fractional nonlinear PDEs with proportional delays by homotopy perturbation method," *Applied Mathematical Modelling*, vol. 40, no. 13-14, pp. 6639–6649, 2016.

[43] A. AK, "Application of differential transform method on nonlinear integro-differential equations with proportional delay," *Neural Computing & Applications*, vol. 24, pp. 391–397, 2014.

Hindawi
Complexity
Volume 2022, Article ID 2219570, 23 pages
https://doi.org/10.1155/2022/2219570

WILEY | Hindawi

Research Article

Marshall–Olkin Extended Gumbel Type-II Distribution: Properties and Applications

Farwa Willayat,[1] Naz Saud,[2] Muhammad Ijaz,[3] Anita Silvianita,[4] and Mahmoud El-Morshedy[5,6]

[1]*Department of Statistics, Gulab Devi Educational Complex, Lahore, Pakistan*
[2]*Department of Statistics, Lahore College for Women University, Lahore, Pakistan*
[3]*Department of Mathematics and Statistics, University of Haripur, Haripur, Pakistan*
[4]*School of communications and business, Telkom University, Jalan Terusan Buah Batu 1, Bandung 40257, Indonesia*
[5]*Department of Mathematics, College of Sciences and Humanities in Al-Kharj, Prince Sattam Bin Abdulaziz University, Al-Kharj 11942, Saudi Arabia*
[6]*Department of Mathematics, Faculty of Science, Mansoura University, Mansoura 35516, Egypt*

Correspondence should be addressed to Muhammad Ijaz; ijaz.statistics@gmail.com

Received 10 November 2021; Accepted 4 December 2021; Published 30 January 2022

Academic Editor: Fathalla A. Rihan

Due to the advance computer technology, the use of probability distributions has been raised up to solve the real life problems. These applications are found in reliability engineering, computer sciences, economics, psychology, survival analysis, and some others. This study offers a new probability model called Marshall–Olkin Extended Gumbel Type-II (MOEGT-II) which can model various shapes of the failure rate function. The proposed distribution is capable to model increasing, decreasing, reverse J-shaped, and upside down bathtub shapes of the failure rate function. Various statistical properties of the proposed distribution are derived such as alternate expressions for the density and distribution function, special cases of MOEGT-II distribution, quantile function, Lorenz curve, and Bonferroni curve. Estimation of the unknown parameters is carried out by the method of maximum likelihood. A simulation study is conducted using three different iterative methods with different samples of sizes n. The usefulness and potentiality of the MOEGT-II distribution have been shown using three real life data sets. The MOEGT-II distribution has been demonstrated as better fit than Exponentiated Gumbel Type-II (EGT-II), Marshall–Olkin Gumbel Type-II (MOGT-II), Gumbel Type-II (GT-II), Marshall–Olkin–Frechet (MOF), Frechet (F), Burr III, Log Logistic (LL), Beta Inverse Weibull (BIW), and Kumaraswamy Inverse Weibull (KIW) distributions.

1. Introduction

Probability distributions are mostly used in survival analysis for modeling data because it provides insight interest in the nature of various parameters and functions mainly in the failure rate function. The lifetime distributions are used in reliability engineering and life data analysis. For example, Aksoy [1] used the Gamma distribution to model the rainfall data, the Weibull distribution has been used by Keshavan et al. [2] to model fracture strength of glass data, Al-Hasan and Nigmatullin [3] worked out the analysis of wind speed data, and environmental radioactivity data were analyzed by Dahm et al. [4] since the real data set values have different structures and we cannot model these complex data sets with the existing distributions. The existing verities of models can only be applied to the data that have monotonic increasing or decreasing failure function. Surprisingly, this gap has been covered by many researchers working in distribution theory. In this way, the exponential distribution has been modified by many researchers; for example, Gupta and Kundu [5, 6] defined new families of exponential distribution; exponentiated generalized class of distributions was introduced by Cordeiro et al. [7]; and Exponentiated Generalized Gumbel distribution was proposed by Andrade et al. [8].

A family of distribution was introduced by Marshall and Olkin [9] by developing a new method for adding a parameter to the existing probability distributions. Special cases of this family were discussed by using Exponential, Weibull, Gamma, and Log Normal distribution. The survival function of a two parametric exponential distribution was obtained by using the survival function of one-parametric exponential distribution. As a result, it was found that the new extended family might seem as much better competitor than the gamma and Weibull families; likewise, two-parametric Weibull distribution was used to derive the survival function of three-parametric Weibull distribution.

The cumulative distribution function (cdf) of Marshall–Olkin family is given by

$$G_X(x) = \frac{F(x)}{1-(1-\alpha)\overline{F}(x)}, \quad -\infty < x < \infty,\ 0 < \alpha < \infty, \tag{1}$$

where $F(x)$ is the cdf of a continuous type distribution and "α" is shape parameter. The corresponding probability density function (pdf) of Marshall–Olkin family is

$$g(x) = \frac{\alpha f(x)}{(1-(1-\alpha))\overline{F}(x)^2}, \quad -\infty < x < \infty,\ 0 < \alpha < \infty. \tag{2}$$

In recent years, many researchers have used Marshall–Olkin technique to modify different existing models. For example, Marshall–Olkin Bivariate semipareto (MO-BSP) distribution and Marshall–Olkin Bivariate Pareto (MO-BP) distribution were proposed by Alice and Jose [10]. A three-parameter lifetime distribution named as Marshall–Olkin extended Weibull distribution was introduced by Ghitany et al. [11]. Ghitany et al. [12] derived a new probability distribution to model life time data by extending the Lomax distribution, and this new distribution is called as the Marshall–Olkin Extended Lomax distribution. A four-parameter continuous distribution named as Marshall–Olkin q Weibull distribution and max-min processes was proposed by Jose et al. [13]. Jose [14] presented a new Marshall–Olkin Extended Uniform distribution by using the Marshall–Olkin model on Extended Uniform distribution. The Marshall–Olkin Extended Lindley distribution was introduced by Ghitany et al. [15]; The Marshall–Olkin–Frechet Distribution was proposed by Krishna et al. [16]. Al-Saiari et al. [17] introduced a new three-parameter distribution named as Marshall–Olkin Extended Burr Type XII Distribution.A four-parameter distribution named as a Marshall–Olkin Exponential Weibull (MOEW) distribution for skewed positive data was proposed by Pogány et al. [18]. Saboor and Pogány [19] suggested a new distribution named as the Marshall–Olkin Gamma Weibull (MOGW) distribution. Marshall–Olkin Extended Weibull Distribution was proposed by Ahmad et al. [20]. Marshall–Olkin additive Weibull distribution was proposed by Afify et al. [21]. Exponentiated Gumbel type-II distributed was discovered by Biswas and Gupta [22]. Gillariose et al. [23] introduced a new Marshall–Olkin Modified Lindley Distribution; Marshall Olkin Power Lomax distribution was proposed by Haq et al. [24]; Ogunde et al. [25] proposed the Extended Gumbel Type-II distribution; and Almetwally et al. [26] derived various properties of Marshall–Olkin Alpha Power Weibull distribution.

The Exponentiated Generalized Gumbel distribution was proposed by Andrade et al. [8]. Okorie et al. [27] introduced the Kumaraswamy G Exponentiated Gumbel type-II distribution.

The generalized form of the standard Gumbel type-II distribution was derived by Okorie et al. [28] called Exponentiated Gumbel type-II (EGT-II). The cdf, survival function, and pdf are

$$F_X(x) = 1-\left(1-\ \exp^{-\lambda x^{-\rho}}\right)^{\theta}, \quad x > 0, \lambda, \rho, \theta > 0, \tag{3}$$

$$S_X(x) = \left(1-\ \exp^{-\lambda x^{-\rho}}\right)^{\theta}, \quad x > 0, \lambda, \rho, \theta > 0, \tag{4}$$

$$f_X(x) = \theta\rho\lambda x^{-\rho-1}\exp^{-\lambda x^{-\rho}}\left(1-\ \exp^{-\lambda x^{-\rho}}\right)^{\theta-1}, \quad x > 0, \lambda, \rho, \theta > 0, \tag{5}$$

where "λ" is the scale parameter and "ρ" and "θ" are shape parameters.

The Exponentiated Gumbel Type-II Distribution is used for modeling complex data sets

However, a Gumbel Type-II distribution cannot handle the analysis of complex data sets. To deal with this problem, some shape parameters have been added to Gumbel Type-II to improve the model flexibility.

The current research study is motivated by producing new probability models by adding a shape and scale parameter. More surprisingly, there was a gap to modify the Gumbel type-II distribution by using the Marshall–Olkin family of distributions. In this study, we derive a new probability distribution by employing the cdf and pdf of Gumbel type-II in the Marshall–Olkin family of distributions called Marshall–Olkin Extended Gumbel Type-II (MOEGT-II) distribution.

This article is organized as follows. In section 2, we present Marshall–Olkin Extended Gumbel Type-II (MOEGT-II) distribution. In section 3, reliability analysis of MOEGT-II distribution is derived. Several mathematical properties of MOEGT-II distribution are derived in section 4. Measure of uncertainty and inequality of our proposed distribution are derived in section 5. Order statistics of the

proposed distribution is derived in section 6. Estimation of the parameters by maximum likelihood is given in section 7, and in section 8, a simulation study is discussed. In section 9, we analyze three real data sets and compared our proposed distribution with different competent distributions. Finally, we conclude the paper in section 10.

2. Marshall–Olkin Extended Gumbel Type-II Distribution

The cdf of MOEGT-II distribution can be obtained using (3) and (4) in (1) as

$$G_X(x) = \frac{1-\left(1-\exp^{-\lambda x^{-\rho}}\right)^{\theta}}{1-(1-\alpha)\left(1-\exp^{-\lambda x^{-\rho}}\right)^{\theta}}, \quad x>0, \alpha, \lambda, \rho, \theta > 0, \tag{6}$$

where "λ" is the scale parameter and "α," "θ," and "ρ" are shape parameters.

The corresponding pdf can be obtained by substituting (4) and (5) in (2), and we have

$$g_X(x) = \frac{\alpha\theta\rho\lambda x^{-\rho-1}\exp^{-\lambda x^{-\rho}}\left(1-\exp^{-\lambda x^{-\rho}}\right)^{\theta-1}}{\left(1-(1-\alpha)\left(1-\exp^{-\lambda x^{-\rho}}\right)^{\theta}\right)^{2}}, \tag{7}$$

$$x>0, \alpha, \lambda, \rho, \theta > 0.$$

Figures 1 and 2 define the plot of pdf with different values of parameters. We observed that the shape of density function is positively skewed, modified bathtub shape, and reverse *J*-shaped curve. From Figure 2, it can be observed that the peak of the curves shows a gradual rising behavior; however, a reverse bathtub curve can be also examined.

3. Reliability Analysis of Marshall–Olkin Extended Gumbel Type-II Distribution

In this section, the survival function (SF), hazard rate function (HRF), reverse hazard rate function (RHRF), and cumulative hazard rate function (CHRF) of MOEGT-II distribution are derived.

The survival function of MOEGT-II distribution is

$$\overline{G}(x) = \frac{\alpha\left(1-\exp^{-\lambda x^{-\rho}}\right)^{\theta}}{1-(1-\alpha)\left(1-\exp^{-\lambda x^{-\rho}}\right)^{\theta}}, \quad x>0, \alpha, \lambda, \rho, \theta > 0, \tag{8}$$

The graph of survival function of MOEGT-II distribution is shown in Figure 3. It is demonstrated from Figures 3(a)–3(c) that curves are in a downward direction; however, varying the parameters produces a decreasing trend also.

The hazard rate function of MOEGT-II distribution is

$$h_X(x) = \frac{\theta\rho\lambda x^{-\rho-1}\exp^{-\lambda x^{-\rho}}\left(1-\exp^{-\lambda x^{-\rho}}\right)^{-1}}{1-(1-\alpha)\left(1-\exp^{-\lambda x^{-\rho}}\right)^{\theta}}, \tag{9}$$

$$x>0, \alpha, \lambda, \rho, \theta > 0.$$

The graph of hazard rate function of MOEGT-II distribution is presented in Figure 4. From Figure 4, it can be observed that for different values of parameters, the failure rate of MOEGT-II distribution is increasing, decreasing, reverse J-shaped, and upside down bathtub shape.

The reverse hazard rate function of MOEGT-II distribution is

$$R_X(x) = \frac{\alpha\theta\rho\lambda x^{-\rho-1}\exp^{-\lambda x^{-\rho}}\left(1-\exp^{-\lambda x^{-\rho}}\right)^{\theta-1}\left[1-\left(1-\exp^{-\lambda x^{-\rho}}\right)^{\theta}\right]^{-1}}{1-(1-\alpha)\left(1-\exp^{-\lambda x^{-\rho}}\right)^{\theta}}. \tag{10}$$

The graph of reverse hazard rate function of MOEGT-II distribution is presented in fig. Figures 5(a)–5(c) clearly show that the reverse hazard rate function has a decreasing behavior.

The cumulative hazard rate function of MOEGT-II distribution is as follows:

$$H_X(x) = -\ln\left[\frac{\alpha\left(1-\exp^{-\lambda x^{\rho}}\right)^{\theta}}{1-(1-\alpha)\left(1-\exp^{-\lambda x^{-\rho}}\right)^{\theta}}\right]. \tag{11}$$

The graph of cumulative hazard rate function of MOEGT-II distribution is presented in Figure 6. Figures 6(a)–6(c) clearly show that the cumulative hazard rate function has an increasing behavior.

4. Properties of MOEGT-II Distribution

4.1. Alternate Expression for Distribution Function. For any positive real number "a" and for $|z|<1$, we have the generalized binomial expansion:

$$(1-z)^{-a} = \sum_{k=0}^{\infty}\frac{\Gamma(a+k)}{\Gamma(a)}\frac{z^k}{k!}. \tag{12}$$

Consider the power series expansion:

$$(1-z)^{\theta-1} = \sum_{k=0}^{\infty}(-1)^k\frac{\Gamma\theta}{\Gamma(\theta-k)}\frac{z^k}{k!}, \tag{13}$$

which is valid for $|z|<1$ and any real noninteger θ.

Applying the generalized binomial expansion (12) and power series expansion (13) twice in (6), we get

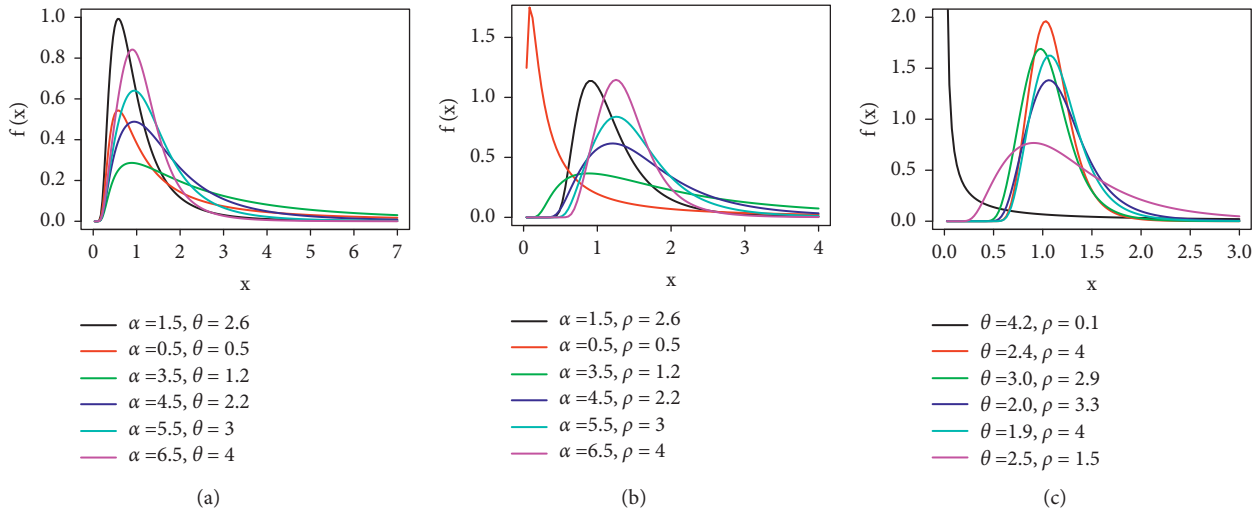

Figure 1: Pdf for different values of parameterα, θ, and ρ with $\lambda = 1$ for (a) $\rho = 1.2$; (b) $\theta = 1.5$; (c) $\alpha = 3.5$.

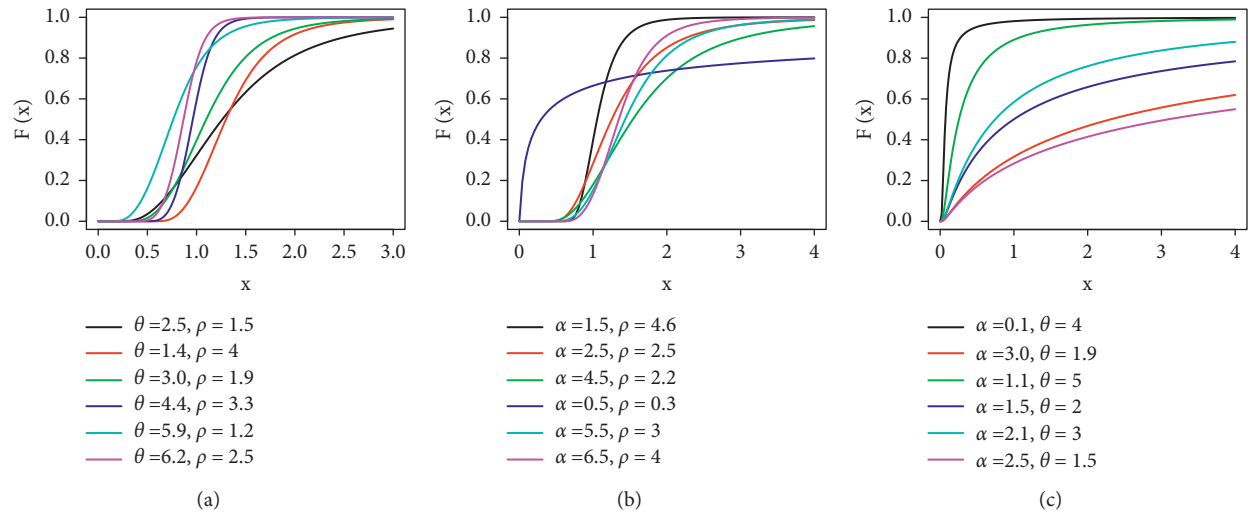

Figure 2: Cdf for different values of parameter α, θ, and ρ with $\lambda = 1$ for (a) $\alpha = 4.5$; (b) $\theta = 1.5$; (c) $\rho = 0.5$.

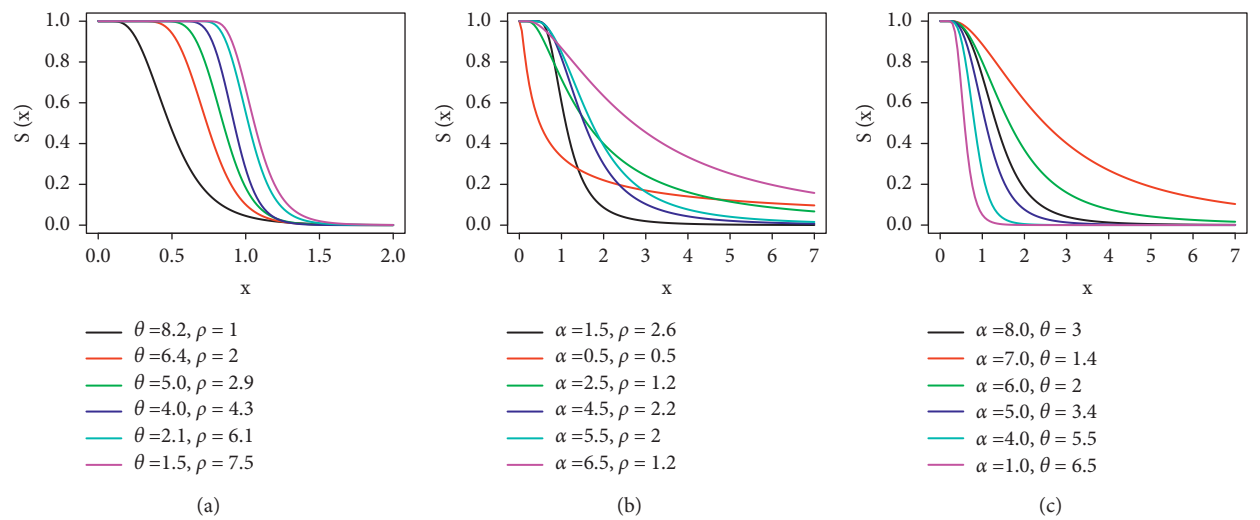

Figure 3: SF for different values of parameterα, θ, and ρ with $\lambda = 1$ for (a) $\alpha = 2$; (b) $\theta = 1.5$; (c) $\rho = 1.5$.

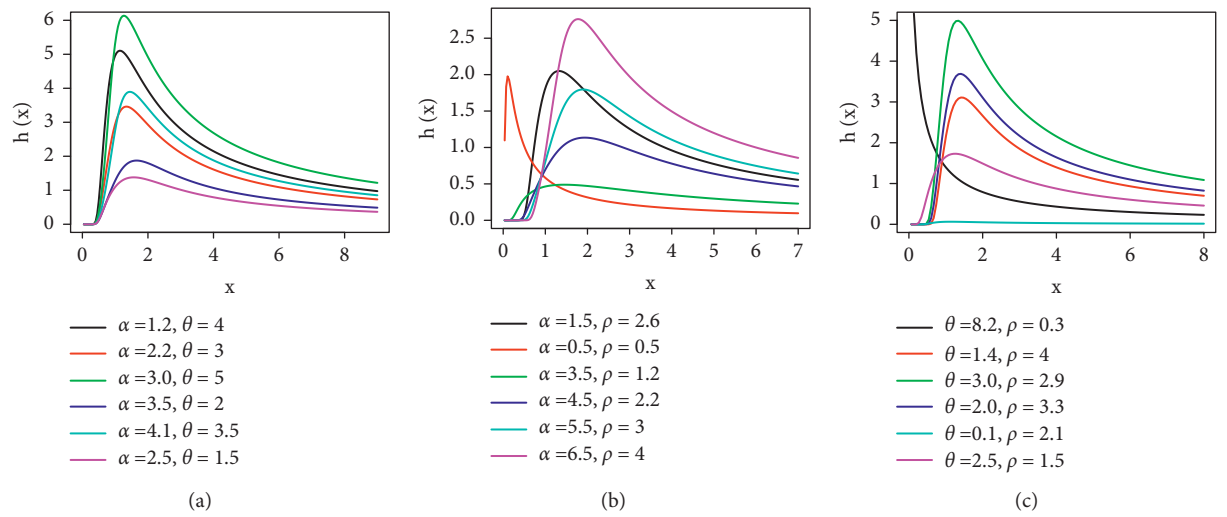

Figure 4: HRF for different values of parameter α, θ, and ρ with $\lambda = 1$ for (a) $\rho = 2.2$; (b) $\theta = 1.5$; (c) $\alpha = 2.0$.

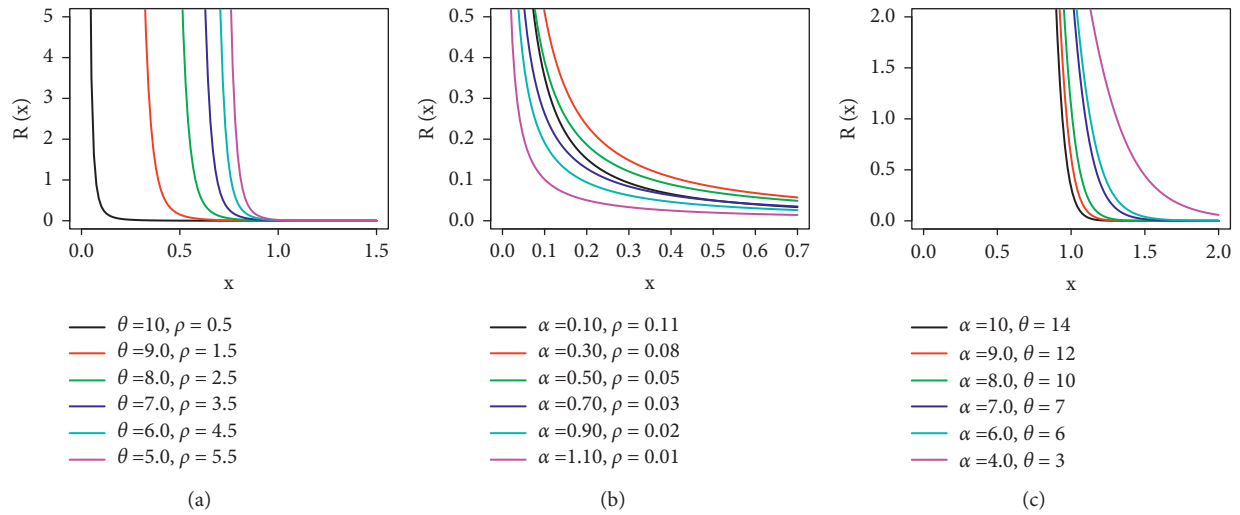

Figure 5: RHRF for different values of parameter α, θ, and ρ with $\lambda = 1$ for (a) $\alpha = 0.01$; (b) $\theta = 1.2$; (c) $\rho = 2.5$.

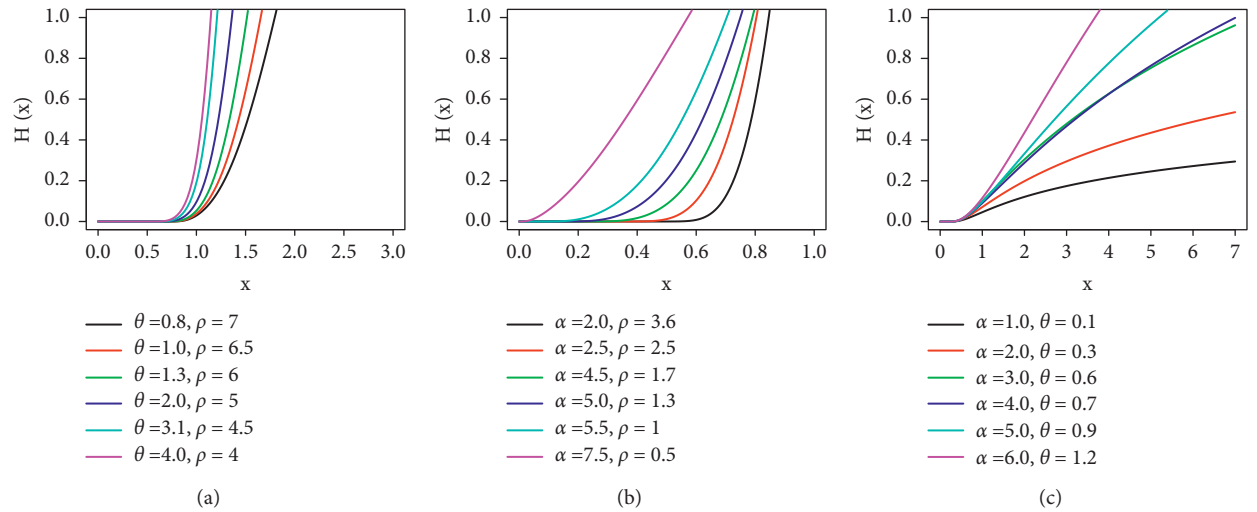

Figure 6: CHRF for different values of parameter α, θ, and ρ with $\lambda = 1$ for (a) $\alpha = 15$; (b) $\theta = 8.5$; (c) $\rho = 1.5$.

$$G_X(x) = \sum_{k=0}^{\infty} w_k\left(\exp^{-k\lambda x^{-\rho}}\right), \tag{14}$$

where

$$w_k = \sum_{i=0}^{\infty}\sum_{j=0}^{\infty} (1-\alpha)^i \frac{(-1)^{j+k}}{i!\,j!k!} \frac{\Gamma(1+i)}{\Gamma(1)} \frac{\Gamma 2}{\Gamma(2-j)} \frac{\Gamma(\theta[i+j]+1)}{\Gamma(\theta[i+j]+1-k)}. \tag{15}$$

4.2. Alternate Expression for Density Function. Applying the generalized binomial expansion (12) and power series expansion (13) in equation (7), we get

$$g_X(x) = \alpha\theta\rho\lambda x^{-\rho-1} \sum_{f=0}^{\infty} t_f\left(\exp^{-(f+1)\lambda x^{-\rho}}\right), \tag{16}$$

where

$$t_f = \sum_{i=0}^{\infty} (\overline{\alpha})^i \frac{(-1)^f}{i!\,f!} \frac{\Gamma(2+i)}{\Gamma(2)} \frac{\Gamma(\theta[i+1])}{\Gamma(\theta[i+1]-f)}. \tag{17}$$

4.3. Special Cases. For different values of parameters, the following distributions are obtained as special cases of MOEGT-II distribution.

Case 1. If substitute $\alpha = 1$ in (6), we get the Exponentiated Gumbel Type-II (EGT-II) distribution.

$$G_X(x) = 1 - \left(1 - \exp^{-\lambda x^{-\rho}}\right)^{\theta}, \quad x > 0, \lambda, \rho, \theta > 0. \tag{18}$$

Case 2. If substitute $\theta = 1$ in (6), we get the Marshall–Olkin Gumbel Type-II (MOGT-II) distribution.

$$G_X(x) = \frac{\exp^{-\lambda x^{-\rho}}}{1-(1-\alpha)\left(1 - \exp^{-\lambda x^{-\rho}}\right)}, \quad x > 0, \lambda, \alpha, \rho > 0. \tag{19}$$

Case 3. If substitute $\alpha = \theta = 1$ in (6), we get the Gumbel Type-II (GT-II) distribution.

$$G_X(x) = \exp^{-\lambda x^{-\rho}}, \quad x > 0, \lambda, \rho > 0. \tag{20}$$

Case 4. If substitute $\alpha = 1$ and $\lambda = \lambda^{\rho}$ in (6), we get the Exponentiated Frechet (EF) distribution.

$$G_X(x) = 1 - \left(1 - \exp^{-(\lambda/x)^{\rho}}\right)^{\theta}, \quad x > 0, \lambda, \theta, \rho > 0. \tag{21}$$

Case 5. If substitute $\alpha = \theta = 1$ and $\lambda = \lambda^{\rho}$, we get the Frechet (F) distribution.

$$G_X(x) = \exp^{-(\lambda/x)^{\rho}}, \quad x > 0, \lambda, \rho > 0. \tag{22}$$

Case 6. If substitute $\theta = 1$ and $\lambda = \lambda^{\rho}$, we get the Marshall–Olkin–Frechet (MOF) distribution.

$$G_X(x) = \frac{\exp^{-(\lambda/x)^{\rho}}}{1-(1-\alpha)\left(1 - \exp^{-(\lambda/x)^{\rho}}\right)}, \quad x > 0, \lambda, \alpha, \rho > 0. \tag{23}$$

4.4. Quantile Function. Quantile function gives the value of the random variable at a particular probability level in the given probability distribution. Quantile function is also known as inverse cumulative distribution.

$$x_q = \left[-\frac{1}{\lambda}\ln\left(1 - \left[\frac{1-q(1-\alpha)}{1-q}\right]^{-1/\theta}\right)\right]^{-1/p}. \tag{24}$$

The median for MOEGT-II distribution can be obtained by substituting $q = 0.5$ in the above expression:

$$\text{median} = \left[-\frac{1}{\lambda}\ln\left(1 - (1+\alpha)^{-1/\theta}\right)\right]^{-1/p}, \tag{25}$$

4.5. Characteristic Function. The characteristic function of MOEGT-II distribution is obtained by substituting (16) in characteristic function formula:

$$\begin{aligned}\rho_x(t) &= \int_0^{\infty} \exp(itx) g_X(x)\mathrm{d}x \\ &= \alpha\theta\rho\lambda \sum_{f=0}^{\infty} t_f \int_0^{\infty} \exp(itx) x^{-\rho-1}\left(\exp^{-(f+1)\lambda x^{-\rho}}\right)\mathrm{d}x.\end{aligned} \tag{26}$$

Making the substitution $\lambda x^{-\rho} = u$ and after simplification, we get

$$\rho_x(t) = \alpha\theta \sum_{f=0}^{\infty} t_f \int_0^{\infty} \exp\left(it\lambda^{1/\rho}u^{-1/\rho}\right)\left(\exp^{-(f+1)u}\right)\mathrm{d}u. \tag{27}$$

We have

$$\exp^{tx} = \sum_{j=0}^{\infty} \frac{(tx)^j}{j!}. \tag{28}$$

Using the above expression, we get

$$\int_0^{\infty} \exp(-at)t^b \mathrm{d}t = \frac{\Gamma(b+1)}{a^{b+1}}. \tag{29}$$

Using expressions (28)and (29) in the above equation, we get the characteristic function of MOEGT-II distribution.

$$\rho_x(t) = \alpha\theta \sum_{f=0}^{\infty} t_f \sum_{s=0}^{\infty} \frac{\left(it\lambda^{1/\rho}\right)^s}{s!} \frac{\Gamma(-s/\rho+1)}{(f+1)^{-s/\rho+1}}, \tag{30}$$

under condition $(s/\rho < 1)$.

4.6. Moment Generating Function. Moment generating function can be defined as follows:

$$M_X(t) = \sum_{r=0}^{\infty} \frac{t^r}{r!} E(X^r), \tag{31}$$

where

$$E(X^r) = \alpha\theta\rho\lambda \sum_{f=0}^{\infty} t_f \int_0^{\infty} x^{r-(\rho+1)} \left(\exp^{-(f+1)\lambda x^{-\rho}}\right) \mathrm{d}x. \tag{32}$$

Making the substitution $\lambda x^{-\rho} = u$ and using expansion (29) in the above equation, we get

$$E(X^r) = \alpha\theta\lambda^{r/\rho} \sum_{f=0}^{\infty} t_f \frac{\Gamma(1 - r/\rho)}{(f+1)^{1-r/\rho}}, \tag{33}$$

under condition $(r/\rho < 1)$.

Substituting (33) in (31), we have

$$M_X(t) = \sum_{r=0}^{\infty} \frac{t^r}{r!} \alpha\theta\lambda^{r/\rho} \sum_{f=0}^{\infty} t_f \frac{\Gamma(1 - r/\rho)}{(f+1)^{1-r/\rho}}, \tag{34}$$

which is the moment generating function of MOEGT-II distribution. For different values of "r," i.e., $r = 1, 2, 3, 4$ in (33), we can obtain first four arbitrary moments:

$$\begin{aligned}
\mu_1' &= E(X) = \alpha\theta\lambda^{1/\rho} \sum_{f=0}^{\infty} t_f \frac{\Gamma(1 - 1/\rho)}{(f+1)^{1-1/\rho}}, \quad \text{under the condition} \left(\frac{1}{\rho} < 1\right), \\
\mu_2' &= E\left(X^2\right) = \alpha\theta\lambda^{2/\rho} \sum_{f=0}^{\infty} t_f \frac{\Gamma(1 - 2/\rho)}{(f+1)^{1-2/\rho}}, \quad \text{under the condition} \left(\frac{2}{\rho} < 1\right), \\
\mu_3' &= E\left(X^3\right) = \alpha\theta\lambda^{3/\rho} \sum_{f=0}^{\infty} t_f \frac{\Gamma(1 - 3/\rho)}{(f+1)^{1-3/\rho}}, \quad \text{under the condition} \left(\frac{3}{\rho} < 1\right), \\
\mu_4' &= E\left(X^4\right) = \alpha\theta\lambda^{4/\rho} \sum_{f=0}^{\infty} t_f \frac{\Gamma(1 - 4/\rho)}{(f+1)^{1-4/\rho}}, \quad \text{under the condition} \left(\frac{4}{\rho} < 1\right).
\end{aligned} \tag{35}$$

4.7. Moments about Mean. Moments about means are

$$\begin{aligned}
\mu_1 &= 0, \\
\mu_2 &= \lambda^{2/\rho} \left(\alpha\theta \sum_{f=0}^{\infty} t_f \frac{\Gamma(1 - 2/\rho)}{(f+1)^{1-2/\rho}} - \left[\alpha\theta \sum_{f=0}^{\infty} t_f \frac{\Gamma(1 - 1/\rho)}{(f+1)^{1-1/\rho}} \right]^2 \right),
\end{aligned} \tag{36}$$

under the condition $(r/\rho < 1)$ for $r = 1, 2$.

$$\cdot\mu_3 = \lambda^{3/\rho} \left[\left[\alpha\theta \sum_{f=0}^{\infty} t_f \frac{\Gamma(1 - 3/\rho)}{(f+1)^{1-3/\rho}} - 3 \left(\alpha\theta \sum_{f=0}^{\infty} t_f \frac{\Gamma(1 - 2/\rho)}{(f+1)^{1-2/\rho}} \right) \left(\alpha\theta \sum_{f=0}^{\infty} t_f \frac{\Gamma(1 - 1/\rho)}{(f+1)^{1-1/\rho}} \right) + 2 \left(\alpha\theta \sum_{f=0}^{\infty} t_f \frac{\Gamma(1 - 1/\rho)}{(f+1)^{1-1/\rho}} \right)^3 \right], \tag{37}$$

under the condition $(r/\rho < 1)$ for $r = 1, 2, 3$.

$$\begin{aligned}
\mu_4 = \lambda^{4/\rho} \Bigg[& \alpha\theta \sum_{f=0}^{\infty} t_f \frac{\Gamma(1 - 4/\rho)}{(f+1)^{1-4/\rho}} - 4 \left(\alpha\theta \sum_{f=0}^{\infty} t_f \frac{\Gamma(1 - 3/\rho)}{(f+1)^{1-3/\rho}} \right) \left(\alpha\theta \sum_{f=0}^{\infty} t_f \frac{\Gamma(1 - 1/\rho)}{(f+1)^{1-1/\rho}} \right) \\
& + 6 \left(\alpha\theta \sum_{f=0}^{\infty} t_f \frac{\Gamma(1 - 2/\rho)}{(f+1)^{1-2/\rho}} \right) \left(\alpha\theta \sum_{f=0}^{\infty} t_f \frac{\Gamma(1 - 1/\rho)}{(f+1)^{1-1/\rho}} \right)^2 - 3 \left(\alpha\theta \sum_{f=0}^{\infty} t_f \frac{\Gamma(1 - 1/\rho)}{(f+1)^{1-1/\rho}} \right)^4 \Bigg],
\end{aligned} \tag{38}$$

under the condition $(r/\rho < 1)$ for $r = 1, 2, 3, 4$.

4.8. Mean, Variance, Skewness, and Kurtosis. The mean and variance are provided in equations (35) and (36), and skewness and kurtosis of MOEGT-II distribution can be obtained as follows:

$$\begin{aligned}\text{skewness} &= \sqrt{\beta_1}\\ &= \frac{\mu_3}{\mu_2^{3/2}},\end{aligned} \tag{39}$$

Using (36) and (37), we have

$$\text{skewness} = \frac{\left(\sum_{f=0}^{\infty} t_f \Gamma(1-3/\rho)/(f+1)^{1-3/\rho} - 3\alpha\theta\left(\sum_{f=0}^{\infty} t_f \Gamma(1-2/\rho)/(f+1)^{1-2/\rho}\right)\left(\sum_{f=0}^{\infty} t_f \Gamma(1-1/\rho)/(f+1)^{1-1/\rho}\right)+2\alpha^2\theta^2\left(\sum_{f=0}^{\infty} t_f \Gamma(1-1/\rho)/(f+1)^{1-1/\rho}\right)^3\right)}{\sqrt{\alpha\theta}\left[\left(\sum_{f=0}^{\infty} t_f \Gamma(1-2/\rho)/(f+1)^{1-2/\rho} - \alpha\theta\left[\sum_{f=0}^{\infty} t_f \Gamma(1-1/\rho)/(f+1)^{1-1/\rho}\right]^2\right)\right]^{3/2}}, \tag{40}$$

under the condition $(r/\rho < 1)$ for $r = 1, 2, 3$.

$$\text{kurtosis} = \beta_2 = \frac{\mu_4}{\mu_2^2}. \tag{41}$$

Using (38) and (36), we have

$$\text{kurtosis} = \frac{\begin{aligned}&\left[\sum_{f=0}^{\infty} t_f \Gamma(1-4/\rho)/(f+1)^{1-4/\rho} - 4\alpha\theta\left(\sum_{f=0}^{\infty} t_f \Gamma(1-3/\rho)/(f+1)^{1-3/\rho}\right)\left(\sum_{f=0}^{\infty} t_f \Gamma(1-1/\rho)/(f+1)^{1-1/\rho}\right)\right.\\ &\left.+6\alpha^2\theta^2\left(\sum_{f=0}^{\infty} t_f\left(\Gamma(1-2/\rho)/(f+1)^{1-2/\rho}\right)\right)\left(\sum_{f=0}^{\infty} t_f\left(\Gamma(1-1/\rho)/(f+1)^{1-1/\rho}\right)\right)^2 - 3\alpha^3\theta^3\left(\sum_{f=0}^{\infty} t_f\left(\Gamma(1-1/\rho)/(f+1)^{1-1/\rho}\right)\right)^4\right]\end{aligned}}{\alpha\theta\left[\left(\sum_{f=0}^{\infty} t_f\left(\Gamma(1-2/\rho)/(f+1)^{1-2/\rho}\right) - \alpha\theta\left[\sum_{f=0}^{\infty} t_f\left(\Gamma(1-1/\rho)/(f+1)^{1-1/\rho}\right)\right]^2\right)\right]^2}, \tag{42}$$

under the condition $(r/\rho < 1)$ for $r = 1, 2, 3, 4$.

4.9. Mean Deviation. The mean deviation can be defined from mean or a median.

4.9.1. Mean Deviation about Mean. The mean deviation about mean is defined by Nadarajah and Kotz [29] with the following form:

$$M.D_{\overline{x}} = 2\left[\mu F(\mu) - \int_0^{\mu} x g(x)\mathrm{d}x\right]. \tag{43}$$

Substitute (16) in the above expression,making the substitution $(f+1)\lambda x^{-\rho} = s$, and after simplification, we get

$$\int_0^{\mu} x g(x)\mathrm{d}x = \alpha\theta\lambda^{1/\rho}\sum_{f=0}^{\infty} t_f (f+1)^{1/\rho-1}\Gamma\left[\left(1-\frac{1}{\rho}\right), (f+1)\lambda\mu^{-\rho}\right]. \tag{44}$$

From (14), substituting $x = \mu$, we get

$$G(\mu) = \sum_{k=0}^{\infty} w_k\left(\exp^{-k\lambda\mu^{-\rho}}\right). \tag{45}$$

By substituting (44) and (45) in (43), we get

$$M.D_{\overline{x}} = 2\mu\left(\sum_{k=0}^{\infty} w_k\left(\exp^{-k\lambda\mu^{-\rho}}\right)\right) - 2\left(\alpha\theta\lambda^{1/\rho}\sum_{f=0}^{\infty} t_f (f+1)^{(1/\rho)-1}\,\Gamma\left[\left(1-\frac{1}{\rho}\right), (f+1)\lambda\mu^{-\rho}\right]\right), \tag{46}$$

under the condition $((1/\rho) < 1)$ where μ is defined in (35).

4.9.2. Mean Deviation about Median. The mean deviation about median is defined by Nadarajah and Kotz [29] with the following form:

$$M \cdot D_{\tilde{x}} = E(x) + 2MF(M) - M - 2\int_0^M xg(x)\mathrm{d}x. \tag{47}$$

Substituting $\mu = M$ in (44), we get

$$\int_0^M xg(x)\mathrm{d}x = \alpha\theta\lambda^{1/\rho}\sum_{f=0}^{\infty} t_f (f+1)^{(1/\rho)-1}\Gamma\left[\left(1-\frac{1}{\rho}\right), (f+1)\lambda M^{-\rho}\right]. \tag{48}$$

Using (35), (25) and (48), then (47) equation becomes

$$\begin{aligned} M.D_{\tilde{x}} = {} & \alpha\theta\lambda^{(1/\rho)}\sum_{f=0}^{\infty} t_f \frac{\Gamma(1-1/\rho)}{(f+1)^{1-1/\rho}} + 2M\left[-\frac{1}{\lambda}\ln\left(1-(1+\alpha)^{(1/\theta)}\right)\right]^{-(1/\rho)} \\ & -M - 2\left(\alpha\theta\lambda^{(1/\rho)}\sum_{f=0}^{\infty} t_f (f+1)^{(1/\rho)-1}\Gamma\left[\left(1-\frac{1}{\rho}\right), (f+1)\lambda M^{-\rho}\right]\right), \end{aligned} \tag{49}$$

under the condition $((1/\rho) < 1)$ where M is median defined in (25).

4.10. Geometric Mean. The geometric mean of a random variable is defined by Abd El-Monsef and Ghoneim [30] with the following form:

$$\log G \cdot M = E(\log x), \tag{50}$$

where

$$E(\log x) = \int_0^{\infty} \log(x) g(x)\mathrm{d}x. \tag{51}$$

Substituting (16) in the above equation, making the substitution $(f+1)\lambda x^{-\rho} = t$, and after simplification, we get

$$\begin{aligned} \log G \cdot M &= E(\log x) \\ &= \alpha\theta\sum_{f=0}^{\infty} t_f (f+1)^{-1}\left[\frac{1}{\rho}\log(f+1) + \frac{1}{\rho}\log\lambda - \frac{1}{\rho}\int_0^{\infty}\log te^{-t}\mathrm{d}t\right], \end{aligned} \tag{52}$$

as

$$\int_0^{\infty}\log te^{-t}\mathrm{d}t = 0.5722. \tag{53}$$

Substituting the result in the above equation, we get the geometric mean of MOEGT-II distribution:

$$\log G \cdot M = \alpha\theta\sum_{f=0}^{\infty} t_f (f+1)^{-1}\left[\frac{1}{\rho}\log(f+1) + \frac{1}{\rho}\log\lambda - \frac{1}{\rho}(0.5722)\right]. \tag{54}$$

4.11. Harmonic Mean. The Harmonic mean is defined as

$$\frac{1}{H} = \int_0^{\infty}\frac{1}{x}g(x)\mathrm{d}x. \tag{55}$$

Substituting (16) in the above expression, making the substitution $(f+1)\lambda x^{-\rho} = t$, and after simplification, we get

$$\frac{1}{H} = \alpha\theta\lambda^{-(1/\rho)}\sum_{f=0}^{\infty} t_f (f+1)^{-(1+(1/\rho))}\int_0^{\infty} t^{(1+(1/\rho))-1}\exp^{-t}\mathrm{d}t. \tag{56}$$

The Gamma function is

$$\Gamma z = \int_0^{\infty} x^{z-1} \exp(-x)\mathrm{d}x. \tag{57}$$

So, using Gamma function (57) in the above equation, we get the Harmonic mean of MOEGT-II distribution:

$$\frac{1}{H} = \alpha\theta\lambda^{-(1/\rho)} \sum_{f=0}^{\infty} t_f (f+1)^{-(1+(1/\rho))}\Gamma\left(1+\frac{1}{\rho}\right). \tag{58}$$

5. Measure of Uncertainty and Inequality

In this section, the measure of uncertainty of MOEGT-II distribution has been derived including Renyi entropy and q^{th} entropy. Lorenz and Bonferroni curves are also derived as a measure of inequalities of MOEGT-II distribution.

5.1. Renyi Entropy. Renyi entropy is defined as

$$I_{X;R}(\delta) = \frac{1}{1-\delta}\log\left[I_X(\delta)\right], \tag{59}$$

where

$$I_X(\delta) = \int_R g_X^{\delta}(x)\mathrm{d}(x), \quad \text{for } \delta > 0 \text{ and } \delta \neq 1. \tag{60}$$

Substituting (7) in the above equation and then applying the generalized binomial expansion (12) and power series expansion (13), we get

$$I_X(\delta) = (\alpha\theta\rho\lambda)^{\delta} \sum_{i=0}^{\infty}\sum_{j=0}^{\infty} (\overline{\alpha})^i \frac{(-1)^j}{i!j!} \frac{\Gamma(2\delta+i)}{\Gamma(2\delta)} \frac{\Gamma(\theta[\delta+i]-\delta+1)}{\Gamma(\theta[\delta+i]-\delta+1-j)} \int_0^{\infty} \left(x^{-\rho-1}\right)^{\delta} \left(\exp^{-\lambda x^{-\rho}}\right)^{\delta+j} \mathrm{d}x. \tag{61}$$

Making the substitution $\lambda x^{-\rho} = u$ and after simplification, we get

$$I_X(\delta) = (\alpha\theta)^{\delta}\lambda^{-(\delta/\rho)+(1/\rho)}\rho^{\delta-1} \sum_{i=0}^{\infty}\sum_{j=0}^{\infty} (\overline{\alpha})^i \frac{(-1)^j}{i!j!} \frac{\Gamma(2\delta+i)}{\Gamma(2\delta)} \frac{\Gamma(\theta[\delta+i]-\delta+1)}{\Gamma(\theta[\delta+i]-\delta+1-j)} \int_0^{\infty} u^{(\delta+(\delta/\rho)-(1/\rho))-1} \left(\exp^{-(\delta+j)u}\right)\mathrm{d}u. \tag{62}$$

As we know,

$$\int_0^{\infty} \exp(-x\theta)x^{\alpha-1}\mathrm{d}x = \frac{\Gamma\alpha}{\theta^{\alpha}}. \tag{63}$$

Using expansion (63) in the above expression,

$$I_X(\delta) = (\alpha\theta)^{\delta}\lambda^{(1/\rho)(1-\delta)}\rho^{-(1-\delta)} \sum_{i=0}^{\infty}\sum_{j=0}^{\infty} (\overline{\alpha})^i \frac{(-1)^j}{i!j!} \frac{\Gamma(2\delta+i)}{\Gamma(2\delta)} \frac{\Gamma(\theta[\delta+i]-\delta+1)}{\Gamma(\theta[\delta+i]-\delta+1-j)} \frac{\Gamma((1/\rho)(\delta-1)+\delta)}{(\delta+j)^{1/\rho(\delta-1)+\delta}}. \tag{64}$$

Applying log on the above equation and then substituting the resulting equation in (59), we get the Renyi entropy of MOEGT-II distribution:

$$I_{X;R}(\delta) = \frac{\delta}{1-\delta}\log(\alpha\theta) + \frac{1}{\rho}\log\lambda - \log\rho + \frac{1}{1-\delta}\log\left[\sum_{i=0}^{\infty}\sum_{j=0}^{\infty} (\overline{\alpha})^i \frac{(-1)^j}{i!j!} \frac{\Gamma(2\delta+i)}{\Gamma(2\delta)} \frac{\Gamma(\theta[\delta+i]-\delta+1)}{\Gamma(\theta[\delta+i]-\delta+1-j)} \frac{\Gamma(1/\rho(\delta-1)+\delta)}{(\delta+j)^{1/\rho(\delta-1)+\delta}}\right], \tag{65}$$

under the condition ($\delta > 1$).

It can be observed from Table 1 that as values of parameters decrease, the value of Renyi entropy increases.

5.2. q^{th} Entropy. q-entropy can be defined as

$$H_X(q) = \frac{1}{q-1}\log\left[1 - I_X(q)\right]. \tag{66}$$

Substituting $\delta = q$ in equation (64) and then substituting the resulting equation in the above expression, we get the q^{th} entropy of MOEGT-II distribution:

$$H_X(q) = \frac{1}{q-1}\log\left(1 - \left[(\alpha\theta)^q \lambda^{(1/\rho)(1-q)} \rho^{-(1-q)} \sum_{j=0}^{\infty} t_j\right]\right), \tag{67}$$

where

$$t_j = \sum_{i=0}^{\infty} (\overline{\alpha})^i \frac{(-1)^j}{i!\,j!} \frac{\Gamma(2q+i)}{\Gamma(2q)} \frac{\Gamma(\theta[q+i]-q+1)}{\Gamma(\theta[q+i]-q+1-j)} \frac{\Gamma(1/\rho(q-1)+q)}{(q+j)^{1/\rho(q-1)+q}}. \tag{68}$$

It can be observed from Table 2 that the value of q-Renyi entropy decreases as the values of parameters decrease.

5.3. Lorenz Curve. $L(x)$ denotes the Lorenz curve and is defined as

$$L(X) = \frac{G^*(x)}{E(x)}, \tag{69}$$

where

$$G^*(x) = \int_0^x \frac{wg(w)}{E(x)}\,\mathrm{d}w. \tag{70}$$

Substituting (16) and (69) in the above equation, we get

$$G^*(x) = \frac{\rho\lambda^{1-(1/\rho)}\sum_{f=0}^{\infty} t_f}{\sum_{f=0}^{\infty} t_f\left(\Gamma(1-1/\rho)/(f+1)^{1-1/\rho}\right)} \int_0^x w^{-\rho}\left(\exp^{-(f+1)\lambda w^{-\rho}}\right)\mathrm{d}w. \tag{71}$$

Making the substitution $(f+1)\lambda w^{-\rho} = z$ and after using upper incomplete gamma function, we get

$$G^*(x) = \frac{\sum_{f=0}^{\infty} t_f (f+1)^{-1+(1/\rho)}\,\Gamma[(1-1/\rho), (f+1)\lambda x^{-\rho}]}{\sum_{f=0}^{\infty} t_f (f+1)^{-1+(1/\rho)}\Gamma(1-1/\rho)}. \tag{72}$$

Putting (72) and (35) in (34), we get the Lorenz curve of MOEGT-II distribution as

$$L(x) = \frac{\sum_{f=0}^{\infty} t_f (f+1)^{-1+(1/\rho)}\Gamma[(1-1/\rho), (f+1)\lambda x^{-\rho}]}{\alpha\theta\lambda^{1/\rho}(\Gamma(1-(1/\rho)))^2\left(\sum_{f=0}^{\infty} t_f (f+1)^{-1+(1/\rho)}\right)^2}. \tag{73}$$

5.4. Bonferroni Curve. $B(x)$ denotes the Bonferroni Curve and is defined as

$$B(X) = \frac{L(x)}{G(x)}. \tag{74}$$

Substituting the result of Lorenz curve (73) and (14) in the above expression, we get the Bonferroni curve of MOEGT-II distribution as follows :

$$B(X) = \frac{\sum_{f=0}^{\infty} t_f (f+1)^{-1+(1/\rho)}\Gamma[(1-1/\rho), (f+1)\lambda x^{-\rho}]}{\alpha\theta\lambda^{(1/\rho)}(\Gamma(1-1/\rho))^2\left(\sum_{f=0}^{\infty} t_f (f+1)^{-1+1/\rho}\right)^2\sum_{k=0}^{\infty} w_k\left(\exp^{-k\lambda x^{-\rho}}\right)}. \tag{75}$$

Figure 7 defines the graph of Bonferroni and Lorenz curve.

6. Order Statistics

In this section, the density of k^{th} order statistics for MOEGT-II distribution has been derived. The r^{th} moments for the density of order statistics are obtained. The distribution of the median is also discussed.

6.1. Density of k^{th} Order Statistics. Let $x_1, x_2, \ldots, x_n$ be a random sample of size n from MOEGT-II density function, $g(x)$. Let $X_{k:n}$ denote the k^{th} order statistics. Then, the density function of k^{th} order statistics of the random variable $X_{k:n}$ can be obtained using

$$f_{X(k:n)}(x) = \frac{n!}{(k-1)!\,(n-k)!} f_X(x) \left[F_X(x)\right]^{k-1}\left[1 - F_X(x)\right]^{n-k}. \tag{76}$$

Substituting (6) and (7) in the above equation, after applying the generalized binomial expansion (12) and power series expansion (13), we get the final expression of density of k^{th} order statistics of MOEGT-II distribution:

$$f_{X(k:n)}(x) = \sum_{h=0}^{\infty} C_{k:n}^{(h)} g(x; \lambda(h+1), \rho), \tag{77}$$

where

Table 1: Renyi entropy of the MOEGT-II for different combinations of parameters.

α	λ	ρ	θ	δ	Renyi entropy
6.5	4.9	3.3	4.2	1.8	0.013
4.0	2.9	2.5	4.1	1.7	0.098
3.5	2.8	2.0	3.2	1.5	0.323
2.9	1.9	1.7	2.5	1.4	0.426
2.8	1.4	1.5	2.3	1.3	0.462
2.4	1.0	0.9	1.8	1.2	0.752
2.3	0.8	0.7	1.6	1.15	0.860
1.5	0.7	0.5	1.3	1.12	0.927
1.4	0.5	0.4	1.0	1.10	0.975
1.3	0.4	0.3	0.99	1.01	0.978

Table 2: q^{th} entropy of the MOEGT-II for different combinations of parameters.

α	λ	ρ	θ	δ	q^{th} entropy
2.0	0.7	3.1	3.0	0.9	16.875
1.9	0.6	2.5	2.9	0.8	11.424
1.5	0.5	2.3	2.8	0.7	10.036
1.3	0.4	2.25	2.7	0.6	6.722
1.2	0.37	2.22	2.6	0.59	6.497
1.0	0.2	1.9	2.5	0.5	2.472
0.9	0.1	1.4	2.3	0.44	1.572
0.5	0.09	1.0	2.2	0.42	1.473
0.4	0.05	0.9	2.1	0.40	1.340
0.01	0.02	0.8	2.0	0.39	0.981

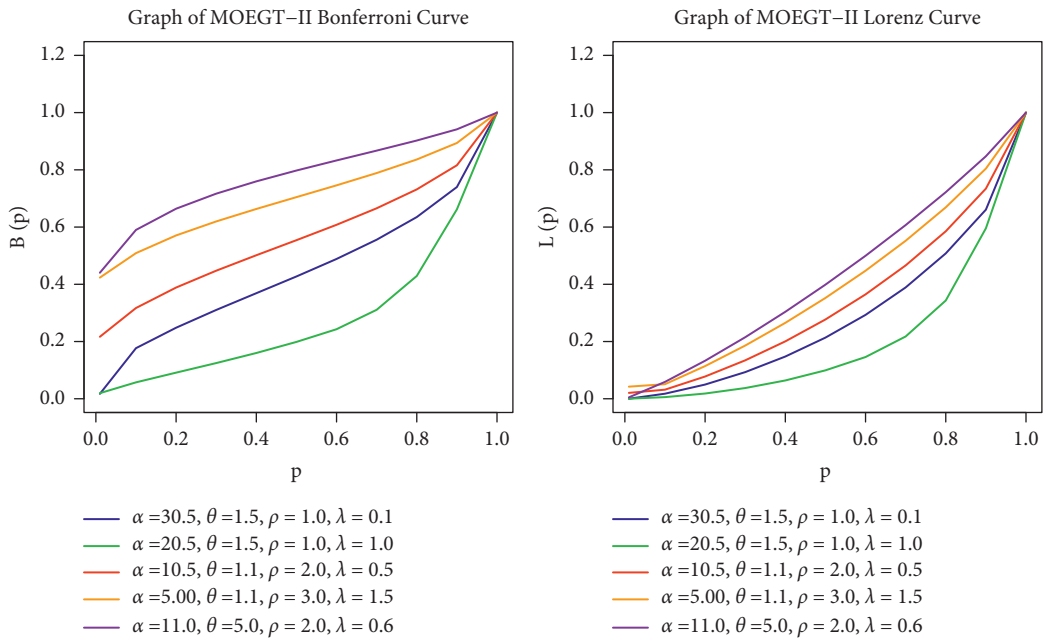

Figure 7: Graphs of Bonferroni and Lorenz curve.

$$C_{k:\,n}^{(h)} = \frac{n!}{(k-1)!(n-k)!}\alpha^{n+1-k}\frac{\theta}{(h+1)}\sum_{i=0}^{\infty}\sum_{j=0}^{\infty}(\overline{\alpha})^{i}\frac{(-1)^{j+h}}{i!\,j!h!}\frac{\Gamma(n+1+i)}{\Gamma(n+1)}\frac{\Gamma k}{\Gamma(k-j)}\frac{\Gamma[\theta(n-k+i+j+1)]}{\Gamma[\theta(n-k+i+j+1)-h]}, \tag{78}$$

and

$$g(x;\lambda(h+1),\rho)=\lambda(h+1)\rho x^{-\rho-1}\exp^{-(h+1)\lambda x^{-\rho}}. \tag{79}$$

$g(x;\lambda(h+1),\rho)$ denotes the Gumbel type-II density function with parameter $\lambda(h+1)$ and ρ. So, the density function of the order statistics is simply an infinite linear combination of Gumbel type-II density.

6.2. Moments of K^{th} Order Statistics. The r^{th} moment for the density of k^{th} order statistics can be obtained as follows:

$$E\left(X_{k:n}^{r}\right)=\int_{0}^{\infty}x^{r}f_{(K:n)}(x)\mathrm{d}x. \tag{80}$$

Substituting (77) in the above expression, making the substitution $(h+1)\lambda x^{-\rho}=z$, and using gamma function (57), we get the r^{th} moment of the k^{th} order statistic from MOEGT-II distribution as follows:

$$E\left(X_{k:n}^{r}\right)=\lambda^{r/\rho}\sum_{h=0}^{\infty}(h+1)^{r/\rho}C_{k:n}^{(h)}\Gamma\left(1-\frac{r}{\rho}\right), \tag{81}$$

under condition $((r/\rho)<1)$.

For different values of "r," i.e., $r=1, 2, 3, 4$, in (81), we can obtain first four arbitrary moments of the k^{th} order statistic.

6.3. Distribution of Median. In many situations, when data are skewed or when the outliers are present in the data, usually the median is found to be the best measure amongst all. The distribution of median can be obtained using the density of k^{th} order statistics for odd and even sample sizes.

When n is odd, say $n=2l+1$, the median is the $(l+1)^{\text{th}}$ order statistic. By substituting $k=l+1$ in the density function of k^{th} order statistic, the distribution of median can be obtained.

From (77), the density of k^{th} order statistic and the density of median (m) are obtained as follows:

$$f_{(l+1:n)}(m)=n!\alpha^{n}\ \theta\lambda\rho m^{-\rho-1}\sum_{i=0}^{\infty}\sum_{j=0}^{\infty}\sum_{h=0}^{\infty}\alpha^{-l}(\overline{\alpha})^{i}\frac{(-1)^{j+h}}{i!j!h!l!(n-l-1)!}\frac{\Gamma(n+1+i)}{\Gamma(n+1)}$$
$$\frac{\Gamma l+1}{\Gamma(l+1-j)}\frac{\Gamma[\theta(n-l+i+j)]}{\Gamma[\theta(n-l+i+j)-h]}\exp^{-(h+1)\lambda m^{-\rho}}. \tag{82}$$

When n is even, say $n=2l$, the median is then obtained as $x_l+x_{l+1}/2$ and density can be obtained from the joint density function of l^{th} and $(l+1)^{\text{th}}$ order statistics.

The joint density function of l^{th} and $(l+1)^{\text{th}}$ can be found using

$$f(x_l,x_{l+1})=\frac{n!}{(l-1)!(n-l-1)!}[F(x_l)]^{l-1}\ f(x_l)[1-F(x_{l+1})]^{n-l-1}f(x_{l+1}). \tag{83}$$

Substituting the distribution function (6) and density function (7) of MOEGT-II distribution in the above expression and after simplification, we get

$$f(x_l,x_{l+1})=\frac{n!\alpha^{n-l+1}\theta^{2}\rho^{2}\lambda^{2}}{(l-1)!(n-l-1)!}\left[1-\left(1-\ \exp^{-\lambda x_l^{-\rho}}\right)^{\theta}\right]^{l-1}\left[\frac{1}{1-(1-\alpha)\left(1-\ \exp^{-\lambda x_l^{-\rho}}\right)^{\theta}}\right]^{l+1}$$
$$x_l^{-\rho-1}\exp^{-\lambda x_l^{-\rho}}x_{l+1}^{-\rho-1}\exp^{-\lambda x_{l+1}^{-\rho}}\left(1-\ \exp^{-\lambda x_l^{-\rho}}\right)^{\theta-1}\left(1-\ \exp^{-\lambda x_{l+1}^{-\rho}}\right)^{\theta(n-l)-1} \tag{84}$$
$$\left[\frac{1}{1-(1-\alpha)\left(1-\ \exp^{-\lambda x_{l+1}^{-\rho}}\right)^{\theta}}\right]^{n-l+1},\quad 0<x_l<x_{l+1}<\infty.$$

Substituting

$$m = \frac{x_l + x_{l+1}}{2} \Rightarrow x_l = 2m - v, \qquad v = x_{l+1}, \tag{85}$$

we get

$$f(m,v) = \frac{2n!\alpha^{n-l+1}\theta^2\rho^2\lambda^2}{(l-1)!(n-l-1)!}\left[1-\left(1-\exp^{-\lambda(2m-v)^{-\rho}}\right)^{\theta}\right]^{l-1}\left[\frac{1}{1-(1-\alpha)\left(1-\exp^{-\lambda(2m-v)^{-\rho}}\right)^{\theta}}\right]^{l+1}$$
$$(2m-v)^{-\rho-1}\exp^{-\lambda(2m-v)^{-\rho}}v^{-\rho-1}\exp^{-\lambda v^{-\rho}}\left(1-\exp^{-\lambda(2m-v)^{-\rho}}\right)^{\theta-1}\left(1-\exp^{-\lambda v^{-\rho}}\right)^{\theta(n-l)-1} \tag{86}$$
$$\left[\frac{1}{1-(1-\alpha)\left(1-\exp^{-\lambda v^{-\rho}}\right)^{\theta}}\right]^{n-l+1}, \quad 0 < m < v < \infty.$$

To get the marginal density of 'm,' we integrate the above expression w.r.t 'v'; then, applying generalized binomial expansion (12) twice and power series expansion (13) thrice, we get

$$f(m) = \frac{2n!\alpha^{n-l+1}\theta^2\rho^2\lambda^2}{(l-1)!(n-l-1)!}\sum_{i=0}^{\infty}\sum_{j=0}^{\infty}\sum_{k=0}^{\infty}\sum_{p=0}^{\infty}\sum_{q=0}^{\infty}(\overline{\alpha})^{i+j}\frac{(-1)^{k+p+q}}{i!j!k!p!q!}\frac{\Gamma(n-l+1+i)}{\Gamma(n-l+1)}\frac{\Gamma(l+1+j)}{\Gamma(l+1)}\frac{\Gamma l}{\Gamma(l-k)}$$
$$\frac{\Gamma(\theta(j+k+1))}{\Gamma((\theta(j+k+1))-p)}\frac{\Gamma(\theta(n+i-l))}{\Gamma((\theta(n+i-l))-q)}\int_m^{\infty}(2m-v)^{-\rho-1}v^{-\rho-1}\exp^{-\lambda\left[(p+1)(2m-v)^{-\rho}+(q+1)v^{-\rho}\right]}\mathrm{d}v. \tag{87}$$

Now, using the expansion,

$$\exp^{-x} = \sum_{i=0}^{\infty}\frac{(-1)^i x^i}{i!}, \tag{88}$$

$$(q+p)^n = \sum_{j=0}^{n}\binom{n}{j}p^j q^{n-j}. \tag{89}$$

Substituting (88) and (89) in the above equation, then applying the binomial expansion (89) twice, then solving integration term, and after simplification, we get the distribution of median for MOEGT-II distribution:

$$f(m) = \frac{2^{-\rho}\ n!\alpha^{n-l+1}\theta^2\rho^2\lambda^2}{(l-1)!(n-l-1)!}\sum_{i=0}^{\infty}\sum_{j=0}^{\infty}\sum_{k=0}^{\infty}\sum_{p=0}^{\infty}\sum_{q=0}^{\infty}\sum_{r=0}^{\infty}\sum_{s=0}^{r}\sum_{u=0}^{\rho(s-r-1)-1}2^{\rho(s-r)-u}\lambda^r(\overline{\alpha})^{i+j}(q+1)^s(p+1)^{r-s}$$
$$\frac{(-1)^{k+p+q+r+u}}{i!j!k!p!q!r!}\frac{\Gamma(n-l+1+i)}{\Gamma(n-l+1)}\frac{\Gamma(l+1+j)}{\Gamma(l+1)}\frac{\Gamma l}{\Gamma(l-k)}\frac{\Gamma(\theta(j+k+1)}{\Gamma((\theta j+k+1)-p)}\frac{\Gamma(\theta(n+i-l))}{\Gamma(\theta(n+i-l)-q)} \tag{90}$$
$$\binom{r}{s}\binom{\rho(s-r-1)-1}{u}\frac{m^{-2\rho-\rho r-1}}{(\rho s+\rho-u)},$$

for $m > 0$.

7. Maximum Likelihood Estimation

Let $x_1, x_2, \ldots, x_n$ be a random sample of size "n" from the MOEGT-II distribution defined in (7). Then, the likelihood function can be expressed as follows:

$$L = \prod_{i=1}^{n}\left(\frac{\alpha\theta\rho\lambda x^{-\rho-1}\exp^{-\lambda x^{-\rho}}\left(1-\exp^{-\lambda x^{-\rho}}\right)^{\theta-1}}{\left(1-(1-\alpha)\left[1-\exp^{-\lambda x^{-\rho}}\right]^{\theta}\right)^{2}}\right). \tag{91}$$

Taking ln on both sides, we get

$$\begin{aligned}\ln L = {} & n\ln\alpha + n\ln\theta + n\ln\rho + n\ln\lambda - (\rho+1)\sum_{i=1}^{n}\ln x - \lambda\sum_{i=1}^{n}x^{-\rho} \\ & + (\theta-1)\sum_{i=1}^{n}\ln\left[1-\exp\left(-\lambda x^{-\rho}\right)\right] - 2\sum_{i=1}^{n}\ln\left(1-(1-\alpha)\left[1-\exp\left(-\lambda x^{-\rho}\right)\right]^{\theta}\right).\end{aligned} \tag{92}$$

Partially differentiating (92) w.r.t "α," "θ," "ρ," and "λ," we get

$$\begin{aligned}\frac{\partial \ln L}{\partial\alpha} &= \frac{n}{\alpha} - 2\sum_{i=1}^{n}\frac{\left[1-\exp\left(-\lambda x^{-\rho}\right)\right]^{\theta}}{1-(1-\alpha)\left[1-\exp\left(-\lambda x^{-\rho}\right)\right]^{\theta}}, \\ \frac{\partial \ln L}{\partial\theta} &= \frac{n}{\theta} + \sum_{i=1}^{n}\ln\left[1-\exp\left(-\lambda x^{-\rho}\right)\right] + 2\sum_{i=1}^{n}\frac{\left[(1-\alpha)\left[1-\exp\left(-\lambda x^{-\rho}\right)\right]^{\theta}\right]\ln\left[1-\exp\left(-\lambda x^{-\rho}\right)\right]}{1-(1-\alpha)\left[1-\exp\left(-\lambda x^{-\rho}\right)\right]^{\theta}}, \\ \frac{\partial \ln L}{\partial\rho} &= \frac{n}{\rho} - \sum_{i=1}^{n}\ln x + \lambda\sum_{i=1}^{n}x^{-\rho}\ln(x) - \sum_{i=1}^{n}\left[\exp\left(-\lambda x^{-\rho}\right)\right]\left(\lambda x^{-\rho}\right)(\ln x)\left[\frac{(\theta-1)}{1-\exp\left(-\lambda x^{-\rho}\right)} + \frac{2\theta(1-\alpha)\left[1-\exp\left(-\lambda x^{-\rho}\right)\right]^{\theta-1}}{1-(1-\alpha)\left[1-\exp\left(-\lambda x^{-\rho}\right)\right]^{\theta}}\right], \\ \frac{\partial \ln L}{\partial\lambda} &= \frac{n}{\lambda} - \sum_{i=1}^{n}x^{-\rho} + \sum_{i=1}^{n}\left[\exp\left(-\lambda x^{-\rho}\right)\right]\left(x^{-\rho}\right)\left[\frac{(\theta-1)}{1-\exp\left(-\lambda x^{-\rho}\right)} + \frac{2\left[\theta(1-\alpha)\left[1-\exp\left(-\lambda x^{-\rho}\right)\right]^{\theta-1}\right]}{1-(1-\alpha)\left[1-\exp\left(-\lambda x^{-\rho}\right)\right]^{\theta}}\right].\end{aligned} \tag{93}$$

The maximum likelihood estimates of parametersα, θ, ρ, and λcan be obtained from the solution of equations given in (93). Since these are nonlinear equations and their solution in closed form cannot be obtained, therefore any numerical method can be used to obtain MLE.

8. Simulation Study

To check the flexibility of the MOEGT-II, we discuss the simulation study of the proposed distribution using Monte Carlo simulations. All results are obtained for 5000 Monte Carlo runs, and the simulations are performed using R. In each replication, random samples of size ($n = 50$, 100, 300, 500, and 1000) are generated for different combinations of parameters from MOEGT-II (α, θ, ρ, λ) distribution, and three different iterative procedures named as Nelder–Mead, Quasi-Newton, and Conjugate-Gradients (CG) method (also known as Fletcher–Reeves method) have been used. The means and standard deviations of the MLEs are listed in Tables 3 and 4.

9. Application

In this section, the MOEGT-II distribution is applied to three real data sets to illustrate the usefulness and applicability of the proposed model. The MLEs of the proposed model parameters are computed, and some goodness-of-fit statistics for the fitted models are computed in *R* by using the BFGS (Broyden–Fletcher–Goldfarb–Shanno) method. The estimated cdfs of the data sets and the pdfs of the fitted distributions are plotted. In

Table 3: MLE and their sample statistics for some simulated samples and true values $\alpha = 1$, $\theta = 1$, $\rho = 1$, and $\lambda = 1$.

		Nelder–Mead				Quasi-Newton				Fletcher–Reeves			
N	Parameters	Min	Max	Mean	Std	Min	Max	Mean	Std	Min	Max	Mean	Std
50	α	0.087	27.866	1.319	1.149	0.090	3.884	1.095	0.387	0.132	4.952	1.017	0.192
	θ	0.245	3.929	1.071	0.386	0.118	2.722	1.041	0.261	0.237	2.869	1.009	0.169
	ρ	0.649	1.791	1.016	0.107	0.772	1.783	1.024	0.095	0.784	1.461	1.025	0.087
	λ	15.934	42.289	1.007	1.252	0.026	2.346	1.005	0.127	0.475	3.853	1.015	0.125
	Iteration	69	279	126	24	4	576	88	39	399	899	813	43
100	α	0.118	8.549	1.141	0.597	0.055	5.072	1.036	0.294	0.058	2.289	1.011	0.119
	θ	0.248	2.652	1.034	0.267	0.099	2.555	1.019	0.191	0.119	1.792	0.009	0.114
	ρ	0.768	1.355	1.007	0.074	0.821	1.339	1.012	0.064	0.862	1.334	1.012	0.058
	λ	7.725	16.290	1.062	0.705	0.492	3.687	1.002	0.117	0.481	2.598	1.007	0.087
	Iteration	65	279	119	23	19	603	112	55	411	953	818	46
300	α	0.366	2.945	1.039	0.285	0.447	2.359	1.017	0.147	0.406	1.558	1.003	0.065
	θ	0.513	1.623	1.008	0.148	0.585	1.492	1.007	0.099	0.566	1.386	1.004	0.067
	ρ	0.861	1.139	1.003	0.042	0.894	1.154	1.004	0.036	0.909	1.119	1.005	0.034
	λ	5.753	5.349	1.078	0.421	0.506	1.608	1.002	0.056	0.599	1.428	1.001	0.039
	Iteration	61	233	112	21	18	502	86	37	440	899	828	38
500	α	0.454	2.129	1.026	0.223	0.502	1.759	1.007	0.116	0.502	1.905	1.003	0.049
	θ	0.649	1.485	1.007	0.117	0.671	1.388	1.005	0.081	0.721	1.401	1.005	0.041
	ρ	0.898	1.124	1.002	0.033	0.899	0.117	1.003	0.026	0.912	1.340	1.002	0.019
	λ	3.133	3.761	1.091	0.333	0.652	1.646	1.004	0.051	0.661	1.627	1.003	0.029
	Iteration	64	234	107	22	24	691	120	60	402	910	835	49
1000	α	0.575	1.747	1.017	0.152	0.513	1.509	1.004	0.081	0.631	1.302	1.002	0.039
	θ	0.759	1.331	1.006	0.082	0.666	1.269	1.002	0.055	0.753	1.215	1.002	0.036
	ρ	0.919	1.091	1.001	0.023	0.934	1.082	1.002	0.019	0.936	1.083	1.001	0.018
	λ	1.785	3.743	1.093	0.264	0.424	1.431	1.001	0.035	0.738	1.253	1.001	0.026
	Iteration	63	221	105	20	24	606	108	45	453	901	839	41

Table 4: MLE and their sample statistics for some simulated samples and true values $\alpha = 2$, $\theta = 4$, $\rho = 6$, and $\lambda = 5$.

		Nelder–Mead				Quasi-Newton				Fletcher–Reeves			
n	Parameters	Min	Max	Mean	Std	Min	Max	Mean	Std	Min	Max	Mean	Std
50	α	0.154	1471.2	4.234	39.642	0.268	11.623	1.813	0.668	0.504	7.319	1.74	0.448
	θ	0.456	22.541	5.175	2.448	0.938	12.668	4.213	0.818	2.018	9.891	4.211	0.44
	ρ	1.815	34.877	5.773	1.590	3.525	11.051	6.099	0.62	3.794	8.582	6.262	0.561
	λ	3672.7	2083.4	3.165	88.678	1.719	11.4	4.865	0.687	4.235	11.538	4.664	0.664
	Iteration	79	501	141	38	16	295	46	25	4	922	835	41
100	α	0.293	430.19	1.963	7.577	0.194	8.17	1.77	0.479	0.595	4.014	1.771	0.335
	θ	0.526	21.514	4.998	1.614	1.336	11.559	4.203	0.713	2.079	7.312	4.169	0.317
	ρ	2.186	32.628	5.594	0.879	3.702	8.454	6.026	0.443	4.291	8.121	6.22	0.423
	λ	854.3	36.5	5.208	13.651	1.443	8.815	4.848	0.594	1.423	7.764	4.725	0.517
	Iteration	79	501	132	27	19	949	50	39	7	921	842	31
300	α	0.565	5.146	1.625	0.505	0.519	13.851	1.81	0.361	0.659	3.602	1.80	0.301
	θ	2.405	9.443	4.908	0.896	2.187	12.288	4.109	0.411	2.612	7.402	4.163	0.265
	ρ	4.187	7.439	5.501	0.421	3.36	7.595	6.049	0.335	4.558	7.328	6.208	0.334
	λ	6.865	13.148	5.534	0.877	0.151	11.046	4.836	0.426	0.838	8.322	4.757	0.424
	Iteration	79	273	127	22	2	1308	51	58	8	924	858	31
500	α	0.73	3.868	1.596	0.378	0.411	4.372	1.805	0.309	0.494	4.341	1.892	0.261
	θ	2.969	7.92	4.899	0.696	1.9	8.282	4.106	0.380	1.945	7.902	4.105	0.236
	ρ	4.442	6.689	5.481	0.325	4.181	7.718	6.039	0.323	3.927	7.240	6.024	0.291
	λ	3.78	17.343	5.553	0.715	1.561	9.143	4.82	0.396	0.928	6.997	4.724	0.387
	Iteration	85	255	127	25	20	934	52	61	14	990	866	30
1000	α	0.893	2.781	1.559	0.261	0.473	4.319	1.779	0.259	0.661	4.016	1.824	0.256
	θ	3.371	6.974	4.861	0.50	2.099	8.383	4.099	0.376	2.569	7.690	4.141	0.228
	ρ	4.721	6.551	5.476	0.233	4.256	7.148	5.984	0.217	4.333	7.307	6.182	0.215
	λ	2.964	13.442	5.566	0.604	0.759	8.398	4.78	0.390	0.325	6.705	4.788	0.385
	Iteration	83	253	128	23	2	1349	54	64	12	950	867	29

From Tables 3 and 4, it can be seen that with increasing sample size, the standard deviations for the estimates tend to decrease and the Fletcher–Reeves method provides a better estimate as compared with the Nelder–Mead method and Quasi-Newton method with increasing sample size.

Table 5: MLEs and their SE (in parentheses) for breaking stress data.

Distribution	α	λ	ρ	θ
MOEGT-II	9.884 777 6 (13.054 577 0)	5.089 054 8 (2.118 862 0)	0.505 807 8 (0.181 352 4)	54.932 699 8 (76.616 613 6)
EGT-II	—	8.346 042 9 (1.091 707 0)	0.507 850 7 (0.101 844 2)	137.719 819 4 (149.254 856 0)
MOGT-II	158.282 337 3 (71.820 618 29)	0.157 871 5 (0.057 381 76)	3.635 606 7 (0.245 951 64)	—
GT-II	—	3.088 187 (0.327 115 2)	1.769 024 (0.111 922 3)	—
MOF	112.389 913 9 (57.785 004 16)	0.627 062 2 (0.069 095 07)	3.482 807 1 (0.248 425 82)	—
F	—	1.891 563 (0.113 794 3)	1.769 022 (0.111 922 3)	—
Burr III	—	—	2.319 184 (0.149 555 1)	5.221 175 (0.598 417 7)
LL	—	43.357 123 (16.039 205 8)	4.117 069 (0.343 907 9)	—
BIW	28.855 093 4 (11.767 038 1)	0.773 766 1 (0.133 844 5)	0.377 652 0 (0.168 107 5)	97.324 915 2 (74.619 980 4)
KIW	3.300 443 3 (2.257 001 01)	0.476 214 9 (0.092 630 72)	4.845 829 4 (1.876 991 23)	176.087 174 1 (189.465 682 34)

Table 6: MLEs and their SE (in parentheses) for service times of windshield data.

Distribution	α	λ	ρ	θ
MOEGT-II	17.343 521 7 (16.476 418 09)	4.401 977 4 (1.267 586 86)	0.208 865 7 (0.058 273 55)	134.686 072 1 (148.932 304 57)
EGT-II	—	5.877 250 7 (0.864 721 37)	0.269 711 1 (0.042 099 34)	118.691 077 6 (95.874 791 74)
MOGT-II	115.845 881 73 (59.952 866 916)	0.020 763 57 (0.009 710 782)	1.740 842 20 (0.146 055 081)	—
GT-II	—	0.943 541 8 (0.128 395 05)	0.810 293 4 (0.065 628 02)	—
MOF	207.295 920 4 (128.468 612 87)	0.092 251 8 (0.023 996 99)	1.829 382 9 (0.161 485 05)	—
F	—	0.930 597 0 (0.154 297 27)	0.810 355 9 (0.065 629 43)	—
Burr III	—	—	1.564 679 (0.153 962 2)	1.641 350 (0.208 898 8)
LL	—	3.514 333 (0.933 951 1)	2.135 245 (0.231 174 2)	—
BIW	125.532 248 4 (58.098 105 90)	0.458 660 7 (0.055 434 43)	0.274 777 9 (0.096 170 21)	105.112 800 2 (70.456 427 40)
KIW	2.709 499 7 (3.362 850 85)	0.227 468 7 (0.031 733 62)	5.441 804 4 (1.702 913 12)	305.607 672 3 (234.649 978 71)

addition, the probability plot (P-P) is also discussed. We compare the MOEGT-II distribution with nine different models that are the Exponentiated Gumbel Type-II (EGT-II) distribution, Marshall–Olkin Gumbel Type-II (MOGT-II) distribution, Gumbel Type-II (GT-II) distribution, Marshall Olkin Frechet (MOF) distribution, Frechet (F) distribution, Burr III distribution, Log Logistic (LL) distribution, Beta Inverse Weibull (BIW) distribution, and Kumaraswamy Inverse Weibull (KIW) distribution.

The first example is a data set from Nichols and Padgett [31] consisting of 100 observations on breaking stress of carbon fibres (in Gba). Recently, Afify et al. [32] and Saboor et al. [33] used these data to analyze the distributions. The data values are 3.7, 2.74, 2.73, 2.5, 3.6, 3.11, 3.27, 2.87, 1.47, 3.11, 4.42, 2.41, 3.19, 3.22, 1.69, 3.28, 3.09, 1.87, 3.15, 4.9, 3.75, 2.43, 2.95, 2.97, 3.39, 2.96, 2.53, 2.67, 2.93, 3.22, 3.39, 2.81, 4.2, 3.33, 2.55, 3.31, 3.31, 2.85, 2.56, 3.56, 3.15, 2.35, 2.55, 2.59, 2.38, 2.81, 2.77, 2.17, 2.83, 1.92, 1.41, 3.68, 2.97, 1.36, 0.98, 2.76, 4.91, 3.68, 1.84, 1.59, 3.19, 1.57, 0.81, 5.56, 1.73, 1.59, 2, 1.22, 1.12, 1.71, 2.17, 1.17, 5.08, 2.48, 1.18, 3.51, 2.17, 1.69, 1.25, 4.38, 1.84, 0.39, 3.68, 2.48, 0.85, 1.61, 2.79, 4.7, 2.03, 1.8, 1.57, 1.08, 2.03, 1.61, 2.12, 1.89, 2.88, 2.82, 2.05, 3.65, 2.341, 4.628, 1.244, 2.435, 4.806, 1.249, 2.464, 4.881, 1.262, 2.543, 5.140.

The second example is a data set corresponding to service times for a particular windshield model including 63 observations that are classified as service times of windshields from Murthy et al. [34]. Recently, Tahir et al. [35] applied these data to the Weibull–Lomax distribution. The data values are 0.046, 1.436, 2.592, 0.140, 1.492, 2.600, 0.150, 1.580, 2.670, 0.248, 1.719, 2.717, 0.280, 1.794, 2.819, 0.313, 1.915, 2.820, 0.389, 1.920, 2.878, 0.487, 1.963, 2.950, 0.622, 1.978, 3.003, 0.900, 2.053, 3.102, 0.952, 2.065, 3.304, 0.996, 2.117, 3.483, 1.003, 2.137, 3.500, 1.010, 2.141, 3.622, 1.085, 2.163, 3.665, 1.092, 2.183, 3.695, 1.152, 2.240, 4.015, 1.183, 2.341, 4.628, 1.244, 2.435, 4.806, 1.249, 2.464, 4.881, 1.262, 2.543, 5.140.

The third data set represents the fracture toughness of alumina (Al_2O_3) (in the units of MPa $m1 = 2$) by Nadarajah [36]. Recently, Arifa et al. [37] and Ghitany et al. [38] used these data to analyze the distributions. The data values are 5.5, 5, 4.9, 6.4, 5.1, 5.2, 5.2, 5, 4.7, 4, 4.5, 4.2, 4.1, 4.56, 5.01, 4.7, 3.13, 3.12, 2.68, 2.77, 2.7, 2.36, 4.38, 5.73, 4.35, 6.81, 1.91, 2.66, 2.61, 1.68, 2.04, 2.08, 2.13, 3.8, 3.73, 3.71, 3.28, 3.9, 4, 3.8, 4.1, 3.9, 4.05, 4, 3.95, 4, 4.5, 4.5, 4.2, 4.55, 4.65, 4.1, 4.25, 4.3, 4.5, 4.7, 5.15, 4.3, 4.5, 4.9, 5, 5.35, 5.15, 5.25, 5.8, 5.85, 5.9, 5.75, 6.25, 6.05, 5.9, 3.6, 4.1, 4.5, 5.3, 4.85, 5.3, 5.45, 5.1, 5.3, 5.2, 5.3, 5.25, 4.75, 4.5, 4.2, 4, 4.15, 4.25, 4.3, 3.75, 3.95, 3.51, 4.13, 5.4, 5, 2.1, 4.6, 3.2, 2.5, 4.1, 3.5, 3.2, 3.3, 4.6, 4.3, 4.3, 4.5, 5.5, 4.6, 4.9, 4.3, 3, 3.4, 3.7, 4.4, 4.9, 4.9, 5.

Tables 5–7 provide the MLEs and their corresponding standard errors (SEs) (in parentheses); and the result of AIC, CAIC, BIC, HQIC, log-likelihood, Cramer-von Mises (W^*), Anderson–Darling (A^*), and Kolmogorov–Smirnov (KS) statistics and its $p$value for each distribution are presented in Tables 8–10. The MOEGT-II distribution has the smallest values for the AIC, CAIC, BIC, HQIC, log-likelihood, Cramer-von Mises (W^*), Anderson–Darling (A^*), and Kolmogorov-Smirnov (KS) statistics as compared with other fitted distributions, suggesting that the MOEGT-II model provides the good fit. The estimated cdfs, histogram of three

Table 7: MLEs and their SE (in parentheses) for the fracture toughness of alumina data.

Distribution	α	λ	ρ	θ
MOEGT-II	15.294 400 5 (14.227 853 1)	10.421 918 7 (2.633 296 1)	0.789 969 1 (0.222 581 7)	69.729 425 3 (70.055 174 4)
EGT-II	—	19.184 216 8 (1.949 256 8)	0.990 687 2 (0.114 450 2)	67.827 826 2 (35.304 429 3)
MOGT-II	368.233 172 (298.072 646 0)	61.918 359 (50.694 638 2)	6.869 485 (0.511 673 3)	—
GT-II	—	48.477 859 (10.825 173 9)	3.022 359 (0.184 929 5)	—
MOF	0.004 179 529 (0.001 304 203)	22.086 001 867 (3.392 175 442)	1.033 172 128 (0.072 468 604)	—
F	—	3.611 630 (0.116 713 1)	3.024 015 (0.185 130 9)	—
Burr III	—	—	3.058 00 (0.179 916)	51.880 55 7 (11.180 150)
LL	—	227.626 726 (54.064 342 1)	3.933 087 (0.176 544 8)	—
BIW	15.446 107 5 (3.741 849 2)	1.509 306 4 (0.335 202 4)	0.312 665 8 (0.150 726 5)	91.427 467 5 (59.284 776 0)
KIW	11.252 737 6 (7.562 136 5)	0.806 074 3 (0.109 693 1)	2.683 321 0 (1.532 909 3)	243.688 695 4 (189.885 147 0)

Table 8: Several goodness-of-fit criteria for breaking stress data.

Distribution	AIC	CAIC	BIC	HQIC	l	W^*	A^*	KS	p value
MOEGT-II	290.86	291.27	301.27	295.07	−141.43	0.075	0.404	0.066	0.772
EGT-II	293.57	293.82	301.38	296.74	−143.78	0.156	0.804	0.102	0.253
MOGT-II	303.78	304.04	311.61	306.95	−148.89	0.269	1.432	0.111	0.176
GT-II	350.28	350.41	355.49	352.39	−173.14	0.756	4.312	0.177	0.004
MOF	305.56	305.81	313.37	308.73	−149.78	0.273	1.459	0.106	0.22
F	350.28	350.41	355.49	352.39	−173.14	0.756	4.312	0.177	0.003 6
Burr III	325.95	326.07	331.16	328.055	−160.97	0.569	3.173	0.139	0.041
LL	296.56	296.68	301.77	298.67	−146.28	0.239	1.241	0.091	0.388
BIW	335.42	335.79	346.26	339.82	−163.71	0.088	0.503	0.082	0.444
KIW	335.96	336.34	346.79	340.36	−163.98	0.108	0.583	0.083	0.427

Table 9: Several goodness-of-fit criteria for service times of windshield data.

Distribution	AIC	CAIC	BIC	HQIC	L	W^*	A^*	KS	p value
MOEGT-II	209.33	210.02	217.91	212.69	−100.66	0.11	0.62	0.09	0.66
EGT-II	220.82	221.23	227.25	223.35	−107.41	0.32	1.91	0.16	0.06
MOGT-II	229.55	229.96	235.98	232.08	−111.77	0.43	2.52	0.15	0.11
GT-II	266.61	266.81	270.89	268.29	−131.31	0.99	5.42	0.22	0.003
MOF	227.26	227.66	233.69	229.78	−110.63	0.399	2.354	0.14	0.15
F	266.61	266.81	270.89	268.29	−131.31	0.99	5.42	0.22	0.004
Burr III	233.53	233.73	237.82	235.22	−114.76	0.53	3.12	0.19	0.02
LL	221.48	221.78	225.77	223.17	−108.74	0.33	1.98	0.12	0.31
BIW	220.33	221.02	228.91	223.71	−106.16	0.27	1.63	0.18	0.023
KIW	220.36	221.05	228.93	223.73	−106.18	0.28	1.71	0.16	0.07

Table 10: Several goodness-of-fit criteria for the fracture toughness of alumina data.

Distribution	AIC	CAIC	BIC	HQIC	L	W^*	A^*	KS	p value
MOEGT-II	345.03	345.38	356.15	349.54	−168.52	0.07	0.52	0.05	0.92
EGT-II	359.03	359.24	367.36	362.41	−176.52	0.36	2.19	0.13	0.05
MOGT-II	363.19	363.41	371.54	366.58	−178.59	0.39	2.42	0.08	0.31
GT-II	425.79	425.89	431.35	428.05	−210.89	1.41	7.87	0.20	0.000 1
MOF	399.23	399.44	407.56	402.62	−196.62	0.94	5.49	0.14	0.03
F	425.79	425.89	431.35	428.05	−210.89	1.41	7.88	0.21	0.000 1
Burr III	423.54	423.64	429.09	425.79	−209.77	1.37	7.66	0.19	0.000 2
LL	409.49	409.59	415.05	411.75	−202.75	0.52	3.13	0.23	0.000 007
BIW	355.07	355.42	366.18	359.58	−173.54	0.27	1.64	0.13	0.051
KIW	356.12	356.46	367.23	360.63	−174.06	0.28	1.72	0.11	0.102

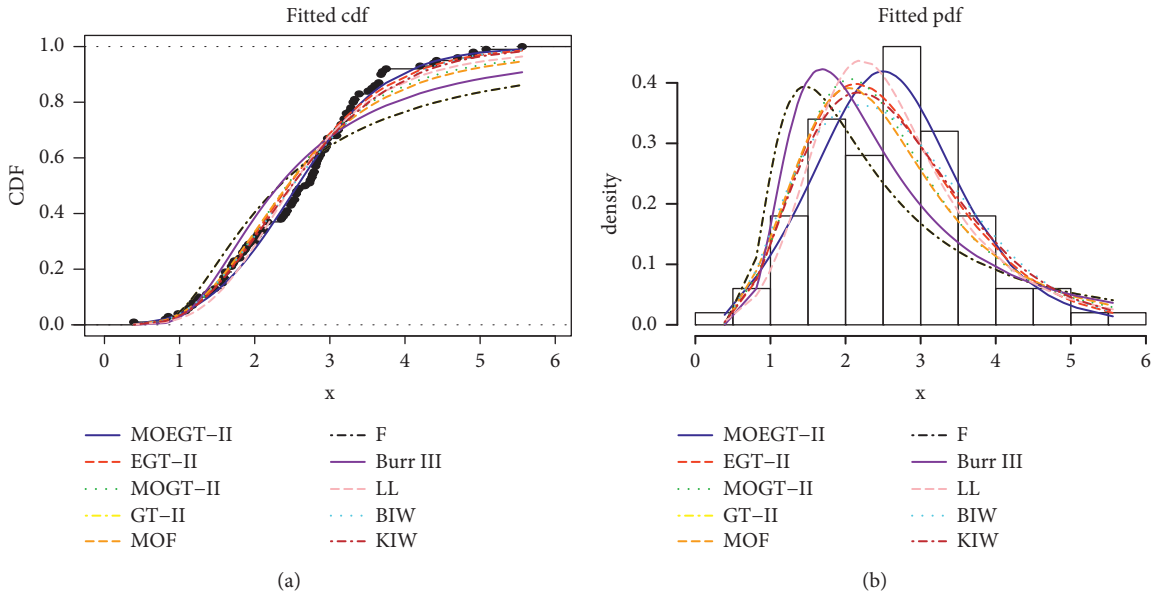

Figure 8: (a) Graphs of estimated cdfs; (b) graphs of estimated pdfs for breaking stress data.

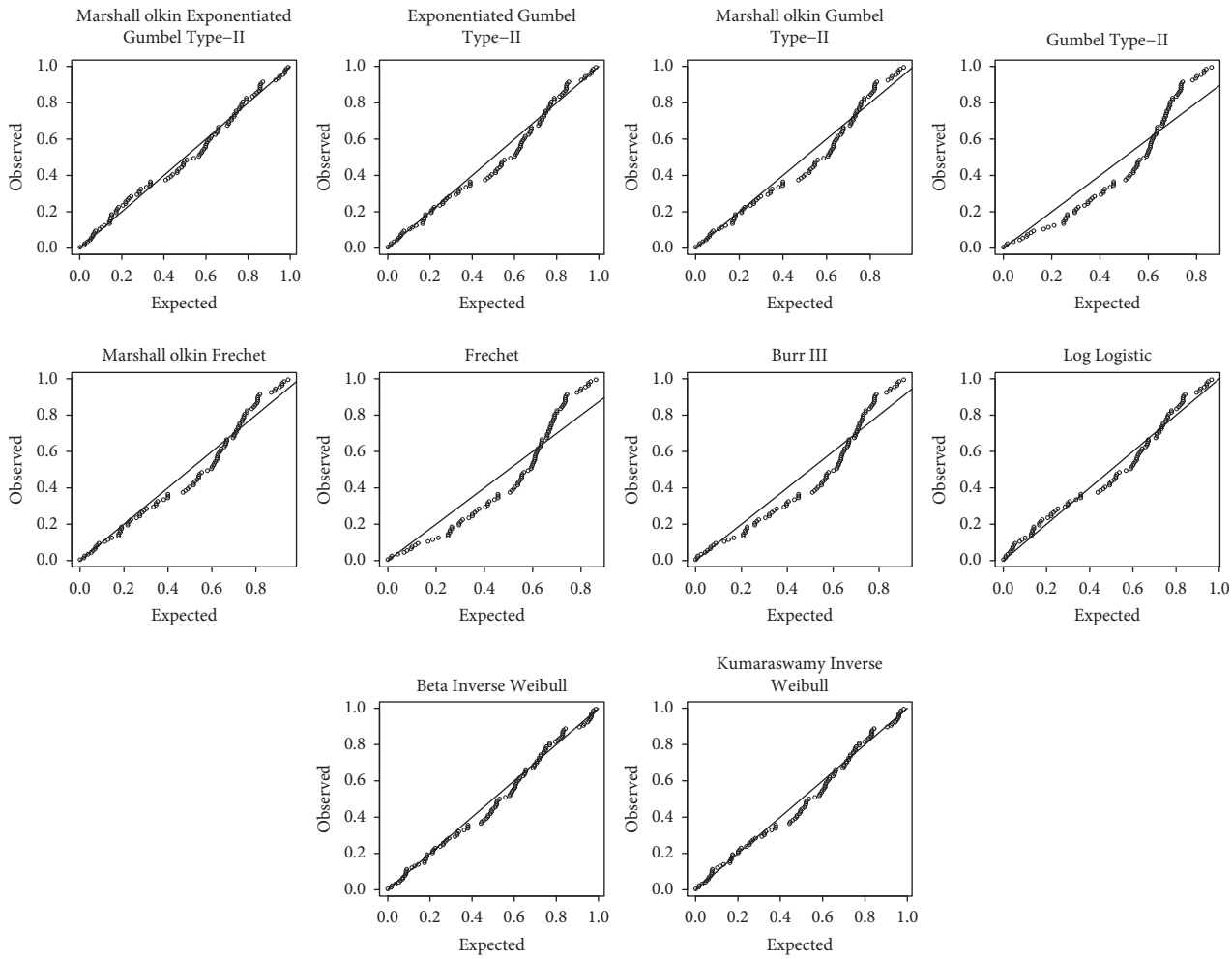

Figure 9: Graphs of P-P for breaking stress data.

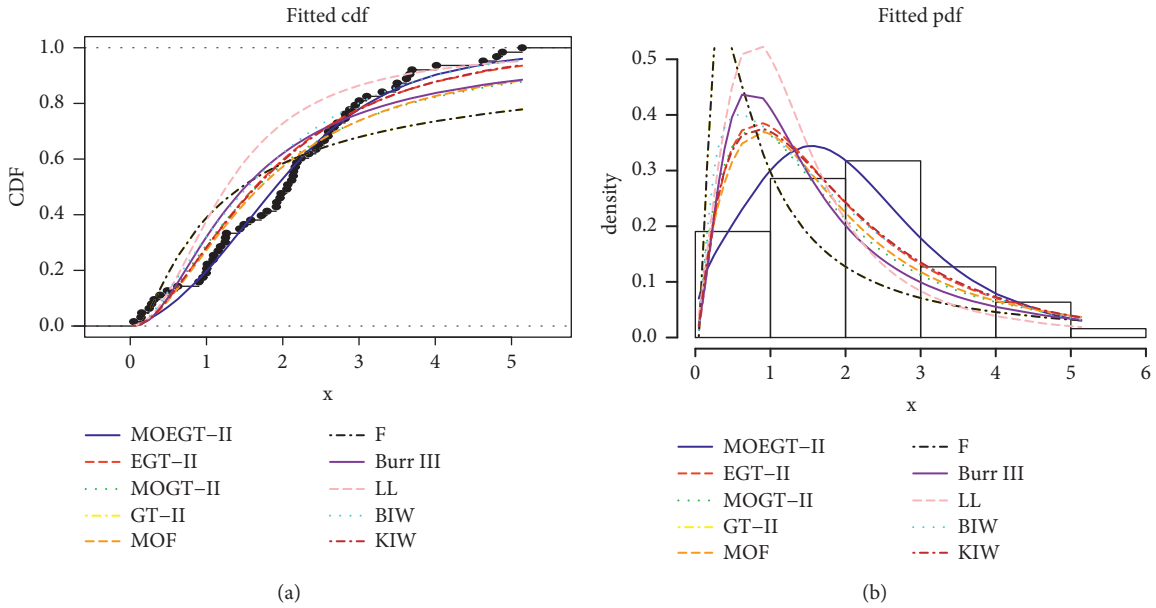

Figure 10: (a) Graphs of estimated cdfs; (b) graphs of estimated pdfs for service times of 63 aircraft windshield.

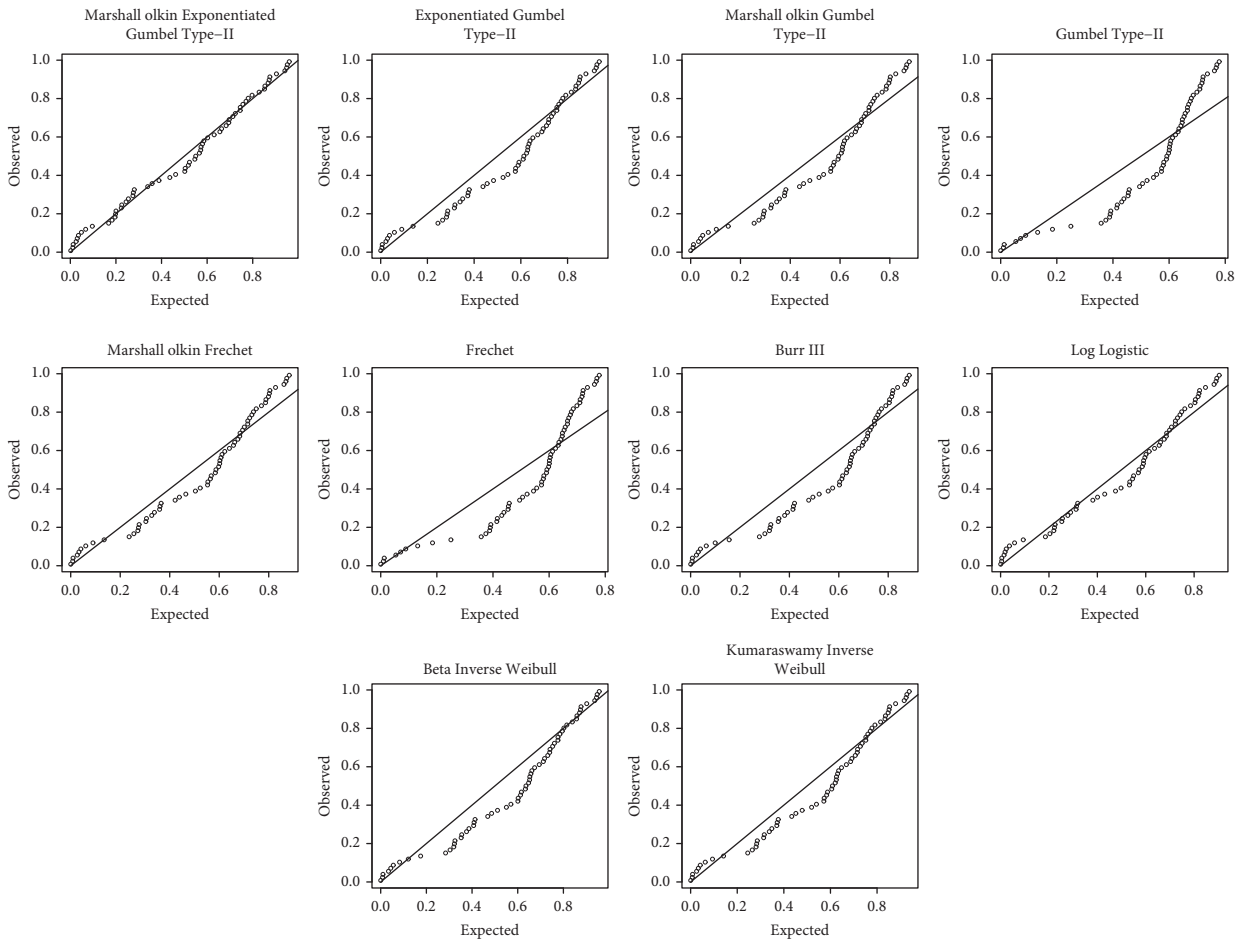

Figure 11: Graphs of P-P for service times of 63 aircraft windshield.

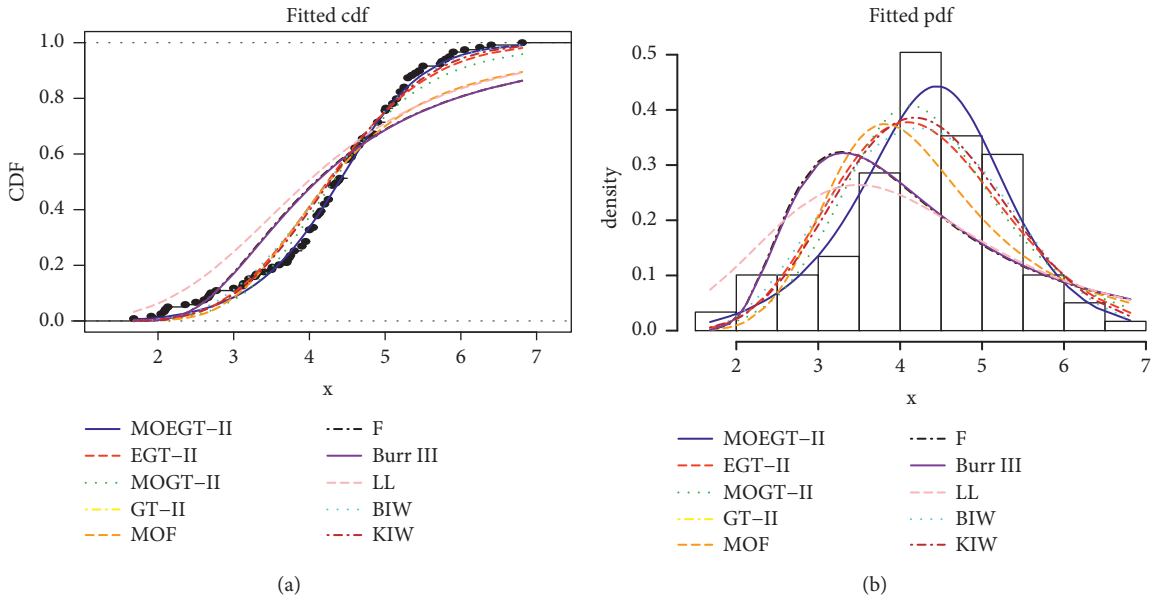

Figure 12: (a) Graphs of estimated cdfs; (b) graphs of estimated pdfs for the fracture toughness of alumina data.

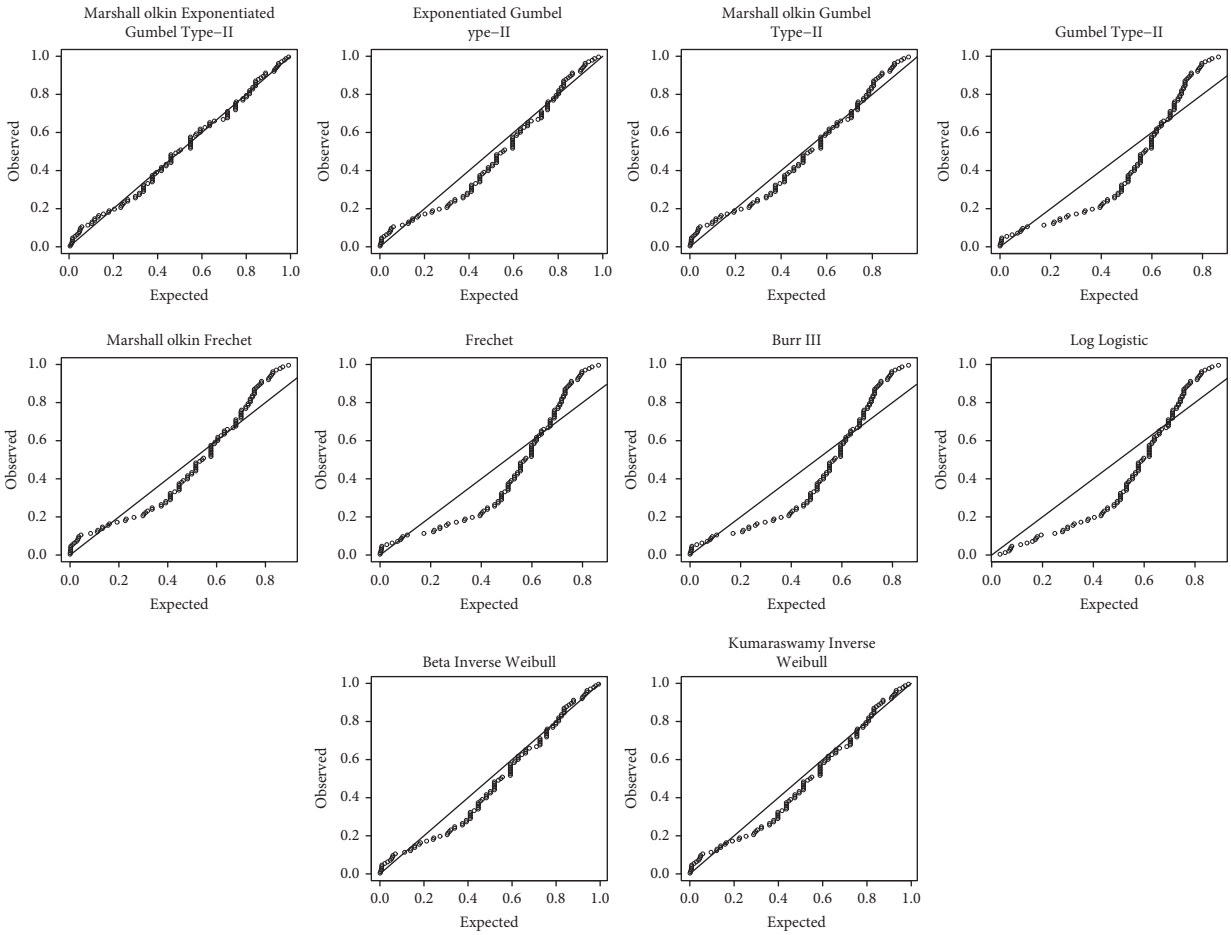

Figure 13: Graphs of P-P for the fracture toughness of alumina (Al_2O_3) data.

data sets, pdfs, and P-P are presented in Figures 8–13, respectively. It is clear from Tables 8–10 and Figures 8–13 that the MOEGT-II distribution provides better fit than EGT-II, MOGT-II, GT-II, MOF, Frechet (F), Burr III, LL, BIW, and KIW models for given three data sets.

10. Conclusion

A new probability model called MOEGT-II is derived by employing the cdf of EGT-II in Marshall–Olkin family of distributions. The proposed model is important due to its modeling of various shapes of the hazard rate function such as increasing, decreasing, reverse J-shaped, and upside down bathtub. The special cases of MOEGT-II are called EGT-II, MOGT-II, GT-II, EF, F, and MOF distribution. Mathematical properties of the proposed distribution were studied including survival function, hazard rate function, reverse hazard rate function, Renyi entropy, q^{th} entropy, Lorenz curve, and Bonferroni curve. Expressions for the k^{th} order statistics and their r^{th} moments are also derived. Performance of the maximum likelihood estimates is also investigated through Monte Carlo simulation. We observed that with the increase in the sample size, the better results for maximum likelihood estimates are obtained. Also, the Conjugate-Gradients (CG) method (Fletcher–Reeves method) provides better estimates as compared with the Nelder–Mead method and Quasi-Newton method with increasing sample size. At the end, we have considered three data sets, and it has been shown that MOEGT-II distribution provides better performance than EGT-II, MOGT-II, GT-II, MOF, F, Burr III, LL, BIW, and KIW distributions.

Data Availability

The data sets have been taken from the literature and the references are given at the end.

Conflicts of Interest

The authors declare that they have no conflicts of interest.

Authors' Contributions

The following are the contributions of each author to the paper. Farwa Willayat was responsible for main analysis wrote original article, provided software, proposed methodology, and visualized the study. Naz Saud wrote original draft, supervised the study, reviewed the article, provided suggestions, developed methodology, and visualized the study. Muhammad Ijaz conceptualized the study, visualized the study, reviewed and edited the article, developed methodology, and provided suggestions. Anita Silvianita and M. Mahmoud El-Morshedy reviewed and edited the manuscript, provide suggestions, and validated the study.

References

[1] H. Aksoy, "Use of gamma distribution in hydrological analysis," *Turkish Journal of Engineering and Environmental Sciences*, vol. 24, no. 6, pp. 419–428, 2000.

[2] M. K. Keshavan, G. A. Sargent, and H. Conrad, "Statistical analysis of the hertzian fracture of pyrex glass using the weibull distribution function," *Journal of Materials Science*, vol. 15, no. 4, pp. 839–844, 1980.

[3] M. Al-Hasan and R. R. Nigmatullin, "Identification of the generalized weibull distribution in wind speed data by the eigen-coordinates method," *Renewable Energy*, vol. 28, no. 1, pp. 93–110, 2003.

[4] H. Dahm, J. Niemeyer, and D. Schröder, "Application of the weibull distribution to describe the vertical distribution of cesium-137 on a slope under permanent pasture in Luxembourg," *Journal of Environmental Radioactivity*, vol. 63, no. 3, pp. 207–219, 2002.

[5] R. D. Gupta and D. Kundu, "Generalized exponential distributions," *Australian New Zealand Journal of Statistics*, vol. 41, no. 2, pp. 173–188, 1999.

[6] R. D. Gupta and D. Kundu, "Exponentiated exponential family: an alternative to gamma and weibull distributions," *Biometrical Journal*, vol. 43, no. 1, pp. 117–130, 2001.

[7] G. M. Cordeiro, E. M. Ortega, and D. C. da Cunha, "The exponentiated generalized class of distributions," *Journal of Data Science*, vol. 11, no. 1, pp. 1–27, 2013.

[8] T. Andrade, H. Rodrigues, M. Bourguignon, and G. Cordeiro, "The exponentiated generalized gumbel distribution," *Revista Colombiana de Estadística*, vol. 38, no. 1, pp. 123–143, 2015.

[9] A. Marshall and I. Olkin, "A new method for adding a parameter to a family of distributions with application to the exponential and weibull families," *Biometrika*, vol. 84, no. 3, pp. 641–652, 1997.

[10] T. Alice and K. Jose, "Marshall-olkin pareto processes," *Far East Journal of Theoretical Statistics*, vol. 9, no. 2, pp. 117–132, 2003.

[11] M. E. Ghitany, E. K. Al-Hussaini, and R. A. Al-Jarallah, "Marshall-Olkin extended weibull distribution and its application to censored data," *Journal of Applied Statistics*, vol. 32, no. 10, pp. 1025–1034, 2005.

[12] M. E. Ghitany, F. A. Al-Awadhi, and L. A. Alkhalfan, "Marshall-Olkin extended lomax distribution and its application to censored data," *Communications in Statistics - Theory and Methods*, vol. 36, no. 10, pp. 1855–1866, 2007.

[13] K. K. Jose, S. R. Naik, and M. M. Ristić, "Marshall-Olkin q-Weibull distribution and max-min processes," *Statistical Papers*, vol. 51, no. 4, pp. 837–851, 2010.

[14] K. Jose, "Marshall-olkin family of distributions and their applications in reliability theory, time series modeling and stress-strength analysis," in *Proceedings of the ISI 58th World Statistics Congress International Statics Institution*, pp. 3918–3923, Dublin, Ireland, 2011 August.

[15] M. Ghitany, D. Al-Mutairi, F. Al-Awadhi, and M. Al-Burais, "Marshall-olkin extended lindley distribution and its application," *International Journal of Applied Mathematics*, vol. 25, no. 5, pp. 709–721, 2012.

[16] E. Krishna, K. K. Jose, T. Alice, and M. M. Ristić, "The Marshall-Olkin Fréchet Distribution," *Communications in Statistics - Theory and Methods*, vol. 42, no. 22, pp. 4091–4107, 2013.

[17] A. Y. Al-Saiari, L. A. Baharith, and S. A. Mousa, "Marshall-olkin extended burr type xii distribution," *International Journal of Statistics and Probability*, vol. 3, no. 1, p. 78, 2014.

[18] T. K. Pogány, A. Saboor, and S. Provost, "The marshall-olkin exponential weibull distribution," *Hacettepe Journal of Mathematics and Statistics*, vol. 45, no. 47, p. 1, 2015.

[19] A. Saboor and T. K. Pogány, "Marshall-Olkin gamma-Weibull distribution with applications," *Communications in Statistics - Theory and Methods*, vol. 45, no. 5, pp. 1550–1563, 2016.

[20] H. H. Ahmad, O. M. Bdair, M. Ahsanullah, and M. Ahsanullah, "On marshall-olkin extended weibull distribution," *Journal of Statistical Theory and Applications*, vol. 16, no. 1, pp. 1–17, 2017.

[21] A. Z. Afify, G. M. Cordeiro, H. M. Yousof, A. Saboor, and E. M. Ortega, "The marshall-olkin additive weibull distribution with variable shapes for the hazard rate," *Hacettepe J Math Stat*, vol. 47, pp. 365–381, 2018.

[22] S. Biswas and N. Gupta, "Some ordering properties of highest and lowest order statistics with exponentiated gumble type-ii distributed components," 2019, https://arxiv.org/abs/1904.08730.

[23] J. Gillariose, L. Tomy, F. Jamal, and C. Chesneau, "The marshall-olkin modified lindley distribution: properties and applications," *Journal of Reliability and Statistical Studies*, pp. 177–198, 2020.

[24] M. A. U. Haq, G. Hamedani, M. Elgarhy, and P. L. Ramos, "Marshall-olkin power lomax distribution: properties and estimation based on complete and censored samples," *International Journal of Statistics and Probability*, vol. 9, no. 1, pp. 1–48, 2020.

[25] A. A. Ogunde, S. T. Fayose, B. Ajayi, and D. O. Omosigho, "Extended gumbel type-2 distribution: properties and applications," *Journal of Applied Mathematics*, vol. 2020, Article ID 2798327, 11 pages, 2020.

[26] E. M. Almetwally, M. A. Sabry, R. Alharbi, D. Alnagar, S. A. Mubarak, and E. H. Hafez, "Marshall–olkin alpha power weibull distribution: different methods of estimation based on type-i and type-ii censoring," *Complexity*, vol. 2021, Article ID 5533799, 18 pages, 2021.

[27] I. E. Okorie, A. C. Akpanta, D. C. Johnson Ohakwe, and E. O. Obi, "The Kumaraswamy G exponentiated gumbel type-2 distribution," *African Journal*, vol. 12, 2017.

[28] I. E. Okorie, A. C. Akpanta, and J. Ohakwe, "The exponentiated gumbel type-2 distribution: properties and application," *International Journal of Mathematics and Mathematical Sciences*, vol. 2016, Article ID 5898356, 10 pages, 2016.

[29] S. Nadarajah and S. Kotz, "The beta exponential distribution," *Reliability Engineering & System Safety*, vol. 91, no. 6, pp. 689–697, 2006.

[30] M. Abd El-Monsef and S. Ghoneim, "The weighted kumaraswamy distribution," *Information*, vol. 18, no. 8, pp. 3289–3300, 2015.

[31] M. D. Nichols and W. J. Padgett, "A bootstrap control chart for weibull percentiles," *Quality and Reliability Engineering International*, vol. 22, no. 2, pp. 141–151, 2006.

[32] Z. Afify, G. G. Hamedani, I. Ghosh, and M. E. Mead, "The Transmuted Marshall-Olkin Fr\'{e}chet Distribution: Properties and Applications," *International Journal of Statistics and Probability*, vol. 4, no. 4, p. 132, 2015.

[33] A. Saboor, M. Kamal, and M. Ahmad, "The transmuted exponential–weibull distribution with applications," *Pakistan Journal of Statistics*, vol. 31, no. 2, pp. 229–250, 2015.

[34] D. P. Murthy, M. Xie, and R. Jiang, *Weibull Models*, John Wiley & Sons, Hoboken, NJ, USA, 2004.

[35] M. H. Tahir, G. M. Cordeiro, M. Mansoor, and M. Zubair, "Weibull-lomax Distribution: Properties and Applications," *Hacettepe Journal of Mathematics and Statistics*, vol. 44, no. 14, p. 1, 2014.

[36] S. Nadarajah, "The model for fracture toughness," *Journal of Mechanical Science and Technology*, vol. 22, no. 7, pp. 1255–1258, 2008.

[37] S. Arifa, M. Z. Yab, and A. Ali, "The modified burr iii g family of distributions," *Journal of Data Science*, vol. 15, no. 1, pp. 41–60, 2017.

[38] M. E. Ghitany, S. M. Aboukhamseen, and E. A. S. Mohammad, "Weighted half exponential power distribution and associated inference," *Applied Mathematical Sciences*, vol. 10, no. 2, pp. 91–108, 2016.

Hindawi
Complexity
Volume 2021, Article ID 9736179, 12 pages
https://doi.org/10.1155/2021/9736179

Research Article

Blended Features Classification of Leaf-Based Cucumber Disease Using Image Processing Techniques

Jaweria Kainat,[1] Syed Sajid Ullah,[2] Fahd S. Alharithi,[3] Roobaea Alroobaea,[3] Saddam Hussain,[4] and Shah Nazir[5]

[1]*Department of Computer Science, COMSATS University Islamabad, Wah Cantt, Pakistan*
[2]*Department of Electrical and Computer Engineering, Villanova University, Villanova, PA, USA*
[3]*Department of Computer Science, College of Computers and Information Technology, Taif University, P.O. Box 11099, Taif 21944, Saudi Arabia*
[4]*School of Digital Science, Universiti Brunei Darussalam, Jalan Tungku Link, Gadong BE1410, Brunei Darussalam*
[5]*Department of Computer Science, University of Swabi, Swabi, Khyber Pakhtunkhwa, Pakistan*

Correspondence should be addressed to Saddam Hussain; saddamicup1993@gmail.com and Shah Nazir; shahnazir@uoswabi.edu.pk

Received 6 October 2021; Revised 19 November 2021; Accepted 10 December 2021; Published 30 December 2021

Academic Editor: Shanmugam Lakshmanan

Existing plant leaf disease detection approaches are based on features of extracting algorithms. These algorithms have some limits in feature selection for the diseased portion, but they can be used in conjunction with other image processing methods. Diseases of a plant can be classified from their symptoms. We proposed a cucumber leaf recognition approach, consisting of five steps: preprocessing, normalization, features extraction, features fusion, and classification. Otsu's thresholding is implemented in preprocessing and Tan–Triggs normalization is applied for normalizing the dataset. During the features extraction step, texture and shape features are extracted. In addition, increasing the instances improves some characteristics. Through a principal component analysis approach, serial feature fusion is employed to provide a feature score. Fused features can be classified through a support vector machine. The accuracy of the Fine KNN is 94.30%, which is higher than the previous work in past papers.

1. Introduction

Plant leaf infections are a very inferior risk and require a robust economy for the nation. The development of farming products and accountability for a valuable part of these products are quite imperative.

In image processing, pipelined techniques have created incredible advancement results with high accuracy, yet there are a few concerns as well. Firstly, proficiency exceedingly relies upon features extraction and after that features selection for infected leaf image, in which the highlighted features are extracted, and secondly pipelined procedures are moderately unpredictable. The boisterous images, irregular lighting, and turmoil background in the dataset are unneglectable. This may damage the feature's eminence and reduce the detection rate. For this reason, a viable technique is utilized to dispense with noise and another hazard [1]. The plant leaf disease detection through the naked eye observes the manifestations, incorporating an extensive level of complications, because of this multifaceted nature and countless disease in crops and current pathology issues, even a ranch expert and vegetable pathologists are generally neglected to dissect specific disease and therefore conducted wrong results and deductions.

An automatically computerized strategy to perceive and classify the plant leaf disease would give full support to the plant pathologists for detection of disease through visual perceptions [2]. With the use of graphical processing units' numerous applications related to artificial intelligence (AI), machine learning has a higher rate of growth, which prompts curiosity in models and methodologies. An automated computerized identification is required for the

detection of classification of plant leaf disease [2]. Features extraction [3] and features selection are essential for image illustration. Many features extraction and classification approaches have been introduced for organic products, such as fruits. The hybrid method is used for the recognition and detection method for the citrus fruit disease. Lesion spot detection and geometric and texture feature fusion are used to select the best features. PCA was used for scoring the features. The proposed method utilizes a dataset of citrus diseased fruit named Anthracnose, canker, scab, greening, and melanoses. The proposed algorithm accomplished diverse accuracy which is 97% on citrus disease, 89% results on the consolidated, and 90.4% accuracy on the local dataset [4]. Different steps of image processing in which preprocessing, segmentation, features extraction, and classification are used are depicted in Figure 1.

Classical image processing contains propelled procedure of Computer Vision (CV) for detection of disease and expands the rate of accuracy in results. Approaches for the segmentation incorporate thresholding [5], adaptable thresholding approach [6] segmentation dependent on Neural Network (NN) [7,8], bend segmentation [9], and edge recognition-based segmentation [10]. These methods can be applied for plant leaf disease detection.

The image processing techniques are used to check different diseases in the crop and the diseases in insects of the crop. Deep learning techniques also help in identifying infections. The detection implementation by using the Convolutional Neural Network (CNN) is improved in terms of accuracy, well-defined results, and precision [11].

When it comes to know about the challenges, then different methods are used to compare the existing work with the previous one. The challenges include detection speed problem, occlusion problem, and lighting problem [5].

1.1. Problem Statement. Generally, Computer Vision- (CV-) based techniques for identification and classification consist of mainly five steps including preprocessing, features extraction, features selection, features fusion, and classification. For these types of structures, many challenges are encountered that are to be addressed to increase the efficiency and accuracy rate for classification.

The visually appealing quality of images of cucumber leaves for accurate feature extraction is the first challenge in the preprocessing stage. The maintenance of low- and high-quality contrast of spots on leaves, curved edges may affect the accuracy of classification. The changes required for the dataset include scale spacing for data augmentation. Feature fusion and feature selection use texture and shape features; therefore, an appropriate method for feature extraction and selection is needed for the improvement of accuracy in results and as well as for classification. Moreover, the domain of computer-based approaches indicates that visually interesting features in features selection are the main challenge for the improvement of accuracy performance and recognition rate.

1.2. Author's Contributions. Significant contribution in this approach is the preprocessing, feature extraction, and classification steps. In preprocessing resized, the greyscale transformed image uses the Otsu threshold, which converts the intensity image into a binary image. Tan–Triggs is used for normalization, which is never utilized in existing work. The second influential contribution in this algorithm is an amalgamation of three features. These features are extracted and further fused by using serial-based feature fusion. The dataset is usually too small for cucumber leaf disease, and preprocessing is the primary issue. The preprocessing step is necessary for this cause. The contrast enhancement problem, as well as the light variation problem, can render detecting cucumber leaf disease difficult.

1.3. Paper Organization. The remaining paper is arranged as follows: Section 2 describes literature work. Section 3 presents a proposed step along with diagram and all proceeding steps. Section 4 presents feature extraction and selection; Section 5 presents features fusion; Section 6 provides classification; in Section 7, results and experiments are presented; and the conclusion is described in Section 8.

2. Related Work

In related work, a number of techniques are presented for recognition and classification of plant leave disease. For the detection of crop disease, the CNN model was used for training and testing purposes, based on a plant leaf dataset of different classes. Existing deep learning models are applied, which are specific and are very easily applicable to crops attack. These models are determined with a small amount of data but give the best results for specific objects [6]. These modeling's contain the very high-performing technique for the development of disease recognition. For the sake of better results, the classification method using many classifiers gives satisfactory results [7].

Zhang et al. [12] described an IoT-based approach that handles the problem of discriminant features selection of disease parts. They explained that equal importance of features fusion, clustering, and PHOG features are extracted. A complete process of segmentation is done, and in this way, plant disease can be recognized.

By comparing different conventional techniques with CNN models using the images taken from the dataset, their results for the conventional perform better than a deep model. The losses may occur due to the mismanagement of CLR infection present on the coffee leaves, resulting in the drop of immature leaves. The severity of plant disease can be described with less amount of work with remote sensing bands and different vegetation catalogs. This is because of the multifaceted relationship between remote sensing catalog and leaf disease complexity [9]. Multiscreening with multifeatures is used for disease detection [10].

The diagnosis of leaf diseases is important in the cultivation of crops. The production can be achieved by observation which requires a high degree of learning and

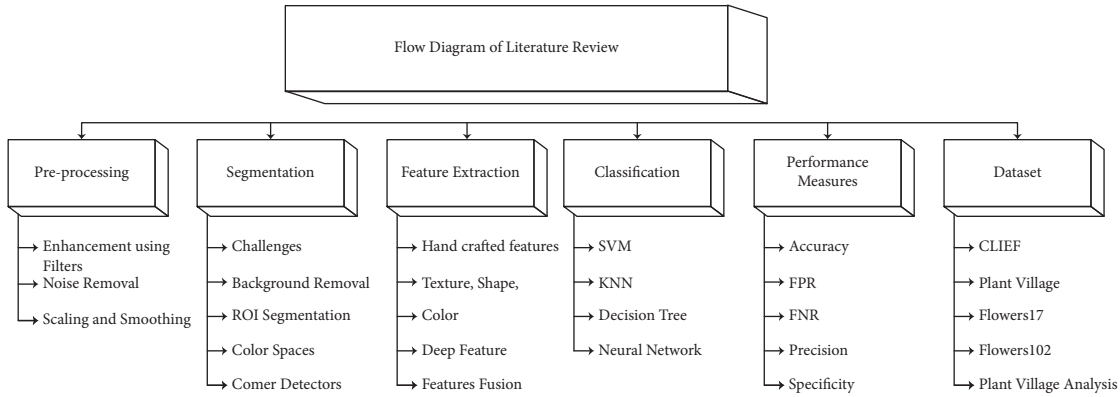

Figure 1: The literature review of different steps in image processing.

practice. The novelty in the domain of Artificial intelligence is the observation of retaining data, which is further enhanced by using different tools merging with the AI techniques helpful in diagnosing the crop diseases. The stimulating task is a visualization of features or interesting parts of a leaf image. This task is difficult in the case of automated detection [13].

The proposed approach for segmentation and detection method for plant leaf disease include the fusion of superpixel and k-mean clustering. Feature extraction method PHOG uses the color components and greyscale image. The accuracy achieved by the proposed method is 92.15% with fivefold cross-validation [12].

3. Proposed Model and Benefit

This section of the proposed model elaborates three major steps like preprocessing, feature extraction, and leave disease classification. Each step is further divided into multiple subparts in a sequence. The first step consists of preprocessing and normalization. Whereas Figure 1 shows the second step of feature extraction based on the texture and shape features of cucumber leaf images, Figure 2 shows the proposed model for cucumber leave disease identification and classification.

3.1. Dataset Expansion. The dataset for cucumber leaf disease is increased by increasing the instances of the dataset. The main reason for enlarging the number of images is to get the improving accuracy and decrease the error rate. A number of instances can be increased by using the MATLAB command and we also increase the dataset by using the flipping function, which also increases the dataset. The main reason for increasing the number of instances is to manage the dataset to get the optimal solution.

3.2. Preprocessing. Preprocessing plays an essential role in image enhancement in order to achieve the milestone to refine edges, eliminate noise, and remove blurriness, and challenge is required for image augmentation. The preprocessing step involves the conversion of a color image into a greyscale image. The intensity of the color image is converted into another channel with the image size of 640×480. Figure 3 shows the cucumber dataset. The purpose of image preprocessing is to encounter the interesting part (i.e., diseased part).

Normalization is a process in which data is rearranged to meet the needs of removing the redundancy from the data and adding all related data (logical data) or interesting parts. All normalization techniques perform in the preprocessing stage. First of all, RGB images from the dataset are converted into greyscale, resized images, and normalization techniques are performed.

Tan–Triggs is a function to normalize the data in a vector and matrix which can be computed through scoring. Our work includes the Tan–Triggs normalization and Otsu threshold to binarize the image into greyscale. The dataset consists of six diseased classes of cucumber containing Downy mildew, Powdery mildew, Anthracnose, Blight, *Corynespora*, and Angular leaf spot. Dataset is collected on the basis of private reference [14] excluding healthy images.

3.3. Tan–Triggs Normalization. Tan–Triggs is used for the enhancement of the local texture features of the image for disease recognition under lighting conditions. The Illumination Normalisation (IN) is used in the prepossessing stage to describe the difference between gamma correction, nonlinear filtering, and Gaussian filtering [15].

Tan–Triggs contains different steps: Gamma correction, the difference of Gaussian, masking, and contrast equalization. Details are as follows [16].

3.4. Illumination Normalization and Reflectance. The amount of illumination is reflected from the image, and components contain the reflectance; these components are

$$m(x, y) = J(x, y) * K(x, y). \quad (1)$$

In the above equation, J is light incident and depends on circumstances, and it varies when compared with reflectance.

We also take the log of J term when the objects are compressed by using the sum.

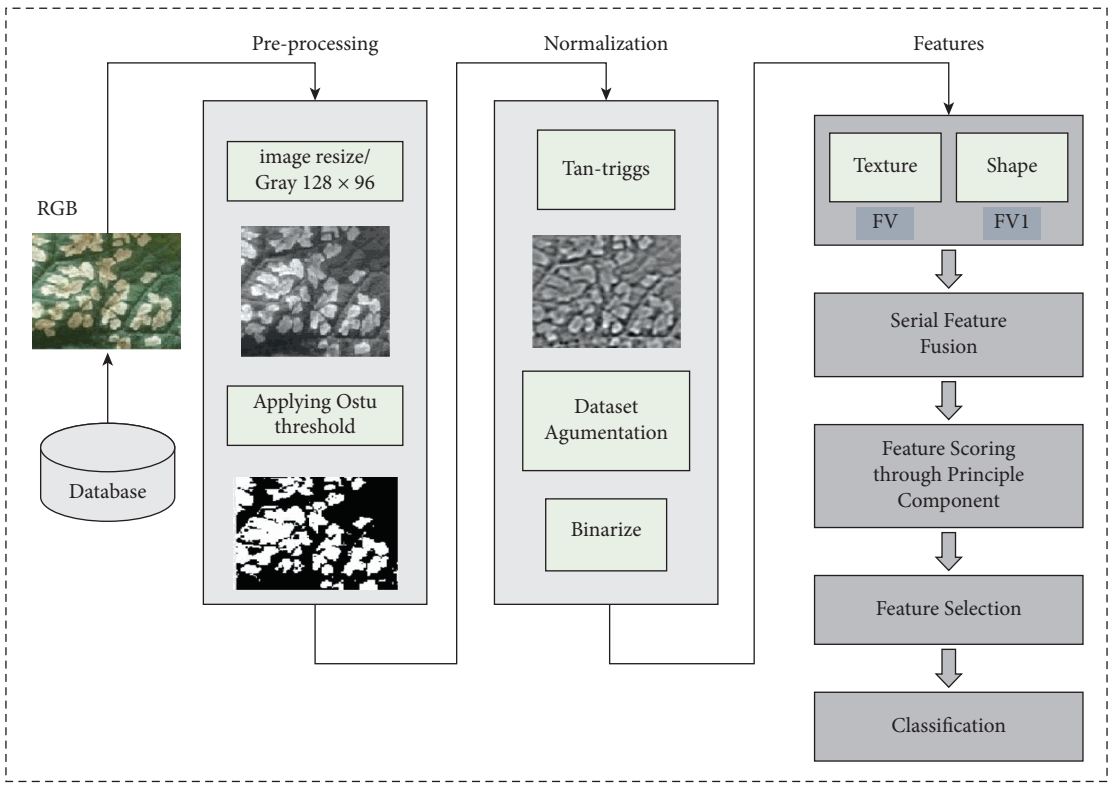

Figure 2: A proposed model for cucumber leaves disease identification and classification.

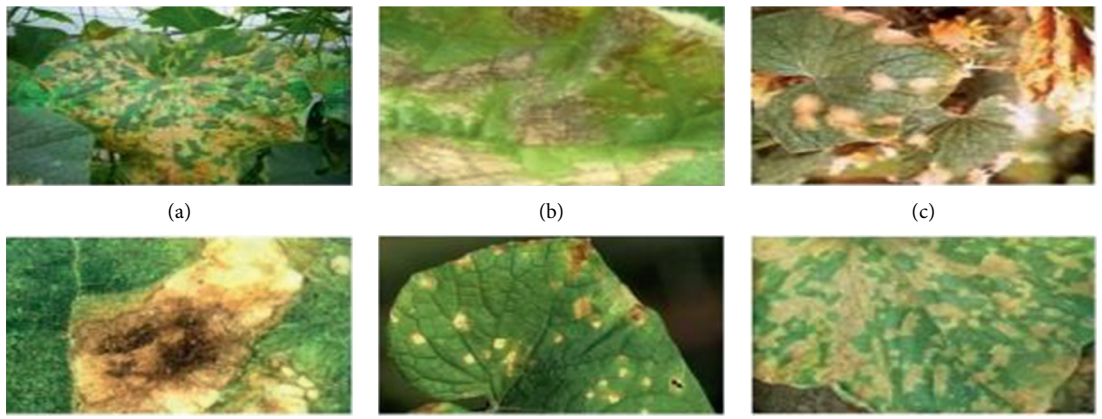

Figure 3: Cucumber diseased leaf dataset. (a) Angular leaf spot. (b) Anthracnose. (c) Blight. (d) *Corynespora*. (e) Downy mildew. (f) Powdery mildew.

$$log\,(J\,(x, y)) + K\,(x, y). \tag{2}$$

3.4.1. Gamma Correction. Gamma correction is a transformation of a grey-level image. Its purpose is to convert every pixel into its intensity as follows:

$$0 \le \gamma \le 1, \tag{3}$$

where $g\,(J)$ increases the dynamic series of pixels. The dynamic range enhances the brightness while doing compression and enhances the dynamic range in dark areas.

3.4.2. Difference of Gaussian Filtering. Normalization for enhancing the contrast does not eliminate shading/intensity effects. Shading effects have a low frequency. Shading effects can be removed by using the high range filters known as Dog filters.

Dog filter used for edge detection and Gaussian can be described by standard deviation sigma. Sigma σ) is used to remove noise only. Another Gaussian removes high-frequency details from the pixels. So, we can obtain a high-frequency edge by subtracting low-frequency pixels.

3.4.3. Contrast Equalization. Pixel intensifies and maintains the contrast. We can get pixel intensity by using the following equations:

$$j = \frac{j}{\left(\text{mean}\left(j^{\alpha}\right)\right)^{(1/\alpha)}},$$
$$j = \frac{j}{\left(\text{mean}\left(\min\left(\tau,\ j^{\text{alpha}}\right)\right)\right)^{(1/\alpha)}}, \tag{4}$$
$$j = \tau * \tanh\left(\frac{1}{\tau}\right).$$

Figure 4 shows the grey scale and Tan–Triggs normalized image of a cucumber leaf.

A complete proposed diagram of the proposed model for the cucumber leaf disease recognition is presented in Figure 2.

4. Features Extraction and Selection

Feature extraction in image processing extracts the interesting part of an image (i.e., the diseased part of an image). The selected features reduce the dimensions. In the proposed system, texture and shape features including HOG, LBP, and COLOR features are extracted. As HOG stands for Histogram of Gradient, LBP stands for Local Binary Pattern, and SVM stands for Support Vector Machine. By using many parameters, every feature returns a different feature vector. The detailed diagram is shown in Figure 5. The details of every feature are described as follows.

HOG features are widely used for object detection, which is represented as a single feature vector where each represents a segment of an object. Mostly computed by using the sliding window for each position in a segment of an image with an SVM classifier. Therefore, we use these features for the detection of disease in the cucumber leaves. Preprocessing phases resize the original image into any type of size through which the position of an image can get through several scales. The visualization of the HOG feature for cucumber anthracnose is shown in Figure 6.

The local binary pattern that is used for the texture feature was first to discover by [17] in 2002. The mathematical modeling of LBP can be described by using blocks. The block is overlapped and divided into the same size. The center and neighboring pixels are matched with the greyscale values. The threshold is fixed to compare the block size value with the grey pixel value. If the equivalent grey-level value is greater than the center pixel value, the position is marked as "1." Otherwise, the position is marked as "0" [18].

The 7 layers of CNN are used with the LBP. The LBP stands for Local Binary Pattern that is used for the features extraction of disease [14].

Color features are used to find out the diseases in the plants or crops. Different colors spaces are explored in [11], and then features are extracted from different color channels.

Binary code: 00100011 and LBP.

In the above figure, the first two tables show the difference of pixels, and the third table shows the threshold value and binary code accordingly.

The formal form of the LBP feature can be explained by using the following equation [18]:

$$lbp\left(L_a,\ M_a\right) = \sum_{q=0}^{q-1} 2^q f\left(i_q - i_a\right). \tag{5}$$

In the above equation, the terms $\mathbf{L_a}$, $\mathbf{M_a}$ show the location of the pixel that is located at the center; i_q and i_a show the brightness of adjacent pixels where the term $\mathbf{f}$ shows symbolic function:

$$f(a) = \begin{cases} 1, & \text{if } x \geq 0, \\ 0, & \text{else.} \end{cases} \tag{6}$$

The local binary pattern has the ability to adapt to the circumstances of different texture features in detail and is used in many fields, including texture recognition [19] and hyperspectral image classification [20]. The diseased anthracnose leaf has LBP feature extraction with pixel-wise LBP image shown in Figures 5 and 7, showing the calculation of features extraction and features scoring of HOG, LBP, and color, respectively.

5. Features Fusion

Feature fusion plays an important role in the field of machine learning and computer vision. Many features are joined together to make a new feature vector by applying the serial-based fusion. To get the optimal solution, the HOG, LBP, and color feature vectors are fused.

Features reduction is substantial in most disease recognition processes as it eliminates the unwanted features and removes the redundant features from the images [14]. As a result, we will get an accurate classification. The fusion method is very helpful for getting better results. This paper implements a probability process for the removal of inappropriate features [21]. Features are named as feature factors F_1, F_2, and F_3; these factors belong to R, where R represents the real values. Hog, LBP, and color features are to be considered, which represent the positive value features.

The feature vector can be described by using the following equation:

$$Fv_{i\times H} = \left\{v_{i\times 1}, v_{i\times 2}, v_{i\times 3}, \ldots, v_{i\times H}\right\}. \tag{7}$$

Equation (7) shows the fused feature vector of HOG, where $i = 1$, F is the feature vector, and H shows the HOG feature.

$$Fv_{j\times L} = \left\{v_{j\times 1}, v_{j\times 2}, v_{j\times 3}, \ldots, v_{j\times L}\right\}. \tag{8}$$

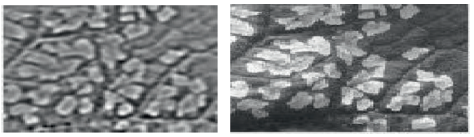

Figure 4: Tan–Triggs normalization.

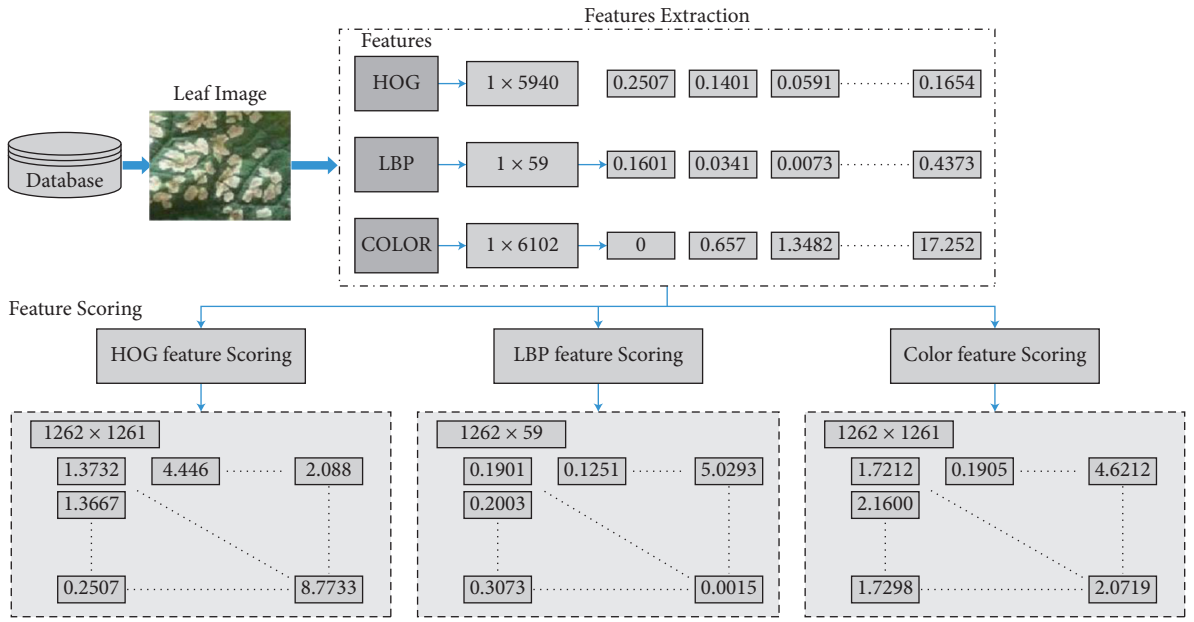

Figure 5: Features extraction and features scoring of HOG, LBP, and color, respectively.

Figure 6: HOG visualization.

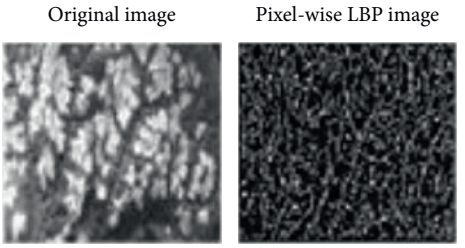

Figure 7: Grey image with LBP pixel-wise extraction.

Equation (8) shows the fused feature vector of LBP, where $j = 1$, F is the feature vector, and L shows the LBP feature.

$$Fv_{k\times C} = \{v_{k\times 1}, v_{k\times 2}, v_{k\times 3}, \ldots, v_{k\times C}\}. \quad (9)$$

Equation (9) shows the fused feature vector of color, where $k = 1$, F is the feature vector, and C shows the color feature.

Features are fused by using the following equation, where D shows the fused vector:

$$\text{FUSED } (FV)_{1\times D} = \sum_{i=1}^{3} \left\{ Fv_{i\times H}, Fv_{j\times L}, Fv_{k\times C} \right\}. \quad (10)$$

HOG, LBP, and color features are extracted and fused together. Figure 8 shows the complete feature extraction of texture, color, and shape features.

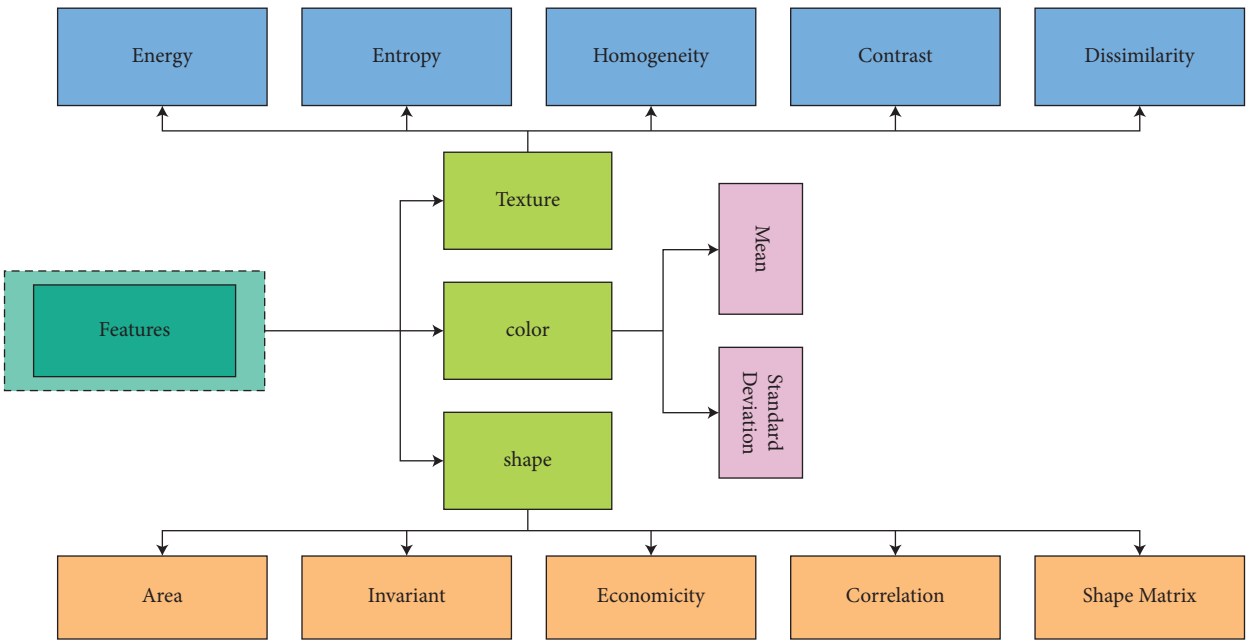

Figure 8: Features extraction of texture, color, and shape features.

6. Classification

Classification plays an essential role in the field of image processing. To attain satisfactory results from the multi-SVM, many experiments have been performed by using the selected feature. In the category of classification, many classifiers are used to classify the disease. KNN classifiers include medium, weighted, and fine KNN.

The geometric family of classifiers includes the diversity of SVM. These can be substantiated by using the functions quadratic, Gaussian kernel, linear, and cubic. The tree category contains the ensemble boosted and bagged trees. Probability classifications include naïve Bayes, multikind of naïve Bayes, Bayesian logistic regression, and Bayesian net. These classifiers are used to evaluate the performance of the cucumber leaf dataset, which is based on different performance measures later used in the result section.

7. Experimental Results and Analysis

A set of models are presented for the final analysis of the suggested framework. In the first experiment, HOG and BRISK features are fused and later fed to the classifiers. In the second test, all types of features (shape, texture, and colors) are fused and given to the classifiers, and in the final test, reduced features using the proposed method are supplied to the classifiers. The key reason behind these experiments is to analyze the performance of each step, involved in this proposed methodology.

7.1. Dataset and Performance Measures. For the evaluation of experimental results, cucumber leaf dataset is used, which is collected through private reference. The six classes for cucumber leaf dataset are angular leaf spot, anthracnose, blight, coryneform, downy mildew, and powdery mildew. The total number of images in the dataset is 1262. Three types of experiments are performed with the help of features extraction. All experiments contain different feature subsets with the variation of HOG, LBP, and COLOR features. Each experimental result varies from the other based on selecting features. Classification results can be measured by using classification methods including Fine KNN, subspace KNN, Bagged trees, Weighted KNN, SVM cubic, Quadratic SVM, boosted trees, Fine Tree, Cosine KNN, and Medium tree. The performance is calculated by using many classification methods. Performance measures include False Positive Rate (FPR), Sensitivity, Classification Rate (CR), Specificity, False Negative Rate (FNR), Precision, Accuracy, and Time.

In true positive rate means diseased samples, and true negative means both actual and predicted values are negative. False-negative means that actual values are positive and predicted values are negative. The mathematical results can be taken by using the formulas for CR, FPR, Sensitivity, Specificity, Precision, and FNR as follows [22]:

$$\begin{aligned} \text{CR} &= \frac{(\text{CC samples})}{(\text{all samples})} \times 100\%, \\ \text{FNR} &= \frac{(\text{false negative})}{(\text{all negatives output})}, \\ \text{FPR} &= \frac{(\text{false positive})}{(\text{all positives output})}, \\ \text{senstivity} &= \frac{\text{true positive}}{\text{true positive} + \text{false negative}}, \\ \text{presicion} &= \frac{\text{true positive}}{\text{TP} + \text{FP}}. \end{aligned} \tag{11}$$

There are many cross-validation (CV) methods available in MATLAB, including *k*-fold, HoldOut, LeaveMout. The method performed by machine learning mainly involves tuning, assembly of the trained model, and performance evaluation of the proposed model. CV methods besides the performance measure also perform estimation and configuration. This is enthusiastically inclined and effective. An effective bootstrap method for cross-validation (BBC-CV) is used for selecting the best results and performance [23]. Features were combined with Principal Component Analysis (PCA) with key point's I-e principal component and index. We perform 10-fold cross-validation on each trial to get better results and generate classifying data for the cucumber dataset. All tests were performed on MATLAB 2018a using the personnel laptop with Windows 8.1, 64-bit operating system, and 6 GB RAM.

7.1.1. Angular Leaf Spot. The spots may consist of different colors of light yellow, and the condition of leaves becomes very severe in case of less nitrogen. Angular leaf spot means that spots appear on veins of leaf caused by the virus pathogens, *P. syringae* PV. Lachrymans. This disease is mostly caused by infection and the pseudomonas virus. For this purpose, medicated protection element Plant Growth-Promoting Rhizobacteria (PGPR) mediated ISR is recycled [24].

7.1.2. Powdery Mildew. Powdery mildew is a severe disease that causes mildew toxicities in leaves of cucumber. Infected fluid from leaves causes reductions in growth, premature vegetation, as a result of loss in economic. A fungal virus that is commonly known as phytopathogenic is present in powdery mildew. There is fast and divergent increase of the fungus-virus in infected leaves preserved with Milana. Milana may be suitable in the case of plant disease defense in the incorporated organization of powdery mildew [25].

7.1.3. Downy Mildew. Fungus bacterial diseased spreads from the leaves, caused by the infection known as *Pseudoperonospora*. The growing reason for downy mildew is the increased rate of leaf temperature. Unhealthy regions with complex backgrounds show infected parts [26].

7.1.4. Anthracnose. Anthracnose is caused by yeast effects and the fungal virus is known as *Colletotrichum*. These viruses cause resistance possessions in the growth rate of cucumber leaves [3].

7.1.5. Corynespora. The infection in leaves starts from slight spots of brown color with increasing the yellow glory. Leaves become uneven in shape and result in leafless plants. Symptoms rapidly increase in the fungal virus known as *Corynespora* [8].

7.2. Results. For measurable results, three separate tests are performed using a distinct number of features in each experiment. The description for each experiment which contains the number of features and number of diseased classes is shown in Table 1.

The description analysis for each experiment is performed on 1262 images with multifeatures selection.

7.2.1. Experiment 1. In experiment 1, the total number of images are 1262 with six diseased classes of a cucumber leaf. For these first results, in the first experiment, HOG, LBP, and color features are extracted. 100 features for HOG and LBP are taken at 10-fold cross-validation. Fine KNN and subspace KNN give the highest accuracy of 94.30% than other classification methods. The accuracy gained for both fine KNN and subspace KNN is similar. The instances for the feature vector (FV) are double. Performance measures include specificity, sensitivity, precision, FNR, FPR, and time. The graphical illustration of certain classification methods is shown in Figure 9. The other classifiers including bagged KNN, weighted KNN, and SVM cubic are also described as below. The first experiment gives the best results as compared with other experiments from the above discussion and analysis our proposed method gives the performance for the feature vector size for HOG is 1×5940, LBP is 1×59, and color is 1×6120. In the confusion matrix ensemble, fine KNN confirms the classification results shown in Table 2. Table 3 shows the experimental results of experiment 1. The confusion matrix of cucumber leaf dataset of Test 1 on ensemble fine KNN is shown in Table 2.

7.2.2. Experiment 2. In the second experiment, HOG, LBP, and color features are extracted. 300 features for HOG and LBP are taken at 10 cross-validations. In the second experiment, fine KNN and subspace KNN give 94.60% and 94.50% accuracy with 84.0% specificity and sensitivity, 84.6% precision, 5.4% FNR rate, and 0.011 FPR rate, respectively. These classifiers give the highest accuracy as compared to others. The instances for the feature vector (FV2) are double. Performance measures include specificity, sensitivity, precision, FNR, FPR, and time. The confusion matrix confirms the classification results in Table 4. Table 5 shows the performance evaluation of experiment 2. Graphical representation of classification methods in terms of accuracy and time for experiment 2 is shown in Figure 10.

7.2.3. Experiment 3. In the third experiment, HOG and LBP features are extracted. 500 features for HOG and LBP are taken at 10 cross-validations. In the first experiment, fine KNN and subspace KNN give 94.2% and 82.5% specificity and 83.66% precision, 5.8% FNR, and 0.011 FPR rate, respectively. These classifiers give the highest accuracy as compared to others. The instances for the feature vector (FV2) are double for the reason of improving accuracy. Performance measures include specificity, sensitivity, precision, FNR, FPR, and time. The confusion matrix approves the result of the classification method in Table 6. The remaining performance of classifiers includes Fine SVM, cubic SVM, and fine Gaussian SVM, fine tree, weighted

Table 1: Selected features in experiments.

		Selected features		
Experiment	Classes	HOG	LBP	Color
Experiment 1	6	100	100	50
Experiment 2	6	150	100	0
Experiment 3	6	100	150	60

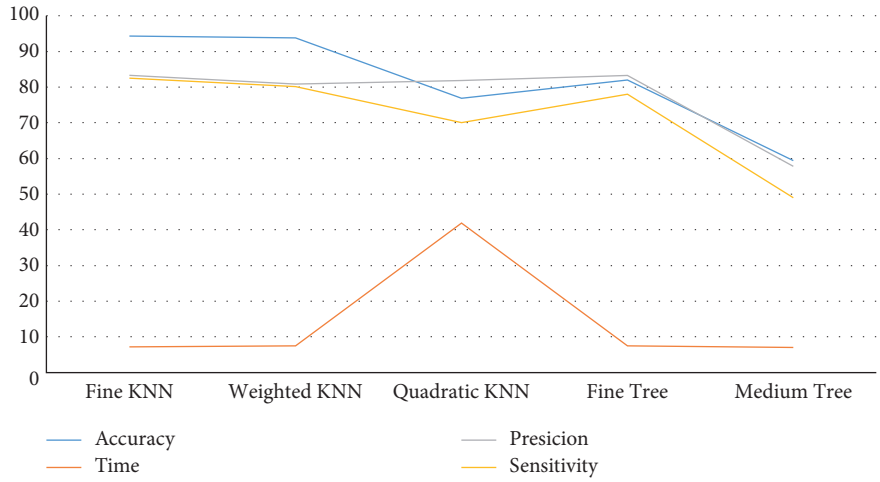

Figure 9: Graphical representation of classification methods in terms of accuracy and time for experiment 1.

Table 2: Confusion matrix of cucumber leaf dataset of test 1 on ensemble fine KNN.

		Classification classes					
Classification classes	Total images	Angular leafspot	Anthracnose	Blight	*Corynespora*	Downy mildew	Powdery mildew
Angular leafspot	204	**96%**	2%	1%	1%		
Anthracnose	54		**99%**	1%			
Blight	130			**98%**			5%
Corynespora	22		25%	56%	**16%**	2%	2
Downy mildew	257	2%	2%	3%	5%	**87%**	1%
Powdery mildew	348			1%			**99%**

Bold shows highest values in terms of accuracy.

Table 3: Result for experiment 1.

Classifier	Performance evaluation					
	Accuracy (%)	Specificity (%)	Sensitivity (%)	Precision (%)	FNR (%)	FPR
Fine KNN	**94.30**	**82.5**	**82.5**	**83.30**	**5.7**	**0.011**
Subspace KNN	**94.30**	**82.5**	**82.5**	**82.50**	7.2	0.011
Bagged trees	94.00	96.0	96.0	79.80	6.0	0.013
Weighted KNN	93.80	80.1	80.1	80.83	6.2	0.013
SVM cubic	91.90	65.5	91.6	94.40	8.1	0.031
Quadratic SVM	76.70	68.9	72.0	81.80	23.3	0.055
Fine tree	82.00	78.0	78.0	83.20	18.0	0.040
Boosted trees	66.20	56.0	56.0	72.40	33.8	0.071
Cosine KNN	68.70	60.0	60.0	64.80	31.3	0.071
Medium tree	59.40	49.4	49.4	57.80	59.4	0.093

Bold shows the highest values in terms of accuracy.

KNN and their specificity, sensitivity, precision, FNR, and FPR, respectively, are also shown in Table 7. The accuracy improves by the subspace classifier by using 10-fold cross-validation. Graphical representation of classification methods in terms of accuracy, time, precision, and specificity for experiment 2 is shown in Figure 11.

Table 4: Confusion matrix of cucumber leaf dataset of test 2 on ensemble fine KNN.

		Classification classes					
Classification classes	Total images	Angular leafspot	Anthracnose	Blight	*Corynespora*	Downy mildew	Powdery mildew
Angular leafspot	204	**97%**		1%	1%		
Anthracnose	54		**99%**	1%			
Blight	130			**98%**	1%		1%
Corynespora	22		25%	56%	**23%**	2%	2
Downy mildew	257	1%	2%	3%	5%	**87%**	1%
Powdery mildew	348						**100%**

Bold shows the highest values in terms of accuracy. Fine KNN and subspace KNN have highest accuracy.

Table 5: Performance evaluation of experiment 2.

Classifier	Performance evaluation					
	Accuracy (%)	Specificity (%)	Sensitivity (%)	Precision (%)	FNR (%)	FPR
Fine KNN	**94.6**	**84.0**	**84.0**	**84.6**	**5.4**	**0.011**
Subspace KNN	94.5	83.8	83.8	84.3	5.6	0.011
Bagged trees	94.2	80.5	80.5	81.0	5.8	0.013
Weighted KNN	93.6	81.0	81.0	82.5	6.4	0.013
SVM cubic	91.6	90.8	90.8	93.6	8.4	0.018
Fine tree	81.8	76.6	76.6	81.6	18.2	0.045

Bold shows the highest values in terms of accuracy. The Fine KNN classifier has the highest accuracy of 94.6%, specificity of 84.0%, sensitivity of 84.0%, precision of 84.6%, FNR rate of 5.4, and FPR is 0.011.

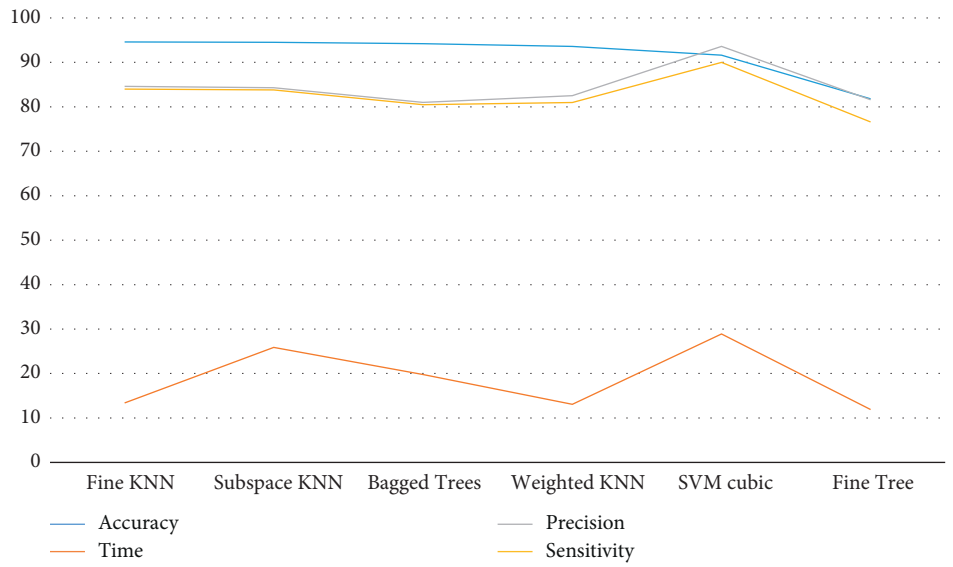

Figure 10: Graphical representation of classification methods in terms of accuracy and time for experiment 2.

Table 6: Confusion matrix of cucumber leaf dataset of test 1 on subspace-KNN.

		Classification classes					
Classification classes	Total images	Angular leafspot	Anthracnose	Blight	*Corynespora*	Downy mildew	Powdery mildew
Angular leafspot	204	**96%**	2%	1%	1%		
Anthracnose	54		**99%**	1%			
Blight	130			**96%**	1%	2%	1%
Corynespora	22		12%	25%	**18%**	45%	22
Downy mildew	257	1%	2%	3%	5%	**87%**	1%
Powdery mildew	348						**99%**

The highest values are shown in bold.

Table 7: Performance evaluation of experiment 3.

Classifier	Performance evaluation					
	Accuracy (%)	Specificity (%)	Sensitivity (%)	Precision (%)	FNR (%)	FPR
Subspace KNN	**94.2**	**82.5**	**82.5**	**83.66**	**5.8**	**0.011**
Bagged trees	93.0	95.2	94.8	79.16	7.0	0.015
Fine KNN	93.9	83.1	82.1	83.66	6.1	0.013
Cubic SVM	91.8	93.6	91.0	94.00	8.2	0.018
Fine Gaussian SVM	71.2	62.2	62.2	81.8	28.2	0.068
Fine tree	82.1	77.6	77.6	83.2	17.9	0.08
Weighted KNN	93.4	95.6	90.7	96.9	6.6	0.016

Bold shows the highest values in terms of accuracy. The subspace classifier has the highest accuracy of 94.2%, specificity of 82.5%, sensitivity of 82.5%, precision of 83.66%, FNR rate of 5.8, and FPR is 0.011.

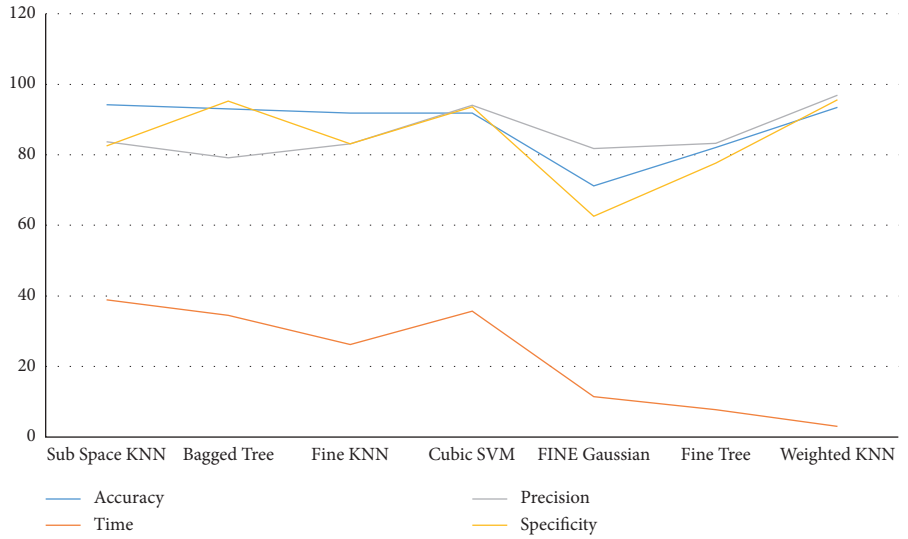

Figure 11: Graphical representation of classification methods in terms of accuracy, time, precision, and specificity for experiment 2.

8. Conclusion

The proposed approach is mainly used for cucumber leaf detection, based on preprocessing, normalization, feature extraction, feature selection, fusion, and classification. From above all discussion and influences, it is concluded that cucumber leaf disease is addressed by using the feature extraction of HOG, LBP, and color features. These texture and shape features help in the recognition of the disease in leaves and color features help in the recognition of diseased part of a leaf. Furthermore, feature selection and feature fusion are important to improve the accuracy of different performance measures, including accuracy, specificity, sensitivity, and precision. The proposed algorithm method shows 94.6% accuracy, which is better than that of existing work.

Data Availability

The data used to support the findings of this study can be obtained from the corresponding author upon request.

Conflicts of Interest

The authors declare that they have no conflicts of interest.

Authors' Contributions

All the authors contributed equally to this work and were involved in its development at every phase. The submitted version of the work has been read and approved by all authors.

Acknowledgments

This study was supported byTaif University Researchers Supporting Project (no. TURSP-2020/347), Taif University, Taif, Saudi Arabia.

References

[1] J. Ma, K. Du, F. Zheng, L. Zhang, Z. Gong, and Z. Sun, "A recognition method for cucumber diseases using leaf symptom images based on deep convolutional neural network," *Computers and Electronics in Agriculture*, vol. 154, pp. 18–24, 2018.

[2] W. Xie, J. A. Noble, and A. Zisserman, "Microscopy cell counting and detection with fully convolutional regression networks," *Computer Methods in Biomechanics and Biomedical Engineering: Imaging & Visualization*, vol. 6, no. 3, pp. 283–292, 2018.

[3] H. D. Gottstein and J. Kuc, "Induction of systemic resistance to anthracnose in cucumber by phosphates," *Phytopathology*, vol. 79, no. 2, pp. 176–179, 1989.

[4] M. Sharif, M. A. Khana, Z. Iqbal, M. F. Azam, M. I. UllahLali, and M. Y. Javed, "Detection and classification of citrus diseases in agriculture based on optimized weighted segmentation and feature selection," *Computers and Electronics in Agriculture*, vol. 150, pp. 220–234, 2018.

[5] J. Liu and X. Wang, "Plant diseases and pests detection based on deep learning: a review," *Plant Methods*, vol. 17, no. 1, pp. 1–18, 2021.

[6] X. E. Pantazi, D. Moshou, A. A. Tamouridou, and S. Kasderidis, "Leaf disease recognition in vine plants based on local binary patterns and one class support vector machines," in *Proceedings of the IFIP International Conference on Artificial Intelligence Applications and Innovations,* Thessaloniki, Greece, Springer, September 2016.

[7] S. H. Lee, C. S. Chan, P. Wilkin, and P. Remagnino, "Deepplant: plant identification with convolutional neural networks," in *Proceedings of the 2015 IEEE International Conference on Image Processing (ICIP),* Quebec City, Canada, IEEE, September 2015.

[8] M. Kwon, B. R. Kang, B. H. Cho, and Y. C. Kim, "Occurrence of target leaf spot disease caused by Corynespora cassicola on cucumber in Korea," *Plant Pathology*, vol. 52, no. 3, p. 424, 2003.

[9] A. Chemura, O. Mutanga, M. Sibanda, and P. Chidoko, "Machine learning prediction of coffee rust severity on leaves using spectroradiometer data," *Tropical Plant Pathology*, vol. 43, no. 2, pp. 117–127, 2018.

[10] P. A. Marin Zapata, S. Roth, D. Schmutzler, T. Wolf, E. Manesso, and D. A. Clevert, "Self-supervised feature extraction from image time series in plant phenotyping using triplet networks," *Bioinformatics*, vol. 37, no. 6, pp. 861–867, 2021.

[11] L. C. Ngugi, M. Abelwahab, and M. Abo-Zahhad, "Recent advances in image processing techniques for automated leaf pest and disease recognition–A review," *Information processing in agriculture*, vol. 8, no. 1, pp. 27–51, 2021.

[12] S. Zhang, H. Wang, W. Huang, and Z. You, "Plant diseased leaf segmentation and recognition by fusion of superpixel, K-means and PHOG," *Optik-International Journal for Light and Electron Optics*, vol. 157, pp. 866–872, 2018.

[13] X. Pantazi, D. Moshou, and A. Tamouridou, "Automated leaf disease detection in different crop species through image features analysis and One Class Classifiers," *Computers and Electronics in Agriculture*, vol. 156, pp. 96–104, 2019.

[14] S. Zhang and Z. Wang, "Cucumber disease recognition based on Global-Local Singular value decomposition," *Neurocomputing*, vol. 205, pp. 341–348, 2016.

[15] X. Tan and W. Triggs, "Enhanced local texture feature sets for face recognition under difficult lighting conditions," *IEEE Transactions on Image Processing*, vol. 19, no. 6, pp. 1635–1650, 2010.

[16] X. Tan and B. Triggs, "Enhanced local texture feature sets for face recognition under difficult lighting conditions," in *Proceedings of the International Workshop on Analysis and Modeling of Faces and Gestures*, Springer, Rio de Janeiro, Brazil, October 2007.

[17] T. Ojala, M. Pietikainen, and T. Maenpaa, "Multiresolution gray-scale and rotation invariant texture classification with local binary patterns," *IEEE Transactions on Pattern Analysis and Machine Intelligence*, vol. 24, no. 7, pp. 971–987, 2002.

[18] Z. Xia, X. Ma, Z. Shen, X. Sun, N. N. Xiong, and B. Jeon, "Secure image lbp feature extraction in cloud-based smart campus," *IEEE Access*, vol. 6, 2018.

[19] R. Mehta and K. Egiazarian, "Dominant rotated local binary patterns (DRLBP) for texture classification," *Pattern Recognition Letters*, vol. 71, pp. 16–22, 2016.

[20] W. Li, C. Chen, H. Su, and Q. Du, "Local binary patterns and extreme learning machine for hyperspectral imagery classification," *IEEE Transactions on Geoscience and Remote Sensing*, vol. 53, no. 7, pp. 3681–3693, 2015.

[21] Z. Wang, D. Ziou, C. Armenakis, D. Li, and Q. Li, "A comparative analysis of image fusion methods," *IEEE Transactions on Geoscience and Remote Sensing*, vol. 43, no. 6, pp. 1391–1402, 2005.

[22] C. Xie, C. Yang, and Y. He, "Hyperspectral imaging for classification of healthy and gray mold diseased tomato leaves with different infection severities," *Computers and Electronics in Agriculture*, vol. 135, pp. 154–162, 2017.

[23] I. Tsamardinos, E. Greasidou, and G. Borboudakis, "Bootstrapping the out-of-sample predictions for efficient and accurate cross-validation," *Machine Learning*, vol. 107, no. 12, pp. 1895–1922, 2018.

[24] L. Liu, J. Kloepper, and S. Tuzun, "Induction of systemic resistance in cucumber against bacterial angular leaf spot by plant growth-promoting rhizobacteria," *Phytopathology*, vol. 85, no. 8, pp. 843–847, 1995.

[25] F. Daayf, A. Schmitt, and R. Belanger, "The effects of plant extracts of Reynoutria sachalinensis on powdery mildew development and leaf physiology of long English cucumber," *Plant Disease*, vol. 79, no. 6, pp. 577–580, 1995.

[26] M. Lindenthal, U. Steiner, H. W. Dehne, and E. C. Oerke, "Effect of downy mildew development on transpiration of cucumber leaves visualized by digital infrared thermography," *Phytopathology*, vol. 95, no. 3, pp. 233–240, 2005.

Hindawi
Complexity
Volume 2021, Article ID 3248376, 21 pages
https://doi.org/10.1155/2021/3248376

Research Article

Analytical Investigation of Noyes–Field Model for Time-Fractional Belousov–Zhabotinsky Reaction

Mohammed Kbiri Alaoui,[1] **Rabia Fayyaz**,[2] **Adnan Khan**,[3] **Rasool Shah**,[3] **and Mohammed S. Abdo**[4]

[1]*Department of Mathematics, College of Sciences, King Khalid University, Abha 61413, Saudi Arabia*
[2]*Department of Mathematics, COMSATS University Islamabad, Islamabad, Pakistan*
[3]*Department of Mathematics, Abdul Wali Khan University, Mardan 23200, Pakistan*
[4]*Department of Mathematics, Hodeidah University, Al-Hodeidah, Yemen*

Correspondence should be addressed to Rabia Fayyaz; rabia_fayyaz@comsats.edu.pk and Mohammed S. Abdo; msabdo@hoduniv.net.ye

Received 11 October 2021; Accepted 15 November 2021; Published 8 December 2021

Academic Editor: Fathalla A. Rihan

In this article, we find the solution of time-fractional Belousov–Zhabotinskii reaction by implementing two well-known analytical techniques. The proposed methods are the modified form of the Adomian decomposition method and homotopy perturbation method with Yang transform. In Caputo manner, the fractional derivative is used. The solution we obtained is in the form of series which helps in investigating the analytical solution of the time-fractional Belousov–Zhabotinskii (B-Z) system. To verify the accuracy of the proposed methods, an illustrative example is taken, and through graphs, the solution is shown. Also, the fractional-order and integer-order solutions are compared with the help of graphs which are easy to understand. It has been verified that the solution obtained by using the given approaches has the desired rate of convergence to the exact solution. The proposed technique's principal benefit is the low amount of calculations required. It can also be used to solve fractional-order physical problems in a variety of domains.

1. Introduction

Fractional calculus is concerned with fractional-order derivatives and integrals [1]. Although fractional calculus has a similar background to classical calculus, it has received little attention for a long time. Fractional calculus and fractional differential equations, on the other hand, have grown in popularity in recent decades as a result of their significant prospective applications in physics and engineering [2–6]. For various physical phenomena, a considerable number of new differential equations (models) including fractional derivatives and integration have been constructed. These models have proven to be effective. Many phenomena in physics, chemistry, engineering, and other sciences can be better understood using fractional calculus methods, such as the theory of fractional noninteger order derivatives and integrals. These mathematical phenomena enable a more accurate description of an actual object than using "integer" methods [7–10].

Fractional partial differential equations (FPDEs) are a contemporary tool in calculus that may be used to simulate a variety of phenomena in applied sciences and engineering. Because it proved difficult to simulate nonlinear real-world processes in ordinary calculus, the subject of fractional calculus became popular among researchers [11–17]. In this context, FPDEs approximation and analytical solutions are critical for accurately describing the dynamics of important physical processes. In view of the above statement, mathematicians have devised and applied a variety of approximate and analytical procedures to identify the solutions to a number of important mathematical models that represent real-world issues. Despite the fact that calculating the analytical and even approximate solutions of certain nonlinear FPDEs and systems of FPDEs is extremely challenging,

mathematicians continue to do their best in this respect. Around the years, a great deal of study has been conducted in the fields of science and engineering all over the world, and various methodologies have been developed to provide the best obtainable solutions. This is an unstoppable process, and new techniques are being developed on a daily basis since the world is confronted with new, insoluble, and challenging difficulties and problems [18–22]. Different methods for solving FDEs have been proposed in the literature, including the fractional differential transform method (FDTM) [23], modified homotopy perturbation method (MHPM) [24], Adomian decomposition method (ADM) [25], Sumudu transform method (STM) [26], differential transform method (DTM) [27], homotopy analysis method (HAM) [28], variational iteration method (VIM) [29], and fractional Fourier transform method (FFTM) [30].

The Yang transform decomposition method (YTDM) and the homotopy perturbation Yang transform method (HPYTM) are expanded for time-fractional Belousov–Zhabotinskii (B-Z) system solution in this article. Xiao-Jun Yang proposed the Yang transform, which may be used to solve a variety of differential equations with constant coefficients. On the other hand, the Adomian decomposition method [31, 32] is a well-known technique for solving linear and nonlinear and homogeneous and nonhomogeneous differential and partial differential equations, and integrodifferential and FDEs that provides exact solutions in the form of a convergent series. He introduced HPM in 1998 [33, 34]. The result is considered to be an in series solution with a high number of terms that quickly converge to the actual derived solution in this technique. The method is capable of adequately solving nonlinear PDEs. When the HPTM results were compared with the real solution to the problems, a higher level of accuracy was proven. Nonlinear wave equations [35], nonlinear problem bifurcation [36], and boundary value problems [37] have all been solved using this technique. In this paper, we used a new approximation analytical method called HPYTM. The hybrid form of Yang transform and HPM is the newly designed technique. The current methods are shown to be quite effective in obtaining the analytical solution of the time-fractional Belousov–Zhabotinskii (B-Z) system. The results of the recommended procedures are convincing, providing exact solutions to the targeted problems. The fractional problem findings obtained utilising the given approaches are also used to analyse the problems from a fractional perspective. The existing techniques can be adjusted to solve various fractional PDEs and related systems, which has been confirmed.

Our goal in this paper is to use two analytical techniques for solving a fractional-order nonlinear oscillatory system known as Belousov–Zhabotinskii (B-Z). The B-Z chemical reaction family is fascinating because it can show both temporal and spatial travelling concentration waves, as well as dramatic colour changes [38]. For the B-Z reaction, the simplified fractional Noyes–Field model is as follows [39]:

$$\begin{aligned} D_\tau^\alpha \xi &= \Psi_1 \xi_{\varphi\varphi} + \beta\rangle\zeta + \xi - \xi^2 - \xi\zeta, \quad 0 < \alpha \le 1, \\ D_\tau^\alpha \zeta &= \Psi_2 \zeta_{\varphi\varphi} + \gamma\zeta - \delta\xi\zeta, \end{aligned} \tag{1}$$

where Ψ_1 and Ψ_2 are the diffusing constants for ξ and ζ concentration, respectively, γ and β are given constants, $\delta \neq 1$ and ϱ are positive parameters, and α is the fractional order.

2. Preliminaries

In this section, we presented some basic definitions of fractional calculus along with Yang transform theory properties.

2.1. Definition. The fractional-order derivative in Caputo manner is given as

$$D_\tau^\alpha \xi(\varphi,\tau) = \frac{1}{\Gamma(k-\alpha)} \int_0^\tau (\tau-\rho)^{k-\alpha-1} \xi^{(k)}(\varphi,\rho)\mathrm{d}\rho, \quad k-1 < \alpha \le k,\ k \in N. \tag{2}$$

2.2. Definition. The Yang–Laplace transform was introduced by Xiao-Jun Yang in 2018. The Yang transform for a function $\xi(\tau)$ is determined by $Y\{\xi(\tau)\}$ or M(u) and is given as

$$\begin{aligned} Y\{\xi(\tau)\} &= M(u) \\ &= \int_0^\infty e^{-\tau/u} \xi(\tau)\mathrm{d}\tau, \quad \tau > 0,\ u \in (-\tau_1, \tau_2). \end{aligned} \tag{3}$$

The inverse transform (inverse symbol) is defined as

$$Y^{-1}\{M(u)\} = \xi(\tau), \tag{4}$$

where Y^{-1} is inverse Yang operator.

2.3. Definition. The Yang transform for nth derivatives is defined as

$$Y\{\xi^n(\tau)\} = \frac{M(u)}{u^n} - \sum_{k=0}^{n-1} \frac{\xi^k(0)}{u^{n-k-1}}, \quad \forall n = 1, 2, 3, \ldots. \tag{5}$$

2.4. Definition. The Yang transform for fractional-order derivatives is defined as

$$Y\{\xi^\alpha(\tau)\} = \frac{M(u)}{u^\gamma} - \sum_{k=0}^{n-1} \frac{\xi^k(0)}{u^{\alpha-(k+1)}}, \quad 0 < \alpha \le n. \tag{6}$$

3. Homotopy Perturbation Yang Transform Method

Consider a general nonlinear homogeneous partial differential equation with initial conditions of the type to demonstrate the basic idea of this method:

$$D_\tau^\alpha \xi(\varphi,\tau) + \mathscr{P}_1 \xi(\varphi,\tau) + \mathscr{Q}_1 \xi(\varphi,\tau) = 0, \quad 0 < \alpha \le 1, \tag{7}$$

with some initial sources such as

$$\xi(\varphi,0) = h(\varphi), \tag{8}$$

where D_τ^α is the fractional differential operator with respect to τ. $\mathscr{P}_1$ and $\mathscr{Q}_1$ are the linear and nonlinear differential operator with respect to φ, respectively.

Using Yang transformation to (7), we have

$$Y\left[D_\tau^\alpha \xi(\varphi,\tau)\right] + Y\left[\mathscr{P}_1 \xi(\varphi,\tau) + \mathscr{Q}_1 \xi(\varphi,\tau)\right] = 0, \tag{9}$$

$$\frac{1}{u^\alpha}\{M(u) - u\xi(0)\} + Y\left[\mathscr{P}_1 \xi(\varphi,\tau) + \mathscr{Q}_1 \xi(\varphi,\tau)\right] = 0. \tag{10}$$

Equation (9) implies that

$$M(\xi) = uh(\varphi) - u^\alpha Y\left[\mathscr{P}_1 \xi(\varphi,\tau) + \mathscr{Q}_1 \xi(\varphi,\tau)\right]. \tag{11}$$

Now, by taking inverse Yang transform, we get

$$\xi(\varphi,\tau) = H(\varphi) - Y^{-1}\left[u^\alpha Y\left[\mathscr{P}_1 \xi(\varphi,\tau) + \mathscr{Q}_1 \xi(\varphi,\tau)\right]\right], \tag{12}$$

where $H(\varphi)$ represents the term arising from the source term and the prescribed initial conditions. Now, we apply the homotopy perturbation method:

$$\xi(\varphi,\tau) = \sum_{k=0}^{\infty} p^k \xi_k(\varphi,\tau), \tag{13}$$

and the nonlinear term can be decomposed as

$$\mathscr{Q}_1 \xi(\varphi,\tau) = \sum_{k=0}^{\infty} p^k H_k(\xi), \tag{14}$$

for a set of He's polynomials H_k defined by

$$H_k(\xi_0,\xi_1,\ldots,\xi_k) = \frac{1}{k!}\frac{\partial^k}{\partial p^k}\left[\mathscr{Q}_1\left(\sum_{i=0}^{\infty} p^i \xi_i\right)\right]_{p=0}, \quad k = 0,1,2,3\ldots \tag{15}$$

Substituting equations (14) and (15) in (12), we get

$$\sum_{k=0}^{\infty} p^k \xi_k(\varphi,\tau) = H(\varphi) - p \times \left(Y^{-1}\left[u^\alpha Y\left\{\mathscr{P}_1 \sum_{k=0}^{\infty} p^k \xi_k(\varphi,\tau) + \sum_{k=0}^{\infty} p^k H_k(\xi)\right\}\right]\right). \tag{16}$$

The Yang transform and the homotopy perturbation approach using He's polynomials are coupled in this method. The following approximations are obtained by comparing the coefficients of like powers of p.

$$\begin{aligned}
&p^0\colon \xi_0(\varphi,\tau) = H(\varphi),\\
&p^1\colon \xi_1(\varphi,\tau) = -Y^{-1}\left[u^\alpha Y\left(\mathscr{P}_1 \xi_0(\varphi,\tau) + H_0(\xi)\right)\right],\\
&p^2\colon \xi_2(\varphi,\tau) = -Y^{-1}\left[u^\alpha Y\left(\mathscr{P}_1 \xi_1(\varphi,\tau) + H_1(\xi)\right)\right],\\
&\quad\vdots\\
&p^k\colon \xi_k(\varphi,\tau) = -Y^{-1}\left[u^\alpha Y\left(\left(\mathscr{P}_1 \xi_{k-1}(\varphi,\tau) + H_{k-1}(\xi)\right)\right)\right], \quad k > 0, k \in N.
\end{aligned} \tag{17}$$

Thus, we can calculate easily component $\xi_k(\varphi,\tau)$, which rapidly leads us to the convergent series. By taking $p \longrightarrow 1$, we get

$$\xi(\varphi,\tau) = \lim_{M \longrightarrow \infty} \sum_{k=1}^{M} \xi_k(\varphi,\tau). \tag{18}$$

The result we get is in form of series and quickly converges to the problem exact solution.

4. Idea of YTDM

The solution by YTDM for partial differential equations having fractional order is described in this section.

$$D_\tau^\alpha \xi(\varphi,\tau) = \mathscr{P}(\varphi,\tau)_1 + \mathscr{Q}_1(\varphi,\tau) + \mathscr{R}_1(\varphi,\tau), \quad 0 < \alpha \le 1, \tag{19}$$

with some initial sources such as

$$\xi(\varphi,0) = \xi(\varphi), \tag{20}$$

where $D_\tau^\alpha = \partial^\alpha/\partial\tau^\alpha$ is the fractional derivative in Caputo manner of order α, $\mathscr{P}_1$ and $\mathscr{Q}_1$ are linear and nonlinear functions, and $\mathscr{R}_1$ is the source term, respectively.

By applying Yang transform on both sides of equation (19), we obtain

$$Y\left[D_\tau^\alpha \xi(\varphi,\tau)\right] = Y\left[\mathscr{P}_1(\varphi,\tau) + \mathscr{Q}_1(\varphi,\tau) + \mathscr{R}_1(\varphi,\tau)\right]. \tag{21}$$

By differentiation property of Yang transform, we obtain

$$\frac{1}{u^\alpha}\{M(u) - u\xi(0)\} = Y\left[\mathscr{P}_1(\varphi,\tau) + \mathscr{Q}_1(\varphi,\tau) + \mathscr{R}_1(\varphi,\tau)\right]. \tag{22}$$

Equation (20) implies that

$$M(\xi) = u\xi(0) + u^\alpha Y\left[\mathscr{P}_1(\varphi,\tau) + \mathscr{Q}_1(\varphi,\tau) + \mathscr{R}_1(\varphi,\tau)\right], \tag{23}$$

and taking the inverse Yang transform of equation (23), we get

$$\xi(\varphi,\tau) = \xi(0) + Y^{-1}\left[u^\alpha Y\left[\mathscr{P}_1(\varphi,\tau) + \mathscr{Q}_1(\varphi,\tau) + \mathscr{R}_1(\varphi,\tau)\right]\right]. \tag{24}$$

YTDM defines the infinite sequence solution of $\xi(\varphi,\tau)$ as

$$\xi(\varphi,\tau) = \sum_{m=0}^{\infty} \xi_m(\varphi,\tau). \tag{25}$$

The Adomian polynomial $\mathscr{Q}_1$ decomposition of nonlinear terms is given as

$$\mathscr{Q}_1(\varphi,\tau) = \sum_{m=0}^{\infty} \mathscr{A}_m. \tag{26}$$

All types of nonlinearity are represented by Adomian polynomials as

$$\mathscr{A}_m = \frac{1}{m!}\left[\frac{\partial^m}{\partial\delta^m}\left\{\mathscr{Q}_1\left(\sum_{k=0}^{\infty}\delta^k\varphi_k, \sum_{k=0}^{\infty}\delta^k\tau_k\right)\right\}\right]_{\delta=0}. \tag{27}$$

Putting equations (23) and (25) into (24) gives

$$\begin{aligned}\sum_{m=0}^{\infty}\xi_m(\varphi,\tau) = \xi(0) + Y^{-1}\left[u^\alpha Y\{\mathscr{R}_1(\varphi,\tau)\}\right] \\ + Y^{-1}u^\alpha\left[Y\left\{\mathscr{P}_1\left(\sum_{m=0}^{\infty}\varphi_m, \sum_{m=0}^{\infty}\tau_m\right)\right.\right. \\ \left.\left. + \sum_{m=0}^{\infty}\mathscr{A}_m\right\}\right].\end{aligned} \tag{28}$$

The following terms are described:

$$\begin{aligned}\xi_0(\varphi,\tau) &= \xi(0) + Y^{-1}\left[u^\alpha Y\{\mathscr{R}_1(\varphi,\tau)\}\right], \\ \xi_1(\varphi,\tau) &= Y^{-1}\left[u^\alpha Y\{\mathscr{P}_1(\varphi_0,\tau_0) + \mathscr{A}_0\}\right].\end{aligned} \tag{29}$$

In general, for $m \geq 1$, it is calculated as

$$\xi_{m+1}(\varphi,\tau) = Y^{-1}\left[u^\alpha Y\{\mathscr{P}_1(\varphi_m,\tau_m) + \mathscr{A}_m\}\right]. \tag{30}$$

5. Applications

The solutions to the time-fractional Belousov–Zhabotinskii (B-Z) system are derived using YTDM and HPYTM in this section.

5.1. Example. Consider the time-fractional B-Z system having $\gamma = \beta = 0$, then equation (1) is reduced to

$$\begin{aligned}\frac{\partial^\alpha \xi}{\partial\tau^\alpha} &= \frac{\partial^2\xi}{\partial\varphi^2} + \xi - \xi^2 - \xi\zeta, \quad 0 < \alpha \leq 1, \\ \frac{\partial^\alpha \zeta}{\partial\tau^\alpha} &= \frac{\partial^2\zeta}{\partial\varphi^2} - \delta\xi\zeta,\end{aligned} \tag{31}$$

having initial conditions as

$$\begin{cases}(\varphi,0) = \dfrac{1}{\left(e^{\sqrt{\delta/6}\varphi} + 1\right)^2}, \\ \zeta(\varphi,0) = \dfrac{(1-\delta)e^{\sqrt{\delta/6}\varphi}\left(e^{\sqrt{\delta/6}\varphi} + 2\right)}{\left(e^{\sqrt{\delta/6}\varphi} + 1\right)^2}.\end{cases} \tag{32}$$

The exact solution of equation (28) when $\alpha = 1$ is

$$\begin{aligned}\xi(\varphi,\tau) &= \frac{e^{5\delta/3\tau}}{\left(e^{\sqrt{\delta/6}\varphi} + e^{5\delta/6\tau}\right)^2}, \\ \zeta(\varphi,\tau) &= \frac{(1-\delta)e^{\sqrt{\delta/6}\varphi}\left(e^{\sqrt{\delta/6}\varphi} + 2e^{5\delta/6\tau}\right)}{\left(e^{\sqrt{\delta/6}\varphi} + e^{5\delta/6\tau}\right)^2\Big\rangle},\end{aligned} \tag{33}$$

where ϱ and $\delta \neq 1$ are positive parameters.

Remark 1. . The exact solution can take the following form as well:

$$\frac{e^{5\delta/3\tau}}{\left(e^{\sqrt{\delta/6}\,\varphi}+e^{5\delta/6\tau}\right)^2}=\frac{1}{4}\left(\tanh^2\left(\sqrt{\frac{\delta}{24}}\varphi-\frac{5\delta}{12}\tau\right)-1\right)^2,$$

$$\frac{(1-\delta)e^{\sqrt{\delta/6}\varphi}\left(e^{\sqrt{\delta/6}\,\varphi}+2e^{5\delta/6\tau}\right)}{\left(e^{\sqrt{\delta/6}\,\varphi}+e^{5\delta/6\tau}\right)^2}=\frac{\delta-1}{4\rangle}\left(\tanh^2\left(\sqrt{\frac{\delta}{24}}\varphi-\frac{5\delta}{12}\tau\right)-2\tanh\left(\sqrt{\frac{\delta}{24}}\varphi-\frac{5\delta}{12}\tau\right)-3\right). \tag{34}$$

Taking Yang transformation of equation (28), we get

$$Y\left\{\frac{\partial^\alpha\xi}{\partial\tau^\alpha}\right\}=Y\left[\frac{\partial^2\xi}{\partial\varphi^2}+\xi-\xi^2-\xi\zeta\right],$$
$$Y\left\{\frac{\partial^\alpha\zeta}{\partial\tau^\alpha}\right\}=Y\left[\frac{\partial^2\zeta}{\partial\varphi^2}-\delta\xi\zeta\right]. \tag{35}$$

Applying the differential property of the Yang transform, we get

$$\frac{1}{u^\alpha}\{M(u)-u\xi(0)\}=Y\left[\frac{\partial^2\xi}{\partial\varphi^2}+\xi-\xi^2-\xi\zeta\right],$$
$$\frac{1}{u^\alpha}\{M(u)-u\zeta(0)\}=Y\left[\frac{\partial^2\zeta}{\partial\varphi^2}-\delta\xi\zeta\right],$$
$$M(u)=u\xi(0)+u^\alpha Y\left[\frac{\partial^2\xi}{\partial\varphi^2}+\xi-\xi^2-\xi\zeta\right],$$
$$M(u)=u\zeta(0)+u^\alpha Y\left[\frac{\partial^2\zeta}{\partial\varphi^2}-\delta\xi\zeta\right]. \tag{36}$$

The inverse Yang transform implies that

$$\xi(\varphi,\tau)=\xi(0)+Y^{-1}\left[u^\alpha\left\{Y\left(\frac{\partial^2\xi}{\partial\varphi^2}+\xi-\xi^2-\xi\zeta\right)\right\}\right],$$
$$\zeta(\varphi,\tau)=\zeta(0)+Y^{-1}\left[u^\alpha\left\{Y\left(\frac{\partial^2\zeta}{\partial\varphi^2}-\delta\xi\zeta\right)\right\}\right],$$
$$(\varphi,\tau)=\frac{1}{\left(e^{\sqrt{\delta/6}\,\varphi}+1\right)^2}+Y^{-1}\left[u^\alpha\left\{Y\left(\frac{\partial^2\xi}{\partial\varphi^2}+\xi-\xi^2-\xi\zeta\right)\right\}\right],$$
$$\zeta(\varphi,\tau)=\frac{(1-\delta)e^{\sqrt{\delta/6}\varphi}\left(e^{\sqrt{\delta/6}\,\varphi}+2\right)}{\left(e^{\sqrt{\delta/6}\,\varphi}+1\right)^2\Big\rangle}+Y^{-1}\left[u^\alpha\left\{Y\left(\frac{\partial^2\zeta}{\partial\varphi^2}-\delta\xi\zeta\right)\right\}\right]. \tag{37}$$

Now, we apply the homotopy perturbation method as follows:

$$\xi(\varphi,\tau)=\xi_0+\xi_1p+\xi_2p^2+\cdots,$$
$$\zeta(\varphi,\tau)=\zeta_0+\zeta_1p+\zeta_2p^2+\cdots,$$
$$\sum_{k=0}^{\infty}p^k\xi_k(\varphi,\tau)=\frac{1}{\left(e^{\sqrt{\delta/6}\,\varphi}+1\right)^2}+p\left(Y^{-1}\left[u^\alpha Y\left[\left(\sum_{k=0}^{\infty}p^k\xi_k(\varphi,\tau)\right)_{\varphi\varphi}+\sum_{k=0}^{\infty}p^k\xi_k(\varphi,\tau)-\sum_{k=0}^{\infty}p^kH_k^1(\varphi,\tau)\right]\right]\right), \tag{38}$$
$$\sum_{k=0}^{\infty}p^k\zeta_k(\varphi,\tau)=\frac{(1-\delta)e^{\sqrt{\delta/6}\varphi}\left(e^{\sqrt{\delta/6}\,\varphi}+2\right)}{\left(e^{\sqrt{\delta/6}\,\varphi}+1\right)^2}+p\left(Y^{-1}\left[u^\alpha Y\left[\left(\sum_{k=0}^{\infty}p^k\zeta_k(\varphi,\tau)\right)_{\varphi\varphi}-\sum_{k=0}^{\infty}p^kH_k^2(\varphi,\tau)\right]\right]\right),$$

where the nonlinear terms are represented by He's polynomials $H_k(\varphi)$. For example, the first few components of He's polynomials are given by

$$
\begin{aligned}
H_0^1(\varphi) &= (2\xi_0\xi_1) + (\xi_0\zeta_1 + \xi_1\zeta_0),\\
H_1^1(\varphi) &= \left(2\xi_0\xi_2 + \xi_1^2\right) + (\xi_0\zeta_2 + \xi_1\zeta_1 + \xi_2\zeta_0),\\
H_2^1(\varphi) &= (2\xi_0\xi_3 + 2\xi_1\xi_2) + (\xi_0\zeta_3 + \xi_1\zeta_2 + \xi_2\zeta_1 + \xi_3\zeta_0),\\
&\vdots\\
H_0^2(\varphi) &= \xi_0\zeta_1 + \xi_1\zeta_0,\\
H_1^2(\varphi) &= \xi_0\zeta_2 + \xi_1\zeta_1 + \xi_2\zeta_0,\\
H_2^2(\varphi) &= \xi_0\zeta_3 + \xi_1\zeta_2 + \xi_2\zeta_1 + \xi_3\zeta_0.
\end{aligned}
\tag{39}
$$

When the coefficients of like powers of p are compared, we get

$$
p^0\colon \xi_0(\varphi,\tau) = \frac{1}{\left(e^{\sqrt{\delta/6}\,\varphi}+1\right)^2},
$$

$$
\zeta_0(\varphi,\tau)\frac{(1-\delta)e^{\sqrt{\delta/6}\varphi}\left(e^{\sqrt{\delta/6}\,\varphi}+2\right)}{\left(e^{\sqrt{\delta/6}\,\varphi}+1\right)^2},
$$

$$
p^1\colon \xi_1(\varphi,\tau) = \frac{5\delta e^{\sqrt{\delta/6}\varphi}}{3\Gamma(\alpha+1)\left(e^{\sqrt{\delta/6}\,\varphi}+1\right)^3},
$$

$$
\zeta_1(\varphi,\tau) = \frac{5\delta(\delta-1)e^{\sqrt{\delta/6}\varphi}}{3\Gamma(\alpha+1)\left(e^{\sqrt{\delta/6}\,\varphi}+1\right)^3},
$$

$$
p^2\colon \xi_2(\varphi,\tau) = \frac{25\delta^2 e^{\sqrt{\delta/6}\varphi}\left(2e^{\sqrt{\delta/6}\,\varphi}-1\right)}{18\Gamma(2\alpha+1)\left(e^{\sqrt{\delta/6}\,\varphi}+1\right)^4},
$$

$$
{}_2(\varphi,\tau) = \frac{25\delta^2(\delta-1)e^{\sqrt{\delta/6}\varphi}\left(2e^{\sqrt{\delta/6}\,\varphi}-1\right)}{18\rangle\Gamma(2\alpha+1)\left(e^{\sqrt{\delta/6}\,\varphi}+1\right)^4},
$$

$$
p^3\colon \xi_3(\varphi,\tau) = -\frac{25\delta^3\Gamma(2\alpha+1)e^{\sqrt{2\delta/3}\varphi}}{9\Gamma(\alpha+1)^2\Gamma(3\alpha+1)\left(e^{\sqrt{\delta/6}\,\varphi}+1\right)^6} - \frac{25\delta^3 e^{\sqrt{\delta/6}\varphi}\left(15e^{\sqrt{2\delta/3}\,\varphi}-20e^{\sqrt{3\delta/2}\,\varphi}+6e^{\sqrt{\delta/6}\,\varphi}-5\right)}{108\Gamma(3\alpha+1)\left(e^{\sqrt{\delta/6}\,\varphi}+1\right)^6},
$$

$$
\zeta_3(\varphi,\tau) = -\frac{25\delta^3(\delta-1)\Gamma(2\alpha+1)e^{\sqrt{2\delta/3}\varphi}}{9\Gamma(\alpha+1)^2\Gamma(3\alpha+1)\left(e^{\sqrt{\delta/6}\,\varphi}+1\right)^6} - \frac{25\delta^3(\delta-1)e^{\sqrt{\delta/6}\varphi}\left(15e^{\sqrt{2\delta/3}\,\varphi}-20e^{\sqrt{3\delta/2}\,\varphi}+6e^{\sqrt{\delta/6}\,\varphi}-5\right)}{108\Gamma(3\alpha+1)\left(e^{\sqrt{\delta/6}\,\varphi}+1\right)^6},
$$

$$
p^4\colon \xi_4(\varphi,\tau) = -\frac{25\delta^4\Gamma(2\alpha+1)e^{\sqrt{2\delta/3}\varphi}\left(11e^{\sqrt{2\delta/3}\,\varphi}-5e^{\sqrt{\delta/6}\,\varphi}-1\right)}{27\Gamma(\alpha+1)^2\Gamma(4\alpha+1)\left(e^{\sqrt{\delta/6}\,\varphi}+1\right)^8} - \frac{125\delta^4\Gamma(3\alpha+1)e^{\sqrt{2\delta/3}\varphi}\left(2e^{\sqrt{\delta/6}\,\varphi}-1\right)}{27\Gamma(\alpha+1)\Gamma(2\alpha+1)\Gamma(4\alpha+1)\left(e^{\sqrt{\delta/6}\,\varphi}+1\right)^7}
$$

$$
\begin{aligned}
&+\frac{25\delta^4 e^{\sqrt{2\delta/3}\varphi}\left(124e^{\sqrt{2\delta/3}\,\varphi}+100e^{\sqrt[3]{2\delta/3}\varphi}+85e^{\sqrt{\delta/6}\,\varphi}-4\right)}{324\Gamma(4\alpha+1)\left(e^{\sqrt{\delta/6}\,\varphi}+1\right)^8}-\frac{625\delta^4 e^{\sqrt{\delta/6}\varphi}\left(17e^{\sqrt[3]{2\delta/3}\varphi}+1\right)}{648\Gamma(4\alpha+1)\left(e^{\sqrt{\delta/6}\,\varphi}+1\right)^8},\\
\zeta_4(\varphi,\tau)=&-\frac{25\delta^4(\delta-1)\Gamma(2\alpha+1)e^{\sqrt{2\delta/3}\varphi}\left(11e^{\sqrt{2\delta/3}\,\varphi}-5e^{\sqrt{\delta/6}\,\varphi}-1\right)}{27\varrho\Gamma(\alpha+1)^2\Gamma(4\alpha+1)\left(e^{\sqrt{\delta/6}\,\varphi}+1\right)^8}-\frac{125\delta^4(\delta-1)\Gamma(3\alpha+1)e^{\sqrt{2\delta/3}\varphi}\left(2e^{\sqrt{\delta/6}\,\varphi}-1\right)}{27\varrho\Gamma(\alpha+1)\Gamma(2\alpha+1)\Gamma(4\alpha+1)\left(e^{\sqrt{\delta/6}\,\varphi}+1\right)^7}\\
&+\frac{25\delta^4(\delta-1)e^{\sqrt{2\delta/3}\varphi}\left(124e^{\sqrt{2\delta/3}\,\varphi}+100e^{\sqrt[3]{2\delta/3}\varphi}+85e^{\sqrt{\delta/6}\,\varphi}-4\right)}{324\varrho\Gamma(4\alpha+1)\left(e^{\sqrt{\delta/6}\,\varphi}+1\right)^8}-\frac{625\delta^4(\delta-1)e^{\sqrt{\delta/6}\varphi}\left(17e^{\sqrt[3]{2\delta/3}\varphi}+1\right)}{648\varrho\Gamma(4\alpha+1)\left(e^{\sqrt{\delta/6}\,\varphi}+1\right)^8},\\
&\vdots
\end{aligned}
\tag{40}
$$

Now, taking $p \longrightarrow 1$ gives the approximate solution as follows:

$$
\begin{aligned}
\xi(\varphi,\tau)&=\xi_0+\xi_1+\xi_2+\xi_3+\xi_4+\cdots\\
&=\frac{1}{\left(e^{\sqrt{\delta/6}\,\varphi}+1\right)^2}+\frac{5\delta e^{\sqrt{\delta/6}\varphi}}{3\Gamma(\alpha+1)\left(e^{\sqrt{\delta/6}\,\varphi}+1\right)^3}+\frac{25\delta^2 e^{\sqrt{\delta/6}\varphi}\left(2e^{\sqrt{\delta/6}\,\varphi}-1\right)}{18\Gamma(2\alpha+1)\left(e^{\sqrt{\delta/6}\,\varphi}+1\right)^4}\\
&-\frac{25\delta^3\Gamma(2\alpha+1)e^{\sqrt{2\delta/3}\varphi}}{9\Gamma(\alpha+1)^2\Gamma(3\alpha+1)\left(e^{\sqrt{\delta/6}\,\varphi}+1\right)^6}-\frac{25\delta^3 e^{\sqrt{\delta/6}\varphi}\left(15e^{\sqrt{2\delta/3}\,\varphi}-20e^{\sqrt{3\delta/2}\,\varphi}+6e^{\sqrt{\delta/6}\,\varphi}-5\right)}{108\Gamma(3\alpha+1)\left(e^{\sqrt{\delta/6}\,\varphi}+1\right)^6}\\
&-\frac{25\delta^4\Gamma(2\alpha+1)e^{\sqrt{2\delta/3}\varphi}\left(11e^{\sqrt{2\delta/3}\,\varphi}-5e^{\sqrt{\delta/6}\,\varphi}-1\right)}{27\Gamma(\alpha+1)^2\Gamma(4\alpha+1)\left(e^{\sqrt{\delta/6}\,\varphi}+1\right)^8}-\frac{125\delta^4\Gamma(3\alpha+1)e^{\sqrt{2\delta/3}\varphi}\left(2e^{\sqrt{\delta/6}\,\varphi}-1\right)}{27\Gamma(\alpha+1)\Gamma(2\alpha+1)\Gamma(4\alpha+1)\left(e^{\sqrt{\delta/6}\,\varphi}+1\right)^7}\\
&+\frac{25\delta^4 e^{\sqrt{2\delta/3}\varphi}\left(124e^{\sqrt{2\delta/3}\,\varphi}+100e^{\sqrt{[2]}\,2\delta/3\varphi}+85e^{\sqrt{\delta/6}\,\varphi}-4\right)}{324\Gamma(4\alpha+1)\left(e^{\sqrt{\delta/6}\,\varphi}+1\right)^8}-\frac{625\delta^4 e^{\sqrt{\delta/6}\varphi}\left(17e^{\sqrt{[2]}\,2\delta/3\varphi}+1\right)}{648\Gamma(4\alpha+1)\left(e^{\sqrt{\delta/6}\,\varphi}+1\right)^8}\cdots.
\end{aligned}
\tag{41}
$$

YTDM Solution

Taking Yang transformation of equation (28), we get

$$
\begin{aligned}
Y\left\{\frac{\partial^\alpha\xi}{\partial\tau^\alpha}\right\}&=Y\left[\frac{\partial^2\xi}{\partial\varphi^2}+\xi-\xi^2-\xi\zeta\right],\\
Y\left\{\frac{\partial^\alpha\zeta}{\partial\tau^\alpha}\right\}&=Y\left[\frac{\partial^2\zeta}{\partial\varphi^2}-\delta\xi\zeta\right].
\end{aligned}
\tag{42}
$$

Applying the differential property of the Yang transform, we get

$$
\begin{aligned}
\frac{1}{u^\alpha}\{M(u)-u\xi(0)\}&=Y\left[\frac{\partial^2\xi}{\partial\varphi^2}+\xi-\xi^2-\xi\zeta\right],\\
\frac{1}{u^\alpha}\{M(u)-u\zeta(0)\}&=Y\left[\frac{\partial^2\zeta}{\partial\varphi^2}-\delta\xi\zeta\right].
\end{aligned}
\tag{43}
$$

The inverse Yang transform implies that

$$\begin{aligned}
\zeta(\varphi,\tau) &= \zeta(0) + Y^{-1}\left[u^{\alpha}\left\{Y\left(\frac{\partial^2\zeta}{\partial\varphi^2} - \delta\xi\zeta\right)\right\}\right],\\
\xi(\varphi,\tau) &= \xi(0) + Y^{-1}\left[u^{\alpha}\left\{Y\left(\frac{\partial^2\xi}{\partial\varphi^2} + \xi - \xi^2 - \xi\zeta\right)\right\}\right],\\
\xi(\varphi,\tau) &= \frac{1}{\left(e^{\sqrt{\delta/6}\,\varphi}+1\right)^2} + Y^{-1}\left[u^{\alpha}\left\{Y\left(\frac{\partial^2\xi}{\partial\varphi^2} + \xi - \xi^2 - \xi\zeta\right)\right\}\right],\\
\zeta(\varphi,\tau) &= \frac{(1-\delta)e^{\sqrt{\delta/6}\varphi}\left(e^{\sqrt{\delta/6}\,\varphi}+2\right)}{\left(e^{\sqrt{\delta/6}\,\varphi}+1\right)^2} + Y^{-1}\left[u^{\alpha}\left\{Y\left(\frac{\partial^2\zeta}{\partial\varphi^2} - \delta\xi\zeta\right)\right\}\right].
\end{aligned} \tag{44}$$

Assume that the unknown $\xi(\varphi,\tau)$ and $\zeta(\varphi,\tau)$ functions, in infinite series form, have the following solution:

$$\begin{aligned}
\xi(\varphi,\tau) &= \sum_{m=0}^{\infty}\xi_m(\varphi,\tau),\\
\zeta(\varphi,\tau) &= \sum_{m=0}^{\infty}\xi_m(\varphi,\tau),
\end{aligned} \tag{45}$$

where the Adomian polynomials $\xi^2 = \sum_{m=0}^{\infty}\mathscr{A}_m$ and $\xi\zeta = \sum_{m=0}^{\infty}\mathscr{B}_m$ and the nonlinear terms have been characterised. Using certain terms, equation (44) can be rewritten in the form

$$\begin{aligned}
\sum_{m=0}^{\infty}\xi_m(\varphi,\tau) &= \xi(\varphi,0) + Y^{-1}\left[u^{\alpha}Y\left[\frac{\partial^2\xi}{\partial\varphi^2} + \xi - \sum_{m=0}^{\infty}\mathscr{A}_m - \sum_{m=0}^{\infty}\mathscr{B}_m\right]\right],\\
\sum_{m=0}^{\infty}\zeta_m(\varphi,\tau) &= \zeta(\varphi,0) + Y^{-1}\left[u^{\alpha}Y\left[\frac{\partial^2\zeta}{\partial\varphi^2} - \delta\sum_{m=0}^{\infty}\mathscr{B}_m\right]\right],\\
\sum_{m=0}^{\infty}\xi_m(\varphi,\tau) &= \frac{1}{\left(e^{\sqrt{\delta/6}\,\varphi}+1\right)^2}\\
&\quad + Y^{-1}\left[u^{\alpha}Y\left[\frac{\partial^2\xi}{\partial\varphi^2} + \xi - \sum_{m=0}^{\infty}\mathscr{A}_m - \sum_{m=0}^{\infty}\mathscr{B}_m\right]\right],\\
\sum_{m=0}^{\infty}\zeta_m(\varphi,\tau) &= \frac{(1-\delta)e^{\sqrt{\delta/6}\varphi}\left(e^{\sqrt{\delta/6}\,\varphi}+2\right)}{\left(e^{\sqrt{\delta/6}\,\varphi}+1\right)^2}\\
&\quad + Y^{-1}\left[u^{\alpha}Y\left[\frac{\partial^2\zeta}{\partial\varphi^2} - \delta\sum_{m=0}^{\infty}\mathscr{B}_m\right]\right].
\end{aligned} \tag{46}$$

All forms of nonlinearity can be represented by the Adomian polynomials as, according to equation (27),

$$\begin{aligned}
\mathscr{A}_0 &= \xi_0^2,\\
\mathscr{A}_1 &= 2\xi_0\xi_1,\\
\mathscr{A}_2 &= 2\xi_0\xi_2 + \xi_1^2,\\
\mathscr{A}_3 &= 2\xi_0\xi_3 + 2\xi_1\xi_2,\\
\mathscr{B}_0 &= \xi_0\omega_0,\\
\mathscr{B}_1 &= \xi_1\zeta_0 + \xi_0\zeta_1,\\
\mathscr{B}_2 &= \xi_0\zeta_2 + \xi_1\zeta_1 + \xi_2\zeta_0,\\
\mathscr{B}_3 &= \xi_0\zeta_3 + \xi_1\zeta_2 + \xi_2\zeta_1 + \xi_3\zeta_0.
\end{aligned} \tag{47}$$

Thus, on comparing both sides of equation (46),

$$\begin{aligned}
\xi_0(\varphi,\tau) &= \frac{1}{\left(e^{\sqrt{\delta/6}\,\varphi}+1\right)^2},\\
\zeta_0(\varphi,\tau) &= \frac{(1-\delta)e^{\sqrt{\delta/6}\varphi}\left(e^{\sqrt{\delta/6}\,\varphi}+2\right)}{\left(e^{\sqrt{\delta/6}\,\varphi}+1\right)^2}.
\end{aligned} \tag{48}$$

For $m = 0$,

$$\begin{aligned}
\xi_1(\varphi,\tau) &= \frac{5\delta e^{\sqrt{\delta/6}\varphi}}{3\Gamma(\alpha+1)\left(e^{\sqrt{\delta/6}\,\varphi}+1\right)^3},\\
\zeta_1(\varphi,\tau) &= \frac{5\delta(\delta-1)e^{\sqrt{\delta/6}\varphi}}{3\Gamma(\alpha+1)\left(e^{\sqrt{\delta/6}\,\varphi}+1\right)^3}.
\end{aligned} \tag{49}$$

For $m = 1$,

$$\xi_2(\varphi,\tau) = \frac{25\delta^2 e^{\sqrt{\delta/6}\varphi}\left(2e^{\sqrt{\delta/6}\,\varphi}-1\right)}{18\Gamma(2\alpha+1)\left(e^{\sqrt{\delta/6}\,\varphi}+1\right)^4},$$
$$\zeta_2(\varphi,\tau) = \frac{25\delta^2(\delta-1)e^{\sqrt{\delta/6}\varphi}\left(2e^{\sqrt{\delta/6}\,\varphi}-1\right)}{18\rangle\Gamma(2\alpha+1)\left(e^{\sqrt{\delta/6}\,\varphi}+1\right)^4}. \tag{50}$$

For $m = 2$,

$$\xi_3(\varphi,\tau) = -\frac{25\delta^3\Gamma(2\alpha+1)e^{\sqrt{2\delta/3}\varphi}}{9\Gamma(\alpha+1)^2\Gamma(3\alpha+1)\left(e^{\sqrt{\delta/6}\,\varphi}+1\right)^6} - \frac{25\delta^3 e^{\sqrt{\delta/6}\varphi}\left(15e^{\sqrt{2\delta/3}\,\varphi}-20e^{\sqrt{3\delta/2}\,\varphi}+6e^{\sqrt{\delta/6}\,\varphi}-5\right)}{108\Gamma(3\alpha+1)\left(e^{\sqrt{\delta/6}\,\varphi}+1\right)^6},$$
$$\zeta_3(\varphi,\tau) = -\frac{25\delta^3(\delta-1)\Gamma(2\alpha+1)e^{\sqrt{2\delta/3}\varphi}}{9\rangle\Gamma(\alpha+1)^2\Gamma(3\alpha+1)\left(e^{\sqrt{\delta/6}\,\varphi}+1\right)^6} - \frac{25\delta^3(\delta-1)e^{\sqrt{\delta/6}\varphi}\left(15e^{\sqrt{2\delta/3}\,\varphi}-20e^{\sqrt{3\delta/2}\,\varphi}+6e^{\sqrt{\delta/6}\,\varphi}-5\right)}{108\rangle\Gamma(3\alpha+1)\left(e^{\sqrt{\delta/6}\,\varphi}+1\right)^6}. \tag{51}$$

For $m = 3$,

$$\xi_4(\varphi,\tau) = -\frac{25\delta^4\Gamma(2\alpha+1)e^{\sqrt{2\delta/3}\varphi}\left(11e^{\sqrt{2\delta/3}\,\varphi}-5e^{\sqrt{\delta/6}\,\varphi}-1\right)}{27\Gamma(\alpha+1)^2\Gamma(4\alpha+1)\left(e^{\sqrt{\delta/6}\,\varphi}+1\right)^8} - \frac{125\delta^4\Gamma(3\alpha+1)e^{\sqrt{2\delta/3}\varphi}\left(2e^{\sqrt{\delta/6}\,\varphi}-1\right)}{27\Gamma(\alpha+1)\Gamma(2\alpha+1)\Gamma(4\alpha+1)\left(e^{\sqrt{\delta/6}\,\varphi}+1\right)^7}$$
$$+\frac{25\delta^4 e^{\sqrt{2\delta/3}\varphi}\left(124e^{\sqrt{2\delta/3}\,\varphi}+100e^{\sqrt{[2]}\,2\delta/3\varphi}+85e^{\sqrt{\delta/6}\,\varphi}-4\right)}{324\Gamma(4\alpha+1)\left(e^{\sqrt{\delta/6}\,\varphi}+1\right)^8} - \frac{625\delta^4 e^{\sqrt{\delta/6}\varphi}\left(17e^{\sqrt{[2]}\,2\delta/3\varphi}+1\right)}{648\Gamma(4\alpha+1)\left(e^{\sqrt{\delta/6}\,\varphi}+1\right)^8},$$
$$\zeta_4(\varphi,\tau) = -\frac{25\delta^4(\delta-1)\Gamma(2\alpha+1)e^{\sqrt{2\delta/3}\varphi}\left(11e^{\sqrt{2\delta/3}\,\varphi}-5e^{\sqrt{\delta/6}\,\varphi}-1\right)}{27\varrho\Gamma(\alpha+1)^2\Gamma(4\alpha+1)\left(e^{\sqrt{\delta/6}\,\varphi}+1\right)^8} - \frac{125\delta^4(\delta-1)\Gamma(3\alpha+1)e^{\sqrt{2\delta/3}\varphi}\left(2e^{\sqrt{\delta/6}\,\varphi}-1\right)}{27\varrho\Gamma(\alpha+1)\Gamma(2\alpha+1)\Gamma(4\alpha+1)\left(e^{\sqrt{\delta/6}\,\varphi}+1\right)^7}$$
$$+\frac{25\delta^4(\delta-1)e^{\sqrt{2\delta/3}\varphi}\left(124e^{\sqrt{2\delta/3}\,\varphi}+100e^{\sqrt{[2]}\,2\delta/3\varphi}+85e^{\sqrt{\delta/6}\,\varphi}-4\right)}{324\varrho\Gamma(4\alpha+1)\left(e^{\sqrt{\delta/6}\,\varphi}+1\right)^8} - \frac{625\delta^4(\delta-1)e^{\sqrt{\delta/6}\varphi}\left(17e^{\sqrt{[2]}\,2\delta/3\varphi}+1\right)}{648\varrho\Gamma(4\alpha+1)\left(e^{\sqrt{\delta/6}\,\varphi}+1\right)^8}. \tag{52}$$

The remaining YTDM solution elements xi_m and ζ_m for $(m \geq 3)$ are similarly simple to get. As a result, we define the series of possibilities as follows:

$$\xi(\varphi,\tau) = \sum_{m=0}^{\infty} \xi_m(\varphi,\tau) = \xi_0(\varphi,\tau) + \xi_1(\varphi,\tau) + \xi_2(\varphi,\tau) + \xi_3(\varphi,\tau) + \xi_4(\varphi,\tau) + \cdots,$$

$$\zeta(\varphi,\tau) = \sum_{m=0}^{\infty} \zeta_m(\varphi,\tau) = \zeta_0(\varphi,\tau) + \zeta_1(\varphi,\tau) + \zeta(\varphi,\tau) + \zeta_3(\varphi,\tau) + \zeta_4(\varphi,\tau) + \cdots,$$

$$\begin{aligned}
\xi(\varphi,\tau) = {} & \frac{1}{\left(e^{\sqrt{\delta/6}\,\varphi}+1\right)^2} + \frac{5\delta e^{\sqrt{\delta/6}\varphi}}{3\Gamma(\alpha+1)\left(e^{\sqrt{\delta/6}\,\varphi}+1\right)^3} + \frac{25\delta^2 e^{\sqrt{\delta/6}\varphi}\left(2e^{\sqrt{\delta/6}\,\varphi}-1\right)}{18\Gamma(2\alpha+1)\left(e^{\sqrt{\delta/6}\,\varphi}+1\right)^4} \\
& - \frac{25\delta^3\Gamma(2\alpha+1)e^{\sqrt{2\delta/3}\varphi}}{9\Gamma(\alpha+1)^2\Gamma(3\alpha+1)\left(e^{\sqrt{\delta/6}\,\varphi}+1\right)^6} - \frac{25\delta^3 e^{\sqrt{\delta/6}\varphi}\left(15e^{\sqrt{2\delta/3}\,\varphi}-20e^{\sqrt{3\delta/2}\,\varphi}+6e^{\sqrt{\delta/6}\,\varphi}-5\right)}{108\Gamma(3\alpha+1)\left(e^{\sqrt{\delta/6}\,\varphi}+1\right)^6} \\
& - \frac{25\delta^4\Gamma(2\alpha+1)e^{\sqrt{2\delta/3}\varphi}\left(11e^{\sqrt{2\delta/3}\,\varphi}-5e^{\sqrt{\delta/6}\,\varphi}-1\right)}{27\Gamma(\alpha+1)^2\Gamma(4\alpha+1)\left(e^{\sqrt{\delta/6}\,\varphi}+1\right)^8} - \frac{125\delta^4\Gamma(3\alpha+1)e^{\sqrt{2\delta/3}\varphi}\left(2e^{\sqrt{\delta/6}\,\varphi}-1\right)}{27\Gamma(\alpha+1)\Gamma(2\alpha+1)\Gamma(4\alpha+1)\left(e^{\sqrt{\delta/6}\,\varphi}+1\right)^7} \\
& + \frac{25\delta^4 e^{\sqrt{2\delta/3}\varphi}\left(124e^{\sqrt{2\delta/3}\,\varphi}+100e^{\sqrt[3]{2\delta/3}\varphi}+85e^{\sqrt{\delta/6}\,\varphi}-4\right)}{324\Gamma(4\alpha+1)\left(e^{\sqrt{\delta/6}\,\varphi}+1\right)^8} - \frac{625\delta^4 e^{\sqrt{\delta/6}\varphi}\left(17e^{\sqrt[3]{2\delta/3}\varphi}+1\right)}{648\Gamma(4\alpha+1)\left(e^{\sqrt{\delta/6}\,\varphi}+1\right)^8}\cdots
\end{aligned} \tag{53}$$

$$\begin{aligned}
\zeta(\varphi,\tau) = {} & \frac{(1-\delta)e^{\sqrt{\delta/6}\varphi}\left(e^{\sqrt{\delta/6}\,\varphi}+2\right)}{\left(e^{\sqrt{\delta/6}\,\varphi}+1\right)^2} + \frac{5\delta(\delta-1)e^{\sqrt{\delta/6}\varphi}}{3\rangle\Gamma(\alpha+1)\left(e^{\sqrt{\delta/6}\,\varphi}\varphi+1\right)^3} + \frac{25\delta^2(\delta-1)e^{\sqrt{\delta/6}\varphi}\left(2e^{\sqrt{\delta/6}\,\varphi}-1\right)}{18\Gamma(2\alpha+1)\left(e^{\sqrt{\delta/6}\,\varphi}+1\right)^4} \\
& - \frac{25\delta^3(\delta-1)\Gamma(2\alpha+1)e^{\sqrt{2\delta/3}\varphi}}{9\Gamma(\alpha+1)^2\Gamma(3\alpha+1)\left(e^{\sqrt{\delta/6}\,\varphi}+1\right)^6} - \frac{25\delta^3(\delta-1)e^{\sqrt{\delta/6}\varphi}\left(15e^{\sqrt{2\delta/3}\,\varphi}-20e^{\sqrt{3\delta/2}\,\varphi}+6e^{\sqrt{\delta/6}\,\varphi}-5\right)}{108\rangle\Gamma(3\alpha+1)\left(e^{\sqrt{\delta/6}\,\varphi}+1\right)^6} \\
& - \frac{25\delta^4(\delta-1)\Gamma(2\alpha+1)e^{\sqrt{2\delta/3}\varphi}\left(11e^{\sqrt{2\delta/3}\,\varphi}-5e^{\sqrt{\delta/6}\,\varphi}-1\right)}{27\Gamma(\alpha+1)^2\Gamma(4\alpha+1)\left(e^{\sqrt{\delta/6}\,\varphi}+1\right)^8} - \frac{125\delta^4(\delta-1)\Gamma(3\alpha+1)e^{\sqrt{2\delta/3}\varphi}\left(2e^{\sqrt{\delta/6}\,\varphi}-1\right)}{27\Gamma(\alpha+1)\Gamma(2\alpha+1)\Gamma(4\alpha+1)\left(e^{\sqrt{\delta/6}\,\varphi}+1\right)^7} \\
& + \frac{25\delta^4(\delta-1)e^{\sqrt{2\delta/3}\varphi}\left(124e^{\sqrt{2\delta/3}\,\varphi}+100e^{\sqrt[3]{2\delta/3}\varphi}+85e^{\sqrt{\delta/6}\,\varphi}-4\right)}{324\Gamma(4\alpha+1)\left(e^{\sqrt{\delta/6}\,\varphi}+1\right)^8} - \frac{625\delta^4(\delta-1)e^{\sqrt{\delta/6}\varphi}\left(17e^{\sqrt[3]{2\delta/3}\varphi}+1\right)}{648\Gamma(4\alpha+1)\left(e^{\sqrt{\delta/6}\,\varphi}+1\right)^8}\cdots.
\end{aligned}$$

In Figure 1, the exact and analytical solution graph of $\xi(\varphi,\tau)$ is shown. In Figure 2, the different fractional graph of $\alpha = 1, 0.7, 0.5$, and 0.3 of $\xi(\varphi,\tau)$ is shown. Similarly, in Figure 3, the exact and analytical solution graph of $\zeta(\varphi,\tau)$ is shown. In Figure 4, the different fractional graph of $\alpha = 1, 0.7, 0.5$, and 0.3 of $\zeta(\varphi,\tau)$ is shown.

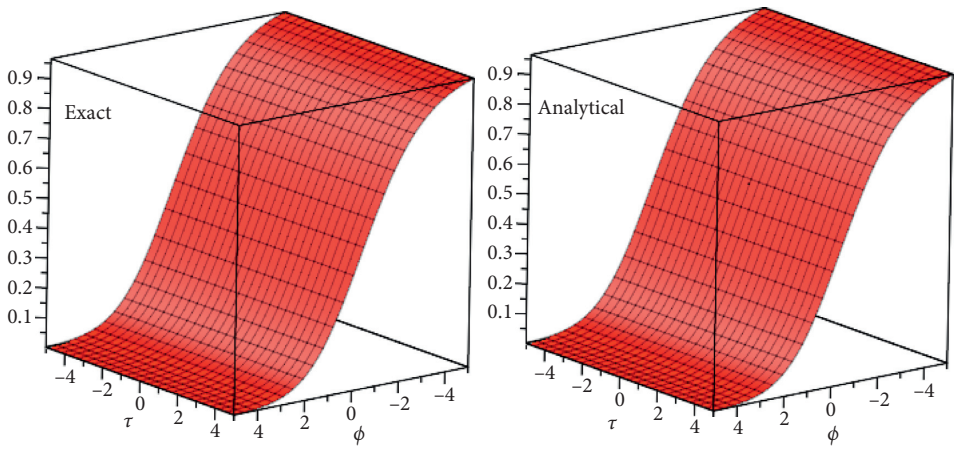

Figure 1: The exact solution and analytical solution graph at $\alpha = 1$ for $\xi(\varphi, \tau)$.

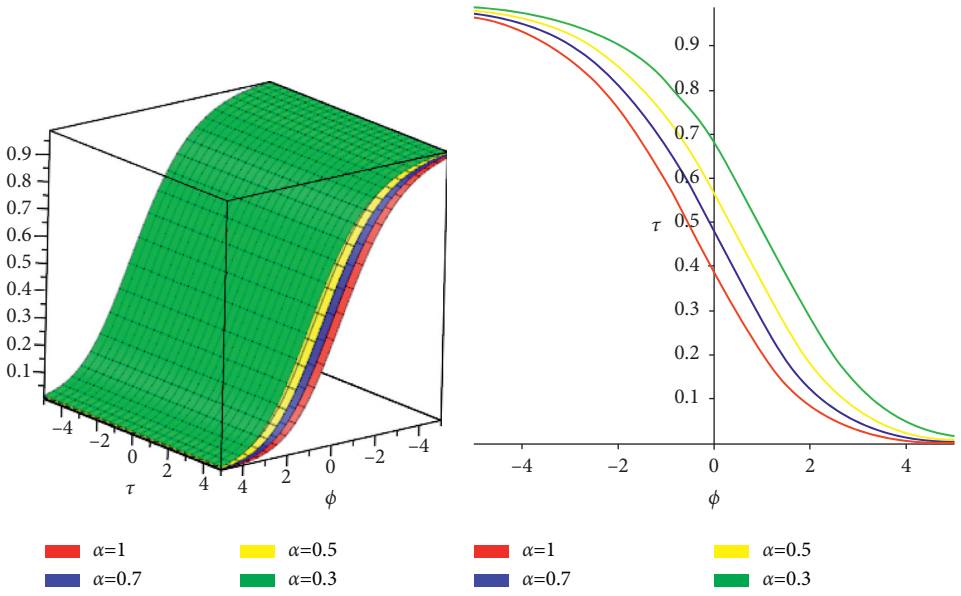

Figure 2: The different fractional-order solution graph of α for $\xi(\varphi, \tau)$.

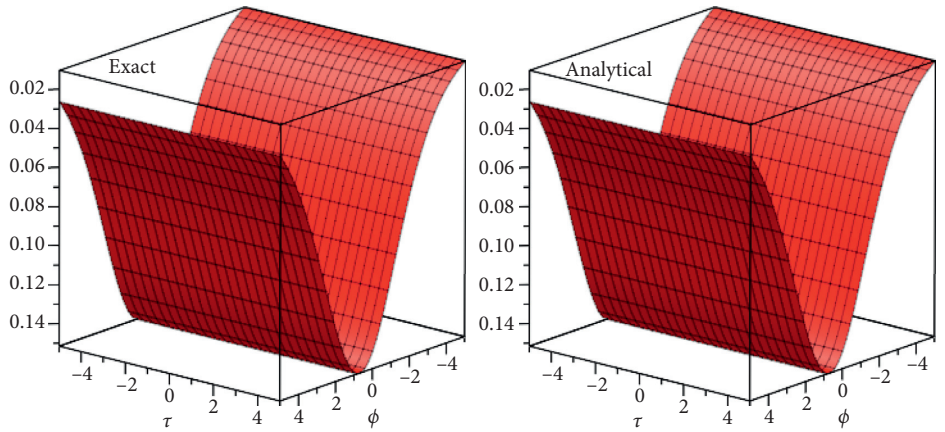

Figure 3: The exact solution and analytical solution graph at $\alpha = 1$ for $\zeta(\varphi, \tau)$.

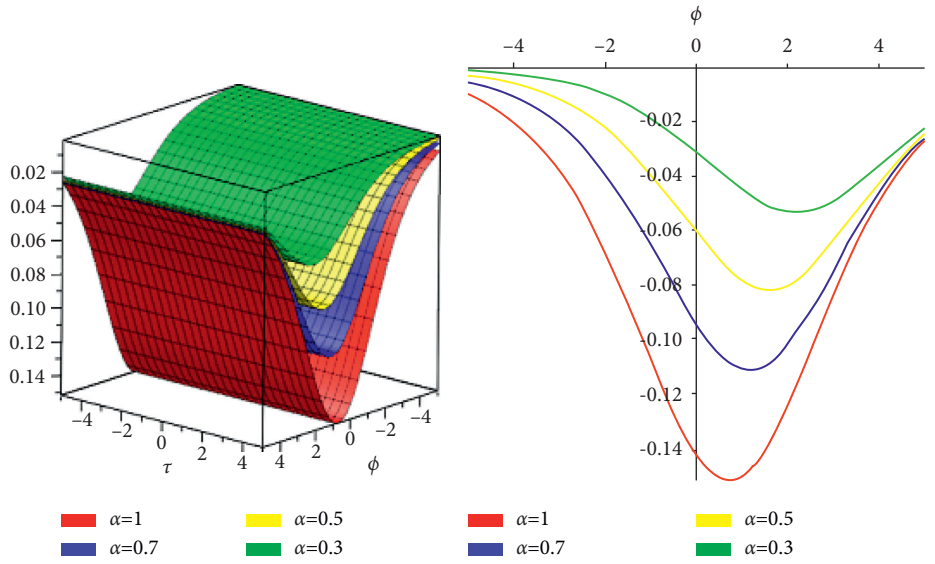

FIGURE 4: The different fractional-order solution graph of α for $\zeta(\varphi, \tau)$.

5.2. Example. Consider the time-fractional B-Z system having $\gamma = \delta$ and $\beta = 1$, then equation (1) is reduced to

$$\begin{aligned} \frac{\partial^{\alpha}\xi}{\partial\tau^{\alpha}} &= \frac{\partial^{2}\xi}{\partial\varphi^{2}} + \zeta + \xi - \xi^{2} - \xi\zeta, \quad 0 < \alpha \le 1, \\ \frac{\partial^{\alpha}\zeta}{\partial\tau^{\alpha}} &= \frac{\partial^{2}\zeta}{\partial\varphi^{2}} + \delta\zeta - \delta\xi\zeta, \end{aligned} \tag{54}$$

having initial conditions

$$\begin{cases} \xi(\varphi, 0) = \dfrac{1}{\left(e^{\sqrt{\delta/6}\,\varphi} + 1\right)^{2}}, \\ \zeta(\varphi, 0) = \dfrac{\delta - 1}{\left(e^{\sqrt{\delta/6}\,\varphi} + 1\right)^{2}}, \end{cases} \tag{55}$$

The exact solution of equation (54) when $\alpha = 1$ is

$$\begin{aligned} \xi(\varphi, \tau) &= \frac{e^{5\delta/3\tau}}{\left(e^{\sqrt{\delta/6}\,\varphi} + e^{5\delta/6\tau}\right)^{2}}, \\ \zeta(\varphi, \tau) &= \frac{(\delta - 1)e^{5\delta/3\tau\tau}}{\left(e^{\sqrt{\delta/6}\,\varphi} + e^{5\delta/6\tau}\right)^{2}}, \end{aligned} \tag{56}$$

where $\delta \neq 1$ is a positive parameter.

Remark 2. . The exact solution can take the following form as well:

$$\begin{aligned} \frac{e^{5\delta/3\tau}}{\left(e^{\sqrt{\delta/6}\,\varphi} + e^{5\delta/6\tau}\right)^{2}} &= \frac{1}{4}\left(\tanh\left(\sqrt{\frac{\delta}{24}}\varphi - \frac{5\delta}{12}\tau\right) - 1\right)^{2}, \\ \frac{(\delta - 1)e^{5\delta/3\tau}}{\left(e^{\sqrt{\delta/6}\,\varphi} + e^{5\delta/6\tau}\right)^{2}} &= \frac{\delta - 1}{4}\left(\tanh\left(\sqrt{\frac{\delta}{24}}\varphi - \frac{5\delta}{12}\tau\right) - 1\right)^{2}. \end{aligned} \tag{57}$$

Taking Yang transformation of equation (54), we get

$$\begin{aligned} Y\left\{\frac{\partial^{\alpha}\xi}{\partial\tau^{\alpha}}\right\} &= Y\left[\frac{\partial^{2}\xi}{\partial\varphi^{2}} + \zeta + t\xi n{-}\rangle\xi^{2} - \xi\zeta\rangle\right], \\ Y\left\{\frac{\partial^{\alpha}\zeta}{\partial\tau^{\alpha}}\right\} &= Y\left[\frac{\partial^{2}\zeta}{\partial\varphi^{2}} + \delta\zeta - \delta\xi\zeta\right]. \end{aligned} \tag{58}$$

Applying the differential property of the Yang transform, we get

$$\begin{aligned} \frac{1}{u^{\alpha}}\{M(u) - u\xi(0)\} &= Y\left[\frac{\partial^{2}\xi}{\partial\varphi^{2}} + \zeta + \xi - \xi^{2} - \xi\zeta\right], \\ \frac{1}{u^{\alpha}}\{M(u) - u\zeta \le (0)\} &= Y\left[\frac{\partial^{2}\zeta}{\partial\varphi^{2}} + \delta\zeta - \delta\xi\zeta\right], \\ M(u) &= u\xi(0) + u^{\alpha}Y\left[\frac{\partial^{2}\xi}{\partial\varphi^{2}} + \zeta + \xi - \xi^{2} - \xi\zeta\right], \\ M(u) &= u\zeta(0) + u^{\alpha}Y\left[\frac{\partial^{2}\zeta}{\partial\varphi^{2}} + \delta\zeta - \delta\xi\zeta\right]. \end{aligned} \tag{59}$$

The inverse Yang transform implies that

$$\begin{aligned}
\xi(\varphi,\tau) &= \xi(0) + Y^{-1}\left[u^{\alpha}\left\{Y\left(\frac{\partial^2\xi}{\partial\varphi^2} + \right\rangle\zeta + \xi - \xi^2 - \xi\zeta\right)\right\}],\\
\zeta(\varphi,\tau) &= \zeta(0) + Y^{-1}\left[u^{\alpha}\left\{Y\left(\frac{\partial^2\zeta}{\partial\varphi^2} + \delta\zeta - \delta\xi\zeta\right)\right\}\right],\\
\xi(\varphi,\tau) &= \frac{1}{\left(e^{\sqrt{\delta/6}\,\varphi}+1\right)^2} + Y^{-1}\left[u^{\alpha}\left\{Y\left(\frac{\partial^2\xi}{\partial\varphi^2} + \right\rangle\zeta + \xi - \xi^2 - \xi\zeta\right)\right\}],\\
\zeta(\varphi,\tau) &= \frac{\delta-1}{\left(e^{\sqrt{\delta/6}\,\varphi}+1\right)^2\rangle} + Y^{-1}\left[u^{\alpha}\left\{Y\left(\frac{\partial^2\zeta}{\partial\varphi^2} + \delta\zeta - \delta\xi\zeta\right)\right\}\right].
\end{aligned} \tag{60}$$

Now, we apply the homotopy perturbation method as follows:

$$\begin{aligned}
\xi(\varphi,\tau) &= \xi_0 + \xi_1 p + \xi_2 p^2 + \xi_3 p^3 + \xi_4 p^4 + \cdots,\\
\zeta(\varphi,\tau) &= \zeta_0 + \zeta_1 p + \zeta_2 p^2 + \zeta_3 p^3 + \zeta_4 p^4 + \cdots,\\
\sum_{k=0}^{\infty} p^k\xi_k(\varphi,\tau) &= \frac{1}{\left(e^{\sqrt{\delta/6}\,\varphi}+1\right)^2} + p\left(Y^{-1}\left[u^{\alpha}Y\left[\left(\sum_{k=0}^{\infty} p^k\xi_k(\varphi,\tau)\right)_{\varphi\varphi} + \left(\sum_{k=0}^{\infty} p^k\xi_k(\varphi,\tau)\right) + \sum_{k=0}^{\infty} p^k\xi_k(\varphi,\tau) - \sum_{k=0}^{\infty} p^k H_k^1(\varphi,\tau)\right]\right]\right),\\
\sum_{k=0}^{\infty} p^k\zeta_k(\varphi,\tau) &= \frac{\delta-1}{\left(e^{\sqrt{\delta/6}\,\varphi}+1\right)^2} + p\left(Y^{-1}\left[u^{\alpha}Y\left[\left(\sum_{k=0}^{\infty} p^k\xi_k(\varphi,\tau)\right)_{\varphi\varphi} + \delta\left(\sum_{k=0}^{\infty} p^k\xi_k(\varphi,\tau)\right) - \sum_{k=0}^{\infty} p^k H_k^2(\varphi,\tau)\right]\right]\right),
\end{aligned} \tag{61}$$

where the nonlinear terms are represented by He's polynomials $H_k(\varphi)$. For example, the first few components of He's polynomials are given by

$$\begin{aligned}
H_0^1(\varphi) &= (2\xi_0\xi_1) + (\xi_0\zeta_1 + \xi_1\zeta_0),\\
H_1^1(\varphi) &= \left(2\xi_0\xi_2 + \xi_1^2\right) + (\xi_0\zeta_2 + \xi_1\zeta_1 + \xi_2\zeta_0),\\
H_2^1(\varphi) &= (2\xi_0\xi_3 + 2\xi_1\xi_2) + (\xi_0\zeta_3 + \xi_1\zeta_2 + \xi_2\zeta_1 + \xi_3\zeta_0),\\
&\vdots\\
H_0^2(\varphi) &= \xi_0\zeta_1 + \xi_1\zeta_0,\\
H_1^2(\varphi) &= \xi_0\zeta_2 + \xi_1\zeta_1 + \xi_2\zeta_0,\\
H_2^2(\varphi) &= \xi_0\zeta_3 + \xi_1\zeta_2 + \xi_2\zeta_1 + \xi_3\zeta_0.
\end{aligned} \tag{62}$$

When the coefficients of like powers of p are compared, we get

$$
\begin{aligned}
p^0\colon \xi_0(\varphi,\tau) &= \frac{1}{\left(e^{\sqrt{\delta/6}\,\varphi}+1\right)^2},\\
\zeta_0(\varphi,\tau) &= \frac{\delta-1}{\varrho\left(e^{\sqrt{\delta/6}\,\varphi}+1\right)^2},\\
p^1\colon \xi_1(\varphi,\tau) &= \frac{5\delta e^{\sqrt{\delta/6}\varphi}}{3\Gamma(\alpha+1)\left(e^{\sqrt{\delta/6}\,\varphi}+1\right)^3},\\
\zeta_1(\varphi,\tau) &= \frac{5\delta(\delta-1)e^{\sqrt{\delta/6}\varphi}}{3\varrho\Gamma(\alpha+1)\left(e^{\sqrt{\delta/6}\,\varphi}+1\right)^3},\\
p^2\colon \xi_2(\varphi,\tau) &= \frac{25\delta^2 e^{\sqrt{\delta/6}\varphi}\left(2e^{\sqrt{\delta/6}\,\varphi}-1\right)}{18\Gamma(2\alpha+1)\left(e^{\sqrt{\delta/6}\,\varphi}+1\right)^4},\\
\zeta_2(\varphi,\tau) &= \frac{25\delta^2(\delta-1)e^{\sqrt{\delta/6}\varphi}\left(2e^{\sqrt{\delta/6}\,\varphi}-1\right)}{18\varrho\Gamma(2\alpha+1)\left(e^{\sqrt{\delta/6}\,\varphi}+1\right)^4},\\
p^3\colon \xi_3(\varphi,\tau) &= -\frac{25\delta^3\Gamma(2\alpha+1)e^{\sqrt{2\delta/3}\varphi}}{9\Gamma(\alpha+1)^2\Gamma(3\alpha+1)\left(e^{\sqrt{\delta/6}\,\varphi}+1\right)^6}-\frac{25\delta^3 e^{\sqrt{\delta/6}\varphi}\left(15e^{\sqrt{2\delta/3}\,\varphi}-20e^{\sqrt{3\delta/2}\,\varphi}+6e^{\sqrt{\delta/6}\,\varphi}-5\right)}{108\Gamma(3\alpha+1)\left(e^{\sqrt{\delta/6}\,\varphi}+1\right)^6},\\
\zeta_3(\varphi,\tau) &= -\frac{25\delta^3(\delta-1)\Gamma(2\alpha+1)e^{\sqrt{2\delta/3}\varphi}}{9\varrho\Gamma(\alpha+1)^2\Gamma(3\alpha+1)\left(e^{\sqrt{\delta/6}\,\varphi}+1\right)^6}-\frac{25\delta^3(\delta-1)e^{\sqrt{\delta/6}\varphi}\left(15e^{\sqrt{2\delta/3}\,\varphi}-20e^{\sqrt{3\delta/2}\,\varphi}+6e^{\sqrt{\delta/6}\,\varphi}-5\right)}{108\varrho\Gamma(3\alpha+1)\left(e^{\sqrt{\delta/6}\,\varphi}+1\right)^6},\\
p^4\colon \xi_4(\varphi,\tau) &= -\frac{25\delta^4\Gamma(2\alpha+1)e^{\sqrt{2\delta/3}\varphi}\left(11e^{\sqrt{2\delta/3}\,\varphi}-5e^{\sqrt{\delta/6}\,\varphi}-1\right)}{27\Gamma(\alpha+1)^2\Gamma(4\alpha+1)\left(e^{\sqrt{\delta/6}\,\varphi}+1\right)^8}-\frac{125\delta^4\Gamma(3\alpha+1)e^{\sqrt{2\delta/3}\varphi}\left(2e^{\sqrt{\delta/6}\,\varphi}-1\right)}{27\Gamma(\alpha+1)\Gamma(2\alpha+1)\Gamma(4\alpha+1)\left(e^{\sqrt{\delta/6}\,\varphi}+1\right)^7}\\
&\quad+\frac{25\delta^4 e^{\sqrt{2\delta/3}\varphi}\left(124e^{\sqrt{2\delta/3}\,\varphi}+100e^{\sqrt[3]{2\delta/3}\varphi}+85e^{\sqrt{\delta/6}\,\varphi}-4\right)}{324\Gamma(4\alpha+1)\left(e^{\sqrt{\delta/6}\,\varphi}+1\right)^8}-\frac{625\delta^4 e^{\sqrt{\delta/6}\varphi}\left(17e^{\sqrt[3]{2\delta/3}\varphi}+1\right)}{648\Gamma(4\alpha+1)\left(e^{\sqrt{\delta/6}\,\varphi}+1\right)^8},\\
\zeta_4(\varphi,\tau) &= -\frac{25\delta^4(\delta-1)\Gamma(2\alpha+1)e^{\sqrt{2\delta/3}\varphi}\left(11e^{\sqrt{2\delta/3}\,\varphi}-5e^{\sqrt{\delta/6}\,\varphi}-1\right)}{27\varrho\Gamma(\alpha+1)^2\Gamma(4\alpha+1)\left(e^{\sqrt{\delta/6}\,\varphi}+1\right)^8}-\frac{125\delta^4(\delta-1)\Gamma(3\alpha+1)e^{\sqrt{2\delta/3}\varphi}\left(2e^{\sqrt{\delta/6}\,\varphi}-1\right)}{27\varrho\Gamma(\alpha+1)\Gamma(2\alpha+1)\Gamma(4\alpha+1)\left(e^{\sqrt{\delta/6}\,\varphi}+1\right)^7}\\
&\quad+\frac{25\delta^4(\delta-1)e^{\sqrt{2\delta/3}\varphi}\left(124e^{\sqrt{2\delta/3}\,\varphi}+100e^{\sqrt[3]{2\delta/3}\varphi}+85e^{\sqrt{\delta/6}\,\varphi}-4\right)}{324\varrho\Gamma(4\alpha+1)\left(e^{\sqrt{\delta/6}\,\varphi}+1\right)^8}-\frac{625\delta^4(\delta-1)e^{\sqrt{\delta/6}\varphi}\left(17e^{\sqrt[3]{2\delta/3}\varphi}+1\right)}{648\varrho\Gamma(4\alpha+1)\left(e^{\sqrt{\delta/6}\,\varphi}+1\right)^8}\\
&\quad\vdots\,.
\end{aligned}
\tag{63}
$$

Now, taking $p \longrightarrow 1$ gives the approximate solution as follows:

$$\xi(\varphi,\tau) = \xi_0 + \xi_1 + \xi_2 + \xi_3 + \xi_4 + \cdots$$

$$= \frac{1}{\left(e^{\sqrt{\delta/6}\,\varphi}+1\right)^2} + \frac{5\delta e^{\sqrt{\delta/6}\varphi}}{3\Gamma(\alpha+1)\left(e^{\sqrt{\delta/6}\,\varphi}+1\right)^3} + \frac{25\delta^2 e^{\sqrt{\delta/6}\varphi}\left(2e^{\sqrt{\delta/6}\,\varphi}-1\right)}{18\Gamma(2\alpha+1)\left(e^{\sqrt{\delta/6}\,\varphi}+1\right)^4}$$

$$- \frac{25\delta^3\Gamma(2\alpha+1)e^{\sqrt{2\delta/3}\varphi}}{9\Gamma(\alpha+1)^2\Gamma(3\alpha+1)\left(e^{\sqrt{\delta/6}\,\varphi}+1\right)^6} - \frac{25\delta^3 e^{\sqrt{\delta/6}\varphi}\left(15e^{\sqrt{2\delta/3}\,\varphi}-20e^{\sqrt{3\delta/2}\,\varphi}+6e^{\sqrt{\delta/6}\,\varphi}-5\right)}{108\Gamma(3\alpha+1)\left(e^{\sqrt{\delta/6}\,\varphi}+1\right)^6}$$

$$- \frac{25\delta^4\Gamma(2\alpha+1)e^{\sqrt{2\delta/3}\varphi}\left(11e^{\sqrt{2\delta/3}\,\varphi}-5e^{\sqrt{\delta/6}\,\varphi}-1\right)}{27\Gamma(\alpha+1)^2\Gamma(4\alpha+1)\left(e^{\sqrt{\delta/6}\,\varphi}+1\right)^8} - \frac{125\delta^4\Gamma(3\alpha+1)e^{\sqrt{2\delta/3}\varphi}\left(2e^{\sqrt{\delta/6}\,\varphi}-1\right)}{27\Gamma(\alpha+1)\Gamma(2\alpha+1)\Gamma(4\alpha+1)\left(e^{\sqrt{\delta/6}\,\varphi}+1\right)^7}$$

$$+ \frac{25\delta^4 e^{\sqrt{2\delta/3}\varphi}\left(124e^{\sqrt{2\delta/3}\,\varphi}+100e^{\sqrt{[2]}\,2\delta/3\varphi}+85e^{\sqrt{\delta/6}\,\varphi}-4\right)}{324\Gamma(4\alpha+1)\left(e^{\sqrt{\delta/6}\,\varphi}+1\right)^8} - \frac{625\delta^4 e^{\sqrt{\delta/6}\varphi}\left(17e^{\sqrt{[2]}\,2\delta/3\varphi}+1\right)}{648\Gamma(4\alpha+1)\left(e^{\sqrt{\delta/6}\,\varphi}+1\right)^8}\cdots,$$

$$\zeta(\varphi,\tau) = \zeta_0 + \zeta_1 + \zeta_2 + \zeta_3 + \zeta_4 + \cdots$$

$$= \frac{\delta-1}{\left(e^{\sqrt{\delta/6}\,\varphi}+1\right)^2\rangle} + \frac{5\delta(\delta-1)e^{\sqrt{\delta/6}\varphi}}{3\rangle\Gamma(\alpha+1)\left(e^{\sqrt{\delta/6}\,\varphi}\varphi+1\right)^3} + \frac{25\delta^2(\delta-1)e^{\sqrt{\delta/6}\varphi}\left(2e^{\sqrt{\delta/6}\,\varphi}-1\right)}{18\Gamma(2\alpha+1)\left(e^{\sqrt{\delta/6}\,\varphi}+1\right)^4}$$

$$- \frac{25\delta^3(\delta-1)\Gamma(2\alpha+1)e^{\sqrt{2\delta/3}\varphi}}{9\Gamma(\alpha+1)^2\Gamma(3\alpha+1)\left(e^{\sqrt{\delta/6}\,\varphi}+1\right)^6} - \frac{25\delta^3(\delta-1)e^{\sqrt{\delta/6}\varphi}\left(15e^{\sqrt{2\delta/3}\,\varphi}-20e^{\sqrt{3\delta/2}\,\varphi}+6e^{\sqrt{\delta/6}\,\varphi}-5\right)}{108\Gamma(3\alpha+1)\left(e^{\sqrt{\delta/6}\,\varphi}+1\right)^6}$$

$$- \frac{25\delta^4(\delta-1)\Gamma(2\alpha+1)e^{\sqrt{2\delta/3}\varphi}\left(11e^{\sqrt{2\delta/3}\,\varphi}-5e^{\sqrt{\delta/6}\,\varphi}-1\right)}{27\Gamma(\alpha+1)^2\Gamma(4\alpha+1)\left(e^{\sqrt{\delta/6}\,\varphi}+1\right)^8} - \frac{125\delta^4(\delta-1)\Gamma(3\alpha+1)e^{\sqrt{2\delta/3}\varphi}\left(2e^{\sqrt{\delta/6}\,\varphi}-1\right)}{27\rangle\Gamma(\alpha+1)\Gamma(2\alpha+1)\Gamma(4\alpha+1)\left(e^{\sqrt{\delta/6}\,\varphi}+1\right)^7}$$

$$+ \frac{25\delta^4(\delta-1)e^{\sqrt{2\delta/3}\varphi}\left(124e^{\sqrt{2\delta/3}\,\varphi}+100e^{\sqrt{[2]}\,2\delta/3\varphi}+85e^{\sqrt{\delta/6}\,\varphi}-4\right)}{324\Gamma(4\alpha+1)\left(e^{\sqrt{\delta/6}\,\varphi}+1\right)^8} - \frac{625\delta^4(\delta-1)e^{\sqrt{\delta/6}\varphi}\left(17e^{\sqrt{[2]}\,2\delta/3\varphi}+1\right)}{648\Gamma(4\alpha+1)\left(e^{\sqrt{\delta/6}\,\varphi}+1\right)^8}\cdots. \tag{64}$$

YTDM Solution

Taking Yang transformation of equation (41), we get

$$Y\left\{\frac{\partial^\alpha \xi}{\partial\tau^\alpha}\right\} = Y\left[\frac{\partial^2\xi}{\partial\varphi^2} + \varrho\zeta + \xi - \xi^2 - \varrho\xi\zeta\right],$$
$$Y\left\{\frac{\partial^\alpha \zeta}{\partial\tau^\alpha}\right\} = Y\left[\frac{\partial^2\zeta}{\partial\varphi^2} - \delta\xi\zeta\right]. \tag{65}$$

Applying the differential property of the Yang transform, we get

$$\frac{1}{u^\alpha}\{M(u) - u\xi(0)\} = Y\left[\frac{\partial^2\xi}{\partial\varphi^2} + \varrho\zeta + \xi - \xi^2 - \varrho\xi\zeta\right],$$
$$\frac{1}{u^\alpha}\{M(u) - u\zeta(0)\} = Y\left[\frac{\partial^2\zeta}{\partial\varphi^2} + \delta\zeta - \delta\xi\zeta\right]. \tag{66}$$

The inverse Yang transform implies that

$$\begin{aligned}
\xi(\varphi,\tau) &= \xi(0) + Y^{-1}\left[u^{\alpha}\left\{Y\left(\frac{\partial^2\xi}{\partial\varphi^2} + \zeta + \xi - \xi^2 - \xi\zeta\right)\right\}\right],\\
\zeta(\varphi,\tau) &= \zeta(0) + Y^{-1}\left[u^{\alpha}\left\{Y\left(\frac{\partial^2\zeta}{\partial\varphi^2} + \delta\zeta - \delta\xi\zeta\right)\right\}\right],\\
\xi(\varphi,\tau) &= \frac{1}{\left(e^{\sqrt{\delta/6}\,\varphi}+1\right)^2} + Y^{-1}\left[u^{\alpha}\left\{Y\left(\frac{\partial^2\xi}{\partial\varphi^2} + \zeta + \xi - \xi^2 - \xi\zeta\right)\right\}\right],\\
\zeta(\varphi,\tau) &= \frac{\delta-1}{\left(e^{\sqrt{\delta/6}\,\varphi}+1\right)^2} + Y^{-1}\left[u^{\alpha}\left\{Y\left(\frac{\partial^2\zeta}{\partial\varphi^2} + \delta\zeta - \delta\xi\zeta\right)\right\}\right].
\end{aligned} \tag{67}$$

Assume that the unknown $\xi(\varphi,\tau)$ and $\zeta(\varphi,\tau)$ functions, in infinite series form, have the following solution:

$$\begin{aligned}
\xi(\varphi,\tau) &= \sum_{m=0}^{\infty}\xi_m(\varphi,\tau),\\
\zeta(\varphi,\tau) &= \sum_{m=0}^{\infty}\zeta_m(\varphi,\tau),
\end{aligned} \tag{68}$$

where the Adomian polynomials $\xi^2 = \sum_{m=0}^{\infty}\mathscr{A}_m$ and $\xi\zeta = \sum_{m=0}^{\infty}\mathscr{B}_m$ and the nonlinear terms have been characterised. Using certain terms, equation (67) can be rewritten in the form as follows:

$$\begin{aligned}
\sum_{m=0}^{\infty}\xi_m(\varphi,\tau) &= \xi(\varphi,0) + Y^{-1}\left[u^{\alpha}Y\left[\frac{\partial^2\xi}{\partial\varphi^2} + \varrho\zeta + \xi - \sum_{m=0}^{\infty}\mathscr{A}_m - \varrho\sum_{m=0}^{\infty}\mathscr{B}_m\right]\right],\\
\sum_{m=0}^{\infty}\zeta_m(\varphi,\tau) &= \zeta(\varphi,0) + Y^{-1}\left[u^{\alpha}Y\left[\frac{\partial^2\zeta}{\partial\varphi^2} + \delta\zeta - \delta\sum_{m=0}^{\infty}\mathscr{B}_m\right]\right],\\
\sum_{m=0}^{\infty}\xi_m(\varphi,\tau) &= \frac{1}{\left(e^{\sqrt{\delta/6}\,\varphi}+1\right)^2} + Y^{-1}\left[u^{\alpha}Y\left[\frac{\partial^2\xi}{\partial\varphi^2} + \varrho\zeta + \xi - \sum_{m=0}^{\infty}\mathscr{A}_m - \varrho\sum_{m=0}^{\infty}\mathscr{B}_m\right]\right],\\
\sum_{m=0}^{\infty}\zeta_m(\varphi,\tau) &= \frac{\delta-1}{\varrho\left(e^{\sqrt{\delta/6}\,\varphi}+1\right)^2} + Y^{-1}\left[u^{\alpha}Y\left[\frac{\partial^2\zeta}{\partial\varphi^2} + \delta\zeta - \delta\sum_{m=0}^{\infty}\mathscr{B}_m\right]\right].
\end{aligned} \tag{69}$$

All forms of nonlinearity can be represented by the Adomian polynomials, according to equation (25), as

$$\begin{aligned}
\mathscr{A}_0 &= \xi_0^2,\\
\mathscr{A}_1 &= 2\xi_0\xi_1,\\
\mathscr{A}_2 &= 2\xi_0\xi_2 + \xi_1^2,\\
\mathscr{A}_3 &= 2\xi_0\xi_3 + 2\xi_1\xi_2,\\
\mathscr{B}_0 &= \xi_0\omega_0,\\
\mathscr{B}_1 &= \xi_1\zeta_0 + \xi_0\zeta_1,\\
\mathscr{B}_2 &= \xi_0\zeta_2 + \xi_1\zeta_1 + \xi_2\zeta_0,\\
\mathscr{B}_3 &= \xi_0\zeta_3 + \xi_1\zeta_2 + \xi_2\zeta_1 + \xi_3\zeta_0.
\end{aligned} \tag{70}$$

Thus, on comparing both side of equation (69),

$$\begin{aligned}
\xi_0(\varphi,\tau) &= \frac{1}{\left(e^{\sqrt{\delta/6\varphi}}+1\right)^2},\\
\zeta_0(\varphi,\tau) &= \frac{\delta-1}{\left(e^{\sqrt{\delta/6\varphi}}+1\right)^2}.
\end{aligned} \tag{71}$$

For $m = 0$,

$$\begin{aligned}
\xi_1(\varphi,\tau) &= \frac{5\delta e^{\sqrt{\delta/6\varphi}}}{3\Gamma(\alpha+1)\left(e^{\sqrt{\delta/6\varphi}}+1\right)^3},\\
\zeta_1(\varphi,\tau) &= \frac{5\delta(\delta-1)e^{\sqrt{\delta/6\varphi}}}{3\Gamma\rangle(\alpha+1)\left(e^{\sqrt{\delta/6\varphi}}+1\right)^3}.
\end{aligned} \tag{72}$$

For $m = 1$,

$$\begin{aligned}
\xi_2(\varphi,\tau) &= \frac{25\delta^2 e^{\sqrt{\delta/6\varphi}}\left(2e^{\sqrt{\delta/6\varphi}}-1\right)}{18\Gamma(2\alpha+1)\left(e^{\sqrt{\delta/6\varphi}}+1\right)^4},\\
\zeta_2(\varphi,\tau)\frac{25\delta^2(\delta-1)e^{\sqrt{\delta/6\varphi}}\left(2e^{\sqrt{\delta/6\varphi}}-1\right)}{18\rangle\Gamma(2\alpha+1)\left(e^{\sqrt{\delta/6\varphi}}+1\right)^4}.
\end{aligned} \tag{73}$$

For $m = 2$,

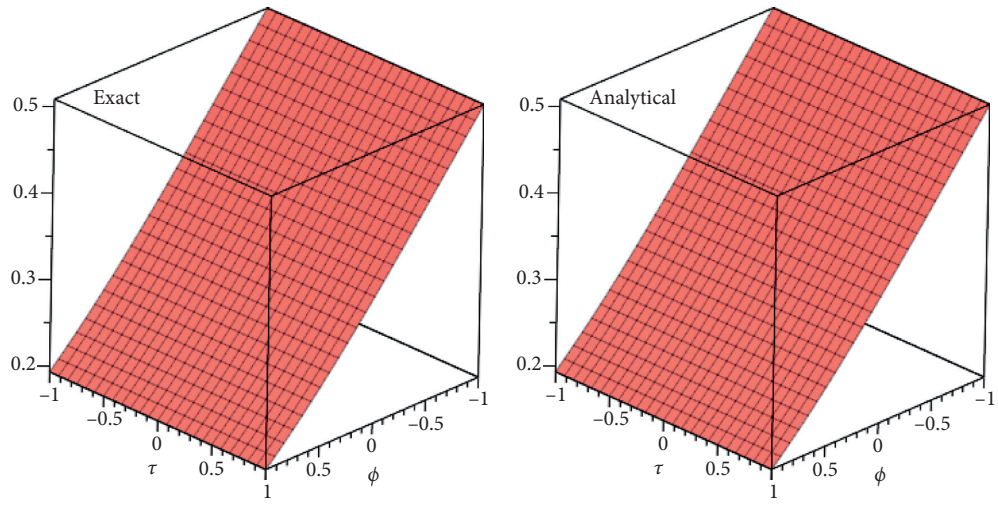

Figure 5: The exact solution and analytical solution graph at $\alpha = 1$ for $\xi(\varphi, \tau)$.

$$\xi_3(\varphi,\tau) = -\frac{25\delta^3\Gamma(2\alpha+1)e^{\sqrt{2\delta/3\varphi}}}{9\Gamma(\alpha+1)^2\Gamma(3\alpha+1)\left(e^{\sqrt{\delta/6\varphi}}+1\right)^6} - \frac{25\delta^3 e^{\sqrt{\delta/6\varphi}}\left(15e^{\sqrt{2\delta/3\varphi}} - 20e^{\sqrt{3\delta/2\varphi}} + 6e^{\sqrt{\delta/6\varphi}} - 5\right)}{108\Gamma(3\alpha+1)\left(e^{\sqrt{\delta/6\varphi}}+1\right)^6},$$

$$\zeta_3(\varphi,\tau) = -\frac{25\delta^3(\delta-1)\Gamma(2\alpha+1)e^{\sqrt{2\delta/3\varphi}}}{9\varrho\Gamma(\alpha+1)^2\Gamma(3\alpha+1)\left(e^{\sqrt{\delta/6\varphi}}+1\right)^6} - \frac{25\delta^3(\delta-1)e^{\sqrt{\delta/6\varphi}}\left(15e^{\sqrt{2\delta/3\varphi}} - 20e^{\sqrt{3\delta/2\varphi}} + 6e^{\sqrt{\delta/6\varphi}} - 5\right)}{108\varrho\Gamma(3\alpha+1)\left(e^{\sqrt{\delta/6\varphi}}+1\right)^6}. \tag{74}$$

For $m = 3$,

$$\xi_4(\varphi,\tau) = -\frac{25\delta^4\Gamma(2\alpha+1)e^{\sqrt{2\delta/3\varphi}}\left(11e^{\sqrt{2\delta/3\varphi}} - 5e^{\sqrt{\delta/6\varphi}} - 1\right)}{27\Gamma(\alpha+1)^2\Gamma(4\alpha+1)\left(e^{\sqrt{\delta/6}\,\varphi}+1\right)^8} - \frac{125\delta^4\Gamma(3\alpha+1)e^{\sqrt{2\delta/3\varphi}}\left(2e^{\sqrt{\delta/6\varphi}} - 1\right)}{27\Gamma(\alpha+1)\Gamma(2\alpha+1)\Gamma(4\alpha+1)\left(e^{\sqrt{\delta/6\varphi}}+1\right)^7}$$
$$+ \frac{25\delta^4 e^{\sqrt{2\delta/3\varphi}}\left(124e^{\sqrt{2\delta/3\varphi}} + 100e^{\sqrt{[2]\,2\delta/3\varphi}} + 85e^{\sqrt{\delta/6\varphi}} - 4\right)}{324\Gamma(4\alpha+1)\left(e^{\sqrt{\delta/6\varphi}}+1\right)^8} - \frac{625\delta^4 e^{\sqrt{\delta/6\varphi}}\left(17e^{\sqrt{[2]\,2\delta/3\varphi}} + 1\right)}{648\Gamma(4\alpha+1)\left(e^{\sqrt{\delta/6\varphi}}+1\right)^8},$$

$$\zeta_4(\varphi,\tau) = -\frac{25\delta^4(\delta-1)\Gamma(2\alpha+1)e^{\sqrt{2\delta/3\varphi}}\left(11e^{\sqrt{2\delta/3\varphi}} - 5e^{\sqrt{\delta/6\varphi}} - 1\right)}{27\varrho\Gamma(\alpha+1)^2\Gamma(4\alpha+1)\left(e^{\sqrt{\delta/6\varphi}}+1\right)^8} - \frac{125\delta^4(\delta-1)\Gamma(3\alpha+1)e^{\sqrt{2\delta/3\varphi}}\left(2e^{\sqrt{\delta/6\varphi}} - 1\right)}{27\varrho\Gamma(\alpha+1)\Gamma(2\alpha+1)\Gamma(4\alpha+1)\left(e^{\sqrt{\delta/6\varphi}}+1\right)^7}$$
$$+ \frac{25\delta^4(\delta-1)e^{\sqrt{2\delta/3\varphi}}\left(124e^{\sqrt{2\delta/3\varphi}} + 100e^{\sqrt{[2]\,2\delta/3\varphi}} + 85e^{\sqrt{\delta/6\varphi}} - 4\right)}{324\varrho\Gamma(4\alpha+1)\left(e^{\sqrt{\delta/6\varphi}}+1\right)^8} - \frac{625\delta^4(\delta-1)e^{\sqrt{\delta/6\varphi}}\left(17e^{\sqrt{[2]\,2\delta/3\varphi}} + 1\right)}{648\varrho\Gamma(4\alpha+1)\left(e^{\sqrt{\delta/6\varphi}}+1\right)^8}. \tag{75}$$

The remaining YTDM solution elements xi_m and ζ_m for $(m \geq 3)$ are similarly simple to get. As a result, we define the series of possibilities as follows:

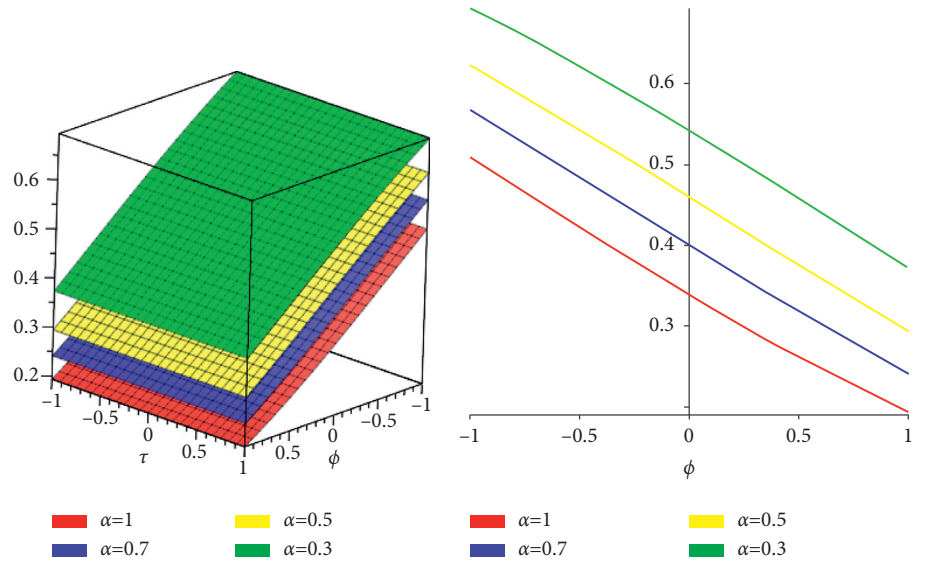

Figure 6: The different fractional-order solution graph of α for $\xi(\varphi, \tau)$.

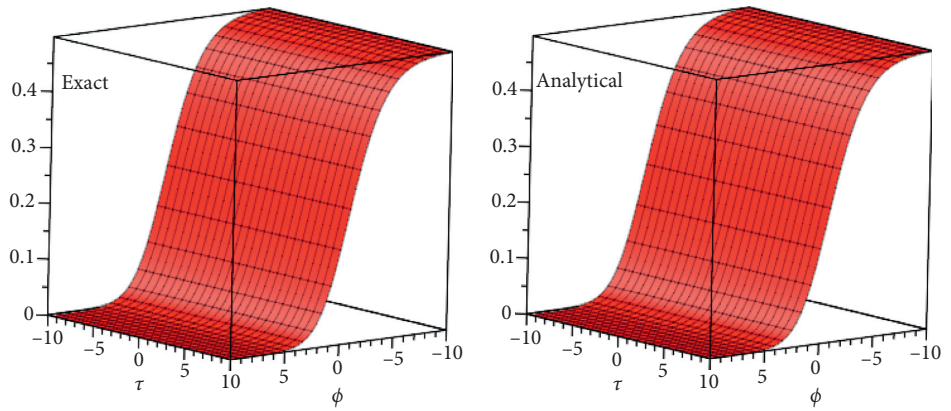

Figure 7: The exact solution and analytical solution graph at $\alpha = 1$ for $\xi(\varphi, \tau)$.

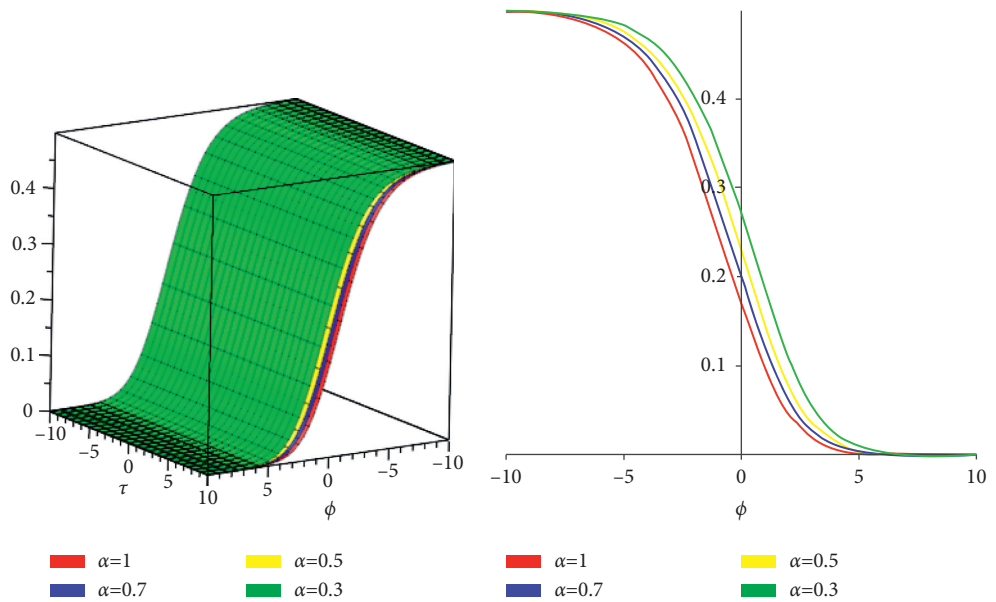

Figure 8: The different fractional-order solution graph of α for $\zeta(\varphi, \tau)$.

$$\xi(\varphi,\tau)=\sum_{m=0}^{\infty}\xi_m(\varphi,\tau)=\xi_0(\varphi,\tau)+\xi_1(\varphi,\tau)+\xi_2(\varphi,\tau)+\xi_3(\varphi,\tau)+\xi_4(\varphi,\tau)+\cdots,$$

$$\zeta(\varphi,\tau)=\sum_{m=0}^{\infty}\zeta_m(\varphi,\tau)=\zeta_0(\varphi,\tau)+\zeta_1(\varphi,\tau)+\zeta(\varphi,\tau)+\zeta_3(\varphi,\tau)+\zeta_4(\varphi,\tau)+\cdots,$$

$$\begin{aligned}\xi(\varphi,\tau)=&\frac{1}{\left(e^{\sqrt{\delta/6}\,\varphi}+1\right)^2}+\frac{5\delta e^{\sqrt{\delta/6}\varphi}}{3\Gamma(\alpha+1)\left(e^{\sqrt{\delta/6}\,\varphi}+1\right)^3}+\frac{25\delta^2 e^{\sqrt{\delta/6}\varphi}\left(2e^{\sqrt{\delta/6}\,\varphi}-1\right)}{18\Gamma(2\alpha+1)\left(e^{\sqrt{\delta/6}\,\varphi}+1\right)^4}\\&-\frac{25\delta^3\Gamma(2\alpha+1)e^{\sqrt{2\delta/3}\varphi}}{9\Gamma(\alpha+1)^2\Gamma(3\alpha+1)\left(e^{\sqrt{\delta/6}\,\varphi}+1\right)^6}-\frac{25\delta^3 e^{\sqrt{\delta/6}\varphi}\left(15e^{\sqrt{2\delta/3}\,\varphi}-20e^{\sqrt{3\delta/2}\,\varphi}+6e^{\sqrt{\delta/6}\,\varphi}-5\right)}{108\Gamma(3\alpha+1)\left(e^{\sqrt{\delta/6}\,\varphi}+1\right)^6}\\&-\frac{25\delta^4\Gamma(2\alpha+1)e^{\sqrt{2\delta/3}\varphi}\left(11e^{\sqrt{2\delta/3}\,\varphi}-5e^{\sqrt{\delta/6}\,\varphi}-1\right)}{27\Gamma(\alpha+1)^2\Gamma(4\alpha+1)\left(e^{\sqrt{\delta/6}\,\varphi}+1\right)^8}-\frac{125\delta^4\Gamma(3\alpha+1)e^{\sqrt{2\delta/3}\varphi}\left(2e^{\sqrt{\delta/6}\,\varphi}-1\right)}{27\Gamma(\alpha+1)\Gamma(2\alpha+1)\Gamma(4\alpha+1)\left(e^{\sqrt{\delta/6}\,\varphi}+1\right)^7}\\&+\frac{25\delta^4 e^{\sqrt{2\delta/3}\varphi}\left(124e^{\sqrt{2\delta/3}\,\varphi}+100e^{\sqrt[3]{2\delta/3}\varphi}+85e^{\sqrt{\delta/6}\,\varphi}-4\right)}{324\Gamma(4\alpha+1)\left(e^{\sqrt{\delta/6}\,\varphi}+1\right)^8}-\frac{625\delta^4 e^{\sqrt{\delta/6}\varphi}\left(17e^{\sqrt[3]{2\delta/3}\varphi}+1\right)}{648\Gamma(4\alpha+1)\left(e^{\sqrt{\delta/6}\,\varphi}+1\right)^8}\cdots,\end{aligned}\tag{76}$$

$$\begin{aligned}\zeta(\varphi,\tau)=&\frac{\delta-1}{\varrho\left(e^{\sqrt{\delta/6}\,\varphi}+1\right)^2}+\frac{5\delta(\delta-1)e^{\sqrt{\delta/6}\varphi}}{3\varrho\Gamma(\alpha+1)\left(e^{\sqrt{\delta/6}\,\varphi}\varphi+1\right)^3}+\frac{25\delta^2(\delta-1)e^{\sqrt{\delta/6}\varphi}\left(2e^{\sqrt{\delta/6}\,\varphi}-1\right)}{18\varrho\Gamma(2\alpha+1)\left(e^{\sqrt{\delta/6}\,\varphi}+1\right)^4}\\&-\frac{25\delta^3(\delta-1)\Gamma(2\alpha+1)e^{\sqrt{2\delta/3}\varphi}}{9\varrho\Gamma(\alpha+1)^2\Gamma(3\alpha+1)\left(e^{\sqrt{\delta/6}\,\varphi}+1\right)^6}-\frac{25\delta^3(\delta-1)e^{\sqrt{\delta/6}\varphi}\left(15e^{\sqrt{2\delta/3}\,\varphi}-20e^{\sqrt{3\delta/2}\,\varphi}+6e^{\sqrt{\delta/6}\,\varphi}-5\right)}{108\varrho\Gamma(3\alpha+1)\left(e^{\sqrt{\delta/6}\,\varphi}+1\right)^6}\\&-\frac{25\delta^4(\delta-1)\Gamma(2\alpha+1)e^{\sqrt{2\delta/3}\varphi}\left(11e^{\sqrt{2\delta/3}\,\varphi}-5e^{\sqrt{\delta/6}\,\varphi}-1\right)}{27\varrho\Gamma(\alpha+1)^2\Gamma(4\alpha+1)\left(e^{\sqrt{\delta/6}\,\varphi}+1\right)^8}-\frac{125\delta^4(\delta-1)\Gamma(3\alpha+1)e^{\sqrt{2\delta/3}\varphi}\left(2e^{\sqrt{\delta/6}\,\varphi}-1\right)}{27\varrho\Gamma(\alpha+1)\Gamma(2\alpha+1)\Gamma(4\alpha+1)\left(e^{\sqrt{\delta/6}\,\varphi}+1\right)^7}\\&+\frac{25\delta^4(\delta-1)e^{\sqrt{2\delta/3}\varphi}\left(124e^{\sqrt{2\delta/3}\,\varphi}+100e^{\sqrt[3]{2\delta/3}\varphi}+85e^{\sqrt{\delta/6}\,\varphi}-4\right)}{324\varrho\Gamma(4\alpha+1)\left(e^{\sqrt{\delta/6}\,\varphi}+1\right)^8}-\frac{625\delta^4(\delta-1)e^{\sqrt{\delta/6}\varphi}\left(17e^{\sqrt[3]{2\delta/3}\varphi}+1\right)}{648\varrho\Gamma(4\alpha+1)\left(e^{\sqrt{\delta/6}\,\varphi}+1\right)^8}\cdots.\end{aligned}$$

In Figure 5, the exact and analytical solution graph of $\xi(\varphi,\tau)$ is shown. In Figure 6, the different fractional graph of $\alpha=1,0.7,0.5$, and 0.3 of $\xi(\varphi,\tau)$ is shown. Similarly, in Figure 7, the exact and analytical solution graph of $\zeta(\varphi,\tau)$ is shown. In Figure 8, the different fractional graph of $\alpha=1,0.7,0.5$, and 0.3 of $\zeta(\varphi,\tau)$ is shown.

6. Conclusion

Finding the analytical solution to fractional partial differential equations is a tough task in most circumstances. This article makes a successful attempt to solve time-fractional Belousov–Zhabotinskii reaction for this purpose. It is confirmed that the proposed methods are the best tool for solving FPDEs. The displayed graphs confirm the strong relationship between the exact and analytical results. The plotted graphs confirmed the accuracy of the suggested techniques. In order to understand the behavior of the given problems, solutions at different fractional order is taken and is shown with the help of graphs. The convergence phenomenon has confirmed the reliability of the suggested method.

Data Availability

The numerical data used to support the findings of this study are included within the article.

Conflicts of Interest

The authors declare that there are no conflicts of interest regarding the publication of this article.

Acknowledgments

The authors extend their appreciation to the Deanship of Scientific Research at King Khalid University, Abha 61413, Saudi Arabia, for funding this work through research groups program under grant number R.G.P-1/192/42.

References

[1] A. Loverro, "Fractional calculus: history, definitions and applications for the engineer," *Rapport Technique*, Univeristy of Notre Dame: Department of Aerospace and Mechanical Engineering, Notre Dame, IN, USA, 2004.

[2] I. Podlubny, *Fractional Differential Equations*, Vol. 198, Academic Press, San Diego, CA, USA, 1999.

[3] J. Wang, Y. Ye, X. Pan, and X. Gao, "Parallel-type fractional zero-phase filtering for ECG signal denoising," *Biomedical Signal Processing and Control*, vol. 18, pp. 36–41, 2015.

[4] H. M. Srivastava, D. Baleanu, and C. Li, *Preface: Recent Advances in Fractional Dynamics*, AIP Publishing LLC, College Park, MD, USA, 2016.

[5] A. A. A. Kilbas, H. M. Srivastava, and J. J. Trujillo, *Theory And Applications Of Fractional Differential Equations*, Vol. 204, Elsevier Science Limited, Amsterdam, Netherlands, 2006.

[6] R. Hilfer, Ed., *Applications of Fractional Calculus in Physics*, World Scientific, Singapore, 2000.

[7] J. Ahmad, M. Mushtaq, and N. Sajjad, "Exact solution of whitham broer-kaup shallow water wave equations," *Journal of Science and Arts*, vol. 15, p. 5, 2015.

[8] M. Inc, "The approximate and exact solutions of the space- and time-fractional Burgers equations with initial conditions by variational iteration method," *Journal of Mathematical Analysis and Applications*, vol. 345, no. 1, pp. 476–484, 2008.

[9] X.-J. Yang, D. Baleanu, and H. M. Srivastava, "Local fractional similarity solution for the diffusion equation defined on Cantor sets," *Applied Mathematics Letters*, vol. 47, pp. 54–60, 2015.

[10] K. Nonlaopon, A. M. Alsharif, A. M. Zidan, A. Khan, Y. S. Hamed, and R. Shah, "Numerical investigation of fractional-order Swift–Hohenberg equations via a Novel transform," *Symmetry*, vol. 13, no. 7, 2021.

[11] F. Liu, P. Zhuang, and Q. Liu, "Numerical methods of fractional partial differential equations and applications," 2015, https://onlinelibrary.wiley.com/journal/10982426.

[12] K. M. Owolabi, A. Atangana, and A. Akgul, "Modelling and analysis of fractal-fractional partial differential equations: application to reaction-diffusion model," *Alexandria Engineering Journal*, vol. 59, no. 4, pp. 2477–2490, 2020.

[13] A. Ara, N. A. Khan, O. A. Razzaq, T. Hameed, and M. A. Z. Raja, "Wavelets optimization method for evaluation of fractional partial differential equations: an application to financial modelling," *Advances in Difference Equations*, vol. 2018, no. 1, pp. 1–13, 2018.

[14] F. Meng and Q. Feng, "A new fractional subequation method and its applications for space-time fractional partial differential equations," *Journal of Applied Mathematics*, vol. 2013, Article ID 481729, 10 pages, 2013.

[15] R. Shah, H. Khan, D. Baleanu, P. Kumam, and M. Arif, "The analytical investigation of time-fractional multi-dimensional Navier-Stokes equation," *Alexandria Engineering Journal*, vol. 59, no. 5, pp. 2941–2956, 2020.

[16] M. Shakeel, I. Hussain, H. Ahmad, I. Ahmad, P. Thounthong, and Y. F. Zhang, "Meshless technique for the solution of time-fractional partial differential equations having real-world applications," *Journal of Function Spaces*, vol. 2020, Article ID 8898309, 17 pages, 2020.

[17] G. W. Wang and T. Z. Xu, "The improved fractional sub-equation method and its applications to nonlinear fractional partial differential equations," *Romanian Reports in Physics*, vol. 66, no. 3, pp. 595–602, 2014.

[18] J. Cresson, "Fractional embedding of differential operators and Lagrangian systems," *Journal of Mathematical Physics*, vol. 48, no. 3, Article ID 033504, 2007.

[19] U. N. Katugampola, "New approach to a generalized fractional integral," *Applied Mathematics and Computation*, vol. 218, no. 3, pp. 860–865, 2011.

[20] H. Khan, R. Shah, P. Kumam, D. Baleanu, and M. Arif, "Laplace decomposition for solving nonlinear system of fractional order partial differential equations," *Advances in Difference Equations*, vol. 2020, no. 1, pp. 1–18, 2020.

[21] M. Klimek, "Lagrangian fractional mechanics - a noncommutative approach," *Czechoslovak Journal of Physics*, vol. 55, no. 11, pp. 1447–1453, 2005.

[22] M. Klimek, *On Solutions of Linear Fractional Differential Equations of a Variational Type*, Publishing Office of Czestochowa University of Technology, Częstochowa, Poland, 2009.

[23] J. Xu, H. Khan, H. Khan et al., "The analytical analysis of nonlinear fractional-order dynamical models," *AIMS Mathematics*, vol. 6, no. 6, pp. 6201–6219, 2021.

[24] H. Khan, R. Shah, J. F. Gómez-Aguilar, D. Shoaib, D. Baleanu, and P. Kumam, "Travelling waves solution for fractional-order biological population model," *Mathematical Modelling of Natural Phenomena*, vol. 16, p. 32, 2021.

[25] S. Momani and Z. Odibat, "Analytical solution of a time-fractional Navier-Stokes equation by Adomian decomposition method," *Applied Mathematics and Computation*, vol. 177, no. 2, pp. 488–494, 2006.

[26] R. Darzi, B. Mohammadzade, S. Mousavi, and R. Beheshti, "Sumudu transform method for solving fractional differential equations and fractional diffusion-wave equation," *Journal of Mathematical and Computational Science*, vol. 6, no. 1, pp. 79–84, 2013.

[27] A. Arikoglu and I. Ozkol, "Solution of fractional differential equations by using differential transform method," *Chaos, Solitons & Fractals*, vol. 34, no. 5, pp. 1473–1481, 2007.

[28] Z. Odibat, S. Momani, and H. Xu, "A reliable algorithm of homotopy analysis method for solving nonlinear fractional differential equations," *Applied Mathematical Modelling*, vol. 34, no. 3, pp. 593–600, 2010.

[29] G.-c. Wu, "A fractional variational iteration method for solving fractional nonlinear differential equations," *Computers & Mathematics with Applications*, vol. 61, no. 8, pp. 2186–2190, 2011.

[30] T. C. Mahor, R. Mishra, and R. Jain, "Analytical solutions of linear fractional partial differential equations using fractional Fourier transform," *Journal of Computational and Applied Mathematics*, vol. 385, Article ID 113202, 2021.

[31] G. Adomian, "Solution of physical problems by decomposition," *Computers & Mathematics with Applications*, vol. 27, no. 9-10, pp. 145–154, 1994.
[32] G. Adomian, "A review of the decomposition method in applied mathematics," *Journal of Mathematical Analysis and Applications*, vol. 135, Article ID 501544, 1988.
[33] J.-H. He, "Homotopy perturbation technique," *Computer Methods in Applied Mechanics and Engineering*, vol. 178, no. 3-4, pp. 257–262, 1999.
[34] J.-H. He, "A coupling method of a homotopy technique and a perturbation technique for non-linear problems," *International Journal of Non-linear Mechanics*, vol. 35, no. 1, pp. 37–43, 2000.
[35] J.-H. He, "Application of homotopy perturbation method to nonlinear wave equations," *Chaos, Solitons & Fractals*, vol. 26, no. 3, pp. 695–700, 2005.
[36] J.-H. He, "Homotopy perturbation method for bifurcation of nonlinear problems," *International Journal of Nonlinear Sciences and Numerical Stimulation*, vol. 6, no. 2, pp. 207-208, 2005.
[37] J.-H. He, "Homotopy perturbation method for solving boundary value problems," *Physics Letters A*, vol. 350, no. 1-2, pp. 87-88, 2006.
[38] R. G. Gibbs, "Traveling waves in the Belousov-Zhabotinskii reaction," *SIAM Journal on Applied Mathematics*, vol. 38, no. 3, pp. 422–444, 1980.
[39] Q.-X. Ye and M.-X. Wang, "Travelling wave front solutions of noyes-field system for Belousov-Zhabotinskii reaction," *Nonlinear Analysis: Theory, Methods & Applications*, vol. 11, no. 11, pp. 1289–1302, 1987.